

*Vid CRDI
for Redbook*

Outer Continental Shelf Environmental Assessment Program

Final Reports of Principal Investigators

Volume 51

December 1986



U.S. DEPARTMENT OF COMMERCE
National Oceanic and Atmospheric Administration
National Ocean Service
Office of Oceanography and Marine Assessment
Ocean Assessments Division
Alaska Office



U.S. DEPARTMENT OF THE INTERIOR
Minerals Management Service
OCS Study, MMS 86-0113

"Outer Continental Shelf Environmental Assessment Program Final Reports of Principal Investigators" ("OCSEAP Final Reports") continues the series entitled "Environmental Assessment of the Alaskan Continental Shelf Final Reports of Principal Investigators."

It is suggested that sections of this publication be cited as follows:

Anderson, J. W., G. Roesijadi, J. M. Augenfeld, R. G. Riley, and E. A. Credilius. 1980. Research to determine the accumulation of organic constituents and heavy metals from petroleum-impacted sediments by marine detritivores of the Alaskan outer continental shelf. U.S. Dep. Commer., NOAA, OCSEAP Final Rep. 51(1986):1-162

Baker, E. T. 1983. Suspended particulate matter distribution, transport, and physical characteristics in the north Aleutian Shelf and St. George Basin lease areas. U.S. Dep. Commer., NOAA, OCSEAP Final Rep. 51(1986):163-307

Cline, J. D., K. Kelly-Hansen, and C. N. Katz. 1982. The production and dispersion of dissolved methane in southeastern Bering Sea. U.S. Dep. Commer., NOAA, OCSEAP Final Rep. 51(1986):309-417

Hayes, M. O. 1980. Oil spill vulnerability, coastal morphology, and sedimentation of outer Kenai Peninsula and Montague Island. U.S. Dep. Commer., NOAA, OCSEAP Final Rep. 51(1986):419-538

Royer, T. C. 1981. Circulation and water masses in the Gulf of Alaska. U.S. Dep. Commer., NOAA, OCSEAP Final Rep. 51(1986):539-684

Muench, R. D., P. R. Temple, J. T. Gunn, and L. E. Hachmeister. 1982. Coastal oceanography of the northeastern Gulf of Alaska. U.S. Dep. Commer., NOAA, OCSEAP Final Rep. 51(1986):685-829

OCSEAP Final Reports are published by the U.S. Department of Commerce, National Oceanic and Atmospheric Administration, National Ocean Service, Office of Oceanography and Marine Assessment, Ocean Assessments Division, Alaska Office, Anchorage, and primarily funded by the Minerals Management Service, U.S. Department of the Interior, through interagency agreement.

Requests for receipt of OCSEAP Final Reports on a continuing basis should be addressed to:

NOAA-OMA-OAD
Alaska Office
701 C Street
P.O. Box 56
Anchorage, AK 99513

The facts, conclusions, and issues appearing in these reports are based on research results of the Outer Continental Shelf Environmental Assessment Program (OCSEAP), which is managed by the National Oceanic and Atmospheric Administration, U.S. Department of Commerce, and funded (wholly or in part) by the Minerals Management Service, U.S. Department of the Interior, through an Interagency Agreement.

Mention of a commercial company or product does not constitute endorsement by the National Oceanic and Atmospheric Administration. Use for publicity or advertising purposes of information from this publication concerning proprietary products or the tests of such products is not authorized.

Content of these reports has not been altered from that submitted by the Principal Investigators. In some instances, minor grammatical, spelling, and punctuation errors have been corrected to improve readability; some figures, charts, and tables have been enhanced to improve clarity in reproduction.



Outer Continental Shelf Environmental Assessment Program

Final Reports of Principal Investigators

VOLUME 51

DECEMBER 1986

C O N T E N T S

J. W. ANDERSON, G. ROESIJADI, J. M. AUGENFELD, R. G. RILEY, and E. A. CREDILIUS: Research to determine the accumulation of organic constituents and heavy metals from petroleum-impacted sediments by marine detritivores of the Alaskan outer continental shelf.	1
E. T. BAKER: Suspended particulate matter distribution, transport, and physical characteristics in the north Aleutian Shelf and St. George Basin lease areas.	163
J. D. CLINE, K. KELLY-HANSEN, and C. N. KATZ: The Production and dispersion of dissolved methane in southeastern Bering Sea.	309
M. O. HAYES: Oil spill vulnerability, coastal morphology, and sedimentation of outer Kenai Peninsula and Montague Island.	419
T. C. ROYER: Circulation and water masses in the Gulf of Alaska.	539
R. D. MUENCH, P. R. TEMPLE, J. T. GUNN, and L. E. HACHMEISTER: Coastal oceanography of the northeastern Gulf of Alaska.	685

RESEARCH TO DETERMINE THE ACCUMULATION OF ORGANIC CONSTITUENTS
AND HEAVY METALS FROM PETROLEUM-IMPACTED SEDIMENTS
BY MARINE DETRITIVORES OF THE ALASKAN OUTER CONTINENTAL SHELF

by

J. W. Anderson, G. Roesijadi, J. M. Augenfeld,
R. G. Riley, and E. A. Credilius

Principal Investigators

D. L. Woodruff, J. W. Blaylock, B. L. Thomas,
S. L. Kiesser, and J. L. Webster

Technical Specialists

Battelle Pacific Northwest Laboratories

Final Report
Outer Continental Shelf Environmental Assessment Program
Research Unit 454

April 1980

Legal Notice

This report was prepared by Battelle as an account of sponsored research activities. Neither Sponsor nor Battelle nor any person acting on behalf of either:

MAKES ANY WARRANTY OR REPRESENTATION, EXPRESS OR IMPLIED, with respect to the accuracy, completeness, or usefulness of the information contained in this report, or that the use of any information, apparatus, process, or composition disclosed in this report may not infringe privately owned rights; or

Assumes any liabilities with respect to the use of, or for damages resulting from the use of, any information, apparatus, process or composition disclosed in this report.

TABLE OF CONTENTS

List of Figures	5
List of Tables	7
Abstract	11
Acknowledgement	11
I. EXECUTIVE SUMMARY	13
II. BIOAVAILABILITY OF PETROLEUM HYDROCARBONS FROM SEDIMENT	21
A. The Fate of Polyaromatic Hydrocarbons in an Intertidal Sediment Exposure System: Bioavailability to <u>Macoma</u> <u>inquinata</u> (Mollusca:Pelecypoda)	23
B. The Fate of Polyaromatic Hydrocarbons in an Intertidal Sediment Exposure System: Bioavailability to <u>Abarenicola</u> <u>pacifica</u> (Annelida:Polychaeta)	49
III. BIOAVAILABILITY OF METALS FROM PETROLEUM-IMPACTED SEDIMENTS	61
A. Bioavailability of Trace Elements from Oil-Contaminated Sediment to <u>Macoma inquina</u> ta and <u>Phascolosoma</u> <u>agassizii</u>	63
B. Uptake of Trace Metals by the Clam <u>Macoma inquina</u> ta from Clean and Oil-Contaminated Detritus	75
IV. SUBLETHAL EFFECTS OF PETROLEUM HYDROCARBON CONTAMINATION OF SEDIMENTS	89
A. Effects of Prudhoe Bay Crude Oil Contaminated Sediments on <u>Protothaca staminea</u> (Mollusca:Pelecypoda): Hydrocarbon Content, Condition Index, Free Amino Acid Level	91
B. Effects of Prudhoe Bay Crude Oil Contamination on Sediment Working Rates of <u>Abarenicola pacifica</u>	105
C. Effects of Prudhoe Bay Crude Oil in Sediment on <u>Abarenicola pacifica</u> in Laboratory and Field Experiments ...	115
V. EFFECTS OF WEATHERING ON OIL	135
A. Changes in the Volatile Hydrocarbon Content of Prudhoe Bay Crude Oil Treated under Different Simulated Weathering Conditions	137
VI. DISTRIBUTION AND FATE OF POLYAROMATIC HYDROCARBONS IN SEDIMENT-WATER SYSTEMS	155
A. Distribution and Fate of Polyaromatic Hydrocarbons in Interstitial Water and Sediment	157
VII. APPENDIX: Publications Resulting from Research Conducted on the NOAA/BLM OSCEAP Program Unit 454	159



LIST OF FIGURES

Section II-A Figures:

- Figure 1. Design of sediment exposure system.
- Figure 2. Scheme for the extraction and analysis of ^{14}C -labelled hydrocarbons from clam tissue and sediment.
- Figure 3. Concentration of phenanthrene in Macoma tissue and sediment (59-day exposure). The curves were fit by eye to connect the means ($n = 3$), and the vertical bars represent standard deviations.
- Figure 4. Concentration of chrysene in Macoma tissue and sediment (58-day exposure). The curves were fit by eye to connect the means ($n = 3$), and the vertical bars represent standard deviations.
- Figure 5. Concentration of benzo(a)pyrene in Macoma tissue and sediment (60-day exposure). The curves were fit by eye to connect the means ($n = 3$), and the vertical bars represent standard deviations.

Section II-B Figures:

- Figure 1. Concentration of phenanthrene in Abarenicola tissue and sediment (60-day exposure).
- Figure 2. Concentration of chrysene in Abarenicola tissue and sediment (58-day exposure).
- Figure 3. Concentration of benzo(a)pyrene in Abarenicola tissue and sediment (60-day exposure).

Section III-B Figures:

- Figure 1. Detritus (mg/g) ingested by Macoma inquinata.
- Figure 2. Incorporation of radio-labelled zinc into Macoma tissue.
- Figure 3. Incorporation of radio-labelled cobalt into Macoma tissue.

Section IV-B Figure:

- Figure 1. Regression of fecal weight per unit body weight on body weight.
- Control: $y = 1.839 - 2.56 x$; $r = -.653$; $n = 8$
250 ppm: $y = 1.600 - 2.56 x$; $r = -.941$; $n = 9$
500 ppm: $y = .449 - .50 x$; $r = -.921$; $n = 8$
1000 ppm: $y = .438 - .50 x$; $r = -.885$; $n = 7$

Section IV-C Figures:

- Figure 1. Regression of weight-specific fecal weight on body weight: effect of Prudhoe Bay crude oil in sediment.
- Figure 2. Free amino acid content of body wall muscle of Abarenicola pacifica ($\mu\text{m/g}$ wet wt.) following laboratory exposure to sediment containing 400 ppm Prudhoe Bay crude oil.
- Figure 3. Free amino acid concentrations in A. pacifica body wall muscle: field exposure to 400 ppm Prudhoe Bay crude oil in sediment.

Section V-A Figures:

- Figure 1. Gas capillary chromatograms of saturate hydrocarbon fraction from original Prudhoe Bay crude oil (top) and saturate hydrocarbon fraction from 24-day weathered oil sample from Tank #1 (bottom).
- Figure 2. Gas capillary chromatograms of aromatic hydrocarbon fraction from original Prudhoe Bay Crude Oil (top) and aromatic hydrocarbon fraction from 24-day weathered oil sample from Tank #1 (bottom). A denotes monoaromatic hydrocarbon region.

LIST OF TABLES

Section II-A Tables:

- Table 1. Concentration of PAH in Macoma tissue and sediment ($\bar{x} \pm$ S.D., $n = 3$), and the ratio between these two (magnification factor).
- Table 2. Percent recovery of ^{14}C -radioactivity from tissue and sediment extracts chromatographed on GPC and reverse-phase liquid chromatographic systems.
- Table 3. PAH contents of sediment and tissues (ppb wet weight).

Section II-B Tables:

- Table 1. Particle size distribution and water content of sediments from Macoma and Abarenicola habitats.
- Table 2. Concentration of PAH in Abarenicola tissue and sediment (pmoles/g ww).
- Table 3. Ratio of tissue concentration of PAH after 60 days exposure to sediment concentration of PAH one day after contamination.

Section III-A Tables:

- Table 1. Trace element concentrations in Prudhoe Bay crude oil. Samples represent oil from two different barrels and were analyzed by neutron activation analysis.
- Table 2. Uptake of trace elements by Phascolosoma agassizii exposed to oil-contaminated sediment.
- Table 3. Uptake of trace elements by Macoma inquinata exposed to oil-contaminated detritus (ca. 2000 $\mu\text{g/g}$ total hydrocarbons).
- Table 4. Analysis of trace elements in Macoma inquinata by x-ray fluorescence. Estimation of sample variability.
- Table 5. Uptake of total gamma-labelled trace metals from detritus by Macoma. Values are counts per 40 minutes per gram (tissue) or per 200 ml (seawater).
- Table 6. Uptake of specific radio-labelled trace metals from detritus by Macoma. Values are counts per 1000 minutes per gram detritus or tissue and per 200 ml seawater.

Section III-B Tables:

- Table 1. Co content of filtered sea water ($\mu\text{g} \times 10^{-5}/\text{ml}$).
- Table 2. Calculated weight of detritus (mg/g d.w.) in Macoma inquinata.
- Table 3. Zn and CO ($\mu\text{g/g}$ d.w. tissue) incorporation into Macoma inquinata exposed to oiled and non-oiled detritus.

Section IV-A Tables:

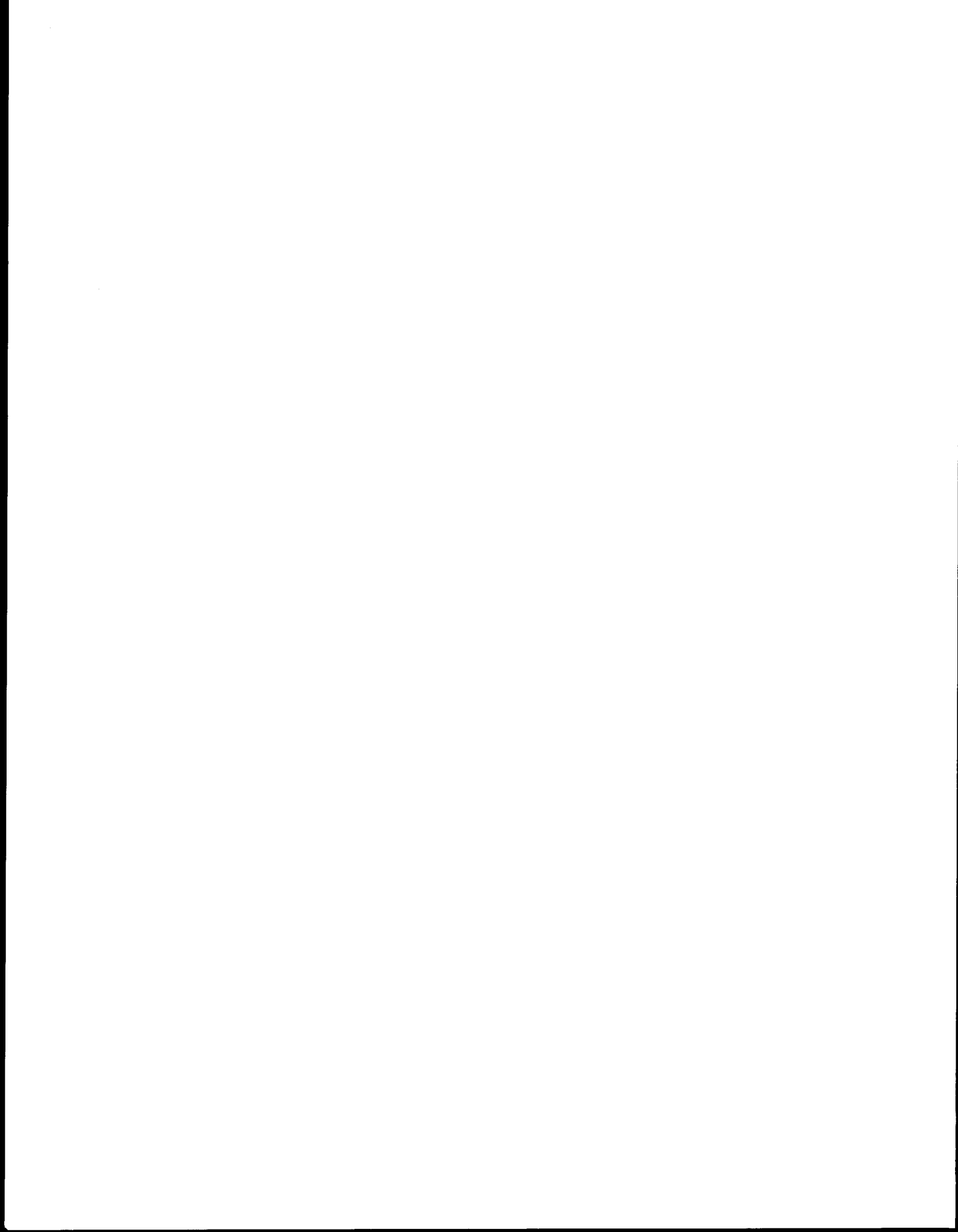
- Table 1. Glass capillary gas chromatographic analyses of petroleum hydrocarbons content ($\mu\text{g/g}$) in Macoma and Protothaca tissue and sediment after 54 days exposure to oil-contaminated sediment.
- Table 2. Condition indices of initial control, field control, and exposed Protothaca staminea.
- Table 3. Free amino acid concentration in gills, mantle, and adductor muscle of Protothaca staminea ($\mu\text{moles/g}$) after 54 days exposure to oil-contaminated sediment.
- Table 4. Survival and condition index of Macoma and Protothaca after exposure to oil-contaminated sediment.
- Table 5. Free amino acid content ($\mu\text{moles/g}$) of Macoma and Protothaca.

Section IV-B Tables:

- Table 1. Particle size distribution in tide flat habitat of Abarenicola pacifica.
- Table 2. Effects of PBC on survival and behavior of Abarenicola pacifica.
- Table 3. Effect of Prudhoe Bay crude oil on fecal production of A. pacifica: laboratory exposure.
- Table 4. Effect of Prudhoe Bay crude oil contamination of fecal production of A. pacifica: field exposure.

Section V-A Tables:

- Table 1. Parameters measured during the course of the weathering experiment.
- Table 2. Concentrations of saturate hydrocarbons in Prudhoe Bay crude oil (PBC) and in 24-day weathered oil samples. Concentrations in mg/gram oil.
- Table 3. nC_{17} /pristane and nC_{18} /phytane ratios from PBC crude oil and PBC oil weathered in three exposure systems.
- Table 4. Concentrations of aromatic hydrocarbons in Prudhoe Bay crude oil (PBC) and in 24-day weathered oil samples. Concentrations in mg/gram oil.
- Table 5. Significance in the relationships between the concentrations of various saturate and aromatic hydrocarbons and hydrocarbon types and the type of exposure. Confidence limits are measured at the 95% level. S.D. = significantly different, N.S.D. = not significantly different.

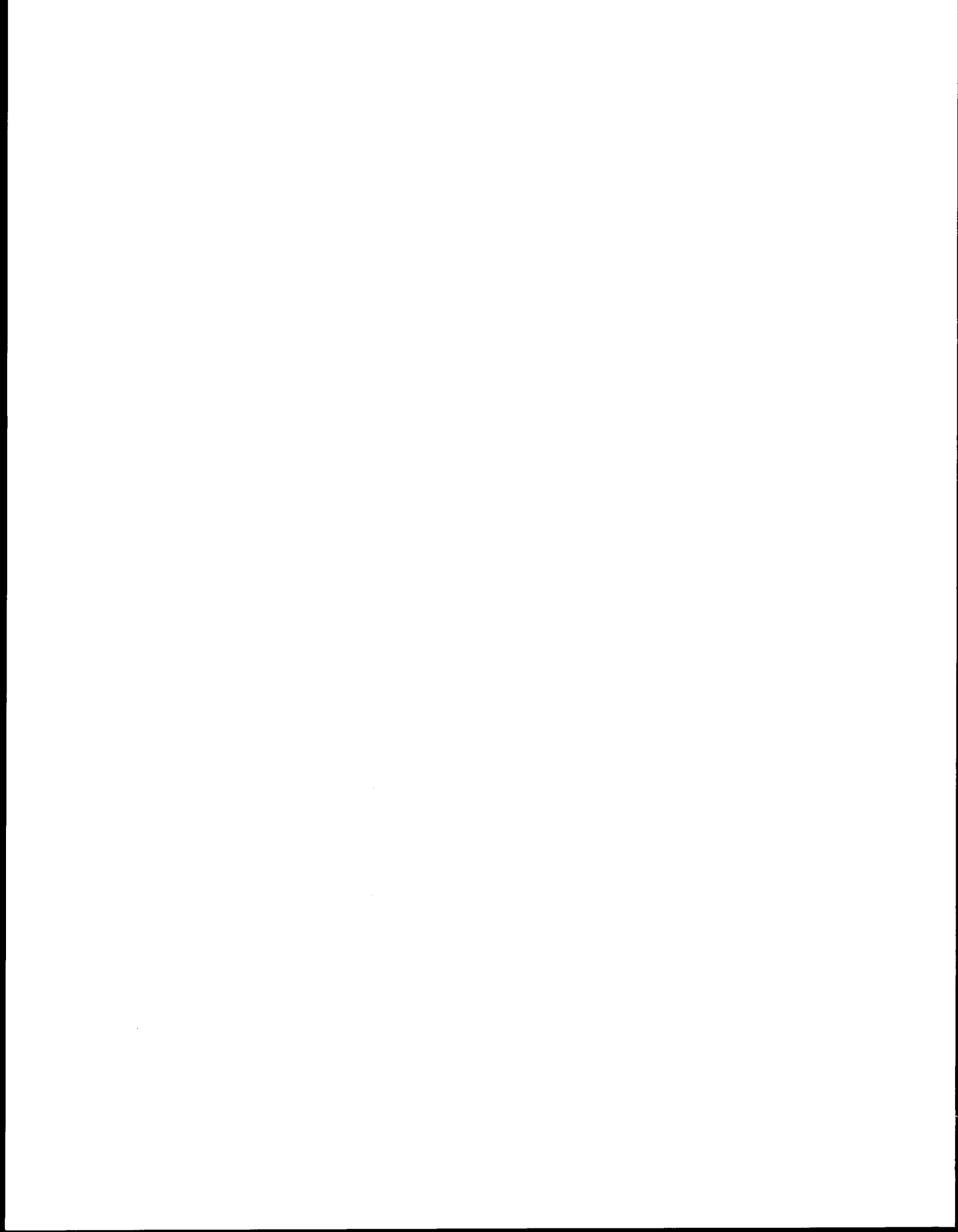


ABSTRACT

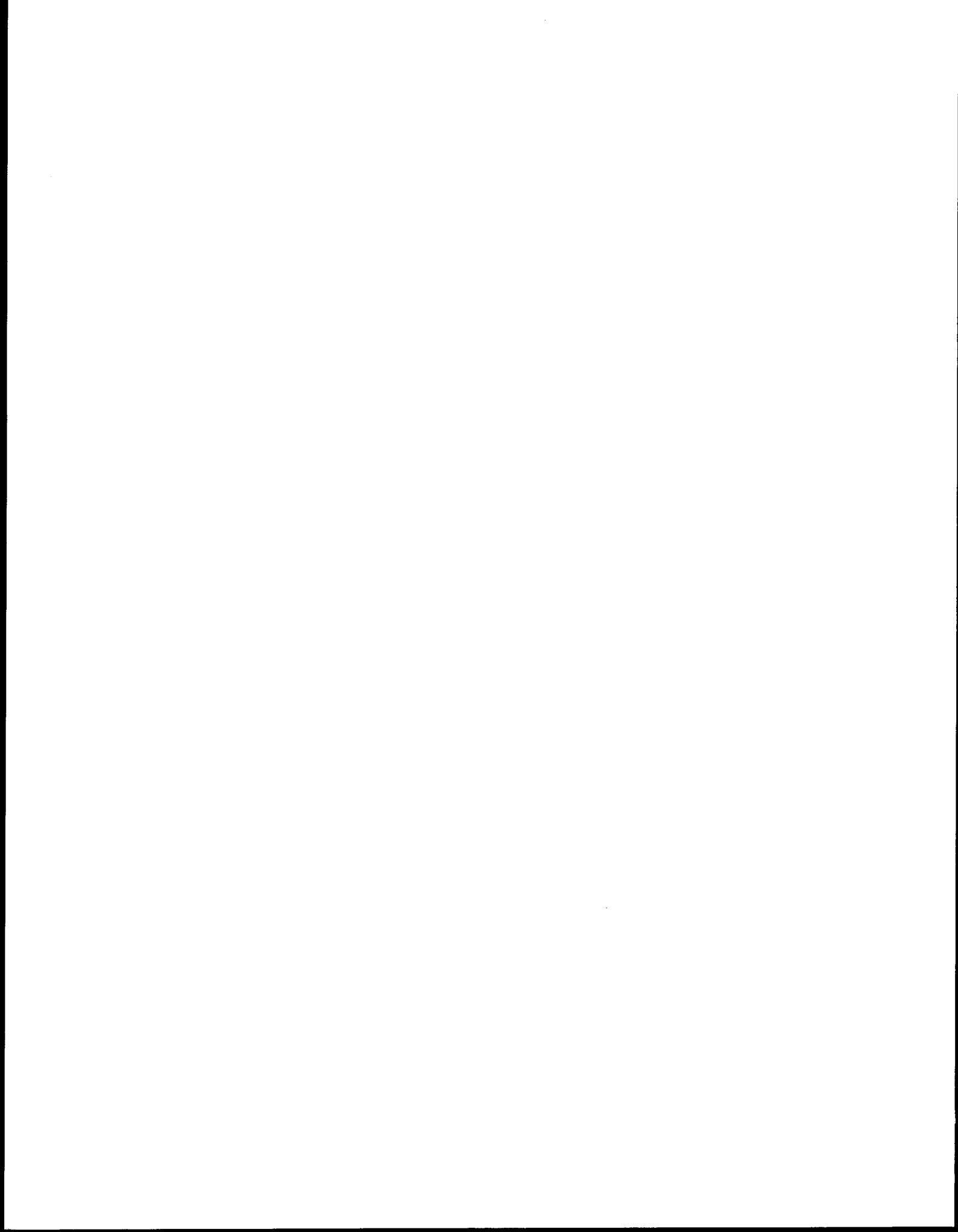
The major objective of this research program was to investigate the fate of petroleum hydrocarbons in the water column and intertidal zone and their bioavailability to, and effects on, the biota. Investigations included two field habitats to supplement laboratory observations. We have learned: 1) That the molecular weight of petroleum hydrocarbon compounds is positively correlated with retention in: (a) weathered oil, (b) oil-impacted sediment, and (c) molluscan tissue; 2) That there was no evidence that the presence of oil enhances the bioavailability of heavy metals to clams (Macoma); 3) That metabolized aromatic hydrocarbons were not found in Macoma tissue, but these polar compounds were present in interstitial water; 4) That petroleum hydrocarbon pollution depresses the feeding rate of marine worms (Abarenicola); and, 5) That pollution is less stressful to a filter feeding clam than to a deposit feeding clam. The work has advanced the level of knowledge by demonstrating that exposure to petroleum hydrocarbons in sediments can result in accumulation and retention of heavier polynuclear aromatic hydrocarbons, but does not enhance uptake of trace metals. These findings have been described in Quarterly Reports and Annual Reports to NOAA/OCSEAP and several journal articles are published, in press, or submitted.

ACKNOWLEDGEMENT

This study was supported by the Bureau of Land Management through inter-agency agreement with the National Oceanic and Atmospheric Administration under which a multi-year program responding to needs of petroleum development of the Alaskan Continental Shelf is managed by the Outer Continental Shelf Environmental Assessment Program (OCSEAP) Office.



I. EXECUTIVE SUMMARY



I. EXECUTIVE SUMMARY

Substantial proportions of the intertidal zone of the lower Cook Inlet shoreline consist of fine-grained muddy sediments. Sites with significant areas of such sediment include: Koyuktolik Bay, China Poot Bay, the north shore of Kachemak Bay, the north side of Homer spit, the northwest coast of the Kenai Peninsula, Tuxedni Bay, Chinitna Bay, Iniskin Bay, Bruin Bay, and McNeill Cove (Sears and Zimmerman, 1977). Petroleum or its products which impact muddy sediments as a result of tanker accidents, platform spills, or chronic leakages may persist and affect local organisms for periods of years (Mayo et al., 1978; Teal et al., 1978, Krebs and Burns, 1977; Sabo and Stegeman, 1977). These effects are of more than local interest. Dames and Moore (1979) conducted ecological studies of the intertidal habitats of lower Cook Inlet and concluded, with respect to the mudflats, that "fish, crabs, and ducks move onto the intertidal flats during high tides, and the shorebirds move in during low tides. Commercially, the most important of these interactions appears to be that of juvenile salmon. The consequence is that a very large proportion of the tissue produced on the flats is exploited by predators from other systems. This is particularly important on the west side of the inlet because of 1) the richness of the mud flats, 2) the large proportion of mud flat habitat in the intertidal zone and, 3) the potential susceptibility of this assemblage to oil pollution."

In view of the significance and vulnerability of this habitat type in lower Cook Inlet a series of investigations has been carried out to determine the extent to which populations of invertebrates might become contaminated by specific components of petroleum hydrocarbons. The effects of crude oil on some measures of the growth, activity, and well-being of the intertidal populations, as well as the effect of weathering on the oil itself have also been examined.

The species of organisms used in these investigations were selected to represent genera and feeding types which are important in the habitats under consideration. They included Macoma inquinata, a species very closely related to Macoma balthica which is among the most abundant bivalves in the

mud flat assemblage at Glacier Spit, Chinitna Bay, studied by Dames and Moore (1979). These clams are surface deposit feeders. Another clam, Protothaca staminea, was chosen to represent the suspension feeders, such as Mya which are also present in large numbers in the Glacier Spit fauna. The polychaete, Abarenicola pacifica represents another phylum and another nutritional type, namely non-selective deposit feeding. It is found in large numbers in the upper intertidal zone of Glacier Spit and in smaller numbers in sandier sites of Deep Creek and Homer Spit in lower Cook Inlet.

The toxicity of petroleum hydrocarbons is correlated with their content of aromatic compounds. Furthermore, concern has been expressed that some polynuclear aromatics, or their metabolites, which are carcinogenic might be taken up from oil-impregnated sediment by invertebrates and transferred to higher trophic levels in the food chain. The accumulation of specific aromatic compounds from contaminated sediment was therefore investigated. In the case of the surface deposit feeding clam Macoma there was a positive correlation between molecular size and accumulation. The two-ring naphthalenes and the three-ring compound phenanthrene were not accumulated to concentrations above those in the sediment after sixty days of exposure. The average accumulation of two and three ring aromatics by the suspension-feeding clam Protothaca was even lower than in the deposit feeder.

By contrast the four-ring compound chrysene and the five-ring benzo(a)-pyrene, which are potential carcinogens or metabolic precursors of carcinogens, continued to be accumulated over a sixty day period by Macoma, tissue magnification factor for the two compounds were 11.7 and 5.3, respectively, (wet weight tissue per wet weight sediment). Abarenicola accumulated and retained chrysene initially, but reached a plateau at a concentration some six times as high as that in the sediment after fifteen days. Phenanthrene and benzo(a)pyrene were also accumulated for fifteen days to levels four and six times as high, respectively, as those in the sediment. But in the polychaete the concentrations of these compounds fell to 53% and 68% of their peak values over the next 45 days, though the sediment concentrations remained high. No carcinogenic metabolites were found to accumulate in the tissues of either Macoma or Abarenicola. These data may be useful in estimating the degree of risk from this source to higher organisms at specific levels of sediment contamination.

Concern has also been expressed that the presence of petroleum hydrocarbons in sediment might, by altering either the physical relations of heavy metals to the sediment or the physiology of invertebrate organisms, result in an increased rate of uptake and retention of the metals by the organisms. However, in several experiments in which they were fed with crude oil contaminated detritus for up to fifteen days Macoma showed no tendency to take in more heavy metals than controls did.

The experiments just mentioned did indicate that Macoma took in less food when the food was covered with oil. This finding is consistent with the fact that the condition index, a measure of nutritional status of bivalves, declined by 16% in Macoma exposed in the field for 38 days in summer to sediment containing 360 ppm crude oil. Another index which has been proposed as a measure of well-being in bivalves is the ratio of taurine to glycine in the intracellular free amino acid pool (Bayne, *et al.*, 1976; Jeffries, 1972). This ratio declined from 0.89 to 0.55 in the oil-exposed Macoma giving further evidence for their stressed condition. When exposed to oil under similar conditions in winter 83% of the Macoma died.

By contrast, when the suspension-feeding clam Protothaca was exposed to 850 ppm oil in sediment 85% survived, their average condition index declined by only 6%, and their taurine:glycine ratio increased. It appears that suspension feeding clams are less susceptible to damage from oil in sediment than are deposit feeding clams. The significance of this finding for areas of fine-grained sediment in lower Cook Inlet lies in the fact that the two most abundant genera of bivalves are the deposit feeding Macoma and the suspension feeding Mya. There is therefore a potential for differential mortality or effects on growth and wellbeing on these two groups by any oil pollution incident, with subsequent effects on the patterns of populations and resource utilization in these habitats.

The behavior of organisms is often a sensitive indicator of environmental change. One form of behavior of burrowing animals such as Abarenicola which can be quantitatively measured is the deposition of fecal casts on the surface which reflects the amount of sediment being swallowed. When exposed to sediment containing 1000 ppm or 250 ppm crude oil in artificial burrows in the laboratory their deposition rate was reduced by 70% and 36% respectively. In the field all Abarenicola exposed to 1000 ppm died, and those exposed to 200 ppm reduced their burrowing rate by 45%. This reduction however was transient, and after

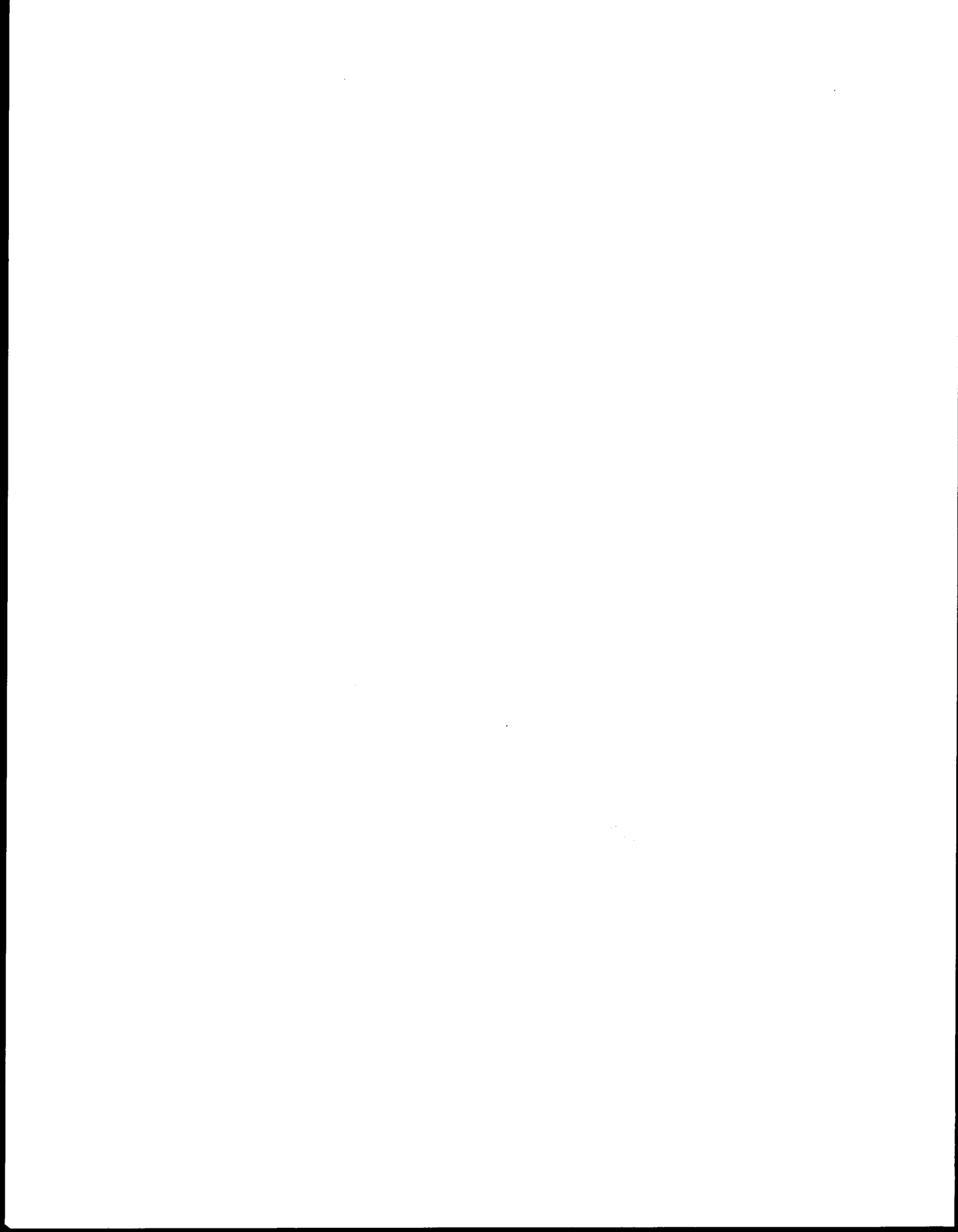
a week these animals were turning over as much sediment as the controls. It seems probable that, at some concentrations, oil in sediment will reduce the amount of material that is transported from subsurface sediment to the surface, which in turn would reduce the rate of chemical and/or microbial degradation of the oil.

The next phase of this investigation dealt with changes in the composition and properties of petroleum which might be anticipated after a spill. Crude oil was layered over sea water and weathered under different conditions of sunlight and agitation. Monoaromatic aromatic hydrocarbons, a toxic fraction, and shorter straight-chain saturates (C_8 to C_{10}) disappeared in 24 days under all conditions used. Simulation of violent agitation by spraying water on the oil resulted in an increased loss of other relatively light fractions, which led to a relative increase in the concentration of three ring aromatic compounds, the heaviest examined. Without violent agitation, only 3,6-dimethyl phenanthrene increased in relative concentration. The presence or absence of direct sunlight had no significant consistent effect on the composition of the oil. The implication of these findings are that oil spilled during periods of storms would be poorer in low molecular weight fractions, probably reducing its immediate toxicity, but would provide relatively more heavy compounds with a greater probability of accumulation from sediment. Photoperiod as such would have less effect.

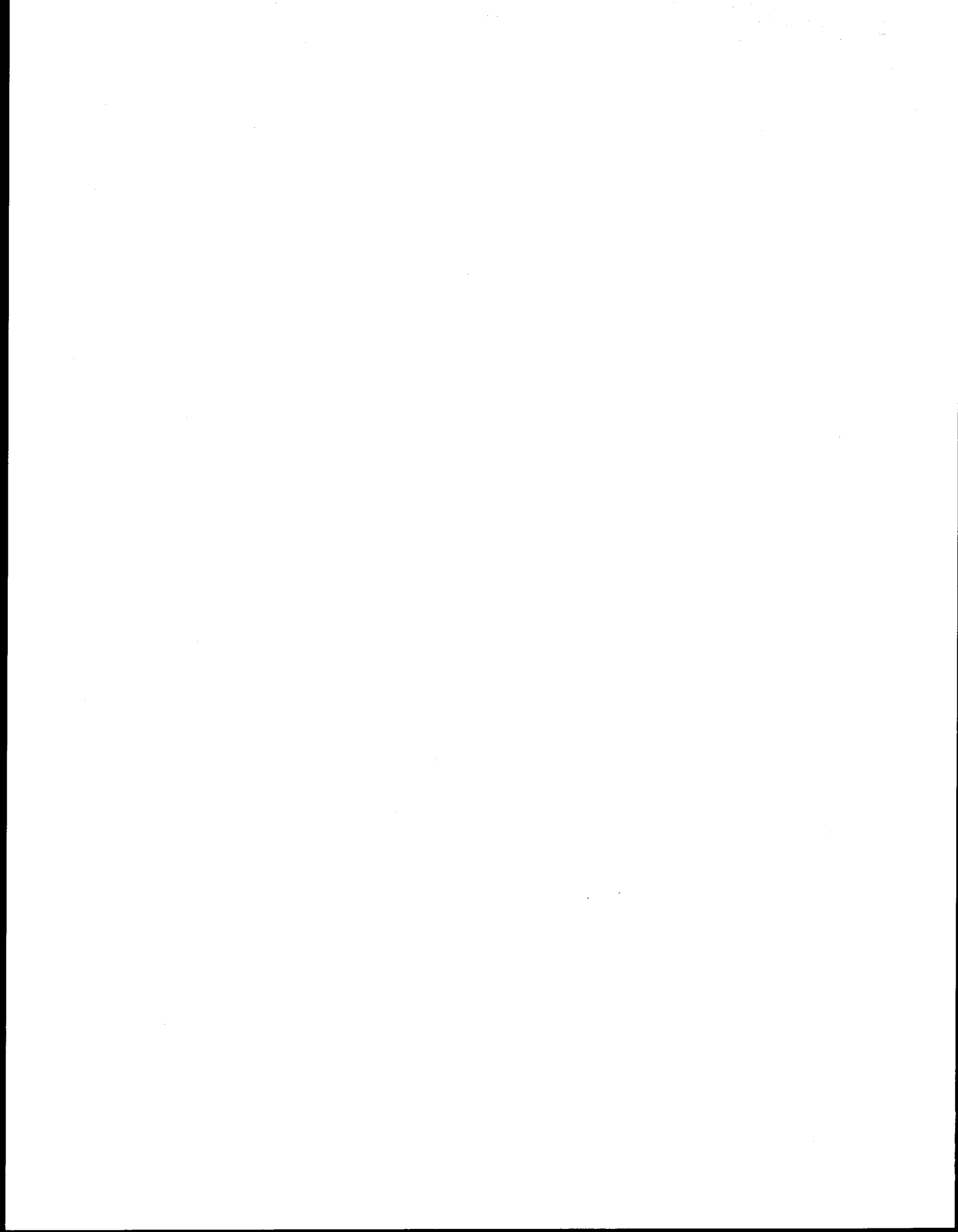
Finally, a study has been made of the fate of those polynuclear aromatic hydrocarbons that become mixed into the intertidal sediment. The most complete data are available for the fate of phenanthrene in a silty sand, containing 28.2% particles smaller than 50 microns in diameter. In this substrate 70% of the added ^{14}C -labelled phenanthrene was still present after sixty days in a simulated intertidal environment. Less than 0.2% of the radioactivity in the sediment was found in the interstitial water at any time, and 75% to 100% of this was present as $^{14}CO_2$. All of the chrysene and 75% of the benzo(a)pyrene mixed into this substrate remained in place after 60 days. In a somewhat coarser substrate, containing fewer than 4% particles smaller than 50 microns, 77%, 67%, and 8% respectively of added benzo(a)pyrene, chrysene and phenanthrene remained after sixty days. As much as 3% of the ^{14}C -label added or phenanthrene appeared in the interstitial water. It is apparent that the heavier the aromatic compound and the finer the grain size the longer is the residence time in sediment. In the

case of phenanthrene, loss from the sediment results at least partially from microbial breakdown of the hydrocarbon to carbon dioxide.

The investigations carried out under this research unit have resulted in a series of publications, and manuscripts submitted for publication. These works and summaries of results of other efforts, which are presented in the following sections of this report, include the details of the procedures and results of the studies.



II. BIOAVAILABILITY OF PETROLEUM HYDROCARBONS FROM SEDIMENT



II-A:
THE FATE OF POLYAROMATIC HYDROCARBONS
IN AN INTERTIDAL SEDIMENT EXPOSURE SYSTEM:
BIOAVAILABILITY TO MACOMA INQUINATA (MOLLUSCA:PELECYPODA)

by

J. M. Augenfeld and J. W. Anderson
Battelle Marine Research Laboratory

and

R. G. Riley and B. L. Thomas
Battelle Pacific Northwest Laboratories

ABSTRACT

Macoma inquinata, a deposit-feeding clam, was exposed for 60 days to sediment containing ^{14}C -labelled phenanthrene, chrysene, or benzo(a)pyrene. Over 70% of the chrysene and benzo(a)pyrene, but only 8% of the phenanthrene, remained in the sediment. The concentrations of chrysene and benzo(a)pyrene in the clams rose steadily, reaching levels 11.6 and 5.2 times as high as those in the sediment. The tissue phenanthrene concentration rose for 3 days, then fell to 1/8 of the initial concentration. No polar metabolites of any of the hydrocarbons were detected in sediment or tissue.

INTRODUCTION

When petroleum or its products are mixed into marine intertidal sediments the heavier aromatic compounds may remain for years (Burns and Teal, 1979). Concern has been expressed that these compounds, some of which are carcinogens or metabolic precursors of carcinogens, may accumulate in the tissues of organisms living in impacted sediments, undergo biomagnification, and be transferred along the food chain, becoming hazardous to the ultimate consumers, including man. A study has therefore been undertaken to investigate the duration of retention of 3-, 4-, and 5-ring polynuclear aromatic hydrocarbons (PAH) in sediment under simulated intertidal conditions and the uptake of these compounds by invertebrate organisms. The distribution of the compounds between sediment particles and interstitial water and the presence of polar metabolites of the PAH were also studied. The first paper of this series describes the fate of phenanthrene, chrysene, and benzo(a)pyrene in a moderately coarse substrate containing the clam Macoma inquinata Deshayes, 1855.

MATERIALS AND METHODS

Exposure system

9-¹⁴C phenanthrene (11.3 m Ci/mmol), 5, 6, (11, 12)-¹⁴C chrysene (6.3 m Ci/mmol), and 7, 10-¹⁴C benzo(a)pyrene (25.3 m Ci/mmol) were purchased from Amersham-Searle Co., Arlington Heights, Illinois. Impurities associated with benzo(a)pyrene degradation have been characterized by reverse phase high pressure liquid chromatography (Clarke, 1976). We have recently used this technique to determine the radio-purity of all three substrates used in these studies. Phenanthrene and chrysene undergo no significant chemical degradation under prolonged storage. Benzo(a)pyrene, however, showed the presence of about 10% impurities and, therefore, was purified by silica gel chromatography

immediately before exposure to assure that no degradative chemical artifacts were introduced to invalidate the radioactivity analyses. The purification procedure was: benzo(a)pyrene (25.3 mCi/mmol, 200 μ Ci in 1 ml benzene) was chromatographed over 10 grams of silica gel (Grace Davison Chemical Co., 100/200 mesh - heated overnight at 120°C) using benzene as the eluent. Ten milliliter fractions were collected and pure benzo(a)pyrene eluted from the column in the second 10 ml fraction. The column and collection tubes were wrapped in aluminum foil to minimize the exposure of the benzo(a)pyrene to light. The benzene was removed under a stream of purified nitrogen and the crystalline benzo(a)-pyrene was stored at -20°C until use the next day.

Previously, 190 M. inquinata and 100 kg sediment were collected from the low intertidal zone of Sequim Bay, Washington State, U.S.A., in an area of coarse sand mixed with fine gravel subject to moderate wave action. The sediment was passed through a 6 mm mesh sieve, and it and the clams were stored in the laboratory under flowing sea water at approximately 10°C and 30‰ salinity. Detritus was collected from the laboratory seawater head tanks, filtered onto #42 Whatman filter paper, and refrigerated.

The labelled hydrocarbon compounds were individually dissolved in solvent as was a measured amount of Prudhoe Bay crude (PBC) oil. The solvent, oil, and labelled PAH were next mixed with detritus, and finally this slurry was incorporated into sieved sediment in a fiberglass-lined cement mixer. The final mixtures contained approximately 80 g detritus, 40 ppm PBC, and between 4.5 and 6.8 μ Ci labelled compound per kg. The final concentration of chrysene was 230 μ g/kg, of phenanthrene 102 μ g/kg, and of benzo(a)pyrene 42 μ g/kg. Unlabelled phenanthrene present in the added PBC made up 23% of the total, while the amounts of chrysene and benzo(a)pyrene in the oil were negligible. These mixtures were poured to a depth of 8 cm into mesh-bottomed trays divided

into three compartments each. The trays were placed on cement blocks in fiberglass tanks at a depth which permitted 5 cm of water to stand above the sediment surface but which did not permit water to rise above the edge of the trays. At 12 hour intervals, water was pumped out of the fiberglass tanks for one hour, allowing the water in the trays to drain out through the mesh bottom and to be replaced by fresh volumes of water after the pumping stopped (Figure 1).

After two flushings, a sediment core was taken from each compartment and replaced by a 12 mm standpipe to facilitate future drainage. At this time, ten M. inquinata were placed in each compartment. The cores from the center compartment of each tray were divided into upper, middle, and lower sections. The radioactivity in replicate samples from each section was measured, and the results indicated that the labelled compounds were evenly distributed throughout the sediment. More than eighty percent of the calculated radioactivity added was recovered in the chrysene and benzo(a)pyrene exposures and 72% in the phenanthrene.

At intervals of one, three, seven, fifteen, thirty, and sixty days after the clams were placed in the trays, a sample of the surface water overlying the sediment was removed from one compartment and passed through a 0.45 μ Millipore filter. The water level was then lowered; ten clams were removed and placed in a mesh basket in clean running sea water for 24 hours depuration, after which they were rinsed with distilled water and frozen. Part of the sediment was also frozen immediately. The remaining sediment was placed in a Wildco CRTM Core Squeezer, in 100 cc batches, and the interstitial water was forced out with compressed air at 50 psi, passing through several layers of Whatman #42 filter paper within the squeezer. This filtrate was then passed through a syringe fitted with a Swinnex-47 Filter Holder (Millipore

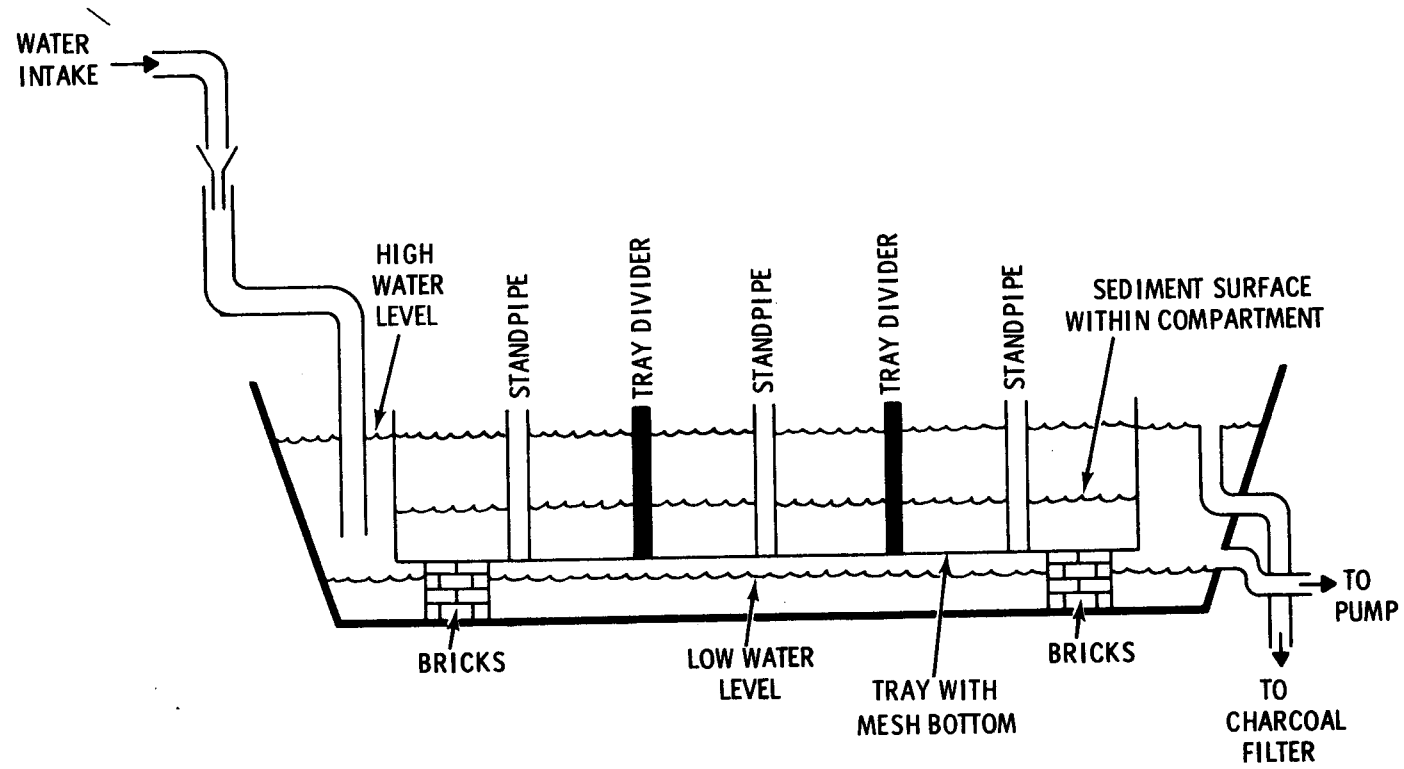


Figure 1. Design of sediment exposure system.

Corporation) containing a pre-filter and a 0.45 μ filter. A slightly different sampling schedule was followed in the benzo(a)pyrene exposure. Glassware containing benzo(a)pyrene in water was protected from light by aluminum foil wrappings. All water was kept in ice and protected from evaporation whenever possible.

Chemical Analyses

The total radioactivity present in the filtered interstitial water was measured by liquid scintillation spectrometry. Radioactive components contained in tissue and sediment samples were separated by reverse phase liquid chromatography and analyzed by liquid scintillation spectrometry. Stress was placed on an analytic approach which enabled us to account for the formation of degradation products other than CO₂ as a result of microbial activity or metabolism within the clams (Figure 2). Conventional tissue digestion techniques such as that described by Warner (1976) could not be used because of the potential chemical destruction of degradation products that might be formed during the experiments. Therefore, Macoma tissue samples were homogenized in 2:1 ethyl acetate/acetone. A similar extraction technique has previously been applied to a study of the metabolism of 7, 12-dimethylbenz(a)-anthracene in mouse skin homogenates (DiGiovanni et al., 1977), and it produced very high recoveries of original substrate and metabolites. A modification of the techniques has been used in a study of benzo(a)pyrene phenols formed by the metabolism of benzo(a)pyrene by rat liver microsomes (Selkirk et al., 1974, 1976).

Tissue from individually shucked clams containing ¹⁴C hydrocarbons was patted dry and weighed into 25 ml corex centrifuge tubes. To each tube was added a solution of ethyl acetate/acetone, 2:1 (3 ml/2.5 g tissue, wet weight).

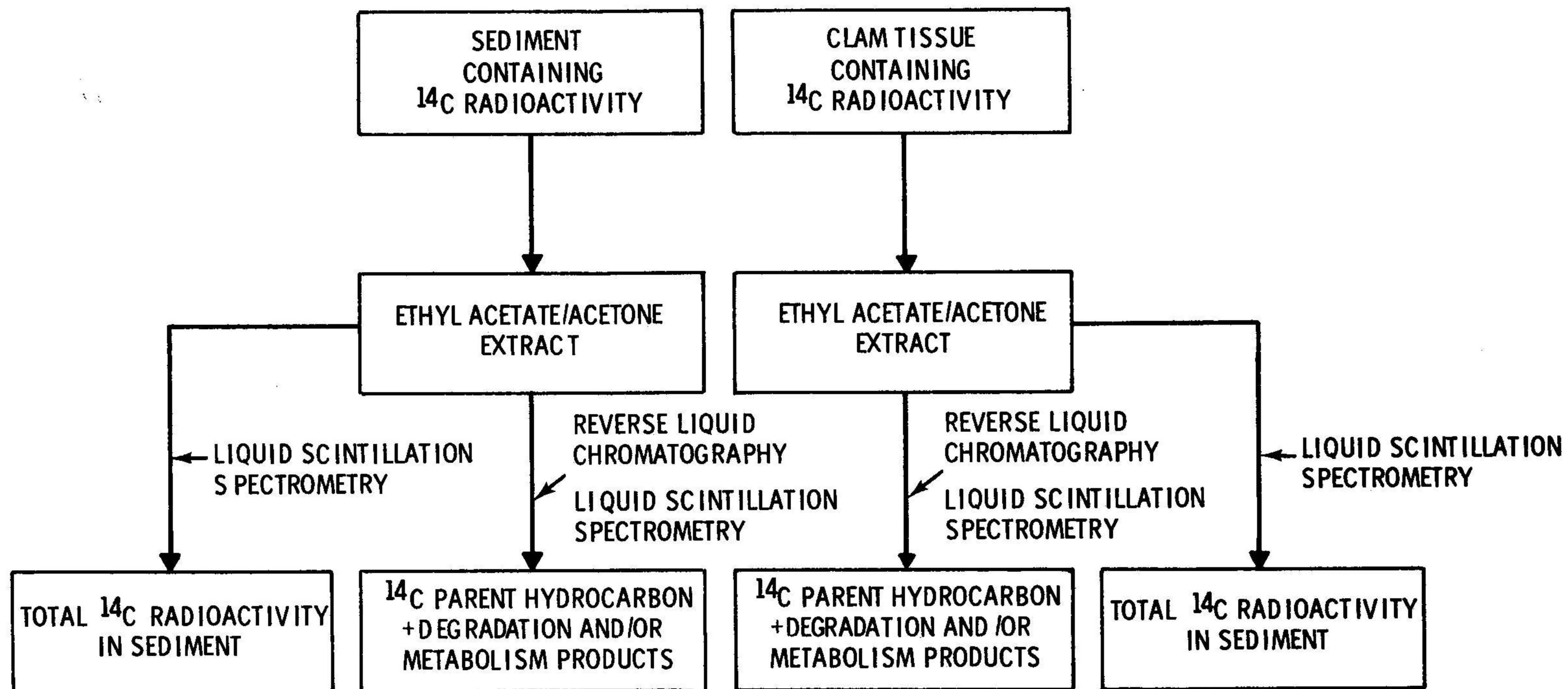


Figure 2. Scheme for the extraction and analysis of ¹⁴C-labelled hydrocarbons from clam tissue and sediment.

The samples were homogenized using a Tekmar Tissumizer and then centrifuged at 5000 rpm for 10 minutes. The organic layer (top) from each sample was transferred to calibrated 15 ml glass-stoppered centrifuge tubes with pasteur pipettes. The extraction sequence was repeated using ethyl acetate/acetone 2:1 (2 ml/2.5 g of tissue) and saturated sodium chloride (1.0 ml/2.5 g of tissue). The organic extracts (two from each tissue sample) were combined and the volume recorded. An aliquot of each sample was analyzed for total ^{14}C -radioactivity by liquid scintillation spectrometry. Recovery of ^{14}C -hydrocarbons from amended tissue was greater than 92%.

Samples of sediment from cores (~ 15 to 30 grams, wet weight) containing ^{14}C -radioactivity were Soxhlet extracted with 50 ml of 2:1 ethyl acetate/acetone overnight. The Soxhlets were cooled in such a manner as to retain as much of the solvent as possible in the Soxhlet cup. The concentrated organic extract from each sample was transferred to calibrated glass-stoppered centrifuge tubes and the volume recorded. An aliquot of each sample was analyzed for total ^{14}C -radioactivity. A second overnight extraction of the sediment samples recovered no additional radioactivity in the solvent. Furthermore, no additional radioactivity was detected from direct liquid scintillation analysis of extracted sediment particles. These results indicated that use of this procedure resulted in high recovery of ^{14}C radioactivity from sediments.

One milliliter concentrates of tissue and sediment extracts were chromatographed on three series coupled μ -Styragel columns with pore sizes of 1000, 500, and 100 Angstroms and/or two series coupled μ Bondapak C-18 columns (reverse-phase). Methylene chloride was used as the mobile phase for the μ -Styragel system at a flow rate of 2.0 ml/min with the UV detector set at 254 nm. The same parameters were used for the reverse

phase system operating in the linear gradient solvent program mode (acetonitrile/water: 60/40 to 80/20 in 20 minutes). For both systems, aliquots of 2.0 ml fractions collected were analyzed for total ^{14}C -radioactivity.

RESULTS

Table 1 and Figures 3 to 5 show the changes in concentration with time of three PAH compounds in tissue and sediment. For convenience of comparison between compounds and between sediment and tissues all the hydrocarbon concentrations are given on a picomole/g wet weight basis. The data reflect the total amounts of hydrocarbon added to the sediment, including unlabelled compounds in the crude oil and radio-labelled material.

The fate of phenanthrene introduced into the sediment system differed from that of chrysene or benzo(a)pyrene (Figures 3-5 and Table 1). Fifteen days after the exposure began 50% of the phenanthrene initially present in the sediment had been removed, and after 60 days only 8% of the original amount remained. By contrast 67 and 77%, respectively, of the originally added chrysene and benzo(a)pyrene remained in the sediment after 60 days. Complementing its more rapid depletion from the sediment, phenanthrene or its metabolites appeared in the interstitial water in concentrations two orders of magnitude higher than chrysene or benzo(a)pyrene, so that after 60 days almost 3% of the activity remaining in the phenanthrene exposure system was found in the water.

The incorporation of radioactivity from phenanthrene into the tissues of Macoma also differed from that of the heavier compounds. The concentrations of chrysene and benzo(a)pyrene in the clams rose steadily over the 60 day period, while the sediment level fell. The tissue magnification factor

Table 1. Concentration of PAH in Macoma tissue and sediment ($\bar{x} \pm S.D.$, $n = 3$), and the ratio between these two (magnification factor).

<u>Days</u>	<u>Macoma</u> (<u>pmoles/g w.w.</u>)	<u>Sediment</u> (<u>pmoles/g w.w.</u>)	<u>Tissue/</u> <u>Sediment</u>	<u>% Initial</u> <u>Sediment Content</u>
Phenanthrene				
0		396 ± 28		100
1	821 ± 234	407 ± 26	2.02	103
3	2486 ± 415	403 ± 84	6.17	102
7	2142 ± 940	364 ± 43	5.88	92
15	1608 ± 908	204 ± 84	7.88	51
30	574 ± 290	109 ± 59	5.27	27
59	103 ± 24	32 ± 5	3.22	8
59	*18 ± 4	*6 ± 1		
Chrysene				
1	617 ± 83	750 ± 59	0.82	100
3	1399 ± 326	777 ± 159	1.80	104
7	1844 ± 754	735 ± 79	2.51	98
15	3697 ± 1697	773 ± 97	4.78	104
30	5013 ± 650	532 ± 79	9.42	71
58	5853 ± 656	503 ± 282	11.64	67
58	*1334 ± 149	*114 ± 76		
Benzo(a)pyrene				
0		146 ± 5		100
1	79 ± 21	144 ± 1	0.55	99
3	167 ± 21	127 ± 110	1.31	87
11	262 ± 11	132 ± 19	1.98	91
20	429 ± 98	124 ± 3	3.46	85
35	453 ± 28	116 ± 28	3.91	80
60	588 ± 213	112 ± 11	5.25	77
60	*148 ± 54	*28 ± 3		

* ppb (wet weight).

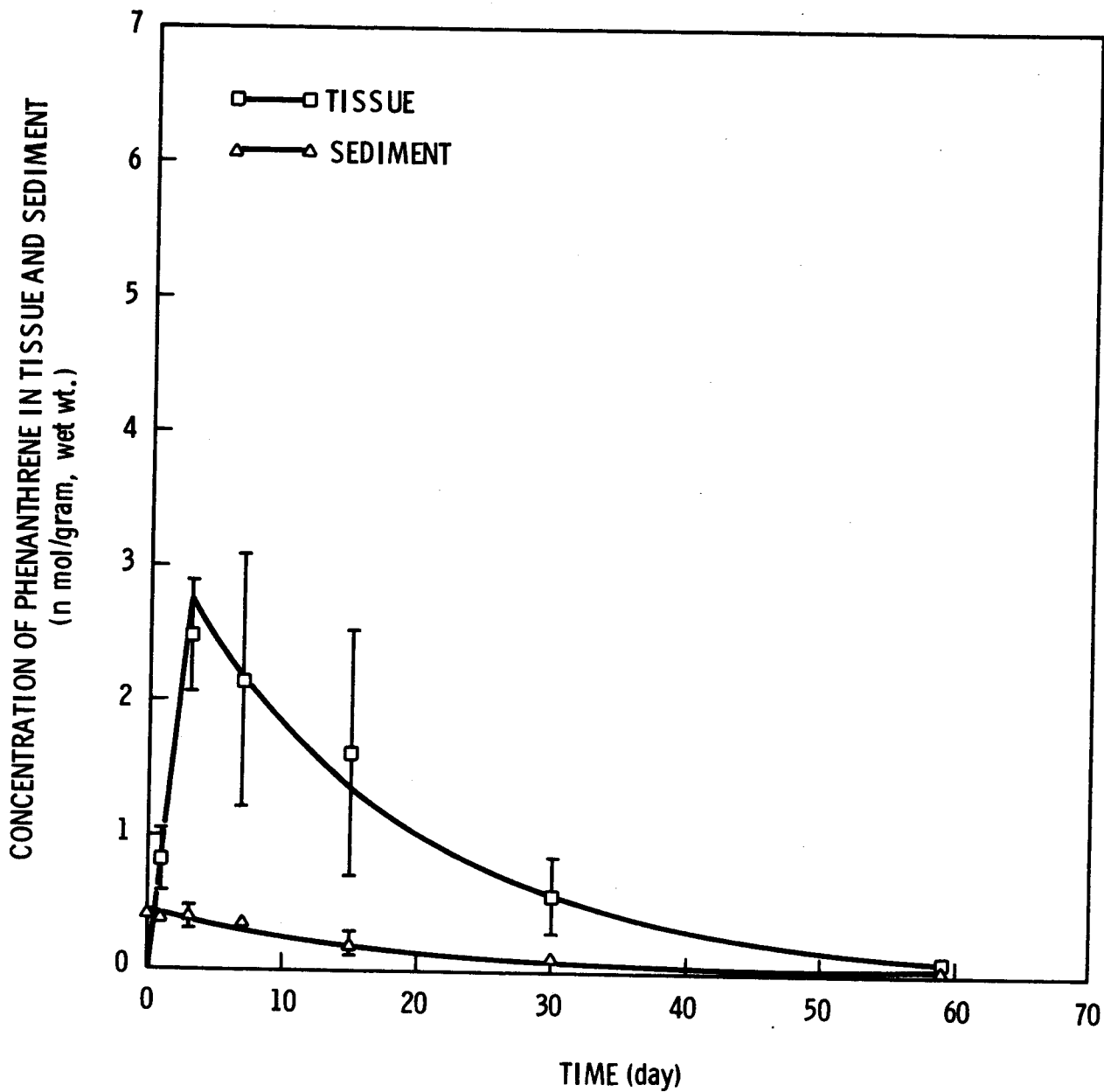


Figure 3. Concentration of phenanthrene in Macoma tissue and sediment (59 day exposure). The curves were fit by eye to connect the means ($n = 3$) and the vertical bars represent standard deviations.

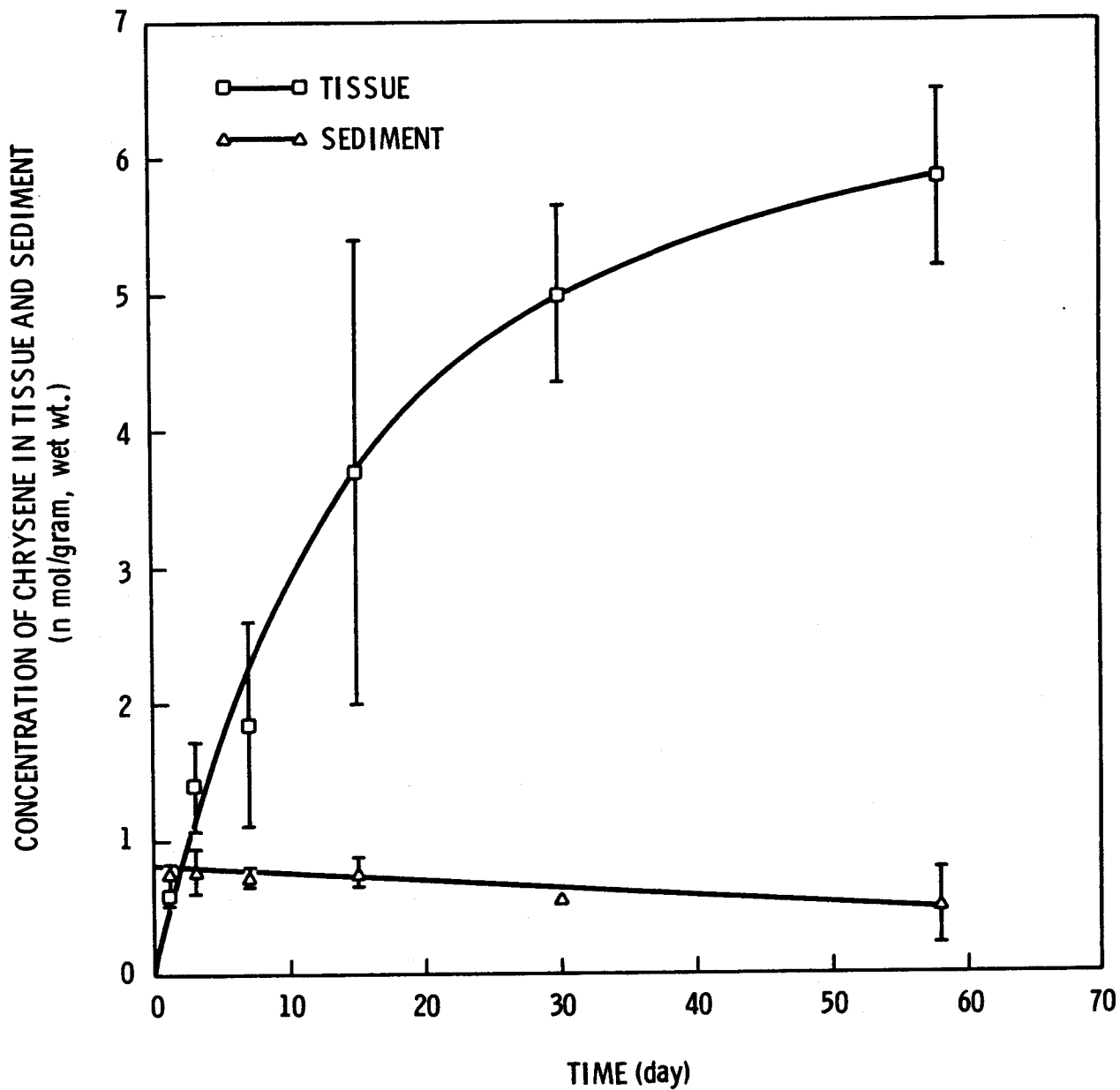


Figure 4. Concentration of chrysene in Macoma tissue and sediment (58 day exposure). The curves were fit by eye to connect the means ($n = 3$) and the vertical bars represent standard deviations.

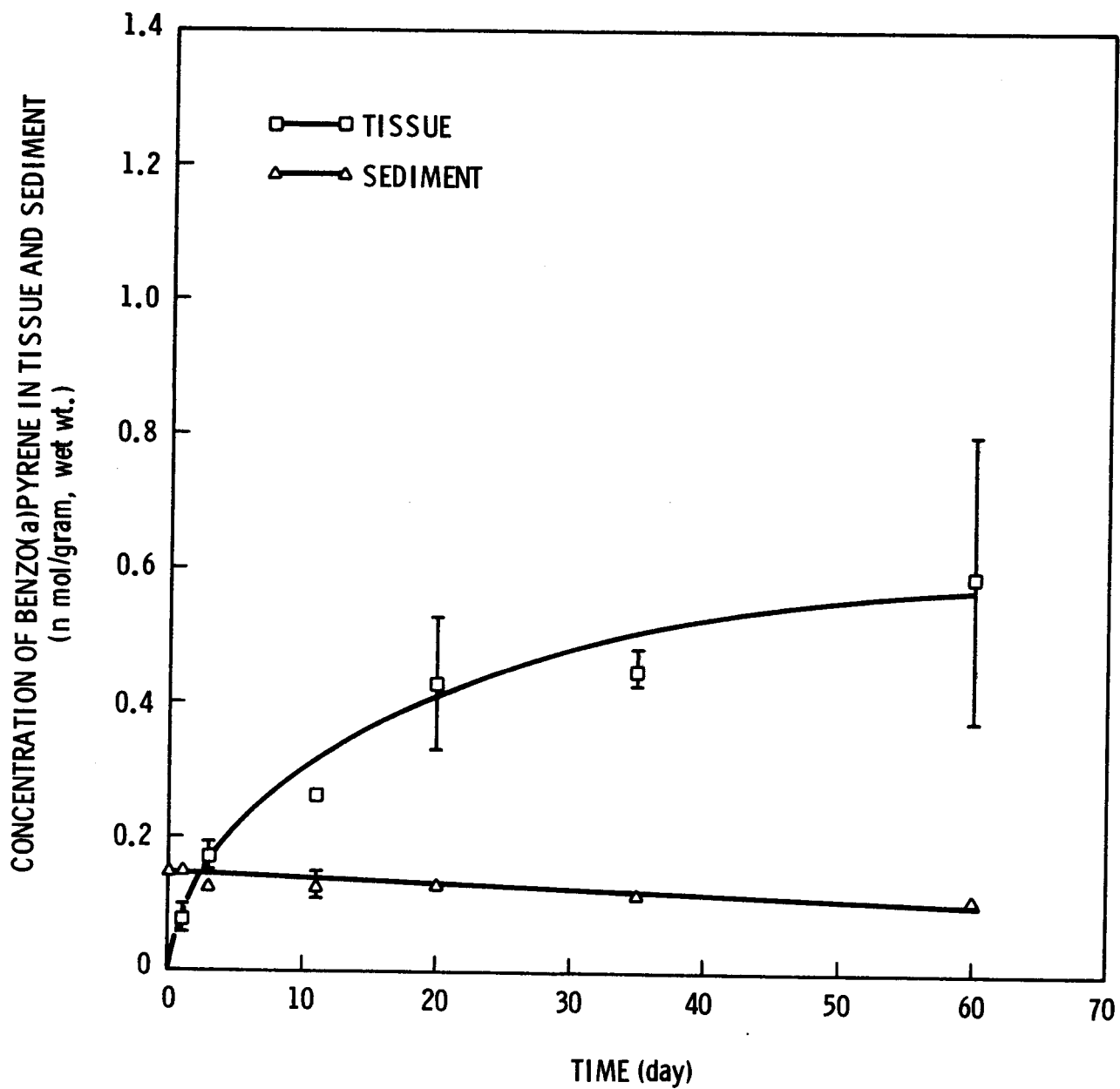


Figure 5. Concentration of benzo(a)pyrene in Macoma tissue and sediment (60 day exposure). The curves were fit by eye to connect the means (n = 3) and the vertical bars represent standard deviations.

therefore also increased continually reaching 11.6 for chrysene and 5.2 for benzo(a)pyrene, on a wet weight to wet weight basis (Table 1). Phenanthrene, on the other hand, was taken up in larger amounts than chrysene or benzo(a)pyrene in the first three days of exposure, but its concentration fell thereafter. Since the sediment concentration of phenanthrene fell rapidly the tissue magnification factor continued to increase for two weeks, but it also declined towards the end of the exposure period. Put another way, the tissue content of chrysene and benzo(a)pyrene after 60 days exposure was 9.5 and 7.4 times as high as on day 1, respectively, while the tissue concentration of phenanthrene was only 1/8 as high on the last day of exposure as on the first (Table 1).

It is possible to roughly estimate the proportion of those hydrocarbon compounds leaving the sediment over 60 days which appeared in the clams at the end of this period by assuming that the total weight of the sediment in each compartment was approximately 6.6 kg and the total weight of the ten Macoma in each was 43 g. These are reasonable assumptions, based on the volumes of the compartments, the density of the sediment, and the average size of individuals of the populations of animals. Calculations based on these assumptions indicate that 15.4% and 11.3%, respectively, of the radioactivity of chrysene and benzo(a)pyrene which left the sediment can be accounted for by its presence in the clams, while only 0.18% of the corresponding phenanthrene remained in the organisms. Therefore, of the hydrocarbons present in the sediment when the clams were originally exposed, approximately 5.1% of the chrysene, 2.6% of the benzo(a)pyrene and 0.179% of the phenanthrene was present in their tissues after 60 days. Since these figures are not based on actual measurements of the animals' weight, they should be taken only as order of magnitude estimates.

No evidence was found for the presence of degradation products or metabolites of any of the three compounds in either tissue or sediment. This conclusion is based on the findings that: (1) separation of tissue and sediment extracts by gel permeation chromatography (GPC) and by reverse phase high pressure liquid chromatography resulted in the generation, in each case, of one radioactive peak which had a retention time identical to that of the parent compound; and (2) recoveries of substrate radioactivity in tissue and sediment extracts from the GPC and reverse phase chromatography steps were high, indicating that no activity which could be ascribed to polar compounds had been lost on the column systems (Table 2).

DISCUSSION

Roesijadi et al. (1978) exposed M. inquinata to labelled phenanthrene, chrysene, and benzo(a)pyrene. Their system differed from the one described here in that the PAH hydrocarbons were distributed only through a thin (1-2 mm) layer of detritus overlying a clean sand substrate which contained the clams. Probably as a result of this arrangement a larger proportion of their added labelled material left the substrate, leaving less than one percent, five percent and twenty-five percent, respectively, of the originally added phenanthrene, chrysene, and benzo(a)pyrene at the end of the experiment. Consequently, in the earlier experiment the concentration of phenanthrene in the clams declined continuously from the start, and chrysene increased in concentration only for 15 days and then declined. Only benzo(a)pyrene followed the same pattern of continual increase in tissue concentration found here. This contrast in results illustrates the importance of the physical relation of the hydrocarbons to the sediment substrate for its bioavailability to the organisms.

Table 2. Percent recovery of ¹⁴C-radioactivity from tissue and sediment extracts chromatographed on GPC and reverse phase liquid chromatographic systems.

<u>Chromatography</u>	<u>Compound</u>	<u>Tissue</u> ¹	<u>Sediment</u> ¹
GPC	Phenanthrene	101.5	97.6
	Chrysene	114.6	99.3
	Benzo(a)pyrene	102.1	102.6
Reverse-Phase	Phenanthrene	96.9	85.6 ²
	Chrysene	103.8	101.4
	Benzo(a)pyrene	87.3 ²	89.9 ²

¹ % recovery of activity injected on column system.

² Due to the low count levels in these samples, the lower recovery values can be accounted for by the greater counting error, which ranged from 10-30% for these samples.

The contrast, in this experiment, between the fate of phenanthrene and the fates of chrysene and benzo(a)pyrene may be accounted for by the tendency of hydrocarbons to remain sequestered in animals' lipids in inverse proportion to their solubility in water. Phenanthrene is more soluble, by three orders of magnitude, than the two heavier compounds (May, et al., 1978).

According to this model, half the added phenanthrene leaves the film surrounding the sediment particles within two weeks of exposure to dissolve in the water. The water-borne compound enters the clam tissue, producing the observed early peak of radioactivity. Once in the clam tissue, relatively more phenanthrene moves from lipids, entering the aqueous compartment which then exchanges with the surrounding water. At later time intervals the availability of phenanthrene in water probably decreases. A portion of this loss is probably due to microbial metabolism acting in the exposure system to alter the hydrocarbons in the interstitial water. Phenanthrene would be converted to soluble products, which would be eliminated from the exposure system by the daily flushing. As the sediment becomes depleted of phenanthrene the level of radioactivity in interstitial water falls, allowing the phenanthrene concentration in the clams to decrease by exchange with the relatively clean water.

Chrysene and benzo(a)pyrene, by contrast, remain within the oil film coating the grains of sediment for longer periods than phenanthrene. Though they enter the water phase more slowly, once they enter Macoma tissue they apparently remain longer in their lipid depots due to their slower rate of exchange with the ambient fluid. Such a sequence of events may be responsible for the time course of changes in tissue magnification factors seen in Table 1. The magnification for phenanthrene remains greater than that for chrysene for the first fifteen days of exposure, and greater than that for benzo(a)pyrene

for the first thirty. Nevertheless, the final tissue magnification factor is greater for the heavier compounds.

The absence of degradation products in tissue and sediments is consistent with the widely held belief that bivalves have very low aromatic hydrocarbon hydroxylase (AHH) activity (Payne, 1977). There is no doubt that bacteria in marine sediments are capable of metabolizing aromatic hydrocarbons. Furthermore, evidence of phenanthrene degradation was found in interstitial water from this experiment, and findings with regard to them will be discussed in a later publication. Probably any metabolites formed were sufficiently soluble in water to readily leave the system during the flushing intervals.

The conditions chosen for these experiments are compared in Table 3 with those present in actual sediments and with those that might be expected after oil spills comparable in severity to the West Falmouth incident of 1969 and the Amoco Cadiz of 1978. In this table some values have been converted to a ppb dry weight basis for sediment and ppb wet or dry weight basis for tissues to facilitate comparison with data from other sources. Since the dry weight of the sediment was 84.3% of the wet weight there is little difference between these two bases. In the 1969 incident over 2000 ppm fuel oil was incorporated into sediment in some areas. If contamination of this degree with South Louisiana crude or Bunker C residual oil took place, the chrysene concentration in the sediment would be 34 or 400 ppb, (dry weight) respectively (Pancirov and Brown, 1975; taken from Neff, 1979). Giger and Blumer (1974) reported the presence of 40 and 240 ppb chrysene in sediment from relatively clean and chronically polluted sites in Buzzard's Bay, Massachusetts. The level of chrysene present at the beginning of this exposure, i.e., 203 ppb, is therefore, in an environmentally realistic range.

Table 3. PAH contents of sediment and tissues (ppb wet weight)

	<u>Chrysene</u>	<u>Benzo(a)pyrene</u>	<u>Ref.</u>
Sediment			
Laboratory, Initial	171 (203*)	37 (44*)	This study
Laboratory, Final	114 (136*)	28 (33*)	This study
Field, Buzzard's Bay, Massachusetts	240 (40*)	75-370*	Giger & Blumer, 1974
Field, Bay of St. Malo-Bassin		170*	Perdriau, 1964
Hypothetical contamination with 2000 ppm:			Pancirov & Brown, 1975
South Louisiana crude	34		
Kuwait crude	400	6	
Bunker C residual		88	
Tissue			
Laboratory, Final (Concentration factor over sediment)	1334 (11.6)	148 (5.2)	This study
Field, Oysters, Norfolk Harbor, VA	20-40		Cahnmann & Kuratsune, 1957
Field, Clams, Seine estuary		187	Perdriau, 1964
Hypothetical contamination of <u>Macoma</u> following 60 days exposure to sediment contaminated with 2000 ppm:			Pancirov & Brown, 1975
South Louisiana crude	265		
Kuwait crude		24	
Bunker C residual	3100	352	

* = ppb dry weight

The same is true for benzo(a)pyrene. Due to the large number of possible sources of this hydrocarbon, extreme values, as high as 15,000 ppb (dry weight) have been found in heavily polluted areas (Mallet et al., 1963). In a hypothetical sediment contamination with 2000 ppm Kuwait crude or Bunker C residual oil, 6 or 88 ppb (wet weight), respectively, of benzo(a)pyrene would be added to otherwise clean sediment (Pancirov and Brown, 1975). The laboratory exposure concentration of 44 ppb is within this range. The levels of 4- and 5-ring PAH accumulated over 60 days by the experimental animals is therefore probably of the same order of magnitude that might be expected in those deposit-feeding clams that survive the initial impact of a high-volume oil spill.

The tissue:sediment ratios of the specific aromatic hydrocarbons used in this study may be compared with the ratios of total aromatic hydrocarbons found in a field situation. Laseter et al. (1980) analyzed oysters and sediment taken from Aber Wrac'h, a site heavily polluted by oil from the Amoco Cadiz. Three months after the spill the total aromatic content of the Japanese oyster (Crassostrea gigas Thunberg 1793) was 1.24 times as high as that of the surrounding sediment. After fourteen months the ratio had increased to 2.30. The flat oyster, Ostrea edulis L., by contrast contained only 0.88 times as much aromatic HC as the sediment after three months, and after fourteen months the ratio had fallen to 0.53. It has been suggested that the difference between the species may reflect differences in the relative amounts of lipids they contain. The fact that the levels of bio-accumulation found here in Macoma were still higher than those in C. gigas, agree with the findings of Roesijadi et al. (1978) that deposit-feeding invertebrates tend to accumulate hydrocarbons at higher rates than suspension feeders.

Far more attention has been focused on the presence of benzo(a)pyrene in potential food organisms than on the presence of chrysene. This is understandable, since the former compound, when applied to mammalian skin, in very low doses (2 g/kg body weight) and in the presence of suitable co-carcinogens, can induce the growth of cancer. Though the lowest reported oral carcinogenic dose is 5 orders of magnitude higher, a degree of caution with regard to such a chemical may be warranted. It is possible, by extrapolating from the uptake observed under realistic conditions in the laboratory to the effects that might be anticipated in a post-spill situation such as those described above, to predict the presence of 25 to 350 ppb of benzo(a)pyrene in the tissues of deposit feeding clams. The upper part of this range is similar to that observed in molluscs taken from highly polluted areas such as the Bay of Naples (Boucart and Mallet, 1965) or the Seine estuary (Perdriau, 1964), or from creosoted pilings in Vancouver, B. C. (Dunn and Stich, 1975). The concentrations of benzo(a)pyrene in smoked food or charcoal-broiled meat, two principal dietary sources, are an order of magnitude less than those in the more heavily contaminated bivalves (Lijinsky, 1967; Panalaks, 1976).

Fewer data are available on the range of concentrations of chrysene in tissues of marine animals, but Cahnmann and Kuratsune (1957) reported a concentration of 20-40 ppb in oysters from the Norfolk, VA., harbor. The potential for accumulation of this compound in bivalve tissue is therefore one to two orders of magnitude higher than that actually found in a fairly heavily polluted environment. The lowest reported carcinogenic dose of chrysene is four orders of magnitude higher than that of benzo(a)pyrene. Nevertheless its higher concentration in oil or oil products and its greater tendency to remain in tissues suggest that this compound may deserve some of the attention now being paid to the 5-ring PAH.

It has been demonstrated that a deposit feeding clam can accumulate heavy aromatic compounds to concentrations several times higher than those in surrounding oil-contaminated sediment. The findings imply that bivalves which survive the initial impact of oil contamination may become reservoirs for these compounds. Therefore, deposit feeding molluscs may be suitable choices for monitoring the long-term effects of oil pollution in sediments. Such monitoring would not only provide significant information on the state of contamination or depuration of an affected area, but also be useful in evaluating the degree of risk to predator organisms, including man, from ingestion of an additional dietary source of suspected carcinogens.

ACKNOWLEDGEMENTS

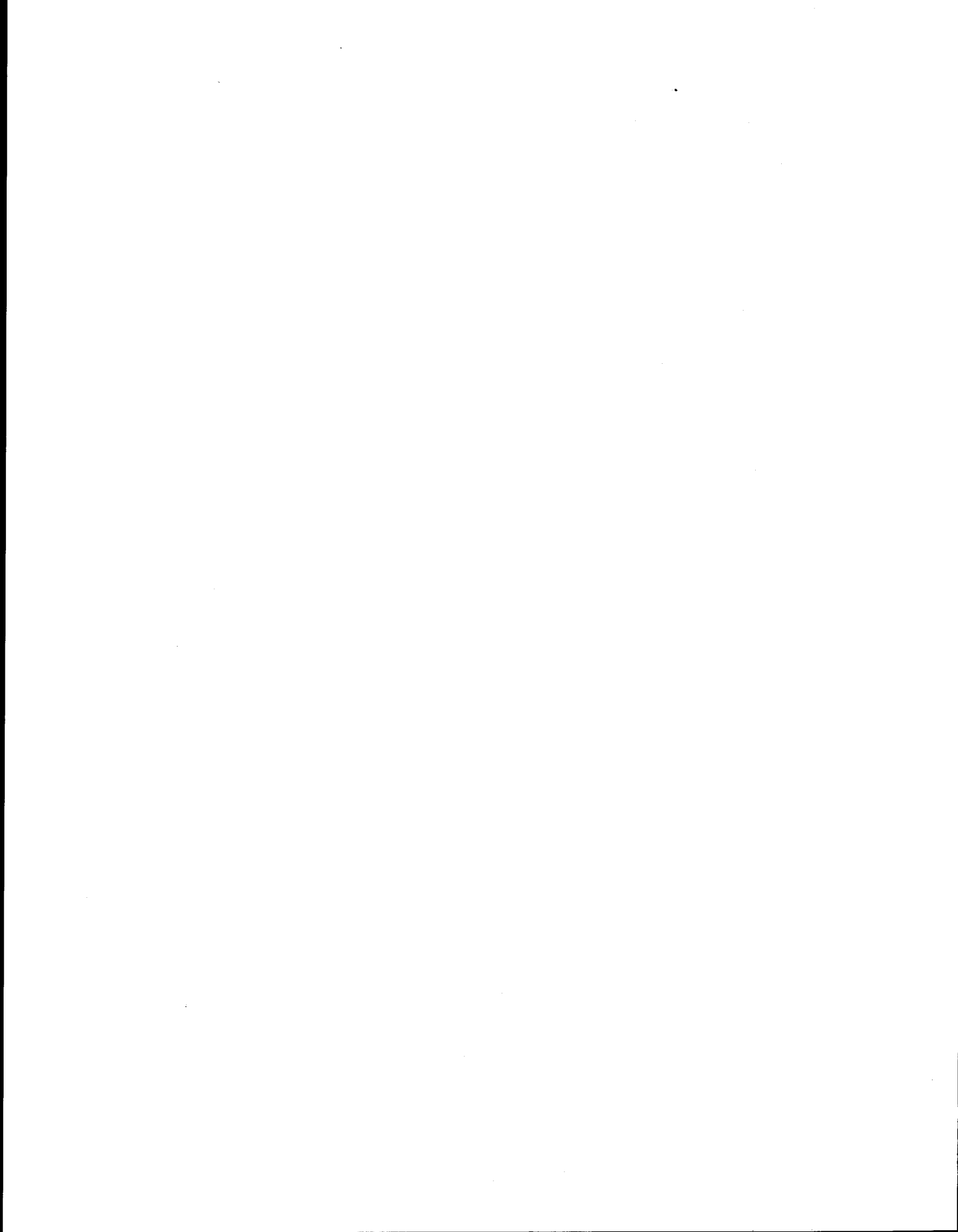
This study was supported by the Bureau of Land Management through interagency agreement with the National Oceanic and Atmospheric Administration, under which a multi-year program responding to needs of petroleum development of the Alaskan continental shelf is managed by the Outer Continental Shelf Environmental Assessment Program (OCSEAP) Office.

LITERATURE CITED

- Boucart, J. and L. Mallet: Marine pollution of the shores of the central region of the Tyrrhenian Sea (Bay of Naples) by benzo-3,4-pyrene-type polycyclic aromatic hydrocarbons. *C. R. Acad. Sci. (Paris) Ser. D.* 260, 3729-3734 (1965).
- Burns, K. A. and J. M. Teal: The West Falmouth oil spill: Hydrocarbons in the salt marsh ecosystem. *Estuar. and Coastal Mar. Sci.* 8 349-360, (1979).
- Cahnmann, H. J. and M. Kuratsune: Determination of polycyclic aromatic hydrocarbons in oysters collected in polluted water. *Anal. Chem.* 29, 1312-1317 (1957).
- Clarke, P. A.: Benzo(a)pyrene metabolite identification - An example of NMR as an analytical technique. *In: Carcinogenesis Vol. 1, Polynuclear Aromatic Hydrocarbons: Chemistry, Metabolism and Carcinogenesis.* Ed. by R. I. Freudenthal and P. W. Jones, New York: Raven Press (1976).
- DiGiovanni, J., T. J. Slaga, D. L. Berry and M. R. Juchau: Metabolism of 7, 12-dimethylbenz(a)anthracene in mouse skin homogenates analyzed with high-pressure liquid chromatography. *Drug Metabolism and Disposition* 5, 295-301 (1977).
- Dunn, B. P. and H. F. Stich: The use of mussels in estimating benzo(a)pyrene contamination of the marine environment. *Proc. Soc. Exper. Biol. Med.* 150 49-51, (1975).
- Giger, W., and M. Blumer: Polycyclic aromatic hydrocarbons in the environment: isolation and characterization by chromatography, visible, ultraviolet and mass spectrometry. *Anal. Chem.* 46, 1663-1671, (1974).

- Laseter, J. L., G. C. Laeler, E. B. Overton, J. R. Patel, J. P. Holmes, M. I. Shields and M. Maberry: Characterization of aliphatic and aromatic hydrocarbons in flat and Japanese type oysters and adjacent sediments collected from L'Aber Wrac'h following the Amoco Cadiz oil spill. In: Colloque International, 19-22 Nov. 1979 AMOCO-CADIZ: Consequences d'une pollution accidentelle par les hydrocarbures Brest: Centre Océanologique le Bretagne, (1980).
- Lijinsky, W.: Detection of carcinogenic chemicals in the environment. *Cancer Bull.* 19 63-64, (1967)
- Mallet, L., V. Perdriau and S. Perdriau: Extent of pollution by polycyclic aromatic hydrocarbons of the benzo-3,4-pyrene type in the North Sea and the glacial Arctic Ocean. *Bull. Acad. Nat. Med. (Paris)* 147, 320-325, (1963).
- May, W. E., S. P. Wasik and D. H. Freeman: Determination of the solubility behavior of some polycyclic aromatic hydrocarbons in water. *Analyt. Chem.* 50, 997-1000 (1978).
- Neff, J. M.: Polycyclic aromatic hydrocarbons in the aquatic environment. London: 262 pp. Applied Science Publishers, Ltd., 1979.
- Panalaks, T.: Determination and identification of polycyclic aromatic hydrocarbons in smoked and charcoal-broiled food products by high pressure liquid chromatography and gas chromatography. *J. Environ. Sci. Health* B11, 299-315, (1976).
- Pancirov, R. J. and R. A. Brown: Analytical methods for polynuclear aromatic hydrocarbons in crude oils, heating oils and marine tissues. pp. 103-113. Proc. 1975 Conference on Prevention and Control of Oil Pollution, Washington, D. C.: American Petroleum Institute, 1975.

- Payne, J. I.: Mixed function oxidase in marine organisms in relation to petroleum hydrocarbon metabolism and detection. *Mar. Poll. Bull.* 8, 112-116 (1977).
- Perdriau, J.: Marine pollution by carcinogenic benzo-3,4-pyrene-type hydrocarbons - biological incidences. Part II. *Cah. Oceanogr.* 16, 205-229 (1964).
- Roesijadi, G., J. W. Anderson and J. W. Blaylock: Uptake of hydrocarbons from marine sediments contaminated with Prudhoe Bay crude oil: Influence of feeding type of test species and availability of polycyclic aromatic hydrocarbons. *J. Fish. Res. Bd. Canada* 35, 608-614 (1978).
- Selkirk, J. K., R. G. Croy and H. V. Gelboin: Benzo(a)pyrene metabolites: Efficient and rapid separation by high pressure liquid chromatography. *Science* 184, 169-175 (1974).
- Selkirk, J. K., R. G. Croy and H. V. Gelboin: High pressure liquid chromatographic separation of 10 benzo(a)pyrene phenol and identification of 1-phenol and 7-phenol as new metabolites. *Cancer Research* 36, 922-926 (1976).
- Warner, J. S.: Determination of aliphatic and aromatic hydrocarbons in marine organisms. *Anal. Chem.* 48, 578-583 (1976).



II-8:

THE FATE OF POLYAROMATIC HYDROCARBONS
IN AN INTERTIDAL SEDIMENT EXPOSURE SYSTEM:
BIOAVAILABILITY TO ABARENICOLA PACIFICA (ANNELIDA:POLYCHAETA)

by

J. M. Augenfeld, R. G. Riley, B. L. Thomas, and J. W. Anderson

Battelle Pacific Northwest Laboratories
Marine Research Laboratory

ABSTRACT

Abarenicola pacifica, a burrowing polychaete, was exposed for 60 days to fine-grained sediment containing ^{14}C -labelled phenanthrene, chrysene, or benzo(a)pyrene. Thirty percent of the phenanthrene, but negligible amounts of the chrysene and benzo(a)pyrene present at the start of the exposure left the sediment. The concentrations of each of the aromatic hydrocarbons in Abarenicola tissue increased for two weeks to 4-6 times the sediment levels. The tissue concentration of chrysene remained constant thereafter, but the levels of phenanthrene and benzo(a)pyrene fell to one half of their peak values.

INTRODUCTION

An earlier paper in this series (Augenfeld, Riley, Thomas and Anderson, 1980) describes an exposure system and analytic scheme for investigating the fate and distribution of several ^{14}C -labelled polyaromatic hydrocarbons (PAH) in a moderately coarse sandy sediment. The uptake by, and fate of, these compounds in the intertidal detritivorous clam, Macoma inquinata, exposed to the sediment, was also examined. The work described in that paper has been extended to include studies of the fate of the same compounds i.e., phenanthrene, chrysene, and benzo(a)pyrene in a more fine-grained silty sand sediment and their uptake by, and fate in, a non-selective deposit feeding polychaete, the lugworm, Abarenicola pacifica.

MATERIALS AND METHODS

Ninety-six A. pacifica and 100 kg sediment were collected from the high intertidal zone of an almost enclosed lagoon usually well protected from wave

action. The collecting site is separated by a narrow tongue of land from Sequim Bay, Washington State, U.S.A., from which the Macoma and sediment used in the earlier experiment had been taken. The grain size distribution of sediment from both sites was determined by the round hole sieve and hydrometer method.

¹⁴C-labelled PAHs were purchased from Amersham-Searle Co., Arlington Heights, Ill. Benzo(a)pyrene was purified before use by the method described in Augenfeld, Riley, Thomas and Anderson (1980). Individual compounds were dissolved in small volumes of solvent together with Prudhoe Bay crude oil and spread over the surface of ca. 200 g sediment. After allowing about 20 minutes for the solvent to evaporate, the oil-PAH-sediment mixture was shaken by hand for two minutes and poured over a larger volume of sediment in a fiberglass lined cement mixer. The material was mixed for one hour and poured into 600-ml beakers whose bottoms had been replaced with 0.8 mm mesh Nitex. The sediment in the beakers contained 40 ppm PBC and a calculated activity of between 9 and 11 μ Ci labelled compound per kg. The calculated hydrocarbon concentrations were: 380 μ g/kg of labelled chrysene, 169 μ g/kg of labelled phenanthrene or 104 μ g/kg of benzo(a)pyrene. The added oil contained negligible quantities of chrysene and benzo(a)pyrene but did include enough phenanthrene to make up 12% of the total phenanthrene in the sediment. In calculating the total concentration of phenanthrene in the sediment and tissues, the contribution of the unlabelled compound in the oil was taken into account.

The beakers were placed on racks in tanks in a sea table and flushed with running sea water for 18 hours. At this time 89% of the calculated amounts of labelled phenanthrene, 45% of the chrysene, and 79% of the benzo(a)pyrene were recovered in the sediment. Two specimens of A. pacifica were placed in 1/6 of the beakers, one each in 1/3 of the beakers, and none in the remaining 1/6. The water level in the tanks was continuously raised and lowered by a clockwork mechanism to produce a simulated "tide" which left the surface of the beakers uncovered for about 6 hours per day. This is similar to the tidal regimen which this population encounters in its natural habitat.

Beakers containing two worms were removed after one and three days, and those containing one worm after 7, 15, 30, and 60 days. Beakers containing only sediment were removed after 30 and 60 days. Sediment cores were taken from each beaker and frozen, and the remaining sediment was centrifuged for 30 minutes at 7500 g. The supernatant water was frozen for subsequent filtration through .45 μ filters. The worms were rinsed and frozen immediately

after removal from the sediment. They were later thawed and rinsed with hexane, and their intestinal tracts were removed and slit open. The sediment within their guts was removed, the interior of the guts was rinsed with hexane, and the body wall and intestinal tracts were frozen together. When two worms were placed into one beaker, their tissues were combined for analysis.

The methods used for extraction and analysis of the tissue and sediment were the same as those described in Augenfeld, Riley, Thomas and Anderson (1980), with one modification. Due to the very fine grain size and high water content of the sediment, it was necessary to continue Soxhlet extraction for two days instead of one.

RESULTS

Table 1 shows the particle size distribution and water content of the sediments from the sites of origin of the Macoma and Abarenicola used in this and in the previous experiment. Approximately one half of the particles from both sites are fine sand, with grain size between 50 and 500 micra. In the Macoma collecting area 49.5% are medium and coarse sand and gravel with diameters greater than 500 micra. In the Abarenicola collecting area only 19.6% of the particles were in this range, while 28.2% were silt or clay with grain size less than 50 micra. The fine grained sediment contained twice as much water as the coarser material.

As Table 2 and Figures 1-3 indicate, the concentration of chrysene and benzo(a)pyrene in sediment changed little during the course of the experiments. The differences between the concentrations one day after and sixty days after the initial measurements are less than the variations among replicate samples. All the benzo(a)pyrene concentrations over this period are about 30% lower than that measured initially. This finding, however, may be due to an anomalously high initial measurement since the variation among replicates of the measurement was four times as great as that of any of the others. The weight of sediment in each beaker was about 1000 times as great as that of the worms they contained. It was therefore possible for the animals to accumulate substantial concentrations of PAH even though the concentrations in the sediment did not decline measurably. The sediment concentration of phenanthrene, by contrast to the two heavier compounds, did decline by about 30% over the course of the experiment. The sediment PAH concentration in beakers containing no worms did not differ significantly from those in beakers with worms.

Table 1. Particle size distribution and water content of sediments from Macoma and Abarenicola habitats.

<u>Habitat</u>	<u>Water Content</u>	<u>Particle Size (μ)</u>						
		Clay	Silt	Fine	Medium	Coarse	Fine	Gravel
				Sand	Sand	Sand	Gravel	
		<.002	.002-.05	.05-5	.5-10	1.0-2.0	2.0-5.0	>5.0
<u>Macoma</u>	15.7%	1.1%	2.1	27.2	21.1	12.1	12.7	3.7
<u>Abarenicola</u>	29.4%	1.6	26.6	52.2	16.2	2.2	1.0	0.2

Table 2. Concentration of PAH in Abarenicola tissue and sediment (pmoles/g ww)

	<u>Days</u>	<u>Abarenicola</u>	<u>(pmoles/g ww)</u>	<u>Sediment</u>	<u>% Initial</u>
					<u>Sediment</u>
Phenanthrene	0			968 \pm 213	
	1	699 \pm 100	.75	927 \pm 95	90
	3	1253 \pm 258	1.30	965 \pm 0	100
	7	2553 \pm 255	3.35	763 \pm 44	79
	15	2940 \pm 604	4.03	730 \pm 45	75
	30	1999 \pm 629	3.13	639 \pm 107	66
	60	1531 \pm 167	2.27	674 \pm 118	70
Chrysene	0			747 \pm 7	
	1	470 \pm 173	.57	828 \pm 27	111
	3	2097 \pm 967	2.73	767 \pm 105	103
	7	3821 \pm 91	4.64	823 \pm 31	110
	15	5014 \pm 225	5.71	878 \pm 68	118
	30	4401 \pm 689	5.76	765 \pm 52	102
	58	4490 \pm 285	5.65	795 \pm 98	106
Benzo(a)pyrene	0			328 \pm 147	
	1	165 \pm 40	.67	231 \pm 7	70
	3	417 \pm 65	1.86	224 \pm 15	68
	7	912 \pm 141	4.15	220 \pm 14	67
	15	1197 \pm 106	5.75	208 \pm 36	63
	30	935 \pm 133	4.63	202 \pm 22	62
	60	699 \pm 88	2.85	245 \pm 2	75

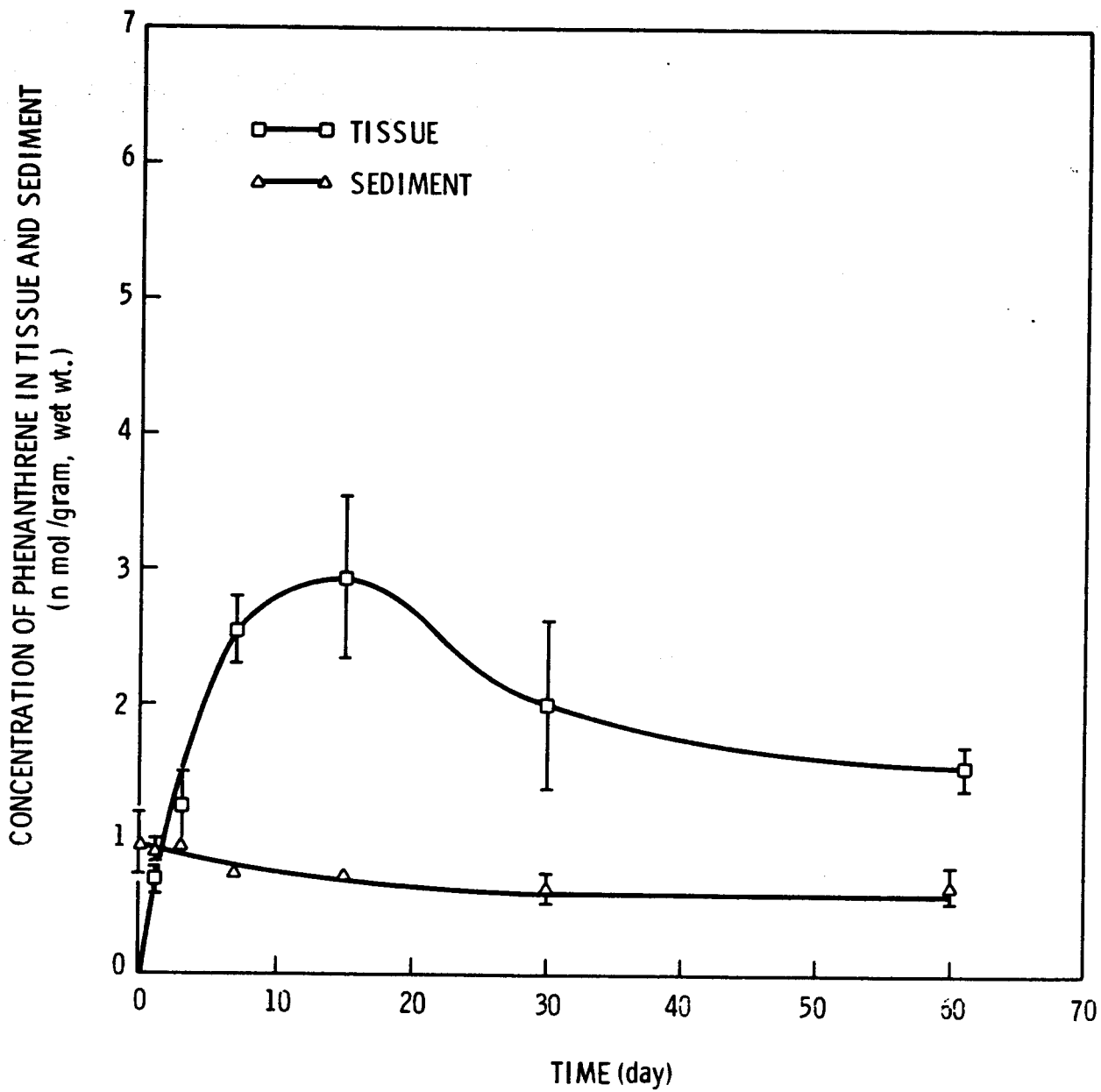


Figure 1. Concentration of phenanthrene in Abarenicola tissue and sediment (60-day exposure).

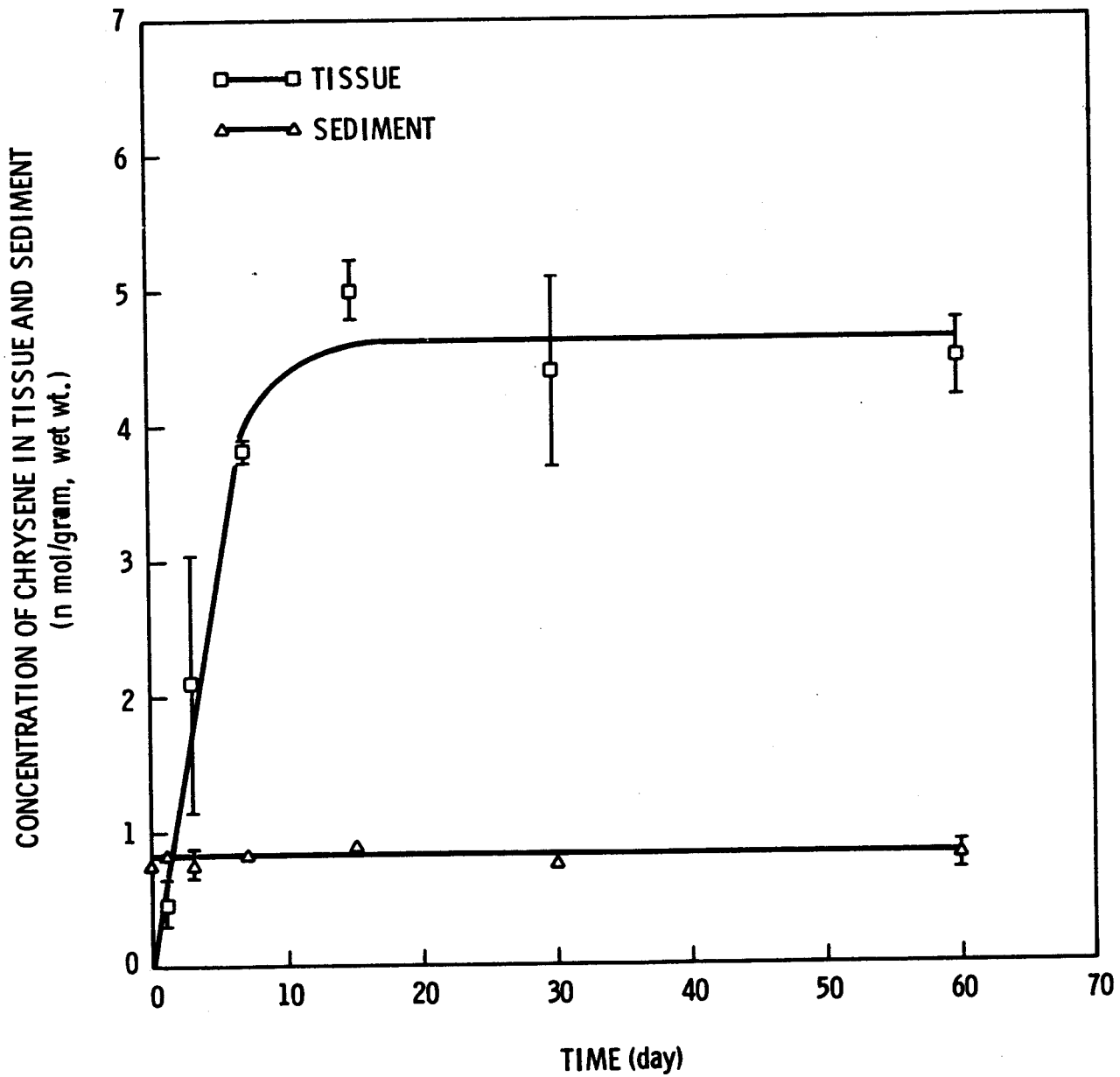


Figure 2. Concentration of chrysene in Abarenicola tissue and sediment (58-day exposure).

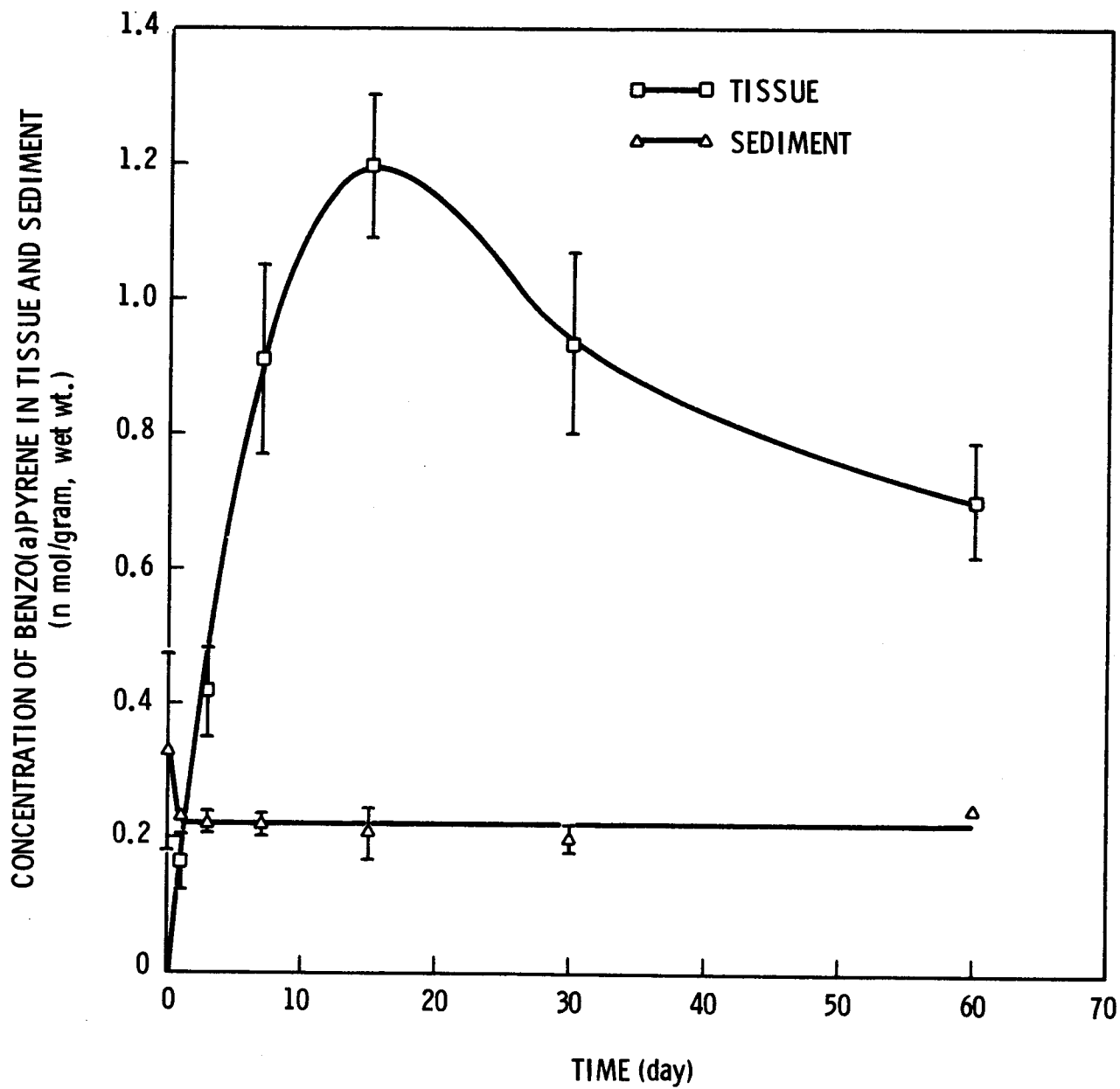


Figure 3. Concentration of benzo(a)pyrene in Abarenicola tissue and sediment (60-day exposure).

The concentrations of each of the PAHs in the worms' bodies reached a peak fifteen days after exposure began. In each case the tissue levels at this point were four to six times as high as the sediment levels at the time. In the case of phenanthrene and benzo(a)pyrene the tissue levels fell over the next 45 days to half of their peak values. After sixty days only two to three times as much PAH was found in the tissues as in the sediment. The tissue level of chrysene however decreased only slightly and the tissue magnification factor hardly changed.

No polar metabolites of any of the three PAH compounds were found in either sediment or tissues.

DISCUSSION

In the coarser, dryer sediment employed in the study of Macoma referred to earlier, 92% of the added phenanthrene disappeared within 60 days, while less than two thirds of the added chrysene and benzo(a)pyrene did so. In the wetter, more fine-grained sediment occupied by Abarenicola all the compounds were held more tightly. The most striking contrast with the earlier findings lies in the fate of phenanthrene, 70% of which was still present after 60 days. Negligible amounts of the two heavier compounds were lost from this sediment. The considerably greater degree of retention is probably due to the lower rate of circulation of water through fine sediments.

Examination of the initial uptake of PAH by Abarenicola shows a steadily increasing concentration in the tissues, both in absolute terms and in proportion to the sediment level. Two weeks after the first contact however, the levels of phenanthrene and benzo(a)pyrene began to fall noticeably, even though sediment levels remained high. The reduction in tissue level following a lag period suggests the presence of an inducible enzyme system which could transform PAH into water soluble metabolites that are more readily excreted.

Mixed function oxidases (MFO) such as aryl hydrocarbon hydroxylases (AHH) capable of converting benzo(a)pyrene into polar metabolites have been found in several polychaetes, e.g., Nereis sp. (Payne, 1977; Lee et al., 1979) and Capitella capitata (Lee & Singer, 1979). Payne and May (1979) reported that they could find no detectable AHH in another lugworm, Arenicola marina, nor could they induce it by one week of exposure to ca. 3000 ppm Venezuelan crude oil. This finding is consistent with the fact that Abarenicola accumulated PAH in its tissue for two weeks before beginning to reduce their level,

since it indicates that an extended period of exposure may be required to stimulate AHH induction in lugworms.

The tissue level of chrysene remained essentially constant after the first fifteen days of exposure. This might indicate that, since chrysene is not as ubiquitous a compound as phenanthrene or benzo(a)pyrene, the MFO system of invertebrates has not developed as rapid a response to its presence. However, in Macoma chrysene also accumulated to a greater extent than either of the two other compounds. Clams are generally held to have no or very low levels of native or inducible AHH, and if this is the case, the higher levels of chrysene in Macoma tissue probably do not reflect a lower effectiveness in inducing enzyme formation. An alternate explanation for the higher level of retention in both species might lie in an affinity between the molecular structure of the compound and some component of invertebrate tissue.

If the effects of potential oil spills in areas inhabited by Abarenicola on the worms' bioaccumulation of PAH are to be compared with similar effects on Macoma, two factors which work in opposite directions must be balanced. On the one hand, the compounds are retained longer in the fine-grained sediment preferred by Abarenicola and are therefore more available for transfer to the tissues, by ingestion or absorption. On the other hand, the polychaetes are more capable of metabolizing and removing them from the tissues. Table 3 summarizes the point at which the balance is struck after 60 days exposure. It shows the ratio of labelled compounds found in the tissues of the two species to the amount of each compound present in the sediment on the first day of exposure. As can be seen, extended physical retention of phenanthrene in sediment outweighs the physiological ability of the worm to remove it during this time span. Since chrysene is retained longer in its surrounding sediment and is not excreted effectively, it too accumulates to a greater extent in Abarenicola than in Macoma. Only benzo(a)pyrene which is retained somewhat more in coarse-grained sediment, and is actively removed from Abarenicola tissue, is found in higher relative concentrations in Macoma

Two points however must be remembered in comparing the two species as depots of hydrocarbon pollutants. One is that the tissue levels found in Macoma may have been reduced during the 24 hour depuration period needed to purge their gut contents, while the Abarenicola were frozen immediately after removal from the sediment, and their gut contents rinsed out

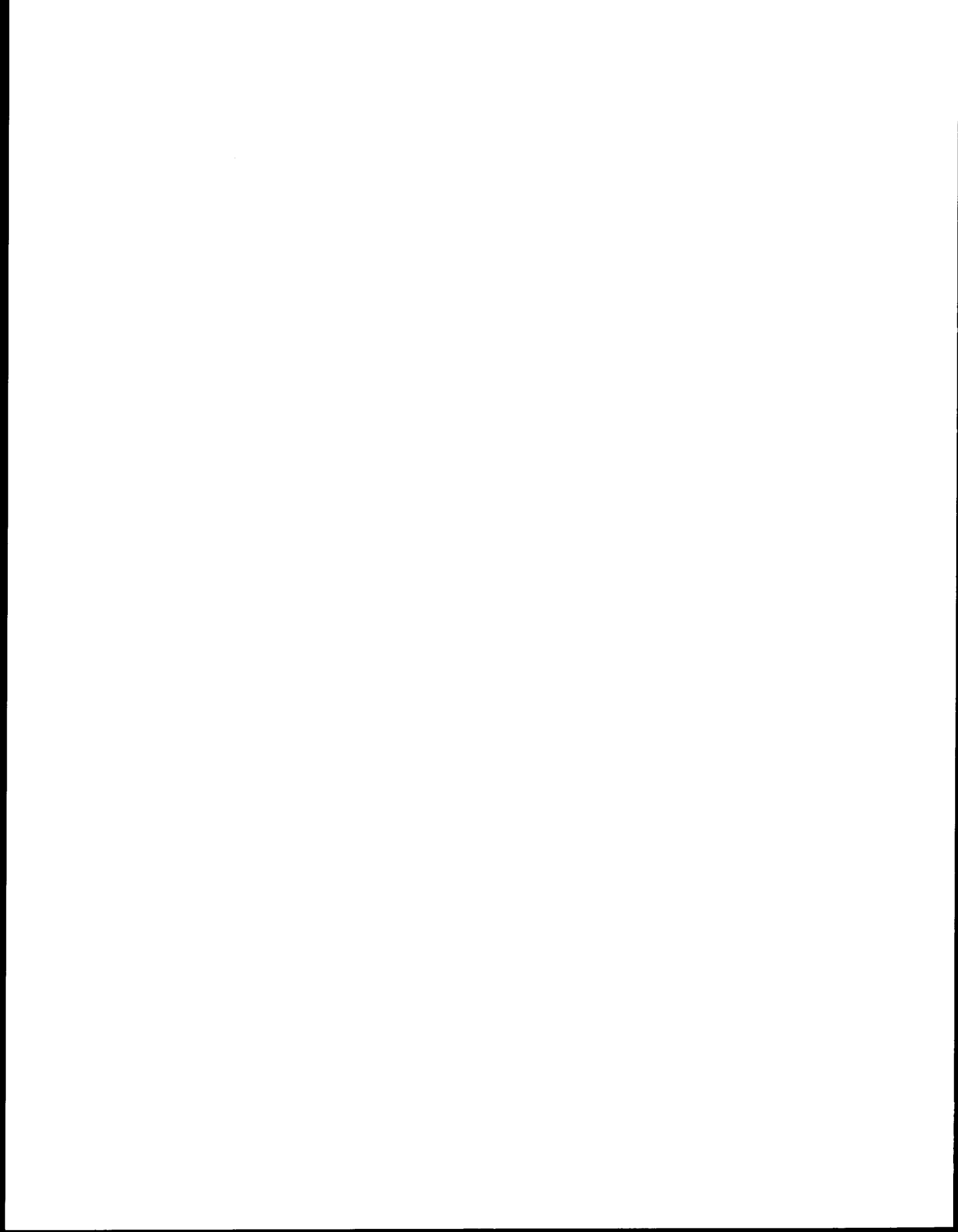
Table 3. Ratio of tissue concentration of PAH after 60 days exposure to sediment concentration of PAH one day after contamination.

	<u>Phenanthrene</u>	<u>Chrysene</u>	<u>Benzo(a)pyrene</u>
<u>Macoma</u>	.25	5.44	4.02
<u>Abarenicola</u>	1.58	7.80	3.03

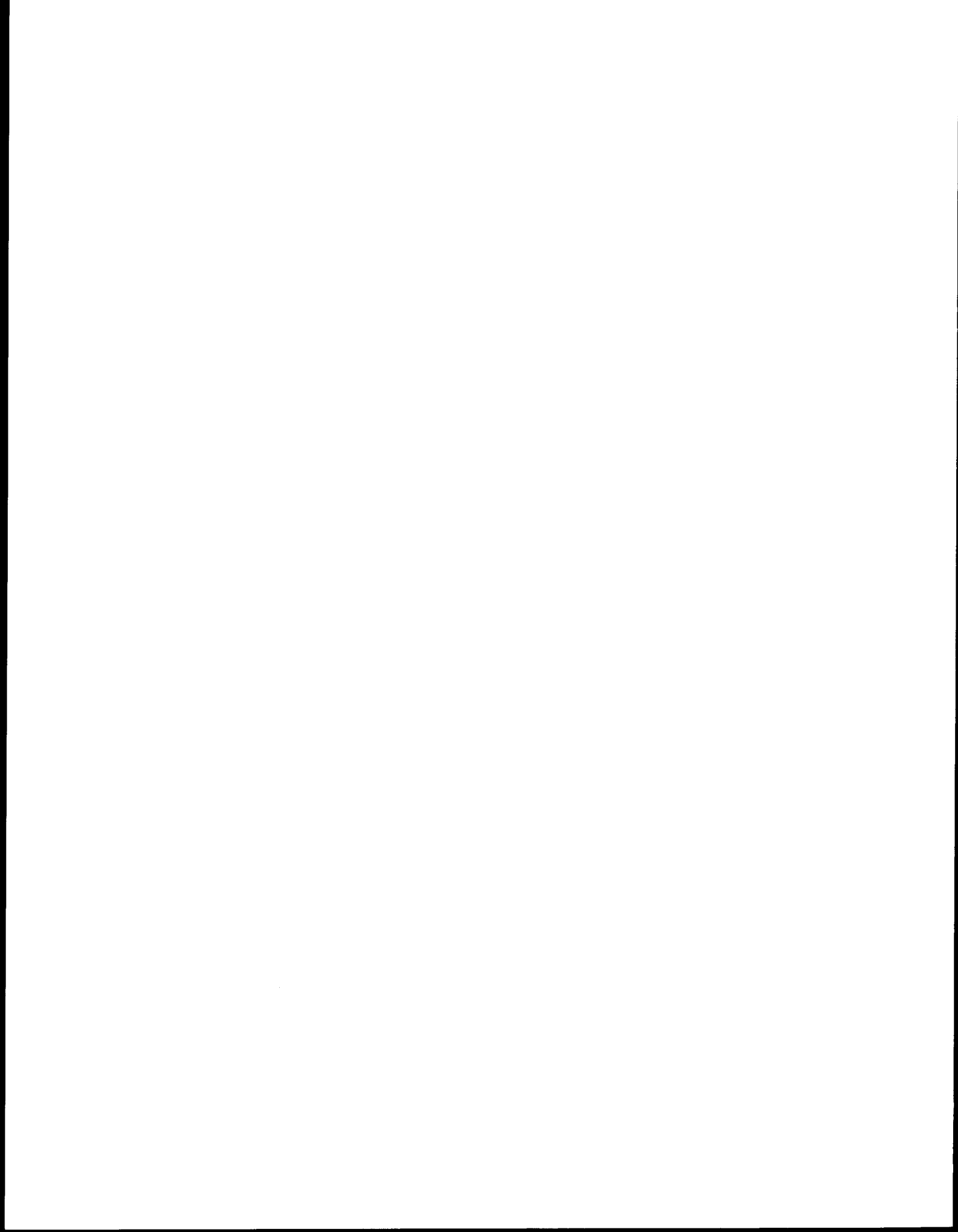
subsequently. The other point is that the tissue levels of phenanthrene and benzo(a)pyrene in the worms were declining at the 60 day interval, and a continuation of this trend for another 70 days would eventually reduce their body burden to sediment levels. In the clam, while phenanthrene was washed out of both tissue and surrounding sediment there was no indication that either chrysene or benzo(a)pyrene was released from the tissues. Therefore, if the results of exposure of invertebrates to PAH after actual oil spills resemble those found in this laboratory simulation, deposit-feeding bivalves such as Macoma could be expected to concentrate both chrysene and benzo(a)-pyrene to levels several times higher than those in the sediment, while polychaetes such as Abarenicola would retain only chrysene. The worms seem able to reduce their body burdens of phenanthrene and benzo(a)pyrene to background levels within about four months.

LITERATURE CITED

- Augenfeld, J. M., R. G. Riley, B. L. Thomas and J. W. Anderson. 1980. The fate of polyaromatic hydrocarbons in an intertidal sediment exposure system: Bioavailability to Macoma inquinata (Mollusca:Pelecypoda). (in preparation).
- Lee, R. F., E. Furlong and S. Singer. 1979. Metabolism of hydrocarbons in marine invertebrates: Aryl hydrocarbon hydroxylase from the tissues of the blue crab, Callinectes sapidus, and the polychaete worm, Nereis sp. Biological Effects Program Workshop held May 16-19, 1976, Texas A&M University, College Station, Texas.
- Lee, R. F. and S. C. Singer. 1979. Detoxification Enzyme System in Marine Polychaetes. Increases in activity after exposure to aromatic hydrocarbons. ICES Workshop on Monitoring Biological Effects of Pollution in the Sea. February 26 to March 2, 1979, Beaufort, North Carolina, USA, No. 23.
- Payne, J. F. 1977. Mixed function oxidases in marine organisms in relation to petroleum hydrocarbon metabolism and detection. Mar. Poll. Bull 8:112-116.
- Payne, J. F. and N. May. 1979. Further studies on the effect of petroleum hydrocarbons on mixed-function oxidases in marine organisms, pp. 339-347 in Pesticide and Xenobiotic Metabolism in Aquatic Organisms, M.A.Q. Khan, J. J. Lech, and J. J. Menn, eds, American Chemical Society Symposium Series.



III. BIOAVAILABILITY OF METALS FROM PETROLEUM-IMPACTED SEDIMENTS



III-A:

BIOAVAILABILITY OF TRACE ELEMENTS FROM OIL-CONTAMINATED SEDIMENT

TO MACOMA INQUINATA AND PHASCOLOSOMA AGASSIZII

Numerous trace elements including heavy metals occur in crude oil at low concentrations (Shah et al., 1970a, 1970b; Hitchon et al., 1975). Little is known about the dynamics of petroleum-derived heavy metals in the marine environment. Accumulation of specific heavy metals from sediment by benthic organisms has been described in numerous studies (Bryan and Hummerstone, 1971, 1973a, 1973b; Renfro, 1973; Hess et al., 1975; Luoma and Jenne, 1975; Renfro and Benayoun, 1975). The results, however, may not be directly applicable to petroleum-sediment-organism interactions since organic coatings on the surface of sediment particles can inhibit metals uptake (Luoma and Jenne, 1975). The presence of petroleum may interfere with the "normal" uptake kinetics of heavy metals from sediment. The low concentrations of trace metals in crude oil (e.g., 24 $\mu\text{g/g}$ in Prudhoe Bay crude oil) suggest that the contribution of those metals to the environment will be very low. For example, sediment contaminated with 2,000 $\mu\text{g/g}$ Prudhoe Bay crude will contain approximately 0.048 μg total trace metals contributed by the oil, assuming that all the metals in oil remain in the sediment. Compared to the normal levels of trace metals in marine sediments, that from oil would be negligible. Feder et al. (1976) were not able to detect any changes in sediment metals content as a result of contamination by Prudhoe Bay crude oil. However, experimental examination of the possible effects of oil on the uptake of trace metals has not been reported.

The uptake of trace metals from sediment contaminated with Prudhoe Bay crude oil has been investigated in two species of deposit-feeders: The sipunculid Phascolosoma agassizii and the clam Macoma inquinata. The animals were collected from intertidal regions of Sequim Bay and held at the Battelle Marine Research Laboratory under raw, flowing seawater at approximately 10°C and 30‰.

In the first experiment individuals of Phascolosoma agassizii were exposed to oil-contaminated sediment (ca. 2000 $\mu\text{g/g}$) prepared by mixing sand and oil in a cement mixer. Exposures were conducted in sediment trays immersed in holding tanks containing flowing seawater. Animals were sampled after 1, 7, and 14 days of exposure and after 14 days depuration. Whole animals or tissue

homogenates were dried and analyzed by x-ray fluorescence. Secondly, Macoma inquinata were exposed for 2 weeks to oil-contaminated detritus. Fifteen g of oil-contaminated detritus (2000 µg/g) were supplied initially and on the seventh day of exposure. Clams were sampled at the end of exposure, allowed to depurate gut contents for 24 h, then dried. Tissue from 10 clams was pooled and analyzed by x-ray fluorescence.

A separate experiment was conducted to determine natural variability of trace metals in Macoma inquinata. Immediately following collection, 100 clams were placed in clean, flowing seawater for 5 days to allow depuration of gut contents. The clams were then dried and analyzed for trace metals by x-ray fluorescence. Ten samples of 9 to 10 clams each were analyzed.

Two samples of Prudhoe Bay crude oil were analyzed by neutron activation analysis. The concentrations of trace elements are presented in Table 1. Only four elements, vanadium, cobalt, zinc, and bromine, were present at levels above detection limits. The total concentration of trace elements was approximately 24 µg/g.

Several difficulties arose in the experiment designed to assess uptake of trace metals by Phascolosoma agassizii. Primary among these was the fact that the exposure sediment became anaerobic in the early stages of exposure, and exposed worms crawled onto the sediment surface. Therefore, worms may have been releasing to seawater rather than taking up metals from sediment during the exposure period. Such observations may account for the decreasing levels of compounds such as chromium, manganese, and nickel during exposure. Most were present at levels below those of the sediment, although a few such as nickel, copper, zinc, and manganese, were elevated compared to sediment concentrations. No discernible differences were observed between control and exposed groups. Values for aluminum, silicon, and titanium can be attributed to metals associated with sediment in the gut (Table 2).

Levels of trace metals in Macoma inquinata (Table 3) were generally similar to those of Phascolosoma agassizii, with a few exceptions: concentrations of chromium, manganese, iron, and nickel were substantially lower in M. inquinata despite the fact that the concentrations of the latter three metals in the respective sediment of the two species were quite similar. Nickel, zinc, and selenium were more concentrated in clam tissue than in sediment. Oil exposure did not affect metals concentrations in M. inquinata. With the exception of titanium and lead, individual variability

Table 1. Trace element concentrations in Prudhoe Bay crude oil. Samples represent oil from two different barrels and were analyzed by neutron activation analysis.

Element	Concentration ($\mu\text{g/g}$)	
	Sample 1	Sample 2
Na	<0.06	0.097
Mg	<30	<33
Al	<0.5	<0.5
Cl	<1	0.95
K	<4	<1.4
Sc	<0.001	<0.001
V	20.9	18.0
Cr	<0.21	<0.15
Mn	<0.04	<0.02
Fe	<1.6	<1.7
Co	0.018	0.017
Cu	<5	<3
Zn	0.31	0.31
As	<0.03	<0.01
Se	--	<0.3
Br	5.73	2.75
Rb	<0.06	<0.08
In	<0.005	<0.003
Sb	<0.002	<0.002
Cs	<0.002	<0.001
Ba	<23	<8
La	<0.01	<0.01
Sm	<0.002	<0.001
Eu	<0.001	<0.001
Tb	<0.007	<0.006
Ta	<0.04	--
Hg	<0.03	<0.03
Th	<0.008	<0.006

Table 2. Uptake of trace elements by *Phascolosoma agassizii* exposed to oil-contaminated sediment.

Treatment	Concentration ($\mu\text{g/g}$ dry weight)									
	Al	Si	P	S	Cl	K	Ca	Ti	V	Cr
Control										
sediment	60,500	35,500	-	-	-	8,200	29,400	4,550	33	690
sediment	60,700	37,200	-	-	-	8,500	30,100	4,810	61	703
animals from field	7,600	3,150	1,905	8,710	43,490	6,706	6,208	204	7.8	42
animals held in lab in sediment	5,070	2,716	1,606	9,953	38,650	7,600	2,344	242	6.0	29
animals held in lab 2 days out of sediment	5,800	1,310	395	10,500	49,700	6,820	3,480	153	<6	45
Exposed										
1 day - whole animals	5,000	437	1,536	11,300	43,400	7,350	1,850	100	<5	14
1 day - homogenate	3,400	1,300	790	9,490	32,034	6,230	2,326	145	<6	142
1 day - homogenate	2,000	1,224	1,680	9,180	40,633	7,100	2,684	210	9.8	94
7 days - homogenate	19,450	1,584	2,408	11,140	46,190	9,174	3,986	128	6	47
14 days - homogenate	12,630	1,636	1,216	11,150	49,320	9,478	2,323	83	<4	29
14 days + 14 days depuration - homogenate	20,990	1,673	<727	13,300	92,050	10,230	3,112	58	<4	15
Control										
	Mn	Fe	Ni	Cu	Zn	Se	Pb	As	Rr	
sediment	443	17,900	<30	<2	<3	14	5.5	1.5	3.9	
sediment	442	17,700	<30	<2	<3	12	2.0	0.8	3.5	
animals from field	1,120	4,647	20	18	132	3.4	6.4	9.4	837	
animals held in lab in sediment	452	4,256	24	9.2	109	8.0	5.9	12	751	
animals held in lab 2 days out of sediment	1,316	3,994	22	15	158	3.8	9.3	10	920	
Exposed										
1 day - whole animals	180	2,824	19	20	154	3.1	5.5	10.5	822	
1 day - homogenate	1,087	3,673	49	21	251	4.5	15.5	13.1	1,026	
1 day - homogenate	1,385	3,947	44	19	185	4.2	19	12	814	
7 days - homogenate	598	3,494	31	12	145	<.3	9	12	712	
14 days - homogenate	273	2,629	13	12	80	<.5	<1	12	696	
14 days + 14 days depuration - homogenate	123	2,241	9	13	112	<.5	<1	11	810	

Table 3. Uptake of trace elements by *Macoma inquinata* exposed to oil-contaminated detritus (ca. 2000 µg/g total hydrocarbons).

Treatment	-----Concentration (µg/g dry weight)-----						
	Cl	K	Ca	Ti	V	Cr	Mn
Control							
Initial sed.	16,800	11,900	21,100	4,690	80	145	668
2-wk sed.	16,400	11,600	20,900	4,610	109	101	706
Initial tissue	52,900	13,000	1,970	21	<4	<2	11
2-wk tissue	55,200	13,900	1,590	29	<4	2.7	12
2-wk tissue	51,100	12,500	2,030	55	□4	5.6	19
Exposed							
Initial sed.	15,400	11,100	19,600	4,460	84	126	682
2-wk sed.	16,600	11,400	20,400	4,500	73	97	706
2-wk tissue	55,500	13,200	1,870	42	<4	5.5	14
	Fe	Ni	Cu	Zn	Se	Pb	As
Control							
Initial sed.	38,800	<36	31	85	1.3	10	9.2
2-wk sed.	38,600	<32	34	92	1.4	12	13.1
Initial tissue	284	4.2	7.7	199	3.1	<1.2	11
2-wk tissue	370	3.5	9.1	210	3.1	<1.3	11
2-wk tissue	516	4.9	10.3	202	2.7	<1.3	11
Exposed							
Initial sed.	37,400	<43	31	84	1.5	10	10.1
2-wk sed.	38,100	<33	35	90	1.3	13	10.1
2-wk tissue	535	3.3	7.5	163	2.9	2.1	8.2

was relatively low for all metals (Table 4) (combined coefficient of variation = 12.3 ± 5.5 S.D.). Titanium was most likely to be associated with sediment remaining in the gut and would therefore be more likely to exhibit a degree of inconsistency. Concentrations of lead approached detection limits of the technique. Only three samples possessed measurable quantities of lead. Only the values for chromium and manganese in the previous experiment fell outside the 95% confidence limits determined in this study.

Since it is possible that x-ray fluorescence techniques may not detect small changes in the tissue content of certain heavy metals, the use of radio-labelled detritus and oil, which would be produced by neutron-activation of these substances, was suggested. By generating gamma-emitting isotopes from the metals contained in the oil and associated with the detritus, very small amounts of isotopes transferred from these substances to the detritivores could be measured. In the fall of 1977 samples of oil and detritus were subjected to neutron-activation, and the products were measured for isotope content and activity. Because the concentration of metals in the oil was so low (Table 1) and the specific metals present did not lend themselves to use in this experimentation, the activated oil was not utilized.

The detritus, however, did possess at least four gamma-emitting isotopes which exhibited activities and half-lives suitable for use in experimentation. In January of 1978, a preliminary experiment was conducted to evaluate the uptake of isotopically labelled heavy metals by the clam Macoma inquinata. Activated natural detritus was mixed with fresh cold detritus (1:10) and the mixture was "aged" in seawater at 10°C for four days. The final product was then filtered on #42 Whatman paper, and divided into two halves. The oil-impacted portion received a calculated 2000 ppm of PBC contamination by the methods described earlier under hydrocarbon exposure. The non-oiled portion received only one ml of ether used as a carrier in the oiled sample. These two samples of activated detritus were placed on the bottom of two separate 5-liter aquaria, and low aeration was supplied. Ten marked clams were placed on the substrate of each tank, and then a basket containing an additional five clams was suspended in the water column above the other animals. The exposure continued for one week, followed by a depuration period of two days. During the exposure, water and clam samples were

Table 4. Analysis of trace elements in Macoma inquinata by x-ray fluorescence. Estimation of sample variability.

Element	Sample Size	Concentration ($\mu\text{g/g}$) $\times \pm 2$ S.E.	
P	10	4,651	± 686
S	10	15,374	± 591
Cl	10	53,859	$\pm 3,695$
K	10	13,504	± 245
Ca	10	2,003	± 140
Ti	10	23.7	± 9.5
V	3	3.58	± 0.45
Cr	5	3.92	± 0.60
Mn	10	9.136	± 1.043
Fe	10	315.2	± 31.3
Co	4	2.497	± 0.442
Ni	10	3.282	± 0.391
Cu	10	8.108	± 0.374
Zn	10	195.2	± 12.5
Ga	10	n.d. ²	
Hg	10	n.d.	
Se	10	3.177	± 0.188
Pb	3	0.815	± 0.680
As	10	10.319	± 0.368
Br	10	262.5	± 17.8
Rb	10	n.d.	
Sr	10	29.59	± 2.46

¹ In sample size <10, the remaining samples (=10-n) were below detection limits. Nine to ten clams composed a single sample.

² n.d. = not detectable.

counted at 1, 3, and 7 days, and animals were also counted after depuration. It was possible to utilize a small number of animals since they could be counted alive and placed back in the aquarium. The same groups of five individuals were counted together, and the configuration within the counting chamber was kept constant. After the one-week exposure and final counting at Sequim for total gamma activity, five of the ten animals on the bottom of each aquarium were transferred to clean water with clean detritus for two days depuration. The remaining five in each group were removed from the shell, and both tissue and shell were analyzed in detail at the Richland laboratory of Battelle, Pacific Northwest Laboratories. The same procedure was used on the 2-day depurated groups and the two groups of five suspended above the detritus. The determinations of total gamma activity and specific isotope content of the various groups and samples are shown in Tables 5 and 6.

During the one-week exposure, the oiled detritus decreased in total hydrocarbon concentration from 1755 ppm to 1138 ppm. The gamma activity associated with the water above the detritus (both oiled and non-oiled) was primarily in solution and was of significant magnitude, except on day 3 (Table 5). Counts generally present in the 200-ml water samples were about twice as high as those found in the clam tissues after seven days of exposure to detritus (200). Clams suspended above the substrate, where activity could only be obtained from the water and very fine suspended particles, exhibited rather consistent counts between 34 and 79. The shells of clams living on the bottom of both aquaria (oiled and unoled detritus) had a total activity of 35 counts/g (per 40 min). Two days of depuration in clean water and detritus reduced all counts, including those clams on and above detritus, with and without oil and shells, to a range of 23 to 52 (Table 5). Since the shell alone gave a count of 28, it is apparent that uptake by clam tissue was extremely small, if present at all.

Samples taken on the seventh day of exposure and after two days of depuration were analyzed for content of specific radioisotopes (Table 6.) It is clear that the detritus contained sufficiently high amounts of these four isotopes to provide the organisms with an opportunity to exhibit uptake. More ^{60}Co than other metals was found in the water, but it amounted to only 1% of the detritus activity. The Zn in water equalled about 4% of its detrital concentration. There are no apparent differences

in the metal contents of clams between the oiled and non-oiled groups, but the sub-groups living above the detritus both exhibited lower contents. Depuration for two days reduced the levels to those of the clams living above the substrate, which were approximately equal to those associated with the shells of those living on the detritus.

It is interesting to note that when the Zn counts in the tissues are converted by use of the Zn specific activity, the amount of Zn accumulated by Macoma represents only about 0.1% of the total Zn found in freshly collected animals. These findings make two facts apparent. First, no other means of analysis would ever detect uptake of Zn at this very low level; and secondly, a short depuration reduces tissue levels to approximately the same activity associated with shell material.

A final experiment was planned using detritus containing a larger number of isotopes and higher specific activity. The results of this study are described in the next section of this report.

Table 5. Uptake of total gamma-labelled trace metals from detritus by Macoma. Values are counts per 40 minutes per gram (tissue) or per 200 ml (seawater).

Type of Sample	Sample Interval (days)				Depuration (after 7 days exposure) 2
	0	Exposure			
		1	3	7	
Seawater (200 ml)					
Filtered (0.5 μ)	370	432	23	440	
Unfiltered	473				
Filtered	268				
<u>Macoma</u>					
On detritus					
with oil		109	141	200	45
without oil		230	59	172	52
Above detritus					
with oil		79	54	68	27
without oil		68	34	55	23
Shell only					
				35	28

Table 6. Uptake of specific radio-labelled trace metals from detritus by Macoma. Values are counts per 1000 minutes per gram detritus or tissue and per 200 ml seawater.

	Isotopes			
	¹⁵² Eu	⁶⁰ Co	⁴⁶ Sc	⁶⁵ Zn
Detritus (after 7 days)				
With oil	25,984	13.456	14,528	1,216
Without oil	17,038	17.038	9,656	913
Seawater (200 ml)				
Filtered on day 7				
With oil	0	131	1	41
Without oil	14	173	7	28
Filter				
With oil	6	1	9	7
Without oil	8	6	5	<1
7-day <u>Macoma</u>				
With oil				
On detritus	101	70	55	16
Above detritus	10	13	4	7
Without oil				
On detritus	81	65	48	13
Above detritus	7	11	4	8
2-day depuration (On detritus)				
With oil	15	19	8	7
Without oil	23	26	10	13
Shell only				
7-day exposed <u>on</u> detritus				
With oil	39	24	22	7
Without oil	50	28	23	8
7-day exposed <u>above</u> detritus				
With oil	16	9	8	5
Without oil	13	9	7	4
2-day depurated (On detritus)				
With oil	37	22	20	7
Without oil	10	10	10	4

LITERATURE CITED

- Bryan, G. W., and L. G. Hummerstone. 1971. Adaptation of the polychaete Nereis diversicolor to estuarine sediments containing high concentrations of heavy metals. I. General observations and adaptation to copper. J. Mar. Biol. Assoc. U.K. 51:845-683.
- Bryan, G. W. and L. G. Hummerstone. 1973a. Adaptation of the polychaete Nereis diversicolor to estuarine sediments containing high concentrations of zinc and cadmium. J. Mar. Biol. Assoc. U.K. 53:839-857.
- Bryan, G. W. and L. G. Hummerstone. 1973b. Adaptation of the polychaete Nereis diversicolor to manganese in estuarine sediments. J. Mar. Biol. Assoc. U.K. 53:859-872.
- Feder, H. M., L. M. Cheek, P. Flanagan, S. C. Jewitt, M. H. Johnston, A. S. Naidu, S. A. Norrell, A. J. Paul, A. Scarborough, and D. Shaw. 1976. The Sediment Environment of Port Valdez, Alaska: The Effects of Oil on this Ecosystem. Ecological Research Series, EPA-600/3-76-086.
- Hess, C. T., C. W. Smith, A. A. Price, II. 1975. Model for the accumulation of radionuclides in oysters and sediments. Nature 258:225-226.
- Hitchon, B., R. H. Filby and K. R. Shah. 1975. Geochemistry of trace elements in crude oils, Alberta, Canada. pp. 111-121 in: The Role of Trace Metals in Petroleum (T. F. Yen, ed.). Ann Arbor Sci. Publ., Ann Arbor, Mich.
- Luoma, S. N. and E. A. Jenne. 1975. Factors affecting the availability of sediment-bound cadmium to the estuarine, deposit-feeding clam, Macoma balthica. pp. 283-290 in: Radioecology and Energy Resources; Proceedings of the Fourth National Symposium on Radioecology, Corvallis, Oregon, May 12-14, 1975 (C. E. Cushing, Jr., ed.). Dowden, Hutchinson and Ross, Stroudsburg, Pa.
- Renfro, W. C. 1973. Transfer of ^{65}Zn from sediments by marine polychaete worms. Mar. Biol. 21:305-316.
- Renfro, W. C. and G. Benayoun. 1975. Sediment-worm interaction: Transfer of ^{65}Zn from marine silt by the polychaete Nereis diversicolor. pp. 250-255 in: Radioecology and Energy Resources; Proceedings of the Fourth National Symposium on Radioecology, Corvallis, Oregon., May 12-14, 1975 (C. E. Cushing, Jr., ed.). Dowden, Hutchinson and Ross, Stroudsburg, Pa.
- Shah, K. R., R. H. Filby and W. A. Haller. 1970a. Determination of trace elements in petroleum by neutron activation analysis. I. Determination of Na, S, Cl, K, Ca, V, Mn, Co, Ga, and Br. J. Radioanal. Chem. 6:185-192.

Shah, K. R., R. H. Filby, and W. A. Haller. 1970b. Determination of trace elements in petroleum by neutron activation analysis. II. Determination of Sc, Cr, Fe, Co, Ni, Zn, As, Se, Sb, Eu, An, Hg and U. J. Radioanal. Chem. 6:413-422.

III-B:

UPTAKE OF TRACE METALS BY THE CLAM MACOMA INQUINATA
FROM CLEAN AND OIL-CONTAMINATED DETRITUS

by

E. A. Crecelius, J. M. Augenfeld, D. L. Woodruff, and J. W. Anderson

Battelle Pacific Northwest Laboratories
Marine Research Laboratory

In recent years there has been increasing concern about the entry of petroleum hydrocarbon (PHC) into the marine environment and the effects of such entry on the composition and functioning of the marine ecosystem. Few reports have been published on the possible effect of oil on the uptake of metals from water or sediments by animals. The possibility of such effects is indicated by the work of Fletcher *et al.* (1979), who showed that crude oil causes a reduction in blood plasma copper concentrations in fish, and Payne *et al.* (1978) who reported that petroleum affected chloride regulation in fish. Luoma and Jenne (1977) have shown that the availability of sediment-bound metals to a deposit-feeding clam depended on the metal-sediment association and sediment-to-water desorption rate.

Here, we exposed a detritivorous clam, Macoma inquinata, to clean and oil-contaminated detritus to determine the effects of the oil on metal accumulation. To measure the uptake of metals, clams were exposed to neutron activated detritus and the uptake of several isotopes (^{51}Cr , ^{60}Co , ^{152}Eu , ^{59}Fe , ^{46}Sc , and ^{65}Zn) measured in the clams.

MATERIALS AND METHODS

Preparation of detritus

The term "detritus" as used in this paper is defined as the suspended matter in Sequim Bay water that settled out in the head tanks of the laboratory flowing seawater system. The element composition of this detritus is similar to both that of Sequim Bay fine grained sediment and shale (Vinogradov, 1962).

Detritus was collected from the bottom of head tanks through which raw Sequim Bay seawater had passed. Dried detritus was neutron activated for two hours at a neutron flux of approximately $1 \times 10^{13} \text{ n cm}^{-2} \text{ sec}^{-1}$, and stored for three months to allow activity to be reduced through radioactive decay. Six g dry weight (d.w.) of neutron activated detritus was added to 100 g wet weight of untreated detritus in 1 L of sea water, and the mixture was shaken by hand for 1 minute. The resulting slurry was aerated for five days at 13°C, then filtered onto #42 Whatman paper and the detritus divided into two portions of approximately 60g each. Enough Prudhoe Bay crude oil to produce a concentration of 1000 ppm oil in 60g of the detritus was dissolved in 1 ml of ether. The ether-oil mixture was then added to 100 ml sea water containing 60g of detritus. To the second 60 g portion of detritus was added 100 ml seawater and 1 ml ether without oil. Each portion of detritus was shaken 4 minutes, filtered again, and samples of the detritus removed for gamma counting.

Exposure system

The exposure system was designed to expose clams to either oiled or non-oiled detritus, and also expose other clams to only water-borne materials defined as less than 100 μm in diameter. The exposure system consisted of

two 4 L aquaria that had been divided into two equal compartments. Oiled or non-oiled detritus was placed in one compartment of each aquaria and 2 L seawater added to each compartment. Water was pumped from the compartment containing detritus through a 100 μm mesh nylon screen into the adjacent compartment. Water returned to the detritus containing compartment by gravity flow over a separating barrier. The clams were dug and stored in a flowing aquarium without food, for two days before the experiment began. Thirty clams were placed in each of the four compartments. To maintain a constant temperature the aquaria were placed in a 13° water bath.

This system provided for the exposure of clams to detritus and water-borne materials (<100 μm) on one side and only water-borne materials (<100 μm) on the other. The pump system provided the necessary aeration without agitating the detritus enough to suspend it in the water column. There was a small amount of solids that accumulated on the bottom in the filtered compartment. These were removed periodically by gentle suction and returned to the compartments with detritus.

Groups of five clams were removed from each compartment after 2, 4, 8, and 15 days of exposure. They were opened, and the meat and shells were rinsed in fresh sea water. If needed, shells were scrubbed before being opened to remove adhering detritus. The meat and shells of each group were dried to constant weight at 80°C. One-hundred ml samples of sea water were taken from the filtered compartment after 2, 8, and 15 days and evaporated to dryness for counting. Samples of oiled and non-oiled detritus were removed and dried on the 15th day of exposure, for gamma counting.

After 15 days of exposure, the remaining clams were transferred to depuration tanks with clean water and non-labelled detritus, both of which were replaced after 2 and 4 days. Groups of five clams were removed

after 2 and 8 days of depuration and prepared for counting. All meat and shells from 1 group were pooled. The gamma activity of samples of detritus, meat, shells, and residue from evaporated sea water was measured on a Ge(Li) diode.

Data treatment

The numbers of net counts at energy levels corresponding to ^{51}Cr , ^{152}Eu , ^{46}Sc , ^{59}Fe , ^{65}Zn , and ^{60}Co were calculated and corrected for the rates of decay of each isotope to determine the count rate/g d.w./1000 minutes at the time each sample was removed from the experiment. The relation between the corrected isotope count and the actual amount of metal present was established by reference to the known metal content of the detritus. These values had been established in this laboratory for K, Ca, Ti, V, Cr, Mn, Fe, Cu, Zn, Se, Pb, and As, by x-ray fluorescence. The elemental values we measured agreed with the trace metal concentrations in shale as reported by Krauskopf (1967); taken from Vinogradov (1962). Since the elemental composition of the collected detritus was similar to that of shale, we used the levels of Eu, Sc, and Co in shale in calculations to determine the amount of metal originating from detritus that was present per g clam meat or shell, or per ml sea water.

Since the clams that were removed from the aquaria during the exposure had not been depurated to purge their intestinal tracts before they were shucked and dried, it was necessary to partition the total isotope content of each metal in meat samples into that portion which was in transit through the animals' digestive systems at the time of sampling and that which had passed through the gut wall and been incorporated into the tissues. This partitioning was made possible by the presence of ^{46}Sc and ^{152}Eu in the

detritus. Based on work by Palumbo (1963) and Peters and Hoss (1974) there is good reason to believe that these two elements, as a result of their chemical form and insolubility, are absorbed very poorly if at all from food into animal tissue. The amount of detritus localized in the gut lumen was, therefore, taken to be equal to the amount of shale which would contain the scandium present in the entire sample. The amounts of other metals localized in the gut were calculated by multiplying the concentration of each metal in shale by the calculated quantity of detritus in the gut. To determine the amount of each labelled metal in tissue, the amount present in the gut was subtracted from the total amount present in the sample.

One example of this treatment of the data is given here:

<u>Metal</u>	<u>Concentration in shale</u>	<u>Concentration in detritus</u>	<u>Corrected Counts /1000 mins/g d.w. detritus</u>	<u>Corrected Counts /1000 mins/g d.w. Macoma (non-oiled, 4 days)</u>
Sc	10µg/g		287,907	4086
Zn	80µg/g	88µg/g	3,493	90

$$\frac{3493}{88} = \frac{90}{x}$$

$$x = 2.27 \mu\text{g Zn/g d.w. total Macoma sample.}$$

$$\frac{287,907}{10} = \frac{4086}{y}$$

$$y = .142 \mu\text{g Sc/g d.w. total Macoma sample.}$$

$$\frac{10}{10^6} = \frac{.142}{z}$$

$$z = 14,200 \mu\text{g} = 14.2 \text{ mg detritus/g d.w. total Macoma sample.}$$

$$\frac{14.2 \times 88}{1000}$$

$$= 1.25 \mu\text{g Zn/g d.w. sample, associated with detritus.}$$

$$2.27 - 1.25 = 1.02 \mu\text{g Zn/g d.w. sample, incorporated into tissue.}$$

RESULTS

The only metal which appeared consistently at detectable levels in sea water was cobalt, whereas Cr, Eu, and Sc appeared sporadically and no Fe or Zn were detected. As shown in Table 1, the amount of Co released to the sea water by oiled and non-oiled sediment did not differ.

Table 1. Co content of filtered sea water ($\mu\text{g} \times 10^{-5}/\text{ml}$).

<u>Days Exposure</u>	<u>Oiled</u>	<u>Non-oiled</u>
2	5.1	4.5
8	4.15	no sample
15	6.0	5.5

The detrital contents, as calculated from the scandium levels of the samples, indicated that the clams fed during the first two days of direct exposure to detritus, and the net amount of food in their digestive tracts declined thereafter as shown in Table 2 and Figure 1. On day 2, in the absence of oil, 25.6 mg/g of body d.w. was composed of detritus. In the presence of oil only one half as much food was ingested initially and it was lost at a greater rate than in the non-oiled clams.

In the filtered compartment of the aquarium to which no oil had been added, less than one tenth as much scandium labelled material, assumed to be detritus, was taken up initially as in the non-oiled detritus compartment. The Sc level in clams in the filtered compartment declined more slowly and irregularly than that in clams in the detritus compartment. Clams receiving filtered water from oiled detritus took in about as much food as the non-oiled controls.

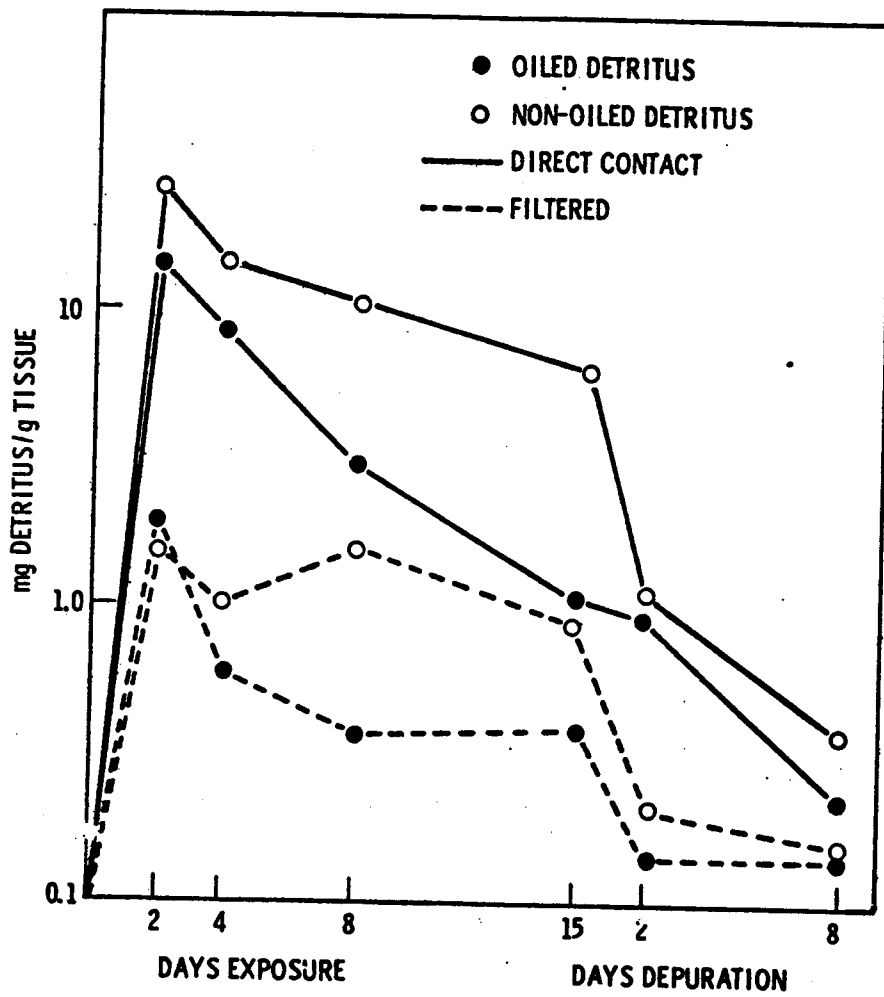


Figure 1. Detritus (mg/g) ingested by *Macoma inquinata*.

Following the transfer of clams to tanks containing non-labelled detritus, part of the radioactive material was quickly lost from the gut, but a fraction, on the order of one to ten percent of the originally ingested material, remained at the end of eight days.

Table 2. Calculated weight of detritus (mg/g d.w.) in Macoma inquinata.

<u>Days Exposure</u>	<u>Non-oiled</u>	<u>Oiled</u>	<u>Non-oiled (filtered)</u>	<u>Oiled (filtered)</u>
2	25.7	13.5	1.53	1.99
4	14.2	8.31	0.96	0.57
8	10	2.97	1.52	0.37
15	6.2	1.07	0.88	0.38
<u>Days Depuration</u>				
2	1.1	0.88	0.22	0.14
8	0.37	0.24	0.15	0.14

Table 3 shows the amounts of Zn and Co per g d.w. incorporated into Macoma tissue. Chromium was detected in only three clam samples. The levels of Eu present in the total samples differed from the amounts calculated to be in the detritus by less than 10^{-2} $\mu\text{g/g}$ in all but one case. Probably, these small differences were artifacts produced by the random nature of the gamma-emitting process, and europium, like other rare earths, is not absorbed from the gut. Similarly, the apparent net uptake of iron was so irregular and represented such a small proportion of the iron present in the detritus that it does not provide firm evidence that any iron was taken into the tissue.

Figures 2 and 3 show the amounts of Co and Zn incorporated into Macoma tissues during two weeks exposure to labelled detritus and one week depuration. Those organisms which received their metal through the water column or on very fine particles incorporated nearly identical amounts whether oil was present

Table 3. Zn and CO ($\mu\text{g/g}$ d.w. tissue) incorporation into Macoma inquinata exposed to oiled and non-oiled detritus.

<u>Days Exposure</u>	<u>Zn</u>				<u>Co</u>			
	<u>NO</u>	<u>O</u>	<u>NOF</u>	<u>OF</u>	<u>NO</u>	<u>O</u>	<u>NOF</u>	<u>OF</u>
2	0.24	0.29	0.26	-	0.024	0.059	0.009	0.019
4	1.02	1.38	0.32	-	0.070	0.112	0.025	0.043
8	1.18	1.09	0.572	0.95	(0.038) 0.175	0.108	0.049	0.043
15	3.41	1.38	1.05	0.87	(0.038) 0.140 (0.051)	(0.033) 0.067	(0.088) 0.042	(0.022) 0.054
<u>Days Depuration</u>								
2	2.23	0.62	0.94	1.01	0.216	0.130	0.043	0.026
8	2.10	0.99	1.10	1.32	0.133	0.080	(0.066) 0.037 (0.038)	(0.026) 0.046

O = oiled
NO = not oiled
F = filtered
 - = no metal present in sample
 figures in () = concentrations in shells

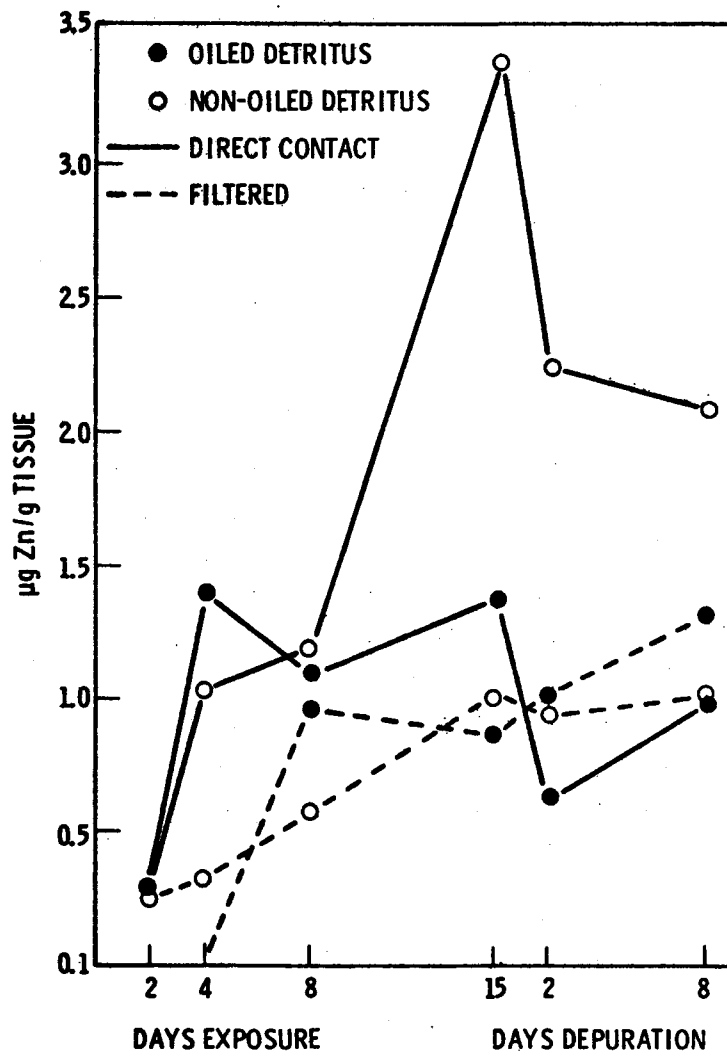


Figure 2. Incorporation of radiolabelled zinc into Macoma tissue.

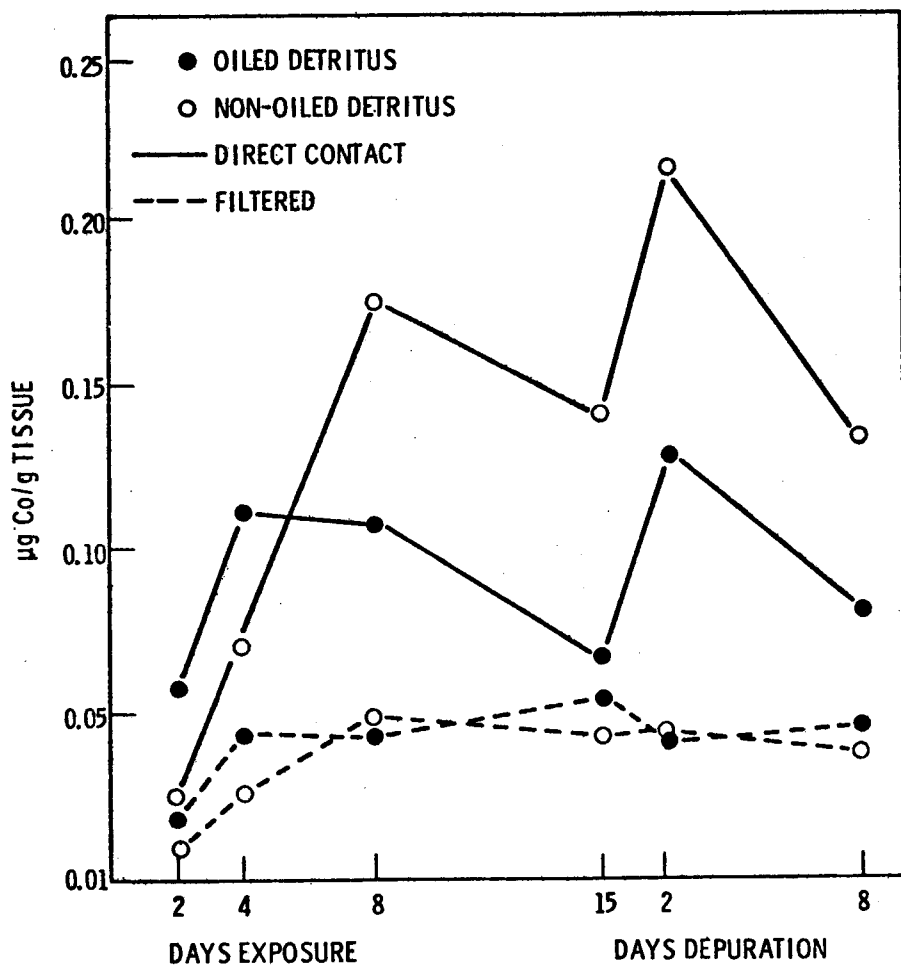


Figure 3. Incorporation of radiolabelled cobalt into Macoma tissue.

or absent. Those which had direct access to detritus incorporated the same amounts early in the exposure period, but later the oiled animals took in less. This difference is probably due to the fact that less oiled than non-oiled detritus was ingested and, therefore, a smaller amount of labelled metal was available for absorption across the walls of the intestinal tract.

The only metal to appear consistently in the shells was cobalt. Its concentration there was of the same order of magnitude as in the clam meat. There was no indication that more cobalt was taken into the shells from oiled than from non-oiled detritus.

DISCUSSION

The detritus on which the clams fed in this experiment was approximately the same material they ingest in nature. There is, therefore, no reason to believe that the concentrations of metals in their food were any higher during than before the experiment or to expect a net increase in metal concentration in the controls, i.e., those animals exposed to non-oiled detritus. The fact that labelled Zn and Co appeared in the controls indicates that a more or less rapid exchange takes place between the metals in the tissue and those in the food or water. The persistence of some labelled metals during the period of depuration may be caused by the retention of old material in the animals' gut after their transfer to clean aquaria.

The normal tissue zinc concentration of Macoma is about 200 ppm. The cobalt concentration is not known, but probably resembles that of other bivalves from unpolluted waters, which is on the order of 0.5 ppm. Thus, the amount of labelled zinc and cobalt taken in by non-oiled Macoma in two weeks,

presumably replacing metals lost to the environment, amounts to about 1% and 30%, respectively, of their normal metal pool. If hydrocarbons enhanced the rate of uptake of metal from detritus, then oil-exposed animals would be expected to accumulate metals from the detritus at a faster rate than that at which they lost them to the environment and so to exhibit a greater increase in radioactivity than is found in the non-oil exposed clams. This was not the case, since the net amount of radioactivity incorporated into the tissues of oil-exposed clams over time was less than that in the tissues of clams exposed to non-oiled detritus. This reduction in metal uptake by tissue, however, does not imply that PHCs reduce the ability of Macoma to absorb metals from detritus, but that PHC reduces the feeding rate of exposed clams.

There seem to be no grounds for believing that exposure to 1000 ppm PHC either increases or decreases the rate at which Macoma absorbs metals, except through a reduction in the rate of food intake. This conclusion is supported by the fact that in the filtered compartment of the aquarium, where the absolute differences between food intakes of oiled and non-oiled animals were less and where more of the metals were probably taken in via the water column, the amounts incorporated by the two groups were quite similar. The results of this experiment therefore indicate that, while the presence of crude oil in sediment may affect the clams' condition through its effect on their feeding behavior, it is not likely to increase the risk of heavy metal toxicity to the population. However, PHC contamination of sediment could alter patterns of metal transfer in the marine benthic community and change the food web due to changes in feeding behavior.

ACKNOWLEDGEMENTS

This study was supported by the Bureau of Land Management through inter-agency agreement with the National Oceanic and Atmospheric Administration, under which a multi-year program responding to needs of petroleum development of the Alaskan continental shelf is managed by the Outer Continental Shelf Environmental Assessment Program (OCSEAP) Office.

REFERENCES

FLETCHER, G. L., J. W. KICENIUK, M. J. KING and J. F. PAYNE: Bull. Environm. Contam. Toxicol. 221, 548 (1979).

KRAUSKOPF, K.: Introduction to Geochemistry, p. 639, McGraw-Hill, New York (1967).

LUOMA, S. N. and E. A. JENNE: The availability of sediment-bound cobalt, silver, and zinc to a deposit-feeding clam, p. 213-230. In H. Drucker and R. C. Wildung (Ed.) Biological implications of metals in the environment. Technical Information Center, Energy Research and Development Administration (1977).

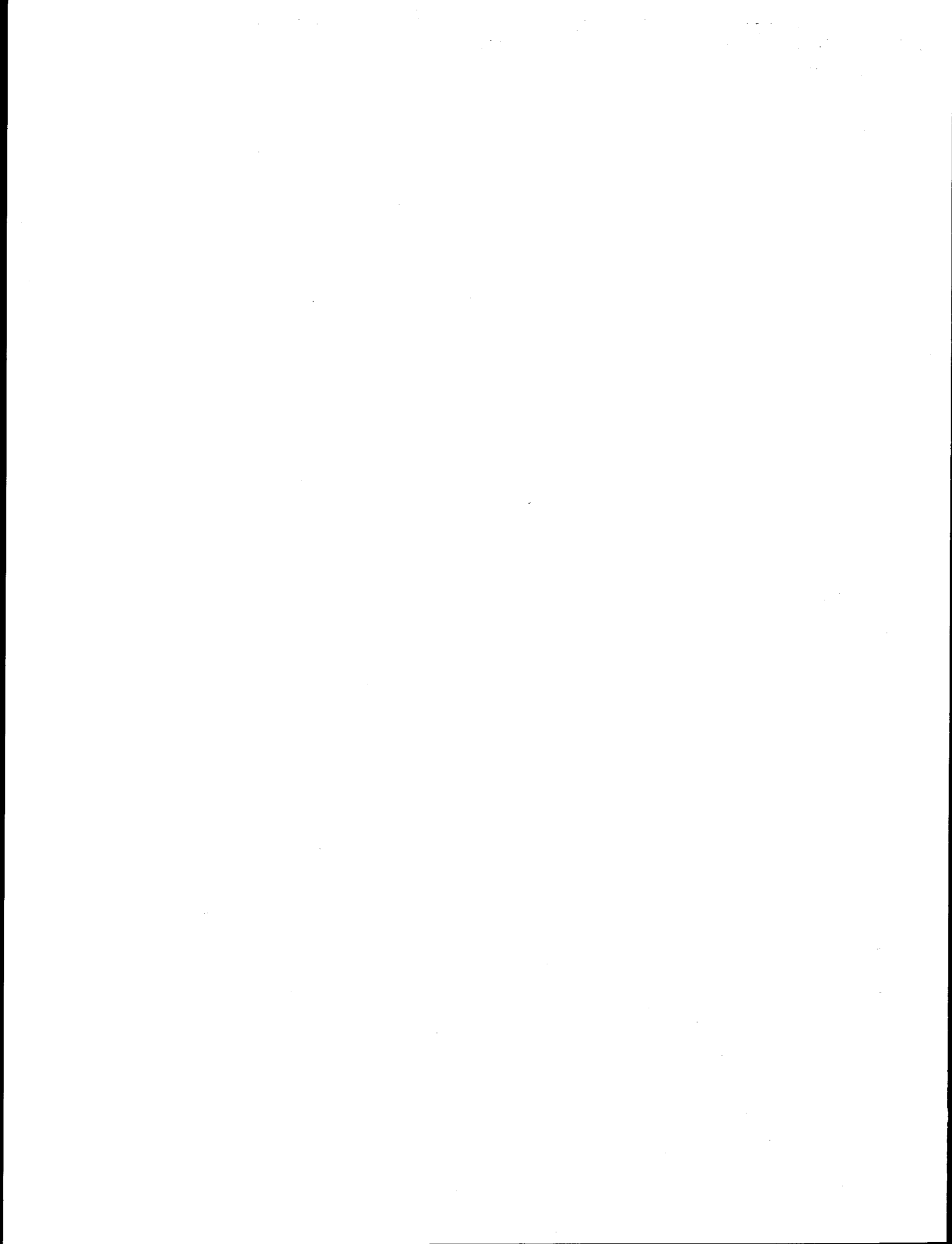
PALUMBO, R. F.: Factors controlling the distribution of the rare earths in the environment and in living organisms, p. 533-538. In V. Schultz and A. Klement (Ed.) Radioecology Reinhold Publishing Corp., New York (1963).

PAYNE, J. F., J. W. KICENIUK, W. R. SQUIRES and G. L. FLETCHER: J. Fish. Res. Bd. Can. 35, 665 (1978).

PETERS, D. S. and D. E. HOSS: Trans. Am. Fish. Soc. 103, 626 (1974).

VINOGRADOV, A. P.: Geokhimiya 7, 555 (1962).

IV. SUBLETHAL EFFECTS OF PETROLEUM HYDROCARBON
CONTAMINATION OF SEDIMENTS



IV-A:

EFFECTS OF PRUDHOE BAY CRUDE OIL CONTAMINATED SEDIMENTS

ON PROTOTHACA STAMINEA (MOLLUSCA:PELECYPODA):

HYDROCARBON CONTENT, CONDITION INDEX, FREE AMINO ACID LEVEL

by

J. M. Augenfeld, J. W. Anderson, D. L. Woodruff, and J. L. Webster

Battelle Pacific Northwest Laboratories

ABSTRACT

Protothaca staminea and Macoma inquinata were exposed to sediment contaminated with 1237 ppm Prudhoe Bay crude oil in the field. Eighty-five percent of the Protothaca and 17% of the Macoma survived 54 days exposure. Body burdens of saturate and di- and tri-aromatic hydrocarbons were less than 2 ppm and quite variable. The condition index of Protothaca was reduced by 6% by exposure to oil. The level of free glycine in mantle, gills and adductor muscle did not change significantly, but the taurine level fell, leading to a decrease in the taurine:glycine ratio. It was concluded that Protothaca, a filter feeder, is affected less severely by oil pollution than Macoma, a detritivore, perhaps because the feeding activity of filter feeders is inhibited less.

INTRODUCTION

Roesijadi and Anderson (1979) reported that exposing the deposit-feeding bivalve, Macoma inquinata to oil-contaminated sediment resulted in reduced survival, reduced condition index (CI), and reduced levels of free amino acids (FAA), principally glycine, in the gills, mantle, and adductor muscle. Roesijadi, Anderson, and Blaylock (1978) had found this species to accumulate substantially larger amounts of diaromatic hydrocarbons from sediment than the filter-feeding bivalve, Protothaca staminea. An experiment has been undertaken, using more severe exposure conditions, in order to examine a wider range of petroleum hydrocarbon (PHC) compounds taken up by the two species and to compare the physiological impact of exposure on P. staminea with that on Macoma.

METHODS

P. staminea, M. inquinata, and the sipunculid Phascolosoma agassizi, in addition to sediment, were collected from the protected side of a sand spit at the mouth of Sequim Bay, Washington State, U.S.A. The animals were kept under running seawater at about 10°C and 30 parts per thousand (‰) salinity for six days before use. The sediment used was that from the animal collection site which passed through a 6 mm mesh screen. Ninety-eight ml of Prudhoe Bay crude oil was emulsified in a blender with two 500 ml portions of sea water. The oil and one l sea water were added to 42 kg of sieved sediment in a cement mixer and mixed for one hour. The oiled sediment was flushed three times with sea water while in mesh bottomed trays, 25 x 47 x 12 cm in size. Unooled control sediment was similarly treated. Sediment samples were taken for determination of initial total hydrocarbon content by IR spectrophotometry (API, 1958). Initial control groups of clams were taken for condition index

and free amino acid determinations by the methods of Roesijadi and Anderson (1979), and the remainder were placed in the sediment trays. Thirty Protothaca were placed in each of three control and three oiled trays. Thirty Macoma and 30 Phascolosoma, a detritivorous sipunculid worm, were placed in one oiled tray, and 20 Macoma and 30 Phascolosoma in one control tray. On January 11, 1978 the trays were placed in the low intertidal zone in the area from which the animals and sediment had been collected.

On March 6, 1978 the trays were removed, and the total hydrocarbon content of the sediment was determined by IR spectrophotometry. Surviving animals were counted, left overnight in running sea water to allow their intestinal contents to be cleared, and frozen at -65°C. Two Macoma, three Protothaca, and samples of the sediment were taken for analysis of individual hydrocarbon compounds by glass capillary gas chromatography (Warner, 1976). Condition indices and free amino acid levels of control and exposed Protothaca were determined by the methods of Roesijadi and Anderson (1979). Condition indices were calculated according to the formula:

$$\text{C. I.} = \frac{\text{g ash free dry weight}}{\text{cm shell length}} \times 1000$$

RESULTS

Initially the oiled sediment contained 1237 ± 112 ppm hydrocarbons ($n = 4$), and the control sediment 10 ± 11 ppm ($n = 2$). After 54 days exposure 850 ± 17 ppm ($n = 4$) remained in the contaminated trays. In the control trays 82 out of 90 Protothaca (91%), all 20 Macoma (100%) and 11 out of 30 Phascolosoma (37%) remained. In the trays containing oiled sediment 77 out of 90 Protothaca (85%), but only 5 out of 30 Macoma (17%) and no Phascolosoma were

recovered alive. The more mobile worms may have migrated from the oiled environment, but the missing clams presumably died. As Table 1 shows, in control animals the level of PHC compounds is below the limit of detection. The PHC content of exposed animals was less than 2 ppm and highly variable within each species. The mean content of the two Macoma tested was twice that of the three Protothaca examined. The most consistent and marked contrast between the two species was the naphthalene level, which was an order of magnitude higher in Macoma.

A difference, significant at the .01 level, was found between the mean condition indices of exposed and control Protothaca (Table 2). There was a decrease of similar proportion among control animals between the beginning and end of the exposure period, but it was not statistically significant. Analysis of the free amino acids in gill, mantle, and adductor muscle (Table 3) showed reductions, significant at the .01 level, in the contents of alanine, histidine, and leucine in controls at the end of the experiment, compared to initial controls. The total FAA content however rose over this period, due to a 29% increase in the level of taurine. Comparison of control and exposed animals taken after 54 days in the field showed highly significant reductions only in the levels of lysine and taurine. The latter was quite variable, being almost absent in some exposed clams. There was a highly significant difference in total amino acid content between the two groups, two thirds of which was accounted for by the decline in the mean level of taurine.

DISCUSSION

In June, 1977 Roesijadi and Anderson (1979) exposed M. inquinata to sediment initially containing 1144 ± 47 ppm hydrocarbons. Their exposure period lasted 38 days, during which time the petroleum hydrocarbon (PHC)

Table 1. Glass capillary gas chromatographic analyses of petroleum hydrocarbons content ($\mu\text{g/g}$) in Macoma and Protothaca tissue and sediment after 54 days exposure to oil-contaminated sediment.

	<u>Macoma</u>			<u>Protothaca</u>				<u>Sediment</u>
	<u>Control</u>	<u>Exposed</u> <u>I</u>	<u>II</u>	<u>Control</u>	<u>Exposed</u> <u>I</u>	<u>II</u>	<u>III</u>	
Saturates n _C ₁₂ -n _C ₂₈	<.047	.381	.514	<.196	<.948	.181	<.154	35.57
Pristane	-*	.020	.009	<.018	.002	.009	-	2.085
Phytane	-	.023	.011	-	-	.010	-	1.170
Naphthalene	-	.021	.032	-	.001	<.001	<.009	0.347
2-MN	-	.022	.048	-	.022	.020	.023	1.401
1-MN	-	.023	.081	-	.025	.024	.019	0.761
1 Ethyl + 2 Ethyl Naphthalene	-	.023	.181	-	.012	.001	.018	0.300
2,6 + 2,7 DMN	-	.023	.092	<.014	.076	.001	.018	0.653
1,3 + 1,6 DMN	-	.023	.135	<.015	.039	.035	.030	0.580
1,7 DMN	-	.023	.021	-	.022	.026	.009	0.822
1,4 + 2,3 + 1,5 DMN	-	.024	.096	-	.057	.002	.024	0.486
1,2 DMN	-	.026	.052	-	.034	-	-	0.162
Phenanthrene	-	.010	.102	-	.017	.010	.036	0.114
C1 Phenanthrenes	-	.014	.225	-	.044	.007	.064	0.028
C2 Phenanthrenes	-	.014	.271	-	.051	.009	.074	0.311
Total Diaromatics	-	.208	.638	<.043	.288	.111	.153	5.512
Total Triaromatics	-	.038	.598	-	.112	.026	.174	0.453
Total PHC Identified	<.074	.670	1.770	.206	1.350	.337	.481	44.791

* To reduce confusion in reading the table, all values <0.008 have been removed. The variability in the detection threshold is a result of differences in the recovery of internal standards and the sample weight.

MN = methyl naphthalenes
 DMN = dimethyl naphthalenes
 C1 = methyl
 C2 = dimethyl

Table. 2. Condition indices of initial control, field control, and exposed Protothaca staminea.

	$\bar{x} \pm S.E.$	n
Initial Control	19.3 \pm .36	10
Field Control - 54 days in clean trays	18.2 \pm .20 n.s.	59
Exposed - 54 days in contaminated trays	17.1 \pm .17 **	64

n.s. Not significantly different at .10 level from initial control.

** Significantly different from field control at .01 level when means are compared by student's t test.

Table 3. Free amino acid concentration in gills, mantle, and adductor muscle of Protothaca staminea (μ moles/g) after 54 days exposure to oil-contaminated sediment.

	<u>Initial Control</u>	<u>Field Control</u>	<u>Field Exposed</u>
Alanine	9.47 \pm 1.48	6.47 \pm 2.23††	4.01 \pm 2.3*
Arginine	2.84 \pm 0.56	2.75 \pm 0.85	1.92 \pm 1.31
Aspartic Acid	1.30 \pm 0.65	1.15 \pm 0.47	0.56 \pm 0.50*
Glutamic Acid	3.89 \pm 1.57	3.26 \pm 0.88	1.99 \pm 1.32*
Glycine	26.7 \pm 6.5	21.9 \pm 7.8	18.33 \pm 12.6
Histidine	0.21 \pm 0.06	0.11 \pm 0.03††	0.34 \pm 0.70
Isoleucine	0.27 \pm 0.05	0.24 \pm 0.10	0.15 \pm 0.10
Leucine	0.43 \pm 0.10	0.24 \pm 0.11††	0.31 \pm 0.16
Lysine	0.34 \pm 0.12	0.37 \pm 0.11	0.21 \pm 0.11**
Methionine	0.08 \pm 0.0	0	0
Phenylalanine	0.31 \pm 0.08	0.22 \pm 0.07†	0.22 \pm 0.17
Proline	0.26 \pm 0.08	0.16 \pm 0.10†	0.10 \pm 0.09
Serine ¹	1.17 \pm 0.30	0.91 \pm 0.18†	0.93 \pm 0.67
Threonine	0.36 \pm 0.13	0.28 \pm 0.08	0.21 \pm 0.13
Tyrosine	0.28 \pm 0.06	0.25 \pm 0.08	0.21 \pm 0.22
Valine	0.37 \pm 0.07	0.33 \pm 0.10	0.23 \pm 0.15
Taurine	33.6 \pm 10.6	43.3 \pm 17.1	18.36 \pm 13.05**
Total	79.94 \pm 17.96	85.56 \pm 26	48.08 \pm 24.5**
Taurine:Glycine	1.23 \pm 0.28	2.04 \pm 0.54	1.38 \pm 0.78

† Significantly different from initial control at .05 level; student's t test.

†† Significantly different from initial control at .01 level; student's t test.

* Significantly different from field control at .05 level; student's t test.

** Significantly different from field control at .01 level; student's t test.

¹ Serine, glutamine, and asparagine co-chromatograph.

content declined to 364 ± 66 ppm. These conditions were obviously less severe than our winter exposure of 54 days, during which the PHC level remained above 800 ppm. The lesser severity is reflected in the fact that in the earlier experiment 59% of the exposed Macoma survived while only 17% did so in this experiment. Earlier, Roesijadi, Anderson and Blaylock, (1978) had exposed Phascolosoma agassizi for 60 days to sediment containing 887 ppm PHC at the beginning and 420 ppm at the end of the period. Their experimental animals survived and remained in their trays, while the sipunculids exposed here either died or migrated out. This contrast also indicates the greater stressfulness of the present exposure. Nevertheless, even under the present harsher conditions 85% of the exposed Protothaca survived.

The number of Macoma surviving the winter exposure was too small to allow comparisons to be made of sublethal physiological effects with those on winter exposed Protothaca. These Protothaca apparently were affected less intensely than the surviving summer exposed Macoma of Roesijadi and Anderson (1979). Thus the average condition index of Macoma inquinata exposed to oil-contaminated sediment for 38 days in June, 1977 was 16% lower than that of control animals (Table 4). By contrast, the condition index of Protothaca exposed in January 1978 was only 6% less than that of the controls. Since it is not likely that the shell length of any individual animal changed significantly during the course of the experiment, the condition indices are directly proportional to the ash free dry weights. The decline from control levels by exposed Protothaca was only one third as large as that exhibited by exposed Macoma. This indicates that the former were not forced to draw on their stored reserves for nutrition to as great an extent as the latter. That the absolute value of the CI of control Protothaca is substantially higher

Table 4. Survival and condition index of Macoma and Protothaca after exposure to oil-contaminated sediment.

	<u>Survival (%)</u>	<u>Condition Index</u>	<u>PHC Content Of Sediment (ppm)</u>	
			<u>Initial</u>	<u>Final</u>
<u>Macoma</u>				
June				
Control	92	8.92 ± 0.18		
Exposed	59	7.46 ± 0.28** (16.3% decrease)	1144 (± 47.3)	364 (± 66.4)
<u>Macoma</u>				
January				
Control	100			
Exposed (54 days)	17		1237 (± 112)	850 (± 17)
<u>Protothaca</u>				
January				
Control	91	18.2 ± 0.20		
Exposed (54 days)	85	17.1 ± 0.17** (6% decrease)		

**Significantly different from control at .01 level by student's t test.

than that of control Macoma is due to the fact that Protothaca is wider in proportion to its length than Macoma. Therefore, in animals of equivalent nutritional status a given unit of shell length corresponds to a larger volume of flesh for Protothaca.

The changes found in free amino acid levels in the tissues of Protothaca differ from those reported in other bivalve species under stress. Roesijadi and Anderson (1979) found a pattern in Macoma resembling the stress syndrome described by Bayne *et al.* (1976) in Mytilus edulis. In their exposed animals the average level of glycine was reduced to 62% of that in the controls, while the taurine level stayed constant, leading to an increase in the taurine:glycine ratio. Jeffries (1972) reported a drop in glycine level in stressed Mercenaria mercenaria accompanied by an increase in taurine levels, again leading to an elevated taurine:glycine ratio.

In the Protothaca exposed in this experiment the reverse was found. The mean glycine level of exposed clams did not differ significantly from that of controls, but the mean level of taurine was reduced by 58%, leading to a decline in the taurine:glycine ratio. Table 5 compares the relevant data. The significance of the decline in taurine is not clear at this time, since its only known role in the metabolism of marine invertebrates is to function in osmoregulation. There is no reason to suspect any difference between the salinity level of the water surrounding the oil-exposed and the control groups. However, there is some evidence to indicate that the taurine levels of Protothaca tissue may fluctuate as a result of conditions not related to stress or osmoregulation. Roesijadi (1979) reported that holding Protothaca in the laboratory for 26 days under constant temperature and salinity resulted in a significant decrease in the taurine level of the gills while the glycine levels remained constant. Stress, in the form of addition of up to 155 µg/ℓ

Table 5. Free amino acid content ($\mu\text{moles/g}$) of Macoma and Protothaca.

<u>Amino Acids</u>	<u>Macoma</u>		<u>Protothaca</u>	
	(June, 38 day exposure)		(January, 54 day exposure)	
	<u>Control</u>	<u>Exposed</u>	<u>Control</u>	<u>Exposed</u>
Glycine	70.25 \pm 4.51	43.56 \pm 4.94	21.9 \pm 7.8	18.33 \pm 12.6 n.s.
Lysine	0.59 \pm 0.04	0.41 \pm 0.04	0.37 \pm 0.11	0.21 \pm 0.11
Threonine	1.16 \pm 0.05	0.87 \pm 0.07	0.28 \pm 0.08	0.21 \pm 0.13 n.s.
Taurine	37.06 \pm 1.94	35.08 \pm 2.39	43.3 \pm 17.1	18.36 \pm 13.05
TOTAL	150.57 \pm 8.15	110.48 \pm 8.24	85.56 \pm 26.0	47.0 \pm 24.5
Taurine:Glycine	0.54 \pm 0.04	0.89 \pm 0.12	2.04 \pm 0.54	1.38 \pm 0.78

n.s. No significant difference, other differences significant at .01 level.

of Na hypochlorite led to a significant decrease in the concentration of glycine but not of taurine (Roesijadi, 1979).

In view of these data, which indicate that taurine levels may change in this species for unknown reasons, it may be more useful to consider the changes in other free amino acids, especially glycine, as indicators of stress. There is only a slight, statistically insignificant, decrease in the glycine levels in the oil-exposed Protothaca. This response, together with the smaller decrease in condition index and the higher rate of survival, all support the conclusion that the suspension feeder Protothaca is less vulnerable to oil-contaminated sediment than the deposit feeder Macoma.

It is difficult to relate this lower vulnerability to a lower body burden of PHC except in the case of naphthalene. Roesijadi, Anderson, and Blaylock (1978) pooled their samples of exposed Macoma and found the level of total diaromatics to be an order of magnitude higher than in exposed Protothaca. If the same procedure had been followed in this work, a qualitatively similar difference would have been found for all aromatics, though of smaller extent. However, one individual exposed Macoma contained lower levels of most hydrocarbon compounds examined than some exposed Protothaca, in agreement with the findings of Roesijadi and Anderson (1979) who found quite low levels (.08 µg/g) of diaromatics in their exposed Macoma. Comparison of body burdens of individual PHC compounds with corresponding levels in the sediment showed no trend toward tissue magnification except in the case of methyl phenanthrene. Other triaromatics and a few diaromatics approached equilibrium with the sediment levels, while most diaromatic and saturate concentrations are one to two orders of magnitude lower in tissue than in sediment.

From these few analyses there was only a slight difference in the level of hydrocarbon accumulation in the tissues of the two species, while there are

clear differences in the severity of physiological impact of oil pollution. Therefore, these data are not sufficient to support the hypothesis that the impact of oil pollution on the survival and physiological state of intertidal bivalves results directly from the toxic effects of hydrocarbon compounds. It is possible that the effects noted are instead the result of a decline in feeding activity induced by the oil. Gilfillan et al. (1977) reported a negative correlation between carbon flux and tissue aromatic HC content in Mya arenaria collected from sites contaminated by an accidental oil spill. Stegeman and Teal (1973) found that Crassostrea virginica reduced its production of faeces and pseudofaeces in proportion to the hydrocarbon concentration in the surrounding water at concentrations between 100 and 400 µg/l. In our laboratory, Augenfeld, Anderson and Crecelius (in preparation) observed a 50% decline in detritus intake by Macoma presented with food tainted with Prudhoe Bay crude oil. Augenfeld (1980, in press) reported an 80% decrease in sediment egestion rate by Abarenicola pacifica, a deposit feeding polychaete, in heavily contaminated sediment. Gordon, Dale and Keizer (1978) noted a decrease of up to 93% in the sediment-working rate of the similar form Arenicola marina in the presence of 275 ppm oil in sediment. The material taken in by filter feeders is in less direct contact with oil associated with sediment than the food taken in by deposit feeders. As a result, Protothaca may have been inhibited in its feeding activity to a lesser degree than Macoma. The enhanced survival and reduced level of stress shown by the former may thus be the direct result of a superior nutritional status.

LITERATURE CITED

- American Petroleum Institute. (1958). Determination of volatile and non-volatile oily material: infrared spectrometric method. API Publication No. 733-748. American Petroleum Institute, Washington, D. C.
- Augenfeld, J. M. (1980). Effect of Prudhoe Bay crude oil contamination on sediment working rates of Abarenicola pacifica. Mar. Env. Res., in press.
- Bayne, B. L., D. R. Livingstone, M. N. Moore, and J. Widdows. (1976). A cytochemical and biochemical index of stress in Mytilus edulis L. Mar. Pollut. Bull. 7,221-224.
- Gilfillan, E. S., D. W. Mayo, D. S. Page, D. Donovan and S. Hanson. (1977). Effects of varying concentrations of petroleum hydrocarbons in sediments on carbon flux in Mya arenaria. In Physiological responses of marine biota to pollutants, ed. by W. B. Vernberg, A. Calabrese, F. Thurberg and F. J. Vernberg, pp. 199-314. New York, Academic Press.
- Gordon, D. C., Jr., J. Dale and P. D. Keizer. (1978). Importance of sediment working by the deposit-feeding polychaete Arenicola marina on the weathering rate of sediment-bound oil. J. Fish. Res. Bd. Canada 35, 591-603.
- Jeffries, H. P. (1972). A stress syndrome in the hard clam, Mercenaria mercenaria. J. Invert. Pathol. 20, 242-287.
- Roesijadi, G. (1979). Taurine and glycine in the gills of the clam Protothaca staminea exposed to chlorinated seawater. Bull. Environm. Contam. Toxicol. 22, 543-547.

- Roesijadi, G. and J. W. Anderson. (1979). Condition index and free amino acid content of Macoma inquinata exposed to oil-contaminated marine sediments. In Marine Pollution: Functional Responses, ed. by W. B. Vernberg, A. Calabrese, F. Thurberg and F. J. Vernberg, pp. 69-83. New York, Academic Press.
- Roesijadi, G., J. W. Anderson and J. W. Blaylock. (1978). Uptake of hydrocarbons from marine sediments contaminated with Prudhoe Bay crude oil: Influence of feeding type of test species and availability of polycyclic aromatic hydrocarbons. J. Fish. Res. Bd. Canada 35, 608-614.
- Stegeman, J. J. and J. M. Teal. (1973). Accumulation, release, and retention of petroleum hydrocarbons by the oyster Crassostrea virginica. Mar. Biol. 22, 37-44.
- Warner, J. S. (1976). Determinations of aliphatic and aromatic hydrocarbons in marine organisms. Analyt. Chem. 48, 578-583.

IV-B:
EFFECTS OF PRUDHOE BAY CRUDE OIL CONTAMINATION
ON SEDIMENT WORKING RATES OF ABARENICOLA PACIFICA

by

J. M. Augenfeld

Battelle Pacific Northwest Laboratories

ABSTRACT

Lugworms (*Abarenicola pacifica*) were exposed to sediment containing 250 to 1000 ppm Prudhoe Bay crude oil. At concentrations of 500 and 1000 ppm the rate of feeding, as measured by faecal production, was reduced by 70%. Smaller control animals turned over more sediment in proportion to their body size than larger ones. Exposure to oil at high levels abolished this difference by greater depression of the rate of faecal production by smaller individuals.

INTRODUCTION

Accidentally spilled petroleum hydrocarbons (PHCs) which impact fine-grained sediments in intertidal zones may remain in situ for periods of years (Mayo et al. 1978; Teal, Burns & Farrington, 1978), resulting in long-term effects on local populations (Krebs & Burns, 1977). One factor which may contribute to this persistence is the existence of anoxic conditions at depths of more than 1 cm below the surface of these habitats (Teal & Kanwisher, 1961; Pamatmat, 1968; Hylleberg, 1975). ZoBell (1964) has reported that PHCs are degraded at much slower rates in anaerobic sediments than under aerobic conditions.

The burrowing and feeding activities of certain organisms transport sediment from the lower anoxic areas to the surface, where aerobic microbes can metabolize hydrocarbons more rapidly. One such organism which occurs in high densities in fine-grained sediment along the shores of the North Pacific is the sedentary polychaete worm, Abarenicola pacifica Healy & Wells. Hobson (1967) has calculated that a population of A. pacifica located in False Bay, San Juan Island, Washington State, U.S.A., could move all the sediment in the upper 10 cm of the area they inhabit to the surface in a little more than two years. Their activity could aid in the recovery of intertidal zones from the effects of oil pollution if they can continue to feed in contaminated sediment.

Gordon, Dale & Keizer (1978) reported that exposure in the laboratory to No. 2 fuel oil, Venezuelan Bunker C., South Louisiana crude, Kuwait crude oil, or to sediment which had been impacted by an accidental spill of Bunker C led to reductions of 51% to 82% in sediment-working rates of Abarenicola marina L. This species is found in sandy beaches on both sides of the North Atlantic and is closely related to A. pacifica. Gordon et al., found that direct contact with sediment containing oil at concentrations as low as 153 ppm for as little as 5 days caused some of their worms to surface, and some died at concentrations of 275 ppm.

In our laboratory A. pacifica has been found to tolerate direct contact with sediment containing 1000 ppm of Prudhoe Bay crude oil (PBC) for more than three weeks. It therefore seemed possible that the mud-dwelling Pacific species is more tolerant of oil contamination than the sand-dwelling Atlantic species. An experiment was designed to learn whether contamination of their habitat with various levels of PBC would reduce the amount of sediment which A. pacifica transports to the surface. This experiment made use of the fact

that the worm deposits its faeces in easily recognizable coils around the entrance to its burrow.

MATERIALS AND METHODS

Forty specimens of A. pacifica and 12 kg sediment were collected from the high intertidal region of an almost enclosed lagoon adjacent to Sequim Bay, Washington State, U.S.A. The upper 10 cm of the sediment consisted of very fine-grained, semi-liquid mud, and a layer of firmer fine-grained sand lay beneath. In the laboratory the worms were kept in sediment under running sea water at 10°C and 30‰ salinity.

Sediment (2.5 kg wet wt.) consisting of equal volumes of the mud and sand strata, was placed in each of four cylindrical metal containers of 3-liter capacity. Three different volumes of PBC (.625, 1.25 or 2.5 g) were added to three containers, and the contents of each, including the uncoiled control, were stirred 6 minutes with a motor-driven impeller. Previous trials with the dispersion of radio-labelled material have shown this time period to be adequate for thorough mixing. The resulting mixtures were injected into 40 pieces of tygon tubing, 40 cm long and 17 mm i.d. The tubes were bent into U-shapes and placed in racks under running sea water for 20 hours to allow the more toxic low molecular weight components of the oil to wash out. Remaining sediment was placed under running sea water as a reserve supply.

One worm was placed in each tube, and plastic trays, 64 mm on a side, were placed around the ends of the tubes. At 24-hour intervals the water levels in the tanks were lowered and the faeces produced by each worm were collected with a stainless steel spatula from the trays and from the surface of the sediment within the tubes. At intervals of several days sediment from the appropriate reserve supply was added to the tubes to replace consumed

material. The faeces were dried in air for 24 hours and weighed. Preliminary studies indicated that this time period was long enough to achieve a constant weight. All calculations of faecal cast production were based on the mean daily dry weight produced by each individual worm.

After 11 days of exposure, the sediment and worms were removed from the tubes. The worms were rinsed with sea water, blotted dry, weighed and frozen. Samples of the sediment were taken from tubes at each treatment level, frozen, and later analyzed for total hydrocarbon content by IR spectrophotometry.

RESULTS

The level of PHC in the sediment changed little during the exposure period. The worms' native substrate used in the experiment has a fairly high endogenous content of organic material which absorbs IR radiation at the same wavelengths as hydrocarbons. The HC content of sediment at the three treatment levels, when corrected for interference by the organic content of the control sediment, was between 80 and 100% of the amount originally added. The actual concentrations of PBC to which the worms were exposed lie somewhere between the levels originally added and the levels measured at the end of the experiment. For the sake of convenience, these levels will be referred to as those originally added, viz. 250 ppm (low), 500 ppm (medium), and 1000 ppm (high).

All the control worms survived, but two of them left their tubes and burrowed into detritus at the bottom of the tank, where their faeces could not be collected. Mortality was slightly higher in the exposed groups, and some signs of behavior stress were observed. When the faeces were collected, at 24-hour intervals, some of the worms exposed to medium and high levels of PBC were seen to extend their posterior segments from the burrows

and slowly move them through the water. This behavior, which would obviously be maladaptive under natural conditions, was never observed in the controls or in the field. Feeding behavior was apparently depressed during the first two days of exposure, to a greater extent in the higher concentrations. During the remaining nine days the frequency of defaecation, based on 24-hour observation periods, was slightly, but not significantly, lower in the exposed animals. Data on faecal production was therefore taken from this nine-day period, as being more representative of the long-term effect of oil exposure.

A strong negative correlation was found between faecal production per unit body weight and body weight. The slope of the regression line relating these parameters was calculated according to the formula

$$b = \frac{\sum xy - \frac{\sum x \sum y}{n}}{\sum x^2 - \frac{(\sum x)^2}{n}}$$

and found to be -2.56 for the control and low-level exposure groups and only -0.50 for the two higher-level exposure groups (Figure 1). The degree of scatter around the regression lines was less in the exposed groups than in the control. Mean faecal production per unit body weight was moderately depressed in low-level exposed groups.

The regression of dry faecal weight, unadjusted for body weight, on body weight, was not significant within any treatment group; i.e., it could not be statistically demonstrated that the total amount of sediment turned over by an individual worm was affected by the weight of the worm. The mean produced faecal weight is markedly reduced by exposure to hydrocarbon levels above 500 ppm. Pairwise comparison of the control with each treatment group by

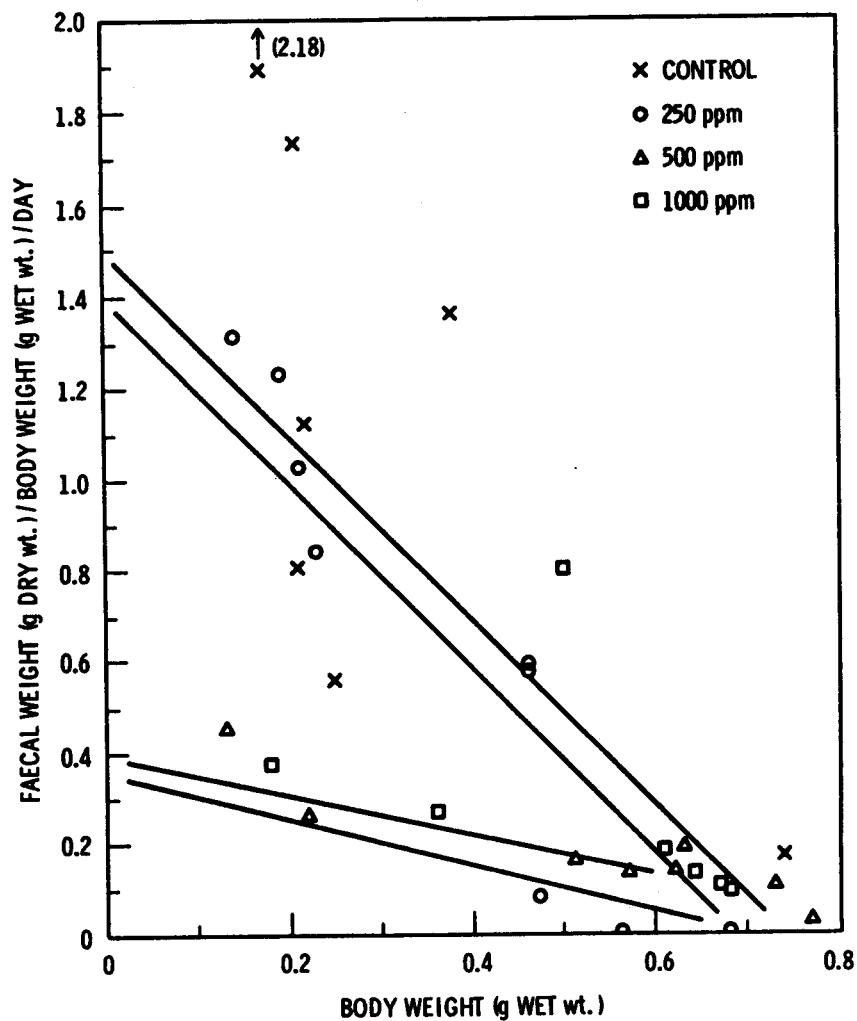


Figure 1. Regression of Faecal Weight Per Unit Body Weight on Body Weight.

Control	$y = 1.839 - 2.56 x; r = -.653; n = 8$
250 ppm	$y = 1.600 - 2.56 x; r = -.941; n = 9$
500 ppm	$y = .449 - .50 x; r = -.921; n = 8$
1000 ppm	$y = .438 - .50 x; r = -.885; n = 7$

the Newman-Keuls test showed no significant difference between it and the low-exposure level, while the mean production rate at the medium- and high-exposure levels differed significantly at the .05 level from that of the controls.

DISCUSSION

Exposure to oil reduces the degree of scatter around the regression lines relating faecal production per unit body weight to body weight of A. pacifica, and at levels above 500 ppm greatly reduces the slope of the lines (Figure 1). Both of these effects may be attributed to a greater impact of exposure to oil on the smaller and more active animals. Among control worms weighing less than 0.25 g, faecal production per unit body weight varied between 0.9 and 2.1 g feces/g worm/day. Production by worms in this size class ranged from 0.84 to 1.3 g/g worm/day under exposure to a low level of oil. At the higher oil levels values for the smaller worms fell to between 0.37 and 0.45 g/g worm/day. By contrast, the maximum production of worms weighing more than 0.6 g was reduced only from 0.2 g/g worm/day in control animals to .08 g/g worm/day at the higher exposure levels. Exposure to oil clearly leads to a greater reduction in feeding activity at the lower end of the size range than at the upper end. The individual variability of production is lessened by a greater decrease in the maximum rate achieved by the smaller animals than in the minimum rates.

These data indicate some of the effects of hydrocarbon pollution on the survival and activity of the worms. However, measures of faecal production per unit body weight such as these, and those reported by

Gordon et al. (1978), are less useful in predicting the effect of the affected worms on sediment turnover, since predictions based on them would require information on the size distribution of the exposed population, which might not be available. Fortunately, the effect of the negative regression of faecal production on body weight is cancelled out by the increasing body weight itself, with the result that within each treatment group the regression of faecal weight, uncorrected for body weight, on body weight is not significant at the .05 level.

The somewhat surprising conclusion is that under uniform conditions and within the weight range examined, which was .14 to .74 g, the size of the worms has no significant effect on the average dry weight of faeces produced per day. Therefore, if suitable control populations were available for comparison the defaecation rate of A. pacifica could be used as an indicator of a particular level of environmental stress, even if the size distribution of the worm population is not known.

The results also suggest that if pollution is not too severe, Abarenicola may continue to turn over the equivalent of its own wet body weight per day in sediment. However, high concentrations of oil may reduce the sediment-working rate of surviving worms by as much as 70%. This effect, together with any mortality due to the environmental pollution, would substantially retard the transportation of sediments to the surface. If these effects are found under actual field conditions, it is possible that sufficiently high levels of oil will retard the rate of sediment recovery by reducing the feeding behavior of ecologically significant species. Measurements of the food intake of deposit-feeders and detritivores may be a valuable means of evaluating effects of oiled substrate, as Roesijadi & Anderson (1979) have shown that condition index and free amino acid content of the deposit-feeding clam, Macoma, decreased during field exposure to oiled sediment.

ACKNOWLEDGEMENTS

This research was funded by Contract No. 03-6-022-35204 from the National Oceanic and Atmospheric Administration as part (Research Unit 454) of the Outer Continental Shelf Environmental Assessment Program (OCSEAP) of the Alaskan Project Office.

LITERATURE CITED

- Gordon, D. C., Jr., J. Dale & P. D. Keizer. (1978). Importance of sediment-working by the deposit-feeding polychaete, Arenicola marina on the weathering rate of sediment-bound oil. J. Fish. Res. Bd. Canada 35: 591-603.
- Hobson, K. D. (1967). The feeding and ecology of two North Pacific Abarenicola species (Arenicolidae, Polychaeta). Biol. Bull. 133: 343-354.
- Hylleberg, J. (1975). Selective feeding by Abarenicola pacifica with notes on Abarenicola vagabunda and a concept of gardening in lugworms. Ophelia 14:113-137.
- Krebs, C. T. & K. A. Burns. (1977). Long-term effects of an oil spill on populations of the salt-marsh crab Uca pugnax. Science 197:484-487.
- Mayo, D. W., D. S. Page, J. Cooley, E. Sorensen, F. Bradley, E. S. Gilfillan & S. A. Hanson. (1978). Weathering characteristics of petroleum hydrocarbons deposited in fine clay marine sediments, Searsport, Maine. J. Fish. Res. Bd. Canada 35:552-562.
- Pamatmat, M. M. (1968). Ecology and metabolism of a benthic community on an intertidal sandflat. Int. Revue ges. Hydrobiol. 53:211-298.
- Roesijadi, G. & J. W. Anderson. (1979, in press). Marine Pollution: Functional Responses. Proceedings of the Symposium on Pollution and Physiology of Marine Organisms. Georgetown, S. C., November 14-17, 1977, New York, Academic Press.
- Teal, J. M. & J. W. Kanwisher. (1961). Gas exchange in a Georgia salt marsh. Limnol. Oceanogr. 6:388-399.
- Teal, J. M., K. Burns & J. Farrington. (1978). Analyses of aromatic hydrocarbons in intertidal sediments resulting from two spills of No. 2 fuel oil in Buzzards Bay, Massachusetts. J. Fish. Res. Bd. Canada 35:510-520.
- ZoBell, C. E. (1964). The occurrence, effects, and fate of oil polluting the sea. In: Adv. In Water Pollution 3:85-109. E. A. Pearson, ed., MacMillan Co., New York.



IV-C:

EFFECTS OF PRUDHOE BAY CRUDE OIL IN SEDIMENT
ON ABARENICOLA PACIFICA IN LABORATORY AND FIELD EXPERIMENTS

by

J. M. Augenfeld and J. W. Anderson
Battelle Pacific Northwest Laboratory

Introduction

Hydrocarbon pollutants are particularly persistent in fine grained intertidal sediments (Mayo et al., 1978; Teal et al., 1978), and, once introduced, may affect local populations for extended periods (Krebs & Burns, 1977; Sabo & Stegeman, 1977). In view of this vulnerability it would be advantageous to identify responses on the part of organisms typically found in such habitats which could provide early warnings of a deterioration in environmental quality. Behavioral responses are often sensitive indicators of changes over short time frames, but observations of organisms buried in mud presents obvious difficulties. There is however one form of behavior taking place within the sediment which can be quantified by an observer at the surface. This is the burrowing and feeding activity of organisms which deposit their feces around the entrance of permanent burrows.

One such group of organisms are the Arenicolidae, or lugworms. Several characteristics of these sedentary worms make them potentially valuable as indicators of environmental quality. They are relatively non-motile, survive well in the laboratory, and are found in large numbers in sensitive habitats. In addition, their pattern of feeding and respiratory behavior increase their

potential exposure to substances both in the substrate surrounding them and the water column above them, since they ingest large amounts of sediment and use undulating body motions to pass large volumes of water over their gills.

Casual observations in our laboratory suggested that the rate of burrowing of Abarenicola pacifica, a species typical of muddy tidal flats, was reduced by hydrocarbons in its environment. Gordon, Dale and Keizer (1978) reached similar conclusions for Arenicola marina, a larger, related form, typical of sandy intertidal areas. Their work was carried out in the laboratory for periods of up to two weeks. The work described here included similar experiments using Abarenicola and was extended to explore the possibility of using burrowing rates of lugworms as an indicator of pollution levels in the field over longer periods of time.

If a reduction in burrowing rates is reflected in reduced food intake, a decline in nutritional status might be expected. In this study we examined the level of free amino acids in the tissues as a possible indicator of nutritional status.

Methods

Animals and sediment were collected from an intertidal mud flat adjacent to Sequim Bay, Washington State, U. S. A. (48°5' N, 112°3'W). The same area was used for field exposures. Table 1 indicates the grain size distribution of the site. As over 25% of the particles present were less than 50 μm in diameter the sediment would be classed as a silty sand. Immediately after collection the sediment was mixed with Prudhoe Bay crude (PBC) oil for one hour in a cement mixer or stirred for shorter periods with a motor driven impeller. Control sediment was mixed in the same way without the addition of

TABLE 1

PARTICLE SIZE DISTRIBUTION IN TIDE FLAT HABITAT OF ABARENICOLA PACIFICA.

117

SIZE	>5.0 MM	2.0-5.0	1.0-2.0	1.0-0.5	0.5-0.05	0.05-0.002	<0.002
%	0.2	1.0	2.2	16.2	52.2	26.6	1.6

oil. After mixing, the oiled sediment was placed in running sea water for 24 hours to allow part of the lighter, more toxic, fractions to be flushed out before the worms were placed in it.

Experiments designed to measure changes in body composition in the laboratory were carried out in fiberglass trays with mesh bottoms. For measurements of burrowing/feeding rates in the laboratory forty artificial burrows, consisting of U-shaped tygon tubes, were set up. Ten contained clean sediment, and ten contained sediment to which Prudhoe Bay crude oil at original concentrations of 250, 500 or 1000 ppm had been added. One A. pacifica was placed in each burrow. Feces were collected daily from plastic trays surrounding the ends of the tubes, dried, and weighed. The experimental procedure is described in more detail in Augenfeld (1980).

To expose worms to known levels of petroleum hydrocarbons under field conditions, the bottoms were removed from 800-ml polyethylene beakers and replaced with 800 micron mesh Nitex screen. One worm was placed in each beaker with uncontaminated sediment or sediment mixed with PBC. The beakers were set into the collection area of the tide flat at such a depth that the surface of the sediment in the beakers was level with the surface outside. Feces were collected daily from the surfaces of the beakers and dried to constant weight.

A second field exposure was set up, using controls and an intermediate concentration of oil, i.e., 400 ppm, in two conditions. Sixteen animals were placed in sediment containing fresh PBC. The sediment-oil mixture in these beakers was only flushed in sea water for 24 hours before the worms were added. A second set of 16 was placed in sediment containing PBC which had been weathered for 24 days by exposure to sunlight and flowing sea water beneath it.

Amino acid determinations were carried out on sections of body wall musculature weighing ca 100 mg. They were minced and shaken with 80% ethanol (1 ml/10 mg tissue) for 24 hours. The extract was centrifuged and the total amino acid content of the supernatant was determined by the method of Clark (1964).

Results

Laboratory exposure: burrowing rates

After eleven days under flowing sea water the low, medium and high oiled sediment contained approximately 250, 400, and 800 ppm oil, respectively, as measured by infrared (IR) spectrophotometry. One, two, and three worms, respectively, died in the low, medium, and high level exposure system, while all the controls survived (see Table 2). Animals exposed to 400 to 500 ppm oil were seen at times to extend the posterior portion of their body from their burrows and move them slowly through the water. Animals exposed to 800 to 1000 ppm did so more often. This behavior was never observed among worms exposed to sediment containing no or low levels of oil.

Control worms began depositing feces at once, and after a lag period of two days, exposed animals did so too. As has been reported earlier (Hylleberg, 1975) the pattern of defecation was irregular, with pauses of varying lengths between intervals of activity. On the average, approximately one set of castings was produced per two days.

As Table 3 shows, A. pacifica exposed to sediment containing more than 400 ppm PBC reduced their burrowing rates on the average by over 75%. Exposure to 250 ppm resulted in a 36% reduction. These effects were not exerted to the same extent on all size ranges in the population. Among control and low level exposed animals the smaller individuals produced a

TABLE 2

EFFECTS OF PBC ON SURVIVAL AND BEHAVIOR OF A. PACIFICA

		<u>EXPOSURE LEVEL</u>			
		CONTROL	LOW	MEDIUM	HIGH
	SURVIVAL	10/10	9/10	8/10	7/10
120	LEFT TUBES	2/10	0	0	0
	TAIL EXTENDED FROM TUBES	0	0	6	12
	CAST PRODUCTION*				
	FIRST 2 DAYS	4.5	3.5	2	1
	CAST PRODUCTION*				
	NEXT 9 DAYS	5	4.9	4.6	4.5

* MEAN NUMBER OF CASTS/DAY PRODUCED BY ALL SURVIVING WORMS

TABLE 3

EFFECT OF PRUDHOE BAY CRUDE OIL ON FECAL PRODUCTION OF *A. PACIFICA*: LABORATORY EXPOSURE

	EXPOSURE LEVEL			
	CONTROL	LOW	MEDIUM	HIGH
MEAN BODY WEIGHT ± STANDARD ERROR	.32 ± .15g	.32 ± .14g	.52 ± .17g	.52 ± .16g
MEAN FECAL DRY WEIGHT/WEEK	1.75 ± .98	1.12 ± .77	.073 ± .06	.077 ± .06
MEAN FECAL DRY WEIGHT/WEEK/ g BODY WEIGHT	6.93 ± 2.10	4.41 ± 1.68	1.26 ± .84	1.19 ± .84
REGRESSION OF MEAN FECAL WEIGHT ON BODY WEIGHT	-.31 n.s.	-.37 n.s.	+.012 n.s.	+.012 n.s.
REGRESSION OF MEAN FECAL WEIGHT/g BODY WEIGHT ON BODY WEIGHT	-2.56	-2.56	-.51	-.50

larger volume of burrowed material per unit body weight than did larger animals. As Figure 1 shows, all individuals weighing less than 0.4 g produced more than 0.5 g dry weight in feces per g body weight per day, in the control and low oil sediments, while all individuals in this size range produced less than 0.5 g dry weight feces per g. body weight per day, when exposed to 400 or 800 ppm oil. Among worms weighing more than 0.5 g the differences in burrowing rates between exposed and control individuals was not significant at the .05 level. Within each treatment group fecal production per unit body weight grew smaller as body weight grew larger. As these two trends cancelled each other out, fecal weight per se did not change significantly with changing body size (cf. Augenfeld, 1980).

Laboratory exposure: amino acid content

At the time that the effect of Prudhoe Bay crude oil on body wall amino acid content was tested, a heavy fungal growth appeared on the surface of oiled sediment in the laboratory and, to a lesser degree, on control sediment. Since the presence of this material, which covered the entrances to the burrows, might impose an additional stress on the worms, the test concentration of oil was reduced to 400 ppm. Nevertheless, there was increased mortality among the exposed animals. While all the controls survived, only six out of nine exposed individuals survived one week and only two out of nine survived two weeks. Half of these survivors left their burrows and stayed on the sediment surface. In spite of the obviously severe conditions the free amino acid levels in the muscle did not change significantly after one week, and declined by only 9% after two weeks (see Figure 2).

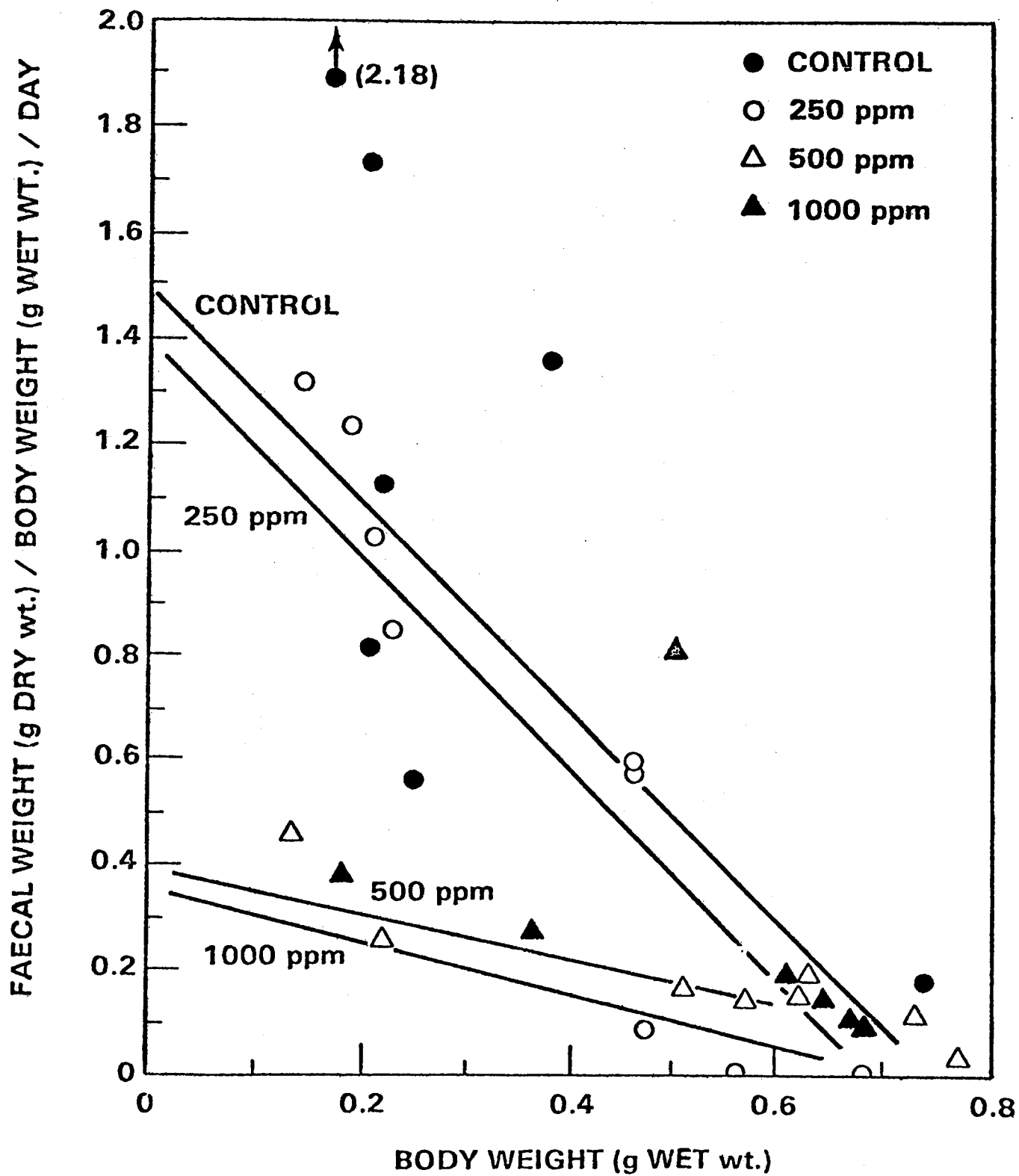


Figure 1. Regression of weight-specific fecal weight on body weight: Effect of Prudhoe Bay crude oil in sediment.

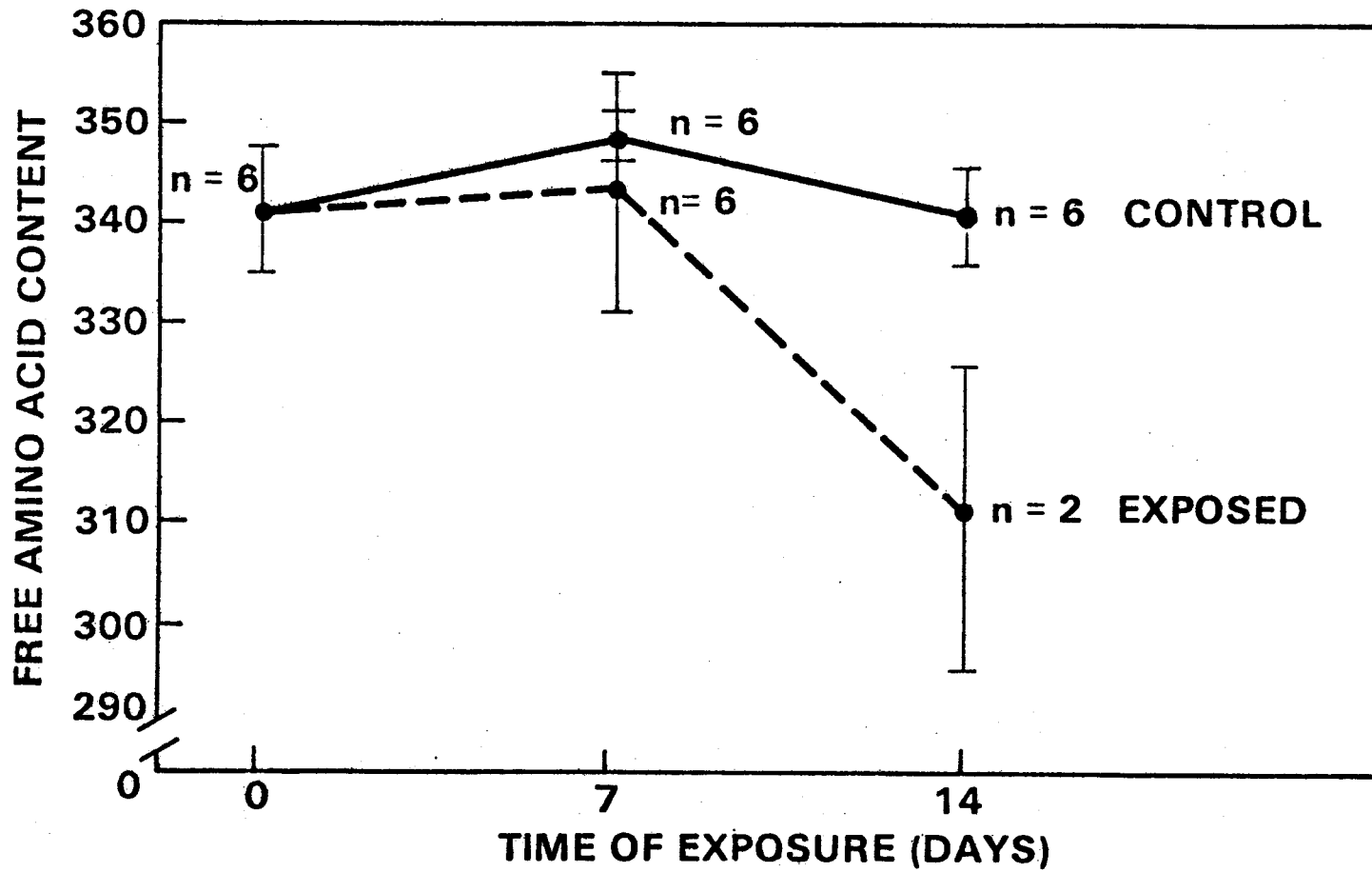


Figure 2. Free amino acid content of body wall muscle of *Abarenicola pacifica* ($\mu\text{m/g}$ wet wt.) following laboratory exposure to sediment containing 400 ppm Prudhoe Bay crude oil.

Field exposure: burrowing rate

The experiments designed to measure burrowing rates in the field were carried out in September, 1978, three months after the lab exposures. At this time the mean weight of the Abarenicola in the collecting area was 0.7 g, a size at which no significant effect had been found in the lab. Since it was not known in advance whether exposure to oiled sediment in the field would have more severe or less severe effects than exposure in the lab, a maximal concentration of 1000 ppm and a minimal concentration of 200 ppm were employed. Over a five week period the concentration of oil in the sediment declined to 600 and 100 ppm.

Twelve individuals were used at each level. No feces appeared in the beakers containing the higher level of pollutant. After two and a half weeks these beakers were examined and found to contain no worms. Partially decayed remains of worms were found in some beakers, indicating that they had died in situ rather than having migrated. A new set of animals was placed in the beakers, on the assumption that the previous group might have been killed or driven out by the presence of toxic low molecular weight compounds such as benzene or naphthalene, which tend to be washed out of sediment sooner than heavier molecules (compounds). The second set of animals also produced no feces, and at the end of five weeks these beakers contained no worms. In the control beakers containing stirred but unoiled sediment, seven out of twelve animals survived and remained, and in the low level exposed group six out of twelve did so.

As is summarized in Table 4, burrowing activity of the worms in the control beakers began at a slow rate, compared to that of the laboratory population. It increased steadily through the five week period of observation until, during the fifth week, it was five times as high as during the first

TABLE 4

EFFECT OF PRUDHOE BAY CRUDE OIL CONTAMINATION ON FECAL PRODUCTION OF A. PACIFICA: FIELD EXPOSURE.

	DRY WEIGHT FECES/WORM/WEEK				
	WEEK 1	WEEK 2	WEEK 3	WEEK 4	WEEK 5
CONTROL	.305 ± .091g	.661 ± .193g	.910 ± .20g	.89 ± .24g	1.53 ± .34g
EXPOSED	.168 ± .069	.685 ± .127	.87 ± .23	.56 ± .16	.98 ± .14

week and not significantly different from that of the control group in the lab. The group exposed to sediment containing a low level of petroleum hydrocarbon (PHC) contamination turned over, on the average, 55% as much material as the control group during the first week. During the next two weeks these animals matched the controls, and during the last two weeks of observation they fell behind again to 64% of the control levels. None of these differences however was statistically significant at the .05 level.

Field exposure: amino acid content

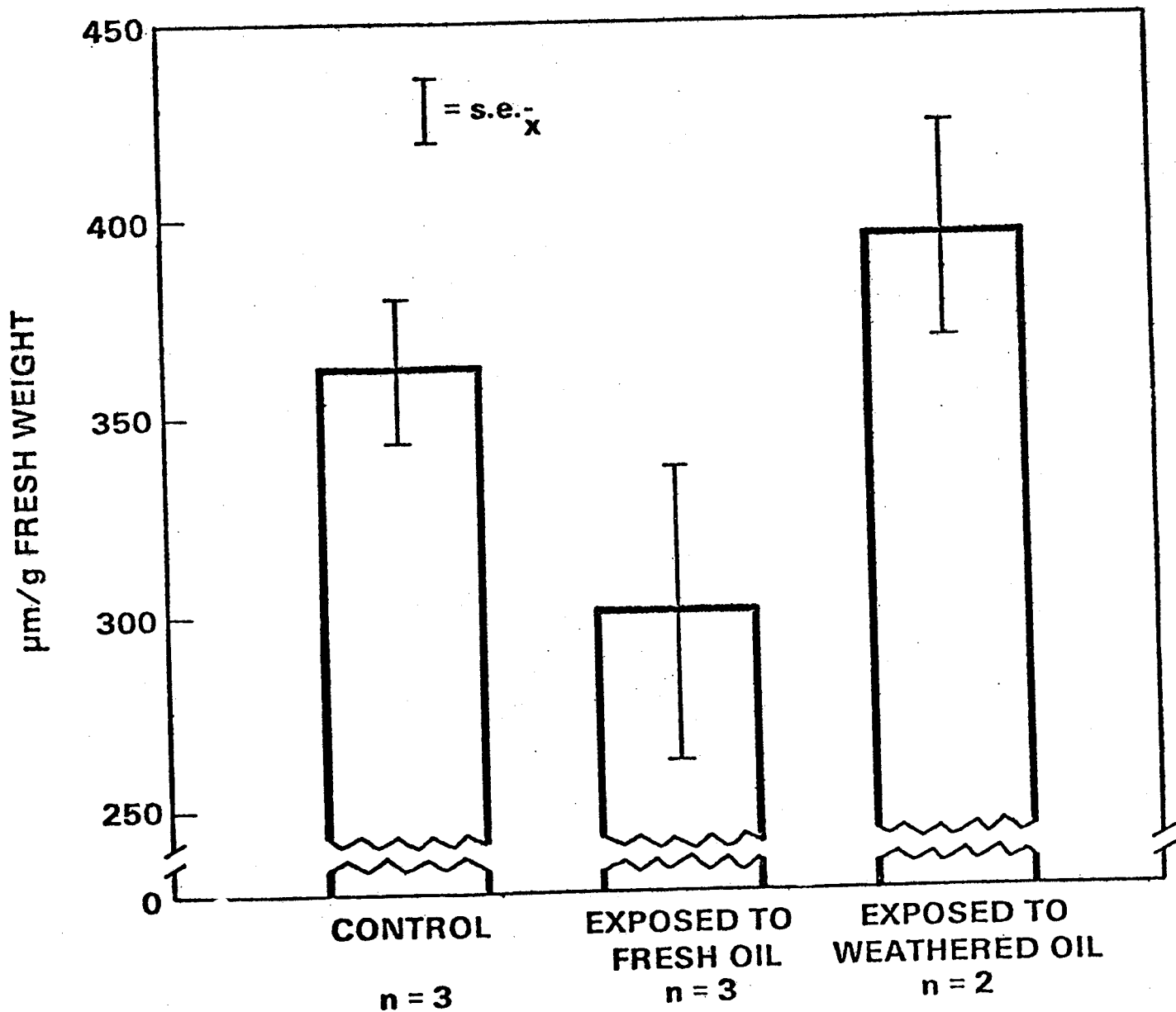
The conditions affecting the organisms during this exposure were evidently more stressful than those present during the earlier field experiment, since only three controls, three animals exposed to fresh oil, and two exposed to weathered oil survived. Further, very few feces were produced by the surviving animals, and most of these were in the form of loose grains of material which was readily dispersed in the water, instead of solid coils, which could be collected. Therefore it was not possible to make quantitative measurements of burrowing rates. As Figure 3 shows, the mean muscle free amino acid contents of the two worms which survived exposure to weathered oil was slightly higher than that of the controls. This in turn was as high as the level found in animals collected directly from their normal habitat. The content of worms exposed to fresh oil was 18% lower than in the controls.

Discussion

While the results obtained in these experiments do not rule out the use of burrowing rates as indicators of stress on Abarenicola populations, they do indicate a need for caution in extrapolating from laboratory results to conditions which might be found in the field, and in planning for and

Figure 3. Free amino acid concentrations in A. pacifica body wall muscle:
field exposure to 400 ppm Prudhoe Bay crude oil in sediment.

FREE AMINO ACID CONCENTRATION IN A. PACIFICA BODY WALL MUSCLE: FIELD EXPOSURE



interpreting the results of field observations. The most striking contrast between laboratory and field results was the difference in mortality of worms exposed to sediment containing more than 600 ppm oil. In the lab 70% of the exposed animals survived. In the field there was 100% mortality. The difference may have resulted from the additional stress on the field population of coping with periodic emersions during low tides. May (1972) described a behavior pattern by which A. pacifica draw air bubbles into their burrows from which oxygen may be absorbed, even if fresh supplies of oxygenated water are not available. If the presence of high levels of oil in the sediment affects this behavior pattern, as it affects burrowing rates in the laboratory, it may interfere with an even more vital function than feeding and so cause the death of the organism. In the laboratory situation, where the supply of oxygenated water is more constant, the behavior pattern described by May would be less critical for survival. Another possible reason for the higher mortality rate in the field lies in the response seen in the lab in which part of the worms' bodies are extended from the burrows. Such a position would make the animal more vulnerable to predation by fish or shore birds. On the other hand, the more vigorous flushing action of the natural tidal cycle apparently resulted in a greater reduction in PHC concentration in the sediment than took place in the lab. Perhaps it was a result of this that the worms exposed to the lower concentration of oil in the field attained a mean burrowing rate that matched that of the controls, after the first week of exposure.

Another cause for caution pointed up by these results lies in the highly irregular pattern of fecal production over time by individual control animals, both in the lab and in the field. In order to separate any "signal" resulting from a response to pollution from the "noise" generated by the animals' own

patterns, it will be necessary to continue observations over longer periods of time. If the responses are of a transient nature, as appears to have been the case in the field burrowing rate experiments a larger number of animals will have to be observed.

Nevertheless, these results may be taken as at least a preliminary suggestion that lugworm burrowing rates may be developed into a useful monitoring tool. At the least the rates could be used in laboratory studies as indicators of the ability of suspected pollutants of sediments to affect the behavior of benthic infaunal organisms.

Their usefulness as a measure of effects in the field, however, may be restricted, at least in the case of PHCs, to a narrow range of concentrations. As we have seen, the effects at low concentrations may be subtle enough to require the use of large numbers of organisms to detect their significance, while at substantially higher concentrations the effects are lethal. This finding is in accord with observations made along the coast of Brittany after the wreck of the Amoco Cadiz. There it was reported (Chasse, 1978) that in the five km of coast line nearest to the wreck, populations of Arenicola marina suffered heavy mortality, while at sites only slightly more distant they appeared to be unaffected. It may be concluded that in order to use lugworm burrowing rates as measures of effects in the field without requiring unrealistically large numbers of animals, more information will have to be gained on normal variations in these rates and on the background factors affecting survival.

There is little indication from these experiments that muscle free amino acid content in these animals is affected to a substantial degree by PHC in the sediment. It is true that a slight reduction was seen after periods of exposure of two weeks or more, but these were in survivors of populations that

had suffered heavy mortality. Some of these survivors were under severe enough stress to have left their burrows, which would certainly result in their death under natural conditions. It therefore seems unlikely that a significant reduction in mean amino acid concentration would be observed at lower levels of stress. While such reductions have been suggested as parameters to be monitored in bivalve mollusks (Jeffries, 1972; Bayne et al., 1976; Roesijadi and Anderson, 1979), their significance in at least one polychaete has not been established.

ACKNOWLEDGEMENTS

This work was performed under a related service agreement for the Environmental Protection Agency and the Department of Energy under Contract No. EY-76-06-1830 and under Contract No. 03-6-022-35204 from the National Oceanic and Atmospheric Administration/Bureau of Land Management.

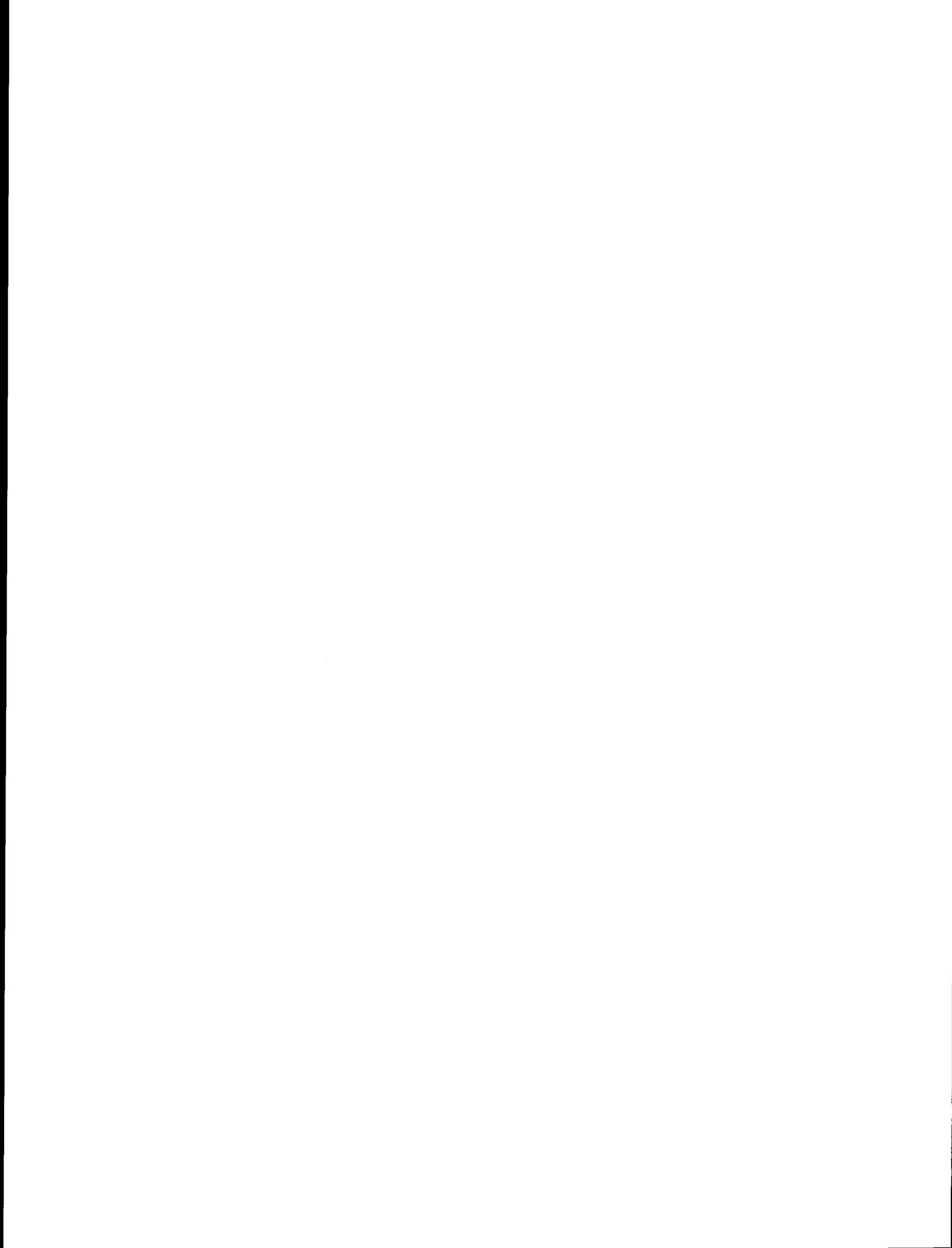
We thank Applied Science Publishers Ltd. for permission to reproduce material which appeared in Marine Environmental Research.

We also thank Gil Fellingham for his assistance with statistical analysis of the data.

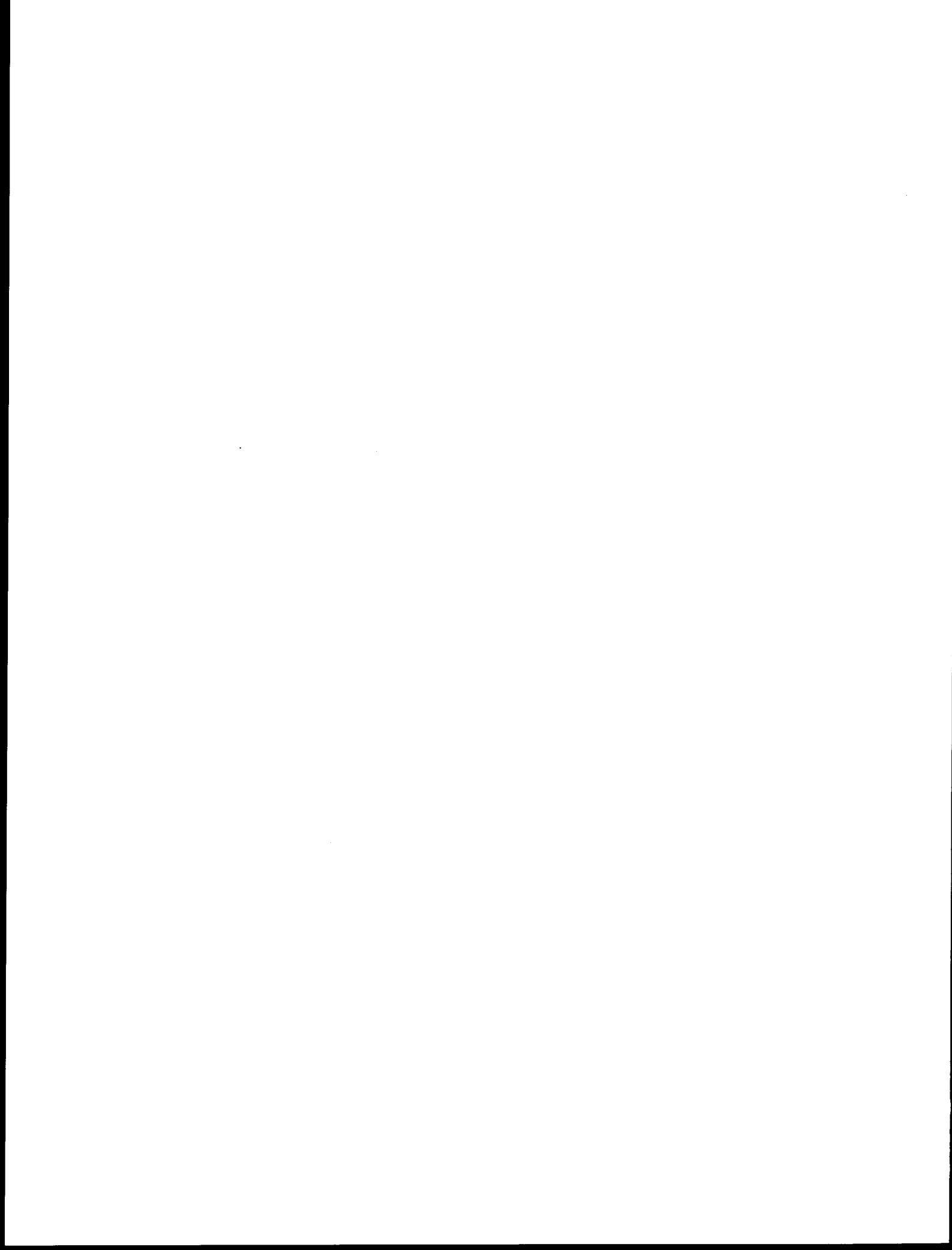
LITERATURE CITED

- Augenfeld, J. M. 1980. Effect of Prudhoe Bay crude oil contamination on sediment working rates of Abarenicola pacifica. Mar. Env. Res., in press.
- Bayne, B. L., D. R. Livingstone, M. N. Moore and J. Widdows. 1976. A cytochemical and biochemical index of stress in Mytilus edulis L. Mar. Pollut. Bull. 7:221-224.
- Chasse, C. 1978. Escisse d'un bilan ecologique provisoire de l' impact de la maree noire de l' Amoco Cadiz sur le littoral. In: Amoco Cadiz: Preliminary observation of the oil spill impact on the marine environment pp. 115-134. Actes de Colloques No. 6. Ed. by G. Conan et al., Brest: Centre National Pour L' Exploitation des Oceans (CNEXO).
- Clark, M. E. 1964. Biochemical studies on the coelomic fluid of Nephtys hombergi (Polychaeta: Nephthyidae), with observations on changes during different physiological states. Bio. Bull. Mar. Biol. Lab., Woods Hole. 127:63-84.
- Gordon, D. C., Jr., J. Dale and P. D. Keizer. 1978. Importance of sediment working by the deposit-feeding polychaete, Arenicola marina on the weathering rate of sediment-bound oil. J. Fish. Res. Bd. Canada 35:591-603.
- Hylleberg, J. 1975. Selective feeding by Abarenicola pacifica with notes on Abarenicola vagabunda and a concept of gardening in lugworms. Ophelia 14:113-137.
- Jeffries, H. P. 1972. A stress syndrome in the hard clam, Mercenaria mercenaria. J. Invert. Pathol. 20:242-287.
- Krebs, C. T. and K. A. Burns. 1977. Long-term effects of an oil spill on populations of the salt-marsh crab Uca pugnax. Science 197:484-487.

- May, D. R. 1972. The effects of oxygen concentration and anoxia on respiration of Abarenicola pacifica and Lumbrineris zonata (Polychaeta). Biol. Bull. Mar. Biol. Lab., Woods Hole 142:71-83.
- Mayo, D. W., D. S. Page and J. Cooley, E. Sorensen, F. Bradley, E. S. Gilfillan and S. A. Hanson. 1978. Weathering characteristics of petroleum hydrocarbons deposited in fine clay marine sediments, Searsport, Maine. J. Fish. Res. Bd. Canada 35:552-562.
- Roesijadi, G. and J. W. Anderson. 1979. Condition index and free amino acid content of Macoma inquinata exposed to oil-contaminated marine sediments. In: Marine Pollution: Functional Responses, pp. 69-83. Ed. by W. B. Vernberg, A. Calabrese, F. Thurberg and F. J. Vernberg. Academic Press, New York.
- Sabo, D. J. and J. J. Stegeman. 1977. Some metabolic effects of petroleum hydrocarbons in marine fish. In: Physiological Responses of Marine Biota to Pollutants, pp. 279-287. Ed. by F. J. Vernberg, A. Calabrese, F. P. Thurberg, and W. B. Vernberg. Academic Press, New York.
- Teal, J. M., K. Burns and J. Farrington. 1978. Analyses of aromatic hydrocarbons in intertidal sediments resulting from two spills of No. 2 Fuel oil in Buzzards Bay, Massachusetts. J. Fish. Res. Bd. Canada 35:510-520.



V. EFFECTS OF WEATHERING ON OIL



V-A:

CHANGES IN THE VOLATILE HYDROCARBON CONTENT OF PRUDHOE BAY CRUDE OIL
TREATED UNDER DIFFERENT SIMULATED WEATHERING CONDITIONS

by

R. G. Riley, B. L. Thomas, J. W. Anderson, and R. M. Bean

Battelle Pacific Northwest Laboratories

ABSTRACT

Changes have been determined in the concentrations of volatile saturate and aromatic hydrocarbons in Prudhoe Bay Crude oil (PBC) weathered under three different simulated environmental conditions. A combination of light and water spray upon the surface of the oil produced the largest relative decreases in volatile saturate and most aromatic hydrocarbons. After 24 days, detectable amounts of monoaromatic hydrocarbons were absent in all three weathered oils as were the saturate hydrocarbons from C_8 to C_{10} . Retention of aromatic hydrocarbons appeared to be related to molecular weight, as enrichments of triaromatics (phenanthrenes) were observed in weathered PBC relative to the original crude oil. These data are discussed with respect to effects resulting from spilled oil impacting benthic organisms residing in intertidal and shallow subtidal communities.

INTRODUCTION

The potential environmental impact to benthic marine organisms and the intertidal environment from spilled oil may depend on the extent to which oil has been exposed to the action of various dissipative factors prior to impact. Major processes which contribute to the weathering of oil include evaporation, dissolution, photo-oxidation, emulsification and biodegradation. (National Academy of Science, 1975). Water soluble fractions rich in aromatic hydrocarbons produced from the dissolution of oils have produced both acute and chronic effects in marine organisms in the laboratory (Neff et al, 1976; Anderson (1977), Malins (1977), Anderson et al. (1978), Anderson et al. (1979). Oil spilled offshore, which impacts near-shore benthic habitats and intertidal sediments would contain reduced levels of these components and, therefore, have the potential of producing different levels of effects on marine organisms, relative to fresh crude oil. There is, therefore, a need to produce quantities of weathered oils to serve as source materials for experimental studies directed toward predicting the environmental effects of weathered oils.

We have designed a research program to produce and characterize weathered Prudhoe Bay Crude oil (PBC), which could subsequently be used by biological investigators in experiments. Analyses were designed to describe changes in the volatile saturate and aromatic hydrocarbons of PBC oil weathered under three different simulated environmental conditions. By altering water agitation and sun exposure, the contribution made by these processes could be evaluated. It is hoped that these data will provide a base for possible correlations of hydrocarbon compositional changes of weathered oils with biological effects observed in future investigations.

MATERIALS AND METHODS

Three large volume tanks measuring 1.6 m in diameter and 0.9 m deep (2 m² area and 1,830 l volume) were each layered with 20 l of Prudhoe Bay crude oil. Each tank received flowing seawater that was maintained at a constant level by an external standpipe.

Each tank simulated a different weathering condition:

- Tank #1: To simulate weathering under violent weathering conditions inflow water was sprayed upon the surface of the oil (without a sun shield).
- Tank #2: To simulate weathering under calm conditions in the presence of sunlight, a slow flow of seawater was injected from below the oil slick.
- Tank #3: To reduce the effects of sunlight (photo-oxidation of hydrocarbons), a system similar to tank #2 was prepared with a sun shield over the oil.

During the 24-day weathering period, several environmental parameters were measured at frequent intervals. Air and water temperatures, salinity,

flow rates and light intensity measurements were taken to aid in characterizing the conditions.

Three replicate 25 ml oil samples were taken from each tank at days 1, 2, 4, 8, 16, and 24. These samples were placed in small vials that were completely filled with oil, wrapped with foil to exclude light, and sealed with teflon-lined caps before refrigeration. Each sample vial was washed in CCl_4 and dried with nitrogen gas before use. At termination (24 days) 1-gallon samples were taken from each tank and immediately shipped to Alaska for use by other investigators under National Oceanic and Atmospheric Administration contract.

Samples of the original and weathered oil were shipped on ice from the Sequim Marine Laboratory to the Pacific Northwest Laboratory, Richland, Washington, for hydrocarbon analyses. Samples (6-100 mg) of oil were chromatographed according to the method of Warner (1976) with the following modifications: fifteen grams of silica gel (Grace Davison Chemical Company, 100-200 mesh) were used to separate the oil into saturate (eluted with 40 ml in hexane) and aromatic (eluted with 86 ml of 20% CH_2Cl_2 in hexane) fractions. The fractions, collected in 40 ml conical tubes, were concentrated under a stream of nitrogen without the aid of external heat, transferred to 5 ml conical vials and concentrated to 1 ml. An internal standard (2,6,10-trimethyldodecane for saturate fraction, hexamethylbenzene for aromatic fraction) was added to each sample, and the samples were analyzed by capillary gas chromatography. Individual hydrocarbons were separated and quantitated on a Hewlett Packard 5840A gas chromatograph employing 30 meter OV-101 glass capillary columns operating at 65° with an initial 4-minute hold and then programmed at $4^\circ/\text{min}$ to 250° . Data were corrected based on the recovery

data of aliphatic and aromatic hydrocarbon standards. Typical recoveries were 82-111% for saturate hydrocarbons (C_{12} to C_{24}) and 84-89% for aromatic hydrocarbons (naphthalene to dimethylphenanthrenes).

The significance in the differences in the concentrations of hydrocarbons and hydrocarbon classes between tanks was determined by comparing calculated t values based on standard deviation of the difference to a table value of t with two degrees of freedom at a $P = 0.05$.

RESULTS

Several weathering parameters monitored during the course of the experiment are summarized in Table 1.

Water and air temperatures varied little over the 24-day period of weathering, as did salinity. The intensity of ambient light over the tanks (1 and 2) ranged from a mean of 2.5×10^5 Lux at noon to about 1×10^5 Lux at 8am and 4pm. Since we attempted to enhance agitations of the oil layer in tank 1 by injections of water streams from above, the flow rate was approximately 3 times (27 l/min) that of the other two tanks. This agitation in tank 1 did indeed produce a weathered product different from the other oils, as a brown "chocolate mousse" was apparent by about 10 days of exposure. This material was strikingly different from the other products, which appeared as the original oil except for the increased viscosity observed in tank 2. When samples of the 3 products were subjected to centrifugation (8,000 RPM for 30 min.) separation of 2 or 3 layers was observed. Tank 1 material separated into 3 distinct layers with a mousse layer over water which

TABLE 1
PARAMETERS MEASURED DURING THE COURSE OF THE WEATHERING EXPERIMENT

	$\bar{x} \pm \text{S.D.}$	N	Range	
			Maximum	Minimum
Air Temperature (C) Randomly taken during day	12.20 \pm 1.65	16	15.5	10.0
Water temperature (C)	9.88 \pm 0.51	16	10.6	9.0
Salinity (o/oo)	30.19 \pm 0.36	16	31.0	30.0
Light (Lux) over tanks @ 0800 hr	9.3x10 ⁴ \pm 5.1x10 ⁴	15	1.75x10 ⁵	2.2x10 ⁴
Light (Lux) over tanks @ 1200 hr	2.54x10 ⁵ \pm 9.0x10 ⁴	10	3.5x10 ⁵	1.31x10 ⁵
Light (Lux) over tanks @ 1600 hr	1.52x10 ⁵ \pm 6.9x10 ⁴	7	2.7x10 ⁵	6.6x10 ⁴
Flow rate l/min Tank #1	26.66 \pm 4.37	16	30.0	15.0
Flow rate l/min Tank #2	8.95 \pm 0.34	16	10.0	8.5
Flow rate l/min	8.58 \pm 1.93	16	15.0	5.0

was covered by an oil layer. Only the oil and water layers were observed in samples from tanks 2 and 3.

Average relative decreases of saturate hydrocarbons (between C_{12} and C_{26}) in tanks #2 and #3 after 24 days of exposure ranged between 45% and 49% (Table 2). These results are in marked contrast to tank #1 where an average relative decrease of 83% was observed. The saturate hydrocarbons $C_8 - C_{10}$, although present in the original oil, were not detectable in any of the 24 day weathered oil samples (Figure 1).

The ratios of nC_{17} /pristane and nC_{18} /phytane did not change significantly in the weathered oils relative to the original crude oil (Table 3).

Relative decreases in the concentrations of aromatic hydrocarbons were different from those observed for the saturate hydrocarbons in the three exposure systems. Decreases in aromatic hydrocarbons (naphthalene through 3,6-dimethylphenanthrene) were 37% for tanks #1 and #2 and 9% for tank #3. The tricyclic aromatic hydrocarbons (phenanthrene through 3,6-dimethylphenanthrene) appeared to have the greatest persistence with relative enrichments occurring in tank #1 (Table 4). 3,6-Dimethylphenanthrene showed relative enrichment in all three exposure systems. Also reported in Table 4 are concentrations for a variety of mono-aromatic hydrocarbons (toluene through 1,2,3,5-tetramethylbenzene). The concentration values reported for these compounds in the original oil were not corrected for recovery, nevertheless, they are reported because, with the exception of the tetramethylbenzenes, none of these compounds was detected in the 24-day weathered oil samples from any of the three exposure systems. These results

TABLE 2

CONCENTRATIONS OF SATURATE HYDROCARBONS IN PRUDHOE BAY CRUDE OIL (PBC) AND IN 24-DAY WEATHERED OIL SAMPLES.
CONCENTRATIONS IN MG/GRAM OIL

Compound	Concentration in Original Oil	Concentration in Weathered Oil			Relative Decrease in Concentration(%)		
		Tank #1	Tank #2	Tank #3	Tank #1	Tank #2	Tank #3
C ₈	4.20 ± 0.12	c	c	c	100	100	100
C ₉	4.42 ± 0.10	c	c	c	100	100	100
C ₁₀	4.44 ± 0.35	c	c	c	100	100	100
C ₁₁	4.68 ± 0.08	0.15 ± 0.02	0.22 ± 0.01	1.68 ± 0.32	96.8	95.3	64.1
C ₁₂	4.62 ± 0.15	0.54 ± 0.01	0.97 ± 0.02	2.19 ± 0.40	88.3	79.0	52.6
C ₁₃	4.46 ± 0.26	0.63 ± 0.02	1.64 ± 0.05	2.38 ± 0.15	85.9	63.2	46.6
C ₁₄	4.16 ± 0.05	0.69 ± 0.01	1.93 ± 0.06	2.26 ± 0.20	83.4	53.6	45.7
C ₁₅	3.99 ± 0.22	0.70 ± 0.01	1.99 ± 0.05	2.15 ± 0.24	82.5	50.1	46.1
C ₁₆	3.74 ± 0.24	0.64 ± 0.02	1.85 ± 0.05	1.99 ± 0.29	82.9	50.5	46.8
C ₁₇	3.39 ± 0.42	0.58 ± 0.03	1.75 ± 0.04	1.85 ± 0.26	82.9	48.4	45.4
Pristane	2.07 ± 0.38	0.33 ± 0.02	1.04 ± 0.02	1.12 ± 0.12	84.1	49.8	45.9
C ₁₈	2.50 ± 0.24	0.48 ± 0.05	1.38 ± 0.04	1.30 ± 0.23	80.8	44.8	48.0
Phytane	1.05 ± 0.24	0.22 ± 0.01	0.57 ± 0.03	0.58 ± 0.04	79.0	45.7	44.8
C ₁₉	3.04 ± 0.76	0.46 ± 0.01	2.07 ± 0.24	1.73 ± 0.10	84.9	31.9	43.1
C ₂₀	1.93 ± 0.24	0.38 ± 0.02	1.08 ± 0.04	0.99 ± 0.17	79.8	44.0	48.7
C ₂₁	1.58 ± 0.20	0.33 ± 0.03	1.05 ± 0.27	0.85 ± 0.19	79.1	33.5	46.2
C ₂₂	1.86 ± 0.30	0.31 ± 0.03	1.18 ± 0.01	1.24 ± 0.30	83.3	36.6	33.3
C ₂₃	1.65 ± 0.29	0.30 ± 0.03	1.20 ± 0.12	1.26 ± 0.31	81.8	27.3	23.6
C ₂₄	1.27 ± 0.26	0.30 ± 0.04	1.11 ± 0.19	1.00 ± 0.24	76.4	12.6	21.3
C ₂₅	1.02 ± 0.55	0.24 ± 0.03	0.79 ± 0.16	0.71 ± 0.13	76.5	22.5	30.4
C ₂₆	0.76 ± 0.23	0.21 ± 0.02	0.60 ± 0.15	0.53 ± 0.07	72.4	21.1	30.3
Total (C ₁₂ -C ₂₆)	43.39 ± 4.27	7.30 ± 0.10	21.98 ± 0.61	23.98 ± 4.27	Avg% 83.1	49.3	44.7

^a Compounds C₈ - C₁₁ were corrected for recovery on the basis of the recovery of C₁₂ hydrocarbon and, therefore, are more than likely somewhat low.

^b
$$\frac{\text{Concentration in original oil} - \text{concentration in weathered oil}}{\text{concentration in original oil}} \times 100$$

^c Indicates compound not detected at the sensitivity level that analyses were conducted.

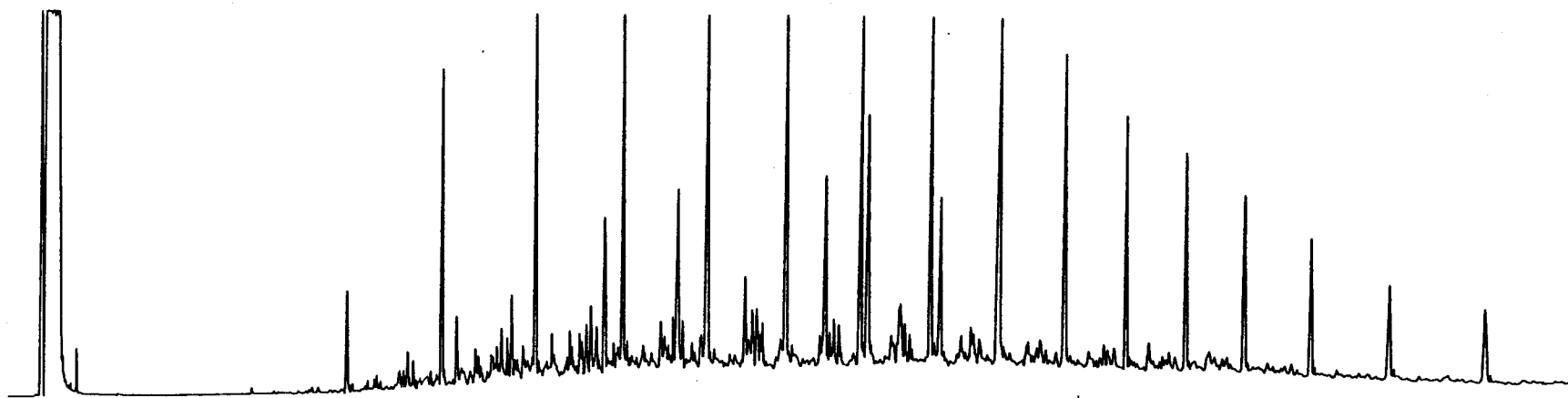
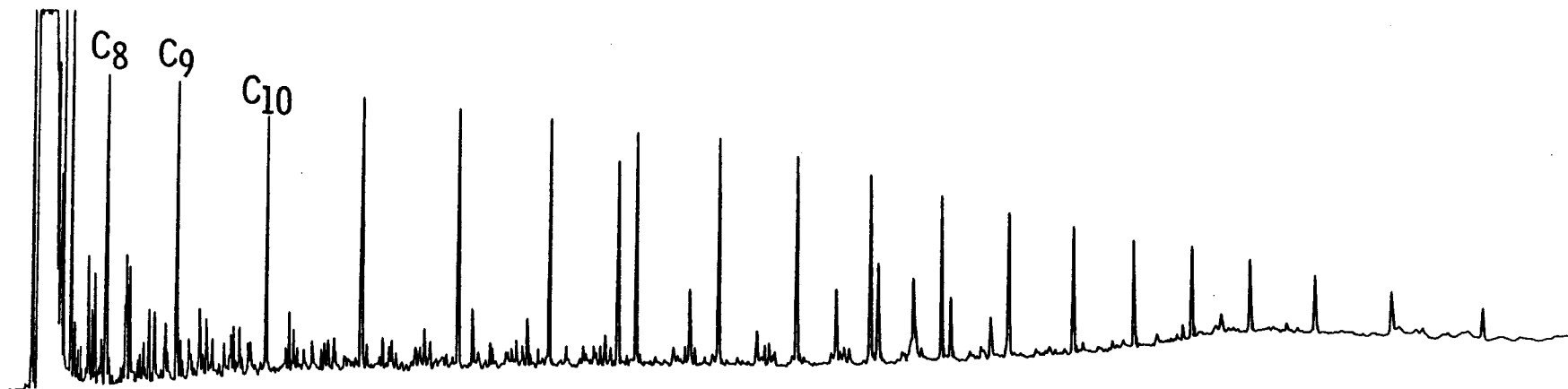


FIGURE 1. Gas capillary chromatograms of saturate hydrocarbon fraction from original Prudhoe Bay crude oil (top) and saturate hydrocarbon fraction from 24-day weathered oil sample from Tank #1 (bottom).

TABLE 3. nC₁₇/pristane and nC₁₈/phytone Ratios from PBC
Crude Oil and PBC Oil Weathered in Three Exposure Systems

<u>Ratio</u>	<u>Initial</u>	<u>Final (24 days)</u>		
		<u>Tank #1</u>	<u>Tank #2</u>	<u>Tank #3</u>
nC ₁₇ /pristane	1.64 ± 0.36	1.75 ± 0.08	1.68 ± 0.03	1.65 ± 0.18
nC ₁₈ /phytane	2.38 ± 0.25	2.18 ± 0.11	2.42 ± 0.06	2.24 ± 0.19

TABLE 4

CONCENTRATIONS OF AROMATIC HYDROCARBONS IN PRUDHOE BAY CRUDE OIL (PBC)
AND IN 24 DAY WEATHERED OIL SAMPLES. CONCENTRATIONS IN MG/GRAM OIL

Compound	Concentration in Original Oil	Concentration in Weathered Oil			Relative Change in Concentration(%)		
		Tank #1	Tank #2	Tank #3	Tank #1	Tank #2	Tank #3
toluene	0.82 ± 0.08	c	c	c	100	100	100
ethylbenzene	0.56 ± 0.01	c	c	c	100	100	100
m+p-xylene	2.05 ± 0.04	c	c	c	100	100	100
o-xylene	0.79 ± 0.01	c	c	c	100	100	100
isopropylbenzene	0.16 ± 0.00	c	c	c	100	100	100
1-ethyl+4-methylbenzene	0.29 ± 0.00	c	c	c	100	100	100
1,3,5-trimethylbenzene	0.41 ± 0.00	c	c	c	100	100	100
1,2,4-trimethylbenzene	1.14 ± 0.01	c	c	c	100	100	100
secbutylbenzene	0.14 ± 0.00	c	c	c	100	100	100
methyl-4-isopropylbenzene	0.12 ± 0.00	c	c	c	100	100	100
indane	0.67 ± 0.00	c	c	c	100	100	100
1,3-dimethyl-5-ethylbenzene	0.27 ± 0.00	c	c	c	100	100	100
1,2-diethylbenzene	0.24 ± 0.02	c	c	c	100	100	100
1,2-dimethyl-4-ethylbenzene	0.24 ± 0.01	c	c	c	100	100	100
1,2,4,5-tetramethylbenzene	0.38 ± 0.00	0.03 ± 0.00	c	0.25 ± 0.03	d	100	d
1,2,3,5-tetramethylbenzene	0.27 ± 0.00	0.03 ± 0.00	c	0.18 ± 0.02	d	100	d
naphthalene	0.92 ± 0.01	0.06 ± 0.01	0.16 ± 0.01	0.51 ± 0.08	93.5	82.6	44.6
2-methylnaphthalene	1.63 ± 0.02	0.53 ± 0.07	0.76 ± 0.08	1.34 ± 0.18	67.5	53.4	17.3
1-methylnaphthalene	1.29 ± 0.02	0.48 ± 0.06	0.69 ± 0.06	1.20 ± 0.16	62.8	46.5	7.0
1-ethyl+2-ethylnaphthalene	0.48 ± 0.00	0.27 ± 0.03	0.43 ± 0.08	0.51 ± 0.06	43.8	10.4	6.3
2,6+2,7-dimethylnaphthalene	0.69 ± 0.01	0.52 ± 0.06	0.83 ± 0.13	0.94 ± 0.12	24.6	+20.3	+36.2
1,3+1,6-dimethylnaphthalene	0.99 ± 0.01	0.51 ± 0.06	0.70 ± 0.05	0.91 ± 0.12	48.5	29.3	8.1
1,7-dimethylnaphthalene	1.10 ± 0.01	0.51 ± 0.04	0.77 ± 0.06	0.94 ± 0.12	53.6	30.0	14.5
1,4+2,3+1,5-dimethylnaphthalene	0.80 ± 0.01	0.52 ± 0.06	0.35 ± 0.11	0.90 ± 0.12	35.0	56.3	+12.5
1,2-dimethylnaphthalene	0.40 ± 0.00	0.23 ± 0.03	0.21 ± 0.01	0.37 ± 0.04	42.5	47.5	7.5
2,3,6-trimethylnaphthalene	0.51 ± 0.07	0.26 ± 0.03	0.39 ± 0.12	0.43 ± 0.04	49.0	23.5	15.7
phenanthrene	0.38 ± 0.05	0.61 ± 0.06	0.34 ± 0.05	0.22 ± 0.00	60.5	10.5	42.1
1-methylphenanthrene	0.33 ± 0.02	0.77 ± 0.15	0.24 ± 0.02	0.31 ± 0.04	+133.3	27.3	6.7
2-methylphenanthrene	0.21 ± 0.01	0.53 ± 0.04	0.19 ± 0.01	0.22 ± 0.02	+152.4	9.5	4.8
3,6-dimethylphenanthrene	0.11 ± 0.00	0.53 ± 0.04	0.24 ± 0.05	0.20 ± 0.04	+381.8	+118.2	+81.8
Total (naphthalene - 3,6-dimethylphenanthrene)	9.91 ± 0.15	6.21 ± 0.42	6.27 ± 0.41	9.03 ± 1.05			

^aMonoaromatic hydrocarbons have not been corrected for recovery.

^b% decrease = $\frac{\text{Concentration in original oil} - \text{concentration in weathered oil}}{\text{found concentration in original oil}} \times 100$; (+) sign indicates higher concentration of compound in weathered oil on weathered oil basis as compared to original oil.

^cCompound not detected at the sensitivity level that analyses were conducted.

^dRelative decrease in concentration % was not calculated because recovery data was not obtained on monoaromatic hydrocarbons.

are more graphically depicted in Figure 2 where the gas capillary chromatogram of the aromatics fraction of the original crude oil is compared to the aromatics fraction derived from the 24-day weathered oil sample of tank #1.

Confidence limits were established and significant differences determined for various saturate and aromatic hydrocarbons and hydrocarbon types in the three exposure systems. These results are compiled in Table 5. Variability associated with the sum of all saturate hydrocarbons $C_{12}-C_{26}$ including pristane and phytane indicated differences between tank #1 vs. tank #2 and #3 to be significant; however, total differences between tanks #2 and #3 were not significant. Significant differences were also found for the concentrations of all aromatic hydrocarbons and hydrocarbon types (naphthalene - 3,6-dimethylnaphthalene) between tanks #1 and #3. Significant trends in the differences in concentrations of the aromatic components of tank #1 vs. tank #2 and tank #2 vs. tank #3 are more subtle. No significant differences in the concentrations of diaromatic hydrocarbons and hydrocarbon types are observed between tanks #1 and #2; however, significant differences are observed for the triaromatics. Although significant differences in the concentrations of naphthalene, methylnaphthalenes, and phenanthrene were observed, no trends were observed for the aromatic components of tanks #2 vs. #3.

DISCUSSION

The combination of light and water exposure parameters of Tank #1 produced the largest relative decreases in volatile saturate (C_{12} to C_{26}) and most aromatic (naphthalene -2, 3, 6-trimethylnaphthalene) hydrocarbons relative to the original oil.

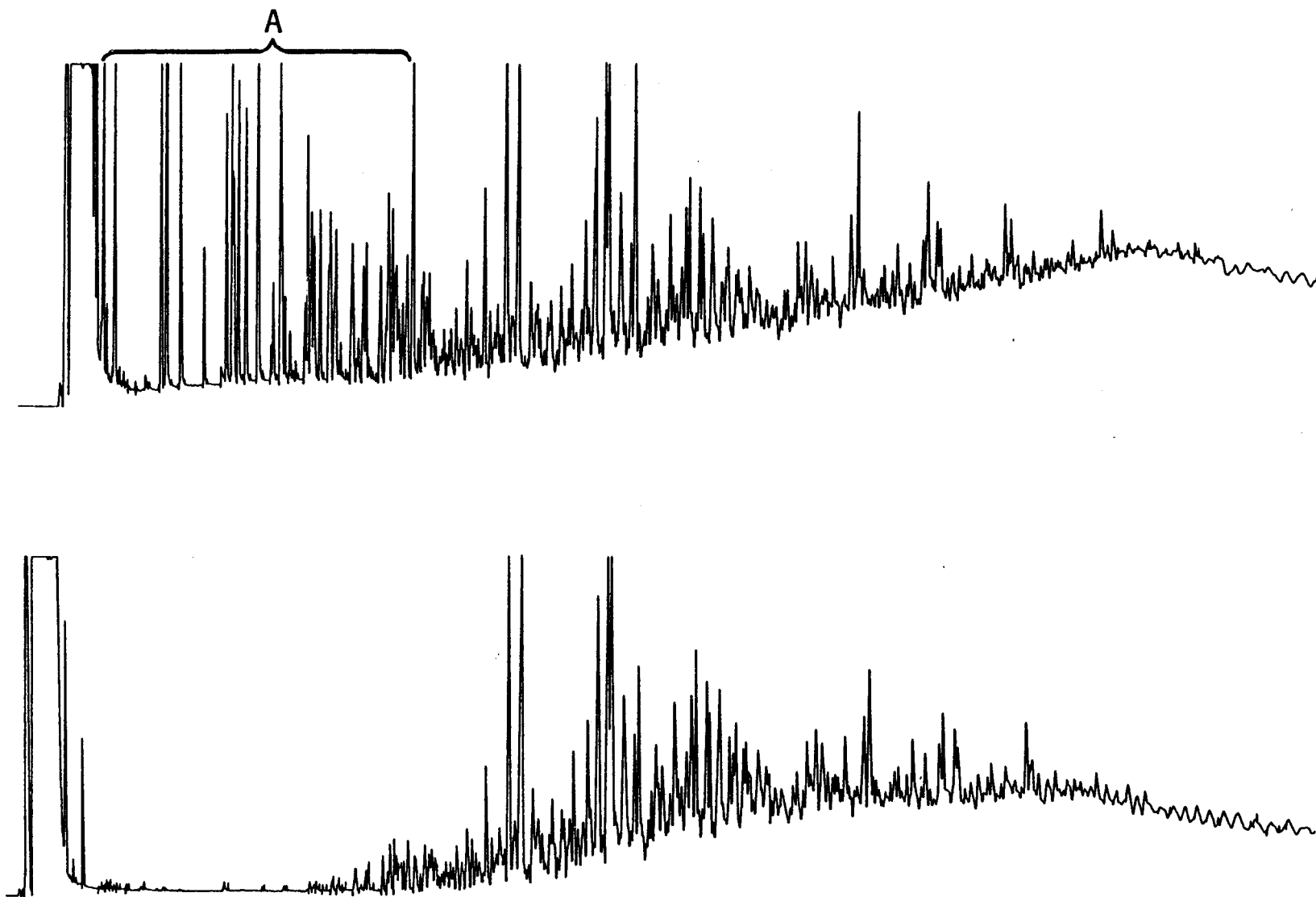


FIGURE 2. Gas capillary chromatograms of aromatic hydrocarbon fraction from original Prudhoe Bay Crude Oil (top) and aromatic hydrocarbon fraction from 24-day weathered oil sample from Tank #1 (bottom). A denotes monoaromatic hydrocarbon region.

TABLE 5 SIGNIFICANCE IN THE RELATIONSHIPS BETWEEN THE CONCENTRATIONS OF VARIOUS SATURATE AND AROMATIC HYDROCARBONS AND HYDROCARBON TYPES AND THE TYPE OF EXPOSURE. CONFIDENCE LIMITS ARE MEASURED AT THE 95% LEVEL. S.D. = SIGNIFICANTLY DIFFERENT, N.S.D. = NOT SIGNIFICANTLY DIFFERENT.

Hydrocarbon or Hydrocarbon Type	Concentration in mg/gram Oil		
	Tank #1	Tank #2	Tank #3
(C ₁₂ - C ₂₆) + Pristane + Phytane	7.30 ± 0.10	21.98 ± 0.61	23.98 ± 4.27
	S.D.		
	S.D. N.S.D.		
Naphthalene	0.06 ± 0.01	0.16 ± 0.01	0.52 ± 0.08
	S.D.		
	N.S.D. S.D.		
Methylnaphthalenes	1.01 ± 0.12	1.43 ± 0.14	2.54 ± 0.34
	S.D.		
	N.S.D. S.D.		
Dimethylnaphthalenes	2.29 ± 0.22	2.83 ± 0.27	4.12 ± 0.54
	S.D.		
	N.S.D. N.S.D.		
2,3,6-Trimethylnaphthalene	0.26 ± 0.03	0.39 ± 0.12	0.43 ± 0.04
	S.D.		
	N.S.D. N.S.D.		
Phenanthrene	0.61 ± 0.06	0.34 ± 0.05	0.22 ± 0.01
	S.D.		
	S.D. S.D.		
Methylphenanthrenes	1.19 ± 0.06	0.43 ± 0.03	0.52 ± 0.05
	S.D.		
	S.D. N.S.D.		
3,6-Dimethylphenanthrene	0.53 ± 0.04	0.26 ± 0.03	0.20 ± 0.04
	S.D.		
	S.D. N.S.D.		
Total Aromatics (Naphthalene - 3,6-dimethylphenanthrene)	6.21 ± 0.42	6.27 ± 0.41	9.03 ± 1.05
	S.D.		
	N.S.D. N.S.D.		

Significant changes have been reported in the ratios of nC_{17} /pristane and nC_{18} /phytane after 6 to 9 months of exposure of oil contaminated intertidal sediments in field recruitment studies (Anderson et al., 1978) which suggested the presence of hydrocarbon utilizing organisms (Blumer & Sass, 1972). No changes were observed in these ratios in weathered oil from these three exposure systems. These data suggest that biodegradation was a minor process in shaping the composition of the weathered oils produced in these exposure systems in this short period of time. Detectable amounts of monoaromatic hydrocarbons were absent in all three weathered oils as were the saturate hydrocarbons from C_8 to C_{10} . Similar, but qualitative results have been reported from the dissolution of #2 fuel oil in laboratory studies (Zucher et al., 1978). The different exposure parameters of Tank #1 and #3 produced the greatest differences in the volatile hydrocarbon content of these oils following 24 days of weathering. The decreases in the content of most aromatic compounds were less for oil protected from light, water agitation and somewhat from air circulation (Tank #3). The sun shield reduced air flow over the oil and the only component shown to increase somewhat in Tank #3 in proportion to the original oil was the heaviest compound, 3, 6-dimethylphenanthrene. This component was enriched to a greater extent in Tank #2 and in Tank #1 its contribution to the total was nearly four times as great. There was an increasing degree of enrichment in the weathered (mousse) oil in Tank #1 as molecular weight increased from phenanthrene to the 3, 6-dimethylphenanthrene. These data may well indicate that higher molecular weight compounds of 4 and 5 rings (polynuclear aromatics) are also enriched in weathered oil, perhaps relative to their molecular weight. This is of

considerable significance, since tissue contamination or effects from these potential carcinogenic or mutagenic compounds could be enhanced by the weathering processes. The polynuclear aromatics are less water soluble than those identified in Table 4, so it is not likely that water column species would be affected. However, the mixing of weathered oil with sediments may produce an environment more hazardous to benthic species than contamination from fresh oil. Oil in sediments containing a higher proportion of higher molecular weight compounds, would appear to have greater potential for tissue contamination (Roesijadi et al., 1978), but the effects of such exposures can not be estimated at this time. To determine the actual significance of the weathered oil to marine organisms, field experiments should be conducted and data on accumulation and effects compared to fresh oil exposures.

ACKNOWLEDGMENTS

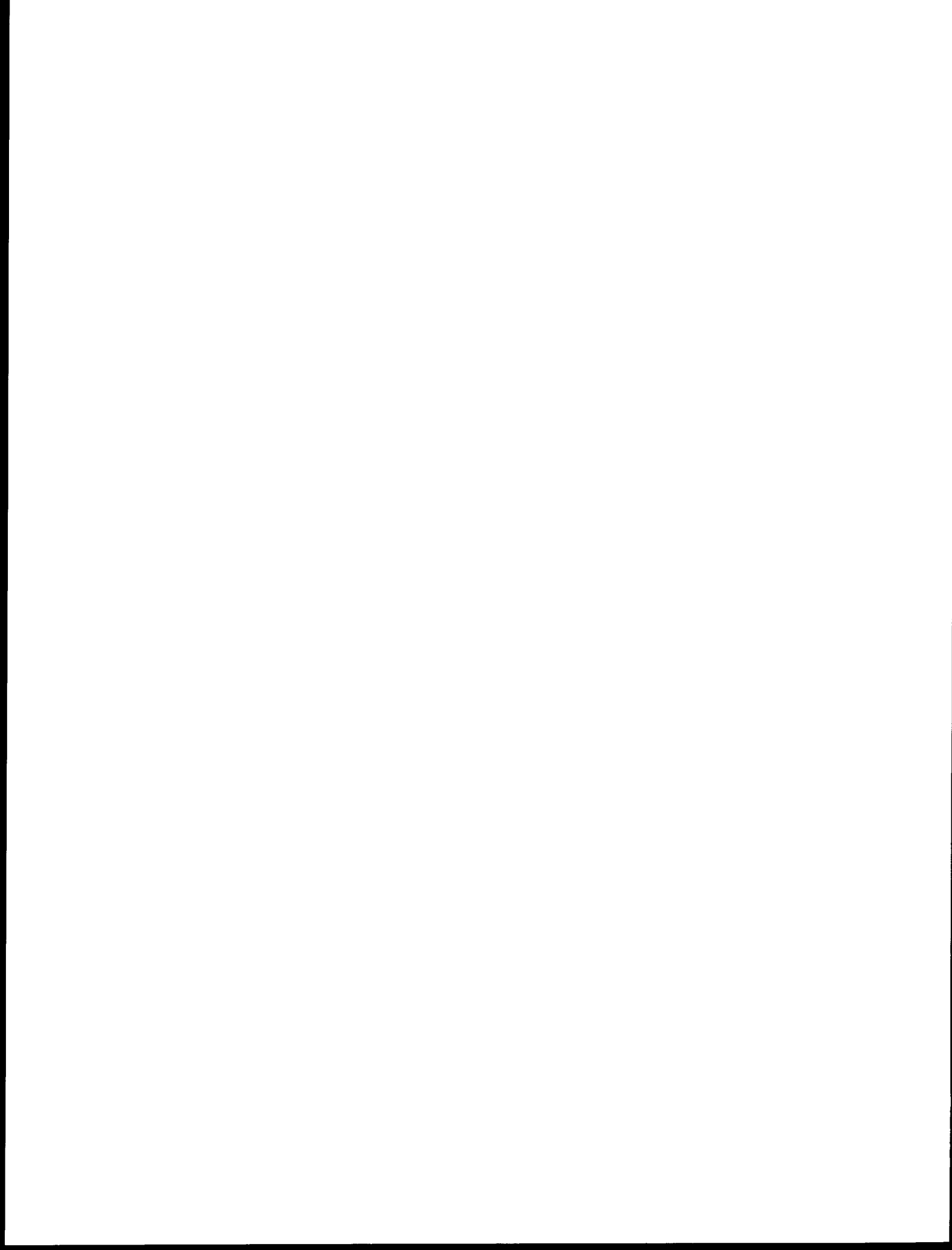
We wish to thank Steve Kiesser for monitoring the exposure tanks during the 24 day experiments.

This work was supported by funds from the National Oceanic and Atmospheric Administration, Outer Continental Shelf Environmental Assessment Program, Juneau, Alaska.

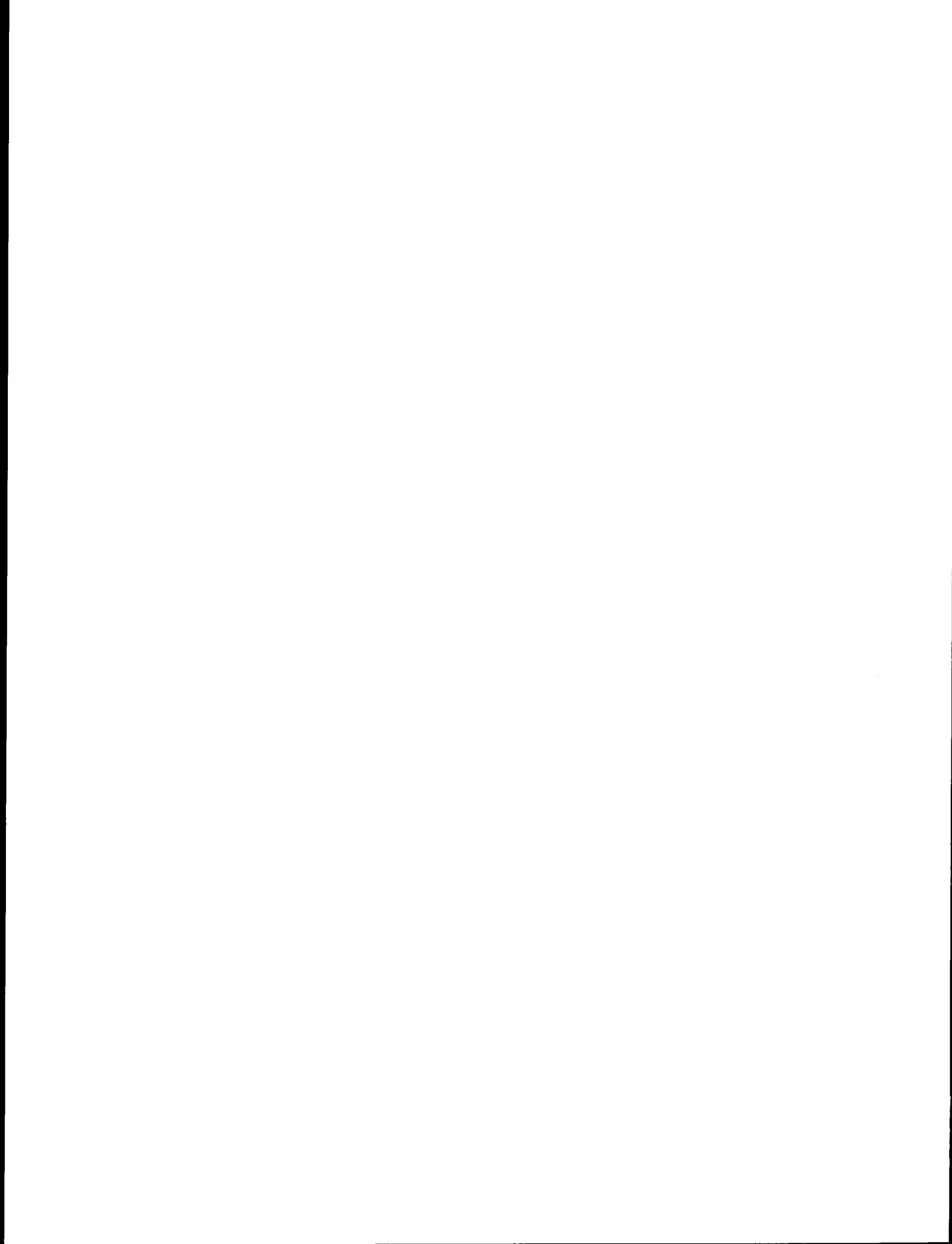
Brand names and manufacturers are cited to assist the reader in replication of the experiments, however, use does not constitute endorsement by Battelle Memorial Institute.

REFERENCES

- ANDERSON, J. W. (1977). Responses to Sublethal Levels of Petroleum Hydrocarbons: Are they Sensitive Indicators and do they Correlate with Tissue Contamination? Fate and Effects of Petroleum Hydrocarbons in Marine Ecosystems and Organisms, Douglas Wolfe, (ed.) Pergamon Press, New York. pp. 95-114.
- ANDERSON, J. W., RILEY, R. G., & BEAN, R. M. (1978). Recruitment of Benthic Animals as a Function of Petroleum Hydrocarbon Concentrations in the Sediment. J. Fish. Res. Board Can., 35(5):776-790.
- ANDERSON, J. W., KIESSER, S. L. & BLAYLOCK, J. W. (1979). Comparative Uptake of Naphthalenes from Water and Oiled Sediment by Benthic Amphipods. Proceedings of the 1979 Oil Spill Conference. American Petroleum Institute, Washington, D.C. pp. 579-584.
- BLUMER, M., & SASS, J. (1972). Oil Pollution: Persistence and Degradation of Spilled Fuel Oil. Science, 176,1120-1122.
- MALINS, D. C. (ed.). (1977). Effects of Petroleum on Arctic and Subarctic Marine Environments and Organisms. Vol. I and II. Academic Press, New York.
- NATIONAL ACADEMY OF SCIENCES. (1975). Petroleum in the Marine Environment. Workshop on Inputs, Fates and the Effects of Petroleum in the Marine Environment, Washington, D.C. pp. 42-72.
- NEFF, J. M., ANDERSON, J. W., COX, B. A., LAUGHLIN, R. B., Jr., ROSSI, S. S. & TATEM, H. E. (1976). Effects of Petroleum on Survival, Respiration, and Growth of Marine Animals. In Sources, Effects and Sinks of Hydrocarbons in the Aquatic Environment. American Institute of Biological Sciences, Arlington, Virginia.
- ROESIJADI, G., J. W. Anderson & J. W. Blaylock (1978). Uptake of Hydrocarbons from Marine Sediments Contaminated with Prudhoe Bay Crude Oil: Influence of Feeding Type of Test Species and Availability of Polycyclic Aromatic Hydrocarbons. J. Fish. Res. Board Can., 35(5): 608-614.
- WARNER, J. S..(1976). Determination of Aliphatic and Aromatic Hydrocarbons in Marine Organisms. Anal. Chem. 48, 578-583.
- ZUCHER, FRITZ & MARKUS THUER. (1978). Rapid weathering Processes of Fuel Oil in Natural Waters: Analyses and Interpretations. Environ. Sci. Technol. 12,838-834.



VI. DISTRIBUTION AND FATE OF POLYAROMATIC HYDROCARBONS
IN SEDIMENT-WATER SYSTEMS

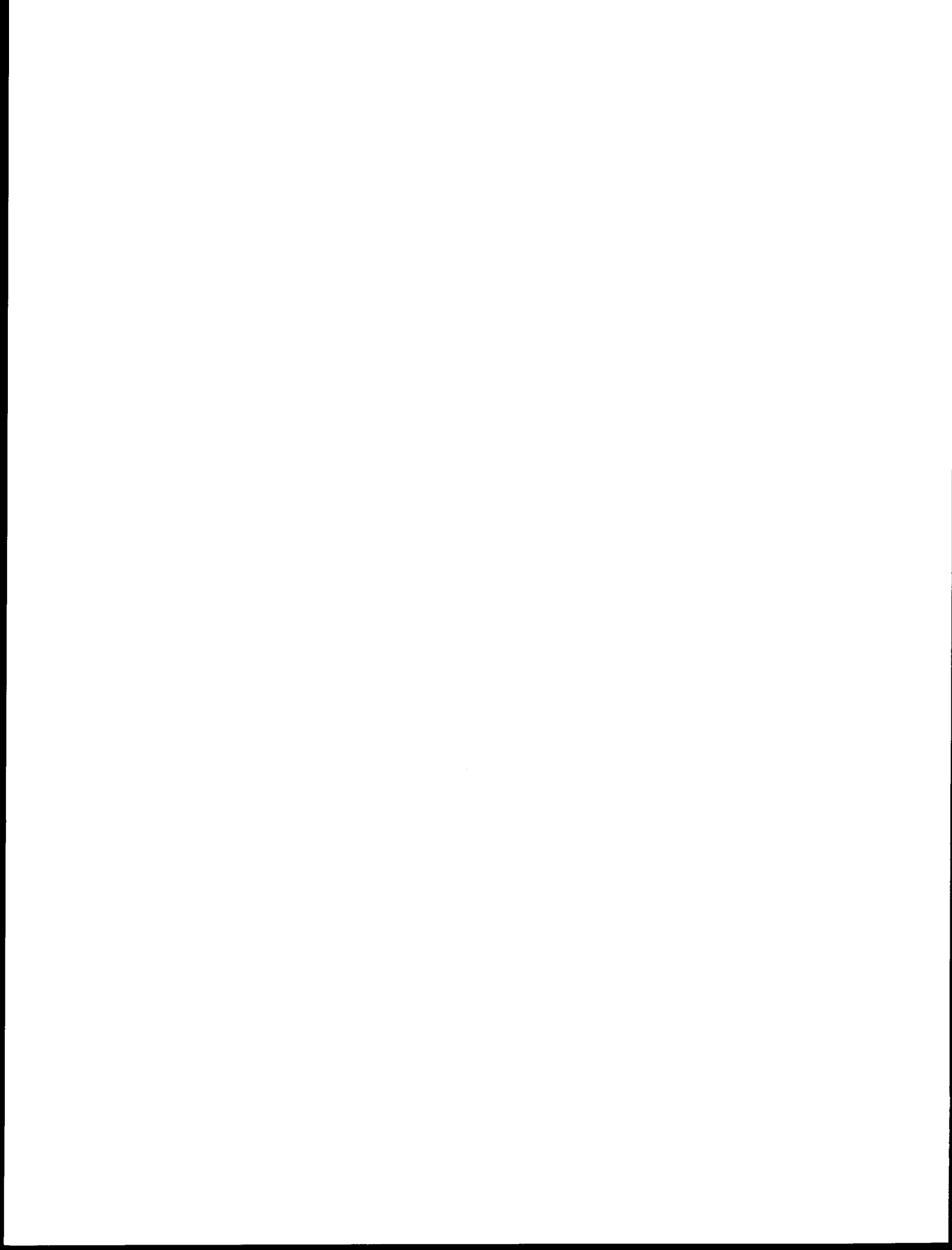


DISTRIBUTION AND FATE OF POLYAROMATIC HYDROCARBONS
IN INTERSTITIAL WATER AND SEDIMENTSUMMARY OF RESULTS

One day after ^{14}C -labelled phenanthrene was added to an oil-contaminated coarse-grained sediment in a simulated intertidal exposure system, about $\frac{1}{2}$ of 1 percent of the radiolabel was present in the interstitial water. The remainder was associated with the sediment, presumably in a film of oil surrounding the individual particles. The proportion of radiolabel in the water gradually increased, reaching 3% after 60 days. The proportion of radiolabel arising from chrysene and benzo(a)pyrene contained in the water was lower by 1 to 3 orders of magnitude. It ranged from 0.05% to 0.1% for chrysene and 0.01 to 0.04% for benzo(a)pyrene after 1 and 60 days, respectively. When ^{14}C -labelled phenanthrene was added to fine-grained sediment in a similar system, only 0.1% of the label appeared in interstitial water after 1 day, 0.53% after a week and 0.16% after 60 days. The proportion of label from chrysene and benzo(a)pyrene in interstitial water was the same in fine as in coarse-grained sediment.

The labelled compounds found in interstitial water from fine-grained sediment exposed to ^{14}C -phenanthrene were further characterized. After 7 days of exposure only 15% of the label was present as parent phenanthrene or moderately polar degradation products. After 60 days this proportion was reduced to 1.5%. $^{14}\text{CO}_2$ comprised approximately 35%, 45%, and 72% of the labelled products after 7, 30, and 60 days, respectively.

The time course of parent compound and CO_2 concentrations are consistent with a gradual degradation of phenanthrene by way of intermediate metabolic products. The metabolites present in interstitial water from fine-grained sediment after 7, 15, and 30 days exposure to labelled phenanthrene were separated by high-pressure liquid chromatography. Three to four different products were present at each time period. The retention times of the major products were approximately 14.5, 16.0, and 4.5 minutes. Conventional microbiological cultures of marine sediments containing ^{14}C -phenanthrene produced metabolites with the same retention times as those found in the simulated intertidal system, though in different proportions. This finding suggests that the degradative processes observed in controlled laboratory experiments are valid models of the processes occurring under natural environmental conditions.

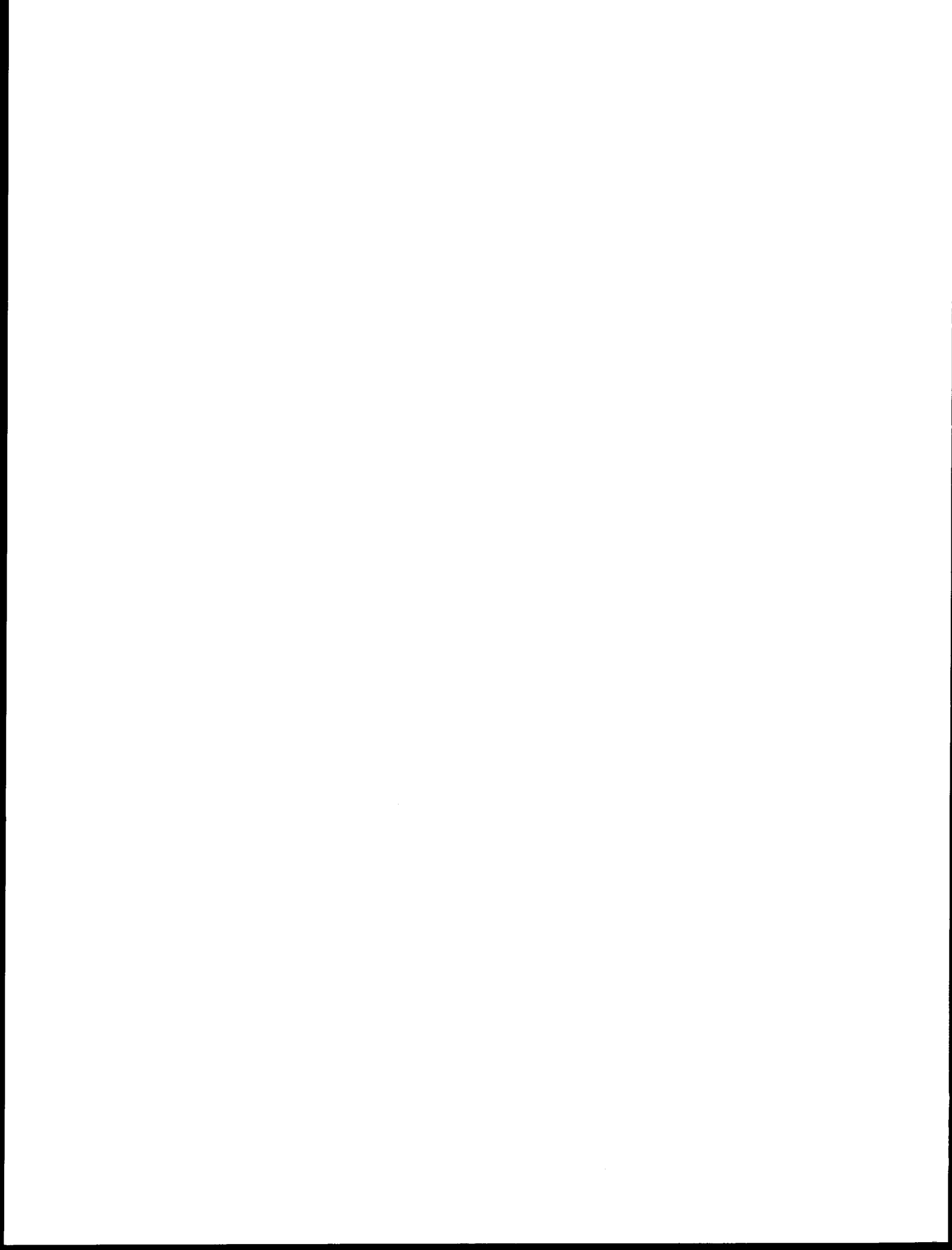


VII. APPENDIX

PUBLICATIONS RESULTING FROM RESEARCH CONDUCTED
ON THE NOAA/BLM OCSEAP PROGRAM UNIT 454

by the Staff of

Battelle Pacific Northwest Laboratories



PUBLICATIONS RESULTING FROM RESEARCH
CONDUCTED ON THE NOAA/BLM OCSEAP PROGRAM UNIT 454

by the staff of

BATTELLE PACIFIC NORTHWEST LABORATORIES

Reports

Anderson, J. W., G. Roesijadi, D. L. Woodruff and E. A. Crecelius. 1977. Research to Determine the Accumulation of Organic Constituents and Heavy Metals from Petroleum-impacted Sediments by Marine Detritivores of the Alaskan Outer Continental Shelf. Annual Report to NOAA, Boulder, CO., April, 1977, pp. 47.

Anderson, J. W., G. Roesijadi and E. A. Crecelius. 1978. Bioavailability of Hydrocarbons and Heavy Metals to Marine Detritivores from Oil-Impacted Sediments. Progress Report on Research Unit 454 of NOAA/BLM OCSEAP Program, Seattle, Washington, November 28-30, 1977. NOAA Technical Report Series.

Anderson, J. W., J. M. Augenfeld, E. A. Crecelius and R. G. Riley. 1978. Research to Determine the Accumulation of Organic Constituents and Heavy Metals From Petroleum-impacted Sediments by Marine Detritivores of the Alaskan Outer Continental Shelf. Annual Report to NOAA, Boulder, CO., April, 1978.

Anderson, J. W., J. M. Augenfeld, E. A. Crecelius and R. G. Riley. 1979. Research to Determine the Accumulation of Organic Constituents and Heavy Metals From Petroleum-impacted Sediments by Marine Detritivores of the Alaskan Outer Continental Shelf. Annual Report to NOAA, Boulder, CO., April, 1979.

Symposia

Anderson, J. W. 1977. Responses to sublethal levels of petroleum hydrocarbons: Are they sensitive indicators and do they correlate with tissue contamination?, pp. 95-114. In: Fate and Effects of Petroleum in Marine Ecosystems and Organisms, ed. by D. Wolfe. Pergamon Press, New York.

Anderson, J. W. 1979. An Assessment of knowledge concerning the fate and effects of petroleum hydrocarbons in the marine environment, pp. 3-22. In: Marine Pollution: Functional Responses, ed. by W. B. Vernberg, A. Calabrese, F. Thurberg and F. J. Vernberg, Academic Press, N. Y.

Anderson, J. W., L. J. Moore, J. W. Blaylock, D. L. Woodruff and S. L. Kiesser. 1977. Bioavailability of sediment-sorbed naphthalenes to the sipunculid worm, Phascolosoma agassizii, pp. 276-285. In: Fate and Effects of Petroleum in Marine Organisms and Ecosystems, ed. by D. A. Wolfe. Pergamon Press, New York.

Roesijadi, G. and J. W. Anderson. 1978. Condition index and free amino acid content of Macoma inquinata exposed to oil-contaminated marine sediments, pp. 69-84. In: Marine Pollution: Functional Responses, ed. by W. B. Vernberg, A. Calabrese, F. Thurberg and F. J. Vernberg. Academic Press, N. Y.

Journal Articles

Roesijadi, G., J. W. Anderson and J. W. Blaylock. 1978. Uptake of hydrocarbons from marine sediments contaminated with Prudhoe Bay crude oil: Influences of feeding type of test species and availability of polycyclic aromatic hydrocarbons. Proceedings of the Oil/Environment 1977 - An International Symposium, Halifax, Nova Scotia, October 10-16, 1977. J. Fish. Res. Bd. Canada 35:608-614.

Roesijadi, G., D. L. Woodruff and J. W. Anderson. 1977. Bioavailability of naphthalenes from marine sediments artificially contaminated with Prudhoe Bay crude oil. Env. Poll. 15:223-229.

Riley, R. G., B. L. Thomas, J. W. Anderson and R. M. Bean. 1980. Changes in the volatile hydrocarbon content of Prudhoe Bay crude oil treated under different simulated weathering conditions. Marine Environmental Research, (in press).

Augenfeld, J. M. 1980. Effects of Prudhoe Bay crude oil contamination on sediment working rates of Abarenicola pacifica. Marine Environmental Research (in press).

Augenfeld, J. M., J. W. Anderson, D. L. Woodruff and J. L. Webster. 1980. Effects of Prudhoe Bay crude oil contaminated sediments on Protothaca staminea (Mollusca:Pelecypoda): Hydrocarbon content, condition index, free amino acid levels. Marine Environmental Research (submitted).

Augenfeld, J. M. 1980. Effects of Prudhoe Bay crude oil in sediment on Abarenicola pacifica in laboratory and field experiments. In: The Proceedings of the Symposium on Pollution and Physiology of Marine Organisms. Milford, Conn., November, 1979, (submitted).

Crecelius, E. A., J. M. Augenfeld, D. L. Woodruff and J. W. Anderson. 1980. Uptake of trace metals by the clam Macoma inquinata from clean and oil-contaminated detritus. Bull. Environ. Contam. Toxicol. (submitted).

SUSPENDED PARTICULATE MATTER DISTRIBUTION, TRANSPORT,
AND PHYSICAL CHARACTERISTICS IN THE NORTH ALEUTIAN SHELF
AND ST. GEORGE BASIN LEASE AREAS

by

Edward T. Baker

Pacific Marine Environmental Laboratory
National Oceanic and Atmospheric Administration

Final Report
Outer Continental Shelf Environmental Assessment Program
Research Unit 594

January 1983

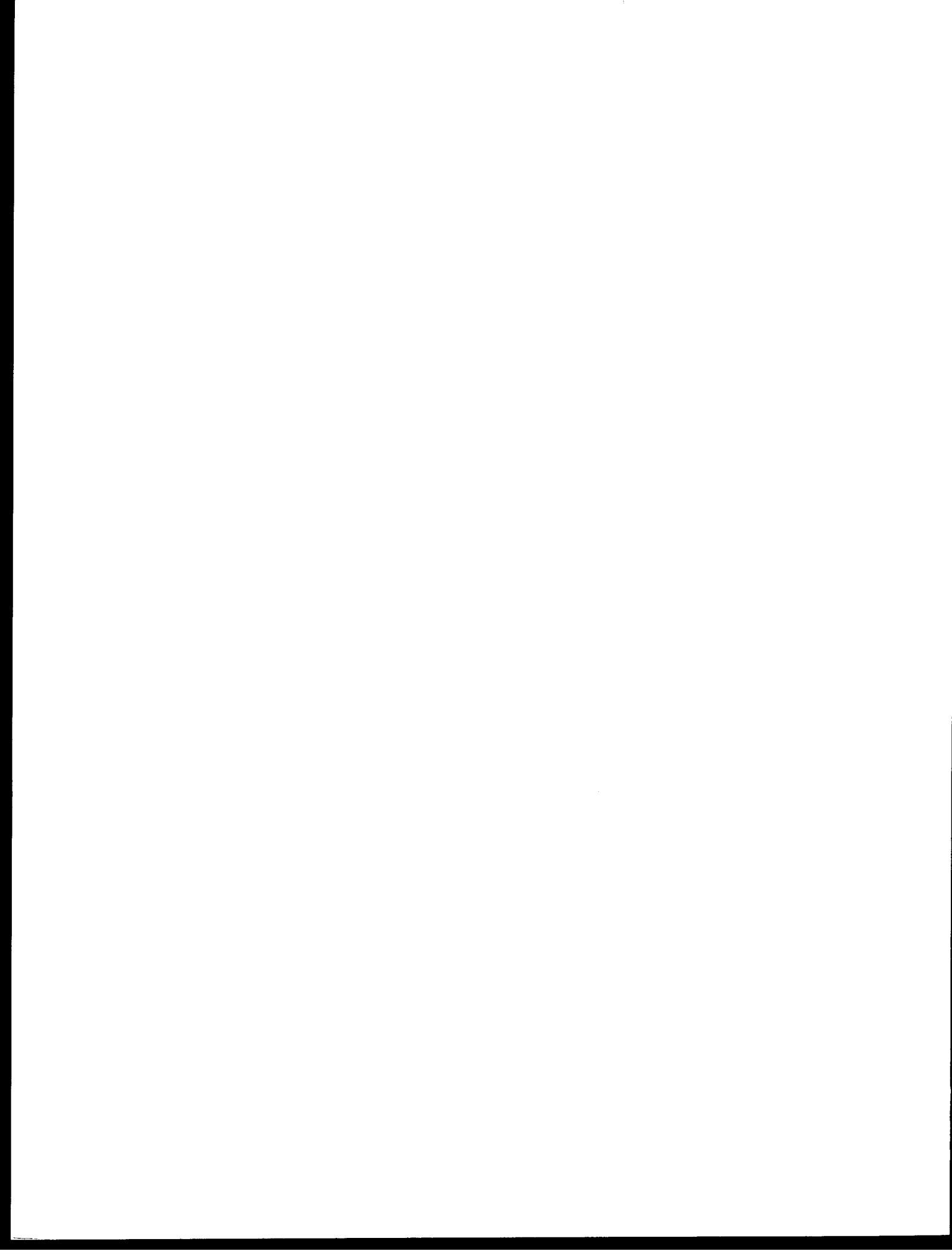


TABLE OF CONTENTS

List of Figures	167
List of Tables	171
I. SUMMARY OF OBJECTIVES, CONCLUSIONS, AND IMPLICATIONS WITH RESPECT TO OCSEAP OIL AND GAS DEVELOPMENT	173
A. Objectives	173
B. Conclusions and Implications	173
II. INTRODUCTION	175
A. Purpose of Study	175
B. Specific Objectives	176
C. Relevance to OCSEAP	176
III. STUDY AREA AND OCEANOGRAPHIC SETTING	177
A. Hydrographic Domains	177
B. Bottom Sediments	182
C. Suspended Particulate Matter	182
IV. METHODOLOGY	184
A. Data Collection	184
1. Water samples	184
2. Light attenuation profiles	185
3. Flux measurements	189
B. Sample Analyses	190
1. Gravimetry	190
2. Particle size	191
3. Organic matter concentration	194
4. X-ray diffraction mineralogy	194
5. Phytoplankton pigments	195
V. RESULTS	196
A. North Aleutian Shelf Region	196
1. Areal suspended matter and salinity distributions	196
2. Density and SPM cross-sections.....	207
3. Particle size distribution	225
4. Organic matter concentrations	230
5. X-ray clay mineralogy	233
6. Particle flux measurements	233

B.	St. George Basin Region	246
1.	Density and SPM cross-sections	246
2.	Particle size distributions	252
VI.	DISCUSSION	258
A.	Relationship between Vertical Distributions of Particles and Density	258
B.	Characteristics of the Particle Domains and Domain Boundaries	265
1.	Offshore transport of suspended particles	265
2.	Vertical mixing of particles	267
C.	Particle Influences on the Transport of Spilled Oil in the Southeastern Bering Sea	272
VII.	ACKNOWLEDGEMENTS	276
VIII.	REFERENCES	276
IX.	APPENDICES	281
A.	Discrete Sample Data from Cruise RP4SU804	283
B.	Discrete Sample Data from Cruise RP4SU81A	291
C.	Discrete Sample Data from Cruise RP4DI81A	299

LIST OF FIGURES

- Figure 1. Map of north Aleutian Shelf (NAS) region showing bathymetry and all NA station locations. Lines 1, 2 and 3 are the locations chosen for the vertical cross-sections of attenuation and density shown in subsequent figures.
- Figure 2. Map of the St. George Basin area showing all SG, PL, Y, and UP station locations occupied during one or more NASTE cruises. PL stations are numbered from 1 to 24 starting at the southwest end of the line.
- Figure 3. Map of the North Aleutian Shelf region near Port Moller showing bathymetry and mooring locations.
- Figure 4. Typical water property and particle concentration profiles for hydrographic domains in the southeastern Bering Sea.
- Figure 5. Bottom sediment data from the Bering Sea (Sharma, 1979) showing the depth control of mean size.
- Figure 6. Transmissometer calibration curves for (top) August 1980, (middle) January 1981, and (bottom) May 1981.
- Figure 7. Incremental particle distribution, dN/dD , for replicate Coulter Counter samples.
- Figure 8. Areal maps of light attenuation (top) and salinity (bottom) at the surface during August 1980. Contour interval is 0.2 m^{-1} for attenuation and 0.2 ‰ for salinity.
- Figure 9. Areal maps of light attenuation (top) and salinity (bottom) at the bottom during August 1980. Contour interval is 0.2 m^{-1} for attenuation and 0.2 ‰ for salinity.
- Figure 10. Areal maps of light attenuation (top) and salinity (bottom) at the surface during January 1981. Contour interval is 0.2 m^{-1} for attenuation and 0.2 ‰ for salinity.
- Figure 11. Areal maps of light attenuation (top) and salinity (bottom) at the bottom during January 1981. Contour interval is 0.2 m^{-1} for attenuation and 0.2 ‰ for salinity.
- Figure 12. Areal maps of light attenuation (top) and salinity (bottom) at the surface during May 1981. Contour interval is 0.2 m^{-1} for attenuation and 0.2 ‰ for salinity.
- Figure 13. Areal maps of light attenuation (top) and salinity (bottom) at the bottom during May 1981. Contour interval is 0.2 m^{-1} for attenuation and 0.2 ‰ for salinity.

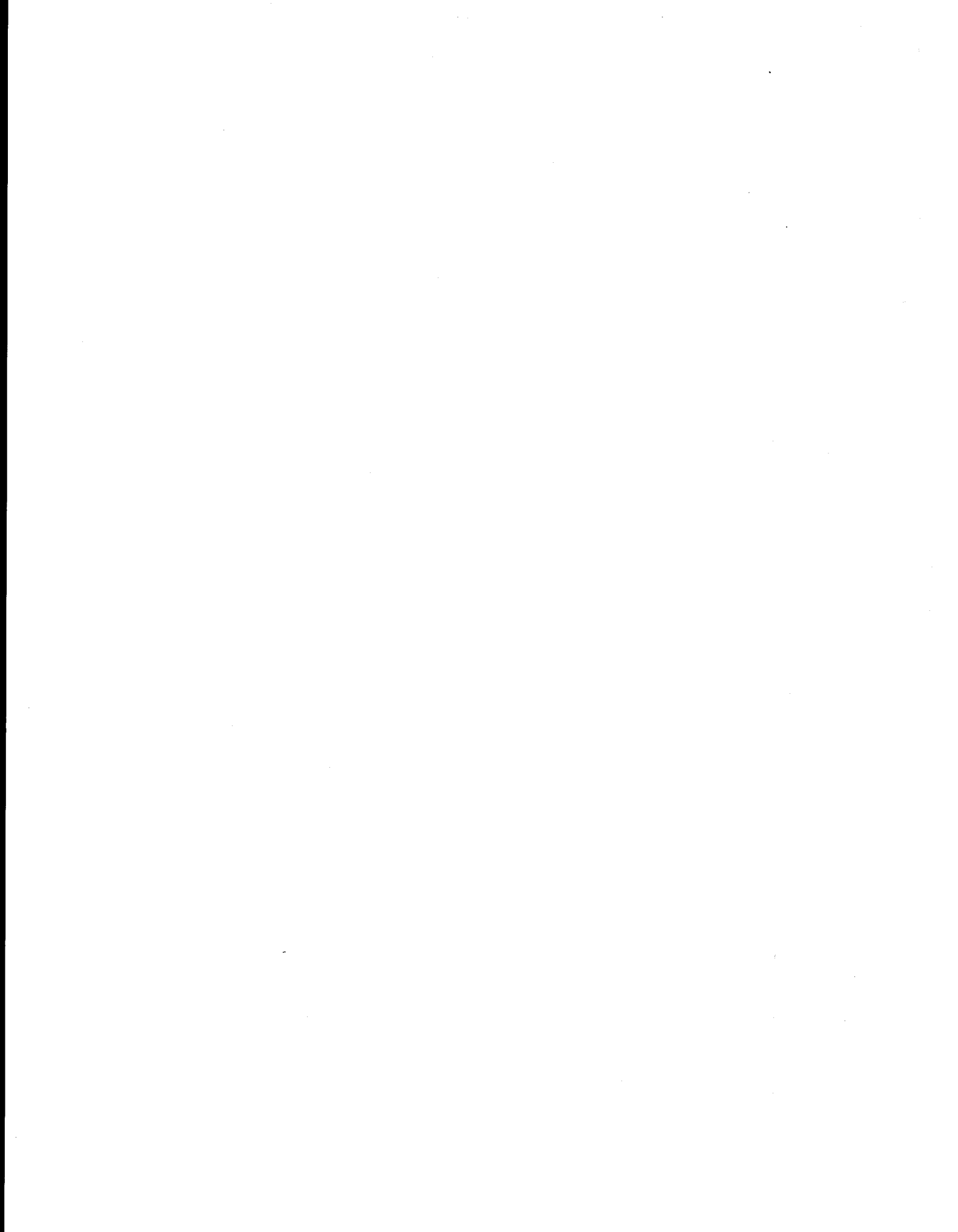
- Figure 14. Light attenuation vs. salinity in the surface water at NA stations for (top) August 1980, (middle) January 1981, and (bottom) May 1981. Inset for NASTE 1 data shows the complete data set.
- Figure 15. Attenuation (top) and density (bottom) cross-sections for line 1 (stations NA17-22), August 1980.
- Figure 16. Attenuation (top) and density (bottom) cross-sections for line 2 (stations NA34-40), August 1980.
- Figure 17. Attenuation (top) and density (bottom) cross-sections for line 3 (stations NA47-52), August 1980.
- Figure 18. Attenuation (top) and density (bottom) cross-sections for line 1 (stations NA17-22), January 1981.
- Figure 19. Attenuation (top) and density (bottom) cross-sections for line 2 (stations NA34-40), January 1981.
- Figure 20. Attenuation (top) and density (bottom) cross-sections for line 3 (stations NA47-52), January 1981.
- Figure 21. Attenuation (top) and density (bottom) cross-sections for line 1 (stations NA17-22), May 1981.
- Figure 22. Attenuation (top) and density (bottom) cross-sections for line 2 (stations NA34-40), May 1981.
- Figure 23. Attenuation (top) and density (bottom) cross-sections for line 3 (stations NA47-52), May 1981.
- Figure 24. Attenuation (top) and density (bottom) cross-sections for stations NA34-40 on August 20 (left), August 24 (middle), and August 31, 1980 (right).
- Figure 25. Attenuation (top) and density (bottom) cross-sections for stations NA41-46 on August 19 (left), and August 24, 1980 (right).
- Figure 26. Attenuation (top) and density (bottom) cross-sections for stations NA41-46 on August 31 (left), and September 2, 1980 (right).
- Figure 27. Attenuation (top) and density (bottom) cross-sections for stations NA34-40 on January 31 (left), and February 8, 1981 (right).
- Figure 28. Attenuation (top) and density (bottom) cross-sections for stations NA41-45 on May 15 (left), May 25 (middle), and May 30, 1981 (right).

- Figure 29. Incremental cumulative curves for particle populations along the NA34-40 station line from surface (A) and bottom (B) samples from NASTE 1, and surface (C) and bottom (D) samples from NASTE 2.
- Figure 30. Incremental cumulative curves for particle populations at (A) an offshore station (NA34) and (B) an inshore station (NA40) during NASTE 1, and offshore (C) and inshore (D) stations during NASTE 2.
- Figure 31. Incremental cumulative curves for particle populations along the NA34-40 station line from surface (top) and bottom (bottom) samples from NASTE 3.
- Figure 32. Incremental cumulative curves for particle populations at the surface and bottom at each station (NA34-40 station line) from NASTE 3. A is the outermost station and F is the innermost station.
- Figure 33. Flux values from NAS sediment traps. Each point represents an 11.25 day average value.
- Figure 34. Flux values for fine- and coarse-grained particles in the NAS sediment traps.
- Figure 35. Variability of particle-size partitioning of sediment trap material.
- Figure 36. Variance spectra for attenuation records. A, TP7; B, TP2; C, TP8; D, TP6; E, TP4; F, TP9. Peaks occur at tidal frequencies.
- Figure 37. Current meter/transmissometer record at TP7.
- Figure 38. Current meter-transmissometer record at TP9. Note change in scales from Figure 37.
- Figure 39. Mean speed and mean attenuation values averaged over sediment trap collection periods.
- Figure 40. Attenuation (top) and density (bottom) cross-sections for the PL line during NASTE 1.
- Figure 41. Attenuation (top) and density (bottom) cross-sections for the PL line, May 17-18, 1981.
- Figure 42. Attenuation (top) and density (bottom) cross-sections for the PL line, May 23-24, 1981.
- Figure 43. Incremental cumulative curves from the PL line during NASTE 1 for surface water (A), minimum turbidity zone (B), bottom water (C). Curve envelopes for each group are also shown.

- Figure 44. Incremental cumulative curves from the NASTE 2 surface (top) and bottom (middle) waters. Curve envelopes (bottom) demonstrate the similarity of the two populations.
- Figure 45. Incremental cumulative curves from NASTE 3 PL₁ surface (A), minimum turbidity (B), and bottom (C) zones. Panels D, E, and F show analogous curves for the PL₂ transect.
- Figure 46. Net particle attenuation profiles, stability profiles, and density profiles from the coastal (top), middle (middle), and oceanic (bottom) domains. Note the stability maximum at the top of each bottom nepheloid layer.
- Figure 47. Attenuation (open circles) and salinity (closed circles) gradients normal to the Alaska Peninsula for each cruise. Mean attenuation and salinity values from each NA station were grouped and averaged over 10-m station depth increments.
- Figure 48. Salinity and $\Delta \sigma_t$ gradients along the PL line during NASTE 1 and NASTE 3.
- Figure 49. Changes in the attenuation value in the turbidity minimum and in the concentration of surface and bottom chlorophyll a along the PL line. Compare the position of these changes with the hydrographic changes in Figure 48.

LIST OF TABLES

- Table 1. Linear least squares parameters for regressions of particle mass concentration (C) and light attenuation (α).
- Table 2. Flux measurements during the NASTE project.
- Table 3. Coulter counter sampling variations.
- Table 4. Percent organic matter in SPM samples from the North Aleutian Shelf region.
- Table 5. Vertical particle flux measurements.
- Table 6. Sediment flux calculations.
- Table 7. Particle size distribution parameters from PL line in St. George Basin.
- Table 8. Calculation of vertical eddy diffusion coefficients (K_z) from SPM profiles.
- Table 9. Estimated oil loading on NAS suspended sediments.
- Table 10. Estimated oil sedimentation rates in NAS waters.



I. SUMMARY OF OBJECTIVES, CONCLUSIONS, AND IMPLICATIONS WITH RESPECT TO
OCS OIL AND GAS DEVELOPMENT

A. Objectives

The principal objective of this research unit was to describe the distribution, transport, and physical characteristics of suspended particulate matter (SPM) in the area of the North Aleutian Shelf (NAS) and St. George Basin (SGB). These data are required to assess the effect that the natural particle population in these waters might have on the transport and dispersal of spilled oil.

B. Conclusions and Implications

1. The oceanographic conditions which result in the creation of hydrographic structural domains and frontal regions (Kinder and Schumacher, 1981a) also create characteristic SPM distributions in each of these domains. Particle gradients in the coastal domain were very low or non-existent in the vertical and very steep in the horizontal, with particle concentrations decreasing rapidly offshore. The middle and outer domains were typified by a three-layer structure: a high-turbidity surface layer resulting from in-situ phytoplankton growth and offshore advection and diffusion of shore and river derived particles, a broad middle zone of horizontally and vertically uniform particle concentrations, and a bottom layer of increased turbidity largely resulting from local resuspension of bottom sediments. This structure was always found in the outer domain. In the middle domain it can be weakened or destroyed when the normal two-layer density structure is weakened or obliterated, as in winter or during severe storms. Frontal zones were

sites of increased horizontal particle concentration gradients, especially in the mid-depth low turbidity layer.

2. Seasonal particle concentrations in the NAS region varied by <25% and were not significantly different during any of the three cruises. Seasonal salinity changes were likewise small but did vary inversely with the particle concentration.

3. The offshore gradient of mean particle concentration fell rapidly from shore to about the 50-m isobath and then varied little with increasing water depth. This pattern was evident irrespective of season (i.e., the presence or absence of the coastal front) or of location along the NAS.

4. The particle size distribution data followed the power law curve characteristic of many aqueous and terrestrial fine-particle suites. The slope of the power curve normally fell between 3.0 and 4.5 in agreement with numerous other marine studies and corresponding to median diameters of ~8-25 μm . Lower slopes, characteristic of a larger proportion of coarse-grained particles in the distribution, were normally found in near-shore waters. Organic matter loading in the SPM ranged from a low of ~25% for inshore stations during the winter to >50% for surface water samples from the offshore stations during the spring.

5. Areal distribution maps depict an SPM distribution in which particles from point sources along the coast are largely retained in the nearshore zone and dispersed parallel to the coast. Particle flux measurements from long term current meter/transmissometer deployments support this view.

Three moorings in the nearshore ($z < 32$ m) waters to the west of Port Moller recorded a net SPM alongshore transport to the southwest, away from Port Moller. A mooring in the coastal front zone ($z = 59$ m) recorded near-bottom SPM flux predominantly onshore. Two moorings seaward of the coastal front ($z > 68$ m) recorded near-bottom SPM flux offshore and to the northeast. This pattern is consistent with a transport divergence creating a particle minimum in the near-bottom waters under the coastal front, an interpretation which agrees with the minimums in SPM concentration around the 50-m isobath observed in fall and spring.

6. Maximum concentrations of particulate-associated oil resulting from an oil spill in NAS waters can be roughly estimated by combining the SPM data from this report with oil-loading studies performed by Payne et al., (1981) at Science Applications, Inc. (SAI). Based on the range of oil loading for different marine sediment types found by SAI, particulate-associated oil concentrations might reach 0.7-7 ppb in the water column of the nearshore zone (10-19 m deep) and 0.06-1.1 ppb in the offshore zone (40-90 m deep). Sedimentation of this oil to the benthos, calculated on the basis of sediment trap data from this report, could be expected to be in the range of 1-10 mg oil $m^{-2} day^{-1}$.

II. INTRODUCTION

A. Purpose of the Study

If petroleum hydrocarbons are introduced into the water column either through natural seepage or unintentional spills, a significant fraction will become associated with the ambient particles (Meyers and Quinn, 1973; Baker et al., 1978; Payne et al., 1981). Oil trajectories and sedimentation

will then be governed not only by the water trajectories but also by the trajectories and sedimentation of natural particles accommodating the oil. The purpose of this study, then, was to quantify the distribution and transport of particles which could affect oil movement. In addition, the study sought to define the relationships between the hydrographic structure of the southeastern Bering Sea (Kinder and Schumacher, 1981a) and the variability in particle distributions.

B. Specific Objectives

Specific objectives under this research unit included:

(1) Seasonal distributions of SPM concentrations in the vicinity of the NAS and SGB lease areas.

(2) Direct information concerning the horizontal and vertical SPM flux at several locations on the NAS by means of moored current meter/transmissometer and sediment trap measurements.

(3) Characterizations of the SPM at several locations along and across the inner front on the NAS in terms of particle size distribution, organic matter content, and x-ray clay mineralogy.

(4) Using pertinent data from other research units, estimate the water column loading and sedimentation rates of sediment accommodated oil for various areas on the NAS and SGB.

C. Relevance to OCSEAP

One factor in determining which potential lease areas may be inappropriate for development is the predicted fate of spilled oil from a particular location. Furthermore, OCSEAP is charged with providing information from which spilled oil trajectories and landfalls may be projected. Because

natural particles will provide vehicles for the transport and sedimentation of spilled oil, knowledge of particle distributions and transport is necessary to improve OCSEAP's predictions concerning the fate of spilled oil.

III. STUDY AREA AND OCEANOGRAPHIC SETTING

The study area for the North Aleutian Shelf Transport Experiment (NASTE) was the southeastern Bering Sea. Sampling was concentrated in two specific areas: (1) along the North Aleutian Shelf (NA stations, Fig. 1), and (2) in St. George Basin between the Pribilof Islands and Unimak Island (SG, PL, UP, and Y stations, Fig. 2). Each area was visited during three cruises: RP4SU80A between 13 August and 8 September, 1980 (NASTE 1); RP4SU81A between 30 January and 17 February, 1981 (NASTE 2); and RP4DI81A between 13 May and 2 June, 1981 (NASTE 3); moored instruments were deployed between NASTE 1 and NASTE 2 and between NASTE 2 and NASTE 3 at the locations shown in Fig. 3.

A. Hydrographic Domains

The hydrographic structure of the southeastern Bering Sea has been summarized by Kinder and Schumacher (1981a). The structure is developed not in response to mean flow patterns but rather as a result of boundary processes: tidal and wind mixing; buoyancy input from surface heating, cooling, and freshwater melt; and lateral exchange with the offshore oceanic water mass. Three distinct hydrographic domains can be identified from the vertical structure of the water column, as illustrated by three stations sampled during NASTE 1 along the PL line in St. George Basin (Fig. 4). The coastal domain (PL 24) is vertically homogeneous in water properties and is separated

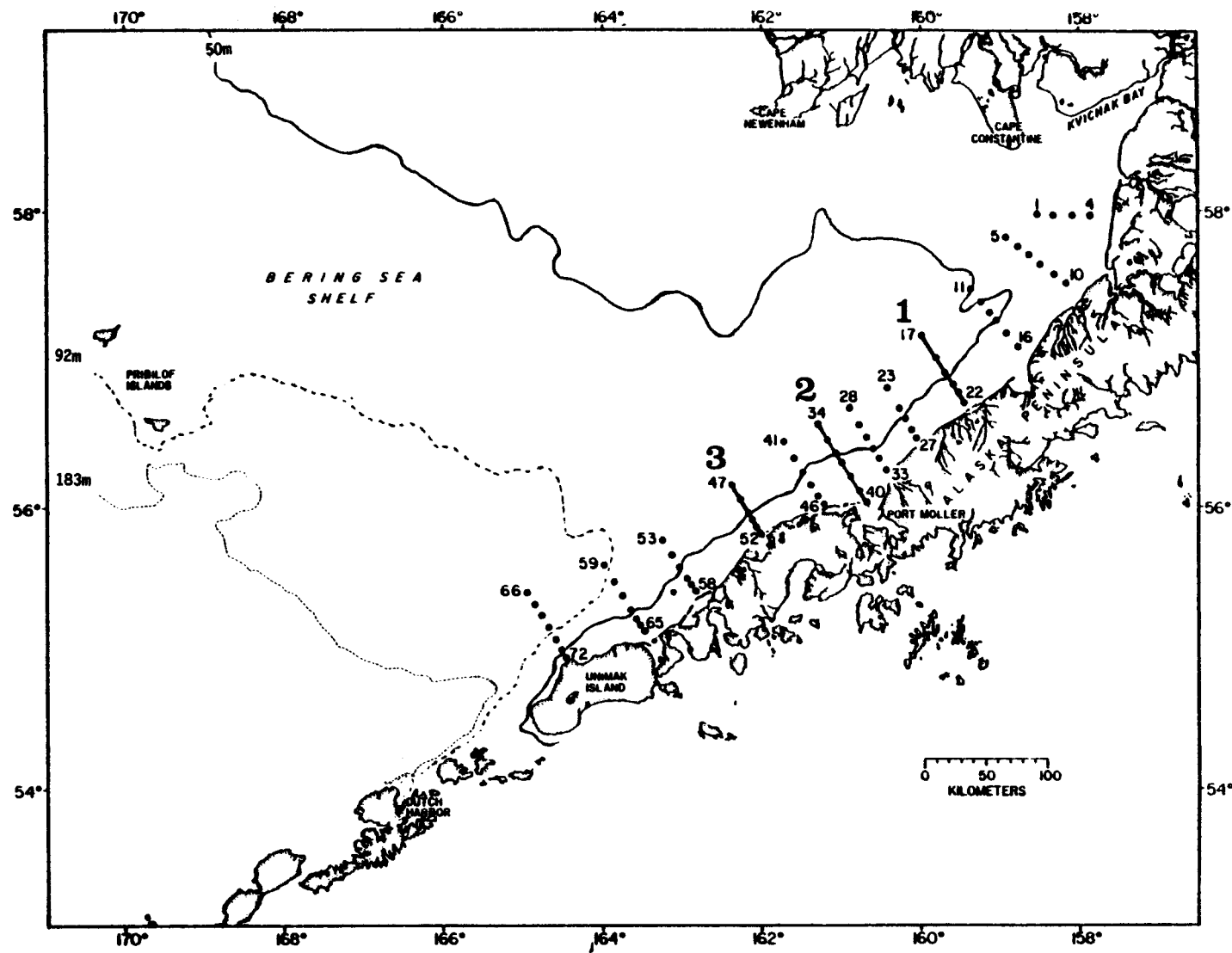


Figure 1. Map of north Aleutian Shelf (NAS) region showing bathymetry and all NA station locations. Lines 1, 2 and 3 are the locations chosen for the vertical cross-sections of attenuation and density shown in subsequent figures.

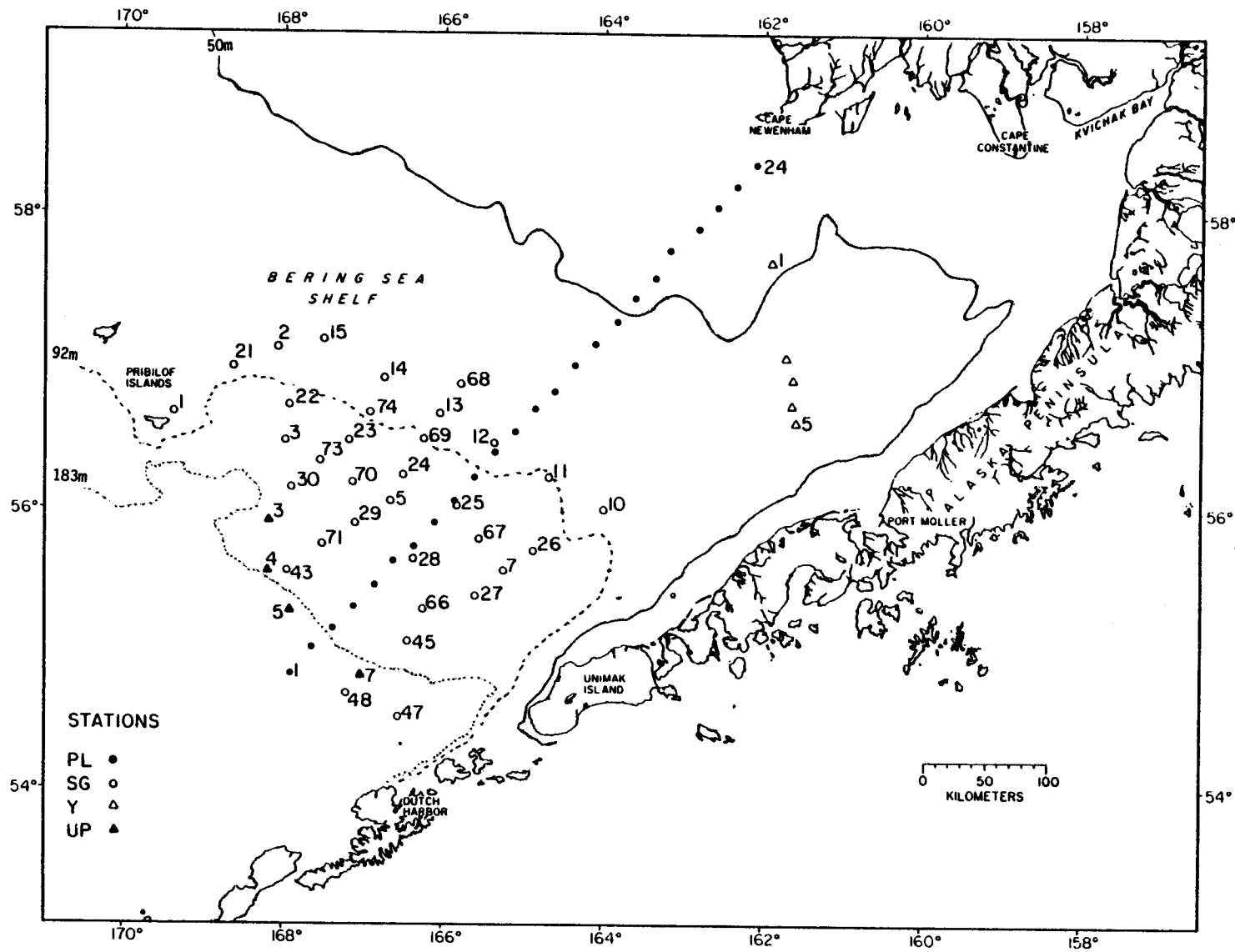


Figure 2. Map of the St. George Basin area showing all SG, PL, Y, and UP station locations occupied during one or more NASTE cruises. PL stations are numbered from 1 to 24 starting at the southwest end of the line.

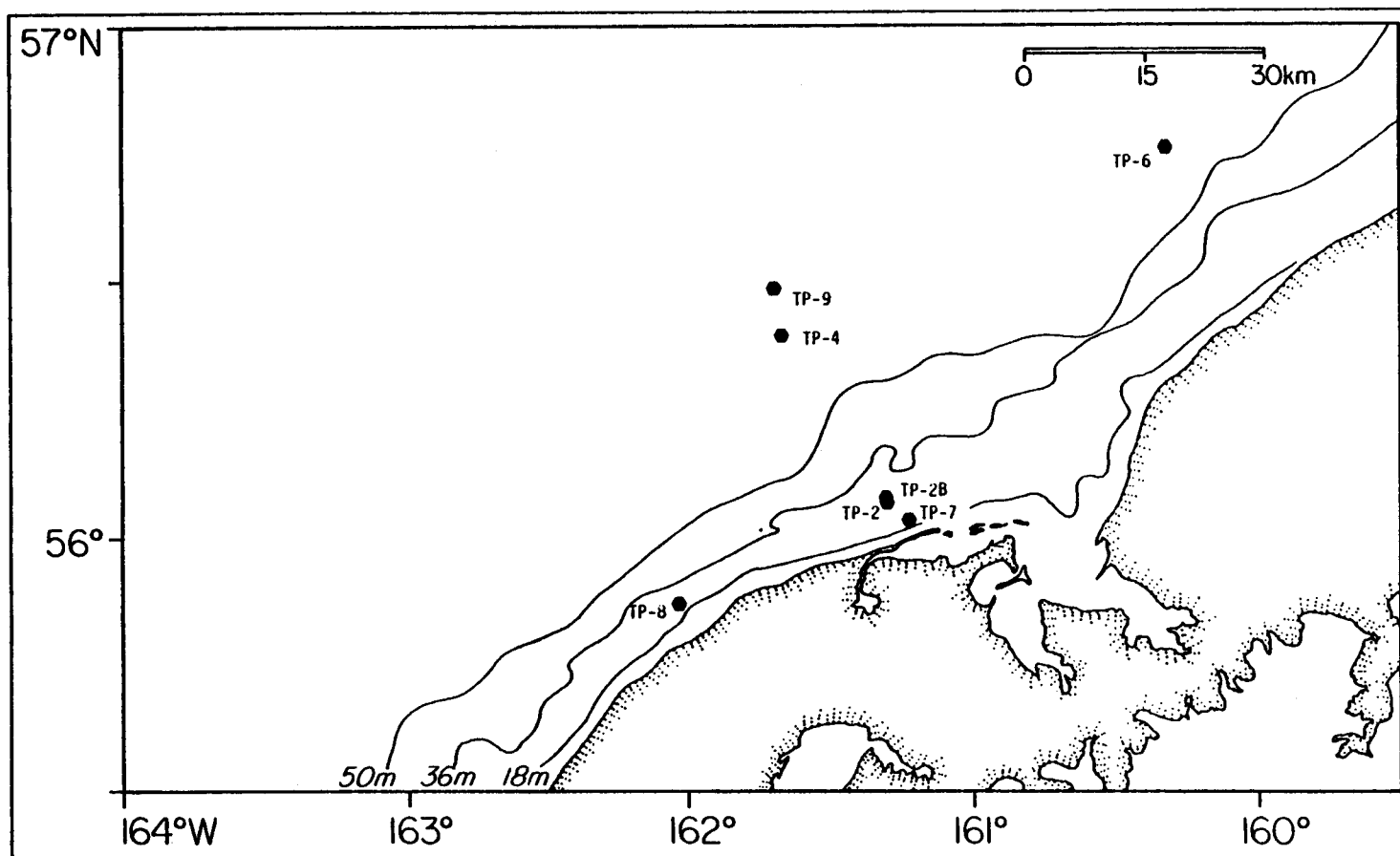


Figure 3. Map of the North Aleutian Shelf region near Port Moller showing bathymetry and mooring locations.

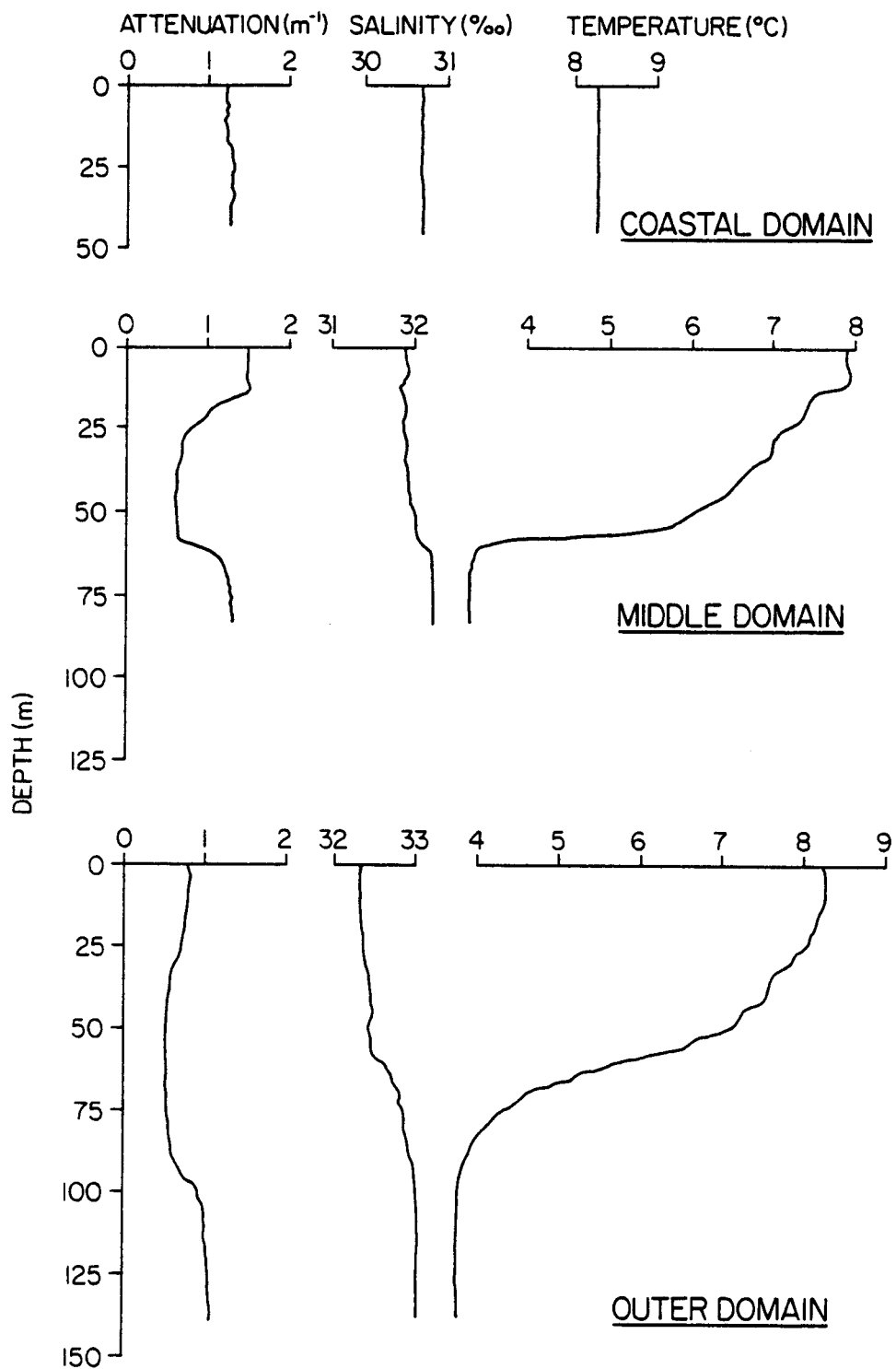


Figure 4. Typical water property and particle concentration profiles for hydrographic domains in the southeastern Bering Sea.

from the middle domain by a narrow (~10 km) front normally centered along the 50-m isobath. Seaward of this front, the middle domain is basically two-layered: a wind-mixed surface layer separated from a tidally-mixed bottom layer by a sharp pycnocline (PL 11). This domain extends to about the 100-m isobath where the broad (~50 km) middle front is located. Seaward of this front is the outer domain. This domain also has surface and bottom mixed layers, but the increased water depths prevent these layers from meeting and results in a broad zone of weak stratification and pronounced temperature and salinity fine structure (PL 4). As will be discussed in this report, these domains, as well as the fronts separating them, also are a major influence on the vertical distribution of suspended particulate matter and its transport through the southeastern Bering Sea.

B. Bottom Sediments

Sharma (1979) has summarized much of the available information on bottom sediments of the southeastern Bering Sea. Most of the NASTE study area is covered by sand and silt, with locally important amounts of gravel and clay. Mean sediment size contours closely follow isobaths, grading from very coarse sand (1-2 mm diameter) in Kvichak Bay to fine silt (8-18 μm) in St. George Basin between Unimak Island and the Pribilofs. Mean size is closely controlled by water depth (Fig. 5): at depths $<\sim 60$ m the mean size is nearly always found to be >125 μm ; at depths $>\sim 75$ m the mean size is <125 μm . The interval between 60 and 75 m is a broad transition zone where mean size is highly variable. This transition zone roughly corresponds to the position of the coastal front.

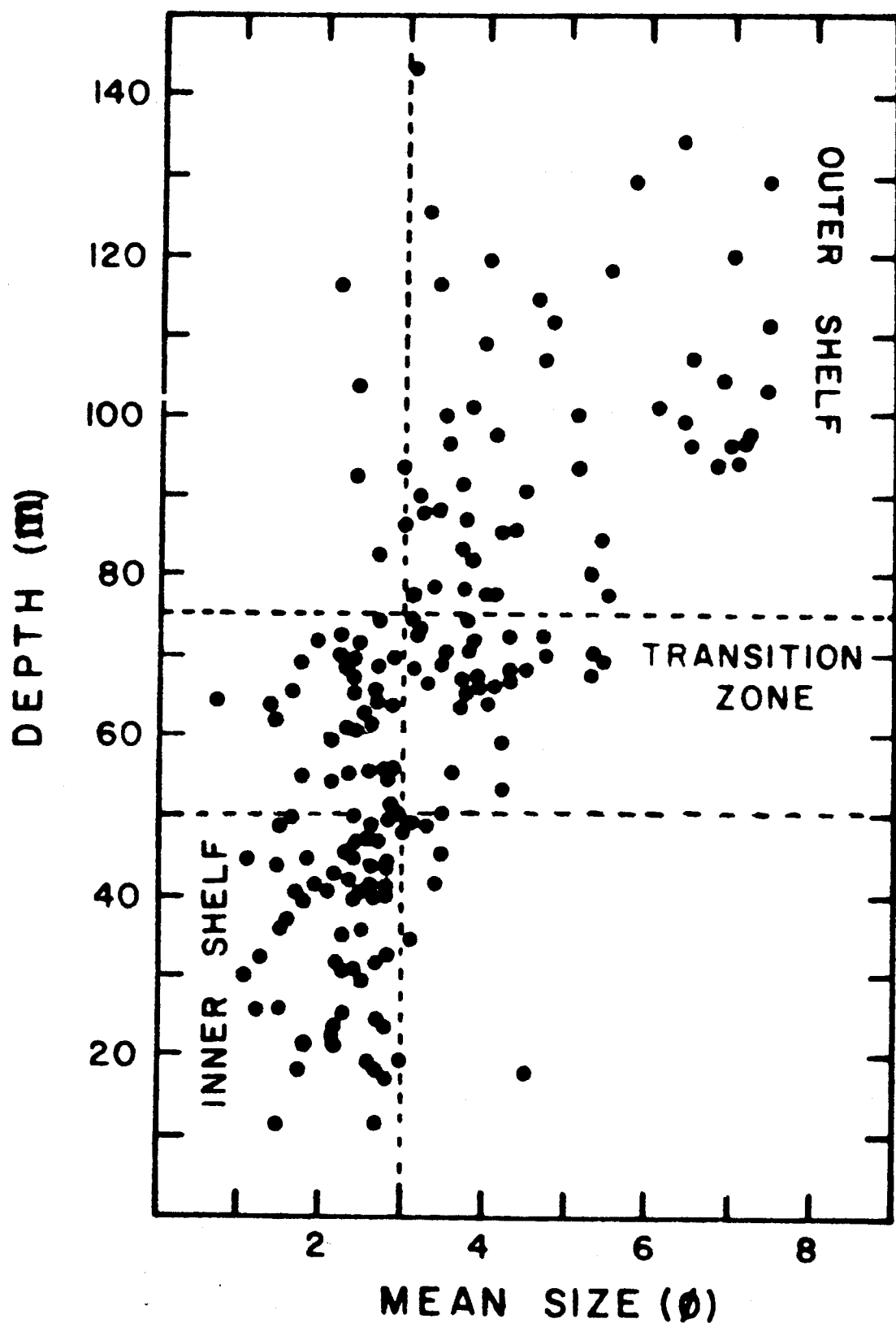


Figure 5. Bottom sediment data from the Bering Sea (Sharma, 1979) showing the depth control of mean size.

C. Suspended Particulate Matter

Detailed information on SPM concentrations in the southeastern Bering Sea is scarce. Sharma (1979) found surface concentrations of 0.2 to 2.2 mg l^{-1} during June and July of 1973, but station spacing was too coarse to define any pattern in the NASTE study area. Feely et al. (1981) occupied ~50 stations at 50 to 100 km spacing in the southeastern Bering Sea during the fall of 1975 and the summer of 1976. Surface concentrations ranged from 1 to $>6 \text{ mg l}^{-1}$ in the near-shore zone and were generally $<1 \text{ mg l}^{-1}$ seaward of ~75 km from the Alaska Peninsula. Near-bottom concentrations also showed a bathymetric influence and were higher than their surface counterparts, indicating that resuspension activity was common. Of particular interest to the present study was the indication in Feely's data of a narrow band of relatively low ($<1.0 \text{ mg l}^{-1}$) near bottom SPM values running parallel to the Alaska Peninsula at or just seaward of the 50 m isobath; that is, at about the position of the coastal front.

IV. METHODOLOGY

A. Data Collection

1. Water samples

Water samples for SPM filtration, mineralogy samples, pigment analyses, and particle size distribution measurements were collected from 5- ℓ Niskin or Go-Flo sampling bottles lowered by a CTD-mounted rosette system. Upon recovery, separate samples were drawn for particle size distribution and pigment analyses. During NASTE 1 and 2, SPM samples were

filtered by transferring a portion of the bottle sample to a separate filtering apparatus. During NASTE 3, SPM samples were filtered directly from the sample bottles. In each case, seawater was drawn through preweighed 0.4 μm pore size, 47 mm diameter polycarbonate filters under a 15 psi vacuum. Filters were rinsed three times with particle-free distilled water to remove sea salts, desiccated at room temperature, sealed, and returned to the laboratory for reweighing and analysis.

2. Light attenuation profiles

Light attenuation data were recorded at every CTD station and on seven of the Aanderaa current meter deployments. The beam transmissometers used are fully described by Bartz et al. (1978). The light source is a light-emitting diode with a wavelength of 660 nm to eliminate attenuation resulting from dissolved humic acids ("yellow matter"). Accuracy and stability are sufficient to provide data with an error of <0.5% of the true light transmission. The path length is 0.25 m to provide excellent resolution in coastal waters where SPM concentrations typically range from 1 mg l^{-1} to 20 mg l^{-1} .

For profiling work, the transmissometer readout was converted from the normal DC output to a frequency modulated signal compatible with the CTD data flow. The transmission signal was then recorded on the CTD data tape along with temperature, salinity, and depth. A realtime strip chart record was also available to provide a guide to choosing appropriate depths for discrete water samples.

By correlating the absolute SPM concentrations from filter samples with the transmissometer reading from the same depth and location, transmissometer calibration curves were developed for each cruise. Light

transmission values were first converted to the optical parameter of attenuation (α) using:

$$\alpha = \frac{-\ln (T/100)}{R}$$

where T = percent transmission and R = path length of the instrument (0.25 m). Plots of particle mass concentration (C) versus light attenuation (α) are shown in Fig. 6; statistical parameters of the least-squares regression are given in Table 1. Figure 6 and Table 1 indicate that correlations between light attenuation and SPM concentration were significant at the 0.05 probability level for each cruise. Furthermore, the 95% confidence intervals for the slope of the lines all overlap, implying that the two variables possessed a similar functional relationship during all three cruises. Inspection of Fig. 6 reveals that for NASTE 2 and 3 the most dilute samples fall below the regression line. To accurately predict SPM values of $<1.5 \text{ mg l}^{-1}$ from attenuation readings, a separate regression line is necessary (Table 1). The most notable change is that the intercept of the lines for the dilute NASTE 2 and 3 samples average $\sim 0.41 \text{ m}^{-1}$. One measure of the effectiveness of transmissometer readings in predicting the true SPM concentration is a comparison of the value of α at the zero SPM intercept to that for particle-free water. Tyler et al. (1974) present laboratory data which show that at 660 nm α lies between 0.34 and 0.43 m^{-1} . Both the NASTE 2 and NASTE 3 intercepts are within or close to that range, indicating that the variation in particle concentration was indeed the primary influence affecting the transmissometer readings. Although mass concentration of particles is commonly the primary influence on attenuation, factors such as size, shape, number, and index of refraction of the particles are also

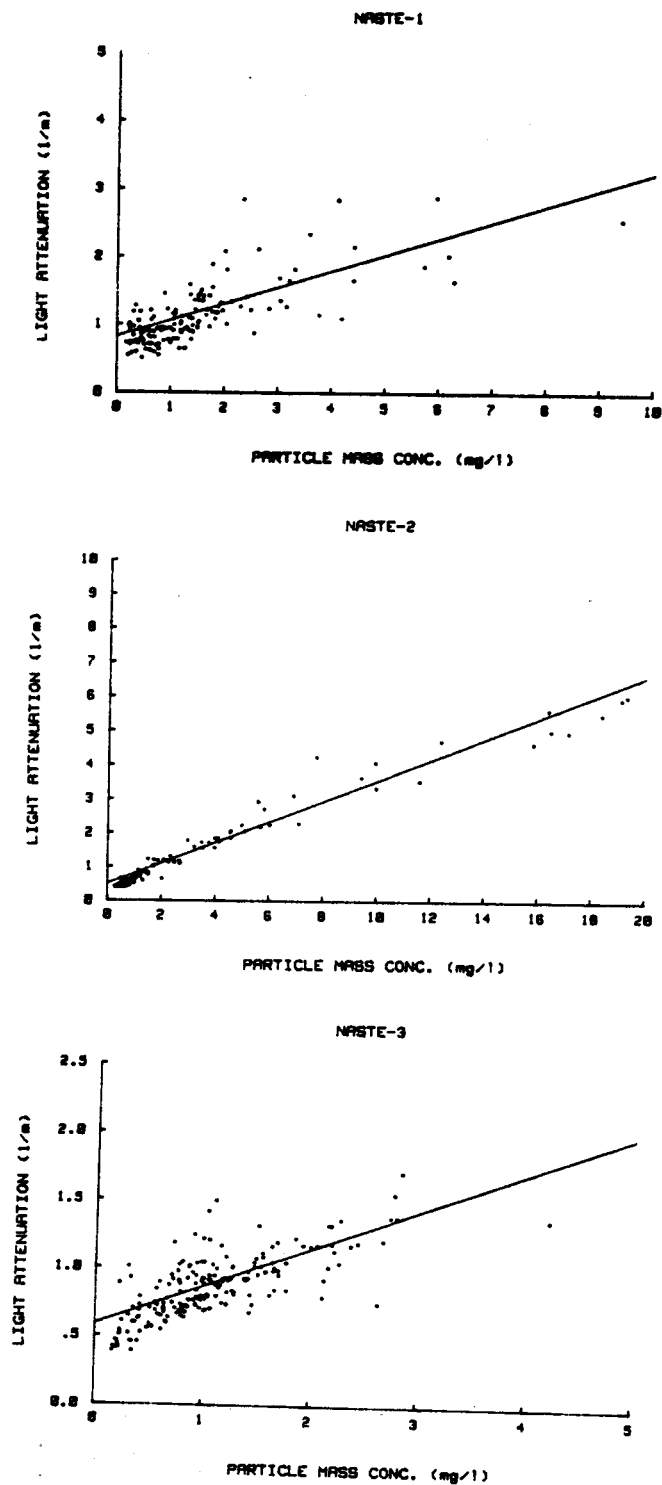


Figure 6. Transmissometer calibration curves for (top) August 1980, (middle) January 1981, and (bottom) May 1981.

important. The consistent difference in regression parameters between NASTE 1 and the following cruises suggests that the particles may have had somewhat different average characteristics during the late summer than during winter and spring.

TABLE 1

Linear least squares parameters for regressions of particle mass concentration (C) and light attenuation (α)

	<u>All Samples</u>		
	NASTE 1	NASTE 2	NASTE 3
No. of samples pairs	144	126	187
Regression equation	$\alpha = .80 + .26C$	$\alpha = .50 + .31C$	$\alpha = .59 + .28C$
Correlation (r)	.72	.98	.74
Standard error of estimate	.30	.26	.16
95% confidence interval			
Slope	.22-.30	.30-.32	.24-.31
Intercept	.72-.88	.45-.55	.54-.64
	<u>Dilute Samples</u>		
SPM range (mg l ⁻¹)	0-1.5	0-1.5	0-1.0
No. of sample pairs	98	79	104
Regression equation	$\alpha = .80 + .22C$	$\alpha = .36 + .41C$	$\alpha = .46 + .47C$
Correlation (r)	.40	.86	.65
Standard error of estimate	.20	.077	.14
95% confidence interval			
Slope	.18-.32	.32-.40	.36-.57
Intercept	.72-.89	.35-.47	.39-.54

3. Flux measurements

Measurements of horizontal SPM flux and vertical mass flux were made at the times and locations given in Table 2. Horizontal SPM flux data were acquired by means of a transmissometer (identical to the profiling model) coupled to the directional vane of Aanderaa current meters deployed by J. Schumacher, PMEL. The attenuation data were recorded internally on the current meter's pressure channel. The record length for the transmissometer data varies from 16 to 93 days depending on equipment failures and degradation of the signal as a result of organic growth on the lens surfaces. Transport flux was obtained by vector addition of the mean and variable portions of the flow along two component axes:

TABLE 2

Flux measurements during the NASTE project

Mooring	Location	Water Depth (m)	Transmissometer		Sediment Trap	
			Sampling Interval	Meter Depth (m)	Sampling Interval	Trap Depth (m)
TP2	56.07°N 161.30°W	32	19 Aug-25 Sep	20	--	--
TP6	56.78°N 160.30°W	59	20 Aug-17 Sep	55	--	--
TP4	56.41°N 161.68°W	68.5	19 Aug-20 Sep	63	--	--
TP7	56.03°N 161.22°W	24.5	30 Jan-5 May	15	3 Feb-15 May	13.5
TP8	55.86°N 162.04°W	31	2 Feb-19 Feb	21	5 Feb-17 May	17
TP2B	56.08°N 161.30°W	35	No record	25	3 Feb-15 May	21
TP9	56.50°N 161.71°W	89	31 Jan-27 Mar	79	4 Feb-16 May	77

$$\text{Flux} = [(\bar{u} \bar{c} + \frac{1}{n} \sum u' c')^2 + (\bar{v} \bar{c} + \frac{1}{n} \sum v' c')^2]^{\frac{1}{2}},$$

where \bar{u} , u' and \bar{v} , v' = the mean and fluctuating components of the flow along the east-west and north-south axes, respectively, and \bar{c} and c' = the mean and fluctuating components of the SPM concentration. Transport direction relative to the component axes is given by

$$\theta = \tan^{-1} \left(\frac{\bar{u} \bar{c} + 1/n \sum u' c'}{\bar{v} \bar{c} + 1/n \sum v' c'} \right)$$

Vertical mass flux was measured by newly designed Sequentially Sampling Sediment Traps (S³T) which collect up to 10 separate flux samples per deployment (Baker and Milburn, in press). The traps are cylindrical with a diameter of 25 cm and a height/width ratio of 3.25. These dimensions follow those recommended by several field and laboratory tests (Gardner, 1980a,b). A steep asymmetric funnel at the bottom of the trap focuses the settling particles into one of 10 acrylic sample collectors which rotate into position beneath the funnel at preset intervals. In this study, a new sample was collected every 11.25 days. Interpretation of the sediment trap data should be made with caution, however. Instantaneous current speeds at the trap locations often exceed 50 cm sec⁻¹, and in high flow conditions sediment traps may be biased samplers in a way that is not yet fully understood (Hannan and Grant, 1982).

B. Sample Analyses

1. Gravimetry

Total suspended matter concentrations were determined gravimetrically. Volumetric samples were collected on 0.4 μm pore size, 47 mm diameter

polycarbonate filters weighed on a Cahn 4700[®] electrobalance before and after filtration. Suspended matter loadings were determined by difference after correction for weight changes due to the freshwater rinse. This correction averaged 0.030 mg, 0.021 mg and 0.099 mg for NASTE 1, 2, and 3 applied to an average sample mass of ~2 mg (1.1 - 2.5%). The weighing precision ($2\sigma = \pm 0.011$ mg) and volume reading error (± 10 ml) yield a combined coefficient of variation in SPM concentration of ~ 1% at mean sample loading and volume.

2. Particle size

Particle size distributions were determined using a Coulter Electronics ZBI[®] particle size analyzer and C1000[®] channelizer. Water samples were analyzed shortly after collection. No preservatives were added. Fifty μm and 200 μm aperture tubes were used for the analyses during NASTE 1 and NASTE 2. Particles with equivalent spherical diameters of 1-80 μm were counted with this combination of aperture tubes. In order to avoid problems in matching the overlap region of the 50 and 200 μm aperture tubes, size analyses during NASTE 3 were run on an intermediate (100 μm) aperture tube only. This tube covered the size range 2-40 μm , which included all particles of interest to this study.

Coulter Counter analyses of particle suspensions yield a very detailed data distribution. The size range covered by each aperture is broken down into 100 logarithmically spaced channels of population information. In order to compare samples, it was necessary to fit the data to a specific distribution. Bader (1970) has shown that many natural collections of small particles, such as cosmic and terrestrial dust, oceanic suspended particles, and fine sediments, have a size distribution well fitted by a

hyperbolic (or power) curve: $N = -K D^{-c}$, where N = the number of particles > a given size, D = particle diameter (or some other parameter), and K and c are constants. The derivative with respect to size of this cumulative distribution is an incremental distribution: $dN/dD = aD^{-b}$, where $a = cK$ and $b = c + 1$. This distribution has been used by several authors to describe the observed particle populations in seawater (Carder and Schlemmer, 1973; Lal and Lerman, 1975; McCave, 1975; Brun-Cottan, 1976; Lerman et al., 1977, Baker et al., 1979): a represents the dN/dD value at $D = 1 \mu\text{m}$, and b represents the slope of the distribution (linear on full logarithmic paper). The slope is thus a measure of the number of large particles relative to the number of small particles; the larger the slope, the greater the relative proportion of small particles. Material having a slope $b = 3$ contains equal volumes of particles in logarithmically increasing size grades (McCave, 1975). Values of $b < 3$ indicate that the volume concentration is skewed towards the larger size grades and values of $b > 3$ indicates a skewness towards the finer size grades. Values of b for deep-sea sediments and suspended particulate matter commonly lie between 3.5 and 4.5 (Lal and Lerman, 1975; Brun-Cottan, 1976; Baker et al., 1979). Inshore and surface waters commonly have values of $b < 3$ due to the influence of large amounts of coarse grained organic (i.e., phytoplankton) and inorganic particles (Carder and Schlemmer, 1973; Kitchen et al., 1978). In the present study, variations in slope and intercept of the power distribution served to distinguish different particle populations.

Sampling variations in the Coulter Counter technique were periodically assessed by comparing measured particle volumes from replicate samples. In the example illustrated in Table 3, two Niskin bottles were tripped at the same depth, two subsamples were drawn from each bottle, and three replicate

TABLE 3
Coulter counter sampling variations
NASTE 1 Sta. SG 2 Depth 72 m

Niskin Bottle	Subsample	Replicate Analysis	Total Particle Volume ($\mu\text{m}^3\text{ml}^{-1}$)	
			1.18-6.32 μm^1	6.36-41.1 μm^1
1	1	1	28.5 x 10 ⁴	36.2 x 10 ⁴
		2	29.6 x 10 ⁴	63.4 x 10 ⁴
		3	30.4 x 10 ⁴	94.9 x 10 ⁴
1	2	1	28.5 x 10 ⁴	68.2 x 10 ⁴
		2	29.2 x 10 ⁴	80.4 x 10 ⁴
		3	29.3 x 10 ⁴	68.6 x 10 ⁴
2	1	1	27.5 x 10 ⁴	74.4 x 10 ⁴
		2	26.4 x 10 ⁴	45.4 x 10 ⁴
		3	27.4 x 10 ⁴	69.4 x 10 ⁴
2	2	1	27.3 x 10 ⁴	33.3 x 10 ⁴
		2	26.4 x 10 ⁴	46.5 x 10 ⁴
		3	27.7 x 10 ⁴	55.4 x 10 ⁴

¹ Diameter (D) range of the volume calculation, assuming all particles are spheres

analyses were performed on each subsample. Comparison of the means of the particle volume for each subsample (Natrella, 1963), at the 0.01 level of significance, indicates that there is no basis for concluding that the average volume for either diameter range (i.e., the 50 μ m and 200 μ m apertures) differs between subsamples or sampling bottles.

Examination of the volume measured in the 6.36 - 41.1 μ m range reveals much larger variations than in the finer size range. This condition arises from the fact that at the coarse end of the particle range ($D > \sim 20\mu$ m) particle counting statistics are poor because of a small concentration of particles ($< \sim 5$ per ml for each one μ m interval; Fig. 7). And since volume is proportional to the cube of the radius, a small change in the number of large particles results in a large change in total volume.

3. Organic matter concentrations

The efficiency of hydrogen peroxide in oxidizing particulate organic matter from seawater samples has been demonstrated by Crecelius et al. (1974) and Landing (1978). The filters were placed in 20 ml of 10% H_2O_2 for 30-45 minutes at room temperature, sonicated for one minute to remove the particles, then taken from the H_2O_2 and rinsed. The particles remained in the hydrogen peroxide for 24 hours in a 60°C oven. Each H_2O_2 -particle suspension was then poured back through the original sample filter, dried in a dessicator, and weighed. The concentration of organic matter was determined by the weight difference after treatment with hydrogen peroxide.

4. X-ray diffraction mineralogy

Selected samples for clay mineral determination were collected on cellulose membrane filters (Baker, 1973). Organic matter was removed from

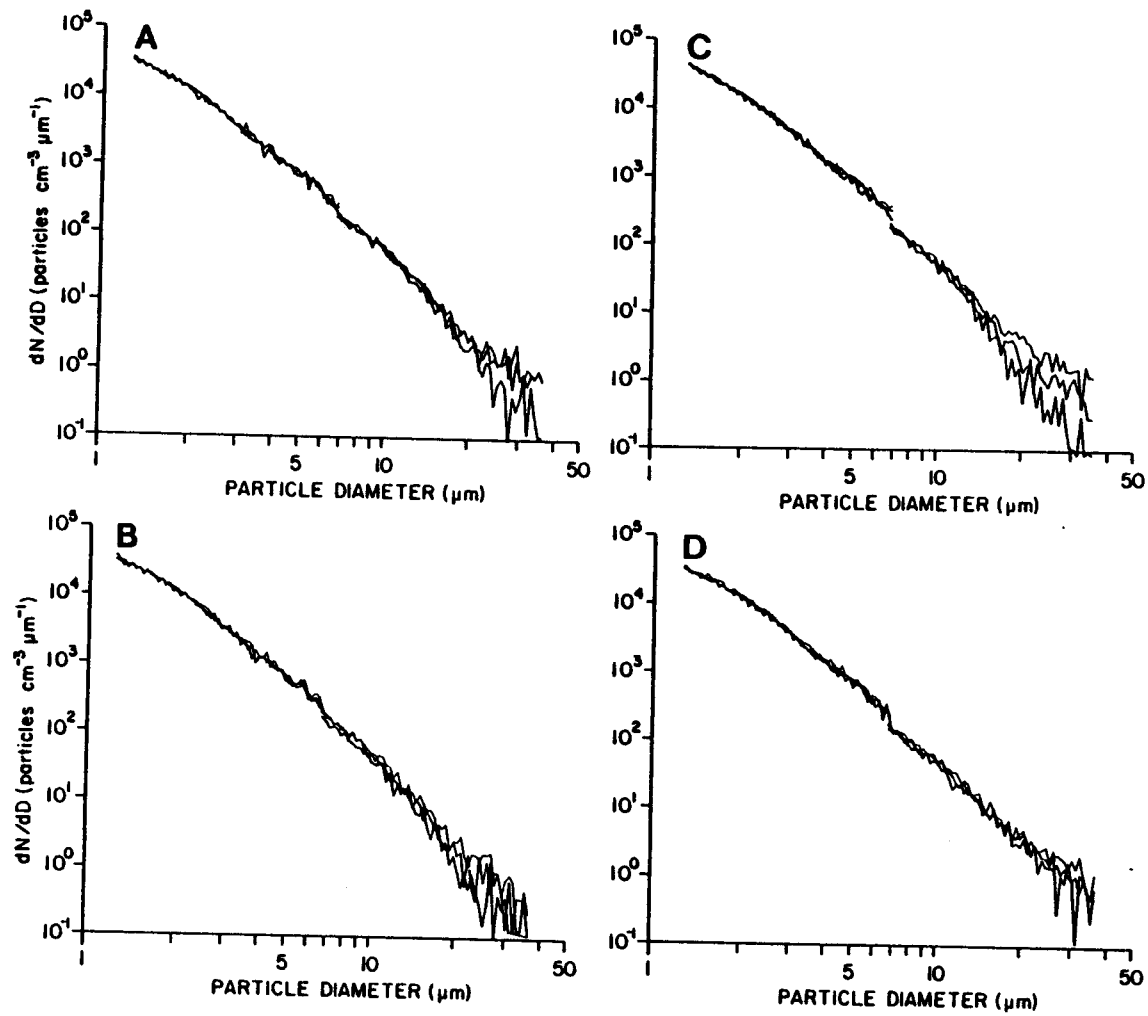


Figure 7. Incremental particle distribution, dN/dD , for replicate Coulter Counter samples.

the samples by hydrogen peroxide treatment in order to improve the quality of the diffractograms. Afterwards, the filters were dissolved in acetone until all traces of the filter material had disappeared. The resulting suspension was then refiltered through a Selas Flotronics[®] pure silver membrane filter (47mm diameter, mean pore size 0.45 μ m) in order to prepare an oriented mount for x-ray analysis. All samples were analyzed on a Phillips diffractometer with CuK α radiation and graphite focusing monochromator, scan speed 1 $^\circ$ 2 θ /min.

5. Phytoplankton pigments

The concentration of phytoplankton pigments was measured in selected samples. Subsamples (100 ml) were drawn from the sample bottles and filtered onto a glass fiber filter. The filter was then immersed in 90% acetone and sonicated for five minutes. Solids were separated by centrifugation. Chlorophyll a and pheophorbide a were measured by the fluorometric method of Holm-Hansen et al. (1965) using a Turner model 111 fluorometer.

V. RESULTS

A. North Aleutian Shelf Region

1. Areal suspended matter and salinity distributions

Comparison of surface attenuation and salinity (Fig. 8) during NASTE 1 shows considerable agreement in terms of source areas and gradients. In

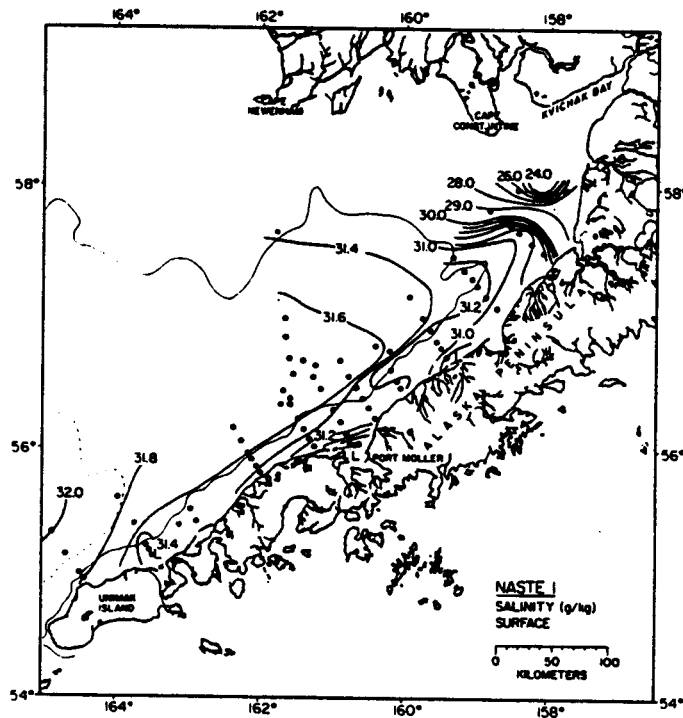
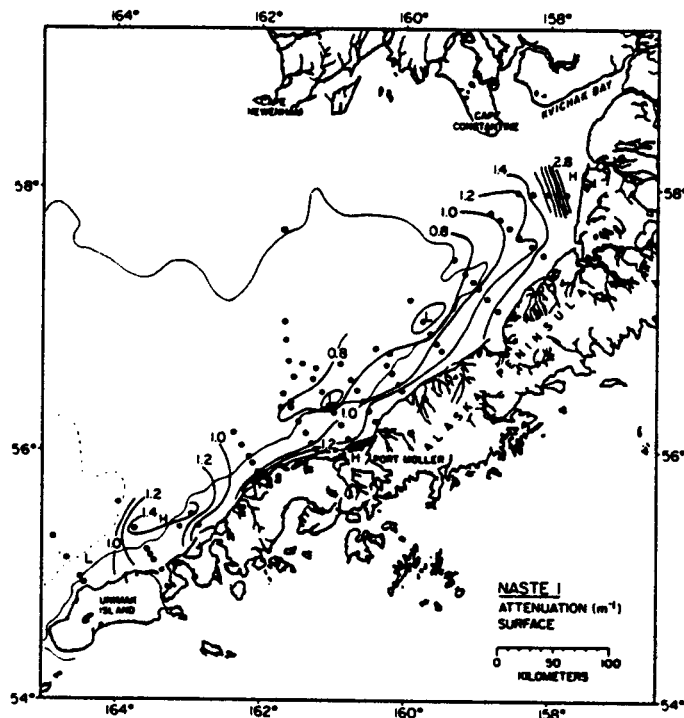


Figure 8. Areal maps of light attenuation (top) and salinity (bottom) at the surface during August 1980. Contour interval is 0.2 m^{-1} for attenuation and 0.2 ‰ for salinity.

general, attenuation and salinity contours ran predominantly alongshore, closely following the trend of the bathymetry. Prominent freshwater sources such as the Izembek Lagoon area (just east of Unimak Island), the Port Moller area, and Kvichak Bay, also showed high attenuation values. Isolated high values of attenuation at nearshore stations (e.g. station NA52, Fig. 1), were caused by tidal resuspension in shallow water.

Attenuation and salinity (Fig. 9) 5m above bottom (mab) showed patterns similar to the surface values, especially for salinity. A source of deep, high salinity water intruded from the northwest. Organization of the salinity contours along isobaths was more pronounced than in the surface waters. The influence of coastal freshwater sources was diminished, except for large sources such as Port Moller and Kvichak Bay. Because near-bottom attenuation is strongly influenced by local changes caused by bottom resuspension (e.g., station NA52), the contour pattern was more complicated than that of salinity. The trend of the contours was still alongshore, however. Superimposed upon this trend was a tendency for low attenuation values to occur near the center of each transect, roughly at the 50-m isobath. This pattern was particularly evident in the transects east of Port Moller. West of Port Moller the pattern was intermittent and not well described by the contour interval of Fig. 9. Note that the 50-m isobath is the approximate dividing line between the middle and coastal domains (Kinder and Schumacher, 1981a).

Oceanographic conditions during the winter (NASTE 2) resulted in a very close association between attenuation and salinity in both surface and bottom waters. Attenuation and salinity (Fig. 10) contours in the surface waters followed the isobath trends closely. Asymmetric trends of attenuation and salinity contours inshore of ~50 m suggest net transport to the northeast.

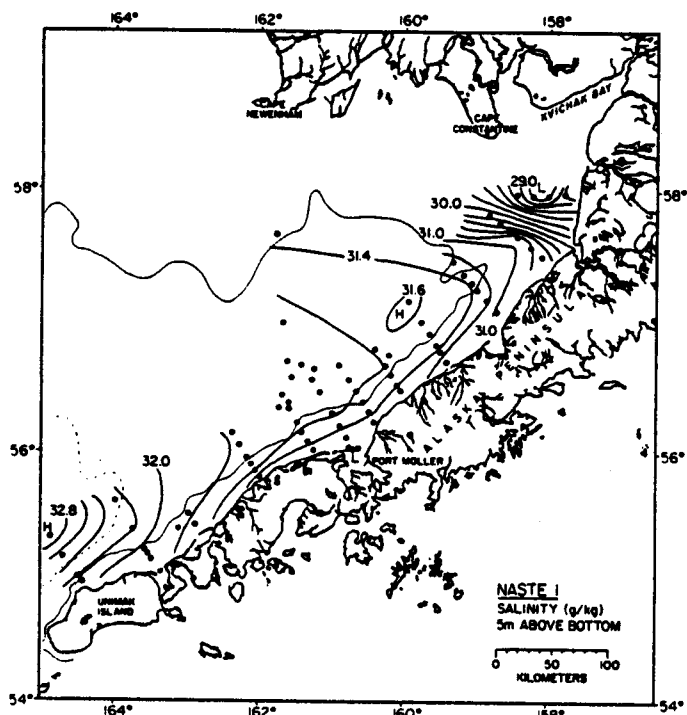
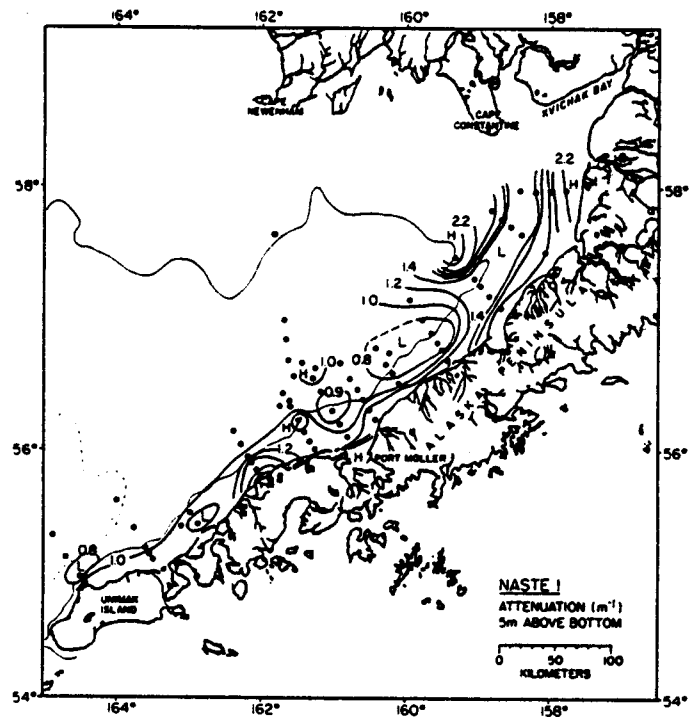


Figure 9. Areal maps of light attenuation (top) and salinity (bottom) at the bottom during August 1980. Contour interval is 0.2 m^{-1} for attenuation and 0.2 ‰ for salinity.

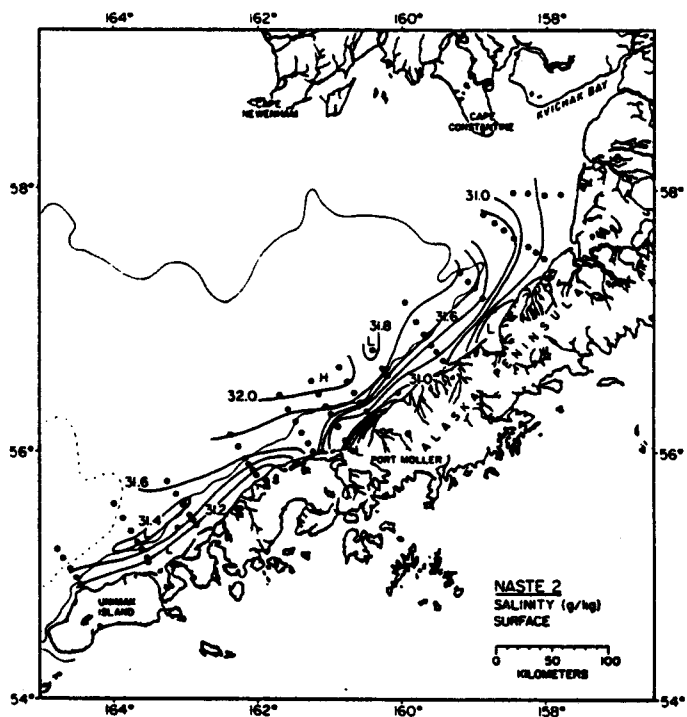
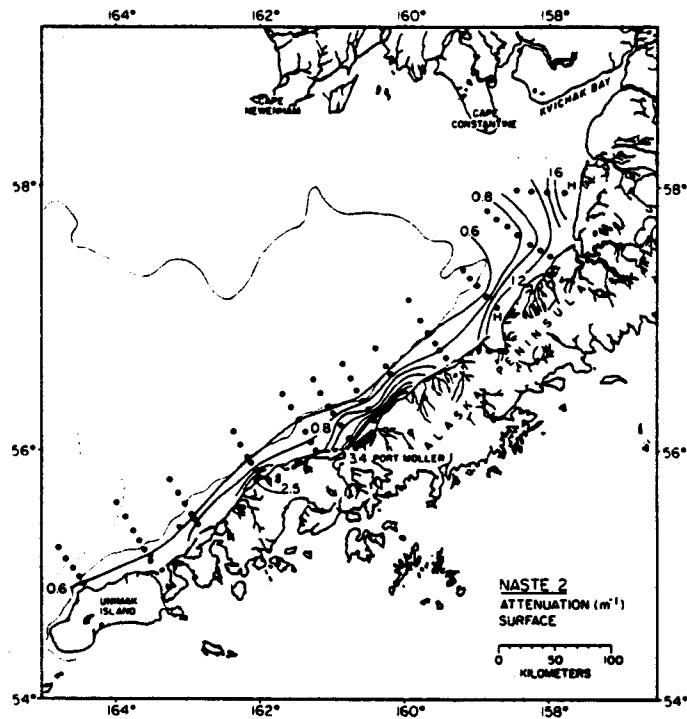


Figure 10. Areal maps of light attenuation (top) and salinity (bottom) at the surface during January 1981. Contour interval is 0.2 m^{-1} for attenuation and 0.2 ‰ for salinity.

A strong particle and freshwater source at Port Moller, for example, appeared to be elongated eastward along the coast. Another fresh water source was the Izembeck Lagoon area, but this area was not a significant particle source. These pockets of high turbidity and/or low salinity were separated by small areas of low attenuation and high salinity (e.g., stations NA46 and NA22). Seaward of ~50 m both alongshore and offshore gradients of salinity and attenuation became very low. Particle concentrations in this zone were nearly identical throughout the study area.

Descriptions of attenuation and salinity (Fig. 11) distributions in the bottom water during NASTE 2 are essentially the same as those presented for the surface water: Stations NA46 and NA22 separated regions of higher attenuation and freshwater content. Alongshore and offshore gradients were very low seaward of the 50-m isobath. Unlike NASTE 1, the near-bottom attenuation distribution showed little indication of isolated highs or lows attributable to resuspension activities. The weak vertical stratification throughout the region in winter (see section V. A2. below) evidently encouraged vertical mixing and thus prevented the creation of a bottom nepheloid layer other than that associated with isolated coastal sites where freshwater input was significant.

The NASTE 3 cruise encountered a return to conditions similar to those observed during NASTE 1. Surface salinity (Fig. 12) contours were parallel to the isobaths as usual and freshwater sources were evident in Port Moller and Port Heiden (no data was collected from the two easternmost transects). Prominent particle sources (Fig. 12) were Izembek Lagoon, Port Moller, and Port Heiden. In addition, isolated highs throughout the region, always associated with a high chlorophyll a concentration, were indicative of phytoplankton patchiness.

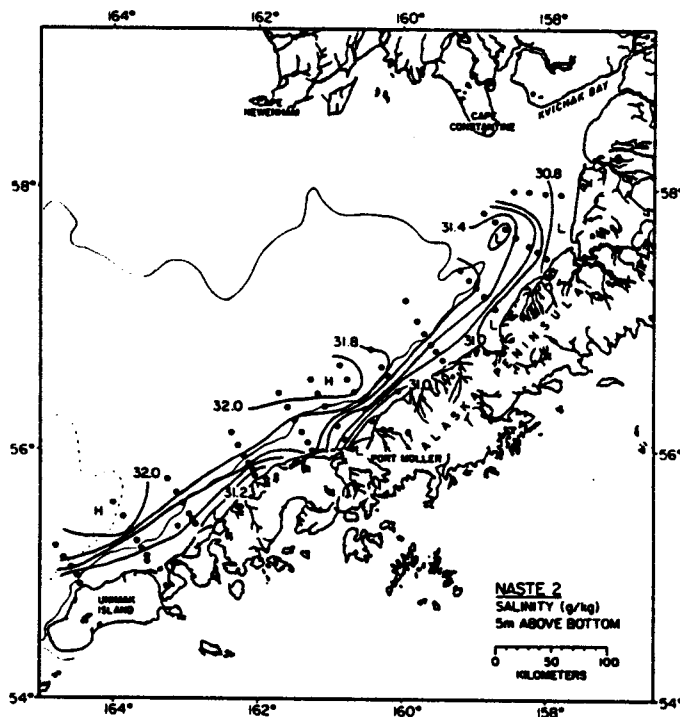
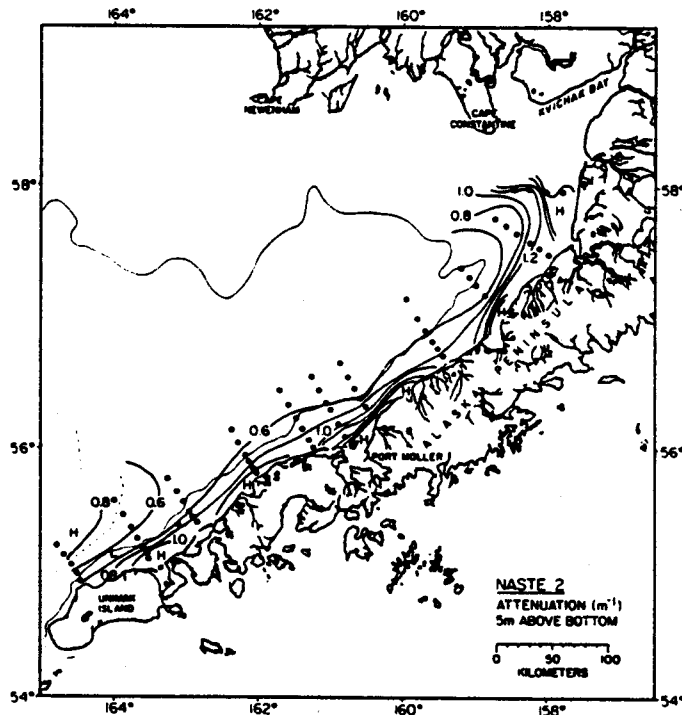


Figure 11. Areal maps of light attenuation (top) and salinity (bottom) at the bottom during January 1981. Contour interval is 0.2 m^{-1} for attenuation and 0.2 ‰ for salinity.

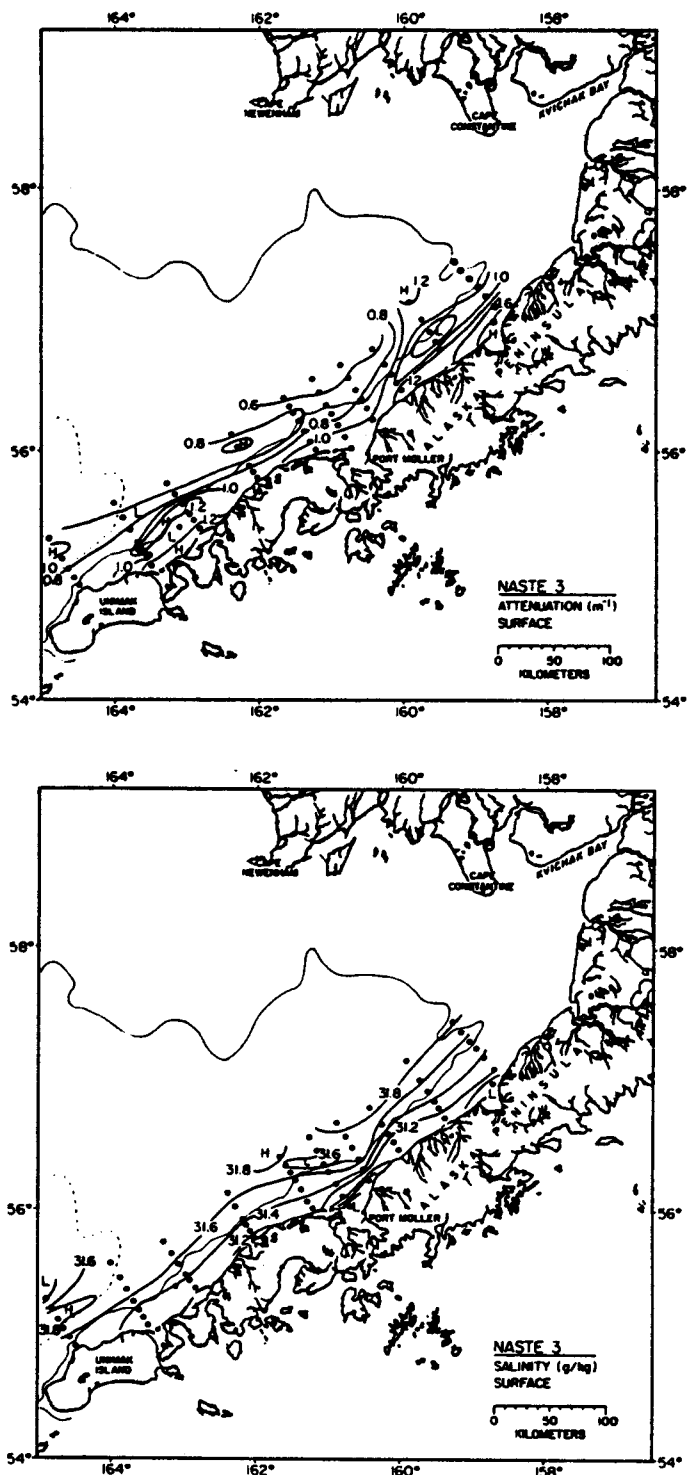


Figure 12. Areal maps of light attenuation (top) and salinity (bottom)₁ at the surface during May 1981. Contour interval is 0.2 m for attenuation and 0.2 ‰ for salinity.

The salinity distribution in the deep water (Fig. 13) again showed an intrusion of high salinity water from the west and a strict correlation between bathymetric and salinity isolines. Offshore gradients became very low seaward of ~50 m. Attenuation contours (Fig. 13) clearly described an SPM minimum zone along the 50-m isobath on every transect but the shallowest (the easternmost transect). This pattern was much more pronounced than during NASTE 1 and generally was not interrupted by isolated highs caused by resuspension.

The relationship between salinity and SPM concentrations in the surface waters of the North Aleutian Shelf region can be described by the use of a salinity vs. attenuation scatter plot analogous to the mixing diagrams used to trace the loss or addition of dissolved (Liss, 1976) or particulate (Baker, 1982) constituents in estuarine regions. During NASTE 1 and 3, correlations between attenuation and salinity were similar: $r \cong -0.56$ with a slope of -0.16 during NASTE 1 and -0.47 during NASTE 3 (Fig. 14). Salinity was a poor predictor of SPM concentration during these times, because particle sources other than freshwater runoff were important. These sources included resuspension and subsequent vertical mixing of particles into the surface waters (in the nearshore zone) and in-situ phytoplankton production.

The shape of the salinity-attenuation scatter plot was noticeably different during NASTE 2 (Fig. 14). Attenuation values fell rapidly with increasing salinity up to ~31.5‰; above that value very little change was observed in attenuation. The areal plots (Fig. 10) indicate that this point marks the transition between steep offshore gradients of attenuation landward of ~50 m and essentially uniform attenuation values to seaward.

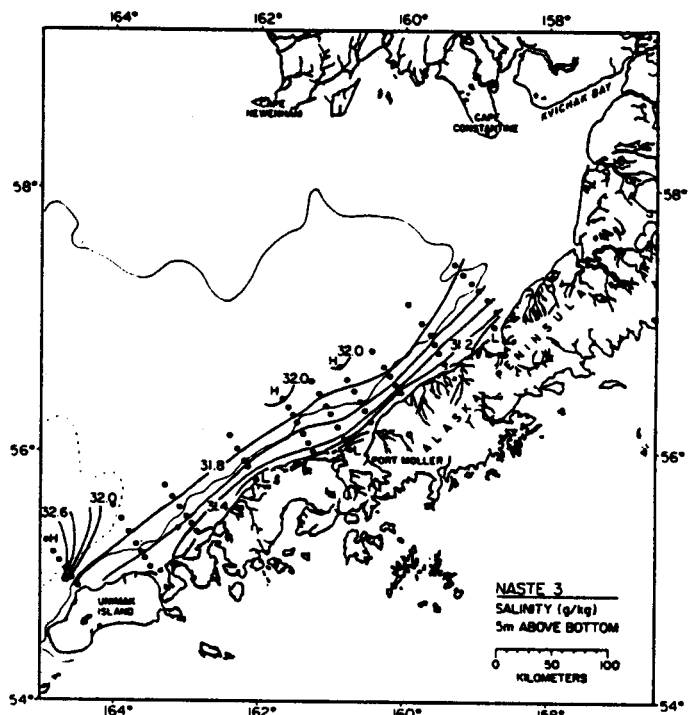
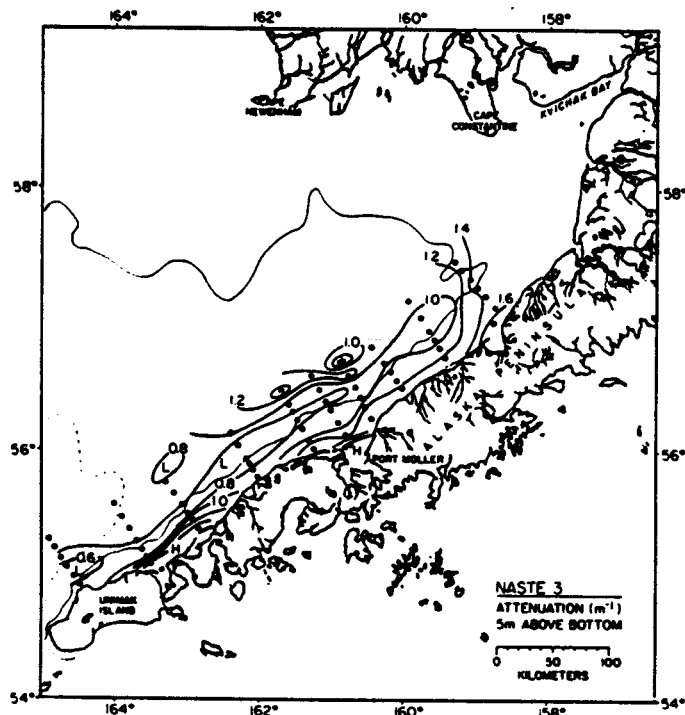


Figure 13. Areal maps of light attenuation (top) and salinity (bottom) at the bottom during May 1981. Contour interval is 0.2 m^{-1} for attenuation and 0.2 ‰ for salinity.

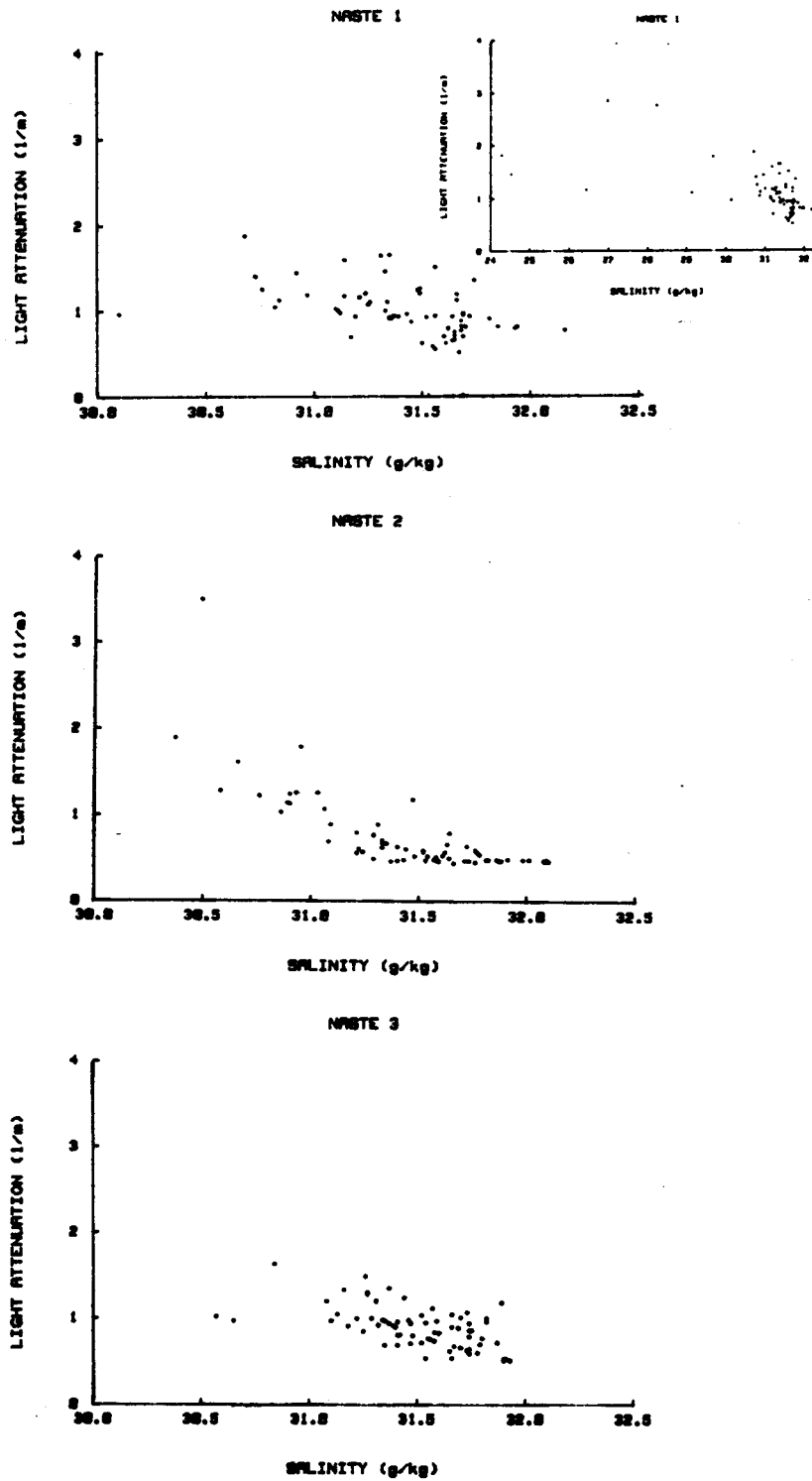


Figure 14. Light attenuation vs. salinity in the surface water at NA stations for (top) August 1980, (middle) January 1981, and (bottom) May 1981. Inset for NASTE 1 data shows the complete data set.

Seasonal changes in the average water column attenuation and salinity (based on 1-m averaged data from CTD casts at each NA station) in the NAS region were small. Attenuation decreased from $1.17 \pm 0.86 \text{ m}^{-1}$ during NASTE 1 to $0.97 \pm 0.90 \text{ m}^{-1}$ and 0.92 ± 0.25 during succeeding cruises. These means are identical at a significance level of 0.05 (Natrella, 1963). Salinity changes are also small and statistically non-significant, but it is instructive to note that the steady increase in salinity from NASTE 1 to 3 mirrored the decrease in attenuation, just as salinity was inversely proportional to attenuation during each cruise.

2. Density and SPM cross-sections

Vertical cross-sections for lines 1 (NA17-NA22), 2 (NA34-NA40), and 3 (NA47-NA52) normal to the Alaskan Peninsula (Fig. 1) were constructed from CTD casts on each cruise. These lines were chosen to reflect SPM conditions in different sections of the NAS study area.

Density cross-sections during NASTE 1 (Figs. 15, 16, and 17) typically showed isopycnals sloping landward, indicative of a weakly stratified two-layer system. Horizontal σ_t contours were found only at the westernmost line, where a reverse slope to the isopycnals clearly indicated an intrusion of relatively dense, deep water as close to shore as the 30-m isobath. Inshore stations on lines 2 and 3 showed nearly complete vertical mixing, whereas the density profile at Station NA22 on line 1 showed a prominent gradient due to freshwater influence from rivers in the Kvichak Bay area.

SPM distributions (Figs. 15, 16, and 17) closely followed the observed density pattern. Sites of strong horizontal density gradients on lines 1 (Station NA20), 2 (Station NA37), and 3 (Station NA51), were also sites of strong horizontal SPM gradients. Landward of these points, SPM contours

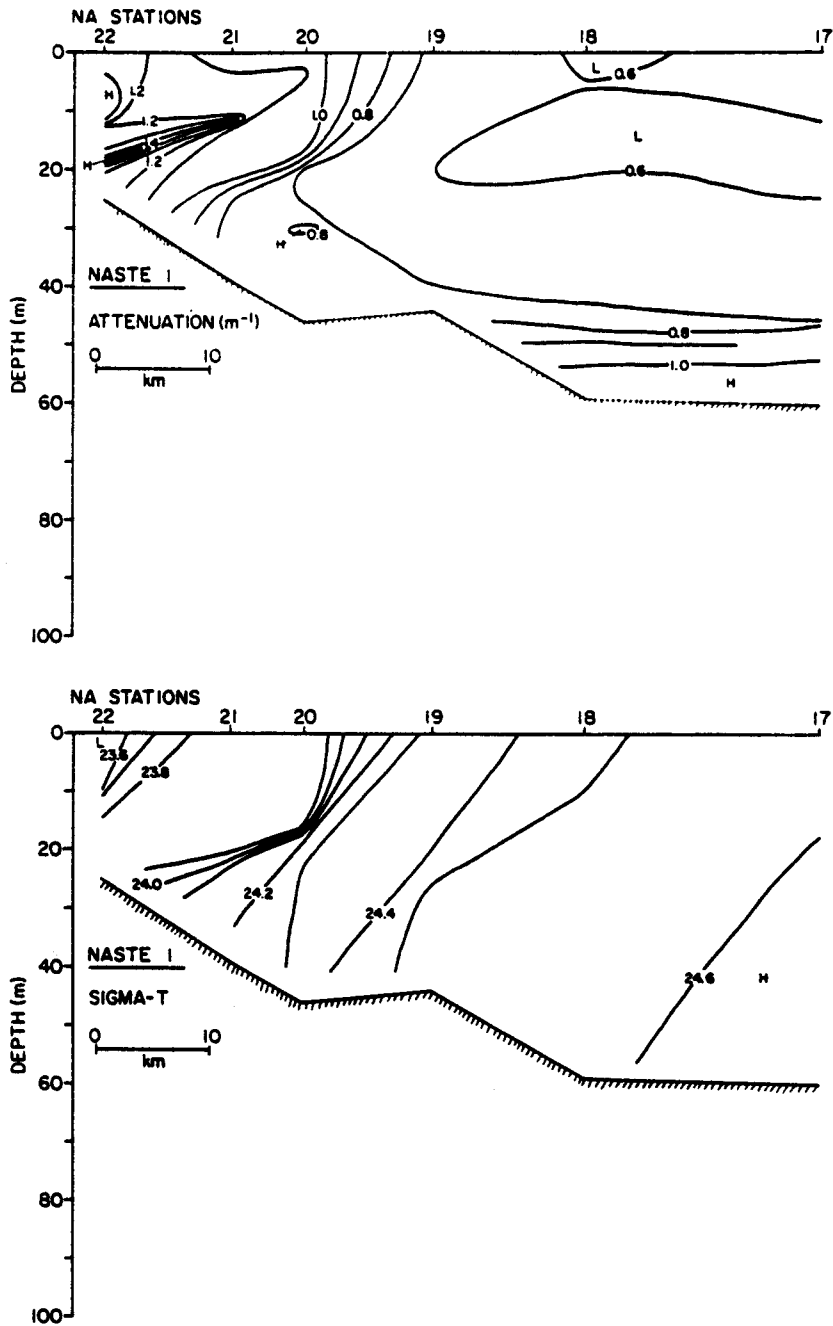


Figure 15. Attenuation (top) and density (bottom) cross-sections for line 1 (stations NA17-22), August 1980.

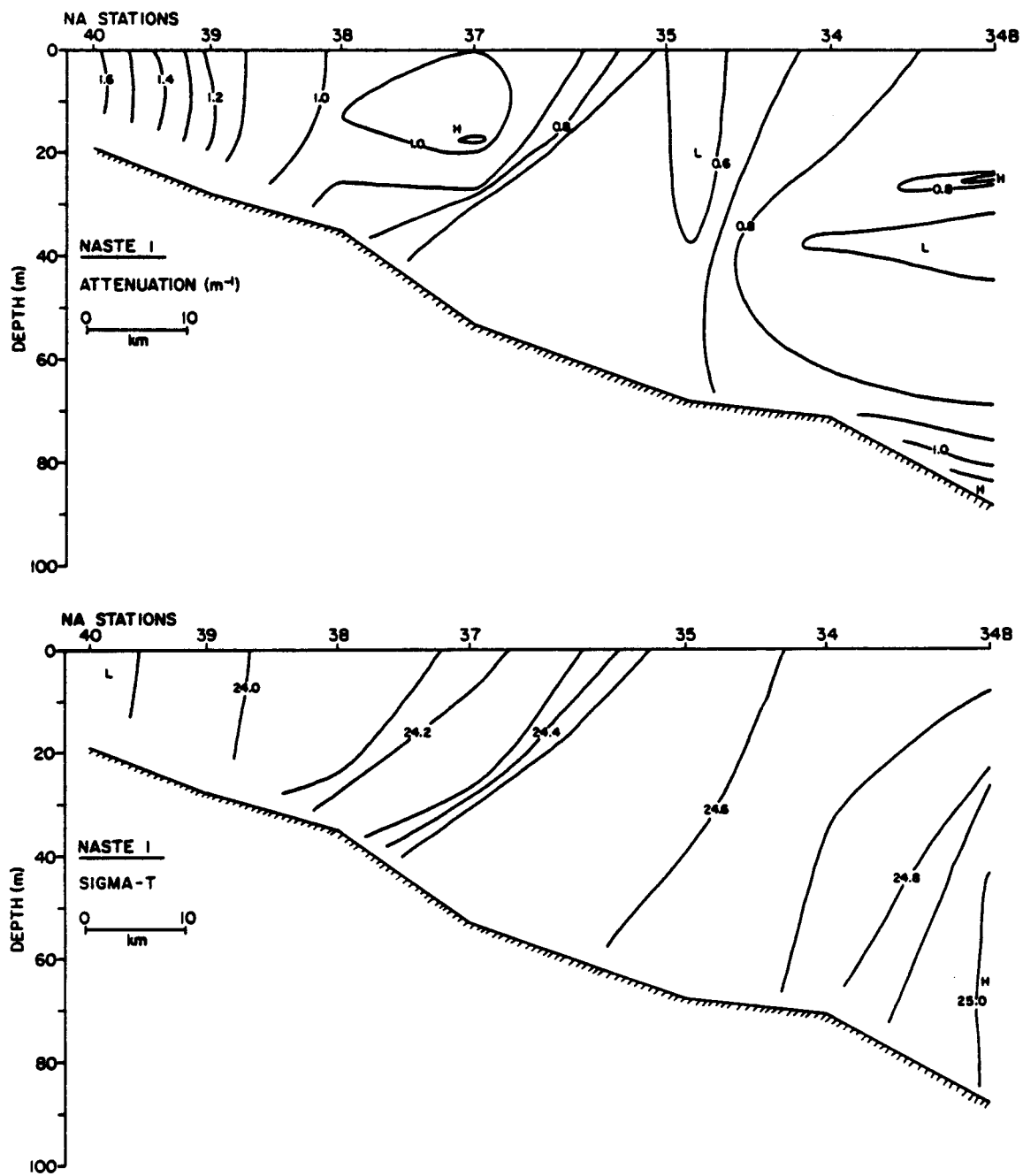


Figure 16. Attenuation (top) and density (bottom) cross-sections for line 2 (stations NA34-40), August 1980.

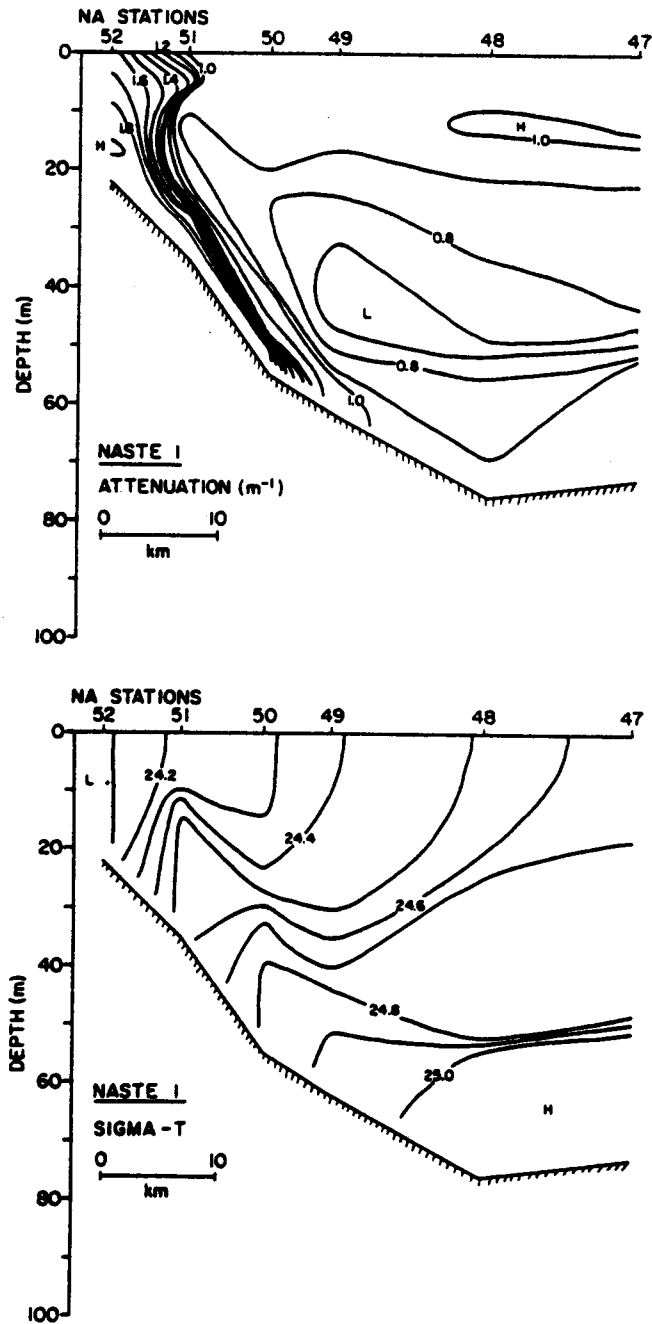


Figure 17. Attenuation (top) and density (bottom) cross-sections for line 3 (stations NA47-52), August 1980.

followed the trend of the σ_t contours, becoming vertically mixed on lines 2 and 3 and vertically stratified on line 1. Seaward of Stations NA20, NA37, and NA51 (i.e., ~the 40-m isobath), the vertical SPM distributions became typical of nearly all offshore stations in the study area. A strong three-layer distribution was well developed; a horizontally uniform mid-depth minimum zone separated horizontally variable layers of higher turbidity in the surface and bottom waters. This distribution is characteristic of the middle domain (Kinder and Schumacher, 1981a) in the southeastern Bering Sea. Line 3 was particularly interesting because it showed an excellent example of relatively clear deep water intruding along the seafloor until blocked by the coastal front produced by strong tidal mixing of water and particulates in the near-shore zone. High attenuation values in the near-bottom waters at Stations NA49, NA50, and NA51 were presumably due to resuspended sediment trapped in a thin bottom nepheloid layer below the intruding deep water.

Conditions during the winter cruise, NASTE 2, were significantly different both for density and SPM distributions (Figs. 18, 19, and 20). Density stratification was weak or absent throughout the region; only line 2, off Port Moller, showed signs of freshwater input in the density structure. SPM distributions were also generally unstratified. Absence of the middle domain stratification characteristics to at least a depth of 80 m resulted in a vertically uniform SPM distribution on all lines.

Late spring (NASTE 3) was a return to a period of strong vertical stratification throughout the study area (Figs. 21, 22, and 23). A surface mixed layer ~10 m thick was present along each line, separated from the underlying waters by 0.2 - 0.4 σ_t units at the offshore stations. Tidal mixing produced vertically homogeneous water landward of about 30 m.

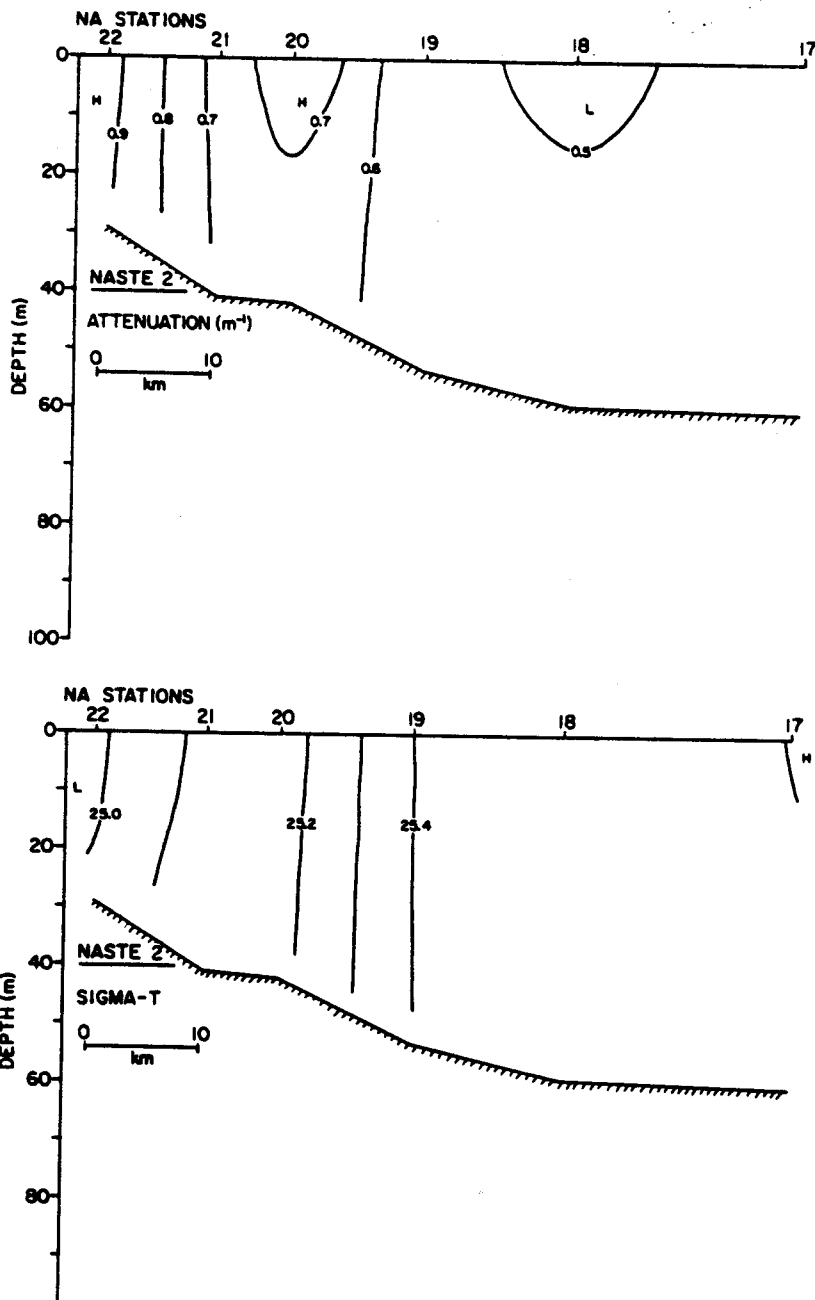


Figure 18. Attenuation (top) and density (bottom) cross-sections for line 1 (stations NA17-22), January 1981.

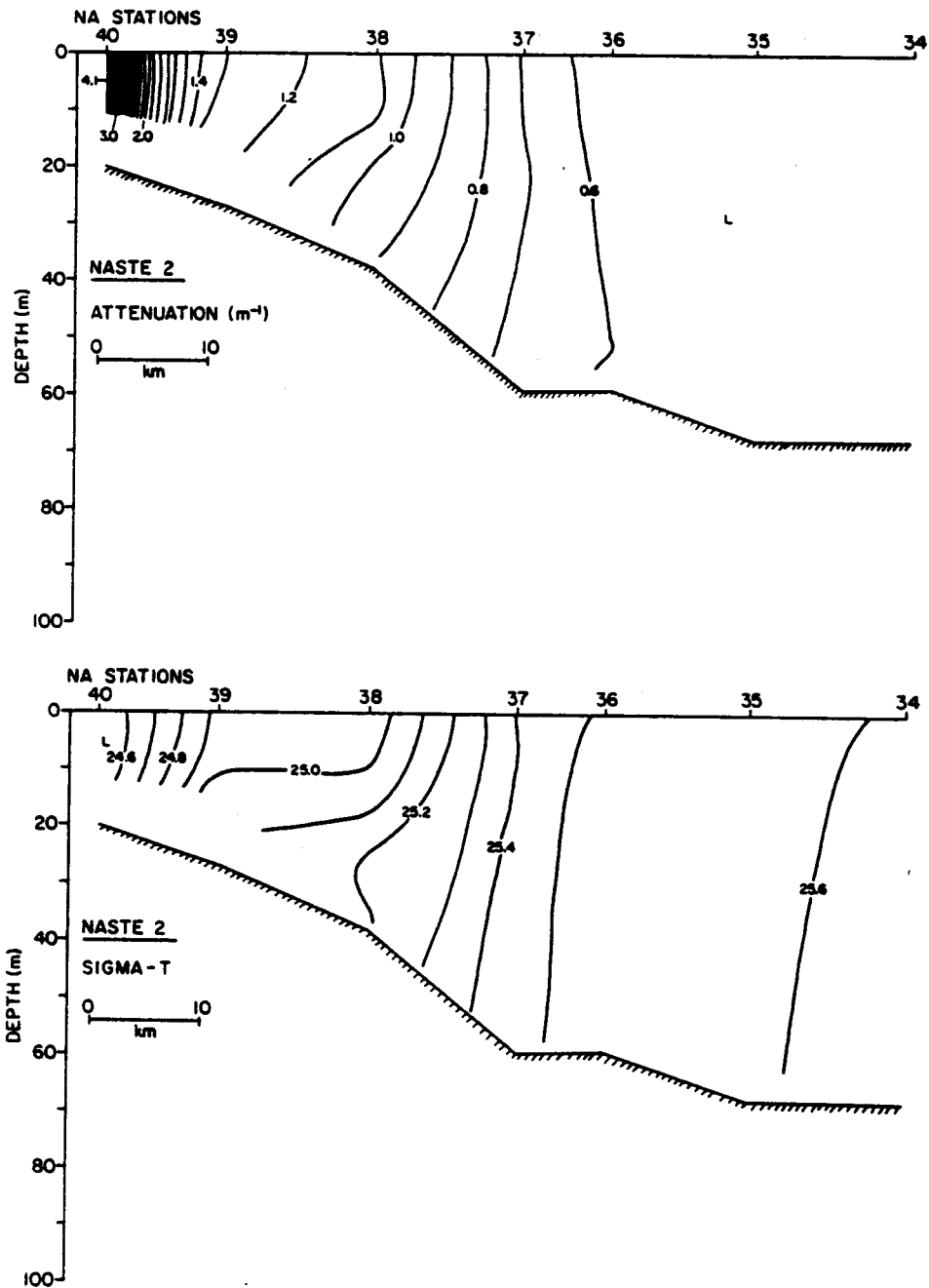


Figure 19. Attenuation (top) and density (bottom) cross-sections for line 2 (stations NA34-40), January 1981.

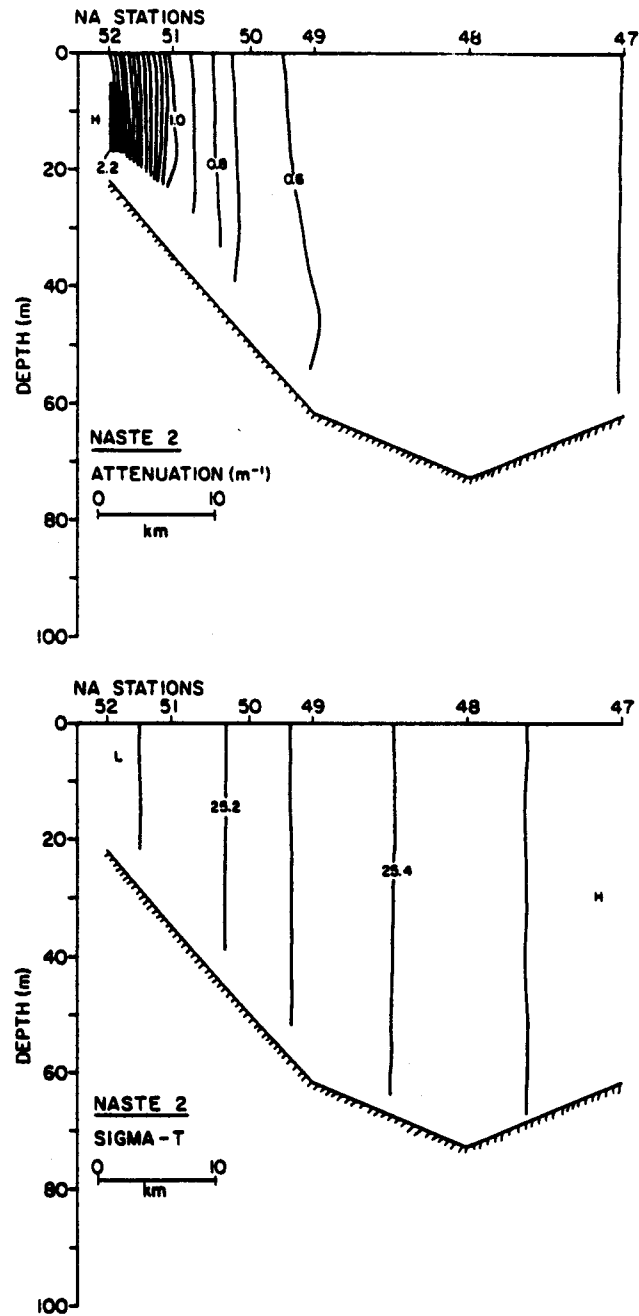


Figure 20. Attenuation (top) and density (bottom) cross-sections for line 3 (stations NA47-52), January 1981.

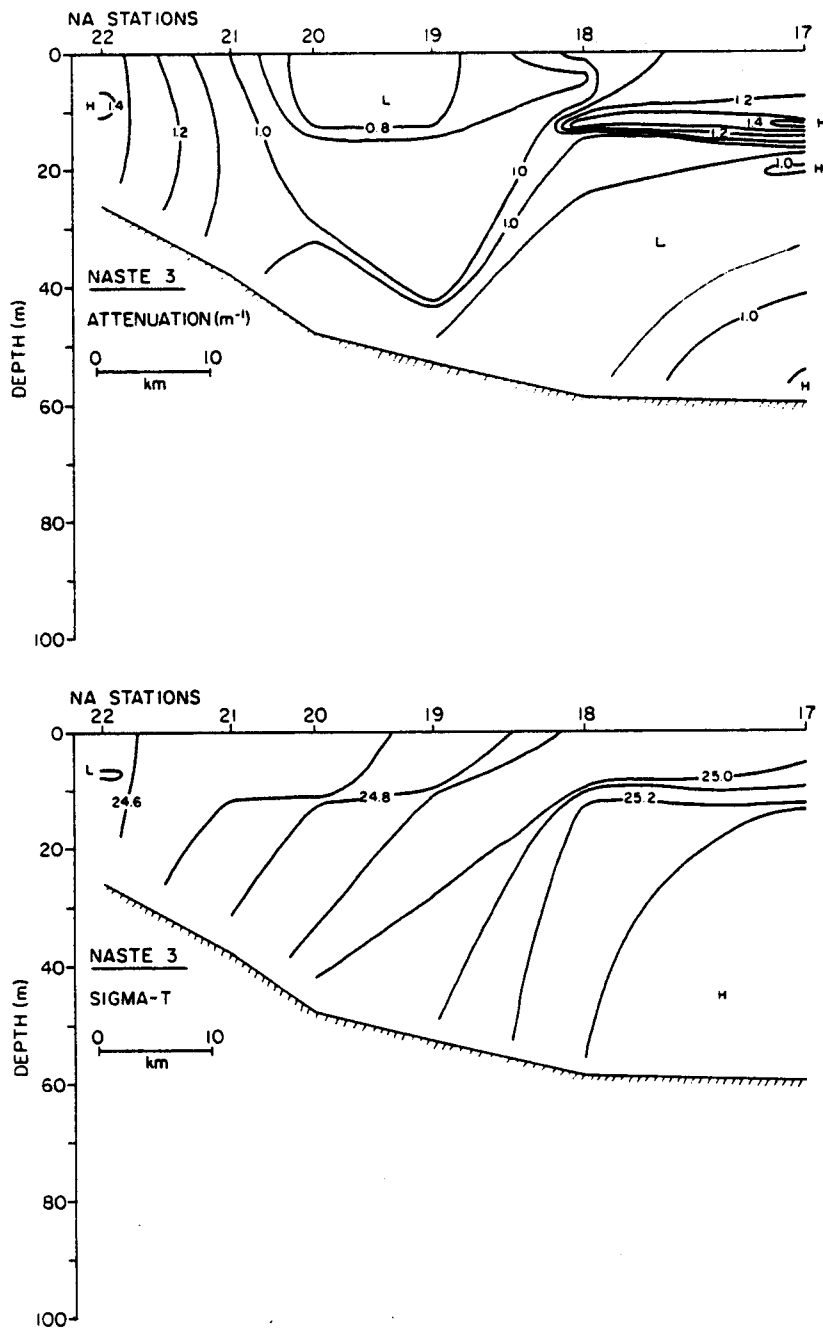


Figure 21. Attenuation (top) and density (bottom) cross-sections for line 1 (stations NA17-22), May 1981.

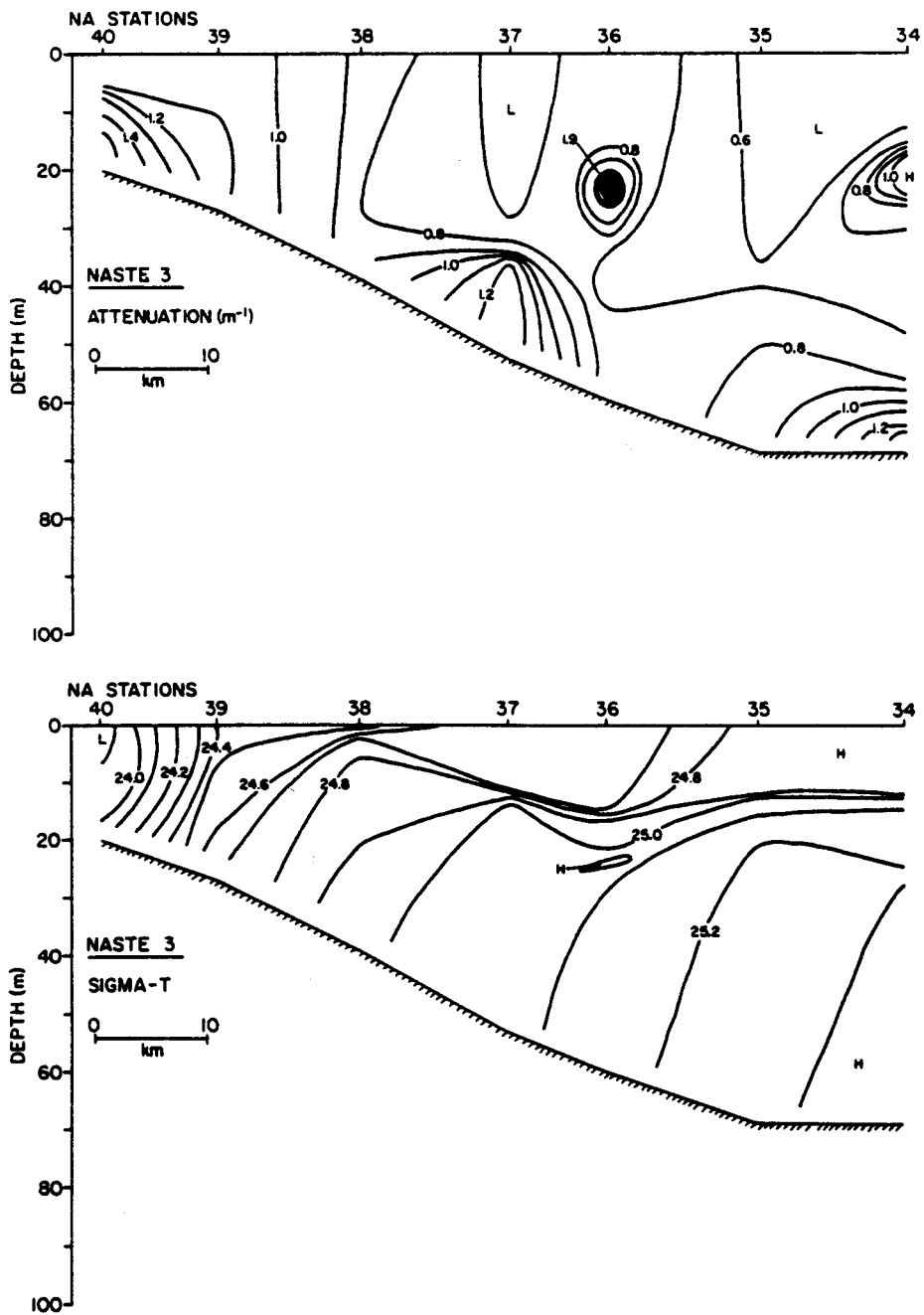


Figure 22. Attenuation (top) and density (bottom) cross-sections for line 2 (stations NA34-40), May 1981.

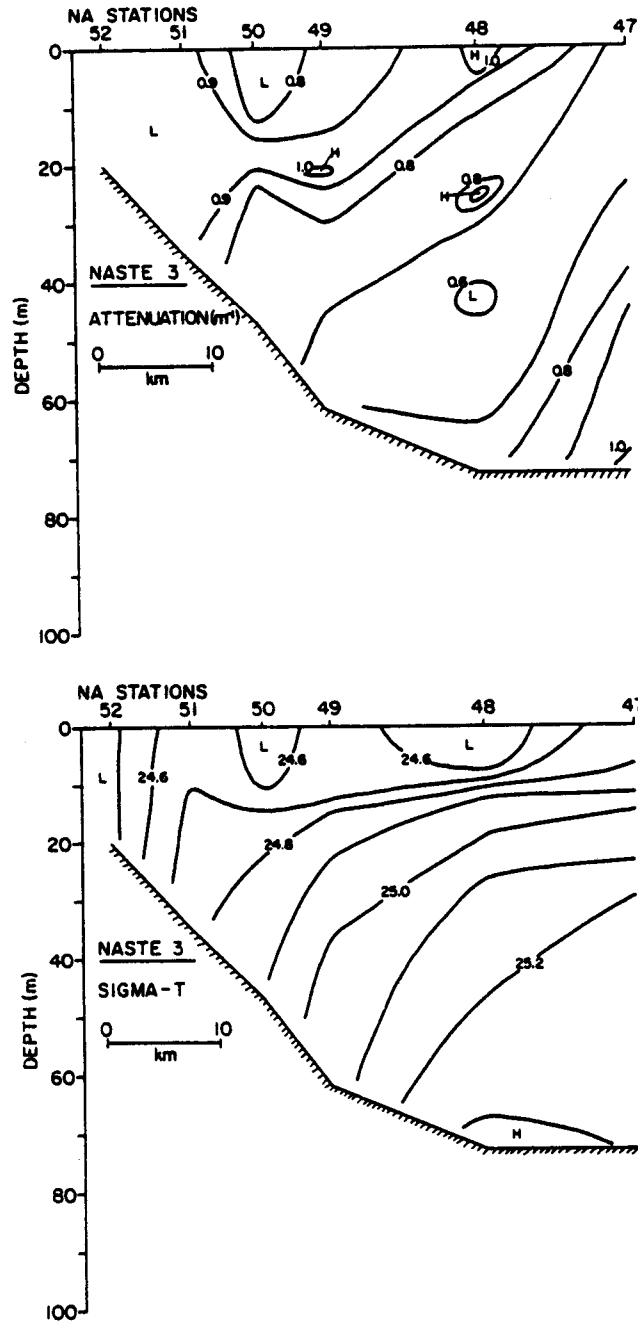


Figure 23. Attenuation (top) and density (bottom) cross-sections for line 3 (stations NA47-52), May 1981.

Beneath the surface mixed layer, σ_t contours dipped steeply landward.

SPM distributions were controlled by the strong pycnocline, weak stratification below the pycnocline, and inshore tidal mixing. Stations where the pycnocline was strongest (NA18, NA17, NA36, and NA34) had intense SPM maxima at the bottom or just below the surface mixed layer. Based on information from particle size distributions and phytoplankton pigment concentrations, these subsurface highs were produced by in-situ phytoplankton growth.

Weak stratification below the pycnocline allowed bottom resuspension to produce a thick nepheloid layer. The mid-depth minimum typical of NASTE 1 was only found along line 3 where vertical stratification below the pycnocline was slightly greater than along lines 1 and 2.

Inshore vertical density stratification was almost nonexistent on lines 1 and 3, and attenuation values were likewise vertically uniform. Freshwater input from Port Moller produced weak stratification at stations NA40 and NA39 (line 2) and induced a similar stratification in attenuation, by preventing the upward mixing of resuspended sediments.

In a highly energetic region such as the North Aleutian Shelf, instantaneous occupations of a station line may be unrepresentative of the "average" conditions typical of an entire season. Transient weather conditions may completely interrupt the seasonal pattern of hydrographic structure and SPM distribution. For these reasons, certain transects were occupied several times during the NASTE 1, 2, and 3 cruises in order to gauge the magnitude of short-term variability in the particle distributions. During NASTE 1, line NA34-NA40 was traversed during the following (GMT) times (Fig. 24): 20 Aug. 1308-2139, 24 Aug. 0706-1436, and 31 Aug. 1702 - 1 Sept. 0010. An adjacent transect, line NA41-NA46, was occupied four separate times (Figs. 25

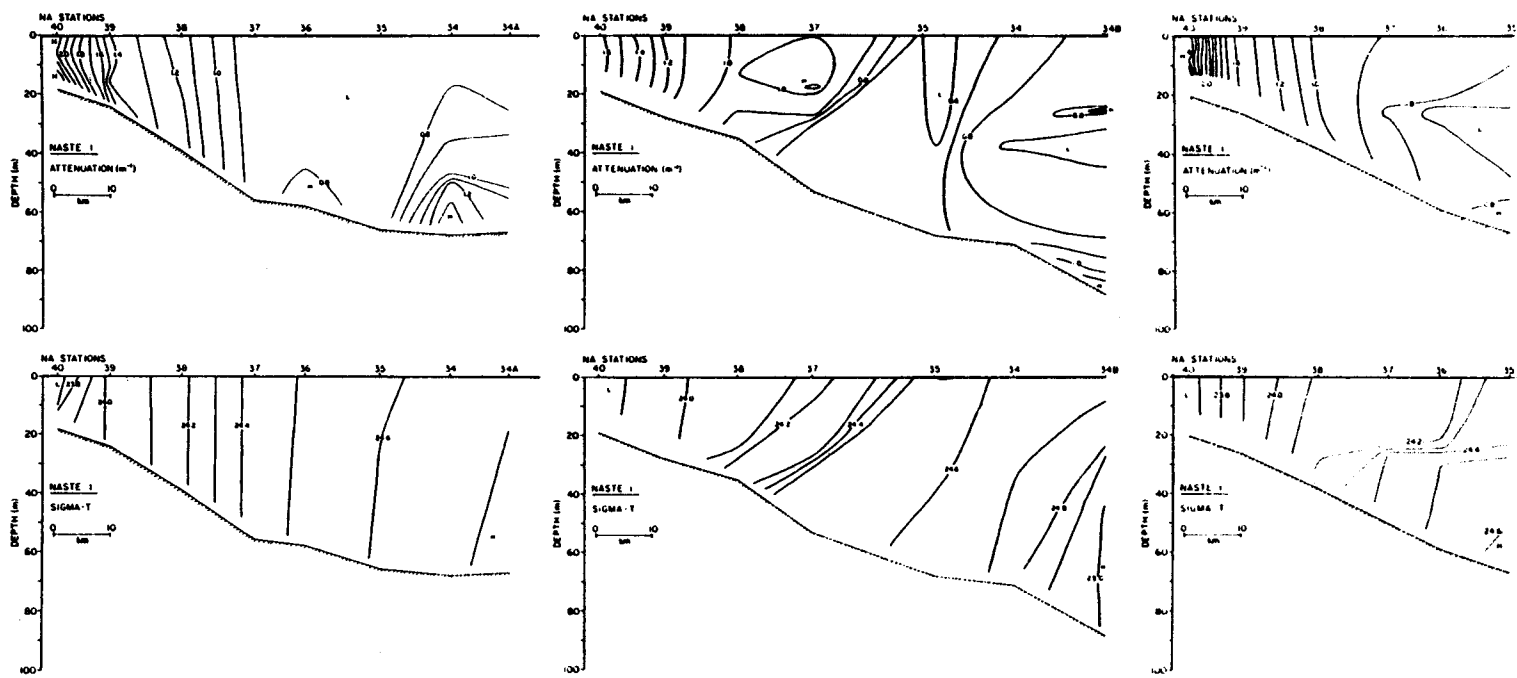


Figure 24. Attenuation (top) and density (bottom) cross-sections for stations NA34-40 on August 20 (left), August 24 (middle), and August 31, 1980 (right).

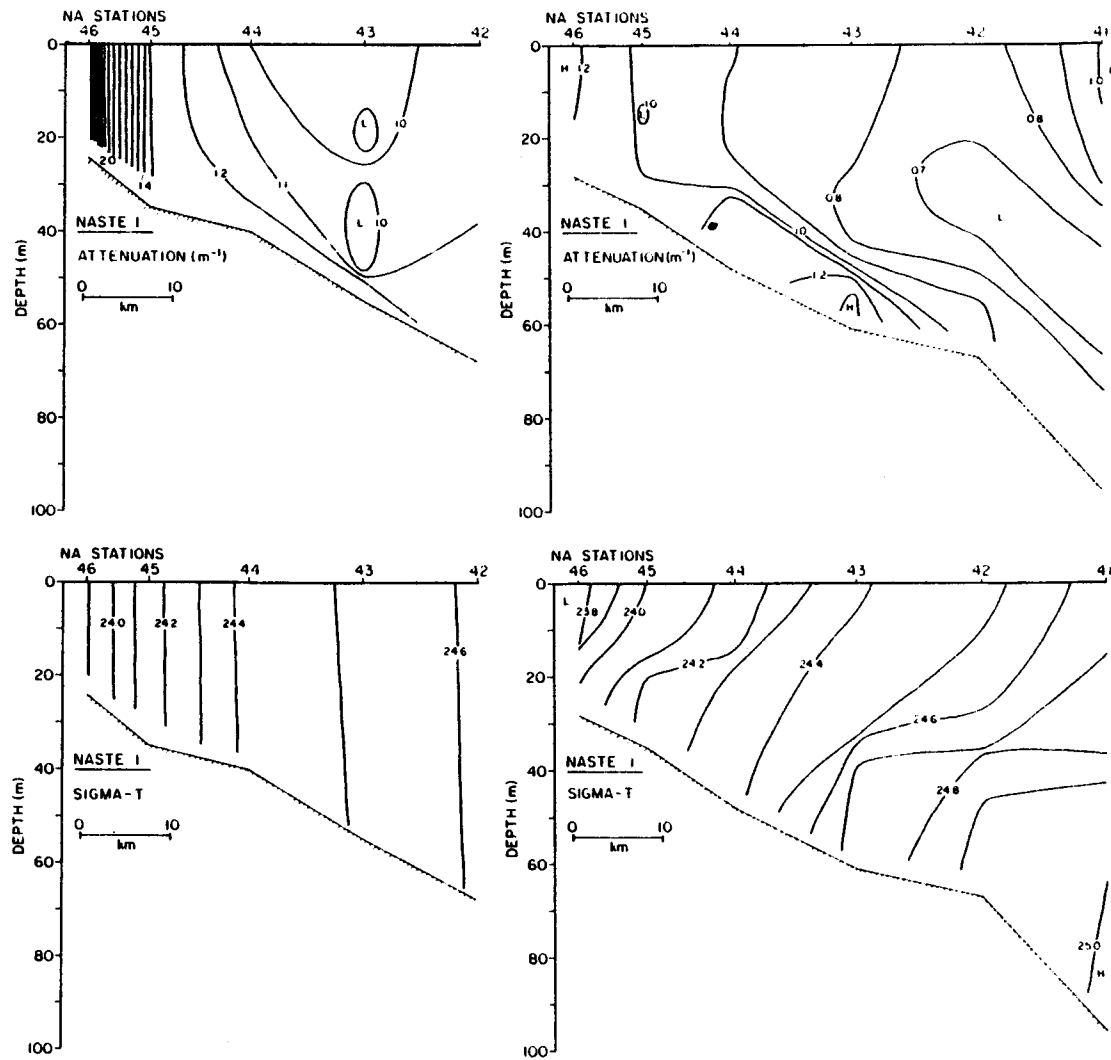


Figure 25. Attenuation (top) and density (bottom) cross-sections for stations NA41-46 on August 19 (left), and August 24, 1980 (right).

and 26): 19 Aug. 0655-1344, 24 Aug. 1740-2354, 31 Aug. 0709-1225, and 2 Sept. 2009 - 3 Sept. 0035. During NASTE 2 line NA34-NA40 was occupied twice (Fig. 27): 31 Jan. 0330-1200 and 8 Feb. 1323-1945. During NASTE 3 line NA41-NA46 was occupied three times (Fig. 28): 15 May 0147-1135, 25 May 0420-1042, and 30 May 1237-1815.

The only significant short-term perturbations were noted during NASTE 1 as the result of a brief storm which destroyed the front separating the coastal and middle shelf hydrographic domains (Pearson et al., 1980). On 17-18 Aug. 1980 the remnant of typhoon MARGE passed through the study area with winds in excess of 30 m sec^{-1} . Transects run the following day (Figs. 24 and 25) showed that the density field was vertically homogeneous at least out to the 60-m isobath, with very weak stratification in deeper water. SPM contours were also vertical out to $\sim 40 \text{ m}$; beyond that depth values increased from surface to bottom as a result of gravitational settling and resuspension. Transects occupied subsequently document the reestablishment of the frontal and domain characteristics typical of late summer. Prior to the 24 Aug. transects, a period of moderate ($5\text{-}10 \text{ m sec}^{-1}$) northeasterly winds appeared to drive an offshore Ekman flux, resulting in vertical density and SPM stratification as far inshore as the 20-m isobath. At this time, however, stratification was best developed in waters deeper than $\sim 60 \text{ m}$ where a prominent SPM minimum had developed in association with the maximum density gradient. By the 31st of August, increasingly strong tides had firmly reestablished the well-mixed coastal domain and the inner front separating it from the two-layer middle domain (Figs. 24 and 26). SPM distribution in the middle domain showed the typical mid-depth minimum zone separating the well-mixed surface layer from the resuspension-induced BNL. The thickness of the BNL was controlled by the thickness of the bottom-mixed

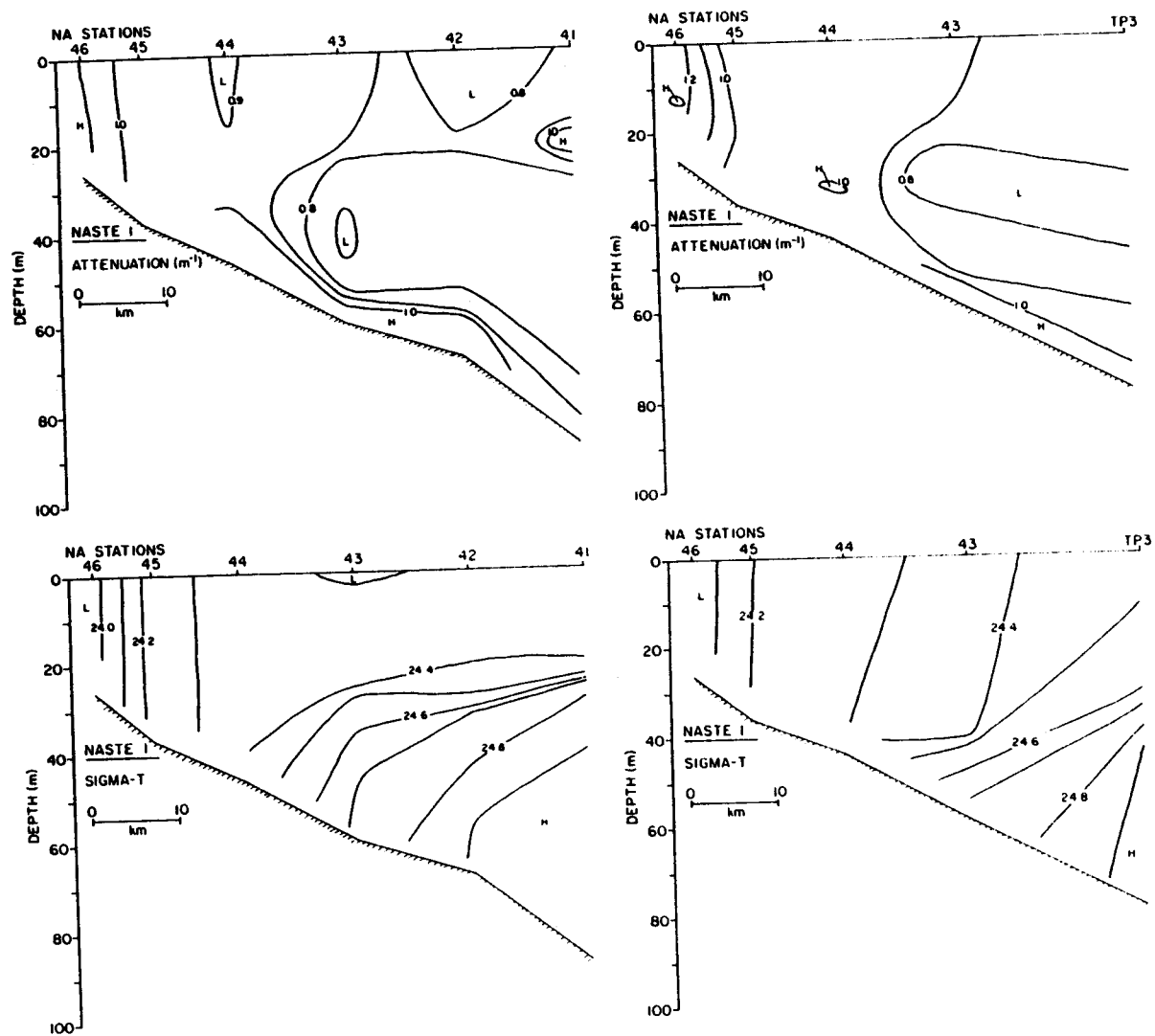


Figure 26. Attenuation (top) and density (bottom) cross-sections for stations NA41-46 on August 31 (left), and September 2, 1980 (right).

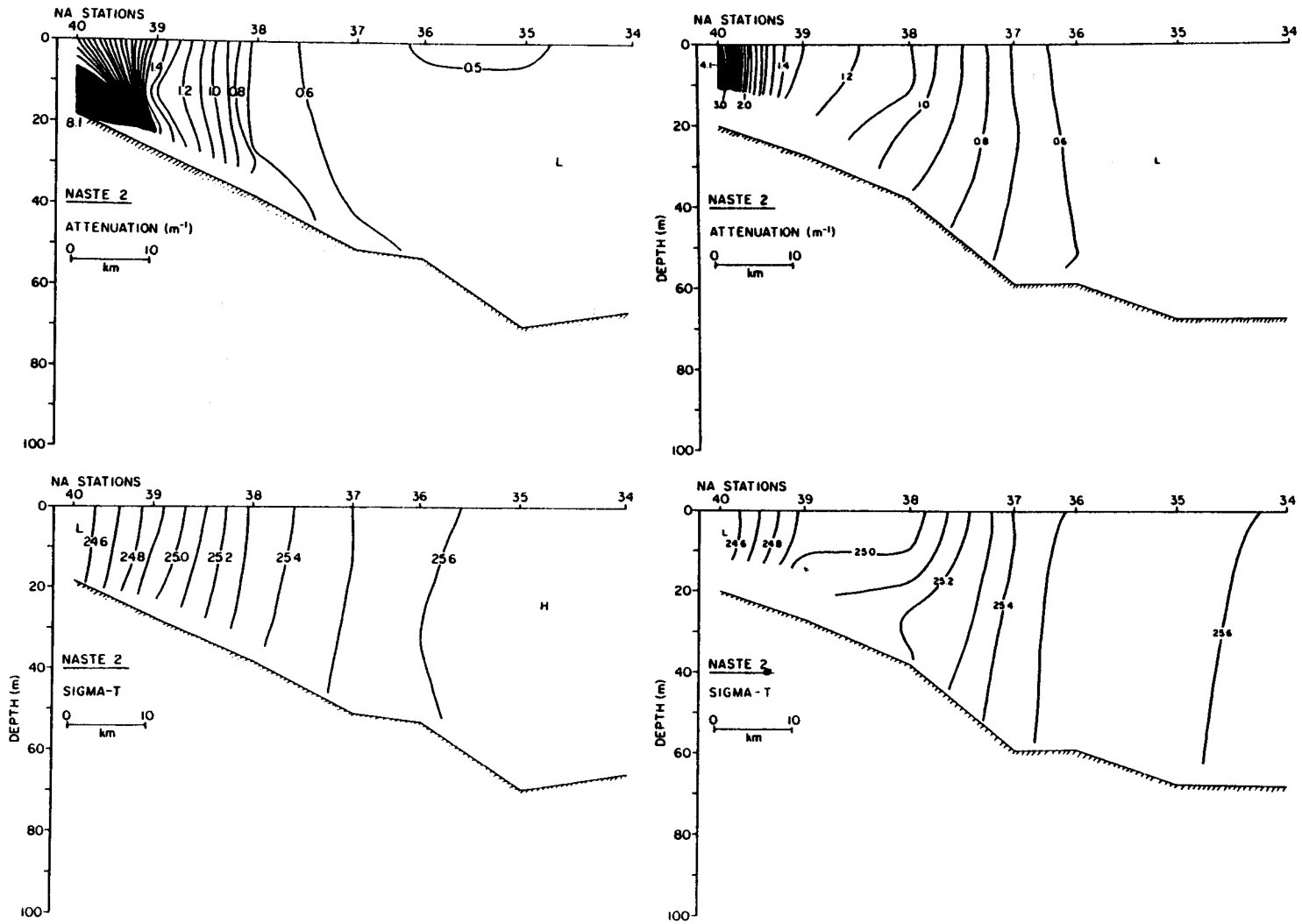


Figure 27. Attenuation (top) and density (bottom) cross-sections for stations NA34-40 on January 31 (left), and February 8, 1981 (right).

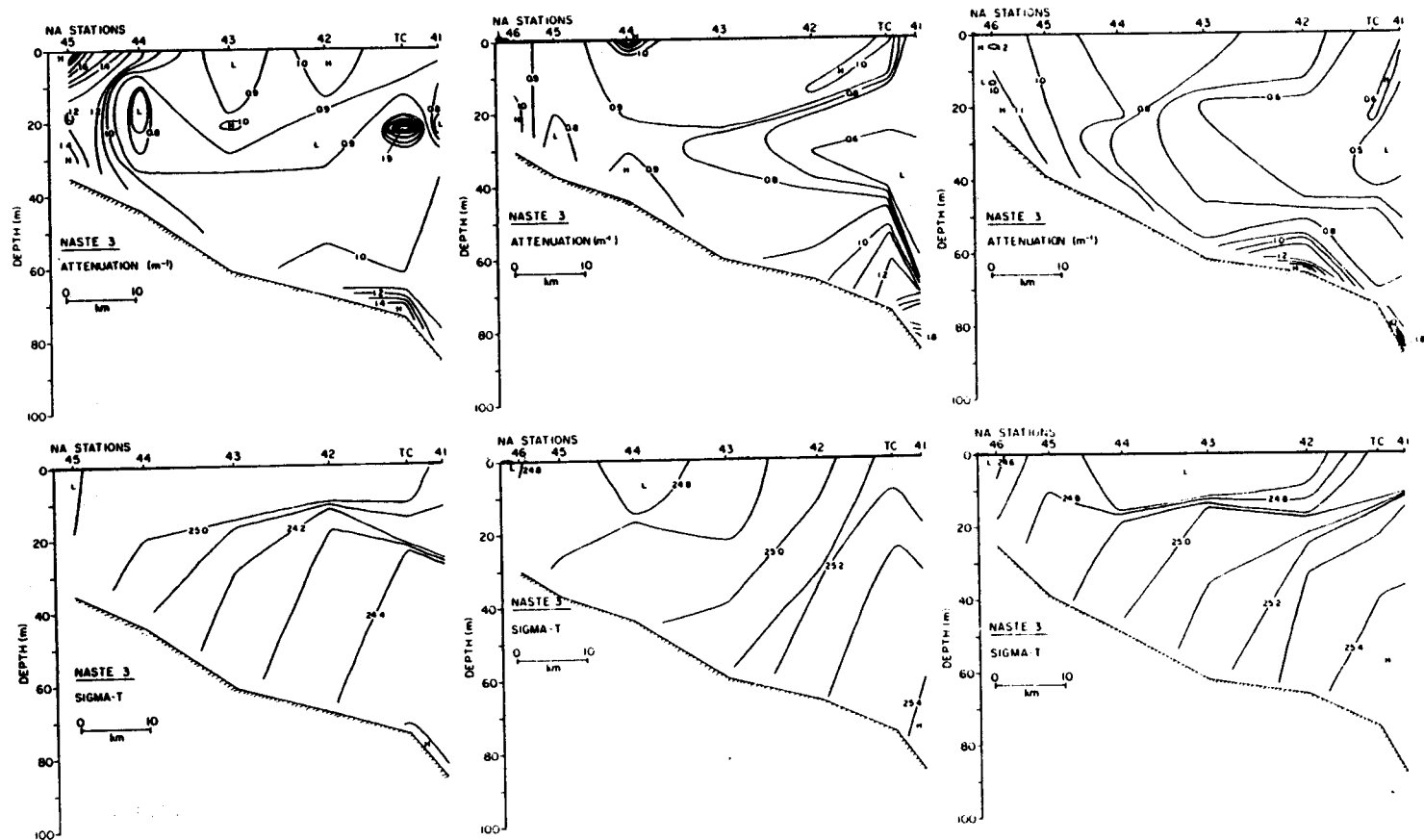


Figure 28. Attenuation (top) and density (bottom) cross-sections for stations NA41-45 on May 15 (left), May 25 (middle), and May 30, 1981 (right).

layer, which was generally greater along the NA40-NA34 line than along the NA41-NA46 line. Line NA41-NA46 was occupied a final time on 2 Sept. and found basically unchanged (Fig. 26).

Winter conditions along the NA34-NA40 line were found to be quite uniform on the scale of a week (Fig. 27). Density stratification was minimal except for just offshore of Port Moller where freshwater outflow caused a low density surface plume and higher attenuation values during the second occupation. Although the general structure of the density and SPM distributions remained constant throughout NASTE 3, the attenuation levels of individual stations showed high variability. During all three occupations of the NA41-NA46 line, a well-developed SPM mid-depth minimum zone was present seaward of Station NA45. Near-bottom attenuation values were always highest at the inner and outer ends of the transect, in good agreement with the regional pattern evident in the areal plot (Fig. 13). The surface layer showed numerous isolated high and low attenuation zones which were largely attributable to phytoplankton patchiness.

3. Particle size distributions

The particle size distribution (PSD) data from the North Aleutian Shelf area are summarized by reference to the NA34-NA40 station line. Variations along other transects during each cruise closely followed the changes observed along the NA34-NA40 line.

Data from NASTE 1 (Fig. 29A and B) indicated good agreement between PSD curves from surface and bottom waters. Slopes averaged 3.24 ± 0.55 in the surface water and 3.35 ± 0.50 5 m above bottom. Intercept values averaged 4.8×10^5 and 3.9×10^5 for surface and bottom samples. The inshore station, NA40, clearly showed the effects of fine-grained particle sources supplied

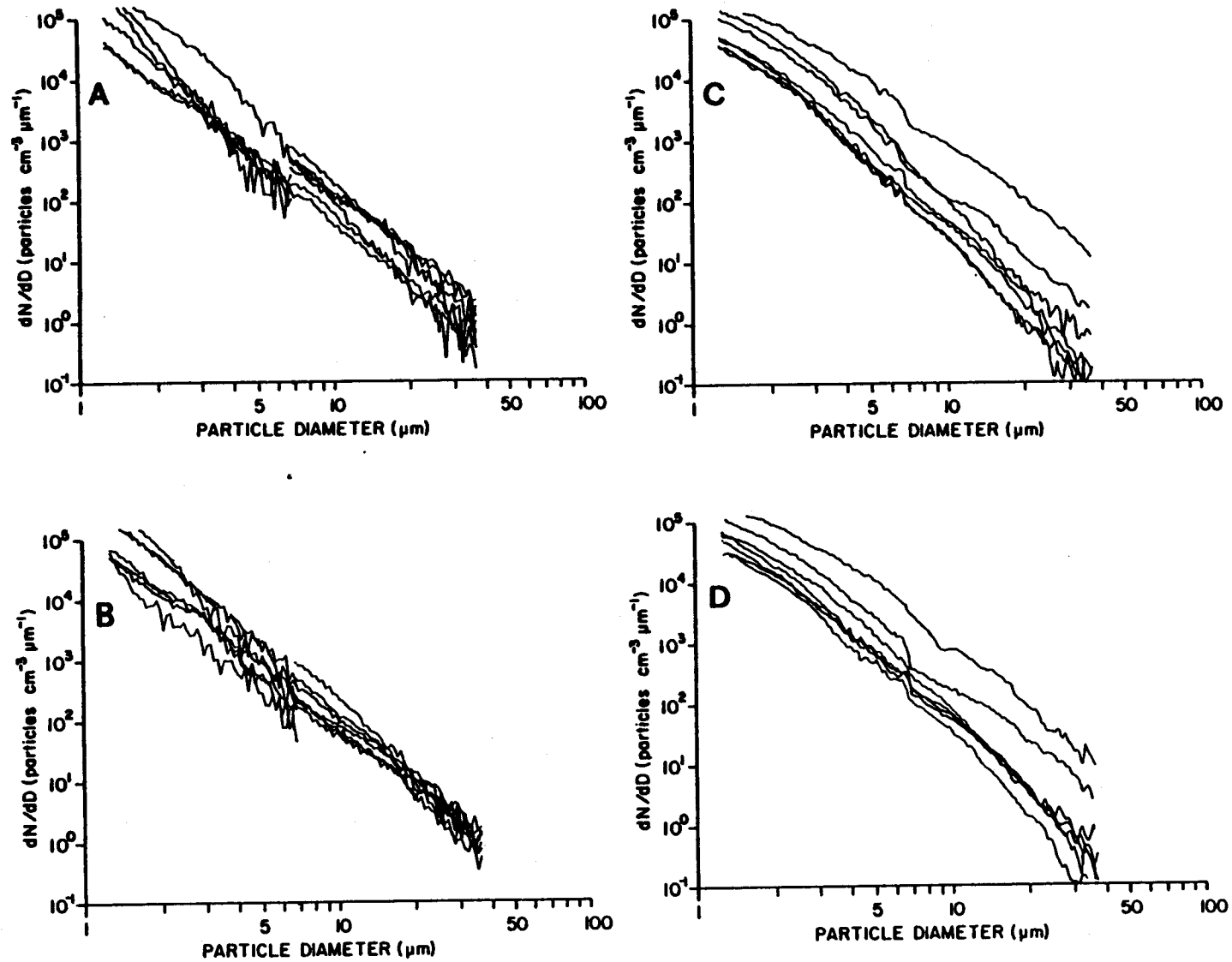


Figure 29. Incremental cumulative curves for particle populations along the NA34-40 station line from surface (A) and bottom (B) samples from NASTE 1, and surface (C) and bottom (D) samples from NASTE 2.

from the adjacent lagoon environment: the slope and intercept for the surface water sample were 4.16 and 27.0×10^5 , indicative of a turbid, fine-grained particle population.

PSD curves from NASTE 2 (Fig. 29C and D) show the influence of strong horizontal and weak vertical gradients in both density and SPM concentration typical of winter conditions. The family of curves for each depth horizon are virtually identical, while variation within each horizon is much greater than at any particular station. Particle populations in both surface and bottom waters became more turbid and relatively coarser grained progressing inward from Station NA34. Slope and intercept for surface and 5 mab at NA34 were 4.08, 3.1×10^5 and 3.74, 3.1×10^5 , respectively. These values are relatively steady seaward of ~50 m (NA37); landward of this position horizontal density and attenuation gradients increased markedly. By NA40, slope and intercept values for surface and 5 mab were 3.10, 14.2×10^5 and 3.24, 17.7×10^5 , significantly different than the surface and bottom averages for the entire line: 3.87 ± 0.41 , 7.6×10^5 and 3.69 ± 0.32 , 5.1×10^5 .

The different conditions prevailing between NASTE 1 and 2 can be illustrated by comparing the individual inshore and offshore stations from each cruise (Fig. 30). Landwardmost and seawardmost stations during NASTE 1 were virtually indistinguishable from each other at the coarse end of the particle size spectrum and gradually diverged towards the fine-grained end. That is, the slope of the PSD curves was highest for the inshore station. The same stations during NASTE 2 showed far greater between-station than within-station variability.

Surface-bottom differences in the particle populations were also observed during NASTE 3 (Fig. 31). Horizontal variability in slope and

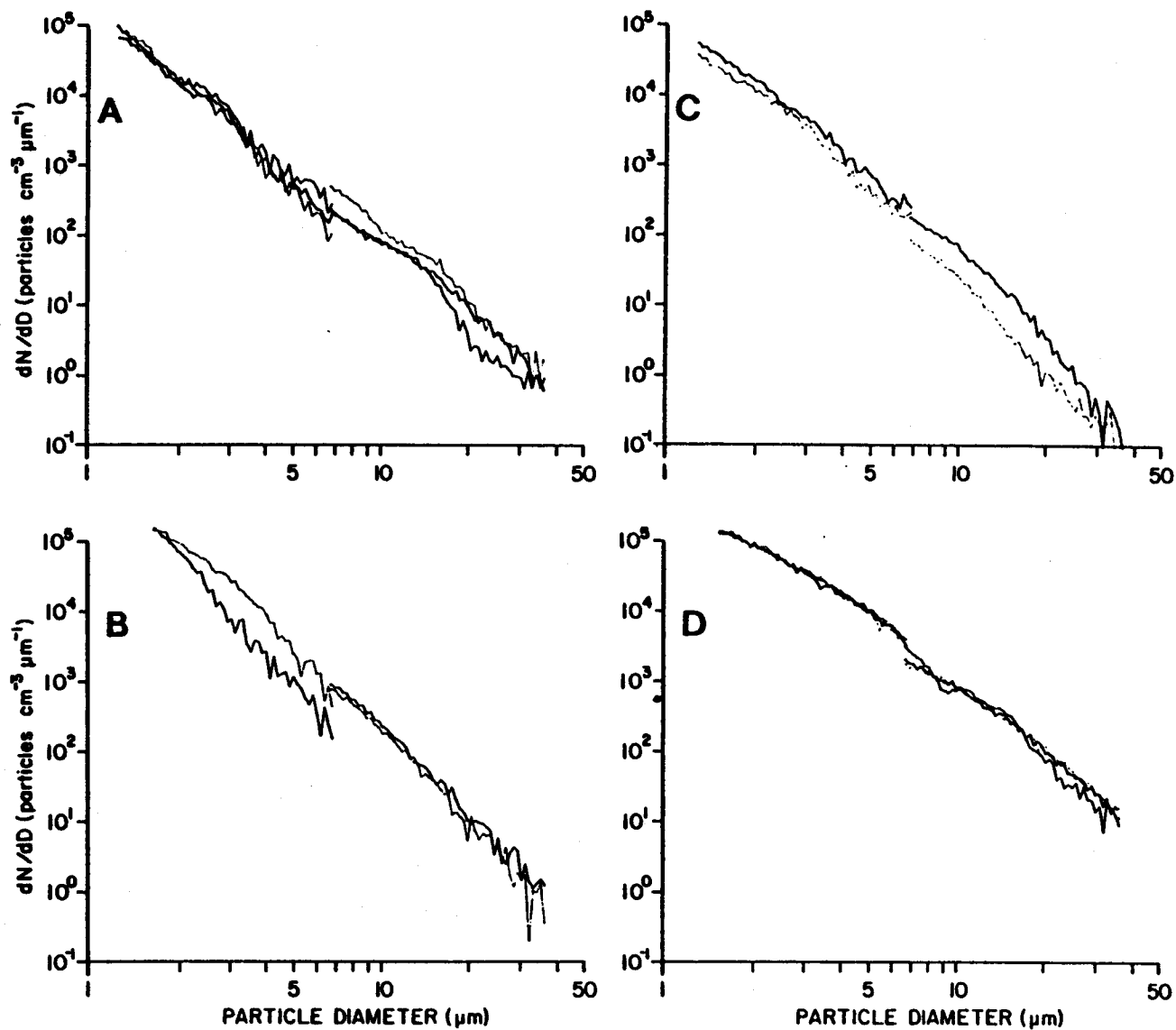


Figure 30. Incremental cumulative curves for particle populations at (A) an offshore station (NA34) and (B) an inshore station (NA40) during NASTE 1, and offshore (C) and inshore (D) stations during NASTE 2.

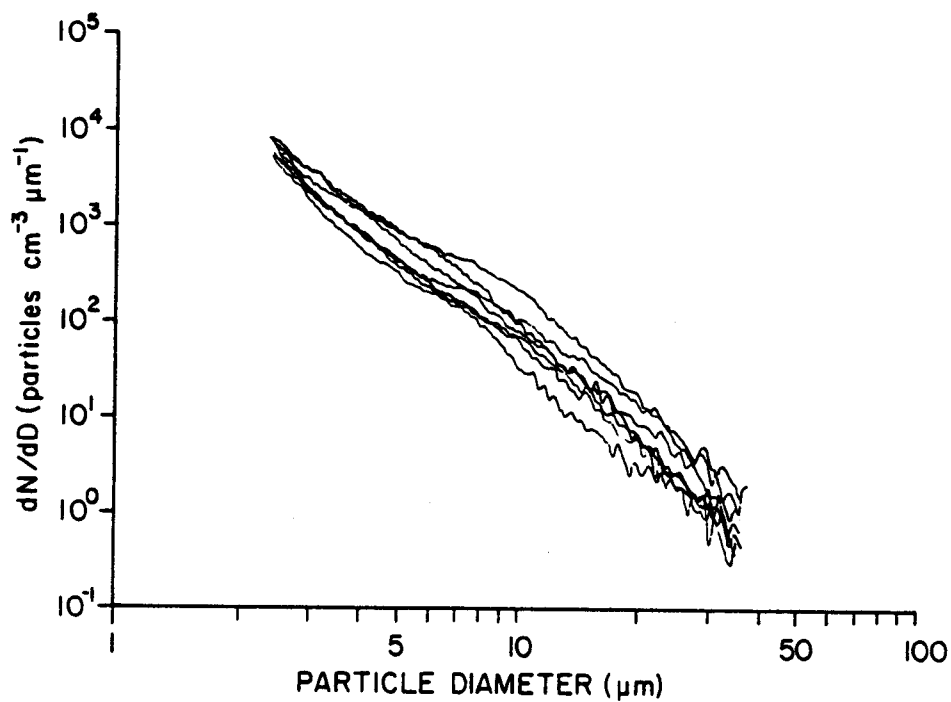
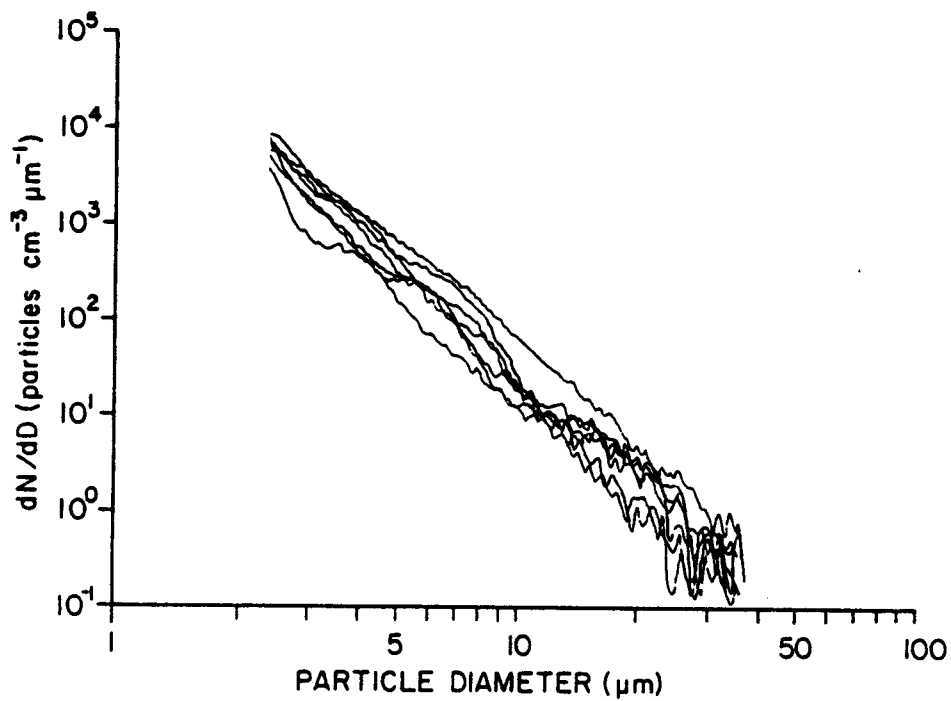


Figure 31. Incremental cumulative curves for particle populations along the NA34-40 station line from surface (top) and bottom (bottom) samples from NASTE 3.

intercept values was lower than in either of the two previous cruises, a fact which can be attributed to the well-developed surface and bottom mixed layers present during the spring (Fig. 32). Average surface values of the slope and intercept were 3.76 ± 0.39 and 1.0×10^5 with no distinct spatial trend. Average bottom values were quite different: 2.91 ± 0.37 and 0.8×10^5 , again with no definite spatial trend. As a group, these bottom samples were the coarsest measured on any cruise.

Although no clear spatial trends are evident within individual horizons, the influence of changing hydrographic regimes between the inshore and offshore stations can nevertheless be detected in the relationship between the surface and near-bottom samples. Figure 32 traces the surface and near-bottom PSD curves from NA34 to NA40 during NASTE 3. Curves from the offshore stations vary independently; particularly obvious are broad peaks in the surface samples which do not occur in the bottom samples and the greater concentration of coarse-grained particles. Moving inshore, the curves become progressively more similar, until at NA40, well inside the well mixed coastal domain, the surface and bottom curves are virtually identical. As during NASTE 2, agreement in the particle population characteristics substantially improves landward of ~40-50 m depth.

4. Organic matter concentrations

Available SPM samples from the seawardmost and landwardmost stations of all NA transects from each cruise were analyzed for organic matter content in order to characterize possible differences between the middle and coastal SPM domains. Table 4 summarizes these results.

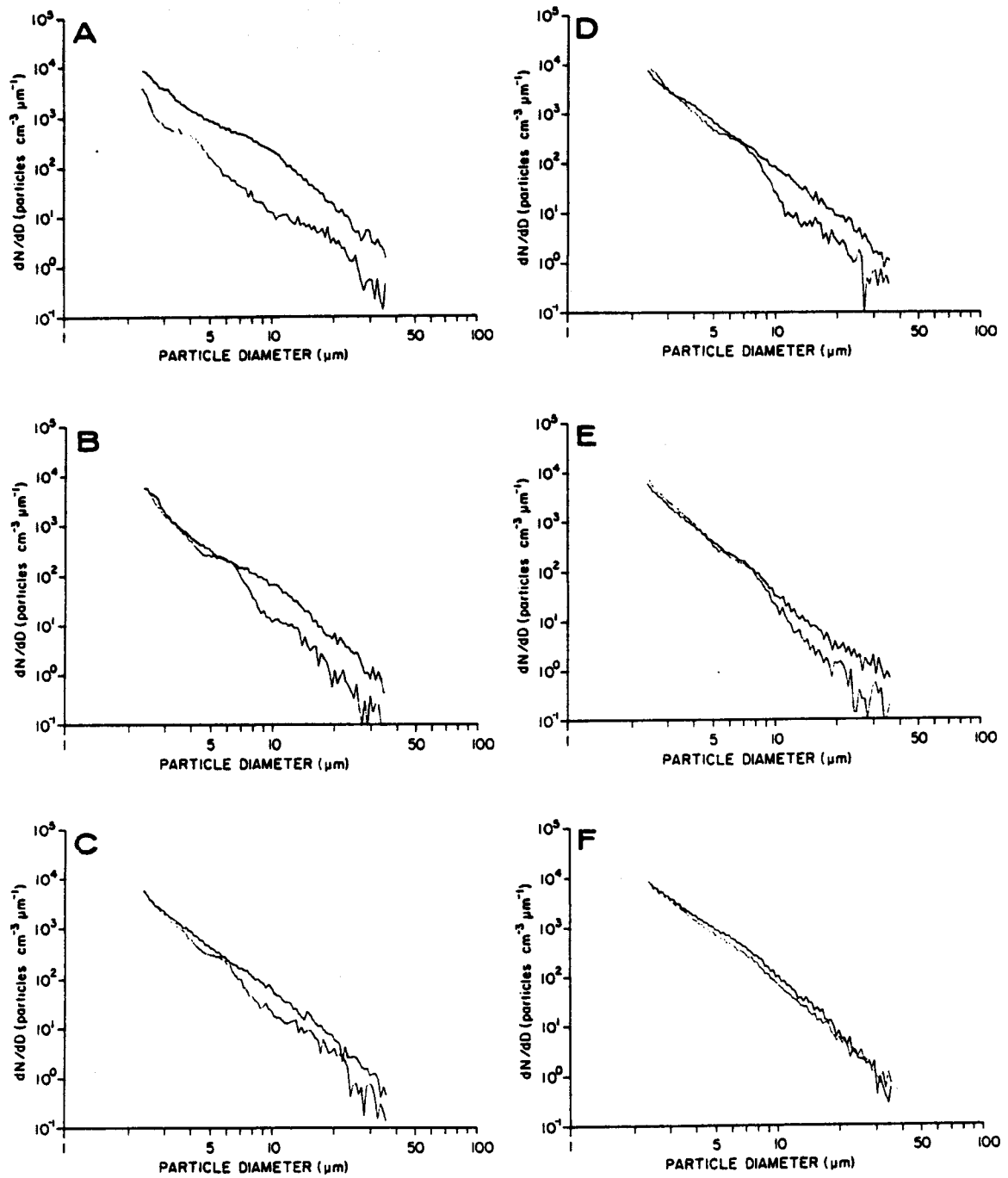


Figure 32. Incremental cumulative curves for particle populations at the surface and bottom at each station (NA34-40 station line) from NASTE 3. A is the outermost station and F is the innermost station.

TABLE 4

Percent organic matter in SPM samples from the North Aleutian Shelf region

Cruise	Surface						5 m above bottom					
	Onshore			Offshore			Onshore			Offshore		
	n	\bar{x}	s	n	\bar{x}	s	n	\bar{x}	s	n	\bar{x}	s
NASTE 1	15	42.8	9.6	12	47.9	7.4	14	38.5	11.4	13	32.8	8.2
NASTE 2	15	25.7	6.4	15	46.3	9.0	15	24.7	5.3	16	40.4	9.2
NASTE 3	7	45.6	15.6	10	57.5	15.3	7	39.7	11.9	10	29.3	5.7

The highest overall percentage of organic matter (43.0%) was recorded during NASTE 3, the cruise conducted during the normally highly productive spring bloom period. The percent organic matter was only slightly less during the late summer (40.5%, NASTE 1) and substantially lower in winter (34.3%). The lowest values recorded (~25%) were the surface and near-bottom values from the inshore winter stations; the offshore winter surface value was only slightly lower than its summer and spring counterparts. Offshore winter near-bottom values were higher than either spring or summer, an anomaly apparently caused by the relatively unimpeded vertical exchange between surface and bottom waters when density stratification is minimal.

Averaged over all three cruises, the surface offshore percent organic matter (50.6%) was significantly greater than the inshore value (38.0%), perhaps due to dilution of phytoplankton-produced organic matter in the coastal zone by inorganic detritus from shore and bottom erosion and re-suspension. Differences in phytoplankton standing stock or primary pro-

duction between the coastal and middle domains, however, were not investigated during this study.

Near-bottom percent organic matter values were always less than the surface values, although the inshore-offshore pattern differed seasonally. Offshore near-bottom values in the spring and summer were lower than the corresponding inshore values because the offshore samples were insulated from the productive surface waters by the regional pycnocline. Resuspension of bottom sediment relatively poor in organic matter was a major source of particles to the offshore near-bottom water at these times. During winter, however, offshore near-bottom organic matter values were greater than the inshore values.

5. X-ray clay mineralogy

Results from the clay mineralogy analyses were inconclusive. The only peaks observed on any diffractogram were from silt-sized particles such as quartz and feldspars. Clay mineral concentrations in the water column were not great enough to yield measurable results by standard sampling techniques. Future efforts to quantify the clay mineral suite in suspension must encompass special techniques to recover, filter, and concentrate large volumes (10-20 l) of seawater.

6. Particle flux measurements

a) Vertical particle flux

Vertical particle flux was measured at Stations TP2B, TP7, TP8, and TP9 between NASTE 1 and NASTE 2 (Fig. 3). Sequentially sampling sediment traps (S^3T) were deployed 11 to 15 m above bottom at each station in conjunction with transmissometers to measure light attenuation and current

meters to measure current flow and water properties. Each sediment trap collected 9 separate flux samples of 11.25 days each, beginning on February 3 0600 (TP2B), February 3 0540 (TP7), February 6 0020 (TP8), and February 4 0400 (TP9) and ending on or around May 16 (all times local).

Average total sedimentation rates (TSR) varied from $<2 \text{ g m}^{-2} \text{ day}^{-1}$ at TP8 to $>9 \text{ g m}^{-2} \text{ day}^{-1}$ at TP7 and TP9, the shallowest and deepest stations, respectively (Table 5). Stations TP7, TP2B, and TP9 were along a transect normal to the coast, while TP8 was located $\sim 56 \text{ km}$ to the southwest at about the same depth as TP2B. Thus the TSR appears to be depth controlled, with large values found both close inshore and seaward of the coastal front, whereas smaller values were found near the zone where the SPM distribution changed from vertically stratified to horizontally stratified during NASTE 3 (see Figs. 21, 22, and 23). This zone may be considered the location of the coastal front along the North Aleutian Shelf region. Other indications also point to a higher energy environment at the TP7 and TP9 locations relative to TP8 and TP2B. The average flux of particles $>38\mu\text{m}$ at TP7 and TP9 was 4 to 16 times greater and comprised 51.2% of the total flux compared to only 31.0% at TP8 and TP2B.

Much of the mixing energy in the nearshore waters of the Alaskan Peninsula is provided by wind events whose energy output varies greatly in time (Kinder and Schumacher, 1981a). Similarly, the flux of organic matter is dependent on seasonal plankton cycles. Thus "average" characterizations of the vertical SPM flux, while useful for defining regional variability, can not adequately describe the processes which control the flux. This point is illustrated by the temporal flux variability as recorded by the 11.25 day samples from each of the S^3T (Fig. 33). The TSR at TP7 and TP9 varied by as much as a factor of 15 between successive collection periods;

TABLE 5
Vertical particle flux measurements

Mooring Location	Water Trap Depth (m)	Trap Depth (m)	Average Sedimentation Rate ($\text{g m}^{-2} \text{day}^{-1}$)				Average Composition (%)			
			Total	Phyto- plankton pigments	Organic matter	Particles <38 μm	Particles >38 μm	Organic matter	Particles <38 μm	Particles >38 μm
TP7	24	13	11.23 \pm 5.54	2.24 \pm 1.18	1.04 \pm 0.56	3.96 \pm 1.64	6.87 \pm 4.24	10.5 \pm 1.8	37.5 \pm 12.7	58.8 \pm 13.1
TP8	31	16.5	1.76 \pm 0.81	0.69 \pm 1.07	0.25 \pm 0.12	1.07 \pm 0.52	0.42 \pm 0.22	14.6 \pm 2.5	61.0 \pm 5.3	23.4 \pm 7.2
TP2B	35	20.5	3.25 \pm 1.72	0.94 \pm 0.87	0.48 \pm 0.20	1.73 \pm 1.20	1.30 \pm 0.75	16.5 \pm 5.5	53.4 \pm 14.0	38.7 \pm 14.5
TP9	89	77	9.60 \pm 8.26	2.22 \pm 3.56	1.17 \pm 0.86	3.94 \pm 2.89	4.96 \pm 6.40	13.8 \pm 2.8	48.3 \pm 14.6	43.6 \pm 15.2

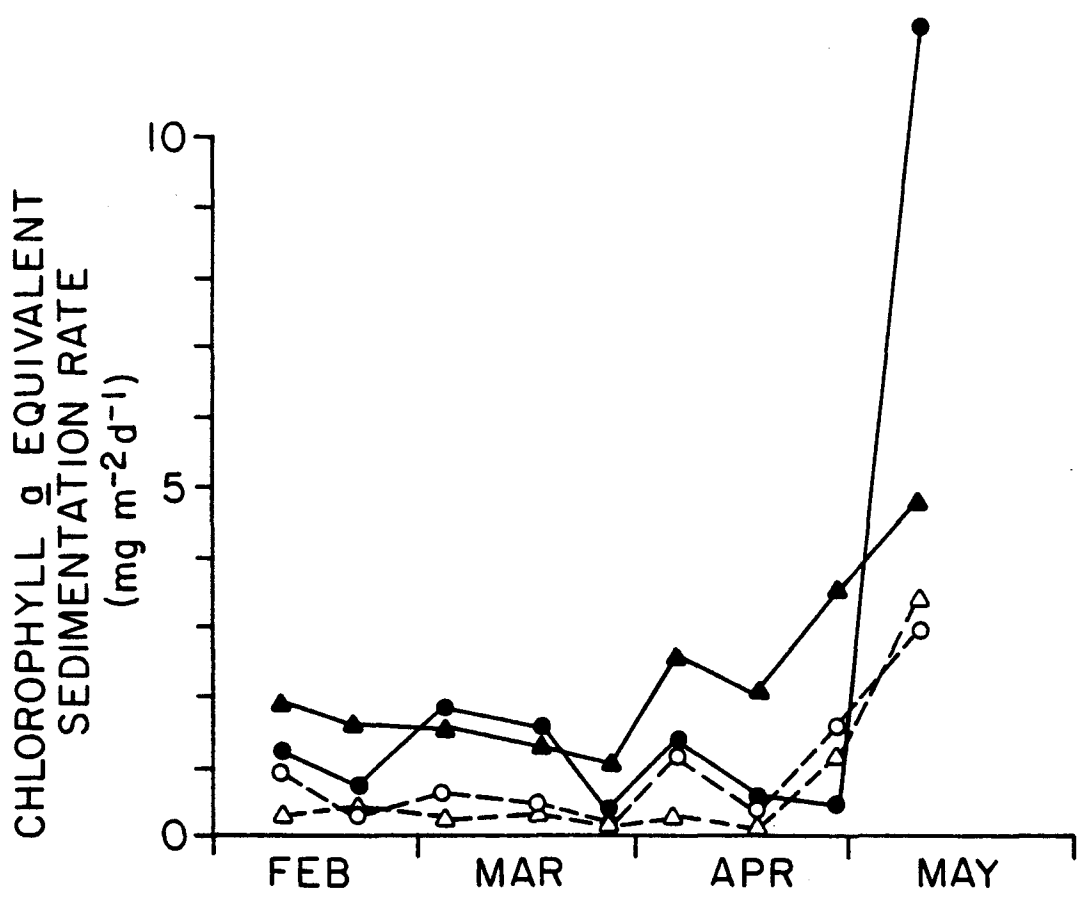
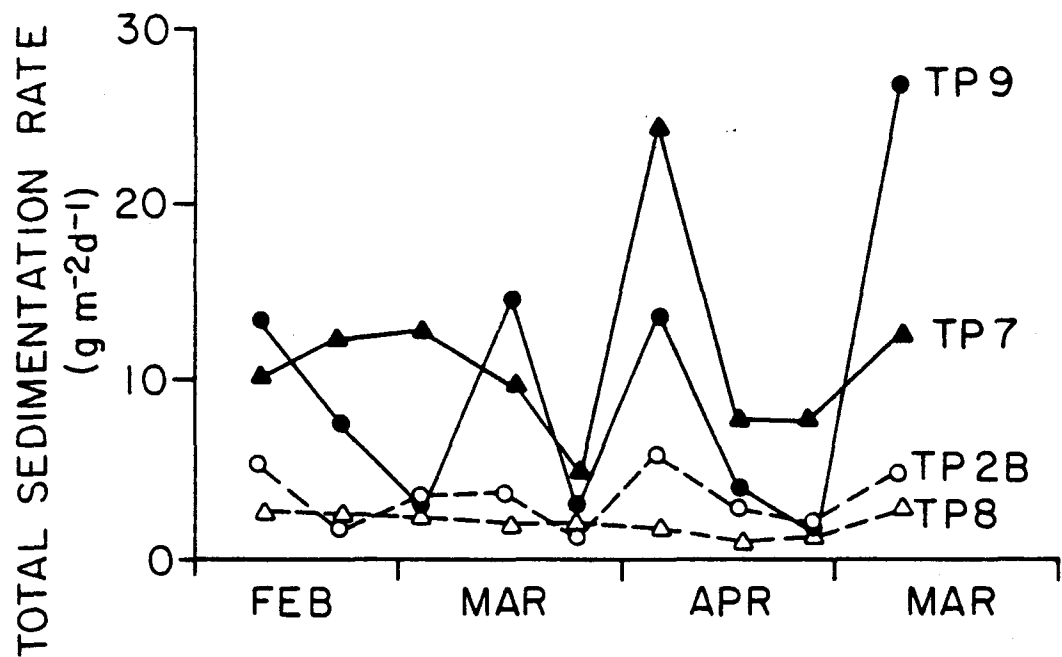


Figure 33. Flux values from NAS sediment traps. Each point represents an 11.25 day average value.

changes on the order of 5x were common. At TP8 and TP2B, however, temporal variability was far lower; the maximum observed was a 7-fold change and changes >2x were rare. Changes in the flux of fine and coarse-grained particles followed the same trends (Fig. 34). It is clear from Figs. 33 and 34 that this variability was not random. Sedimentation rates showed clear maxima in collection periods 4 (March 8-19), 6 (March 31-April 1), and 9 (May 3-14) at TP9. The same sequence was recorded at TP7 (except for a shift from period 4 to period 3) and, in reduced fashion, at TP2B. TP8, located 56 km down the coast from the others, showed no clear pattern in its much lower flux rate. Although the grain-size composition was highly variable at each site (Fig. 35), there was no clear pattern to the changes.

The temporal pattern of the biogenic portion of the flux was dominated by onset of increased phytoplankton production in the spring (Fig. 33). The flux of phytoplankton pigments, expressed as chlorophyll a equivalents [= chlorophyll a + (1.52) pheophorbide, the chlorophyll a degradation product; see Shuman and Lorenzen (1975)], varied only slightly at all stations through the first seven collection periods. Towards the end of the deployment, however, the pigment flux rose sharply, especially at TP9 where density stratification could produce a stable surface mixed layer to encourage primary production.

b) Horizontal particle flux

Variations in attenuation at the mooring sites were primarily the result of tidal forcing. Both inshore and offshore records (Fig. 36) showed significant (at the 0.05 level) spectral peaks in the attenuation record at periods of approximately 1, 0.5, 0.33, and 0.25 days. Significant variations were also caused by longer period events such as the fortnightly waxing and

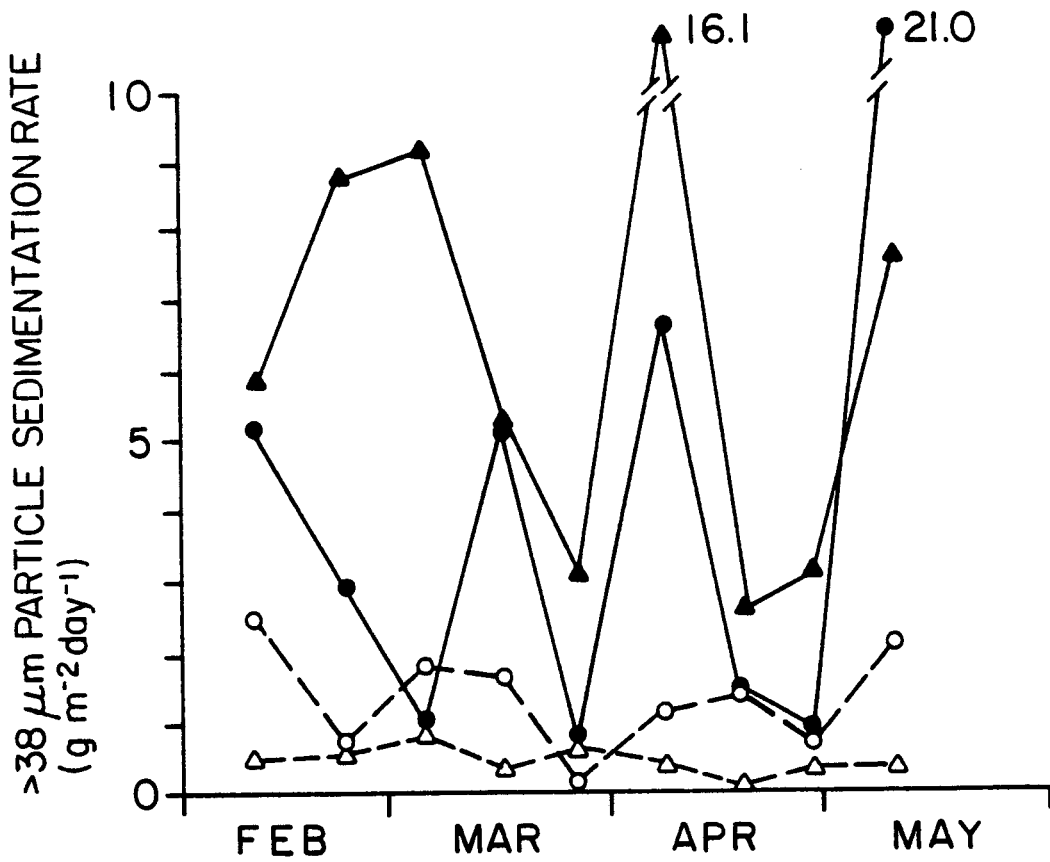
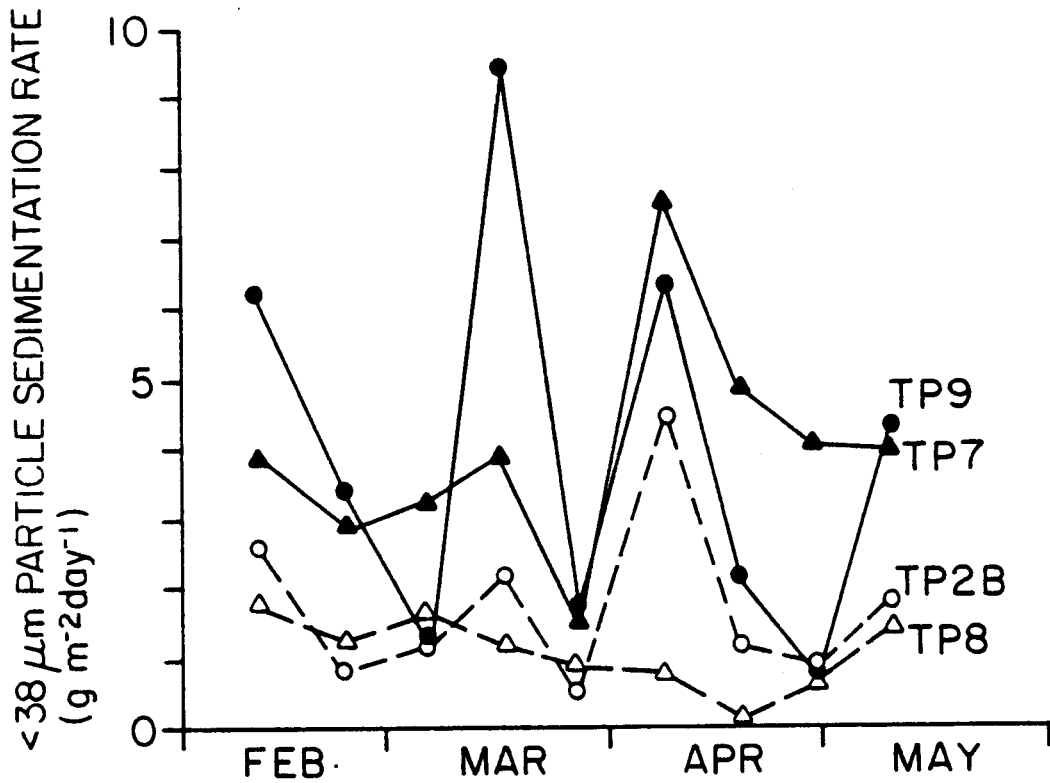


Figure 34. Flux values for fine- and coarse-grained particles in the NAS sediment traps.

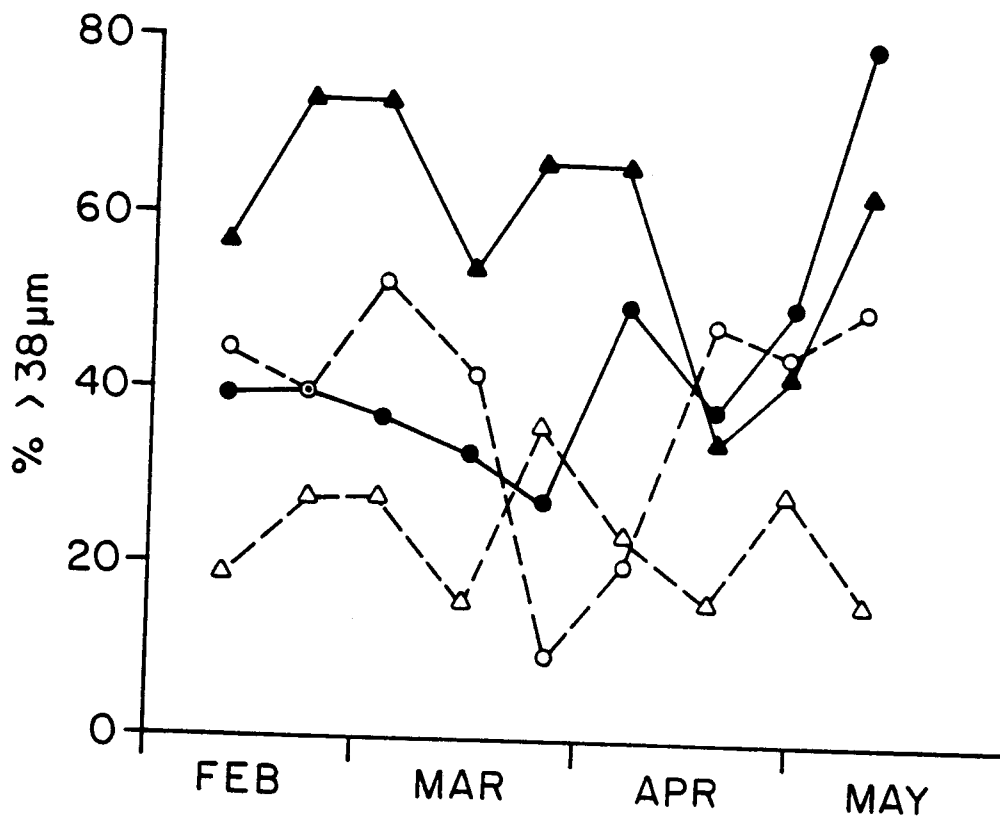
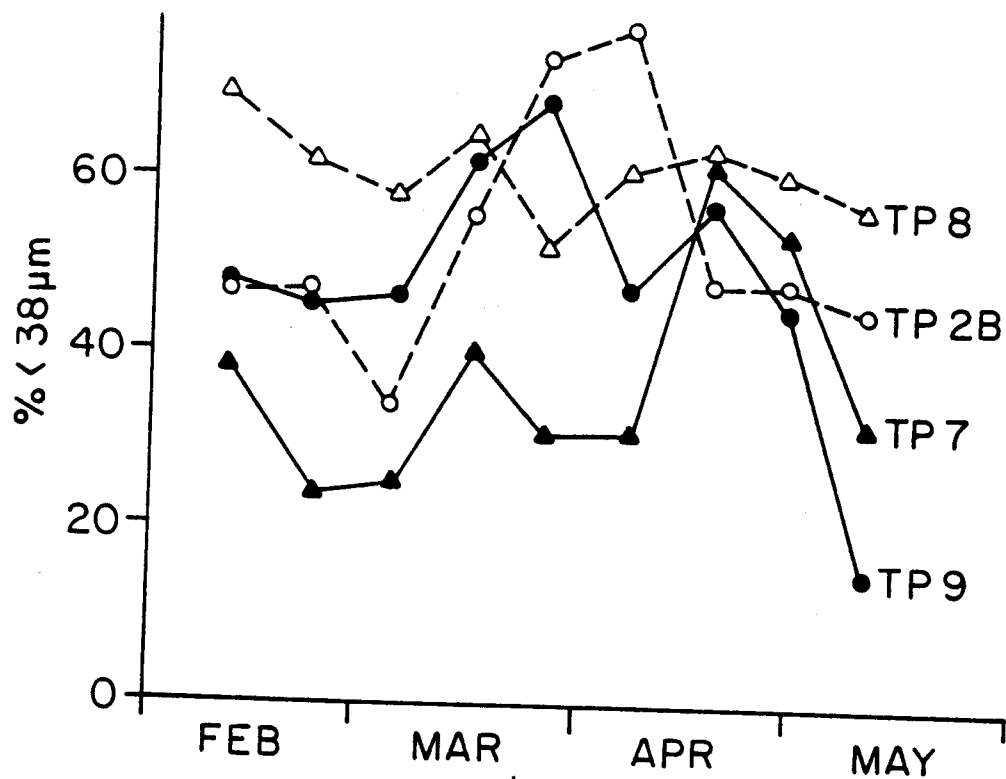


Figure 35. Variability of particle-size partitioning of sediment trap material.

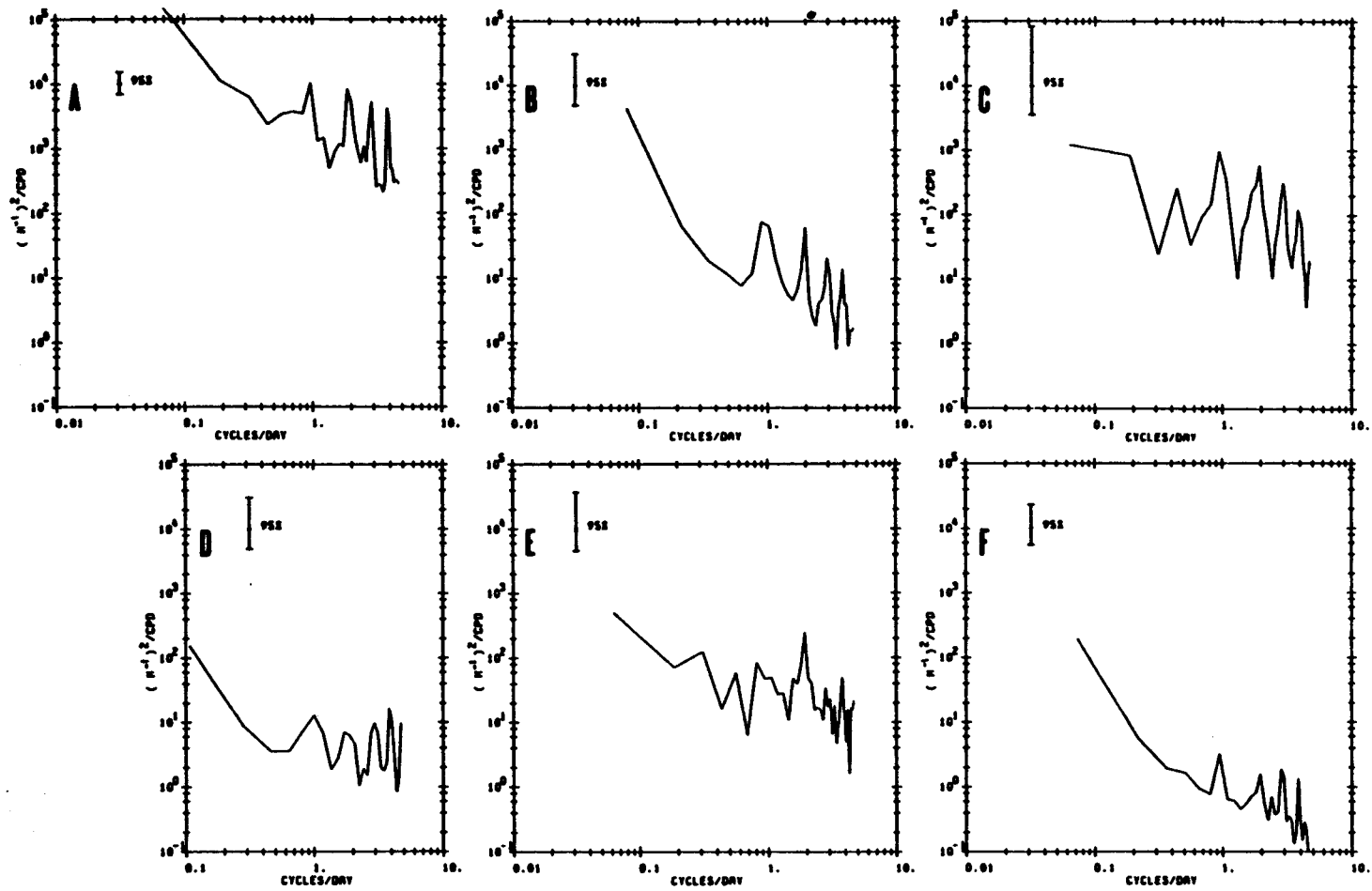


Figure 36. Variance spectra for attenuation records. A, TP7; B, TP2; C, TP8; D, TP6; E, TP4; F, TP9. Peaks occur at tidal frequencies.

waning of tidal energy, as expressed by the large proportion of spectral variance at periods of ~ 10 days. Attenuation variance levels were greatest at TP7, the shallowest station, and least at TP9, the deepest station. Variance at other stations was roughly proportional to the depth, but did not vary in a strictly linear fashion.

Figs. 37 and 38 illustrate the character of the mooring records from the landwardmost and seawardmost stations. Station TP7 shows very large daily variations throughout the record, as well as several 5- to 10-day intervals where the turbidity values were routinely $4\times$ the "normal" value of $\sim 2 \text{ m}^{-1}$. These aperiodic events are probably related to the local weather (at present, the local wind record from the temporary shore station has not finished the data processing routine). Station TP9 (Fig. 39) shows a very different attenuation record. (The record has been terminated at Mar. 27 since past that time fouling of the transmissometer lenses rapidly deteriorated the attenuation signal. Fouling was not found to be a problem in the much more energetic environment at TP7.) Daily changes are very small.

Sediment flux calculations (Table 6) show clear differences between inshore and offshore stations. SPM fluxes were $>7 \mu\text{g cm}^{-2} \text{ sec}^{-1}$ at TP7, TP2, and TP8, but $< \sim 2 \mu\text{g cm}^{-2} \text{ sec}^{-1}$ in deeper waters. No consistent transport direction was found, but it should be remembered that net flow in this environment is difficult to interpret due to its very small magnitude relative to the tidal variations (Kinder and Schumacher, 1981b). The direction of net sediment flux usually agreed closely with that of the net water flow. Sediment flux at the offshore moorings was directed alongshore at the deepest two sites (TP4 and TP9) and inshore at TP6, a slightly shallower site. Sediment flux at the three inshore stations had a strong alongshore component to the southwest, away from Port Moller.

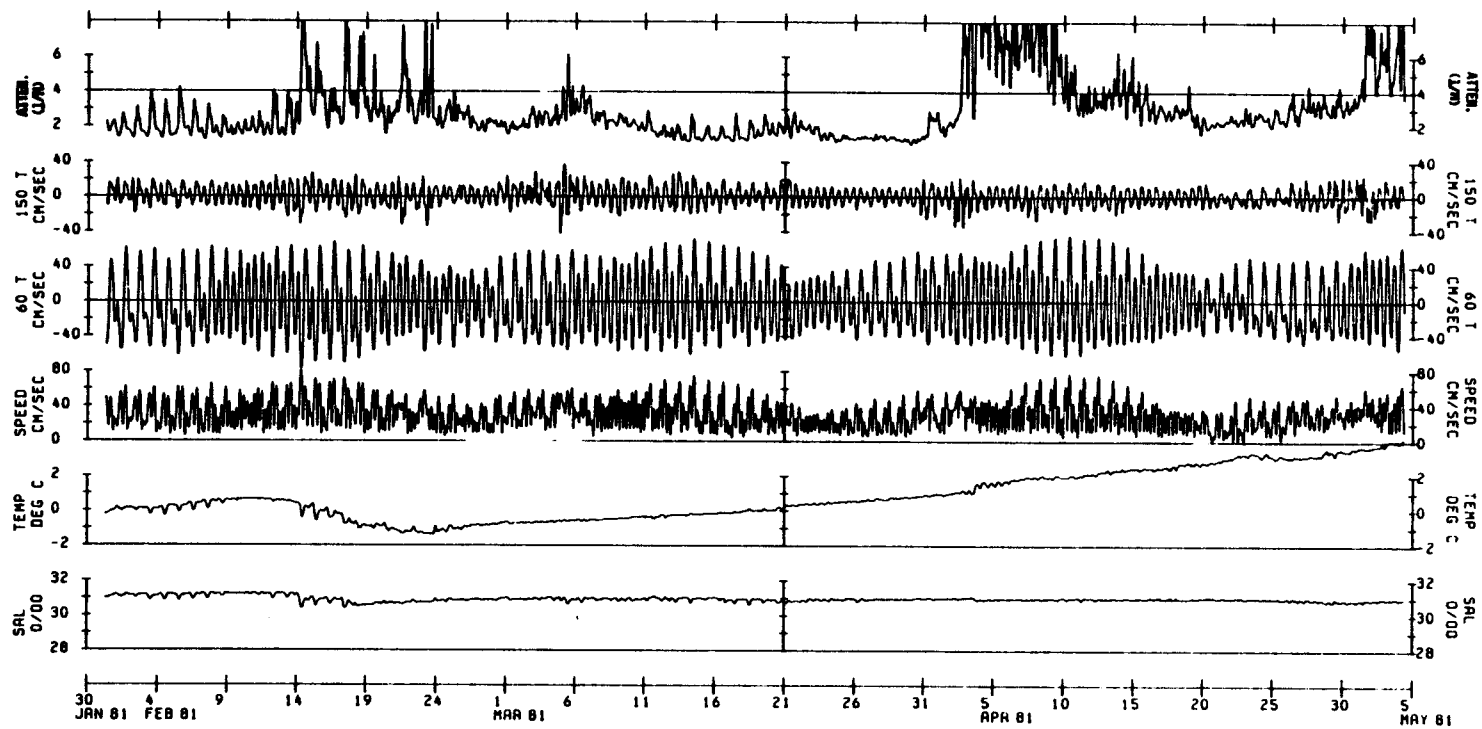


Figure 37. Current meter/transmissometer record at TP7.

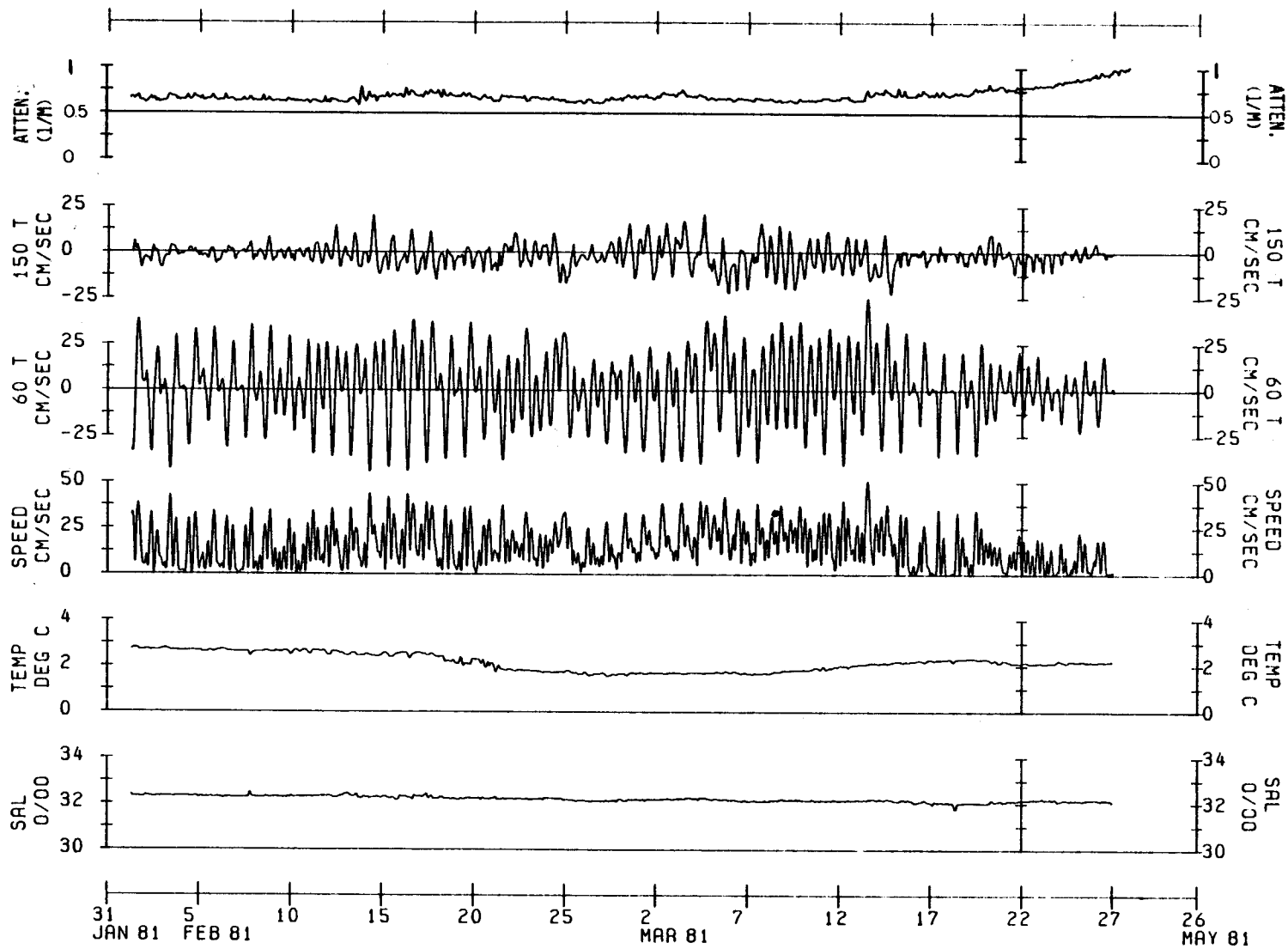


Figure 38. Current meter/transmissometer record at TP9. Note change in scales from Figure 37.

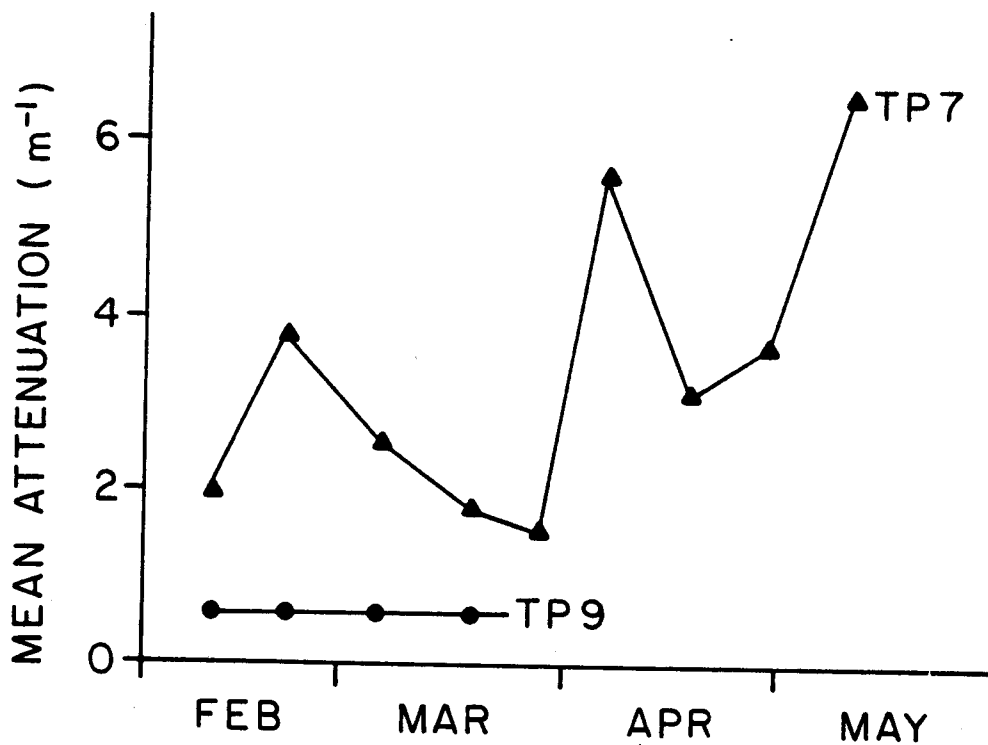
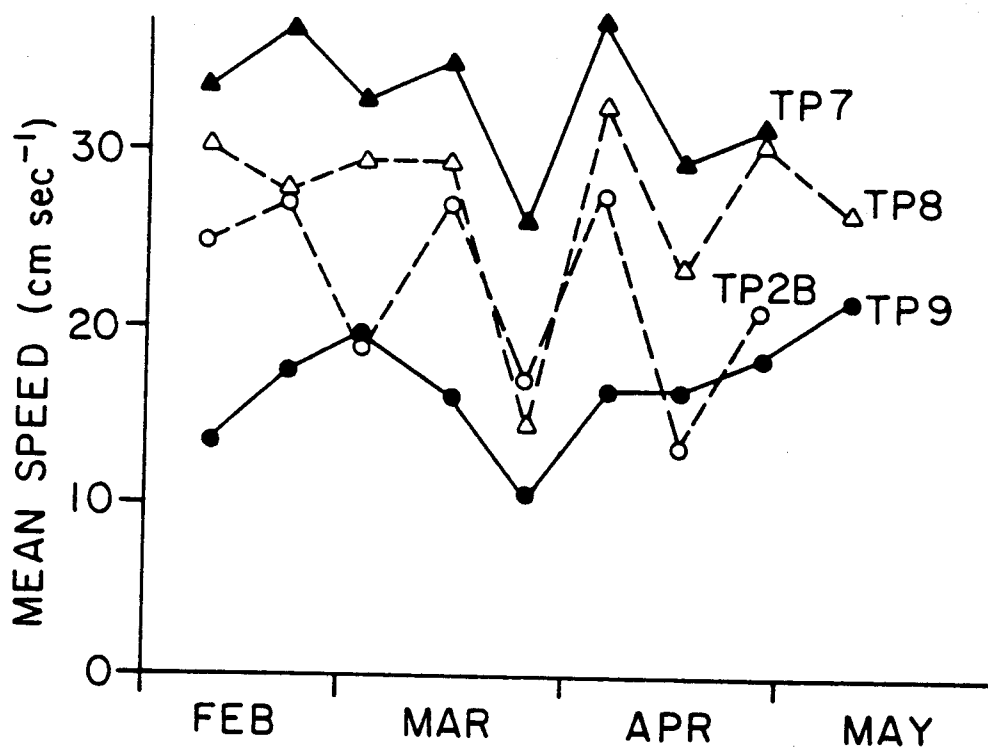


Figure 39. Mean speed and mean attenuation values averaged over sediment trap collection periods.

TABLE 6

Sediment flux calculations

Mooring	Meter Depth (m)	Sampling Interval	Particle Flux ($\mu\text{g cm}^{-2} \text{sec}^{-1}$)	Dir. ($^{\circ}$)	Mean Speed (cm sec^{-1})	Dir. ($^{\circ}$)
<u>Inshore</u>						
TP7	15	30 Jan-5 May	17.5	238	33.0	206
TP2	20	19 Aug-25 May	7.6	219	27.8	212
TP8	21	2 Feb-19 Feb	7.0	205	30.4	210
<u>Offshore</u>						
TP6	55	20 Aug-17 Sep	1.1	153	22.4	150
TP4	63	19 Aug-20 Sep	2.1	45	14.9	47
TP9	Ø9	31 Jan-27 Mar	1.2	15	15.5	13

It is also interesting to note that the correlation between mean current speed and sediment transport magnitude is poor. Mean current speed about doubles from TP9 to TP7, whereas sediment flux increases approximately fifteenfold. This difference can be explained on the basis of particle availability; the high SPM concentrations typical of the near-shore region result in much greater mass transport with only a moderate increase in current flow.

Comparison of the incremental sedimentation rate, mean current speed, and mean attenuation (Fig. 39) shows clear differences between nearshore and offshore environments. All three parameters follow similar trends at TP7, implying that the particles are thoroughly mixed throughout the water column and that these mixing processes are more important in controlling the distribution and transport of particles in the water than are sedimentation processes. At TP9, the TSR and mean speed trends are nearly

independent, except for a mutual minimum during period 5 (a quiescent time over the entire region). Similarly, the truncated attenuation record shows essentially no change even with a near doubling of mean speed between periods 1 and 3. These results arise from the fact that the TSR at TP9 is strongly influenced by settling particles originating in the surface layers as well particles resuspended and advected within the BNL. TP8 and TP2B appear to be intermediate between these extremes in the relationship between sedimentation and current speed.

B. St. George Basin Region

Field work in this region was done to ascertain SPM distributions characteristic of the hydrographic domains as described by Kinder and Schumacher (1981a). Extensive descriptions of the physical oceanography of the southeastern Bering Sea are available, but data on the particle distributions are sketchy and related almost exclusively to purely biological processes (e.g., chlorophyll a distributions; Iverson et al., 1979).

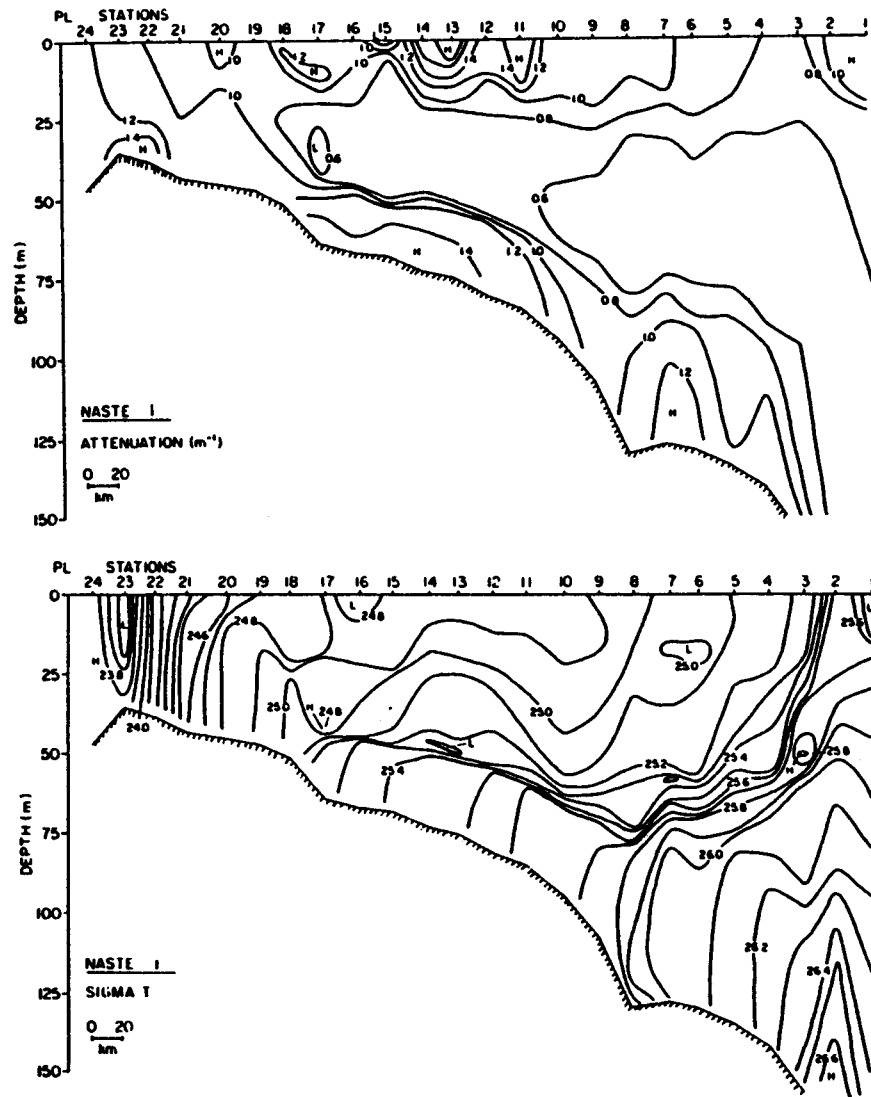
Because the field emphasis in this project was the North Aleutian Shelf region, station coverage in St. George Basin was not uniform for all three cruises. Furthermore, equipment problems during NASTE 2 resulted in only a few CTD casts having acceptable transmissometer data. Data coverage was most complete during NASTE 3.

1. Density and SPM cross-sections

The longest continuous line of stations across the southeastern Bering Sea hydrographic domains was occupied during NASTE 1 and encompassed

Stations PL1 to PL24 (Fig. 40). (This line duplicated a standard station line used by the NSF PROBES Program.) The density cross-section clearly reveals the various hydrographic domains. The coastal domain, identified by vertically homogeneous water, was found inshore of about Station PL19 (approximately the 45-m isobath). The inner front, characterized by a high horizontal density gradient in the bottom water, occurred between Stations PL18 and PL16. Seaward of this zone, a strong two-layer stratification marks the middle domain. The broad middle front appeared to be centered around Station PL8. Further seaward the stratification separating the wind mixed surface layer and the tidally mixed bottom layer became more moderate and typical of the outer shelf domain. Surface expression of the shelf break front was seen between Stations PL2 and PL3.

Several features of the SPM distribution reflect these hydrographic domains. In the coastal domain, particles were well mixed throughout the water column with only slight increases in near-bottom attenuation levels due to gravitational sinking of large particles. Both the middle and outer shelf domains were characterized by a three layer SPM distribution. Particles in the bottom water were trapped below the regional pycnocline and created a bottom nepheloid layer with a sharp vertical gradient. Both bottom nepheloid layer concentrations and vertical gradients appeared substantially lessened at stations where horizontal near-bottom density gradients increased (i.e., Stations PL9 and PL18). Above the nepheloid layer was a broad zone where SPM concentration gradients were low in both horizontal and vertical directions. This zone was terminated in the landward direction by the inner front. Above the mid-depth minimum zone, SPM concentrations are highly variable and probably controlled by phytoplankton patchiness.



The data set from NASTE 3 is both geographically and temporally more extensive. An abbreviated portion of the PL line was occupied twice, once on May 17 and May 18 (Fig. 41) and again May 23 and 24 (Fig. 42).

The middle and outer shelf domains were again identified during the spring cruise. Sampling did not extend landward far enough to reach the coastal domain. The most significant change appeared to be in the strength and position of the pycnocline in the middle domain. During NASTE 1, Brunt-Väisälä frequencies averaged 10.9 ± 1.4 cph in the middle shelf pycnocline; during NASTE 3 the stability averaged 10.1 ± 1.2 cph during the first PL occupation and only 8.7 ± 0.6 cph during the second. Maximum Brunt-Väisälä values were found an average of 16 ± 4 m above bottom during NASTE 1; during NASTE 3 the average was 47 ± 8 m above bottom during the first occupation, lowering to 25 ± 9 m above bottom during the second.

Although the general character of the SPM distribution was similar to NASTE 1, these alterations in the density distribution had demonstrable effects on the details of the SPM cross-sections. During the first PL occupation (Fig. 41), the extreme thickness of the bottom mixed layer effectively destroyed the mid-depth minimum zone landward of the middle shelf by allowing resuspended particles to be mixed high into the water column. Six days later, during the second PL occupation, the horizon of maximum stability had lowered to within ~ 25 m of the seafloor and thus allowed the reestablishment of a mid-depth minimum zone throughout the PL line (Fig. 42).

Data collected along three other lines parallel to the PL line (Fig. 2) also exhibited similar relationships between the density stratification and the vertical SPM distribution.

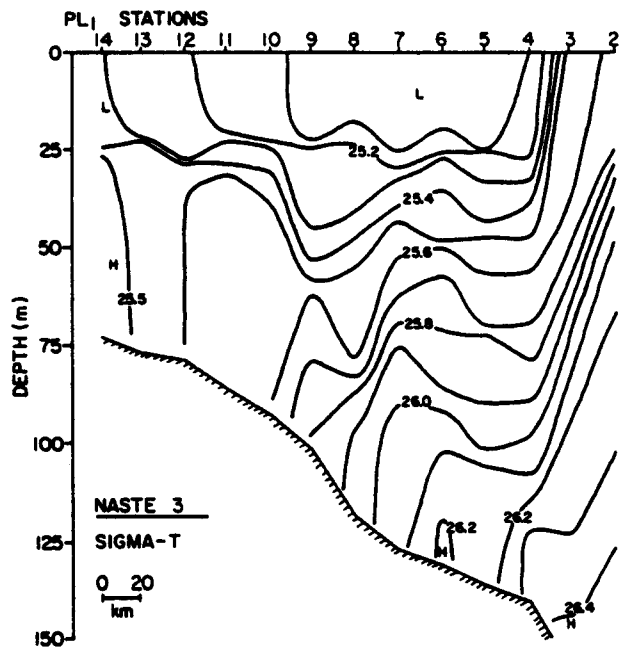
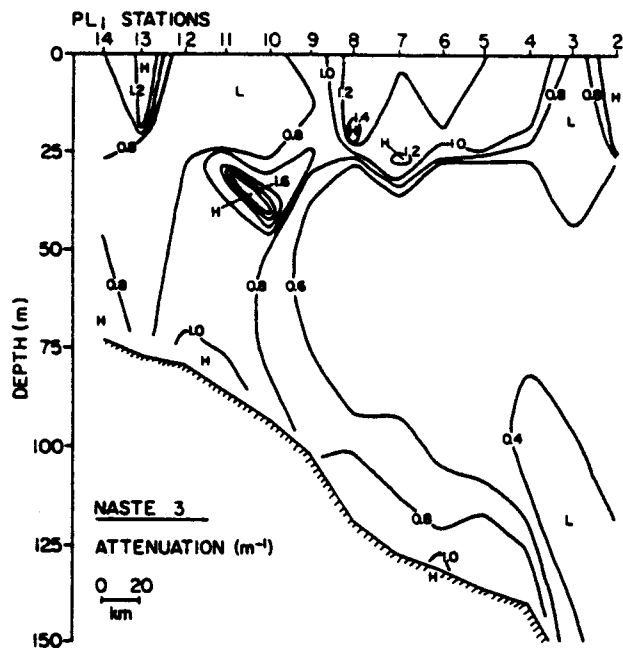


Figure 41. Attenuation (top) and density (bottom) cross-sections for the PL line, May 17-18, 1981.

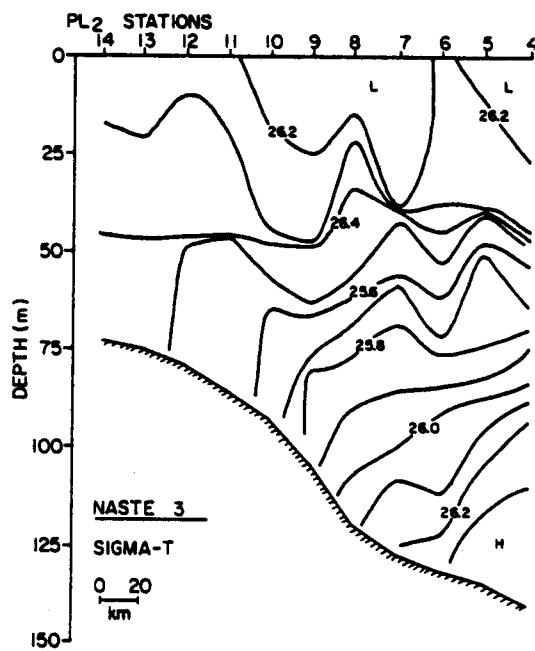
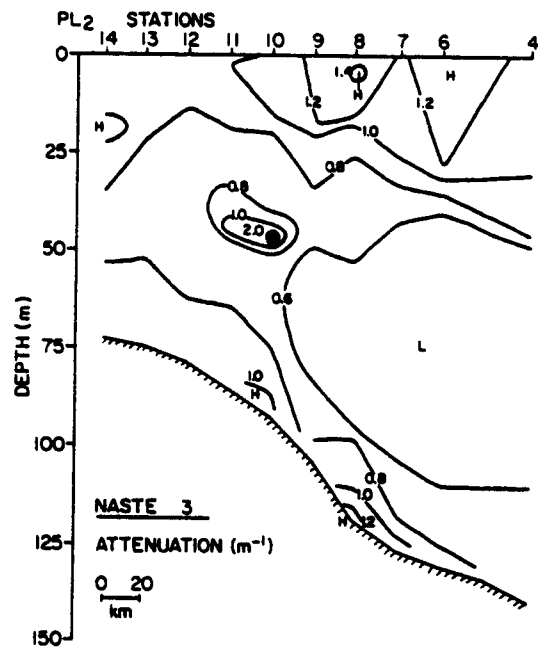


Figure 42. Attenuation (top) and density (bottom) cross-sections for the PL line, May 23-24, 1981.

2. Particle size distributions

Although particle size distribution data was collected at all St. George Basin stations, only samples from stations along the PL line will be discussed in detail. This transect was the only one occupied on each cruise and is representative of the entire region.

All distributions show excellent correlation with a power law distribution (see Section IV. B.1.). Correlation coefficients (r^2) for all samples were >0.95 . The power law distribution fails only at diameters $>\sim 20 \mu\text{m}$ in the surface water where large concentrations of particles over a narrow size range (i.e., phytoplankton) result in deviations from the linear trend. During NASTE 1 and 2, a slight change of slope was observed at $\sim 4 \mu\text{m}$ diameter (see Fig. 43; data from NASTE 3 was inconclusive on this point). This intersection has been noted in other oceanic samples processed by Coulter Counter techniques (Bader, 1970; Brun-Cottan, 1976; and McCave, 1975). Its origins and implications are unknown at present. To compare distribution slopes between cruises and depths, then, only the range between 4 and $20 \mu\text{m}$ was considered in calculating the power law regression coefficients.

Surface water along the PL line during NASTE 1 contained particle size distributions (PSD) with both the steepest slope and highest particle concentrations of any portion of the water column during any cruise (Table 7, Fig. 43). Variability in the family of PSD curves is high, with peaks in both the $\sim 20 \mu\text{m}$ and 3 - $5 \mu\text{m}$ range perhaps indicative of specific kinds of phytoplankton. PSD curves in the mid-depth minimum zone are much more coherent. The average slope (4.19) shows a marked decrease from the surface samples (4.54) and the intercept value is lower by an order of magnitude (Table 7). The slope of the near-bottom samples decreases still further,

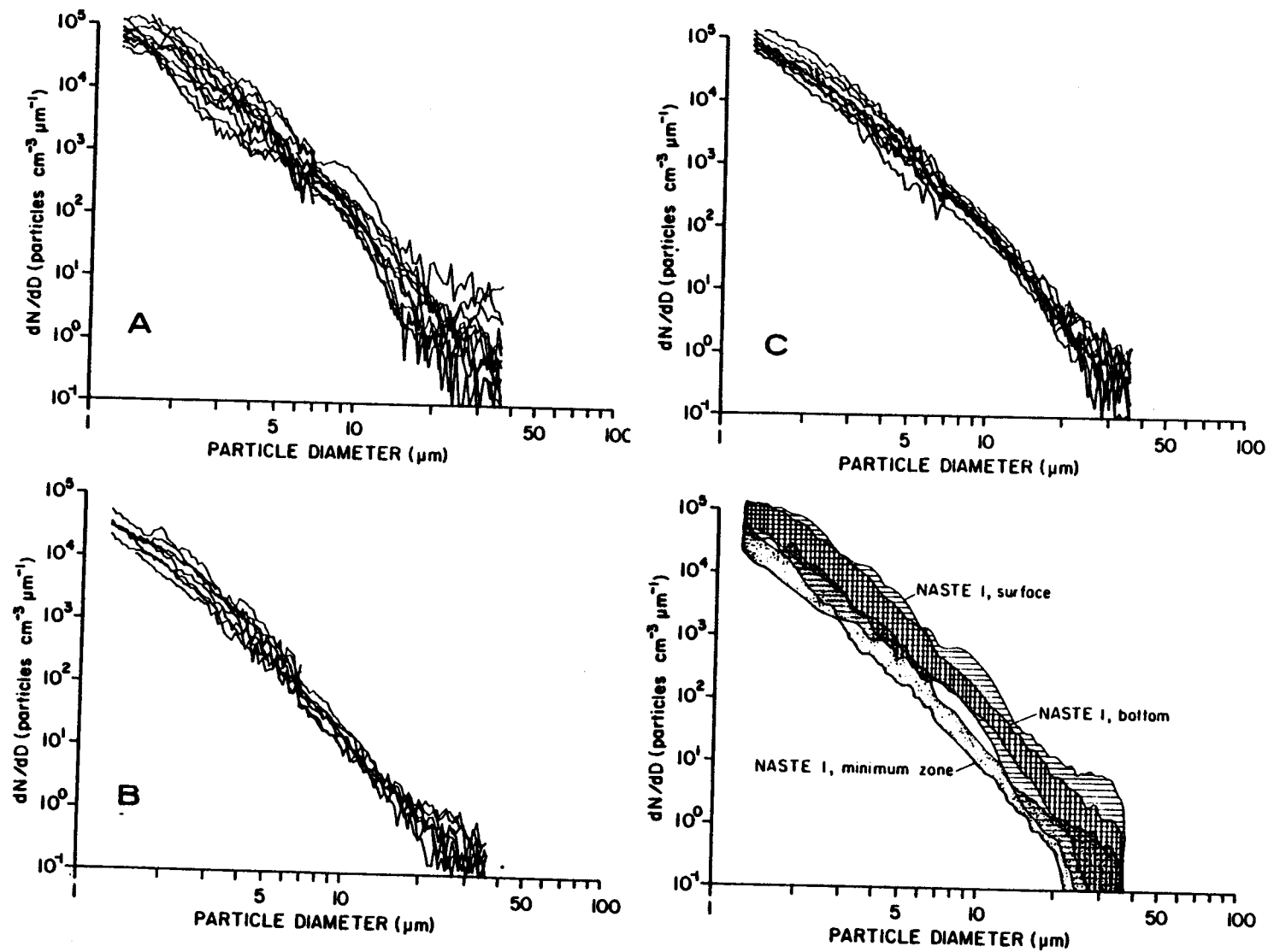


Figure 43. Incremental cumulative curves from the PL line during NASTE 1 for surface water (A), minimum turbidity zone (B), bottom water (C). Curve envelopes for each group are also shown.

TABLE 7
Particle size distribution parameters from
PL line in St. George Basin

Cruise	Depth Zone	a ¹ (x10 ⁵)	b ¹	n ²
NASTE 1	surface	40.3 ± 90.0	4.54 ± 0.62	10
	mid-depth	4.0 ± 3.0	4.19 ± 0.32	9
	bottom	12.8 ± 7.4	4.06 ± 0.22	9
NASTE 2	surface	3.0 ± 1.6	4.04 ± 0.17	6
	bottom	12.6 ± 14.4	4.13 ± 0.43	7
NASTE 3-PL ₁	surface	1.1 ± 6.6	3.34 ± 0.27	13
	mid-depth			
	stas. 2-8	0.4 ± 0.2	3.79 ± 0.34	6
	stas. 9-14	1.2 ± 0.9	3.44 ± 0.45	6
	bottom			
stas. 9-9, 13-14	3.1 ± 1.2	4.00 ± 0.18	7	
stas. 10-12	0.8 ± 0.4	3.04 ± 0.78	3	
NASTE 3-PL ₂	surface	0.8 ± 0.2	3.40 ± 0.14	10
	mid-depth			
	stas. 4-9	0.6 ± 0.4	3.88 ± 0.30	6
	stas. 10-14	0.8 ± 0.3	3.42 ± 0.16	5
	bottom			
	stas. 4-8, 14	4.8 ± 2.0	4.14 ± 0.27	6
stas. 10-13	0.6 ± 0.2	2.98 ± 0.05	4	

¹ Mean and standard deviation of constants determined from fitting the observed distributions to the form $dN/dD = aN^{-b}$.

² Sample size for each depth zone.

although the intercept value is greater than for the minimum zone samples.

The relative characteristics of the family of PSD curves from each depth horizon are compared in Fig. 43. Samples from the surface and bottom are seen to occupy very similar plot coordinates, while those from the minimum zone are distinct. Furthermore, PSD curves in all three horizons are uniform throughout the PL line (through PL20). This uniformity may be traced to the strong vertical stratification which prevailed during NASTE 1 (Fig. 40), thereby allowing the particle populations in the surface and bottom mixed layers to be internally consistent and distinct from the intermediate minimum zone.

PSD curves from the surface and bottom waters along the PL line during NASTE 2 are shown in Fig. 44 (no minimum zone data was collected). The average slopes of these lines are similar to each other and to the minimum zone and near-bottom samples from NASTE 1 (Table 7). Concentrations are slightly higher in the near-bottom samples. Comparison of the family of PSD curves from the minimum zone of NASTE 1 and the surface waters of NASTE 2 (Fig. 44) shows them to be nearly identical. This agreement indicates that in the absence of active phytoplankton growth and strong vertical stratification (as is the case in January-February in the southeastern Bering Sea), the particle populations of the surface layer and the mid-depth zone are indistinguishable and form what may be considered the "background" population of this region. Changes to this background thus occur when additional sources, such as bottom resuspension, phytoplankton growth, or river runoff, are influential.

Particle populations in the surface water during NASTE 3 again showed the strong influence of phytoplankton peaks (Fig. 45) at diameters $>20 \mu\text{m}$. Below $20 \mu\text{m}$, the PSD curves are quite coherent with slopes less than those

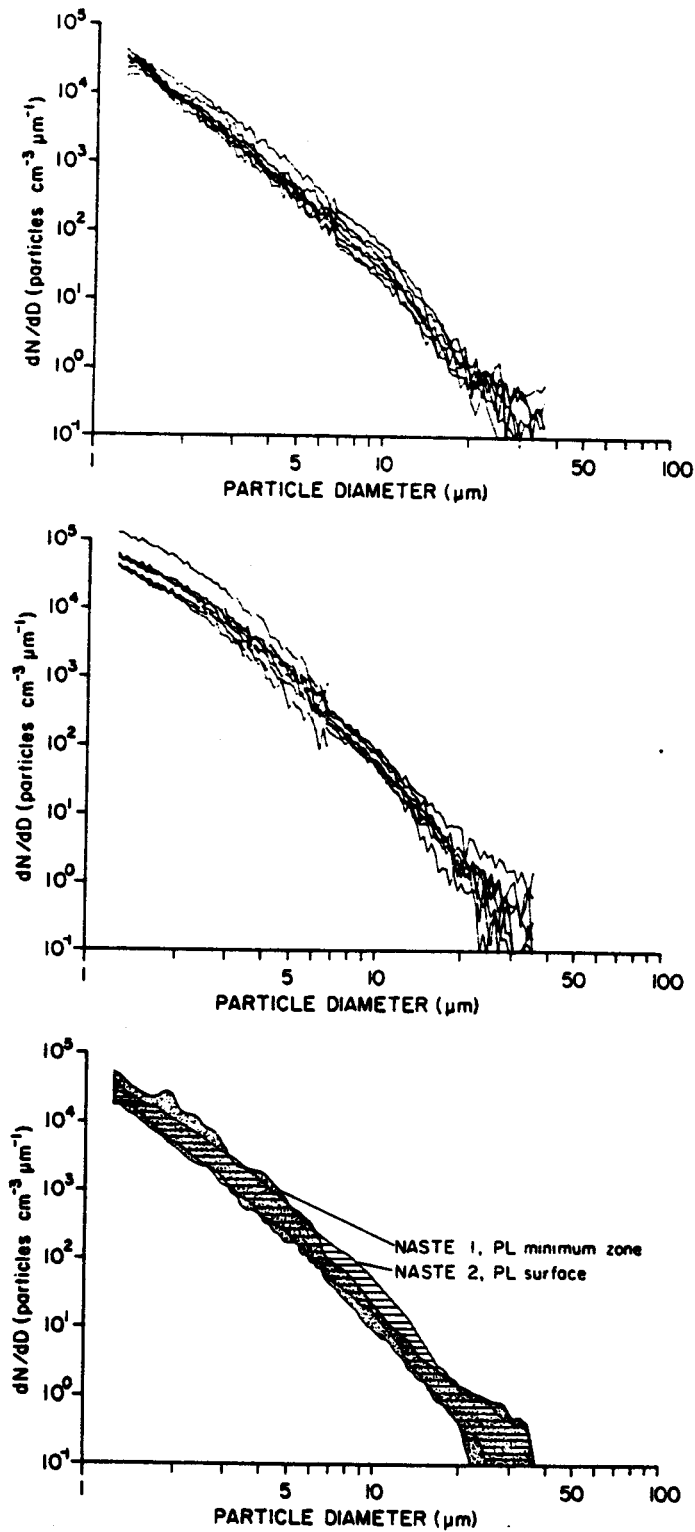


Figure 44. Incremental cumulative curves from NASTE 2 surface (top) and bottom (middle) waters. Curve envelopes (bottom) demonstrate the similarity of the two populations.

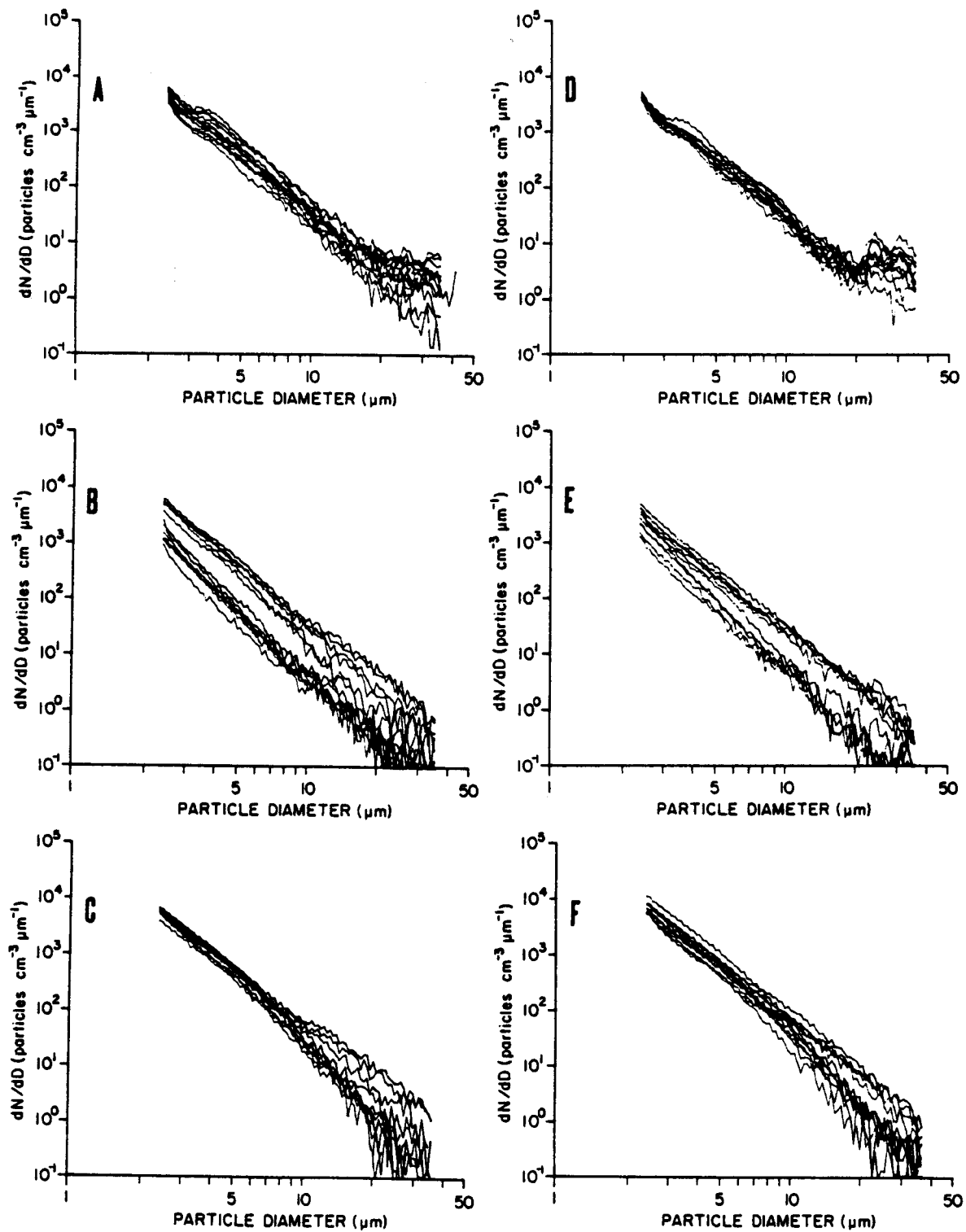


Figure 45. Incremental cumulative curves from NASTE 3 PL₁ surface (A), minimum turbidity (B), and bottom (C) zones. Panels D,E, and F show analogous curves for the PL₂ transect.

typical of the late summer and winter periods (Table 7). During both occupations of the PL line, there was a definite indication of a non-linearity in the PSD curves centered at $\sim 3.5 \mu\text{m}$, the same size range where prominent peaks were observed in the NASTE 1 surface data. Below the surface water, the mid-depth minimum zone can be separated into two distinct sub-populations (Fig. 45B and E): one sub-population, seaward of stations PL8 or 9, is characterized by slopes of ~ 3.8 ; another sub-population, inshore of these stations, is characterized by slopes of ~ 3.4 , similar to the surface waters (Table 7). A similar, but less exaggerated situation also exists in the near-bottom water (Fig. 45C and F; Table 7). In the bottom water, however, the region of PSD curves with low slopes is more restricted and does not include the landwardmost stations.

VI. DISCUSSION

A. Relationship Between Vertical Distributions of Particles and Density

The vertical distribution of fine-grained particles in the ocean is principally governed by the density structure, since the density structure controls the vertical distribution of turbulence. 'Fine-grained' in this context is taken to mean those particles whose settling velocity is much less than the mean horizontal current speeds of a given environment. For inorganic particles, the upper limit is $\sim 10 \mu\text{m}$; for organic particles and floccules, the upper limit may be several times larger. Since the hydrographic domains of the southeastern Bering Sea are also determined by the density structure (Kinder and Schumacher, 1981a), it is reasonable to expect that the various

hydrographic domains are characterized by specific kinds of particle distributions.

Figure 46 summarizes the types of particle distributions found during this study and illustrates their dependence on the density distribution. In the outer domain (PL6), the particle distribution consists of well-mixed layers at the boundaries of the water column and a mid-depth low turbidity zone. These layers are separated by zones of relatively uniform change in the particle concentration. In this figure, values of total light attenuation have been uniformly reduced by the clear water attenuation value of 0.4 m^{-1} (see Section IV. A.2.) in order to plot only the curvature resulting from the particle attenuation. Plotting the resultant values on semi-log paper identifies zones where the eddy diffusion is uniform. These zones are characterized by a uniform slope in the particle attenuation curve. Several such increments are apparent at PL6. The bottom nepheloid layer consists of two such layers, a layer of relatively high diffusion (steep slope) in the bottom 30m and an overlying layer of much lower diffusion between 70 and 95 m. According to Bassin (1974), the maintenance of a nepheloid layer requires both a particle source and an overlying layer of increased stability (minimum turbulence) to inhibit diffusion of the particles upward and out of the nepheloid layer. At PL6 there was excellent agreement between the attenuation profile and the shape of the stability distribution (Brunt-Väisälä frequency). Tidal mixing along the bottom created a zone of low and uniform stability in which the particles were well mixed. Above this zone, mixing diminished and the stability increased towards a maximum at ~70 m. Particle concentrations decreased rapidly through this zone. Close correspondence between particle and density gradients at the top of the bottom nepheloid layer has been previously observed in other environments as

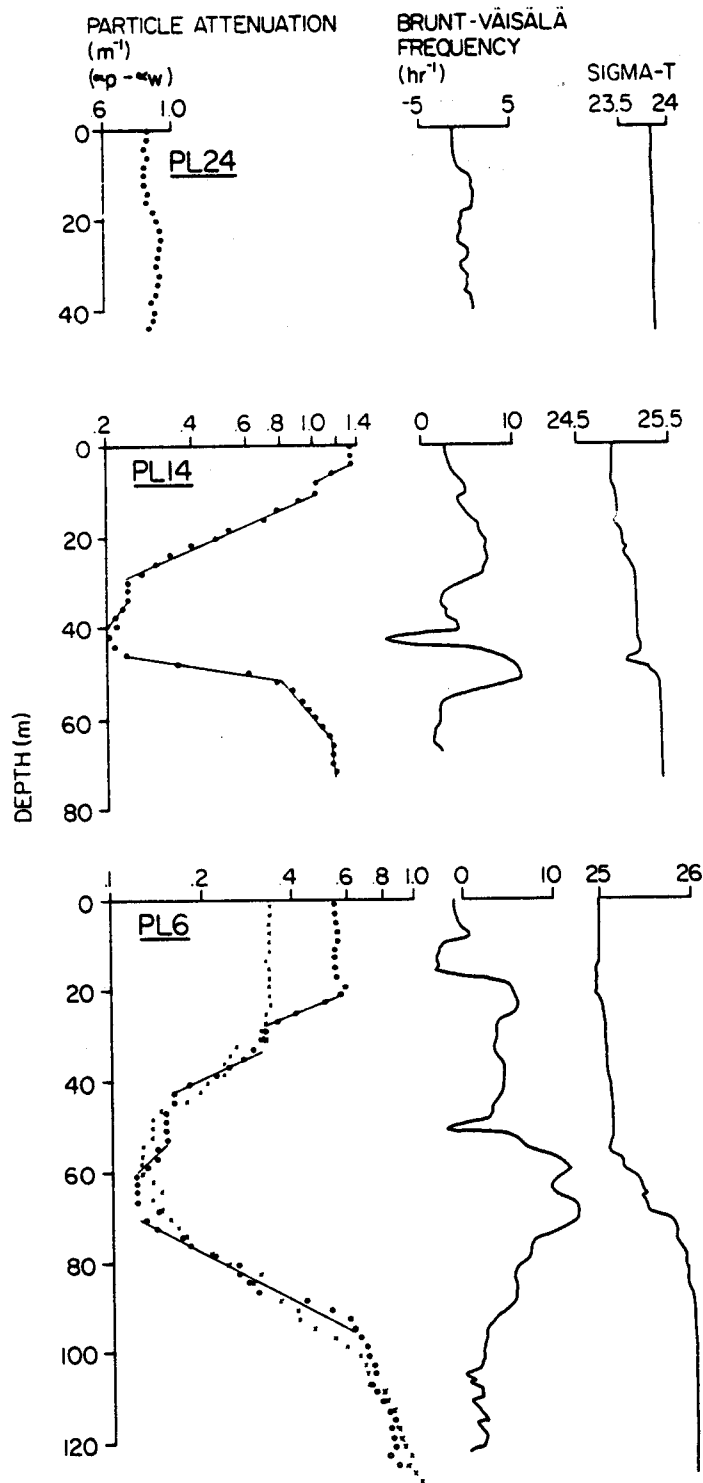


Figure 46. Net particle attenuation profiles, stability profiles, and density profiles from the coastal (top), middle (middle), and oceanic (bottom) domains. Note the stability maximum at the top of each bottom nepheloid layer.

diverse as the northwest Atlantic Ocean (Biscaye and Eitrem, 1974), Vema Channel in the southwest Atlantic (Johnson et al., 1976), and over the continental shelf off Oregon (Newberger and Caldwell, 1981).

A similar situation prevailed in the surface waters. Wind mixing created a layer of uniform density and particle concentrations underlain by a series of stability maxima and minima. Zones of low and uniform diffusion on Aug. 29 (e.g., 20-28 m, 34-44 m, and 54-62 m) were associated with stability peaks, while the relatively well-mixed layers separating them were associated with stability minima. This step-like decrease in particle concentrations, also seen during the Sept. 3 station occupation at PL6, may be attributable to discrete mixing events affecting the upper water column.

Distributions in the middle domain (Fig. 46, PL 14) were similar although the vertical particle gradients were generally steeper because of the sharper density gradients. The sigma-t curve, for instance, exhibited more of a discrete two-layer character without the intermediate middle layer seen in the outer domain. This change was reflected in a very low diffusion cap on the bottom nepheloid layer. Also, this layer at PL14 was partitioned into three mixing zones instead of the two observed at PL6.

As expected, distributions in the coastal zone were vertically uniform (Fig. 46, PL24). Water column stability was near zero everywhere and turbulence had thoroughly mixed the particles.

Coefficients of vertical eddy diffusion for particles can be estimated from the attenuation profiles in Fig. 45 using a sediment mass continuity equation:

$$\frac{\delta C}{\delta t} + \bar{u} \frac{\delta C}{\delta x} + \bar{v} \frac{\delta C}{\delta y} + (\bar{w} - w_s) \frac{\delta C}{\delta z} =$$

$$\frac{\delta}{\delta y} (K_y \frac{\delta C}{\delta y}) + \frac{\delta}{\delta z} (K_z \frac{\delta C}{\delta z})$$

where C is the SPM concentration in mass per unit volume; \bar{u} , \bar{v} , and \bar{w} are the mean advective flows in the horizontal and vertical directions; w_s is the SPM settling velocity; and K_y and K_z are the horizontal and vertical eddy diffusion coefficients. This equation can be simplified by assuming a steady state situation ($\delta C/\delta t = 0$), and $\delta C/\delta y$ and $\delta C/\delta x$ negligible compared to $\delta C/\delta z$; thus:

$$0 = \frac{\delta}{\delta z} \left[K_z \frac{\delta}{\delta z} + (\bar{w} - w_s) C \right]$$

and

$$\frac{C_z}{C_a} = \exp \left[- \int_a^z \frac{(\bar{w} - w_s)}{K_z} dz \right]$$

where C_z is the concentration level of SPM at some level z above a reference level C_a . Levels of approximately constant K_z are assumed wherever a semi-log plot of C vs. depth yields a straight line, and K_z in these intervals may be evaluated by the expression:

$$K_z = \frac{(\bar{w} - w_s) (z-a)}{\ln (C_z/C_a)}$$

Station PL6 was visited twice (August 29 and September 3) and showed little change in the vertical gradients, justifying the steady state assumption.

K_z can be accurately estimated for each interval only if the term $\bar{w} - w_s$ (the sum of vertical advection and particle settling velocity) is known. The settling velocity can be estimated from the Stokes equation

$$w_s = \frac{2g (\rho_s - \rho)r^2}{9 \eta}$$

if the particles are assumed to be spherical and their radius (r) and net density ($\rho_s - \rho$) is known, and if the viscosity of the water (η) is known. The PSD's yield limits on the size range at various depths, but the in-situ density of the particles is unknown at present. Furthermore, since w_s for most particles is likely to be in the range of 10^{-2} to 10^{-4} cm sec $^{-1}$, the vertical advection term is likely to be an important factor. J. Schumacher (personal communication) has suggested that the vertical advection term in the southeastern Bering Sea, particularly in frontal areas, may be on the order of 10^{-3} cm sec $^{-1}$.

For comparative purposes, then, Table 8 gives values of $K_z/(w - w_s)$ for each interval. Values of K_z are also calculated for some reasonable values of $(\bar{w} - w_s)$. Certain trends are clear from these data. Turbulent mixing is always highest in the tidally mixed bottom layer. Above this layer, values of K_z decrease either abruptly or by means of a transition layer into a layer of low K_z which ends in the uniform concentrations of the mid-depth low turbidity zone. At PL14, this decrease in K_z was a factor of 100 in the space of ~20 m.

The presence of diffusive barriers to particle mixing from the surface and bottom layers implies that transport of fine-grained particles from the surface to the bottom layers must occur primarily by large particles (e.g., biological aggregates such as fecal pellets) whose transit is not seriously impeded by the density structure. Similarly, fine-grained particles in the bottom layer are not easily mixed up into the overlying waters except when stratification breaks down, as in the coastal domain and in the middle domain during winter or during major storm events.

Table 8
 Calculation of vertical eddy diffusion coefficients
 (K_z) from SPM profiles

STA.	z (m above bottom)	a	$\ln(C_z/C_a)$	$K_z/(\bar{w} - w_s)$	K_z ($\text{cm}^2\text{sec}^{-1}$)			
					$\bar{w} = 0$	$\bar{w} = 0$	$\bar{w} = 10^{-3}$	$\bar{w} = 10^{-3}$
					$r = 5 \mu\text{m}$ $(\rho_{s1.5} - \rho) =$	$r = 5 \mu\text{m}$ $(\rho_{s0.15} - \rho) =$	$r = 5 \mu\text{m}$ $(\rho_{s1.5} - \rho) =$	$r = 5 \mu\text{m}$ $(\rho_{s0.15} - \rho) =$
PL-6	35	5	-0.38	-7905	14.8	1.5	6.9	0.7
	60	35	-1.47	-1700	3.2	0.3	1.5	0.2
PL-14	12	5	-0.01	-74549	139.4	13.5	64.9	6.5
	24	12	-0.31	-3912	7.3	0.7	3.4	0.3
	31	24	-1.18	-594	1.1	0.1	0.5	0.1

B. Characteristics of the particle domains and domain boundaries

1. Offshore transport of suspended particles

One of the goals of this project was to evaluate the effectiveness of the coastal front off the NAS region in prohibiting offshore transport of particles. To examine this question, offshore trends of average attenuation and average salinity were plotted against water depth for each survey period (Fig. 47). Figure 47 was constructed by averaging all NA stations (except NA 1-16, where properties were largely controlled by rivers in Kvichak Bay) within each of eight successive depth increments: 10-19, 20-29, 30-39, 40-49, 50-59, 60-69, 70-79, and ≥ 80 m. Average water column attenuation and salinity from each of these intervals then gave a meaningful picture of the offshore gradations of these properties.

The offshore trends of salinity and attenuation followed each other closely during each survey period. The steepest gradients were always found inshore of the 50-m isobath, with attenuation increasing sharply in the 10-19 m interval. Average attenuation seaward of 50 m was essentially uniform, with a value of $\sim 0.8 \text{ m}^{-1}$ during NASTE 1, 0.5 m^{-1} during NASTE 2, and 0.7 m^{-1} during NASTE 3. Salinity showed a continual decline in the deeper waters, however, except during the winter when values were stable.

As reported in the RESULTS section, the coastal front was best developed during NASTE 1 and 3; during NASTE 2 vertical stratification was absent throughout the region and so the coastal front, defined as the zone separating two differing structural domains, did not exist. Nevertheless, offshore attenuation gradients were virtually identical to the fall and spring cruises. This situation implies that the coastal front should not be thought of as a "barrier" to the passage of suspended particles in the

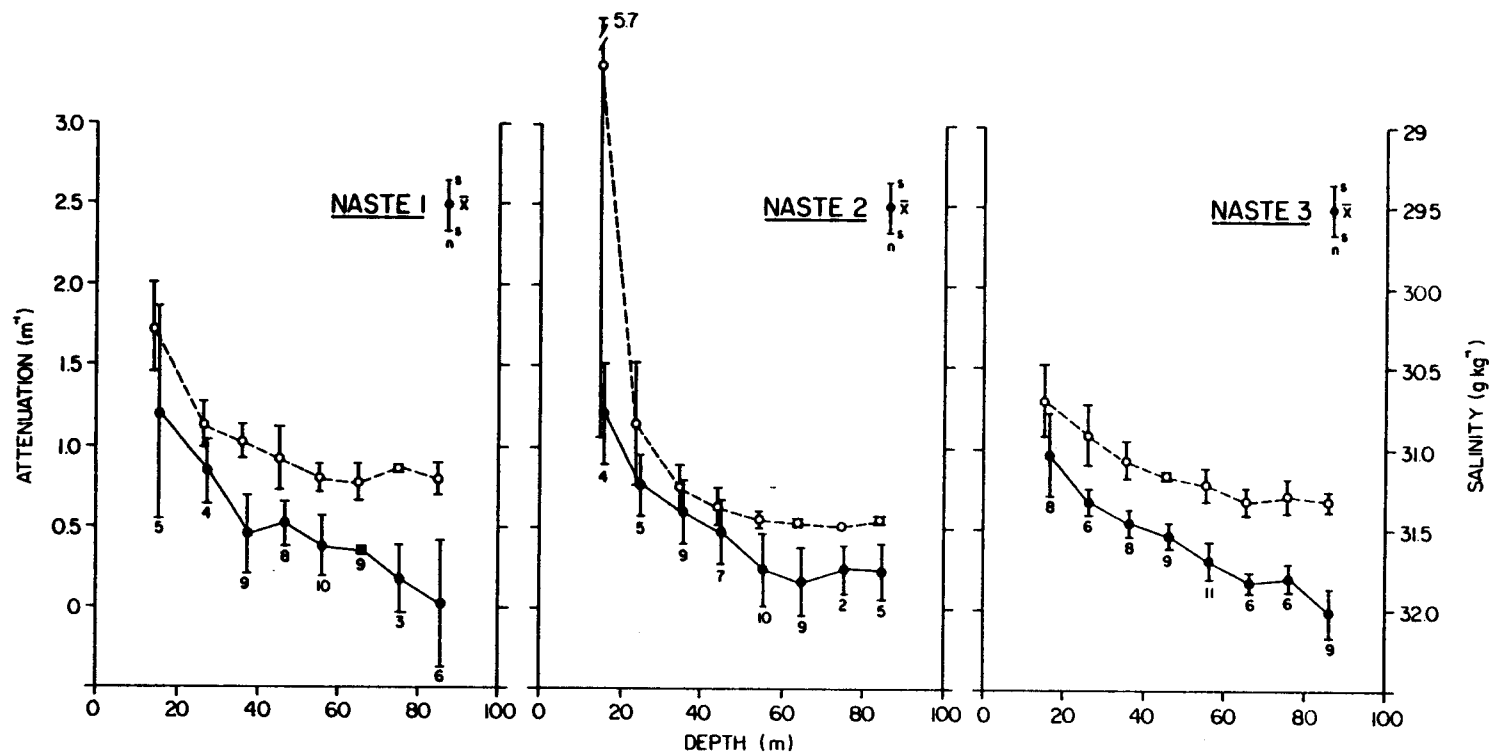


Figure 47. Attenuation (open circles) and salinity (closed circles) gradients normal to the Alaska Peninsula for each cruise. Mean attenuation and salinity values from each NA station were grouped and averaged over 10-m station depth increments.

water column. Particle concentrations are high inshore of 50 m because mixing energy, both tidal and wind, is highest there. Mean near-bottom current speeds at stations TP4, TP6, and TP9 ($z > 59\text{m}$) ranged from 15 to 22 cm sec^{-1} . At stations TP2, TP2B, TP8, and TP7 ($z < 35\text{ m}$), the range was 28 to 33 cm sec^{-1} . Bathymetry determines the positions of the fronts in the southeastern Bering Sea (Kinder and Schumacher, 1981a) and also exerts a powerful influence on the offshore transport of particles. This influence can most clearly be seen during winter, when in-situ particle sources (phytoplankton) are minor and local particle maxima and minima are reduced by vigorous vertical mixing. Examination of the areal distribution of attenuation during NASTE 2 (Figs. 10 and 11) shows that the 0.6 m^{-1} contour precisely follows the 50-m isobath. The 50-m isobath also marks the onset of a change in the bottom sediment texture (Fig. 5). Inshore, the mean size is almost exclusively $125\text{ }\mu\text{m}$ or greater. Seaward of 50m, the mean grain sizes become more variable and finer grained, attributes of a lower energy environment.

2. Vertical mixing of particles

Vertical mixing of particles is complete in the coastal zone except for isolated instances where large freshwater sources form a low-density surface plume. Direct evidence for this mixing comes from the many transmissometer casts taken in the nearshore zone. Records from the moored transmissometers showed significant peaks in the attenuation spectra at tidal frequencies (Fig. 36), implying that variation in current speeds is a principal controlling element in the variation of particle concentrations. The correlation of sedimentation rate, turbidity record, and mean current

speed was also highest at TP7 in the nearshore zone (Fig. 39).

These results describe a high energy environment where particles are routinely cycled throughout the water column. Median particle sizes in the water column are typically an order of magnitude lower than the bottom sediments. The suspended particles are thus largely in a state of transit through this zone, with little deposition occurring. The major particle sources are local rivers, shore erosion, and biogenic detritus; the influence of rivers such as the Kvichak and Nushagak is not important south of about 57°N along the coast. Port Moller is the only major source of particles in the study region, and even its influence is not felt beyond about 100 km from its mouth (Fig. 10). Particle losses to the middle domain occur by mixing and diffusion of low-salinity coastal water with the higher salinity offshore water, as well as by advective processes such as upwelling by which coastal water is replaced by offshore water.

Vertical mixing in the middle and outer domains is highly dependent on density stratification. Following Coachman and Charnell (1979), the fronts separating the middle and outer domains can be identified by a sharp increase in the horizontal gradient of the 0-100 m average salinity (Fig. 48). Increases in the vicinity of PL8-9 (~110 m) and PL3 (~150 m) were apparent during NASTE 3, agreeing with historical values of $\sim 9.3 \times 10^{-3} \text{ g kg}^{-3} \text{ m}^{-1}$ (Coachman and Charnell, 1979). Frontal characteristics were much less apparent during NASTE 1.

These hydrographic differences directly influenced the horizontal and vertical distributions of particles. During NASTE 3, the mid-depth low-turbidity zone was well developed and uniform seaward of PL9; the minimum attenuation value for these stations averaged $0.42 \pm 0.026 \text{ m}^{-1}$ (Fig. 49). Landward of PL9, the comparable value was 0.76 ± 0.093 , a 76% increase.

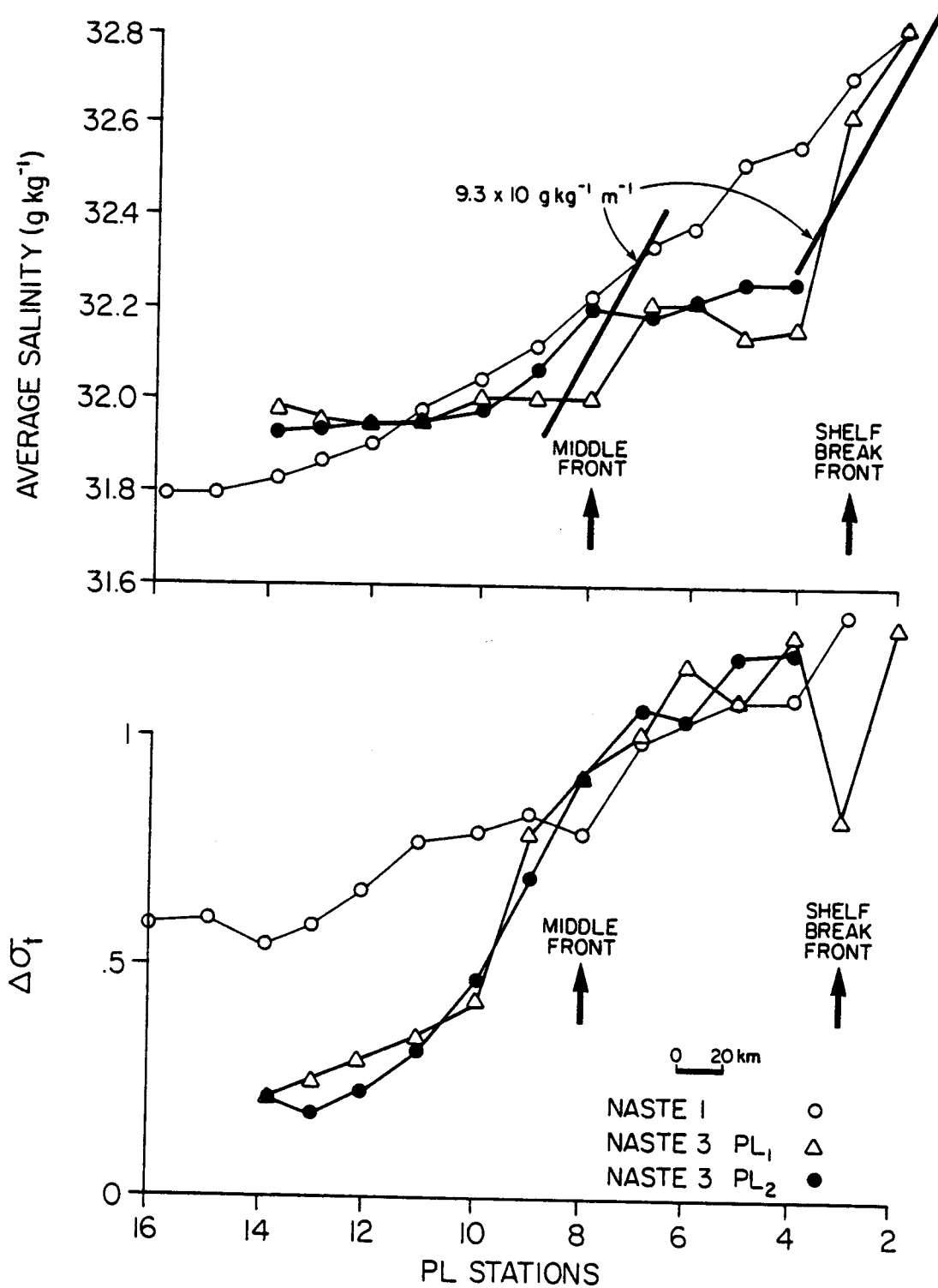


Figure 48. Salinity and $\Delta\sigma_t$ gradients along the PL line during NASTE 1 and NASTE 3.

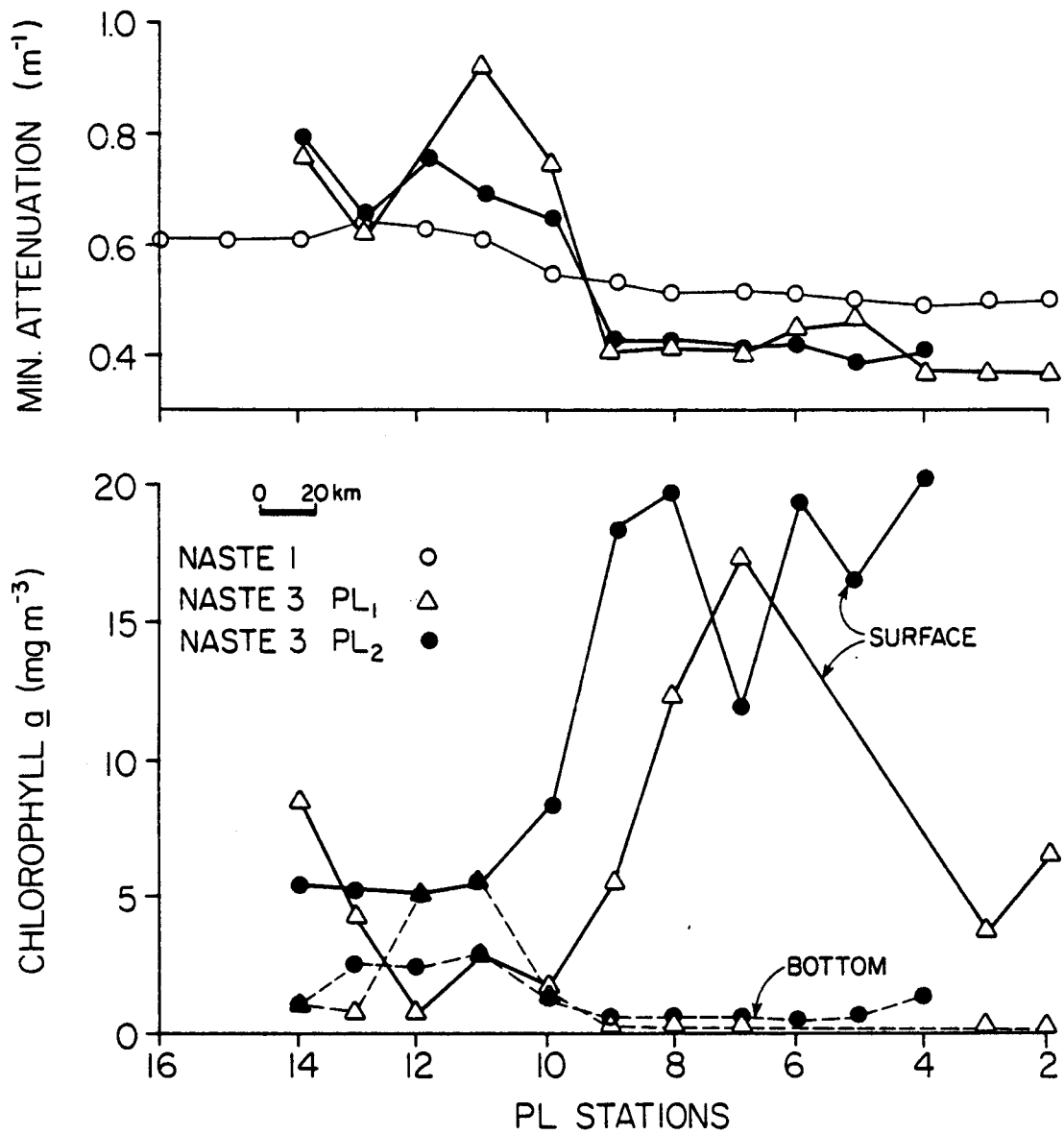


Figure 49. Changes in the attenuation value in the turbidity minimum and in the concentration of surface and bottom chlorophyll a along the PL line. Compare the position of these changes with the hydrographic changes in Figure 48.

Average attenuation over the entire water column increased by only 22% (from $0.70 \pm 0.056 \text{ m}^{-1}$ to $0.86 \pm 0.051 \text{ m}^{-1}$) from the outer to middle domain. These figures imply that increases in the mid-depth region of the water column are attributable to enhanced vertical mixing of the surface and bottom layers which were previously isolated by high $\Delta\sigma_t$ values. This interpretation is supported by the PL cross-sections in Figs. 41 and 42. Particle concentrations in the surface and bottom layers decline crossing the middle front region from outer domain to middle domain. This vertical mixing is also graphically demonstrated by a plot of the surface and bottom chlorophyll a concentration along the PL line during NASTE 3 (Fig. 49). In the outer domain, surface values are $\sim 30 \times$ greater than bottom values. In the middle domain, however, surface values decline and bottom values increase until both are about equal. Particle size distribution curves similarly show dramatic differences between middle and outer domain stations (Fig. 45).

During NASTE 1, however, stratification remained relatively high throughout the middle domain (Fig. 48), resulting in the maintenance of a well-defined, three-layer particle distribution seaward of PL18 (Fig. 40). Average value of the minimum attenuation between PL2 and PL10 was $0.52 \pm 0.02 \text{ m}^{-1}$; between PL11 and 16 this value increased only 19%, to $0.62 \pm 0.01 \text{ m}^{-1}$. The change in the average water column attenuation over the same interval was 28%, from $0.78 \pm 0.06 \text{ m}^{-1}$ to $1.00 \pm 0.09 \text{ m}^{-1}$. Unlike the situation during NASTE 3, vertical mixing of fine-grained particles was inhibited throughout the middle domain. The particle size distribution data also showed homogeneity in the minimum zone throughout the middle and outer domains (Fig. 43).

The mixing processes described above should not be interpreted to mean that no particle exchange occurs between the surface and bottom layers.

Fine-grained particles of both biogenic and non-biogenic origin are continually packaged into large biological particles such as fecal pellets which rapidly fall to the seafloor. On the seafloor, or in the water column, these large particles may be broken up and their constituent particles dispersed into the water column. This transport method is only applicable to particles dense enough to overcome the buoyancy effects of stratification and turbulence in the surface layer. Thus large organic-rich, low-density flocs may not be important in the vertical transport of material in stratified waters.

C. Particle Influences on the Transport of Spilled Oil in the Southeastern Bering Sea

The vertical sediment flux measurements reported here, combined with data on oil loading on various sediment types from SAI studies (Payne et al., 1981), can be used to produce crude estimates of the vertical transport of spilled oil to the seafloor. It must be emphasized that such calculations are extremely speculative. Sediment trap data give the mass of particles passing through a particular depth horizon over a given time with no implications about the origin of such material. Material may be added by surface fallout, mid-depth horizontal advection, or bottom sediment resuspension, and so the interpretation of sediment trap data as it affects the removal of oil from the water column is difficult.

Similarly, the SAI data relating oil loading on various sediment types may not be directly applicable to suspended particles. The SAI studies were all performed on samples of deposited sediments, which may have oil

absorption characteristics quite different from the suspended particles described in this report.

Bearing these difficulties in mind, we may use the available data to generate some oil transport figures to set the scale of the problem. Five sediment types were tested in the SAI study: (1) Kasitsna Bay 1: fine-grained terrestrial sediment plus diatoms, many flakes $\leq 5 \mu\text{m}$, total aliphatic plus aromatic loading of 527 mg per kg of sediment; (2) Kasitsna Bay 2A: surface (< 1 cm deep) sediment mostly $> 5 \mu\text{m}$, terrestrial material plus some plant debris, 1216 mg oil per kg sediment; (3) Kasitsna Bay 2B: below surface (1-8 cm) sediment mostly $> 5 \mu\text{m}$, 744 mg oil per kg sediment; (4) Kasitsna Bay 3: consolidated sediment >90% diatoms, some terrigenous material $\leq 5 \mu\text{m}$, 122 mg oil per kg sediment; and (5) Kasitsna Bay 4: salt marsh material, organic matter plus fecal pellets, 694 mg oil per kg sediment.

The oil loading data can be combined with the sediment data in two ways. First, the range of oil loadings observed can be combined with typical sediment concentrations from different depth zones of the North Aleutian Shelf (Fig. 47) to derive a range of accommodated oil loadings for the NAS waters. Average attenuation values from Fig. 47 were transformed into particle mass concentrations using the regression equations in Table 1. The calculations in Table 9 indicate that sediment accommodated oil loadings might vary from ~ 10 to 100 mg m^{-2} in the near-shore zone, and from ~ 5 to 60 mg m^{-2} in the offshore zone if all the suspended particles were loaded with oil in the manner of the sediments tested by SAI. These loadings translate into ~ 0.7 to 7 ppb total concentration of oil in the near-shore zone water column and ~ 0.06 to 1.1 ppb in the offshore zone. Oil not associated with particles, of course, is not considered here.

A second method of treating the data is to consider the possible

delivery rates of accommodated oil to the benthos by combining the sediment trap data with the oil-loading studies. The figures in Table 10 represent the oil sedimentation expected under the minimum, mean, and maximum fluxes observed at each trap site if the sedimenting material had the characteristics of the various sediments tested in the SAI study. The maximum value is $\sim 30 \text{ mg m}^{-2} \text{ day}^{-1}$ for KB2A at either TP7 or TP9. Mid-shelf values (TP8 and TP2B) never exceed $7 \text{ mg m}^{-2} \text{ day}^{-1}$. Mean values are generally in the range $1\text{-}10 \text{ mg m}^{-2} \text{ day}^{-1}$.

Table 9
Estimated oil loading on NAS suspended sediments

Depth Zone (m)	Average Sediment Loading (gm^{-2})	Sediment Accommodated Oil Loading (mg m^{-2})				
		KBI (527 mg kg^{-1}) ¹	KB2A (1216 mg kg^{-1})	KB2B (747 mg kg^{-1})	KB3 (122 mg kg^{-1})	KB4 (694 mg kg^{-1})
10-19	79.0	41.6	96.1	58.8	9.6	54.8
40-49	41.1	21.7	50.0	30.6	5.0	28.5
80-89	48.4	25.5	58.8	36.0	5.9	33.6

¹Measured SAI oil loading per kg of sediment (Payne et al., 1981).

Table 10
 Estimated oil sedimentation rates in NAS waters

Trap Site	Water Depth (m)	Oil Sedimentation Rate ($\text{mg m}^{-2} \text{ day}^{-1}$)														
		KBI			KB2H			K2B			KB3			KB4		
		min	mean	max	min	mean	max	min	mean	max	min	mean	max	min	mean	max
TP 7	24	2.4	5.9	12.8	5.6	13.6	29.4	3.4	8.3	18.0	0.6	1.4	3.0	3.2	7.8	16.8
TP8	31	0.1	0.9	1.3	0.3	2.2	2.9	0.2	1.3	1.8	0.03	0.2	0.3	0.2	1.2	1.7
TP2B	35	0.4	1.7	3.0	1.0	3.9	6.9	0.6	2.4	4.2	0.1	0.4	0.7	0.5	2.2	4.0
TP9	89	0.9	5.1	13.9	2.2	11.7	32.1	1.3	7.1	19.6	0.2	1.2	3.2	1.2	6.7	18.3

VII. ACKNOWLEDGEMENTS

This study could not have been conducted without the support of many other people in both the field and the laboratory. D.A. Tennant and S.L. Walker were of continuing help throughout this project. The captains and crews of the NOAA ships *Surveyor* and *Discoverer* made the field studies possible. The work was supported by the Office of Marine Pollution Assessment, Alaska Office.

VIII. REFERENCES

- Bader, H. (1970). The hyperbolic distribution of particle size. J. Geophys. Res. 75, 2822-2830.
- Baker, E.T. (1973). Nephelometry and mineralogy of suspended particulate matter in the waters over the Washington Continental slope and Nitinat Deep-Sea Fan. Ph.D. dissertation, Univ. of Washington, Seattle, 142 pp.
- Baker, E.T. (1982). Suspended particulate matter in Elliott Bay. NOAA Tech. Rept. ERL 417-PMEL 35, 44 pp.
- Baker E.T., J.D. Cline, R.A. Feely, and J. Quan (1978). Seasonal distribution, trajectory studies, and sorption characteristics of suspended particulate matter in the northern Puget Sound region. EPA-600 17-78-126, 140 pp.

- Baker, E.T., R.A. Feely, and K. Takahashi (1979). Chemical composition, size distribution, and particle morphology of suspended particulate matter at DOMES sties A, B, and C: Relationships with local sediment composition. In Marine Geology and Oceanography of the Pacific Manganese Nodule Province (J. Bischoff and D.Z. Piper, eds.), Plenum, New York, pp. 163-201.
- Baker, E.T., and H.B. Milburn (in press). An instrument system for the investigation of particle fluxes. Cont. Shelf Res.
- Bartz, R., J.R.V. Zaneveld, and M. Pak (1978). A transmissometer for profiling and moored observations in water. SPIE Ocean Optics V, 106, 102-108.
- Bassin, N.J. (1974). Suspended matter and the stability of the water column: Central Caribbean Sea. In Suspended Solids in Water (R.J. Gibbs, ed.), Plenum, New York, pp. 271-279.
- Biscaye, P.E. and S.L. Eithreim (1974). Variations in benthic boundary layer phenomena: Nepheloid layer in the North American Basin. In Suspended Solids in Water (R.J. Gibbs, ed.), Plenum, New York, pp. 271-279.
- Brun-Cottan, J.C. (1976). Stokes settling and dissolution rate model for marine particles as a functioning size distribution. J. Geophys. Res., 81, 1601-1606.
- Carder, K.L., and F.C. Schlemmer, II (1973). Distribution of particles in the surface waters of the eastern Gulf of Mexico: An indicator of circulation. J. Geophys. Res., 78, 6286-6299.

- Coachmen, L.K., and R.L. Charnell (1979). On lateral water mass interaction--A case study, Bristol Bay, Alaska. J. Phys. Oceanogr., 9, 278-297.
- Crececius, E.A., M.M. Bothner, and R. Carpenter (1974). Geochemistries of arsenic, antimony, mercury, and related elements in sediments of Puget Sound. Env. Sci. Tech., 9: 325-333.
- Feely, R.A., G.J. Massoth, A.J. Paulson, M.F. Lamb, and E.A. Martin (1981). Distribution and elemental composition of suspended matter in Alaskan coastal waters. NOAA Tech. Memo. ERL PMEL-27, 119 pp.
- Gardner, W.D. (1980a). Sediment trap dynamics and calibration: a laboratory evaluation. J. Mar. Res., 38, 17-39.
- Gardner, W.D. (1980b). Field assessment of sediment traps. J. Mar. Res., 38, 41-52.
- Hannan, C.A., and W.D. Grant (1982). Evaluating sediment trap biases in natural flows. EOS, 63, 46.
- Holm-Hansen, O., C.J. Lorenzen, R.W. Holmes, and J.D.H. Strickland (1965). Fluorometric determination of chlorophyll. J. Cons. Int. Explor. Mer., 30, 3-15.
- Iverson, R.L. L.K. Coachman, R.T. Cooney, T.S. English, J.J. Goering, G.L. Hunt, Jr., M.C. MacCauley, C.D. McRoy, W.S. Reeburgh, and T.E. Whitledge (1979). Ecological significance of fronts in the southeastern Bering Sea. In Ecological Processes in Coastal and Marine Systems (R.S. Livingston, ed.), Plenum, New York, pp. 437-466.

Johnson, D.A., S.E. McDowell, L.G. Sullivan, and P.E. Biscaye (1976).

Abyssal hydrography, nephelometry, currents, and benthic boundary layer structure in the Vema Channel. J. Geophys. Res., 81, 5771-5786.

Kinder, T.H. and J.D. Schumacher (1981a). Hydrographic structure over the continental shelf of the southeastern Bering Sea. In The Eastern Bering Sea Shelf: Oceanography and Resources, vol. 1, (D.W. Hood and J.A. Calder, eds.), NOAA/Office of Marine Pollution Assessment, pp. 31-52.

Kinder, T.H. and J.D. Schumacher (1981b). Circulation over the continental shelf of the southeastern Bering Sea. In The Eastern Bering Sea Shelf: Oceanography and Resources, vol. 1, (D.W. Hood and J.A. Calder, eds.), NOAA/Office of Marine Pollution Assessment, pp. 53-75.

Kitchen, J.C., J.R.V. Zaneveld, and M. Pak (1978). The vertical structure and size distributions of suspended particles off Oregon during the upwelling season. Deep-Sea Res., 25, 453-468.

Lal, D. and A. Lerman (1973). Dissolution and behavior of particulate biogenic matter in the ocean: Some theoretical considerations. J. Geophys. Res., 78, 7100-7111.

Landing, W.M. (1978). The chemistry and vertical flux of particulate materials in the N.E. Gulf of Alaska. M.S. Thesis, Univ. of Washington, Seattle, 101 pp.

Lerman, A., K.L. Carder, P.R. Betzer (1977). Elimination of fine suspensoids in the oceanic water column. Earth Planet. Sci. Lett., 37: 61-70.

- Liss, P.S. (1976). Conservative and non-conservative behavior of dissolved constituents during estuarine mixing. In Estuarine Chemistry (J.D. Burton and P.S. Liss, eds.), Academic Press, London, pp. 93-130.
- McCave, I.N. (1975). Vertical flux of particles in the ocean. Deep-Sea Res., 22, 297-310.
- Meyers, P.A. and J.G. Quinn (1973). Factors affecting the association of fatty acids with mineral particles in seawater. Geochim. Cosmochim. Acta, 37, 1745-1759.
- Natrella, M.G. (1963). Experimental Statistics, Nat. Bureau of Standards, 504 pp.
- Newberger, P.A. and D.R. Caldwell (1981). Mixing and the bottom nepheloid layer. Mar. Geol., 41, 321-327.
- Payne, J.R., B.E. Kirstein, R.E. Jordan, G.D. McNabb, Jr., J.L. Lambach, M. Frydrych, W.J. Paplawsky, G.S. Smith, P.L. Mankiewicz, R.T. Redding, D.M. Baxter, R.E. Spenser, R.F. Shokes, and D.J. Maiero (1981). Multi-variate analysis of petroleum weathering in the marine environment-- Sub Arctic. Annual Rept. to NOAA/Office of Marine Pollution Assessment (Alaska Office).
- Pearson, C.A., E.T. Baker, and J.D. Schumacher (1980). CTD and SPM observations during reestablishment of a structural front: Bristol Bay, Alaska. EOS, 61, 1002.
- Sharma, G.D. (1979). The Alaskan Shelf: Hydrographic, Sedimentary, and Geochemical Environment. Springer Verlag, New York.
- Schuman, F.R. and C.J. Lorenzen (1975). Quantitative degradation of chlorophyll by a marine herbivore. Limnol. Oceanogr., 20, 580-586.
- Tyler, J.E., R.W. Austin, and T.J. Petzald (1974). Beam transmissometers for oceanographic measurements. In Suspended Solids in Water (R.J. Gibbs, ed.), Plenum, New York, pp. 51-60.

IX. APPENDICES

Appendix A: Discrete sample data from Cruise RP4SU804.

NASTE 1

Station	Cast #	Depth m	SPM mg/l	% Organic Matter	Size Distribution Slope
NA46	6	2	2.304	42	
		17	5.908	32	
NA44	8	2	1.262		
		35	1.412		
NA42	10	2	0.350		
		66	1.356		
PM1	11	2	0.459		
NA40	12	2	1.958	36	
PM3	13	2	1.725		
NA38	15	2	1.782		
		35	0.263		
NA36	17	2	0.736		
		55	0.451		
NA34	19	2	0.600	37	
		40	1.158		
		63	1.642	29	
NA4-A	24	2	4.068	39	
		17	2.586	42	
NA3-A	26	2	1.996	32	
NA2-A	27	2	1.490	34	
		25	2.448	27	
NA1-A	28	2	0.994	52	
		36	2.792	40	
NA5	29	2	0.636	61	
		37	6.134	32	

Station	Cast #	Depth m	SPM mg/l	% Organic Matter	Size Distribution Slope
NA6	30	2	0.793	47	
		36	1.730	30	
NA7	31	2	1.484		
		38	1.872	31	
NA8	32	2	1.036	38	
		34	1.046	41	
NA9	33	2	1.165	32	
		28	2.984	35	
NA10	34	2	1.320	65	
		24	4.371	45	
NA16	36	2	1.683		
		25	3.264	66	
NA15	37	2	1.020	43	
		37	1.614	21	
NA14	38	2	1.303	55	
		44	6.241	32	
NA12	40	2	0.840	48	
		40	3.721	32	
NA18	44	2	0.732	46	
		30	5.591		
		55	1.996	32	
NA20	46	2	0.194	4	
		41	0.952	33	
NN22	48	2	1.837	44	
		17	2.253	40	

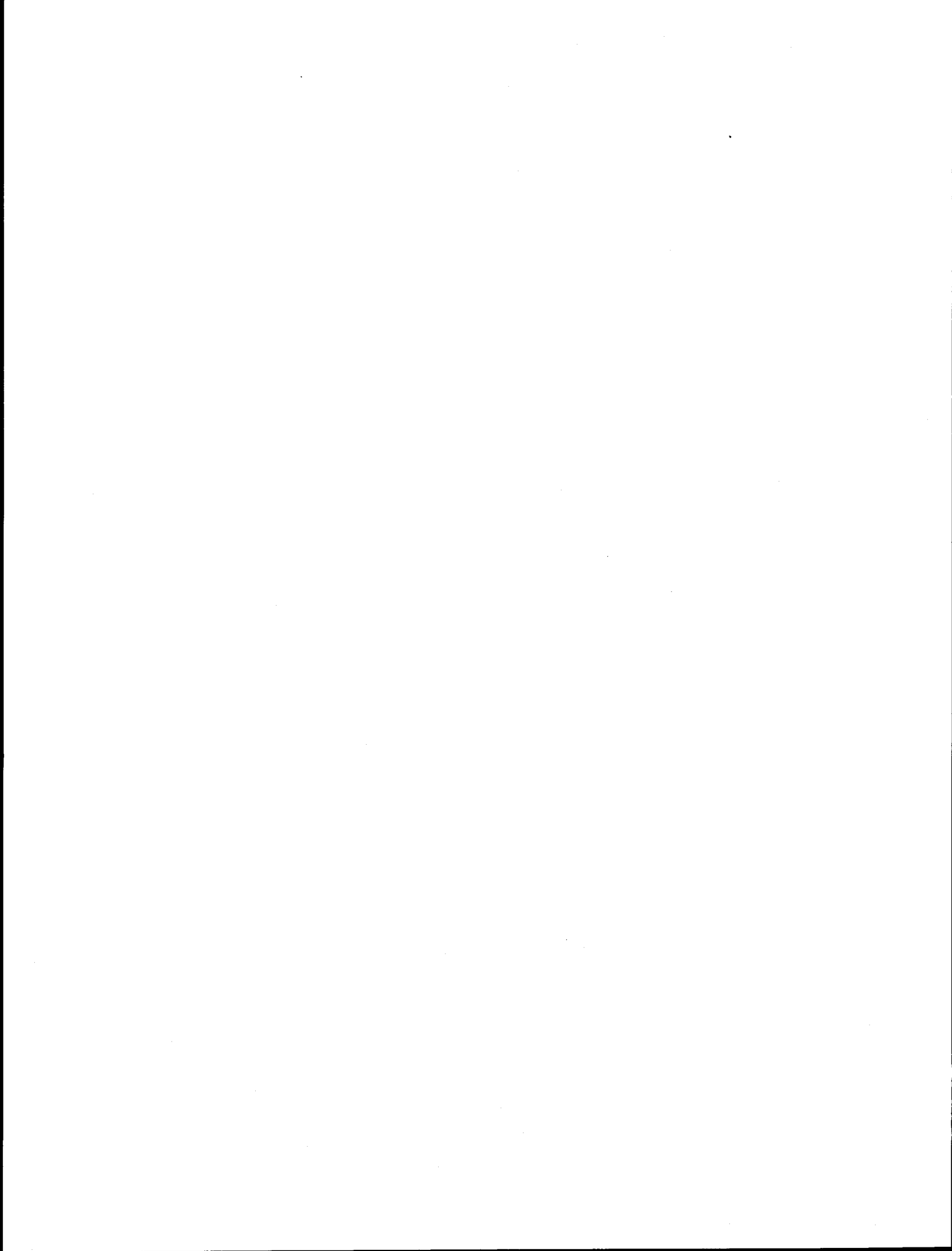
Station	Cast #	Depth m	SPM mg/l	% Organic Matter	Size Distribution Slope
NA27	49	2	2.315	34	
		18	3.004	35	
NA25	51	2	1.221	42	
		45	1.222	57	
NA23	53	3	0.575	57	
		59	1.117	45	
NA29	55	2	0.461	53	
		58	2.509	28	
NA31	57	2	0.196	44	
		45	1.304	15	
NA33	59	2	1.805	47	
		22	1.731	48	
NA40	61	2	1.308	35	4.16
		12	3.168	27	3.23
NA39	62	2			2.84
		17			3.62
NA38	63	2	0.873		2.75
		32	0.999		4.14
NA37	64	2			3.10
		47			3.40
NA35	65	2	0.426		3.73
		64	0.649		3.45
NA34	66	2			3.38
		65			2.50
NA34-B	67	2	0.589	36	2.70
		84	0.595	44	3.12

Station	Cast #	Depth m	SPM mg/l	% Organic Matter	Size Distribution Slope
NA41	68	2	0.273	46	
		86	1.340	27	
NA43	70	2	0.421		
		56	3.116		
NA45	73	2	0.789		
		31	1.456		
NA52	75	4	4.363	26	
		19	5.685	22	
NA50	77	2	0.867	40	
		50	2.371	22	
NA48	79	2	0.383	45	
		72	0.413	32	
NA47	80	2	0.404	44	
		68	0.518	30	
NA58-A	81	2	0.713	50	
		32	0.643	44	
NA40	83	2	3.535	33	
		10	9.376	26	
NA59	86	2	0.464	44	
		50	0.163		
		94	1.010	23	
NA61	87	2	1.397	40	
		76	1.156	26	
NA64	89	3	0.894	48	
		35	1.682	31	

Station	Cast #	Depth m	SPM mg/l	% Organic Matter	Size Distribution Slope
NA72	91	2	1.144	46	
		34	1.078	35	
NA69	93	2	0.392	74	
		99	0.908	22	
SG7	95	2	0.261	51	
		105	1.147	20	
SG5	96	2	1.021		
		124	1.822		
SG4	97	2	0.395		
		72	0.355		
SG2	98	3	0.195		
		75	0.692		
SG1	99	2	0.692		
		66	0.555		
UP5	103	2	0.180		
		50	0.132		
		150	0.204		
		200	0.287		
		296	0.222		
PL3	106	2			4.26
		50			4.12
PL4	107/108	2	0.205		3.52
		50			3.95
		100	0.265		
		137	1.024		4.15

Station	Cast #	Depth m	SPM mg/l	% Organic Matter	Size Distribution Slope
PL6	110	2	0.409		4.75
		50			4.88
		126	1.924		4.26
PL8	112	2			5.32
		60			4.09
		118	1.463		4.10
PL10	114	2	0.048		4.97
		40	0.494		
		60			4.41
		85	1.144		4.26
PL12	116	2	0.303		5.30
		40	0.317		4.27
		75	1.915		4.26
PL14	118	2			4.75
		40	0.231		4.25
		60	1.554		
		72	1.526		4.16
PL16	120	2	0.362		4.75
		30			3.86
		50	1.627		
		63	1.477		3.92
PL18	122	2	0.590		3.81
		30			3.86
		46	4.148		3.71
PL20	125	2			4.01
		40			3.73

Station	Cast #	Depth m	SPM mg/l	% Organic Matter	Size Distribution Slope
NA45	139	2	0.564		
		31	1.370		
NA36	142	2	0.550		
		52	0.735		
NA38	144	2	0.439		
		30	1.364		
NA40	147	2	0.201	53	
NA33	149	2	1.566	44	
		10	1.464	46	
NA31	151	2	0.651	68	
		39	0.452	67	
NA29	153	58	0.308	45	
NA24	156	2	0.497	94	
		54	0.823	39	
NA26	158	2	0.942	58	
		24	0.193		



Appendix B: Discrete sample data from cruise RP4SU81A

NASTE 2

Station	Cast #	Depth m	SPM mg/l	% Organic Matter	Size Distribution Slope
NA28	2	2	0.435	54	
		17	0.544		
		65	0.518	57	
NA31	5	2	0.940	38	
		36	1.418	33	
NA40	8	2	5.506	27	
		16	16.202	20	
NA38	10	2	0.871	51	
		31	1.125	37	
NA36	12	2	0.434	39	
		25	0.435		
		49	0.578	45	
NA34	15	2	0.438	40	
		24	0.422		
		54	0.520	56	
NA46	16	2	2.250	27	
		21	2.183	32	
NA44	18	2	0.991	47	
		30	0.954	51	
NA41	21	2	0.326	50	
		80	0.459	41	
SG11	22	2	0.146		
		44	0.208		
		50	0.216		
		78	0.811		

Station	Cast #	Depth m	SPM mg/l	% Organic Matter	Size Distribution Slope
PL10	24	2	0.217		
		48	0.217		
		68	0.562		
		79	1.032		
NA52-B	29	2	9.851	18	
		10	7.662	23	
NA50	31	2	0.569	48	
		42	0.649	45	
NA47	34	2	0.416	43	
		55	0.511	40	
NA1-A	35	2	2.601	25	
		7	2.401		
		24	3.454	26	
NA4-A	39	2	3.893	17	
		11	2.890	23	
NA10	41	2	1.789	24	
		17	2.008	23	
NA8	43	2	0.905	48	
		23	1.228	68	
NA5	46	2	0.786	50	
		15	0.821		
		31	1.065	45	
NA11	47	2	0.495	38	
		45	0.638	43	
NA14	50	2	0.546	46	
		31	0.742	60	

Station	Cast #	Depth m	SPM mg/l	% Organic Matter	Size Distribution Slope
NA16	52	2	1.417	34	
		14	1,634	30	
PM3(A)	57	2	6,821		
		14	5,596		
PM3(B)	59	2	4.051		
		12	3.404		
PM3(C)	60	2	4.898		
		5	5.031		
		10	4.481		
PM3(D)	62	2	17.058		
		12	19.022		
		15	18.302		
PM3(F)	65	2	12.300		
		13	16.408		
PM3(G)	67	2	4.464		
		15	4.489		
PM3(H)	69	2	3.996		
		13	4.016		
PM3(I)	71	2	7.015		
		13	5.736		
NA22	73	2	1.293	31	
		23	1.361	33	
NA20	75	2	1.933		
		35	0.874	47	

Station	Cast #	Depth m	SPM mg/l	% Organic Matter	Size Distribution Slope
NA17	78	2	0.497	50	
		49	0.481	39	
NA23	79	2	0.552	35	
		60	0.629	40	
NA25	81	2	0.518		
		45	0.737	7	
NA27	83	2	3.687	31	
		21	3.134	28	
NA33	84	2	3.890	23	
		19	5.925	23	
NA31	86	2	0.729	30	
		35	0.897	29	
NA28	89	2	0.329	45	
		61	0.471	48	
NA34	90	2	0.371	47	4.08
		63	0.591	40	3.74
NA35	91	2			4.29
		62			3.93
NA36	92	2	0.440	43	3.84
		54	0.561	35	3.67
NA37	93	2			3.94
		47			3.70
NA38	94	2	1.606	33	4.24
		10	1.633		
		31	1.417	29	4.17

Station	Cast #	Depth m	SPM mg/l	% Organic Matter	Size Distribution Slope
NA39	95	2			3.59
		14			3.36
NA40	96	2	11.506	17	3.10
		5	9.339		
		10	9.893	17	3.24
NA46	97	2	2.588	25	
		18	2.384	27	
NA44	99	2	0.702	42	
		40	0.832	25	
NA41	102	2	0.234	52	
		84	0.479	42	
NA47	103	2	0.212	53	
		67	0.417	42	
NA50	106	2	0.447	45	
		55	0.568	33	
NA52	108	2	3.556	16	
		16	4.697	16	
NA53	109	2	0.208	61	
		60	0.456		
		83	0.533	33	
NA56	112	2	0.444	45	
		39	0.489	37	
NA58	114	2	0.920	35	
		21	1.250	24	
NA65	115	2	0.538	29	
		15	0.423		
		31	1.601	21	

Station	Cast #	Depth m	SPM mg/l	% Organic Matter	Size Distribution Slope
NA63	117	2	0.328	44	
		44	0.496	35	
NA61	119	2	0.226	60	
		60	0.286		
		75	0.805	30	
NA59	121	2	0.264	57	
		50	0.186		
		90	1.026	31	
NA72	122	2	0.628	32	
		45	0.749	31	
NA70	124	2	0.368	39	
		66	0.596	31	
NA68	126	2	0.322		
		102	1.139	23	
PL4	127	2	0.175		3.84
		120	0.762		
		133	0.794		3.72
PL6	128	2			4.30
		123			4.58
SG28	129	116			4.08
PL8	131	2			3.95
		115			4.77
PL10	132	2	0.181		4.11
		77	1.147		
		85	0.989		4.22

Station	Cast #	Depth m	SPM mg/ℓ	% Organic Matter	Size Distribution Slope
PL12	133	2			3.91
		76			3.61
PL14	134	2			4.16
		70			3.92
SG14	136	2	0.237		
		69	0.603		
SG23	140	2	0.175		
		38	0.182		
		78	1.204		
		110	1.165		
SG26	143	2	0.260		
		60	0.200		
		90	1.198		
SG43	146	2	0.183		
		60	0.216		
		128	0.599		
SG29	150	2	0.181		
		92	0.164		
		130	1.446		
SG46	152	2	0.250		
		200	0.167		
		435	0.333		
UP10	153	2	0.394		
		50	0.230		
		285	0.220		

Station	Cast #	Depth m	SPM mg/l	% Organic Matter	Size Distribution Slope
UP12	155	2	0.465		
		56	0.439		
		74	0.385		
UP14	157	2	0.930		
		82	0.378		
		105	0.377		

Appendix C: Discrete sample data from cruise RP4DI81A

Station	Cast #	Depth m	SPM mg/l	% Organic Matter	Size Distribution Slope
NA41	9	2	0.664	64	
		40	1.069		
		81	1.189	30	
NA42	11	2	0.854	53	
		40	0.973		
		63	1.250	38	
NA43	12	2	0.649	37	
		30	1.265		
		56	1.185	36	
NA44	13	2	0.468	45	
		20	0.777		
		37	2.242	39	
NA45	14	2	0.893	52	
		20	1.679		
		27	2.714	35	
NA46	15	2	1.637	58	
		15	2.237	58	
NA40	16	2	2.139	20	
		11	2.749	31	
NA39	17	2	1.036	38	
		15	1.159	47	
NA38	19	2	0.535	49	
		20	0.396		
		28	0.769	47	

Station	Cast #	Depth m	SPM mg/l	% Organic Matter	Size Distribution Slope
NA37	20	2	0.559	37	
		30	1.601		
		45	2.172	40	
NA36	21	2	0.757	55	
		30	1.234		
		55	1.535	43	
NA35	22	2	0.787	42	
		40	1.400		
		65	1.518	34	
NA34	23	2	1.413	72	
		40	1.415		
		63	1.263	33	
SG10	25	2	0.331		
		30	0.332		
		88	1.253		
SG26	27	2	1.394		
		30	0.214		
		92	0.778		
SG27	29	2	0.806		
		30	0.184		
		112	0.591		
SG45	31	2	0.540		
		30	0.308		
		138	0.658		

Station	Cast #	Depth m	SPM mg/l	% Organic Matter	Size Distribution Slope
PL2	33	2	1.142		3.02
		30	0.206		3.30
		365	0.377		3.65
PL3	34	2	0.591		3.64
		153	0.193		3.79
PL4	35	2	0.283		3.93
		100			3.44
		137	0.962		3.97
PL5	36	2	1.904		3.29
		50	0.175		4.16
		120	0.932		
		132	0.915		4.00
PL6	37	2	2.411		3.39
		80			3.87
		127	1.487		4.14
PL7	38	2	2.034		3.64
		50	0.179		3.89
		110	0.761		
		126	1.161		4.22
PL8	39	2	1.665		3.31
		80			4.07
		117	0.203		
PL9	40	2	0.996		3.36
		40	0.402		
		80	0.629		2.97
		97	0.912		4.07

Station	Cast #	Depth m	SPM mg/l	% Organic Matter	Size Distribution Slope
PL10	41	2	0.617		3.66
		70	0.836		3.53
		86	1.246		3.36
PL11	42	2	0.961		3.79
		40	1.213		3.18
		65	1.357		
		81	1.619		2.94
PL12	43	2	0.961		3.79
		40	1.213		3.18
		65	1.357		
		81	1.619		2.94
PL12	43	2	0.483		3.39
		30			3.07
		60	1.091		
		74	1.750		2.82
PL13	44	2	1.032		3.04
		30	0.640		4.09
		55	0.739		
		72	0.794		3.97
PL14	45	2	0.882		3.37
		50	0.922		3.83
		66	1.098		3.65
SG69	46	2	0.769		
		65	0.615		
SG69	48	2	1.102		
		90	0.851		
SG5	51	2	1.122		
		113	0.933		
SG29	52	2	0.701		
		126	0.914		

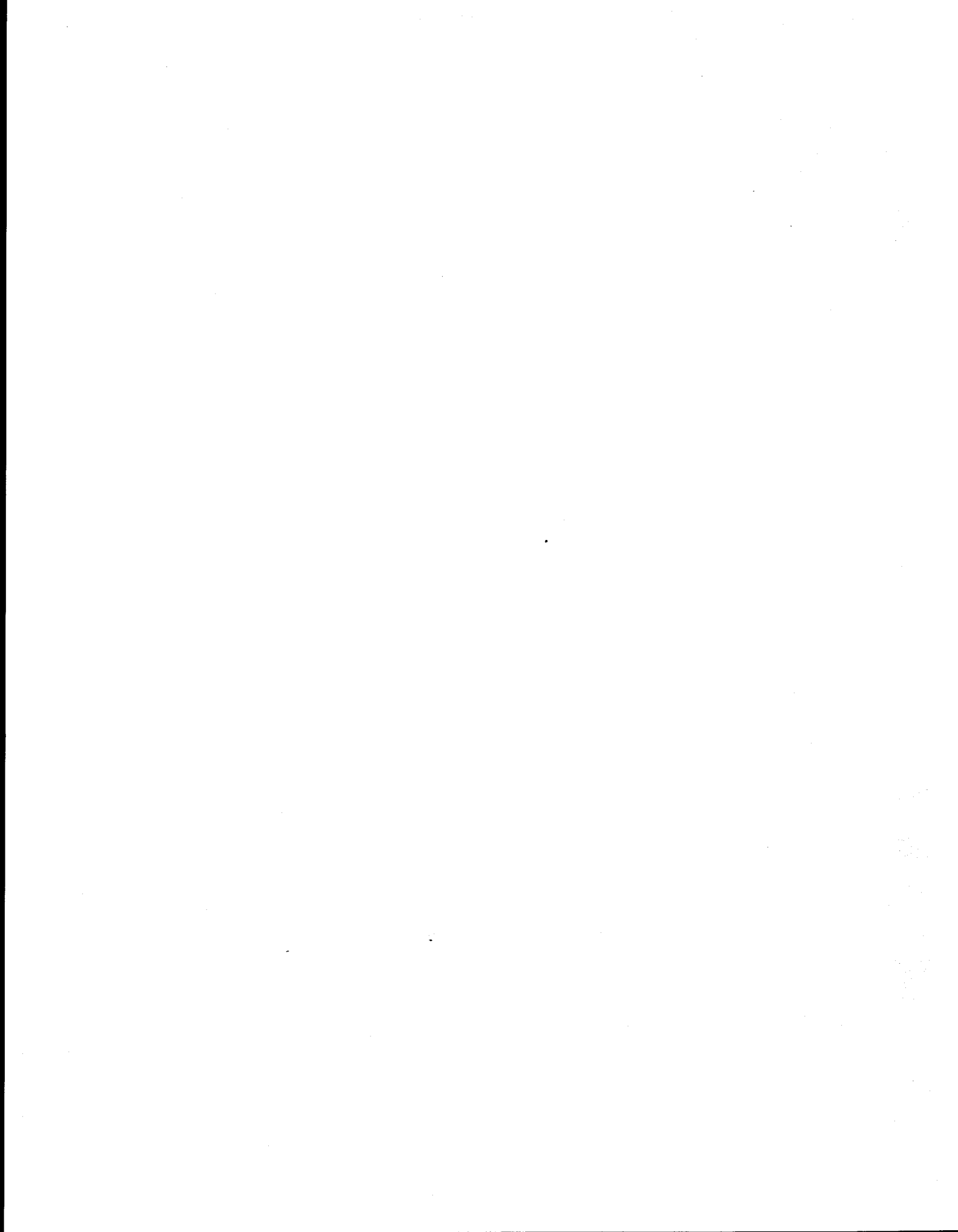
Station	Cast #	Depth m	SPM mg/l	% Organic Matter	Size Distribution Slope
UP3	54	2	0.915		
		70	0.324		
		138	0.324		
SG30	55	2	0.921		
		130	0.510		
SG21	56	2	0.391		
		72	0.721		
SG2	57	2	0.393		
		73	0.613		
SG15	58	2	0.576		
		70	0.458		
SG14	59	2	0.757		
		40	0.986		
		70	0.694		
SG74	60	2	1.060		
		87	0.949		
SG22	61	2	0.548		
		97	0.989		
SG3	62	2	0.912		
		120	0.963		
SG73	63	2	1.371		
		123	1.034		
SG5	66	2	2.194		
		60	0.199		
		121	1.644		

Station	Cast #	Depth m	SPM mg/l	% Organic Matter	Size Distribution Slope
PL4	67	2	1.531		3.56
		70	0.143		
		100			4.16
		136	0.618		4.61
PL5	68	2	2.281		3.34
		70			3.76
		130	0.984		4.17
PL6	69	2	2.165		3.50
		50	0.152		3.88
		127	1.52		4.09
PL7	70	2	1.977		3.63
		70			3.73
		123	1.134		3.92
PL8	71	2	2.248		3.27
		50	0.228		3.46
		116	1.616		4.23
PL9	72	2	1.835		3.40
		60			4.29
		95	0.910		
PL10	73	2	1.456		3.50
		43	2.617		
		70			3.56
		87	1.633		3.06
PL11	74	2	0.837		3.24
		50			3.30
		81	2.101		2.94

Station	Cast #	Depth m	SPM mg/l	% Organic Matter	Size Distribution Slope
PL12	75	2			3.34
		40			3.37
		74			2.99
PL13	76	2			3.21
		30			3.28
		70			2.95
PL14	77	2			
		20			3.63
		68			3.84
NA41	78	2	0.392	43	
		82	2.815	28	
NA43	81	55	1.198	40	
NA44	82	2	0.746	46	
		38	1.086	44	
NA46	84	2	0.307		
		22	1.640	40	
NA39B-2	89	17	0.965		
NA39A-3	91	2	2.615		
		20	1.256		
NA39B-3	92	2	1.465		
		21	1.935		
NA39C-3	93	2	1.420		
		14	2.185		
NA11	94	2	0.847	38	
		48	0.893	35	

Station	Cast #	Depth m	SPM mg/ℓ	% Organic Matter	Size Distribution Slope
NA16	99	21	1.017	53	
NA22	101	19	1.489	38	
NA19	104	2	0.487	31	
		48	0.768		
NA17	106	2	0.705	45	
		55	1.453	27	
NA23	107	2	0.291	52	
		61	2.345	28	
NA25	109	2	1.103	42	
		46	4.194	25	
NA27	111	2	0.977	54	
		19	1.085	25	
NA39A-4	112	2	0.971		
NA39B-4	113	2	0.788		
NA39C-4	114	2	1.082		
NA39B-8	125	2	0.960		
NA39C-8	126	2	1.150		
NA33	130	2	1.559	66	
NA30	133	2	0.289	39	
		56	1.024	40	
NA29	134	65	2.773	39	
NA28	135	2	0.211	51	
		67	0.378	31	
NA34	136	2	0.349	52	3.28
		65	2.646	32	2.50

Station	Cast #	Depth m	SPM mg/l	% Organic Matter	Size Distribution Slope
NA35	137	2			3.96
		65			2.80
NA36	138	2	0.555	45	3.59
		56	1.049	38	3.11
NA37	139	2			3.80
		48			2.43
NA38	140	2	1.016	46	4.13
		33	2.605	45	2.96
NA39	141	2			4.26
		22			3.50
NA40	142	2	2.140	34	3.28
		16			3.07
NA52	146	2	1.047	46	
NA50	148	2	1.003	63	
		42	1.196	38	
NA48	150	2	1.675	73	
		69	1.438	34	
NA45	153	2	0.688	42	
		35	0.988	54	
NA43	155	2	1.755	77	
		57	0.808	17	
NA72	175	2	0.989	41	
		30	0.813	33	
NA69	178	2	0.993	60	
		98	0.785	22	
NA66	181	2	2.091	85	
		105	0.840	15	
PL8	183	114	1.470		



**THE PRODUCTION AND DISPERSION OF DISSOLVED METHANE
IN SOUTHEASTERN BERING SEA**

by

**Joel D. Cline, Kimberly Kelly-Hansen,
and Charles N. Katz**

**Pacific Marine Environmental Laboratory
National Oceanic and Atmospheric Administration**

**Final Report
Outer Continental Shelf Environmental Assessment Program
Research Unit 153**

1982

309

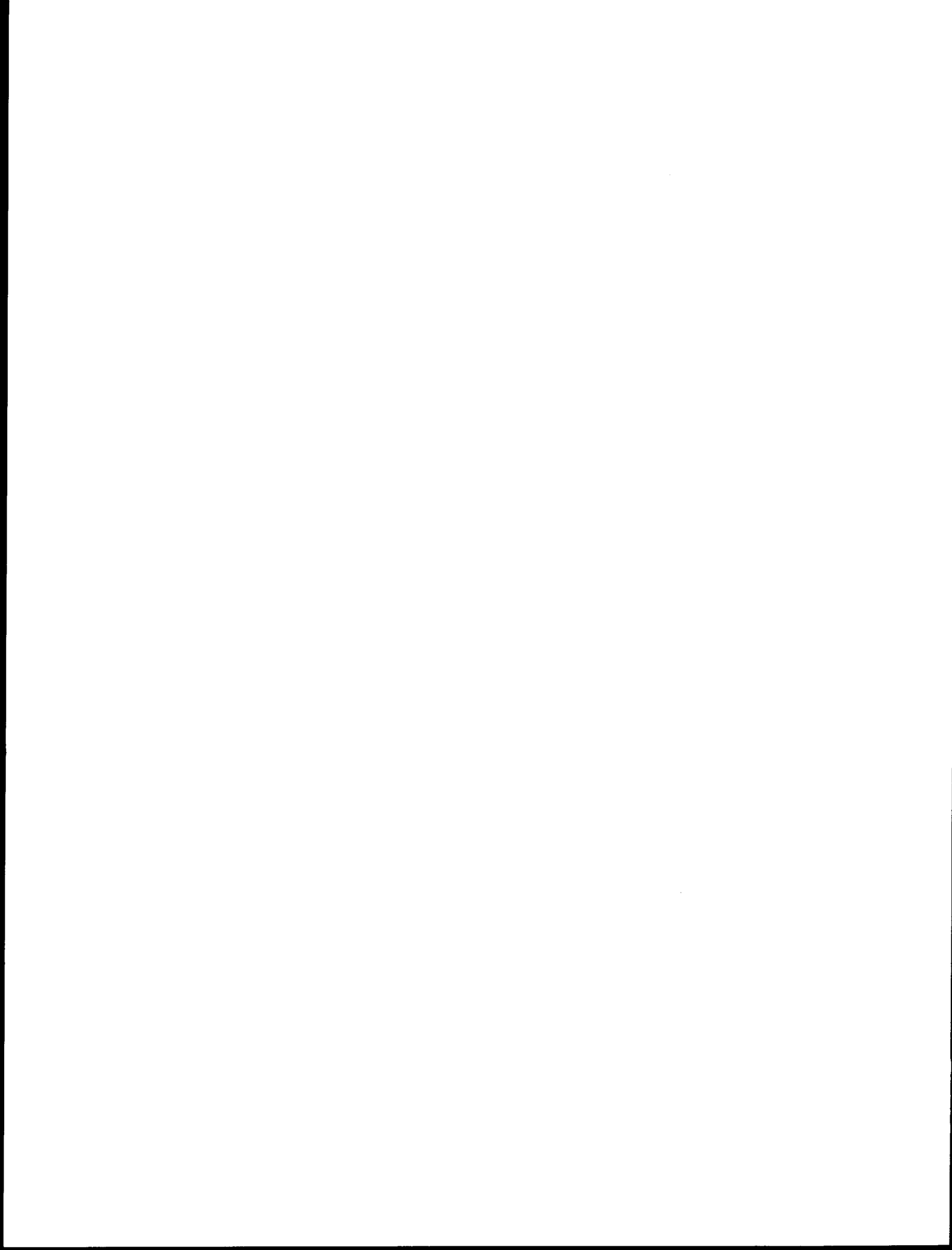


TABLE OF CONTENTS

List of Figures	313
List of Tables	317
1. INTRODUCTION	319
1.1 Purpose of Study	319
1.2 Objectives	319
1.3 Relevance to OCSEAP	320
2. BACKGROUND	322
2.1 Chemical Tracers	322
2.2 Southeastern Bering Sea	323
2.3 North Aleutian Shelf	325
2.4 St. George Basin	326
3. METHODOLOGY	327
3.1 Sample Collection	327
3.2 Preconcentration	327
3.3 Gas Chromatography	327
4. RESULTS	329
4.1 St. George Basin	329
4.2 North Aleutian Shelf	340
5. TRANSPORT MODELS	358
5.1 Horizontal Trajectory Model	358
5.2 Vertical Flux Model	363
6. DISCUSSION	366
6.1 North Aleutian Shelf	366
6.1.1 August 1980	369
6.1.2 February 1981	376
6.1.3 May 1981	378
6.1.4 Port Moller Tidal Flux	383
6.1.5 North Aleutian Shelf Summary	385

6.2	St. George Basin	387
6.2.1	August 1980	391
6.2.2	February 1981	393
6.2.3	May 1981	393
6.2.4	Summary of St. George Basin Studies	396
6.2.5	Oil Spill Scenario, St. George Basin	398
6.2.6	Horizontal Transport of Methane	406
6.2.7	Vertical Transport of Methane	409
7.	CONCLUSIONS	413
7.1	North Aleutian Shelf Studies	413
7.2	St. George Basin Studies	414
8.	REFERENCES	415

LIST OF FIGURES

Figure

1. Study regions and regional setting in the southeastern Bering Sea.
2. Stations occupied in St. George Basin in (a) August 1980, (b) February 1981, and (c) May 1981. Station prefixes are Unimak Pass (UP), St. George Basin (SG), North Aleutian Shelf (NA) and PROBES line (PL).
3. The vertical distributions of (a) salt, (b) temperature, (c) density, and (d) dissolved methane along the PROBES line in August 1980. See Fig. (2a) for the station positions.
4. The vertical distributions of (a) salt, (b) temperature, (c) density, and (d) dissolved methane along the PROBES line in February 1981. See Fig. (2b) for the station positions.
5. The vertical distributions of (a) salt, (b) temperature, (c) density, and (d) dissolved methane along the PROBES line in May 1981. See Fig. (2c) for the station positions.
6. The near-bottom distribution of dissolved methane in (a) August 1980, (b) February 1981, and (c) May 1981. Concentrations were averaged over the lower 20 m of the water column.
7. The vertical distribution of (a) density and (b) methane at Station PL6. Measurements were made on 29 August and 3 September 1980. Small but significant inversions in the density profile are the result of lateral mixing and the formation of salt fingering (Coachman and Charnell, 1979).
8. The vertical distribution of (a) dissolved methane and (b) density (σ_t) at Station SG 70. Measurements were made May 19, 23 and June 1, 1981, and show the temporal variability in circulation across St. George Basin.
- 9a. The location of stations occupied in August 1980 along the NAS.
- 9b. The location of stations occupied in February 1981 along the NAS.
- 9c. The location of stations occupied in May 1981 along the NAS.
10. The seasonal distribution of salinity and temperature along the NAS. The coastal zone was defined to include all waters whose depth was less than 40 m.
11. The seasonal distribution of salinity and temperature along the southern boundary of the middle shelf. The middle shelf was operationally defined to include all stations at which the depth of water exceeded 41 m.

12. The seasonal distribution of salinity, temperature, and density (σ_t) at Station 27 in the coastal zone. Note the well-mixed water column.
13. The seasonal distribution of salinity, temperature, and density (σ_t) at Station 23 in the middle shelf. Note the isothermal, isohaline conditions in February 1981.
14. The average longitudinal distribution of salinity along the NAS coastal zone. Only stations at which the depth of water was less than 40 m were included in the analysis. The dashed arrows indicate the range of values about the mean. Note the large variations at the entrance to Port Moller.
15. The distribution of methane at the surface along the NAS in (a) August 1980, (b) February 1981, and (c) May 1981. Concentrations are in nL/L (STP).
16. The vertical distributions of methane along sections IV and V east of Port Moller (see Fig. 9a). Measurements were made in August 1980.
17. The location of 24-hour time series stations at the entrance to Port Moller. Stations PM1, PM2, PM3 were occupied in August 1980; Station PM3 in February 1981; and Stations 39A, 38B, and 39C in May 1981.
18. The time-averaged distribution of methane across the entrance to Port Moller in (a) August 1980, (b) February 1981, and (c) May 1981. In those cases where more than one measurement was made, the vertical lines indicate the range of values about the mean.
19. The diel variation in temperature, salinity, and methane at Station PM3. Measurements were made on 5-6 February 1981. Note that low salinity, methane-enriched water is found at the entrance to Port Moller during ebb tide.
20. A schematic diagram of the NAS region. The significant transport terms include longshore advection vC' , and the flux divergence KyC'' . The well mixed coastal zone is approximately 20 m deep and 32 km wide. Not shown in the diagram is the air-sea exchange of methane, which is proportional to the concentration of methane.
21. The average distribution of dissolved methane across the entrance to Port Moller. Observations were conducted in August 1980. The mean and range of values (n observations) are shown by the closed triangles and dashed arrows. The concentration of methane shoreward of Station PM13 was assumed constant. A background of 0.45 $\mu\text{L/L}$ was subtracted to give the concentration of excess methane from Port Moller.
22. The depth-averaged distribution of (a) dissolved methane and (b) salinity and Port Moller in August 1980. A background concentration of 0.45 $\mu\text{L/L}$ was subtracted from the observed field, leaving a residual concentration of 0.03 $\mu\text{L/L}$ north of the inner front. The inner front is located near the dashed line (approximately 45 m).

23. Model simulation of the distribution of methane for $u = 3.8$ cm/s and $k = 5.0 \times 10^{-7}$ /s. This is the best fit to the observations shown in Fig. 22a. Concentrations are in $\mu\text{L/L}$. The position of the 45 m isobath is indicated by the dashed line.
24. Model simulations of the distribution of methane for (a) $u = 2.5$ cm/s, $k = 25 \times 10^{-7}$ /s and (b) $u = 5.0$ cm/s and $k = 7.5 \times 10^{-7}$ /s in August 1980. Concentrations are expressed in $\mu\text{L/L}$. The position of the 45 m isobath is indicated by the dashed line.
25. Model simulation of the distribution of methane for $u = 7.5$ cm/s and $k = 5.0 \times 10^{-7}$ /s in August 1980. Concentrations are in $\mu\text{L/L}$. The position of the 45 m isobath is indicated by the dashed line.
26. The depth-averaged distribution of (a) dissolved methane and (b) salinity in February 1981. A background concentration of 0.11 $\mu\text{L/L}$ has been subtracted from the concentration field, leaving a mean residual of 0.014 $\mu\text{L/L}$. The inner front is located near the 45 m isobath and is indicated by the dashed line.
27. Model simulations of the distributions of methane for (a) $u = 3.0$ cm/s and $k = 4.3 \times 10^{-7}$ /s and (b) $u = 7.0$ cm/s and $k = 1.2 \times 10^{-7}$ /s in February 1981. Both distributions are reasonably good fits to the observed distributions. Concentrations are in $\mu\text{L/L}$. The position of the inner front is indicated by the dashed line.
28. The depth-averaged distribution of dissolved methane in May 1981. A background concentration of 0.1 $\mu\text{L/L}$ has been subtracted from the concentration field, leaving a mean residual of 0.013 $\mu\text{L/L}$. The inner front is located near the 45 m isobath and is indicated by the dashed line.
29. Model simulations of the distribution of dissolved methane for (a) $u = 2.0$ cm/s and $k = 2.4 \times 10^{-7}$ /s and (b) $u = 3.0$ cm/s and $k = 4.8 \times 10^{-7}$ /s in May 1981. Both distributions are reasonably good fits to the observed distribution. Concentrations are in $\mu\text{L/L}$. The position of the inner front is near the 45 m isobath and is indicated by the dashed line.
30. Distributions of (a) clay content and (b) total carbon in the surface sediments of St. George Basin. The locus of the high carbon concentrations is approximately 56°N 167°W , which is the location of Stations SG5, SG29, SG24, and SG70 (see Fig. 2). This figure was taken from the report by Gardner et al., 1978.
31. The average excess concentration of methane in the benthic boundary layer across the center of the plume. Data were collected in (a) August 1980, (b) February 1981, and (c) May 1981. Concentrations are expressed $\mu\text{L/L}$.
32. (a) The average near-bottom concentration of dissolved methane in St. George Basin in August 1980. The axes show the position of the model grid. (b) The model simulation of the methane distribution using the source function shown in Fig. (31a). The best fit was obtained for $u = 2.0$ cm/s and $k = 8.6 \times 10^{-8}$ /s.

33. (a) The average near-bottom concentration of dissolved methane in St. George Basin in February 1981. The axes show the position of the model grid. (b) The model simulation of the methane distribution using the source function shown in Fig. (31b). The best fit was obtained for $u = 2.0$ cm/s and $k = 5.6 \times 10^{-8}$ /s.
34. (a) The average near-bottom concentration of dissolved methane in St. George Basin in May 1981. The axes show the position of the model grid. (b) The model simulation of the methane distribution using the source function shown in Fig. (31c). The best fit was obtained for $u = 2.0$ cm/s and $k = 9.2 \times 10^{-8}$ /s.
35. The development of a plume of 'dissolved' oil resulting from an instantaneous release of 6.7×10^8 g (50,000 bbls) confined to a 40 m, vertical-lens of water. The centerline distribution shows the temporal history of the spill locus for a mean current speed of 2.5 cm/s. Reference concentrations of 0.1 and 1.0 ppm 'dissolved' oil also are indicated.
36. The development of a plume of 'dissolved' oil resulting from an instantaneous release of 6.7×10^8 g (50,000 bbls) confined to a 40 m, vertical-lens of water. The centerline distribution shows the temporal history of the spill locus for a mean current speed of 5.0 cm/s. Reference concentrations of 0.1 and 1.0 ppm 'dissolved' oil also are indicated.
37. The development of a plume of 'dissolved' oil resulting from an instantaneous release of 6.7×10^8 g (50,000 bbls) confined to a 40 m, vertical-lens of water. The centerline distribution shows the temporal history of the spill locus for a mean current speed of 10 cm/s. Reference concentrations of 0.1 and 1.0 ppm 'dissolved' oil also are indicated.
38. The vertical distribution of methane in the water column and surficial sediments at (a) Station SG67 and (b) SG70. These data were collected in May-June 1981. Note the scale change in concentrations between the water and the pore fluids.
39. The relationship between salinity and methane at Station PL-6 in August 1980. The linear relationship suggests conservative mixing between the surface and bottom waters.
40. The relationship between the apparent vertical eddy diffusivity, K_z , and the Brunt-Vaaisaala Frequency, N^2 , at Station PL6 in August 1980. The theoretical relationship for shear-induced turbulence is -0.5, which is shown by the dashed lines.

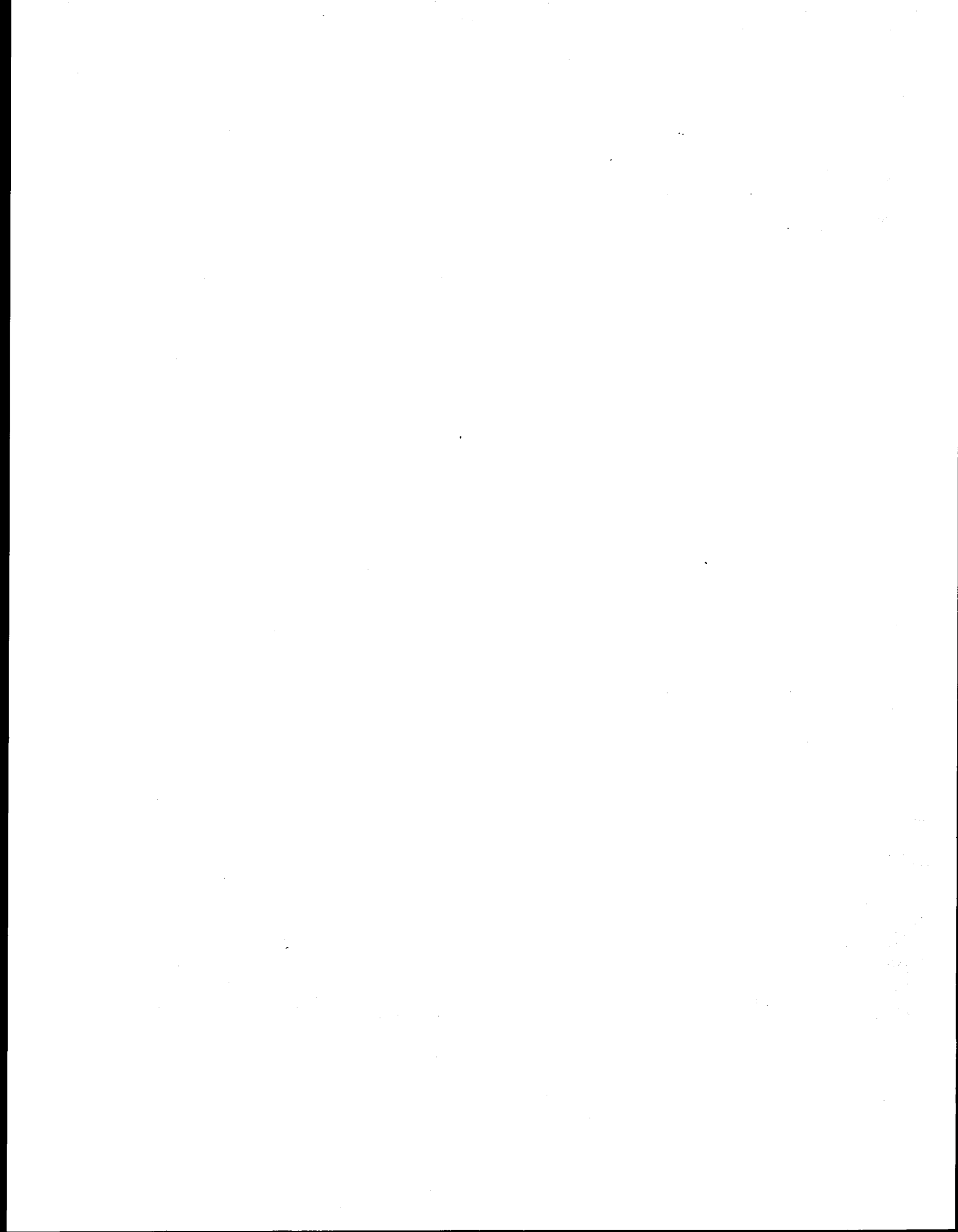
LIST OF TABLES

Table

1. A summary of parameters used to estimate the air-sea exchange rate (R) of methane along the NAS coastal zone. The model is

$$R = - \frac{D}{h \cdot \Delta z} (C) = -k_{a/s} (C)$$

2. A comparison of the tidal transport of methane (T_t) from Port Moller with the transport of methane at the tidal boundary (T_m). The mean tidal velocity is \bar{v} and the mean coastal current is \bar{u} .
3. A summary of the mean velocities along the coastal zone of the North Aleutian Shelf as determined from the distributions of dissolved methane. The air-sea exchange and biological rate constant (combined) was varied by $\pm 50\%$.



1. INTRODUCTION

1.1. Purpose of Study

The purpose of this study was to use dissolved methane as a tracer of mean circulation and to define vertical and horizontal mixing scales in local regions of the southeastern Bering Sea. The subregions selected for study included St. George Basin, a fault basin located on the outer shelf of Bristol Bay, and the North Aleutian Shelf. Both regions were identified as potential off-shore leasing sites for gas and oil production.

Based on previous investigations in Bristol Bay (Cline, 1976, 1977), it was known that localized sources of methane occurred in both areas. By carefully examining the seasonal distributions of methane and by quantifying the extent and magnitude of these sources, it might be possible to delineate horizontal and vertical mixing scales as well as confirming the mean current field.

Methane is a common component of petroleum and is also produced by microorganisms. The origin of methane in petroleum is via thermal cracking of larger organic molecules, whereas methane derived biologically is from the exothermic reduction of carbon dioxide by specialized anaerobic bacteria (Claypool and Kaplan, 1974). In either case, methane is a dissolved gas observed at moderate concentrations in the shelf waters of the Bering Sea and becomes a natural chemical tracer of the movement of the dissolved fractions of crude oil, whether they arise from a tanker spill, pipeline rupture, or well blowouts.

1.2. Objectives

The principal goal of this research was to use dissolved methane as a quantitative tracer of circulation processes and mixing dynamics in selected areas of the southeastern Bering Sea. This report deals with two site-specific areas, the North Aleutian Shelf (NAS) and St. George Basin (SGB).

Specifically, the objectives were:

1. To quantify the longshore mean current and cross-shelf dispersion coefficients along the NAS using the tidal flux of methane from the Port Moller estuary as a chemical tracer.
2. To estimate near-bottom current trajectories and lateral dispersion coefficients in St. George Basin, using the bottom source of methane as a chemical tracer.
3. To estimate the depth dependent vertical eddy diffusivity in St. George Basin using a one-dimensional vertical flux model.
4. To analyze the distributions of methane in terms of a two-dimensional diffusion-advection model for the purpose of confirming mean current velocities and estimating the magnitude of horizontal and vertical mixing processes.

1.3. Relevance to OCSEAP

The persistence of oil in Bristol Bay depends on physical, chemical and biological processes that act in concert to disperse and degrade petroleum. These processes, each with their characteristic time scales (i.e., half-life), must be considered together in order to determine a characteristic time (or space) scale for the persistence of oil or some fraction thereof. Circulation and mixing processes are characterized by relatively short time scales and thus represent a first-order process. Given that the volume of spilled oil is likely to be small compared to the volume of water in the region, it is anticipated that harmful impacts due to petroleum development will be limited to small areas, probably less than 500 km².

Utilization of methane as a chemical tracer of circulation and dispersion allows mesoscale mixing processes to be more clearly defined. In

particular, these studies permit quantitative predictions of water mass trajectories, dispersion characteristics and water mass residence times, all of which are required to quantify the potential impact of oil on living resources.

2. BACKGROUND

2.1. Chemical Tracers

The natural occurrence of dissolved methane is normally due to the metabolic activities of specialized marine bacteria that either selectively reduce molecular CO_2 or ferment simple fatty acids into CO_2 and methane (Claypool, 1974). Regardless of which mechanism prevails in nature, the net result is that a small portion of the annually fixed carbon is reduced to methane. Methanogenesis is normally considered an anaerobic process, usually occurring within oxygen-deficient environments (Reeburgh and Heggie, 1977).

Once methane is released to the water column, usually by diffusion, or in some cases, by bubble injection, the water parcel is chemically marked. The resulting distribution of methane is a function of the input rate, the velocity field, eddy diffusion, air-sea exchange, and biological oxidation. Each of these processes will be discussed below, but suffice it to say that under certain limiting conditions, methane may behave as a conservative property so long as the spatial scales are not too great. This condition presumes that biological oxidation and air-sea exchange are insignificant over the time scale of interest. If air-sea exchange and biological oxidation of CH_4 to CO_2 are relatively small effects, then the distribution of methane is largely governed by the magnitude of the source term and the mixing characteristics of the system.

Baseline studies conducted in 1975 and 1976 indicated that anomalously high concentrations of methane were present in St. George Basin and along the North Aleutian Shelf near the Port Moller estuary. Whereas both sources appeared to be localized, a detailed observational program was initiated to assess the seasonal distributions and derive independent estimates of mixing

parameters based on model interpretation of the distributions. These distributions were similar in scale (actually larger) to proposed oil spill scenarios; thus methane served as a natural analog tracer of oil impacts associated with petroleum development.

We now proceed to discuss the geography, hydrology and oceanography of the two regions as necessary introductory information to the discussion to follow.

2.2. Southeastern Bering Sea

The area and volume of the southeastern Bering Sea, computed out to the 200 m isobath, is 419,000 km² and 30,000 km³, respectively, which calculates a mean depth of approximately 70 m. Freshwater input occurs primarily from the Kuskokwim and Kvichak Rivers, located on the northern and eastern sides of the region (Fig. 1), which results in a 2‰ salinity difference between the offshore waters and the near-shore areas (Schumacher et al., 1979).

Bristol Bay is characterized by a series of frontal features, primarily located at distinct bathymetric depths (Kinder and Schumacher, 1981a). These fronts occur roughly at the 200 m (shelf break front), 100 m (middle shelf) and 50 m (inner front) isobaths (see Fig. 4-1; Kinder and Schumacher, 1981a). Mean circulation landward of the middle front is presumed weak (≤ 2 cm s⁻¹) and hydrographic structures are largely determined by buoyancy input, wind stirring and tidal mixing (Kinder and Schumacher, 1981a; see their report for details). There appears to be a weak cyclonic circulation around the perimeter of Bristol Bay, largely confined to the coastal zone ($z \leq 50$ m).

The region is partially ice covered in winter, usually beginning in protected bays in November and building to a maximum in March. The spring melting results in considerable freshwater added to the surface (Schumacher

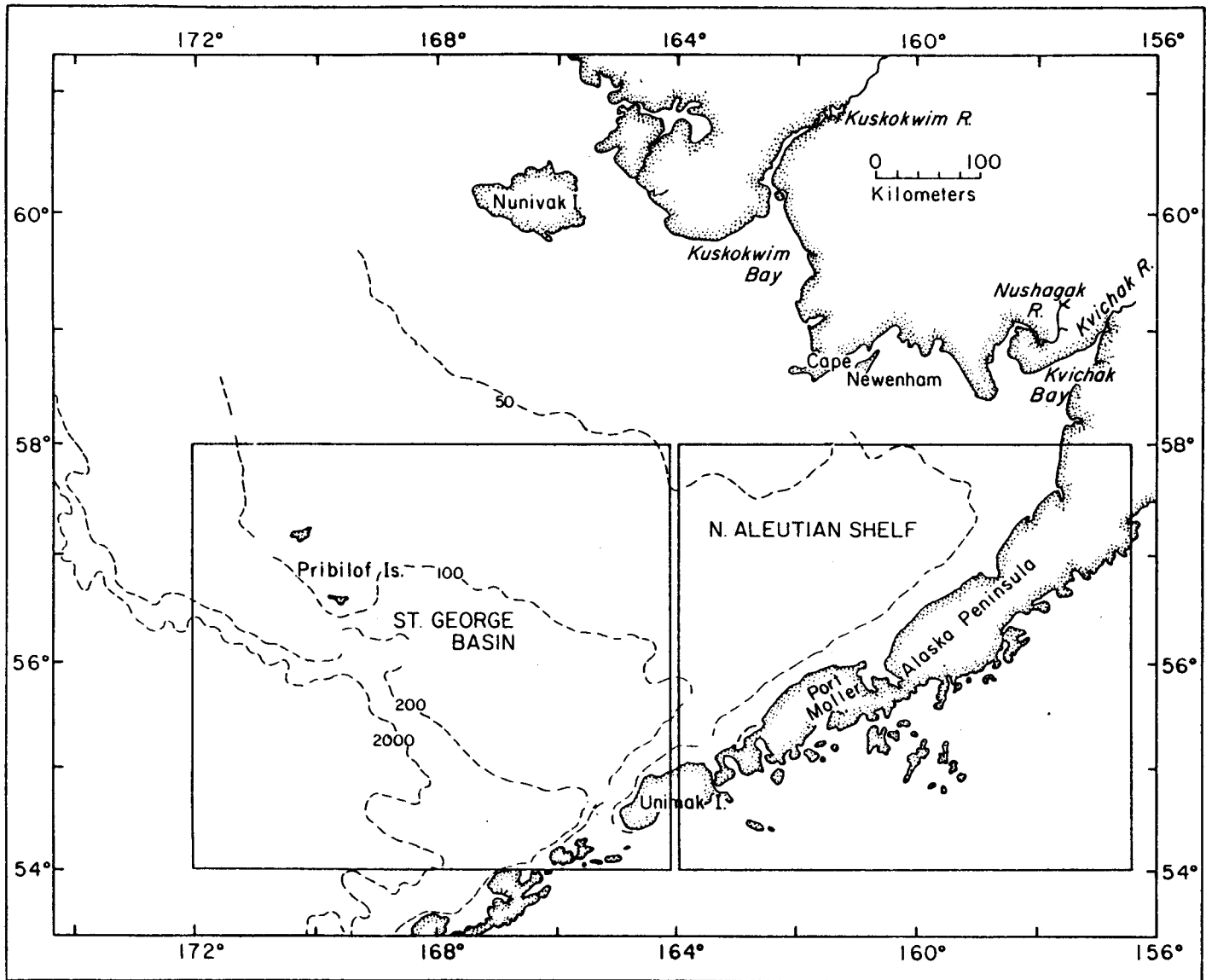


Figure 1. Study regions and regional setting in the southeastern Bering Sea.

et al., 1979). Maximum areal ice coverage is approximately 60%; thickness is usually less than 1 m. Details on hydrography and climate of the region can be found in reports by Kinder and Schumacher, 1981a; Kinder and Schumacher, 1981b; Coachman and Charnell, 1979; Overland, 1981; and references contained therein.

2.3. North Aleutian Shelf (NAS)

The NAS region encompasses the near shore areas from Unimak Island on the west to the Kvichak River on the east (Fig. 1). This region is characterized by a vertically well mixed coastal zone ($z \leq 50$ m), which is hydrographically separated from the seasonally stratified regime located seaward. Stratification is most intense in the summer and nearly vanishes during winter. The breakdown of vertical stratification in the coastal zone is reportedly due to wind and tidal mixing (Kinder and Schumacher, 1981a).

There appears to be no major source of freshwater along the NAS, except the Kvichak River at the eastern extremity. There are undoubtedly numerous diffuse sources, including the possibility of submarine aquifers originating in the mountains of the Alaska Peninsula. Mean velocities are estimated at no more than $3\text{-}5 \text{ cm s}^{-1}$ to the east (Schumacher et al., 1979), with a strong seasonal variability in direction and magnitude (Personal communication, J. Schumacher).

The principal embayment along the NAS is Port Moller, which has two arms, each approximately 38 km in length, with mean depths ranging from 5 m to 15 m. The western arm, Herendeen Bay, is the deeper of the two with depths to 100 m in a small inner basin. Tidal currents within the Port Moller-Herendeen Bay complex are relatively strong, reaching maximum ebb and flood velocities of approximately 150 cm s^{-1} (Department of Commerce, 1980).

Measurements made in September-October of 1975 and again in July of 1976 (Cline, 1981), revealed that the Port Moller estuary was a significant

source of dissolved methane to the surface waters, which could be traced to the northeast for distances of 200 km. The source of methane within Port Moller was not specifically known at that time, but was believed to arise from methanogenesis in anoxic marine muds or possibly from the discharge of cannery wastes at Port Moller.

2.4. St. George Basin

St. George Basin is an offshore fault basin located near the shelf break (Fig. 1). The axis of the basin is northwest-southeast, running roughly from Unimak Pass to the Pribilof Islands. The basin proper is largely contained between the 100-200 m isobaths.

The basin waters are separated from the inner shelf by the middle front at about 100 m and from the Bering Sea water located seaward of the 200 m isobath (Kinder and Schumacher, 1981a; see their Fig. 4-1). Dynamic topographies are largely oriented parallel to the isobaths and reflect weak mean currents toward the northwest (Coachman and Charnell, 1979). Although seasonal variations do exist, surface and near-bottom mean currents are usually $\leq 5 \text{ cm s}^{-1}$ (Coachman and Charnell, 1979; Kinder and Schumacher, 1981a).

The waters overlying SGB appear to be seasonally stratified with a strong erosion and deepening of the pycnocline in winter. Because the Alaska Stream-Bering Sea water penetrates the shelf seasonally (Kinder and Schumacher, 1981a), it is expected that the basin water is modified seasonally by cross-shelf advection and diffusion.

3. METHODOLOGY

3.1. Sample Collection

Water samples were collected using standard 5 L Niskin[®] bottles mounted on a General Oceanics Rosette. Once on deck, water was transferred to clean 1 L glass-stoppered bottles such that air bubbles were not trapped. The samples were stored in the dark at approximately 5°C until analyzed, which was usually within two hours.

3.2. Preconcentration

The analysis of methane was accomplished using a procedure adopted from that originally proposed by Swinnerton and Linnenbom (1967). A detailed discussion of the methods used for analyzing methane and other LMW hydrocarbons can be found in Katz (1980). Briefly, the method is as follows: Dissolved methane was removed from approximately 250 mL of seawater by helium stripping. Gases removed from solution were passed through Drierite[®], Ascarite[®] and Tenax G.C.[®] traps to remove water vapor, carbon dioxide and heavier hydrocarbons. Methane was concentrated on an activated alumina trap at -196°C. After quantitative removal from solution, (~ 5 minutes at a helium flow rate of 100 mL min⁻¹) the trap was warmed to 100°C and the methane was backflushed directly into a gas chromatograph.

3.3. Gas Chromatography

Detection of methane was carried out on a Hewlett-Packard 5710A gas chromatograph equipped with dual flame ionization detectors. In order to insure separation of methane from the air gases (N₂ and O₂), chromatography was accomplished with an activated-alumina, 60-80 mesh, column (1.8 m x 0.48 cm). Chromatography was completed in less than two minutes at a carrier flow rate of 50 mL min⁻¹ and the oven held isothermally at 100°C. Quantita-

tion was accomplished by comparing the samples with methane standards of known concentration. The precision of the analysis is $\pm 5\%$ at one standard deviation. Intercalibration with NBS showed our analysis to be accurate to 5%.

4. RESULTS

4.1. St. George Basin

Based on measurements made in 1975 and 1976 (Cline, 1980), large accumulations of methane were discovered in the near bottom waters of St. George Basin. The methane plume indicated a northwest current trajectory in agreement with observations (Kinder and Schumacher, 1981), although the nature of the source of CH_4 was poorly defined. In an attempt to clarify the mean circulation and lateral mixing characteristics of the basin, and in particular the near-bottom waters, we examined the distribution of methane seasonally and attempted to determine its source. From these measurements, together with the usual hydrographic parameters (e.g., $\text{S}^\circ/\text{o}_\text{o}$, T°C), we explored methane as a natural tracer of dissolved and emulsified oil that might be released during exploration and production activities.

The station grids occupied during the seasonal visits are shown in Figures (2a-2c). Station prefixes are: UP (Unimak Pass), SG (St. George Basin), and PL (Probes Line). The last of these was a line of stations occupied frequently by the PROBES Program and thus was included in our compliment of stations for purposes of continuity, since there was significant overlap in the objectives of the two programs.

In August of 1980, not all of the stations were occupied in St. George Basin due to a priority allocation of time to the North Aleutian Shelf work. More complete coverage was accomplished in February and May of 1981, although in every case, insufficient time was available to trace the methane plume to the northwest beyond the Pribilofs.

In order to summarize the seasonal hydrography of the region, we present the distribution of properties along the PROBES Line. Hydrographic conditions

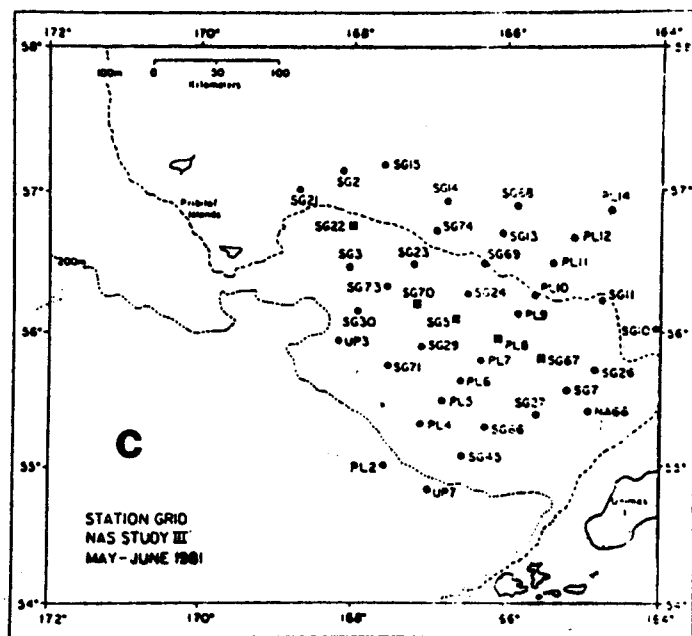
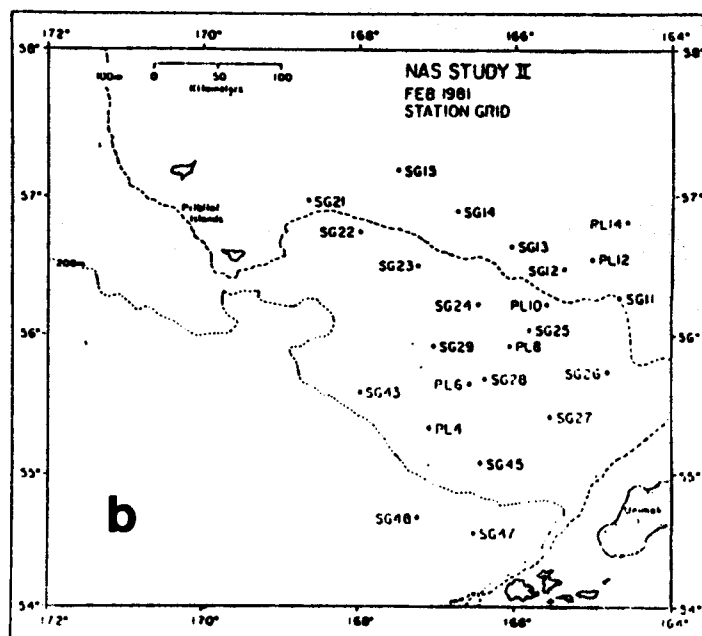
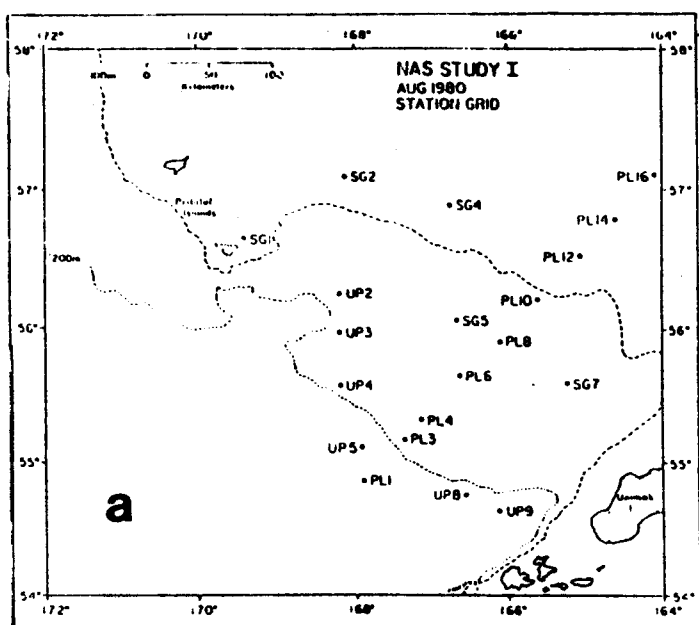


Figure 2. Stations occupied in St. George Basin (a) August 1980, (b) February 1981, and (c) May 1981. Station prefixes are Unimak Pass (UP), St. George Basin (SG), North Aleutian Shelf (NA) and PROBES line (PL).

for August 1980 are shown in Figures (3a-3d), including dissolved methane which reveals strong vertical and lateral gradients along the section. The highest concentrations observed were in the near-bottom waters of St. George Basin (near PL-6) and a smaller maximum near PL-14. Inshore of PL-14 little vertical structure in the distribution of CH_4 was observed with concentrations between 400-500 nL/L (STP). The lowest concentration of methane was found in the offshore surface waters, where concentrations approached 280 nL/L. If the water column were in equilibrium with the atmosphere, the concentration of methane would range between 50-70 nL/L, depending mostly on the water temperature (Yamamoto et al., 1976). Thus, methane is seen to be highly supersaturated, even in the surface layers, with enrichment factors of at least five. The source of methane is most probably biological, although it remains difficult to pinpoint the exact source that contributes to the general background levels. Near-bottom and benthic microbial activity as well as zooplankton excretion seem the most likely sources (Scranton and Brewer, 1977).

Salinity and temperature distributions for August are shown in Figures (3b,c). The haline structure revealed characteristic surface outflow of low salinity water, principally from the Kvichak and Kuskokwim Rivers and the intrusion of high salinity, cold water onto the shelf from the west or southwest. Inshore of PL-20, water properties were uniform with depth, showing the effects of strong vertical turbulence generated by winds and tides (Kinder and Schumacher, 1981a). Within St. George Basin and particularly the middle shelf region ($100 \text{ m} < z < 50 \text{ m}$), the lateral gradient in salt was suggestive of diffusive salt exchange (Coachman et al., 1981) rather than vigorous advective processes. In fact, Kinder and Schumacher, (1981b) have shown that the mean currents are everywhere less than 5 cm/s throughout the year. The strongest vertical stratification observed along

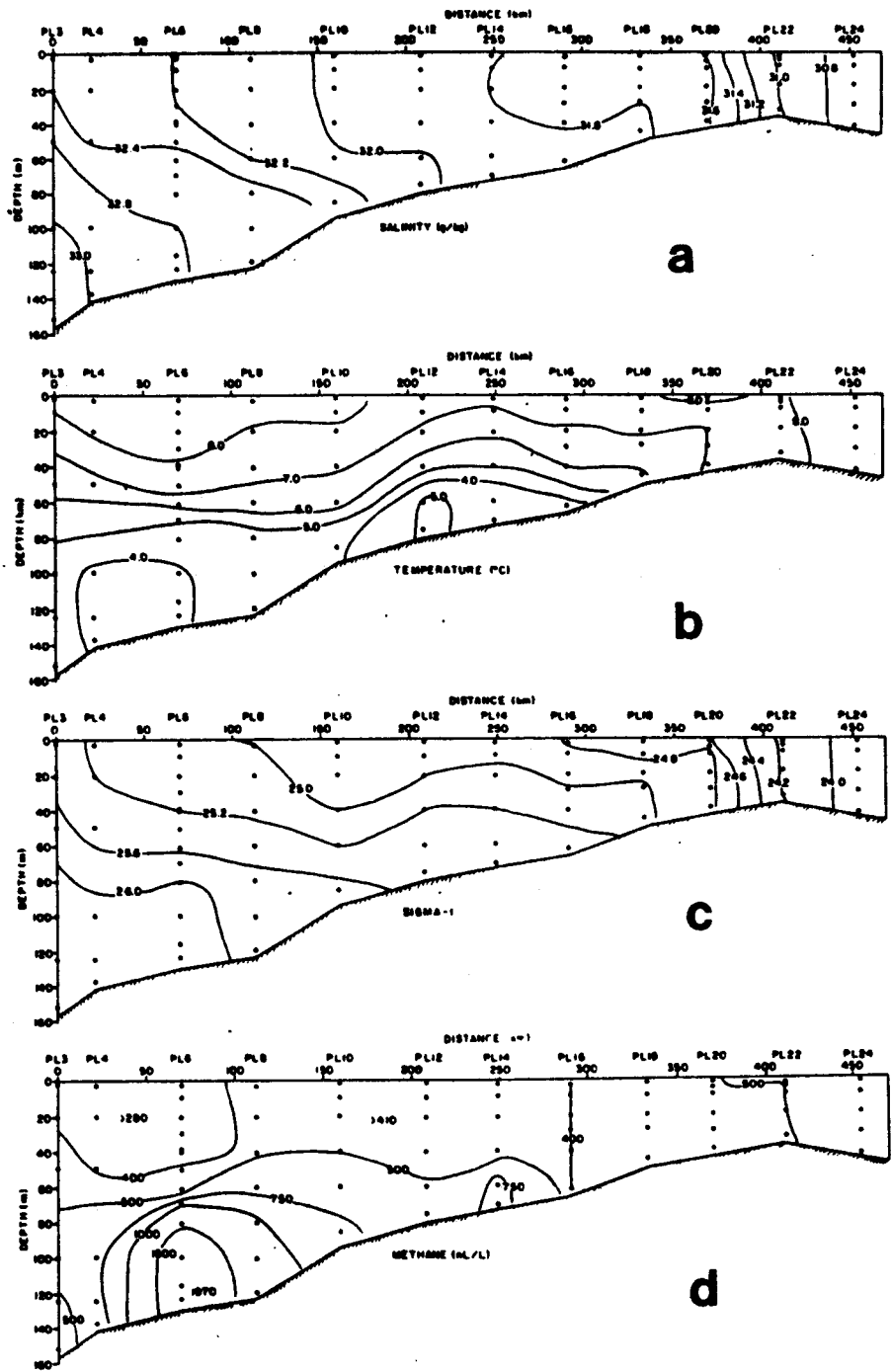


Figure 3. The vertical distributions of (a) salt, (b) temperature, (c) density, and (d) dissolved methane along the PROBES line in August 1980. See Fig. (2a) for the station positions.

the section was near PL-6 (Fig. 3d), which coincides with the maximum thermal and methane gradients. Later on in the discussion, we will elaborate on the significance of this seasonal stratification as it relates to the fate of oil released in this environment.

Figures (4a-4d) show conditions for February 1981. Concentrations of methane were significantly lower than those observed in August, both at the surface and at depth (Fig. 4d). The maximum concentration of methane was near PL-6/PL-8 as observed previously, but was reduced to approximately 25% of the August value. Concentrations in the surface layers remained high at 200 nL/L or about a factor of 3 above saturation (Yamamoto et al., 1976). A reduction in biological activity, and a decrease in vertical stability (Fig. 4c) acted in concert to reduce the near-bottom concentration of dissolved methane. Near-bottom circulation also may have increased during the winter period.

Salinity and temperature distributions are shown in Figures (4a) and (4b). Salinity varied from 31.70‰ in the surface layers at PL-10 to slightly more than 32.75‰ in the near-bottom water at PL-4. Not unlike the situation observed in August 1980, the change in salinity was about 1‰. In contrast however, was the small vertical temperature gradient observed in February. Over St. George Basin, the vertical temperature variation was about 1.2°C in February and 4°C in August, which led to a decrease in the vertical stability (Fig. 4c). The effects of winter cooling was evident in the eastern portion of the section where temperatures had decreased to less than 2.7°C. At this time of the year, the warmest temperatures were found near the bottom of St. George Basin.

The distribution of properties in May-June of 1981 are shown in Figures (5a-5d). Near-bottom concentrations of methane are similar to that observed in February 1981 and again are located near the center of St. George Basin

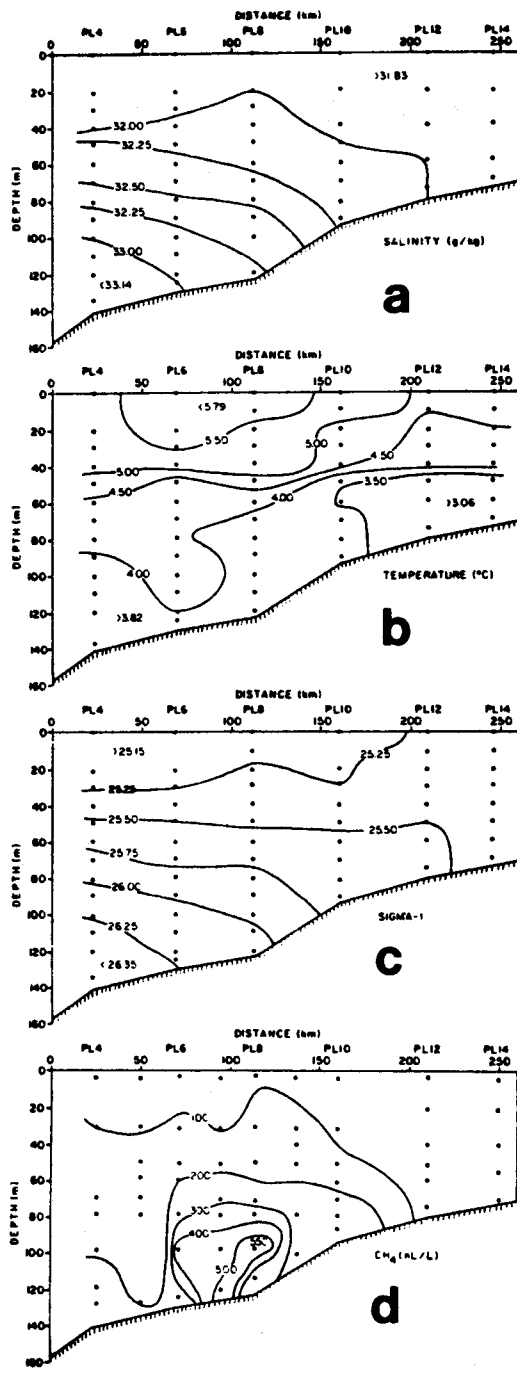


Figure 4. The vertical distributions of (a) salt, (b) temperature, (c) density, and (d) dissolved methane along the PROBES line in February 1981. See Fig. (2b) for the station positions.

(PL-6 to PL-8). In contrast to the previous measurements, surface concentrations were now less than 100 nL/L and suggest a gradual net degassing of the upper water column from February through May. Surface waters over St. George Basin were both isohaline and isothermal (Figs. 5a and 5b). The highest salinity was observed in the bottom waters of St. George Basin, about 33‰, with the surface layers uniform at about 32‰. Temperature varied from 4°C in the bottom waters to nearly 6°C in the surface layers. Once again, the coldest waters were found over the middle shelf region (PL-10 to PL-14). Thermal stratification was developing due to increased solar insolation, which caused an increase in stability and dissolved methane below the pycnocline (Fig. 5c). Of particular note is that although primary production had been increasing since late April or early May, the concentration of dissolved methane was no higher than was observed in February, presumably a time of minimum production. There appears to be a significant lag between the annual fixation of carbon and the maximum concentration of methane. Based on these sparse measurements, the lag appears to be at least 3 or 4 months (see Figs. 3a and 5a).

The distribution of dissolved methane within 5 m of the bottom is shown in Figures (6a-6c). In general, the near-bottom plume is bathymetrically contained within St. George Basin and reveals an ellipsoidal distribution to the north-northwest. The maximum concentration was always found near station SG5 (see Fig. 2c) and was seasonally variable. As noted earlier, the maximum observed concentration of methane was 2500 nL/L in August, followed by a minimum of 1000 nL/L in February and May. The orientation of the plume is determined by the local mixing characteristics and the mean velocity field.

Several obvious conclusions can be drawn about circulation by examining the distribution of methane. The plume appears elongated in the northwest-

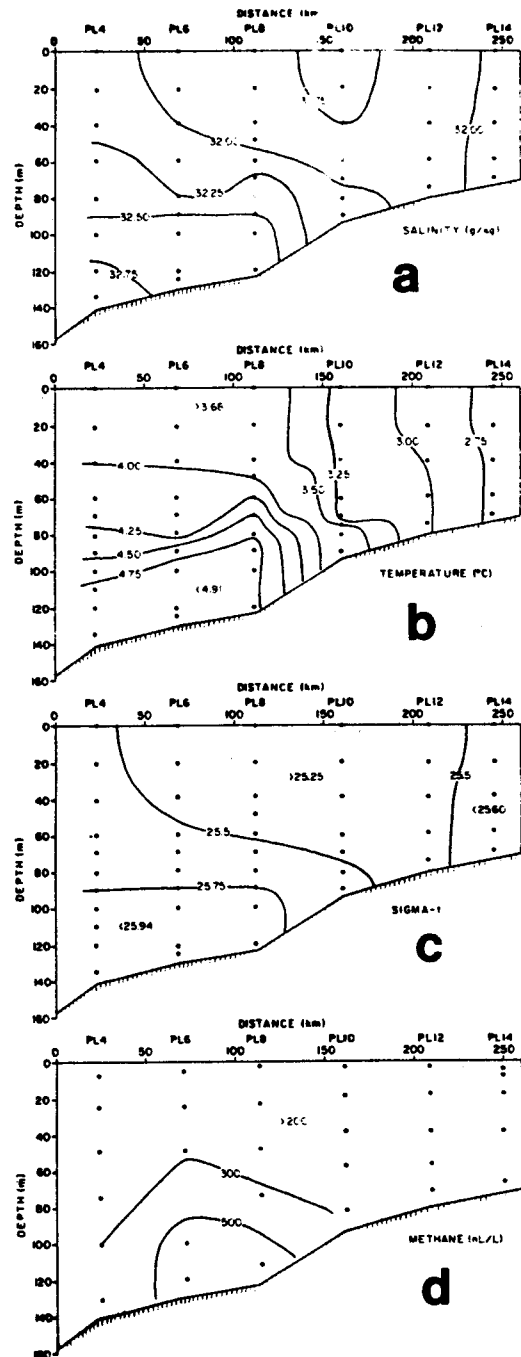


Figure 5. The vertical distributions of (a) salt, (b) temperature, (c) density, and (d) dissolved methane along the PROBES line in May 1981. See Fig. (2c) for the station positions.

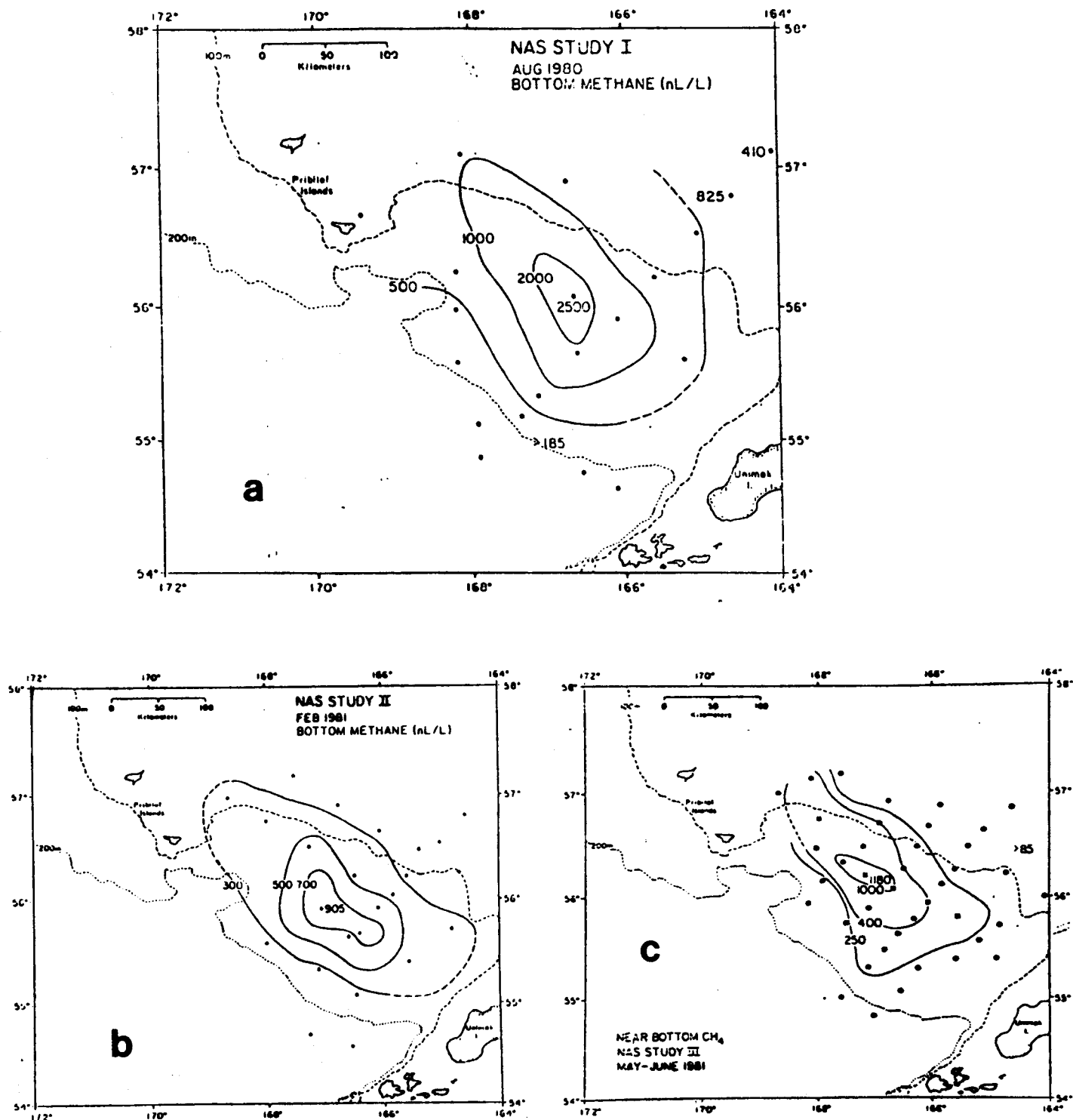


Figure 6. The near-bottom distribution of dissolved methane in (a) August 1980, (b) February 1981, and (c) May 1981. Concentrations were averaged over the lower 20 m of the water column.

southeast dissection in general agreement with the mean velocity field (Kinder and Schumacher, 1981b). The apparent source, located near SG5, coincides with the locus of fine-grained, organic rich sediments (Gardner et al., 1978). Organic carbon concentrations within the region of the plume range from 0.5 to about 1%. The zone of maximum organic carbon roughly coincides with the area circumscribed by the 2000 nL/L isopleth in Figure (6a). Beyond that region, organic carbon decreases and presumably so would the flux of CH₄ to the overlying waters. The absence of a strong trajectory to the northwest suggests that circulation is weak and that the currents are variable.

The distributions of methane shown in Figure (6) are entirely restricted to the near-bottom waters and show no surface outcropping. Even in February 1981 a weak pycnocline over the basin was sufficiently strong so as to inhibit vertical exchange. The vertical distribution of density (σ_t) and methane at station PL-6 in August is shown in Figures (7a,b). This station was occupied twice during a six-day period with little significant change in either the distribution of methane or density. The pycnocline was located between 60 and 80 m with an observed stability of 0.05 m⁻¹. Methane, shown in Figure (7a), showed a sharp gradient in the same region, suggesting that the vertical flux of CH₄ is strongly controlled by stability.

The time dependent nature of the bottom boundary layer is reflected in Figure (8). This station (SG-70) was occupied three times over a 13 day period in May 1981 and revealed the effects of subsurface water replacement on the distribution of methane. The lowest density water was observed on May 23 and it contained the highest concentration of methane. By June 1, however, water of increased density had penetrated the shelf ($\Delta\sigma_t = 0.11$), reducing the concentration of methane from 1200 nL/L to 800 nL/L. It appears that episodic intrusions of water onto the shelf occur with regularity that results in a compression or erosion of the methane plume. Our original

hypothesis was that methane would diffuse off the shelf as had been noted earlier in the Gulf of Alaska (Cline et al, 1978). However, none of our observations to date shows significant dispersion of CH_4 off the shelf, suggesting that any dissolved contaminant introduced into the bottom waters of St. George Basin would be similarly confined to the outer shelf region.

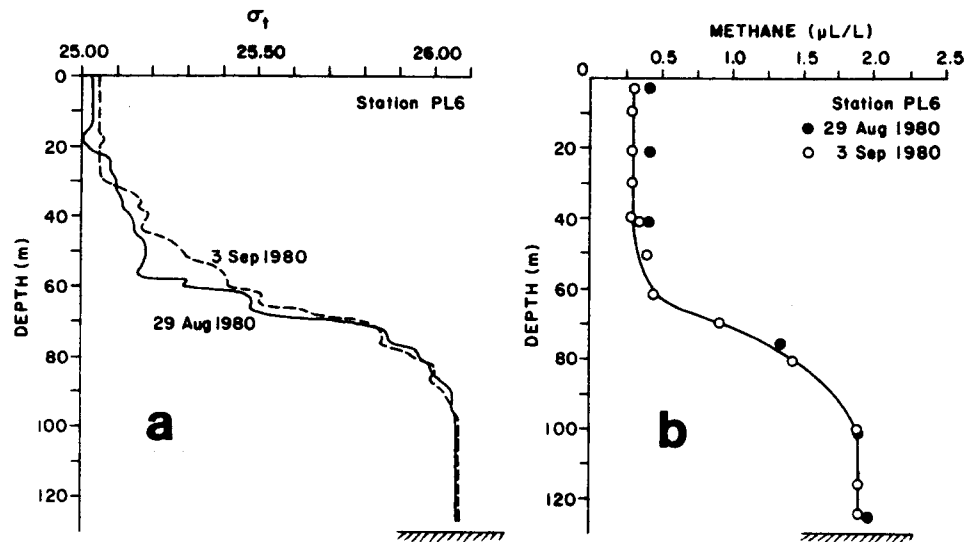


Figure 7. The vertical distribution of (a) density and (b) methane at Station PL6. Measurements were made on 29 August and 3 September 1980. Small but significant inversions in the density profile are the result of lateral mixing and the formation of salt fingering (Coachman and Charnell, 1979).

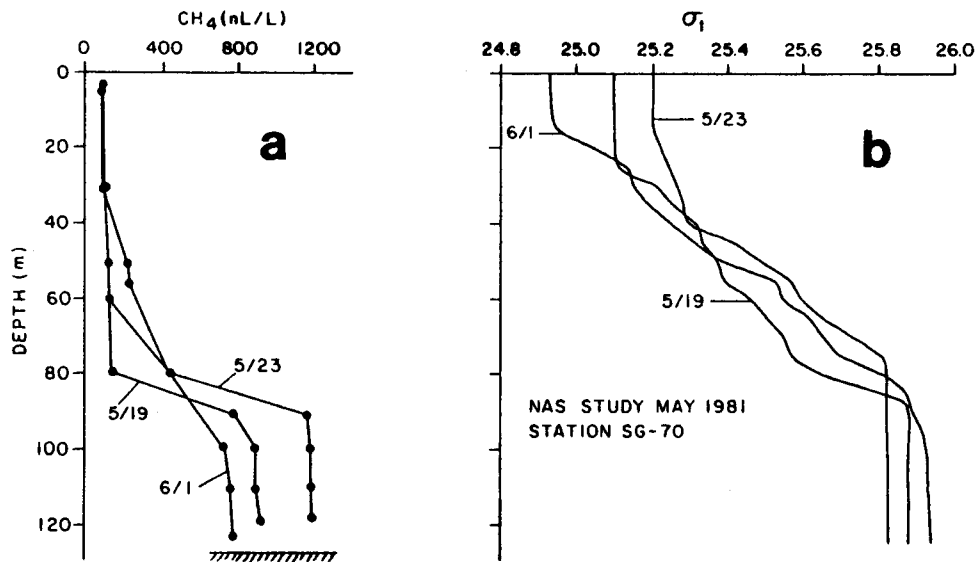


Figure 8. The vertical distribution of (a) dissolved methane and (b) density (σ_t) at Station SG 70. Measurements were made May 19, 23 and June 1, 1981, and show the temporal variability in circulation across St. George Basin.

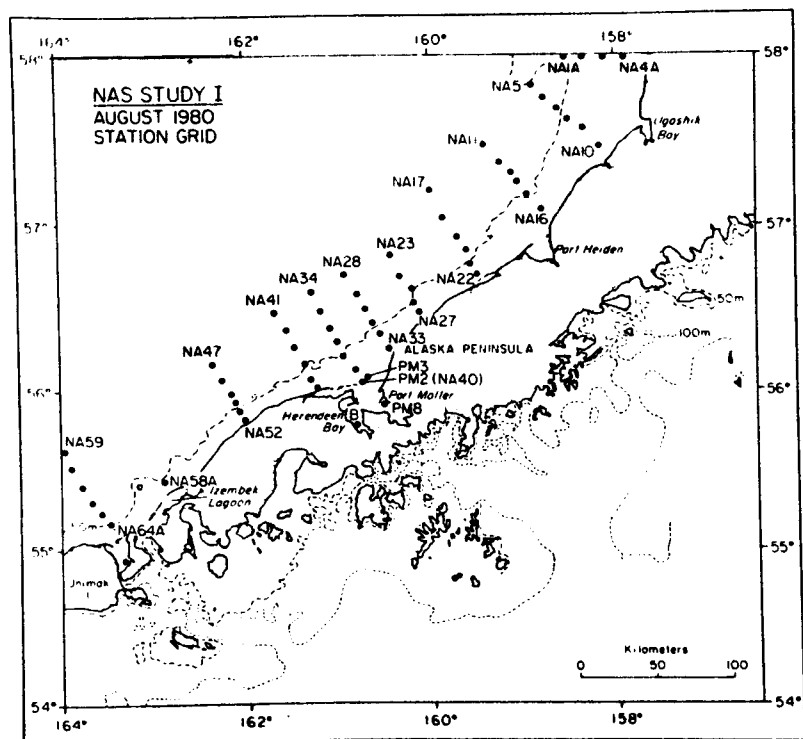


Figure 9a. The location of stations occupied in August 1980 along the NAS.

4.2 North Aleutian Shelf

The North Aleutian Shelf (NAS) extends from Unimak Pass on the west to the Kvichak River on the east (see Fig. 1). Two hydrographic regimes are described in this section, the coastal zone characterized by water depths less than 50 m and the middle shelf representing the slightly deeper offshore water. The coastal zone is usually well mixed due to the dissipation of wind and tidal energy, whereas the middle shelf is seasonally stratified (Schumacher et al., 1979). Because of these hydrographic differences, a frontal-type structure near the 50 m isobath is observed, which may influence the trajectory and dispersion of spilled oil.

The NAS region was surveyed three times to describe its seasonal characteristics. The station locations for each cruise are shown in Figures (9a-9c). The grid pattern was altered slightly during each cruise

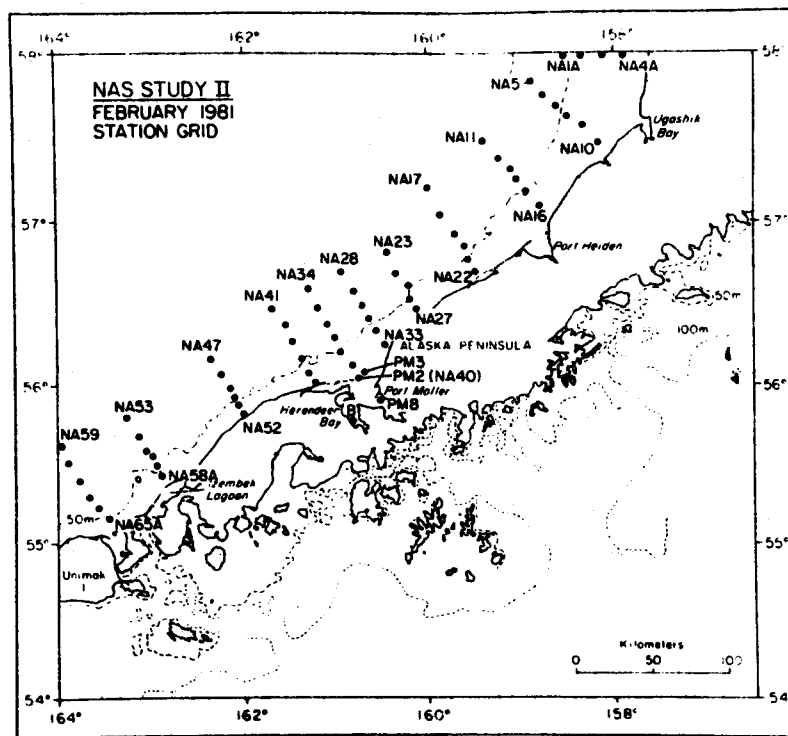


Figure 9b. The location of stations occupied in February 1981 along the NAS.

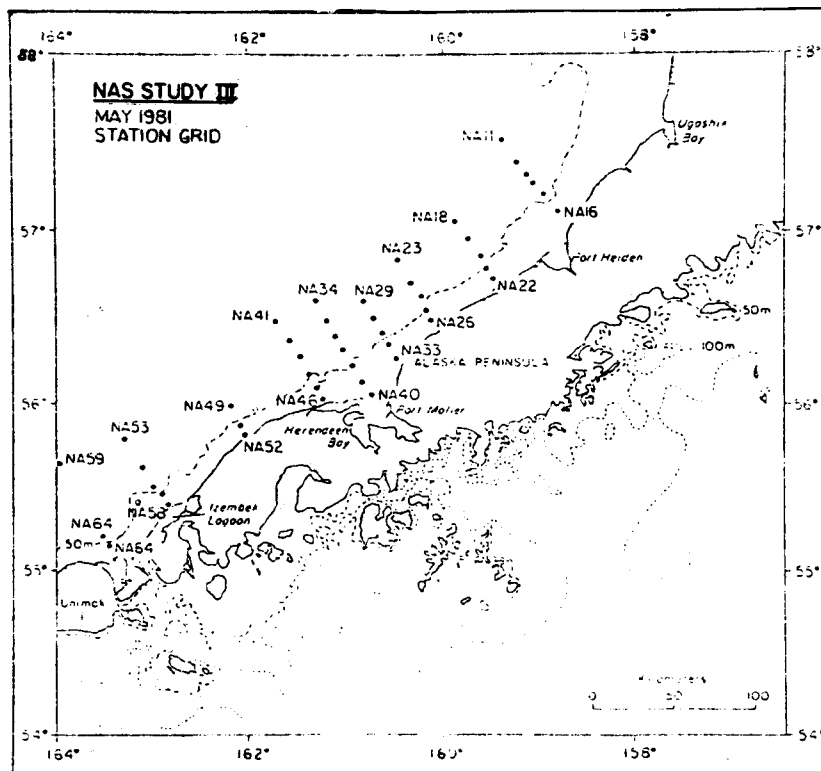


Figure 9c. The location of stations occupied in May 1981 along the NAS.

to account for seasonal hydrography and weather conditions. The methane tracer study emphasized the area adjacent to Port Moller (source) and the downstream region, which extends northeastward to approximately Port Heiden.

In order to summarize the hydrographic conditions for the coastal zone and the middle shelf region, the seasonal T-S relationships for each sub-region are discussed. These relationships are shown in Figures (10) and (11) for the survey periods of August 1980, February 1981, and May 1981.

August, a period of relatively high runoff to the coastal region, is characterized by a strong east-west salinity gradient (Fig. 10). The dominant source of freshwater is the Kvichak River, located at the eastern extremity of the region. There are numerous small sources of freshwater along the NAS, the major source being Port Moller. Diffuse sources of freshwater along the coast lead to relatively low salinities ($S \sim 30\text{‰}$) and warm temperatures ($\cong 12^\circ\text{C}$). Over most of the coastal regime, however, salinities and temperatures range from $30\text{-}32\text{‰}$ and $8\text{-}11^\circ\text{C}$, values typical of summer conditions.

In February, temperatures had decreased to near zero, while salinities remained in the range of $30\text{-}32\text{‰}$ (Fig. 10). While it is likely that freshwater runoff had diminished significantly because of subzero temperatures, the salinities remained nearly constant. The reason for this lies in the mechanisms by which salt is transported across the shelf. One possible explanation is that a decrease in freshwater input results in a reduction in estuarine transport of salt, particularly within the cyclonic circulation of the coastal zone (Kinder and Schumacher, 1981b).

Water temperatures along the coast in May were intermediate between those observed in August of 1980 and February 1981 (Fig. 10). Temperatures had increased to $5\text{-}8^\circ\text{C}$, while salinities remained in the typical range $30\text{-}31\text{‰}$. The mean salinity decreased slightly compared to the previous winter, presumably in response to renewed input of freshwater.

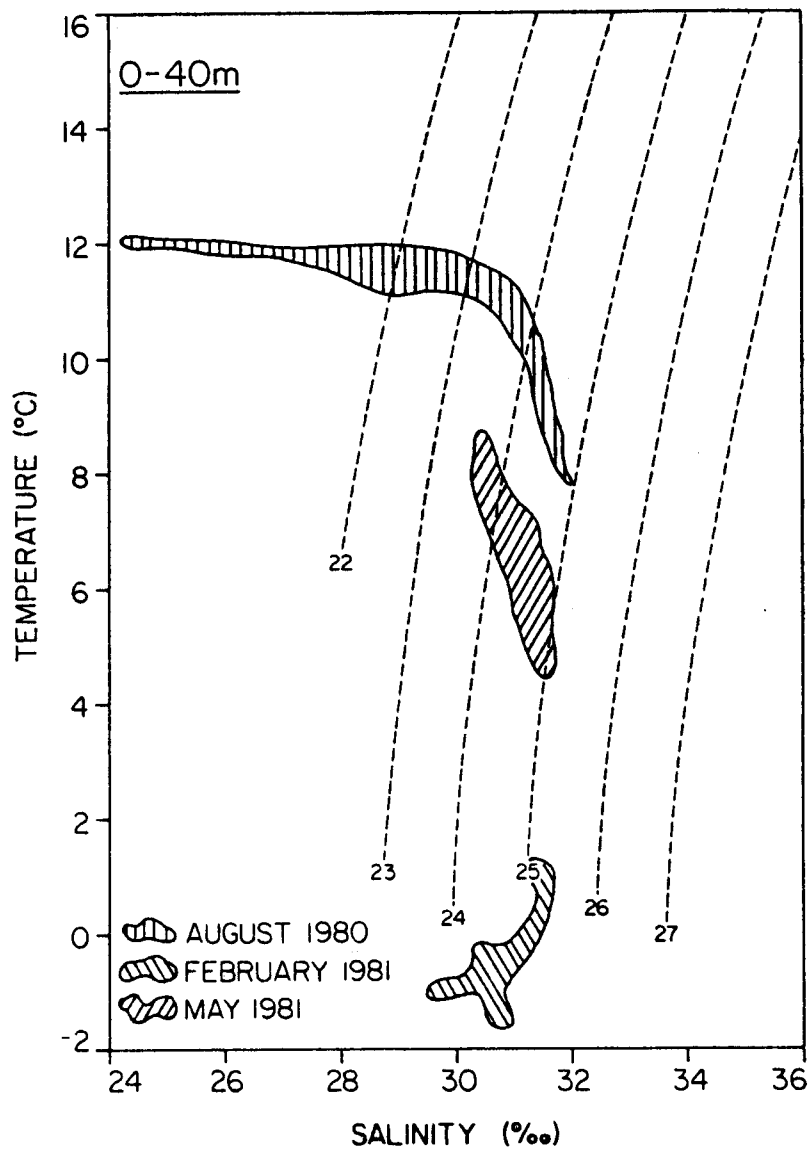


Figure 10. The seasonal distribution of salinity and temperature along the NAS. The coastal zone was defined to include all waters whose depth was less than 40 m.

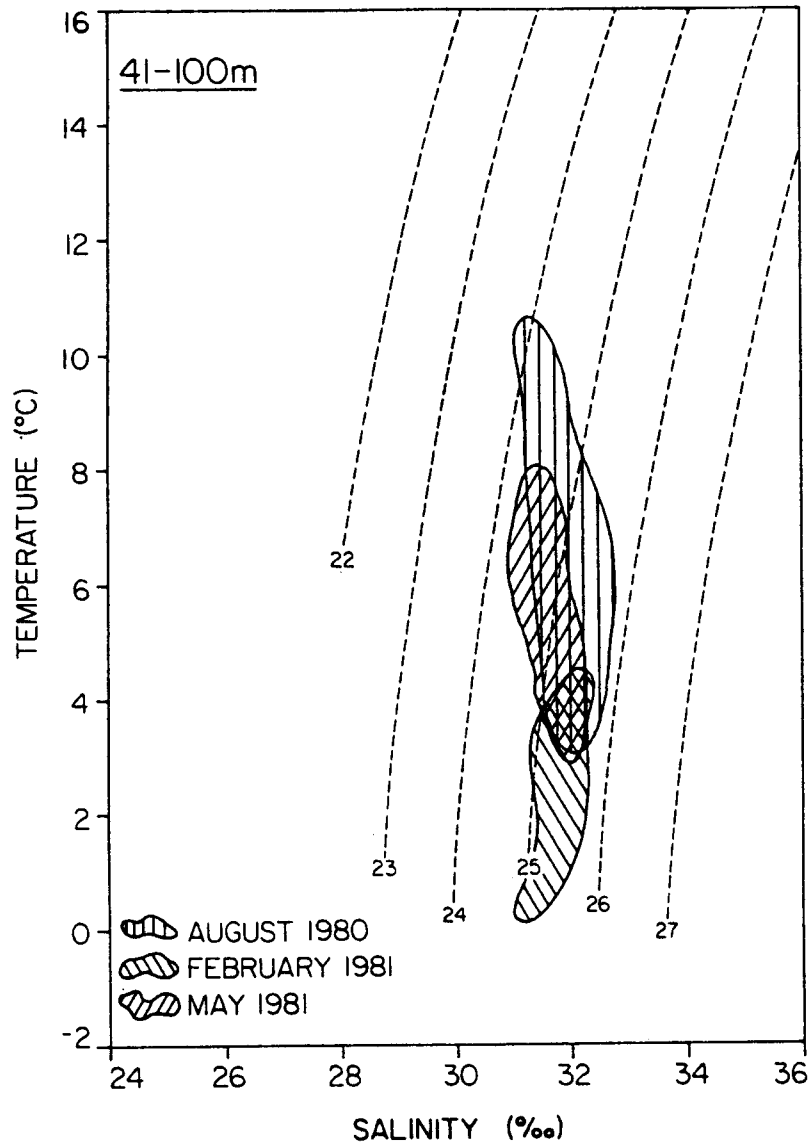


Figure 11. The seasonal distribution of salinity and temperature along the southern boundary of the middle shelf. The middle shelf was operationally defined to include all stations at which the depth of water exceeded 41 m.

The density field, regardless of season, was largely controlled by salinity. The density range (σ_t) was 23 to 25, and largely reflected the longshore distribution of salt.

The seasonal T-S relationships for the southern sector of the middle shelf are shown in Figure 11. In August, the water was nearly isohaline at 31-32‰. Temperature ranged from 3°C to 10°C, the colder waters originating during the previous winter. As noted in the coastal zone, warmer water was associated with lower salinities. On the average, however, salinities were higher in this region compared to the coastal zone (compare Figs. 10 and 11). Temperatures as high as 11°C and salinities as low as 29‰ were observed at the eastern extremity of Bristol Bay.

In February, colder water temperatures prevailed (0 to 4°C), but salinities remained constant at 31-32‰ (Fig. 11). Little horizontal or vertical stratification existed; hence, the T-S trajectory was parallel to the isopycnals. Densities were uniformly 25 to 25.5 σ_t units, slightly higher than the range of 24 to 25.5 observed in August, 1980.

By May, solar insolation had increased temperatures to 8°C, but salinities remained nearly constant at 31-32‰. Stratification had increased as indicated by the intersection of the isopycnal and T-S surfaces. The temperature range over the region was 2 to 8°C, the colder water being a relict feature from the previous winter (Kinder and Schumacher, 1981b).

Examples of the seasonal changes in water column stratification are shown for each hydrographic regime in Figures (12a-12c) and (13a-13c). Station 27 and 23 are representative stations in the coastal zone and in the southern sector of the middle shelf respectively. Station 27, which was occupied on each of the three cruises, was located approximately 5 km offshore in 25 m of water. The vertical distribution of properties indicates that the water column normally was well mixed, although some stratification was

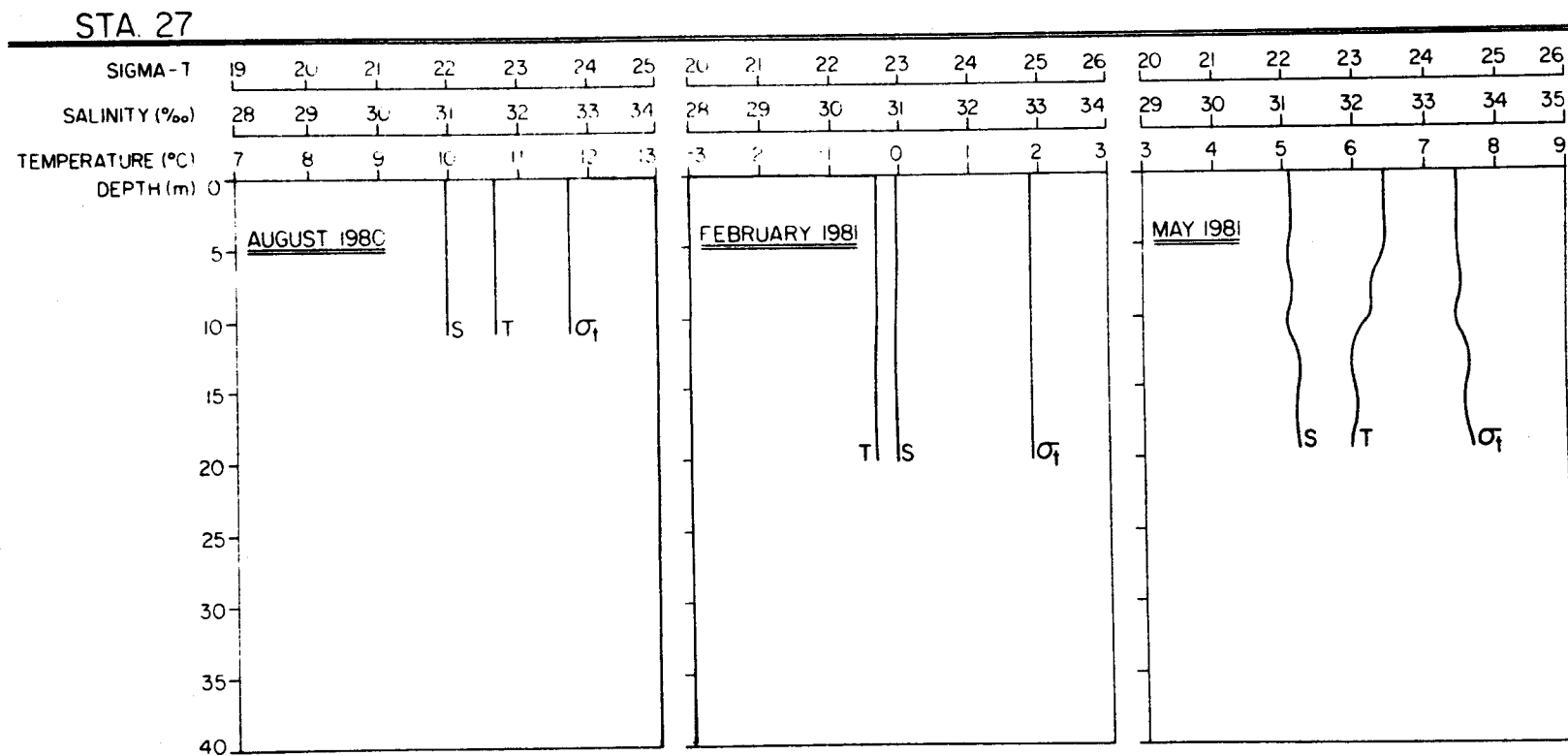


Figure 12. The seasonal distribution of salinity, temperature, and density (σ_t) at Station 27 in the coastal zone. Note the well-mixed water column.

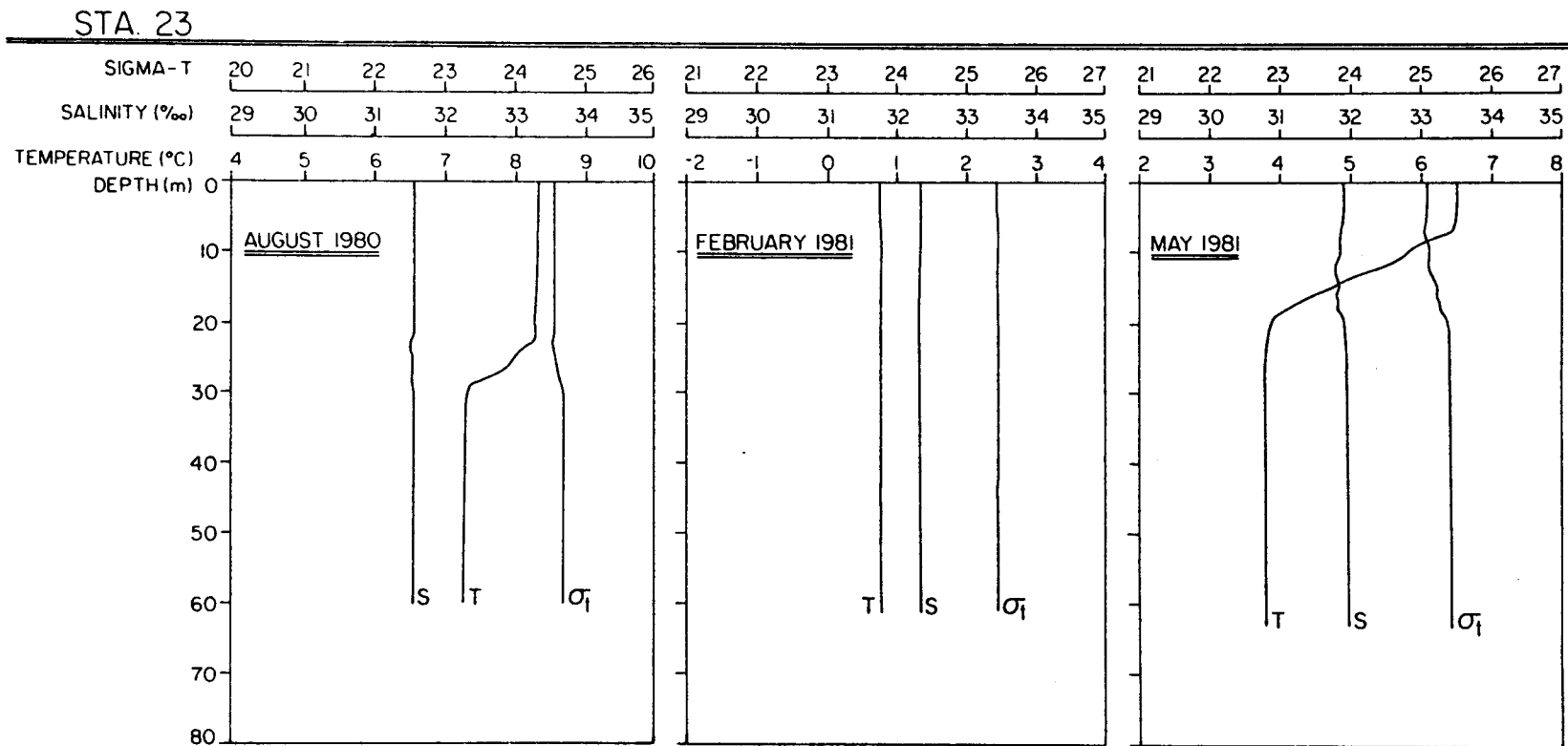


Figure 13. The seasonal distribution of salinity, temperature, and density (σ_t) at Station 23 in the middle shelf. Note the isothermal, isohaline conditions in February 1981.

observed in May 1981 (Fig. 12c). This may have been a transient feature, however. As noted above, the salinity remained remarkably constant at 31‰, while the temperature varied from 10°C in August 1980 to less than zero in February 1981.

In contrast to the well-mixed conditions in the coastal zone, the middle shelf region is characterized by weak seasonal stratification (Figures 13a-13c). Station 23, located about 50 km offshore (Figure 9) and at a depth of 68 m, is an example of middle-shelf conditions near the inner front. Salinity was at a minimum in August, increasing to nearly 32‰ in May. With the exception of February, in which the water column was totally unstratified, a weak thermocline was present in the upper 30 m of the water column. Because salinity was largely invariant, seasonal warming of the surface layers led to weak stratification, which was strongest in May. Under the influence of solar insolation and wind mixing, the thermocline deepens during the summer, but the gradient actually decreases due to the concomitant warming of the bottom waters. The net effect was to decrease the density gradient slightly. Because of large interannual variations in sea surface temperatures and the amount of ice formed locally, bottom water temperatures may vary widely from year to year (Niebauer, 1981).

There appear to be numerous diffuse sources of freshwater along the NAS. In Figure 14 are shown the mean salinities for the coastal zone ($z \leq 40$ m) as a function of distance from Unimak Pass. Salinity data from all stations located in less than 40 m of water were averaged horizontally and vertically for each of the three cruises.

In general, the salinity decreases from west to east along the shelf. The most dramatic decrease occurred in August in which salinities decreased from approximately 32‰ at Unimak Pass to a low of 28‰ near the Kvichak River. During all three cruises, a local salinity minimum occurred at Port

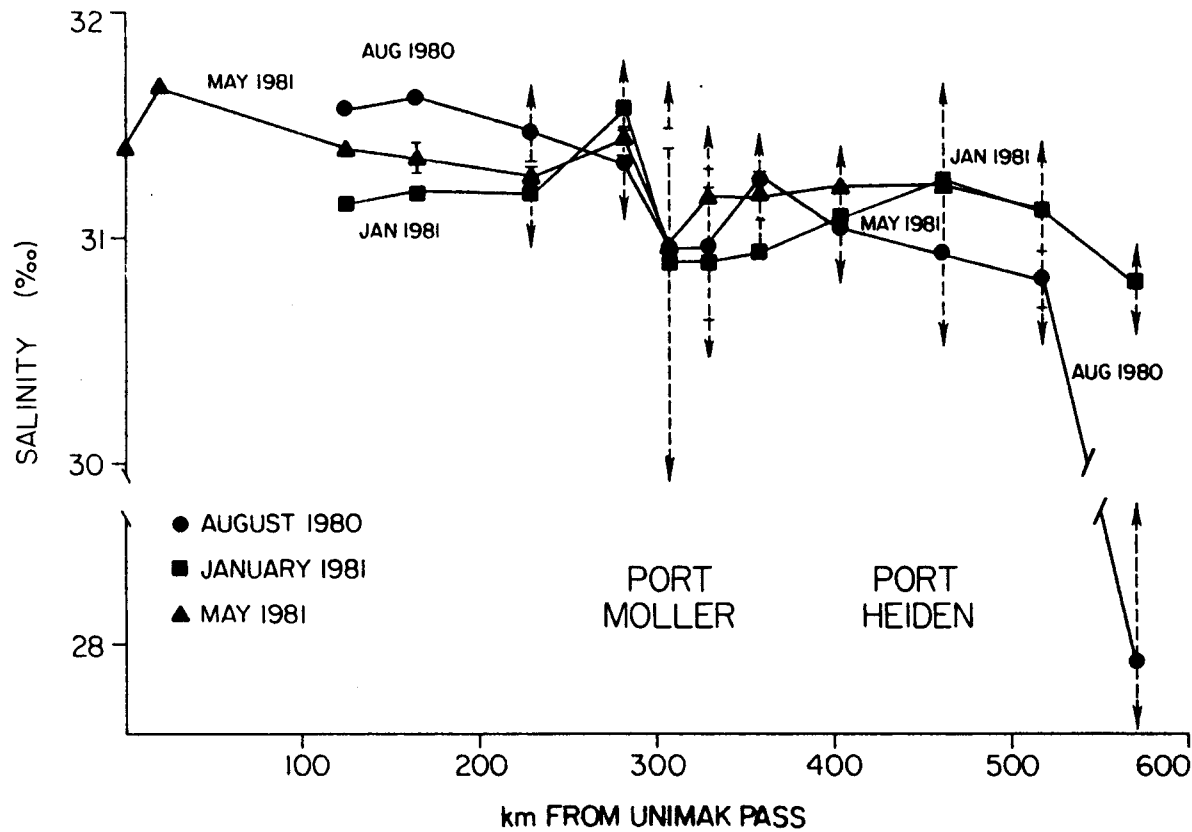


Figure 14. The average longitudinal distribution of salinity along the NAS coastal zone. Only stations at which the depth of water was less than 40 m were included in the analysis. The dashed arrows indicate the range of values about the mean. Note the large variations at the entrance to Port Moller.

Moller, indicating the significance of this source. The salinity profiles for February 1981 and May 1981 indicate that the mean drift of the coastal water is toward the east, in agreement with the cyclonic circulation through Bristol Bay. During February, the freshwater influence of Port Moller was evident to Port Heiden, a distance of about 150 km. To the east of Port Heiden, the effect of the Kvichak River is evident in the systematic decrease in salinities.

A decrease in the mean salinities along the NAS can be interpreted in two ways. The first is that cyclonic circulation through Bristol Bay results in a continual freshening of the high salinity water entering through Unimak Pass. This assumes that the flux of salt across the inner front is not totally sufficient to balance the freshwater input. The second case assumes that circulation is anticyclonic and that the salinity of the coastal water steadily increases due to cross-frontal salt flux and a decrease in the freshwater supply to the west along the shelf. Current meter measurements suggest that the circulation is indeed cyclonic (Kinder and Schumacher, 1981b), an interpretation that is supported by the distribution of methane as well.

The horizontal surface distribution of dissolved methane in the coastal zone and the adjacent middle shelf region is shown in Figures 15a,b,c. In August (Fig. 15a), the middle shelf region was characterized by surface concentrations of methane of 400 nL/L or nearly 8 times supersaturation. Concentrations of methane along the inner front were approximately 500 nL/L, decreasing toward the northeast. The highest concentration of methane observed was 22,000 nL/L inside the Port Moller estuary, decreasing to approximately 1200 nL/L at the entrance. The concentration of methane at the entrance to Port Moller depends on the stage of the tide, as one might expect.

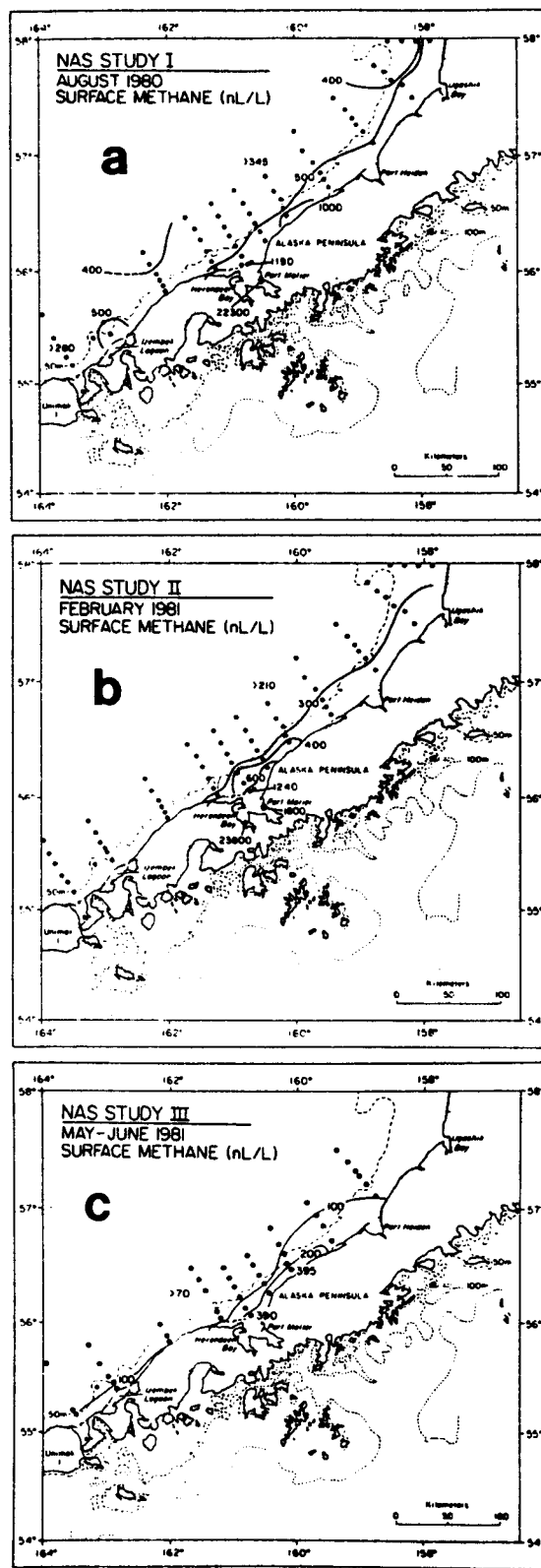


Figure 15. The distribution of methane at the surface along the NAS in (a) August 1980, (b) February 1981, and (c) May 1981. Concentrations are in nL/L (STP).

In February (Fig. 15b), the offshore concentrations had decreased to less than 300 nL/L, whereas the average value near the entrance was about the same as seen the previous August. The inner front was characterized by concentrations of methane of 300 nL/L. The observed systematic decrease in the ambient levels of methane between August and February is attributed to a decrease in biological activity and a seasonal drop in temperature.

The following May, concentrations of methane had decreased to the lowest levels observed (Fig. 15c). Offshore values were approaching saturation levels (~70 nL/L), while the coastal concentrations had fallen to 100-400 nL/L. This observation was unexpected because the spring bloom had commenced, but apparently the microbial production of methane lags the production of carbon by several months. This fact was also observed earlier during the initial baseline study (Cline, 1976).

For each of the observational periods, the trajectory of methane was toward the northeast in agreement with previous observations (see above). The dominant source of CH_4 to the coastal zone was from Port Moller, but other diffuse sources along the coast could not be totally evaluated. We will show below that the tidal flux of methane from Port Moller is sufficient to account for the along-shore distribution of methane without invoking additional sources. In particular, the bottom sediments are not believed to be a significant source of methane because of their coarse texture (coarse sand) and low organic carbon content (Sharma, 1974).

Once the dissolved methane from Port Moller enters the coastal zone, it is rapidly mixed vertically and laterally out to the inner front. This is shown in Figure 16 for two orthogonal sections near Port Moller during the August cruise (see Fig. 9 for ref.). Section IV, located east of Port Moller, shows the offshore decrease in dissolved methane, and the vertical homogeneity of the water column. Only station NA-33 reveals a surface

maximum. Near the front (NA-31), the concentration had fallen to about 450 nL/L and systematically decreased in the offshore direction. Section V, located farther to the east, shows the same vertical homogeneity as was seen in the previous section. Concentrations of methane near the front are approximately 400 nL/L. A vertically homogeneous water column with respect to methane indicates that mixing of the low salinity, high methane waters from Port Moller is essentially complete within 10-20 km of the entrance, or approximately 1-2 tidal excursions.

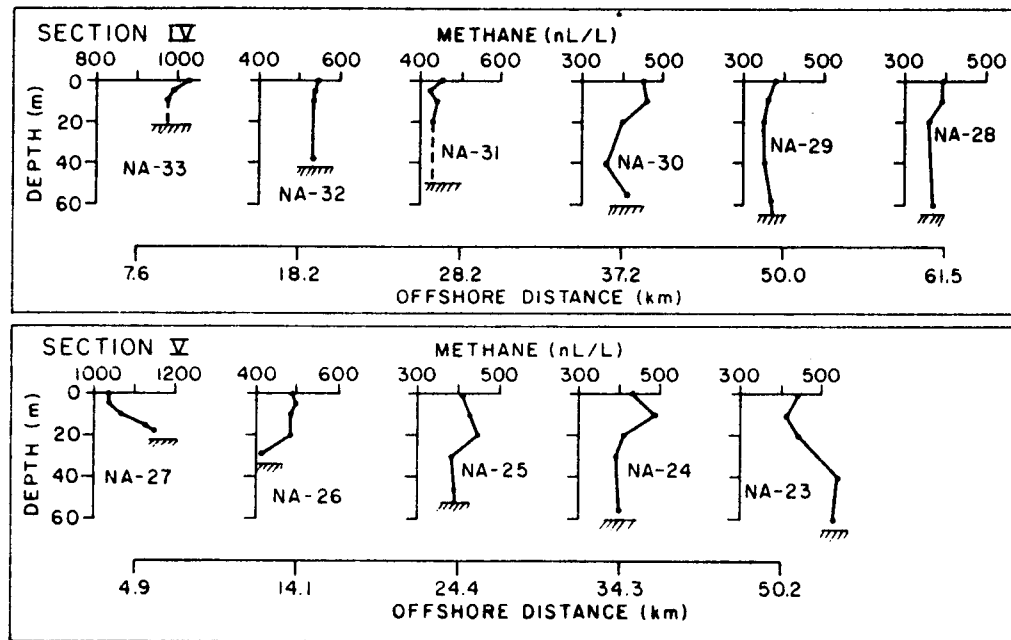


Figure 16. The vertical distributions of methane along sections IV and V east of Port Moller (see Fig. 9a). Measurements were made in August 1980.

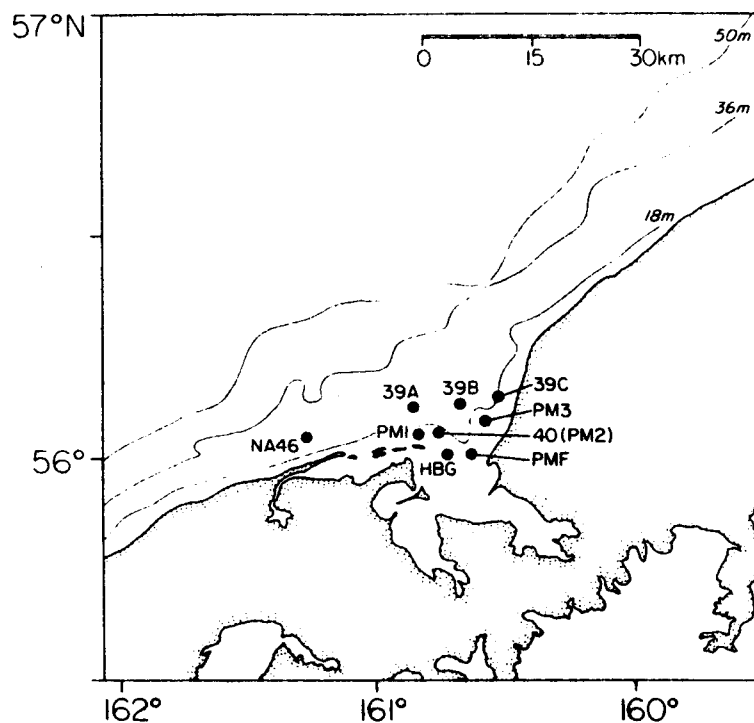


Figure 17. The location of 24-hour time series stations at the entrance to Port Moller. Stations PM1, PM2, PM3 were occupied in August 1980; Station PM3 in February 1981; and Stations 39A, 38B, and 39C in May 1981.

In order to quantify the flux of methane from Port Moller, which was required to satisfy the boundary conditions of the model (see page 362), a time series was conducted near the entrance during all three visits. The location of these stations is given in Figure (17). Stations PM1, PM2(NA40), and PM3 were occupied in a cyclic fashion over a period of 24 hours during the August and February cruises, while stations NA-39A, B, C were occupied during the May cruise. These stations were used to establish the tidal flux conditions for the model.

The methane enriched water was always found along the eastern shore of the estuary as depicted in Figures (18a,b,c). In August, the largest concentrations (3-4 $\mu\text{L/L}$) of methane were observed at PM-3, decreasing abruptly to $1\mu\text{L/L}$ at PM-2. Stations NA-38 (Figure 9), located at the inner front,

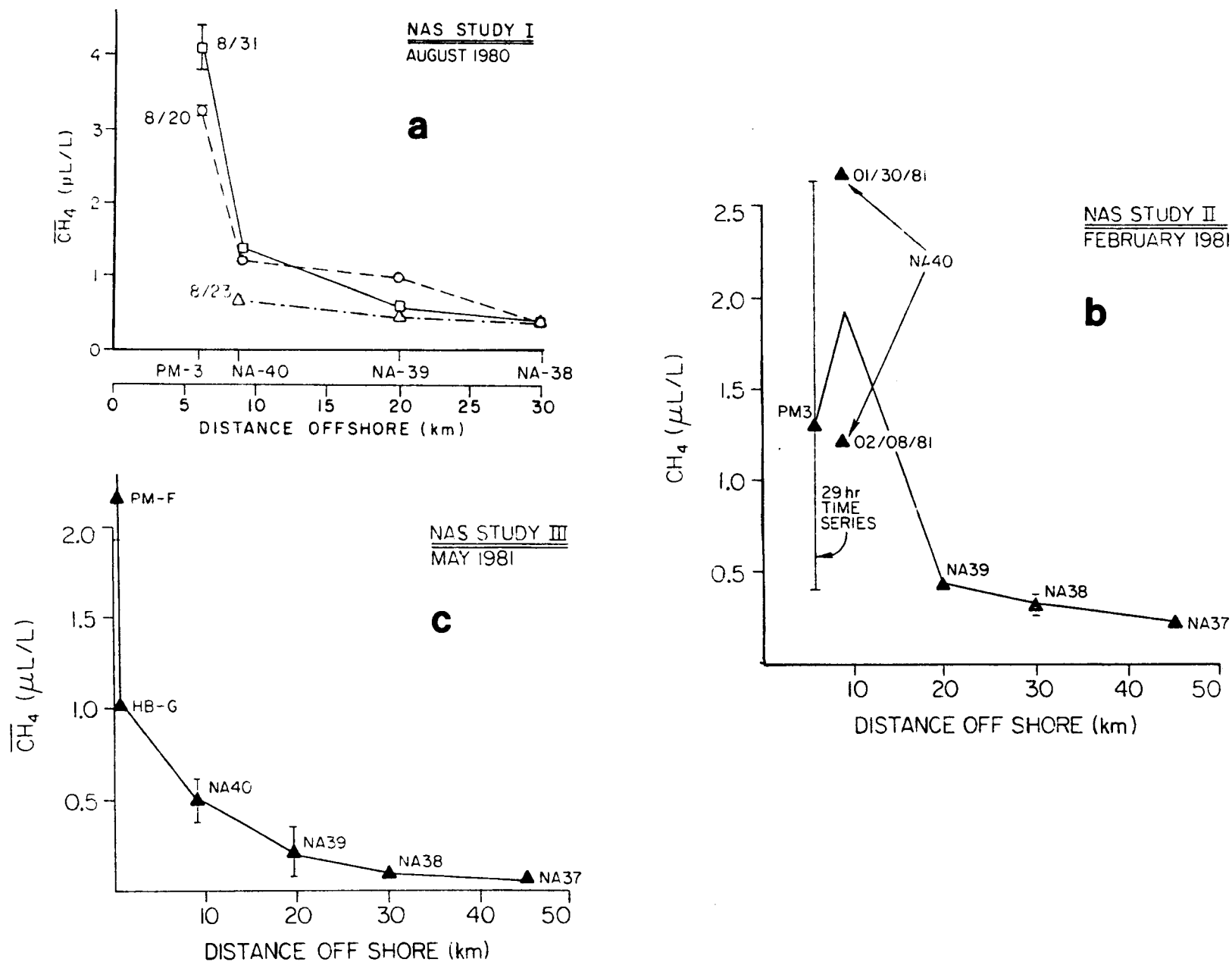


Figure 18. The time-averaged distribution of methane across the entrance to Port Moller in (a) August 1980, (b) February 1981, and (c) May 1981. In those cases where more than one measurement was made, the vertical lines indicate the range of values about the mean.

showed a relatively constant concentration of methane of $0.5\mu\text{L/L}$, the background level observed for that time of year. As we will show later, the concentration of methane (i.e., depth averaged) at the entrance shows large variations due to tidal influences; however, the highest concentrations of methane are always found along the eastern shore, regardless of the stage of the tide.

In February (Fig. 18b), the highest concentrations were observed at PM-3 and NA-40 (PM-2). The mean at each of these stations was $1.3\mu\text{L/L}$ and $1.9\mu\text{L/L}$ respectively as compared to a background level of $0.2\mu\text{L/L}$. The large ranges (e.g., extrema) observed at PM-3 and NA-40 are due to the stage of the tide.

As noted earlier, the concentration of methane over the entire NAS in May was lower than had previously been observed. This was the case for Port Moller as well (Figure 18c). As before, the highest concentrations of methane were observed at PM-F and HB-G, stations located at the entrance to Port Moller. Ambient levels offshore fell to approximately $0.1\mu\text{L/L}$ or 100nL/L as noted earlier.

The influence of tides on the fluxes of salt and methane is shown in Figure 19, which describes the observations taken at PM-3 over a 24-hr period. Temperature showed little variation over the period, whereas salinity varied from 30 to 31‰ , depending on the stage of the tide. The concentration of methane varied from $0.3\mu\text{L/L}$ to over $2.5\mu\text{L/L}$ in concert with the flood and ebb of water from Port Moller. It is this tidal flux that sustains the plume of methane observed along the coast.

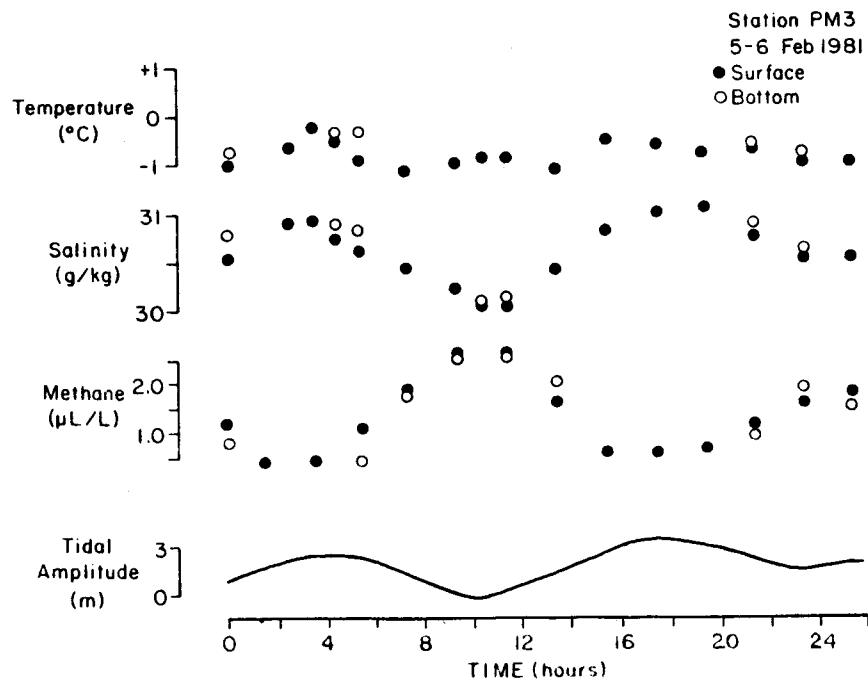


Figure 19. The diel variation in temperature, salinity, and methane at Station PM3. Measurements were made on 5-6 February 1981. Note that low salinity, methane-enriched water is found at the entrance to Port Moller during ebb tide.

5. TRANSPORT MODELS

5.1 Horizontal Trajectory Model

The distribution of dissolved methane in the two survey regions was modeled to provide limits on the horizontal and vertical scales of mixing. The model also provides a comparative check on the magnitude of the mean current speeds, which under most conditions will govern the transport of both surface and 'dissolved' oil.

The usefulness of dissolved methane as a chemical tracer depends critically on the characteristics and strength of the source. For a point source of uniform strength, the spatial distribution of methane can be used to define limits on mixing and transport processes. The most straightforward use of this tracer was found along the North Aleutian Shelf (NAS), where the biological production of methane within Port Moller (see Figure 18) resulted in a significant tidal flux to the coastal zone. This region is hydrographically complex (Csanady, 1981), seasonally and spatially variable, and strongly under the influence of coastal winds. Moreover, subtidal frequencies are strongly dependent on the frequency and duration of storms (Schumacher, 1981). Our purpose here was not to attempt to resolve short-term spatial variations, but rather to clarify the mean condition that exists along the shelf for time periods >30 d.

To examine the salient spatial features of dissolved methane along the NAS, we adopted a stationary, two-dimensional model described by Csanady (1973). This particular model has been used to predict the dispersion characteristics of wastewater injected along a pipe (line source) into a coastal zone environment. The particular model chosen assumes steady state, balances lateral diffusion against horizontal advection, and includes a first order decay term, which incorporates both biological consumption and the air-sea exchange of methane. The assumption of steady state is not valid

for transient events, but should be valid for time scales in excess of one month ($u \geq 3$ cm/s), given a Lagrangian tracer scale of 75 km or more. The model is

$$\frac{\partial}{\partial y} \left\{ K_y \frac{\partial C}{\partial y} \right\} - u \frac{\partial C}{\partial x} - kC = 0, \quad (1)$$

where the space dependency of the horizontal eddy diffusivity is retained. The solution to (1) for a line source of length b is

$$C = (C_0/2) \exp\{-kx/u\} [\operatorname{erf}(y_1) + \operatorname{erf}(y_2)] \quad (2)$$

where

$$y_1 = \frac{b/2+y}{0.1039(x/u)^{1.17}}$$

$$y_2 = \frac{b/2-y}{0.1039(x/u)^{1.17}}$$

x = longshore direction
 y = cross-shelf direction
 u = longshore mean velocity
 k = first order decay constant
 C_0 = concentration of methane at the source

In this description, we ignore diffusion in the x -direction and scale the horizontal diffusivity (K_y) in the y -direction according to the Lagrangian time scale. For simplicity, we assume that mixing is isotropic in the x - and y -directions. However, Okubo (1971) has shown that dispersion is enhanced in the direction of mean flow. The magnitude of the difference is approximately a factor of three for those coastal situations that have been studied (Okubo, 1971). Along the NAS, tidal currents are strongly rectilinear, which presumably results in an enhanced mixing alongshore. In the presence

of a mean flow, u , it can be shown that:

$$\sigma_{rc}^2 = 2\sigma_x\sigma_y, \quad (3a)$$

where σ_{rc} is the mean square radius of diffusing substance, σ_x and σ_y are the respective standard deviations of the plume in the x - and y -directions (Okubo, 1971). If we assume uniform horizontal mixing ($\sigma_{rc}^2 = 2\sigma_y^2$) the apparent diffusivity defined by Okubo is:

$$K_y = \sigma_y^2/4t \quad (3b)$$

or

$$K_y = \sigma_y^2/2t, \quad (3c)$$

where $\sigma_{rc}^2 = 2\sigma_y^2$ and t is the diffusion time. The characteristic time (or length) scale can be computed from $t = x/u$. Substituting into (3c), we obtain:

$$K_y = \sigma_y^2 u/2x \quad (3d)$$

Based on dye patch studies, Okubo (1971) has given estimates of K_y in terms of the characteristic length scale ℓ . He found that the 4/3 law overestimated the magnitude of K_y and presented a log regression diagram that shows:

$$K_y \propto \ell^{1.1} \quad (3e)$$

or that

$$\sigma_{rc}^2 = 0.0108 t^{2.34} \quad (3f)$$

In equation (2), the horizontal eddy diffusivity is formulated in terms of the variance of the plume in the y-direction $\sqrt{2} S_y$. After substitution of $t = x/u$ into (3f) we find:

$$\sqrt{2}s_y = 0.1039 t^{1.17} \quad (3g)$$

Based on the diffusion diagram given by Okubo (1971), we expect

$10^5 \text{cm}^2/\text{s} \leq K_y \leq 10^7 \text{cm}^2/\text{s}$ for length scales between 10 and 100 km. If we assume that K_y is proportional to the tidal excursion, which is approximately 10 km, then $K_y \cong 10^5 \text{cm}^2/\text{s}$.

Dissolved methane may be lost from the water column via air-sea exchange and biological oxidation. Since both processes can be formulated in terms of first order kinetics, they are included in the model as a single term:

$$k = k_{a/s} + k_{\text{biol}} \quad (4)$$

Computation of $k_{a/s}$ requires knowledge of sea-surface roughness (a function of wind speed), the molecular diffusion and Bunsen solubility coefficients as a function of salinity and temperature. All of these parameters are known to within 30% (Broecker and Peng, 1974), thus $k_{a/s}$ can be estimated (see Cline, 1981 for details on the calculation of $k_{a/s}$).

Biological oxidation rates of methane, not previously known for these waters, have been determined by Griffiths et al., (1982). Water samples were inoculated with a known amount of $^{14}\text{CH}_4$ and incubated for 24 to 48 hours. The $^{14}\text{CO}_2$ given off after oxidation was counted and the rate constant computed. The kinetics generally obeyed a first order reaction when incubation time and substrate levels were varied.

The model is formulated in terms of a line source of length b . If the depth of the mixed layer (Δz) is known, then the mass transport of methane out of Port Moller is simply:

$$Q_{\text{CH}_4} = (b) \cdot (\Delta z) \cdot (u) \cdot (C_0), \quad (5)$$

where the mass transport Q has dimensions Mt^{-1} . Thus, the diffusion-advection model is sensitive to the boundary conditions: b , source length; Δz , mixed layer depth; u , mean alongshore velocity; C_0 , initial concentration at the boundary.

A schematic representation of the NAS and the major transport terms used in the model are shown in Figure (20). Because the water depth increases offshore, the methane distribution in the surface layer must be vertically averaged to provide a realistic representation of the actual distribution.

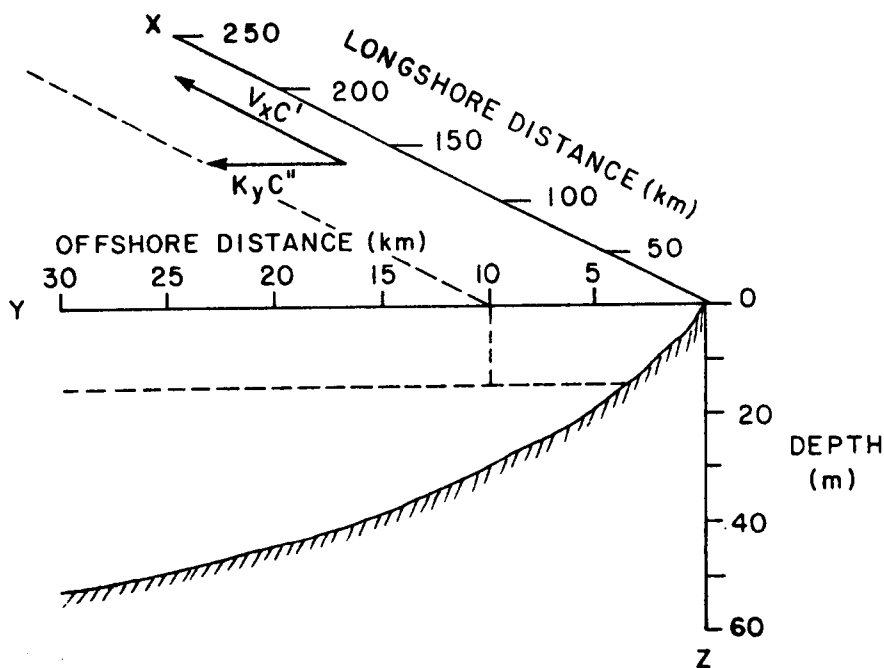


Figure 20. A schematic diagram of the NAS region. The significant transport terms include longshore advection vC' , and the flux divergence KyC'' . The well mixed coastal zone is approximately 20 m deep and 32 km wide. Not shown in the diagram is the air-sea exchange of methane, which is proportional to the concentration of methane.

In the following discussions, we will use this model to estimate mean currents along the NAS and to compare these results with the current meter observations. Along any orthogonal section to the flow, the transport of methane must be balanced by the tidal source at the entrance to Port Moller. Time series measurements made at the entrance allow us to estimate C_0 , b , and Q ; thus the model is constrained by both a concentration at the boundary and the flux. Because the air-sea exchange and biological oxidation of methane are seasonally dependent, appropriate values will be used in the individual modeling comparisons.

5.2 Vertical Flux Model

In a stratified water column, a portion of the methane produced at the bottom diffuses vertically through the pycnocline. In the absence of biological consumption, the curvature in the methane profile provides an independent estimate of the magnitude of K_v within the pycnocline. In the situation where oil may be released at the bottom, vertical transport is limited by strength of the pycnocline. In St. George Basin, the water column is seasonally stratified, thus if oil (dissolved and emulsified) is released into the bottom waters, it will largely remain in the lower boundary layer. To estimate the rate at which dissolved material might be transported vertically in stratified waters of St. George Basin, we used methane as a dissolved tracer.

To quantify the magnitude of the vertical transport parameter K_v within the pycnocline, we adopted a one-dimensional flux model describing the vertical distribution of dissolved methane. The one-dimensional flux model assumes that the curvature in the methane profile is the result of variable shear within the pycnocline and not due to in situ consumption. This assumption is not totally valid in all instances, but it does place a lower

limit on the magnitude of K_v . The essence of the model is that methane is produced at the bottom and is removed by horizontal and vertical transport processes. Most of the biologically produced methane is removed by horizontal advection, but a small portion diffuses vertically through the pycnocline and is removed by air-sea exchange. In the absence of biological processes, the model describing the distribution of methane within the pycnocline is

$$K_v \{dC/dz\} = \text{constant}, \quad (6)$$

where K_v is the depth dependent vertical eddy diffusivity. Since the flux across any horizontal plane is a constant, that constant must be equal to the air-sea evasion flux.

$$F_{a/s} = \frac{D}{h} \{C - C^*\}, \quad (7)$$

where D is the molecular diffusivity of dissolved methane, h is the thickness of the laminar boundary layer, and C^* is the equilibrium solubility of methane at the sea surface. The equilibrium concentration of methane is a function of its atmospheric mixing ratios, salinity, and temperature (Yamamoto et al., 1976). The constants D and h are known parameters, the latter being largely a function of wind velocity (Emerson, 1975). By combining equations 6 and 7, the vertical eddy diffusivity can be calculated from the methane gradient. To compute the gradient, the vertical distribution of methane was smoothed by eye, fit with a cubic spline function, and differentiated to provide a smooth distribution of K_v as a function of depth.

The magnitude of K_v is not actually depth dependent, but rather depends in a complicated way on the local velocity shear and stability of the water column (Welander, 1967). In the discussion to follow, K_v will be plotted as

a function of the Brunt- Vaaisala frequency, which is equal to

$$N^2 = (d\rho/dz)/\rho g \quad (8)$$

The stability of the water column is proportional to the density gradient, $d\rho/dz$. The factor g is the acceleration due to gravity.

6. DISCUSSION

6.1 North Aleutian Shelf

The distributions of methane observed along the North Aleutian Shelf were modeled to estimate the mean trajectory of the water mass, its mean velocity, and mixing characteristics. The model is simplistic and does not include such variables as velocity shear, complex bathymetry, and short term variability in the source of methane or the currents. All of these variables as well as complex frontal interactions will result in significant deviations between the observed data and the model predictions. However, the model does reproduce general features and is useful in corroborating the mean velocity and diffusion fields.

The model is two dimensional and stationary (see section 6.1). This does not imply that the distribution of methane is temporarily invariant-- only that the model is not responsive to time intervals less than about a month. This estimate was made on the assumption that the mean velocity is about 3 cm/s and that the tracer scale is ≥ 75 km.

The only adjustable parameters in the model are the mean velocity, u , and the air-sea exchange rate parameter, k . The constant k also includes the biological oxidation rate (Griffiths, et al., 1982), which was a factor of about 3 less than the air-sea exchange rate. Also included explicitly in k is the depth of water. Because the depth changes systematically from zero at the shore to about 50m at the inner front, we selected a mean depth of 20m. By doing this, the significance of the air sea exchange term is minimized in shallow water ($z < 20\text{m}$) and maximized in deeper water ($z > 20\text{m}$). Similarly, we assume no horizontal shear ($\partial u / \partial y = 0$), divergence or convergence within the coastal zone. Transport across the inner front is by diffusive mixing only.

The principal source of methane is Port Moller and all other sources including bottom sediments are considered insignificant. The modeling of such a distribution is relatively simple as the model need only include source flux at the entrance to the estuary. Dissolved methane is fluxed into the coastal zone by tidal pumping, hence the large diel excursions observed in the concentrations. The source term was tidally averaged to provide a stationary source flux, but was spatially digitized to more accurately describe the offshore dilution of the source. As methane-enriched water is transported out to the inner front, it mixes with water of lower methane concentration. The diluted water from Port Moller is then transported northeast along the coast in the coastal drift. To account for the variable source in the y-direction (see Fig. 18), the time and depth averaged source function was subdivided into 8 individual line sources, each 4 km in length. The total dispersion field was obtained by summing the individual contributions, including that reflected from the coastline. To avoid other model complexities, the ambient background concentrations of methane were subtracted from both the source and the coastal waters to give the distribution of excess methane, or that portion contributed by the Port Moller estuary.

As an example, we show the average distribution of methane at the entrance to Port Moller in August 1980 (Fig. 21). This distribution was based on all measurements taken, including the 24-hour measurements taken at Stations PM3, PM2, and PM1. The mean and the range are shown by closed triangles and dashed lines, based on 'n' measurements. This source was subdivided into 4 km source increments, after removing the background concentration of 0.45 $\mu\text{L/L}$. PM13, sampled only twice, was approximately 5 km offshore. For modeling purposes, we assumed the concentration was constant between PM13 and the shore. By making this assumption, no serious error is envisioned because the depth of water was less than 5 m.

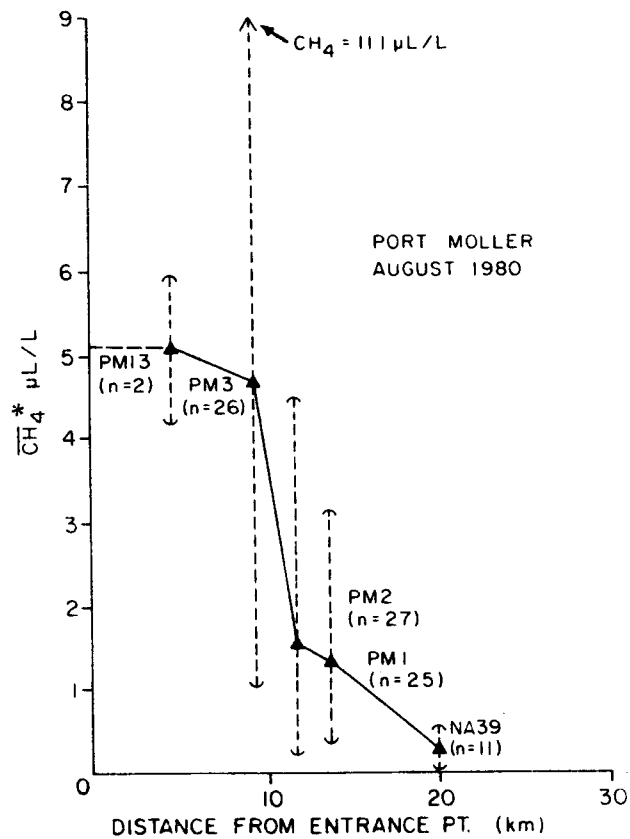


Figure 21. The average distribution of dissolved methane across the entrance to Port Moller. Observations were conducted in August 1980. The mean and range of values (n observations) are shown by the closed triangles and dashed arrows. The concentration of methane shoreward of Station PM13 was assumed constant. A background of 0.45 µL/L was subtracted to give the concentration of excess methane from Port Moller.

One of the major deficiencies of the model is its inability to predict the effects of variable bottom bathymetry. To partially offset this problem, the model concentrations were depth averaged to sill depth (i.e. 20m). After summing all the plumes, the resultant concentration field was then depth averaged to the actual bottom depth. The reason for this was to see if the model simulation would improve the observed relationship between bathymetry and methane distribution. In reality, however, a mixing does not occur in this way. Mixing is essentially complete near the entrance of Port Moller and the distribution of methane is determined by spatial variations

in the mean velocity and by cross-frontal exchange processes. In the absence of any cross-frontal transport, varying the depth of water must result in a systematic change in the local velocity field.

6.1.1. August 1980

The depth-averaged, normalized distribution of excess methane is shown in Figure (22a). The background concentration of methane was 450 nL/L, which was removed from the concentration field. A residual mean concentration of 30 nL/L represents normal spatial variability. Near the source, the concentration of excess methane was approximately 5 μ L/L (5000 nL/L), decreasing to about 0.1 μ L/L at 180 km. The plume trajectory indicates a mean flow to the northeast, paralleling the shoreline.

The distributions of methane and salinity near Port Moller appear influenced by bottom bathymetry (Fig. 22a,b), and in particular the location of the inner front (see 45 m isobath on Figs. 22a,b). Because both constituents are related to freshwater discharge from Port Moller, the observed correlation between water depth and distributions may reflect two processes. The first is that offshore dilution of the freshwater (i.e. vertical mixing) results in the apparent distribution. This must be accompanied by a compression of the streamlines to preserve the apparent offshore intrusion of high salinity water (see $x = 60$ km). Density is closely related to salinity in these waters, which is why the isopycnal surface shows strong correlation with salinity and provides additional evidence that the coastal flow is controlled by bathymetry. The remaining explanation is that the inner front forms a hydrographic barrier to the onshore transport of salt. This might be envisioned as a surface convergence along the front accompanied by a near bottom divergence. Within the front, the onshore transport of salt would be inhibited by a diffusive barrier. However, there appears to be little

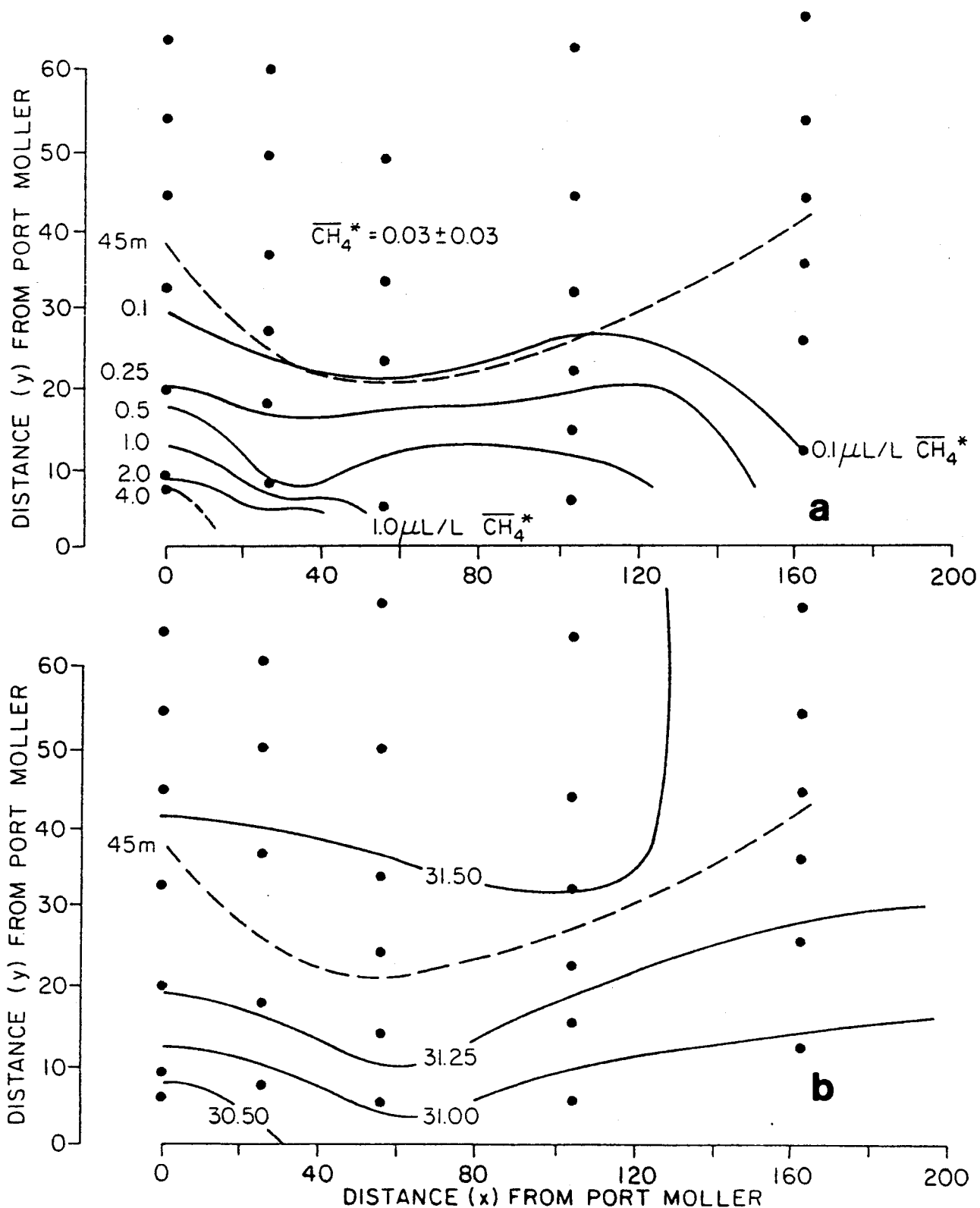


Figure 22. The depth-averaged distribution of (a) dissolved methane and (b) salinity and Port Moller in August 1980. A background concentration of 0.45 $\mu\text{L/L}$ was subtracted from the observed field, leaving a residual concentration of 0.03 $\mu\text{L/L}$ north of the inner front. The inner front is located near the dashed line (approximately 45 m).

evidence that the front is little more than a demarcation between the strong mixing of the coast zone and the seasonally stratified offshore waters (Jim Schumacher, personal communication). At this point, and because our analyses do not disprove it, we provisionally favor the latter explanation.

The constant k is the sum of the air-sea exchange rate and the biological oxidation term. The air-sea exchange term was computed from the mean wind velocity and the sea surface temperature. For a mean wind speed of 6 m/s and a sea surface temperature of 11°C, the computed air-sea exchange coefficient was 4.0×10^{-7} /s (Table 1). Adding to that the biological oxidation rate of 1×10^{-7} /s (Griffiths et al., 1982), the value of k is 5.0×10^{-7} /s. An uncertainty in the mean wind results in an uncertainty in k of about 50%. Using a mean k of 5.0×10^{-7} /s and an uncertainty of 50% ($\pm 2.5 \times 10^{-7}$ /s), mean velocities were arbitrarily chosen until the best visual fit was obtained.

Table 1. A summary of parameters used to estimate the air-sea exchange rate (R) of methane along the NAS coastal zone. The model is

$$R = - \frac{D}{h \cdot \Delta z} (C) = -k_{a/s} (C)$$

Date month/yr	Wind Speed m/s	Temp. °C	D cm ² /s	Δz m	h μ m	$k_{a/s}$ s ⁻¹
Aug. 1980	6	10.7	1.12×10^{-5}	40	70	4.0×10^{-7}
Feb. 1981	9.5	0.0	0.68×10^{-5}	40	20	8.5×10^{-7}
May 1981	7.5	6.5	0.96×10^{-5}	40	50	4.8×10^{-7}

The best fit was obtained for $u = 3.8$ cm/s and a $k = 5.0 \times 10^{-7}$ /s (Fig. 23). The model fit overestimates the transport in the near field ($x \leq 120$ km), but is in good agreement beyond that point. Increasing k or decreasing u would improve the fit in the near field, but only at the expense of the far field. The fit is quite sensitive to the magnitude of u and to a less extent k . Increasing k to a maximum acceptable level of 7.5×10^{-7} /s did not change the coastline intercepts appreciably, but did reduce the offshore penetration of dissolved methane.

Allowing k to vary between the limits 2.5×10^{-7} /s and 7.5×10^{-7} /s, u was arbitrarily chosen to provide the best fit. These results are shown in Figures (24a,b). Because the model contains the ratio, k/u , in the die-off term (see eq. 2), it is not surprising that minor adjustments in k require similar adjustments in u to maintain goodness of fit. For example, if $u = 2.5$ cm/s and $k = 2.5 \times 10^{-7}$ /s, the plume geometry is largely determined by lateral diffusion (Fig. 24a). If the velocity were decreased even further to improve the coastline fit, offshore diffusive transport would increase markedly, resulting in a poorer fit. However, mean velocities less than 2.5 cm/s were not used because the model formulation does not include diffusive transport in the x -direction, which would be required as $u \rightarrow 0$. Increasing k to 7.5×10^{-7} /s requires that u be at least 5 cm/s to maintain goodness of fit (Fig. 24b).

To demonstrate the effect of increasing the mean velocity, the mean flow was increased to 7.5 cm/s while keeping $k = 5.0 \times 10^{-7}$ /s. These results are shown in Figure (25). Note the flat distribution, indicating the dominance of advection. Clearly, this distribution is not similar to the observations shown in Figure (22a), where the 2.0 $\mu\text{L/L}$ and 1.0 $\mu\text{L/L}$ isopleths intersect the coastline axes between 40-60 km.

NORTH ALEUTIAN SHELF

AUGUST 1980

$U = 3.8 \text{ cm/s}$

$k = 5.0 \times 10^{-7} / \text{s}$

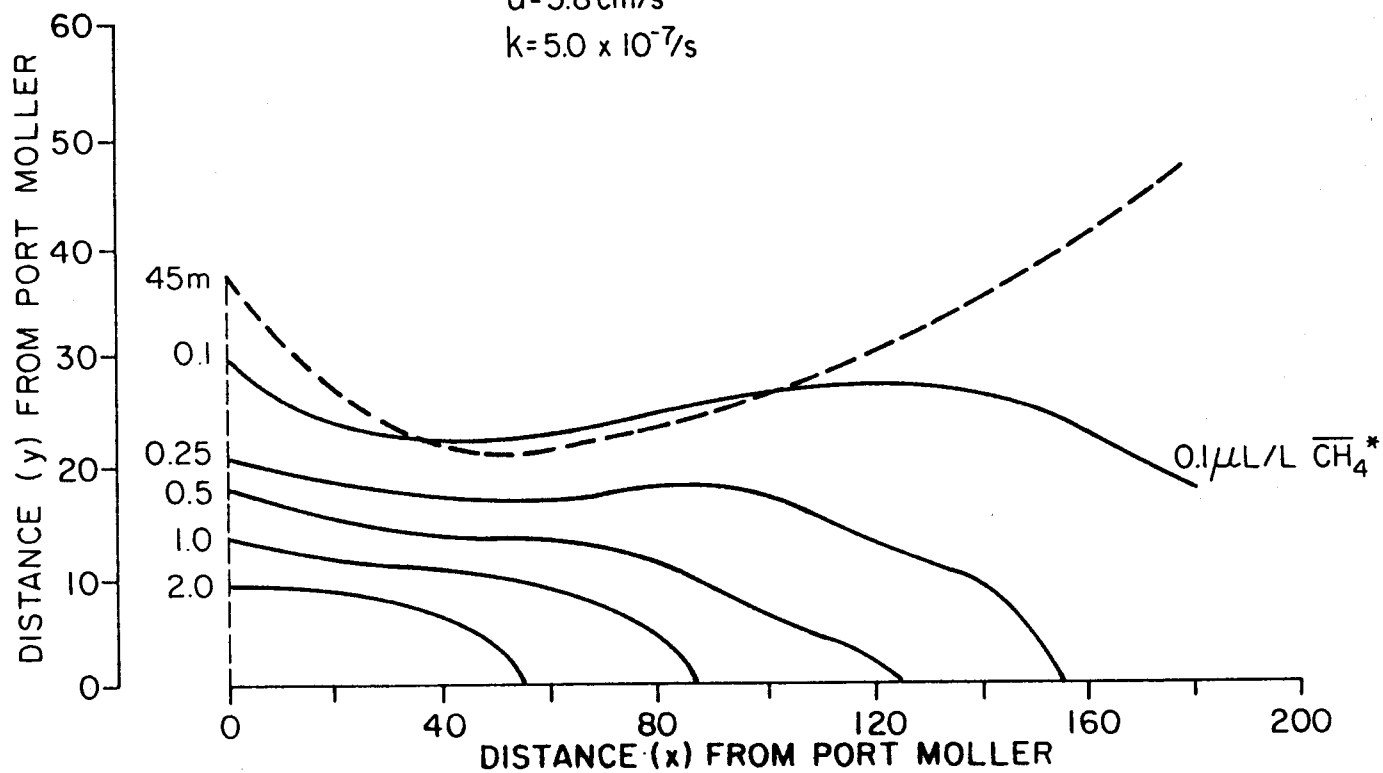


Figure 23. Model simulation of the distribution of methane for $u = 3.8 \text{ cm/s}$ and $k = 5.0 \times 10^{-7} / \text{s}$. This is the best fit to the observations shown in Fig. 22a. Concentrations are in $\mu\text{L/L}$. The position of the 45 m isobath is indicated by the dashed line.

NORTH ALEUTIAN SHELF
AUGUST 1980

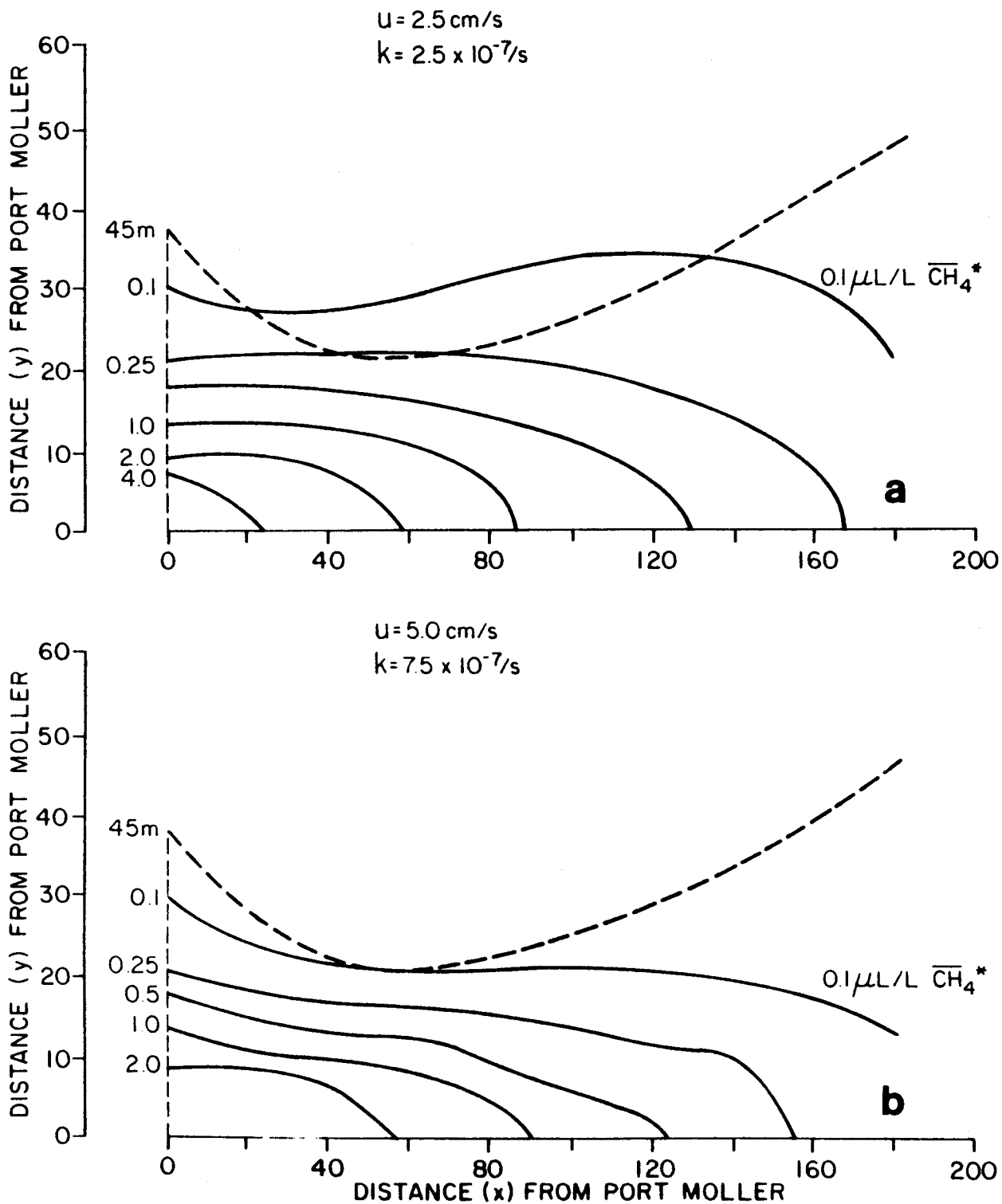


Figure 24. Model simulation of the distribution of methane for (a) $u = 2.5 \text{ cm/s}$, $k = 2.5 \times 10^{-7}/\text{s}$ and (b) $u = 5.0 \text{ cm/s}$ and $k = 7.5 \times 10^{-7}/\text{s}$ in August 1980. Concentrations are expressed in $\mu\text{L/L}$. The position of the 45 m isobath is indicated by the dashed line.

NORTH ALEUTIAN SHELF
AUGUST 1980

$U = 7.5 \text{ cm/s}$
 $k = 5.0 \times 10^{-7} / \text{s}$

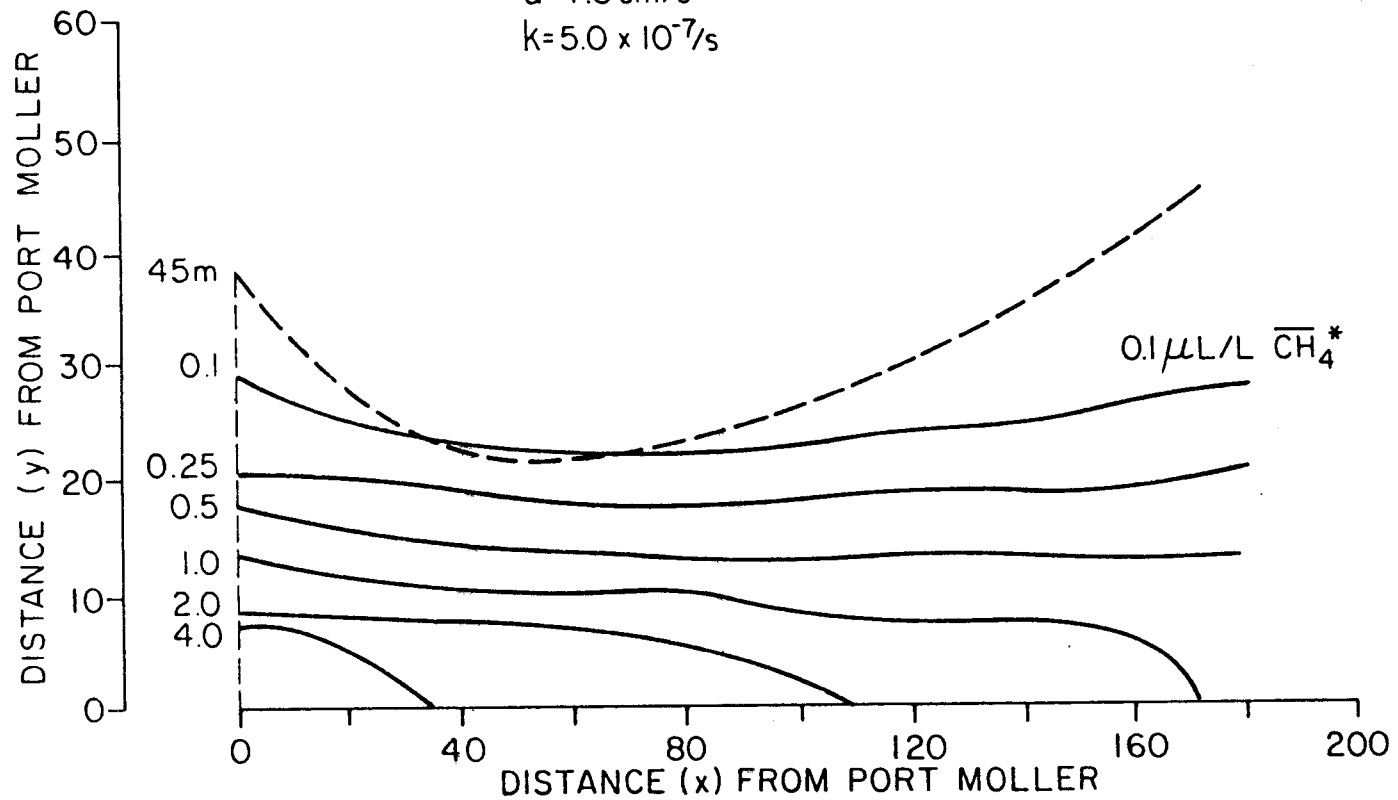


Figure 25. Model simulation of the distribution of methane for $u = 7.5 \text{ cm/s}$ and $k = 5.0 \times 10^{-7} / \text{s}$ in August 1980. Concentrations are in $\mu\text{L/L}$. The position of the 45 m isobath is indicated by the dashed line.

The diffusive scale (K_y) is functionally dependent on the Lagrangian scale, about 200 km in the present case. From the monograms presented by Okubo (1971), K_y varies from $2 \times 10^{-5} \text{ cm}^2/\text{s}$ to about $2 \times 10^6 \text{ cm}^2/\text{s}$, assuming a minimum and maximum scale of 20 km and 200 km respectively. The corresponding K_x would be about a factor of three greater than these estimates. Because our simplistic model does not take into account temporal variations in circulation, horizontal shear, or the effects of a complex bottom bathymetry, there is no reason to adopt other mixing parameters unless a more rigorous diagnostic model were to be developed.

In summary, our best estimate of the mean velocity in August 1980 was 3-5 cm/s, in good agreement with the estimate of 1-6 cm/s given by J. Schumacher (personal communication). Our estimate is, however, higher than the value of 1-2 cm/s given previously by Kinder and Schumacher (1980).

6.1.2. February 1981

The flux of methane from Port Moller in winter was significantly less than observed the previous August. Concentrations at the entrance were a factor of 5 less, which was presumably due to a seasonal drop in temperature (11° to 1°C) and the concomitant decrease in microbial activity. Although the concentration of methane was significantly reduced, so were the background concentrations, permitting the plume to be distinguishable for at least 200 km as before (Fig. 15b).

The distribution of methane observed in February 1981, after depth averaging and removing a background concentration of 110 nL/L, is shown in Figure (26a). Note that the plume is clearly developed for approximately 60 km and less so for distances beyond that point. As we noted earlier, bathymetric influences on the distribution of methane were clearly evident as it was with salinity (Fig. 26b).

NORTH ALEUTIAN SHELF
FEBRUARY 1981

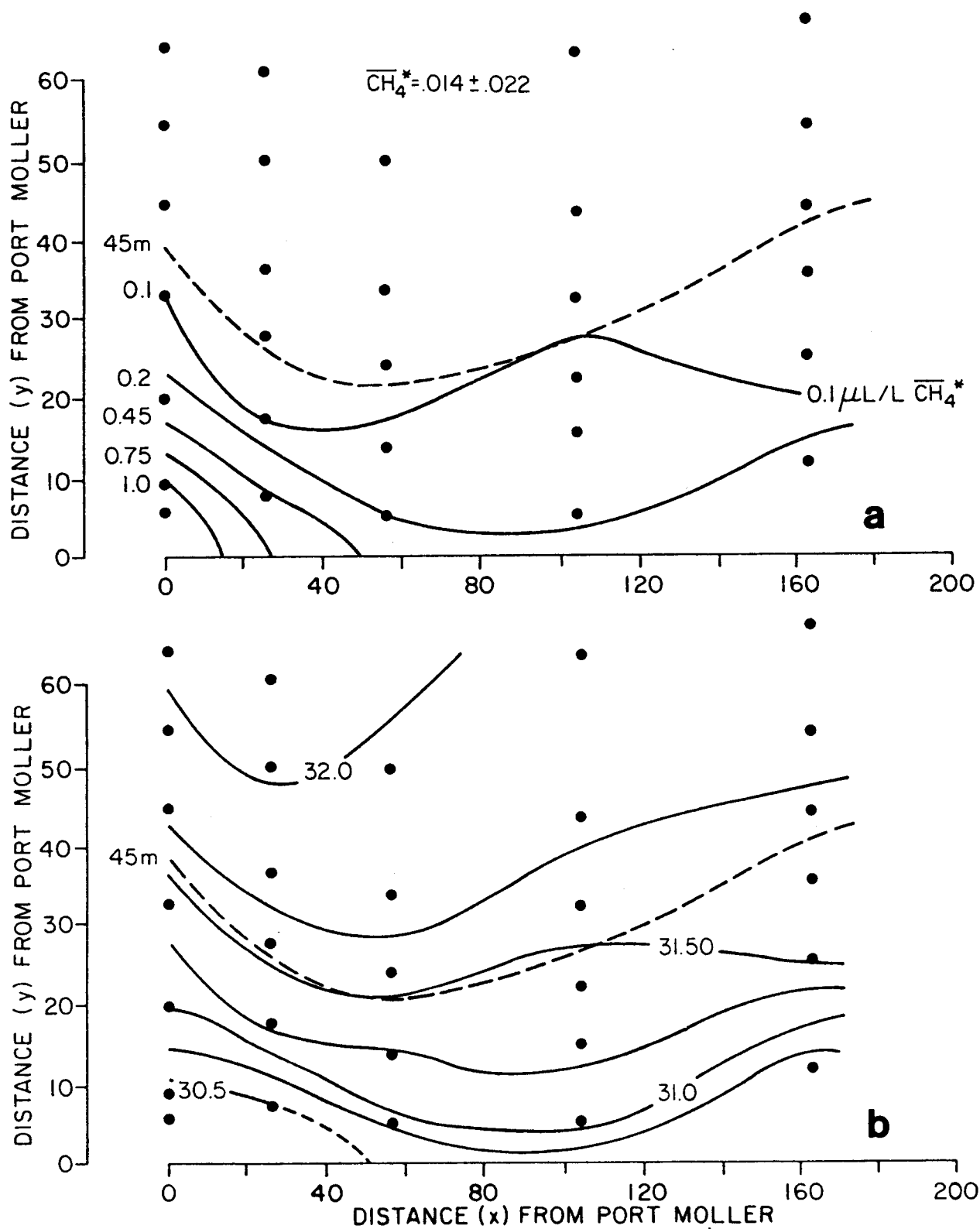


Figure 26. The depth-averaged distribution of (a) dissolved methane and (b) salinity in February 1981. A background concentration of 0.11 $\mu\text{L/L}$ has been subtracted from the concentration field, leaving a mean residual of 0.014 $\mu\text{L/L}$. The inner front is located near the 45 m isobath and is indicated by the dashed line.

The methane source distribution is shown in Figure (18b). Only PM3, located about 5 km from shore, was occupied for 24 hrs; all others were sampled twice. Because of paucity of data, average values for these stations are poorly known. For example, NA40(PM2) appeared to have the highest mean, but that may be due to the sampling frequency and the stage of the tide during which sampling occurred. The source function reflected in Figure (18b) was adjusted downward by 210 nL/L before being digitized into line sources, each 4 km in length.

The air-sea exchange rate constant in February was estimated to be 8.5×10^{-7} , based on a mean wind of 9.5 m/s and a mean sea surface temperature of 0°C (Table 1). The larger value of k is due to higher wind velocity and a concomitant decrease in the stagnant film boundary layer thickness. As described above, k was allowed to vary by 50% or $\pm 4.2 \times 10^{-7}$ /s. Biological oxidation was not a significant factor during winter (Griffiths et al., 1982).

The best simulations of the observations are shown in Figures (27a,b). The predicted velocity range was 3-7 cm/s, given the uncertainties in k and other characteristics of shelf circulation. The wider range of predicted velocities for February was due to a diminished source and poor model resolution. The velocity estimate for February is not statistically different than that observed in August and falls within the estimate of 1-6 cm/s.

The estimates of lateral eddy diffusivities (K_y) are the same as observed in August because the Lagrangian scale is similar.

6.1.3 May 1981

The depth-averaged distribution of methane is shown in Figure (28). The pattern is similar to previous observations, but the concentrations are generally lower. Maximum concentrations at the entrance were about 2 $\mu\text{L/L}$, decreasing to 0.1 $\mu\text{L/L}$ at about 100 km.

NORTH ALEUTIAN SHELF
FEBRUARY 1981

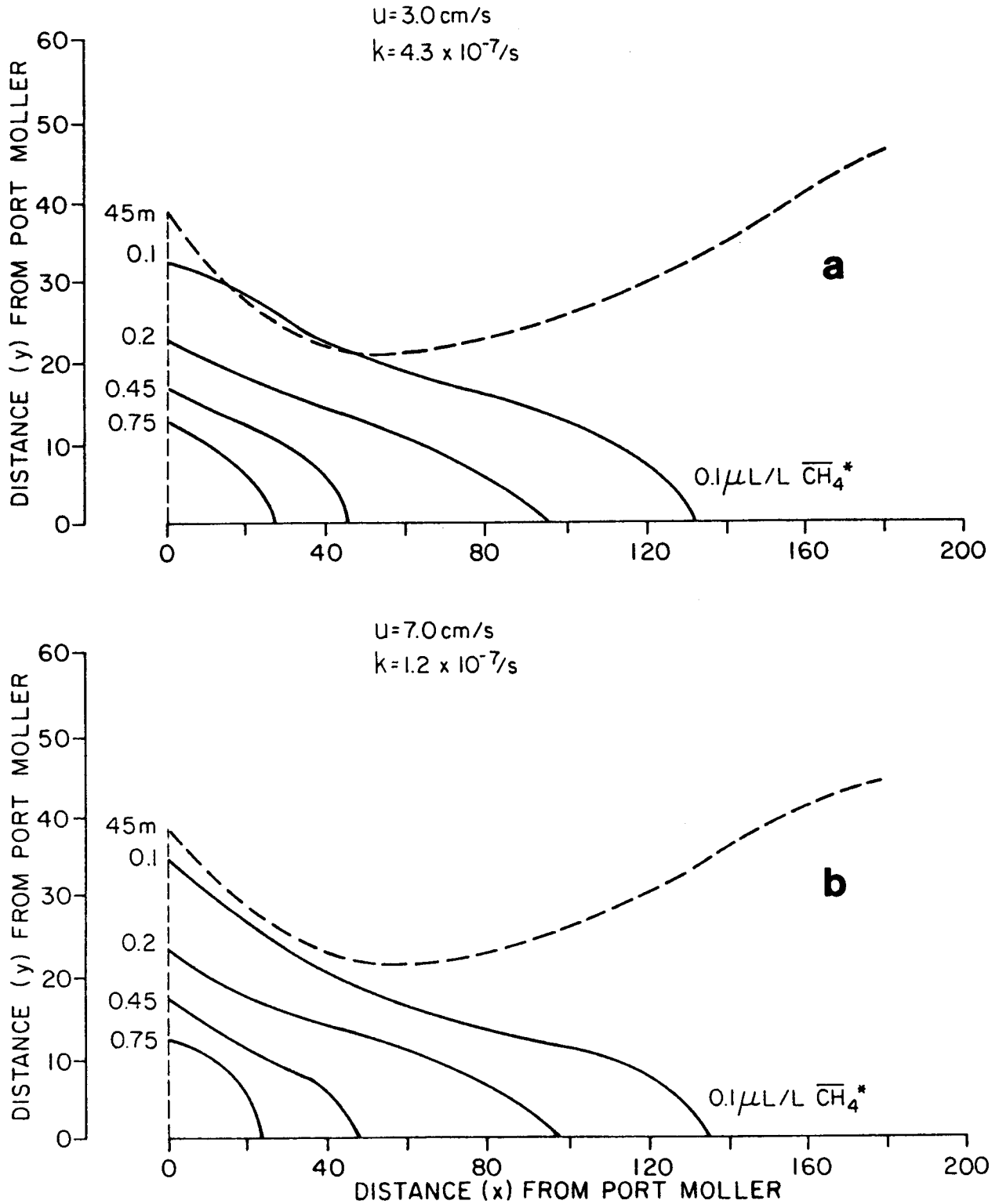


Figure 27. Model simulations of the distributions of methane for (a) $u = 3.0 \text{ cm/s}$ and $k = 4.3 \times 10^{-7} / \text{s}$ and (b) $u = 7.0 \text{ cm/s}$ and $k = 1.2 \times 10^{-7} / \text{s}$ in February 1981. Both distributions are reasonably good fits to the observed distributions. Concentrations are in $\mu\text{L/L}$. The position of the inner front is indicated by the dashed line.

NORTH ALEUTIAN SHELF
MAY, 1981

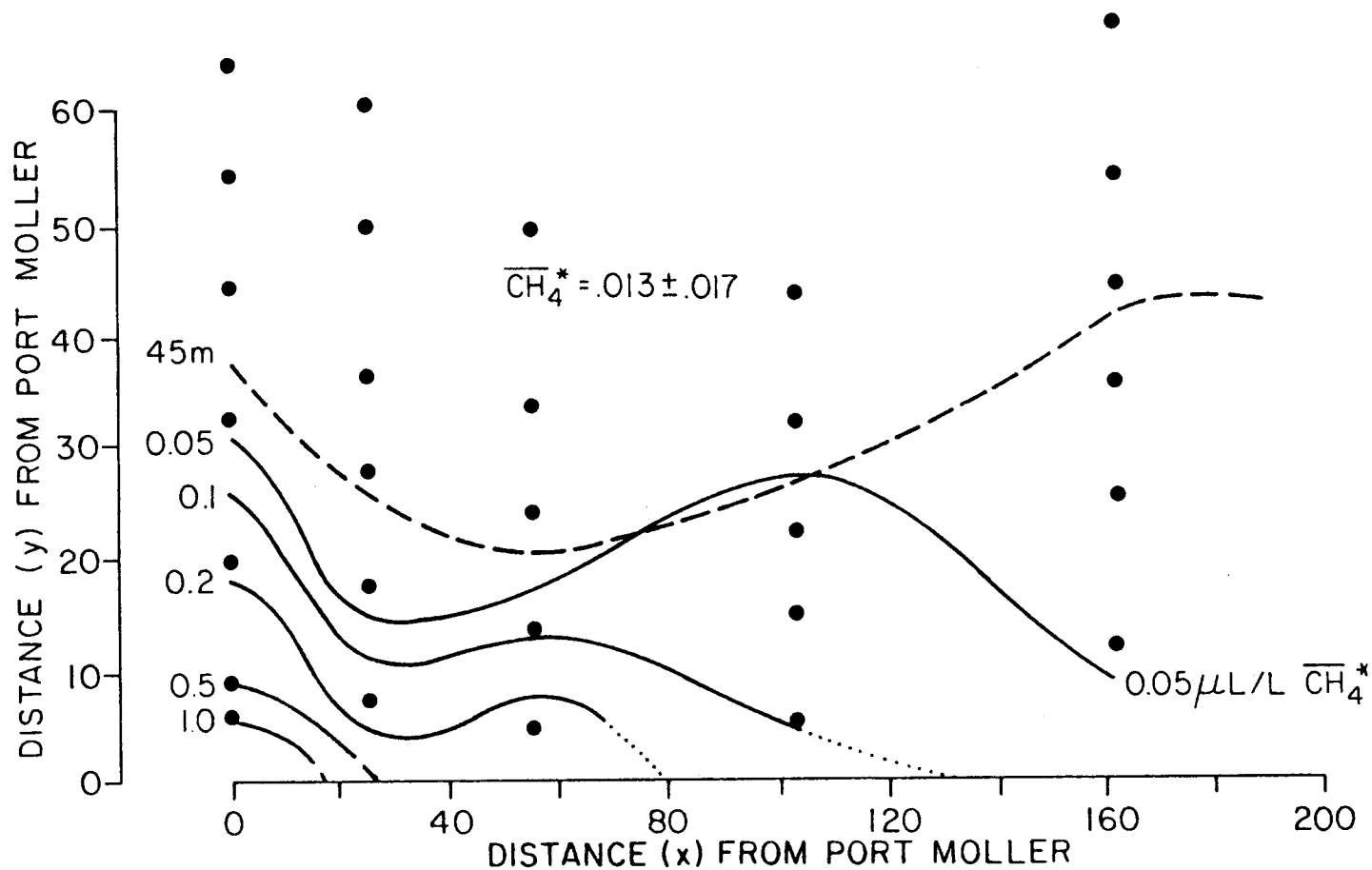


Figure 28. The depth-averaged distribution of dissolved methane in May 1981. A background concentration of 0.1 $\mu\text{L/L}$ has been subtracted from the concentration field, leaving a mean residual of 0.013 $\mu\text{L/L}$. The inner front is located near the 45 m isobath and is indicated by the dashed line.

In May, the surface concentration of methane seaward of the front was 80-100 nL/L, indicating minimum production in the offshore waters. Equilibrium concentrations for this time of year were 60 nL/L; consequently, percent saturation levels ranged from 130 to 160%. In contrast, the saturation levels in August were 900%. The interannual variations in the surface concentrations are strongly a function of water temperature and degree of ice formation the previous winter (Cline et al., 1981).

The time average distribution of methane at the entrance to Port Moller is shown in Figure (18c). Maximum concentrations of 2 μ L/L were observed at PM-F, decreasing markedly to background concentrations of 100 nL/L at station NA38. As noted earlier, the source is hyperbolic and decays rapidly to background levels at about 30 km. This source was subdivided equally into 8 individual line sources, as before.

The air-sea exchange constant, k , was found to be 4.8×10^{-7} /s, based on mean wind of 7.5 m/s and a mean sea surface temperature of 6.5°C (Table 1). The calculated thickness of the diffusion layer was 50 μ m. Biological oxidation, proportional to water temperature and the concentration of methane, was at a minimum ($<1 \times 10^{-8}$ /s) and was not included in the above rate constant (Griffiths et al., 1982).

The best model fits to the methane distribution are shown in Figures (29a,b). Assuming a mean k of 4.8×10^{-7} /s and a variance of $\pm 2.4 \times 10^{-7}$ /s, a range of velocities was fit to the observations. The best simulations were obtained for $u = 2-3$ cm/s. Larger velocities gave elongated plumes that were not in good agreement with the observations. We conclude that in May, the mean velocity along the coast was in the range of 2-3 cm/s and did not exceed 5 cm/s. Horizontal diffusivities are in the range of 1×10^5 cm² /s to 5×10^6 cm² /s for the plume dimensions described here.

NORTH ALEUTIAN SHELF
MAY 1981

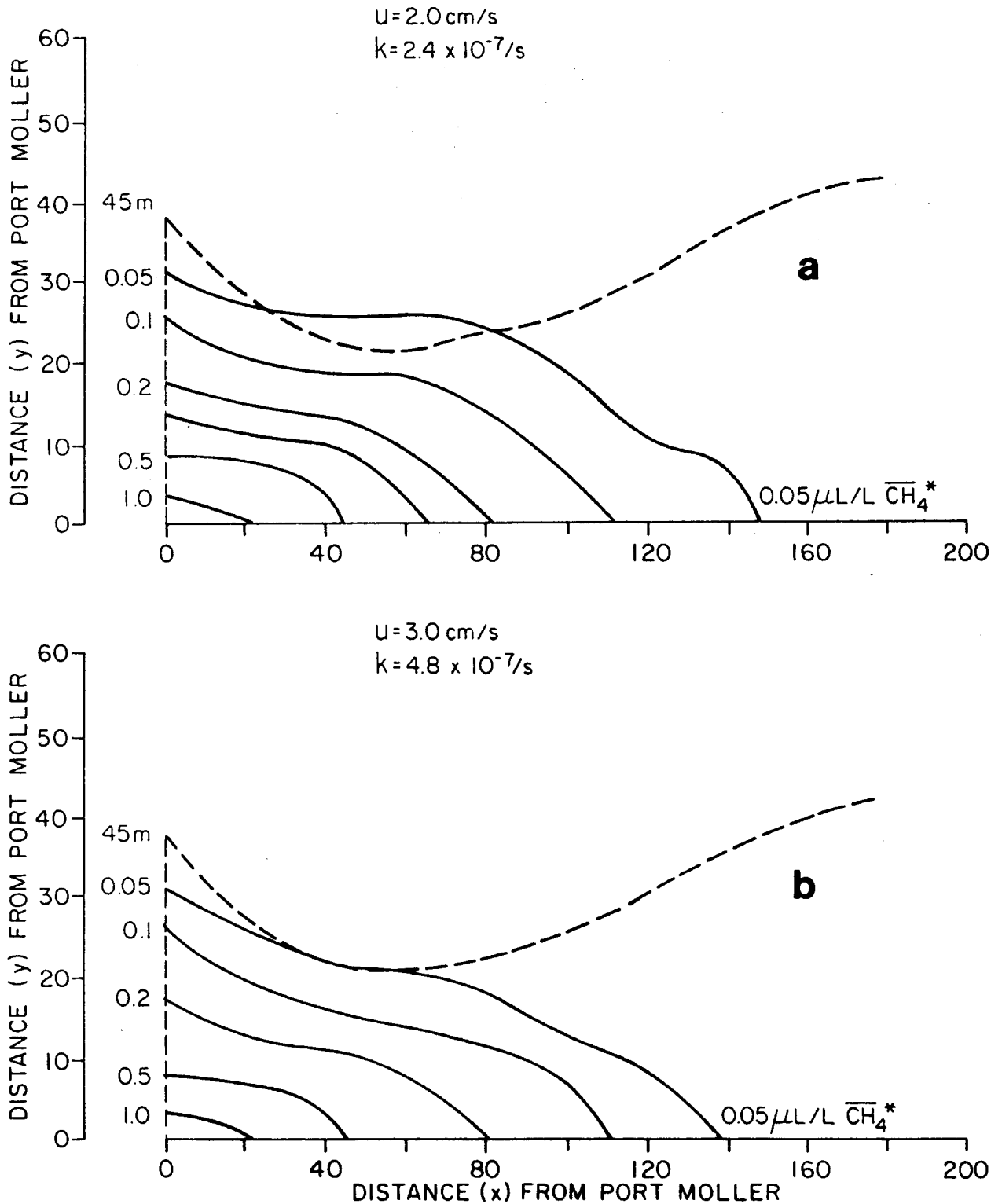


Figure 29. Model simulations of the distribution of dissolved methane for (a) $u = 2.0$ cm/s and $k = 2.4 \times 10^{-7}$ /s and (b) $u = 3.0$ cm/s and $k = 4.8 \times 10^{-7}$ /s in May 1981. Both distributions are reasonably good fits to the observed distribution. Concentrations are in $\mu\text{L/L}$. The position of the inner front is near the 45 m isobath and is indicated by the dashed line.

6.1.4. Port Moller Tidal Flux

In describing the horizontal distribution of methane along the NAS, we established concentrations along the shelf boundary perpendicular to the coast. Because the concentrations of methane are temporally variable near the entrance to Port Moller, we occupied a series of stations repetitively to estimate the average diel flux at the boundary. The boundary was placed near the entrance to Port Moller but was of sufficient distance to avoid the large tidal currents at the entrance. A check on our model can be made by comparing the estimated transport of methane through the entrance on each ebb tide with the time average distribution determined by the model. The implicit assumptions are that air-sea exchange and biological consumption are insignificant over the distance between the entrance and the model boundary (approximately 15 km).

The minimum distance across the entrance to Port Moller is between Entrance Point on the east and Fawn Point in the west. The main channel is approximately 5 km wide, 16 m deep and located toward the eastern shore. A large sand bar extends eastward from Fawn Point and is exposed during low water. At low water the effective channel width is about 9 km. Tidal currents are strong at the entrance, reaching average maximum velocities of 1.7 kts 3 miles west of Entrance Point and 1.2 kts at Entrance Point (Department of Commerce, 1979). For the purpose of calculations, we will assume an average maximum tidal current of 1.5 kts, or 0.8 m/s.

The principal assumption is that during any given tidal cycle, there is little or no recycling of water within the entrance of Port Moller. If this condition is met, then the tidal driven transport of methane to the coastal zone is proportional to the average concentration at the entrance, the width and depth, and the ebb velocity.

$$T_t = \sum C_i \ell \Delta z_i \bar{v} \quad (6)$$

For the sake of simplicity, we assume that C_i , the average excess methane concentration decreases linearly across the entrance from a maximum measured value on the east side to zero on the west. This is a crude approximation to the observations shown in Figure (18). The increment of length, ℓ , is set to 2 km, while the depth, Δz_i , is varied according to the bottom bathymetry. The mean velocity, \bar{v} , across the entrance was calculated from the average maximum velocity according to the formula $\bar{v} = v_{\max}/\pi/2$ (Sverdrup et al., 1942). The results of the tidal transport calculations for each of the three visits are shown in Table 2.

If the model assumptions are reasonably correct, then the tidal flux must equal the flux of methane across the model boundary. To calculate the latter, we used equation (6) and estimates of C_0 from Figure (18). The mean depth was set equal to 20 m and the velocity was estimated from the model fits. The length of the model boundary varied seasonally from 24 to 36 km, which was subdivided into 4 km increments for the purpose of calculation. The results of these calculations also are shown in Table 2.

Table 2. A comparison of the tidal transport of methane (T_t) from Port Moller with the transport of methane at the tidal boundary (T_m). The mean tidal velocity is \bar{v} and the mean coastal current is \bar{u} .

Date	\bar{v} m/s	\bar{u}	T_t ML CH ₄ (STP)/s	T_m
August 1980	0.5	0.038	5.7×10^4	4.9×10^4
February 1981	0.5	0.050	3.4×10^4	4.2×10^4
May 1981	0.5	0.025	2.3×10^4	0.8×10^4

In August the two transport figures are in good agreement; they only differ by 16%. The comparison in February is also reasonably good, although the coastal transport, T_m , exceeds the source strength by 23%. Uncertainty in the mean coastal velocity could easily account for this difference. The comparison in May is poor. There, the source strength exceeded the coastal transport by a factor of nearly three. The reason for the discrepancy may lie in our choice of the concentration distribution across the entrance. Apparently the concentration gradient across the entrance was more nearly hyperbolic (see Fig. 18) than linear as assumed above.

The near agreement between the two transport terms suggests that the model assumptions are nearly correct, conditions during May notwithstanding. This implies that the Port Moller estuary is the dominant source of methane to the coastal zone and that the model fits to the distributions and therefore gives reasonable estimates of the mean velocity field and the eddy diffusivities. Clearly more sophisticated models could be applied to the transport of methane from Port Moller, but non-linear perturbations to the mean velocity field coupled to an incomplete observational record precludes a detailed effort at this time.

6.1.5. North Aleutian Shelf Summary

A summary of the estimated velocities determined from the distributions of methane is presented in Table 3. While the model is crude and numerous approximations were made, the mean velocities range from 2-7 cm/s, depending on season. These estimates are in excellent agreement with current meter observations (J. Schumacher, personal communications). The small variances in the mean velocity field suggest that the flow is baroclinic and responds to the freshwater input. The small seasonal variation in the salinity field also indicates that seasonal variations in the baroclinic field should be small.

Table 3. A summary of the mean velocities along the coastal zone of the North Aleutian Shelf as determined from the distributions of dissolved methane. The air-sea exchange and biological rate constant (combined) was varied by $\pm 50\%$.

Month/year	k s^{-1}	l km	u cm/s
Aug. 1980	$4.0 \pm 2.0 \times 10^{-7}$	>200	3.8 ± 1.3
Feb. 1981	$8.5 \pm 4.2 \times 10^{-7}$	>200	5.0 ± 2.0
May 1981	$4.8 \pm 2.4 \times 10^{-7}$	200	2.5 ± 0.5

Model simulations of the methane distributions explicitly contain a cross-stream horizontal eddy diffusivity (K_y). This parameter was scaled to the mean velocity through equations (3a-3g), which allow the turbulent scale to grow as the plume increases in size. In the model simulations, the value of K_y ranged from $10^4 \text{ cm}^2/\text{s}$ at $x=0$ (4 km wide) to $10^6 \text{ cm}^2/\text{s}$ at $x=200$ km. Given the transient behavior in the current field and the complex bottom bathymetry, the model simulations do not permit a close examination of the magnitude of the turbulent field as a function of the Lagrangian scale. However, suffice it to say, that the cross-stream diffusion of methane is not inconsistent with the empirical formulations given by Okubo (1971). For a point source release, the variance of the plume grows at a rate

$$\sigma_{rc}^2 = 0.0108t^{2.34}, \quad (3f)$$

which also can be used to predict the behavior of point source releases of soluble or dispersed materials.

The simulations showed markedly the influence of the mean velocity field on the observed distributions. At velocities below 5 cm/s, eddy diffusion on the x- and y-directions should be included to improve the model fits. However, at velocities in excess of 5 cm/s and over limited space scales ($l \leq 200$ km), the diffusive terms are relatively insignificant in determining the observed distributions.

6.2. St. George Basin

Enhanced production of methane occurs whenever elevated concentrations of organic carbon are present. This is the case in St. George Basin where relatively high concentrations of organic carbon are found in the surface sediments. The distribution of carbon (Gardner, et al., 1978) is nearly circular and occupies an area of about 8000 km^2 near the center of St. George Basin (56°N ; 167°W) (Fig. 30). In cross section, the surface distribution of organic carbon is nearly Gaussian in form, which implies that the production rate of methane is also Gaussian in form. We will return to this point later in the discussion concerning the methane source term.

The concentration of methane, which depends on the strength of the local source and the intensity of mixing over the basin, is elevated in the fall when microbial production and water column stability are at maximums. Minimum concentrations were observed in the spring and are related to minimum microbial production. Both water temperature and the lack of a suitable organic substrate precluded a significant release of methane in the spring.

The model adopted for the simulation of the near-bottom distribution of methane in St. George Basin is the same model used along the North Aleutian Shelf (see Sec. 5.1). The description is two-dimensional, steady state, and balances lateral diffusion against horizontal advection and biological

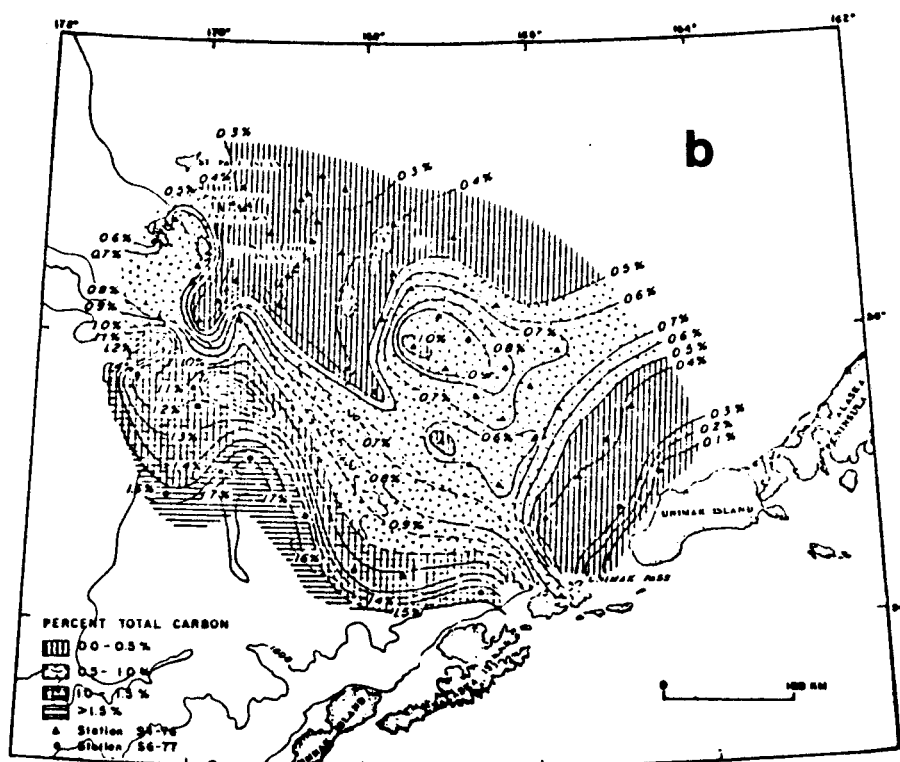
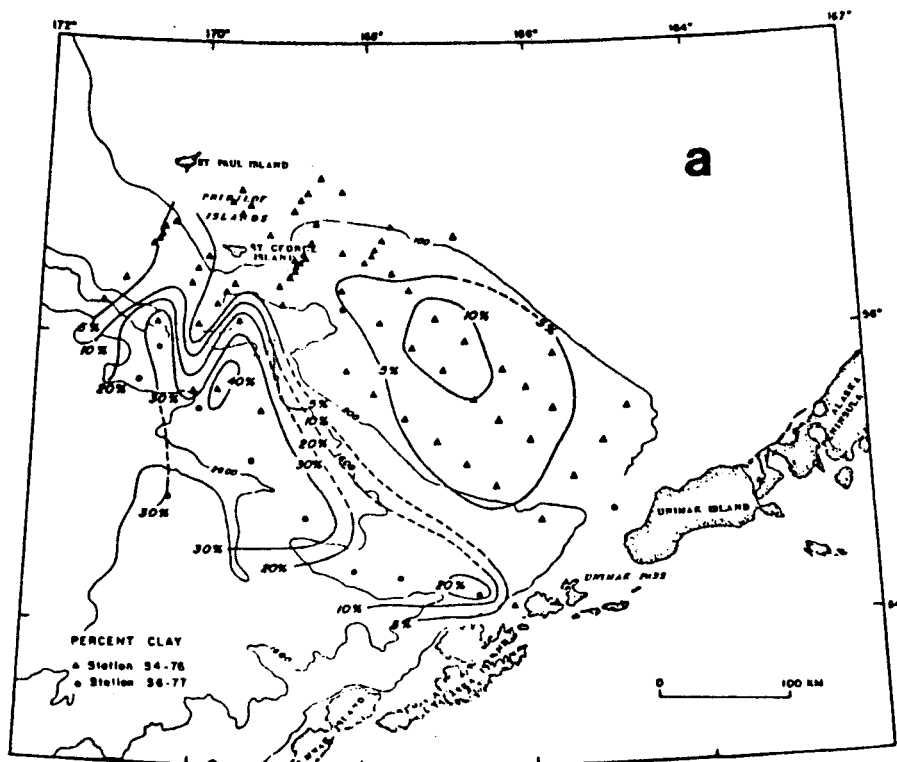


Figure 30. Distributions of (a) clay content and (b) total carbon in the surface sediments of St. George Basin. The locus of the high carbon concentrations is approximately $56^{\circ}\text{N } 167^{\circ}\text{W}$, which is the location of Stations SG5, SG29, SG24, and SG70 (see Fig. 2). This figure was taken from the report by Gardiner et al., 1978.

consumption. The oxidation of methane is considered first order as determined by Griffiths, et al., (1982).

The most serious deficiencies of the model include the source function and the vertical flux of methane across the pycnocline. For modeling purposes, we assume that the source of methane is a plane whose width is the y-dimension of the plume and whose height is the distance from the sea bottom to the base of the benthic boundary layer. This line source is subdivided into individual plane sources, each of which is 4 km in length and approximately 40 m in depth. Because the concentration varies across the source, each planar segment is assigned an initial concentration, C_0 . The source functions used for each of the three simulations are shown in Figure (31). Note that the initial concentration at the source is nearly normal as hypothesized earlier. Each planar section is treated as a separate plume; the total distribution results from the sum of all of the individual plumes.

An examination of the distribution of methane suggests that the source is circular or perhaps elliptical as indicated by the distribution of organic carbon (Fig. 30). By assuming a line source, the source of methane is confined to plane rather than an area. This simplifies the arithmetic at the expense of physical reality. However, the simulation does result in physical bounds on the diffusive and advective transports.

Another serious drawback to the simulation is the lack of a vertical flux term (see eq. 1). We have assumed that this term is small because of the stability above the bottom boundary layer, which inhibits the vertical exchange of materials. Our estimate is that the vertical eddy diffusivity is $\leq 0.5 \text{ cm}^2/\text{s}$, which minimizes the vertical transport of CH_4 . In section 6.3, a scaling argument is presented to show that the vertical processes are indeed small compared to the horizontal transport terms and thus the former can be ignored to the first approximation.

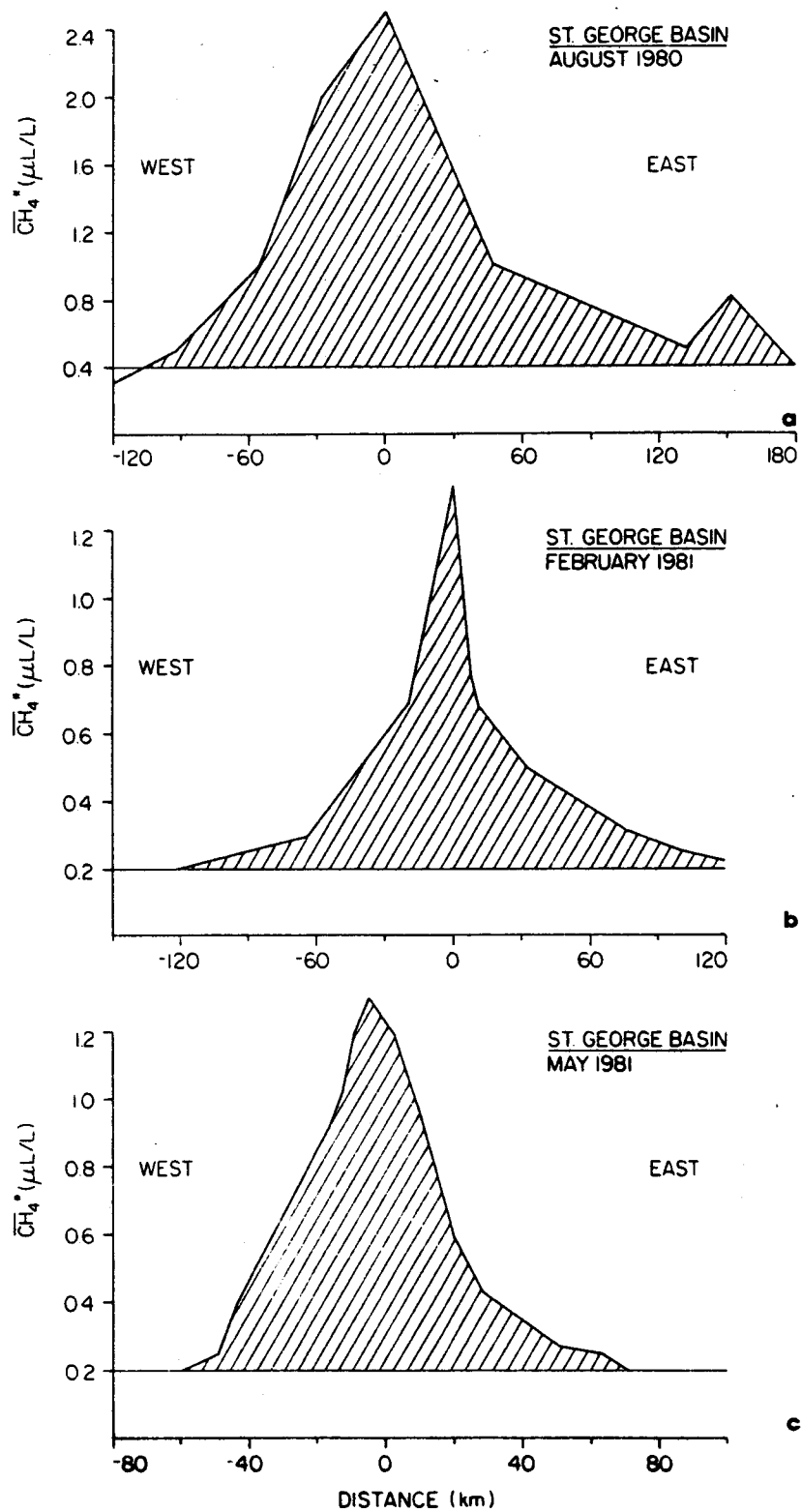


Figure 31. The average excess concentration of methane in the benthic boundary layer across the center of the plume. Data are collected in (a) August 1980, (b) February 1981, and (c) May 1981. Concentrations are expressed $\mu\text{L/L}$.

The areal distributions of methane in the near bottom waters appear as ellipses, elongated in the direction of the axis of the basin (see Figs. 6a,b,c). For modeling purposes, we chose the bottom boundary layer thickness to be 20-30 m, depending on the season, and a planar source of sufficient width to mimic the concentration field at the source. Initial concentrations along the source are interpolated from depth-averaged observations. The mean velocity, u , is the only adjustable parameter, because the biological rate constant that governs the consumption rate of methane was measured. The value of the K_y is scale dependent and is calculated as a function of the Lagrangian distance (see Sec. 5.1).

6.2.1. August 1980

The depth-averaged distribution of methane in August 1980 is shown in Figure (6a) and is redrawn onto rectangular coordinates shown in Figure (32a). The best model fit to the observations is shown in Figure 32b for $u = 2$ cm/s and $k = 8.6 \times 10^{-8}$ /s. Because the source ($x=0$) bisects the plume, the model fit shown in Figure (32b) is only representative of the downstream portion of the plume. A velocity of 3 cm/s also was assumed, but resulted in unrealistically large concentrations along the axis of the plume. Thus, we conclude that the mean velocity in August 1980 was ≤ 2 cm/s. Because of the scale of the plume, K_y ranges from 1×10^6 cm²/s to 2×10^6 cm²/s (Okubo, 1971).

The elongation of the plume in the northwest direction suggests a weak current along the shelf in general agreement with the observations (Kinder and Schumacher, 1981). However, an onshore component is also evident in Figure (32a). This is also in agreement with refinements in the current trajectories that recently have been made (J. Schumacher, personal communication). Current meter deployments made between March and December 1976

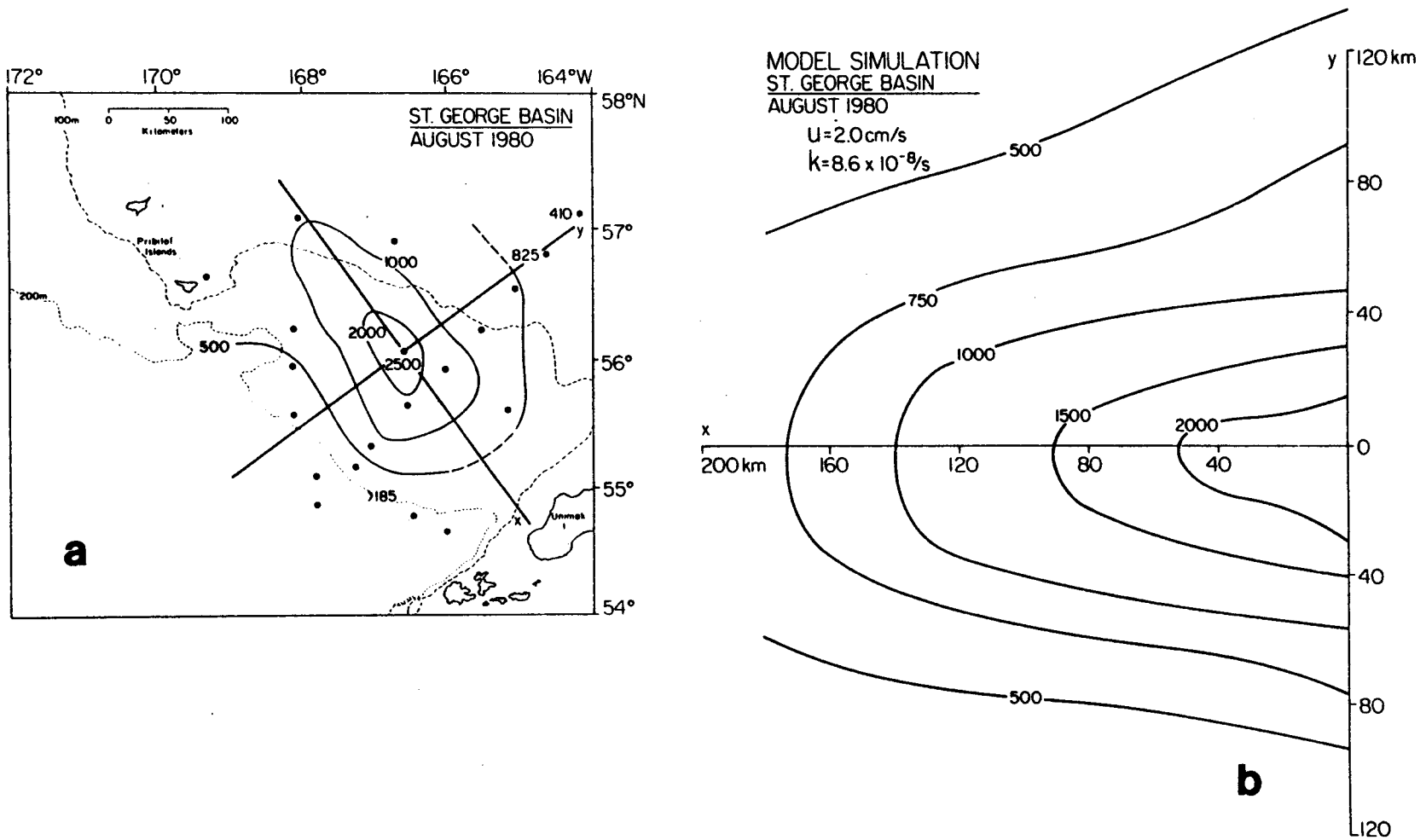


Figure 32. (a) The average near-bottom concentration of dissolved methane in St. George Basin in August 1980. The axes show the position of the model grid. (b) The model simulation of the methane distribution using the source function shown in Fig. (31a). The best fit was obtained for $u = 2.0 \text{ cm/s}$ and $k = 8.6 \times 10^{-8} \text{ /s}$.

indicate vector mean speeds of 2-4 cm/s in the lower 15 to 20 m of the water column (Kinder and Schumacher, 1981). Our model simulation suggests that the mean current speed will fall in the lower range when the effects of diffusion in the x-direction are taken into account.

The presence of significant concentrations upstream of the source demonstrates the broad extent of the source and the importance of alongshelf diffusion. The model used here did not explicitly include alongshelf diffusion; consequently, this effect is accounted for in the velocity term.

6.2.2. February 1981

The depth-averaged distribution of methane during February 1981 is shown in Figure (6b) and has been remapped onto a rectangular grid for model simulation (Fig. 33a).

The average concentration in February 1980 was lower than that measured in August. The plume trajectory is the same as August, and extends about 200 km downstream of the source (e.g. 300 nL/L contour). The width was reduced to about 120 km as compared to 280 km in August.

The best fit to the observed distribution was again obtained with $u = 2$ cm/s and $k = 5.6 \times 10^{-8}$ /s (Figure 33b). The biological rate term was smaller in February, presumably due to the reduced water temperature. As before, the mean velocity, u , was arbitrarily increased to 3 cm/s to test model sensitivity. The fit to the distribution was not improved. Therefore, we conclude that the mean velocity in February was less than 2 cm/s in agreement with the model predictions for August 1980.

6.2.3. May 1981

The depth averaged distribution of methane observed in May 1981 is shown in Figure (6c) and is remapped into the model grid shown in Figure (34a). The maximum concentration of methane (near SG70) was 1200 nL/L and was lower

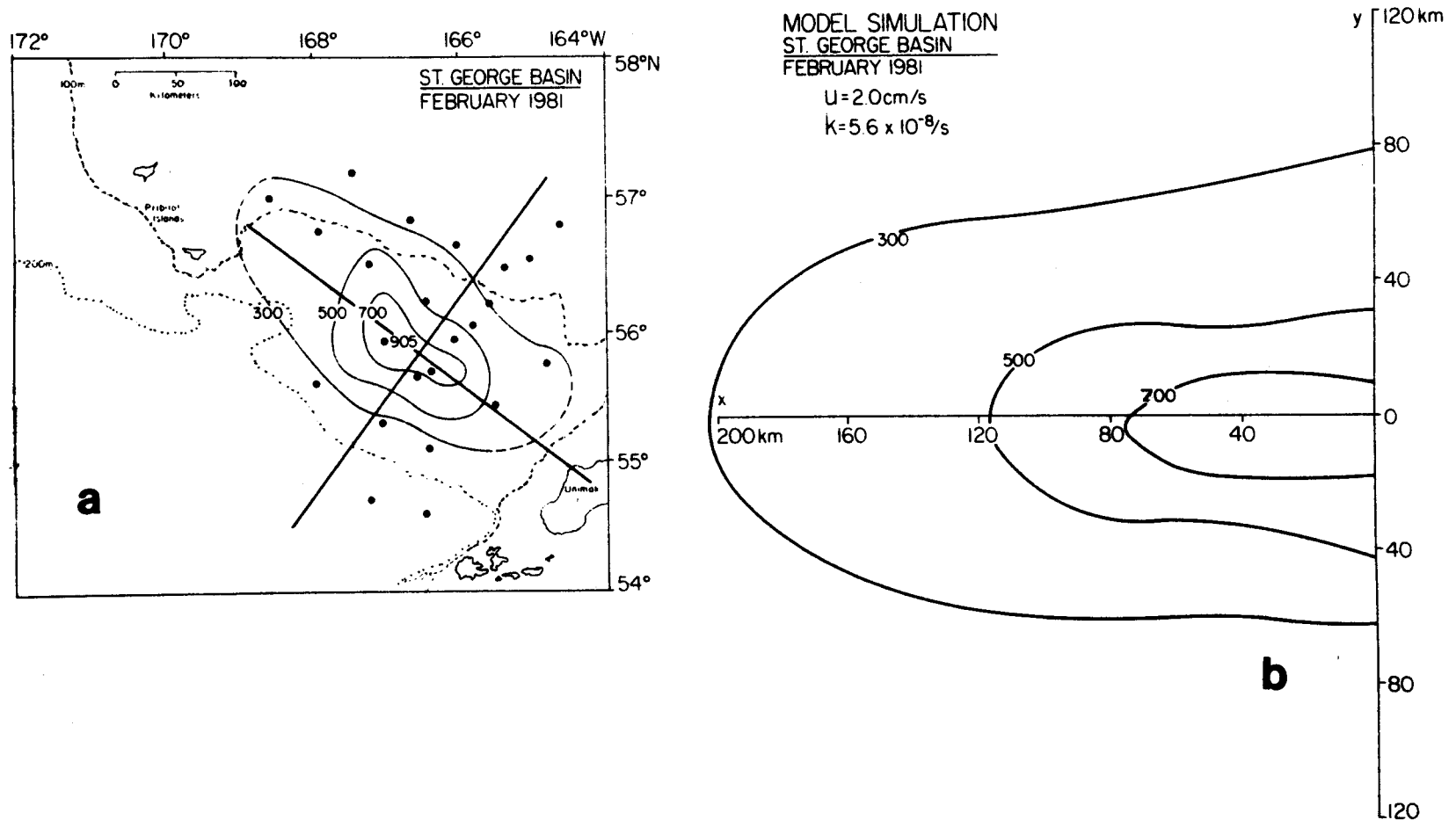


Figure 33. (a) The average near-bottom concentration of dissolved methane in St. George Basin in February 1981. The axes show the position of the model grid. (b) The model simulation of the methane distribution using the source function shown in Fig. (31b). The best fit was obtained for $u = 2.0 \text{ cm/s}$ and $k = 5.6 \times 10^{-8} \text{ /s}$.

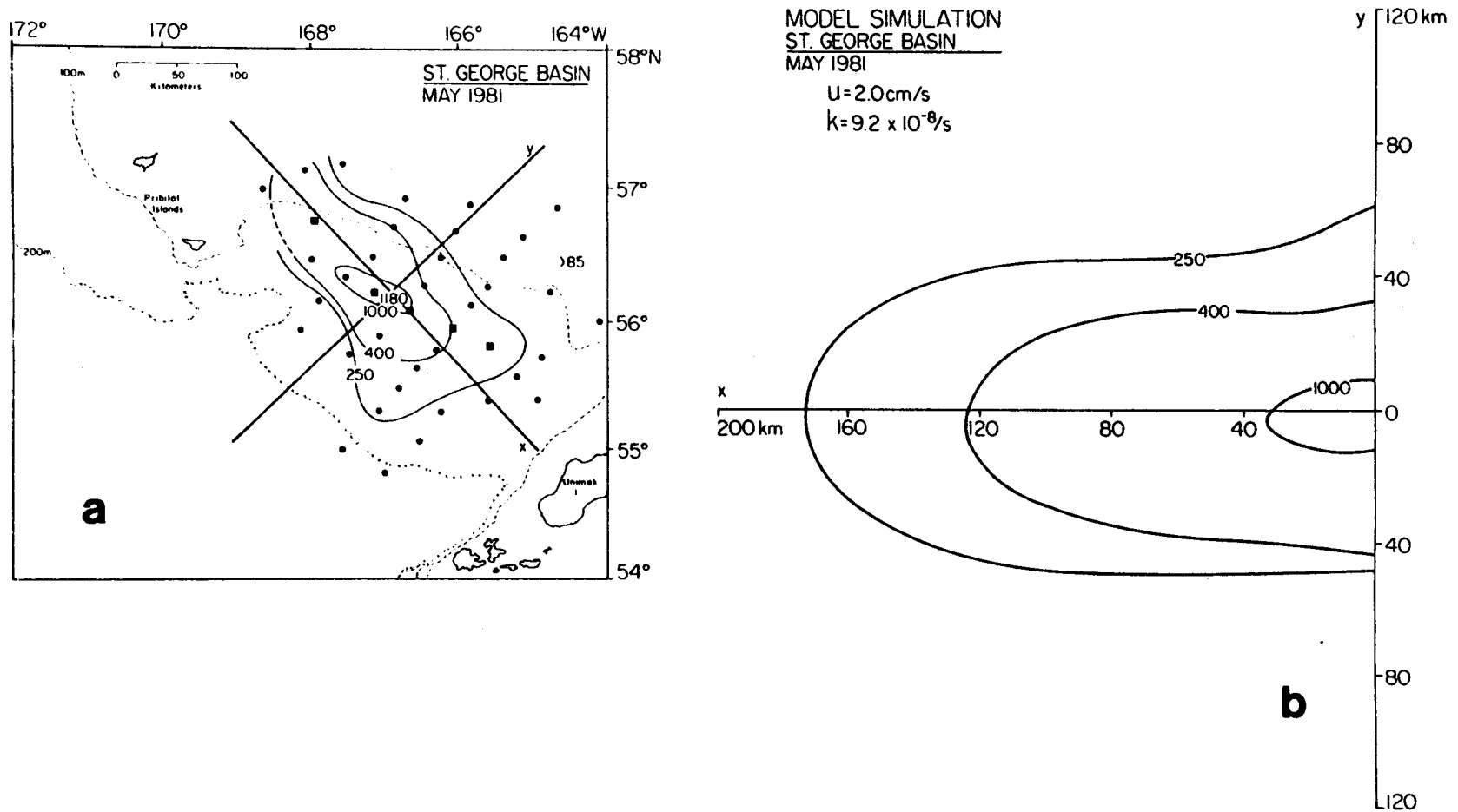


Figure 34. (a) The average near-bottom concentration of dissolved methane in St. George Basin in May 1981. The axes show the position of the model grid. (b) The model simulation of the methane distribution using the source function shown in Fig. (31c). The best fit was obtained for $u = 2.0 \text{ cm/s}$ and $k = 9.2 \times 10^{-8} \text{ /s}$.

than was observed during the two previous visits. The relatively low abundance of methane in May is believed to be related to the vertical carbon flux and possibly the bottom temperatures, as described earlier. The orientation of the plume is as before, except that its cross-shelf extent is much smaller than was observed in August 1980. Asymmetry of the plume suggests short term variations (< 1 month) in the speed and trajectory of the flow, which is not unexpected in the dynamic outer shelf region of the Bering Sea (Kinder and Schumacher, 1981a). As noted before the plume is elongated toward the northeast, suggesting a weak flow in that direction.

The best fit to data was achieved with the source function shown in Figure (31b), $u = 2$ cm/s, and $k = 9.2 \times 10^{-8}$ /s. The biological rate constant, which was determined by in vitro experiments aboard ship, is larger than was observed during the two previous visits. The goodness of fit was not improved by increasing the velocity, indicating as before, that the mean velocity was probably ≤ 2 cm/s.

6.2.4. Summary of St. George Basin Studies

The distributions of methane in the benthic boundary layer were modeled to determine the mean current trajectory, mesoscale mean current velocities, and the characteristic of diffusive mixing. Model simulations were made on three distributions observed in August 1980, February 1981, and May 1981.

The source of the methane is believed to be organic-rich sediments deposited on the basin floor of St. George Basin. The organic carbon content varied from about 0.5% at the edges of the basin to slightly more than 1% at the center of the distribution. The distribution of carbon is nearly circular and appears to be related to circulation processes over the outer shelf. A cursory examination of the dynamic height field suggests a divergent flow near the location of high carbon concentration, which might result in the

accumulation of fine detrital and organic materials. On the basis of sedimentary size analysis, we would expect the accumulation of organic carbon to correlate with weak circulation.

The distribution of methane was modeled by establishing a variable concentration at the boundary and summing the individual plumes. We also assumed that lateral mixing was isentropic, which may not be valid for these waters. Vertical flux calculations demonstrated that insignificant amounts of methane were lost through the pycnocline, which reduced the model to two dimensions. Biological oxidation of methane was included in the model in the basis of in vitro experiments performed on the ship.

The results of the modeling analyses indicated that the mean velocity was no greater than 2 cm/s, and probably less. This is in complete agreement with mean flow measurements of 1-2 cm/s. Plume trajectories also showed an onshore component, which was also in agreement with current meter measurements.

The plumes observed in August 1980, February 1981 and May 1981 all showed trajectories to the north-northwest, but significant amounts of methane were found to the southwest as well. This is indicative of the low mean velocities and the significance of horizontal diffusion in the x-direction, which was not accounted for in the model. We conclude that a more sophisticated model that includes flux divergence in the x-direction as well as the y-direction would predict a lower mean velocity than the 2 cm/s cited above. There is also reason to believe that the mixing is anisentropic, namely that diffusive transport in the x-direction is larger than in the y-direction. The reason for this belief lies in the distribution of the mass field. Flow parallel to the isobaths is along isopycnal surfaces, while cross-shelf flow is across isopycnals. On this basis we would expect that $K_x > K_y$ and that the plume asymmetry is strongly influenced by the imbalance in the horizontal flux divergence terms, particularly at these low mean velocities.

The impact of these findings is particularly relevant to offshore exploration and production activities. These analyses as well as the current meter measurements show the St. George Basin region to be characterized by weak currents and relatively long residence times. Oil spilled or retained in the near-bottom waters will not be removed rapidly by circulation processes; therefore the risk to marine habitats is elevated. However, the actual impact depends on the nature of the spill and the quantity of oil spilled. This point will be treated in the next section.

6.2.5 Oil Spill Scenario, St. George Basin

In the preceding discussion, we have considered the circulation characteristics of two subregions of the southeastern Bering Sea. Specifically the studies centered on the near-bottom circulation of St. George Basin and the coastal zone along the North Aleutian Shelf. In each case, we used a localized source of dissolved methane to describe advective and diffusive scales applicable to each region. This information is directly applicable to estimating or predicting how spilled oil might behave in these areas. We now proceed to develop and test a simple model that will be useful in describing the concentration field resulting from a spill event. These models are only applicable to the dissolved or emulsified fractions and do not describe the behavior of a surface slick.

The situation we wish to simulate here is an instantaneous release of oil at a fixed location, such as might occur in the collision or grounding of a tanker. The three dimensional model that describes the subsequent dispersion of oil under these conditions is given by the following equation (Brubaker and Rote, 1978):

$$C(x,y,z,t) = \left[\frac{Q}{(2\pi)^{3/2} \sigma_x \sigma_y \sigma_z} \right] \exp \left\{ - \frac{(x-ut)^2}{2\sigma_x^2} - \frac{y^2}{2\sigma_y^2} - \frac{z^2}{2\sigma_z^2} \right\}, \quad (7)$$

where Q is the mass of material released, σ_x , σ_y , σ_z , are the standard deviations of the plume as a function of time (t), and u is the mean velocity in the x-direction. To simplify equation (7), we will only consider the centerline distribution ($y=0$) for a constant depth interval, z. Setting $y=z=0$, equation (7) becomes

$$C(x,t) = \left[\frac{Q}{(2\pi)^{3/2} \sigma_x \sigma_y \sigma_z} \right] \exp \left\{ - \frac{(x-ut)^2}{2\sigma_x^2} \right\} \quad (8)$$

This model describes the time dependent behavior of spilled oil contained within a well-mixed lens of water (e.g., surface-mixed layer above the pycnocline). This model also predicts the maximum concentration of oil that will occur along the centerline of the plume. By inspection of equation (8) it is readily apparent that the concentration decreased exponentially in the x-direction. To solve equation (8), we need estimates of Q, u, σ_x , σ_y , and σ_z .

The model represented by equation (8) was solved for a given spill scenario stipulated for St. George Basin (April 1981). The amount of oil spilled was 50,000 bbl or 6.7×10^8 kg. To solve equation (8), a few assumptions were made concerning the duration of the spill as well as the size of the initial plume. In this particular prediction, we will assume that 'worst-case scenario,' which will lead to the largest volumetric impact.

The assumptions imposed on the spill scenario are the following. The spill occurs in the surface waters of St. George Basin in summer. The oil is instantaneously released and all of it is rapidly mixed downward to

the top of the thermocline, or about 40 m. The oil is considered conservative (i.e., does not evaporate nor is it biologically degraded). Also, no flux through the thermocline is permitted. This computation will maximize the concentration of dissolved and emulsified oil and its impact area.

The concentration of oil at any point in time and space depends critically on the rate of mixing. The mixing parameters are implicitly embodied in σ_x , σ_y , and σ_z , the standard deviation of the plume as a function of time or distance. The parameters are linked through the mean velocity $u = x/t$. For the purpose of the model, we assume σ_z is a constant, whereas σ_x , σ_y are allowed to vary with t according to the empirical relationships given by Okubo (1971). The relevant relationships are:

$$\sigma_{rc}^2 = 2\sigma_x\sigma_y \quad (3a)$$

$$\sigma_x\sigma_y = 0.0054 t^{2.34} \quad (9)$$

$$\sigma_y = 0.074 \sigma_x \quad (10)$$

$$\sigma_x = 0.0197t^{2.34} \quad (11)$$

The initial size of the spill is somewhat arbitrary, but for our purpose here we assume a radial spill of 200 m and a mean depth of 40 m. Consequently, the average concentration of oil is $C_0 = (6.7 \times 10^8 \text{ kg}) / (200 \text{ m})^2 (40 \text{ m}) = 425 \text{ kg/m}^3$ or 425 g/L. This amount of oil could not be dissolved in one liter of seawater. For the sake of simplicity, we will retain these initial conditions, recognizing that more realistic scenarios can be easily scaled from these results. By analogy with equation (8), the initial plume disper-

sion parameters are easily calculated, $\sqrt{2\pi} \sigma_x^0 = \sqrt{2\pi} \sigma_y^0 = 200$ m; $\sqrt{2\pi} \sigma_z^0 = 40$ m. Hence $\sigma_x^0 = \sigma_y^0 = 80$ m and $\sigma_z^0 = 16$ m. The initial concentration of oil in the spill, C^0 , is equal to $C_0 = Q/(2\pi)^{3/2} \sigma_x \sigma_y \sigma_z = 425$ g/L.

To examine the temporal development of the spill scenario described above, we assume mean velocities of 2.5, 5.0, and 10 cm/s, which are in the range of observed velocities for St. George Basin (Kinder and Schumacher, 1981a). The results of the modeling are described in Figures (35), (36), and (37), for periods of 2d, 5d, 10d, and 30 d. To express the results generically, we have chosen a relative concentration scale, where C_0 is the initial concentration of oil at the spill. For reference purposes, the 1 ppm and 0.1 ppm concentration lines are also included for comparison. Organisms are stressed or killed at oil concentrations (water soluble fraction) in the range 0.1 to 1 ppm.

Figure (35) depicts the plume development for a period of 30 d at a mean velocity of 2 cm/s. The maximum concentration of oil at 2 d is 1% of the original concentration and occurs at about 4 km downstream. At the fifth day, the center of mass has moved to 10 km, but lateral diffusion has decreased the relative concentration to 0.1%. Similar exponential decreases are noted for the subsequent time periods.

The impact of oil on organisms depends on both duration of exposure and concentration. The spill being considered here was instantaneous and decays according to the mathematical representation of the mixing. If we arbitrarily choose the 0.1 ppm reference level, the concentration of oil is everywhere less than this value after 16 or 17 d.

In Figure (36) is shown the same spill event except the mean velocity was increased to 5 cm/s. The immediate effect of the increased velocity is to elongate the plume in the downstream direction. At comparable distances, the maximum concentration of oil is greater at the higher velocities because

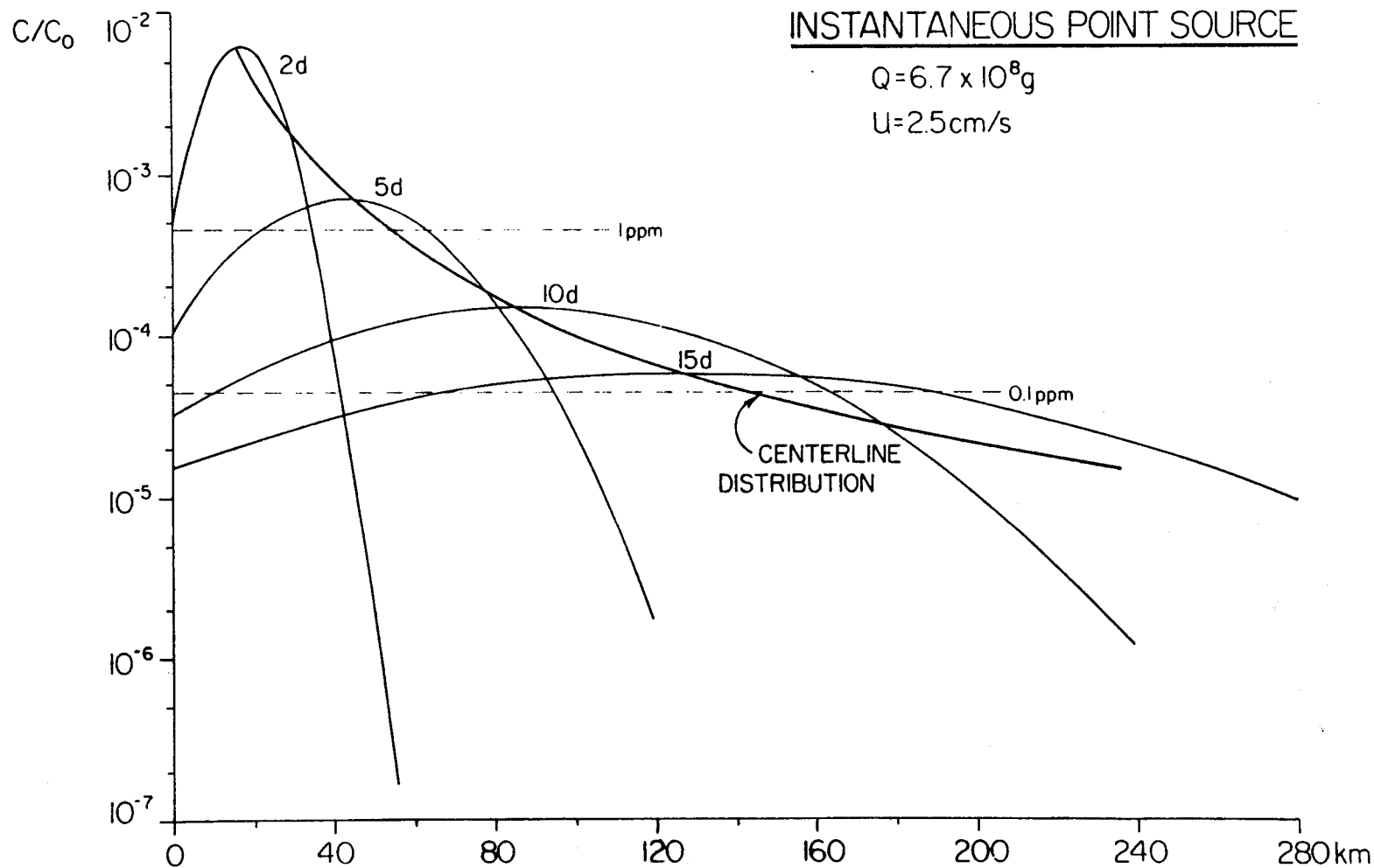


Figure 35. The development of a plume of 'dissolved' oil resulting from an instantaneous release of $6.7 \times 10^8 \text{ g}$ (50,000 bbls) confined to a 40 m, vertical-lens of water. The centerline distribution shows the temporal history of the spill locus for a mean current speed of 2.5 cm/s. Reference concentrations of 0.1 and 1.0 ppm 'dissolved' oil also are indicated.

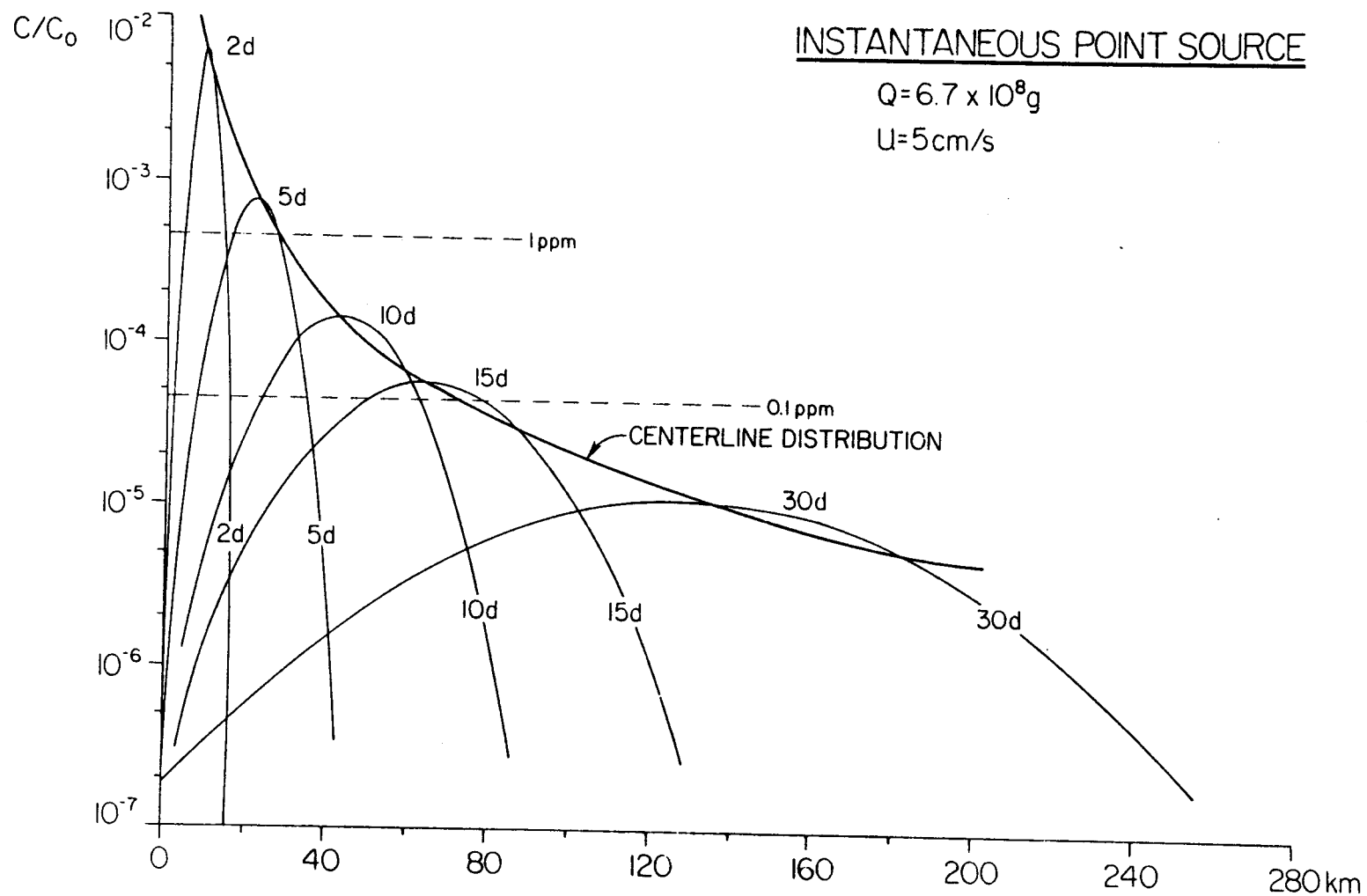


Figure 36. The development of a plume of 'dissolved' oil resulting from an instantaneous release of $6.7 \times 10^8 \text{ g}$ (50,000 bbls) confined to a 40 m, vertical-lens of water. The centerline distribution shows the temporal history of the spill locus for a mean current speed of 5.0 cm/s. Reference concentrations of 0.1 and 1.0 ppm 'dissolved' oil also are indicated.

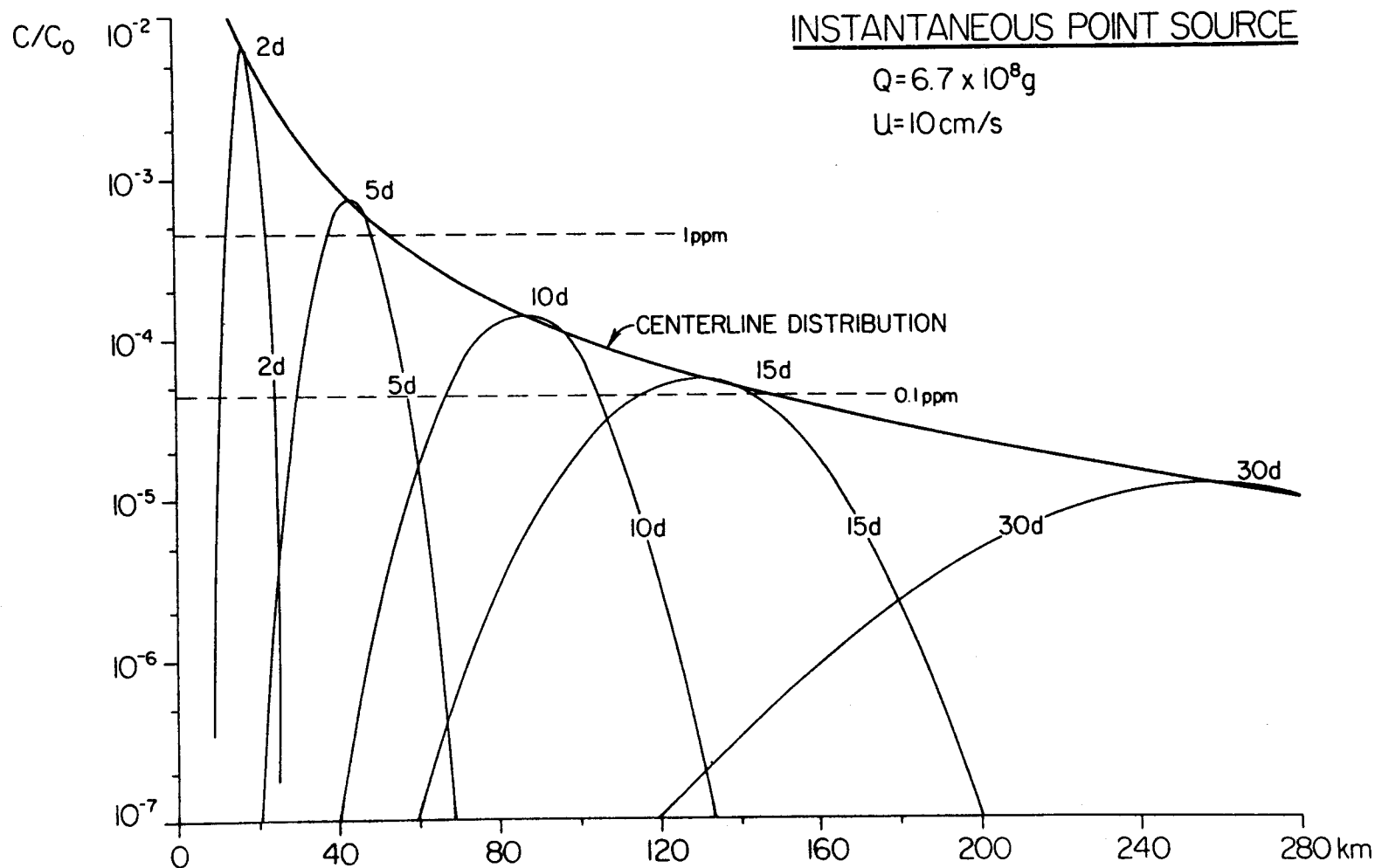


Figure 37. The development of a plume of 'dissolved' oil resulting from an instantaneous release of $6.7 \times 10^8 \text{ g}$ (50,000 bbls) confined to a 40 m, vertical-lens of water. The centerline distribution shows the temporal history of the spill locus for a mean current speed of 10 cm/s. Reference concentrations of 0.1 and 1.0 ppm 'dissolved' oil also are indicated.

the flux of oil across any orthogonal plane must be conserved (i.e. oil is conservative). At 15 d, the maximum concentration of oil has fallen to 0.01% of the original concentration at a distance of 64 km. In the present case, the concentration of oil would be about 0.3 ppm. After 30 d, the concentration of oil is everywhere less than 0.001% or 50 ppb.

The situation for 10 cm/s is shown in Figure (37). The plume is elongated in the x-direction, as noted above. The maximum concentration after 15 d is about 0.1 ppm and occurs 130 km downstream of the spill site.

In the foregoing, the effect of increasing the velocity was to increase the longitudinal transport at the expense of lateral diffusion. However, the amount of oil spilled was constant; therefore, we expect the environmental impact volume to be the same regardless of the velocity. The geometry of the plume will, however, be different. To estimate the impact volume of the hypothetical spill given above, we need only consider the temporal development of the plume and the concentration of oil above any given threshold level, say 0.1 ppm. Considering the 5 cm/s case (Fig. 36), the plume length to width was estimated for each period of time in which the concentration exceeded 0.1 ppm. For example, at 10 d (5 cm/s), the length (x) of the plume was 38 km and its width (y) was about 10 km. As the center of mass of oil is transported, it diffuses laterally and becomes more dilute. Because the diffusion coefficient is increasing as the size of the plume grows, these two effects combine to form a maximum extent in the y-direction to which we might expect biological effects. That downstream distance is about 40 km in the case where $u = 5$ cm/s. Beyond 40 km, the plume continues to grow, but its biological impact is diminishing due to dilution with surrounding water. According to our calculations, the maximum areal extent of the plume is 450 km^2 and would persist for about 15 d. It should be noted that the calculated area represents an accumulated effect area, not an instantaneous

effect area. The maximum instantaneous area affected would occur at about 40 km downstream and would be about $38 \text{ km} \times 10 \text{ km} = 380 \text{ km}^2$. Since we assumed initially a homogeneous lens of water 40 m deep, the volume impact area would be about 18 km^3 .

The scenario discussed above is not totally realistic in that only a small fraction of spilled oil is actually going to be accommodated in the water column as dissolved or emulsified oil. If we assume that only 10% of the total oil is accommodated, then the potential impact area is reduced to about $40\text{-}50 \text{ km}^2$, an area very much smaller than the surface area of St. George Basin.

These elementary calculations suggest that a point source injection of oil (i.e., well blowout or tanker spill) of the magnitude of 50,000 bbl's will result in relatively small amounts of dissolved and/or emulsified oil in the water column and that a reasonable impact area from such an injection is no larger than 450 km^2 (given a 0.1 ppm threshold). More than likely it is a factor of ten less. These results only apply to the open reaches of St. George Basin and do not apply to the coastal zone of the NAS, where the hydrography and the proximity of the beach result in a much different set of conditions.

6.2.6 Horizontal Transport of Methane

In fitting the model to the observed distributions, a source function was hypothesized in terms of the concentration along a line bisecting the source region (e.g. see Figure 32a). It was assumed that the source of the methane was diffusive flux from the underlying sediments, or perhaps from methane production arising from microbial activity at the sediment-water interface. In either event, the near-bottom transport of methane must equal the integrated benthic production rate corrected for biological loss.

To evaluate the bottom flux of methane, we collected five vertical methane profiles to 50 cm in May 1981. Two such profiles taken in May 1981 are shown in Figure (38), where the vertical distributions of methane in the water column and in the sediments are shown. In each case, the maximum concentration in the sediment is approximately a factor of 10 above the bottom boundary layer concentration. The gradient across the sediment-water interface in part explains the accumulation of methane in the bottom waters of St. George Basin. The average flux to the water column, based on a molecular diffusivity of CH_4 of $8.5 \times 10^{-5} \text{ cm}^2/\text{s}$ (Witherspoon and Bonoli, 1968), was $1 \times 10^{-14} \text{ g/cm}^2/\text{s}$ (Katz et al., 1982). Assuming an area of $2.0 \times 10^{14} \text{ cm}^2$ ($r=80 \text{ km}$), the integrated methane production rate is 2 g/s. Integrating the production curve shown in Figure (31c) and assuming a mean velocity of 2 cm/s, we obtain a horizontal transport of 23 g/s, a factor of 10 higher than the benthic flux would suggest. The explanation for the difference may lie in the assumptions. By assuming a slightly larger molecular diffusivity (e.g. bioturbation in the upper 10 cm of the sediment column, Berner, 1980) or decreasing the mean velocity, a match could be achieved. Both of these parameters could be adjusted by appropriate factors to achieve the end result without perturbing seriously the known variances. Also, the interstitial water measurements do not measure production that might occur at the sediment water interface. Consequently, we conclude that methane production rate in the region of elevated carbon concentrations is in agreement with the horizontal transport derived from the model, if we assume a larger molecular diffusivity and/or a lower mean velocity. Our intuition is that the mean velocity is no larger than 2 cm/s and could very well be much lower if anisotropic mixing were invoked.

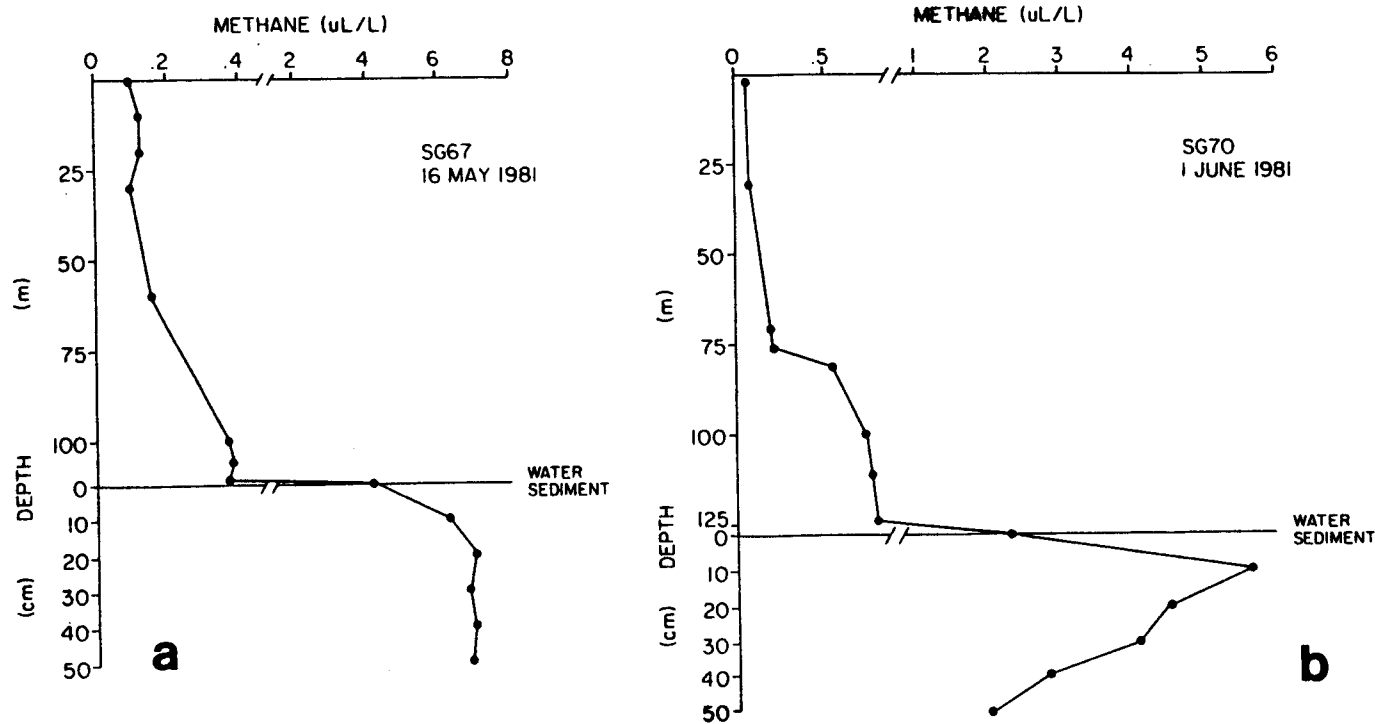


Figure 38. The vertical distribution of methane in the water column and surficial sediments at (a) Station SG67 and (b) SG70. These data were collected in May-June 1981. Note the scale change in concentrations between the water and the pore fluids.

6.2.7. Vertical Transport of Methane

St. George Basin is normally stratified due to seasonal changes in solar insolation and freshwater input. The strength of the pycnocline varies seasonally depending on buoyancy input and the depth of the mixed layer, but appears to be a maximum in late summer or early fall, and a minimum in late winter. Regardless of season, the density difference between the surface layers and the bottom is about one sigma-t unit (e.g., 25 to 26), but the gradient changes significantly over the year. This change in the gradient results in a variable vertical flux of dissolved constituents because the apparent vertical eddy diffusivity is a function of stability (Welander, 1975). In this section we test a simple model that estimates the magnitude of K_v .

On previous visits to St. George Basin it was observed that the vertical distributions of salt and methane were similar, suggesting that methane was quasi-conservative. A plot of methane versus salinity was usually linear (Fig. 39), implying that the vertical flux of methane from bottom sediments was impeded by the pycnocline. In an analogous fashion, the vertical transport of dissolved components of petroleum or micro-droplets of oil would be similarly inhibited.

In order to quantify the magnitude of K_v within the pycnocline, Station PL6 was occupied on two occasions in August 1980. Detailed measurements of salinity, temperature, and methane were made. The results of these measurements are shown in Figure (7). Note that the concentration of methane decreases approximately a factor of five between the bottom and the surface (100 m to 60 m), while σ_t decreases abruptly over the same depth range.

Assuming for the moment that methane is conservative, the vertical flux of methane across any horizontal plane is equal to the bottom flux or to the

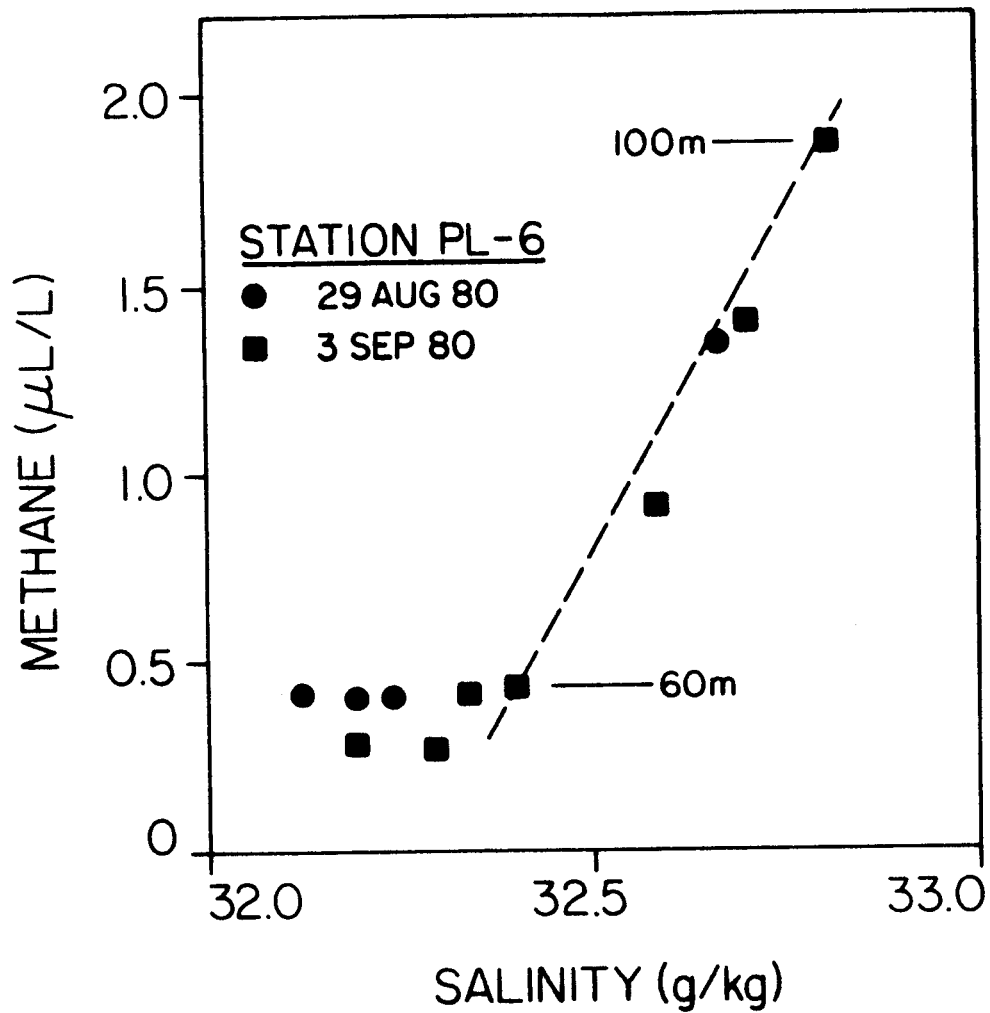


Figure 39. The relationship between salinity and methane at Station PL-6 in August 1980. The linear relationship suggests conservative mixing between the surface and bottom waters.

air-sea evasion rate (see Section 5.2). Since the latter is more easily estimated, a monthly mean air-sea flux was calculated from a knowledge of mean winds and sea surface temperatures. This value is equal to the product of the methane gradient and the apparent vertical eddy diffusivity (eq. 6).

The estimated K_z within the pycnocline was plotted against stability (Brunt-Vaaisaala Frequency) and is shown in Figure (40). In the near surface layers, K_z ranged from 20-50 cm^2/s in agreement with the high shear stresses below the mixed layer. Below 50 m, K_z decreased dramatically to a minimum of 0.2 cm^2/s near 65 m, then again increased to values in excess of 1 cm^2/s as the bottom boundary layer was approached. The slope of the line was -0.5, which indicates that vertical mixing is the result of vertical shear rather than the cascade of energy from large scale turbulence (Welander, 1975).

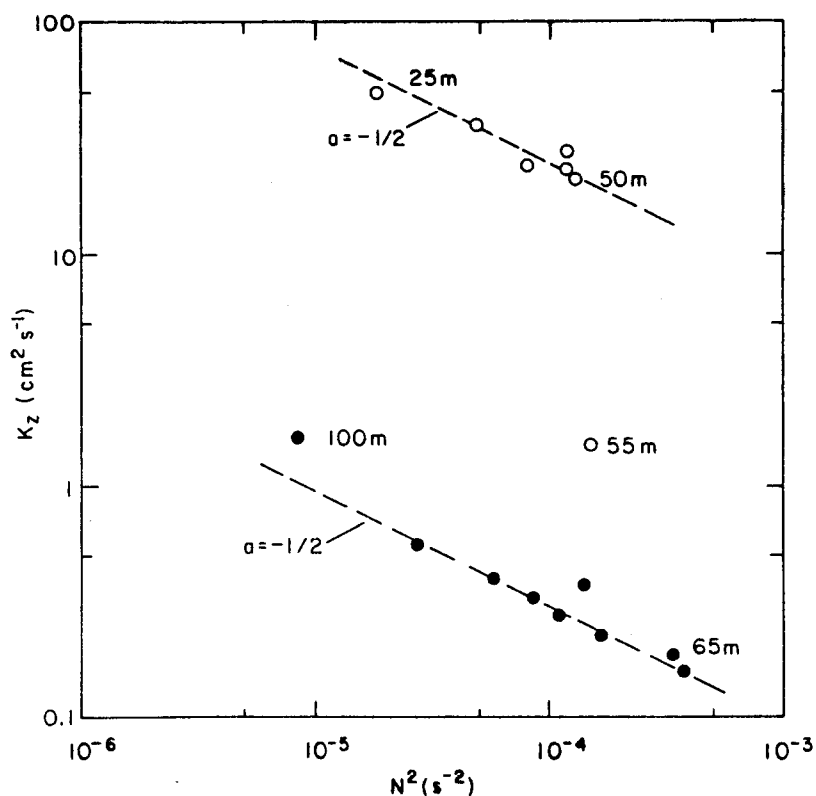


Figure 40. The relationship between the apparent vertical eddy diffusivity, K_z , and the Brunt-Vaaisaala Frequency, N^2 , at Station PL6 in August 1980. The theoretical relationship for shear-induced turbulence is -0.5, which is shown by the dashed lines.

The conditions modeled were typical for late summer and fall and indicate that vertical exchange is strongly retarded by the density gradient. However, what is of interest is the relative magnitude of the vertical flux of methane across the pycnocline compared to the horizontal flux. For this scaling exercise, we assume the following conditions, which existed in August 1980:

$$K_z = 0.2 \text{ cm}^2/\text{s}, \quad d(\text{CH}_4)/dz = 5.0 \times 10^{-4} \text{ nL/cm}^4$$
$$K_h = 1.0 \times 10^6 \text{ cm}^2/\text{s}, \quad d(\text{CH}_4)/dx = 1.1 \times 10^{-7} \text{ nL/cm}^4$$

It is readily apparent that $F_h \gg F_z$, thus to a first approximation, the horizontal flux terms dominate the distribution of methane in the bottom boundary layer and our original assumption that the vertical flux divergence term could be ignored appears valid (see section 6.2). Even if one increases K_v to $1 \text{ cm}^2/\text{s}$ and reduces K_h to $1 \times 10^5 \text{ cm}^2/\text{s}$, the horizontal terms remain dominant for a plume of the observed dimension.

This argument holds true for the velocity terms as well. The advective flux is the product of the mean velocity and the concentration at a specified point. Assuming a mean velocity of 2 cm/s and a methane concentration of 1000 nL/L (1.0 nL/cm^3), the advective flux is $3 \text{ nL/cm}^2/\text{s}$ compared to the horizontal flux divergence of $0.1 \text{ nL/cm}^2/\text{s}$. Clearly, the distributions of methane in the bottom waters of St. George Basin are strongly influenced by the weakest mean flows, even those that are at or below the threshold of conventional current meters.

7. CONCLUSIONS

7.1. North Aleutian Shelf Studies

Dissolved methane, tidally-fluxed from Port Moller, was used as a quasi-conservative tracer of circulation along the North Aleutian Shelf. Three separate observational periods were covered, August 1980, February 1981, and May, 1981. The distribution of dissolved methane along the coast was described using a two dimensional diffusion-advection model, which included a term for biological oxidation and sea-to-air exchange.

The results of the modeling effort predicted mean velocities along the shelf ($z < 50$ m) of 3-6 cm/s. These estimates represent mean velocities over the scale length of the tracer, or about two months. Short term variations in the velocity field (i.e. storm surges) were not detected by the tracer as the characteristic time scale is much shorter than one month.

The seasonal distributions of methane clearly showed the importance of bottom bathymetry and horizontal shear. The model was modified to partially account for bathymetry, but not for a variable u and k . The inner front, located at about 50 m, separates the well mixed shelf water from the seasonally stratified offshore water. Both salinity and methane distributions showed clearly the location of the front, but because the cross frontal gradients were weak, it was impossible to quantify the significance of the front relative to offshore transport. Because of these factors the model fits were not good, but parametric analysis demonstrated that the mean velocity is certainly within the above-stated range.

The model included a variable horizontal eddy diffusivity, K_y , which was scaled to the Lagrangian distance, ut . From our analysis, it appears that the empirical relationships presented by Okubo, 1971, are valid for K_y . K_y varied from about $2 \times 10^5 \text{ cm}^2/\text{s}$ to $2 \times 10^6 \text{ cm}^2/\text{s}$, depending on the size of

the plume. For smaller sources, such as an oil spill, the horizontal eddy diffusivities would be correspondingly smaller.

7.2. St. George Basin Studies

St. George Basin is a fault graben located on the outer continental shelf of the southeastern Bering Sea and is a potential lease area for gas and oil development. First observed in 1975 and again in 1976, the organic-rich sediments of the basin represent a significant source of biogenic methane, which could be used as a Lagrangian tracer of mean circulation. To accomplish this, however, a much tighter observational grid was implemented and a series of seasonal observations was conducted in August 1980, February 1981, and May 1981.

The distribution of dissolved methane in the lower boundary layer was simulated using a two-dimensional diffusion-advection model like the one used for the North Aleutian Shelf. It differed, however, in that no air-sea evasion term was included. The results of the modeling indicated that the mean velocity was 1-2 cm/s and independent of season. These velocities are quite low and are in complete agreement with the measured currents. The above velocities may be an over estimate, because diffusion in the x-direction was not explicitly included in the model. Consequently, the inclusion of anisotropic mixing could result in the same distribution as was modeled with a variable K_y and constant u . There is some basis for this belief as mixing along shelf is isopycnal in contrast to mixing across shelf which is not. In either event, the mean velocities are low, which is supported by current meter measurements and the accumulation of fine-grained sediments.

8. REFERENCES

- Berner, R.A. 1980. Early Diagenesis, A Theoretical Approach. Princeton University Press, Princeton, N.J., 241 pp.
- Broecker, W.S. and T.H. Peng. 1974. Gas exchange rates between air and sea. Tellus 26: 21-35.
- Brubaker, K.L. and P.M. Rote. 1978. Dispersal models for sulfur oxides in urban environments. In: Sulfur in the Environment, Part I, 172-241, J.O. Nriagu (ed.), John Wiley and Sons, New York, 463 pp.
- Claypool, G.E. 1974. Anoxic diagenesis and bacterial methane production in deep-sea sediments. Ph.D. Thesis, University of California at Los Angeles, 277 pp.
- Claypool, G.E. and I.R. Kaplan. 1974. The origin and distribution of methane in marine sediments, In: Natural Bases in Marine Sediments, 99-140, I.R. Kaplan (ed.), Plenum Press, New York, 324 pp.
- Cline, J.D. and R. Feely. 1976. Distribution of light hydrocarbons, C₁-C₄, in the Gulf of Alaska and southeastern Bering Shelf. In: Environmental Assessment of the Alaskan Continental Shelf, 9: 443-547, DOC/NOAA, Boulder, Colo.
- Cline, J.D. 1977. Distribution of light hydrocarbons, C₁-C₄ in the northeast Gulf of Alaska, Lower Cook Inlet, southeastern Chukchi Sea. In: Environmental Assessment of the Alaskan Continental Shelf, 8: 180-268, DOC/NOAA, Boulder, Colo.
- Cline, J.D., C. Katz, and H. Curl, Jr. 1981a. Circulation processes in Bristol Bay, Alaska using dissolved methane as a tracer. OCSEAP/OMPA Annual Report, August 1981, 53 pp.
- Cline, J.D., C.N. Katz, and H.C. Curl, Jr. 1981b. Dynamics of dissolved methane in Bristol Bay, Alaska. IAMAP Third Scientific Assembly, Hamburg, ACGP-1, ROAC, August 17-28, (Abstr.).
- Cline, J.D. 1981. Distribution of dissolved LMLO hydrocarbons in Bristol Bay, Alaska: Implications for future gas and oil development. In: The Eastern Bering Sea Shelf: Oceanography and Resources, 425-444, D.W. Hood and J.A. Calder (eds.), Vol. I, DOC/NOAA/OMPA, University of Washington Press, Seattle, Wash., 625 pp.
- Coachman, L.K. and R.L. Charnell. 1979. On lateral water mass interaction- A case study, Bristol Bay, Alaska, J. Phys. Oceanogr., 9: 278-297.
- Csanady, G.T. 1973. Turbulent Diffusion in the Environment. D. Reidel Publishing, Boston.
- Csanady, G.T. 1981. Circulation in the coastal ocean. EOS 62: 9-11.

- Department of Commerce. 1980. Tidal Current Tables, Pacific Coast of North America and Asia, DOC/NOAA/NOS, Rockville, Md., 260 pp.
- Emerson, S. 1975. Gas exchange rates in small Canadian shield lakes. Limnol. Oceanogr. 20: 754-761.
- Gardner, J.U., T.L. Vallier, W.E. Dean, K.A. Kvenvolden, and G.D. Redden. 1978. Distributions of grain size, total carbon, heavy and light minerals, clay mineralogy, and inorganic geochemistry of the outer continental shelf, southern Bering Sea. In: Annual Report, Environmental Assessment of the Alaskan Continental Shelf, Vol. XI, 300-353, DOC/DOI, OCSEAP, Boulder, Colo., 688 pp.
- Griffiths, R.P., B.A. Caldwell, J.D. Cline, W.A. Broich and R.Y. Morita. 1982. Field observations of methane concentrations and oxidation rates in the southeastern Bering Sea. Appl. and Environ. Microbiol., 44: 435-446.
- Katz, C.N. 1980. Processes affecting the distribution of low molecular weight aliphatic hydrocarbons in Cook Inlet, Alaska. M.S. Thesis, University of Washington, 131 pp.
- Katz, C.N., J.D. Cline, and R.P. Griffiths. 1982. The seasonal distribution of methane in the Bering Sea; a relationship between source and dispersion. EOS 63: 83.
- Kinder, T.H. and J.D. Schumacher. 1981a. Hydrographic structure over the continental shelf of the southeastern Bering Sea. In: The Eastern Bering Sea Shelf: Oceanography and Resources, 31-52, D.W. Hood and J.A. Calder (eds.), Vol. I, DOC/NOAA/OMPA, University of Washington Press, Seattle, Wash., 625 pp.
- Kinder, T.H. and J.D. Schumacher. 1981b. Circulation over the continental shelf of the southeastern Bering Sea. In: The Eastern Bering Sea Shelf: Oceanography and Resources, 53-76, D.W. Hood and J.A. Calder (eds.), Vol. I, DOC/NOAA/OMPA, University of Washington Press, Seattle, Wash., 625 pp.
- Niebauer, H.J. 1981. Recent short-period winter time climate fluctuations and their effect on sea-surface temperatures in the eastern Bering Sea. In: The Eastern Bering Sea Shelf: Oceanography and Resources, 23-30, D.W. Hood and J.A. Calder (eds.), Vol. I, DOC/NOAA/OMPA, University of Washington Press, Seattle, Wash., 625 pp.
- Okubo, A. 1971. Oceanic diffusion diagrams. Deep-Sea Res. 18: 789-802.
- Overland, J.E. 1981. Marine climatology of the Bering Sea. In: The Eastern Bering Sea Shelf: Oceanography and Resources, 15-22, D.W. Hood and J.A. Calder (eds.), Vol. I, DOC/NOAA/OMPA, University of Washington Press, Seattle, Wash., 625 pp.
- Reeburgh, W.S. and D.T. Heggie. 1977. Microbial methane consumption reactions and their effect on methane distributions in freshwater and marine environments. Limnol. Oceanogr. 22: 1-9.

- Schumacher, J.D., T.H. Kinder, D.H. Pashinski, and R.L. Charnell. 1979. A structural front over the continental shelf of the eastern Bering Sea. J. Phys. Oceanogr. 9: 79-87.
- Scranton, M.I. and P.G. Brewer. 1977. Occurrence of methane in near-surface waters of the western subtropical North Atlantic. Deep-Sea Res. 24: 127-138.
- Sverdrup, H.U., M.W. Johnson, and R.H. Fleming. 1942. The Oceans. Prentice-Hall, Inc. Englewood Cliffs, N.J., 1087 pp.
- Swinnerton, J.W. and V.J. Linnenbom. 1967. Determination of the C₁ to C₄₅ hydrocarbons in seawater by gas chromatography. J. Chromatogr. Sci. 45: 570-573.
- Welander, P. 1967. Theoretical forms for the vertical exchange coefficients in a stratified fluid with application to lakes and seas. Acta Geophysica 1: 1-27.
- Witherspoon, P.A. and L. Bonoli. 1969. Correlation of diffusion coefficients for paraffin, aromatic, and cycloparaffin hydrocarbons in water. Indust. Eng. Chem. Funds 8: 589-591.
- Yamamoto, S., J.B. Aleaskas, and T.E. Grozier. 1976. Solubility of methane in distilled water and seawater. J. Chem. Eng. Data 21: 78-80.



**OIL SPILL VULNERABILITY, COASTAL MORPHOLOGY, AND SEDIMENTATION
OF OUTER KENAI PENINSULA AND MONTAGUE ISLAND**

by

Miles O. Hayes

**Coastal Research Division
Department of Geology
University of South Carolina**

**Final Report
Outer Continental Shelf Environmental Assessment Program
Research Unit 59**

April 1980

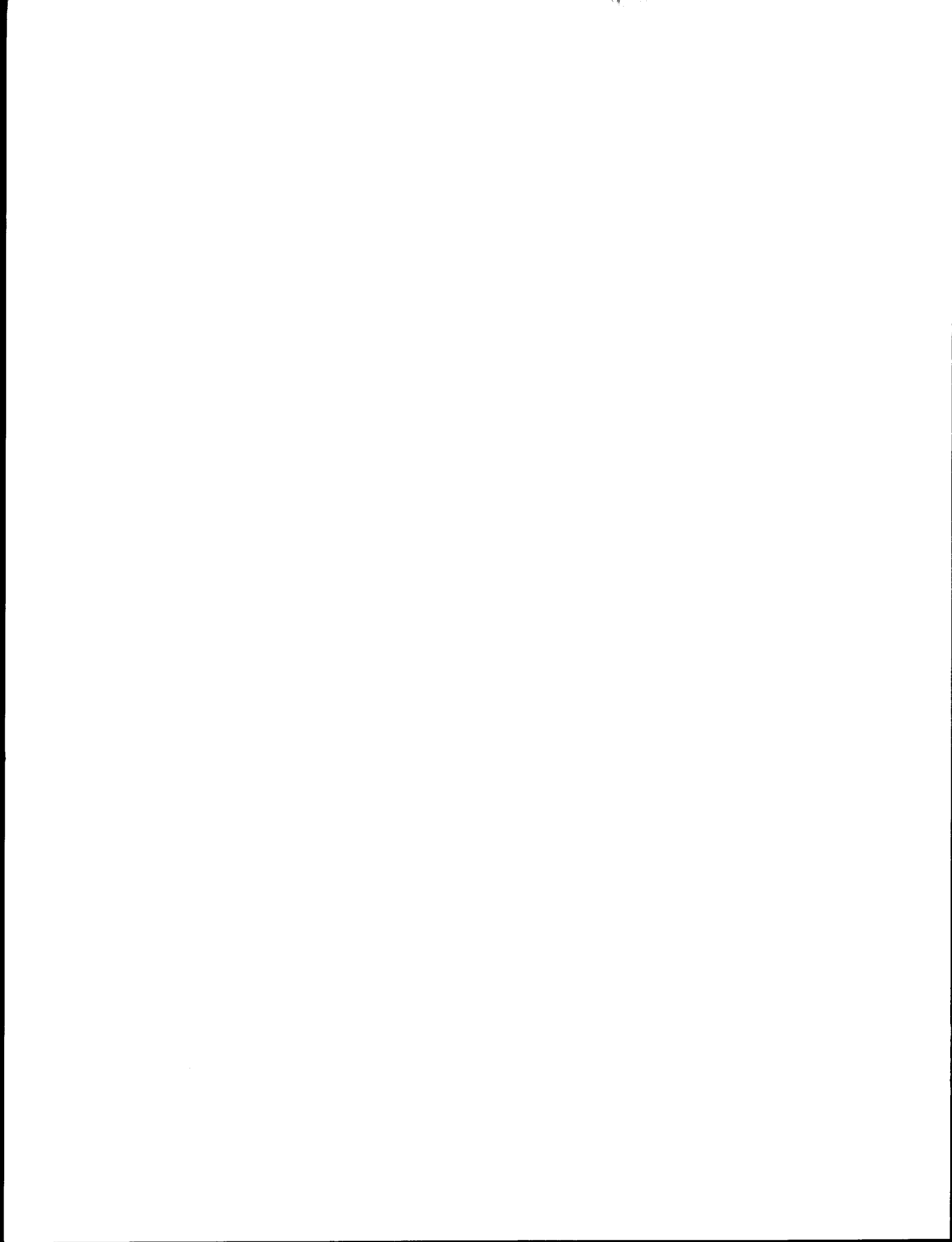


TABLE OF CONTENTS

List of Figures	423
List of Tables	424
Abstract	425
Objectives	425
 INTRODUCTION	 427
 GEOMORPHIC SETTING	 429
General	429
Outer Kenai Peninsula	429
Southwestern Prince William Sound	430
 TECTONIC SETTING	 431
Regional	431
Earthquake Activity	431
 GEOLOGIC SETTING	 435
Regional	435
Lithologies	435
Valdez group	437
Orca group	437
Intrusives	440
Unconsolidated sediments	440
Bedrock Influences on Shoreline Morphology	440
 OCEANOGRAPHIC AND METEOROLOGIC SETTING	 441
Tides	441
Wind and Wave Regime	441
 METHODOLOGY	 444
 COASTAL MORPHOLOGY	 446
General	446
Exposed bedrock shorelines	447
Bedrock cliffs	447
Wave-cut platforms	451
Sheltered Bedrock Shorelines	451
Beaches	455
Continuous linear beaches	455
Pocket beaches	455
Bayhead beaches	460
Spits	460
Uplifted beaches	460
River Mouth Delta-Tidal Flat and Salt Marsh Systems	467

OIL SPILL VULNERABILITY	470
Introduction	470
Oil Spill Vulnerability Index	471
1. Straight rocky headlands	472
2. Wave-cut platforms	472
3. Flat, fine-grained sandy beaches	472
4. Steeper, medium to coarse-grained sandy beaches	473
5. Impermeable exposed tidal flats	473
6. Mixed sand and gravel beaches	474
7. Gravel beaches	474
8. Sheltered rocky headlands	474
9. Protected tidal flats	475
10. Protected salt marshes	475
Applications to the Kenai Peninsula and Montague Island	475
REFERENCES	478
APPENDICES	483
Appendix I: Oil Spill Vulnerability	483
Appendix II: Survey Station Locations and Tasks Completed	517
Appendix III: Beach Profiles	523
Appendix IV: Grain Size Statistics	535

LIST OF FIGURES

- Figure 1. Map showing the location of the 100 stations monitored for this report along the outer Kenai Peninsula and Montague Island. Every 10th station is numbered. The index map shows the relative location of the study area within southeastern Alaska.
- Figure 2. Structural setting and tectonic framework of the Kenai Peninsula and Montague Island within the southern island arc system (King, 1969; modified from Jones and Clark, 1973).
- Figure 3. Regional setting of the Kenai Peninsula and Montague Island with respect to tectonic deformation and seismicity that accompanied the March 27 "Good Friday" earthquake, 1964.
- Figure 4. Idealized vertical section through Kenai Peninsula and Montague Island showing selected rock units and structural features of south central Alaska.
- Figure 5. Generalized geologic map of the Prince William Sound region, southeastern Alaska.
- Figure 6. Wind frequency and wave energy flux distributions taken from SSMO data (1970) for the Seward square in southeastern Alaska.
- Figure 7. Typical examples of exposed bedrock cliffs. These features are very common within the study area and display extreme variability in slope and relief.
- Figure 8. The southwestern end of Montague Island, one of the best examples of an uplifted wave cut platform. The features are backed by erosional scarps and composed almost entirely of bedrock.
- Figure 9. Sheltered bedrock cliffs found in areas of little or no wave energy and typically have an average relief of only 5-10 m.
- Figure 10. Continuous linear beaches most common in the uplifted portions of the study area and found fronting both sheltered and high-energy bedrock scarps and glacial till deposits.
- Figure 11. Small pocket beach (Sta. KNP-5) typical of those found throughout the study area.
- Figure 12. Bayhead beach typical of those found at the heads of the larger embayments in the study area.
- Figure 13. Profile station KNP-100 and KNP-17--both prime examples of cusped spits.

- Figure 14. Recurved spit located at profile station KNP-28. These features are often found at the entrance to small open lagoons. Beach sediments are composed of sand and gravel.
- Figure 15. Profile station KNP-82 located at San Juan Bay on Montague Island. The present day beach was produced by uplift from the 1964 Good Friday Earthquake.
- Figure 16. River mouth delta-tidal flat systems at profile stations KNP-22 and KNP-50. Tidal flats are predominantly composed of sand and fine gravel and have wide, intertidal areas with abundant biota.
- Figure 17. Embayed tidal flats located on northwestern Montague Island. These features are found independent of river mouth deltas in protected low-wave energy environments. Sediments are fine-grained and intertidal life is abundant.

LIST OF TABLES

- Table 1. Shoreline morphology - Kenai Peninsula to Montague Island.
- Table 2. Oil spill vulnerability index, Kenai Peninsula and Montague Island.

- I. Abstract. This report discusses the results of an extensive study of the geomorphology, sedimentology, and oil spill vulnerability of the outer Kenai Peninsula and Montague Island shorelines. Major emphasis is placed on the application of an Oil Spill Vulnerability Index (O.S.V.I.). Large segments of the shoreline are high risk environments with respect to oil spill residence time. Nearly 60% of the study area falls into O.S.V.I. classes 6-10, which indicates any oil spilled would have residence times from one to more than ten years. The remaining 40% of shoreline falls into classes 1-5, which are considerably lower risk areas. Any oil spilled in these environments would be cleaned by natural processes quite rapidly.
- II. Task Objectives. This project falls under Task D-4 which is to: evaluate present rates of change in coastal morphology, with particular emphasis on rates and patterns of man-induced changes, and locate areas where coastal morphology is likely to be changed by man's activities, if any. The relative susceptibility of different coastal areas will be evaluated, especially with regard to potential oil spill impacts.
- III. Field and Laboratory Activities. Included in the body of this report.
- IV. Results. The results have been summarized in the text of this report as well as on the set of basemaps included in the Appendix. The original set of basemaps is being sent under separate cover.
- V. Preliminary Interpretations. Does not apply.
- VI. Auxiliary Material. Original set of 31 U.S.G.S. Quadrangle maps with the number coded Oil Spill Vulnerability Index.
- VII. Problems Encountered. None.

[The page contains a large, faint watermark or bleed-through from the reverse side, which is illegible.]

INTRODUCTION

This report contains the results of an extensive field and laboratory study of the coastal region from the westernmost tip of Kenai Peninsula to Montague Island, approximately 2157 km of shoreline (Fig. 1). The purpose of the investigation was to describe the morphology and sedimentology of the coastline and delineate the vulnerability of the area to massive oil spills. This work was done to aid any agency charged with the responsibility of handling a massive crude oil spill in the region. The major emphasis of this report is placed on the application of the Oil Spill Vulnerability Index (O.S.V.I.) to the study area. The O.S.V.I. is a scale which rates a particular type of shoreline's vulnerability to oil based on the residence time of oil in that particular environment. The O.S.V.I. ranges from 1, for coastlines having the lowest vulnerability, to 10 for coastlines that are the most vulnerable to oil spills (see section on Oil Spill Vulnerability).

Included with this report are 31 standard United States Geological Survey Quadrangle Maps with O.S.V.I. classes labelled for the entire study area. Reductions of these maps are found in Appendix I. Also included in the Appendices are a list of all survey stations visited and the tasks completed, reproductions of all beach profiles run, and summary statistics on all grain size analysis.

This is our final report for the project entitled "Oil Spill Vulnerability, Coastal Morphology and Sedimentation of the Outer Kenai Peninsula and Montague Island."

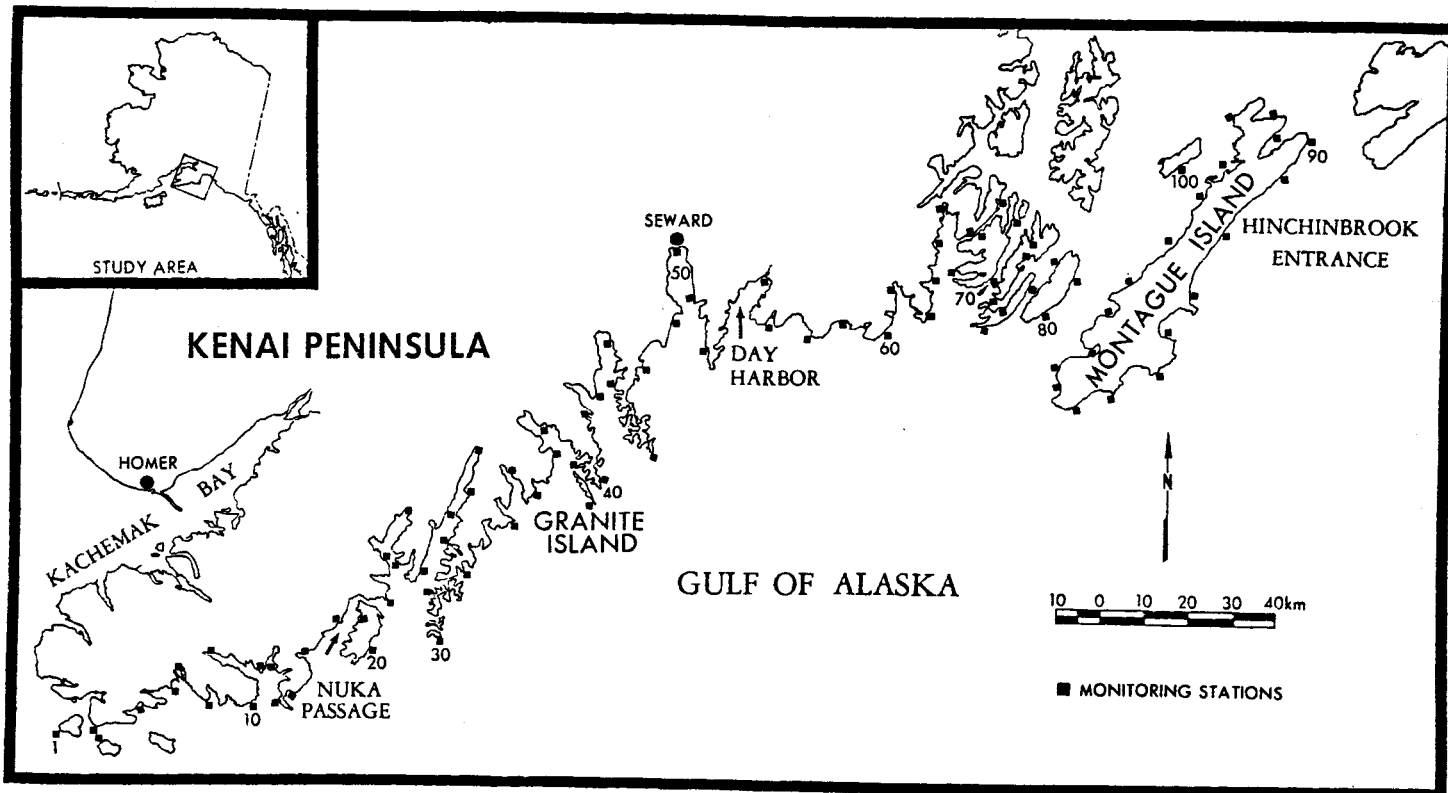


Figure 1. Map showing the location of the 100 stations monitored for this report along the outer Kenai Peninsula and Montague Island. Every 10th station is numbered. The index map (upper left) shows the relative location of the study area within southeastern Alaska.

GEOMORPHIC SETTING

General

The study area consists of 2157 km of shoreline bordering the Gulf of Alaska and Prince William Sound in south-central Alaska (Fig. 1). The area extends northeast from Elizabeth Island at the mouth of Cook Inlet to Hinchbrook Pass and includes: (a) the southern part of the Kenai Peninsula coastline fronting the Gulf of Alaska; (b) the coastlines of Bainbridge, Evans, Elrington, Fleming, and Latouche Islands in the southeastern tip of the outer Kenai Peninsula; and (c) Montague and Green Islands coastlines in the southwestern part of Prince William Sound. Resurrection Bay and the town of Seward provide a precise geographic center for the area of investigation, dividing it into two halves of almost equal shoreline length. Seward is the only town in the study area with a year-round populace. The entire region is largely pristine and incredibly beautiful with only a minimal man-induced impact of the environment.

Outer Kenai Peninsula

The Kenai Peninsula is divided into two major physiographic units. The northern half of the peninsula is a region of rolling lowlands that border Cook Inlet. The southern or seaward-facing portion of the peninsula is comprised of the rugged Kenai-Chugach Mountains. The Kenai Mountains are underlain by rocks of Mesozoic age and form a ria type shoreline made up of deep embayments flanked by sheer rock cliffs. This section of the coast comprises roughly four-fifths of the study area. The region is cut extensively by streams and several large glaciers whose related moraines and outwash features are relatively abundant.

High segments of the Kenai-Chugach Mountains are dominated by east-trending ridges, 2,100 to 4,000 m high. Lower segments consist of discrete massive mountains from 1,000 to 1,800 m high, separated by a system of valleys and passes 1 to 2 km wide that have eroded along joints and bedding planes (Wahrhaftig, 1965). Such jointing and bedding patterns can play an important role in the bedrock control of shoreline orientation. The entire mountain range has been heavily glaciated. Many areas along the outer Kenai Peninsula are dominated by horns, aretes, cirques and U-shaped valleys.

Southwestern Prince William Sound

Montague Island is the largest and most southerly of five long narrow islands that trend northeast across the south side of Prince William Sound (Fig. 1). The island, which is 82 km long by 6 to 20 km wide, consists of a mountainous backbone ridge with an average summit altitude of 730 m and a maximum altitude of 866 m (Plafker, 1971). The other four islands, Latouche, Elrington, Evans, and Bainbridge, vary from 18 to 26 km in length and 2.5 to 7.2 km in width. They are also topographically lower with average summit elevations of roughly 300 m.

Bainbridge, Evans and Elrington Islands all have highly irregular shorelines dominated by large, deep, fjord-type embayments. The islands are separated by long, narrow, quiet water passages typical of a ria type of coastline. Montague and Latouche Islands display similar trends in coastal morphology. Both islands are more regular in outline with a dominance of erosional coastal features on their eastern shorelines. High vertical bedrock scarps and wave-cut platforms are especially prominent on the eastern and southern shorelines of Montague Island. Shallow, quiet water coves, small bays, tidal flats and fine- to coarse-grained sand beaches typify the more depositional western shorelines of Montague and LaTouche Islands. Unlike the outer Kenai Peninsula, the shorelines of these five

mountainous islands have only a very minor contribution from glacially derived sediments. The dominant control on the shoreline morphology of the Prince William Sound Islands is the active tectonic uplift in the area.

TECTONIC SETTING

Regional

The entire study area is underlain by rocks that are part of an extensive arcuate belt of thick Mesozoic and Tertiary marine deposits that extend through the Chugach-Kenai-Kodiak Mountains (Fig. 2). In terms of their tectonic settings, the outer Kenai Peninsula and Montague Island shorelines are examples of young mountain range coasts (Hayes, 1964), or continental collision coasts (Inman and Nordstrom, 1971; Davies, 1973). Rapid tectonic uplift related to Cenozoic orogenic activity typifies this type of shoreline. The coastline is characterized by high rugged cliffs and a narrow continental shelf.

The outer Kenai Peninsula and Prince William Sound areas have undergone tectonic change for millions of years. Broad areas of wave-cut platforms in the eastern half of the study area (uplift) and numerous drowned glacial valleys (downwarp) in the western part are common. It is obvious that tectonics plays a major role in the formation and modification of the island and peninsular shorelines both in the long-term geologic sense and on a much shorter historical time scale.

Earthquake Activity

Sudden, often violent, earthquake activity is associated with continental collision coasts and can exert a strong influence on local morphology and shoreline orientation. This fact was documented within the study area by the sudden tectonic movements, both vertical and horizontal,

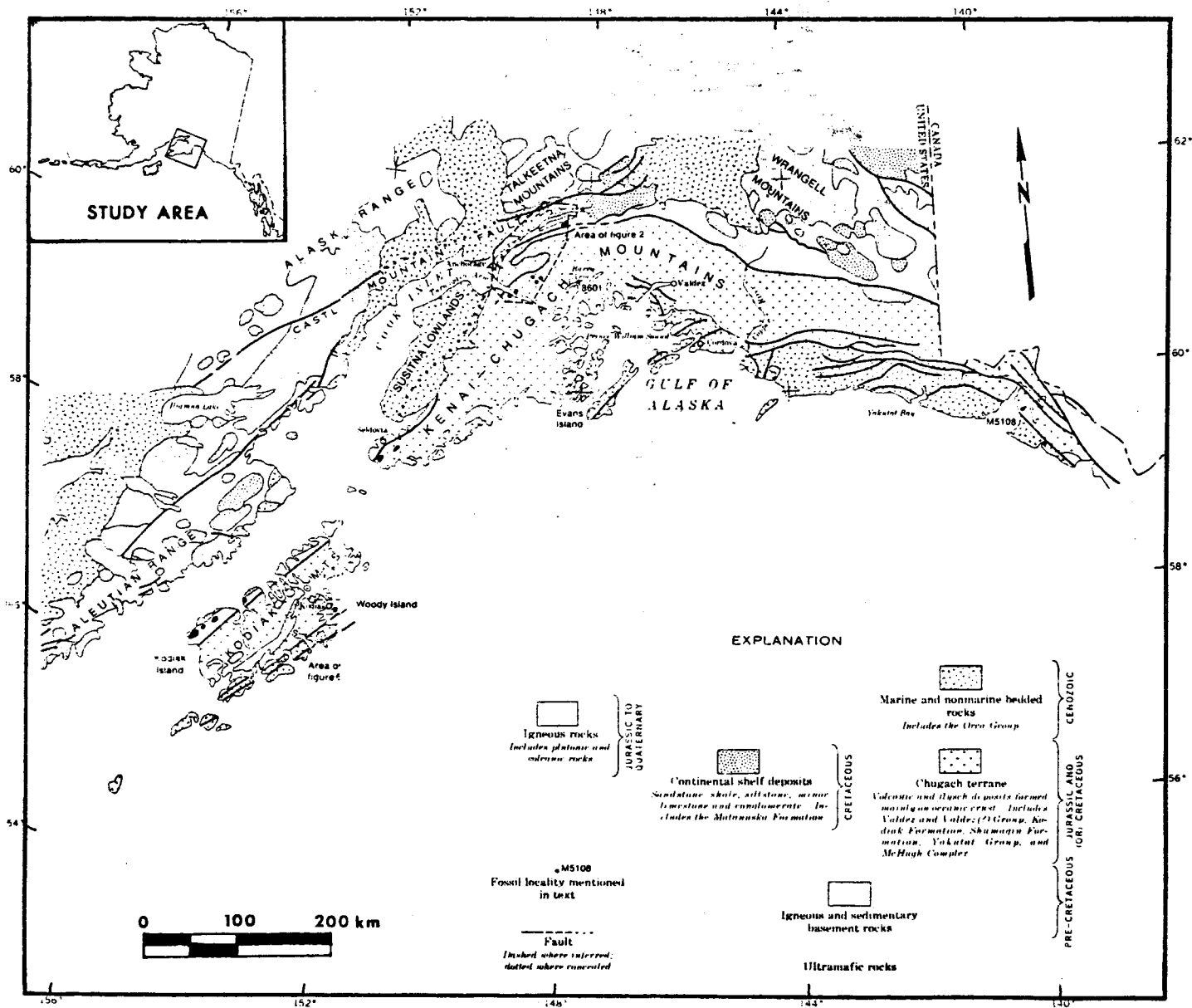


Figure 2. Structural setting and tectonic framework of the Kenai Peninsula and Montague Island within the southern Alaska island arc system (King, 1969; modified from Jones and Clark, 1973).

associated with the 1964 Good Friday Earthquake. Regional deformation produced by this earthquake occurred over an area of at least 112,000 square kilometers in south central Alaska from Kodiak Island to Prince William Sound. The study area for this report lies entirely within this area. Evidence of this tectonic activity is a major zone of uplift to the northeast of Day Harbor (Fig. 3) and a major zone of subsidence to the southwest of Day Harbor.

The zone of subsidence includes most of Kodiak Island, Cook Inlet and roughly four-fifths of the outer Kenai Peninsula. The axis of maximum subsidence within this zone trends northeast along the crest of the Kodiak-Kenai-Chugach Mountains intersecting the study area along the western margin of Nuka Island (Fig. 3). A maximum downwarp of 2.3 m was recorded on the southwest coast of the Kenai Peninsula (Plafker, 1971). Montague Island lies within the 1964 earthquake focal region and is along the axis of maximum tectonic uplift (Fig. 3). Surface faulting and regional warping produced by the earthquake elevated the southwestern end of the island by as much as 11.5 m (Plafker, 1971). Southwest of Montague Island, the nearshore shelf may have been uplifted more than 15 m based on pre- and post-earthquake bottom soundings (Malloy and Merrill, 1971).

Kenai Peninsula and Montague Island have undergone tectonic change (both uplift and submergence) for millions of years. Geologic data (Plafker, 1966) indicates that the 1964 earthquake-related movements were but the most recent pulse in an episode of deformation that probably began in late Pliocene time and continued intermittently to the present.

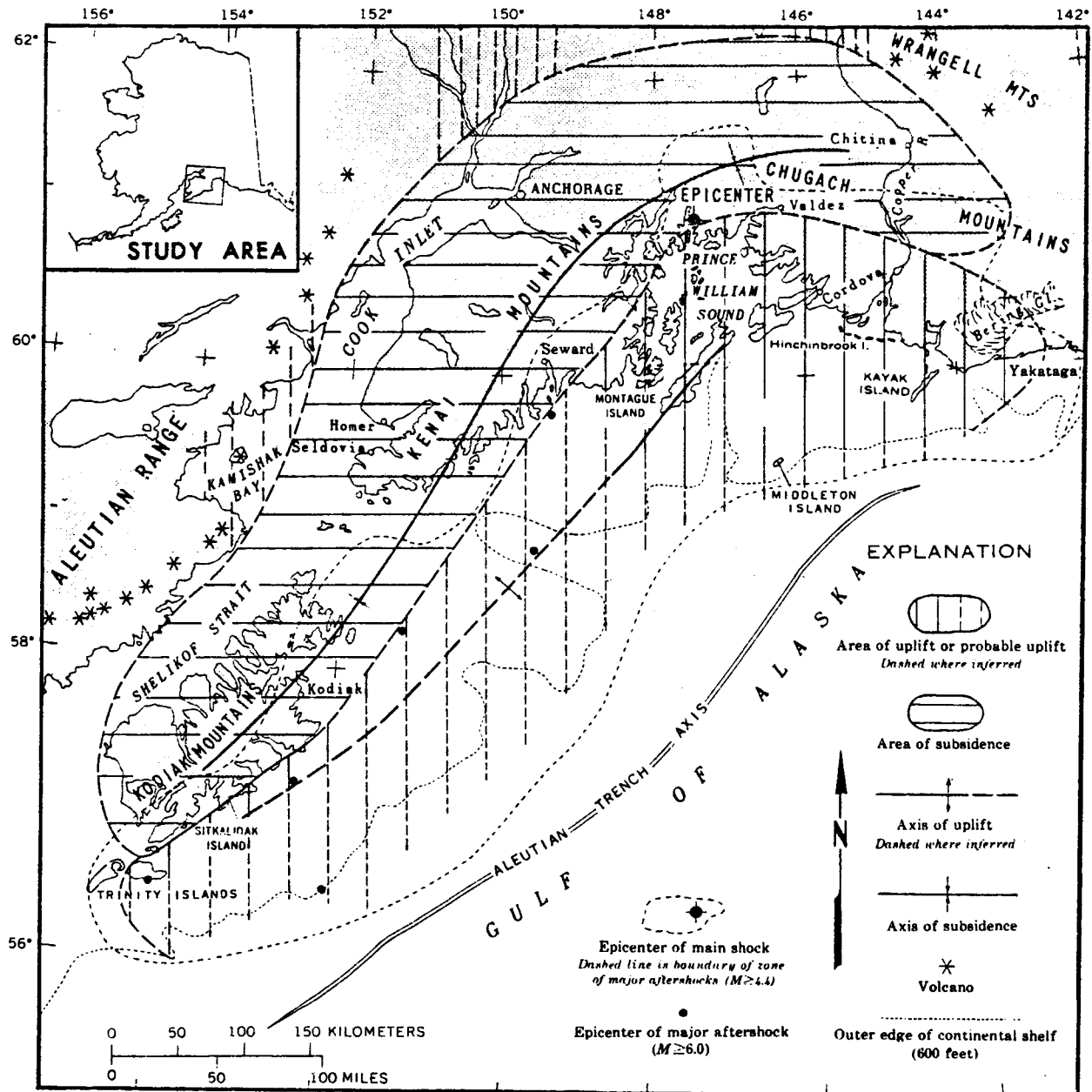


Figure 3. Regional setting of the Kenai Peninsula and Montague Island with respect to tectonic deformation and seismicity that accompanied the March 27 "Good Friday" earthquake, 1964. Note that the axis of maximum uplift parallels the eastern shoreline of Montague Island, while the axis of subsidence intersects the study area at Nuka Passage (stations 17-18; see Fig. 1 for locations). (From Plafker, 1966).

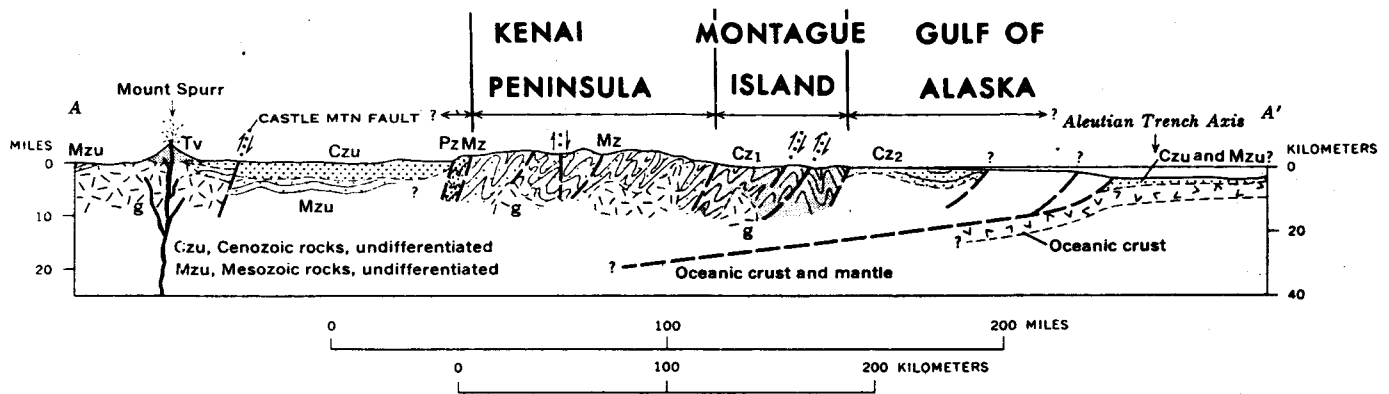
GEOLOGIC SETTING

Regional

The Kenai Peninsula and western Prince William Sound Islands are located within the central margin of the continuous Kodiak-Kenai-Chugach mountain belt (Fig. 2). The Kenai-Chugach Mountains are composed chiefly of dark-gray metasandstone, slate and argillite of Mesozoic and Tertiary age (Plafker, 1966; Wahrhaftig, 1966). The main mass of the mountains is primarily Jurassic and Cretaceous bedded rocks with a narrow, discontinuously exposed section of older rocks along the northern flanks (Clark, 1972). Almost all of the rocks in the Kenai Mountains are mildly metamorphosed and cut in a few places along the southern peninsular coast by granitoid masses. Montague and other Prince William Sound islands contain large bodies of greenstone in association with the argillite and greywacke.

Lithologies

The geologic units in the Kenai Peninsula and Prince William Sound areas shown in Figure 2 include: 1) the Valdez Group, a sequence of eugeosynclinal rocks that comprise the vast majority of the outer Kenai Peninsula; 2) the Orca Group, a sequence of early Tertiary age rocks which can be divided into a lower volcanic unit and an upper sedimentary unit (Case *et al.*, 1966). Elrington, Evans, Latouche, Green, Montague and the eastern half of Bainbridge Islands are all comprised of rocks from the Orca Group (Fig. 2). These rocks are faulted into contact with the Valdez Group of the outer Kenai Peninsula along a north-south line that divides Bainbridge Island into two halves (Fig. 4); 3) bodies of intrusive granitic rocks found within the Valdez Group along the outer Kenai Peninsula in the vicinity of Granite Island (Figs. 2 and 4); 4) unconsolidated sediments and marine deposits of Quaternary age. These are the sediments that comprise the beaches, spits,



EXPLANATION

-  Andesitic extrusive rocks of active or dormant volcanoes
-  Late Cenozoic bedded rocks
Lighter pattern where projected offshore
-  Early Cenozoic bedded rocks
Lighter pattern where projected offshore
-  Late Mesozoic bedded rocks
Lighter pattern where projected offshore
-  Paleozoic and early Mesozoic bedded rocks
Lighter pattern where projected offshore
-  Granitic plutonic rocks
-  Undifferentiated rocks

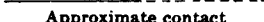
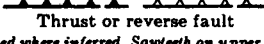
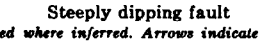
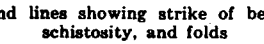
-  Approximate contact
Includes possible fault contacts, Dashed where inferred or concealed
-  Thrust or reverse fault
Dashed where inferred. Sawtooth on upper plate. Open teeth indicate major fault
-  Steeply dipping fault
Dashed where inferred. Arrows indicate relative lateral displacement; bar and ball on relatively downthrown side
-  Trend lines showing strike of bedding, schistosity, and folds

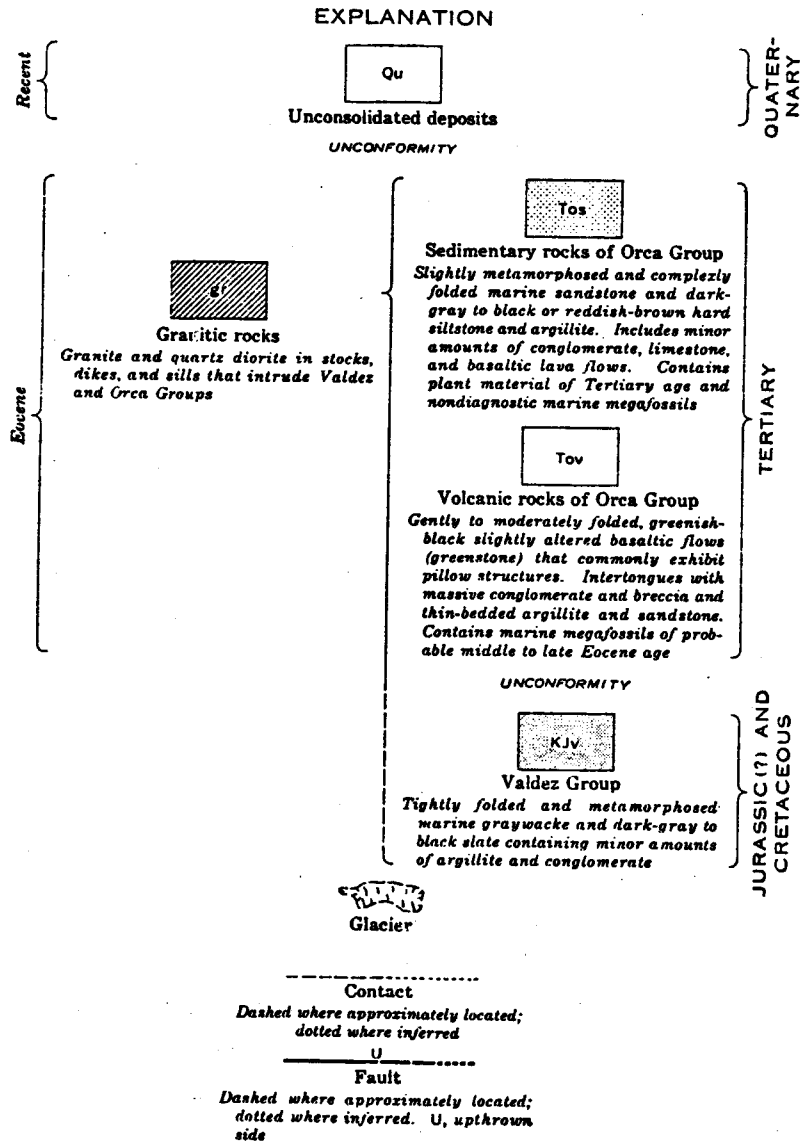
Figure 4. Idealized vertical section through Kenai Peninsula and Montague Island showing selected rock units and structural features of south central Alaska. Note that the structural-tectonic setting is dominated by the subduction of oceanic crust beneath the over-riding continental rocks (collision coast). (After P. B. King, 1969; modified from Plafker, 1966).

and other depositional features in the study area. A more detailed description of the lithologies within these units is given below.

Valdez group. - A thick unit of metasandstone (mostly metagreywacke), metasilstone, and argillite is exposed over four-fifths of the outer Kenai Peninsula (Clark, 1972). Those rocks are part of a belt that extends more than 600 km through the Kenai-Chugach-Kodiak Mountains (Payne, 1955; Burk, 1965; Moore, 1971). The sequence is characterized by thin to thick beds of light-grey or tan, poorly-sorted sandstone of greywacke type interbedded by dark-grey to black argillite and slate (Case et al., 1966). The Valdez Group is a widespread flysch sequence that in some areas retains sedimentary features associated with turbidites (Clark, 1972).

Orca group. - The predominantly volcanic unit that forms the lower part of the Orca Group crops out in a discontinuous belt within the study area on Elrington, Evans and Bainbridge Islands (Fig. 5). This unit consists of altered, green-black basaltic lava flows, pillow lavas, flow breccias, and coarser textured diabase intrusives collectively termed "greenstone" (Case et al., 1966). This volcanic unit is of Tertiary (probably mid to late Eocene) age (Plafker and MacNeil, 1966).

The sedimentary unit that comprises the upper part of the Orca Group includes the rocks that occur on all of Montague, Green and Latouche Islands and most of Evans, Elrington and Bainbridge Islands (Fig. 5). The sequence consists mainly of thin to thick beds of greywacke sandstone and minor amounts of light-colored arkosic, carbonaceous, tuffaceous, calcareous and conglomeratic sandstones (Case et al., 1966). The unit is distinguished from the Valdez Group by a more variable lithology and slighter degree of metamorphism.



Explanation for Figure 5.

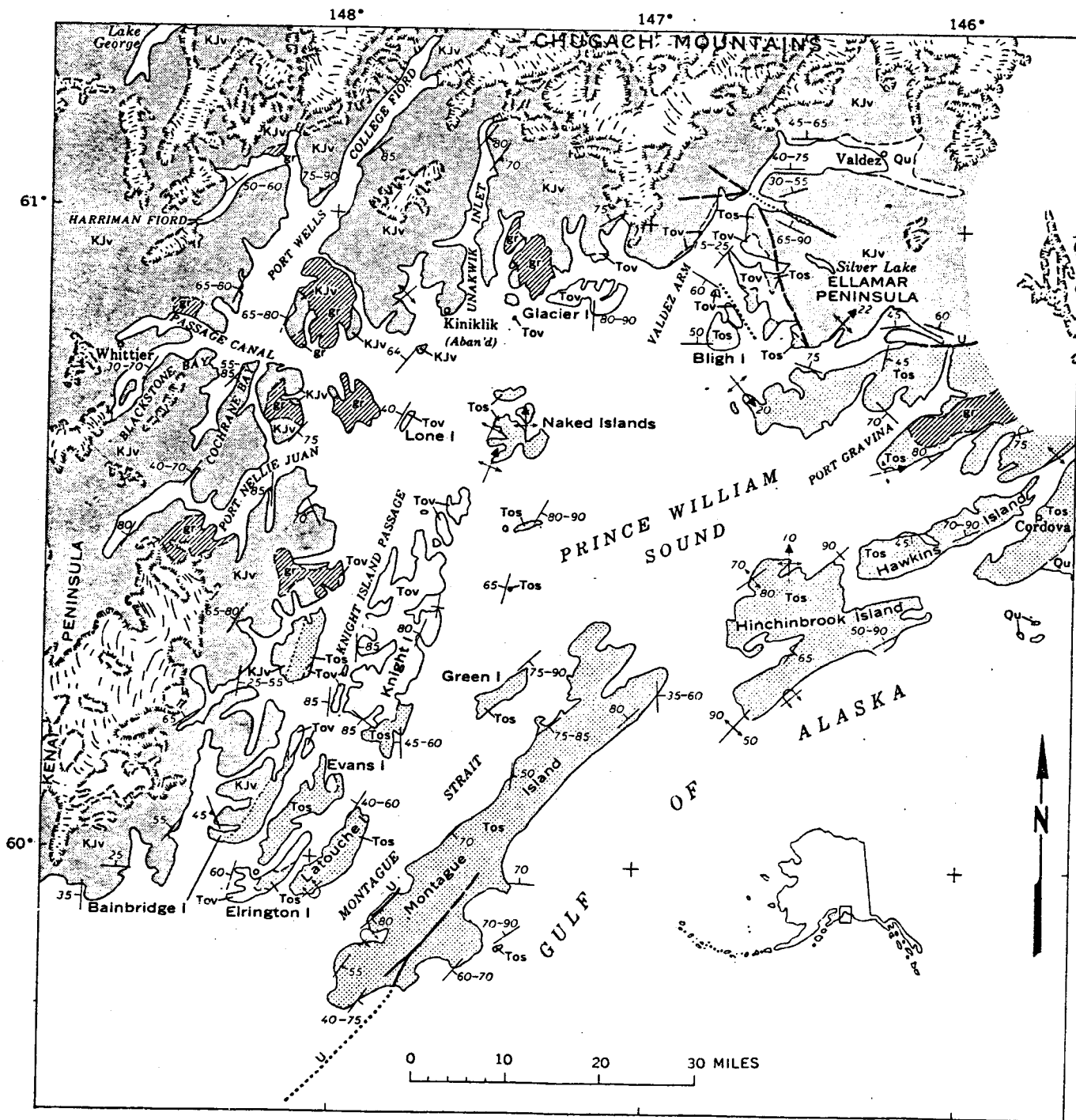


Figure 5. Generalized geologic map of the Prince William Sound region, southeastern Alaska. Note the sharp break in bedrock lithologies from the easternmost Kenai Peninsula (KJv) to Evans, Elrington, Latouche and Montague Islands (Tov and Tos). The nature and composition of bedrock can play a very important role in shoreline orientation and morphology (From Case *et al.*, 1966)

Intrusives. - Granitic rocks intrude the Valdez Group within the study area in the vicinity of Granite Island (Fig. 2). The intrusive rocks are highly resistant to weathering and marine erosion, producing highly irregular trends in shoreline orientation. These rocks consist mainly of pinkish-gray biotite granite and quartz diorite (Clark, 1972).

Unconsolidated sediments. - Flat lying fluvial, glacial and marine deposits of gravel, sand and mud overlie the Mesozoic and Tertiary rocks in the study area. These sediments comprise all the depositional features discussed in this report.

Bedrock Influences on Shoreline Morphology

The structure and lithology of the bedrock along a section of shoreline can play a major role in the weathering patterns and orientation of the coast. In their study of Kodiak Island, Ruby et al. (1979) made the following observations on the bedrock compositional and structural control of beach morphology:

Highly bedded rock types like slates and shales can form a variety of scarp configurations, dependent on the dip of the bedding planes. Where bedding planes are nearly horizontal, the scarps will be very irregular and wave-cut platforms will be quite flat and uniform. If the bedding planes are near vertical, the scarps will be uniform and wall-like, broken and displaced by fracture and fault patterns, while associated wave-cut platforms will be very irregular containing numerous tidal pools. Bedding planes dipping from near vertical to about 50 or 60° will often result in a dip-slope scarp. These scarps are flat and slope downward at the angle of dip of the bedding. Dips from 50° to about 20° will usually result in an irregular scarp and an irregular wave-cut platform.

Bedded rock types yield platy fragments to the beachface. Thus, gravels, cobbles and boulders will generally be flat regardless of their degree of rounding. Very well rounded gravels will look like discs and are referred to as discoidal gravels.

Unbedded rock species like quartz diorite have a more uniform strength and thus the shape of scarps and wave-cut platforms becomes a function of fracture and fault patterns in the rock rather than their own internal structure. The scarps usually appear rather massive and rather steep. The wave-cut platforms

at their base are moderately uniform with undulatory surfaces and scattered tidal pools. Gravels and boulders of this rock type will usually be equant in shape regardless of the degree of rounding. Well rounded gravels will be spherical.

Slate and quartz diorite are two end members of rock species which control scarp and platform shapes as well as gravel shapes. Most other rock types will fall behaviorally somewhere between them. Thus, scarps, platforms and beach sediment can take an extremely wide variety of shapes.

OCEANOGRAPHIC AND METEOROLOGIC SETTING

Tides

The Kenai Peninsula to Montague Island coastline has semi-diurnal tides with a strong diurnal component. Mean tidal ranges, recorded in the Climatic Atlas of the Outer Continental Shelf Waters and Coastal Regions of Alaska, Volume 1 (1977), vary from 2.4 meters at the eastern limit of the study area (Patton Bay, Montague Island) to 3.2 meters at the western limit of the study area (Picnic Harbor, Rocky Bay). There is some amplification of tidal ranges within the embayments, but this is limited due to the relative deepness of most of the fjords.

Wind and Wave Regime

The positioning of two major fronts, the Pacific Polar and Pacific Arctic fronts, largely govern the wind patterns and resultant wave energy flux of southeastern Alaska (Hayes et al., 1976). The high frequency and intensity of storms produced by both of these fronts make the maritime region of the Gulf of Alaska the most severe cyclogenetic region (during winter) in the Northern Hemisphere (Petterssen, 1969). During the summer, cyclonic activity decreases markedly, and storms are of less intensity. Wind and wave data taken from the 1970 Survey of Synoptic Meteorological Observations (SSMO) and the Climatic Atlas of the Outer Continental Shelf Waters and Coastal Regions of Alaska, Volume I (1977) indicate a prevailing

and predominant wind frequency distribution out of both the east and west (Fig. 6). The average wind regime for the Gulf of Alaska over a seven year period from 1963 to 1970 demonstrates that both dominant and prevailing winds are aligned with the general trend of the shoreline (Nummedal and Stephens, 1976). In some instances, fjords generate local wind systems, especially near their heads. They are usually backed by relatively high mountains which can generate catabatic winds which blow downslope toward the mouth of the fjord.

The combination of wind frequency distribution with observed wave heights and periods (SSMO data) provides a wave energy flux value which can be directly related to longshore sediment transport rates (Coastal Engineering Research Center, 1973). The resultant wave energy flux vector for the study area (Seward data square) points northeast. The direction of this vector should correspond to the direction of net coarse sediment transport on adjacent exposed beaches. In the Gulf of Alaska, calculations show a convergence of wave energy toward Montague Island and Prince William Sound (Nummedal and Stephens, 1976). The Seward data square contains the highest average annual wave energy flux value among those computed for the Gulf of Alaska (Nummedal and Stephens, 1978). These values range from 1.5 to 5.7×10^{10} ergs/m sec (Fig. 6).

Ocean bathymetry rapidly deepens off the coastline within both the Gulf of Alaska and the numerous fjords along the outer coast of the Kenai Peninsula. Depths of 120 to 300 m are common within one kilometer of the shoreline. There is tremendous variability in relative wave energy from one area to another. This is due to the variable fetch distance as well as the orientation of the shoreline with respect to incoming waves.

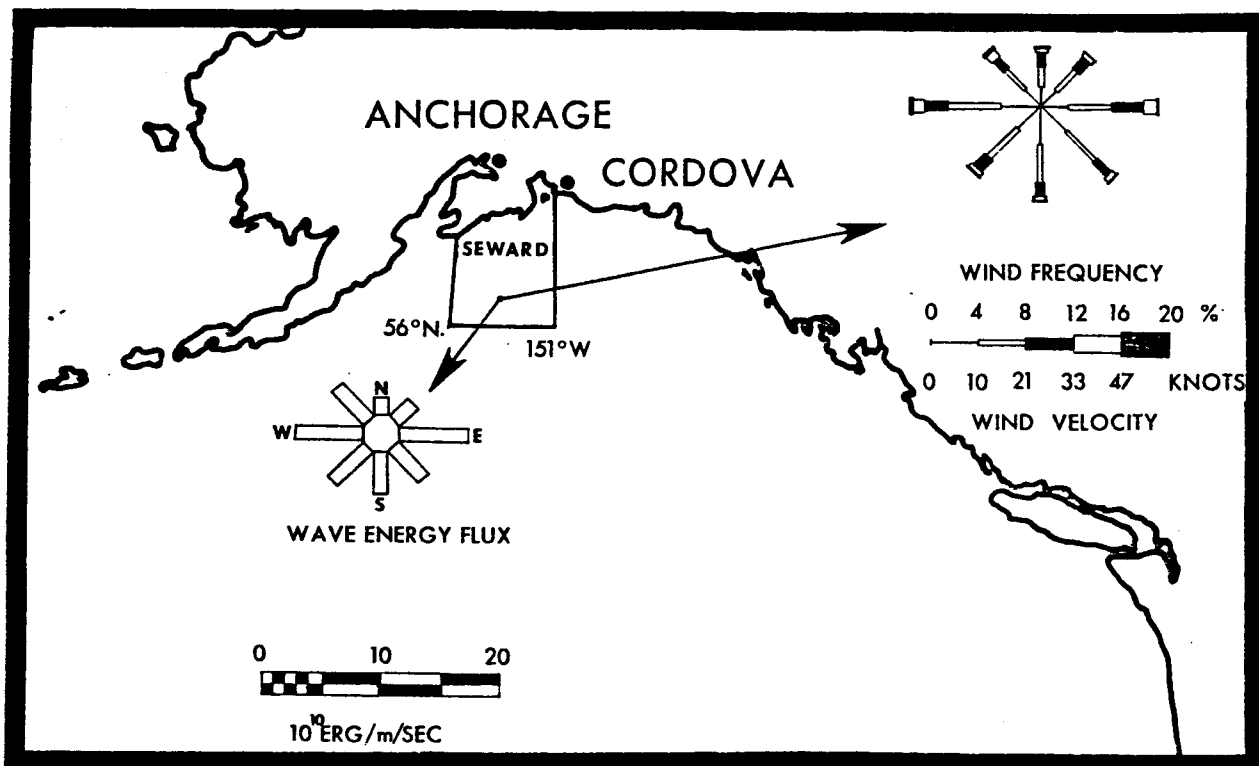


Figure 6. Wind frequency and wave energy flux distributions taken from SSMO data (1970) for the Seward square in southeastern Alaska. Note the difference of winds out of the east and west and resultant wave energy flux (from Nummedal and Stephen, 1976).

In general, there is a uniform decrease in wave energy as the fjord heads are approached. The exposed shorelines usually have well developed high depositional berms indicative of frequent large storm waves. The more protected fjords have much lower, generally vegetated berms, indicative of lower wave energy. Many of the fjords, as well as the other numerous protected areas on the outer Kenai coastline, have exceptionally low wave energy at their heads.

METHODOLOGY

In order to survey large sections of coastline in a reasonable amount of time, a modified zonal method of field study was utilized. The zonal method was developed by the Coastal Research Division at the University of South Carolina (Hayes et al., 1976). Essentially, the method has the following steps:

1. Preceding field work, aerial photographs, maps and charts of the area and pertinent literature are studied.
2. Field work is begun by an aerial reconnaissance of the study area during which:
 - a. Detailed oblique aerial photos are taken using both color and infra-red film.
 - b. Coastal morphologic features such as beaches, cusped spits, bedrock cliffs, etc., are mapped on 1:63,360 topographic maps.
 - c. Changes in coastal geomorphology, which have taken place since the original topographic mapping, are added to the base maps.
 - d. A detailed description of the general geomorphology and sediments is recorded verbally on tape.

3. Based upon observations made during the aerial reconnaissance, equally spaced survey stations are chosen for more detailed work. For the present study, a 20 km interval was selected.

4. For the remainder of the field work, each station is photographed in detail from the air and, where feasible, visited on the ground.

5. At most of the ground stations, the following is done:

- a. A transit line of the active beach zone is made to delineate beach morphology. These profiles are plotted by computer.
- b. Sediment samples are taken using a 10 cm coring tube in the upper, mid and lower beachface.
- c. A field sketch of each site is made to show surrounding geomorphology and geology and to aid the field observer's perception.
- d. Ground photos of the profile site and sediments are taken.
- e. A tape-recorded description of the site and its surrounding geology, geomorphology, sediments and marine processes is made.

6. Oil spill vulnerability classes are recorded on 1:63,360 topographic maps. This is done in the field to allow questionable areas to be rechecked.

Standard laboratory techniques (settling tube and Ro-tap) are used for determination of the textural qualities of sediment samples collected in the field. All samples are analyzed for composition, grain size, sorting, skewness and kurtosis. The beach profiles are computer plotted and studied to help determine the morphology of the beaches. Aerial and ground photographs are reviewed and catalogued. In many instances, where taking samples is impractical due to the large size of the material, photographs are taken of the sediment (i.e., boulders). Grain size and other textural properties are then determined from the photographs.

COASTAL MORPHOLOGY

General

The Kenai Peninsula to Montague Island coastal region is an extremely diverse area that is strongly influenced by tectonic activity, marine processes and glaciation. Recent tectonic activity has resulted in the study area being divided into distinct morphologic zones. The coastline west of Day Harbor to the western tip of Kenai Peninsula (approximately 1180 km of shoreline or 55% of the total study area) shows dramatic evidence of submergence (Fig. 3). The dominant features in this region are high vertical scarps cut into bedrock which are often fronted by narrow gravel and boulder beaches. There are also numerous pocket beaches located in small (less than 1 to 2 km) indentations in the scarps. Other indicators of submergence found west of Day Harbor are: 1) wave-cut notches into bedrock; 2) dead tree lines along beaches backed by forests; and 3) subtidal bedrock platforms. East of Day Harbor, the coastline shows strong evidence of uplift, especially in the Montague Island area. This 880 km stretch of shoreline (41% of the study area) is characterized by uplifted wave-cut platforms, stranded gravel beaches and infilled lagoons.

The coastline is strongly affected by the wave regime. Areas that are exposed to the open ocean or have a large fetch fronting them are subjected to relatively large waves. These exposed areas typically have high vertical bedrock cliffs (often greater than 100 to 200 m). In more sheltered areas, bedrock scarps tend to have low relief. Sheltered or protected areas have more depositional features such as wide sand and gravel beaches, stream mouth deltas, tidal flats and salt marshes.

Glacial activity has also influenced the coastal morphology. Extensive Pleistocene glaciation cut deep fjords that dominate much of the study area. Present glacial activity, although very limited, locally

supplies a great deal of sediment, forming deltas, tidal flats and large bayhead beaches.

Due to the processes discussed above, the coastline along the outer Kenai Peninsula and Montague Island is dominated by four main morphologic types (Table 1). These include: 1) exposed bedrock shorelines; 2) sheltered bedrock shorelines; 3) beaches; and 4) river mouth delta-tidal flats and salt marsh systems (Table 1). In the following section, each one of these environments and their subenvironments will be discussed and typical examples given.

Exposed Bedrock Shorelines

Bedrock cliffs. - Exposed bedrock cliffs comprise 678 km (31%) of the shoreline. They are most abundant in the western portion of the study area where maximum submergence has occurred. The cliffs range in height from a few to over 250 meters (Fig. 7). Generally, bedrock cliffs directly exposed to large waves have maximum relief. In high energy areas, the cliffs are often fronted by sea stacks and large talus slopes (Fig. 7). Exposed bedrock cliffs in emergent areas may have narrow boulder beaches at their base.

Exposed bedrock cliffs are subjected to wave attack, even at low tide. Consequently, these features will clean themselves in the event of an oil spill within a few weeks. In addition, waves reflect off the vertical scarps and tend to "push" floating oil away from the rocks. Therefore, any oil that may be spilled in a coastal area composed of exposed bedrock cliffs would not remain there for very long. These environments are assigned an O.S.V.I. value of 1, the lowest class (see section on Oil Spill Vulnerability).

Table 1. SHORELINE MORPHOLOGY - KENAI PENINSULA TO MONTAGUE ISLAND

<u>ENVIRONMENT</u>	<u>TOTAL SHORELINE (KM)</u>	<u>% OF TOTAL SHORELINE</u>
I. Exposed Bedrock		
A. Bedrock scarps	678 km	31%
B. Wave-cut platforms	212 km	10%
II. Sheltered Bedrock	529 km	24%
III. Beaches	556 km	26%
A. Continuous linear	Abundant	
B. Pocket	Abundant	
C. Bayhead	Common	
D. Spits	Rare	
E. Uplifted	Rare	
IV. River Mouth Deltas-Tidal Flats Systems	81 km	4%
Tidal Flat-Salt Marsh Systems	<u>101 km</u>	<u>5%</u>
TOTALS	2157 km	100%

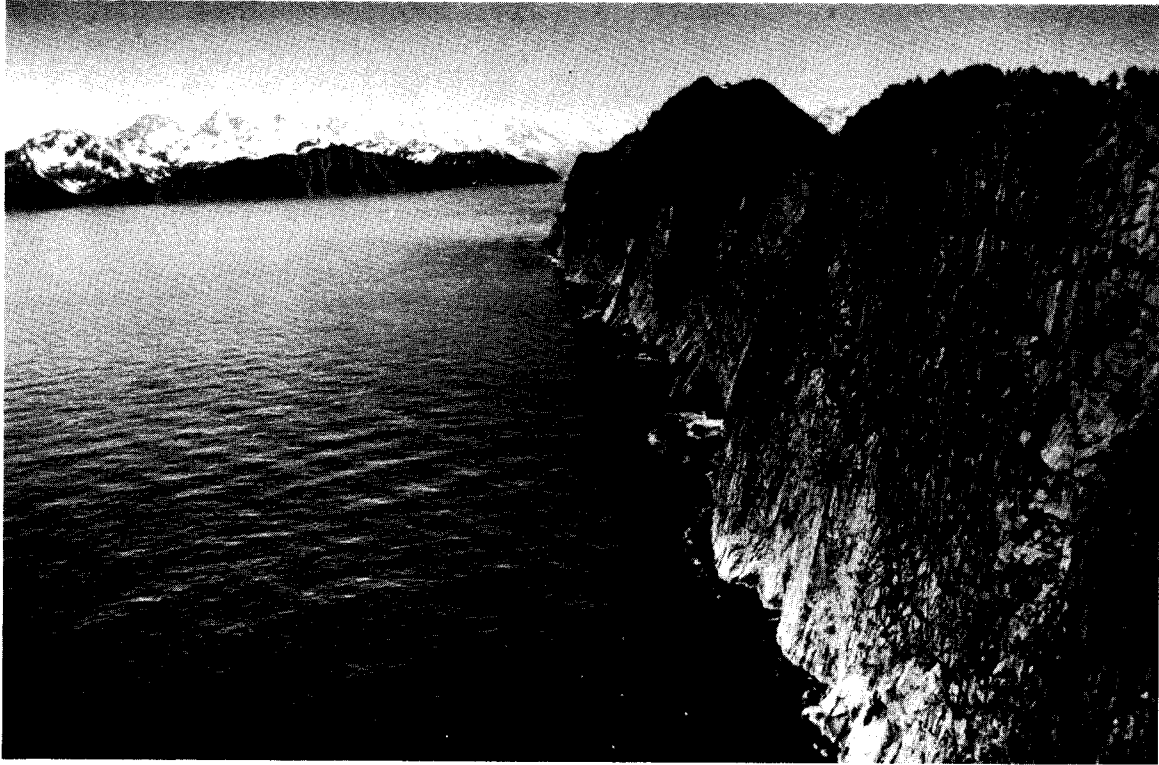
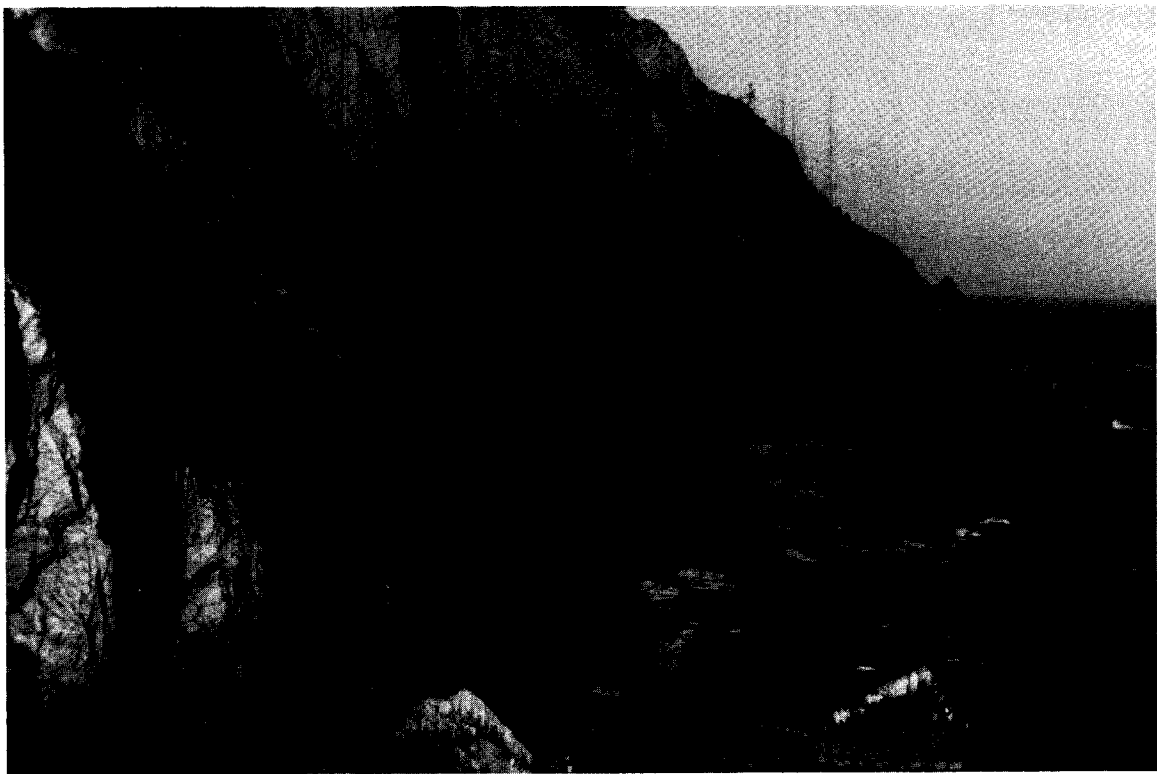
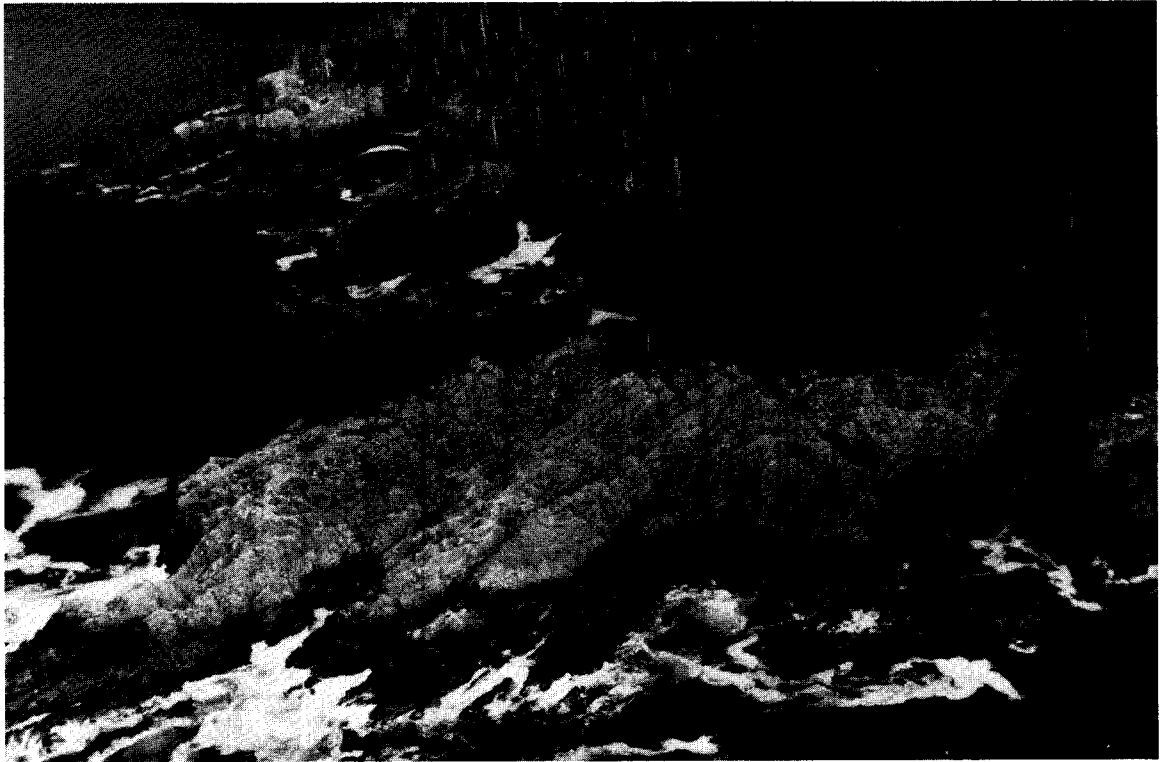


Figure 7. Typical examples of exposed bedrock cliffs. These features are very common within the study area and display extreme variability in slope and relief. The near vertical bedrock cliff shown above (Sta. KNP-39, Granite Island) is over 250 m high. The more gently sloping bedrock cliff at Harrington Point (following page, top) has a relief of only 5-10 meters. In uplifted areas, sediment from avalanche fans and talus slopes form narrow boulder, cobble beaches at the base of the cliff (following page, bottom). Bedrock cliffs are directly exposed to high wave energy. Thus, they are assigned an O.S.V.I. of 1, the lowest class.



Examples of exposed bedrock cliffs are survey station numbers: KNPl, 3, 10, 14, 18, 20, 23, 24, 29, 30, 31, 32, 33, 35, 38, 39, 40, 42, 44, 45, 46, 47, 48, 49, 51, 42, 53, 54, 55, 58, 60, 62, 63, 67, 69, and 84.

Wave-cut platforms. - Wave-cut platforms constitute 212 km (10%) of the study area, being most abundant in locations that have undergone maximum emergence (i.e., Montague Island). Very often, these features are backed by erosional scarps that were uplifted out of wave action. The wave-cut platforms are composed almost entirely of bedrock, but may have a scattering of very coarse, angular gravel and boulders (Fig. 8).

Wave-cut platforms have abundant intertidal life that would suffer from the initial impact of a massive oil spill. Despite this, they are assigned an O.S.V.I. value of 2. Exposure to wave attack causes any oil that may impact one of these areas to be removed relatively quickly. As the O.S.V.I. is based on residence time of the oil, exposed wave-cut platforms are given a low classification.

Examples are survey stations KNP-9, 77, 80, 83, 85, 88, 89, and 90.

Sheltered Bedrock Shorelines

Bedrock cliffs found in sheltered areas (locations that have little or no wave activity) comprise 528 km (25%) of the study area. These scarps typically have an average relief of less than 5 to 10 meters, but may be backed by relatively high, steep vegetated slopes (Fig. 9). Narrow gravel beaches (less than 10 m wide) are often found at the base of the scarps, especially in uplifted areas (Fig. 9). Sheltered rocky shorelines, unlike exposed bedrock shorelines, are assigned a high O.S.V.I. Lack of significant wave energy reduces natural cleansing processes, and any oil that may impact the area would remain for a long period of time. In addition, the relatively coarse nature of the beach sediments often

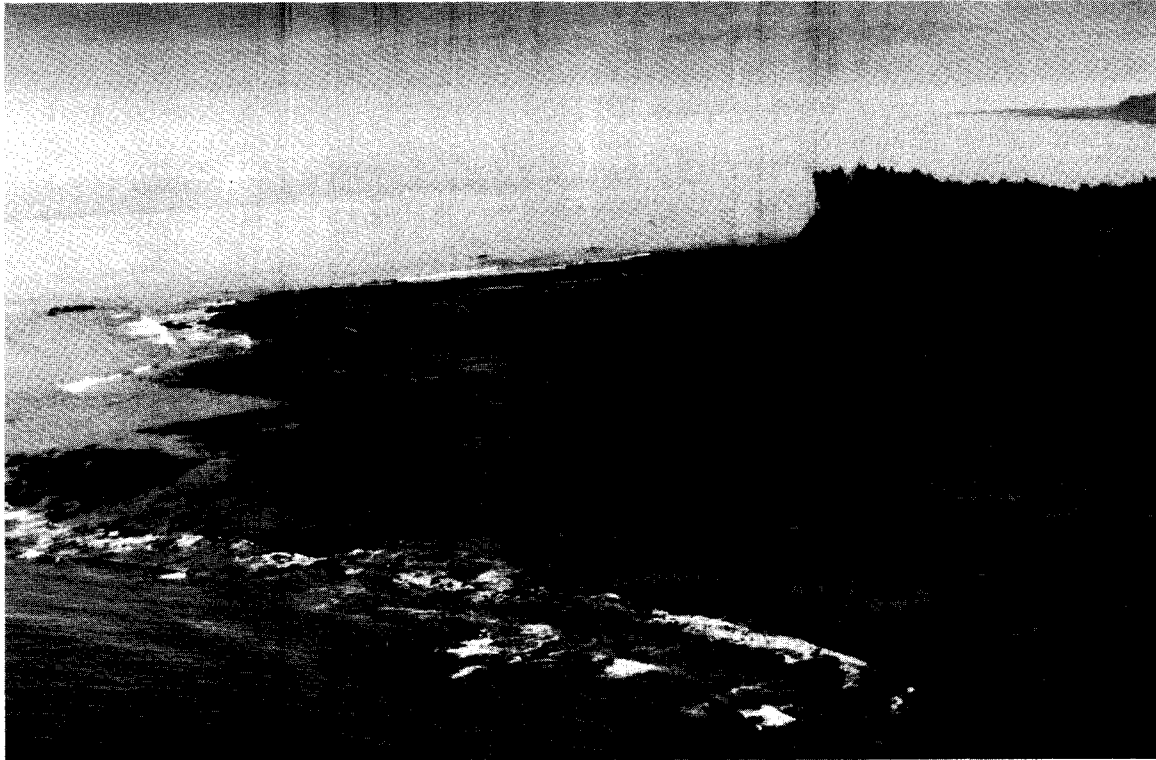
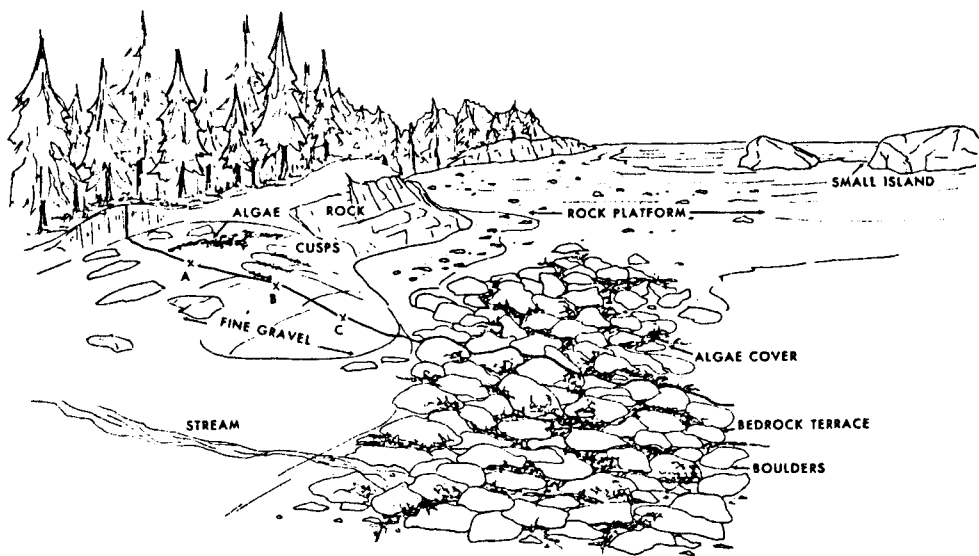


Figure 8. The southwestern end of Montague Island is one of the best examples of an uplifted wave cut platform (above). The features are backed by erosional scarps and composed almost entirely of bedrock. However, they may have a thin, discontinuous scattering of angular gravel and bedrock (following page, top). Rock platforms of this type generally have quite low oil residence times due to their impermeable character and high wave energy. However, as shown in the sketch of station KNP-9 (following page, bottom), the coarse beach face is more sensitive to oil spill impact where a heavy intertidal biota coats the bedrock.



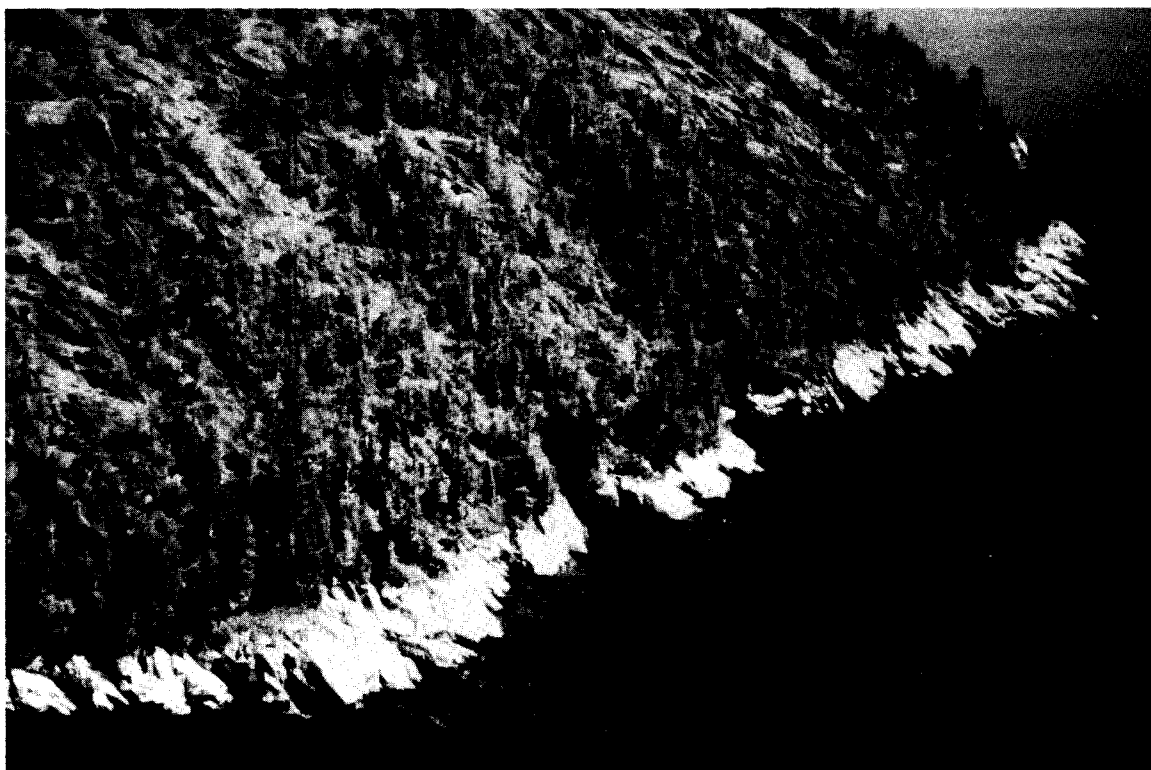
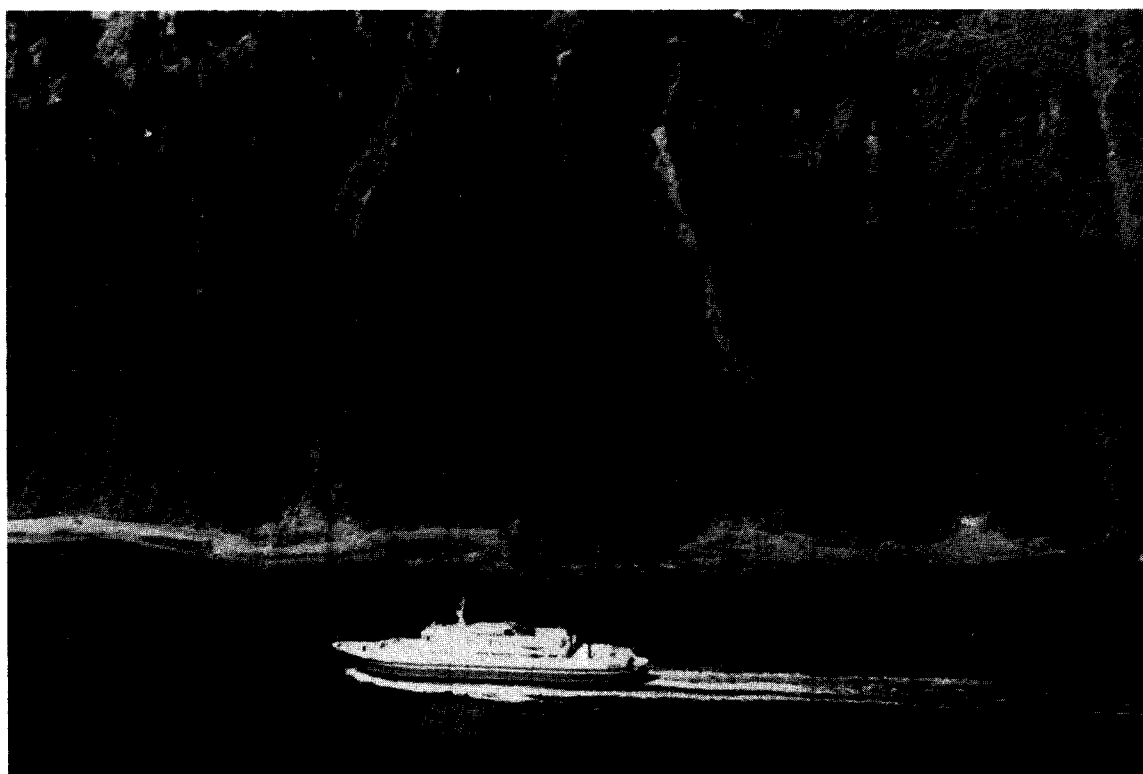


Figure 9. Sheltered bedrock cliffs are found in areas of little or no wave energy and typically have an average relief of only 5-10 m. They are often backed by a steep vegetated slope (Sta. KNP-73, above) or fronted by a narrow gravel beach (KNP-68, below).



associated with these features allows oil to penetrate the substrate, increasing oil retention. The diverse and abundant intertidal life that characterizes these areas would be severely damaged by oil impact. Sheltered bedrock shorelines have an O.S.V.I. of 8.

Examples are survey stations KNP-8, 12, 16, 21, 65, 68 and 72.

Beaches

In total, beach environments comprise 556 km (26%) of the shoreline. There are five morphologically distinct types of beaches commonly found within the study area. They are discussed separately below.

Continuous linear beaches. - These features are extremely common and are the most abundant type of beach in emergent areas. Continuous linear beaches are found fronting sheltered bedrock scarps, glacial till deposits and even high energy exposed scarps in uplifted areas. They normally are narrow, less than 5 to 10 meters wide, but may extend laterally for several kilometers (Fig. 10). Sediment sizes range from gravel in sheltered areas to cobbles and boulders in exposed areas. Continuous linear beaches are assigned O.S.V.I. values of 4, 6, or 7, depending on the texture of the beach. A 4 is assigned to pure sand beaches, 6 to mixed sand and gravel beaches, and 7 to pure gravel beaches. Higher O.S.V.I. values with increasing grain size is due to the relative permeability of the sediments. Normally, coarser sediments have higher permeabilities, increasing the residence time of oil and the O.S.V.I.

Examples are KNP-4, 9, 61, 70, 75, 78 and 79.

Pocket beaches. - Pocket beaches are ubiquitous in the study area, being found in both exposed and sheltered environments. They normally are located in small indentations in the shoreline and are bounded on either end by bedrock scarps (Fig. 11). Sediments are locally derived

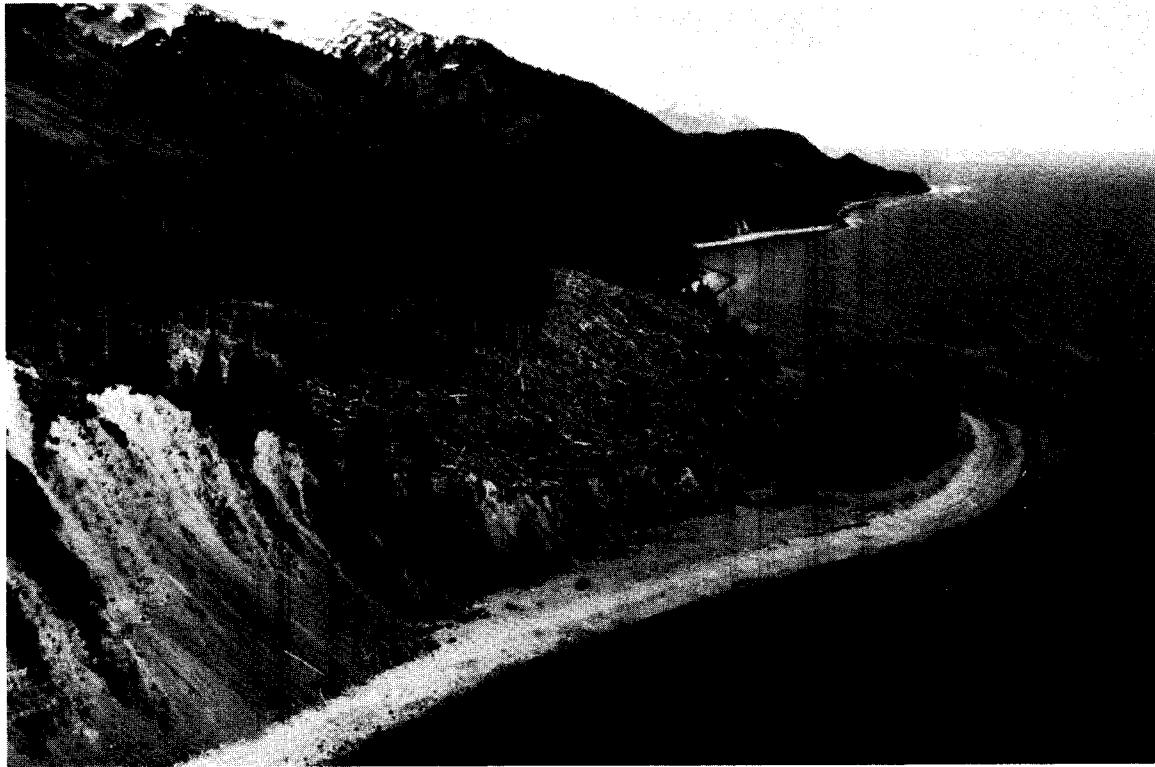
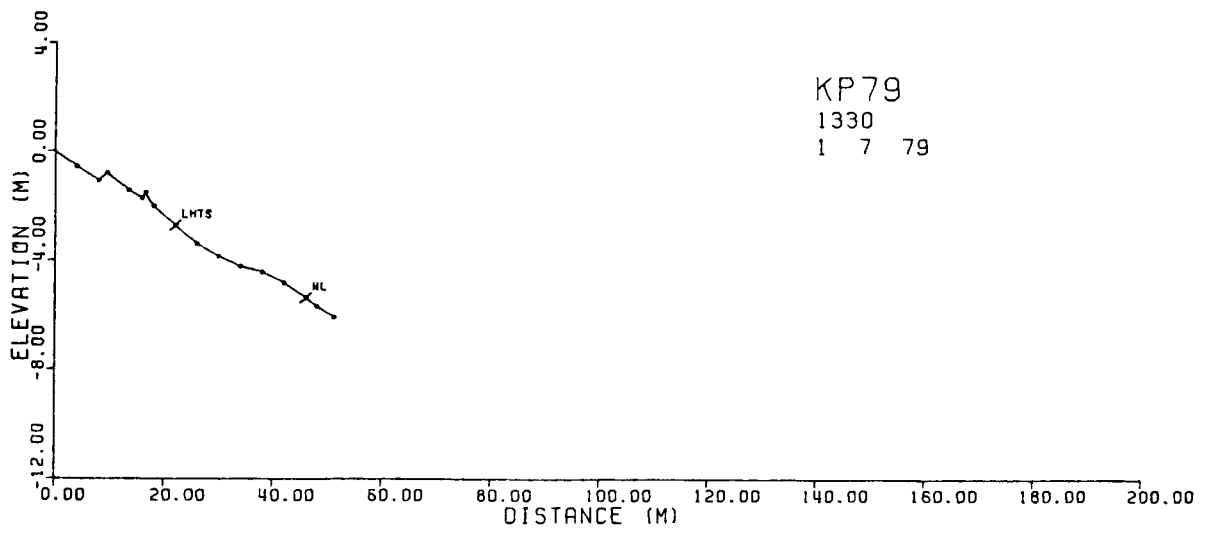


Figure 10. Continuous linear beaches are most common in the uplifted portions of the study area and are found fronting both sheltered and high energy bedrock scarps and glacial till deposits. As shown above, these beaches are normally 5-10 m wide, but may extend laterally for several kilometers. Sediments range from gravel to cobbles and boulders, and are typically angular to subangular (KNP-39, following page, top). The beach profile is narrow and relatively featureless (KNP-79, following page, bottom). Most gravel beaches of this type are classified as O.S.V.I. values 6-8, depending on sediment size and wave energy.



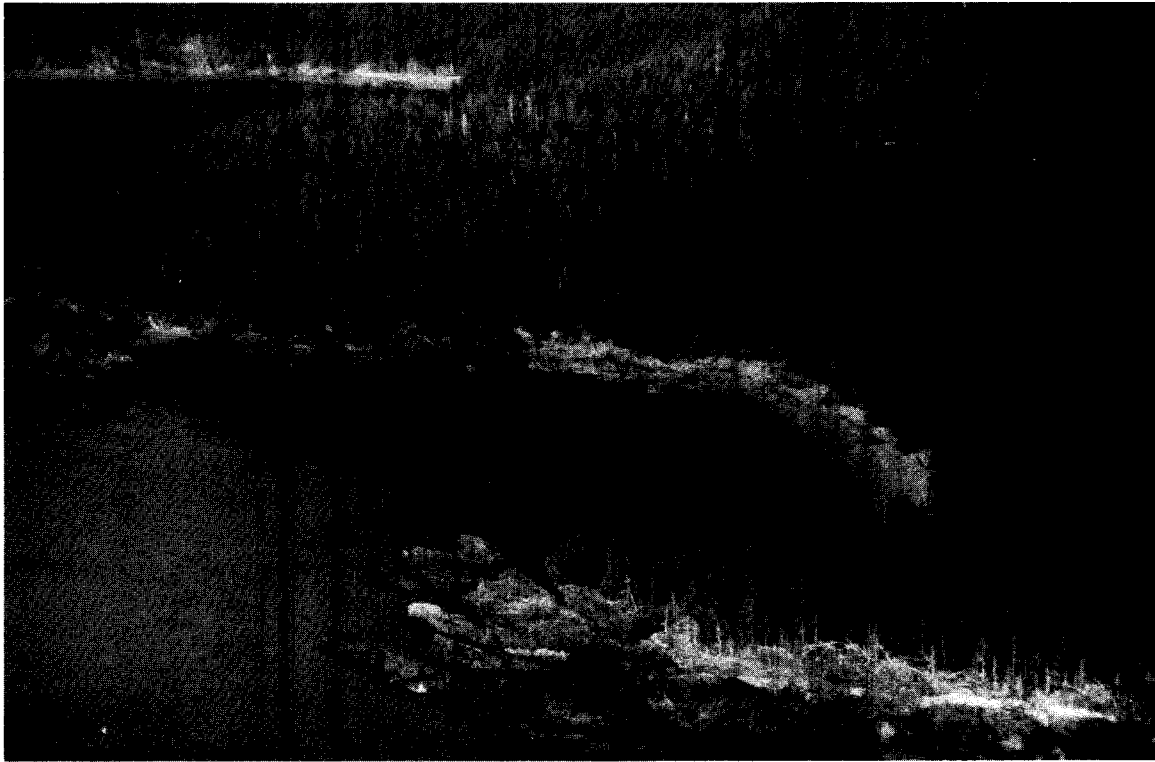
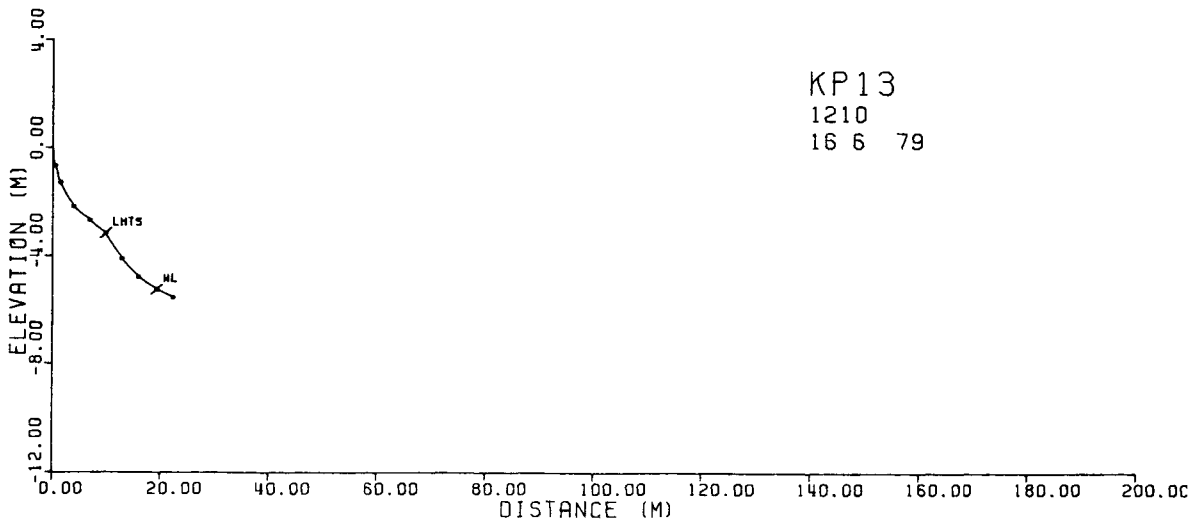
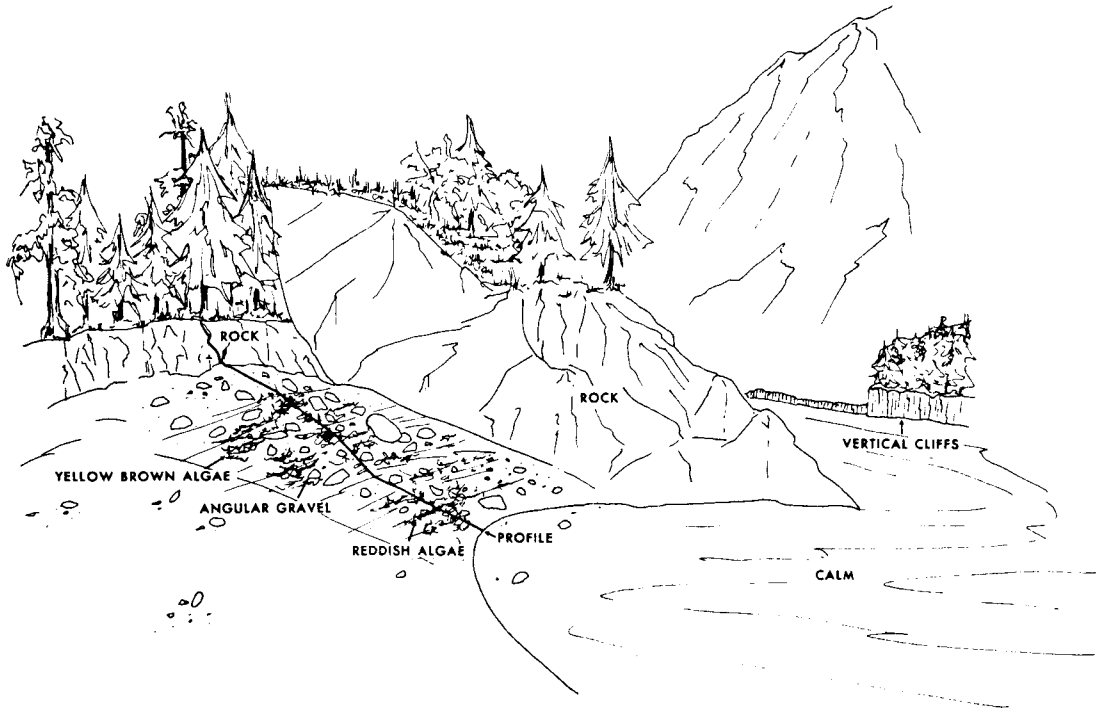


Figure 11. The small pocket beach shown above (Sta. KNP-5) is typical of those found throughout the study area. The sediments are immature and composed of coarse-sand and gravel (KNP-19, below). The sketch and beach profile from Station KNP-13 (following page) shows the narrow, steep nature of the beachface.





from eroding bedrock; consequently, the material is immature and composed of relatively coarse sand and medium gravels.

Pocket beaches are relatively vulnerable to oil spills. The sediment composing these beaches is permeable, allowing oil to penetrate into the substrate. Assigned O.S.V.I. values are 4, 6, and 7.

Examples are survey stations KNP-5, 7, 13, 15 and 19.

Bayhead beaches. - These beaches are commonly found at the heads of many of the shoreline embayments. They are arcuate-shaped features that are relatively wide (30 to 50 meters) and long (Fig. 12). Sediments are mostly sand and gravel. Bayhead beaches are moderately vulnerable to oil spills, again, due to their relatively high permeability, allowing oil to penetrate the substrate. Assigned O.S.V.I. values are 4, 6, or 7.

Examples are survey stations KNP-41, 56, 59 and 64.

Spits. - Two types of spits are occasionally found in the study area. Cuspate spits (Fig. 13) are found in the numerous passageways between islands. Recurved spits are rare, but are typically found at the entrance to lagoons (Fig. 14). Both cuspate and recurved spit beaches are composed of sand and gravel. O.S.V.I. values are 4, 6 or 7.

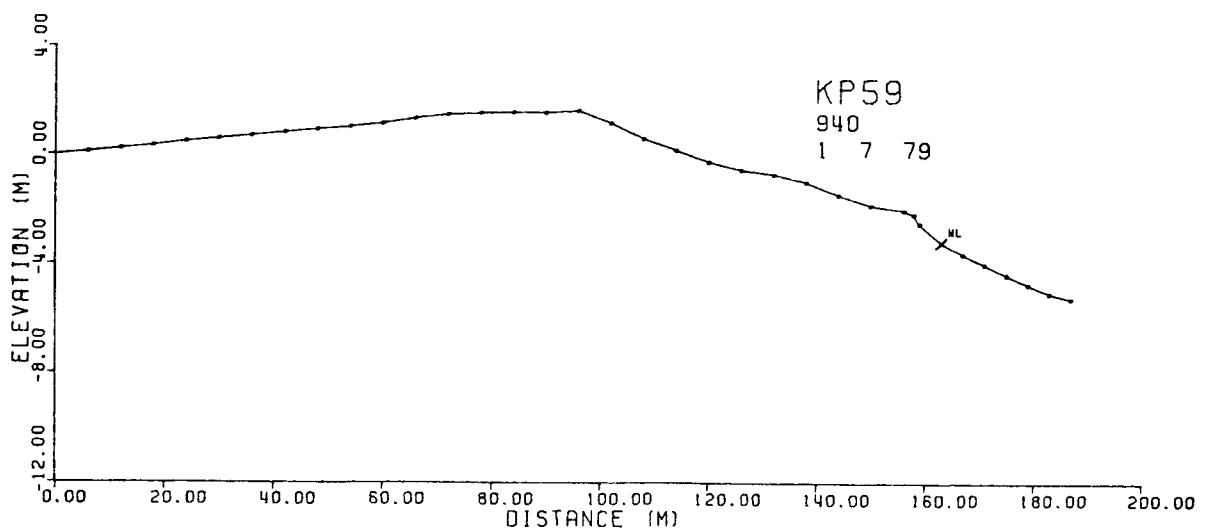
Examples of the cuspate spits are survey stations KNP-2, 17, 25b, and 100.

Examples of recurved spits are survey stations KNP28, 36 and 43.

Uplifted beaches. - Uplifted beaches are common in the eastern portion of the study area, especially around Montague Island. These beaches often have large depositional berms, now above the reach of wave activity, in-filled lagoons, cutoff inlets and wide flat areas between the uplifted berm and the active beach system (Fig. 15). O.S.V.I. values depend on the presently active beach system fronting the uplifted beaches, but normally are 4, 6 or 7.



Figure 12. The bayhead beach shown above is typical of those found at the heads of the larger embayments in the study area. They are generally narrow, arcuate in shape and backed by open lagoons. Beach sediments are usually sand and gravel. The strongly convex upward nature of the beach profile is shown in the profile from station KNP-59 (below).



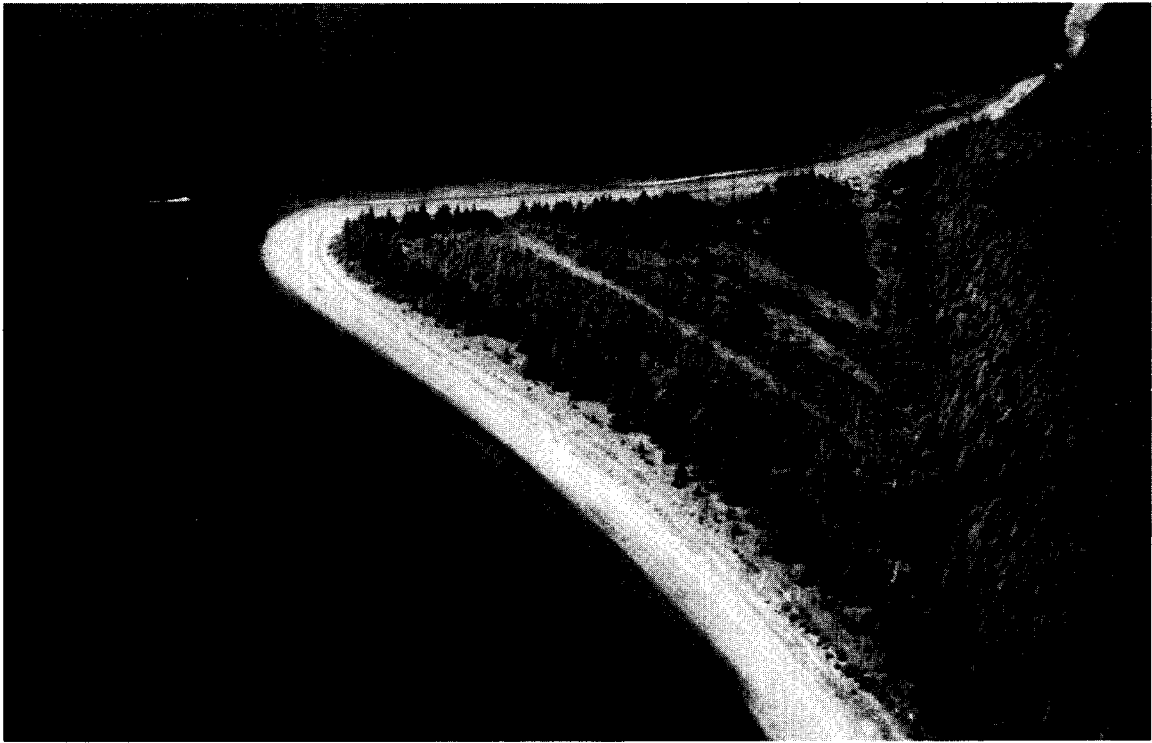


Figure 13. Profile station KNP-100 (above) and KNP-17 (below) are both prime examples of cuspate spits. These depositional features are typically found in the narrow restricted passageways between islands. The sketch and profile of station KNP-17 (following page) show the steep sand and gravel beachface and flat, cobble low-tide terrace typical of cuspate spits.



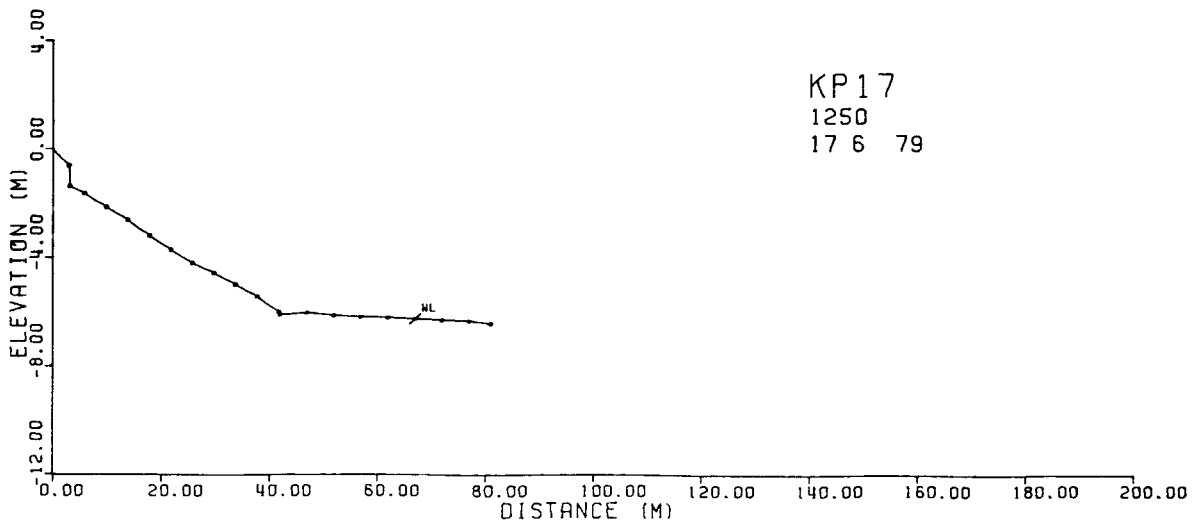
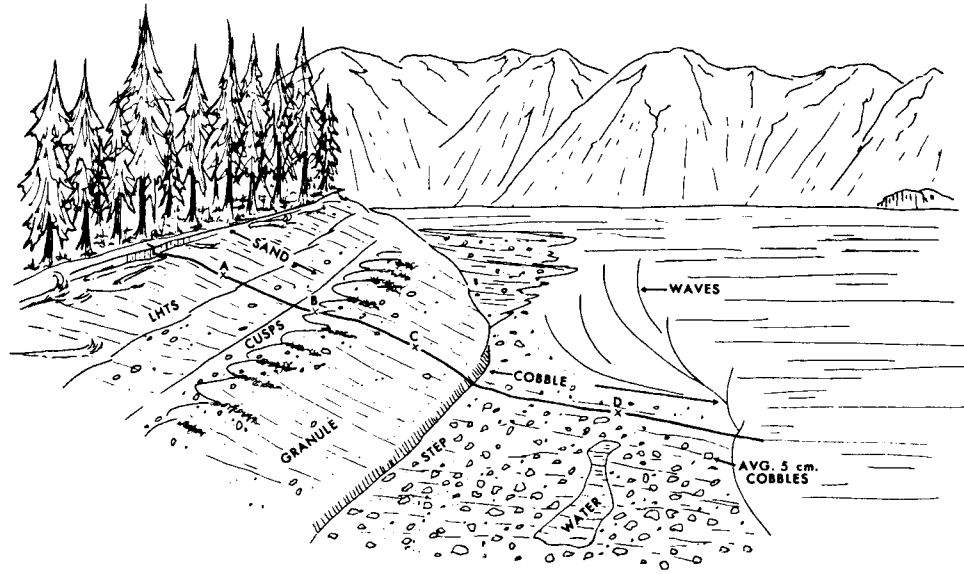
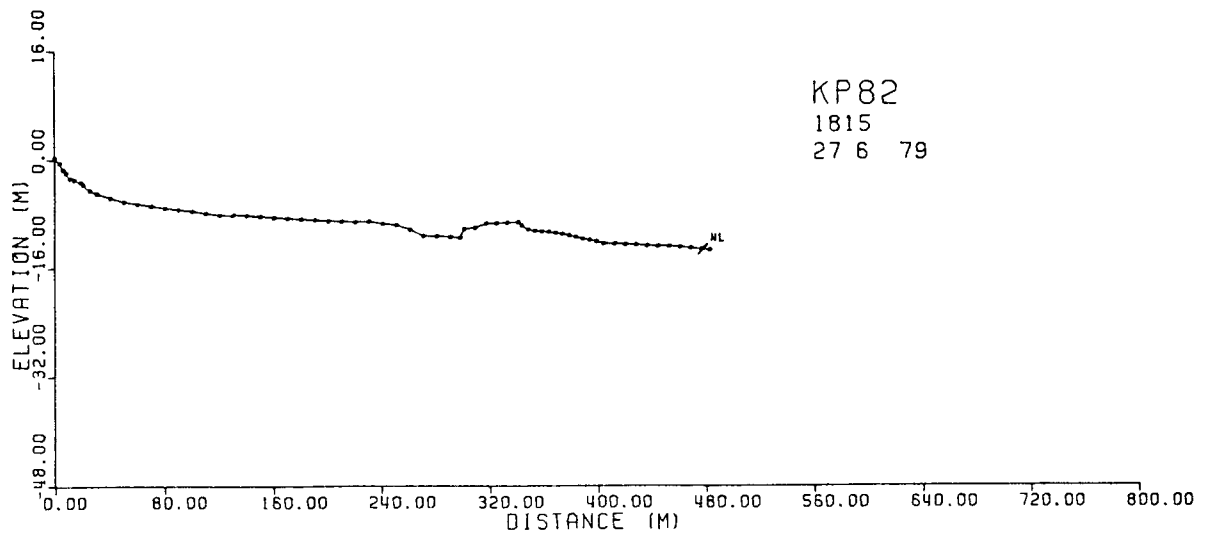




Figure 14. Recurved spit located at profile station KNP-28. These features are often found at the entrance to small open lagoons. Beach sediments are composed of sand and gravel. Note the broad, flat, cobble low-tide terrace at the recurved end of the spit. These terraces are often covered with abundant intertidal life. O.S.V.I. values range from 4-7 for recurved spit beaches.



Figure 15. Profile station KNP-82 located at San Juan Bay on Montague Island. The present day beach was produced by uplift from the 1964 Good Friday Earthquake. The low tree line running parallel to the beach is the site of the pre-uplift depositional berm. Other features produced by the sudden emergence of this area include infilled lagoons and cutoff inlets (above and following page, top). A profile of station KNP-82 was run from the pre-uplifted berm to the present day beach, a distance of roughly 480 m (following page, bottom).



Examples are survey stations KNP-82, 86, 87, 91, 93, 94, 95, 96, 97, 98 and 99.

River Mouth Delta-Tidal Flat and Salt Marsh Systems

River mouth delta-tidal flat systems are primarily found in relatively protected environments where small rivers intersect the coast. Due to the continual influx of sediments from the rivers, wide intertidal areas are formed (Fig. 16). They are dominantly composed of sand and fine gravel. Intertidal life is abundant. The delta-tidal flat systems are occasionally backed by fringing marshes. Approximately 81 km (4%) of the study area is composed of these features.

Examples are survey stations KNP-6, 11, 22, 27, 34, 50, 66 and 76.

Tidal flats and salt marshes are also found independent of river mouth deltas and comprise 101 km (5%) of the shoreline. These features are found in protected or embayed areas that have very little wave energy (Fig. 17). Consequently, the sediments are often fine-grained. Again, intertidal life is abundant.

Examples are the northernmost embayment in Port Bainbridge and the Port Chambers and Stockdale Harbor areas on the northwest side of Montague Island.

Both the delta-tidal flat and salt marsh systems are highly vulnerable to oil spills. Intertidal life can be severely damaged and, due to the protected nature of these environments, oil may remain for extremely long periods of time. These areas should be protected if at all possible. Assigned O.S.V.I. values are 9 or 10. In some instances, if the sediment size of the tidal flats is fine (silts and clays) and the wave or tidal energy is relatively high, the environment is less vulnerable to oil spills. Low permeability of the sediments prevents oil from penetrating the substrate allowing waves and tidal currents to naturally clean the flats.

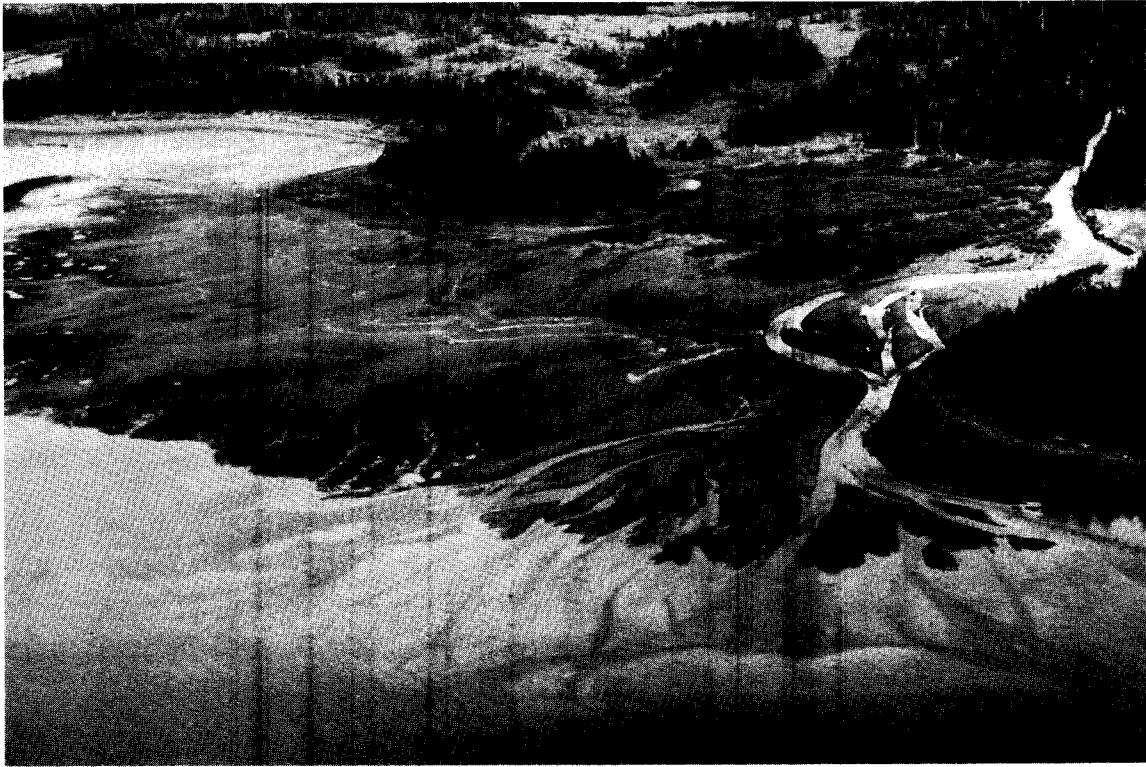
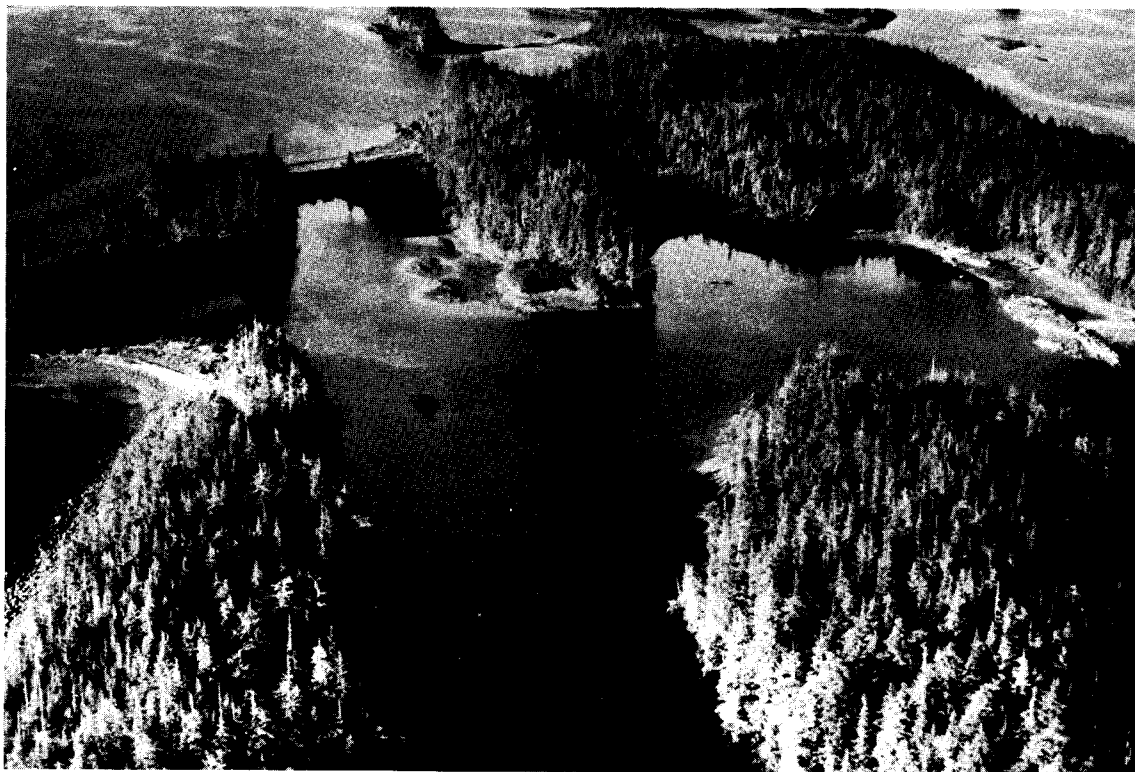


Figure 16. River mouth delta-tidal flat systems are shown here at profile stations KNP-22 (above) and KNP-50 (below). Tidal flats are dominantly composed of sand and fine gravel and have wide, intertidal areas with abundant biota. O.S.V.I. values are 9 or 10.





Figure 17. Embayed tidal flats (above and below), located on northwestern Montague Island. These features are found independent of river mouth deltas in protected low-wave energy environments. Sediments are fine-grained and intertidal life is abundant. O.S.V.I. values are 9 or 10.



In this case, the assigned O.S.V.I. value is 5.

OIL SPILL VULNERABILITY

Introduction

The major purpose of this study has been to supply baseline data regarding shoreline geomorphology and to indicate how that morphology may interact with potential oil spills. Of primary importance is the ranking of coastal environments with regard to the residence time of spilled contaminants. Thus, the primary product of our research is a set of 31 standard U.S.G.S. Quadrangle base maps at a 1:63,360 scale. These 31 topo sheets cover all of the outer Kenai Peninsula and Montague Island. Each map classifies the shoreline into 1 of 10 subclasses, described in this section. The maps are reproduced at page size and are shown in Appendix I. The original maps are submitted as an enclosure.

Our group has been studying oil spills and doing baseline analyses of various coastal areas for about 5 years. There is currently available a large number of publications dealing with specific spills (Blount, 1978; Blount and Gundlach, 1977; Gundlach and Hayes, 1977; Gundlach, Fischer and Stein, 1977; Gundlach, Ruby and Blount, 1977; Gundlach et al., 1977; Hayes and Gundlach, 1975; Hayes et al., 1976; Ruby et al., 1977) as well as many dealing specifically with our coastal work in parts of Alaska (Gundlach et al., 1977; Hayes, Michel and Brown, 1977; Ruby and Hayes, 1978, Hayes et al., 1976; Nummedal and Stephen, 1976; Nummedal, Stephen and Ruby, 1977; Nummedal and Ruby, 1979; and a number of Annual and Progress Reports to OCSEAP). These reports detail the controls that beach morphology, grain size and incoming energy can have on oil spill behavior and longevity. Several of the reports address the potential impacts of spills on various Alaskan marine assemblages. These earlier results will not be repeated in this report. They strongly support the concept that physical degradation of spilled oil is directly related to the marine energy in the spill en-

vironment. There is an abundance of literature dealing with case studies of the numerous major and minor oil spills that have taken place in the coastal waters of the lower 48 states and around the world. Predictive models for oil spill dispersal, spreading, bio-degradation and physical degradation have been developed from these studies. The sub-arctic areas, however, have been to a large extent omitted due to the difficulties inherent in any study of these environments and a general lack of actual oil spills in these environments from which to base detailed case studies. The Arrow oil spill in Chedabucto Bay, Nova Scotia, probably comes closest to a comparative model for the sub-Arctic. However, the clean-up effort and later studies (Owens, 1971; Owens and Drapeau, 1973; Owens, 1973; Drapeau, 1974; Owens and Rashid, 1976) made very little reference to the special problems encountered as a result of the colder environment (i.e., oil on ice and snow; ice-oil interaction with beach sediments; oil dispersal in heavily iced environments, etc.). Our investigation of the Buzzards Bay oil spill (Ruby et al., 1977) and the Ethyl H. spill in the frozen Hudson River have given new insight into the effects of oil spills in ice-choked waters.

Evaporation losses and biodegradation are slower in colder environments. Biodegradation can be reduced as much as 90% in water of 0°C when compared to water of 25°C (Robertson et al. 1972). Isakson et al. (1975) states that burning may be the only feasible method of cleaning oil spills in iced areas; however, this may represent a trade of one type of pollution for another. During the Buzzards Bay spill clean-up, burning was an effective method for cleaning oil which was not accessible from the shore. Only a small amount of particulate matter resulting from the fires was noticed.

Oil Spill Vulnerability Index

This scale has been devised on the basis of actual spill analysis and

a careful study of the literature. It is based primarily on the residence time of oil in each sub-environment, which is generally a function of the intensity of the marine processes, sediment grain size and transport trends. The biologic sensitivity has also been utilized to modify that ratings of various environments.

Coastal environments are listed and discussed below in order of increasing vulnerability to oil spills.

1. Straight rocky headlands:

Most areas of this type are exposed to maximum wave energy. Waves reflect off of the rocky scarps with great force, readily dispersing the oil. In fact, waves reflecting off the scarps at high tide tend to generate a surficial return flow that keeps the oil off the rocks (observed at the Urquiola site in Spain and the Amoco Cadiz spill in France). Even if oiled, natural cleaning will only require a few days or weeks. No human intervention is necessary. They represent the largest single class within the study area, 28.2%.

2. Wave-cut platforms:

These areas are also swept clean by wave action. All of the wave-cut platforms at the Metula site were cleaned of oil after one year. The rate of removal of the oil is a function of wave climate and the irregularity of the platform. In general, no clean-up measures are needed for wave-cut platforms. However, there are large biologic populations in these areas. Most of this classification, 9.3% of the study area, occurs on Montague Island in highly exposed, recently uplifted areas.

3. Flat, fine-grained sandy beaches:

Beaches of this type are generally flat and hard packed. Oil that is emplaced on such beaches will not penetrate more than a few centimeters at most. Usually the oil will be deposited on the surface of the sand where it can be removed by elevated scrapers or other road grading machinery.

Furthermore, these types of beaches change slowly, so sand deposition and resultant burial of oil will take place at a slow rate. If left to natural processes, these beaches will be cleaned within several months. This type of beach is very rare in the study area, representing only 0.8% of the shoreline.

4. Steeper, medium to coarse-grained sandy beaches:

On these beaches, the depth of penetration would be greater than for the fine-grained beaches (though still only a few centimeters), but rates of burial of the oil would be greatly increased. Based on our earlier studies, it is possible for oil to be buried as much as 50-100 cm within a period of a few days on beaches of this class. In this situation, removal of the oil becomes a serious problem, since removal of the oiled sediments will often result in large scale erosion as the beach changes into a new equilibrium state. This was a common problem encountered during the clean-up of the Arrow spill in Chedabucto Bay, Nova Scotia (Owens and Rashid, 1976). Another problem is that burial of the oil preserves it for release at a later date when the beach erodes as part of the natural beach cycle, thus causing longer term pollution of the environment. This class represents only 1.5 % of the study area.

5. Impermeable exposed tidal flats:

One of the major surprises in the study of the Metula site was the discovery that oil had not remained on the mud flats. At the Urquiola site, oil was observed as it became refloated with rising tides on the mud flats. Penetration of the oil is prevented by the extremely fine sediment size, saturated with water. Therefore, if an oiled tidal flat is subject to winds and currents, the oil will tend to be removed, although not at the rapid rate encountered on exposed beaches. Mechanized cleanup is considered impossible. These are often areas of high biologic importance. These areas are very rare in the study area due to a lack of fine sediment. They rep-

resent only 0.3% of the total study area.

6. Mixed sand and gravel beaches:

On beaches of this type, the oil may penetrate several centimeters, and rates of burial are quite high (a few days in Spain). Any attempt to remove the oiled sediment will result in considerable erosion. These beaches occur primarily as pocket beaches between headlands or where till or glacial deposits are being reworked by marine processes. The longevity of the oil at the Metula site, particularly on the low-tide terraces and berm top areas, attests to the high susceptibility of this type of beach to long-term oil spill damage. Natural cleaning may require many years. This type of beach is relatively common in the study area, representing 11.9%.

7. Gravel beaches:

Pure gravel beaches allow the oil to penetrate to considerable depth (up to 45 cm in Spain). Furthermore, rapid burial is also possible. A heavily-oiled gravel beach will be impossible to clean up without completely removing the gravel. Natural cleaning will be quite slow for this type of beach; the exact time required will depend on the intensity of the marine processes. Pure gravel beaches are quite common in the study area representing almost 18.0% of the shoreline. They occur mostly as pocket beaches and linear beaches fronting rock scarps. In some cases, they can be quite long.

8. Sheltered rocky headlands:

Our experience in Spain indicates that oil tends to stick to rough rocky surfaces. In the absence of abrasion by wave action, oil could remain on such areas for years, with only chemical and biological processes left to degrade it. These headlands usually have gravel beaches associated with them; therefore, for the purposes of this study, sheltered gravel beaches are classified with sheltered rocky headlands. They represent the second largest single class

or 23.1% of the study area. Most of these areas are in the quiet water passages and channels between Evans, Elrington and Bainbridge Islands and in the fjords along the western Kenai Peninsula shoreline.

9. Protected tidal flats:

If oil reaches a quiet, protected tidal flat, it will remain there for long periods because natural cleaning progresses at an extremely slow rate. Because of the low intensity of marine process parameters, removal of the oil will have to be accomplished by natural chemical and biogenic processes. This will take many years, dependent on the amount of oil deposited. Because of their high biologic populations, these environments are very sensitive to the toxic effects of oil. These areas are relatively rare in the study area occurring only at fjord heads and at river mouth estuaries. Protected tidal flats comprise 5.12% of the shoreline.

10. Protected salt marshes:

In sheltered salt marshes, oil from a spill may have long-term deleterious effects. We observed oil from the Metula on the salt marshes of East Estuary, in the south shore of the Strait of Magellan, that had shown essentially no change in 1½ years. We predict a life span of at least 10 years for that oil. These areas are extremely important biologically, supporting large communities of organisms. These areas are generally associated with the protected tidal flats (#9) and are also rare, representing only 1.89% of the study area.

Applications to the Kenai Peninsula and Montague Island

Using the vulnerability classification just described, it is possible to make a few generalizations regarding the Kenai area and its reaction to potential oil spills. In general, the area is quite "high risk". Nearly 60% of the shoreline falls in classes 6 - 10 (Table 2). These classes will have a spill residence time of a year or two to more than 10

TABLE 2. Oil Spill Vulnerability Index, Kenai Peninsula
and Montague Island

Class Description	Kilometers of Shoreline	% Total Study Area
1. Straight rocky headlands	609.8	28.3
2. Wave-cut platforms	198.8	9.3
3. Flat, fine-grained sandy beaches	16.6	0.8
4. Steeper, medium-to-coarse grained sandy beaches	30.0	1.3
5. Impermeable exposed tidal flats	6.3	0.3
6. Mixed sand and gravel beaches	258.5	11.9
7. Pure gravel beaches	389.1	18.0
8. Sheltered rocky headlands	496.9	23.0
9. Protected tidal flats	110.7	5.2
10. Protected salt marshes	<u>40.3</u>	<u>1.9</u>
	2157.0	100.0

NOTE: In general, classes 1 and 2 are highly erosional in nature. Classes 5, 9 and 10 are depositional. Classes 3, 4, 6, 7 and 8 can be either erosional or depositional, but in this area they tend to be more erosional.

years. The remaining 40% of the shorelines fall into classes 1 - 5, which are considerably lower risk areas where spilled oil would generally be expected to be cleaned by natural processes within a year.

Unfortunately, the study area is very complex and the higher risk areas do not lend themselves well to being protected during a spill. In many instances, a low-risk rock scarp will lie just seaward of a large embayment with high-risk pure gravel beaches. The fact that the environments change so frequently and rapidly along the shoreline makes the entire shoreline a fairly high-risk area. The indented (fjord) character of the coast will act as "oil traps" for floating oil. Oil will tend to be moved deeper into the fjords rather than to be flushed out. In general, this will result in an oiling of increasingly sensitive environments, since higher risk, lower energy classes are located deeper in fjords and embayments.

Since the Oil Spill Vulnerability Index is based partly on the residence time of potential oil spills within each of the subenvironments, the following guidelines are given:

<u>OSVI</u>	<u>Spill Residence Time</u>
1 + 2	A few days to a few weeks
3 + 4	A month to six months
5 + 6	Six to 24 months
7 + 8	A year or two to as much as 8 years
9 + 10	Up to ten years

These figures are highly dependent on the wave energy during the spill and partly dependent on the temperature. They can vary and are meant to be estimates only. They give a relative indication of the residence time from one environment to another.

REFERENCES

- Blount, A.E., 1978, Two years after the Metula oil spill, Strait of Magellan, Chile: Oil interaction with coastal environments: Tech. Rept. No 16-CRD, University of South Carolina.
- Blount, A.E., and Gundlach, E.R., 1977, Response of coastal environments to the Metula oil spill in the Strait of Magellan, southern Chile: Geol. Soc. Am. Annual Meeting, Seattle, Washington, pp. 902-903.
- Burk, C. A., 1965, Geology of the Alaska Peninsula-Island arc and continental margin: Geol. Soc. America Mem. 99, 250 p.
- Case, J. E., Barnes, D. F., Plafker, G., and Robbins, S. L., 1966, Gravity survey and regional geology of the Prince William Sound epicentral region: U.S. Geological Survey Prof. Paper 543-C, p. 1-12.
- Clark, S.H.B., 1972, Reconnaissance bedrock geologic map of the Chugach Mountains near Anchorage, Alaska: U.S. Geol. Survey Misc. Geol. Inv. Map MF-350.
- Climatic Atlas of the Outer Continental Shelf Waters and Coastal Regions of Alaska, Volume 1, 1977, U.S. Department of Commerce, National Oceanic and Atmospheric Administration, Alaska Outer Continental Shelf Environmental Assessment Program, 439 p.
- Davies, J. L., 1973, Geographical variation in coastal development: Hafner Publishing Company, New York, N. Y. 204 p.
- Drapeau, G., Harrison, W., Bien, W., and Leinonen, P., 1974, Oil slick fate in a region of strong tidal currents: Proc. 14th Coastal Eng. Conf., pp. 2245-2259.
- Gundlach, E. R., Fischer, I.A., and Stein, R. J., 1977, The black tide of La Coruna: Oceans, Vol. 10, No. 2, pp. 56-60.
- Gundlach, E. R., and Hayes, M. O., 1977, The Urquiola oil spill: Case history and discussion of clean-up and control methods: Marine Pollution Bull., Vol. 8, pp. 132-136.
- Gundlach, E. R., Hayes, M. O., Ruby, C. H., Ward, L. G., Blount, A. E., Fischer, I. A., and Stein, R. J., 1977, Some guidelines for oil spill control in coastal environments, based on field studies of four oil spills: ASTM Symposium on Chemical Dispersants for the Control of Oil Spills, Williamsburg, Va., pp. 98-118.
- Gundlach, E. R., Ruby, C.H., and Blount, A. E., 1977, Massive oil spill in La Coruna, Spain: Short-term impact on beaches and rocky coasts as a function of coastal geomorphology and marine processes: Abstr., Geol. Soc. Am. Annual Meeting, Seattle, Washington, p. 999.

- Hayes, M. O., 1964, Lognormal distribution of inner continental shelf widths and slopes: *Deep Sea Res.*, V. 11, p. 53-78.
- Hayes, M. O. and Gundlach, E. R., 1975, Coastal geomorphology and sedimentation of the Metula oil spill site in the Strait of Magellan: Rept. National Science Foundation, Washington, D. C., 103 p.
- Hayes, M. O., Brown, P. J., Michel, J., 1976, Coastal morphology and sedimentation, lower Cook Inlet, Alaska: Tech. Rept No. 12-CRD, Univ. of South Carolina, Columbia, S. C. 107p.
- Hayes, M. O., Michel, J., and Brown, P. J., 1977, Lower Cook Inlet, Alaska: Application of oil spill vulnerability index: 4th Inter. Conf. on Port and Ocean Eng. under Arctic Conditions, St. Johns, Newfoundland, pp. 828-843.
- Hayes, M. O., Ruby, C. H., Stephen, M. F., and Wilson, S. J., 1976, Geomorphology of the southern coast of Alaska: Proc. 15th Inter. Coastal Eng. Conf., Hawaii, pp. 1992-2008.
- Inman, D. L. and Nordstrom, C. E., 1971, On the tectonic and morphologic classification of coasts: *Jour of Geol.*, Vol. 79, pp. 1-21.
- Isakson, J.S., et al., 1975, Comparison of ecological impacts of postulated oil spills at selected Alaskan locations: U.S.G.S. Rept. No. CG-D-155-75, Vol. 1, 633 p., Vol. 2, 865 p.
- Jones, D. L., and Clark, S.H.B., 1973, Upper Cretaceous (Maestrichtian) fossils from the Kenai-Chugach Mountains, Kodiak and Shumagin Islands, southern Alaska: *U.S. Geol. Survey Jour. Research*, v. 1, pp. 125-136,
- King, P.B., 1969, Tectonic map of North America: U.S. Geological Survey special map.
- Malloy, R.J. and Merrill, G. F., 1971, Vertical crustal movement of the sea floor associated with the Prince William Sound, Alaska, earthquake: *U.S. Coast & Geodetic Survey Vol. II. B, C: Seismology and Marine Geology.*
- Moore, J. C., 1971, Structural evolution of the Cretaceous pre-Aleutian Trench, Alaska (abs.): *Geol. Soc. Am. Program with Abstracts*, V. 3, No. 1, p. 650-651.
- Nummedal, Dag, and Ruby, C. H., 1979, Spilled oil retention potential Beaufort Sea, Proc. 5th Inter. Conf. on Port and Ocean Eng. Under Arctic Conditions, Trondheim, Norway, Aug. 13, 1979.
- Nummedal, Dag and Stephen, M.F., 1976, Coastal dynamics and sediment transportation: northeast Gulf of Alaska: Tech. Rept. No. 9-CRD, Univ. of South Carolina, 148 p.

- Nummedal, Dag, Stephen, M. F., and Ruby, C. H., 1977, Reconnaissance evaluation of longshore sediment transport, northeast Gulf of Alaska: Proceedings, 4th Int. Conf. on Port and Ocean Eng. under Arctic Conditions, St. Johns, Newfoundland, Sept., pp. 892-903.
- Nummedal, Dag, and Stephen, M.F., 1978, Wave climate and littoral sediment transport, northeast Gulf of Alaska: Journal of Sed. Petrology, V. 48, No. 2, p. 359-377.
- Owens, E.H., 1971, The restoration of beaches contaminated by oil in Chedabucto Bay, Nova Scotia: Marine Sci. Branch, Ottawa, Can., Manus., Rep. Serv., No. 19, 75 p.
- Owens, E. H., 1973, The cleaning of gravel beaches polluted by oil: Proc. 13th Coastal Eng. Conf., Vancouver, B.C., pp. 2543-2556.
- Owens, E.H., and Drapeau, G., 1973, Changes in beach profiles at Chedabucto Bay, Nova Scotia, following large scale removal of sediments: Can Jour. Earth Sci., 10, pp. 1226-1232.
- Owens, E.H., and Rashid, M. A., 1976, Coastal environments and oil spill residues in Chedabucto Bay, Nova Scotia: Can Jour. Earth Sci., 13, pp. 908-928.
- Payne, T. G., 1955, Mesozoic and Cenozoic tectonic elements of Alaska: U.S. Geol. Survey Misc. Geol. Inv. Map I-84, scale 1:5,000,000.
- Petterssen, S., 1969, Introduction to meteorology: McGraw-Hill Book Co., New York, 333 p.
- Plafker, G., 1966, Surface faults on Montague Island associated with the 1964 Alaska earthquake: U.S. Geol. Survey Prof. Paper 543-G, p. 1-42.
- Plafker, G., 1971, Tectonics of the March 27, 1964, Alaska earthquake, U.S. Geol. Survey Prof. Paper 543-I: in The Great Alaska Earthquake of 1964, Part A - Geology, National Academy of Sciences, Washington, D. C., p. 47-122.
- Plafker, G., and Kachadoorian, R., 1966, Geologic effects of the March 1964 earthquake and associated seismic sea waves on Kodiak and nearby islands, Alaska: Geological Survey Prof. Paper 543-D, 45 p.
- Plafker, G., and MacNeil, F. S., 1966, Stratigraphic significance of fossils from the Orca Group in the Prince William Sound region, Alaska, in Geological Survey Research 1966, U.S. Geol. Survey Prof. Paper 550-B, p. B62-B68.
- Robertson, B., Arhelger, S., Kinney, P. J., and Button, D. K., 1972, Hydrocarbon biodegradation in Alaskan waters: Center for Wetlands Resources, Louisiana State Univ., LSU-SG 73-01.
- Ruby, C. H., and Hayes, M. O., 1978, Application of an oil spill vulnerability index to the Copper River Delta, Alaska: Proceedings, Coastal Zone 1978, San Francisco, Calif., March, pp. 2204-2220.

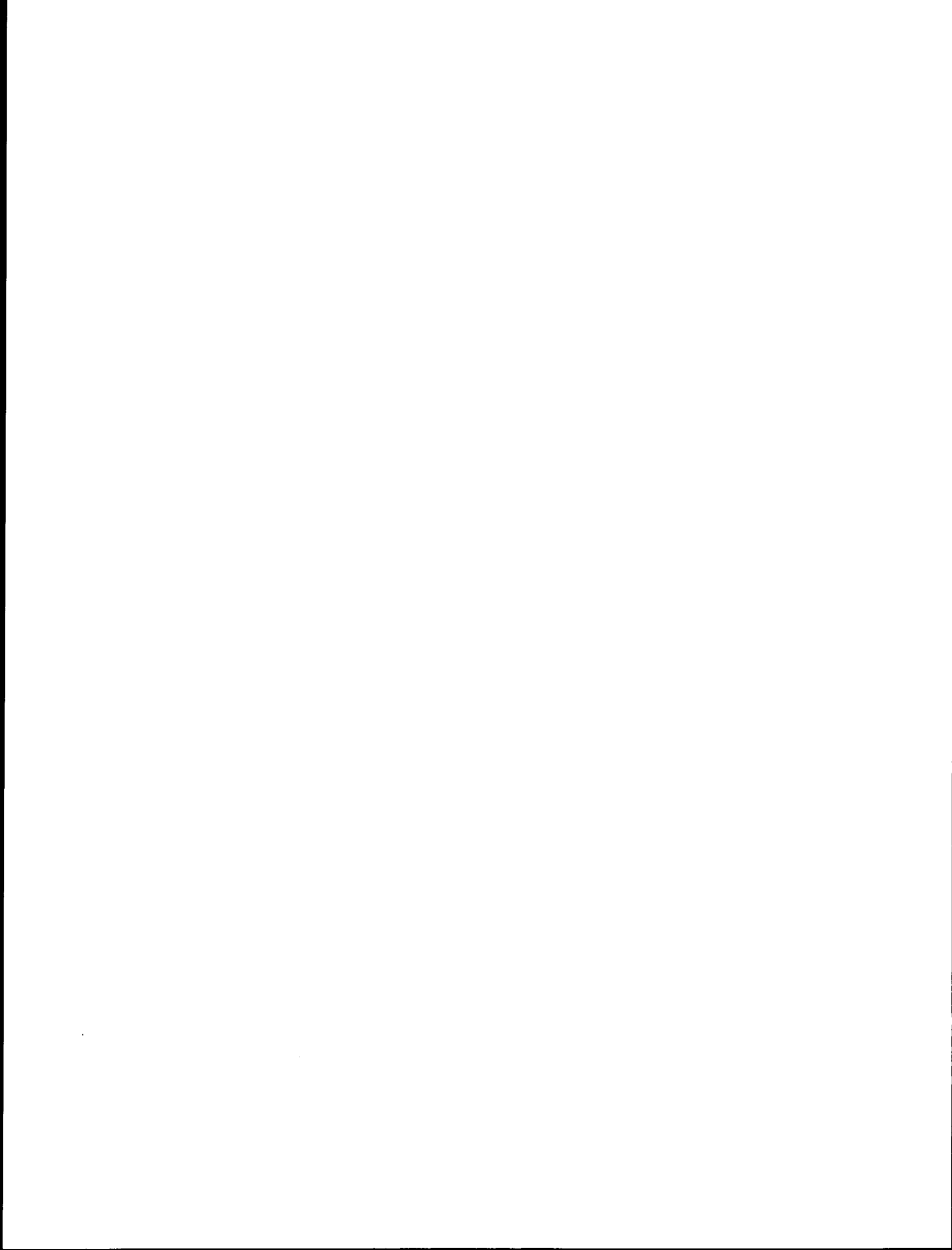
- Ruby, C.H., Ward, L.G., Fischer, I. A., and Brown, P. J., 1977, Buzzards Bay oil spill - an Arctic analogue: 4th International Conf. on Port and Ocean Eng. under Arctic Conditions, St. Johns, Newfoundland, September, pp. 844-855.
- Ruby, C.H., Hayes, M. O., Reinhart, P. J., and Finkelstein, K., 1979, Oil spill vulnerability, coastal morphology, and sedimentation of the Kodiak Archipelago: Final report to the Outer Continental Shelf Environmental Assessment Program, NOAA, 150 p.
- Stanley, K.W., 1966, Effects of the Alaska earthquake of March 27, 1964 on shore processes and beach morphology: Geological Survey Prof. Paper 543-J, 21 p.
- Stanley, K.W., 1971, Effects on shore processes and beach morphology: U.S. Geol. Survey Prof. Paper 543-J: in The Great Alaska Earthquake of 1964, Part A - Geology, National Academy of Sciences, Washington, D. C., p. 229 - 249.
- U.S. Army Coastal Engineering Research Center, 1973, Shore Protection Manual, Vol. 1, Second Edition.
- U.S. Naval Weather Service Command, 1970, Summary of Synoptic Meteorological Observations, North American Coastal Marine Areas: National Climatic Center, Asheville, North Carolina.
- Wahrhaftig, D., 1965, Physiographic divisions of Alaska: U.S. Geol. Survey Prof. Paper 482, 52 p.



APPENDIX I

OIL SPILL VULNERABILITY

This section is prefaced by a table showing the percent shoreline in each Oil Spill Vulnerability Index (O.S.V.I.) class for each topographic sheet (1:63,360 scale) in the study area. The total shoreline length in kilometers for each map is given in the right-hand column of the table. Following this are photographic reductions of all 31 topographic sheets, showing the number-coded O.S.V.I. class for every section of coastline within the study area. The O.S.V.I. number code is outlined in the text of this report.

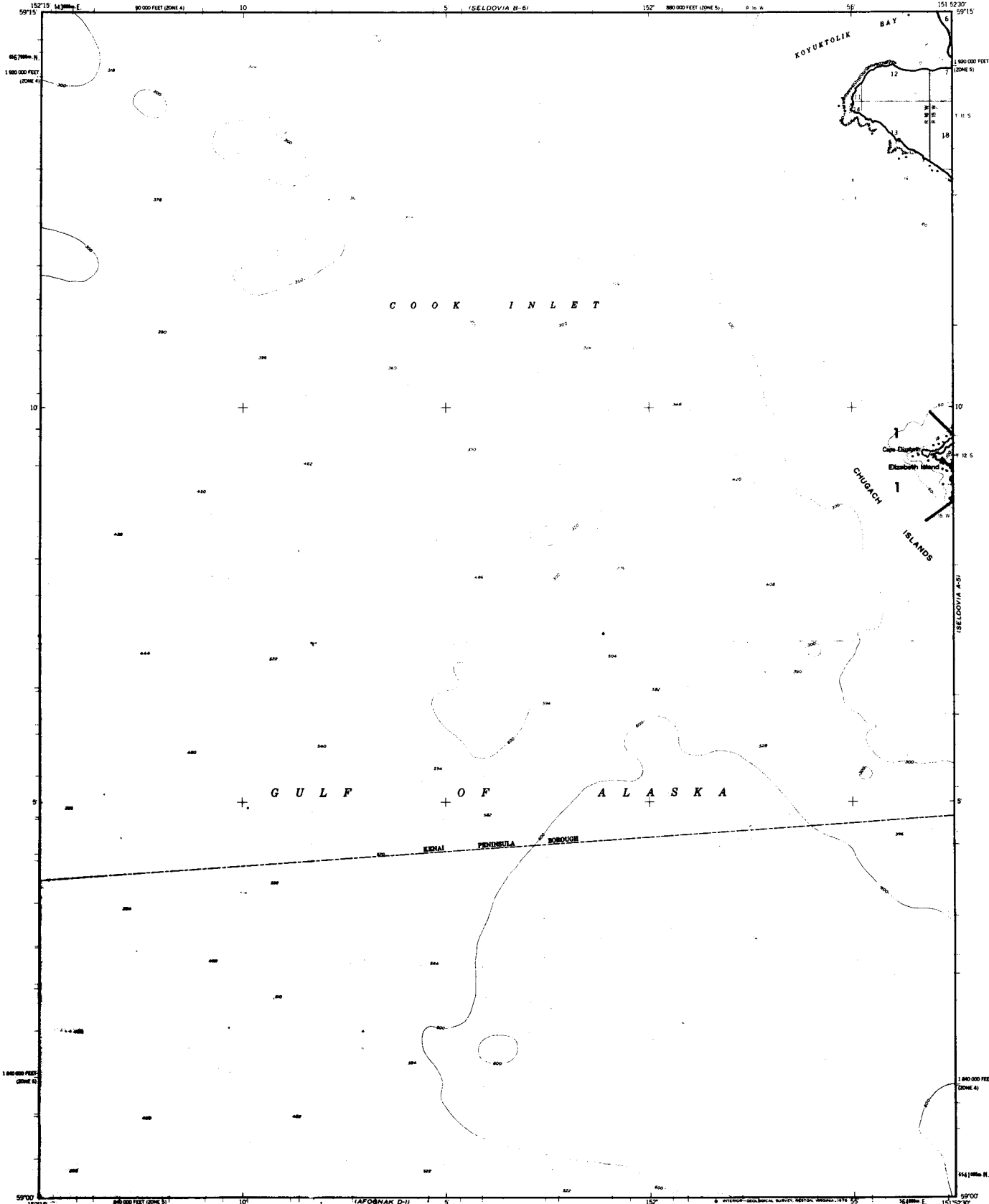


% Shoreline in Each Oil Spill Vulnerability Index Class (for each 1:63,360 topographic sheet).

Map	O.S.V.I. Class										Shoreline length in km	
	1	2	3	4	5	6	7	8	9	10		
Seldovia A-6	100%											1.9
Seldovia A-5	36	3%		14%		27%	2%	10%	7%	2%		
Seldovia A-4	47	8		18		19	1	8				64.4
Seldovia B-4	2			6		14		41	25	12		53.1
Seldovia B-3	31			2		18	6	35	6	2		81.9
Seldovia A-3	65					23	5	5		2		26.9
Seldovia B-2	40				1%	9	3	42	6			178.2
Seldovia C-2	4					8	12	55	12	8		76.3
Seldovia C-2	26					25	12	32	5	1		150.6
Seldovia B-1	62							38				58.1
Bly. Sd. C-8	19					25	8	47	2			81.9
Seldovia D-1							36	64				13.8
Bly. Sd. D-8	14					2	33	41	9			108.8
Bly. Sd. D-7	68					4	12	15				144.4
Bly. Ds. C-7	80						1	20				53.4
Seward A-7	19					14	23	15	19	11		46.3
Bly. Sd. D-6	74		4%	3		4	11	4				46.3
Seward A-6	32					16	21	7	16	7		35.0
Bly. Sd. D-5	58					23	11		5	4		35.6
Seward A-5	27					2	36	9	13	13		14.1
Bly. Sd. D-4	47					11	38	5				53.1
Seward A-4	27	1	1			13	23	29	5	2		139.1
Seward A-3	17	3				12	34	31	2			201.3
Bly. Sd. D-3	3	45	6		2	10	26	4	4	2		82.5
Bly. Sd. D-1 and D-2	7	52	9		5	6	20		2			80.0
Seward A-1		58				6	24		11	1		63.1
Cordova A-7 and A-8		100										2.5
Cordova B-8		87				4	9					14.4
Seward B-1		28				11	47		7	7		100.6
Seward A-2		40	5			2	53					38.8
Seward B-2		37				21	37		4	1		30.3

UNITED STATES
DEPARTMENT OF THE INTERIOR
GEOLOGICAL SURVEY

SELDOVIA (A-6) QUADRANGLE
ALASKA
1:63 360 SERIES (TOPOGRAPHIC)



Maped, edited, and published by the Geological Survey
Control by NGS/NOAA
Topography by photogrammetric methods from aerial photographs
taken 1951. Map not field checked.
Selected hydrographic data compiled from USCGS Charts
1831, 8532, and 8554 (1:200,000 scale). This information
is not intended for navigational purposes.
Universal Transverse Mercator projection, 1927 North American datum
10,000-foot grid based on Alaska coordinate system, zones 5 and 4
1000-meter Universal Transverse Mercator grid ticks,
zone 5, shown in blue.
Land lines represent unsurveyed and unmarked locations
determined by the Bureau of Land Management
Folio S-16, Seward Meridian



SCALE 1:63 360

4 MILES
21000 FEET
3 MILES
15750 FEET
2 MILES
10500 FEET
1 MILE
5250 FEET

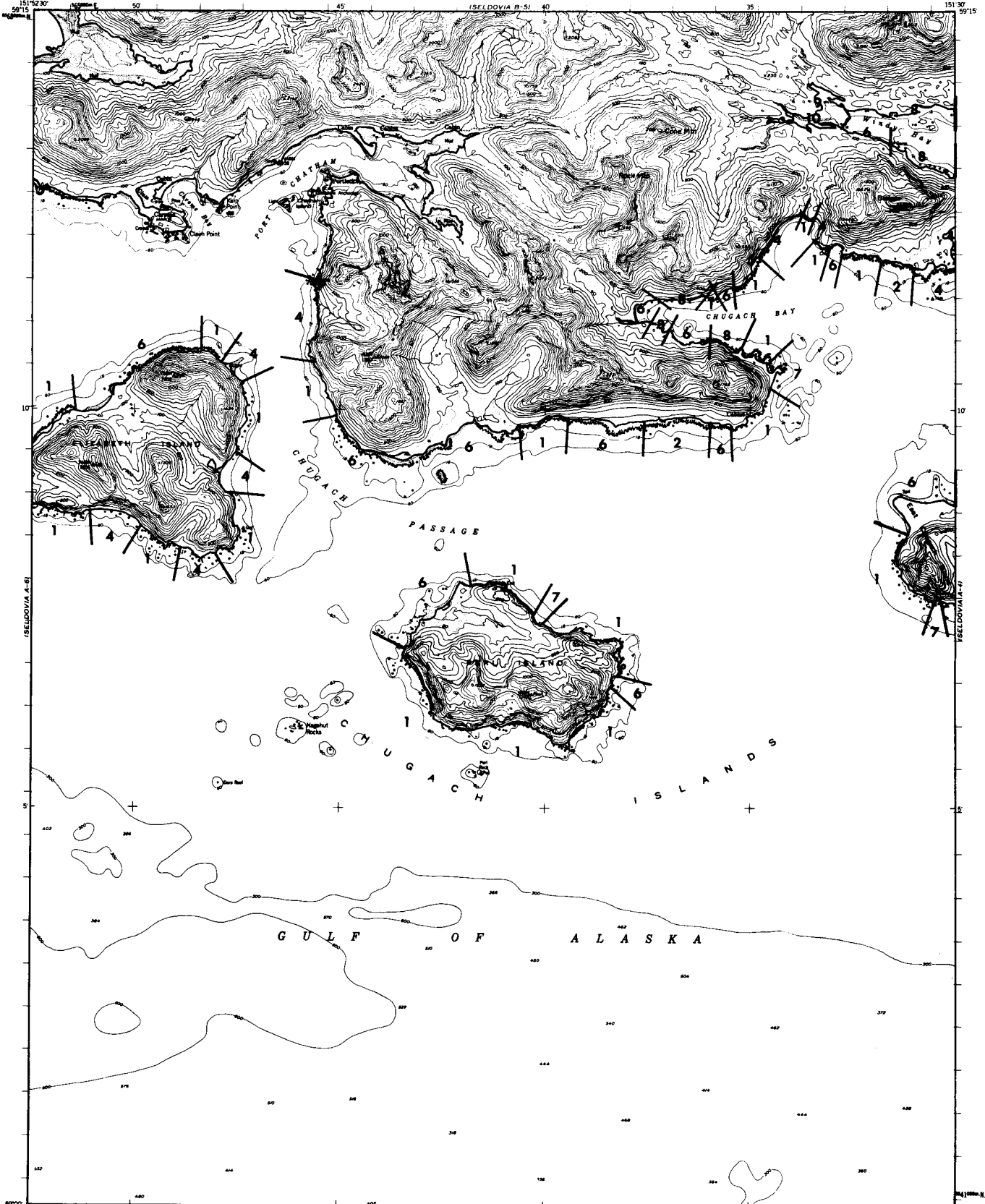
CONTOUR INTERVAL 100 FEET
NATIONAL GEODESIC VERTICAL DATUM OF 1929
DEPTH CURVES AND SOUNDINGS IN FEET DATUM IS MEAN LOWER LOW WATER
SHORELINE SHOWS REPRESENTS THE APPROXIMATE LINE OF MEAN HIGH WATER
THE WEDGE SHAPED OF THIS S REPRESENTS 1/2 FEET

FOR SALE BY U. S. GEOLOGICAL SURVEY
FAIRBANKS, ALASKA 99701, DENVER, COLORADO 80225, OR RESTON, VIRGINIA 22092
A FOLDER DESCRIBING TOPOGRAPHIC MAPS AND SYMBOLS IS AVAILABLE ON REQUEST

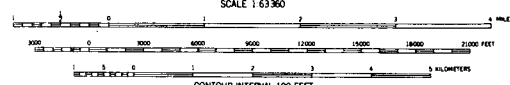


ROAD CLASSIFICATION
No roads or trails in this area

SELDOVIA (A-6), ALASKA
N5900-W15152.5/13A22.5
1951
MAP NUMBER 1317



Mapped, edited, and published by the Geological Survey
Control by USCG&S and USCE
Hydrography compiled from USCG&S charts
8531, 8532, 8554 (1:200,000 scale), and 8558
Topography from aerial photographs by multiple methods 1953
Aerial photographs taken 1951
Universal Transverse Mercator projection, zone 5
1927 North American datum
Unchecked elevations are shown in brown
1000-meter Universal Transverse Mercator grid ticks,
zone 5, shown in blue

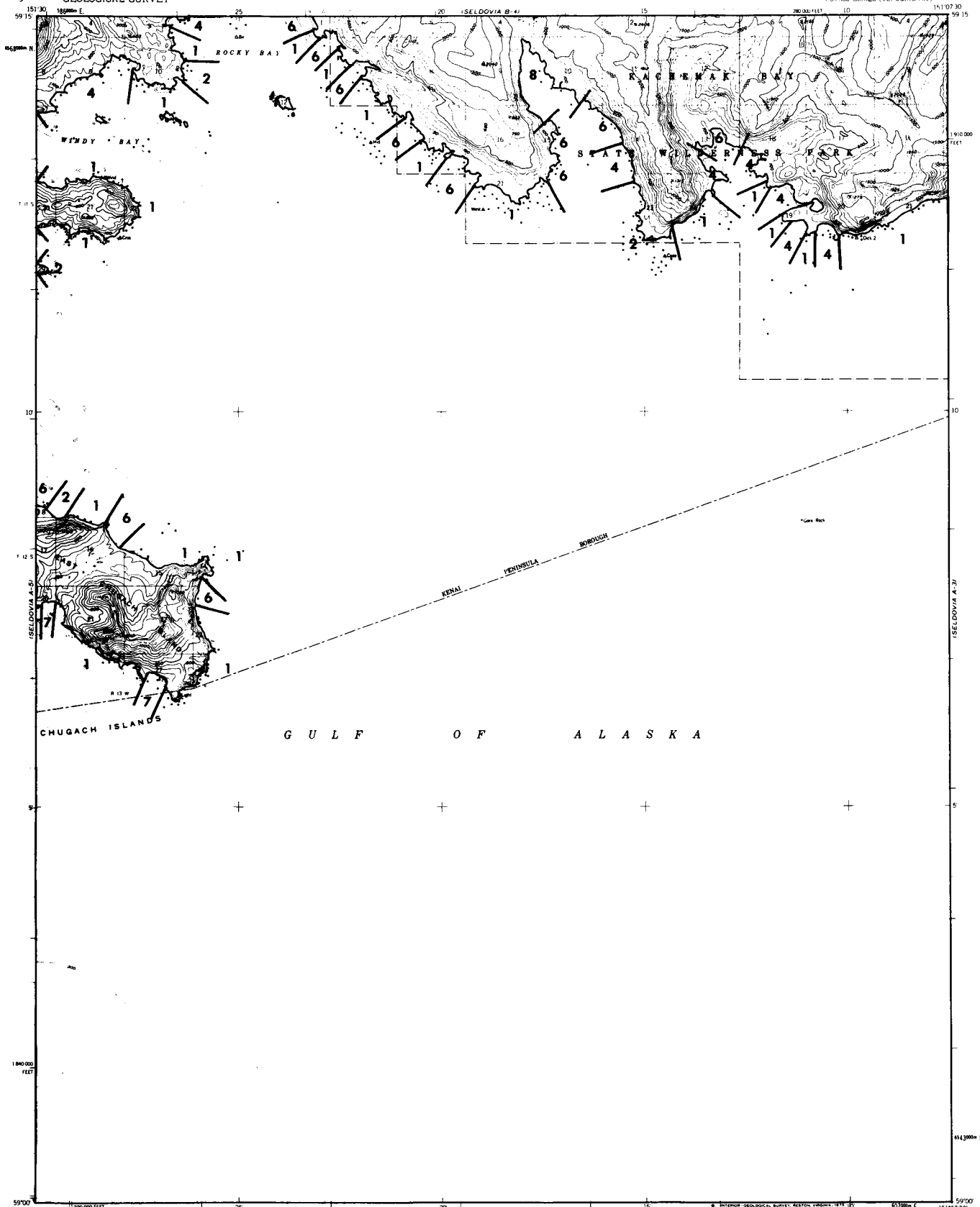


ROAD CLASSIFICATION

ALL WEATHER ROADS	DRY WEATHER ROADS
Hard surface.....None	Improved dirt.....None
Other.....None	Unimproved dirt.....None
Trails.....	

SELDOVIA (A-5), ALASKA
N5900—W15130/15X22.5
1953

FOR SALE BY U. S. GEOLOGICAL SURVEY
FAIRBANKS, ALASKA FEDERAL CENTER, DENVER, COLORADO WASHINGTON 25, D. C.
A FOLDER DESCRIBING TOPOGRAPHIC MAPS AND SYMBOLS IS AVAILABLE ON REQUEST



Mapped, edited, and published by the Geological Survey
Control by NOS/NOAA and USGS
Topography by photogrammetric methods from aerial photographs taken 1951. Map not field checked
Selected hydrographic data compiled from USCGS Charts 8531 (1951), 8532 (1952), 8552 (1952), and 8554 (1952) (1:200 000 scale). This information is not intended for navigational purposes.
Universal Transverse Mercator projection, 1927 North American datum
10,000-foot grid based on Alaska coordinate system, zone 4
1000-meter Universal Transverse Mercator grid ticks, zone 5, shown in blue
Land lines represent unsurveyed and unmarked locations predetermined by the Bureau of Land Management
Folio S-16, Seward Meridian



SCALE 1:63 900
CONTOUR INTERVAL 100 FEET
DOTTED LINES REPRESENT 50 FOOT CONTOURS
NATIONAL GEODESIC VERTICAL DATUM OF 1929
DEPTH CURVES IN FEET DATUM IS MEAN LOW LOW WATER
SHORELINE SHOWN REPRESENTS THE APPROXIMATE LINE OF MEAN HIGH WATER
THE MEANING OF THE SYMBOLS IS INDICATED IN THE
FOR SALE BY U. S. GEOLOGICAL SURVEY
FAIRBANKS, ALASKA 99701, DENVER, COLORADO 80225, OR RESTON, VIRGINIA 22092
A FOLDER DESCRIBING TOPOGRAPHIC MAPS AND SYMBOLS IS AVAILABLE ON REQUEST



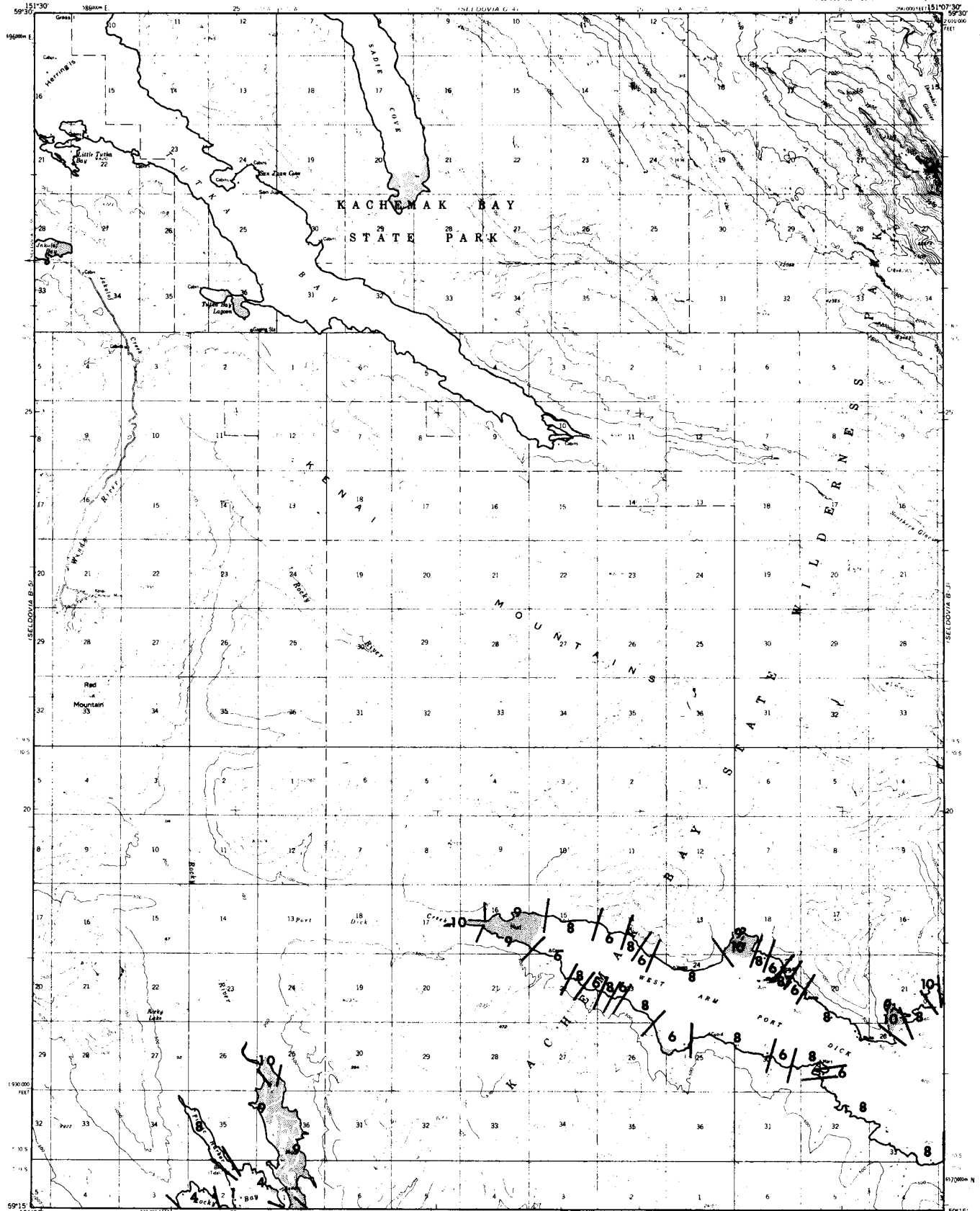
ROAD CLASSIFICATION
No roads or trails in this area

SELDOVIA (A-4), ALASKA
N5900 - W15107 5/15422 5
1951

SELDOVIA C-11
SELDOVIA B-5
SELDOVIA B-5
SELDOVIA A-4
SELDOVIA A-4

UNITED STATES
DEPARTMENT OF THE INTERIOR
GEOLOGICAL SURVEY

SELDOVIA (B-4) QUADRANGLE
ALASKA - KENAI PENINSULA BOROUGH
1:63,360 SERIES (TOPOGRAPHIC)



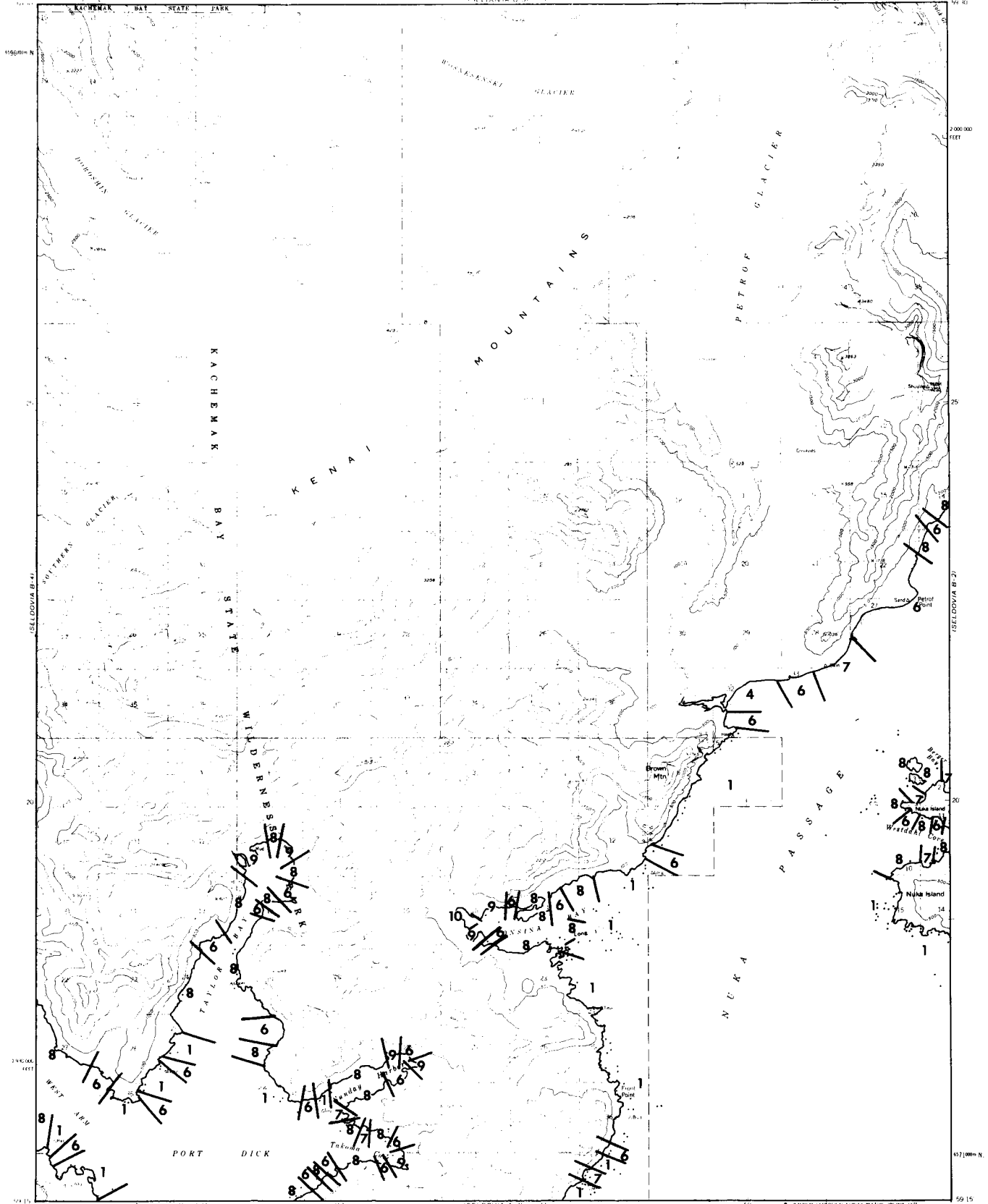
Mapped, edited, and published by the Geological Survey
 Consent by the GCS and USCE
 Topography by photogrammetric methods from aerial photographs
 taken 1951. Map not field checked
 Selected hydrographic data compiled from USCG Charts
 8531, 8552, and 8804 (1:200,000 scale)
 This information is not intended for navigational purposes
 Universal Transverse Mercator projection 1927 North American datum
 10,000-foot grid based on Alaska coordinate system, zone 4
 Contour interval 100 feet
 Land lines represent unsurveyed and unmarked locations
 determined by the Bureau of Land Management
 File S 16, Sheet Number
 Symbols as portrayed indicate only the writer's interpretation
 usually of the relief as shown from aerial photographs
 Examination of original

SCALE 1:63,360

ROAD CLASSIFICATION
 Light duty
 Unimproved dirt

SELDOVIA (B-4) ALASKA
 1951
 MINOR REVISIONS 1976

FOR SALE BY U.S. GEOLOGICAL SURVEY
 FAIRBANKS, ALASKA 99701, DENVER, COLORADO 80225 OR RESTON, VIRGINIA 22092
 A FOLDER DESCRIBING TOPOGRAPHIC MAPS AND SYMBOLS IS AVAILABLE ON REQUEST



Mapped, edited, and published by the Geological Survey
Checked by NOS/NOMA
Engineering by the Geological Survey
Cartography by the Geological Survey
Published by the Geological Survey
Copyright © 1951 by the Geological Survey
This map is a reproduction of the original map
published by the Geological Survey in 1951.
The original map is available for sale from the
Geological Survey, Reston, Virginia 22092.
For more information, contact the
Geological Survey, Reston, Virginia 22092.
Pub. No. 16, Seward Service

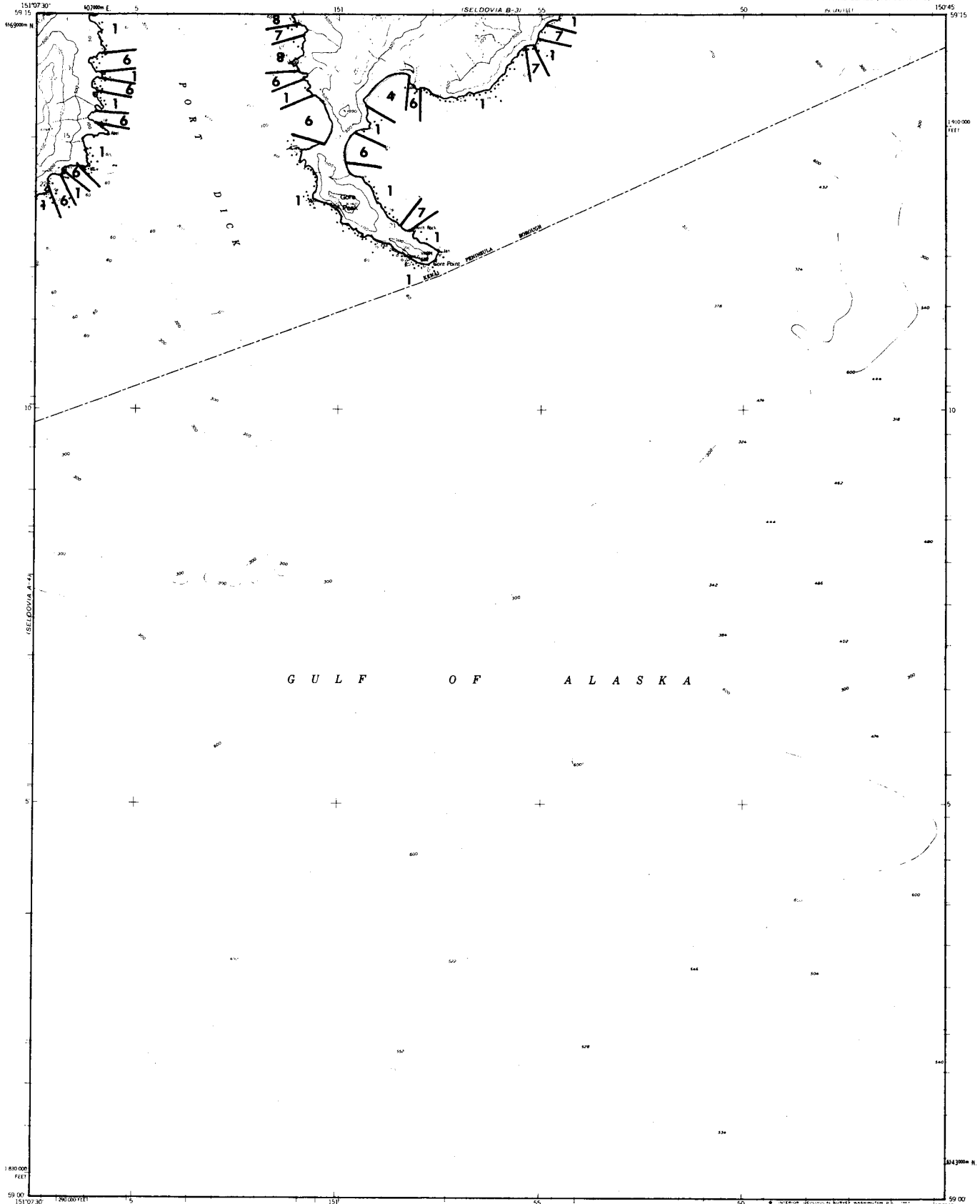
UNIVERSITY MICROFILMS
SERIALS ACQUISITION
300 N. ZEEB RD.
ANN ARBOR, MI 48106

FOR SALE BY U. S. GEOLOGICAL SURVEY
FAIRBANKS, ALASKA 99701, DENVER, COLORADO 80225, OR RESTON, VIRGINIA 22092
A GLENN DESCRIBING TOPOGRAPHIC MAPS AND SYMBOLS IS AVAILABLE ON REQUEST

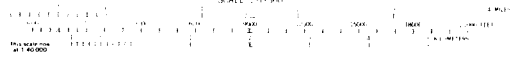


SELDOVIA (B-3), ALASKA
1945, WITH 1945/15422 S.
1951

ROAD CLASSIFICATION
No route or track on this area



Mapped, edited, and published by the Geological Survey
Control by USCGS and USCE
Topography by photogrammetric methods from aerial photographs
taken 1951. Field annotations 1951. Map not field checked
Selected hydrographic data compiled from USCGS Charts 8530
8531, (1961); 8552 (1951); and 8554 (1952) (1:50,000 scale)
This information is not intended for navigational purposes
Universal Transverse Mercator projection, 1927 North American datum
10,000-foot grid based on Alaska coordinate system, zone 4
1000-meter Universal Transverse Mercator grid (T.M.)
zone 5 shown in blue
Land lines represent unsurveyed and unmarked locations
presumed by the Bureau of Land Management
Folio 5, 16, Seward Meridian



CONTOUR INTERVAL 100 FEET
DOTTED AND DASHED LINES INDICATE
DAILY MEAN SEA LEVEL
DEPTH CURVES AND SOUNDINGS IN FEET (DASHES) MEAN LOWER LOW WATER
DOTTED LINES SHOW MEAN HIGH WATER AND MEAN LOWER LOW WATER
DOTTED LINES SHOW MEAN HIGH WATER AND MEAN LOWER LOW WATER



ROAD CLASSIFICATION
No roads or trails in this area

SELDOVIA (A-3), ALASKA
N5900 W15045/15422.5
1951

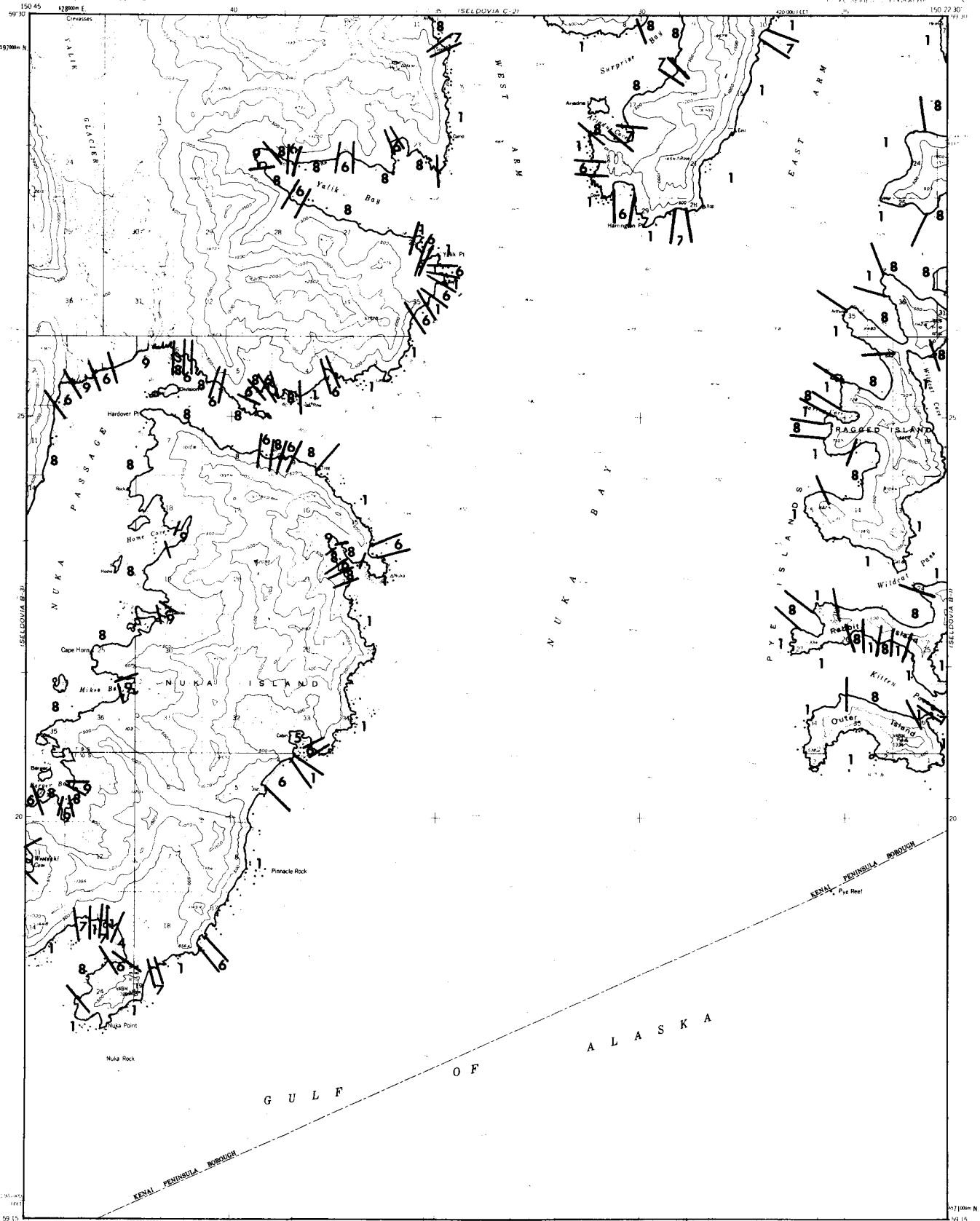
FOR SALE BY U. S. GEOLOGICAL SURVEY
FAIRBANKS, ALASKA 99701, DENVER, COLORADO 80225, OR WASHINGTON, D. C. 20242
A FOLDER DESCRIBING TOPOGRAPHIC MAPS AND SYMBOLS IS AVAILABLE ON REQUEST

SELDOVIA C-1

SELDOVIA G-1

UNITED STATES
DEPARTMENT OF THE INTERIOR
GEOLOGICAL SURVEY

SELDOVIA (B-2) QUADRANGLE
ALASKA



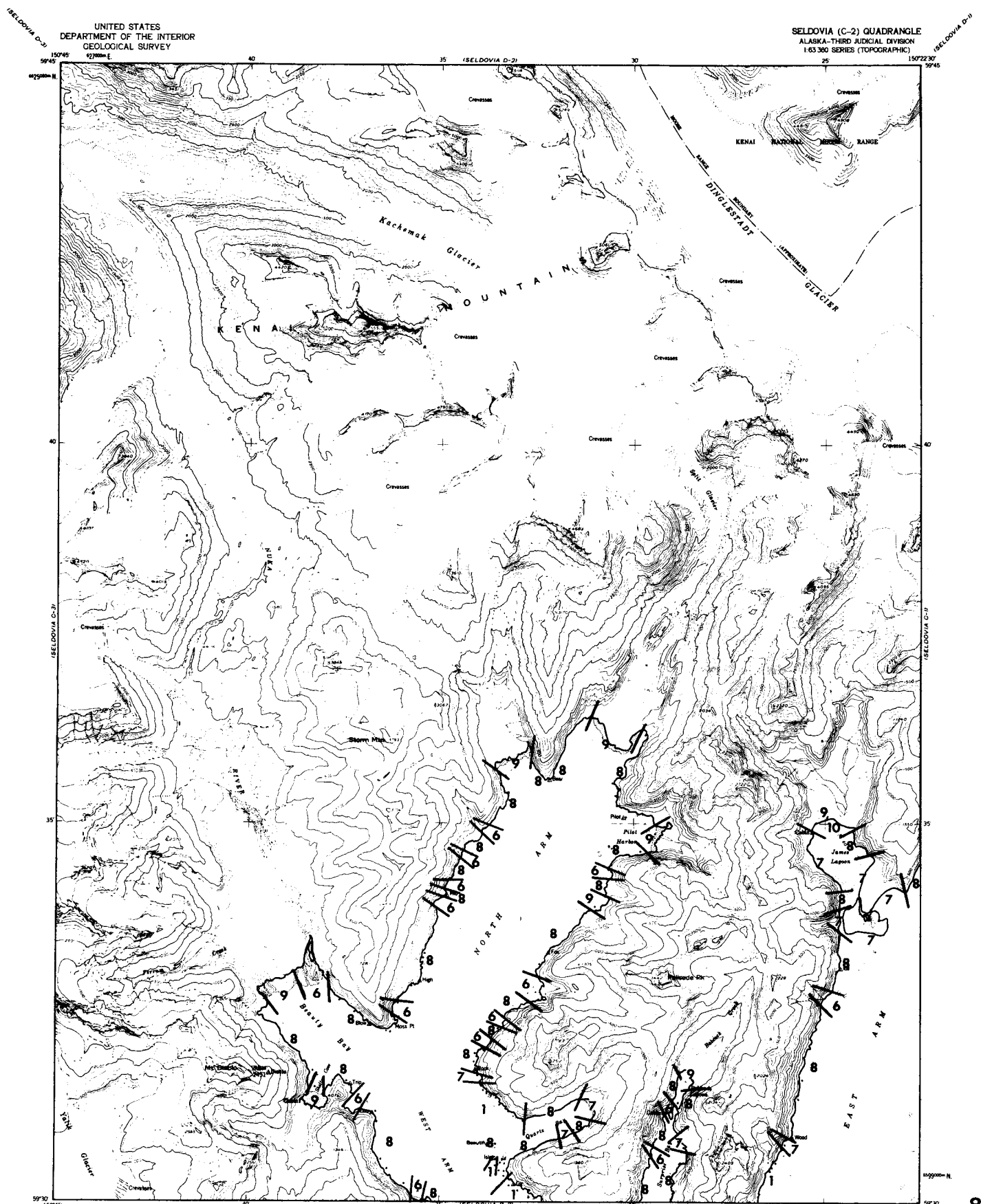
Maped, edited, and published by the Geological Survey
Controlled by USGS and USCE
Topography by photogrammetric methods from aerial photography
taken 1951. Map not held in the field.
Sole red hydrographic data compiled from USCG Charts
8530 and 8532 (1:200,000 scale). This information is not
intended for navigational purposes.
Universal Transverse Mercator projection, 1927 North American datum.
10,000 foot grid based on Alaska coordinate system, Zone 4.
Bathymetric data from the U.S. Hydrographic Survey,
Zone 4, 1950-1952.
Land lines represent contour and contour elevations
predetermined by the Bureau of Land Management.
Elev. in FEET, Seward-Bentley.
Lake elevation in parentheses.

GULF OF ALASKA

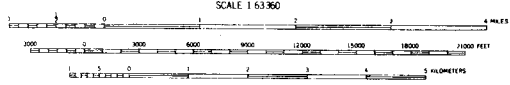
ROAD CLASSIFICATION
No mark on this map

CONTOUR INTERVAL: 100 FEET
FOR SALE BY U.S. GEOLOGICAL SURVEY
FAIRBANKS, ALASKA 99701, DENVER, COLORADO 80225, OR WASHINGTON, D.C. 20242
A FOLDER OF DESCRIBING TOPOGRAPHIC MAPS AND SYMBOLS IS AVAILABLE ON REQUEST

SELDOVIA (B-2), ALASKA
1951



Mapped, edited, and published by the Geological Survey
Control by USCGS and USCE
Hydrography compiled from USCGS charts 8530
and 8552 (1:200,000 Scale)
Topography from aerial photographs by multiple methods, 1953
Aerial photographs taken 1951
Universal Transverse Mercator projection, zone 5
1927 North American datum
Unchecked elevations are shown in brown
1000 meter Universal Transverse Mercator grid lines,
zone 5, shown in blue



ROAD CLASSIFICATION

ALL WEATHER ROADS	(BY WEATHER ZONES)	None	None
Hard surface	None	Improved dirt	None
Other	None	Unimproved dirt	None
Trails	None	None	None

FOR SALE BY U. S. GEOLOGICAL SURVEY
DENVER 2, COLORADO WASHINGTON 25, D. C.
A FOLDER DESCRIBING TOPOGRAPHIC MAPS AND SYMBOLS IS AVAILABLE ON REQUEST

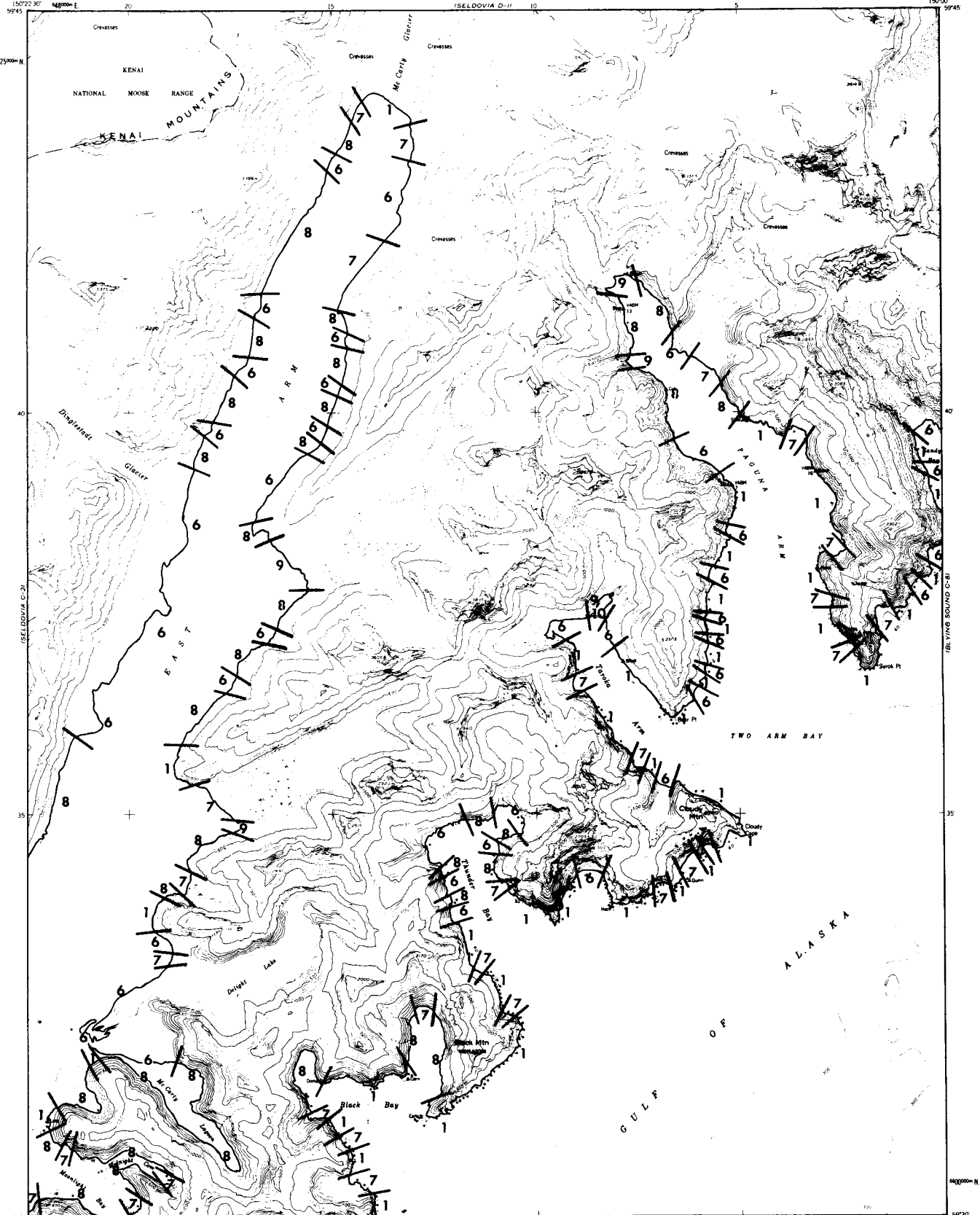
SELDOVIA (C-2), ALASKA
N5930-W15022.5/15X22.5
1953

SELDOVIA C-1

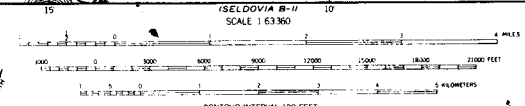
UNITED STATES
DEPARTMENT OF THE INTERIOR
GEOLOGICAL SURVEY

SELDOVIA (C-1) QUADRANGLE
ALASKA—THIRD JUDICIAL DIVISION
1:63,360 SERIES (TOPOGRAPHIC)

SELDOVIA D-11
SELDOVIA B-2
SELDOVIA C-2
SELDOVIA C-3
SELDOVIA D-10
SELDOVIA D-12



Mapped, edited, and published by the Geological Survey
Control by USCGS and USCE
Hydrography compiled from USCGS charts 8529,
8530 and 8552 (1:200,000 scale)
Topography from aerial photographs by multiple methods 1953
Aerial photographs taken 1950
Universal Transverse Mercator projection, zone 5
1927 North American datum
Unchecked elevations are shown in brown and blue
1000-meter Universal Transverse Mercator grid lines,
zone 5, shown in blue



ROAD CLASSIFICATION

ALL WEATHER ROADS		DRY WEATHER ROADS	
Hard surface	None	Improved dirt	None
Other	None	Unimproved dirt	None
		Trails	None

SELDOVIA (C-1), ALASKA
N5930-W15000/15X25 5
1953

FOR SALE BY U. S. GEOLOGICAL SURVEY WASHINGTON 25, D. C.
DENVER 2, COLORADO
FAIRBANKS, ALASKA
A FOLDER DESCRIBING TOPOGRAPHIC MAPS AND SYMBOLS IS AVAILABLE ON REQUEST

SELDOVIA C-2

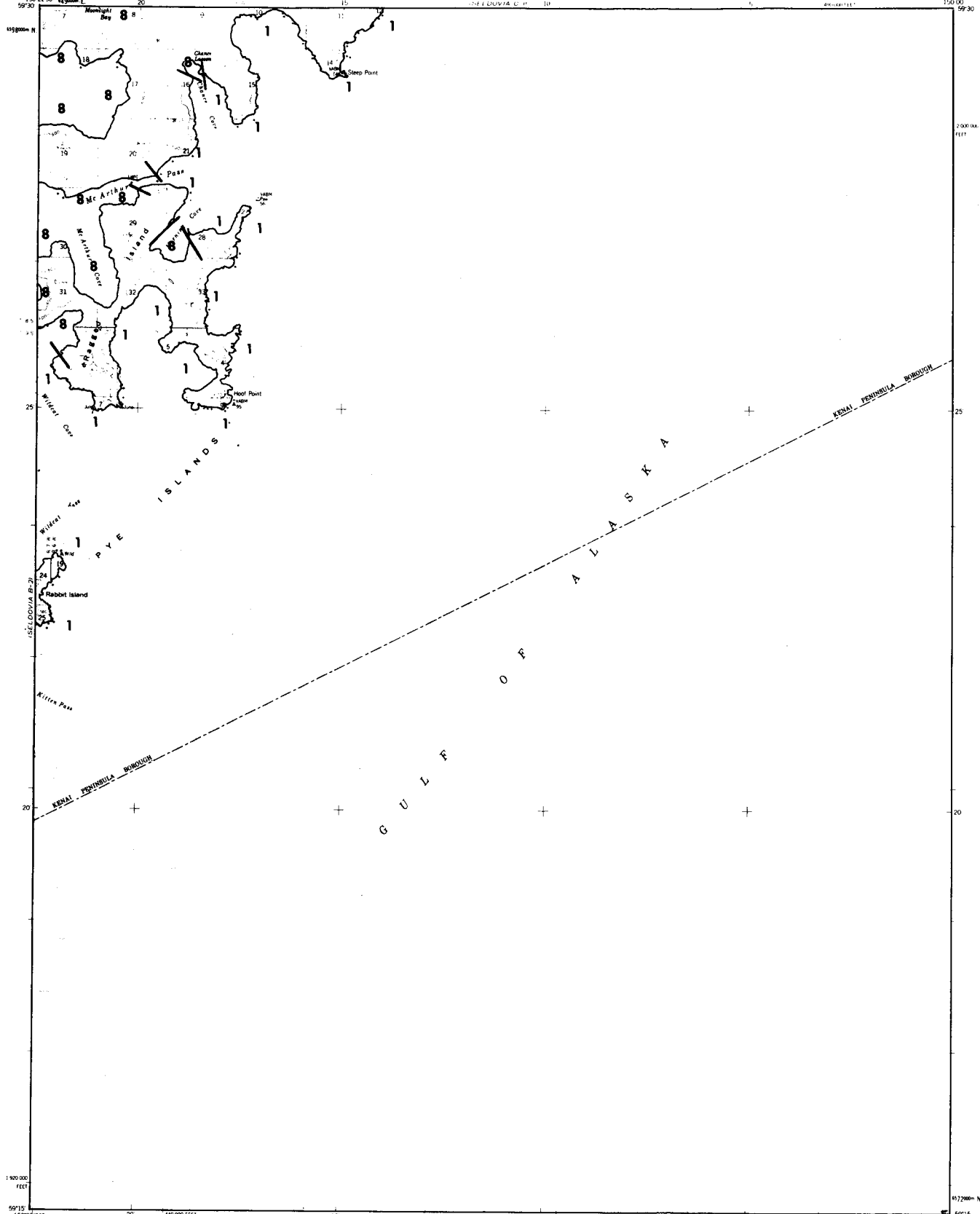
IBBYING SOUND C-6

UNITED STATES
DEPARTMENT OF THE INTERIOR
GEOLOGICAL SURVEY

SELDOVIA (B-1) QUADRANGLE

ALASKA

1:63,360 SERIES (TOPOGRAPHIC)



Mapped, edited, and published by the Geological Survey
Control by USCGS and USGS
Topography by photogrammetric methods from aerial photographs taken 1951; bathymetry 1953. Map not field checked.
Selected hydrographic data compiled from USCGS Charts 8530, 1951 (1:83,074 scale); 8552, 1952 (1:200,000 scale); and 8529, 1951 (1:81,847 scale). This information is not intended for navigational purposes.
Universal Transverse Mercator projection, 1927, North American datum, 10,000 meter; Universal Transverse Mercator grid ticks, zone 5, shown in blue.
Land lines represent unsurveyed and unmarked locations determined by the Bureau of Land Management, Folio S 16, Seward Meridian.

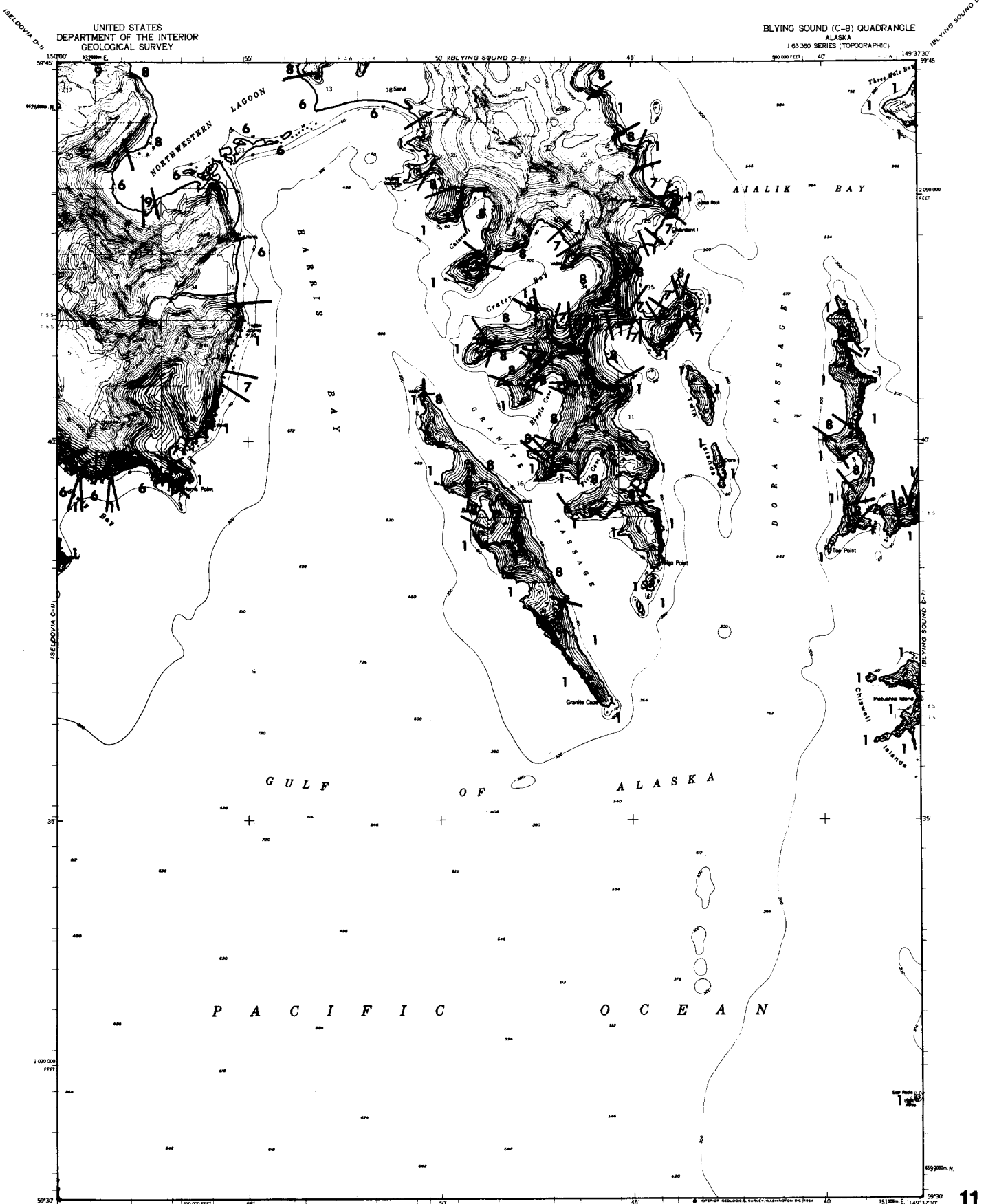
SCALE 1:63,360

CONTOUR INTERVAL 100 FEET
(BASED ON MEAN SEA LEVEL)
DEPTH CURVES AND SOUNDINGS IN FEET GALELLO'S MEAN LOWER LOW WATER
(DEPTH MEASUREMENTS NOT APPROXIMATELY LINE OR MEAN HIGH WATER)
(THE HORIZONTAL RANGE OF TIDE IS APPROXIMATELY 10 FEET)

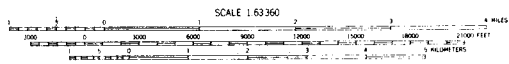
FOR SALE BY U. S. GEOLOGICAL SURVEY
FAIRBANKS, ALASKA 99701, DENVER, COLORADO 80225, OR RESTON, VIRGINIA 22092
A FOLDER DESCRIBING TOPOGRAPHIC MAPS AND SYMBOLS IS AVAILABLE ON REQUEST

ROAD CLASSIFICATION
No roads or trails in this area

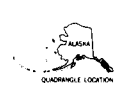
SELDOVIA (B-1), ALASKA
N5915-W15000/15422.5
1953



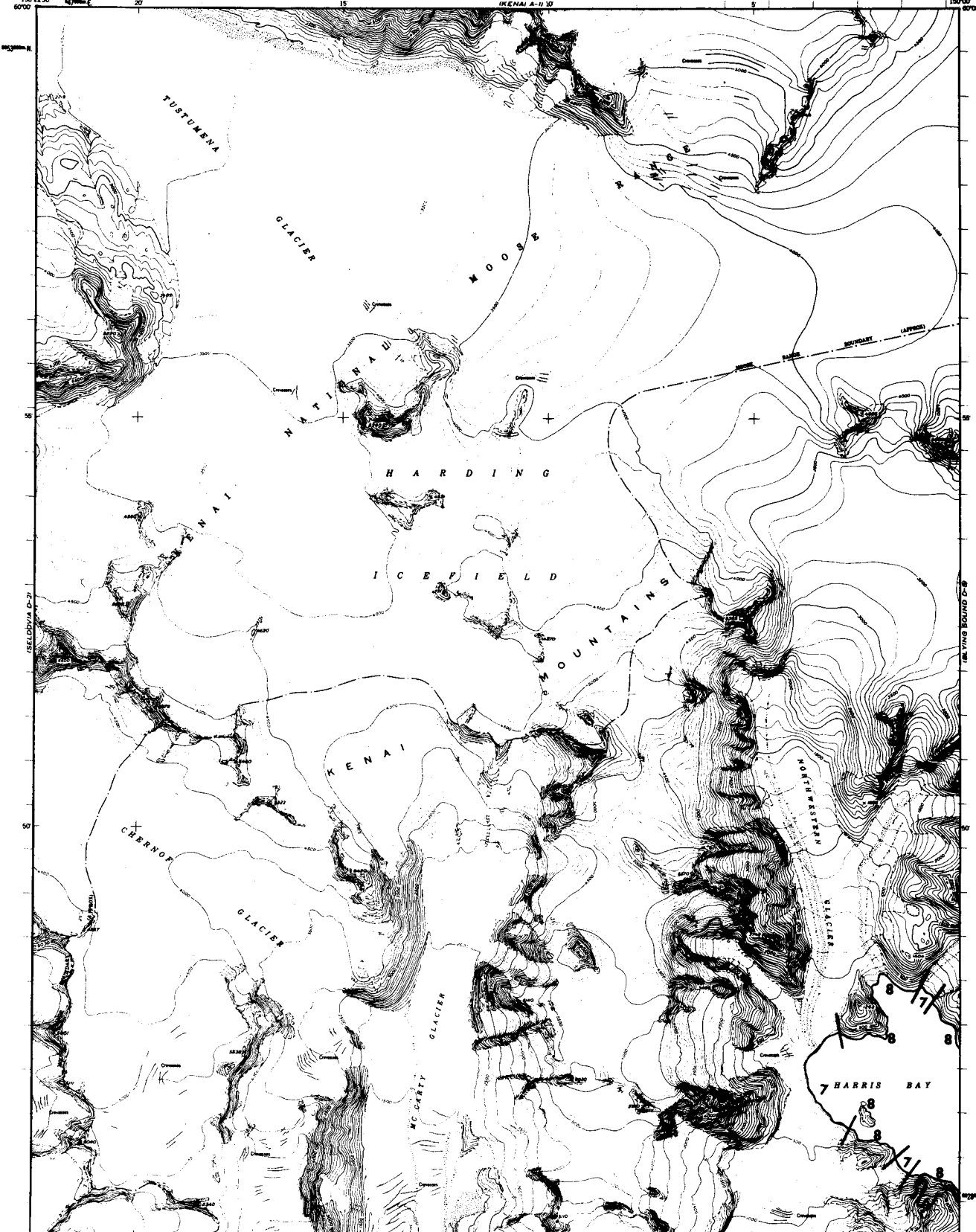
Maped, edited, and published by the Geological Survey
Control by USCGS and USCE
Topography by photogrammetric methods from aerial photographs
taken 1950; field annotated 1951. Map not later checked.
Selected hydrographic data compiled from USCGS
Chart 8529 (1951). This information is not intended
for navigational purposes.
Universal Transverse Mercator projection, 1927 North American datum
10,000 foot grid based on Alaska coordinate system, zone 4
1000 meter Universal Transverse Mercator grid ticks,
zone 5, shown in blue.
Land lines represent unsurveyed and unmarked locations
determined by the Bureau of Land Management
Foto S-16, Seward Meridian



SCALE 1:63,360
CONTOUR INTERVAL 100 FEET
DARTON 0 MEAN SEA LEVEL
DEPTH CURVES AND SOUNDINGS IN FEET (DARTON 0 MEAN LOWER LOW WATER)
WIRELESS SHIP REPRESENTS THE APPROXIMATE LINE OF MEAN HIGH WATER
THE MIDDLE RING OF ICE IS INDICATED BY (11)
FOR SALE BY U. S. GEOLOGICAL SURVEY
FAIRBANKS, ALASKA DENVER 25, COLORADO WASHINGTON 25, D. C.
A FOLDER DESCRIBING TOPOGRAPHIC MAPS AND SYMBOLS IS AVAILABLE ON REQUEST



ROAD CLASSIFICATION
No roads or trails in this area
BLYLING SOUND (C-8), ALASKA
N5930-W14937.5/15K22.5
1951
MICH. REVIEWS 1963

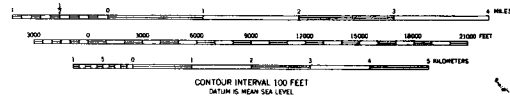


150°22'30"
59°45'
150°22'30"
20
15
10
5
0
5
10
15
20
150°00'

Maped, edited, and published by the Geological Survey
Control by USCGS and USCE
Topography from aerial photographs by multiplex methods 1953
Aerial photographs taken 1950
Universal Transverse Mercator projection, zone 5
1927 North American datum
Unchecked elevations are shown in brown and blue
1000-meter Universal Transverse Mercator grid ticks,
zone 5, shown in blue



APPROXIMATE MEAN
DECLINATION, 1953

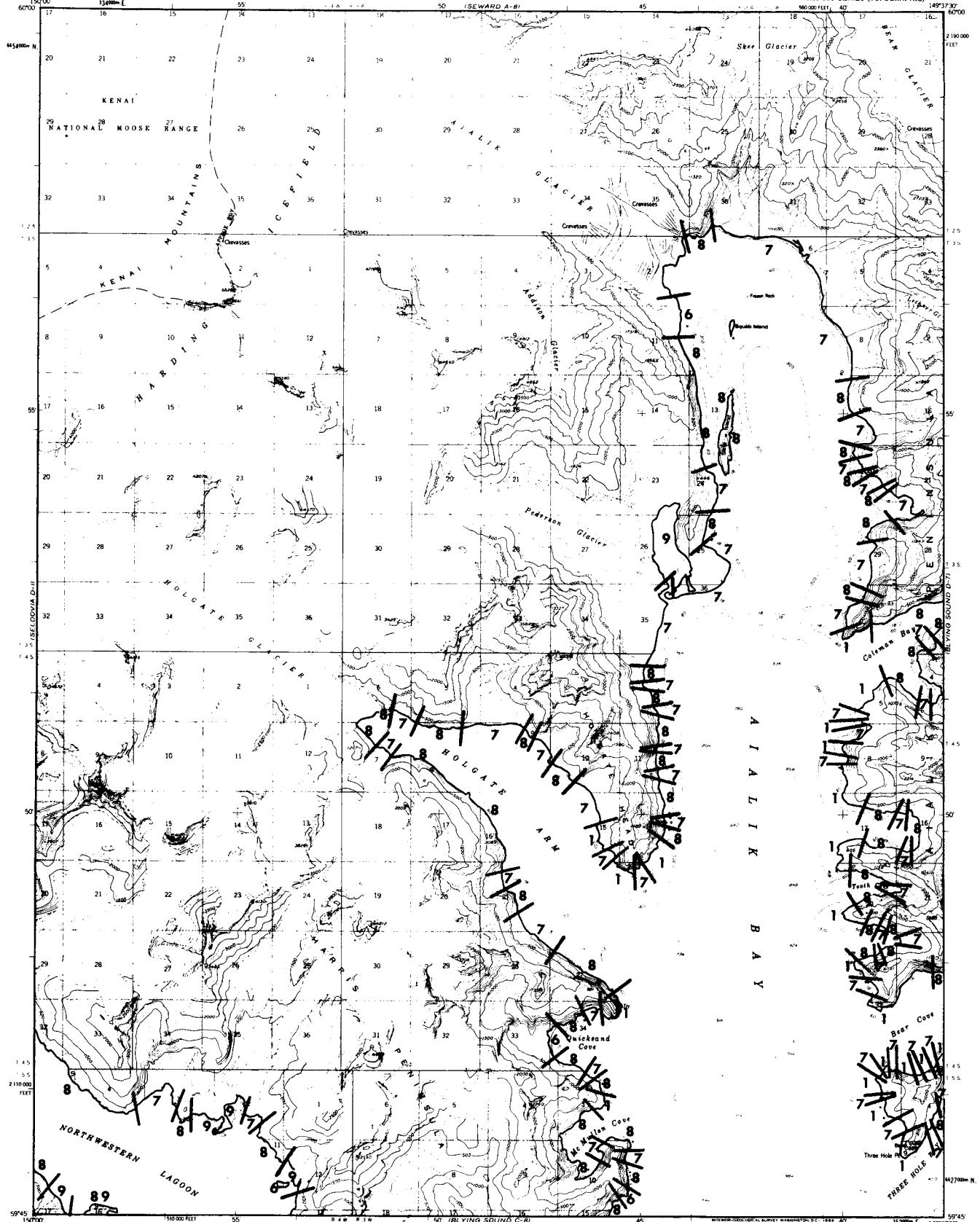


ROAD CLASSIFICATION

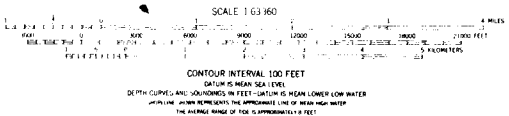
ALL WEATHER ROADS	DRY WEATHER ROADS
Hard surface	None
Improved dirt	None
Other	None
Unimproved dirt	None
Trails	None

FOR SALE BY U. S. GEOLOGICAL SURVEY
FAIRBANKS, ALASKA DENVER 2, COLORADO WASHINGTON 25, D. C.

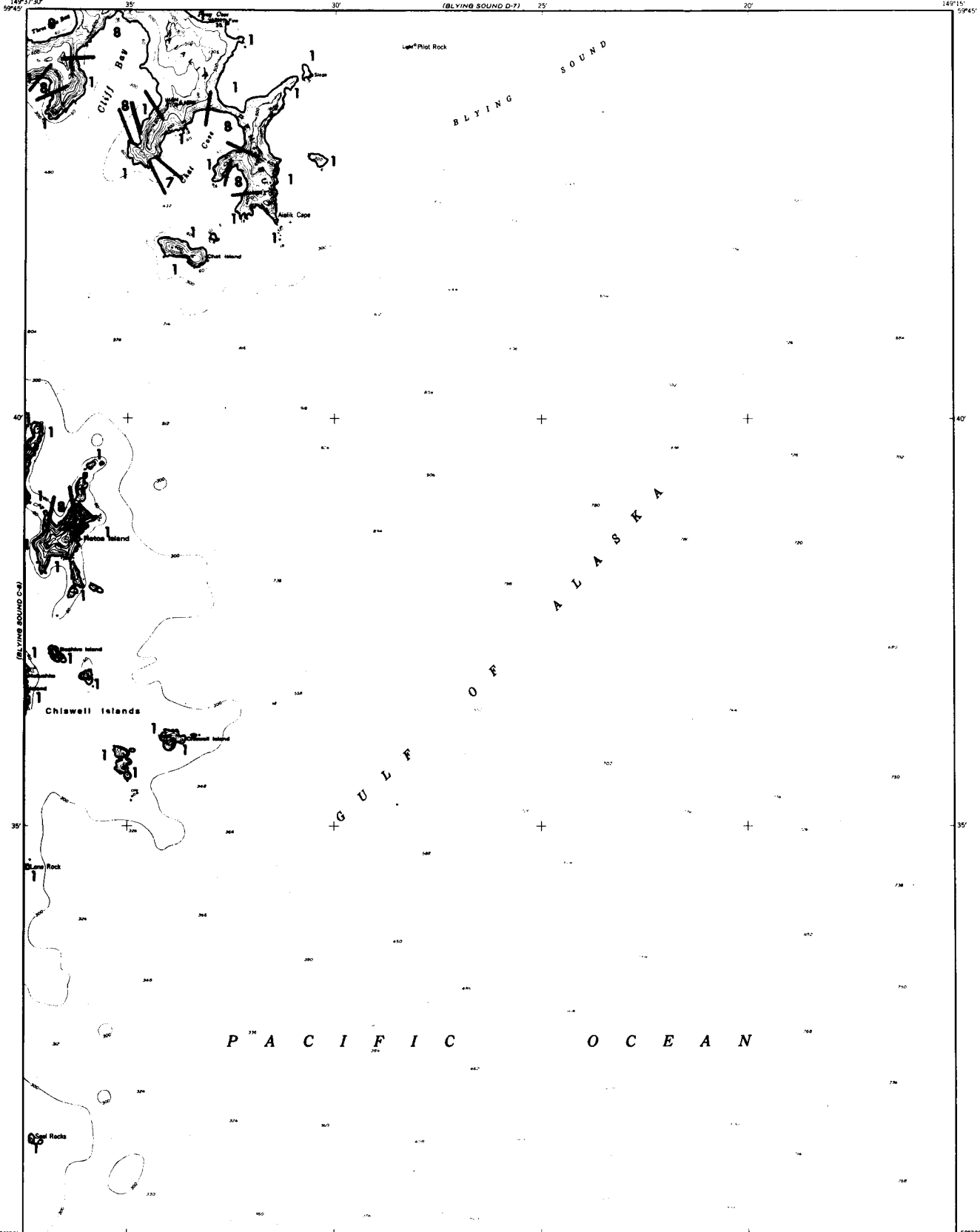
SELDOVIA (D-1), ALASKA
N5945-W15000/15X22.5
1953



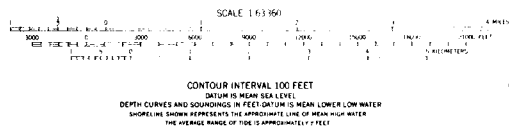
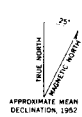
Maped, edited, and published by the Geological Survey
Control by USCGS and USCE
Topography by photogrammetric methods from aerial photographs
taken 1950, field annotated 1951. Map not field checked
Selected hydrographic data compiled from USC&GS Charts
8529 (1951) and 8552 (1951) (1:200,000 scale)
This information is not intended for navigational purposes
Universal Transverse Mercator projection, 1927 North American datum
10,000-foot grid based on Alaska coordinate system, zone 4
1,000-meter Universal Transverse Mercator grid (4-
zone 6, shown in blue)
Land lines represent unsurveyed and unmarked locations
as determined by the Bureau of Land Management
Folio S 16, Seward Meridian



ROAD CLASSIFICATION
No roads or trails in this area
BLYING SOUND (D-8), ALASKA
N5945-W14937.5/15222.5
1951
MAP POSITION 783



Mapped, edited, and published by the Geological Survey
Control by USCGS and USCE
Hydrography compiled from USCGS Chart 8529
Topography from aerial photographs by multiple methods 1952
Aerial photographs taken 1950
Universal Transverse Mercator projection, zone 6
1927 North American datum
Unchecked elevations are shown in brown

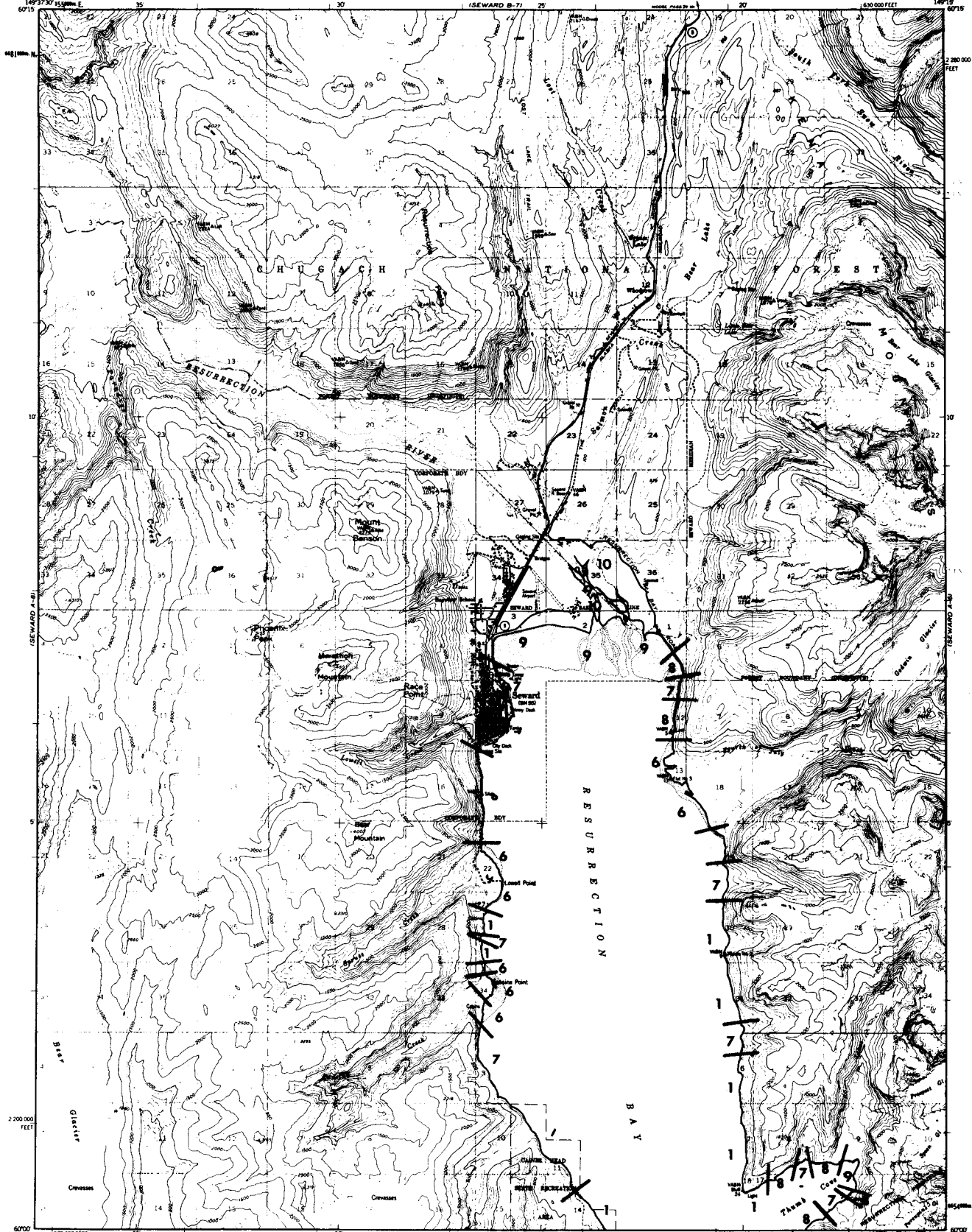


ROAD CLASSIFICATION

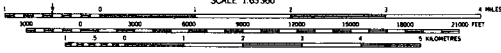
ALL WEATHER ROADS	DRY WEATHER ROADS
Hard surface	None
Other	None
Trails	None

BLYING SOUND (C-7), ALASKA
H5930-W14915/15x22.5
1952

FOR SALE BY U. S. GEOLOGICAL SURVEY, FEDERAL CENTER, DENVER, COLORADO OR WASHINGTON 25, D. C.
A FOLDER DESCRIBING TOPOGRAPHIC MAPS AND SYMBOLS IS AVAILABLE ON REQUEST



Mapped, edited, and published by the Geological Survey
Control by USGS and USCE
Topography by photogrammetric methods from aerial photographs taken 1950. Map not field checked.
Selected hydrographic data compiled from USCGS Charts 8552 (1951) (scale 1:200,000), and 8529 (1951) (scale 1:81,847). This information is not intended for navigational purposes.
Universal Transverse Mercator projection, 1927 North American datum, 10,000-foot grid based on Alaska coordinate system, zone 4.
1,000-metre Universal Transverse Mercator grid ticks, zone 4, shown in blue.
Gray land lines represent unsurveyed and unmarked locations predetermined by the Bureau of Land Management.
Folios S-14, S-15, and S-16, Seward Meridian.
Contours as portrayed indicate only the wetter areas; visibility of low relief as interpreted from aerial photographs.
Lake elevations are unchecked.



CONTOUR INTERVAL 100 FEET
NATIONAL GEODETIC VERTICAL DATUM OF 1929
DEPTH CURVES AND SOUNDINGS IN FEET-DATUM IS MEAN LOWER LOW WATER
SOUNDING CURVES RETAINING THE APPROXIMATE LINE OF MEAN HIGH WATER
THE AVERAGE RANGE OF TIDE IS APPROXIMATELY 8 FEET

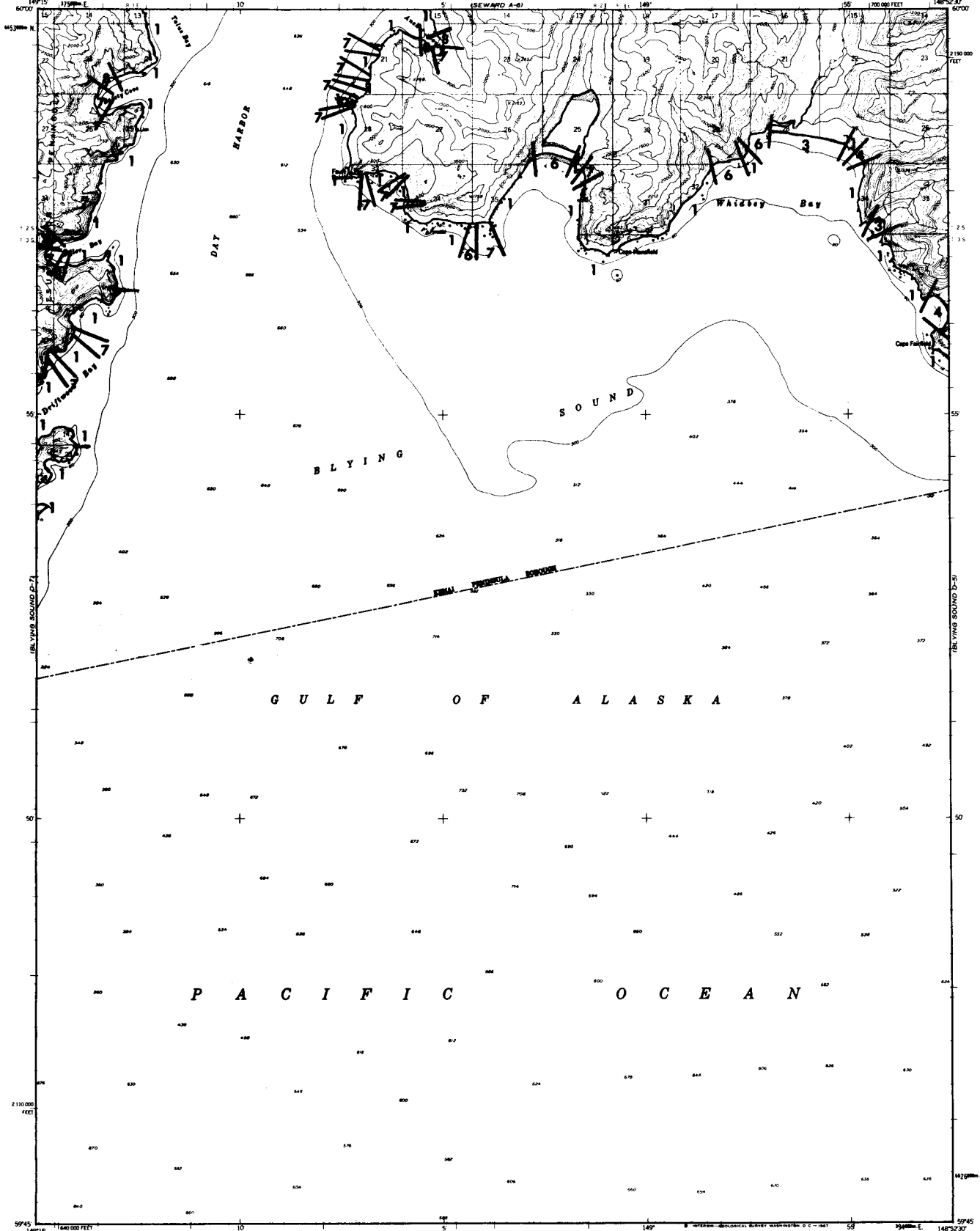


ROAD CLASSIFICATION

Medium-duty	Light-duty
Unimproved dirt	State Route

FOR SALE BY U.S. GEOLOGICAL SURVEY
FAIRBANKS, ALASKA 99701, DENVER, COLORADO 80226, OR RESTON, VIRGINIA 22092
A FOLDER DESCRIBING TOPOGRAPHIC MAPS AND SYMBOLS IS AVAILABLE ON REQUEST

SEWARD (A-7), ALASKA
1:63,360—W14915/15422 5
1950
HONG KONG 1975



BL Y I N G S O U N D C - 7 1

Mapped, edited, and published by the Geological Survey
Control by USCE and USC&GS
Topography by photogrammetric methods from aerial photographs
taken 1950. Map not field checked.
Selected hydrographic data compiled from USCGC Charts 8528
and 8552 (1:200 000 scale). This information is not intended for
navigational purposes.
Universal Transverse Mercator projection, 1927 North American datum
10 000-foot grid based on Alaska coordinate system, zone 4
1000-meter Universal Transverse Mercator grid ticks,
zone 6, shown in blue.
Land lines represent unsurveyed and unmarked locations
determined by the Bureau of Land Management.
Folio S-15, Seward Meridian.



CONTOUR INTERVAL 100 FEET
DATUM IS MEAN SEA LEVEL
DEPTH CURVES AND SOUNDINGS IN FEET - DATUM IS MEAN LOWER LOW WATER
SHORELINE SHOWS APPROXIMATE LINE OF MEAN HIGH WATER
THE AVERAGE RANGE OF TIDE IS APPROXIMATELY 8 FEET

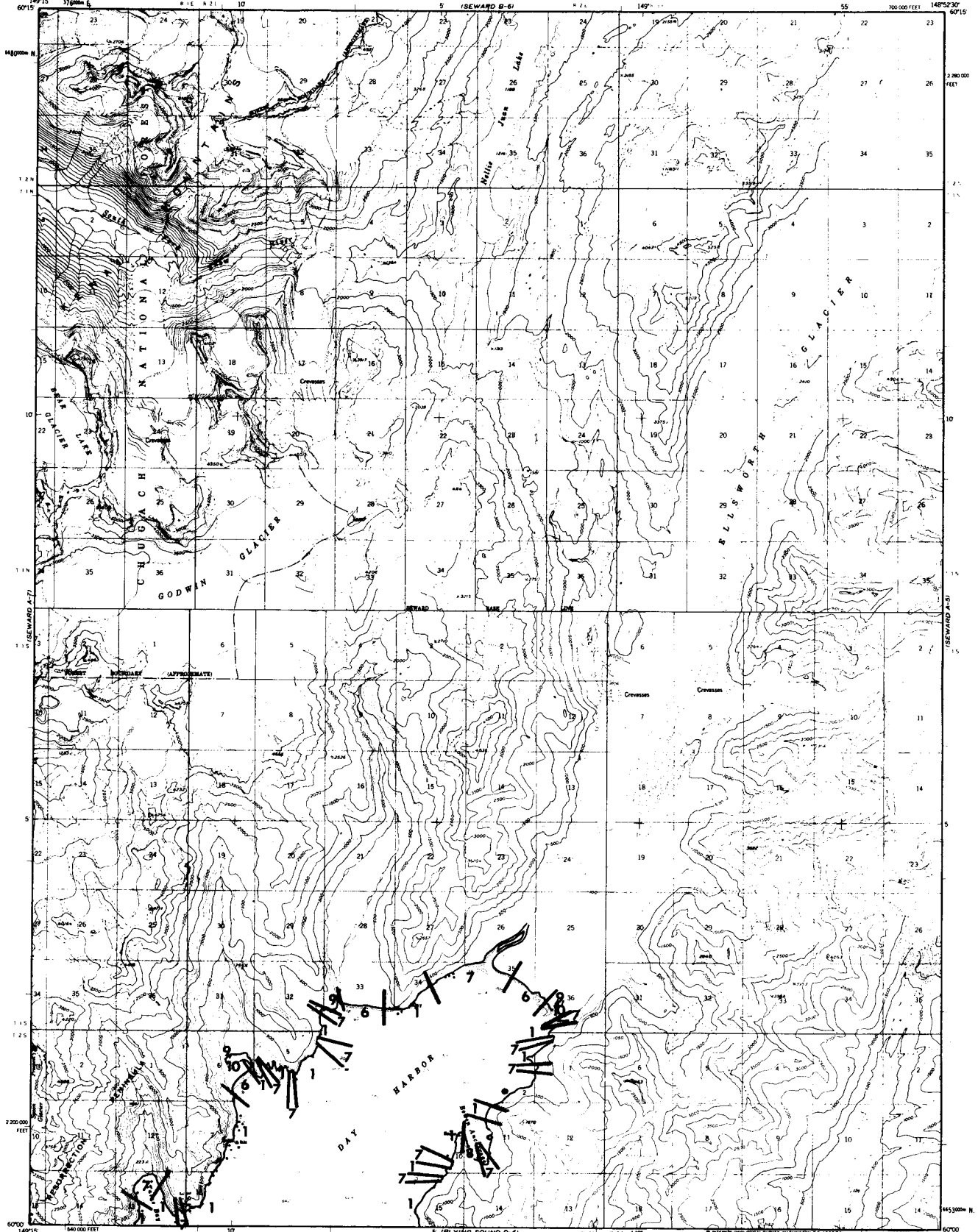


ROAD CLASSIFICATION
No roads or trails in this area

BL Y I N G S O U N D (D-6), ALASKA
N5945-W14852 5/15422 5

1950
7808 84606 184

FOR SALE BY U. S. GEOLOGICAL SURVEY
FAIRBANKS, ALASKA 99701, DENVER, COLORADO 80225, OR WASHINGTON, D. C. 20242
A FOLDER DESCRIBING TOPOGRAPHIC MAPS AND SYMBOLS IS AVAILABLE ON REQUEST



Mapped, edited, and published by the Geological Survey
Control by USCGS and USCE
Topography by photogrammetric methods from aerial photographs
taken 1950. Map not field checked.
Selected hydrographic data compiled from USCGS Charts
8528 and 8552 (1:200,000 scale). This information is not
intended for navigational purposes.
Universal Transverse Mercator projection, 1927 North American datum,
10,000 foot grid based on Alaska coordinate system, zone 4
1000 meter Universal Transverse Mercator grid ticks,
zone 5, shown in blue.
Land lines represent unsurveyed and unmarked locations
determined by the Bureau of Land Management
Forms 5-14 and 5-15, Seward Meridian
Lake elevations are uncheckd

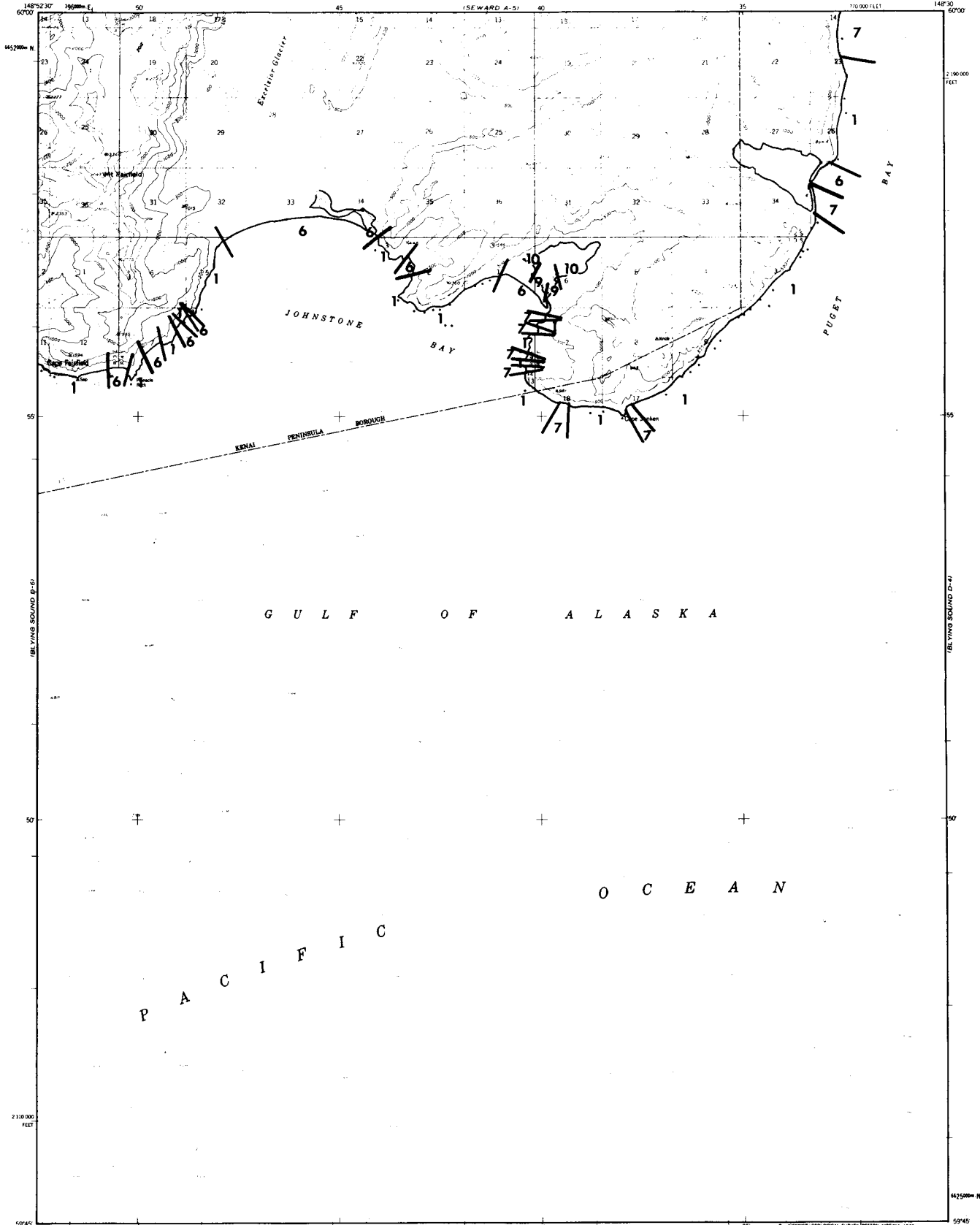


CONTOUR INTERVAL 100 FEET
DOTTED IS MEAN SEA LEVEL
DEPTH CURVES AND SOUNDINGS IN FEET OUT TO 50 FEET MEAN LOWER LOW WATER
DASHED LINE REPRESENTS THE APPROXIMATE LINE OF MEAN LOWER WATER
THE SHORELINE REPRESENTS THE APPROXIMATE LINE OF MEAN SEA LEVEL

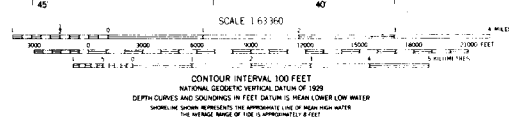


ROAD CLASSIFICATION
No roads or trails in this area
SEWARD (A-6), ALASKA
N6000-W14852-15222-5
1950
WHOLE SHEET NO. 18

FOR SALE BY U. S. GEOLOGICAL SURVEY
FAIRBANKS, ALASKA 99701, DENVER, COLORADO 80225 OR WASHINGTON, D. C. 20242
A FOLDER DESCRIBING TOPOGRAPHIC MAPS AND SYMBOLS IS AVAILABLE ON REQUEST



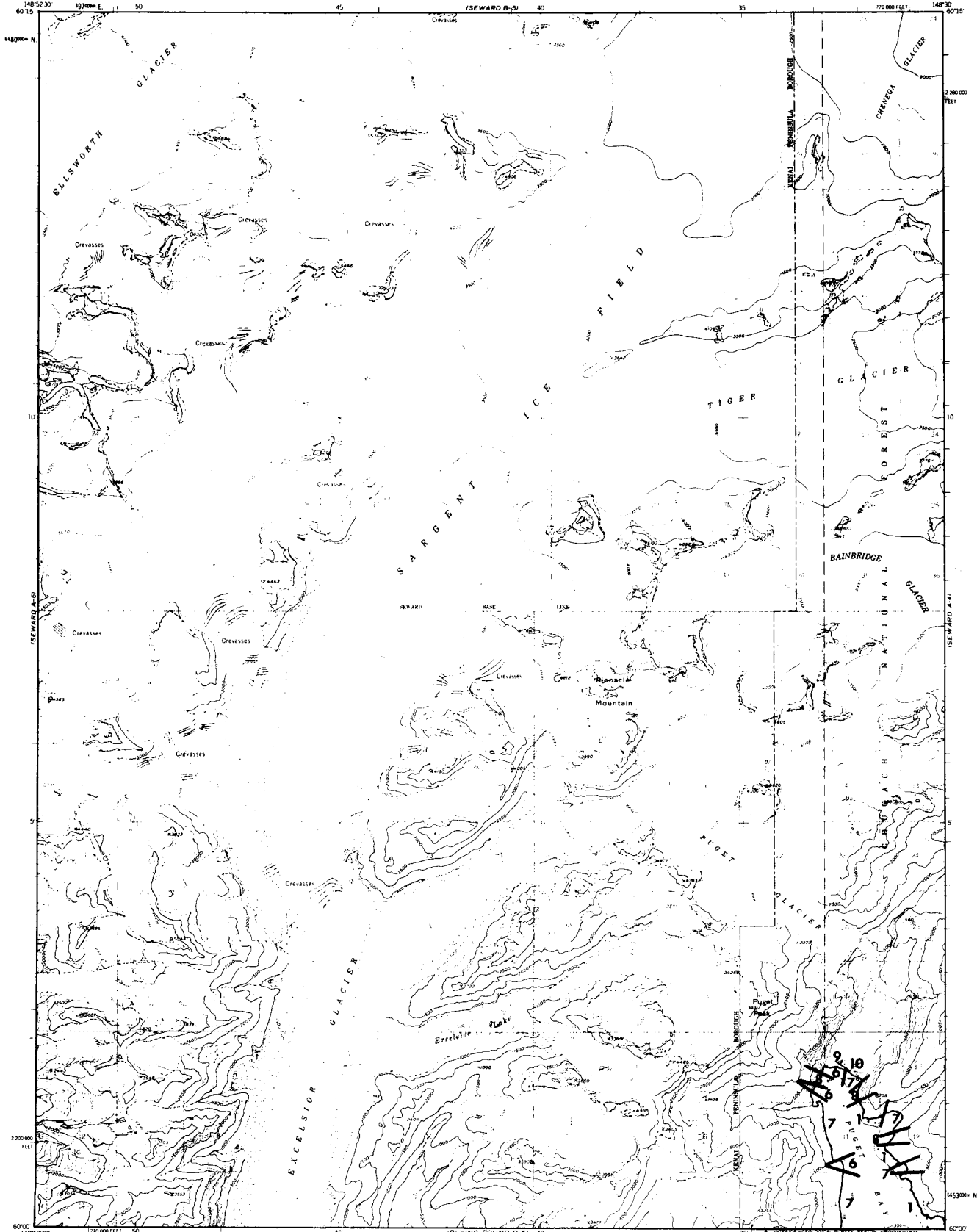
Mapped, edited, and published by the Geological Survey
Control by USCGS and USCE
Topography by photogrammetric methods from aerial photographs
taken 1950. Map not field checked.
Selected hydrographic data compiled from USCGS Charts
8528 (1951) and 8552 (1952) (1:200,000 scale).
This information is not intended for navigational purposes.
Universal Transverse Mercator projection, 1927 North American datum
10,000-foot grid based on Alaska coordinate system, zone 4
1,000-meter Universal Transverse Mercator grid ticks,
zone 6, shown in blue.
Land lines represent unurveyed and unmarked locations
determined by the Bureau of Land Management
Folio S-15, Seward Meridian.
Swamps, as portrayed, indicate only the wetter areas.
Usualy of low relief, as interpreted from aerial photographs.
Lake elevations are uncharted.



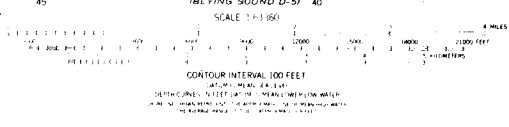
ROAD CLASSIFICATION
No roads or trails in this area

BLYLING SOUND (D-5), ALASKA
NS945-W-14830/15422.5
1952
HATCH 809206, 1952

FOR SALE BY U. S. GEOLOGICAL SURVEY
FAIRBANKS, ALASKA 99701, DENVER, COLORADO 80225, OR RESTON, VIRGINIA 22092
A FOLDER DESCRIBING TOPOGRAPHIC MAPS AND SYMBOLS IS AVAILABLE ON REQUEST



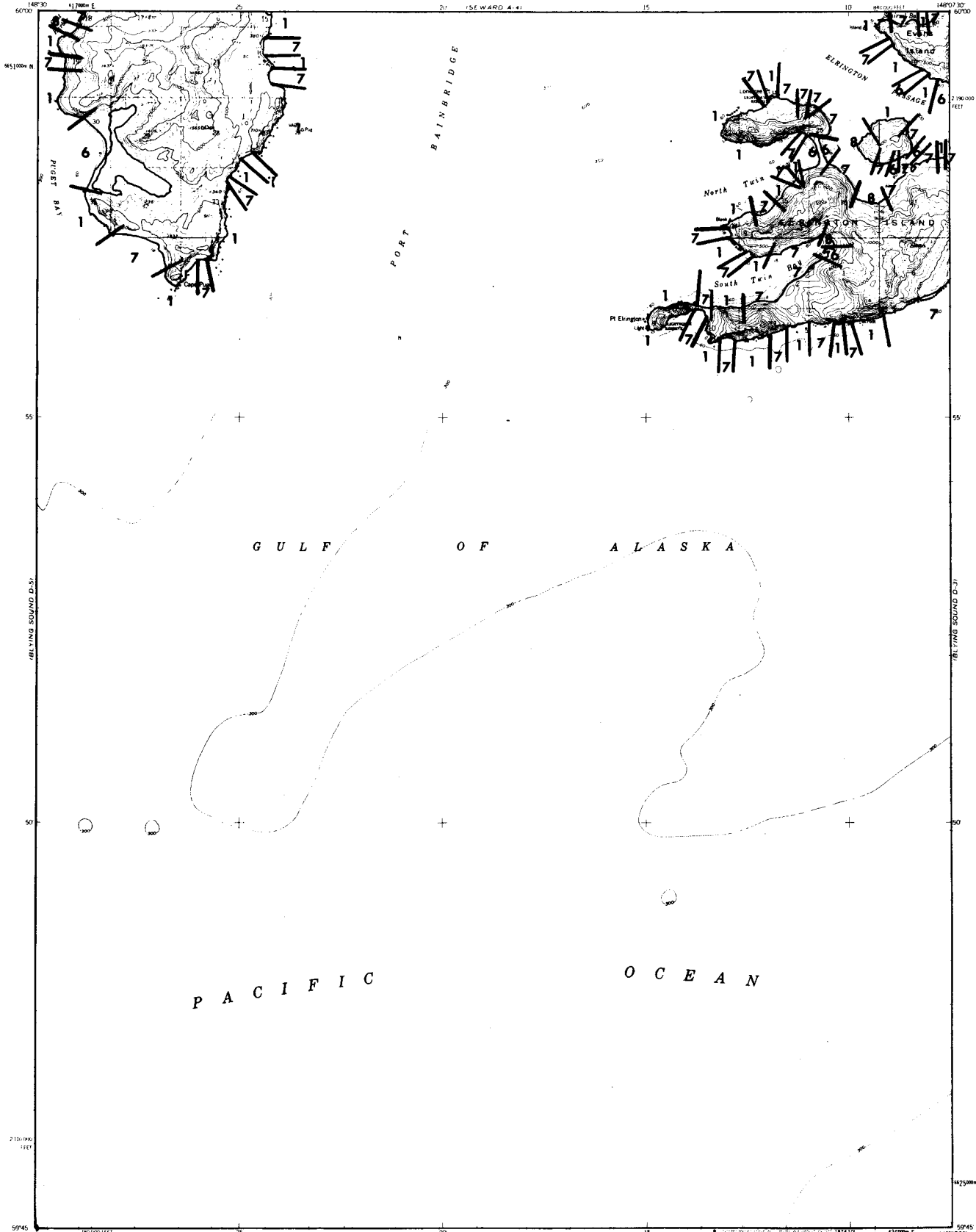
Mapped, edited, and published by the Geological Survey
Control by USCGS and USCE
Topography by photogrammetric methods from aerial photographs
taken 1950, field annotated 1951. Map not field checked.
Selected hydrographic data compiled from USCGS Chart
8028 (1950) (1:81,436 scale). This information is not intended
for navigational purposes.
Universal Transverse Mercator projection, 1927 North American datum
10,000-foot grid based on Alaska coordinate system, zone 4
1000-meter Universal Transverse Mercator grid lines,
zone 6, shown in blue.
Land lines represent unsurveyed and unmarked locations
predetermined by the Bureau of Land Management
Folios 5, 14, and 15, Seward Meridian.
Swamps as portrayed indicate only the water areas
usually of low relief as interpreted from aerial photographs.



ROAD CLASSIFICATION
No roads or trails in this area

FOR SALE BY U. S. GEOLOGICAL SURVEY
FAIRBANKS, ALASKA 99701, DENVER, COLORADO 80225, OR WASHINGTON, D. C. 20242
A FOLDER DESCRIBING TOPOGRAPHIC MAPS AND SYMBOLS IS AVAILABLE ON REQUEST

SEWARD (A-5), ALASKA
N6300-W14830/15422.5
1951



Maped, edited, and published by the Geological Survey
Control by USCGO's and USCE
Topography by photogrammetric methods from aerial photographs
taken 1950. Major road shown
Selected hydrographic data compiled from U.S. Charts 8515,
8523, 8528, and 8531 (1:200,000 scale). This information
is not intended for navigational purposes.
Universal Transverse Mercator projection, 1927 North American datum,
10,000 foot grid based on Alaska coordinate system, zone 4
1000 meter Universal Transverse Mercator grid ticks
shown by shorter tick marks.
Land lines represent unsurveyed and unmarked locations
predetermined by the Bureau of Land Management
Folio S 15, Seaward Mission.
Entire land area is within the Chugach National Forest

CONTOUR INTERVAL 100 FEET
DATUM: MEAN SEA LEVEL
GEODETIC COORDINATE SYSTEM: NORTH AMERICAN 1927
THE POLAR PROJECTION OF THIS MAP IS AVAILABLE ON REQUEST
FOR SALE BY U. S. GEOLOGICAL SURVEY
FAIRBANKS, ALASKA 99701, DENVER, COLORADO 80225, OR WASHINGTON, D. C. 20242
A FOLDER DESCRIBING TOPOGRAPHIC MAPS AND SYMBOLS IS AVAILABLE ON REQUEST



ROAD CLASSIFICATION
No roads or trails in this area

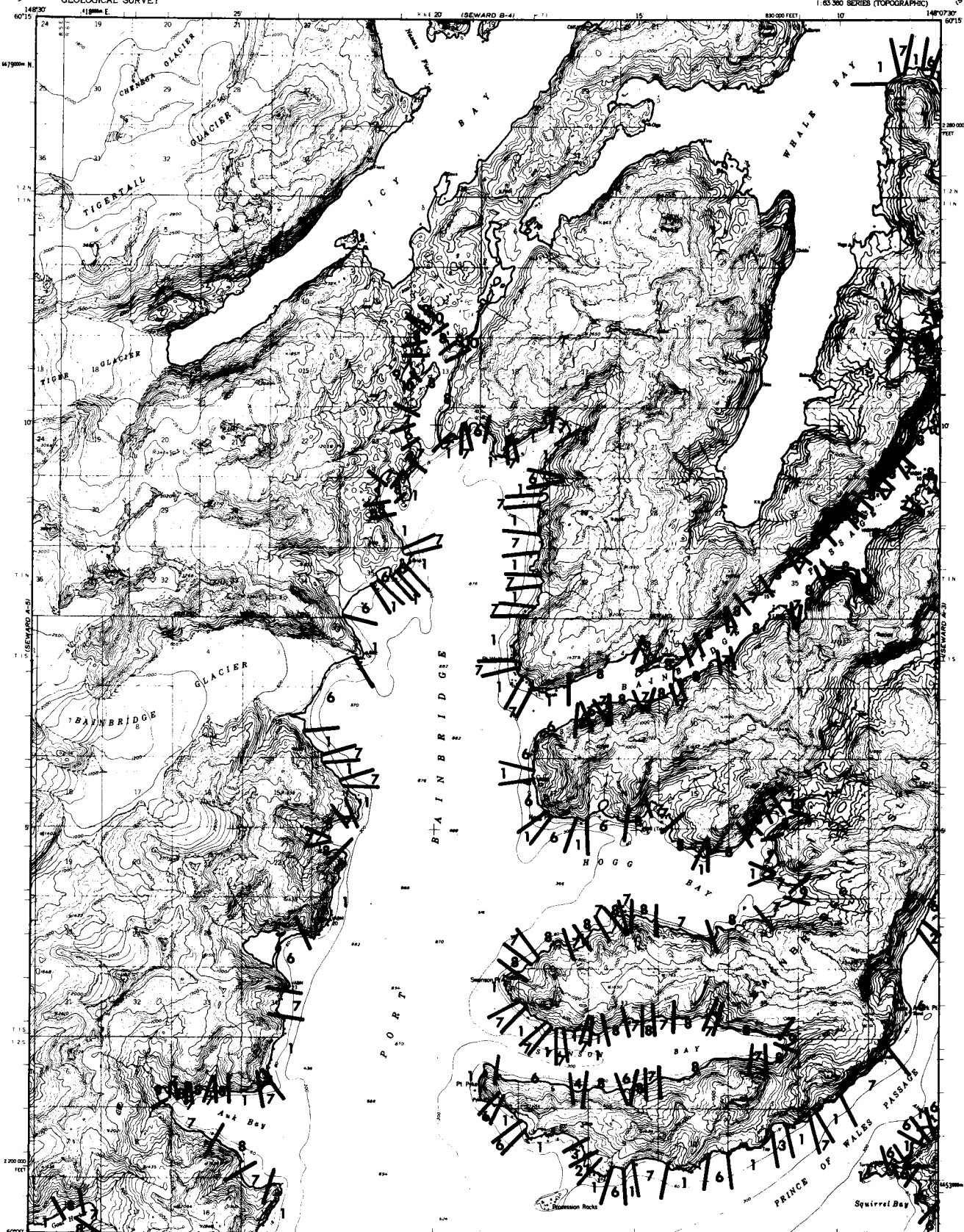
BLYLING SOUND (D-4), ALASKA
N5945 - W14807.5/15422.5
1950
www.gsa.gov

SEWARD B-3

UNITED STATES
DEPARTMENT OF THE INTERIOR
GEOLOGICAL SURVEY

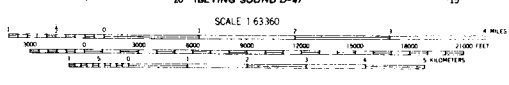
SEWARD (A-4) QUADRANGLE
ALASKA
1:63 360 SERIES (TOPOGRAPHIC)

SEWARD B-2



SEWARD D-2

Mapped, edited, and published by the Geological Survey
Control by USCGS and USCE
Topography by photogrammetric methods from aerial photographs
taken 1950, field annotated 1951. Map not field checked.
Selected hydrographic data compiled from USCGS Charts
8515 (1949), 8523 (1951), 8528 (1950), and 8551 (1950)
This information is not intended for navigational purposes.
Universal Transverse Mercator projection, 1927 North American datum
10,000 foot grid based on Alaska coordinate system, zone 4
1,000 meter Universal Transverse Mercator grid ticks,
zone 6, shown in blue.
Land lines represent unimproved and unmarked locations
determined by the Bureau of Land Management
Folios S-14 and S-15, Seward Meridian
Entire land area is within the Chugach National Forest
Lake elevations are unchecked



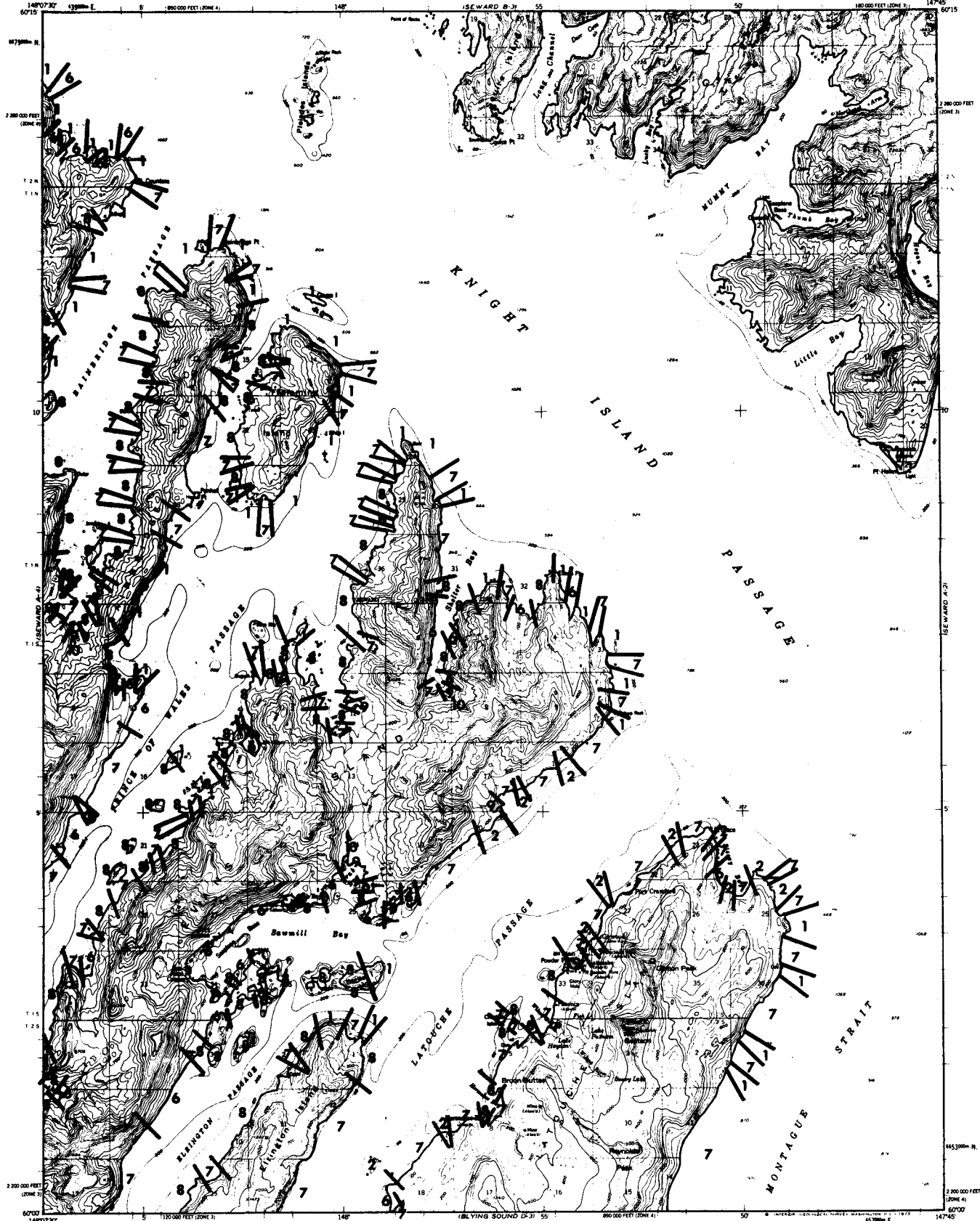
CONTOUR INTERVAL 100 FEET
DATUM IS MEAN SEA LEVEL
DEPTH CURVES AND SOUNDINGS IN FEET-DATUM IS MEAN LOWER LOW WATER
SOUNDING CURVE REPRESENTS THE APPROXIMATE LINE OF MEAN HIGH WATER
THE MEAN RANGE OF TIDE IS APPROXIMATELY 10 FEET



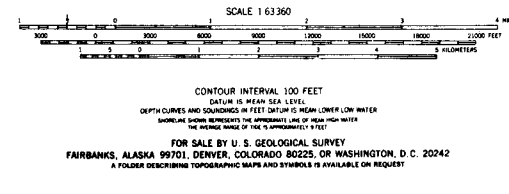
ROAD CLASSIFICATION
No roads or trails in this area
SEWARD (A-4), ALASKA
16000-114807 5/15x22 5
1951
MADE BY USGS, 1951

FOR SALE BY U. S. GEOLOGICAL SURVEY
FAIRBANKS, ALASKA 99701, DENVER, COLORADO 80225, OR WASHINGTON, D. C. 20242
A FOLDER DESCRIBING TOPOGRAPHIC MAPS AND SYMBOLS IS AVAILABLE ON REQUEST

SEWARD D-2



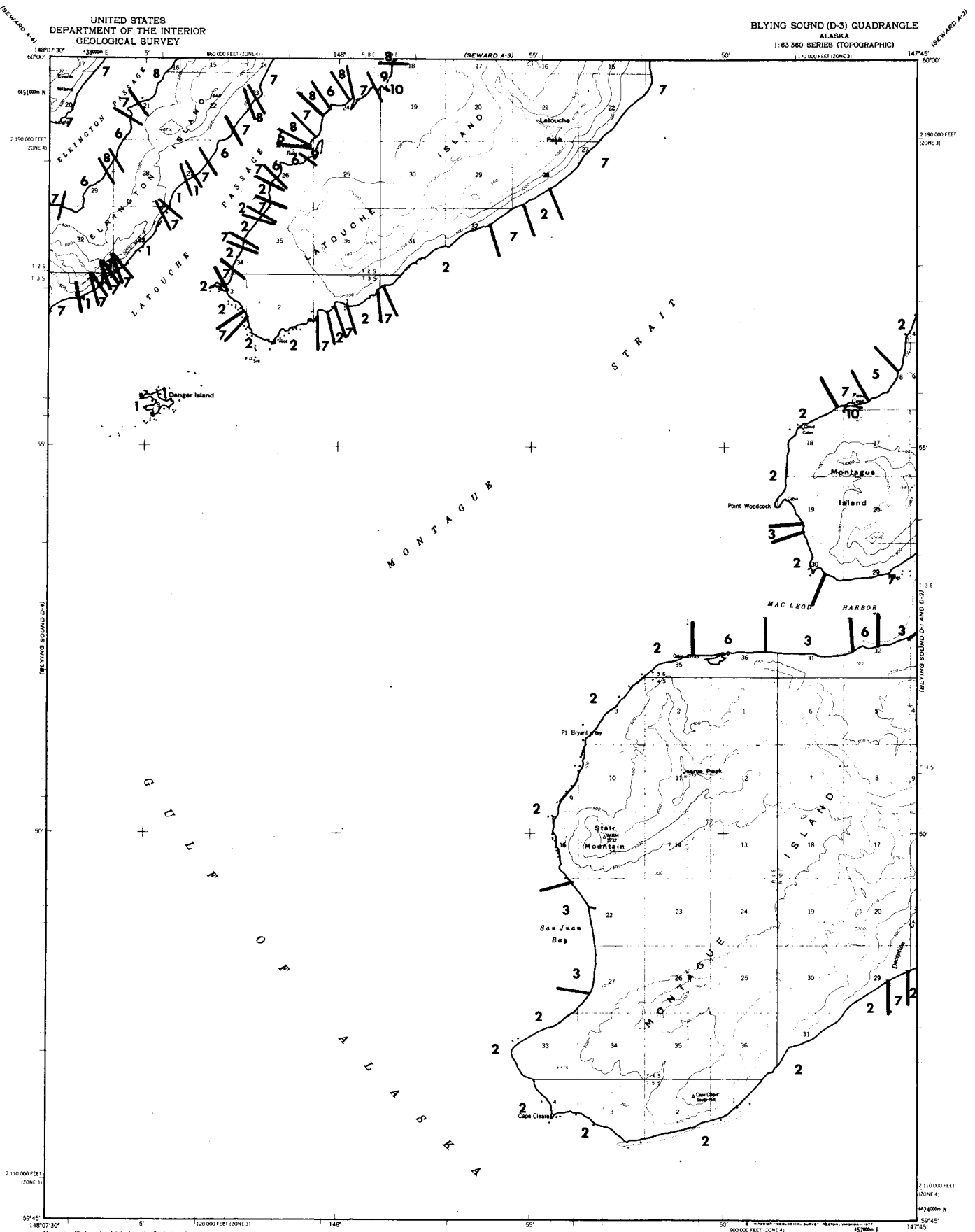
Mapped, edited, and published by the Geological Survey
Control by USCGS and USCE
Topography by photogrammetric methods from aerial photographs taken 1950; level annotated 1951. Map not field checked.
Selected hydrographic data compiled from USCGS Charts 8515 (1949), 8523 (1951), and 8524 (1943). This information is not intended for navigational purposes.
Universal Transverse Mercator projection, 1927 North American datum, 10,000-foot grid based on Alaska coordinate system, zones 3 and 4, 1000-meter Universal Transverse Mercator grid ticks, zone 6, shown in blue.
Land lines represent unsurveyed and unmarked locations predetermined by the Bureau of Land Management, Folios S-14 and S-15, Seward Meridian.
Entire land area is within the Chugach National Forest except Latochee exclusion area.



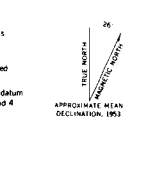
ROAD CLASSIFICATION
Trails

ALASKA
QUADRANGLE LOCATION

SEWARD (A-3), ALASKA
N6000-W14745/15K22.5
1951
MICH. REVISION 1971



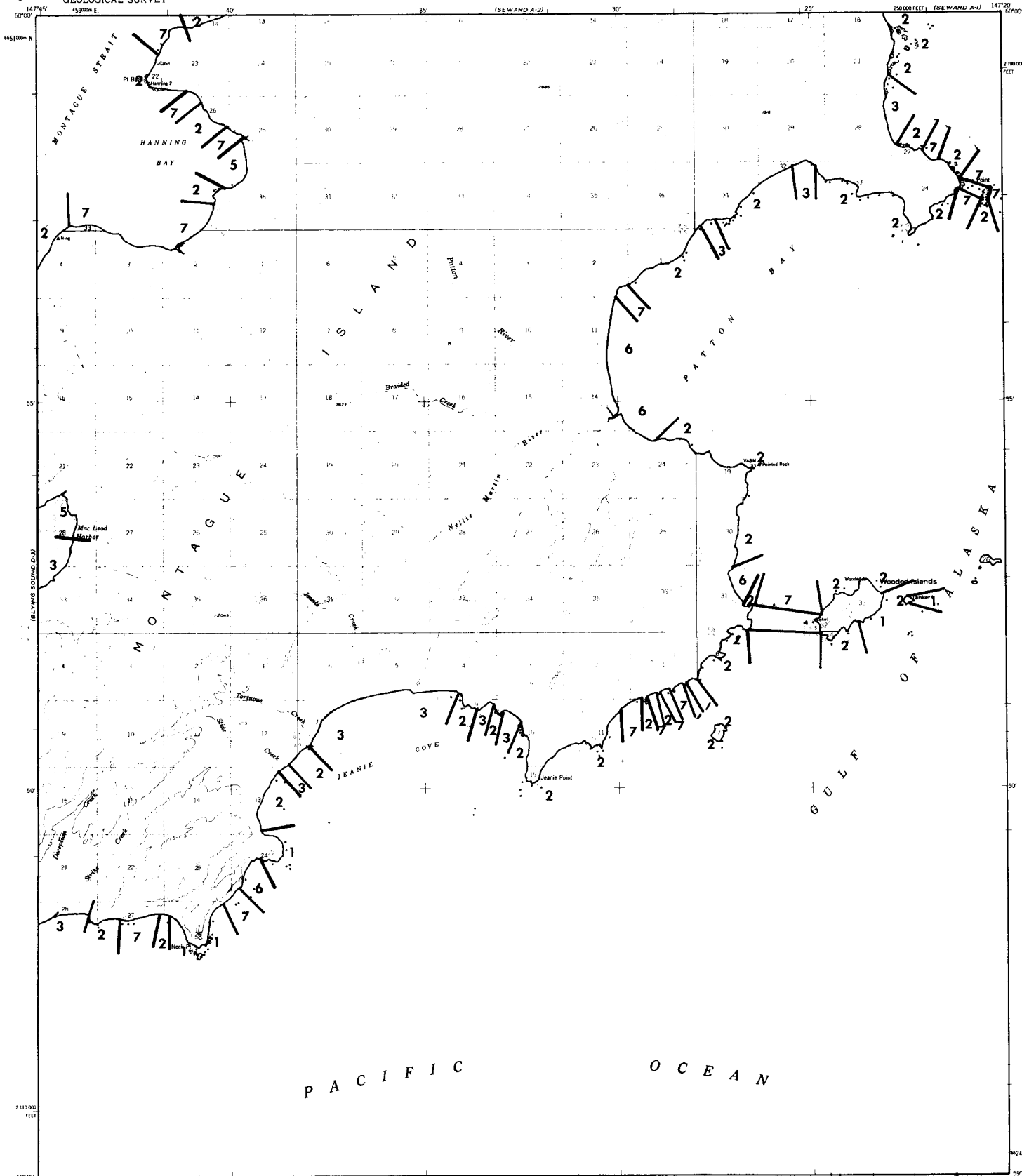
Map compiled, edited, and published by the Geological Survey
Control by USCGS and USCE
Topography by photogrammetric methods from aerial photographs taken 1950, fields annotated 1953. Map not field checked.
Selected hydrographic data compiled from USCGS Charts 8515 (1949) and 8523 (1951). This information is not intended for navigational purposes.
Universal Transverse Mercator projection, 1927 North American datum 10 000-foot grid based on Alaska coordinate system, zones 3 and 4 zone 6 shown in blue.
Land lines represent unsurveyed and unmarked locations determined by the Bureau of Land Management 360 S. 15, Seward Meridian.
Entire land area is within the Chugach National Forest.



SCALE 1:63 360
CONTOUR INTERVAL 100 FEET
NATIONAL GEODETIC VERTICAL DATUM OF 1929
DEPTH CURVES AND SOUNDINGS IN FEET; DATUM IS MEAN LOWER LOW WATER
SHORELINE SHOWS APPROXIMATE LINE OF MEAN HIGH WATER
THE MEAN RANGE OF TIDES IS APPROXIMATELY 9 FEET
FOR SALE BY U.S. GEOLOGICAL SURVEY
FAIRBANKS, ALASKA 99701, DENVER, COLORADO 80225, OR RESTON, VIRGINIA 22092
A FOLDER DESCRIBING TOPOGRAPHIC MAPS AND SYMBOLS IS AVAILABLE ON REQUEST



ROAD CLASSIFICATION
No roads or trails in this area
BLYING SOUND (D-3), ALASKA
N9945-W14745/15222 5
1993



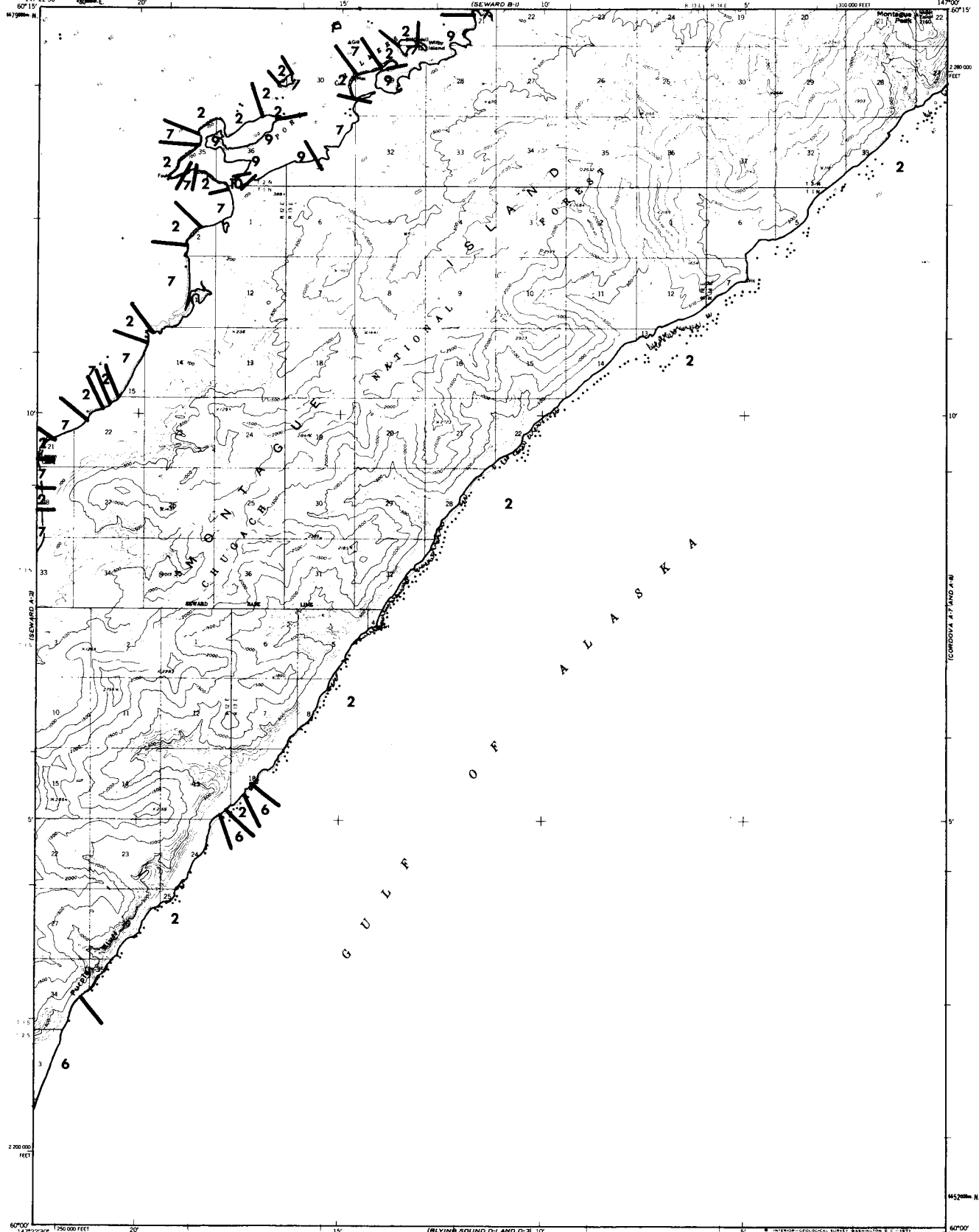
Mapped, edited, and published by the Geological Survey
Control by USCGS and USCE
Topography by photogrammetric methods from aerial photographs
taken 1951 and 1952. Field annotations 1951. Map not later checked.
Selected hydrographic data compiled from USCGS Chart
6315 (1949). This information is not intended for
navigational purposes.
Universal Transverse Mercator projection, 1927 North American datum
10,000-foot grid based on Alaska coordinate system, zone 3
1000-meter Universal Transverse Mercator grid lines,
zone 6, shown in blue.
Land lines represent unsurveyed and unmarked locations
determined by the Bureau of Land Management
Foto S. 15, Seward Meridian
Entire land area is within the Chugach National Forest

SCALE 1:63,360
CONTOUR INTERVAL 100 FEET
NATIONAL GEODETIC VERTICAL DATUM OF 1929
HEIGHTS IN FEET EXCEPT WHERE SHOWN LOWER
FOR SALE BY U.S. GEOLOGICAL SURVEY
FAIRBANKS, ALASKA 99701; DENVER, COLORADO 80225; OR RESTON, VIRGINIA 20192
A FOLDER IN SCREENING TOPOGRAPHIC MAPS AND SYMBOLS IS AVAILABLE ON REQUEST

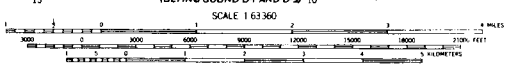
ROAD CLASSIFICATION
No roads or trails in this area



BLYLING SOUND (D-1 AND D-2), ALASKA
NS945-W14720/15A25
1951



Mapped, edited, and published by the Geological Survey
Control by USCGS and USCE
Topography by photogrammetric methods from aerial photographs taken 1951. Field annotated 1951. Map not field checked.
Selected hydrographic data compiled from USC&GS Charts 8515 (1949), 8520 (1951), and 8551 (1950) (1:200 000 scale). This information is not intended for navigational purposes.
Universal Transverse Mercator projection, 3227, North American datum 10 000 foot grid based on Alaska coordinate system, zone 3 1000 meter Universal Transverse Mercator grid ticks, zone 6, shown in blue.
Land lines represent unsurveyed and unmarked locations determined by the Bureau of Land Management
Folios S 14 and S 15, Seward Meridian



CONTOUR INTERVAL 100 FEET
DATUM IS MEAN SEA LEVEL
DEPTH CURVES AND SOUNDINGS IN FEET; DATUM IS MEAN LOWER LOW WATER
SHORELINE SHOWN REPRESENTS THE APPROXIMATE LINE OF MEAN HIGH WATER
THE AVERAGE RANGE OF TIDE IS APPROXIMATELY 9 FEET



ROAD CLASSIFICATION
No roads or trails in this area

SEWARD (A-1), ALASKA
N6000-W14700/15A22 5

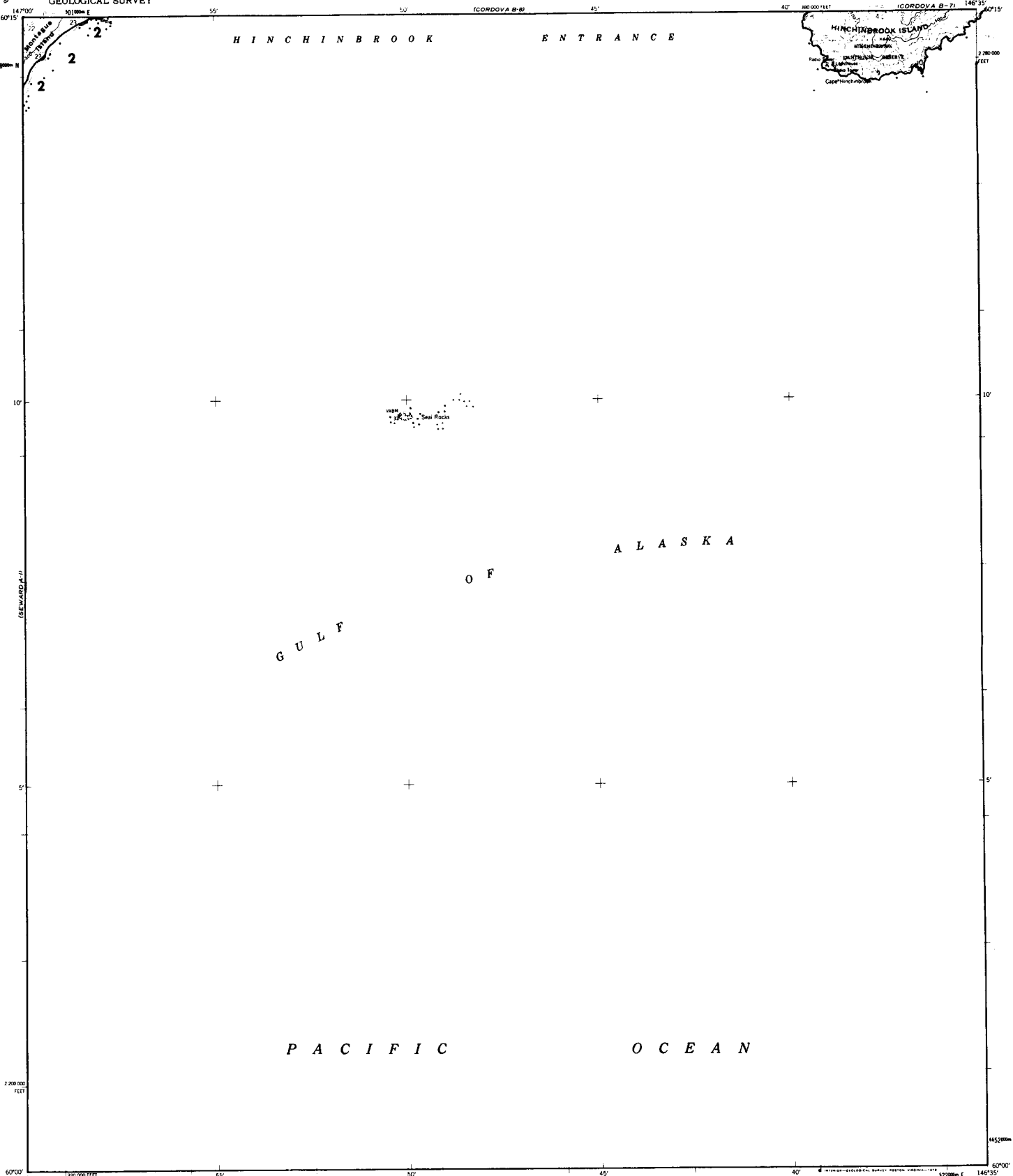
FOR SALE BY U. S. GEOLOGICAL SURVEY
FAIRBANKS, ALASKA 99701, DENVER, COLORADO 80225 OR WASHINGTON, D. C. 20242
A FOLDER DESCRIBING TOPOGRAPHIC MAPS AND SYMBOLS IS AVAILABLE ON REQUEST

H I N C H I N B R O O K E N T R A N C E



A L A S K A
O F
G U L F

P A C I F I C O C E A N



Mapped, edited, and published by the Geological Survey
Control by USGS and USC&GS
Topography by photogrammetric methods from aerial photographs
taken 1950 and 1951. Map not field checked.
Selected hydrographic data compiled from USC&GS Charts
8520 (1951), and 8551 (1:200,000 scale) (1950).
This information is not intended for navigational purposes.
Universal Transverse Mercator projection, 1927 North American datum
10 000-foot grid based on Alaska coordinate system, zone 3
1000 meter Universal Transverse Mercator grid ticks,
zone 6, shown in blue.
Land lines represent unsurveyed and unmarked locations
determined by the Bureau of Land Management
Folios S 14, Seward Meridian and CR 5, Copper River Meridian



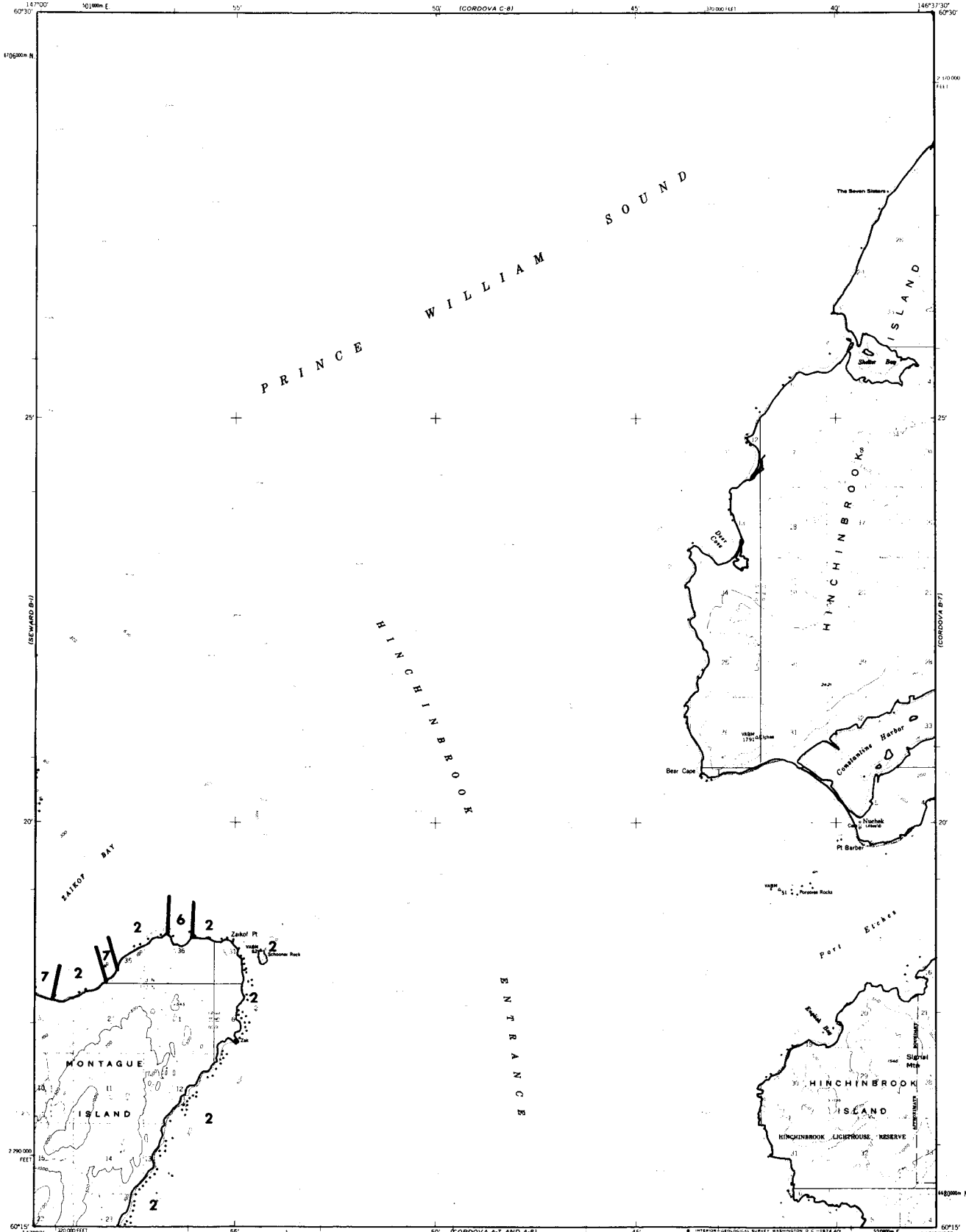
CONTOUR INTERVAL, 100 FEET
NATIONAL GEOGRAPHIC VERTICAL DATUM OF 1929
DEPTH CURVES AND SOUNDINGS IN FEET DATUM IS MEAN LOWER LOW WATER
(WORKING LINES REPRESENT THE APPROXIMATE LINE OF MEAN HIGH WATER
THE AVERAGE RANGE OF TIDE IS APPROXIMATELY 8 FEET)
FOR SALE BY U. S. GEOLOGICAL SURVEY
FAIRBANKS, ALASKA 99701, DENVER, COLORADO 80225, OR RESTON, VIRGINIA 22092
A FOLDER DESCRIBING TOPOGRAPHIC MAPS AND SYMBOLS IS AVAILABLE ON REQUEST



ROAD CLASSIFICATION
No roads or trails in this area

CORDOVA (A-7 AND A-8), ALASKA
N6000-W14635/15X25
1951
HORIZONTAL SCALE

BLANK SOUND D1 AND D2

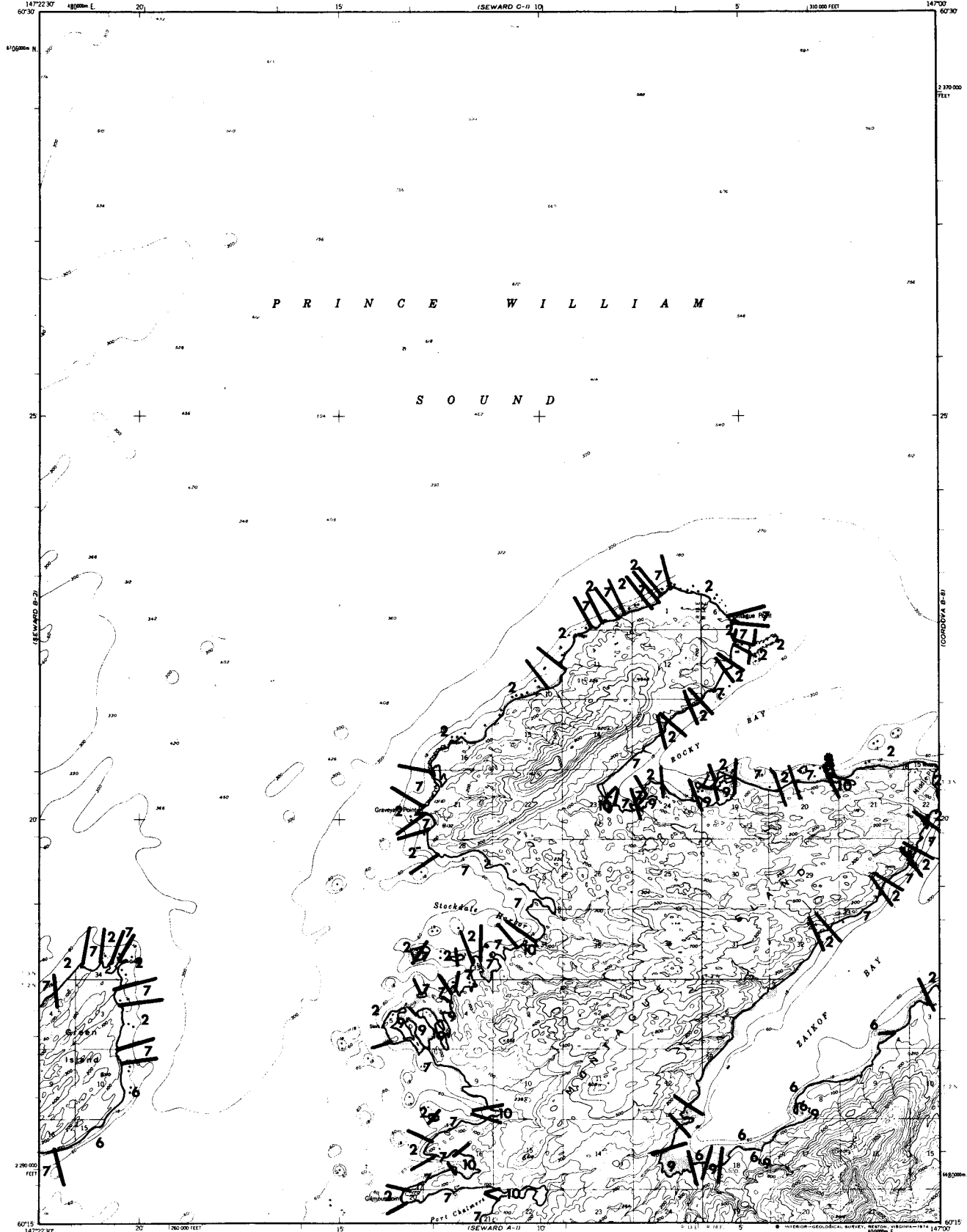


Mapped, edited, and published by the Geological Survey
Control by USGS and USC&GS
Topography by photogrammetric methods from aerial photographs
taken 1950 and 1951; data annotated 1951. Map not field checked.
Selected hydrographic data compiled from USC&GS Charts
8520 (1951) and 8551 (1:200 000 scale) (1950).
This information is not intended for navigational purposes.
Universal Transverse Mercator projection; 1927 North American datum
10,000 foot grid based on Alaska coordinate system, zone 3
1,000 meter Universal Transverse Mercator grid ticks,
zone 5. Shown in blue.
Land lines represent unsurveyed and unmarked locations
determined by the Bureau of Land Management.
Folios S 14, Seward Meridian and CR 5, Cooper River Meridian.
Entire land area is within the Chugach National Forest.

SCALE 1:63 380
CONTOUR INTERVAL 100 FEET
DATUM IS MEAN SEA LEVEL
DEPTH CURVES AND SOUNDINGS IN FEET (DEPTH IS MEAN LOWER LOW WATER)
SHORELINE SHOWN REPRESENTS THE APPROXIMATE LINE OF MEAN HIGH WATER
THE MEAN RANGE OF TIDE IS APPROXIMATELY 19 FEET
FOR SALE BY U. S. GEOLOGICAL SURVEY
FAIRBANKS, ALASKA 99701, DENVER, COLORADO 80225, OR WASHINGTON, D. C. 20242
A FOLDER DESCRIBING TOPOGRAPHIC MAPS AND SYMBOLS IS AVAILABLE ON REQUEST



ROAD CLASSIFICATION
No roads or trails in this area
CORDOVA (B-8), ALASKA
N6015-W14637 5/13/22 5
1951
www.gsa.gov



Mapped, edited, and published by the Geological Survey
Control by USCGS and USCE

Topography by photogrammetric methods from aerial photographs
taken 1950-1951; field annotated 1961. Map not field checked.
Selected hydrographic data compiled from USCGS Charts
8515, 8517, and 8551 (1:200,000 scale). This information
is not intended for navigational purposes.

Universal Transverse Mercator projection, 1927 North American datum
10,000 meter Universal Transverse Mercator grid ticks,
zone 6, shown in blue

Land lines represent unsurveyed and unmarked locations
determined by the Bureau of Land Management
Folio S-14, Seward Meridian

Other land area is within the Chugach National Forest
Line elevations are uncheck



SCALE 1:63,360

CONTOUR INTERVAL 100 FEET
DOTTED LINES REPRESENT 50, 1000 CONTOURS
DATHUM IS MEAN SEA LEVEL
DEPTH CURVES AND SOUNDINGS IN FEET, DATUM IS MEAN LOWER LOW WATER
WATER DEPTHS IN METERS FOR APPROXIMATE LINE OF MEAN HIGH WATER
THE FULL RANGE OF TIDE IS APPROXIMATELY 9 FEET



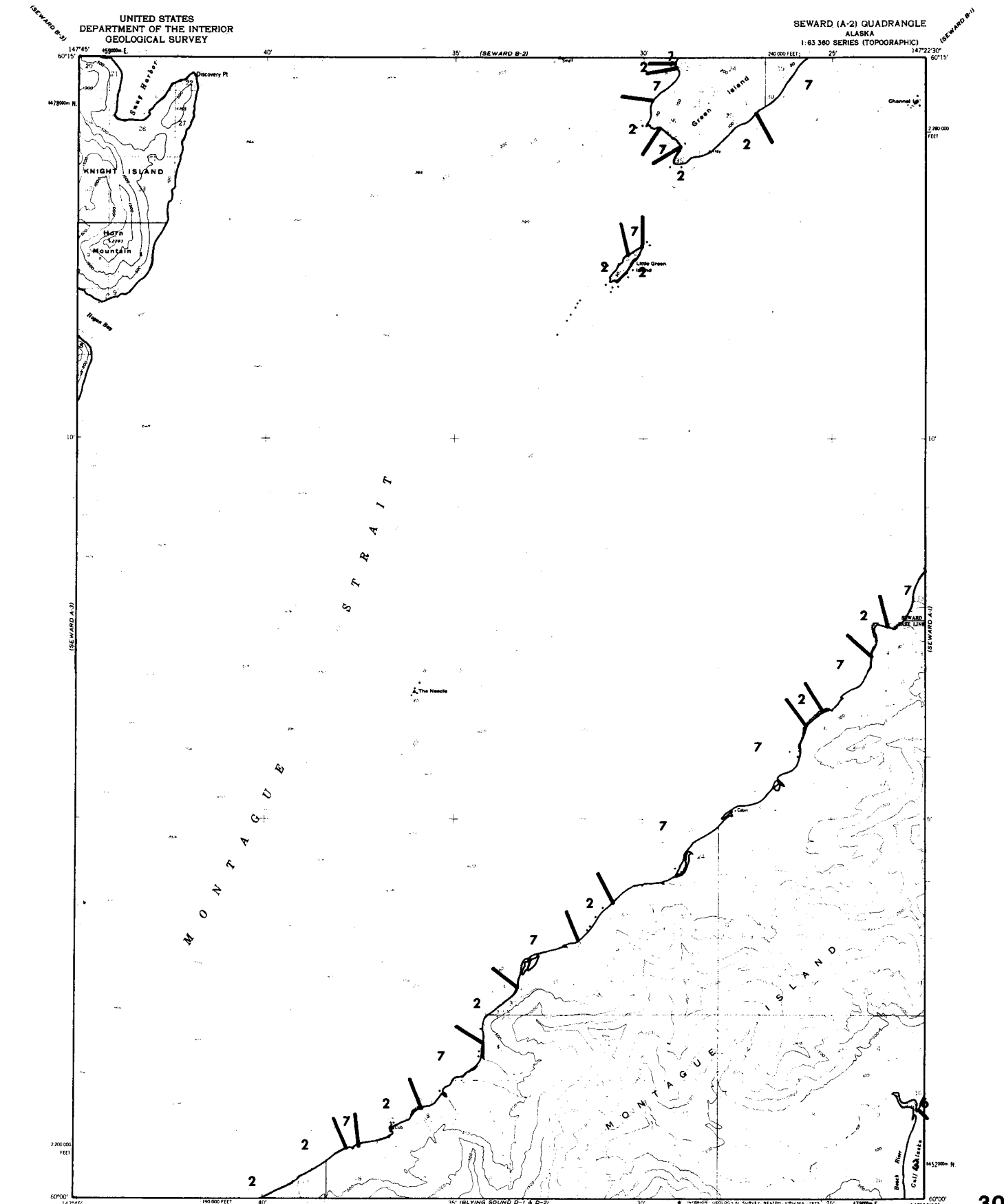
QUADRANGLE LOCATION

ROAD CLASSIFICATION
No roads or trails in this area

SEWARD (B-1), ALASKA
N6015-W14700/15222.5

1951
HONOR 105085 184

FOR SALE BY U S GEOLOGICAL SURVEY
FAIRBANKS ALASKA 99701 DENVER COLORADO 80225 OR RESTON VIRGINIA 22092
A FOLDER DESCRIBING TOPOGRAPHIC MAPS AND SYMBOLS IS AVAILABLE ON REQUEST



Maped, edited, and published by the Geological Survey
Control by USCGS and USCE
Topography by photogrammetric methods from aerial photographs taken 1951. Map not field checked.
Selected hydrographic data compiled from USCG Charts 8515 and 8551 (1:200 000 scale). This information is not intended for navigational purposes.
Universal Transverse Mercator projection, 1927 North American datum
10 000 foot grid based on Alaska coordinate system, zone 3
1000 metre Universal Transverse Mercator grid (4x3), zone 6, shown in blue
Land lines represent unsurveyed and unmarked locations predetermined by the Bureau of Land Management
Folios S 14 and S 15, Seward Meridian
Entire land area is within the Chugach National Forest

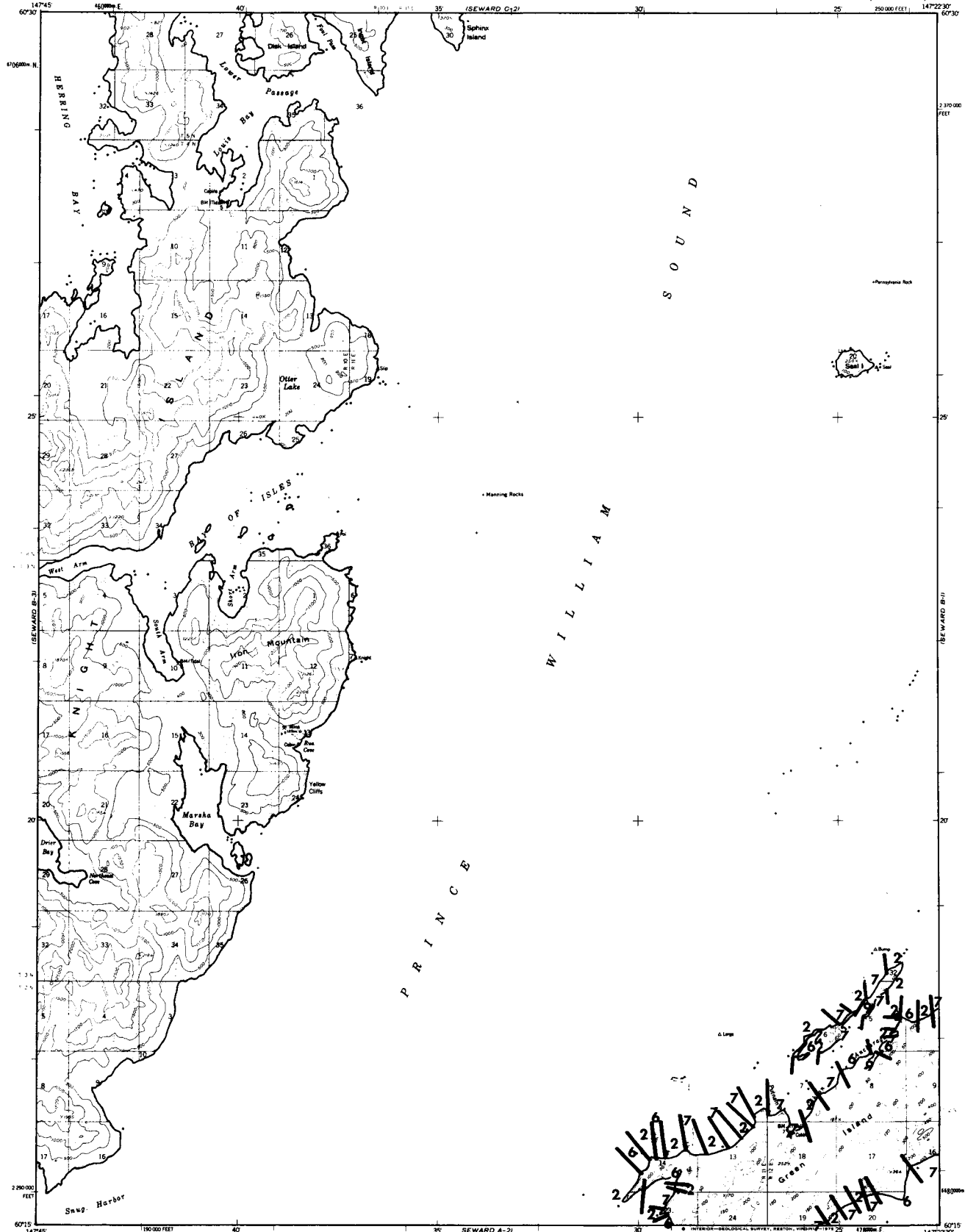
SCALE 1:63 360

CONTOUR INTERVAL 100 FEET
DOTTED LINES REPRESENT 50 FOOT CONTOUR
NATIONAL GEODESIC VERTICAL DATUM OF 1929
DEPTH CURVES AND SOUNDINGS IN FEET-DATUM TO MEAN LOWER LOW WATER
DASHED LINE SHOWN REPRESENTS THE APPROXIMATE LINE OF MEAN HIGH WATER
THE AVERAGE RANGE OF TIDE IS APPROXIMATELY 1:14:1

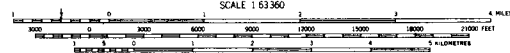
FOR SALE BY U.S. GEOLOGICAL SURVEY
FAIRBANKS, ALASKA 99701, DENVER, COLORADO 80225 OR RESTON, VIRGINIA 22092
A FOLDER DESCRIBING TOPOGRAPHIC MAPS AND SYMBOLS IS AVAILABLE ON REQUEST

ROAD CLASSIFICATION
No roads or trails in this area

SEWARD (A-2), ALASKA
N6000-W14722.5/15X22.5
1951
MADE REVISION 1963



Mapped, edited and published by the Geological Survey
Control by USCGS and USCE
Topography by photogrammetric methods from aerial photographs
taken 1951, field annotated 1951. Map not field checked.
Selected hydrographic data compiled from USCGS Charts
8515 (1949), 8517 (1952), and 8551 (1950) (1:200,000 scale).
This information is not intended for navigational purposes.
Universal Transverse Mercator projection, 1927 North American datum
10,000-foot grid based on Alaska coordinate system, zone 3
1000-metre Universal Transverse Mercator grid ticks,
zone 6, shown in blue.
Land lines represent unimproved and unmarked locations
determined by the Bureau of Land Management
Folio S 14, Seward Meridian
Entire land area is within the Chugach National Forest



CONTOUR INTERVAL 100 FEET
DOTTED LINES REPRESENT 50 FOOT CONTOURS
NATIONAL GEODETIC VERTICAL DATUM OF 1929
DEPTH CURVES AND SOUNDINGS IN FEET - DATUM 0, MEAN LOWER LOW WATER
SHOULDER SHOWS REPRESENTS THE APPROXIMATE LINE OF MEAN HIGH WATER
THE HEIGHT RANGE OF TIDE IS APPROXIMATELY 8 FEET



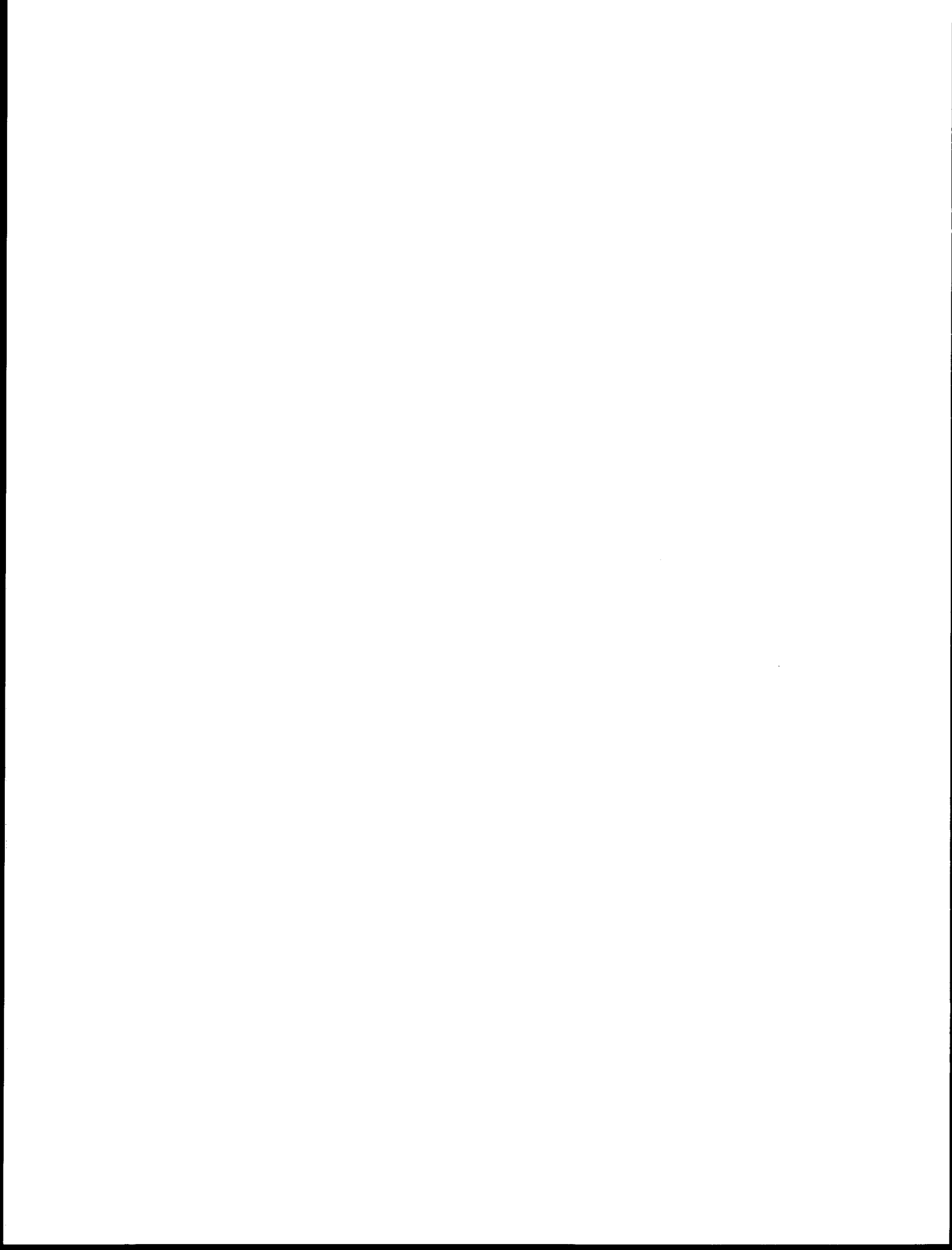
ROAD CLASSIFICATION
Trails
SEWARD (B-2), ALASKA
N6015-W14722.5/15K22.5
1951
MAKER: HUGHSON, 1954

FOR SALE BY U. S. GEOLOGICAL SURVEY
FAIRBANKS, ALASKA 99701, DENVER, COLORADO 80225, OR RESTON, VIRGINIA 22092
A FOLDER DESCRIBING TOPOGRAPHIC MAPS AND SYMBOLS IS AVAILABLE ON REQUEST

APPENDIX II

SURVEY STATION LOCATIONS AND TASKS COMPLETED

This gives the exact locations (latitude and longitude) of all 100 survey stations monitored for this study. The tasks completed at each station (aerial reconnaissance, ground reconnaissance, beach profile, and sediment analysis) are indicated by asterisks.



SURVEY STATION LOCATION AND TASKS COMPLETED

<u>Station Number</u>	<u>LOCATION</u>		<u>TASKS COMPLETED</u>		
	<u>Latitude</u>	<u>Longitude</u>	<u>Aerial Reconn.</u>	<u>Ground Reconn.</u>	<u>Beach profile and sed. analysis</u>
KNP-1	59°8'50"N	151°51'50"W	*		
2	59°7'30"	151°42'17"	*	*	
3	59°6'48"	151°27'59"	*		
4	59°9'30"	151°43'10"	*	*	
5	59°11'52"	151°32'30"	*	*	*
6	59°13'45"	151°33'5"	*	*	
7	59°14'9"	151°26'18"	*	*	*
8	59°15'10"	151°23'35"	*	*	
9	59°12'40"	151°18'29"	*		
10	59°12'29"	151°8'00"	*		
11	59°18'35"	151°18'25"	*		
12	59°17'30"	151°5'40"	*		
13	59°18'30"	151°1'50"	*		
14	59°13'5"	151°1'00"	*		
15	59°14'5"	150°58'05"	*	*	*
16	59°18'30"	150°55'20"	*		
17	59°22'22"	150°46'15"	*	*	*
18	59°25'43"	150°36'00"	*		
19	59°22'58"	150°42'00"	*	*	*
20	59°19'10"	150°39'50"	*		
21	59°31'09"	150°36'40"	*		
22	59°36'02"	150°30'50"	*	*	
23	59°30'11"	150°33'03"	*		
24	59°29'00"	150°27'30"	*	*	*
25	59°35'49"	150°21'30"	*	*	
26	54°43'50"	150°13'27"	*		

<u>Station Number</u>	<u>Latitude</u>	<u>Longitude</u>	<u>Aerial Recon.</u>	<u>Ground Recon.</u>	<u>Beach profile and sed. analysis</u>
KNP-27	59°37'59"	150°15'40"	*	*	
28	59°32'10"	150°21'05"	*	*	
29	59°26'31"	150°23'30"	*		
30	59°20'35"	150°22'59"	*		
31	59°28'38"	150°17'20"	*		
32	59°31'51"	150°10'59"	*		
33	59°34'31"	150° 5'35"	*		
34	59°40'35"	150° 5'55"	*	*	*
35	59°38'24"	149°59'48"	*		
36	59°43'30"	149°55'32"	*	*	
37	59°50'13"	149°56'30"	*	*	*
38	59°41'20"	149°49'05"	*		
39	59°36'50"	149°46'10"	*		
40	39°39'15"	149°44'40"	*		
41	59°47'20"	149°47'05"	*	*	*
42	59°49'39"	149°44'33"	*		
43	59°57'10"	149°41'30"	*	*	*
44	59°50'21"	149°41'00"	*		
45	59°45'55"	149°36'39"	*		
46	59°43'30"	149°31'40"	*		
47	59°46'17"	149°35'25"	*		
48	59°52'42"	149°33'05"	*		
49	59°58'18"	149°25'55"	*		
50	60°7' 21"	149°24'10"	*	*	
51	60°0' 33"	149°20'04"	*		
52	59°53'25"	149°51'30"	*		
53	59°55'18"	149°21'12"	*		
54	59°50'39"	149°24'08"	*		
55	59°58'29"	149°12'30"	*		
56	60°2'55"	149° 2'45"	*	*	*
57	59°57'22"	149° 4'22"	*	*	*
58	59°55'40"	148°52'34"	*		
59	59°57'27"	148°46'00"	*	*	*

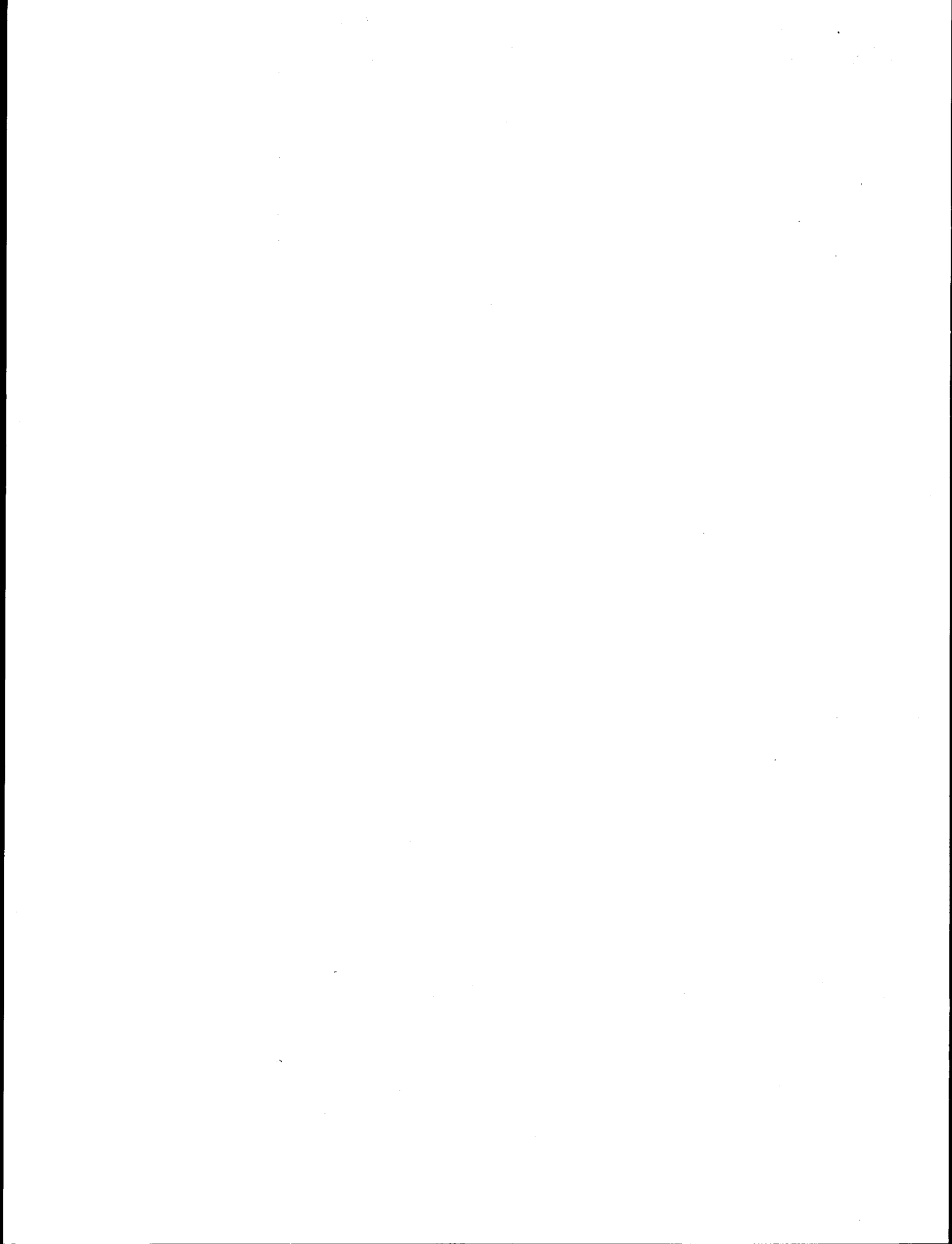
<u>Station Number</u>	<u>Latitude</u>	<u>Longitude</u>	<u>Aerial Recon.</u>	<u>Ground Recon.</u>	<u>Beach profile and sed. analysis</u>
KNP-60	59°55'51"	148°35'50"	*		
61	60°01'18"	148°33'00"	*	*	*
62	59°57'30"	148°25'30"	*		
63	60°02'28"	148°23'41"	*	*	*
64	60°06'41"	148°22'40"	*	*	
65	60°10'29"	148°20'18"	*	*	*
66	60°07'07"	148°14'42"	*	*	
67	60°11'12"	148°06'58"	*		
68	60°07'18"	148°12'25"	*		
69	60°03'04"	148°18'20"	*		
70	60°01'59"	148°09'20"	*		
71	60°08'45"	148°04'02"	*	*	*
72	60°06'50"	147°59'52"	*	*	
73	59°59'22"	148°08'40"	*		
74	59°55'57"	148°13'00"	*		
75	60°01'24"	148°00'00"	*		
76	59°58'01"	148°06'41"	*	*	
77	60°03'51"	148°00'40"	*	*	*
78	60°03'24"	147°53'45"	*	*	
79	60°01'41"	147°50'31"	*	*	*
80	59°56'48"	147°59'28"	*		
81	59°51'00"	147°53'35"	*	*	
82	59°48'34"	147°53'19"	*	*	*
83	59°46'15"	147°50'22"	*		
84	59°48'02"	147°45'41"	*		
85	59°50'28"	147°31'28"	*	*	*
86	59°54'42"	147°29'40"	*	*	
87	59°58'40"	147°23'00"	*	*	*
88	60°06'35"	147°15'20"	*		
89	60°13'46"	147°01'00"	*		
90	60°18'00"	146°54'45"	*		

<u>Station Number</u>	<u>Latitude</u>	<u>Longitude</u>	<u>Aerial Recon.</u>	<u>Ground Recon.</u>	<u>Beach profile and sed. analysis</u>
KNP-91	60°18'21"	147°03'08"	*	*	
92	60°20'25"	147°04'52"	*	*	*
93	60°20'01"	147°12'48"	*	*	*
94	60°14'38"	147°13'20"	*	*	
95	60°10'39"	147°19'50"	*	*	*
96	60°05'42"	147°26'00"	*		
97	60°01'14"	147°35'49"	*	*	*
98	59°57'01"	147°42'10"	*		
99	59°53'18"	147°44'00"	*	*	*
100	60°15'19"	147°23'25"	*	*	*

APPENDIX III

BEACH PROFILES

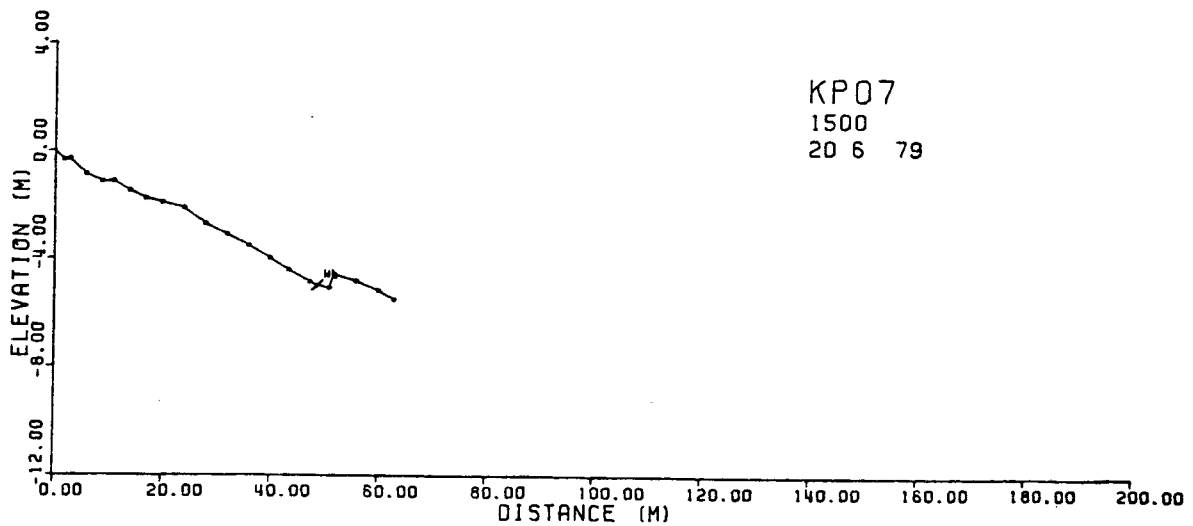
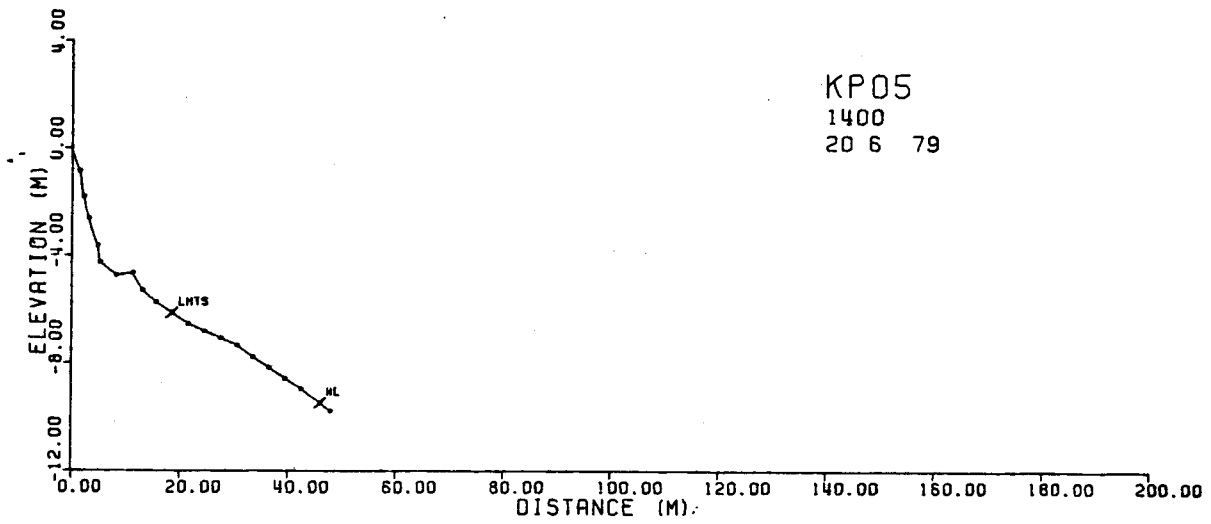
Computer plots of the 28 survey stations that were profiled for this report are given here. Profiles are at a 1:5 vertical exaggeration.

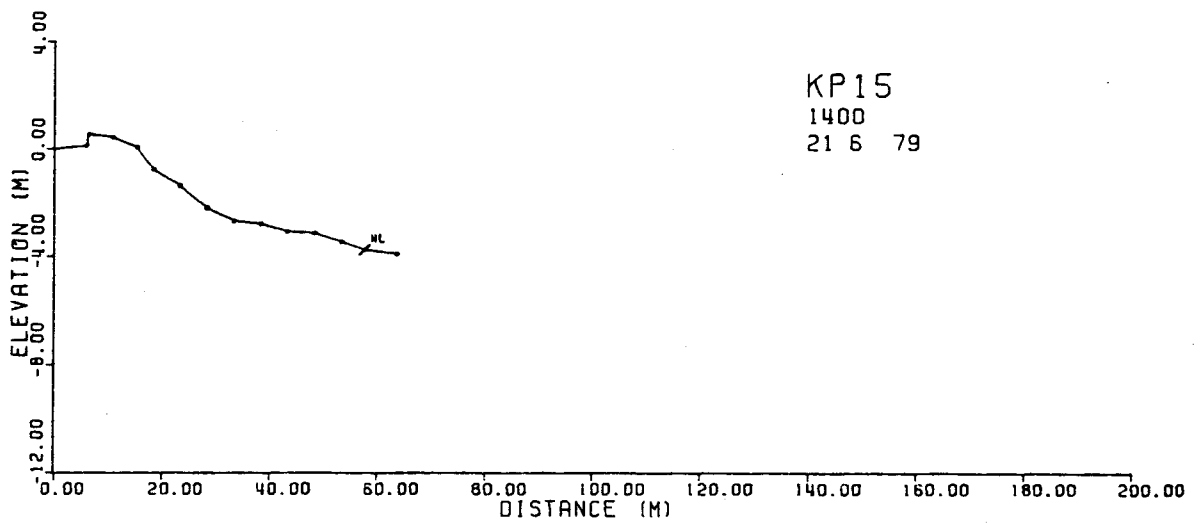
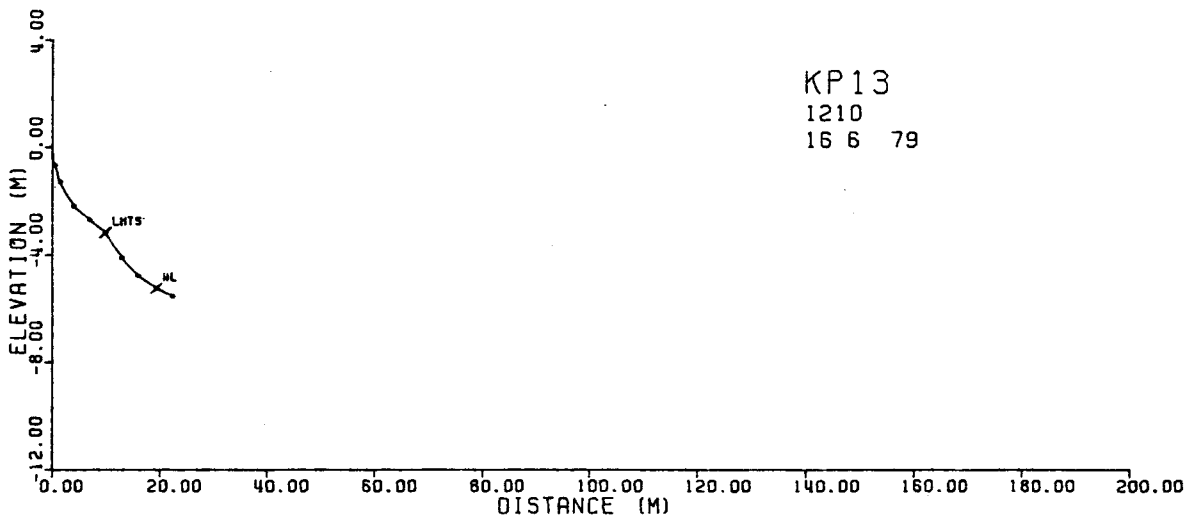
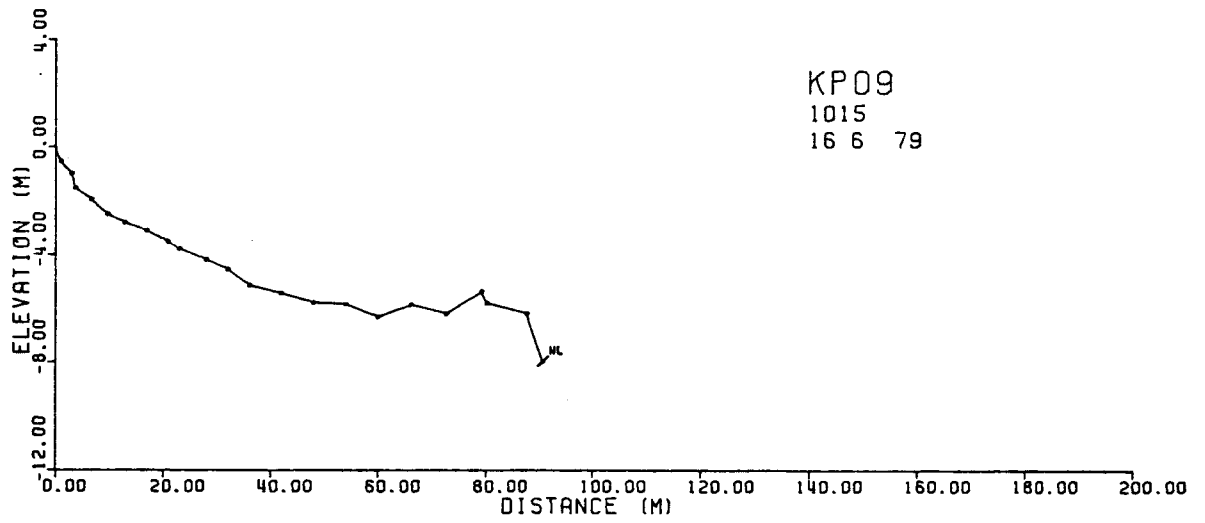


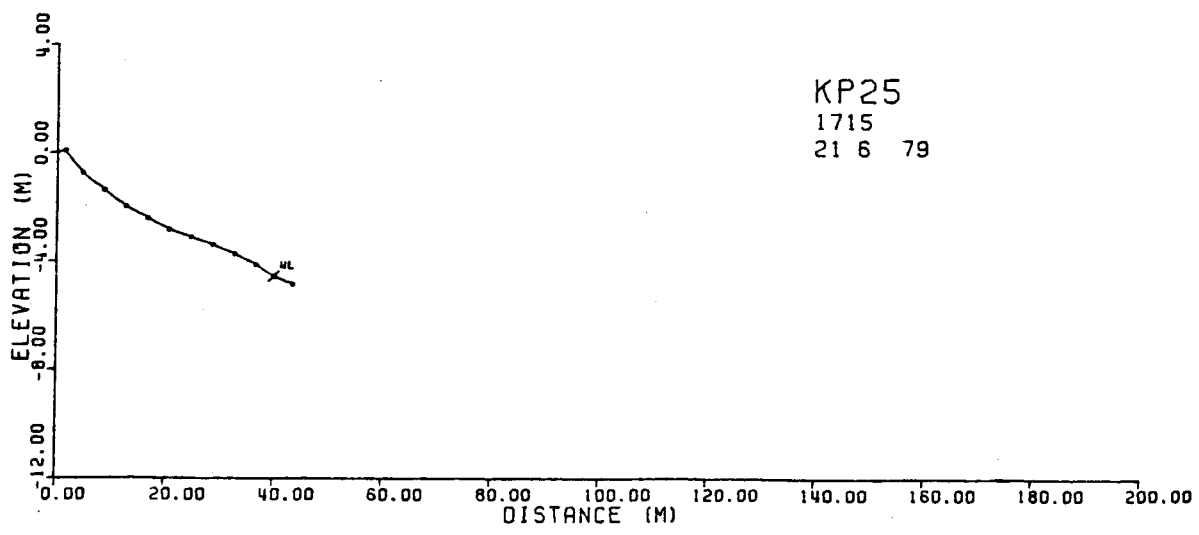
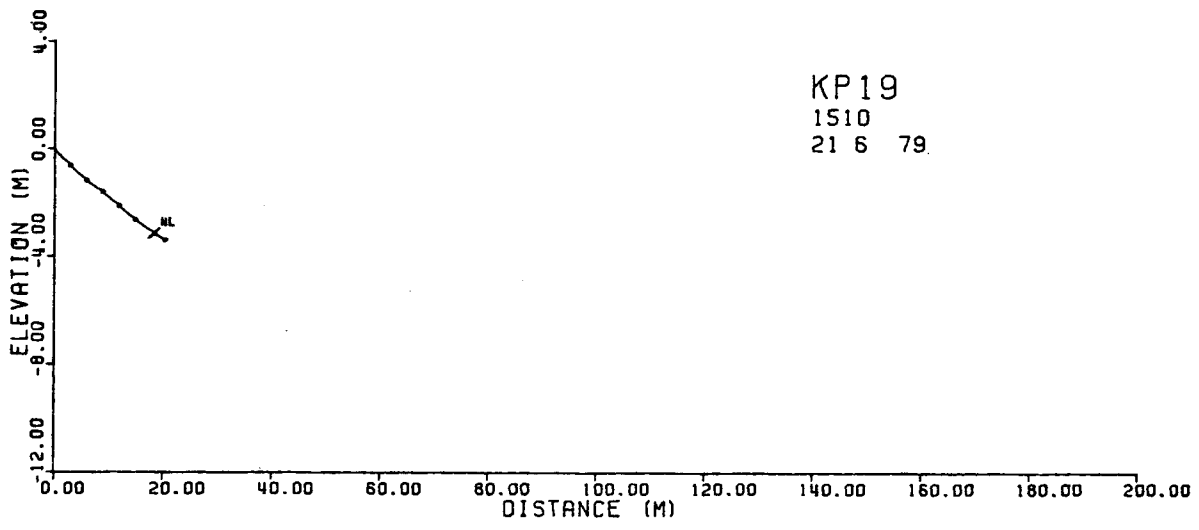
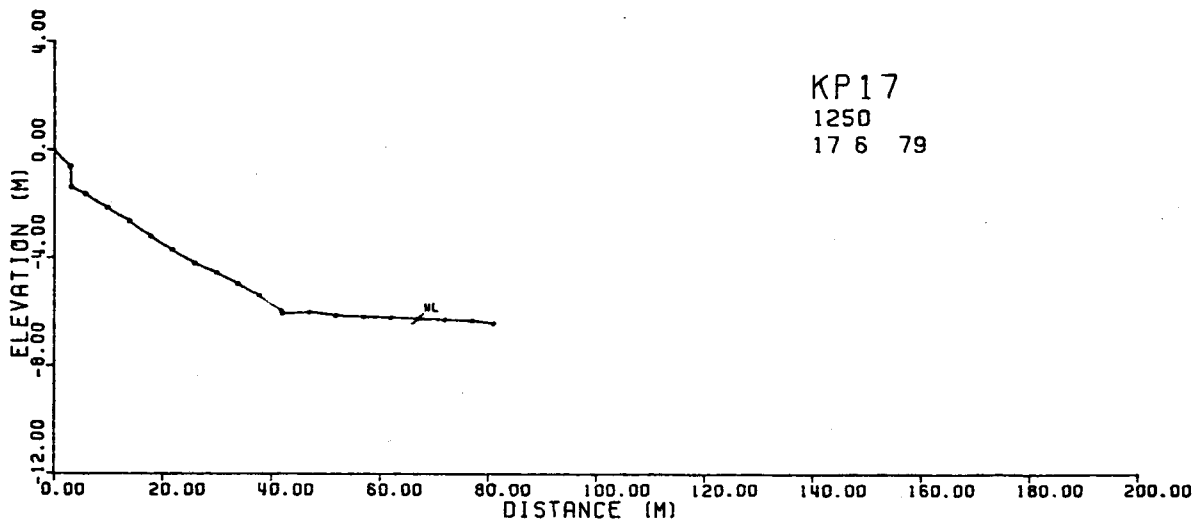
BEACH PROFILES

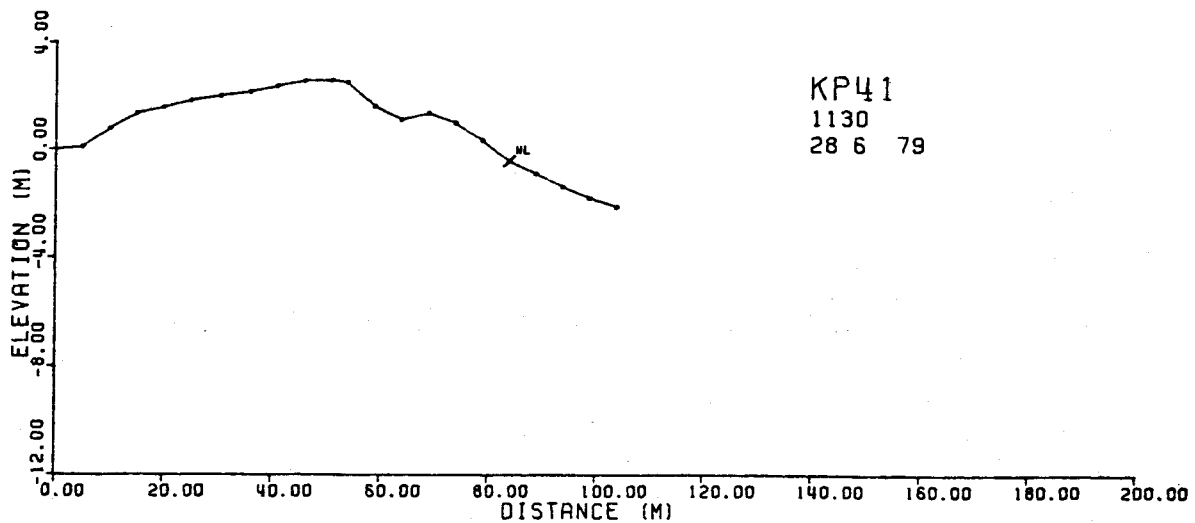
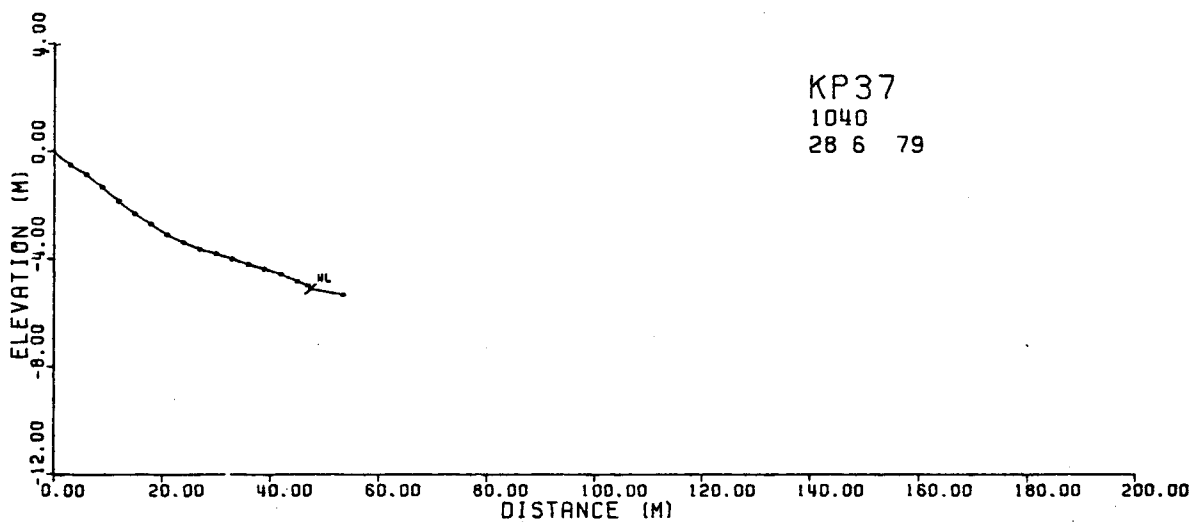
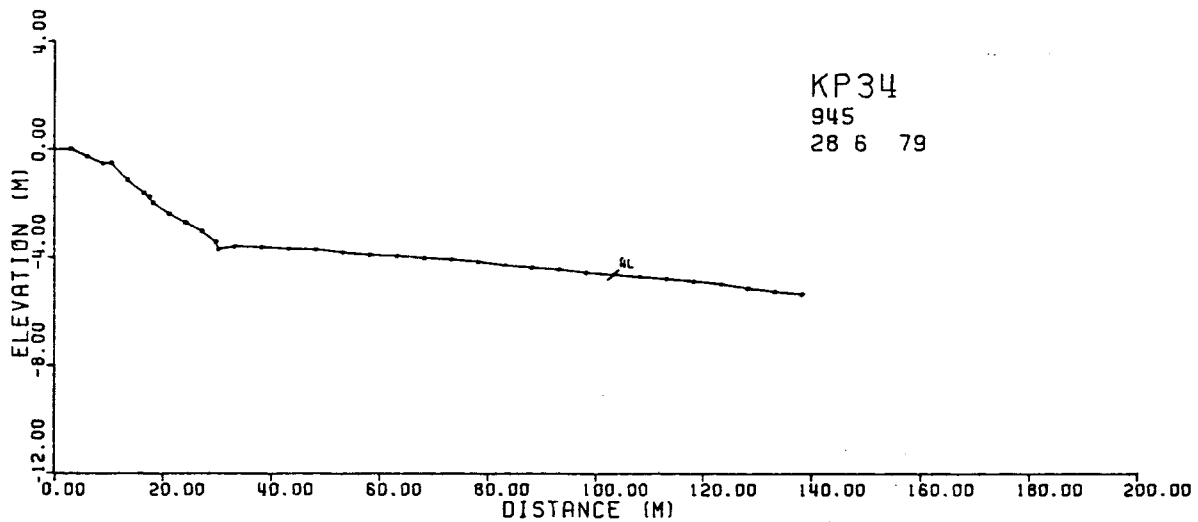
KENAI PENINSULA - MONTAGUE ISLAND

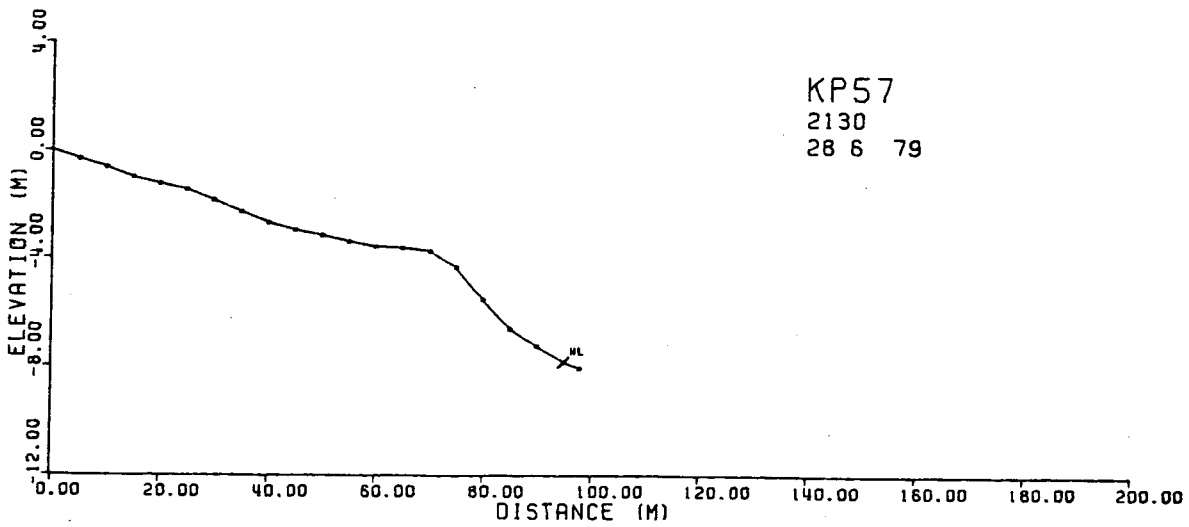
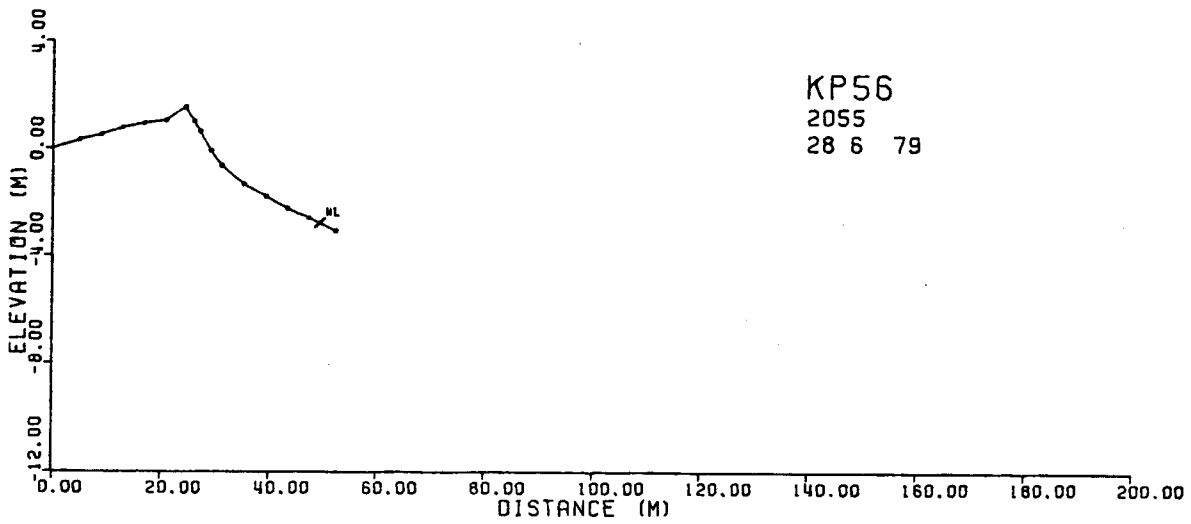
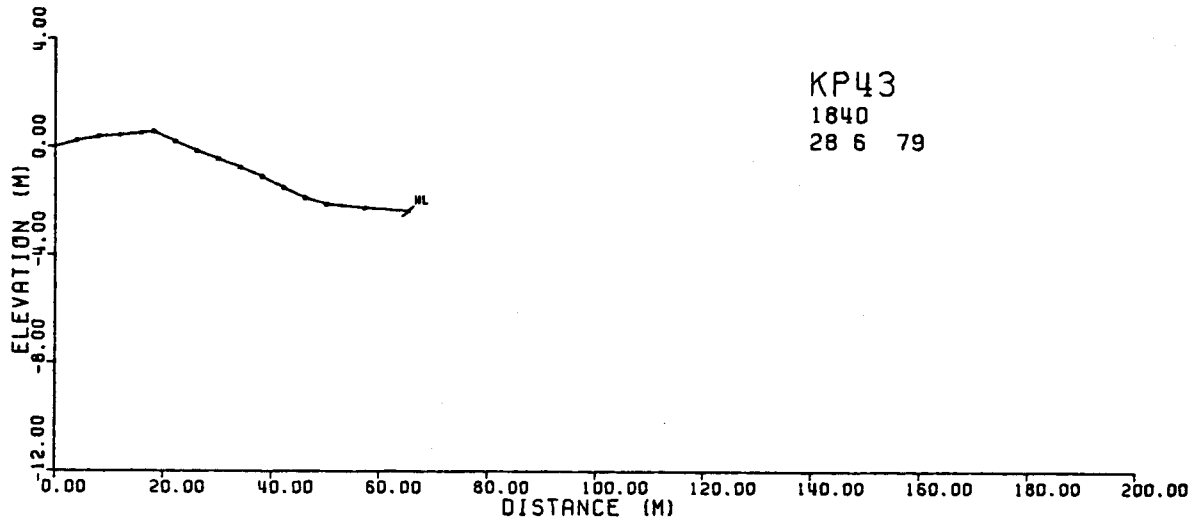
1979

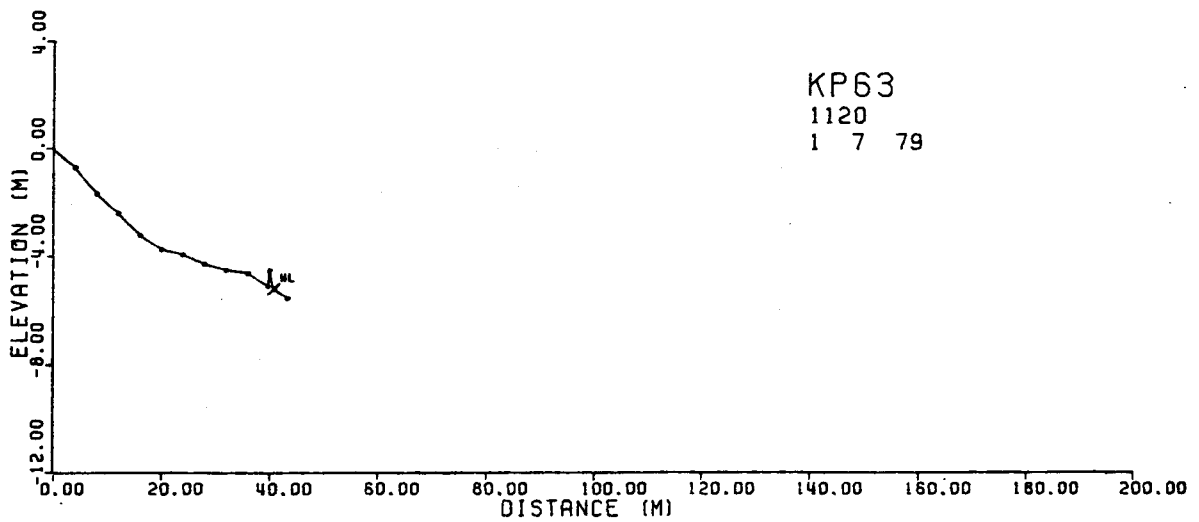
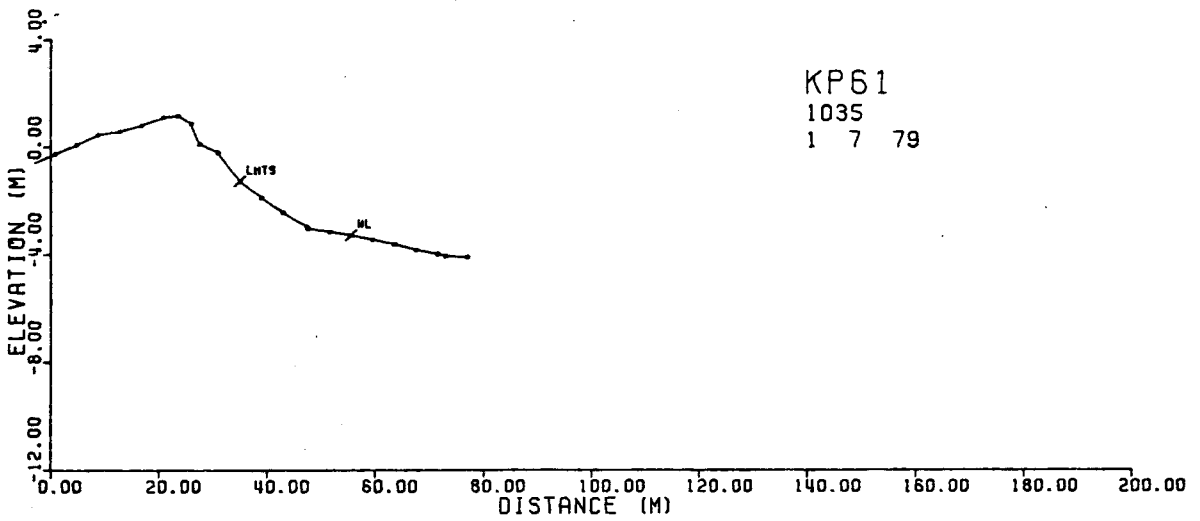
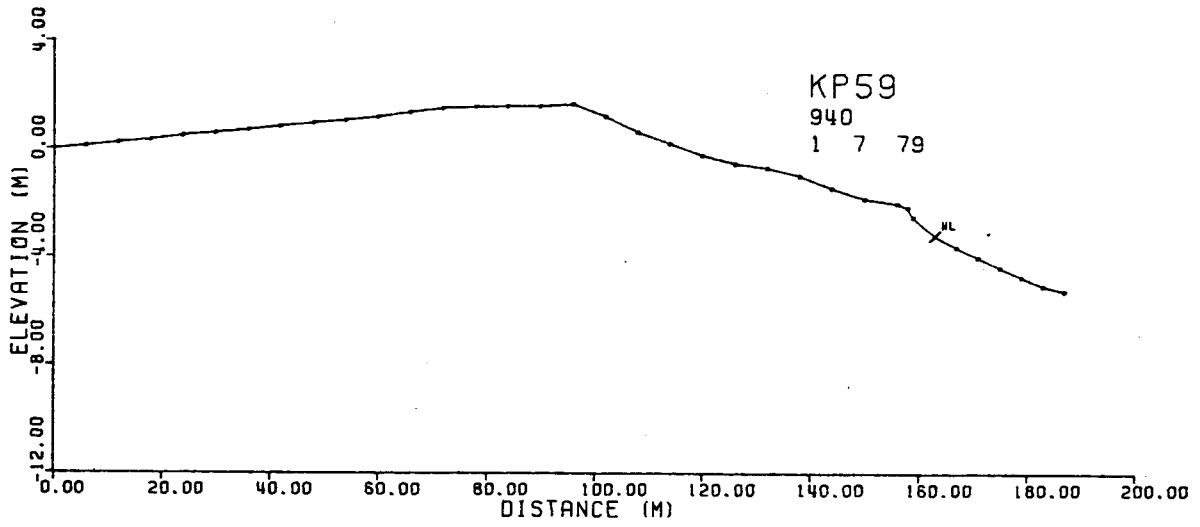


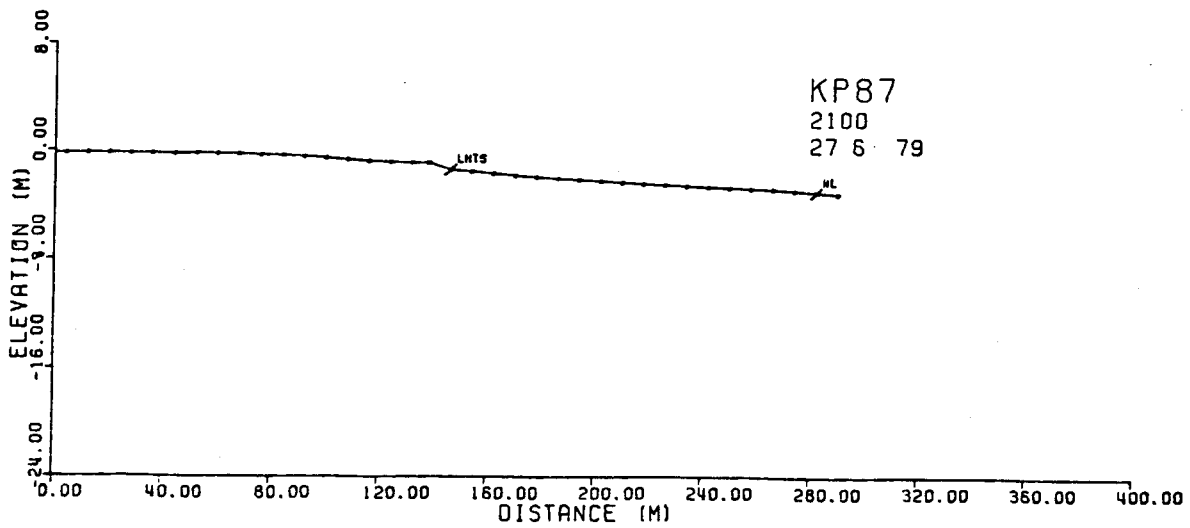
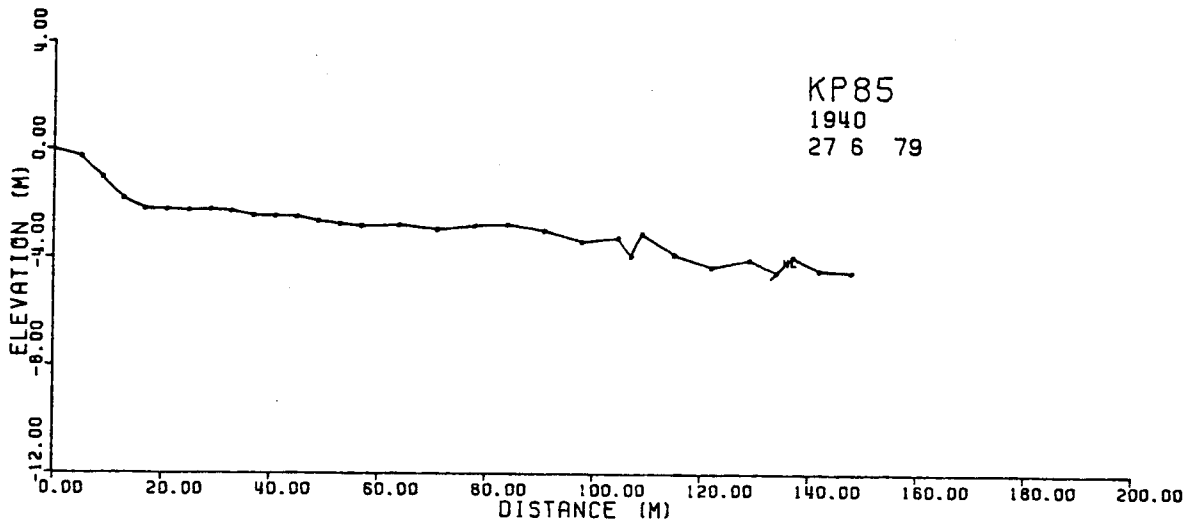
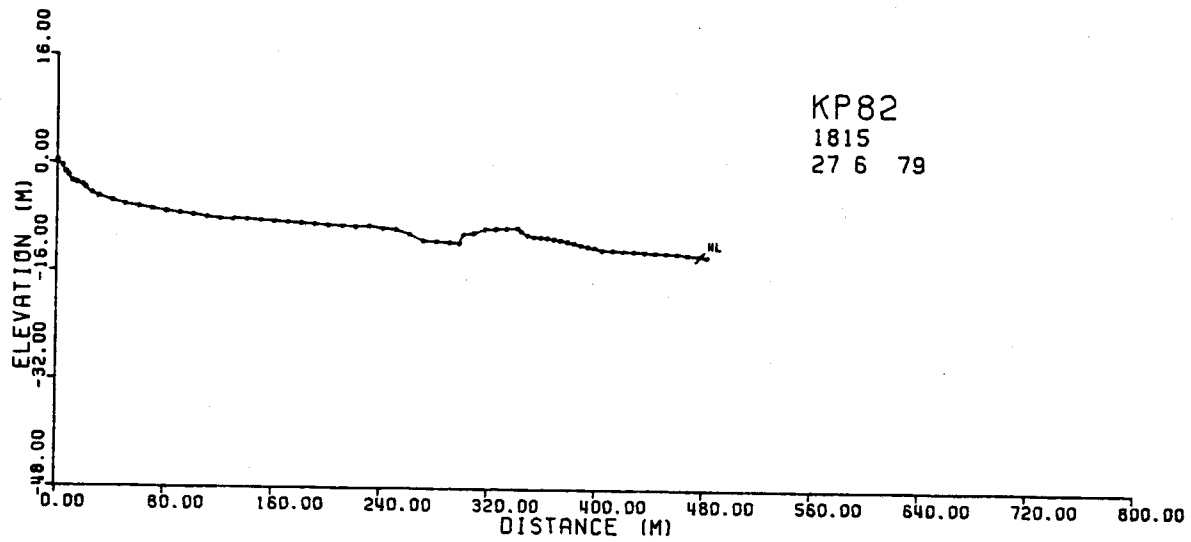


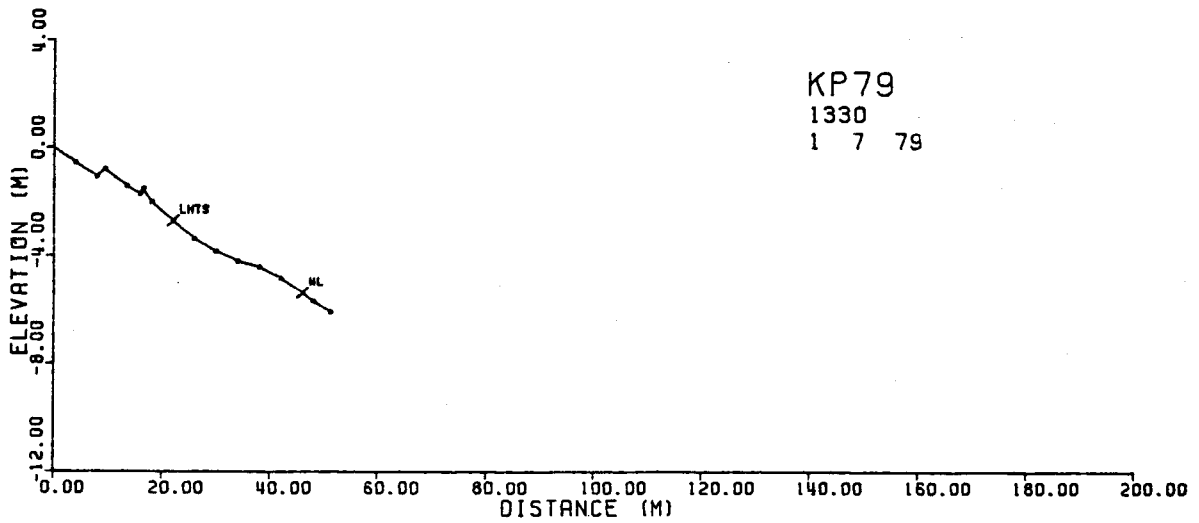
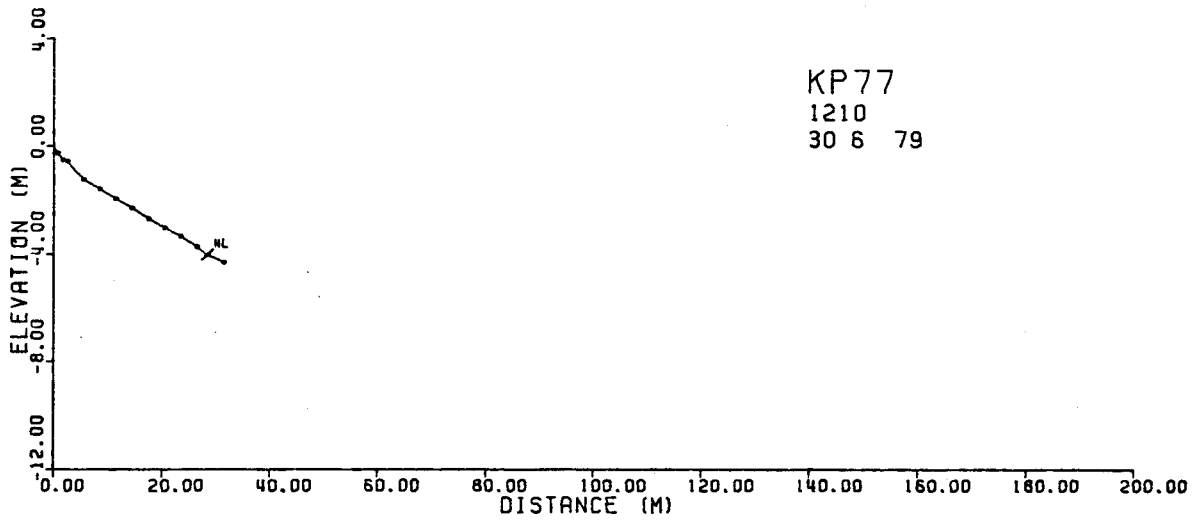
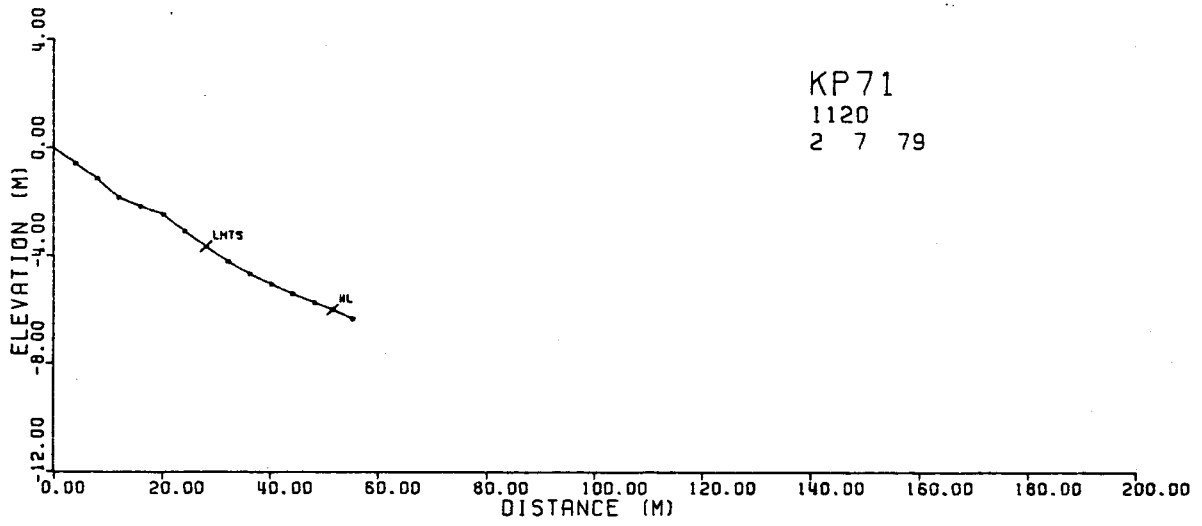


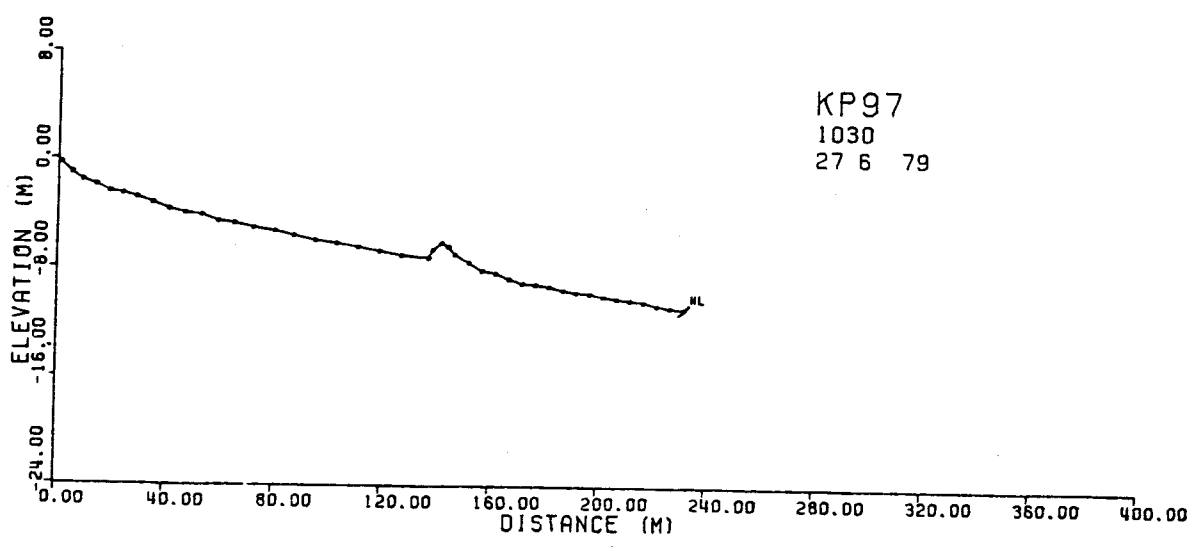
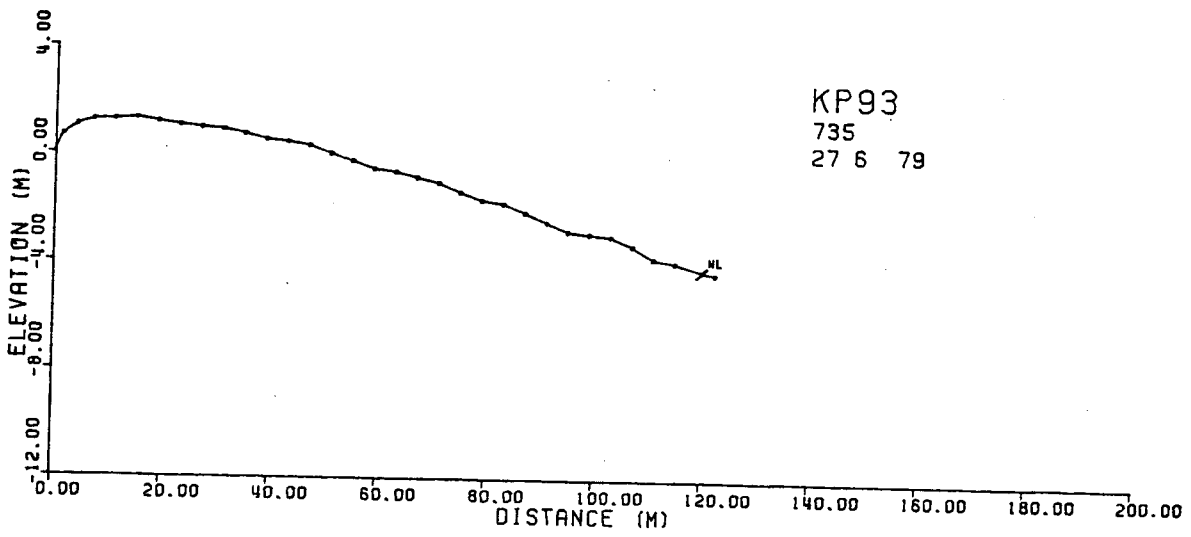
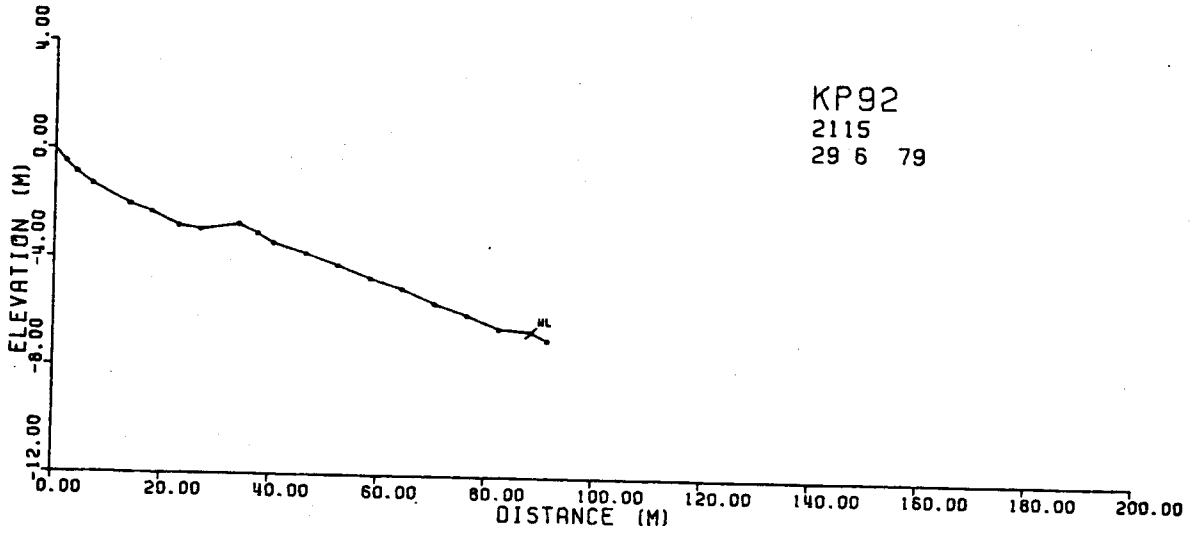


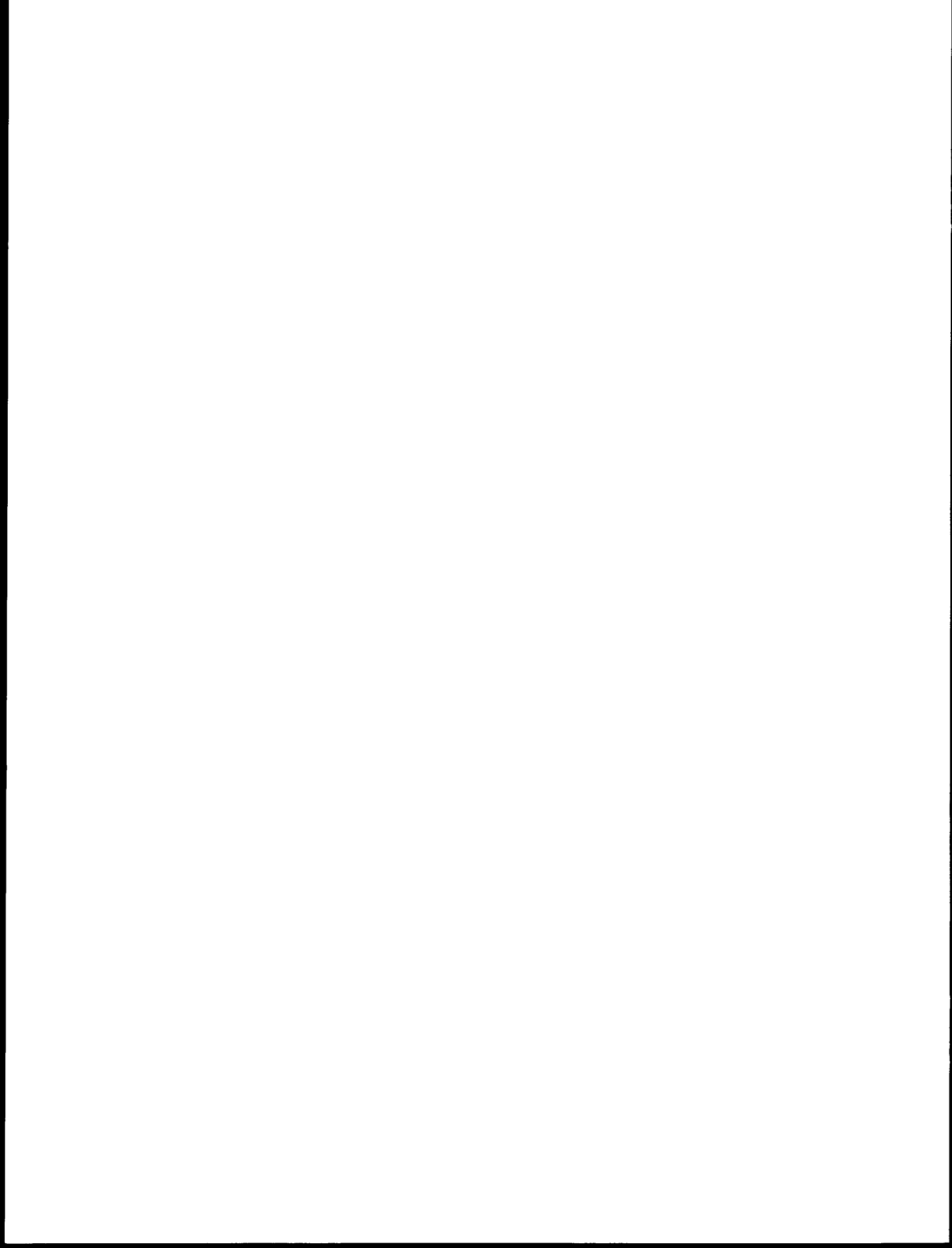








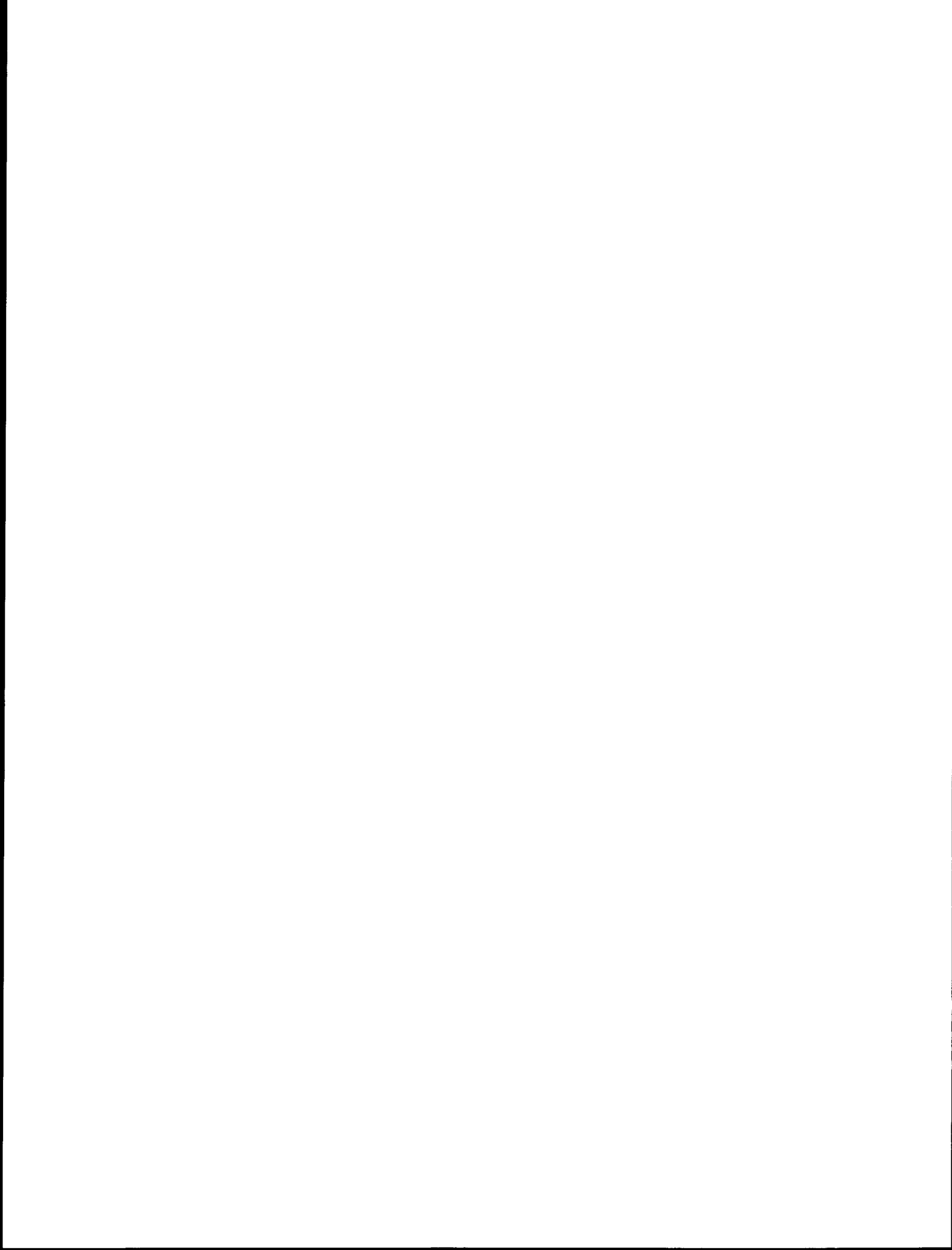




APPENDIX IV.

GRAIN SIZE STATISTICS

The results are shown of both sieve and settling tube grain size analysis and later computer synthesis for all sediment data collected. Samples were taken along profile lines with the same designation shown in Appendix III. Samples A, B and C were spaced $1/4$, $1/2$ and $3/4$ the length of the profile lines, respectively. This corresponds to the upper, mid and lower beachface.



<u>Station No.</u>	<u>Mean Grain Size (ϕ)</u>	<u>Standard Deviation (ϕ)</u>	<u>Skewness</u>	<u>Kurtosis</u>
KNP-1 B	-1.67	1.55	0.40	0.97
KNP-5 A	-4.32	0.74	0.43	0.98
B	-4.38	0.43	-.41	0.88
C	-4.13	0.79	0.34	1.11
KNP-7 A	-3.27	1.45	0.34	0.98
B	-3.40	1.05	-0.26	0.72
C	-3.20	1.20	-0.13	0.88
KNP-9 A	-0.56	1.73	-0.72	0.98
B	-1.14	0.52	0.10	0.99
C	-2.26	1.03	-0.09	0.68
KNP-11 B	0.46	2.52	-0.63	0.81
KNP-15 B	-4.00	1.03	0.47	1.17
KNP-17 A	1.37	0.35	-0.01	1.01
B	-1.15	2.48	-0.67	0.52
C	-1.06	2.43	-0.75	0.56
KNP-19 B	-3.08	0.81	0.14	1.39
KNP-25 A	-0.20	0.36	-0.04	1.04
KNP-34 A	-3.03	1.48	-0.24	1.32
B	-2.61	2.06	0.31	1.17
KNP-36 A	-2.05	1.45	-0.12	0.73
B	0.16	0.48	-0.03	1.00
KNP-37 B	-2.34	0.78	0.10	1.25
C	-0.65	0.39	0.02	0.96
KNP-41 A	-2.78	1.93	0.43	0.53
B	-1.41	2.65	-0.79	2.38
C	0.23	1.36	-0.56	3.52
KNP-43 A	-0.51	1.01	-0.53	4.66
B	-0.82	2.38	-0.81	3.07
C	-0.66	2.14	-0.79	1.64
KNP-59 B	-2.12	-1.56	-0.37	0.61
C	-3.20	1.97	0.64	0.54
KNP-71 A	-1.61	1.66	-0.61	0.67
B	-1.96	2.05	-0.71	1.07
C	-2.33	1.66	-0.24	0.59

<u>Station No.</u>	<u>Mean Grain Size (ϕ)</u>	<u>Standard Deviation (ϕ)</u>	<u>Skewness</u>	<u>Kurtosis</u>	
KNP-75	A	-2.41	2.16	0.23	0.55
	B	-1.87	1.26	0.06	0.87
	C	-5.13	1.03	0.88	0.90
KNP-82	A	1.79	0.33	-0.11	1.15
	B	1.25	0.24	-0.45	1.12
	C	1.37	0.32	-0.02	0.90
KNP-87	A	2.15	0.18	0.05	1.22
	B	2.13	0.13	0.06	1.31
	C	1.86	0.17	-0.04	1.26
KNP-95	A	-3.53	0.42	0.14	1.52
	B	-2.06	2.64	0.42	0.46
	C	-4.62	0.69	0.77	0.72
KNP-97	A	-4.36	0.50	0.48	1.76
KNP-99	A	2.44	0.19	0.03	1.12
	C	-2.71	2.31	0.49	0.76
KNP-100	A	-3.57	0.49	-0.14	1.75
	C	-0.37	0.90	-0.36	2.98

CIRCULATION AND WATER MASSES IN THE GULF OF ALASKA

by

Thomas C. Royer

**Institute of Marine Science
University of Alaska**

**Final Report
Outer Continental Shelf Environmental Assessment Program
Research Unit 289**

March 1981

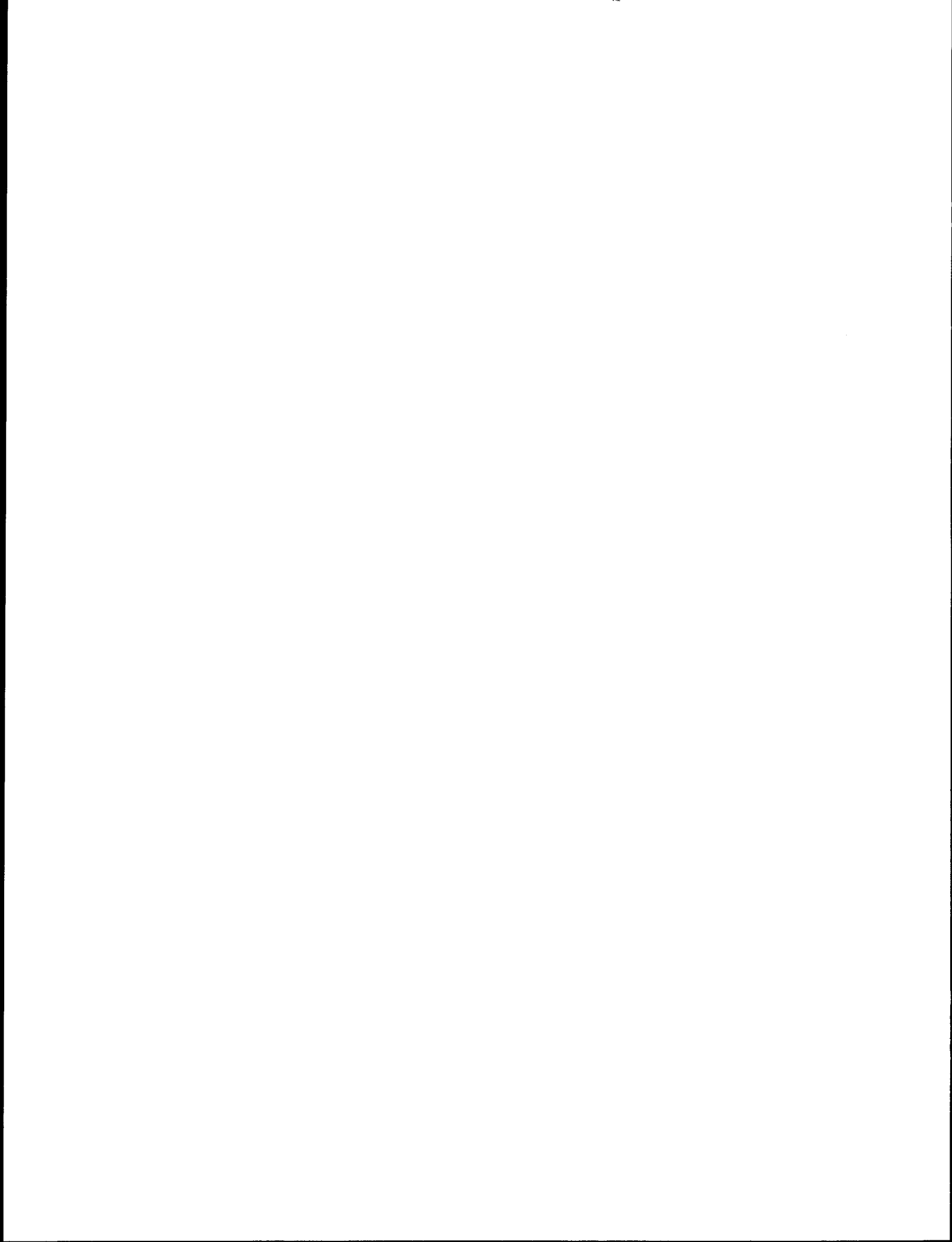


TABLE OF CONTENTS

CIRCULATION AND WATER MASSES IN THE GULF OF ALASKA
 T. C. Royer 539

I. SUMMARY 543

II. INTRODUCTION 544

III. CURRENT STATE OF KNOWLEDGE 544

IV. STUDY AREA 545

V. SERVICES, METHODS, AND RATIONALE OF DATA COLLECTION 545

VI. RESULTS AND DISCUSSION 546

 Remote Sensing Activities 546

 Coastal Circulation in the Gulf of Alaska 548

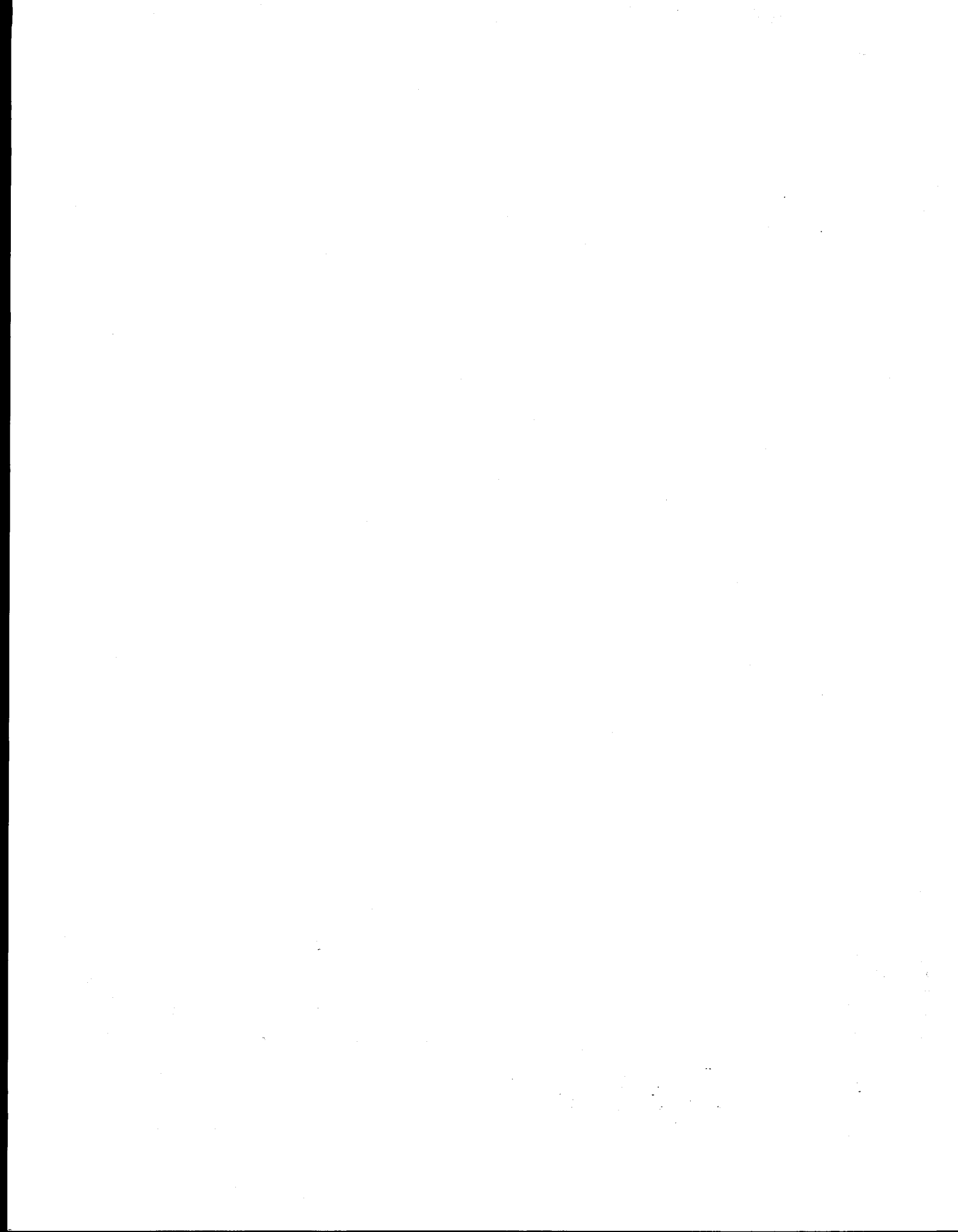
VII. CONCLUSIONS AND OUTLOOK 552

 REFERENCES 553

 APPENDIX: Reviewed Journal Papers Sponsored by BLM/NOAA
 OCS Program - Research Unit 289 555

COASTAL FRESHWATER DISCHARGE IN THE NORTHEAST PACIFIC
 T. C. Royer 559

SURFACE TEMPERATURE ENHANCED NOAA-SATELLITE INFRARED IMAGERY FOR THE
 BERING, CHUKCHI, AND BEAUFORT SEAS AND THE GULF OF ALASKA
 (May 1974-September 1980)
 Kristina Ahlnäs 585



I. SUMMARY

In the last year of this OCS project, analysis of prior oceanographic data from the Gulf of Alaska has continued with several new ideas and concepts evolving. In addition to the continued treatment of archived OCS data, more recent hydrographic and meteorological data gathered on other projects, are being incorporated into the analysis. For example, two cruises in Fall 1980 occupied many of the stations in the OCS grid. These additional data have provided new insights into the coastal circulation in the Gulf of Alaska. In particular, an hypothesis has been developed that suggests that processes affecting sea level in the estuaries can drive an alongshore coastal flow and/or vice-versa. We have evidence of a closely-coupled Prince William Sound - Alaska Coastal Current system which supports this idea. The time scale for circulation responses in this system are of the order of hours to days.

The major milestone of the past year's OCSEAP work is the determination of a vast coastal fresh water discharge for Southeast and Southcoast Alaska, which is slightly greater than the discharge from the Mississippi River. This discharge is in the form of numerous small streams, not major rivers, and thus has generally been overlooked as a major fresh water source. The coastal current responds to this discharge on both an annual and inter-annual basis. Wind stress also plays an important role in modifying this coastal flow. The fresh water discharge is speculated to be an important influence on the circulation of the Alaska Current and hence the circulation of the North Pacific Ocean.

II. INTRODUCTION

No new hydrographic data have been gathered during the past year under sponsorship of OCS. Analysis of previous data has continued, however. This recent work has resulted in three additional reviewed-journal papers on the circulation of the Gulf of Alaska and its forcing mechanisms. A preprint of the discussion of the fresh water discharge in the northeast Pacific is included as the first appended report following this report.

The majority of the funds for the past year's research was allocated to the continued satellite monitoring of Alaskan coastal waters. We have achieved both the visible and IR data with many enhanced images. A list of these data is included as Appendix I of the second appended report.

III. CURRENT STATE OF KNOWLEDGE

The most complete reference for the state of knowledge of the circulation of the Gulf of Alaska is the "Review of the physical oceanography of the northeast Gulf of Alaska, with emphasis on its implications to oil and gas development," which was included as an appendix to the 1980 annual report of RU289.

Within the past year, the research on this contract has evolved to a level where the use of analytic models is appropriate. While no models have been directly applied to our data, the general results of these models are useful. For example, the analytic estuary-coastal current model of Klinck *et al.* (1981) suggests that sea levels within an estuary and along the coast are related. Thus, a mechanism for driving the circulation of either exists; that is, a change in either will affect the other. These models allow us to think more clearly about the importance of various processes on the coastal

circulation. The models do not mimic the observations as numerical models might do, but instead address the physics of the problem. The use of these models is discussed in more detail in Section VI.

IV. STUDY AREA

Field work under this research unit has ranged over the continental shelf of the southern Alaska coastline from Yakutat to Umiak Pass from the coastline to tens of kilometers beyond the shelf break. The satellite data collected for OCSEAP by this unit covers the entire Alaskan coastline from the Beaufort Sea to Southeast. The analysis portion of the past year's work has addressed the entire Gulf of Alaska region.

V. SERVICES, METHODS AND RATIONALE OF DATA COLLECTION

The primary data collection method used in previous years by this research unit was the CTD/STD (salinity - temperature - depth) profile. Some current meter and bottom pressure gauge deployments have also been undertaken to supplement the hydrographic data. From the CTD/STD data, contour maps of salinity, temperature, density and dynamic height were constructed. The contours provide information on the direction and intensity of the flow. The current meter measurements provide a means of "calibrating" the currents obtained from the density fields. The sea level as measured at the coastline by NOS (National Ocean Survey) stations was used in conjunction with the bottom pressure data to determine changes in the slope of sea level between the positions and hence provide a measure of current changes.

The CTD/STD station positions were chosen by 1) a knowledge of the spatial scales of the features to be measured and 2) requirements to continue a time history of oceanographic parameters at a particular location. The objective has been an improved understanding of changes in the oceanographic parameters, spatially and temporally.

VI. RESULTS AND DISCUSSION

Remote Sensing Activities

During the last half year of the project until September 15, 1980 all incoming NOAA-AVHRR satellite imagery has been monitored at the NOAA-NESS CDA-Satellite Station at Gilmore. During this time, a total of 846 prints, including 46 gray scale enhancements and 114 enlargements, made specifically for us, were produced by the tracking station. This number also includes copies of 142 enhancements originated by the Satellite Service Station in Anchorage. The collection of satellite imagery is contained in 41 ring-binders and is divided into two geographical areas: (a) the Arctic Ocean and Bering Sea and (b) the Gulf of Alaska. Most of these binders have been transferred to the Remote Sensing Library of the Geophysical Institute for archiving.

About 25% of the 846 prints produced were requested by persons working outside this project. More than half of that imagery was produced in support of a Master of Science Thesis for an Institute of Marine Science student studying processes along the shelf break in the SE Bering Sea. The next largest request for satellite support was made by a Sea Grant project studying the Bering Sea ice edge. In addition, the temperature structure along the

ice edge in the Chukchi Sea was kept under surveillance in support of an OCS study to predict bird migrations.

The satellite facility, as in years past, has maintained some international connections through discussions of the use of satellite data with visiting Japanese scientists and instructions in the use of satellite data for a student from Taiwan. A request for satellite data for the Russian Arctic, however, had to be referred to other sources.

Some joint work on the sea-ice conditions in the Bering Sea was conducted during March and July with a visiting OCS-supported scientist from PMEL in Seattle. When the funding for this project ended in September, a ringbinder containing 125 satellite enlargements for the Norton Sound area, from 5 December 1979-21 May 1980, was mailed to PMEL to be analyzed there.

This satellite project was supported by NOAA-NESS and then OCS grants from 1974 to 1980. Numerous gray scale enhanced negatives for surface temperature studies have been produced. To make this information available to other scientists, a report entitled "Surface temperature enhanced NOAA-satellite infrared imagery for the Bering, Chukchi, and Beaufort Seas and the Gulf of Alaska, May 1974 - September 1980" was prepared (University of Alaska, Institute of Marine Science Technical Report R80-2). This report, which we have included as our second appended report, contains a listing of all negatives and digitized tapes of special interest that have been saved. The report also shows how the enhanced imagery has been used and gives a background and summary of the NOAA-satellite project since the tracking station at Gilmore became operational for real-time Alaskan imagery in 1974.

Coastal Circulation in the Gulf of Alaska

The bulk of the principal investigator's research effort in the last year has been devoted to analysis of nearshore circulation in the northern Gulf of Alaska and Prince William Sound. The influence of fresh water and winds on this coastal circulation has been discussed in previous annual reports and will soon be published in the May 1981 issue of the Journal of Marine Research. For that work, a very simple hydrology model is used. In the past year, a more advanced treatment of the fresh water discharge has been undertaken with some significant results. The details of this work are contained in our first appended report, "Coastal fresh water discharge in the northeast Pacific," a brief summary of which is given below.

The Yukon has long been considered as the largest Alaskan river; however, there is a larger fresh water source in Alaska. Recent studies of the coastal flow in the Gulf of Alaska at the Institute of Marine Science have revealed a large, river-like, fresh water coastal jet along Southcoast and Southeast Alaska. This jet moves from Southeast toward the north at speeds in excess of two knots (1 knot = 1 nautical mile per hour). It is approximately 10 miles wide, and because of the earth's rotation it generally stays near the coast. The flow continues around the Gulf of Alaska; a portion enters Prince William Sound, then moves past Kodiak Island and along the Aleutian Islands.

The average flow in this jet is considerably greater than that of the Yukon River ($23,000 \text{ m}^3/\text{s}$ versus $6,796 \text{ m}^3/\text{s}$). Incidentally, the average flow is greater than that of the Mississippi River which is $18,123 \text{ m}^3/\text{s}$, in effect giving Alaska a claim to the largest U.S. river. The maximum seasonal flow occurs approximately in October coincident with the maximum precipitation.

The minimum coastal flow is in March. Its maximum flow is also greater than the maximum Mississippi River discharge.

Why has this significant fresh water source gone unnoticed until now? The primary reason is the absence of large rivers in the region. Though residents of Southeast Alaska brag about their high rates of precipitation, no major rivers are associated with that rainfall. The enormous annual rainfall, which occasionally exceeds 8 meters (26 feet), enters the ocean by way of numerous small streams rather than joining to form large river networks. Since few of these streams are gauged, the water in this coastal jet has to be determined indirectly from drainage areas and precipitation rates. These rates are subject to considerable error, so the estimates given here are very rough.

This section of coastline contains over two-thirds of the North American ice fields. Climatic changes which alter the size of these ice fields could affect the amount of fresh water available to the coastal jet. Thus, this coastal circulation might be very sensitive to climatic changes.

There are numerous consequences of this coastal jet. Because the flow is quite steady, vessels navigating the coastal areas in the Gulf of Alaska can use it to their advantage when traveling west-northwest from Southeast to Southcentral Alaska, but should avoid it when moving in the opposite direction. The coastal jet probably has important biological implications and may influence the distributions of fishes and marine mammals. Unfortunately, this current is also a mechanism that can transport pollutants from one coastal harbor to another without significant offshore dilution.

If the analytic two-layer model of Heaps (1980) is applied to our system, it predicts that there will be an offshore flow of about 20% of the alongshore

flow. Thus, after several hundred miles of travel along the coast, the fresh water should be spread over the entire shelf. Since it appears that this does not occur, a mechanism must exist to concentrate the flow at the coast. The predicted offshore fresh water movement has a very similar appearance to an Ekman upwelling situation. Therefore, if Ekman downwelling conditions are superimposed on this fresh water coastal current, a very intense narrow flow will occur. This type of response coincides with recent observations of this coastal jet near Seward. It is less than 10 km wide and it has speeds at the surface in excess of one knot. Apparently the sampling along the Seward line and elsewhere on the hydrographic grid used in the OCSEAP studies was too coarse to resolve adequately the baroclinic velocities. As suggested previously in earlier annual reports, the baroclinic transports are correct as they do not depend on station spacing.

In addition to the previous hydrographic stations being too far apart, recent non-OCSEAP data from November 1980 indicate that the Seward line poorly represents direction and width of the coastal flow. This is a consequence of downstream topographic features--a peninsula and several islands. These obstructions divert the flow offshore as it crosses the Seward line, making it appear to separate from the coast at the point. This also causes an apparent counterflow on the adjacent downstream hydrographic section at Seal Rocks. Thus, the Seward line should be used to determine baroclinic transports only--not baroclinic speeds or the position of the coastal current.

The use of the analytic model by Heaps (1980) also predicts that the barotropic effect of adding fresh water to a coastal current is small. Instead, the alteration of the cross-shelf density by the fresh water is the important dynamic consequence. Incidentally, the fresh water discharge for the northern

Gulf of Alaska is approximately twice the discharge that Heaps used in his model for the Norwegian coast. Similarly, our transports are about twice his values.

An analytic model developed by Klinck *et al.* (1981) of fjord and coastal circulation helps shed light on the interactions between the sea level within an estuary and the coastal current flowing alongshore. Their model indicates that an elevation in sea level within the estuary will accompany an acceleration in the alongshore flow. The implication of this effect is that routine sea level observations can be used to estimate the alongshore flow. Of course, this phenomenon has not yet been verified for the Gulf of Alaska. This application of the analytic model serves not only to understand better the physics of the system but also may provide an inexpensive monitoring scheme.

The relatively narrow, intense coastal flow found throughout southeast and southcoast Alaska presents an interesting problem in estuarine circulation. For estuaries with below average fresh water discharge, the coastal current can serve to drive the circulation in a reverse manner, that is, in at the top and out at the bottom. Even for the usual estuarine circulation, the coastal current would serve to reduce the flow since fresher water could be found outside the estuary.

The other major feature of the circulation of the Gulf of Alaska is the Alaska Current which flows westerly along the shelf break. The coastal current and Alaska current are weakly coupled in several ways. First, the coastal current can mix directly with the Alaska Current south of Kayak Island where the coastal current is directed southward and the shelf becomes very narrow. To the west, the Alaska Current displays the low salinity signature of the coastal current. The Alaska Current also appears to shed eddies which

propagate from west to east along the shelf break. These perturbations accelerate the cross-shelf mixing over the shelf. The third manner in which the coastal and shelf-break currents interact is through the continuous supply of fresh water at the coast. This maintains a cross-shelf density gradient which can in turn drive the Alaska Current. If this latter conjecture is true, the coastal precipitation would be important to the circulation of the entire North Pacific.

In any case, the high rate of coastal precipitation presents an interesting meteorology problem since a vast amount of latent heat will be released to the atmosphere. Combine this warm air with the continental air masses found over the interior of Alaska and very abrupt thermal gradients will be created over the coastal mountain range. This atmospheric system is responsible for the glacial fields found along the coastal margin. Thus, the hydrology, glaciology and oceanography are closely coupled here.

VII. CONCLUSIONS AND OUTLOOK

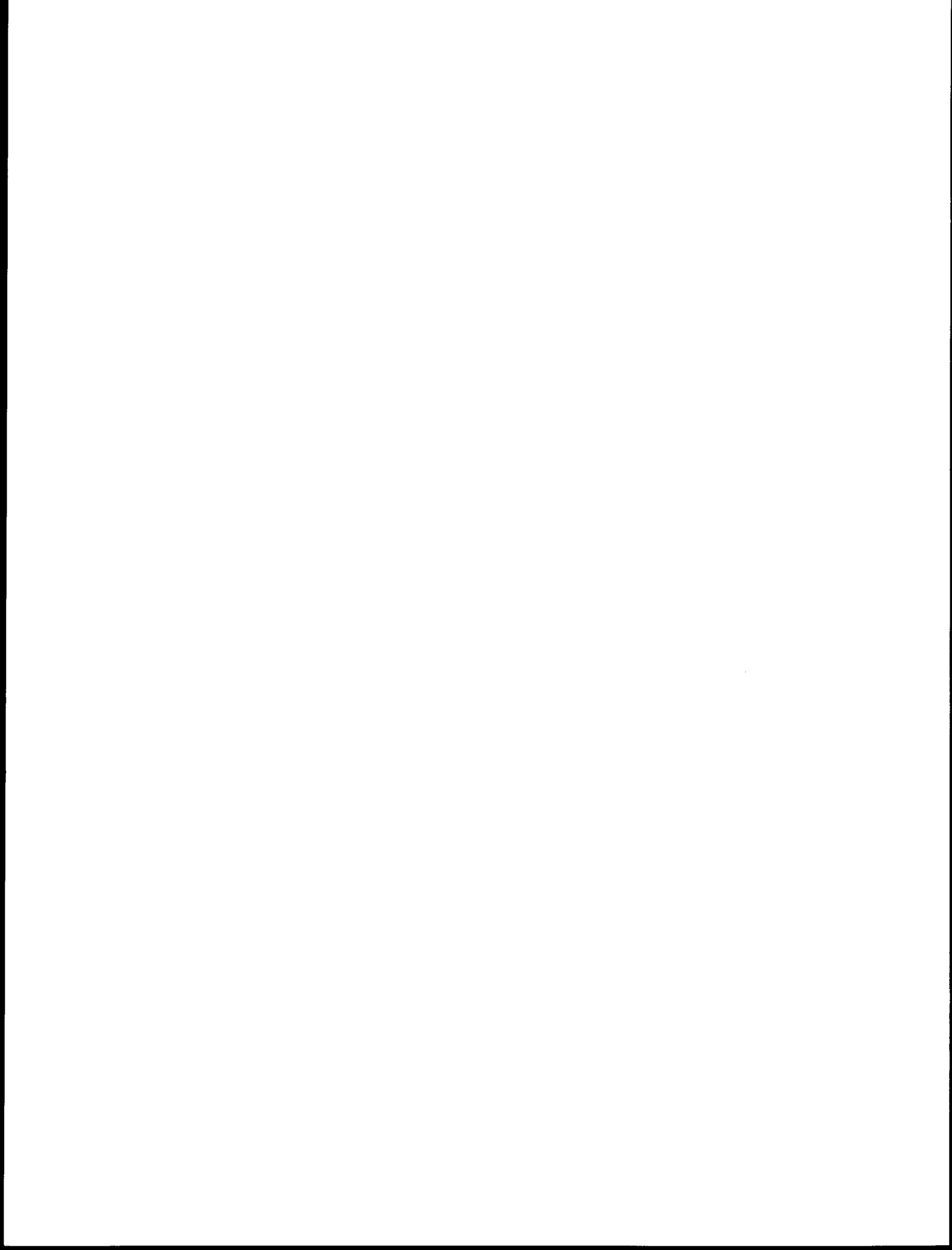
The continued support of this research unit by BLM and NOAA over the past seven years is gratefully acknowledged. I especially appreciate the opportunity, in the past several years, to be allowed to pursue the research of the coastal flows, which has led to a better understanding of the circulation of the northern Gulf of Alaska.

As a consequence of these OCS studies, new programs are being initiated for the continued study of the Alaska Coastal Current. Support for this work is being sought from the National Science Foundation with some contribution requested from BLM. The focus of these new studies is the dynamics of the coastal current. An analytic model is expected to be developed in this effort.

The coastal current is also the object of studies into the biology, chemistry and geology of the northern Gulf of Alaska which are being organized at the Institute of Marine Science. Researchers in fisheries and marine mammals are frequently requesting information on this flow. This coastal flow is vital to studies of estuary circulation in the Gulf of Alaska. It also serves as an important medium to transfer pollutants along the coast, while limiting the pollutant movement across the shelf. Studies of the circulation of the Gulf of Alaska will continue, building upon the knowledge gained in this OCS research program.

REFERENCES

- Heaps, N. S. 1980. Density currents in a two-layered coastal system, with application to the Norwegian Coastal Current. *Geophys. J. R. Astr. Soc.*, 63: 289-310.
- Klinck, J. M, J. J. O'Brien and H. Svendsen. 1981. Simple model of fjord and coastal circulation interaction. Submitted to *J. Phys. Oceanogr.*

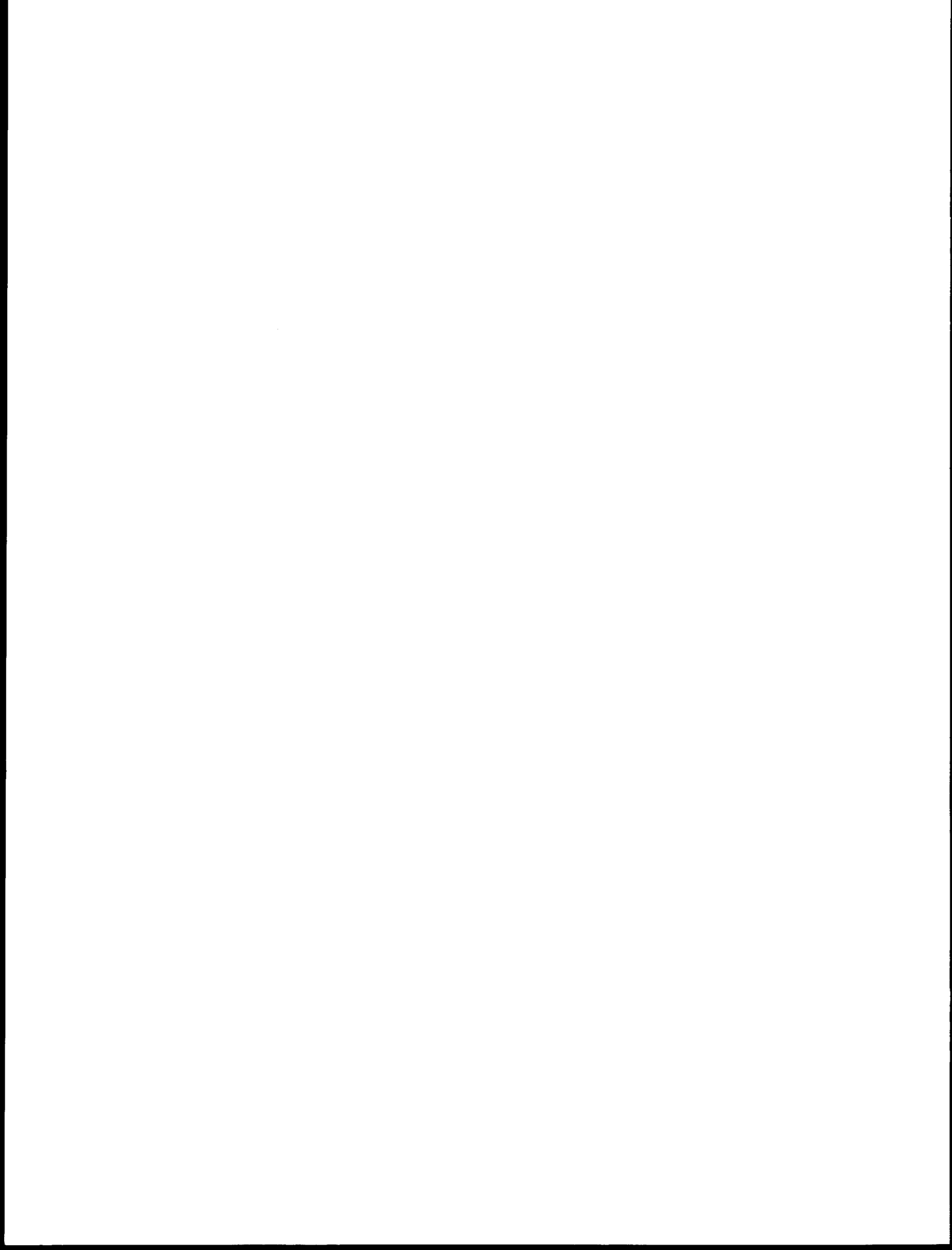


APPENDIX

REVIEWED JOURNAL PAPERS SPONSORED BY BLM/NOAA OCS PROGRAM -
RESEARCH UNIT 289

Thomas C. Royer
Institute of Marine Science
University of Alaska

March 1981



APPENDIX

Reviewed Journal Papers Sponsored by BLM/NOAA OCS Program - Research Unit 289

- Ahlnäs, K. 1979. IR Enhancement Techniques to Delineate Surface Temperature and Sea-Ice Distributions. Proc. 13th Int. Symp. on Remote Sensing of Environment, Ann Arbor, Mich. April 1979. II. 1067-1076.
- Ahlnäs, K. and H. Solomon. 1979. Eddy-like Features in the Kamchatka Current. Polymode News 60.
- Ahlnäs, K. and G. Wendler. 1979. Arctic Sea Ice, Invited summary report for "1978 Arctic Directory" Proc. 7th Northern Library Colloquy, Paris, France September 1978 (in press).
- Livingstone, D. and T. C. Royer. 1980. An analysis of observed surface winds at Middleton Island, Gulf of Alaska. *J. Phys. Ocean.* 10:753-764.
- Livingstone, D. and T. C. Royer. 1980. Eddy propagation determined from rotary spectra. *Deep-Sea Res.* 27A:823-835.
- Roberts, J. and T. C. Royer. 1977. Comparison of storm wave spectra from the Gulf of Alaska. *Dt. Hydrogr. Z.* 30:9-19.
- Royer, T. C. and R. D. Muench. 1977. On the ocean temperature distribution in the Gulf of Alaska, 1974-1975. *J. Phys. Ocean.* 7:92-99.
- Royer, T. C. 1978. Ocean eddies generated by seamounts in the North Pacific. *Science* 199:1063-4.
- Royer, T. C. 1979. On the effect of precipitation and runoff on coastal circulation in the Gulf of Alaska. *J. Phys. Ocean.* 9:555-563.
- Royer, T. C., D. V. Hansen and D. J. Pashinski. 1979. Coastal flow in the northern Gulf of Alaska as observed by dynamic topography and satellite-tracked drogued drift buoys. *J. Phys. Ocean.* 9:785-801.
- Royer, T. C. 1981. Baroclinic transport in the Gulf of Alaska. Part I. Seasonal variations of the Alaska Current. *J. Mar. Res.* Vol. 39 (In press).
- Royer, T. C. 1981. Baroclinic transport in the Gulf of Alaska. Part II. Fresh Water Driven Alaska Coastal Current. *J. Mar. Res.* Vol. 39 (In press).
- Royer, T. C. (with Niebauer and Roberts). 1981. Current fluctuations near the shelf break in the northern Gulf of Alaska, 1976-77. *J. Geop. Res.* Vol. 86 (In press).

Royer, T. C. 1981. Coastal fresh water discharge in the Northeast Pacific. (Submitted to *J. Phys. Oceanogr.*).

Solomon, H. and K. Ahlnäs. 1978. Eddies in the Kamchatka Current. *Deep-Sea Res.* 25:403-410.

Solomon, H. and K. Ahlnäs. 1980. Ice spirals off Barrow as seen by satellite. *Arctic* 33:184-188.

In Preparation

Royer, T. C. Coastal sea level influences in the Northeast Pacific. (To be submitted to *J. Geop. Res.*).

Royer, T. C. Circulation of Prince William Sound and adjacent waters. (To be submitted to *Coastal & Est. Mar. Sci.*).

Solomon, H., K. Ahlnäs, and G. R. Garrison. 1981. Satellite and Oceanographic Observations of the Warm Alaskan Coastal Current in Bering Strait and the Chukchi Sea. (in preparation).

COASTAL FRESH WATER DISCHARGE IN THE NORTHEAST PACIFIC

by

Thomas C. Royer

Institute of Marine Sciences
University of Alaska

March 1981



TABLE OF CONTENTS

List of Figures 563

Abstract 565

1. INTRODUCTION 566

2. THE DISCHARGE COMPUTATIONS 567

3. FRESH WATER DISCHARGE 570

4. OCEANIC RESPONSE 575

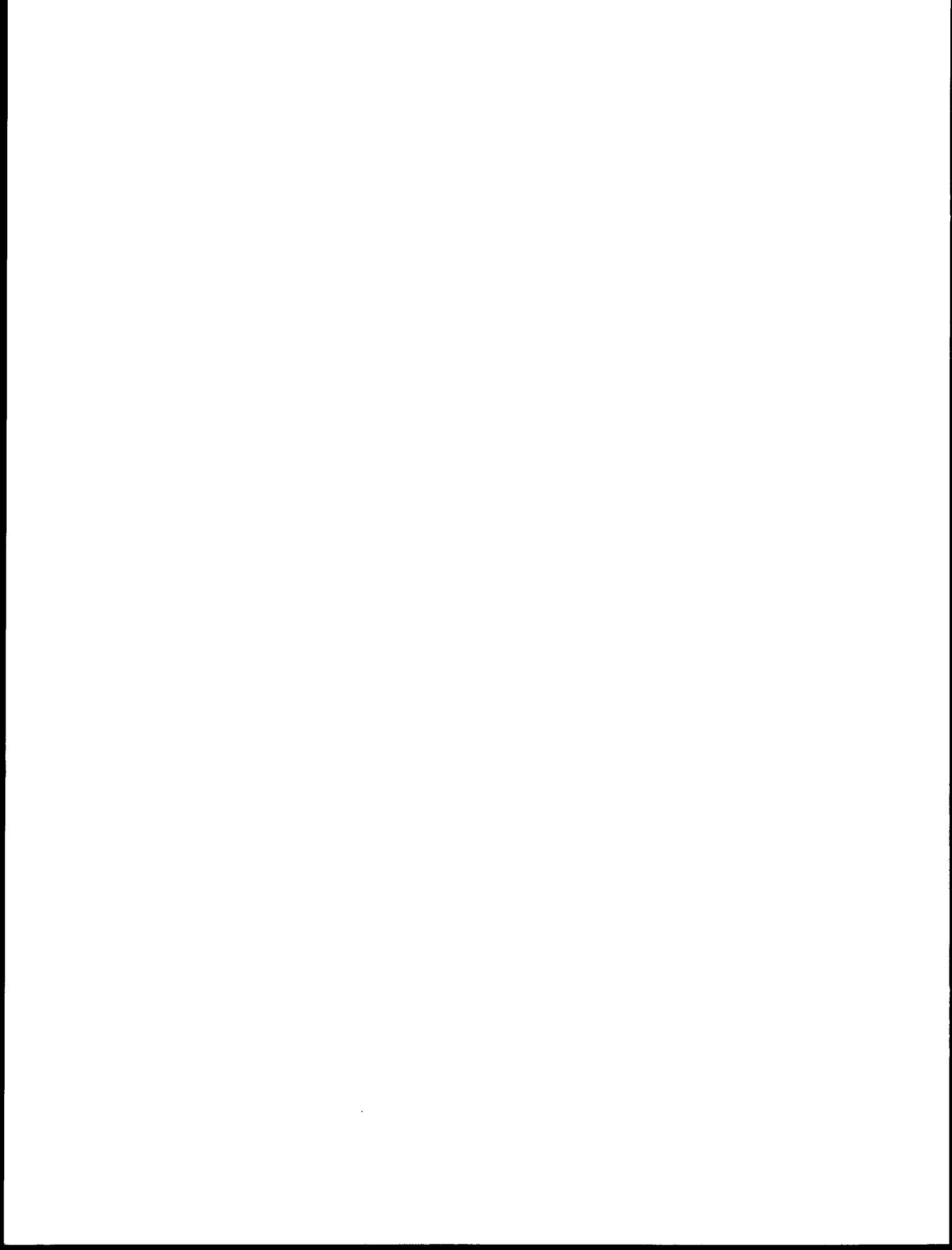
5. CONCLUSIONS 581

ACKNOWLEDGEMENTS 582

REFERENCES 583

LIST OF FIGURES

- Figure 1. Coastal region of northeast Pacific Ocean.
- Figure 2. Monthly fresh water discharge for northeast Pacific with southeast Alaska discharge lagging southcoast Alaska discharge by one month.
- Figure 3. Mean monthly fresh water discharge determined in same manner as Figure 2, using data from 1931 to 1979.
- Figure 4. Annual mean air temperature (top panel) for southeast Alaska (SE) and southcoast Alaska (SC), precipitation (middle panel) and fresh water discharge (lower panel).
- Figure 5. Monthly fresh water discharge (same as Figure 2) for 1974 to 1979 (line) with baroclinic transport (dots) for 1-7 σ_{θ} superimposed. Range of the baroclinic transport is 0 to $1.5 \times 10^6 \text{ m}^3 \text{ s}^{-1}$.
- Figure 6. Salinity cross-section for Seward line looking eastward (see Figure 1), November 1980.
- Figure 7. Cross-sections of temperature (top panel), salinity (middle panel), and density (lower panel) at Cape Fairfield, November 1980 (see Figure 1 for locations).



Abstract

Very high annual rates of precipitation in the coastal mountains which border the northeast Pacific Ocean produce large fresh water discharges ($23000 \text{ m}^3 \text{ s}^{-1}$). This discharge has been ignored previously since it does not enter the ocean in the form of large rivers, but instead, the water enters by way of numerous small rivers and streams. This coastal discharge contributes approximately 40% of the fresh water that enters the northeast Pacific from the atmosphere. The discharge is comparable to the mean annual discharge of the Mississippi River system.

The fresh water creates a density gradient which drives an along-shore baroclinic jet. The width of this jet is less than 25 km with velocities in excess of 100 cm s^{-1} . It extends along the coast from southeast Alaska to at least Kodiak Island. Apparently, the flow is maintained as a narrow current adjacent to the coast by wind stress which causes downwelling conditions here throughout most of the year.

1. Introduction

The importance of fresh water to the ocean circulation of the northeast Pacific has been recognized since Tully and Barber (1960) treated it as an estuary. More recently, coastal fresh water discharge has been identified as being a primary driving mechanism of local coastal circulation in the northwest Gulf of Alaska (Schumacher and Reed, 1980) and throughout the northern Gulf of Alaska (Royer, 1981). Baroclinic flow controlled by salinity distributions is possible here because of the relatively low water temperatures and high rates of fresh water discharge.

Previous discussions of the availability of the fresh water in the northeast Pacific are based either on river discharges or precipitation rates. Roden (1967) addresses the discharge of major river systems into the northeast Pacific and Bering Sea. The major river discharges are the Fraser River ($2.69 \times 10^3 \text{ m}^3 \text{ s}^{-1}$) in British Columbia and the Copper River ($1.05 \times 10^3 \text{ m}^3 \text{ s}^{-1}$) in Alaska. Roden also included six other minor rivers which have a combined average discharge of less than $3 \times 10^3 \text{ m}^3 \text{ s}^{-1}$. Another method of assessing the availability of fresh water in the northeast Pacific is through the use of oceanic precipitation estimates. However, as can be seen by two recent estimates of maximum precipitation rates for the northeast Pacific, the calculated fresh water input can differ considerably. Reed and Elliott (1979) report a precipitation rate of 100 cm yr^{-1} while Dorman and Bourke (1979) show a rate of 180 cm yr^{-1} for the same area. This discrepancy is primarily caused by Dorman and Bourke correcting the oceanic precipitation using Tucker's method. They correct using coastal station data, and because coastal rainfall rates are high in the northeast Pacific the oceanic rates are enhanced.

2. The Discharge Computations

The high precipitation rates suggested by Dorman and Bourke (1979) are consistent with the rates used by Royer (1979, 1981) to obtain the coastal fresh water discharge in the northern Gulf of Alaska. The coastal discharges are determined using a 150 x 600 km drainage area to represent the coastal region. To calculate discharges, the monthly mean U.S. Weather Service divisional precipitation rates for southcoast Alaska are used. Two U.S. Weather Service climatic divisions are used in this work; the southcoast Alaska (approximately 140°W to 150°W) and the southeast Alaska (approximately 130°W to 140°W) (see Figure 1). Depending on the monthly mean air temperature, the precipitation is allowed either to runoff during the month or be stored as snow. The snow is released later when the air temperature is above freezing. It is released gradually over a period of several months, with a pattern that closely approximates the river discharge of those rivers which drain the coastal mountain ranges. An approach involving indirect computations is required here because direct measurements of the discharges of the myriad of rivers and streams is not possible.

To improve the estimate of coastal fresh water discharge into the northeast Pacific, the simple computations have been modified to better approximate actual drainage areas. This improved method still uses the monthly mean divisional precipitation and air temperatures as its input, but incorporates more realistic drainage areas and allows the interannual ablation or growth of the glacial fields which are found in these coastal mountains. This type of response is necessary since glaciers occupy approximately 20% of this coastal drainage area. Abnormally high summer air temperatures are permitted to cause a higher than normal fresh water discharge with abnormally low temperatures causing low fresh water drainages.

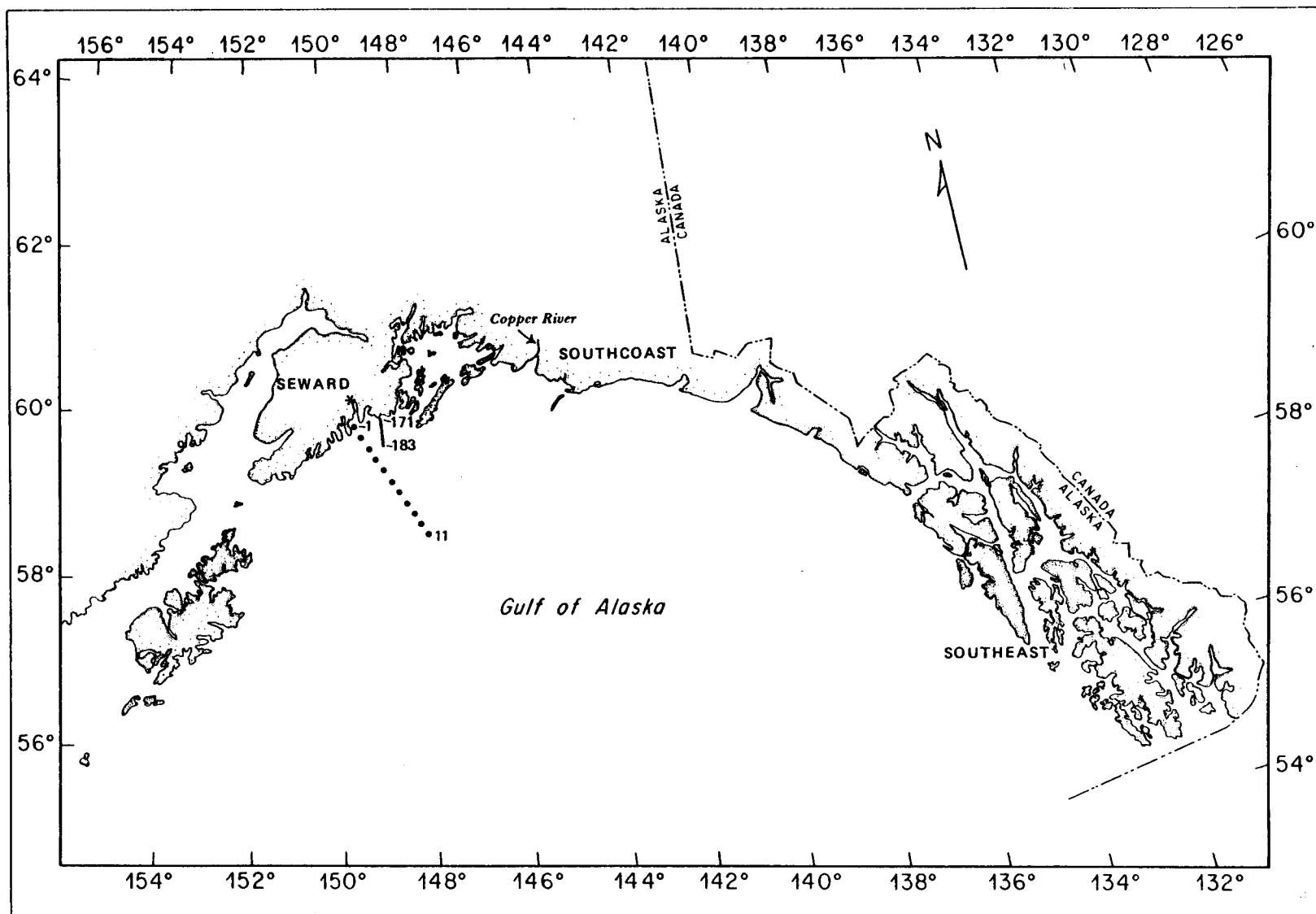


Figure 1. Coastal region of northeast Pacific Ocean.

Two separate drainage areas, southeast and southcoast Alaska are used in the computations (Fig. 1). Precipitation and air temperatures are available for each of the two divisions. Transit times in the form of phase shifts in the discharge are incorporated in this method. A northwestward coastal flow averaging about 30 cm s^{-1} from southeast to southcoast Alaska is approximated by lagging the southeast discharge by one month. The discharges from streams and rivers that are gauged are not included separately. The contribution from the Copper River, which drains a portion of interior Alaska, is not included because its records do not cover the same time period as the precipitation and air temperature records. As will become more evident later in this paper, its contribution ($1000 \text{ m}^3 \text{ s}^{-1}$) is less than 5% of the total coastal discharge and is insignificant in comparison with other errors in the hydrology model.

The coastal topography and the precipitation distributions here are similar to other high latitude regions, such as the coast of Scandinavia (Bergeron, 1949). Along that coast the moist marine air masses impinging on the coastal mountain ranges are elevated adiabatically and precipitation takes place. Analogous processes occur at the northeast Pacific Coast where mountains with heights exceeding 4 km are common in the Alaska Coastal Range. The orographic control of precipitation causes higher rates at higher elevations. Thus, the 180 cm yr^{-1} precipitation rate measured at sea level probably translates into a much greater rate at the higher elevations. The location of meteorological observing sites in coastal communities, therefore, leads to an underestimate of regional precipitation rates. However, other areas on the leeward side of the mountains will have lower rates. It is beyond the scope of this paper to evaluate the magnitude of these errors, since

precipitation rates over these sparsely inhabited areas are not well known. Though detailed seasonal variations in rainfall are not well documented, the most complete representation of the spatial distribution of precipitation is given by Selkregg (1979). Annual precipitation rates in excess of 240 inches (610 cm) are present for the glacial areas, with one area in southeast Alaska having a 320 inch (813 cm) contour. Thus, while the use of the divisional precipitation averages (about 240 cm) might be an underestimate it will be used in lieu of a suitable substitute. The high rate of coastal precipitation extends to the south along the British Columbia coast. Kendrew and Kerr (1955) indicate that the 100 inch (254 cm) precipitation contour is continuous along the British Columbia coast from Alaska to Washington. The effects of the British Columbia discharge will not be included in this study, though they are undoubtedly important.

3. Fresh Water Discharge

The addition of the monthly fresh water discharges for southcoast and southeast (lagged by one month) Alaska from 1931 through 1979 (Fig. 2) demonstrates a large seasonal signal (Fig. 3). This seasonal cycle in the fresh water discharge closely resembles the discharge reported in Royer (1979). The minimum in February-March coincides with oceanographic winter. The sub-maximum in May represents spring runoff followed by a general increase toward the October maximum. This increase is a result of the meltwater discharge and increased seasonal precipitation rate. The sharp decline in November-December is a consequence of air temperatures becoming less than 0°C.

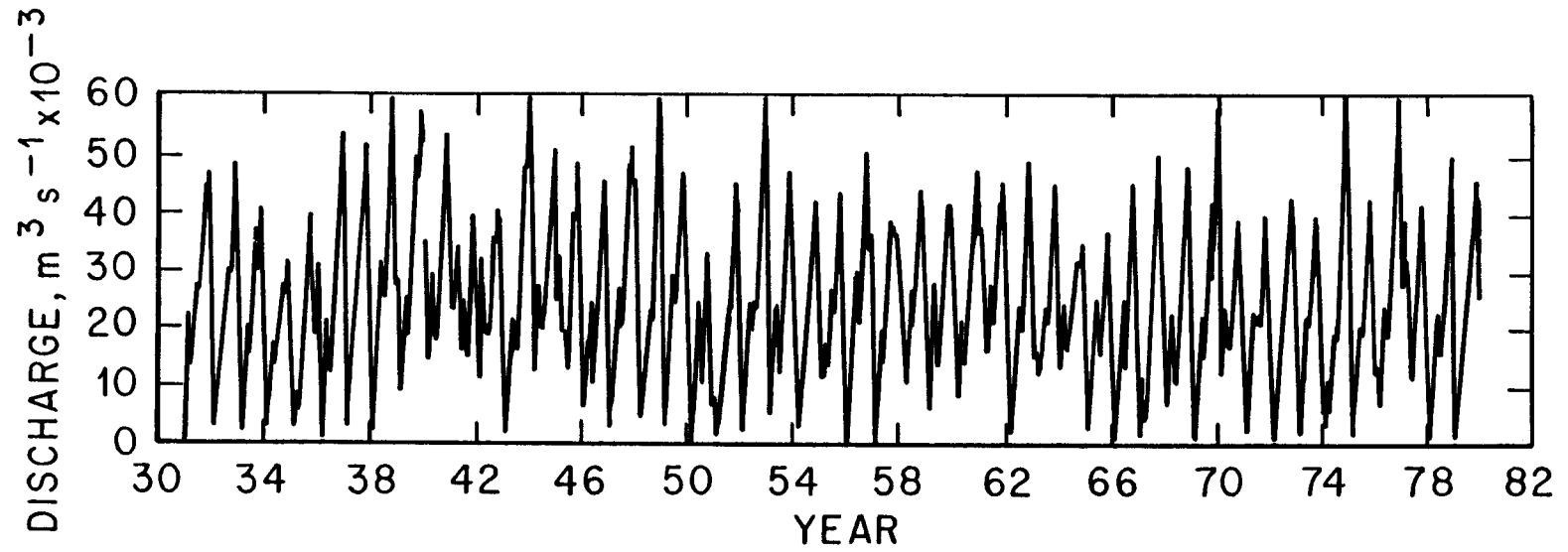


Figure 2. Monthly fresh water discharge for northeast Pacific with southeast Alaska discharge lagging southcoast Alaska discharge by one month.

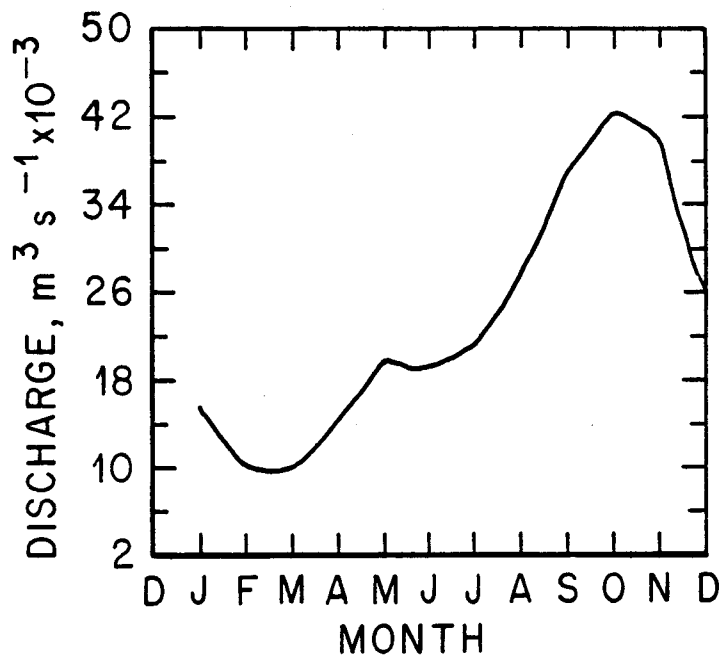


Figure 3. Mean monthly fresh water discharge determined in same manner as Figure 2, using data from 1931 to 1979.

The total discharge (Fig. 2) varies from nearly zero to greater than $60,000 \text{ m}^3 \text{ s}^{-1}$. To better illustrate long-term trends the monthly air temperatures, precipitation and discharges are used to determine annual means (Fig. 4). As expected, the air temperatures for southcoast Alaska are always less than those for southeast. The curves of mean annual temperature and precipitation are quite similar for southcoast and southeast Alaska, indicating that the same atmospheric system probably influences both regions. The below freezing annual mean southcoast air temperatures for 1934 (-0.31°C) and 1935 (-0.16°C) are especially interesting since they were more than two degrees below any others and were accompanied by a subnormal precipitation rate. The discharge for 1934 and 1935 were $16000 \text{ m}^3 \text{ s}^{-1}$ and $18000 \text{ m}^3 \text{ s}^{-1}$ respectively which are well below the 1931-1979 average of $23000 \text{ m}^3 \text{ s}^{-1}$. The minimum annual discharge occurred in 1950 when the average was slightly less than $16000 \text{ m}^3 \text{ s}^{-1}$. This decreased discharge was the result of subnormal temperatures and precipitation rates in November 1950, yielding a discharge of only $16000 \text{ m}^3 \text{ s}^{-1}$ compared with the normal, $40,000 \text{ m}^3 \text{ s}^{-1}$. Throughout 1950, the monthly discharges were slightly below normal also. The maximum discharge occurred in 1940 with $33,000 \text{ m}^3 \text{ s}^{-1}$ after which there was a general decline in discharge until about 1971. The precipitation and air temperatures contain similar patterns. Because oceanographers commonly deal with transports of the order of $10^6 \text{ m}^3 \text{ s}^{-1}$ these discharges seem to be insignificant. However, the mean annual discharge of the Mississippi River is about $18000 \text{ m}^3 \text{ s}^{-1}$.

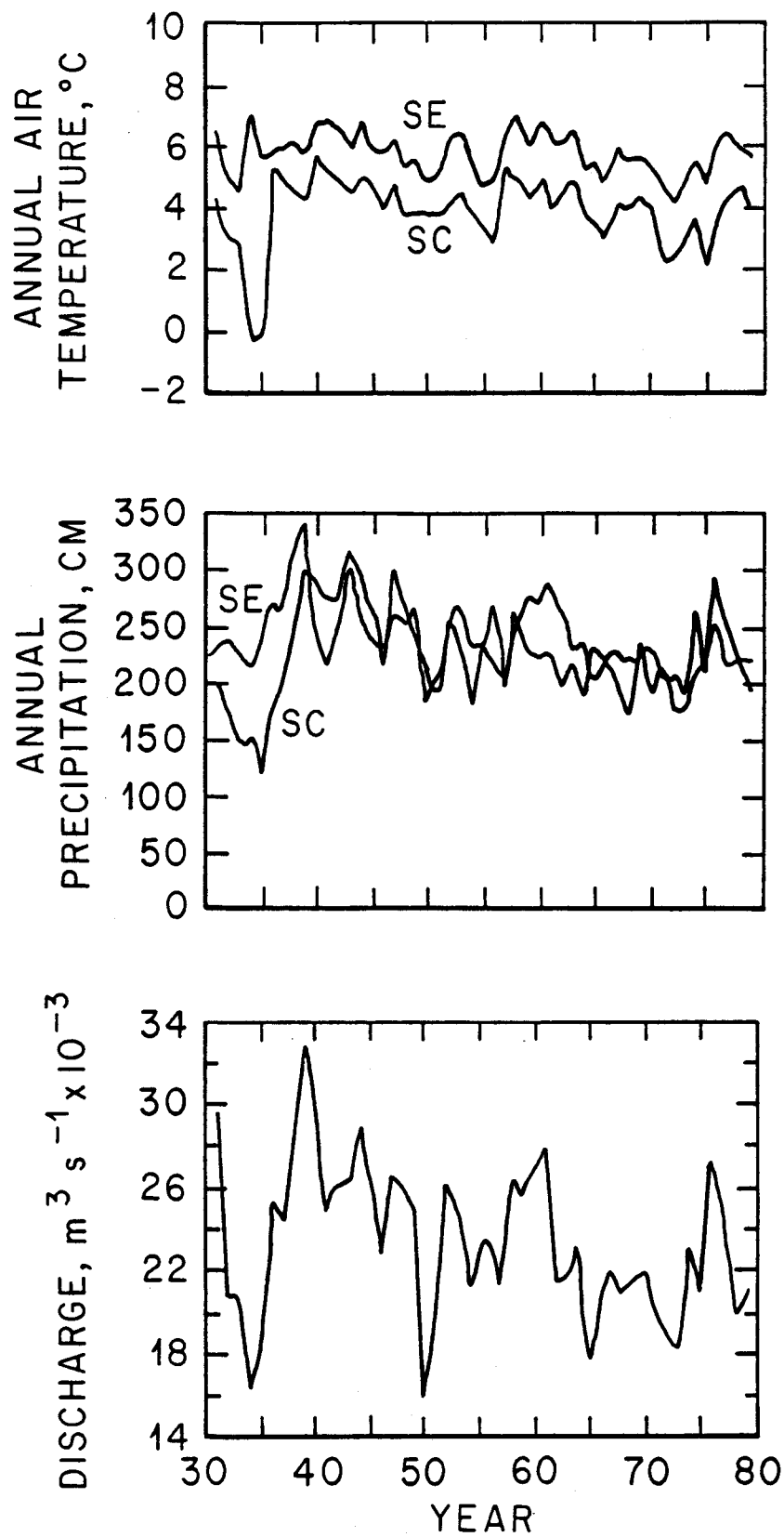


Figure 4. Annual mean air temperature (top panel) for southeast Alaska (SE) and southcoast Alaska (SC), precipitation (middle panel) and fresh water discharge (lower panel).

4. Oceanic Response

The availability of hydrographic data for the Seward Line (Fig. 1) from 1974 through 1979 permits the comparison of the fresh water discharge with the alongshore baroclinic flow for this period (Fig. 5). The alongshore transport (0/100 db) between station pairs 1 and 2 and 1 and 7 (Fig. 1) are used for the correlation. Alongshore is defined here as being orthogonal to the section line (See Fig. 1). Lags for 0 to 3 months for the southeast discharge relative to the southcoast discharge are also used. Based on 22 samples, the best correlation (.763) between baroclinic transport and fresh water discharge occurs where the southeast discharge is lagged by one month. The confidence interval for this correlation is greater than 99.9%. The reduction in the correlation depending on lags is not sharp since the autocorrelation of discharge decreases slightly .847 at two months.

The above correlation between (0/100 db) transport and fresh water discharge contains a very large seasonal signal, so that the high correlation could be simply due to both responses having this annual signature. A better test of the relationship between fresh water discharge and baroclinic flow is done on the anomalies, that is, the time series remaining after the removal of each of their respective annual signals. The cross-correlation of the anomalies of (0/100 db) baroclinic transport for stations 1 - 7 and fresh water discharge with southeast lagged by one month is 0.603, which has a confidence interval of greater than 99.5%. This correlation is slightly higher than that determined previously for the simple runoff computations which was .580 (Royer, 1981). The more realistic methods used in this work probably better estimate the actual discharge.

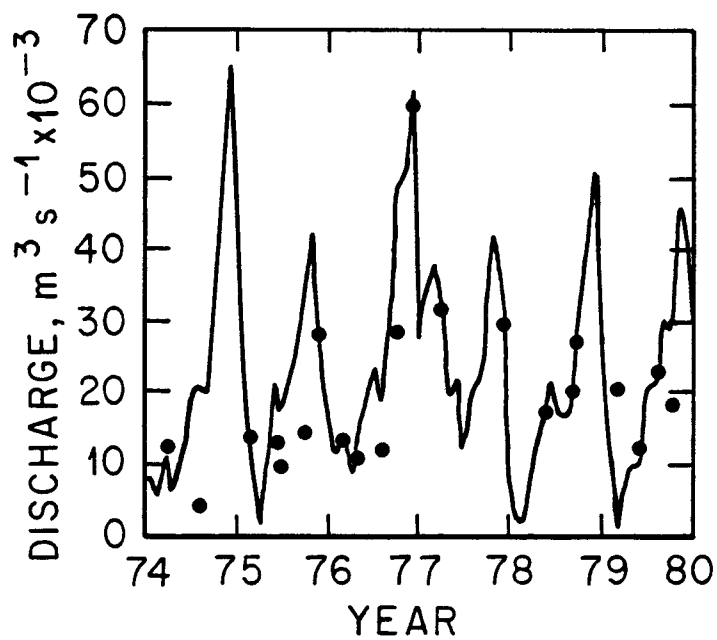


Figure 5. Monthly fresh water discharge (same as Figure 2) for 1974 to 1979 (line) with baroclinic transport (dots) for 1-7 $\sigma_{\theta}/100$ db superimposed. Range of the baroclinic transport is 0 to $1.5 \times 10^6 \text{ m}^3 \text{ s}^{-1}$.

The representation of the coastal circulation by the flow across the Seward line is questionable in light of some more recent temperature and salinity cross-sections taken upstream from this line. In November 1980, the coastal current can be seen as a lens of low salinity water ($< 31\text{‰}$) near the surface between stations 1 and 2 on the Seward line (Fig. 6). The width of this lens is approximately 25 km. Because the flow is adjacent to the coastline, its direction will be strongly influenced by it. Islands and peninsulas to the west divert the flow southward across the Seward line, making that transect oblique to the current. This is verified by a section at Cape Fairfield (Fig. 7) taken a few hours prior to the Seward transect. At Cape Fairfield, the 31‰ salinity band is only about 15 km wide. The difference could be a consequence of the cross-shelf spreading of the coastal current; however, for another section to the west of the Seward line, the coastal current is approximately 18 km wide. The conclusion is that the Seward line does not intersect the coastal current normal to the flow but rather obliquely. Thus, while the transports are valid, the width appears greater than it actually is, and the baroclinic current speeds are underestimated. These current widths are similar to the internal Rossby radius of deformation which ranges from 4 to 10 km for the Cape Fairfield line.

The dynamics of fresh water coastal currents has been investigated in the Norwegian Sea by Heaps (1980). He uses a two layer analytic model on a deep shelf similar to that of the Gulf of Alaska. The major difference between the two situations is that his fresh water discharge per unit length of coastline is about half of that for the Gulf of Alaska. As expected, his transports are about half of those for the Seward line. One feature that

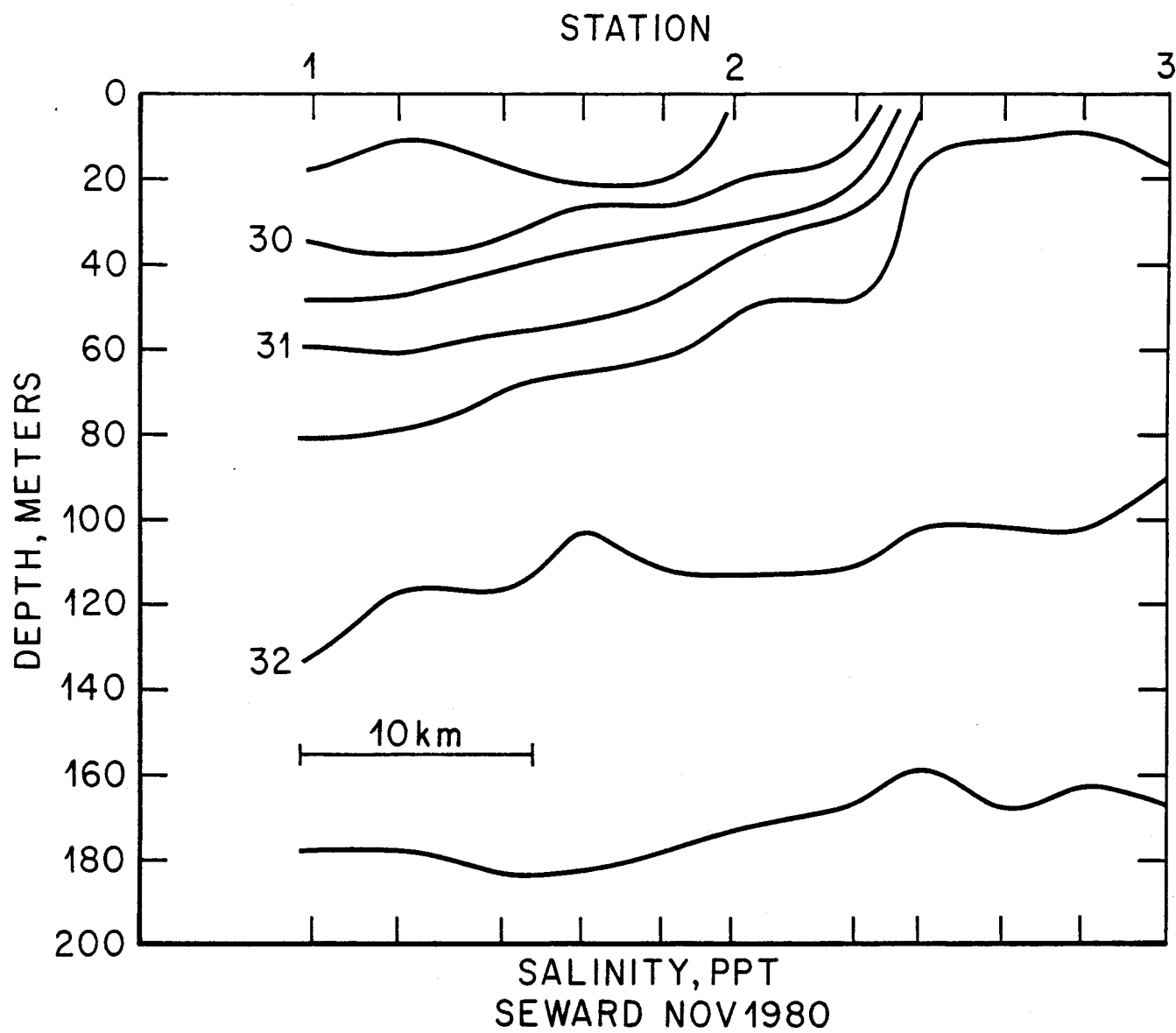


Figure 6. Salinity cross-section for Seward line looking eastward (see Figure 1), November 1980.

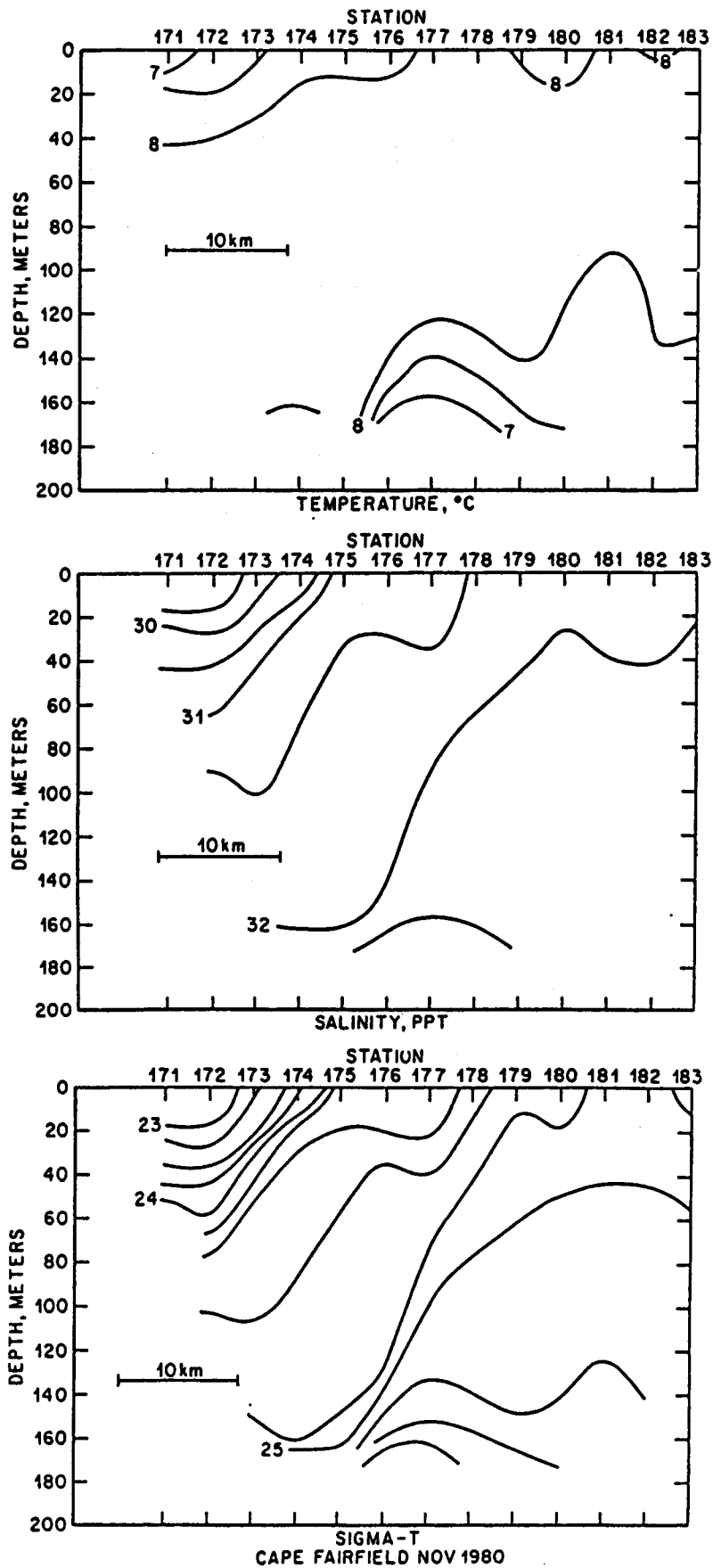


Figure 7. Cross-sections of temperature (top panel), salinity (middle panel), and density (lower panel) at Cape Fairfield, November 1980 (see Figure 1 for locations).

he predicts but is not observed in our situation is a fairly rapid cross-shelf dissipation of the coastal flow. He predicts a cross-shelf velocity at the surface that is approximately 20% of the alongshore component. Thus, the coastal current should spread to encompass the entire shelf after travelling several hundred kilometers downstream. As can be observed in Figure 6, this does not occur here. The narrow current could be a result of flow being constricted as it exits Prince William Sound. However, other observations in the northern Gulf of Alaska (Royer *et al.*, 1979; Schumacher and Reed, 1980) verify a narrow flow elsewhere.

A mechanism which could concentrate this flow at the coast is wind stress. The wind stress, here expressed as upwelling indices, changes by an order of magnitude from summer to winter in the northern Gulf of Alaska (Royer, 1975). Throughout the year easterly winds are common so that the northern Gulf of Alaska usually has downwelling conditions (Livingstone and Royer, 1980). During the November 1980 cruise the mean downwelling index was $69 \text{ m}^3 \text{ s}^{-1} (100 \text{ m of coastline})^{-1}$ (Bakun, personal communication), which is typical for that time of year (Royer, 1979). The offshore transport in the upper layers as predicted by the Heaps (1980) model can be compensated by the onshore Ekman transport. Each of these processes has a lower layer of comparable thickness that moves in the opposite direction of the upper layer. Downwelling is phased so that it lags the maximum fresh water discharge by approximately three months; however, the maximum baroclinic transport remains in phase with the fresh water discharge (Royer, 1979). The narrow, intense coastal current can be considered to be created by the fresh water discharge and then modified by the winds.

Eddies are predicted for salinity induced flows under similar conditions (Elliott and Reid, 1976), but in this case the available hydrographic data are inadequate to address this problem. Eddies will form if there is cross-isobathic flow. Their existence will be investigated in a future study.

5. Conclusions

Through the use of runoff computations, the coastal fresh water discharge for southeast and southcoast Alaska is estimated as about $2300 \text{ m}^3 \text{ s}^{-1}$. This computation does not include the Copper River or discharge from British Columbia, though the latter is probably significant. This water enters as a line source at the coast rather than as a point source as would be typical of large river input. This fresh water creates a cross-shelf horizontal density gradient driving an alongshore baroclinic flow which can exceed $1.3 \times 10^6 \text{ m}^3 \text{ s}^{-1}$. The winds, which are typically easterlies, converge this upper Ekman layer water at the coast and maintain the flow as an intense narrow current, generally less than 20 km wide.

The coastal mountain ranges bordering the Gulf of Alaska act as a barrier to the storms which move easterly across the North Pacific. Adiabatic elevation of these moist air masses cause very high rates of precipitation ($> 8 \text{ m yr}^{-1}$) in the form of rain and snow. The precipitation can be retained for months or even years in the glacial fields which occupy approximately 20% of the region. Better estimates of the growth or ablation of these ice sheets would improve this method of determination of fresh water discharge. For example, what effect would be observed in the coastal current under glacial advance or retreat? With any increase in the fresh water discharge, the

baroclinic transport would probably increase, what would be the current response? Will it become wider, deeper or simply faster? These types of questions should be answered through the application of the two layer baroclinic model.

Though it was stated that the volume of fresh water discharge was comparable to the flow of the Mississippi River, it is equally important to stress the significance of this source of fresh water to the Northeast Pacific circulation. The area of the Northeast Pacific from 60°N to 50°N, 150° to 140°W at 60°N and 150° to 130°W at 50°N is $1.11 \times 10^6 \text{ km}^2$ and the annual precipitation rate is between 0.9 m yr^{-1} (Reed and Elliott, 1979) and 1.1 m yr^{-1} (Dorman and Bourke, 1979). Thus, the coastal fresh water discharge in the Northeast Pacific contributes between 38 and 43% of the total amount of fresh water that enters from the atmosphere. More importantly, this large coastal discharge can affect the dynamics since it creates a sharp horizontal density gradient which might drive alongshore flows at distances offshore.

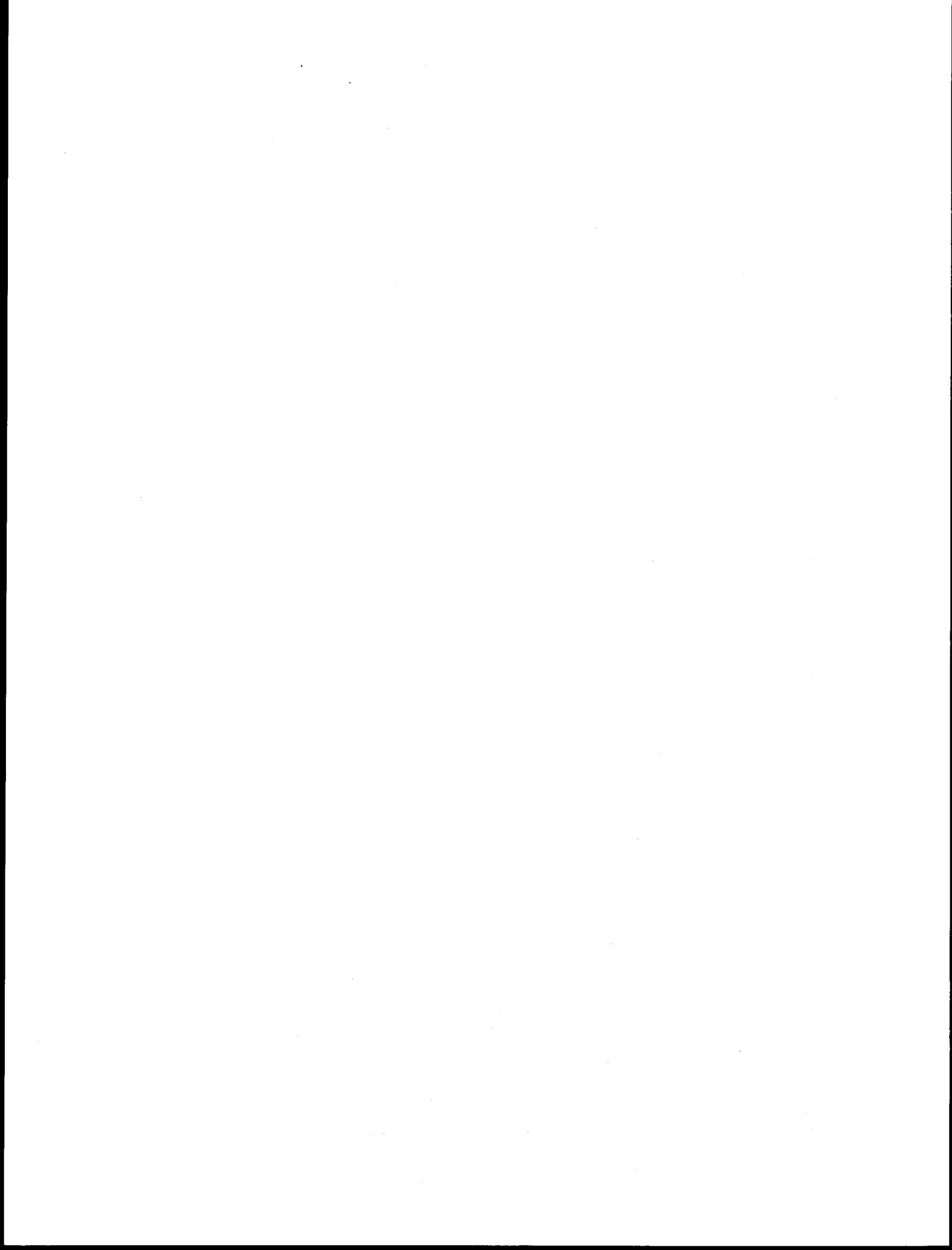
Acknowledgements

The hydrology model was developed under sponsorship of the BLM/NOAA Outer Continental Shelf Environmental Assessment Program. The hydrographic data for November 1980 were obtained aboard *Alpha Helix* on the NSF/IDOE Seagrass Ecosystem Study (SES). Appreciation is extended to C. P. McRoy for making that sampling possible.

Valuable discussions with Professor Reid on this fresh water problem helped produce earlier papers, which form the base for this work.

References

- Bergeron, T. 1949. The problem of artificial control of rainfall on the globe. II. The coastal orographic maxima of precipitation in autumn and winter. *Tellus*, 3, 1832.
- Dorman, C. E. and R. H. Bourke. 1979. Precipitation over the Pacific Ocean, 30°S to 60°N. *Monthly Weather Review*, 107, 896-910.
- Elliott, B. A. and Robert O. Reid. 1976. Salinity induced horizontal estuarine circulation, *Jour. of the Waterways, Harbors and Coastal Engineering Division, ASCE*, 102, WW4, 425-442.
- Heaps, N. S. 1980. Density currents in a two-layered coastal system, with application to the Norwegian Coastal Current. *Geophys. J. R. Astr. Soc.*, 63, 289-310.
- Kendrew, W. G. and D. Kerr. 1955. The climate of British Columbia and the Yukon Territory. Edmond Cloutier, Ottawa, 222 pp.
- Livingstone, D. And T. C. Royer. 1980. Observed surface winds at Middleton Island, Gulf of Alaska and their influence on ocean circulation. *J. Phys. Oceanogr.*, 10, 753-764.
- Reed, R. K. and W. P. Elliott. 1979. New precipitation maps for the North Atlantic and North Pacific Oceans. *Jour. Geophys. Res.*, 84, 7839-7846.
- Roden, G. I. 1967. On river discharge into the Northeastern Pacific Ocean and the Bering Sea. *Jour. Geophys. Res.*, 72, 5613-5629.
- Royer, T. C. 1975. Seasonal variations of waters in the northern Gulf of Alaska. *Deep Sea Res.*, 22, 403-16.
- Royer T. C. 1979. On the effect of precipitation and runoff on coastal circulation in the Gulf of Alaska. *J. Phys. Oceanogr.*, 9, 555-63.
- Royer, T. C. 1981. Baroclinic transport in the Gulf of Alaska. Part II. Fresh water driven coastal current. *J. Mar. Res.*, 39, (In Press).
- Royer, T. C., D. V. Hansen and D. J. Pashinski. 1979. Coastal flow in the northern Gulf of Alaska as observed by dynamic topography and satellite-tracked drogued drift buoys. *J. Phys. Oceanogr.*, 9, 785-801.
- Selkregg, L. L. 1979. Alaska regional profiles - Southeast region, Arctic Environmental Information and Data Center, Univ. of Alaska, 233 pp.
- Schumacher, J. D. and R. K. Reed. 1980. Coastal flow in the Northwest Gulf of Alaska: The Kenai Current. *J. Geophys. Res.*, 85, 6680-6688.
- Tully, J. P. and F. G. Barber. 1960. An estuarine analogy in the sub-arctic Pacific Ocean. *J. Fish. Res. Bd. Can.*, 17, 91-112.



SURFACE TEMPERATURE ENHANCED NOAA-SATELLITE INFRARED IMAGERY FOR THE
BERING, CHUKCHI, AND BEAUFORT SEAS AND THE GULF OF ALASKA

May 1974 - September 1980

by

Kristina Ahlnäs

Institute of Marine Sciences
University of Alaska

March 1981

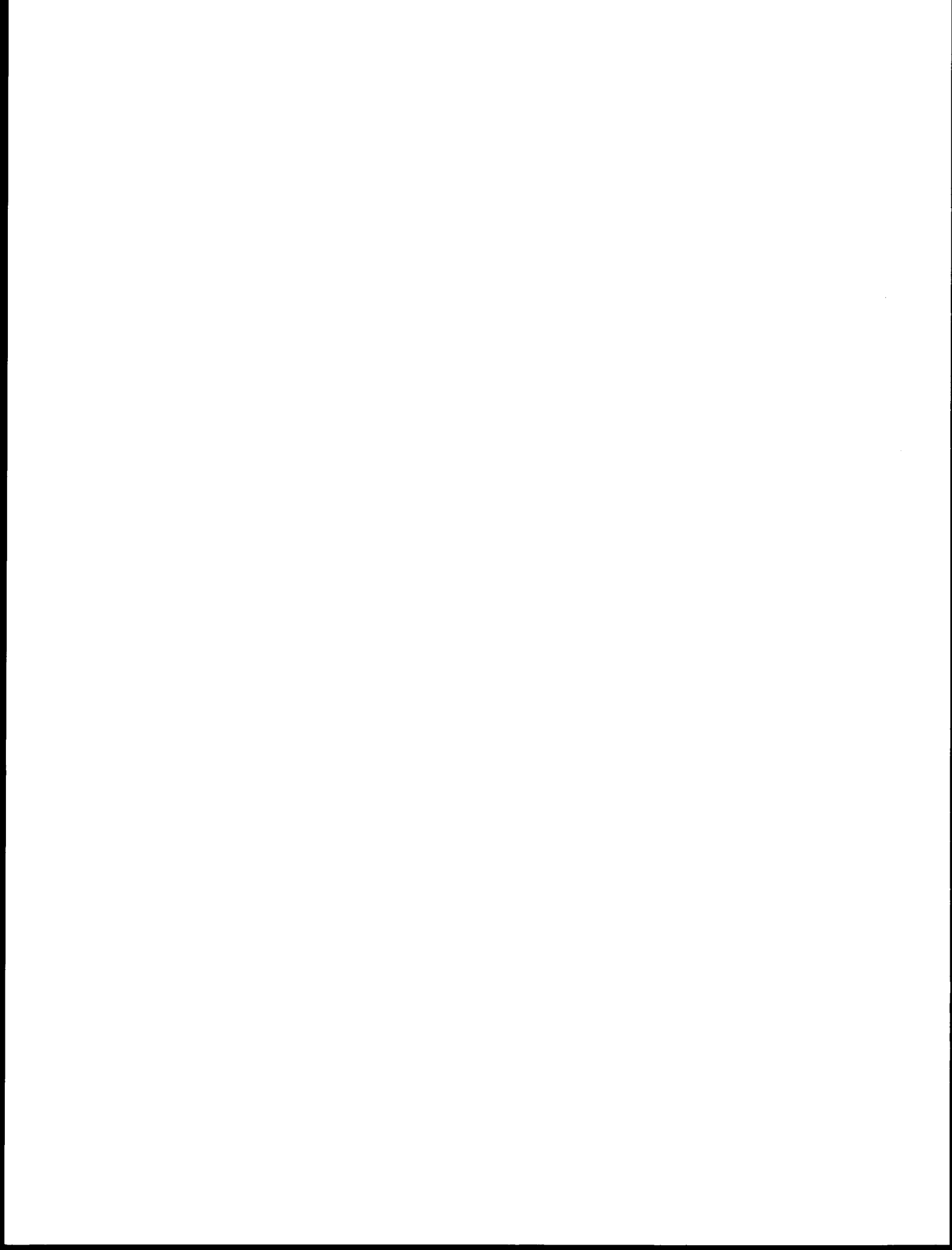
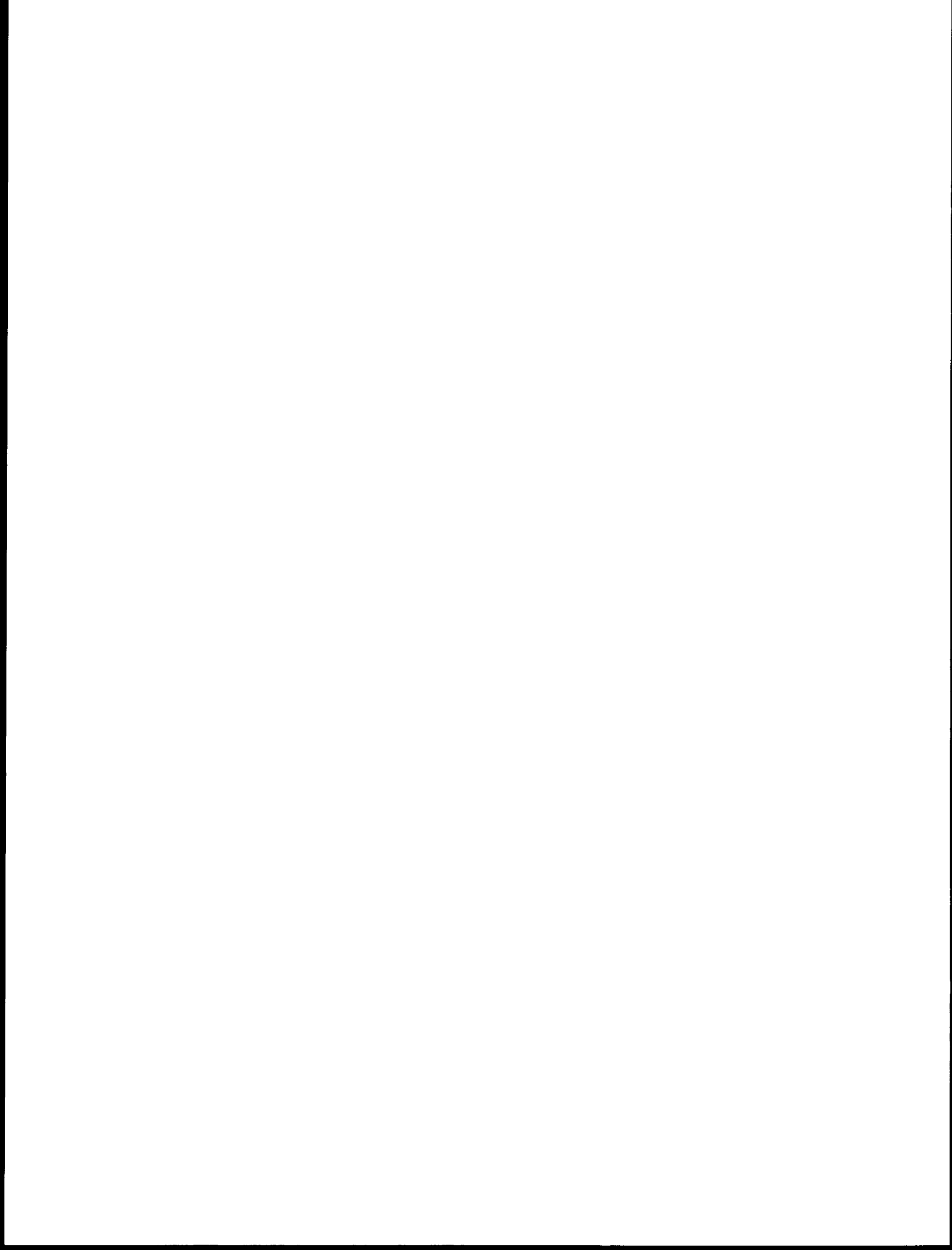


TABLE OF CONTENTS

List of Figures	589
Abstract	591
SATELLITE BACKGROUND	592
THE ALASKA PILOT PROJECT	597
Forest Fire Control	600
The Auroral Zone	601
IR ENHANCEMENTS	601
Birds as Temperature Detectors	608
IR Enhancements with Special Identity	613
Sea-Ice Intrusions	615
Kamchatka Eddies	615
SEA-ICE STUDIES	617
CORRECTIONS FOR GEOGRAPHIC DISTORTION	625
SATELLITE DATA ARCHIVES	628
ACKNOWLEDGEMENTS	630
REFERENCES	631
APPENDIX I: IR ENHANCEMENTS FOR SURFACE TEMPERATURE	633
APPENDIX II: NOAA-VHRR DIGITIZED TAPES SAVED	673



LIST OF FIGURES

- Figure 1. Areal coverage of the NOAA-VHRR and AVHRR satellites with orbits through Gilmore Tracking Station.
- Figure 2. Mosaic of NOAA-VHRR daytime descending orbits on 7 January 1975.
- Figure 3. Mosaic of NOAA-VHRR nighttime ascending orbits on 8 January 1975.
- Figure 4. Standard-size image of Alaska, 12 March 1974.
- Figure 5. Harding Lake (H) and Birch Lake (B) along the Tanana River. NOAA-VHRR IR. Super enlargement, scale 1:235,000.
- Figure 6. Prospective build-up of thunderstorms over Interior Alaska, 29 May 1974, N3-2530 VIS + IR composite.
- Figure 7. Area of enhanced radiation north of Siberia, 30 March 1975.
- Figure 8a. Temperature-enhanced meanders in the Alaska current, 22 May 1974, N3-2443; enhanced IR -3 to 6°C.
- Figure 8b. Visible image of a cloud-free Gulf of Alaska, 22 May 1974, N3-2443.
- Figure 8c. Standard IR image showing thin coastal clouds, 22 May 1974, N3-2443.
- Figure 9. Surface temperatures structure in the Gulf of Alaska, 1 March 1978.
- Figure 10. Northward flow of warm water through Bering Strait, 22 October 1974.
- Figure 11. Band of warm water along the Beaufort Sea coast, 14 August 1977.
- Figure 12. Beaufort Sea leads, 17 March 1975.
- Figure 13. Flow of cold Chukchi Sea ice into the Bering Sea, 20 March 1978.
- Figure 14. Oceanic eddies with cold cores east of Kamchatka, 26 September 1977.
- Figure 15. Ice edge between the Pribilof Islands of St. Paul and St. George, 29 March 1977.

- Figure 16. IR enhancement curve used in Figure 15 from "Polar spacecraft AVHRR sensor enhancement curves" NESS-CDA station (1980).
- Figure 17. IR enhancement curve, "ice table," 64P/N4P used in Figure 18.
- Figure 18. Ice edge structure in Bristol Bay and the warm Alaska current SW of Kodiak, 29 January 1980.
- Figure 19. Bering Sea ice edge with surface temperature structure in waters over the continental shelf, 14 December 1979.
- Figure 20. Image from Figure 19 with temperature table offset -4°C and stretched to rectify geographic distortion in Bristol Bay.

ABSTRACT

A brief history is given of the NOAA-VHRR satellite project in Alaska, starting with the experimental NOAA-NESS supported Pilot Project in 1974. From 1975 to 1980 the project, under the sponsorship of OCS, has also addressed the needs of other scientists, particularly those supported by OCS grants.

During the progress of six years of satellite surveillance of Alaska and the surrounding oceans, numerous gray scale enhancements for surface temperature analysis have been performed. An introductory explanation of the theory behind the enhancements is given. All archived enhanced negatives are listed by date, temperature range and geographical location. Some digitized tapes that were saved because of special features are listed in the same manner. Some enhancements were performed for specific research interests. They are used as illustrations to show the applicability of enhanced infrared imagery.

The NOAA-NESS CDA Station at Gilmore generated all satellite products used by the satellite project. The final archiving, however, is spread out among different facilities in Alaska and Washington D.C. The specific locations for each product is given.

The purpose of this report is to bring the vast quantity of partly unused satellite data to the attention of the inquiring scientist.

SATELLITE BACKGROUND

Since 1960, American weather satellites have orbited the earth. In October 1972 a second generation of environmental satellites of the Improved TIROS Operational Satellites (ITOS) series, the NOAA-2, was launched. These satellites were in near-polar, sun-synchronous circular orbits at an altitude around 1500 km. On the NOAA-2 a new sensor was added, the dual-channel Very High Resolution Radiometer (VHRR). It scanned simultaneously in the visible (VIS), 0.6-0.7 μm , and the infrared (IR) 10.5-12.5 μm , bands. With the advent in October 1978 of the latest, third generation of polar orbiting environmental satellites, the TIROS-N, new sensors were again added to the spacecraft. The 2-channel VHRR of the previous satellites was replaced by the 4-channel AVHRR (Advanced Very High Resolution Radiometer). The scanning radiometers are sensitive to visible/near IR and IR radiation. Following is a table of the AVHRR channel characteristics from Hussey (1979).

Channel	Resolution at subpoint	Wavelength (μm)	Primary use
1	1 km	0.58 - 0.68*	Daytime cloud and surface mapping
2	1 km	0.725- 1.10	Surface water delineation
3	1 km	3.55 - 3.93	SST, Nighttime cloud mapping
4	1 km	10.5 -11.5	SST, Day/night cloud mapping
5	1 km	11.5 -12.5	SST

(Channel 5 to be added later to the AVHRR/2 instrument)

*0.55-0.90 μm on the TIROS-N

Channel 1 is almost identical to the VHRR VIS of 0.6-0.7 μm while the VHRR IR of 10.5-12.5 μm channel will be divided into two. The higher portion

of the IR spectrum will make it possible to remove radiant contributions from atmospheric water vapor when determining surface temperatures. The lowest IR band, channel 3, used together with channel 4 will remove the ambiguity introduced by clouds in a portion of the image. The imagery produced by channels 1 and 2 look similar, but when compared, they provide an indication of ice/snow melt inception. Individually they are used to discern clouds, land-water boundaries and snow and ice extent. The spatial resolution for both systems is 1 km at nadir.

At NOAA's satellite Command and Data Acquisition (CDA) station at Gilmore Creek near Fairbanks, the area of coverage for the VHRR reached from NW Greenland to Seattle or south of the Aleutians. Another orbit covers the region from Hudson Bay to the East Siberian Sea. Thus, one satellite pass covered an area of about 2200 to 6600 km (Fig. 1). The satellites equipped with AVHRR fly at a lower altitude, around 850 km. Thus they cover a smaller area per orbit, but show it in a larger scale. The scale of the old NOAA imagery is about 1:9 million and the new AVHRR about 1:7.5 million. Figure 2 shows a typical mosaic of all descending NOAA-VHRR passes on 7 January 1975. The first pass comes across Baffin Bay, the NW Territories and British Columbia at 8:00 am AST. The second pass covers the Gulf and SE Alaska about 2 hours later. Around noon the third pass crosses over the Beaufort and Bering Seas and around 2:00 pm the last descending pass goes from Baffin Island to the Kamchatka Peninsula. The five ascending nighttime passes on 8 January 1975, cover the same area but from the opposite direction (Fig. 3). Due to the wintertime season both of the above mosaics are covered by infrared imagery only.

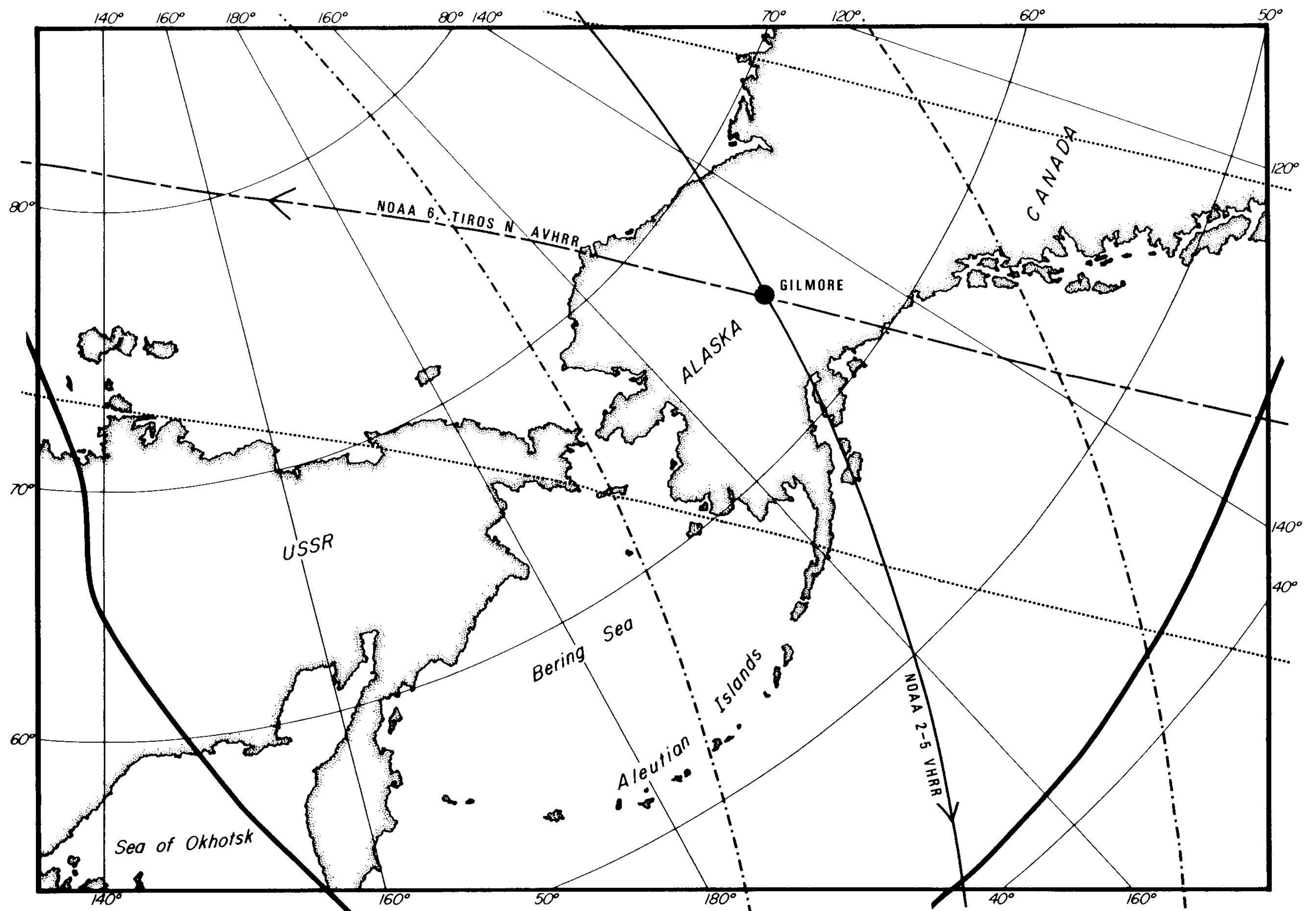


Figure 1. Areal coverage of the NOAA-VHRR and AVHRR satellites with sample orbits over the Gilmore Tracking Station.

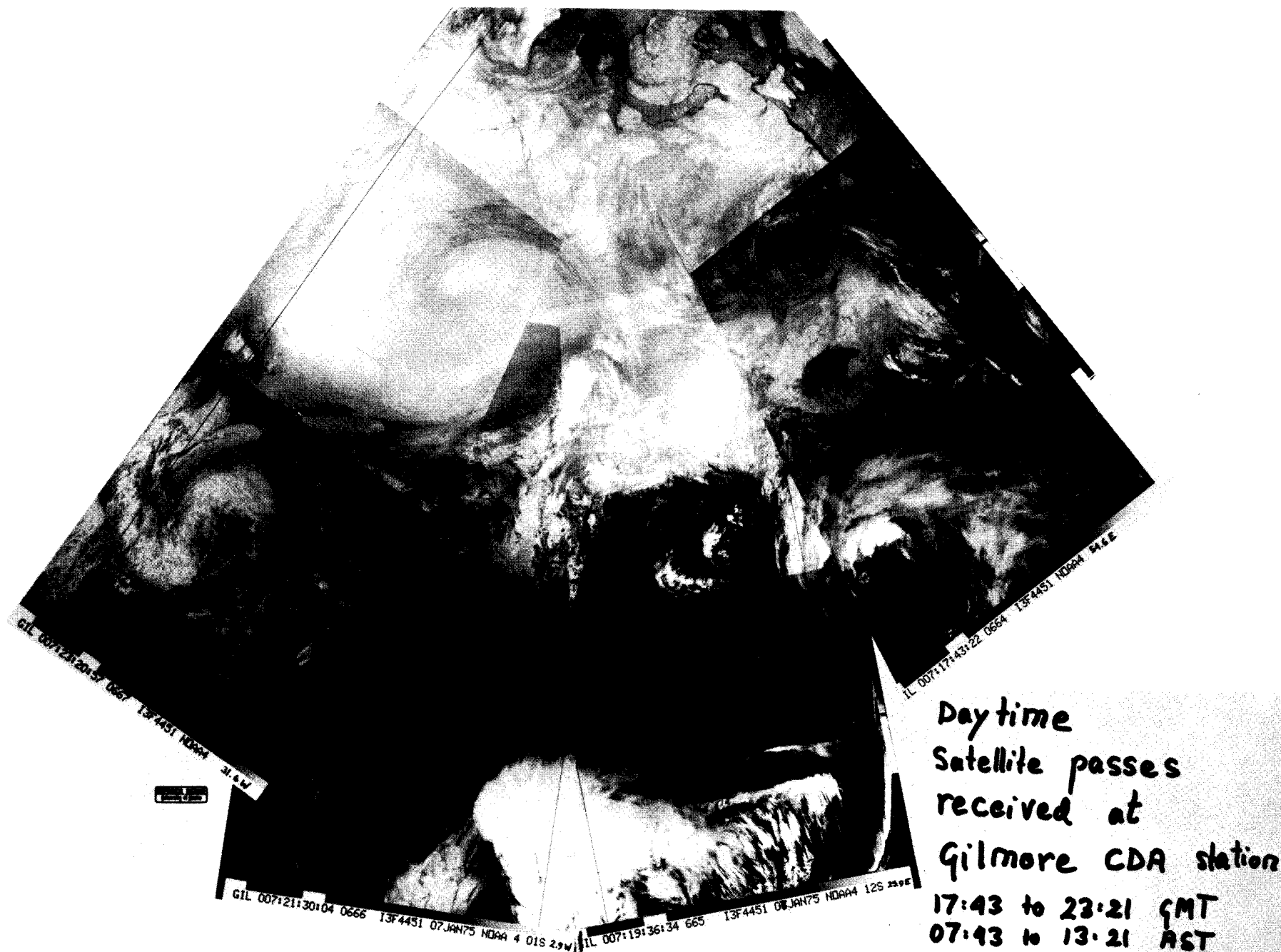


Figure 2. Mosaic of NOAA-VHRR daytime descending orbits on 7 January 1975.

For special features, enlargements in about 1:3 million have been made. Figure 4 shows a standard NOAA-2 VIS image of Alaska on 12 March 1974 in 1:9 million. The small white dot at the arrow is Harding Lake north of the Tanana River. Figure 5 is an extreme enlargement in 1:235,000 of a NOAA-VHRR IR imagery centered around Harding Lake. In this image the scan lines of the satellite radiometer are obvious as the distance between them is 1 km caused by the resolution.

In Alaska and the Arctic, the VIS band is only operational during part of the year, when the polar regions have daylight. The thermal IR band operates continuously, being independent of sunlight but sensitive to emitted terrestrial radiation. The purpose of this paper is to show some applications of the IR imagery and to list the NOAA-VHRR and AVHRR IR imagery that has been specially enhanced for surface temperature distribution.

THE ALASKA PILOT PROJECT

The NOAA satellite, equipped with the VHRR sensors, became operational with direct read-out at the Gilmore Creek station in March 1974. To investigate the usefulness and applicability of the satellite imagery to environmental needs in Alaska, a multi-disciplinary team from the University of Alaska was contracted by NOAA-NESS to carry out the pilot project (McClain 1975). This project operated for two years. In that time we demonstrated the usefulness of the satellite imagery to the Weather Service in Alaska, the Bureau of Land Management (BLM) for forest fire control and to the Arctic Sea Lift to Prudhoe Bay. In part as a result of our work, a satellite field service station was established in Anchorage. That station now distributes



Figure 4. Standard size image of Alaska. Note Harding Lake at arrow by H. 12 March 1974, N2-6425 VIS. Scale 1:8.7x10

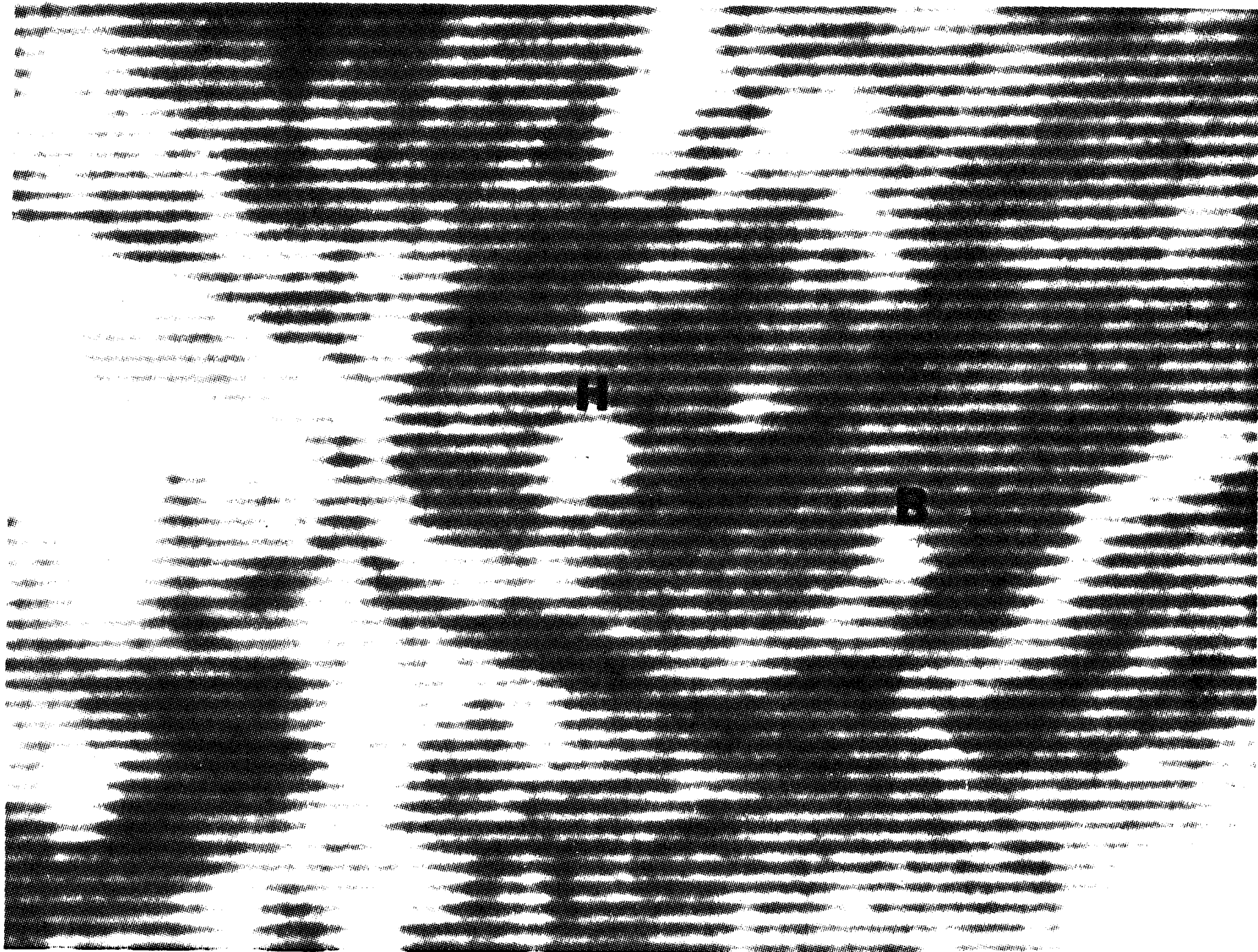


Figure 5. Harding Lake (H) and Birch Lake (B) along the Tanana River. NOAA-VHRR IR. Super enlargement, scale 1:235,000.

sea surface thermal and ice analysis charts for Bristol Bay and the Gulf of Alaska. After the pilot project ended, the Outer Continental Shelf Environmental Assessment Program (OCSEAP) took over sponsorship of the continued surveillance of satellite imagery for Alaska with surrounding ocean areas. As part of the program, gray scale enhancements were performed for surface temperature distribution of cloudfree ocean areas. A list of these enhancements is provided in this publication.

In most studies, the VIS and IR imagery were used to complement each other. The visible band shows the cloud cover and indicates which areas are cloudfree and hence applicable to surface temperature studies by the infrared band. Occasionally in the Arctic, thin, high clouds are transparent enough to let the surface features show through in the visible range. In the IR band, these same clouds are opaque and prevent the underlying higher surface temperature from being registered. Instead, the low temperature of the cloud tops is seen.

Forest Fire Control

About 90% of the acreage annually lost to forest fires in Alaska is caused by lightning fires. To survey the build-up of thunderstorms, aircraft were previously used extensively. During the pilot project, our research team found that thunderstorms could also be identified on the NOAA/VHRR imagery (Jayaweera and Ahlnäs, 1974). Thunderstorms are built up of towering cumulus clouds which are very compact and easy to detect by their form and high reflectance in the VIS band. Since the clouds reach high altitudes, their tops are cold and consequently appear very bright also in the IR band. By convention, the gray tone in the NOAA-satellite

IR imagery is inversely proportional to the radiative temperature. By superimposing the simultaneous visible and IR imagery of the same orbit, the net imagery will show both the coldest clouds and the brightest areas (Fig. 6). Such bright areas can be attributed to large cumulus or possible thunderstorms.

The Auroral Zone

Enhancements of radiation have been observed by balloon measurements in the spectral interval 10-13 μm at auroral latitudes. This spectral window is slightly wider than the 10.5-12.5 μm IR band of the NOAA-VHRR. Thus, it appeared reasonable to assume that evidence of auroral activity would also be manifested in the NOAA imagery. Studying the standard IR imagery, areas of enhanced radiation were also found in the Arctic (Henriksen *et al.*, 1976; Fig. 7). However, no direct correlation was found to the auroral oval.

IR ENHANCEMENTS

The IR sensitivity of the NOAA satellites is 256 digital steps or 8 bits spread out over a temperature range from about -60 to 40°C . However, the capacity of the display device or satellite image is only 32 gray steps. When studying the surface temperature distribution, a narrow range is advantageous for gray scale contrast. Through a minicomputer that operates on the original digital tape of a specific satellite orbit, a chosen scene can be programmed to show any selected temperature range (Ahlnäs, 1979). On the 32-step gray scale the lowest temperature chosen will correspond to white and the highest to black with the temperature

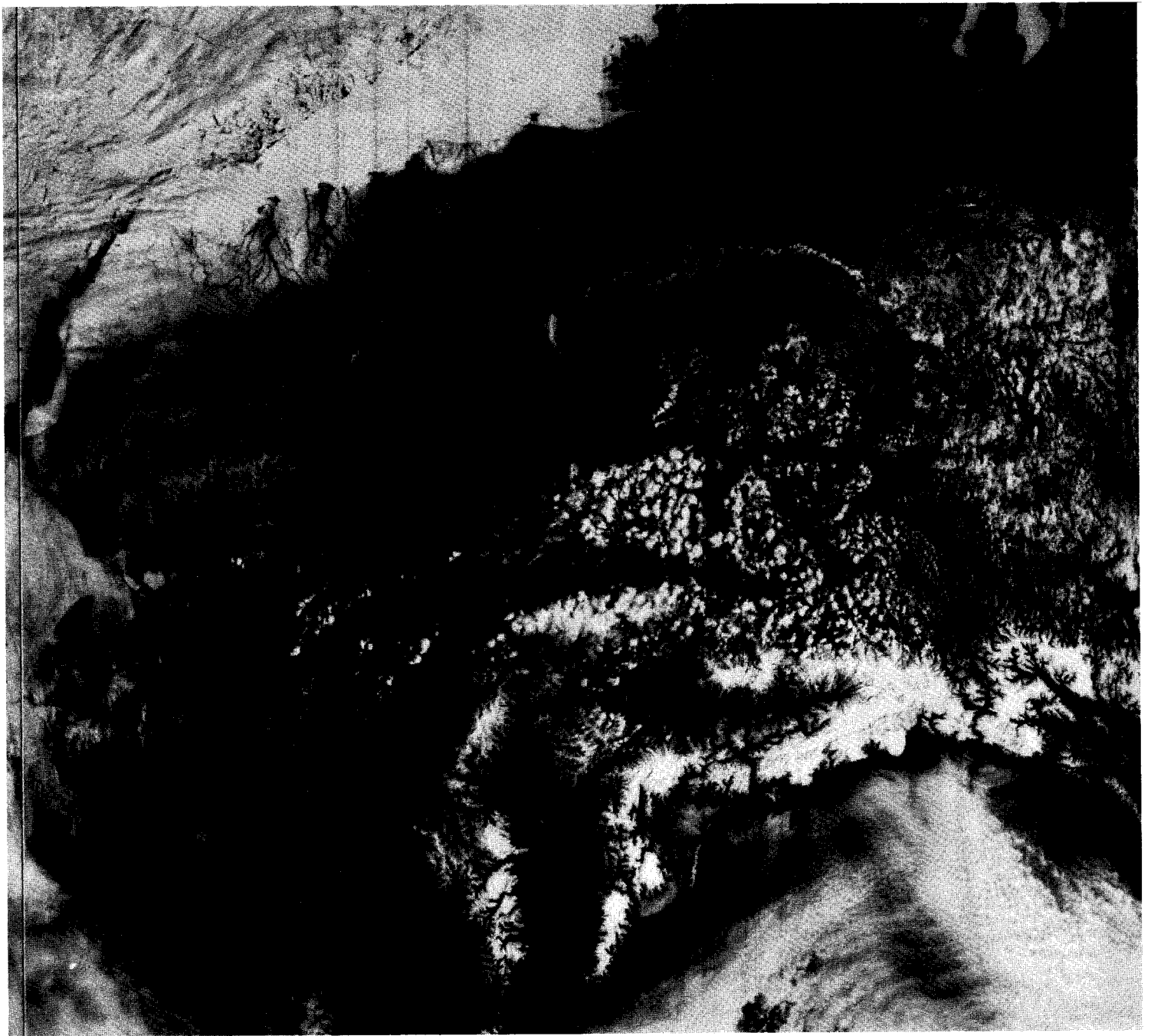


Figure 6. Prospective build-up of thunderstorms over Interior Alaska, 29 May 1974, N3-2530 VIS + IR composite.

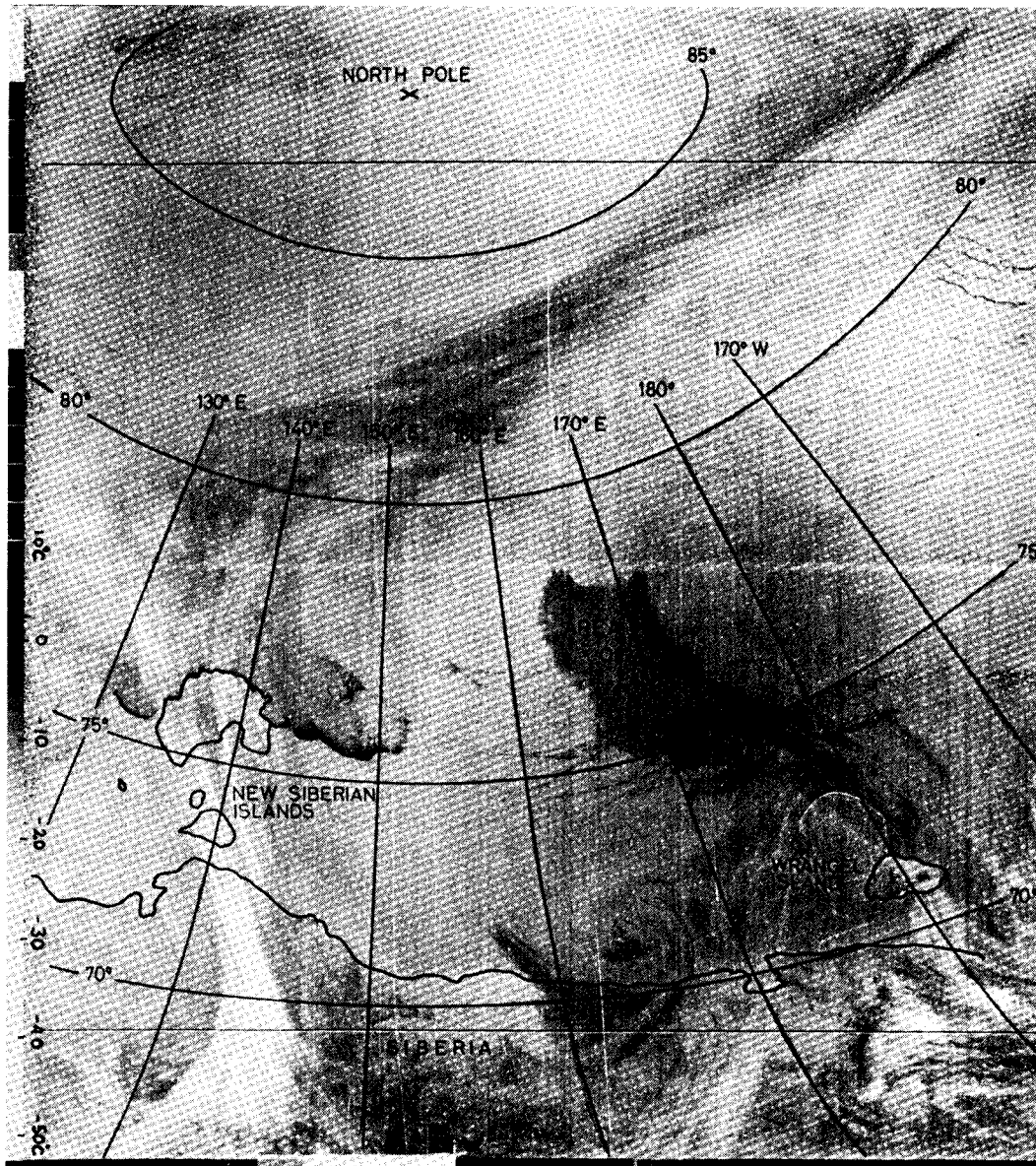


Figure 7. Area of enhanced radiation north of Siberia, 30 March 1975, N4-1684 IR.

range between white and black displayed by various shades of gray. The simplest enhancement uses a single scale with temperatures beyond the scale shown as black or white. This enhancement works well for sea-surface temperatures in summer when the surrounding land is very much warmer and any clouds present are colder. The resulting enhancement thus emphasizes the water areas, while the land shows in contrasting black for geographical orientation and the clouds are white. Figure 8a is a single scale enhancement from -3 to 6°C for the Gulf of Alaska on 22 May 1974. Part of the relatively warm Alaska Current with some meanders shows up very distinctly around 6°C . For comparison, the simultaneous visible image (Fig. 8b) shows that the offshore Gulf of Alaska is cloud free. However, the standard IR (Fig. 8c) shows some low cloud bands extending from the coast over the nearshore area. These cloud bands obstruct the temperature structure close to the coast. The black areas showing between the cloud bands indicate that the temperature is around or above 6°C . Royer and Muench (1977) used this same image among many others to study the ocean temperature distribution in the Gulf of Alaska.

In the wintertime, when both the land areas and the clouds are cold, coast definition can not be achieved from a single scale enhancement. In this case a double scale enhancement gives a more pleasing result. For this enhancement, the entire 32-step gray scale is used independently for two adjoining temperature ranges. The ocean area will still appear the same as it would on a single scale enhancement, but in addition details in another temperature range, such as land areas or sea ice, can be emphasized. The scale break, or temperature where the scales join, is chosen to coincide with the largest temperature gradient, such as the edge of open water at a

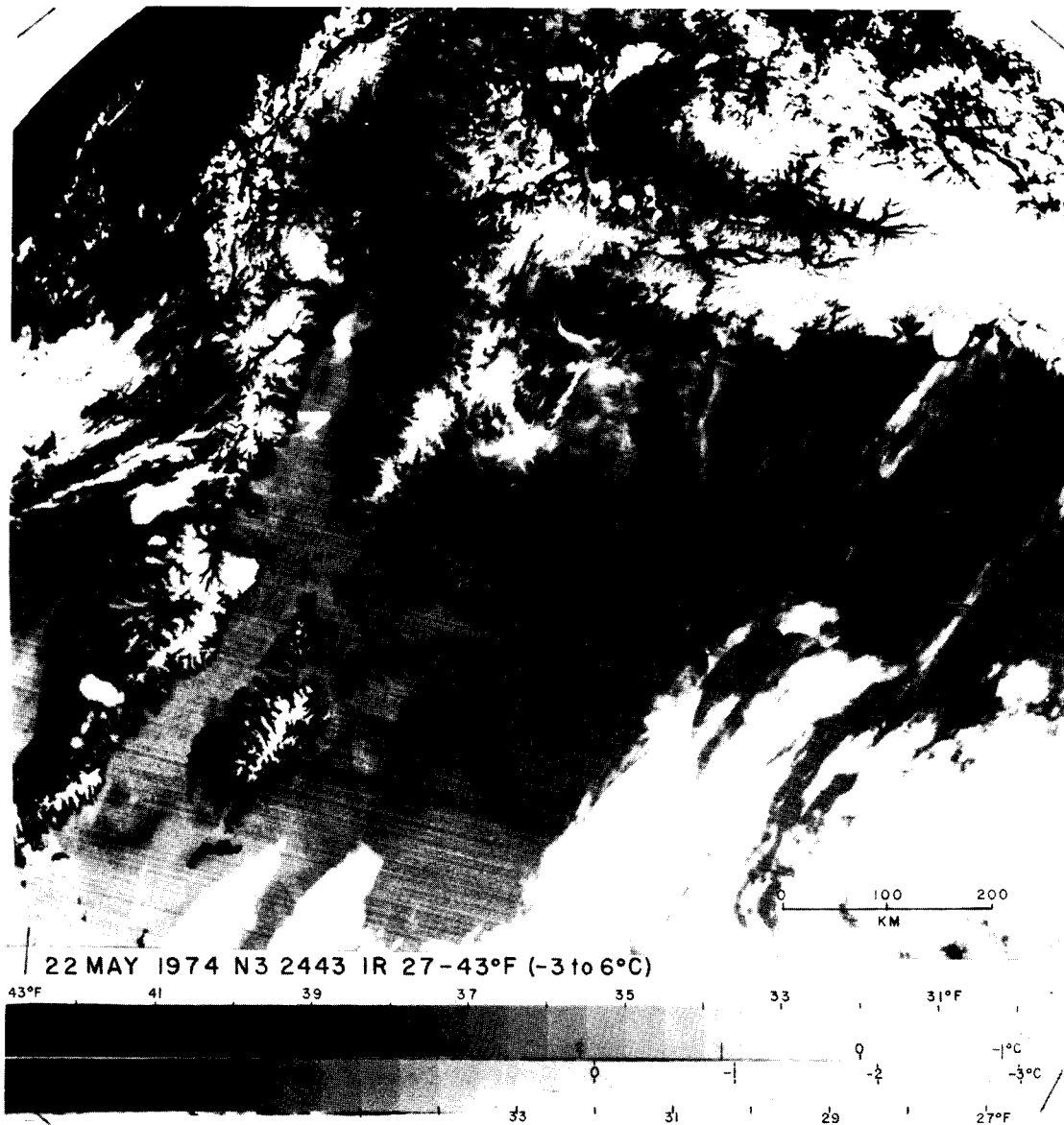


Figure 8a. Temperature-enhanced meanders in the Alaska current, 22 May 1974, N3-2443, enhanced IR -3 to 6°C.

22 MAY 1974 N3 2443 VIS

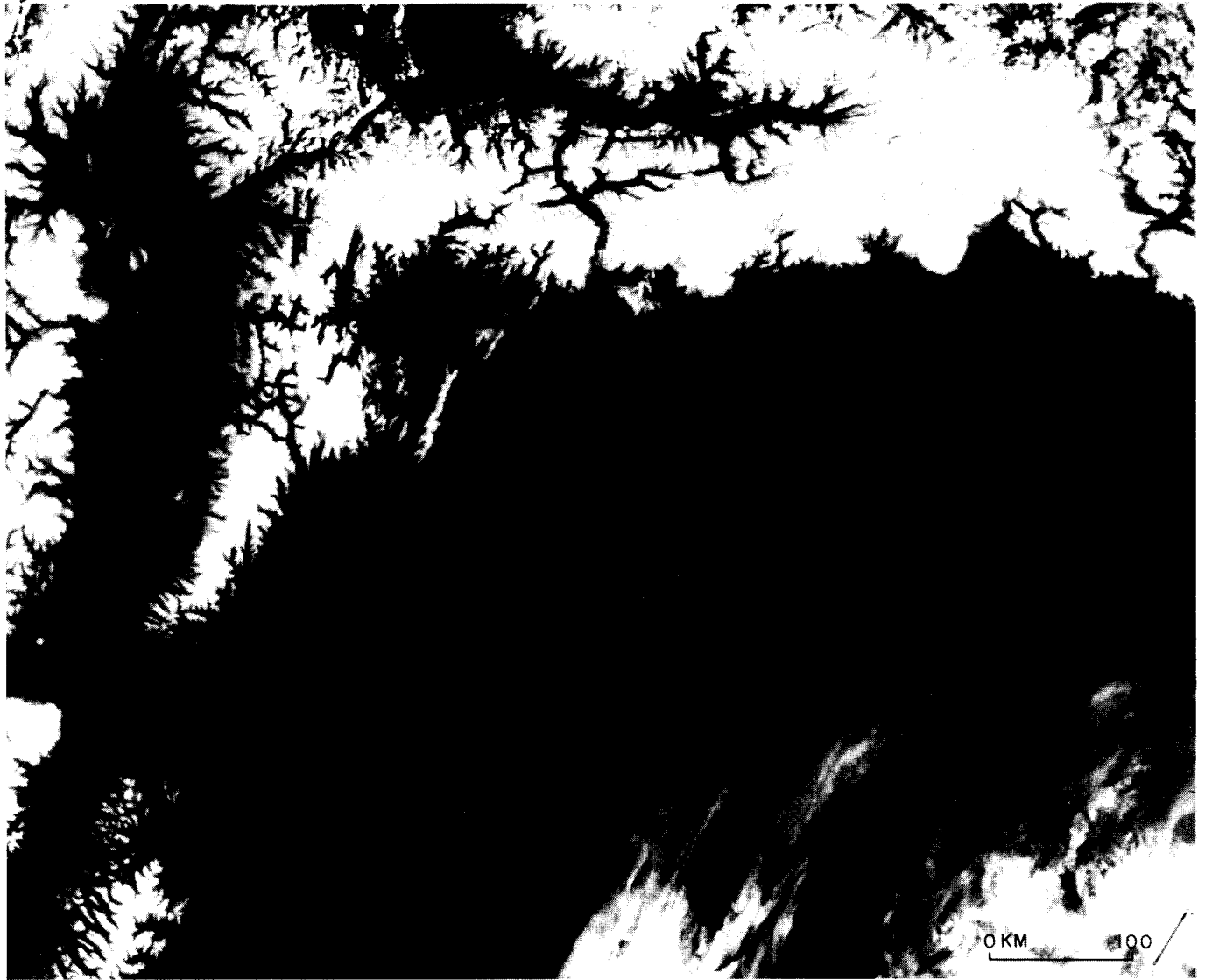


Figure 8b. Visible image of a cloud-free Gulf of Alaska, 22 May 1974, N3-2443.

22 MAY 1974 N3 2443 IR

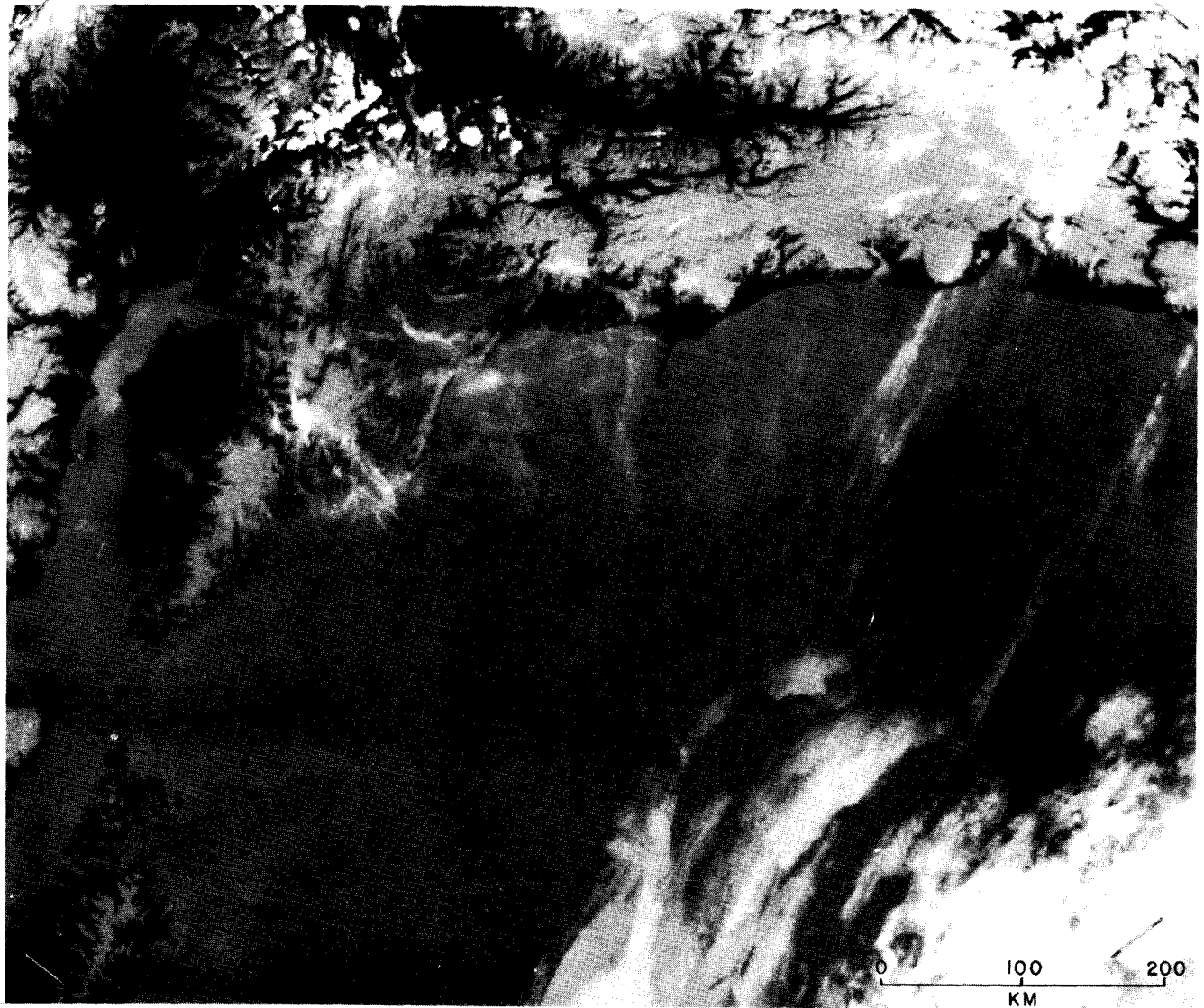


Figure 8c. Standard IR image showing thin coastal clouds, 22 May 1974, N3-2443.

coastline or ice edge. Figure 9 shows such an enhancement for the Gulf of Alaska on 1 March 1978. The scale break is chosen at the freezing point of sea water at -2°C . In the lower (-29 to -2°C) scale, -2° is black and in the higher (-2 to 5°C) scale, -2° is white. The abrupt black/white change coincides with the coastline, except in the ice covered Cook Inlet where it indicates the ice/water interface. The surface water circulation with the warm Alaska Current slightly offshore and the cold coastal jet hugging the northern coast is shown in detail in the higher -2 to 5°C scale. A similar double scale enhancement for 7 February 1975 was used by Royer (1977) to show ocean currents in the Gulf of Alaska.

When Coachman, Aagaard and Tripp (1975) wrote their book about the Bering Strait, the Alaska pilot project group was contacted to provide some satellite imagery for illustrations. A single enhancement from -8 to 6°C for 22 October 1974 showing a northward flowing warm current through the eastern part of the Bering Strait was chosen for the book. Figure 10 shows a double enhancement from (-8 to -2) and (-1 to 4) $^{\circ}\text{C}$ for the same satellite orbit. The scale break at the freezing point literally brings out the coastline around the Seward Peninsula and north of Kotzebue Sound. The northward flowing warm current through Bering Strait is frequently seen in satellite imagery. Its northeastward extension has been observed to extend beyond Barrow, Alaska. A paper investigating the warm water intruding into the Chukchi Sea is presently being prepared together with Solomon and Garrison.

Birds as Temperature Detectors

The warm water entering the Chukchi Sea is also rich in biomass and has been observed to attract feeding birds. Cloudfree temperature enhanced

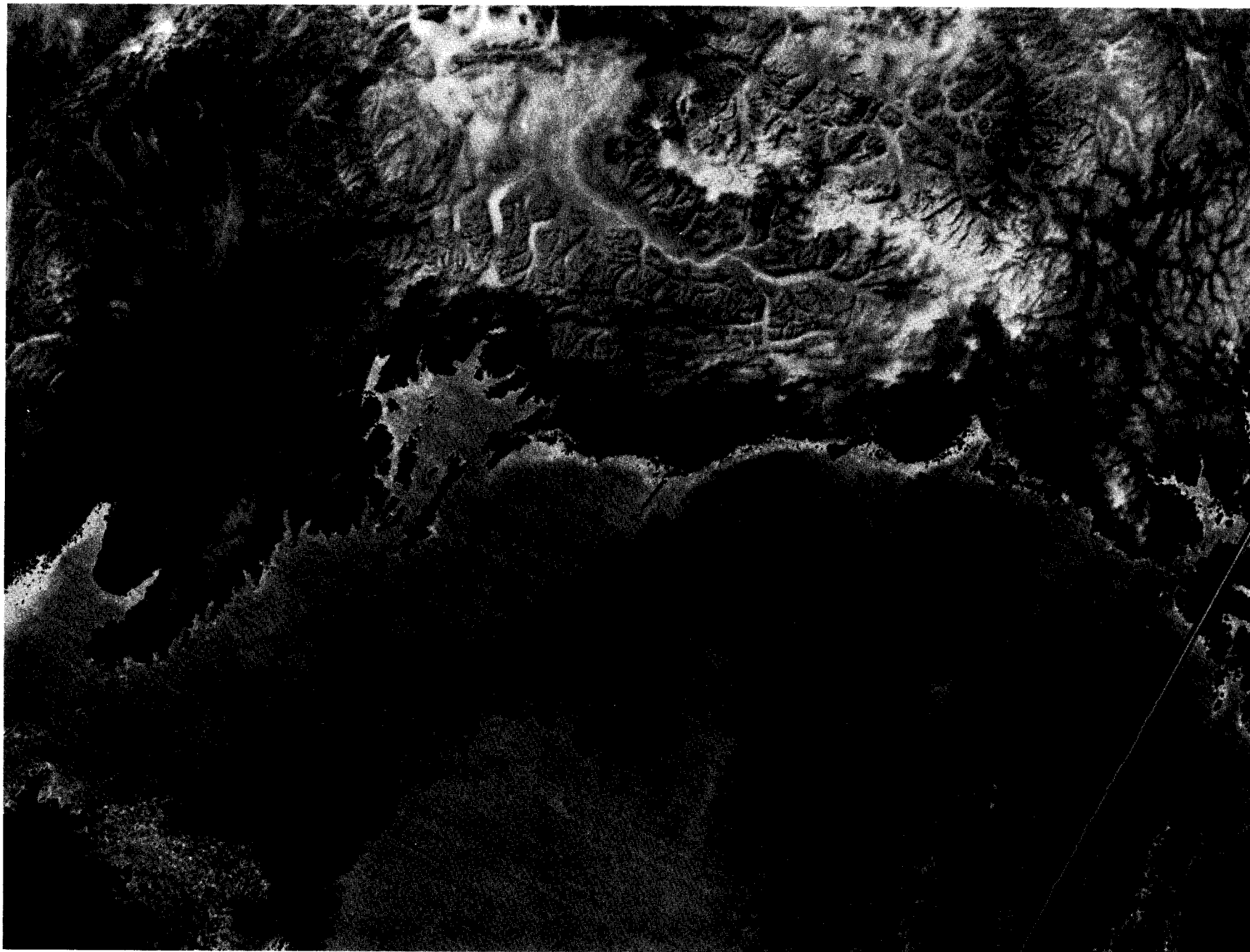


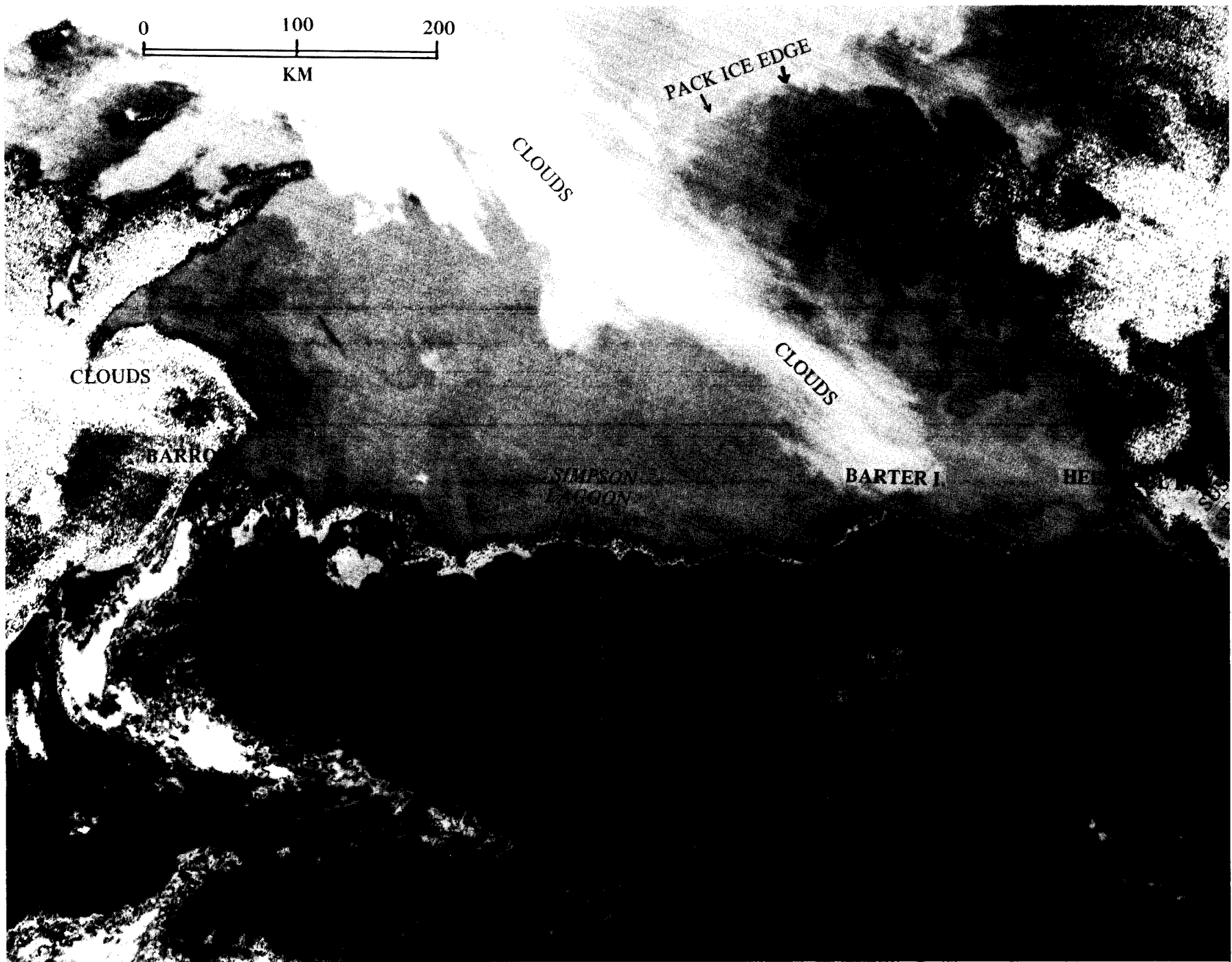
Figure 9. Surface temperatures structure in the Gulf of Alaska, 1 March 1978, N5-7181 IR; $(-29 \text{ to } -2) + (-2 \text{ to } 5)^\circ\text{C}$.



Figure 10. Northward flow of warm water through Bering Strait, 22 October 1974, N3-4340 IR; (-8 to -2)+(-1 to 4)°C.

IR satellite imagery for the first half of July is available from 1974 to 1979 for Ledyard Bay north of Cape Lisburne where Alan Springer has conducted bird observations. The satellite imagery shows a decline in surface temperature from 1974 to 1976 and an increase from 1976 to 1979. Springer (personal communication) has observed major changes in the productivity of the kittiwakes and food habits of birds in general during these years with a direct linear relation between the surface water temperature and the productivity. The surface temperature was also directly related to the extent of the sea-ice cover and the retreat of the ice edge. 1976 showed the lowest temperatures and productivity while 1979 had the highest. Springer could relate the kittiwake abundance to the timing of the fish, but has not yet established a relationship between the biomass and the temperature. Satellite imagery for July 1980, coinciding with Springer's observations off Cape Lisburne, show a band of warm surface water offshore. The birds were observed to be feeding in this area of warm water or along its interface with the cold Arctic water inshore. Since birds can respond to changes in surface water temperature, the distribution of birds might be used to indicate physical parameters.

Figure 11 is another example of how a coastline can be emphasized through a double scale enhancement. The figure shows the Beaufort Sea coast on 14 August 1977. The temperature scale is -2 to 7 and 7 to 16°C . The 7°C scale break distinctly shows a narrow band of warm water along the coast between Barrow and Herschel Island. The outer edge of the warm water is fringed by black dots corresponding to 7°C in the lower scale, that continues into various gray shades in the offshore waters. The inner edge of the warm water is white to very light gray corresponding to



612

Figure 11. Band of warm water along the Beaufort Sea coast, 14 August 1977, N5-4718 IR; (-2 to 7)+(7 to 16)°C.

7°C in the lower part of the higher scale that continues into black, corresponding to 16°C and above over the land. The existence of this warm coastal water was confirmed by data from the Simpson Lagoon and this same Figure 11 was given to Matthews for use in his OCS (1978) annual report.

IR Enhancements with Special Identity

In an IR enhancement any chosen temperature can be specially identified by matching the gray shade of the image with the appropriate shade in the 32-step gray scale. For rapid identification, a specific temperature or range of temperatures can be made either black or white. The first example of this by the Alaska pilot group was presented at the POAC-75 conference (Ahlnäs and Wendler, 1976). In that study we tried to detect open water in the Arctic Ocean in winter using satellite imagery. Figure 12 shows the ice cover in the Beaufort Sea on 17 March 1975. Integrated into the single scale enhancement from -43 to -3°C are -29°C shown by black dots in the medium gray section of the scale and -18°C shown by white dots in the dark gray part of the scale. Densitometer readings showed the coldest ice surface to be -41°C. The warmest ice is seen in a frozen lead just outside the shorefast ice. The only white dots corresponding to -18°C are seen along the southern edge of the lead. North of the lead is a wide belt of black dots corresponding to -29°C. From that area, strings of black dots extend to the northeast indicating the transition from the warmer ice in the refrozen leads to the surrounding cold ice of -41°C.

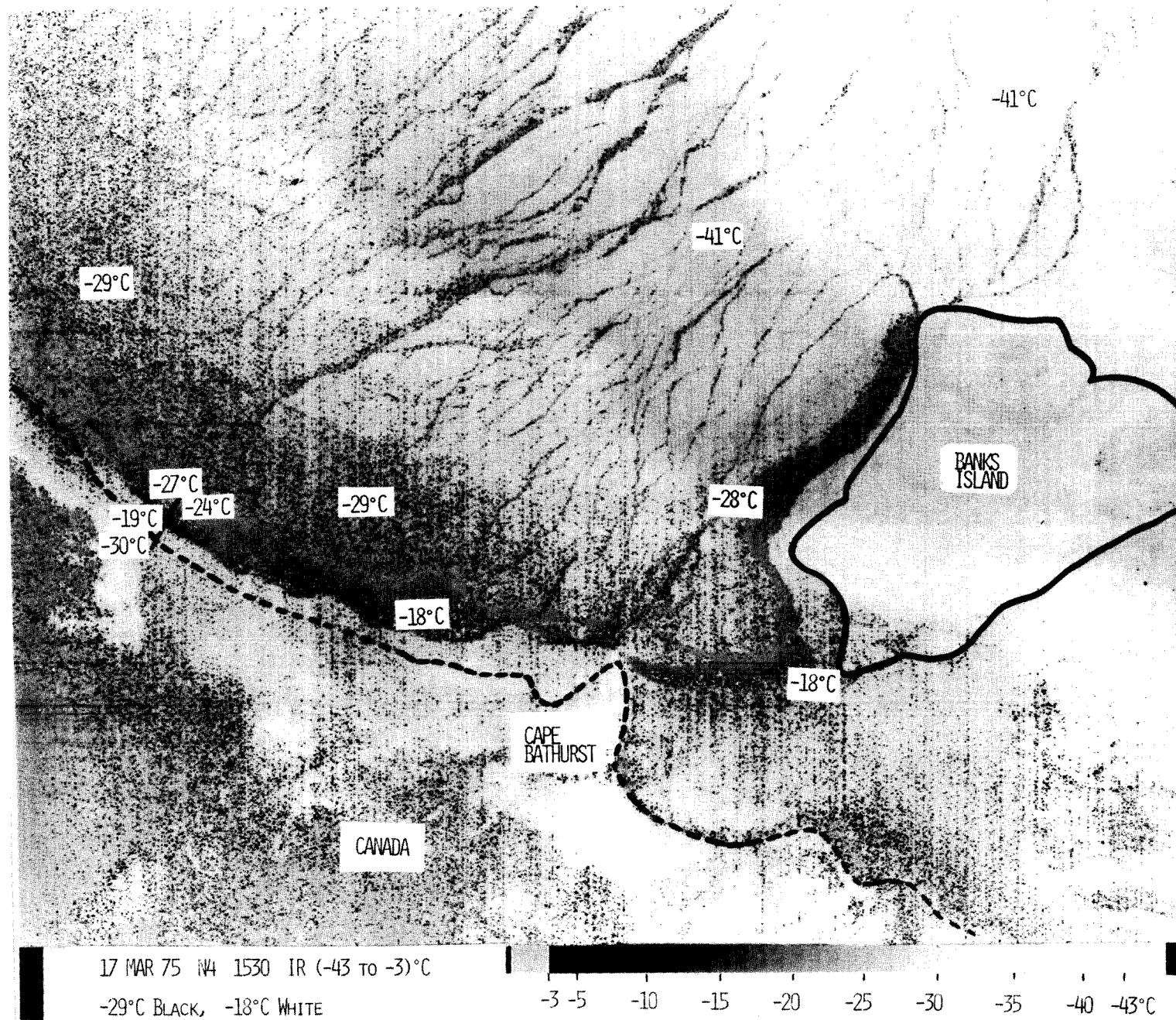


Figure 12. Beaufort Sea leads, 17 March 1975, N4-1530 IR; (-43 to -3)°C; -29°Bl, -18°Wh.

Sea-Ice Intrusions

Figure 13 shows a similar enhancement from -40 to -2°C , but the shades of gray for the special temperatures are the opposite, that is -18°C is black and -29°C is white. The enhancement shows an event of export of cold ice from the Chukchi Sea into the Bering Sea. The cold ice is recognized by its light gray color with the edges of the intrusion outlined by black dots corresponding to -18°C . The rest of the ice in the Bering Sea is dark gray and warmer. The only white dots are seen in the Chukchi Sea where the coldest ice is. Ahlnäs and Wendler (1979) studied two cases of ice transport through the Bering Strait. In both cases we found the reason for this transport to be the prevailing strong northerly winds associated with decreasing temperatures. Because of the well delineated extent of the ice intrusion on the satellite imagery we could measure the area of the cold ice. From that the mean speed with which the ice moved through the strait was calculated. For the longer lasting March episode the speed was 2.8 km/hr.

Kamchatka Eddies

In the above cases the specially selected temperatures outlined a transition between ice masses of different temperatures. When studying oceanic features a smaller temperature range is covered. From time to time, infrared satellite imagery has revealed eddies in the waters east of the Kamchatka Peninsula. Solomon and Ahlnäs (1978) made a study of these eddies using a single scale from 2 to 11°C . Through densitometer readings of the gray scale we found the cold core centers to be 3°C . The most likely source of that cold water is upwelling from greater depths. This seems to be a paradoxical explanation since the eddies are wound in an anticyclonic



Figure 13. Flow of cold Chukchi Sea ice into the Bering Sea, 20 March 1978, N5-7417 IR; (-40 to -2)°C; -29°Wh, -18°Bl.

sense. However, it is beyond the goal of this paper to address the physics of these eddies. In the paper describing IR enhancement techniques, Ahlnäs (1979) used another case when the Kamchatka eddies were observed on 26 September 1977 to demonstrate some applications (Fig. 14). The cold cores of these eddies were also 3°C and they were wound anticyclonically as the ones observed a year earlier. The same single scale enhancement, 2 to 11°C was used. Within this range 3°C was made black and 6°C white. Consequently, the cold cores turned black. Some of the eddies have a warm 6°C rim which is white. This type of special enhancement makes the feature of interest, such as the cold cores in this case, stand out in a striking way.

SEA-ICE STUDIES

The Bering Sea harbors an annual sea-ice cover that for 6 months of the year extends far enough to the south to conflict with fishing interests. To guarantee safety to fishermen and their gear, the location of the exact ice edge and its predicted movements are important. In the absence of clouds, the visible imagery pin-points the ice edge. Its advancement is governed by wind speed and direction in addition to the surface temperature of the waters at the ice edge. Figure 15 shows a special double scale enhancement for the Bering Sea on 29 March 1977. The major part of the sea ice matches the lower scale (-46 to -4°C) while the higher scale, (-2 to 5°C) shows the temperature of the open water. The division -4 to -2°C between these scales is wider than normal and is shown in black. This range indicates newly frozen thin ice, that may not show up on the visible imagery. In addition, ice that may be ready to melt is in this range. Theoretically, the -2°C transition from black to white should coincide with

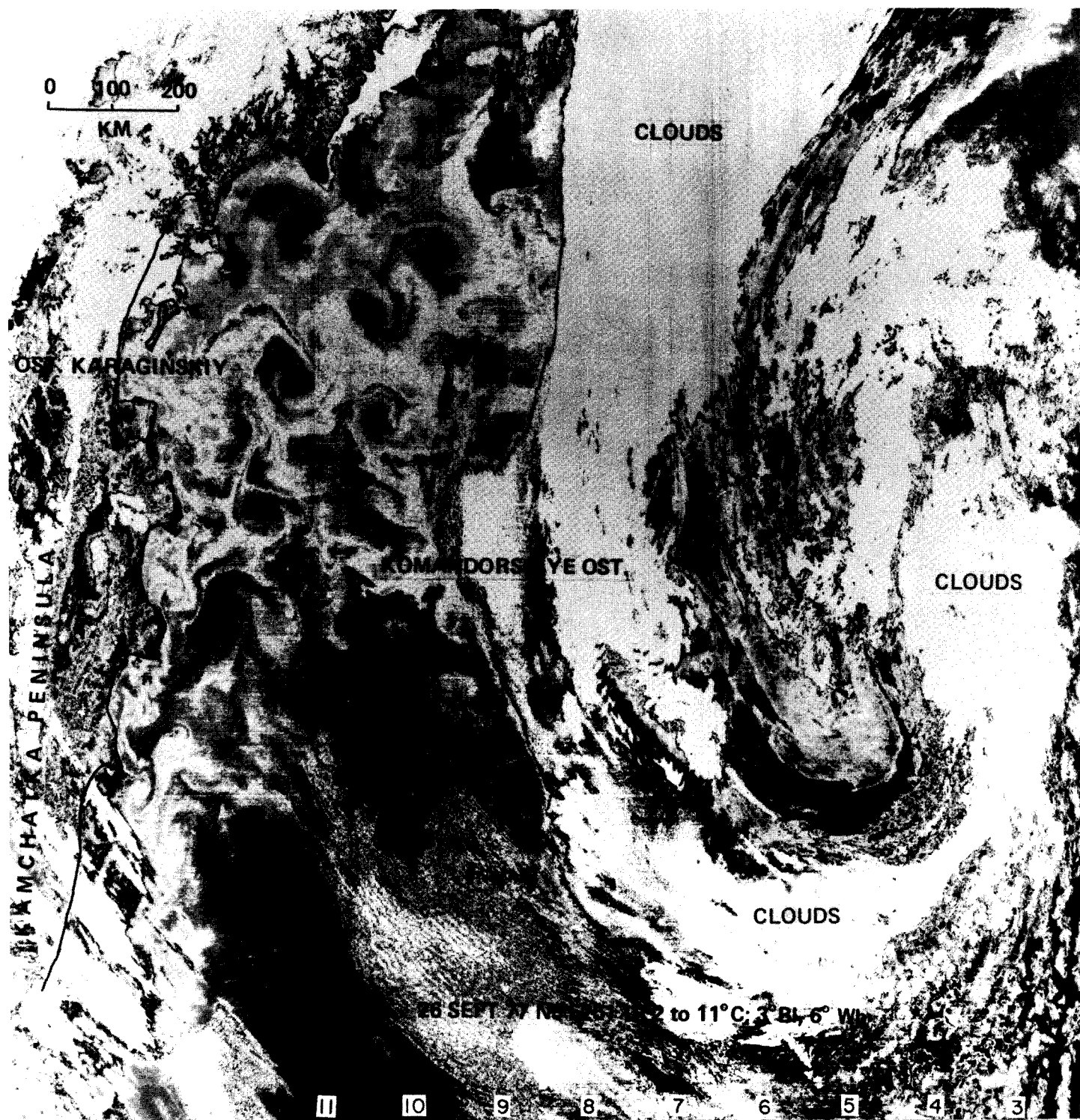


Figure 14. Oceanic eddies with cold cores east of Kamchatka, 26 September 1977, N5-5251 IR; (2 to 11)°C; 3°Bl, 6°Wh.

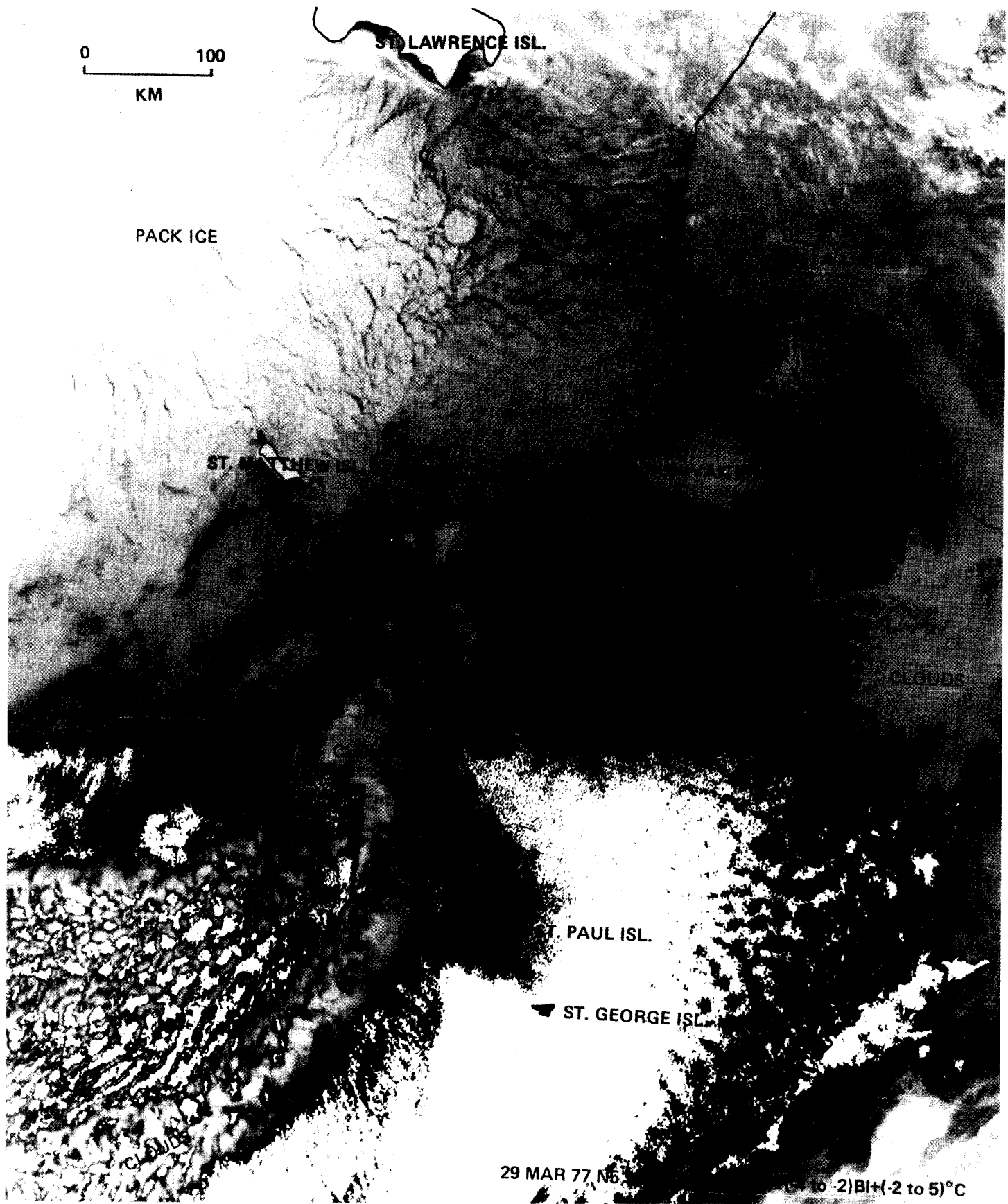
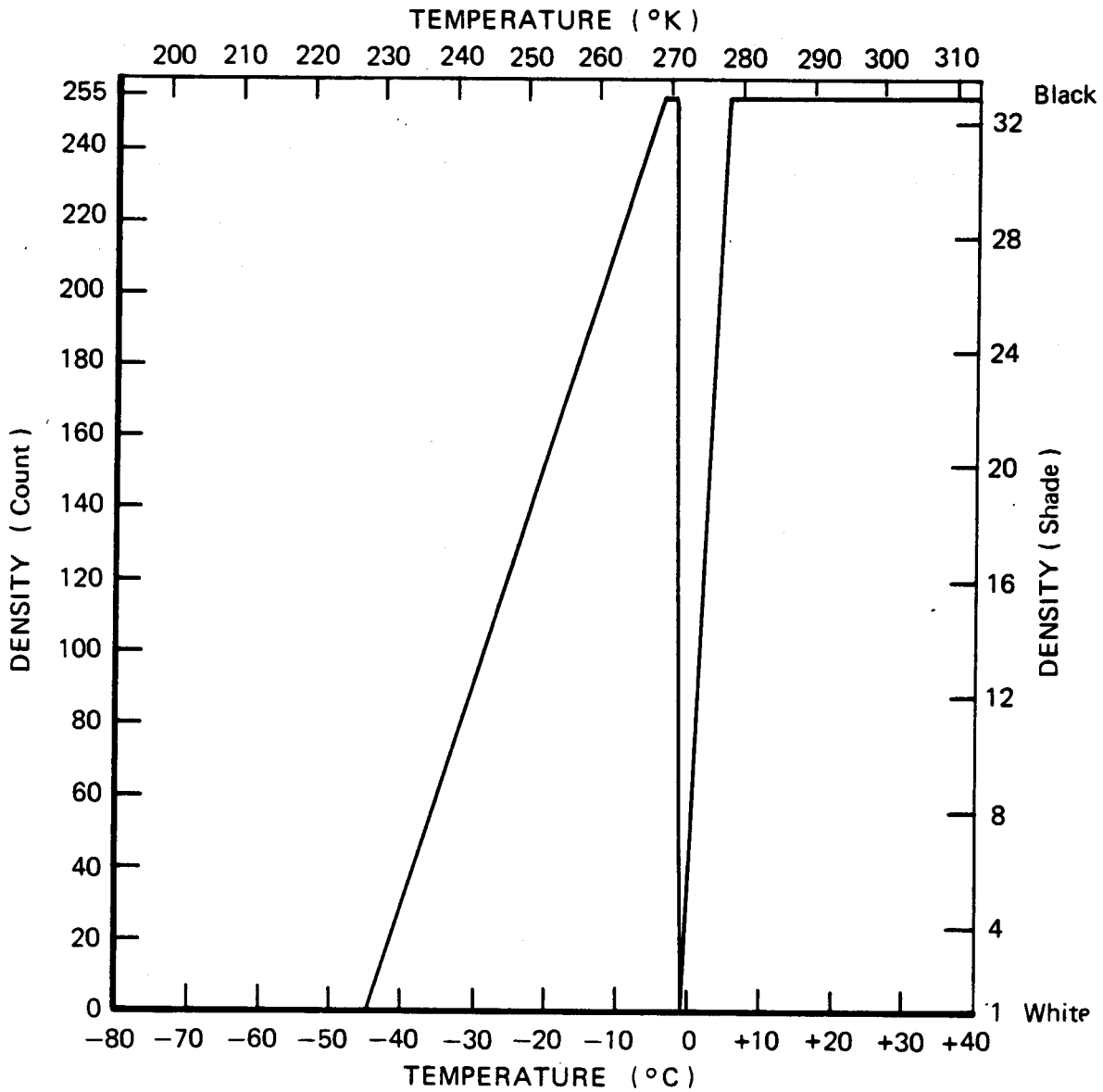


Figure 15. Ice edge between the Pribilof Islands of St. Paul and St. George, 29 March 1977, N5-3010 IR; $(-45 \text{ to } -4)+(-4 \text{ to } -2)B1 + (-2 \text{ to } 5)^\circ\text{C}$.

the ice edge. Due to the effects of atmospheric interference, the precision of the sensors and the digital tape, the true accuracy of the satellite derived sea surface temperatures is $\pm 1.5^{\circ}\text{C}$. Through comparison with the visible imagery it appears that the ice edge in Figure 15 is delineated by -4°C .

It is interesting to note that the black area of cold water surrounds St. Paul Island but leaves nearby St. George Island outside its reach. This is a common occurrence frequently observed on satellite imagery. When the ice edge does extend further south, it often stays between these two islands of the Pribilofs. Another commonly observed feature is a narrow ring of cold water individually surrounding these islands. The above mentioned features were brought to attention after an inquiry from a bird observer, George Hunt (personal communication). Hunt had observed a delay in migration and nesting habits of birds on St. Paul as compared to St. George. Cloud free imagery was sent to Hunt from 1975. Starting with the field season of 1977, the Pribilof Islands were kept under continuous surveillance and temperature enhancements were made when the area was clear. This imagery provided an explanation for the timing of the birds' arrival to the two islands. By supplementing hydrographic data with the satellite data, Hunt and Kinder (personal communication) found the cool surface waters ringing the islands to be caused by tidal mixing. In addition, they could show bird densities inside the rings of well-mixed water to be higher than outside.

IR enhancements produced by the AVHRR have a better resolution and contrast than the VHRR although the true accuracy is the same or $\pm 1.5^{\circ}\text{C}$. The IR enhancement table (Fig. 16) used in Figure 15 to show the ice edge,



Segment	BREAKPOINTS	
	From	To
1	<-80°C/000	-45°C/000
2	-45°C/000	- 4°C/255
3	- 4°C/255	- 2°C/255
4	- 2°C/255	- 1°C/000
5	- 1°C/000	5°C/255
6	5°C/255	>40°C/255

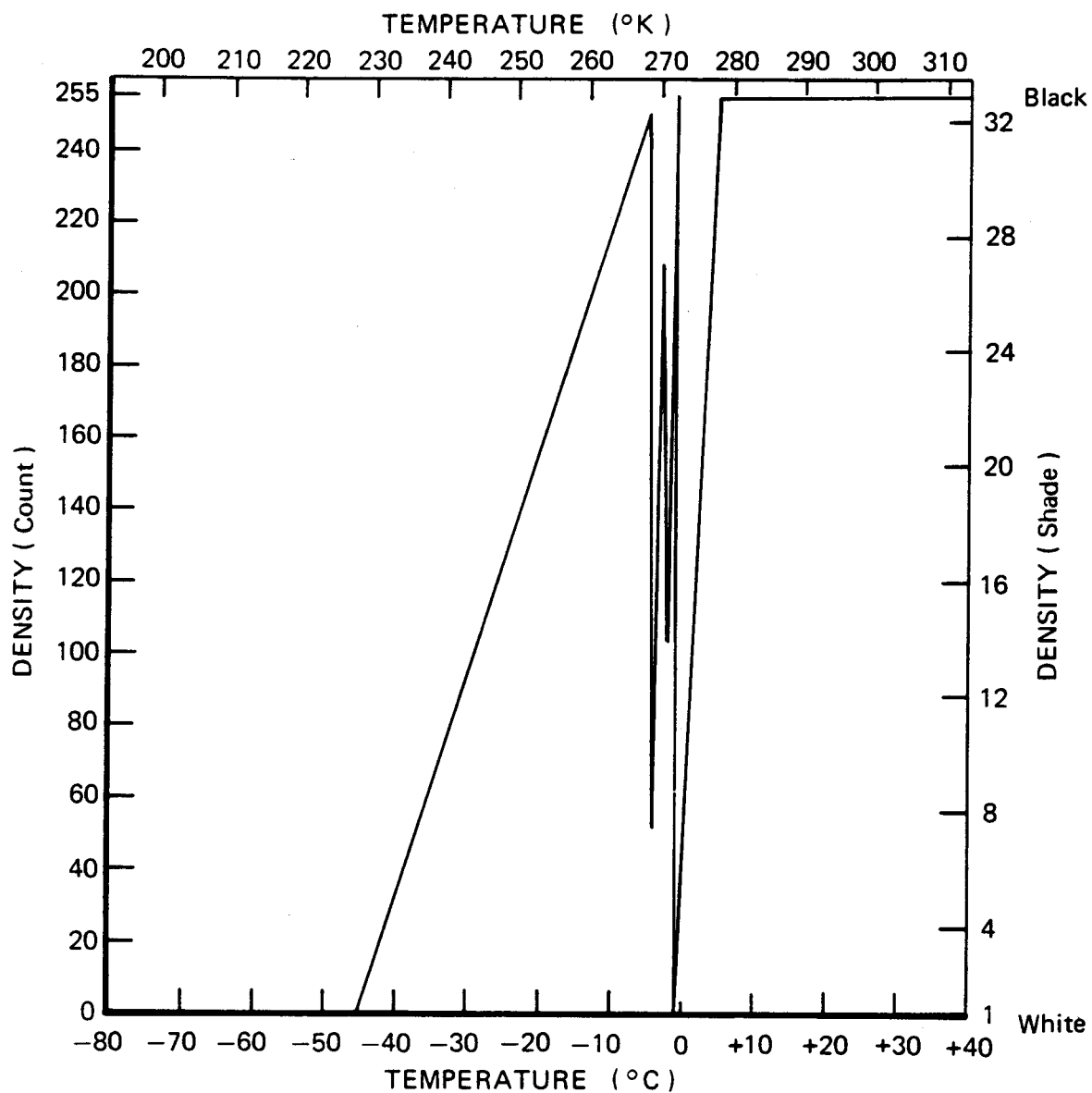
Figure 16. IR enhancement curve used in Figure 15 from "Polar spacecraft AVHRR sensor enhancement curves" NESS-CDA station (1980).

shows the entire temperature range from -4 to -2°C freezing/melting conditions in black. After discussing the problem with Don Sundgren at the Gilmore Tracking Station, he devised a table that divided the temperature range from -4 to -1°C into 4 contrasting shades of gray between limits of black (Fig. 17). This table is called 64P, where 6 stands for the spacecraft used, NOAA-6, and 4 for IR Channel 4. The same table using the TIROS-N satellite would consequently be called N4P. Spelled out table 64P would read:

(-45 to -5)	(-5 to -4)	(-4 to -3.5)	(-3.5 to -3)	(-3 to -2)	(-2 to -1.5)	
000	250	52	156	208	104	255
WH	BL	LLG	DG	DDG	LG	BL
white	black	light light grey	dark grey	dark dark grey	light grey	black

(-1.5 to -1)	(-1 to 5)	$^{\circ}\text{C}$
255	000	255
BL	WH	BL
black	white	black

The numbers under the temperatures indicate the density count on a scale from 000 for white to 255 for black. This table borders on the accuracy of the system, but during suitable temperature conditions the result can be striking. Figure 18 is a demonstration of table 64P, informally called the ice table. On 29 January 1980 the ice edge extended to Bristol Bay and bordered the Bering Sea side of the Alaska Peninsula. The black edge is nearly freezing water at -1.5°C forming an intrusion into Bristol Bay. The light gray band inside is the actual ice edge at -2°C followed by a dark gray band of -3°C ice, a medium gray at -3.5°C and a very light gray at -4°C ; -5°C is almost black. The temperature of the rest of the ice cover south of Nunivak Island is in the upper part of the -45 to -5°C range. With this table, open water within the ice pack or along the coast



BREAKPOINTS

Segment	From	To
1	<-80°C/000	-45°C/000
2	-45°C/000	- 5°C/250
3	- 5°C/250	- 4°C/052
4	- 4°C/052	-3.5°C/156
5	-3.5°C/156	- 3°C/208
6	- 3°C/208	- 2°C/104
7	- 2°C/104	- 1°C/255
8	- 1°C/255	- 1 C/000
9	- 1°C/000	5°C/255
10	5°C/255	>40°C/255

Figure 17. IR Enhancement curve, "ice table", 64P/N4P used in Figure 18.

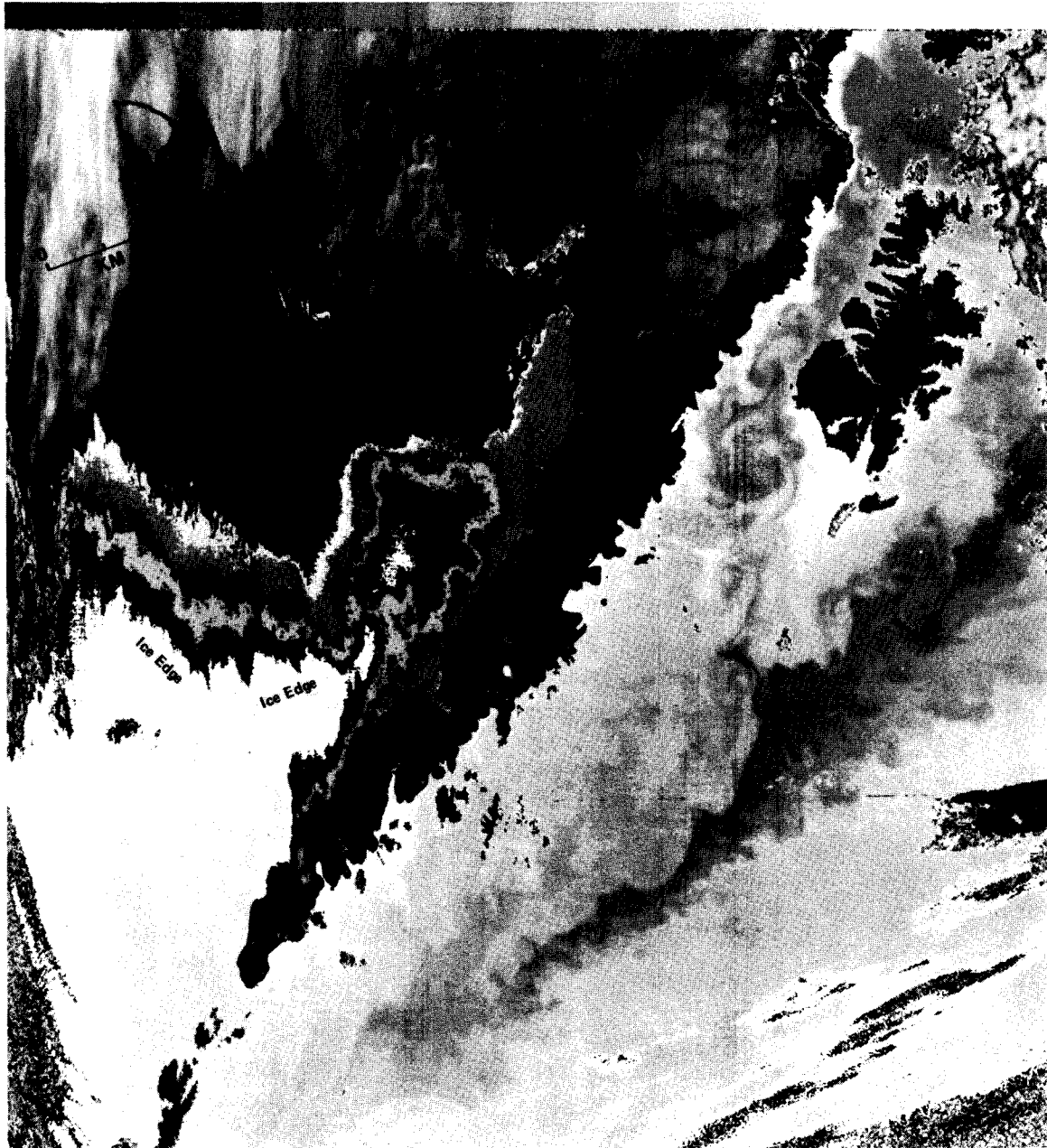


Figure 18. Ice edge structure in Bristol Bay and the warm Alaska current SW of Kodiak, 29 January 1980, N6-3072 IR; "ice table" 64P.

can be readily seen as for example in Nushagak and Kvichak Bay in the eastern Bristol Bay. The warmest part of this ice table, -1 to 5°C , shows the surface temperature of open water. The warm Alaska Current can be seen east of Kodiak Island directed to the southwest. This possibly accounts for the warmer water seen in the Bering Sea extending north through Unimak Pass. The waters west and southwest of Kodiak Island have an irregular distribution, as evidenced by the spiral type surface temperature structure.

Figure 19 is another example of the use of the ice table, N4P, for the TIROS-N satellite on 14 December 1979. The ice edge in this figure is colder than on 29 January and does not show the gradual temperature decrease over a wide area. Instead, great detail is seen in the open water south of the ice edge in the -1 to 5°C range. The isotherms are roughly concentric with the ice edge and both seem to be connected with the bathymetry. Theresa Paluszkiwicz is presently working on this relationship in addition to frontal systems based on satellite evidence for her master's thesis at the Institute of Marine Science, University of Alaska.

CORRECTIONS FOR GEOGRAPHIC DISTORTION

The satellite imagery is produced by horizontally scanning radiometers on the spacecraft passing vertically through the center of the image. This causes geographical distortion along the edges of the image. New software at the tracking station now makes it possible to rectify this distortion by stretching the image. Figure 20 is a stretched version of Figure 19. The correction here is most obvious in Bristol Bay, located at the edge of the image. In addition, the temperature range is offset -4°C . This brings

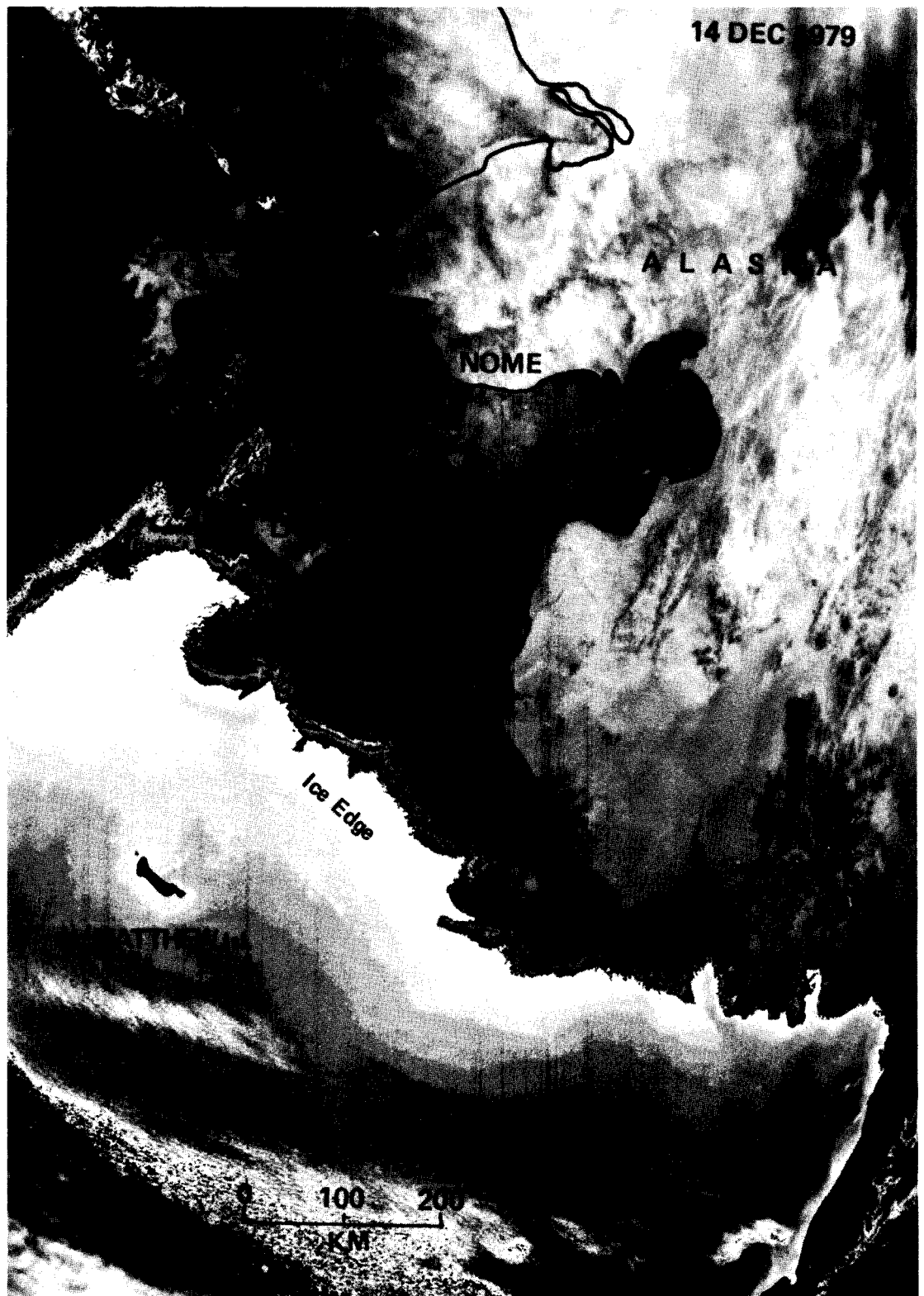


Figure 19. Bering Sea ice edge with surface temperature structure in waters over the continental shelf, 14 December 1979, TN-6025 IR; "ice table" N4P.

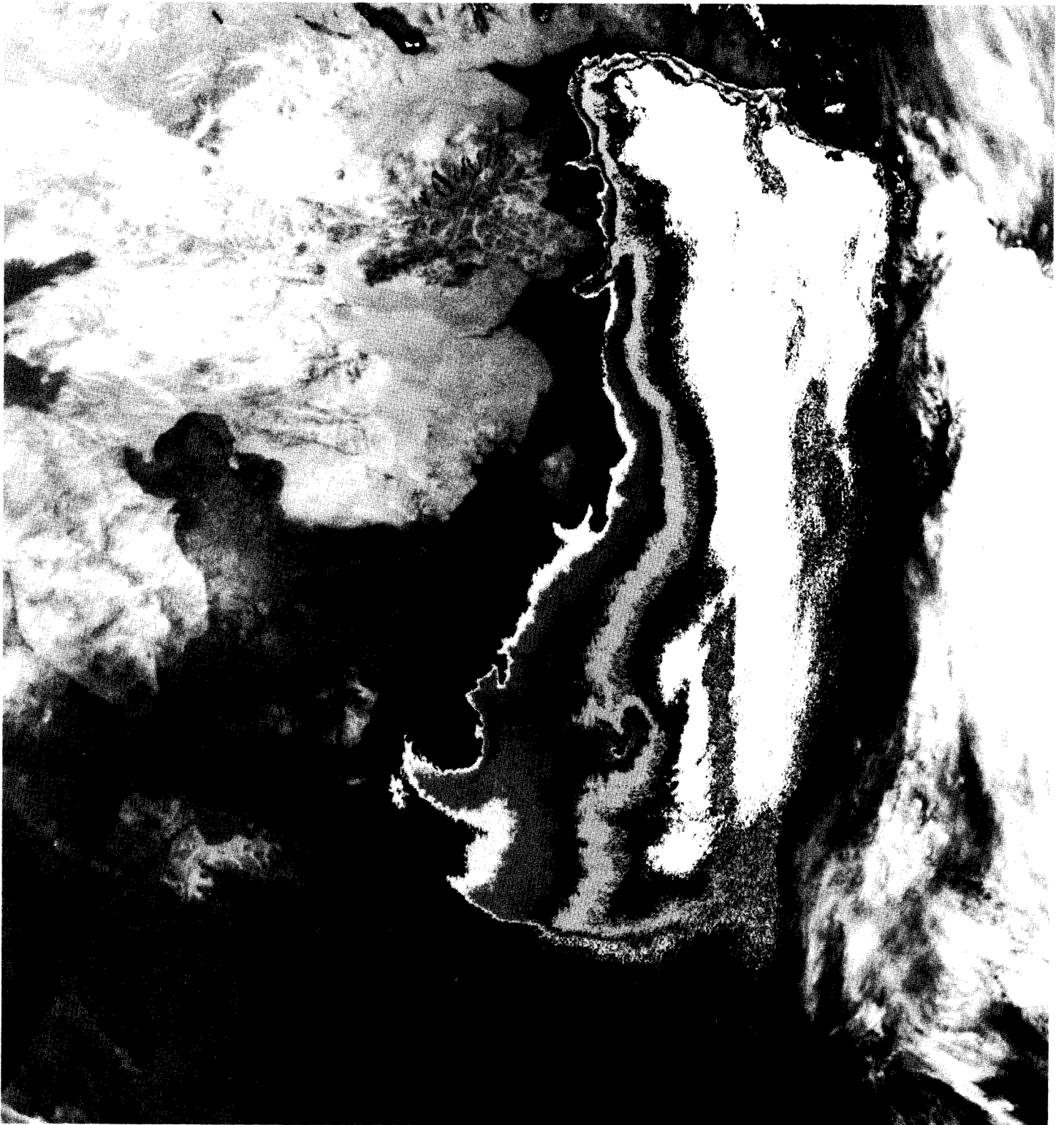


Figure 20. Image from Figure 19 with temperature table offset -4°C and stretched to rectify geographic distortion in Bristol Bay.

detail designed for the ice edge into the open water, where great contrast in the sea surface temperature structure can be observed over the continental shelf.

SATELLITE DATA ARCHIVES

Since the first satellite imagery was produced, its use has rapidly increased. New applications are continuously incorporated as technology advances. As more people become aware of the vast possibilities satellite imagery offers, its use will increase even further. When approaching a problem, historical comparisons are important and so there is always a new use for the previous imagery. The early negatives for the enhancements listed in this publication (Appendix I) are stored at the University of Alaska while most of the negatives since 1976 are stored at the Gilmore Tracking Station. The enhancements are produced from the original satellite digitized tapes which are normally only kept for 30 days before being reused. Over 100 tapes of special interest have been permanently stored at the University of Alaska Remote Sensing Library at the Geophysical Institute. A listing of these tapes is attached (Appendix II). Standard VIS and IR negatives for all Alaska passes processed at the tracking station are mailed monthly to:

Satellite Data Services Branch
National Climatic Center
World Weather Bldg. Rm. 606
Washington, D.C. 20233
Attn: Mr. Gene Hoppe

Standard VIS and IR contact prints can be ordered from there.

A NOAA-satellite pass is divided into three frames. For a descending orbit frame 1 covers the Arctic, frame 2 Alaska and the central Bering Sea

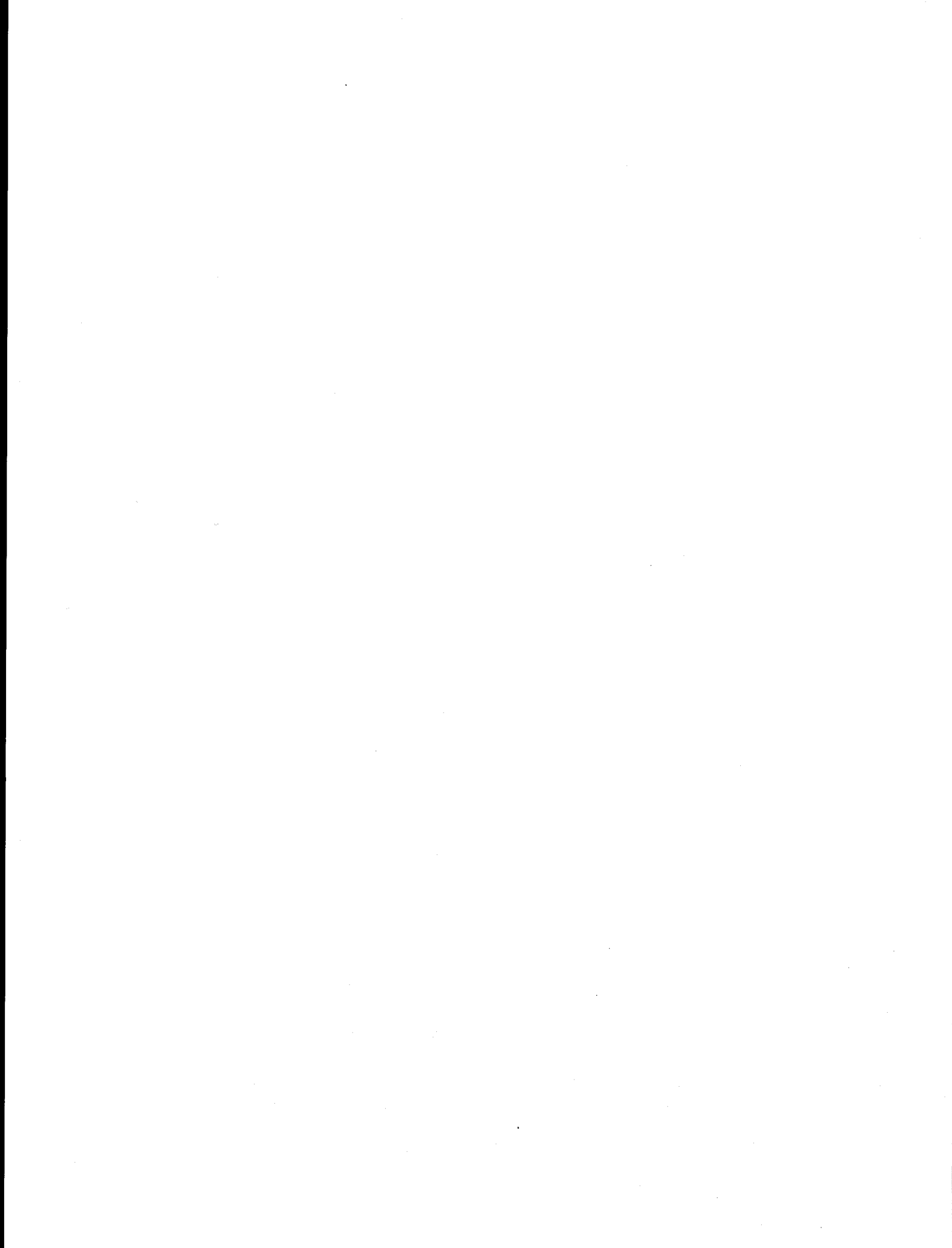
and frame 3 SE Alaska and the Aleutian chain. Positive transparencies of frames 2 and 3 for the orbit covering central Alaska and the Bering Sea are archived at the Geophysical Institute, Remote Sensing Library where they can be reviewed on a light table. During the time period of the Alaska Pilot Project, from March 1974 to 31 October 1975, the three frames for each satellite pass were taped together. During that period, we received up to three daytime passes and one night IR pass. This imagery is archived at the Gilmore Tracking Station. About a thousand copies of this imagery including other cloudfree imagery of interest through 1976 is stored in 12 ringbinders. From 1977 to 15 September 1980 cloudfree imagery concentrating on the Gulf of Alaska and Arctic Ocean/Bering Sea has been archived in 28 additional binders including the enhanced imagery listed here and selected enlargements. Altogether this image collection consists of about 5000 prints stored at the Remote Sensing Library.

ACKNOWLEDGEMENTS

The compilation of this work was supported under contract 03-5-022-56 between the University of Alaska and NOAA, Department of Commerce through the Outer Continental Shelf Environmental Assessment Program to which funds were provided by the Bureau of Land Management, Department of the Interior. The NOAA-NESS CDA Station manager at Gilmore, Gregory White, and former managers, Everitt Kendall and Edward Wrightsman, have been most helpful in providing necessary assistance. All station personnel have shown continuous interest and have been very willing to help throughout the entire satellite project. Special appreciation and thanks are extended to Donald Sundgren for performing most of the IR enhancements and to Kenneth Meyer for all of the photographic processing of the imagery. The careful reviewing of the manuscript by Thomas Royer and help in preparation by the Institute of Marine Science Publications department, led by Helen Stockholm, are also gratefully acknowledged.

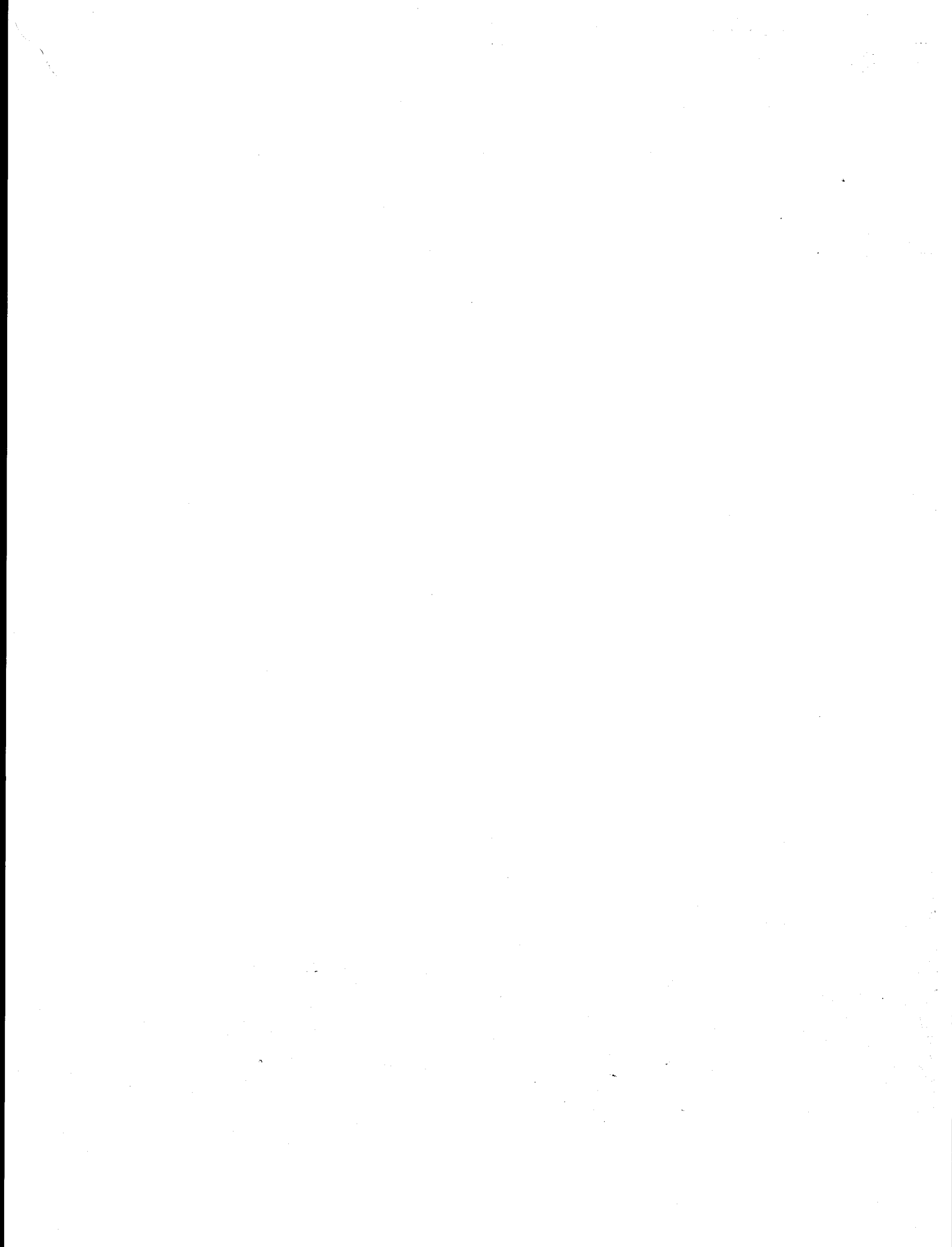
REFERENCES

- Ahlnäs, K. 1979. IR Enhancement Techniques to Delineate Surface Temperature and Sea-Ice Distributions. Proc. 13th Int. Symp. on Remote Sensing of Environment, Ann Arbor, Michigan. April 1979. II:1067-1076.
- Ahlnäs, K. and G. Wendler. 1976. Sea-ice Conditions in the Chukchi, Beaufort, East Siberian and Northern Bering Seas During March 1973, 1974, and 1975 as Seen From the NOAA 2, 3, and 4 Satellites. Proc. 3rd Int. Conf. on Port and Ocean Eng. Under Arctic Conditions (POAC-75) Univ. Alaska, Fairbanks. pp. 83-104.
- Ahlnäs, K. and G. Wendler. 1979. Sea-Ice Observations by Satellite in the Bering, Chukchi, and Beaufort Seas. Proc. 5th Int. Conf. Port and Ocean Eng. Under Arctic Conditions (POAC 79) Univ. Trondheim, Norway. 1:313-328.
- Coachman, L. K., K. Aagaard and R. B. Tripp. 1975. *Bering Strait - The Regional Physical Oceanography*. Seattle, University of Washington Press. 172 p.
- Henriksen, K., C. S. Deehr, and K. Ahlnäs. 1976. Comments on the Origin of Infrared Emissions in the Auroral Regions. *Physica Norvegica* 8(4):183-186.
- Hussey, W. J. 1979. The TIROS-N/NOAA Operational Satellite System. NOAA-NESS, Washington, D.C. 35 p.
- Jayaweera, K. O. L. F., and K. Ahlnäs. 1974. Detection of Thunderstorms from Satellite Imagery for Forest Fire Control. *Journal of Forestry* Vol. 72, No. 12.
- McClain, E. P. 1975. Environmental Research and Application Using the Very High Resolution Radiometer (VHRR) on the NOAA-2 satellite--A Pilot Project in Alaska. In: *Climate of the Arctic*, G. Weller and S. A. Bowling, eds. 415-429.
- Matthews, J. B. 1978. Characterization of the Nearshore Hydrodynamics of an Arctic Barrier Island-Lagoon System. Environmental Assessment of the Alaskan Continental Shelf Annual Report X. pp. 607-627.
- NESS-CDA Station. 1980. Polar Spacecraft AVHRR Sensor Enhancement Curves. Gilmore Creek, Alaska, Unpublished Catalog.
- Royer, T. C. 1977. Wind and Water; Ocean Currents in the Gulf of Alaska. *Alaska Seas and Coasts* 5(1):1-3.
- Royer, T. C. and R. D. Muench. 1977. On the Ocean Temperature Distribution in the Gulf of Alaska, 1974-75. *J. Phys. Ocean.* 7(1):92-99.
- Solomon, H. and K. Ahlnäs. 1978. Eddies in the Kamchatka Current. *Deep-Sea Res.* 25:403-410.



APPENDIX I

IR ENHANCEMENTS FOR SURFACE TEMPERATURE



IR ENHANCEMENTS FOR SURFACE TEMPERATURE

DATE	ORBIT	FRAME	TEMPERATURE (°F)	AREA
1974 May 22	N3-2443	I3500	27 to 43	Gulf of Alaska
"	"	"	36 to 44	"
June 25	N3-2865	I2600	34 to 66	Bering Strait
"	"	I2700	35 to 45	"
June 25	N3-2865	I3700	32 to 50	Aleutians, Unalaska
"	"	"	35 to 45	"
June 25	N3-2865	I3700	41 to 45	Aleutians, Unalaska
July 1	N3-2940	I2800	32 to 48	Bering Strait
"	"	"	34 to 58	"
"	"	"	32 to 64	"
July 13	N3-3089	I2600	34 to 58	Chukchi Sea
"	"	"	34 to 66	"
July 13	N3-3089	I2700	32 to 50	Chukchi Sea
"	"	"	(?)25 to 40	Siberia topography
July 14	N3-3101	I1, 2	34 to 66	Ellesmere, Bering Strait
"	"	I2	(?)25 to <40	Siberia-Alaska
July 14	N3-3101	I2700	32 to 50	Siberia, Bering Strait
"	"	"	(?)25 to <40	"
July 17	N3-3137	I2	42 to 50	Gulf of Alaska
"	"	"	42 to 66	"
July 17	N3-3137	I2400	42 to 60	Gulf of Alaska
"	"	"	42 to 66	"
Aug 14	N3-3484	I2	42 to 66	Gulf of Alaska
Aug 16	N3-3509	I3800	40 to 60	Gulf, "Octopus legs"
Aug 21	N3-3572	I2555	49 to 57	Norton Sound, Kotzebue Sound
"	"	"	34 to 66	"

DATE	ORBIT	FRAME	TEMPERATURE (°F)	AREA
1974 Aug 30	N3-3687	I1, 2	28 to 66	Seattle-Anchorage
Sept 4	N3-3745	I2700	49 to 58	Norton, Bristol, Iliamna Lake
"	"	"	28 to 62	"
Sept 5	N3-3758	I1	(18 to 29)+(30 to 45)	Chukchi Sea
"	"	"	28 to 66	"
Sept 8	N3-3795	I2480	(18 to 29)+(30 to 45)+(46 to 61)	Chukchi, Barrow Canyon
"	"	I2481	28 to 50	Chukchi, Bering Strait
Sept 8	N3-3795	I2	30 to 64	Chukchi, sediments
Sept 29	N3-4055	I2	29 to 62	Cook Inlet, Alaska Peninsula
"	"	I3125	29 to 62	Aleutians, Alaska Stream
"	"	"	49 to 58	"
Sept 30	N3-4067	I2	30 to 63	Prince William Sound
Oct 3	N3-4104	I2	28 to 41	P. William, Norton Sound
"	"	"	32 to 48	"
Oct 11	N3-4203	I2930	28 to 41	Gulf of Alaska Low
"	"	I5205	8 to 57	"
Oct 14	N3-4241	I2	28 to 51	N. Bering Strait
"	"	"	-1 to 36	Warm plume NW Alaska
Oct 18	N3-4921	I2	18 to 43	Alaska W. coast
Oct 21	N3-4328	I2	28 to 39	Bering Strait
Oct 22	N3-4340	I2	18 to 43	Bering Strait
"	"	"	(18 to 28)+(29 to 40)	"
Nov 8	N3-4551	I2	(0 to 28)+(29 to 40)	N. Bering Sea, Chukchi Sea
Nov 16	N3-4649	I2	28 to 41	Gulf of Alaska
Nov 18	N3-4679	I1515	24 to 46	Gulf, Alaska Peninsula

DATE	ORBIT	FRAME	TEMPERATURE (°F)	AREA
1974 Nov 18	N3-4679	I2	(?)20 to 42	Gulf, Alaska Peninsula
Nov 20	N3-4700	I2840	18 to 36	Bering Sea
Nov 26	N3-4774	I0880	18 to 34	Bering Sea
Nov 28	N3-4799	I0880	18 to 34	N. Bering Sea
Nov 30	N3-4824	I2090	-70 to 50; -4 to 4 B1	Chukchi leads
"	"	"	-70 to 50; -4 to 4 Wh	"
Nov 30	N3-4824	I2090	-70 to 50; -4 to 4 B1, 28 to 32 Wh	Chukchi leads
"	"	"	-70 to 50; -4 to 4 Wh, 28 to 32 B1	"
Nov 30	N3-4824	I2090	-26 to -14	Chukchi leads
"	"	"	-40 to 33	"
Nov 30	N3-4824	I2090	21 to 33	Chukchi leads
"	"	"	-16 to 12	"
Nov 30	N3-4824	I2090	-26 to -16	Chukchi leads
"	"	"	-33 to -22	"
Nov 30	N3-4824	I2090	-38 to -28	Chukchi leads
"	"	"	-20 to -10	"
Dec 1	N3-4836	I1700	-40 to 33	Bering, Chukchi Sea
"	"	"	27 to 38	"
Dec 2	N3-4848	I3	(-30 to 25)+(25 to 50)	Bristol, Aleutians
"	"	I2900	(-30 to 25)+(25 to 50)	Bering Sea
Dec 2	N3-4848	I2900	-40 to 33	Bering Sea
"	"	"	27 to 38	Bering, ice edge
Dec 2	N3-4849	I3400	(?)(0 to 27)+(28 to 38)	Bering Sea
"	"	I3000	27 to 38	Bering, ice edge
Dec 3	N3-4861	I3090	27 to 38	Bering, Chukchi Sea
"	"	"	-40 to 33	"
Dec 3	N3-4861	I3200	(?)(0 to 27)+(28 to 38)	Bering Sea
Dec 4	N3-4873	I2	-40 to 32	Bering, Chukchi Sea
"	"	I2750	-40 to 35	"

DATE	ORBIT	FRAME	TEMPERATURE (°F)	AREA
1974 Dec 5	N3-4885	I2	-41 to 33	NW Alaska coast
Dec 6	N3-4898	I2	-40 to 32	Chukchi Sea
Dec 7	N3-4910	I2650	-40 to 19	Chukchi Sea
Dec 8	N3-4923	I2700	26 to 38	Chukchi Sea
"	"	"	-40 to 33	"
Dec 9	N3-4935	I2	-40 to 32	Chukchi Sea
"	"	I2500	-40 to 35	Chukchi, Cook Inlet
Dec 10	N3-4947	I2	-40 to 32	NW Alaska coast
Dec 13	N3-4985	I2890	-40 to 33	Bering Sea
Dec 14	N3-4997	I2626	-40 to 33	Bering Sea
Dec 15	N3-5009	I2730	-50 to 29	Bering Sea
Dec 16	N4-0390	I2	8 to 42	Gulf of Alaska, N. Bering
"	"	"	-40 to 39	"
Dec 16	N4-0390	I2400	-40 to 32	Gulf of Alaska, N. Bering
"	"	I3030	-30 to 32	"
Dec 17	N4-0403	I2800	-50 to 32	Bering Sea
Dec 18	N4-0415	I1850	-50 to 35	E. Chukchi & Bering Sea
Dec 19	N4-0428	I2700	-50 to 35	Bering Sea
Dec 26	N4-0516	I3200	(?)(0 to 27)+(28 to 38)	Bering Sea
Dec 27	N4-0520	I1850	-50 to 50	Bering Sea
"	N4-0528	I2800	-50 to 32	Gulf of Alaska, Bering
Dec 28	N4-0541	I3160	(-48 to 28)+(29 to 41); -20B1, OWh	Bering Sea
Dec 29	N4-0553	I2400	-50 to 32	Gulf of Alaska, Bering
"	"	"	(-70 to 3); -50B1, -34/-20 spec.	"
Dec 31	N3-0578	I2880	(-60 to 28)+(29 to 40); -20B1, OWh	Gulf of Alaska, Bering Sea
"	"	I3200	(?)(0 to 27)+(28 to 38)	"

DATE	ORBIT	FRAME	TEMPERATURE (°F)	AREA
1975 Jan 2	N4-0603	I3500	-50 to 31	Gulf of Alaska, Bering Sea
Jan 5	N4-0641	I3260	(-20 to -1)+(0 to 23)+(24 to 43)	Bering Sea
Jan 6	N4-6053	I2750	-40 to 40	Cook Inlet, E. Bering Sea
"	"	I2752	-50 to 50	"
Jan 7	N4-0665	I2940	(-42 to 27)+(28 to 45)	Gulf to Kodiak
"	"	"	30 to 48	"
Jan 7	N4-0666	I3260	(-20 to -1)+(0 to 23)+(24 to 43)	Bering Sea
Jan 8	N4-0678	I2500	(-70 to 5); -70B1, 2Wh	Bering Sea, Alaska
"	"	"	(-70 to 6); -60B1, -20Wh	"
Jan 8	N4-0678	I2500	(-60 to 31); -50B1, 0Wh	Bering Sea, Alaska
"	"	"	(-60 to 31); -44 to -40B1	"
Jan 8	N4-0678	I2500	(-60 to 31)	Bering Sea, Alaska
"	"	I2700	(-52 to 27)+(28 to 49)	Bering Sea, Alaska Weather map
Jan 9	N4-0683	I1260	(-50 to 28)	Bering Sea
"	N4-0691	I3400	?(-20 to -1)Wh to 3/4B1+(0 to 24)3/4B1	Bering Sea
Jan 9	N4-0691	I4000	to B1+(25 to 43)	
Jan 9	N4-0691	I4000	(-20 to 24)+(25 to 35)	Bering Sea
Jan 10	N4-0703	I2667	(-34 to 28)+(30 to 45)	Unimak Pass
Jan 13	N4-0741	I3165	(-52 to 2); -40B1, -20Wh	Bering Sea
"	"	"	(-30 to 18); -20B1, 0Wh	"
Jan 20	N4-0829	I0875	(-50 to 30); -20B1, 28/29Wh	Arctic Ocean
"	"	I2392	(-50 to 30); -20B1, 28/29Wh	Bering Sea
Jan 29	N4-0941	I2	(-27 to 28)+(30 to 45)	Cook Inlet-Unimak Pass
Jan 31	N4-0966	I2	(-30 to 27)+(28 to 46)	Gulf of Alaska
"	"	"	(-43 to 28)+(29 to 37)	"
Feb 1	N4-0978	I2	(-30 to 27)+(28 to 46)	Gulf of Alaska
		(2/3 res)		

DATE	ORBIT	FRAME	TEMPERATURE (°F)	AREA
1975 Feb 3	N4-1003	I2	(-30 to 27)+(28 to 46)	Gulf of Alaska coast line
"	"	I1800	(-44 to 28)+(29 to 38)	"
Feb 4	N4-1016	I1517=I2 (2/3 res)	(-44 to 28)+(29 to 42)	P. William to SE Alaska
Feb 5	N4-1028	I1815	(-45 to 27)+(28 to 41)	P. William to SE Alaska
Feb 6	N4-1041	I1735	(-45 to 27)+(28 to 41)	P. William to SE Alaska
Feb 7	N4-1053	I1900	(-31 to 27)+(28 to 45)	Gulf of Alaska with Stream
Feb 8	N4-1058	I1, 2	(-30 to 28)+(29 to 46)	Seattle-Anchorage
Feb 9	N4-1078	I2	(-31 to 26)+(27 to 45)	P. William, SE Alaska
"	"	I2300	(-31 to 28)+(29 to 43)	P. William, Alaska Stream
Feb 9	N4-1079	I1980	(-31 to 26)+(27 to 45)	Alaska Stream
"	"	I2500	(-31 to 28)+(29 to 43)	"
Feb 13	N4-1129	I1640	(-60 to -40)+(-39 to 29)+(30 to 40)	Bering Sea, Cook Inlet
"	"	"	(-46 to 10); -40B1, -20Wh	"
Feb 13	N4-1129	I1640	(10 to 30); -15B1, 29Wh	Bering Sea, Cook Inlet
Feb 14	N4-1142	I1880	(-60 to -40)+(-38 to 27); -20B1	Bering Sea, Chukchi Sea
"	"	"	(-33 to 29)+(30 to 45)	"
Feb 14	N4-1142	I2400	(-8 to 24)+(25 to 35)	Bering Sea
Feb 16	N4-1167	I0230	(-60 to -31)+(-30 to -1)+(0 to 29)	Beaufort leads
"	"	I1500	(-60 to -31)+(-30 to -1)+(0 to 29)	Bering Sea, Chukchi Sea
Feb 16	N4-1167	I0825	(-45 to 30); -30B1, OWh	Beaufort leads
"	"	I1760	(-45 to 30); -30B1, OWh	Bering Sea
Feb 16	N4-1167	I0230	-31 to 29	Beaufort leads
"	"	I2505	(-31 to 29)+(30 to 48)	Bering Sea
Feb 23	N4-1254	I2330	(-45 to 28)+(29 to 37)	Bristol Bay
Feb 24	N4-1267	I1940	(-45 to 28)+(29 to 37)	Bering Sea
Mar 1	N4-1329	I1840	(-29 to 28)+(29 to 46)	Gulf of Alaska
"	"	"	(-29 to 28)+(29 to 40)	"

DATE	ORBIT	FRAME	TEMPERATURE (°F)	AREA
1975 Mar 4	N4-1367	I2180	(-38 to 0)+(1 to 29)	Norton Sound-Bristol Bay
Mar 5	N4-1379	I2300	(-28 to 28)+(29 to 46)	Alaska Stream
"	"	"	(-28 to 28)+(29 to 40)	"
Mar 5	N4-1379	I2300	(-28 to 28)+(29 to 34)	Alaska Stream
Mar 6	N4-1392	I2340	(0 to 28)	Cook Inlet
"	"	"	(0 to 28)+(29 to 40)	Cook, P. William Sound
Mar 9	N4-1429	I0940	(-52 to 12); -20B1, OWh	Arctic leads
Mar 14	N4-1492	I0710	(-40 to 0); -20Wh	Arctic leads
"	"	"	(-42 to 28); -1/OWh	"
Mar 14	N4-1492	I0710	(-50 to 12); -40B1, -20Wh	Arctic leads
"	"	I1700	(-10 to 17)	Interior, Arctic leads
Mar 14	N4-1492	I1700	(-2 to 27)	Interior, Norton, Cook
"	"	"	(-2 to 36)	"
Mar 14	N4-1492	I1700	(20 to 34)	Cook Inlet, Kodiak Island
"	"	"	(-19 to 27)+(28 to 45)	Cook, Kodiak, Interior
Mar 14	N4-1492	I2100	(0 to 31); 29/30Wh	Cook Inlet, Kodiak Island
"	"	"	(0 to 15)+(16 to 25)	Cook Inlet, Bristol Bay
Mar 15	N4-1505	I2222	(0 to 29)+(30 to 46)	Bering ice edge
"	"	"	(-20 to 31)+(32 to 42)	Bering ice edge, Pribilofs
Mar 15	N4-1505	I2222	(-40 to 0)+(1 to 32)	Bering ice edge, Pribilofs
Mar 17	N4-1529	I1880	(-27 to 28)+(29 to 46)	Gulf of Alaska
Mar 17	N4-1530	I0855	(-45 to 26); OWh	Arctic leads
"	"	"	(-45 to 26); -20B1, OWh	"
Mar 17	N4-1530	I0855	(-45 to -1)+(0 to 29)	Arctic leads
"	"	I2347	(-45 to -1)+(0 to 29)	Bering Sea
Mar 17	N4-1530	I2347	(-45 to 26); OWh	"
Mar 19	N4-1555	I1000	(-42 to 0)+(2 to 27); 30 B1, 10Wh	Arctic leads
"	"	I2087	(-42 to 0)+(2 to 27)+(28 to 41)	Beaufort Sea-St. Lawrence
Mar 19	N4-1555	I3180	(-42 to 0)+(2 to 27); -30B1, 10Wh	Bering Sea
Mar 21	N4-1580	I1492=I2	(-42 to 27); -20B1, OWh	Bering Sea

DATE	ORBIT	FRAME	TEMPERATURE (°F)	AREA
1975 Mar 23	N4-1605	I2340	(-42 to 27); -19B1, OWh	Bering Sea
Mar 25	N4-1630	I0565	(-42 to -10); -40B1	Arctic leads
"	"	"	(-42 to 27); -20B1, OWh	"
Mar 25	N4-1630	I2057	(-42 to 27); -20B1, OWh	Bering Sea
"	"	"	(-18 to 14); -10B1, 10Wh	"
Mar 28	N4-1667	I0715	(-42 to 27); -20B1, OWh	Arctic leads
Mar 30	N4-1692	I0500	(-40 to 28); 20Wh	Arctic leads
"	"	"	(-50 to 12); -20B1, OWh	"
Apr 2	N4-1730	I2060	(-28 to 28)+(29 to 40)	Gulf of Alaska, Bering Strait
"	"	"	-38 to 30; 28/29Wh	"
Apr 3	N4-1742	I2790	(-28 to 27)+(29 to 40)	Gulf of Alaska
Apr 4	N4-1754	I1492=I2	(-27 to 28)+(29 to 41)	SE Alaska
Apr 6	N4-1781	I2	-28 to 30; 28/29Wh	Chukchi Sea
Apr 7	N4-1793	I2640	(-25 to 28)+(29 to 40)	Bering Sea
Apr 10	N4-1829	I2530	(-27 to 29)+(30 to 45)	"Octopus legs", W. Seattle
Apr 10	N4-1830	I2467	(-27 to 28)+(29 to 45)	E. Bering, Unimak
Apr 13	N4-1868	I0500	-28 to 8; -20B1, OWh	Beaufort Sea
Apr 17	N4-1918	I1950	(-18 to 28)+(29 to 45)	Bering Sea
Apr 21	N4-1968	I0845	-30 to 34; 10 to 15 Wh	Beaufort Sea
"	"	"	-30 to 3; -20B1, OWh	"
Apr 22	N4-1980	I1800	(-40 to 24)+(25 to 28)B1+29 to 34)	Gulf of Alaska
"	"	I2238=I2	(-11 to 28)+(29 to 45) (vertical compression)	Gulf of Alaska
Apr 23	N4-1993	I3000	(-18 to 28)+(29 to 45)	Gulf of Alaska, Bering
Apr 24	N4-2005	I2 (2/3 res)	(-17 to 28)+(29 to 45)	Gulf of Alaska

DATE	ORBIT	FRAME	TEMPERATURE (°F)	AREA
1975 Apr 24	N4-2006	I0685	(-34 to 10)+(11 to 27)Bl+ (28 to 32)Wh; 33Bl	Beaufort Sea
Apr 25	N4-2018	I0910	-30 to 10; 28 to 32Wh	Beaufort Sea
Apr 26	N4-2031	I2050	(-16 to 28)+(29 to 45) (vertical compression)	Bering Sea
Apr 30	N4-2081	I2800	(0 to 28)+(29 to 46)	Bering Sea
May 8	N4-2181	IR	(-28 to -2)+(-2 to 3)	Banks Island polynya
May 14	N4-2256	I2	(0 to 31)+(32 to 34)Wh+(35 to 50)Bl	Alaska snow melt
May 16	N4-2281	I2828	(1 to 28)+(29 to 50)	Norton Sound
"	"	"	25 to 45	Norton Sound, Bristol Bay
May 17	N4-2294	I3660	25 to 46	Bering Sea
"	"	"	20 to 50	"
May 17	N4-2294	I2380	(-2 to 28)+(29 to 45)	Norton Sound
"	"	I3130	(-2 to 23)+(24 to 40)	Bering Sea
May 21	N4-2344	I3160	25 to 46	Bering Sea
"	"	"	17 to 42	"
May 22	N4-2356	I3530	24 to 46	Gulf of Alaska
May 23	N4-2368	I2790	20 to 49	Gulf of Alaska
"	"	"	(-2 to 28)+(29 to 45)	"
May 23	N4-2368	I3030	24 to 45	Gulf of Alaska
May 26	N4-2407	I3388	24 to 45	W. Bering Sea
May 29	N4-2444	I2900	24 to 45	Bering Sea
May 31	N4-2469	I3380	24 to 45	Bering Sea
June 1	N4-2482	I2335	24 to 45	Norton Sound
June 2	N4-2492	I2980	24 to 45	Norton Sound, Bristol Bay

DATE	ORBIT	FRAME	TEMPERATURE (°F)	AREA
1975 June 4	N4-2519	I2700	24 to 45	Norton Sound
June 5	N4-2532	I2238=I2	24 to 45	Norton Sound, Gulf of Anadir
June 6	N4-2544	I2	24 to 45	N. Bering Sea
June 9	N4-2582	I2940	17 to 42	Bering Sea, Pribilofs
June 10	N4-2594	I2920	17 to 42	Bering Sea
June 14	N4-2644	I2	18 to 42	Norton Sound
June 24	N4-2769	I3080	18 to 42	Aleutians
June 26	N4-2794	I2	18 to 42	Gulf of Alaska, Mackenzie Delta
July 3	N4-2882	I2	22 to 45	Bering Strait, Norton Sound
July 5	N4-2907	I2810	22 to 46	Bering Strait, Gulf of Alaska
July 10	N4-2969	I2	26 to 49	Gulf of Alaska
"	"	"	42 to 66	"
July 20	N4-3095	I2	28 to 59	Bering Sea
"	"	"	22 to 46	"
July 22	N4-3120	I2	22 to 46	Bering Sea, Chukchi Sea
July 24	N4-3137	I2	28 to 59	Bering Strait
July 25	N4-3158	I3300	22 to 46	Bering Sea, Chukchi Sea
July 27	N4-3182	I2900	26 to 49	Gulf of Alaska, Alaska Stream
July 28	N4-3196	I4451=I3	(10 to 29)+(30 to 50)	Kamchatka volcanoe eruption
Aug 2	N4-3258	I2920	26 to 50	Bering Sea
Aug 3	N4-3270	I2430	26 to 49	Gulf of Alaska, Alaska Stream
Aug 4	N4-3282	I2	26 to 49	Gulf of Alaska
"	"	"	28 to 59	"

DATE	ORBIT	FRAME	TEMPERATURE (°F)	AREA
1975 Aug 5	N4-3295	I2808	22 to 46	Nunivak-Kodiak
"	"	"	28 to 59	"
Aug 6	N4-3307	I2	26 to 49	Gulf of Alaska
"	"	"	28 to 59	"
Aug 7	N4-3321	I3270	28 to 59	Bering Sea, Chukchi Sea
Aug 8	N4-3333	I2600	22 to 46	Bering Sea
"	"	"	28 to 59	"
Aug 9	N4-3345	I3070	22 to 46	Bering, Pribilofs, Gulf of Alaska
"	"	"	28 to 59	"
Aug 26	N4-3557	I2	27 to 59	SE Alaska
Aug 27	N4-3570	I2	27 to 59	Prince William Sound
Aug 28	N4-3583	I2	27 to 59	Gulf of Alaska
Aug 29	N4-3595	I2790	27 to 59	Gulf of Alaska
Aug 30	N4-3600	I0780	27 to 59	Gulf of Alaska
Aug 30	N4-3609	I3	23 to 48	Aleutians
Sept 13	N4-3783	I2858	28 to 60	Alaska Stream, Cook Inlet
Sept 25	N4-3934	I2500	(-1 to 27)+(28 to 51)	Chukchi-Norton Sound
Oct 6	N4-4071	I2	30 to 62	Gulf of Alaska, Kodiak
Oct 7	N4-4076	I1250	28 to 60	Gulf of Alaska, Kodiak
Oct 9	N4-4101	I0710	29 to 61	Gulf of Alaska, Kodiak
Oct 25	N4-4309	I2808	(-1 to 27)+(28 to 51)	Gulf of Alaska, Alaska Stream
Oct 26	N4-4322	I3000	(-1 to 27)+(28 to 51)	Alaska Stream
Oct 27	N4-4334	I2	(-1 to 27)+(28 to 51)	Gulf of Alaska
"	"	I3000	(-1 to 27)+(28 to 51)	Gulf of Alaska, Alaska Stream
Nov 30	N4-4760	I3140	(0 to 28)+(29 to 44)	Alaska Stream, Aleutians

DATE	ORBIT	FRAME	TEMPERATURE (°F)	AREA
1976 Feb 28	N4-5887	I3238	(-30 to 28)+(29 to 41)	Gulf of Alaska to 10°E
Feb 29	N4-5892	I2	(-30 to 28)+(29 to 41)	Gulf of Alaska
"	"	"	23 to 50	"
Feb 29	N4-5899	I2820	-30 to 28)+(29 to 41)	Gulf of Alaska to 25°E
Apr 14	N4-6463	I3300	-4 to 28)+(29 to 45)	Gulf of Alaska
"	"	"	26 to 34	"
Apr 29	N4-6650	I3300	(-4 to 28)+(29 to 45)	Gulf to SE Alaska
Apr 30	N4-6663	I3300	(-4 to 28)+(29 to 45)	Gulf of Alaska
May 20	N4-6914	I3300	30 to 38	Alaska Stream
"	"	"	32 to 36	"
May 20	N4-6914	I3300	34 to 42	Alaska Stream
May 29	N4-7026	I3500	30 to 38	Alaska Stream
May 30	N4-7039	I3400	30 to 38 (too cold)	Prince William Sound
"	"	"	34 to 50	"
May 31	N4-7051	I3300	30 to 38 (too cold)	Prince William Sound
"	"	"	34 to 50	"
June 8	N3-11714	I3450	30 to 38 (too cold)	Gulf of Alaska
June 10	N3-11739	I2238	30 to 38	Bering Strait
June 11	N4-7189	I3500	30 to 38 (too cold)	Alaska Stream
June 12	N3-11764	I0775	30 to 38	Bering Sea & Pribilofs
July 3	N4-7465	I4180	32 to 48	Alaska Stream, eddies
"	"	"	40 to 48	"
July 10	N4-7553	I2	32 to 48	Bering Strait
July 11	N4-7565	IR	32 to 48	Bering Strait
"	"	"	28 to 60	"

DATE	ORBIT	FRAME	TEMPERATURE (°F)	AREA
1976 July 12	N4-7578	I2	32 to 48	Bering Strait
" "	" "	" "	28 to 60	" "
July 23	N4-7715	I2	28 to 60	Norton Sound
July 25	N4-7740	I3200	28 to 60	Gulf of Alaska
July 31	N4-7816	I0004	0 to 32	Stratus clouds
" "	" "	I2279	0 to 32	" "
Aug 1	N4-7827	I3200	28 to 60	Gulf of Alaska
Aug 21	N4-8078	I3600	28 to 60	Gulf, Alaska Stream
Aug 22	N4-8090	I3500	28 to 60	Gulf of Alaska
Aug 25	N5-0336	I2200	28 to 50	Arctic coast
Aug 26	N5-0349	I2200	28 to 50	Arctic
Sep 7-20	N5-0496+0657	IR	32 to 59	British Columbia coast (Coast Guard Study)
Sep 16	N5-0609	I3000	28 to 60	Kamchatka eddies
" "	" "	I3001	36 to 52	" "
Sep 18	N5-0634	I3500	29 to 52	Kamchatka eddies
Oct 1	N5-0794	I2	(0 to 28)+(29 to 52)	Gulf of Alaska
" "	" "	" "	32 to 48	Gulf of Alaska, Yakutat sediments
Oct 2	N5-0806	I3000	36 to 48; <35B1	Gulf of Alaska
" "	" "	" "	(0 to 19)+(20 to 28)B1+(29 to 48)	" "
Oct 2	N5-0806	I3000	(0 to 31)+(32 to 48)	Gulf of Alaska
" "	" "	I2	(0 to 28)+(29 to 52)	" "
Oct 2	N5-0807	I3000	(0 to 28)+(29 to 44)	Bering Sea, Norton Sound
" "	" "	" "	(0 to 28)+(29 to 52)	" "
Oct 2	N5-0807	I3000	(0 to 31)B1+(32 to 46)	Bering Sea, Norton Sound
" "	" "	" "	40 to 48	Norton Sound

DATE	ORBIT	FRAME	TEMPERATURE (°F)	AREA
1976 Oct 3	N5-0819	I2	(0 to 28)+(29 to 44)	Norton Sound
Oct 7	N5-0869	I3	(0 to 28)+(29 to 44)	Islands of 4 Mountains
Oct 8	N5-0880	I3200	(0 to 28)+(29 to 52)	Gulf of Alaska
Oct 10	N5-0906	I2	(0 to 28)+(29 to 44)	Kotzebue Sound
Oct 14	N5-0955	I1160	(0 to 28)+(29 to 44)	Mackenzie, Amundsen Gulf
Oct 14	N5-0956	I3	(0 to 28)+(29 to 44)	Kamchatka eddies
Oct 15	N5-0968	I3	(0 to 28)+(29 to 44)	Cape Olyutorskiy, Kamchatka
Oct 23	N5-1066	I3400	32 to 48	N. Gulf of Alaska coast
Oct 23	N5-1067	I2	(-20 to 28)+(29 to 44)	Arctic ice, Pt. Hope
Oct 24	N5-1079	I2	(-20 to 28)+(29 to 44)	Chukchi Sea, Norton Sound
Oct 25	N5-1092	I3600	(-20 to 28)+(29 to 37)	Cape Olyutorskiy, Kamchatka
Oct 28	N5-1129	I3300	(-20 to 28)+(29 to 37)	Chukchi, Cape Olyutorskiy
Oct 29	N5-1141	I3400	(-20 to 28)+(29 to 37)	Cape Olyutorskiy, Kamchatka
"	"	I3600	(-20 to 28)+(29 to 45)	Cape Olyutorskiy, Aleutians
Oct 30	N5-1154	I3200	(-20 to 28)+(29 to 37)	Chukchi, Cape Olyutorskiy
Oct 31	N5-1166	I2920	(-30 to 20)+(21 to 28)B1+(29 to 37)	Chukchi, Cape Olyutorskiy
"	"	"	(-20 to 28)+(29 to 37)	"
Nov 4	N5-1215	I2888	(-20 to 28)+(29 to 37)	E. Bering: Pt. Hope-Nunivak
Nov 5	N5-1228	I2888	(-20 to 28)+(29 to 37)	E. Bering, Chukchi
"	"	"	(-30 to 24)+(25 to 28)B1+(29 to 37)	"
Nov 9	N5-1277	I3500	(-30 to 24)+(25 to 28)B1+(29 to 45)	Bristol Bay, Norton Sound
Nov 10	N5-1290	I2, 3	(-30 to 24)+(25 to 28)B1+(29 to 37)	Bering Sea, Kamchatka
Nov 29	N5-1525	I2626	(-40 to 24)+(25 to 28)B1+(29 to 37)	Chukchi, Bering Sea
Nov 30	N5-1537	I2626	(-40 to 24)+(25 to 28)B1+(29 to 37)	Chukchi, Bering Sea

DATE	ORBIT	FRAME	TEMPERATURE (°F)	AREA
1976 Dec 1	N5-1550	I2920	(-40 to 24)+(25 to 28)B1+(29 to 37)	Chukchi, Bering Sea
Dec 2	N5-1562	I2820	(-50 to 24)+(25 to 28)B1+(29 to 37)	Chukchi, Bering Sea
Dec 6	N5-1611	I3200	(-50 to 28)+(29 to 41)	Gulf of Alaska
"	"	"	(-50 to 24)+(25 to 28)B1+(29 to 37)	"
Dec 6	N5-1611	I3200	(-50 to 28)+(29 to 37)	Gulf of Alaska
Dec 7	N5-1624	I2880	(-50 to 24)+(25 to 28)B1+(29 to 37)	Chukchi, Bering Sea
Dec 8	N5-1636	I2920	(-50 to 24)+(25 to 28)B1+(29 to 37)	Chukchi, Bering Sea, Cook Inlet
Dec 9	N5-1649	I3300	(-50 to 24)+(25 to 28)B1+(29 to 37)	Chukchi, Bering Sea
Dec 10	N5-1661	I3200	(-50 to 24)+(25 to 28)B1+(29 to 37)	Chukchi, Bering Sea
Dec 12	N5-1686	I4000	(-50 to 24)+(25 to 28)B1+(29 to 37)	Kamchatka
Dec 16	N5-1735	I3100	(-50 to 28)+(29 to 37)	Cook Inlet, Aleutians
Dec 17	N5-1747	I2626	(-50 to 28)+(29 to 41)	Yakutat coast
"	"	"	(-50 to 28)+(29 to 37)	"
Dec 18	N5-1760	I2820	(-50 to 24)+(25 to 28)B1+(29 to 37)	Bering Sea
Dec 22	N5-1810	I4000	(-50 to 24)+(25 to 28)B1+(29 to 37)	Kamchatka
Dec 28	N5-1884	I3100	(-50 to 24)+(25 to 28)B1+(29 to 37)	Bering Sea

DATE	ORBIT	FRAME	TEMPERATURE (°F)	AREA
1977 Jan 5	N5-1982	I3200	(-50 to 28)+(29 to 41)	Cook Inlet, Kodiak Island
Jan 6	N5-1995	I1650	(-50 to 24)+(25 to 28)B1+(29 to 37)	NW Alaska coast
Jan 14	N5-2094	I1940	(-50 to 24)+(25 to 28)B1+(29 to 37)	Arctic coast to Pt. Hope
Jan 21	N5-2181	I3150	(-50 to 24)+(25 to 28)B1+(29 to 37)	Bering Sea
Jan 26	N5-2243	I3250	(-50 to 24)+(25 to 28)B1+(29 to 37)	W. Bering Sea
Jan 29	N5-2279	I1800	(-50 to 28)+(29 to 45)	"Octopus legs" in Gulf of Alaska
Jan 29	N5-2280	I2920	(-50 to 24)+(25 to 28)B1+(29 to 37)	Bering Sea, E. Chukchi leads
Jan 30	N5-2292	I2720	(-50 to 24)+(25 to 28)B1+(29 to 37)	Bering Sea, E. Chukchi leads
Jan 31	N5-2305	I3065	(-50 to 24)+(25 to 28)B1+(29 to 37)	Bering Sea, plume N. St. Lawrence
"	"	I3070	(-30 to 24)+(25 to 28)B1+(29 to 37)	Bering Sea
Feb 1	N5-2317	I2480	(-50 to 24)+(25 to 28)B1+(29 to 37)	Bering Sea, NW Alaska coast
"	"	"	(-60 to 24)+(25 to 28)B1+(29 to 37)	"
Feb 2	N5-2330	I2676	(-50 to 24)+(25 to 28)B1+(29 to 37)	Bering Sea, NW Alaska coast
Feb 3	N5-2342	I2960	(-50 to 24)+(25 to 28)B1+(29 to 37)	Bering Sea, NW Alaska coast
Feb 6	N5-2379	I3200	(-50 to 24)+(25 to 28)B1+(29 to 37)	Bering Sea
Feb 9	N5-2416	I0485	(-50 to 24)+(25 to 28)B1+(29 to 37)	Arctic leads, breakup Barrow
Feb 11	N5-2441	I2670	(-50 to 24)+(25 to 28)B1+(29 to 37)	Arctic leads, Bering floebergs
Feb 12	N5-2453	I2770	(-50 to 24)+(25 to 28)B1+(29 to 37)	W. Bering-Barrow "plume" N. St. Lawrence Island
Feb 13	N5-2466	I2044	(-50 to 24)+(25 to 28)B1+(29 to 37)	Chukchi floebergs
"	"	I3700	(-50 to 24)+(25 to 28)B1+(29 to 37)	W. Bering Sea
Feb 14	N5-2478	I2820	(-50 to 24)+(25 to 28)B1+(29 to 37)	W. Bering, Chukchi Sea
Feb 16	N5-2503	I3	(-50 to 24)+(25 to 28)B1+(29 to 37)	W. Bering, Kamchatka
Feb 18	N5-2528	I2, 3	(-50 to 24)+(25 to 28)B1+(29 to 37)	NW Alaska coast, Kamchatka ice eddies

DATE	ORBIT	FRAME	TEMPERATURE (°F)	AREA
1977 Feb 20	N5-2552	I3600	(-50 to 28)+(29 to 45)	Aleutians
Feb 21	N5-2565	I3	(-50 to 24)+(25 to 28)B1+(29 to 37)	Ice eddies off Kamchatka
Feb 22	N5-2577	I2725	(-50 to 24)+(25 to 28)B1+(29 to 37)	NW Alaska coast breakup, Bristol
Feb 23	N5-2589	I2100	(-50 to 28)+(29 to 45)	NW Alaska coast, Prince William
Feb 24	N5-2602	I1, 2	(-50 to 24)+(25 to 28)B1+(29 to 37)	NW Alaska coast breakup
Feb 25	N5-2613	I2	(-50 to 28)+(29 to 45)	Gulf, Arctic coast
Feb 25	N5-2614	I1, 2	(-50 to 28)+(29 to 45)	Gulf, Arctic coast
Feb 27	N5-2639	I1000	(-50 to 24)+(25 to 28)B1+(29 to 37)	Chukchi Sea
"	"	I3200	(-50 to 24)+(25 to 28)B1+(29 to 37)	Bering Sea, Bristol Bay
Feb 28	N5-2651	I2040	(-50 to 24)+(25 to 28)B1+(29 to 37)	Chukchi Sea
Mar 2	N5-2676	I2920	(-50 to 24)+(25 to 28)B1+(29 to 37)	Bering Sea
Mar 3	N5-2688	I2	(-70 to -30)+(-29 to 28)+(29 to 37)	Bering ice edge ~250 km north of St. Paul
"	"	I2240	(-30 to 24)+(25 to 28)B1+(29 to 41)	"
Mar 4	N5-2701	I2	(-50 to 24)+(25 to 28)B1+(29 to 37)	Bristol ice free, Bering ice edge,
"	"	I2240	(-30 to 24)+(25 to 28)B1+(29 to 41)	~175 km south of Nunivak
Mar 5	N5-2713	I2	(-50 to 24)+(25 to 28)B1+(29 to 37)	Bering Sea
Mar 6	N5-2726	I4240	(-50 to 24)+(25 to 28)B1+(29 to 37)	W. Bering ice edge, Kamchatka
Mar 7	N5-2737	I2	(-50 to 24)+(25 to 28)B1+(29 to 41)	Gulf of Alaska, Prince William
Mar 7	N5-2738	I2725	(-50 to 24)+(25 to 28)B1+(29 to 37)	Bering Sea
"	"	I2726	(-30 to 24)+(25 to 28)B1+(29 to 41)	Bering Sea
Mar 8	N5-2750	I2	(-50 to 24)+(25 to 28)B1+(29 to 41)	Bering Sea/Gulf of Alaska
"	"	I2240	(-30 to 24)+(25 to 28)B1+(29 to 41)	"
Mar 9	N5-2763	I3200	(-50 to 24)+(25 to 28)B1+(29 to 37)	Bering Sea/Gulf of Alaska
"	"	I3201	(-30 to 24)+(25 to 28)B1+(29 to 41)	"

DATE	ORBIT	FRAME	TEMPERATURE (°F)	AREA
1977 Mar 10	N5-2775	I3100	(-50 to 24)+(25 to 28)B1+(29 to 37)	Bering Sea/Gulf of Alaska
"	"	I3101	(-30 to 24)+(25 to 28)B1+(29 to 41)	"
Mar 11	N5-2787	I2	(-50 to 24)+(25 to 28)B1+(29 to 41)	Gulf/Kodiak warm current
Mar 12	N5-2799	I2	(-50 to 24)+(25 to 28)B1+(29 to 41)	Prince William Sound
Mar 13	N5-2811	I3100	(-50 to 24)+(25 to 28)B1+(29 to 41)	Kodiak Island
Mar 13	N5-2812	I2	(-50 to 24)+(25 to 28)B1+(29 to 41)	Bristol Bay
Mar 14	N5-2824	I1300	(-50 to 24)+(25 to 28)B1+(29 to 41)	Prince William Sound
Mar 14	N5-2825	I1, 2	(-50 to 24)+(25 to 28)B1+(29 to 37)	Arctic leads, Kamchatka
Mar 15	N5-2837	I1560	(-50 to 24)+(25 to 28)B1+(29 to 37)	Arctic leads, Kamchatka
Mar 17	N5-2861	I2500	(-50 to 24)+(25 to 28)B1+(29 to 41)	Gulf of Alaska
Mar 17	N5-2862	I1, 2, 3	(-50 to 24)+(25 to 28)B1+(29 to 37)	W. Bering, Barrow leads
"	"	I0775	(-50 to -18); OWh	Beaufort Sea leads
Mar 18	N5-2873	I2	(-50 to 24)+(25 to 28)B1+(29 to 41)	Gulf of Alaska
Mar 18	N5-2874	I0900	(-50 to 24)+(25 to 28)B1+(29 to 37)	Barrow lead
Mar 18	N5-2874	I0901	(-50 to -18); OWh	Barrow lead
"	"	I3150	(-50 to 24)+(25 to 28)B1+(29 to 37)	W. Bering Sea
Mar 19	N5-2887	I2, 3	(-50 to 24)+(25 to 28)B1+(29 to 41)	W. Bering, Arctic leads
Mar 20	N5-2899	I2	(-50 to 24)+(25 to 28)B1+(29 to 41)	Bering Sea
Mar 21	N5-2910	I2	(-50 to 24)+(25 to 28)B1+(29 to 41)	Prince William Sound
Mar 21	N5-2911	I0440	(-50 to 24)+(25 to 28)B1+(29 to 41)	Arctic leads
"	"	I2678	(-50 to 24)+(25 to 28)B1+(29 to 41)	Bering Sea
Mar 22	N5-2923	I2820	(-50 to 24)+(25 to 28)B1+(29 to 41)	E. Bering Sea
Mar 22	N5-2924	I3500	(-50 to 24)+(25 to 28)B1+(29 to 41)	W. Bering Sea
Mar 23	N5-2935	I3600	(-50 to 24)+(25 to 28)B1+(29 to 41)	Gulf of Alaska
Mar 23	N5-2936	I2530	(-50 to 24)+(25 to 28)B1+(29 to 41)	Bering Sea
Mar 25	N5-2961	I3200	(-50 to 24)+(25 to 28)B1+(29 to 41)	Bering (Chukchi very cold, Barrow (-30 to -35°F 3/27))

DATE	ORBIT	FRAME	TEMPERATURE (°F)	AREA
1977 Mar 27	N5-2985	I2	(-50 to 24)+(25 to 28)B1+(29 to 41)	Gulf of Alaska
"	"	I1	-50 to -18; 0Wh	Banks Island leads
Mar 28	N5-2998	I1450	-50 to 0; -30B1, -10Wh	Chukchi leads
Mar 29	N5-3010	I3500	(-50 to 24)+(25 to 28)B1+(29 to 41)	Bering Sea, Pribilofs
"	"	I3501	"N4P" (see p. 114)	"
Mar 30	N5-3022	I3200	(-50 to 24)+(25 to 28)B1+(29 to 41)	Gulf of Alaska
Mar 30	N5-3023	I3800	(-50 to 24)+(25 to 28)B1+(29 to 41)	W. Bering, Pribilofs, Kamchatka
Mar 31	N5-3035	I2820	(-50 to 24)+(25 to 28)B1+(29 to 41)	Bering Sea
Apr 4	N5-3085	I2	(-50 to 0); -30B1, -10Wh	Chukchi lead
Apr 5	N5-3097	I2	(-50 to 0); -30B1, -10Wh	Chukchi lead
Apr 8	N5-3133	I2	(-50 to 24)+(25 to 28)B1+(29 to 41)	Kayak-Yakutat
"	"	"	(0 to 28)+(29 to 45)	"
Apr 8	N5-3134	I3200	(-50 to 24)+(25 to 28)B1+(29 to 41)	W. Bering ice edge eddies
Apr 15	N5-3221	I3	(-50 to 28)+(29 to 41)	S. Kamchatka
"	"	I4470	24 to 32	"
Apr 15	N5-3221	I4471	16 to 32	S. Kamchatka
"	"	I4472	(0 to 28)+(29 to 41)	"
Apr 15	N5-3221	I4473	24 to 32 rerun	S. Kamchatka
Apr 16	N5-3232	I2600	(0 to 28)+(29 to 45)	Gulf of Alaska
Apr 18	N5-3258	I2	-50 to 0; -20B1, -10Wh	Chukchi Sea
"	"	I2240	0 to 32	"
Apr 18	N5-3258	I2241	(-32 to -1)+(0 to 32)	Chukchi Sea
Apr 21	N5-3294	I2	(0 to 28)+(29 to 45)	Gulf of Alaska
Apr 23	N5-3319	I2	(0 to 28)+(29 to 45)	Prince William Sound
Apr 23	N5-3320	I3600	20 to 36	Kamchatka ice eddies
Apr 26	N5-3357	I2920	(0 to 28)+(29 to 45)	E. Bering Sea, Pribilofs

DATE	ORBIT	FRAME	TEMPERATURE (°F)	AREA
1977 Apr 27	N5-3368	I3200	(0 to 28)+(29 to 45)	Gulf of Alaska
Apr 27	N5-3369	I3000	(0 to 28)+(29 to 45)	Bering Sea/Gulf of Alaska
Apr 28	N5-3381	I2	(0 to 28)+(29 to 45)	Gulf of Alaska
May 4	N5-3455	I3100	(0 to 28)+(29 to 45)	Gulf of Alaska
May 13	N5-3566	I3000	(0 to 28)+(29 to 45)	Gulf of Alaska
May 15	N5-3591	I3200	(0 to 28)+(29 to 45)	SE Alaska
May 17	N5-3617	I3800	(0 to 28)+(29 to 45)	SW Bering Sea
"	"	I3801	24 to 41	"
May 18	N5-3628	I2820	(0 to 28)+(29 to 45)	SE Alaska
"	"	I2821	34 to 50	"
May 18	N5-3628	I2822	30 to 50	SE Alaska
May 19	N5-3642	I3	(0 to 28)+(29 to 45)	Kamchatka oceanic eddies
May 21	N5-3666	I2	(0 to 28)+(29 to 41)	Bering Sea, Norton Sound
May 26	N5-3727	I3000	34 to 50	Gulf of Alaska
May 30	N5-3777	I2	34 to 50	Gulf, Middleton upwelling
June 1	N5-3802	I2850	34 to 50	Cook Inlet, Alaska Peninsula
June 7	N5-3876	I2	34 to 50 (slightly >50F)	Gulf of Alaska
June 12	N5-3939	I3	29 to 45	Kamchatka
June 15	N5-3976	I2820	34 to 50	Upwelling St. Paul, Pribilofs
"	"	I2821	36 to 44	"
June 15	N5-3976	I2822	29 to 45	Upwelling St. Paul, Pribilofs
June 26	N5-4112	I2	28 to 60	Yukon sediments, Norton warm
June 30	N5-4161	I2725	28 to 60	Yukon sediments, eddies
"	"	"	34 to 66	S. Aleutians

DATE	ORBIT	FRAME	TEMPERATURE (°F)	AREA
1977 July 7	N5-4247	I2240	34 to 50	SE Alaska
" "	" "	" "	34 to 66	"
July 10	N5-4284	I2920	40 to 64	Gulf, Alaska Stream
July 12	N5-4310	I1560	28 to 44	Chukchi Sea
" "	" "	I1700	(28 to 52)+(53 to 70)	Interior, sand dunes
July 15	N5-4347	I1750	20 to 36	Chukchi Sea
" "	" "	I1751	32 to 48	"
July 15	N5-4347	I1850	(32 to 48)+(49 to 65)	Chukchi Sea
July 17	N5-4371	I3200	40 to 64	Gulf of Alaska
July 18	N5-4383	I3200	40 to 56	Kodiak, Alaska Stream
July 19	N5-4396	I2920	40 to 56	Pribilofs, Alaska Stream
" "	" "	I2921	(36 to 44)+(45 to 61)	"
July 22	N5-4434	I1840	32 to 48	Pribilofs, Chukchi Sea
" "	" "	I1841	(32 to 48)+(49 to 65)	"
July 28	N5-4507	I2	40 to 64	Gulf of Alaska
July 31	N5-4545	I2300	28 to 60	B. Strait, flow through smoke
" "	" "	I2301	30 to 46	"
July 31	N5-4545	I2440	34 to 66	B. Strait, flow through smoke
" "	" "	I2441	(34 to 66)+(67 to 99)	"
Aug 1	N5-4557	I2000	28 to 60	Pribilofs, Arctic coast
" "	" "	I2001	30 to 46	"
Aug 1	N5-4557	I2002	(28 to 44)+(45 to 68)	Pribilofs, Arctic coast
" "	" "	I2003	(28 to 42)+(43 to 68)	"
Aug 1	N5-4557	I2004	(28 to 40)+(41 to 68)	Pribilofs, Arctic coast
" "	" "	I2005	(28 to 44)+(45 to 60)	"
Aug 1	N5-4557	I3500	36 to 52	Pribilofs, Arctic coast
" "	" "	I3501	36 to 68	"
Aug 1	N5-4558	I3	36 to 52	Kamchatka oceanic eddies

DATE	ORBIT	FRAME	TEMPERATURE (°F)	AREA
1977 Aug 8	N5-4644	I3800	40 to 64	St. Matthew & Pribilofs
Aug 12	N5-4694	I3	40 to 64	Komandorskiy & W. Aleutians
Aug 13	N5-4706	I3	40 to 56	Amchitka upwelling
Aug 14	N5-4718	I1 0001	28 to 44	Arctic coast open
"	"	I0002	(28 to 44)+(45 to 60)	Arctic coast open
Aug 20	N5-4792	I2	40 to 56	Gulf of Alaska
"	"	I2240	40 to 64	"
Aug 21	N5-4805	I2820	40 to 56	Bering Sea, Pribilofs
Aug 23	N5-4830	I2725	40 to 56	Bering Sea
"	"	I2726	36 to 68	"
Aug 27	N5-4879	I2530	36 to 68	E. Bering Sea, St. Paul Island
"	"	I2531	(36 to 52)+(53 to 68)	"
Sept 12	N5-5077	I2240	36 to 52	Gulf→Kodiak ("noisy")
Sept 16	N5-5127	I4470	36 to 52	Kamchatka eddies
"	"	I4471	36 to 52; 37/38B1, 42/43Wh	"
Sept 17	N5-5139	I4140	36 to 52	Pribilof upwelling N. Kamchatka eddies
Sept 26	N5-5251	I4470	36 to 52	Kamchatka eddies
"	"	I4471	36 to 52; 37/38B1, 42/43Wh	"
Sept 26	N5-5251	I4472	36 to 44; 37/38B1, 42/43Wh	Kamchatka eddies
Nov 19	N5-5918	I2240	(-20 to 28)+(29 to 45)	SE Alaska
Nov 21	N5-5943	I3200	(-20 to 28)+(29 to 45)	P. William Sound, Cook Inlet
Nov 21	N5-5944	I4470	(-40 to 28)+(29 to 37)	Kamchatka
Nov 22	N5-5955	I3200	(-20 to 28)+(29 to 45)	Gulf of Alaska
Nov 22	N5-5956	I2820	(-40 to 28)+(29 to 45)	Bering Sea
Nov 23	N5-5968	I2600	(-40 to 28)+(29 to 45)	Gulf of Alaska/Bering Sea
Nov 23	N5-5969	I2820	(-40 to 28)+(29 to 45)	Bering Sea

DATE	ORBIT	FRAME	TEMPERATURE (°F)	AREA
1977 Nov 24	N5-5980	I2400	(-40 to 28)+(29 to 45)	Gulf of Alaska
Nov 24	N5-5981	I2725	(-40 to 28)+(29 to 45)	Bering Strait flow, Bristol
Nov 28	N5-6031	I4475	(-40 to 28)+(29 to 45)	Kamchatka ice/water: <<45
Nov 30	N5-6055	I2240	(-40 to 28)+(29 to 45)	Aleutians, Bristol, Karman vort.
Dec 1	N5-6067	I3600	(-40 to 28)+(29 to 45)	Gulf of Alaska cloud free
Dec 2	N5-6079	I3200	(-40 to 28)+(29 to 45)	Gulf of Alaska
Dec 3	N5-6092	I3500	(-40 to 28)+(29 to 45)	Alaska Stream
Dec 6	N5-6129	I2820	(-40 to 28)+(29 to 45)	Bristol Bay/Gulf of Alaska
Dec 10	N5-6179	I3675	(-40 to 28)+(29 to 45)	Bering Sea, Pribilofs
Dec 13	N5-6216	I3300	(-40 to 28)+(29 to 45)	Bristol Bay, Karman vortices

DATE	ORBIT	FRAME	TEMPERATURE (°F)	AREA
1978 Jan 2	N5-6463	I2400	(-40 to 28)+(29 to 45)	Gulf coast sediment or cold water
Jan 3	N5-6475	I3000	(-40 to 28)+(29 to 45)	SE Alaska, Gulf of Alaska
Jan 7	N5-6526	I3800	(-40 to 28)+(29 to 37)	Kamchatka, Bering Sea
Jan 8	N5-6538	I2000	(-40 to 28)+(29 to 37)	Bering ice edge
Jan 15	N5-6624	I3200	(-40 to 28)+(29 to 41)	Gulf of Alaska
Feb 27	N5-7156	I3000	(-20 to 28)+(29 to 41)	SE Alaska
Feb 28	N5-7168	I2725	(-20 to 28)+(29 to 41)	Gulf of Alaska
Feb 28	N5-7169	I2725	(-40 to 28)+(29 to 37)	Alaska coastline: Norton-Bristol
Mar 1	N5-7181	I2626	(-20 to 28)+(29 to 41)	Gulf of Alaska, Bristol Bay
Mar 2	N5-7194	I2820	(-40 to 28)+(29 to 37)	Bering Sea
"	"	"	(-40 to 20)+(21 to 37)	"
Mar 3	N5-7206	I2920	(-40 to 28)+(29 to 37)	Bering Sea
"	"	I2921	(-40 to 20)+(21 to 37)	"
Mar 18	N5-7392	I2240	(-40 to 4)+(5 to 37)	Bering ice; cloud free
Mar 19	N5-7404	I2530	(-40 to 4)+(5 to 37)	Bering Sea
"	"	I2531	(-40 to 28)+(29 to 37); OB1, -20Wh	"
Mar 20	N5-7417	I2530	(-40 to 28)+(29 to 37); OB1, -20Wh	Bering Sea
Mar 21	N5-7429	I2240	(-40 to 28)+(29 to 37); OB1, -20Wh	Bering Sea, Bristol ice edge
Mar 22	N5-7441	I2300	(-40 to 28)+(29 to 37); OB1, -20Wh	Bering Sea
"	"	I2301	(-20 to 19)+(20 to 36)	"
Mar 23	N5-7454	I3150	(-40 to 28)+(29 to 37); OB1, -20Wh	Bering Sea, Pribilofs, Bristol
Mar 26	N5-7491	I2920	(-20 to 28)+(29 to 37); OWh	Bering Sea
Apr 2	N5-7577	I2240	(-20 to 28)+(29 to 27); OWh	Ice edge Bristol, Alaska Stream

DATE	ORBIT	FRAME	TEMPERATURE (°F)	AREA
1978 Apr 10	N5-7676	I3400	(0 to 28)+(29 to 45) (table adjusted)	Gulf of Alaska
Apr 12	N5-7701	I2675	(0 to 28)+(29 to 45)	Gulf of Alaska
Apr 13	N5-7713	I2240	(0 to 28)+(29 to 45) water apparently colder than Apr 10, 12, 14: Rerun	Gulf of Alaska
Apr 13	N5-7713	I2241	(0 to 28)+(29 to 45) no change!	Gulf of Alaska
Apr 14	N5-7725	I3100	(0 to 28)+(29 to 45)	Gulf of Alaska
Apr 16	N5-7750	I3400	(0 to 28)+(29 to 45)	Gulf, Kodiak, Alaska Stream
Apr 18	N5-7775	I2500	(0 to 28)+(29 to 45)	Gulf, Kodiak, Alaska Stream
Apr 19	N5-7787	I3000	(0 to 28)+(29 to 45)	Gulf of Alaska, ~45°F
Apr 26	N5-7875	I2950	(0 to 28)+(29 to 45)	Bering Sea, Norton Sound
Apr 28	N5-7899	I3000	(0 to 28)+(29 to 45)	Norton Sound
May 14	N5-8097	I2400	34 to 50	Gulf of Alaska
"	"	I2401	(0 to 28)+(29 to 45)	"
May 16	N5-8122	I2300	(0 to 28)+(29 to 45)	Norton Sound
May 20	N5-8171	I2300	(0 to 28)+(29 to 45)	Gulf of Alaska
"	"	I2301	34 to 50	"
May 27	N5-8258	I2820	(0 to 28)+(29 to 45)	Norton Sound
May 27	N5-8259	I3500	(0 to 28)+(29 to 45)	Bering Strait, Gulf of Anadyr
June 7	N5-8394	I3200	34 to 50	E. Kodiak
June 11	N5-8443	I3000	34 to 50	Gulf of Alaska
"	"	I3001	34 to 66	"
June 11	N5-8443	I3002	40 to 56	Gulf of Alaska
June 20	N5-8554	I2626	34 to 66	Gulf of Alaska
July 3	N5-8716	I2626	34 to 66	Bering Strait

DATE	ORBIT	FRAME	TEMPERATURE (°F)	AREA
1978 July 6	N5-8754	I4475	34 to 50	Kamchatka eddies
"	"	I4476	34 to 66	"
July 15	N5-8865	I1540	(32 to 48)+(49 to 65)	E. Chukchi, Kotzebue Sound
July 29	N5-9037	I3000	40 to 56	Gulf of Alaska
July 30	N5-9050	I2240	40 to 56	Gulf of Alaska, Bristol Bay
"	"	I2241	40 to 64	"
July 31	N5-9062	I2820	40 to 56	Gulf of Alaska & SE Alaska
"	"	I2821	40 to 64	"
Aug 5	N5-9125	I3700	36 to 52	Pribilof Islands
Aug 6	N5-9137	I3300	40 to 64	Yukon delta, Pribilofs
Aug 15	N5-9248	I2240	40 to 64	Cook Inlet, P. William Sound
Aug 18	N5-9285	I2820	40 to 64	Gulf of Alaska
Aug 21	N5-9322	I2600	40 to 64	Gulf of Alaska
Aug 25	N5-9372	I3400	40 to 64	Kodiak Island
Sept 2	N5-9471	I2500	40 to 64	Gulf of Alaska
Sept 9	N5-9557	I2240	40 to 64	Gulf of Alaska rivers
Sept 16	N5-9644	I3400	40 to 56	Alaska Stream, Kodiak
Sept 17	N5-9656	I3000	40 to 56	Gulf coast & SE Alaska
"	"	I3001	(30 to 39)+(40 to 64)	"
Sept 23	N5-9731	I3100	40 to 56	Alaska Stream
Sept 29	N5-9805	I2240	32 to 48	Gulf of Alaska, Norton Sound
"	"	I2241	(30 to 39)+(40 to 56)	"
Oct 1	N5-9830	I3200	(30 to 39)+(40 to 56)	Norton Sound, Bristol Bay

DATE	ORBIT	FRAME	TEMPERATURE (°F)	AREA
1978 Oct 2	N5-9843	I2920	(30 to 39)+(40 to 56)	Kotzebue Sound, Bristol Bay
Nov 8	N5-10300	I3000	(0 to 28)+(29 to 45)	Gulf of Alaska, coastal sediments
"	"	I3001	(-20 to 28)+(29 to 53)	"
Nov 11	N5-10337	I2240	(0 to 28)+(29 to 45)	Kayak-Glacier Bay
"	"	I2241	(-20 to 28)+(29 to 53)	"
Nov 12	N5-10350	I4275	(-20 to 28)+(29 to 53)	Atka-Umnak, tidal mixing
Nov 17	N5-10411	I2600	(-20 to 28)+(29 to 53)	Gulf coast & SE Alaska
Dec 26	N5-10894	I2240	(-20 to 28)+(29 to 53)	P. William Sound-SE Alaska

661

DATE	ORBIT	FRAME	TEMPERATURE (°F)	AREA
1979 Jan 3	N5-10993	I2240	(-40 to 28)+(29 to 45)	Kayak Island-SE Alaska
Jan 8	N5-11056	I2530	(-40 to 28)+(29 to 37)	Bering Sea ice
Jan 9	N5-11068	I2240	(-40 to 28)+(29 to 37)	Bering Sea, open ~ Nunivak
Feb 5	N5-11402	I2200	(-60 to 28)+(29 to 37)	Bristol Bay, Pribilofs
Feb 6	N5-11415	I2600	(-60 to 28)+(29 to 37)	Bering Sea ~ St. Matthews
Feb 11	N5-11476	I3500	(-40 to 28)+(29 to 45)	Gulf of Alaska
Feb 22	N5-11612	I2240	(-40 to 28)+(29 to 45)	Gulf of Alaska, SE Alaska-Kodiak
"	"	I2241	(-40 to 28)+(29 to 37)	"
Feb 23	N5-11624	I3300	(-40 to 28)+(29 to 45)	Gulf of Alaska, SE Alaska-Kodiak
"	"	I3301	(-40 to 28)+(29 to 37)	"
Feb 25	N5-11650	I3400	(-60 to 28)+(29 to 37)	Eddies along ice edge West of St. Matthew

DATE	ORBIT	START TIME	START POINT	ZOOM/ ENLARG.	TABLE	TEMPERATURE (°C)	AREA
1979 Mar 27	TN-2334	23:18:15				2 to 12	Vancouver Island
Apr 12	TN-2560	23:54:17				(-18 to -2)+(-2 to 7)	Gulf of Alaska
Apr 22	TN-2701				N4W	0 to 13	Vancouver Island
June 30	TN-3661	01:22:50				(0 to 9)+(9 to 18)	Bering, Chukchi Sea
July 10	TN-3802	01:15:45				4 to 13	Pribilof Islands
July 11	TN-3816	01:03:45				4 to 13 (<<13)	Alaska Stream, Aleutians
July 16	TN-3886	00:14:15				(0 to 9)+(9 to 18)	Beaufort Sea coast
July 19	TN-3942	23:31:15				(0 to 9)+(9 to 18)	Beaufort coast, P. William
July 26	TN-4027	00:08:00	0896	R3	N4X	(?) 0 to 13 step	Cook Inlet
July 26	TN-4035	14:01:36	0512	R3	N4X	(?) 0 to 13 step	Cook Inlet, Kodiak
Sept 24	TN-4882	15:09:41	1024	R2	N4W	0 to 13 smooth	Cook Inlet, Kodiak
"	"	"	"	"	N4X	0 to 13 step	"
Oct 11	TN-5121	13:48:40	0256	R3	N4W, N4X	0 to 13	Kodiak
"	"	"	"	"	N4Z	(?) 3 to 12	Kodiak
Oct 11	TN-5122	15:30:28	0640	R3	N4X	(?) 0 to 13	Yukon delta
Oct 19	TN-5234	14:03:26	0512	R2	N4W, N4X	0 to 13	Cook Inlet & Kodiak
Oct 20	TN-5248	13:52:36	0384	R2	N4X	0 to 13	Cook Inlet-Yakutat
Oct 23	TN-5291	15:01:21	0384	R3	N4X	(?) 0 to 13	Yukon & Kuskokwim delta
"	"	15:02:11	1024	R3	N4X	0 to 13	Bristol Bay
Oct 24	TN-5305	14:53:46	0640	R2	N4W, N4X	0 to 13	S. Kodiak & Bristol Bay
Oct 27	TN-5347	14:19:19	0256	R2	N4W, N4X	0 to 13	S. Kodiak & Bristol Bay
Oct 28	TN-5353	00:13:16	0896	R2	N4W, N4X	0 to 13	S. Kodiak & Bristol Bay
Nov 5	TN-5474	14:21:00	0930	R2	N4X	0 to 13	Gulf of Alaska

DATE	ORBIT	START TIME	START POINT	ZOOM/ ENLARG.	TABLE	TEMPERATURE (°C)	AREA
1979 Nov 11	N6-1940	03:12:28	0896	R2	64W	0 to 13 smooth	Queen Charlotte Sound
"	"	"	"	R2	64X	0 to 13 step	"
Nov 13	TN-5587	14:36:09	0512	R2	N4W, N4X	0 to 13	Kodiak & Bristol Bay
Nov 14	TN-5593	00:31:25	0640	R2	N4W, N4X	0 to 13	Alaska Current
Nov 14	TN-5601	14:25:00	0512	R2	N4W, N4X	0 to 13	Alaska Current→Kodiak
Nov 15	TN-5607	00:20:19	0640	R2	N4W, N4X	0 to 13	Kodiak
Nov 16	N6-2020	18:34:36	0512	R2	64W, 64X	0 to 13	Montague Island
Nov 26	TN-5770	13:55:23	0123/4	R2	N4W, N4X	0 to 13	Kodiak
Nov 26	N6-2162	18:19:21	0257/8	R2	64W, 64X	0 to 13	Kodiak
Dec 3	N6-2254	05:20:58	0257/8	R2	64W, 64X	0 to 13	Kodiak
Dec 5	N6-2290	18:24:48	0384	R2	64W, 64X	0 to 13	Kodiak-Montague
Dec 11	TN-5974	00:39:07	0123/4	R2	N4W, N4X	0 to 13	Kodiak
Dec 11	TN-5982	14:33:05	0893/4	R2	N4W, N4X	0 to 13	Kodiak-P. William Sound
"	"	14:34:05	0893/4	R2	N4W, N4X	0 to 13	Kodiak
Dec 13	TN-6010	14:11:18	0123	R2	N4W	0 to 13	Kodiak-P. William Sound
"	"	"	1023	R2	N4W	0 to 13	Cordova-Yakutat
Dec 13	TN-6010	14:11:18	0124	R2	N4X	0 to 13	Kodiak-P. William Sound
"	"	"	1024	R2	N4X	0 to 13	Cordova-Yakutat
Dec 13	TN-6011	15:52:41	0123/4	R2	N4W, N4X	0 to 13	St. Matthew
"	"	"	1023/4	R2	N4W, N4X	0 to 13	Bristol Bay
Dec 14	TN-6025	15:40:01	0	--	N4P*		St. Matthew, Bering
"	"	15:40:02	0	--		(-45 to -1)+(0 to 5)	St. Matthew, Bering
Dec 14	TN-6025	15:40:06	0	--		(-45 to -3)+(-2 to 5)	St. Matthew, Bering
"	"	15:40:05	0	--		(-45 to -4)+(-3 to 5)	St. Matthew, Bering

* N4P = (-45 to -5)+(-5 to -4)+(-4 to -3.5)+(-3.5 to -3)+(-3 to -2)+(-2 to -1.5)+(-1.5 to -1)+(-1 to 5)

64P	000	250	052	156	208	104	255	000	255
	WH	BL	LLG	DG	DDG	LG	BL	WH	BL
	white	black	light light grey	dark grey	dark dark grey	light grey	black	white	black

DATE	ORBIT	START TIME	START POINT	ZOOM/ ENLARG.	TABLE	TEMPERATURE (°C)	AREA
1979 Dec 14	TN-6025	15:40:04	0	--		(-45 to -5)+(-4 to 5)	St. Matthew, Bering
"	"	15:40:03	0	--		(-45 to -6)+(-5 to 5)	St. Matthew, Bering
Dec 14	TN-6025	15:40:07	DY348	STRECH	N4P*		St. Matthew, Bristol
Dec 15	TN-6031	01:36:31	0	--	N4P		St. Matthew, Bering
"	"	01:36:32	0	--		(-51 to -1)+(0 to 5)	St. Matthew, Bering
Dec 16	TN-6053	15:17:51	0	--	N4P		St. Matthew, Bering
"	"	15:17:52	0	--		(-51 to -1)+(0 to 5)	St. Matthew, Bering
Dec 17	TN-6067	15:08:48	0004	R2	N4Y	-3 to 10 smooth	St. Matthew
"	"	"	0003	R2	N4Z	-3 to 10 step	St. Matthew
Dec 17	TN-6067	15:07:03	0001	R2	N4P		Bering Strait
"	"	15:08:48		R2	N4P		St. Matthew
Dec 18	TN-6073	01:04:01	0	--	N4P		St. Matthew, Bering
"	"	01:04:02	0	--		(51 to -1)+(0 to 5)	St. Matthew, Bering
Dec 18	TN-6073	01:03:33	0	--	N4R	(-11 to -1); 0Wh, >OLG	St. Matthew, Bristol
"	"	01:03:34	DY352	STRECH	N4P		St. Matthew, Bristol
Dec 23	N6-2538	04:47:28	0767/8	R2	64Y, 64Z	-3 to 10	Kodiak
Dec 30	N6-2638	05:38:24	0384	R2	64P		Norton, St. Lawrence
"	"	05:36:43	0384	R2	64P		Bristol Bay
Dec 31	TN-6256	00:22:20	0763/4	R3	N4Y, N4Z	-3 to 10	N. Kodiak
"	"	00:22:05	0123/4	R3	N4Y, N4Z	-3 to 10	P. William-Cross Sound
Dec 31	TN-6256	00:20:50	0003/4	R3	N4Y, N4Z	-3 to 10	SE Alaska
Dec 31	N6-2660	19:03:18	0513/4	R3	64Y, 64Z	-3 to 10	Bristol Bay
"	"	"	0512	R3	?		Bristol Bay

DATE	ORBIT	START TIME	START POINT	ZOOM/ ENLARG.	TABLE	TEMPERATURE (°C)	AREA
1980 Jan 1	TN-6270	00:11:18	0893/4	R3	N4Y, N4Z	-3 to 10	North Kodiak
"	"	00:11:03	0383/4	R3	N4Y, N4Z	-3 to 10	Prince William
Jan 1	TN-6270	00:11:18	0896	R3	N4P*		Cook Inlet
Jan 2	TN-6293	15:34:50	0640	R2	N4P		Nunivak, ice edge
Jan 2	N6-2688	18:19:05	0127/8	R2	64Y, 64Z	-3 to 10	Kodiak
"	"	"	0128	R2	64P*		Kodiak
Jan 3	TN-6312	23:37:57	1024	R2	N4P		Prince William Sound
Jan 8	TN-6377	14:28:19	0763/4	R2	N4Y, N4Z	-3 to 10	Kodiak
"	"	14:28:49	0003/4	R2	N4Y, N4Z	-3 to 10	Bristol, Kodiak
Jan 8	TN-6377	14:27:41	0	--	NMA	(-45 to -2)+(-1 to 7)	Gulf, Alaska Current
"	"	14:28:19	0768	R2	N4P		Kodiak
Jan 9	N6-2779	03:39:28	0897/8	R2	64Y, 64Z	-3 to 10	Cook Inlet-Cross Sound
"	"	03:37:43	0647/8	R2	64Y	-3 to 10	SE Alaska-BC coast
Jan 9	N6-2780	05:20:59	0128	R3	64P		Cook Inlet
Jan 10	TN-6397	00:11:51	0	--	NMA	(-45 to -2)+(-1 to 7)	Gulf of Alaska
Jan 10	TN-6405	14:06:17	0384	R3	N4P		Cook Inlet
Jan 10	TN-6406	15:47:02	0001	R2	N4P		Ice edge, St. Matthew
"	"	15:47:17	0896	R2	N4P		Ice edge, Bristol
Jan 10	TN-6406	15:46:21	0	--	N4P		Bering, St. George eddy
"	"	15:46:22	0	--	NMC	(-45 to -1)+(0 to 5)	Bering, St. George eddy
Jan 11	TN-6412	01:42:21	0	--	N4P		Bering, St. George eddy
"	"	01:42:22	0	--	NMC	(-45 to -1)+(0 to 5)	Bering, St. George eddy
Jan 11	TN-6420	15:36:21	0	--	N4P		Bering Sea
"	"	15:36:22	0	--	NMC	(-45 to -2)+(-1 to 5)	Bering Sea
Jan 12	N6-2822	04:15:35	1024	R3	64P		Cook Inlet
Jan 16	N6-2888	19:55:56	0256	R3	64P		Ice edge, St. Matthew
"	"	"	0896	R3	64P		Ice edge, Nunivak

* N4P = (-45 to -5)+(-5 to -4)+(-4 to -3.5)+(-3.5 to -3)+(-3 to -2)+(-2 to -1.5)+(-1.5 to -1)+(-1 to 5)
64P 000 250 052 156 208 104 255 000 255
 WH BL LLG DG DDG LG BL WH BL

DATE	ORBIT	START TIME	START POINT	ZOOM/ ENLARG.	TABLE	TEMPERATURE (°C)	AREA
1980 Jan 17	TN-6505	16:10:46	0256	R2	N4P		Ice edge, W. Bering
"	"	"	1024	R2	N4P		Central Bering
Jan 21	N6-2959	19:47:35	0256	R3	64P		Ice edge @ St. Matthew
"	"	"	0896	R3	64P		Ice edge, E. Bering
Jan 21	N6-2959	19:47:35	1280	R3	64P		Bristol Bay
Jan 22	N6-2973	19:24:31	0001	R2	64P		St. Lawrence, Norton
"	"	19:26:01	0001	R2	64P		Nunivak, Pribilofs
Jan 22	N6-2973	19:24:31	0896	R2	64P		SW Alaska
"	"	19:26:01	0896	R2	64P		Bristol, Kodiak
Jan 23	N6-2979	05:16:09	0896	R2	64P		Bristol, Nunivak
"	"	"	0001	R2	64P		Kodiak, Alaska Current
Jan 23	N6-2987	19:03:10	1027/8	R2	64Y, 64Z	-3 to 12	Prince William Sound
Jan 25	N6-3007	04:31:43	0133/4	R2	64Y, 64Z	-3 to 12	Prince William→SE Alaska
Jan 26	N6-3021	04:09:44	0133/4	R2	64Y, 64Z	-3 to 12	Prince William→SE Alaska
Jan 28	N6-3058	18:55:38	0256	R2	64P		Bristol, S. Kodiak
"	"	18:54:38	1024	R3	64P		Cook Inlet-Prince William
Jan 29	N6-3072	19:38:27	0001	R2	64P		Bristol Bay, Kodiak
"	"	18:35:50	0640	R2	64P		Cook Inlet, Kodiak
Jan 30	N6-3087	19:51:27	0128	R2	64P		St. Lawrence-St. Matthew
"	"	19:51:42	1024	R2	64P		Bristol Bay
Jan 31	N6-3093	05:42:01	0	--	64P		Bering Sea
"	"	05:43:30	0384	R2	64P		Norton Sound-Nunivak
Jan 31	N6-3093	05:42:45	0384	R2	64P		Bristol Bay
Jan 31	N6-3101	19:30:05	0512	R2	64P		Bristol Bay, Pribilofs
Feb 5	TN-6773	16:03:23	0128	R2	N4P		Olyutorskiy-St. Matthew
"	"	16:03:23	1024	R2	N4P		St. Matthew Island
Feb 13	N6-3285	18:06:15	0256	R2	64P		Prince William Sound

DATE	ORBIT	START TIME	START POINT	ZOOM/ ENLARG.	TABLE	TEMPERATURE (°C)	AREA
1980 Feb 14	N6-3291	03:54:52	0	--	6MA	(-45 to -2)+(-1 to 7)	P. William-Vancouver Isl.
Feb 14	N6-3299	17:45:11	0123	R2	N4Y	-3 to 12 smooth	Yakutat
"	"	"	1023/4	R2	N4Y, N4Z	-3 to 12	Queen Charlotte Island
Feb 15	N6-3305	03:33:32	0	--	6MA	(-45 to -2)+(-1 to 7)	P. William-Vancouver Isl.
Feb 15	N6-3313	17:22:02	0	--	6MA	(-45 to -2)+(-1 to 7)	SE Alaska
Feb 18	N6-3356	17:58:15	0256	R3	64P*		Cook Inlet-Prince William
Feb 19	TN-6970	15:08:18	0001	R2	N4P*	TN IR sensors ~2°C off	Norton Sound-St. Matthew
Feb 20	TN-6976	01:05:49	1024	R2	N4P		St. Lawrence Island
"	"	01:04:39	1024	R2	N4P		Bristol Bay
Feb 20	TN-6976	01:04:01	0	--	NME†		Bering Sea
Feb 26	TN-7069	15:31:33	0128	R2	N4P		St. Lawrence Island
"	"	"	1024	R2	N4P		E. Norton, N. Bristol
Feb 26	TN-7069	15:33:34	0128	R2	N4P		Pribilof Islands
"	"	"	1024	R2	N4P		Bristol Bay
Feb 26	TN-7069	15:31:01	0	--	NME		Bering Sea
Feb 26	N6-3471	20:03:21	0	--	6ME†		Bering ice edge
Feb 27	N6-3477	01:29:34	0640	R2	?		St. Lawrence Island
"	"	01:27:03	0512	R2	?		Bristol Bay
Feb 27	N6-3477	05:55:11	0	--	6ME		Bering Sea
Feb 27	N6-3485	19:41:31	0	--	6ME		Bering Sea, Pribilofs
Feb 29	TN-7111	14:58:25	1152	R3	N4L**	"cloud top table"	Cook, Prince William
"	"	"	1152	R3	N4P		Cook, Prince William

* N4P = (-45 to -5)+(-5 to -4)+(-4 to -3.5)+(-3.5 to -3)+(-3 to -2)+(-2 to -1.5)+(-1.5 to -1)+(-1 to 5)
64P 000 250 052 156 208 104 255 000 255
WH BL LLG DG DDG LG BL WH BL

† NME = (-45 to -5)+(-5 to -4)+(-4 to -3.5)+(-3.5 to -3)+(-3 to -2)+(-2 to -1.5)+(-1.5 to -1)+(-1 to 7)
6ME 000 250 052 156 208 104 255 000 255
WH BL LLG DG DDG LG BL WH BL

**N4L = (-35 to -35)+(-35 to -21)+(-21 to -21)+(-21 to -14)+(-14 to -14)+(-14 to -4)+(-4 to -4)
255 050 050 165 165 100 100 000

DATE	ORBIT	START TIME	START POINT	ZOOM/ ENLARG.	TABLE	TEMPERATURE (°C)	AREA
1980 Mar 5	N6-3585	20:30:46	1024	R2	64P		Bristol Bay
Mar 9	N6-3641	19:02:45	1152	R3	64P		Cook-Prince William
Mar 10	TN-7252	14:48:11	1152	R3	N4Y, N4Z	-3 to 12	Prince William Sound
Mar 12	N6-3684	19:37:15	0128	R2	64P		Norton-St. Lawrence
"	"	"	1024	R2	64P		N. Bristol Bay
Mar 12	N6-3684	19:39:00	0128	R2	64P		Pribilof Islands
"	"	"	1024	R2	64P		Bristol Bay
Mar 17	N6-3746	04:01:53	1280	R3	64P		Cook Inlet
Mar 19	TN-7371	00:55:58	0007/8	R3	N4Y, N4Z	-3 to 12	Cook-Prince William
Mar 19	N6-3775	04:57:58	0256	R3	64Y	-3 to 12	Cook-Prince William
"	"	"	0256	R3	64P		Cook-Prince William
Mar 26	N6-3883	19:31:45	0	--	64P		Norton, St. Lawrence
Mar 28	N6-3911	18:48:32	0648	R2	64Z	-3 to 12 step	N. Kodiak
Apr 3	TN-7590	14:44:04	0768	R2	N4Z	-3 to 12 step	SE Alaska
Apr 4	N6-4011	19:36:21	0750	R2	6ME		Bristol Bay
Apr 7	TN-7639	00:47:36	0768	R2	N4P		Norton Sound-Point Hope
Apr 8	N6-4068	19:48:01	0	--	6ME		E. Bering Sea
Apr 9	TN-7667	00:22:12	0124	R3	N4Z	-3 to 12 step	SE Alaska
Apr 10	TN-7681	00:11:32	0512	R4	N4Y	-3 to 12 smooth	Cook Inlet-Yakutat
Apr 10	N6-4096	19:04:21	0	--	6ME		E. Bering Sea
Apr 11	N6-4102	04:55:11	0	--	6ME		E. Bering Sea
Apr 18	N6-4210	19:28:51	0	--	64P		E. Bering Sea
"	"	19:30:36	0780	R2	6MB	-4 to 4	Bristol Bay
May 5	N6-4452	19:58:19	1027/8	R2	N4Y, N4Z	-3 to 12	Bristol Bay
May 8	N6-4494	18:51:20			6MA	(-45 to -2)+(-1 to 7)	Bristol Bay

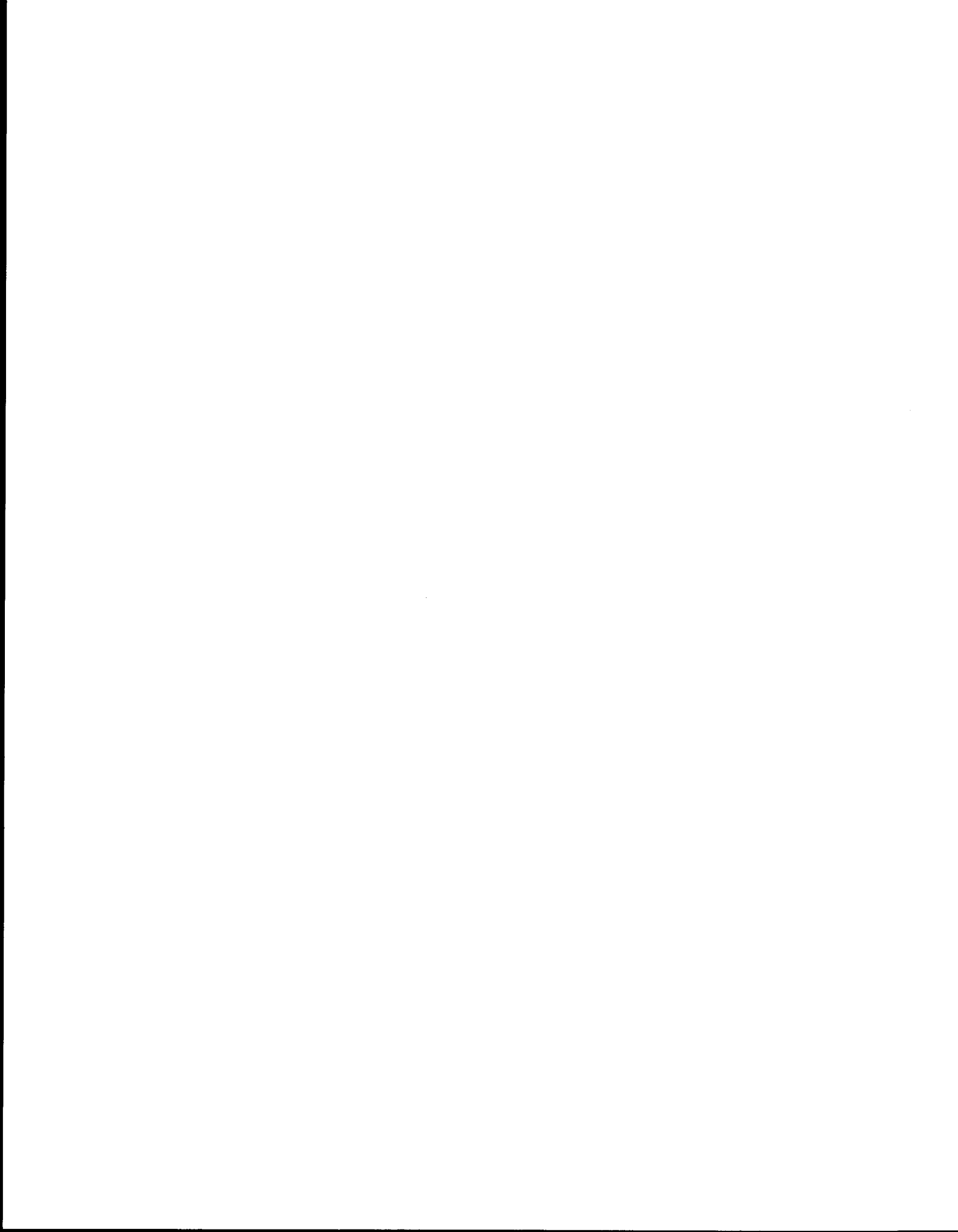
DATE	ORBIT	START TIME	START POINT	ZOOM/ ENLARG.	TABLE	TEMPERATURE (°C)	AREA
1980 May 9	N6-4508	18:30:00	900	R2	6MA	(-45 to -2)+(-1 to 7)	Gulf of Alaska
May 10	N6-4514	04:18:20	0	--	6MA	(-45 to -2)+(-1 to 7)	Kayak Isl.→Q. Charlotte Sound
May 15	N6-4585	04:09:34	0001	R2	64X	0 to 14 step	SE Alaska
May 20	N6-4665	19:29:26	0256	R2	64X	0 to 14 step	Bristol Bay
May 21	N6-8260	00:57:44	0800	R2	N4P		Bering Strait
May 26	TN-8344	23:44:50	0128	R2	N4X	0 to 14 step	Q. Charlotte Island
"	"	23:46:35	0128	R2	N4Z	0 to 14 step	SE Alaska
June 1	N6-4835	18:25:28	0512	R2	64V	3 to 16 step	Kayak Island→N. Kodiak
"	"	"	"	R2	64W, 64X	0 to 14	Kayak Island→N. Kodiak
June 2	N6-4849	18:03:09	1024	R2	64X	0 to 14 step	SE Alaska
June 5	TN-8479	13:40:00	0128	R2	N4X	0 to 14 step	Gulf of Alaska
"	"	"	1024	R2	N4X	0 to 14 step	SE Alaska
June 8	TN-8514	00:53:34	0512	R2	N4X	0 to 14 step	Kodiak, Bristol Bay
June 9	N6-4949	18:49:37	1152	R3	64V	3 to 16 step	Prince William Sound
June 15	N6-5035	19:54:40	0	--	64P		Chukchi Sea-Prudhoe Bay
June 16	N6-5049	19:33:23	0	--	64P		Chukchi Sea-Barter Island
June 23	N6-5140	04:54:20	0512	R2	64V	3 to 16 step	S. Kodiak, N. Bristol Bay
June 23	TN-8739	23:32:45	0896	R2	N4X	0 to 14 step	Kayak Island-Cape Spencer
June 24	TN-8753	23:19:06	0768	R2	N4W, N4X	0 to 14	Queen Charlotte Island
"	"	23:20:49	"	R2	N4X	0 to 14 step	Yakutat-SE Alaska
June 24	TN-8753	23:21:06	0768	R2	N4W	0 to 14 smooth	Yakutat-SE Alaska
June 28	TN-8796	00:28:23	0700	R2	N4V	3 to 16 step	Kodiak
July 2	N6-5267	03:19:15	1024	R2	64T	"thunderstorm table"	North Slope clouds
July 3	TN-8880	23:20:51	0224	R2	N4T	"thunderstorm table"	Clouds around Great Bear Lake

DATE	ORBIT	START TIME	START POINT	ZOOM/ ENLARG.	TABLE	TEMPERATURE (°C)	AREA
1980 July 9	N6-5368	05:42:20	--	--	6MA	(-45 to -2)+(-1 to 7)	SE Bering Sea
July 11	N6-5405	20:23:25	--	--	64Z	3 to 12 step	Bering Strait
July 18	N6-5504	19:29:00	--	--	64Z	3 to 12 step	Bering Sea
July 19	N6-5518	19:08:15	--	--	64V	3 to 16 step	Norton Sound, Bristol Bay
"	"	19:06:59	--	--	64Z	3 to 12 step	Bering Sea
July 19	N6-5519	20:47:12	--	--	64Z	3 to 12 step	Bering Strait
July 20	TN-9107	01:23:40	--	--	N4U, N4V	3 to 16	Bering Strait
"	"	01:21:25	--	--	N4V	3 to 16 step	Bristol Bay
July 20	N6-5532	18:47:11	--	--	64V	3 to 16 step	Bristol Bay, Kodiak
July 21	TN-9121	01:11:56	0768	R2	N4V	3 to 16 step	Norton, Nunivak
"	"	01:10:00	0512	R2	N4V	3 to 16 step	Bristol Bay, Kodiak
July 21	N6-5547	20:04:13	--	--	64V	3 to 16 step	Bristol Bay
July 22	N6-5553	05:56:20	--	--	64V	3 to 16 step	Bering Sea
July 22	N6-5561	19:42:30	--	--	64V	3 to 16 step	Bering Sea
July 23	N6-5567	05:34:15	--	--	64V	3 to 16 step	Bering Sea
July 23	N6-5575	19:18:51	--	--	64Z	-3 to 12 step	Chukchi Sea
July 24	N6-5589	18:59:00	--	--	64V	3 to 16 step	Bristol Bay
July 25	N6-5596	06:28:50	--	--	64V	3 to 16 step	SE Bering Sea
July 28	TN-9233	23:36:02	0256	R2	N4V	3 to 16 step	Vancouver Island
July 29	TN-9234	01:23:32	0256	R2	N4Z	-3 to 12 step	Chukchi Sea
July 30	N6-5675	20:04:43	--	--	N4P		Chukchi Sea
Aug 3	N6-5731	18:38:56	0128	R2	64U, 64V	3 to 16	Cook Inlet, Kodiak
"	"	"	1024	R2	64U	3 to 16 smooth	Prince William
Aug 4	N6-5745	18:16:38	0768	R2	64V	3 to 16 step	Prince William-Yakutat
Aug 5	N6-5759	17:54:31	0128	R2	64V	3 to 16 step	Prince William-Yakutat
"	"	"	1024	R2	64V	3 to 16 step	SE Alaska

DATE	ORBIT	START TIME	START POINT	ZOOM/ ENLARG.	TABLE	TEMPERATURE (°C)	AREA
1980 Aug 11	N6-5844	17:22:06	0500	R2	64U, 64V	3 to 16	SE Alaska
Aug 19	TN-9538	14:35:43	0640	R2	N4U, N4V	3 to 16	Gulf of Alaska
Aug 21	N6-5988	20:20:30	--	--	64V	3 to 16 step	Bering and Chukchi Sea
Aug 22	N6-6002	20:00:00	--	--	64V	3 to 16 step, Stretch	SE Bering Sea
Aug 23	N6-6015	17:55:20	--	--	64Z	-3 to 12 step, Stretch	Cook-Yakutat
Aug 23	N6-6016	19:34:19	--	--	64P*		Beaufort Sea coast
"	"	19:38:10	--	--	64X	0 to 14 step, Stretch	SE Bering Sea
Aug 24	N6-6030	19:16:00	--	--	64X	0 to 14 step, Stretch	SE Bering Sea
Aug 25	TN-9615	01:14:51	0128	R2	N4V	3 to 16 step	Bristol-Prince William
"	"	"	1024	R2	N4V	3 to 16 step	Bristol, Pribilofs
Aug 25	N6-6036	05:05:30	--	--	64X	0 to 14 step, Stretch	Bristol, Alaska Peninsula
Aug 25	N6-6044	18:54:00	--	--	64X	0 to 14 step, Stretch	Kodiak
Aug 26	TN-9629	01:03:44	0128	R2	N4V	3 to 16 step	Kodiak-P. William
Sep 1	TN-9727	23:42:58	0768	R2	N4V	3 to 16 step	Prince William-SE Alaska
Sep 2	N6-6149	03:48:56	0768	R2	64V	3 to 16 step	Prince William-SE Alaska
Sep 9	N6-6258	20:00:01	--	--	6ME†		Norton Sound, Chukchi
Sep 9	TN 9840	23:56:42	0896	R2	N4Z	-3 to 12 step	Chukchi Sea
Sep 10	N6-6272	19:36:45	--	--	64P*		Chukchi Sea
Sep 12	N6-6299	17:15:35	--	--	64X	0 to 14 step	SE Alaska

*N4P = (-45 to -5)+(-5 to -4)+(-4 to -3.5)+(-3.5 to -3)+(-3 to -2)+(-2 to -1.5)+(-1.5 to -1)+(-1 to 5)
64P 000 250 052 156 208 104 255 000 255
WH BL LLG DG DDG LG BL WH BL

†NME = (-45 to -5)+(-5 to -4)+(-4 to -3.5)+(-3.5 to -3)+(-3 to -2)+(-2 to -1.5)+(-1.5 to -1)+(-1 to 7)
6ME 000 250 052 156 208 104 255 000 255
WH BL LLG DG DDG LG BL WH BL



APPENDIX II

NOAA VHRR DIGITIZED TAPES SAVED
(September 1980)

...the first of the ...

...the second of the ...

...the third of the ...

...the fourth of the ...

...the fifth of the ...

...the sixth of the ...

...the seventh of the ...

...the eighth of the ...

...the ninth of the ...

...the tenth of the ...

...the eleventh of the ...

...the twelfth of the ...

...the thirteenth of the ...

...the fourteenth of the ...

...the fifteenth of the ...

...the sixteenth of the ...

...the seventeenth of the ...

...the eighteenth of the ...

NOAA VHRR DIGITIZED TAPES SAVED

(September 1980)

DATE	GMT	ORBIT #	EQUATOR CROSSING	COMMENTS	ENLARGEMENT Δ IR*	STORAGE**
		<u>N3</u>				
9/ 8/74	21:28	3795 IR	7W	Good Arctic Ocean ice edge; maximum ice retreat; cold water west Bering Strait; Yukon sediment plume; warm current northwest Barrow		A
9/ 8/74	21:28	3795 VIS			A	
10/22/74	20:50	4340 IR	2E	Warm current east Bering Strait	Δ IR	A
11/ 9/74	20:40	4563 VIS	5E	Most of Aleutians clear; Carman vortices		A
11/26/74	21:16	4774 IR	4W	Good ice; frozen east of line: Cape Point Wales - east St. Lawrence - west Nunivak	Δ IR	A
		<u>N4</u>				
12/28/74	21:40	0541 IR	9W	Bering Strait, Bering Sea clear		A
12/31/74	20:37	0578 IR	7E	Bering Strait; Alaska Pen- insula; Illiamna freeze-up	2.5	A
1/29/75	22:17	0942 IR	18W	Chukchi/Beaufort, Arctic leads		A
2/ 8/75	04:26	1058 IR	113W	Night IR; clear Cook Inlet - Seattle		A
3/ 5/75	19:55	1379 IR	18E	Bristol Bay, west Gulf of Alaska clear	Δ IR	A
3/14/75	20:30	1492 IR	9E	Cook Inlet; Beaufort leads	Δ IR	A
3/19/75	21:15	1555 IR	2W	Bering/Beaufort, clear, very good		A
4/ 3/75	19:41	1742 IR	22E	Gulf of Alaska	Δ IR	A
4/ 3/75	19:41	1742 VIS				A

* Temperature enhancement.

**Storage: A - Geophysical Institute Archives Room 118, Shelf 151.
GEO - Geophysical Institute (Jayaweera).
IWR - Institute of Water Resources (Seifert).

DATE	GMT	ORBIT #	EQUATOR CROSSING	COMMENTS	ENLARGEMENT ΔIR*	STORAGE**
<u>AIDJEX TAPES</u>						
		<u>N4</u>				
4/13/75	21:10	1868 IR	1W	First Convair 990 flight.		A
4/13/75	21:10	1868 VIS		New floebergs(?) east Wrangel		A
4/16/75	21:58	1906 IR	13W	Convair to Greenland. Bering		A
4/16/75	21:58	1906 VIS		Sea ice edge clear, motion around floeberg		A
4/17/75	21:00	1918 IR	2E	New floebergs. Ice movement		A
4/17/75	21:00	1918 VIS		through Bering Strait		A
4/19/75	20:55	1943 IR	3E	Convair 990 return from Green-		A
4/19/75	20:55	1943 VIS		land, Beaufort Sea cloudy		A
4/21/75	20:50	1968 IR	4E	Convair flight, KA aboard,	ΔIR	A
				AIDJEX camp cloudy		
4/21/75	22:43	1969 IR	25W			A
4/21/75	22:43	1969 VIS				A
4/22/75	17:57	1979 IR	48E	Convair flight		A
4/22/75	19:51	1980 IR	19E	Interior and Prince William		A
4/22/75	19:51	1980 VIS		clear, Arctic cloudy		A
4/23/75	20:45	1993 IR	5E	Cook Inlet, Prince William,		A
4/23/75	20:45	1993 VIS		north Bristol Bay. Eye in Karman vortices		A
4/24/75	19:46	2005 IR	20E	Convair flight, KA on board;	ΔIR	A
				Gulf clear		
4/24/75	21:39	2006 IR	8W			A
4/24/75	21:39	2006 VIS				A
4/26/75	21:35	2031 IR	7W	Convair flight. Bering Sea		A
4/26/75	21:35	2031 VIS		clear, Beaufort Sea partly clear		A
4/29/75	20:31	2068 IR	9E	Open north Bristol Bay, partly clear Interior and Bering Sea		IWR
5/ 1/75	20:27	2093 IR	10E	Open south of land areas in Bering Sea		IWR
5/ 8/75	21:05	2181 IR	0E	Clear: East central Bering Sea.		IWR
5/ 8/75	21:05	2181 VIS		Polynya west Banks Island, ice patch Bristol Bay		IWR

DATE	GMT	ORBIT #	EQUATOR CROSSING	COMMENTS	ENLARGEMENT Δ IR*	STORAGE**
5/10/75	21:00	<u>N4</u> 2206 IR	1E	Bering Sea mainly cloudy, Beaufort Sea transparent clouds		IWR
5/11/75	20:01	2218 IR	16E	Interior clear, open along Barrow-Point Hope coast		A
5/12/75	20:55	2231 IR	3E	Bering Sea partly clear,		IWR
5/12/75	20:55	2231 VIS		wide polynya Barrow-Point Hope		IWR
5/13/75	19:56	2243 IR	18E	Interior to Brooks clear, Beaufort Sea thin clouds		IWR
5/14/75	20:50	2256 IR	4E	Most of Alaska clear, Bering	1:3.7	IWR
5/14/75	20:50	2256 VIS		Sea cloudy, polynya Barrow- Point Hope		IWR
5/16/75	20:46	2281 IR	5E	Clear Barrow polynya and Bering Sea coastal water	Δ IR 1:3.7	A
5/19/75	21:35	2319 IR	7W	Only north Gulf of Anadyr partly clear		GEO
5/20/75	20:36	2331 IR	8E	Northwest Alaska clear.		IWR
5/20/75	20:36	2331 VIS		West Barrow - Point Hope polynya		IWR
5/22/75	20:31	2356 IR	9E	\sim 100 km wide clear area Nunivak-Unalaska	Δ IR 1:3.7	GEO
5/23/75	19:32	2368 IR	24E	Gulf of Alaska and Cook Inlet clear		IWR
5/24/75	20:26	2381	10E	Yukon-Anvik river flooding		IWR
5/25/75	21:21	2394	4W	Bering Sea cloudy		IWR
5/27/75	21:16	2419	2W	East Norton Sound clear		IWR
5/29/75	21:12	2444	1W	Flooding Yukon river delta	Δ IR 1:3.7	IWR
5/31/75	21:06	2469 IR	0E	Ice flow along east Bering Sea	1:3.7	A
6/ 1/75	20:07	2481 IR	15E	Northwest Alaska clear, floes in Banks Island polynya		IWR
6/ 2/75	21:01	2494 IR	1E	Norton Sound and east Bering		IWR
6/ 2/75	21:01	2494 VIS		Strait clear		IWR

DATE	GMT	ORBIT #	EQUATOR CROSSING	COMMENTS	ENLARGEMENT ΔIR*	STORAGE**
6/ 5/75	21:50	^{N4} 2532 IR	11W	Clear north St. Lawrence	ΔIR 1:3.7	A
6/ 6/75	20:55	2544	4E	Clear and open south facing coasts and north Bering Sea		IWR
6/ 9/75	21:40	2582 IR	9W	Bering Sea (St. George open, St. Paul ice)		A
6/10/75	20:41	2594 IR	6E	Bering Sea ice patch-east Lawrence-Yukon Delta-west Nunivak-St. Mathew Island	ΔIR 1:3.7	GEO
6/16/75	20:28	2669 IR	10E	Clear west Banks Island		GEO
6/22/75	20:13	2744 IR	14E	Cloudy		GEO
6/24/75	20:09	2769 IR	15E	Temperature structure in North waters, clear around Kodiak Island, Cook Inlet and Canadian Archipelago, east Beaufort Sea good	ΔIR	A
6/25/75	21:03	2782 IR	1E	Sharp, clear broken ice in east Beaufort Sea. Large lead Banks Island-Ellesmere		A
6/27/75		2807 IR	2E	Arctic clouds		GEO
7/ 3/75	20:42	2882 IR	6E	Hot spots north of Galena and on Seward Peninsula >75°F. Norton Sound clear	ΔIR	A
7/ 5/75	20:38	2907 VIS	7E	North Bering Strait, head of Norton Sound and Bristol Bay clear	ΔIR	IWR
7/ 6/75	19:39	2919 VIS	22E	Interior clear (dark)		IWR
7/ 6/75	21:32	2920 IR	7W	Arctic coast clear, "floeberg"		GEO
7/ 6/75	21:32	2920 VIS				IWR
7/ 7/75	20:32	2932 IR	9E	Open Mackenzie mouth-Banks Island	1:3.7	A
7/ 7/75	20:32	2932 VIS				IWR
7/10/75	19:28	2969 IR	25E	Gulf of Alaska clear	ΔIR	A
7/15/75	20:13	3032 VIS	13E	(print missing)		IWR

DATE	GMT	ORBIT #	EQUATOR CROSSING	COMMENTS	ENLARGEMENT Δ IR*	STORAGE**
7/18/75	21:02	<u>N4</u> 3070 VIS	1E	Beaufort Sea, Chukchi Sea, Norton Sound clear		IWR
7/19/75	20:03	3082 VIS	16E	North Slope clear		IWR
7/20/75	20:57	3095 IR	2E	North Bering Sea clear		GEO
7/22/75	20:52	3120 IR	3E	North Bering Sea and north- west Arctic coast clear; open to Barrow; (to McClain)	Δ IR	A
7/22/75	20:52	3120 VIS			1:3.7	IWR
7/23/75	19:53	3132 IR	18E	North Slope clear		GEO
7/23/75	05:13	3137 IR	125W	Bering Sea clear		A
7/24/75	20:47	3145 IR	5E	Bering Sea clear	Δ IR	A
7/24/75	20:47	3145 VIS				IWR
7/25/75	21:41	3158 IR	9W	Bering Sea clear	Δ IR	A
7/25/75	21:41	3158 VIS				IWR
7/27/75	19:44	3182 IR	21E	East Kodiak Island clear	Δ IR	A
7/28/75	22:30	3196 IR	22W	Kamchatka Volcanoe erup- tion (first seen July 9) Smoke plume 174 km (860 km)	1:2.5	IWR
7/28/75	22:30	3196 VIS				IWR
7/31/75	21:28	3233 IR	5W	Norton Sound, Gulf of Anadyr clear		GEO
8/ 2/75	21:23	3258 IR	4W	East Aleutians, north Bering Strait clear	Δ IR	A
8/ 4/75	19:25	3282 IR	26E	Northwest Gulf of Alaska clear	Δ IR	A
8/ 5/75	20:19	3295 IR	12E	North Bristol Bay, Canadian Archipelago clear	Δ IR	A
8/ 6/75	19:20	3307 IR	27E	Southeast Kodiak Island clear	Δ IR	A
8/ 6/75	21:13	3308 IR	2W	East Beaufort Sea, Kotzebue Sound clear		A
8/ 7/75	20:14	3320 IR	13E	East Bering Strait clear		A
8/ 7/75	22:06	3321 IR	15W	East Bering Strait clear, Kamchatka volcanoe plume.	Δ IR	A

DATE	GMT	ORBIT #	EQUATOR CROSSING	COMMENTS	ENLARGEMENT Δ IR*	STORAGE**
		<u>N4</u>				
8/ 8/75	21:07	3333 IR	0W	East Bering Sea clear		GEO
8/ 9/75	20:09	3345 IR	14E	East Bering Sea clear	Δ IR	A
8/10/75	21:03	3358 IR	1E	Gulf of Alaska clear; ice moved in past Icy Cape		A
8/11/75	20:04	3370 IR	16E	Beaufort Sea, Barrow, Interior Alaska clear		A
8/12/75	20:58	3383 IR	2E	East Beaufort Sea, west Chukchi Sea, Interior clear		A
8/13/75	19:59	3395 IR	17E	Mackenzie Delta, Barrow clear		GEO
8/15/75	19:54	3420 IR	18E	North Alaska to Mackenzie Delta clear		A
8/16/75	20:48	3433 IR	4E	East Beaufort Sea clear, Amundsen Gulf open		A
8/17/75	19:49	3445 IR	19E	Mackenzie River and Delta clear		A
8/19/75	21:38	3471 IR	8W	Bering Strait partly clear	Δ IR	A
8/20/75	20:39	3483 IR	7E	Beaufort Sea clear. (Pass to McClain)		GEO
8/21/75	21:33	3496 IR	7W	Bering Strait cloudy, clear Chukchi Sea to Icy Cape		A
8/22/75	20:34	3508 IR	8E	Kuskokwim-Nushagak coast clear		A
8/23/75	21:28	3521 IR	6W	Contrail (?) northeast from Barter Island; Barrow clear and iced in, clouds southwest	1:3.7	A
8/24/75	20:30	3533 IR	9E	Coastal clouds ~ Barrow and Wainwright + shorefast (?) pack		A
8/26/75	18:39	3557 IR	39E	Southeast Alaska clear	Δ IR	A
8/28/75	20:20	3583 IR	12E	Prince William Sound clear with cloud streaks		GEO
8/29/75	19:21	3595 IR	27E	Gulf of Alaska clear	Δ IR	A

DATE	GMT	ORBIT #	EQUATOR CROSSING	COMMENTS	ENLARGEMENT Δ IR*	STORAGE**
		<u>N4</u>				
8/30/75	04:40	3600 IR	117W	Gulf of Alaska clear	Δ IR	A
8/30/75	22:07	3609 IR	16W	West Aleutians clear	Δ IR	A
8/31/75	21:08	3621 IR	1W	Arctic ice edge (bordering		A
8/31/75	21:08	3621 VIS		cloud bank) clear		A
9/ 5/75	19:59	3683 IR	17E	Cloudy. Tight Low east Beaufort Sea		A
9/ 6/75	20:53	3696 IR	3E	Cloudy, North Slope ice edge visible		A
9/ 9/75	21:43	3734 IR	10W	West Bering Sea and Aleutians clear		A
9/10/75	20:44	3746 IR	6E	St. Matthew Island clear, strong front northeast Pacific to Arctic		A
9/11/75	21:39	3759 IR	8W	Chukchi Sea, central Bering Sea clear		A
9/12/75	20:39	3771 IR	7E	Clear around Queen Charlotte Island. Weak "Octopus" legs off coast. Ice apparently shorefast around Barrow. Pack off coast to east		GEO
9/13/75	19:40	3783 IR	22E	Cook Inlet and Alaska Range clear		A
9/21/75	21:13	3884 IR	2W	North Slope, Norton Sound partly clear		A
9/23/75	21:10	3909 IR				GEO
9/24/75	22:03	3922 IR	15W	Arctic ice edge clear		A
9/25/75	21:04	3934 IR	0E	Interior and Bering Sea clear. Open around Barrow		GEO
9/26/75	21:58	3947 IR	13W	Bering Strait and Chukchi Sea clear		A
9/27/75	20:59	3959 IR	2W	Yukon clear		A
10/ 3/75	20:44	4034 IR	5E	East Beaufort Sea partly clear		GEO

DATE	GMT	ORBIT #	EQUATOR CROSSING	COMMENTS	ENLARGEMENT Δ IR*	STORAGE**
		<u>N4</u>				
10/ 6/75	19:40	4071 IR	22E	Gulf of Alaska clear		GEO
10/ 6/75	21:34	4072 IR	7W	Central Chukchi Sea ice edge clear		A
10/ 6/75	05:01	4076 IR	122W	Gulf of Alaska clear		GEO
10/ 8/75	21:29	4097 IR	6W	Northwest Alaska clear		GEO
10/ 9/75	04:56	4101 IR	121W	East Kodiak Island clear		GEO
10/14/75	21:15	4172 IR	2W	West Coast and Chukchi Sea clear		GEO
10/25/75	19:51	4309 IR	19E	Gulf of Alaska clear		GEO
10/26/75	20:45	4322 IR	5E	West Gulf of Alaska clear	Δ IR	GEO
10/27/75	19:46	4334 IR	20E	Gulf of Alaska, Chukchi Sea and Brooks Range clear		A
10/29/75	05:09	4364 IR	\sim 100W	Alaska coast clear from Barrow to Cook Inlet		A
11/30/75	20:24	4760 IR	12E	Bristol Bay, Alaska peninsula	Δ IR	A
END OF SPION PROJECT						

Satellite

2/29/76	N4	5899 IR	25E	Gulf of Alaska warm current	Δ IR	A
7/ 3/76	N4	7465 IR	1E	Eddies along Gulf side of Aleutians	Δ IR	A
9/16/76	N5	0609 IR		Eddies off Cape Olyutorskiy,		A
9/16/76	N5	0609 VIS		Kamchatka		A

1/31/77	N5	2305 IR		Bering Sea, plume of cold ice north St. Lawrence		A
2/ 1/77	N5	2317 IR		Bering Sea, cold ice plume, northwest Alaska coast break up		A

DATE	SATELLITE	ORBIT #	EQUATOR CROSSING	COMMENTS	ENLARGEMENT ΔIR*	STORAGE**
2/ 3/77	N5	2342	IR	Bering Sea, cold ice plume, northwest Alaska coast break up		A
2/11/77	N5	2441	IR	Bering Sea, Arctic leads, floe- bergs in Chukchi Sea		A
3/18/77	N5	2873	IR	Gulf of Alaska		A
3/20/77	N5	2899	IR	Bering Sea		A
3/20/77	N5	2899	VIS			A
3/21/77	N5	2911	IR	Bering Sea, Arctic leads		A
3/23/77	N5	2935	IR	Alaska Stream off Kodiak		A
3/23/77	N5	2935	VIS	Island		A
3/23/77	N5	2936	IR	Southwest Bering Sea		A
3/23/77	N5	2936	VIS	(beautiful)		A
3/29/77	N5	3010	IR	Bering Sea, Pribilofs. (tape copies from here on)		A
5/17/77	N5	3617	IR	11W Southwest Bering Sea		A
5/18/77	N5	3628	IR	29E Southeast Alaska		A
5/19/77	N5	3642	IR	18W Kamchatka water eddies		A
6/30/77	N5	4161	IR	6E Alaskan Stream eddies		A
7/12/77	N5	4310	IR	Chukchi Sea		A
7/31/77	N5	4545	IR	Bering Strait flow through smoke		?
8/ 1/77	N5	4557	IR	Arctic coast, Pribilofs		A
9/16/77	N5	5127	IR	Kamchatka water eddies		A
9/26/77	N5	5251	IR	Kamchatka water eddies		A
11/19/77	N5	5918	IR	Southeast Alaska		A
11/24/77	N5	5981	IR	Bering Strait flow, Bristol Bay		A
12/ 1/77	N5	6067	IR	Gulf of Alaska clear		A

DATE	SATELLITE	ORBIT #	EQUATOR CROSSING	COMMENTS	ENLARGEMENT ΔIR*	STORAGE**
1/ 3/78	N5	6475 IR		Southeast Alaska, Gulf of Alaska		A
2/ 5/78	N5	6884 IR		Bering Sea ice, Unimak volcano eruption		A
3/ 1/78	N5	7181 IR		Gulf of Alaska, Bristol Bay		A
4/ 2/78	N5	7577 VIS	16E	Gulf of Alaska, cloud free Interior		A
12/14/79	TN	6025 IR		Bering Sea ice edge		A
12/18/79	TN	6073 IR		Bering Sea ice edge		A
						<u>A</u> A:123

COASTAL OCEANOGRAPHY OF THE NORTHEASTERN GULF OF ALASKA

by

**Robin D. Muench, Paul R. Temple,
John T. Gunn, and Lon E. Hachmeister**

Science Applications, Inc.

**Final Report
Outer Continental Shelf Environmental Assessment Program
Research Unit 600**

January 1982

TABLE OF CONTENTS

List of Figures	689
List of Tables	692
1. INTRODUCTION	693
1.1 Statement of Purpose	693
1.2 Geographical Setting	695
1.3 Meteorological Conditions	697
1.4 Regional Oceanographic Conditions	698
2. OBSERVATIONAL PROGRAM	703
2.1 Program Rationale	703
2.2 Current Observation Program	704
2.2.1 Moored Current Meters	704
2.2.2 Lagrangian Current Observations	709
2.2.3 Littoral Current Observations	711
2.3 Temperature and Salinity Observations	714
2.3.1 CTD Observations	714
2.3.2 Temperature and Conductivity Time Series	717
2.4 Wind Observations	718
3. THE AUTUMN EXPERIMENT	720
3.1 Autumn Distributions of Temperature and Salinity	720
3.2 Observed Autumn Near-shore Circulation	731
3.2.1 Autumn Moored Current Observations	731
3.2.2 Autumn Drogued Buoy Observations	742
3.2.3 Autumn Littoral Currents	750
3.2.4 Autumn Wind Observations	756
3.3 Discussion of the Autumn Experiment	756
3.3.1 Temperature-Salinity Analyses	758
3.3.2 Circulation Analyses	762
3.3.3 Littoral Currents	765
3.3.4 Summary	765

4.	THE SPRING EXPERIMENT	767
4.1	Spring Distributions of Temperature and Salinity	767
4.2	Observed Spring Near-shore Circulation	781
4.2.1	Spring Moored Current Observations	781
4.2.2	Spring Drogued Buoy Observations.....	789
4.2.3	Spring Littoral Currents	796
4.2.4	Spring Wind Observations	798
4.3	Discussion of the Spring Experiment	802
4.3.1	Temperature-Salinity Analyses	802
4.3.2	Circulation Analyses	806
4.3.3	Littoral Currents	808
4.3.4	Summary	808
5.	OVER-WINTER WINDS AND CURRENTS	810
5.1	Over-Winter Currents at Mooring 6	810
5.2	Over-Winter Local Winds	812
5.3	Summary	818
6.	SUMMARY AND DISCUSSION	819
7.	REFERENCES	827

LIST OF FIGURES

1. Geographical setting of the study area in the northeast Gulf of Alaska
2. Locations of moored current meter deployments in the northeast Gulf of Alaska
3. Configurations of current meter moorings using vector-averaging current meters (a) and Aanderaa current meters (b)
4. Configuration of radar-tracked drogued drifter used for Lagrangian drift studies
5. Launch site and schematic sea bed drifter paths from study of littoral currents in October-November 1980 and March-April 1981
6. Locations of CTD stations occupied in October-November 1980
7. Locations of CTD stations occupied in March-April 1981
8. Horizontal distributions of temperature (a) and salinity (b) at 5-m depth for 23 October-4 November 1980
9. Horizontal distributions of temperature (a) and salinity (b) at 100-m depth for 23 October-4 November 1980
10. Vertical distributions of temperature (a) and salinity (b) along a transect normal to the coastline on 2 November 1980
11. Vertical distributions of temperature along four transects normal to the coast and having closely-spaced stations
12. Vertical profiles of temperature, salinity, and density at Station 1a in Yakutat Bay
13. Vertical profiles of temperature, salinity, and density at Station B1 just off Ocean Cape
14. Vertical profiles of temperature, salinity, and density of Station D5 on mid-shelf
15. Vertical profiles of temperature, salinity, and density at Station 13 near the shelfbreak
16. One-hour lowpass-filtered time series of currents from autumn Mooring 1
17. One-hour lowpass-filtered time series of currents from autumn Mooring 4
18. Direction histogram illustrating the bimodal flow direction at autumn Mooring 1

19. One-hour lowpass-filtered time series of currents from the 40-m deep meter at autumn Mooring 2
20. One-hour lowpass-filtered time series of currents from the 129-m deep meter at autumn Mooring 2
21. Histogram illustrating the flow direction tendencies at the shallow meter on autumn Mooring 2
22. One-hour lowpass-filtered time series of currents from the 17-m deep meter at autumn Mooring 5
23. One-hour lowpass-filtered time series of currents from the 29-m deep meter at autumn Mooring 6
24. One-hour lowpass-filtered time series of currents from the 102-m deep meter at autumn Mooring 6
25. Composite picture showing all drogued drifter tracks observed in autumn 1980
26. Individual drogue tracks (a), (b), (c) followed by Drifters 1, 2, 3 respectively in the first autumn 1980 drogue experiment
27. Individual drogue tracks (a), (b), (c) followed by Drifters 1, 2, 3 respectively for the second autumn 1980 drogue experiment
28. Plot of separation between drogues as a function of time for the autumn 1980 drifter experiment
29. Plot of drogue speeds as a function of time and vector wind observed at Dry Bay
30. Histograms of longshore speed for Group 1 (a), Group 2 (b), and Group 3 (c) fall 1980 seabed drifter studies
31. One-hour lowpass-filtered time series plots of wind speed, along-shore and cross-shelf components at the Dry Bay (a) and Ocean Cape (b) meteorological stations during the autumn field program
32. Composite temperature-salinity diagram for autumn 1980, showing the relationships between near-shore, shelf and deep ocean water masses
- 33a. Horizontal distribution of temperature ($^{\circ}\text{C}$) at 5-m depth, 20 March-3 April 1981
- 33b. Horizontal distribution of salinity ($^{\circ}/\text{oo}$) at 5-m depth, 20 March-3 April 1981
- 34a. Horizontal distribution of temperature ($^{\circ}\text{C}$) at 100-m depth, 20 March-3 April 1981
- 34b. Horizontal distribution of salinity ($^{\circ}/\text{oo}$) at 100-m depth, 20 March-3 April 1981

- 35a. Vertical distribution of temperature ($^{\circ}\text{C}$) along a cross-shelf transect 30 March 1981
- 35b. Vertical distribution of salinity ($^{\circ}/\text{oo}$) along a cross-shelf transect 30 March 1981
36. Vertical distribution of temperature ($^{\circ}\text{C}$) at four transects normal to the coastline 20-24 March 1981
37. Vertical profiles of temperature, salinity and density at Station 18 in Yakutat Bay
38. Vertical profiles of temperature, salinity and density at Station 43 near the coast
39. Vertical profiles of temperature, salinity and density at Station 6 at mid-shelf
40. Vertical profiles of temperature, salinity and density at Station 40 seaward of the shelfbreak
41. Time-series plots of one-hour filtered current velocity, alongshore and cross-shore speed and temperature at 17 m, Mooring 1
42. Time-series plots of one-hour filtered current velocity, alongshore and cross-shore speed and temperature at 34 m, Mooring 4
43. Time-series plots of one-hour filtered current velocity, alongshore and cross-shore speed and density at 52 m, Mooring 5
44. Time-series plots of one-hour filtered current velocity, alongshore and cross-shore speed and density at 37 m, Mooring 3
45. Time-series plots for one-hour filtered current velocity, alongshore and cross-shore speed and density at 120 m, Mooring 3
46. Time-series plots for one-hour filtered current velocity, alongshore and cross-shore speed and density at 102 m, Mooring 6
47. Plot of separation between drogues 5 and 6 as a function of time
48. Drift tracks for drogues 5 (a) and 6 (b) during the first spring drogue experiment
49. Drift tracks for drogues 4 (a), 5 (b) and 6 (c) during the second spring drogue experiment
50. Plots of wind velocity as a function of time and drogue velocity derived from trajectories as a function of time
51. Histogram of alongshore speed for seabed drifters from groups 1 (a), 2 (b), and 3 (c)
52. Time-series plots of one-hour filtered wind velocity, alongshore and cross-shelf speed at Ocean Cape (a) and Dry Bay (b)

53. Composite temperature-salinity plot for the northeast Gulf of Alaska in spring 1981
54. One-hour filtered currents at Mooring 6 for the 102-m deep current meter plotted as a function of time
55. Thirty-hour filtered winds as observed at Yakutat airport and as computed geostrophic winds plotted as a function of time for September 1980-April 1981
56. Thirty-hour filtered east and north wind speed components from Yakutat airport and as computed geostrophic winds plotted as a function of time for September-December 1980
57. Thirty-hour filtered east and north wind speed components from Yakutat airport and as computed geostrophic winds plotted as a function of time for January-April 1981
58. Normalized spectral estimate for computed geostrophic wind speeds during November 1980, computed using a Maximum Entropy Method routine
59. Surface current vectors constructed by application of a diagnostic model to March 1979 density data, assuming presence of a moderate south-easterly wind stress
60. Vector-averaged currents from current meters deployed in March-April 1981 and for the October 1980-April 1981 record obtained at Mooring 6
61. Vector-averaged currents from current meters deployed in October-November 1980

LIST OF TABLES

1. Summary of Information Concerning Deployment of, and Information Obtained From, Current Meter Moorings Utilized in the Autumn 1980 Field Program in the Northeast Gulf of Alaska
2. Summary of Information Concerning Deployment of, and Information Obtained From, Current Meter Moorings Utilized in the Spring 1981 Field Program in the Northeast Gulf of Alaska
3. Autumn Drogued Buoy Speed Statistics
4. Autumn Surface Current Velocity Estimated From Wave Parameters
5. Spring Survey Drogued Buoy Speed Statistics
6. Spring Surface Current Velocity Estimated From Wave Parameters

1. INTRODUCTION

1.1 Statement of Purpose

The primary objective of the Alaska Outer Continental Shelf (OCS) Environmental Studies Program is to develop an information base permitting prediction of the spatial and temporal distribution of petroleum-related contaminants following their hypothetical release in coastal waters. Such information, taken in conjunction with seasonal and spatial descriptions of potentially vulnerable marine resources, provides a critical input to the Bureau of Land Management (BLM) environmental assessment program. BLM's program requires background information for management decisions which may be necessary to protect the OCS marine environment from possible damage during oil and gas exploration and development. To enable performance of this protective duty (a direct outgrowth of the National Environmental Policy Act of 1969), pertinent data must be available in readily useable form so that informed management decisions can be made before serious environmental damage occurs.

In assessing the potential impact of OCS development upon the marine environment, information on transport and transformation of petroleum-related contaminants is of key importance. When introduced into the environment, such contaminants can be transported in the atmosphere, in the water, or by sea ice. During transport these contaminants undergo continual physical and chemical changes brought about by processes such as evaporation, flocculation, emulsification, weathering, biodegradation, and chemical decomposition.

The study discussed in this report addresses problems relating to transport of contaminants. The OCS Environmental Studies Program transport studies have been designed specifically to provide data that will enable BLM and other agencies to:

- Plan stages and siting of offshore petroleum development so as to minimize potential risk to environmentally sensitive areas;
- Provide trajectory, coastal landfall and impact predictions required for cleanup operations in the event of an oil spill or the introduction of other contaminants;
- Assist in planning the locations of long-term environmental monitoring stations in the study area.

Several inter-disciplinary studies have resulted from this program; the coastal oceanography and meteorology element directly addresses the problem of contaminants movement in continental shelf waters.

The primary objective of OCSEAP oceanography and meteorology studies in the northeast Gulf of Alaska coastal region has been to provide, through interactive field programs and analytical techniques, a capability for predicting movement and distribution of OCS contaminants in the northeast Gulf of Alaska coastal environment. Specific program elements have required methodology development and implementation of studies to supply information on:

- Temporal and spatial variability of coastal oceanic circulation in the northeast Gulf of Alaska;
- Local wind fields and their influence on coastal circulation;
- Influence of regional climatological factors, especially coastal runoff, upon coastal circulation and water mass structure;
- Influence of bottom topography upon circulation and mixing;
- Methods of applying data to the prediction of potential pollutant pathways and impact sites in order to aid in assessing the vulnerability of biotic resources and in design of effective cleanup strategies.

These information requirements have been addressed through an integrated program combining field and analytical research. Circulation has been addressed by comparing currents inferred from the temperature and salinity distributions with those observed directly using taut-wire moorings and drogues; inferred and observed currents have also been compared qualitatively with local freshwater input. Littoral currents have been estimated from the incident wavefield and from seabed drifter studies. Local wind effects have been estimated by comparing locally observed and computed regional geostrophic winds with the observed currents. The remainder of this report addresses the results of these analyses. The topographical, oceanographic and meteorological setting and the scientific background are covered in the remainder of Section 1; the observational program is detailed in Section 2; observational results are presented and discussed in Sections 3 - 5, and Section 5 integrates these results and summarizes them within the context of OCSEAP program needs.

1.2 Geographical Setting

In addressing physical oceanographic processes in the northeast Gulf of Alaska, the focus is upon coastal and continental shelf regimes. Physical factors which are known to exert primary control over circulation and mixing processes in such regions include bottom slope and depth, continental shelf width, and orientation of the coastline relative to the earth's rotational axis. On a smaller scale, coastline and bottom topographic irregularities can exert significant influence over local circulation patterns. Since a range of temporal and spatial scales of oceanographic processes are addressed, those geographical and bottom features which are expected a priori to significantly affect oceanographic conditions must be discussed in some detail.

The northern Gulf of Alaska coastline forms an arcuate east-west trending bight which comprises the extreme northern portion of the northeastern Pacific Ocean (Figure 1). The study reported here has focused upon the northeast Gulf of Alaska continental shelf portion of this region. The study area extended seaward from the coastline to the continental shelfbreak (defined approximately by the 200-m isobath) and extended alongshore from about Point Manby, marking the westernmost entry to Yakutat Bay, to Cape Spencer on the northern coast of Cross Sound. Although temperature and salinity data were obtained throughout this continental shelf area, the program's major emphasis was upon the coastal region within about 10 km of shore.

The continental shelf region encompassed by the study area has complex bottom topography. While the overall shelf width is about 100 km, the presence of transverse troughs effectively decreases the width in some places (Figure 1). Off Yakutat Bay, the shelf is transected by Yakutat Canyon, with depths of about 200 m, which extends to the northwest across the mouth of the Bay and then seaward. To the southeast, off Dry Bay, the shelf is again transected by a major trough -- Alsek Canyon -- which also has depths of about 200 m. Both Yakutat and Alsek canyons are about 20-km wide. The Fairweather Ground, an extensive bank with depths of less than about 100 m, lies southeast of Alsek Canyon and near the shelfbreak.

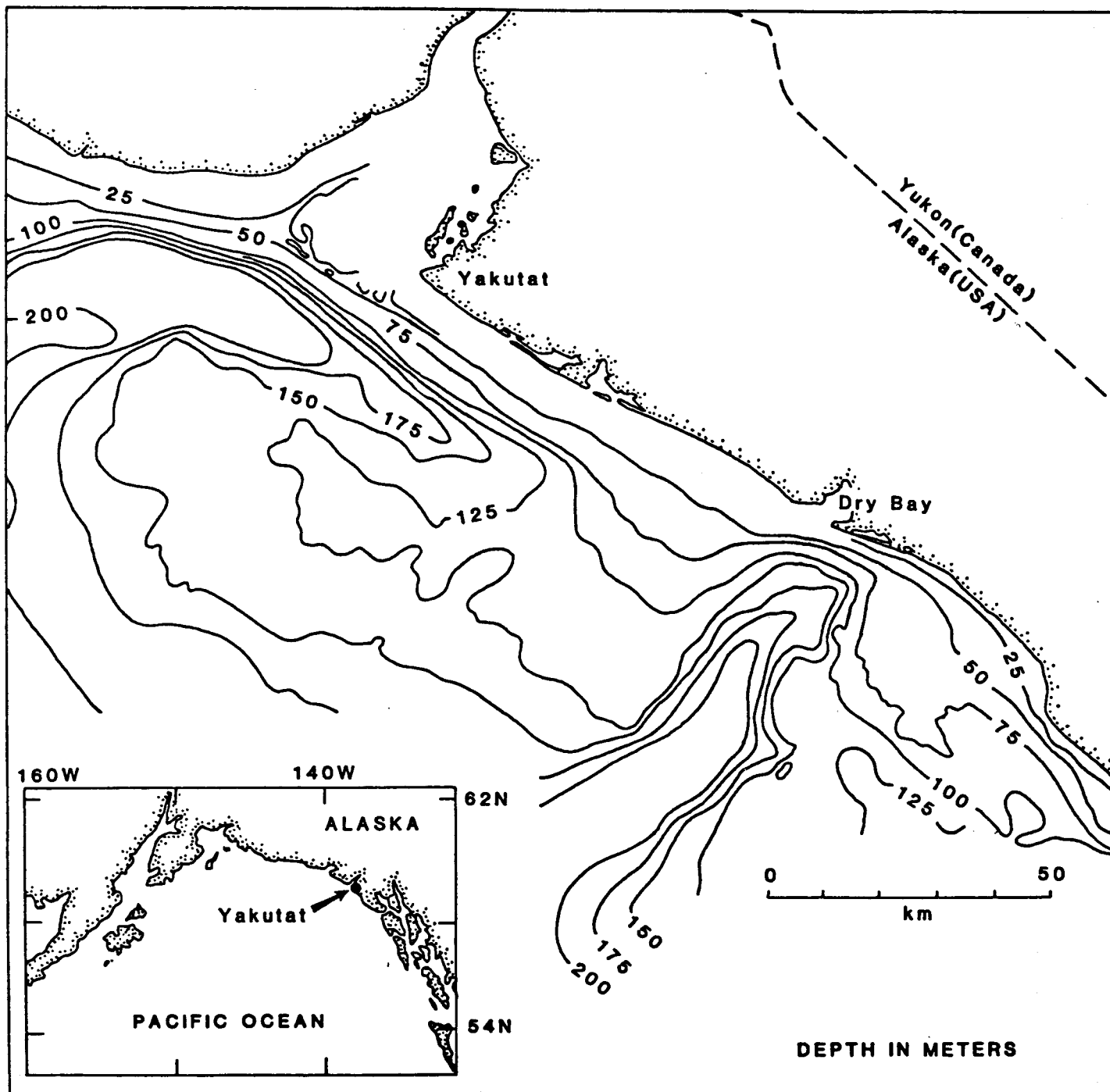


Figure 1. Geographical setting of the study area in the northeast Gulf of Alaska.

The coastline within the study region is nearly linear between Yakutat Bay and Cross Sound, showing little of the curvature which characterizes the northern Gulf of Alaska coast on a larger scale. Major gaps in the coast are formed only by Yakutat Bay and Cross Sound at the northwestern and southeastern boundaries, respectively, of the study area. The coastline itself is composed of nearly continuous mountains with elevations in excess of 1000 m, including isolated peaks as high as about 4000 m. Breaks in these mountains, in the form of transverse valleys which lead through the mountain ranges, occur at Yakutat and Dry bays and at the mouth of the Dangerous River.

1.3 Meteorological Conditions

Meteorological conditions in the northeast Gulf of Alaska coastal region are dominated by seasonal variability. Atmospheric circulation over the northern Gulf of Alaska is dominated during winter by a low-pressure trough, the Aleutian Low, which defines a mean trajectory for severe cyclonic storms which originate to the west along the Aleutian Islands, then migrate to the northeast and intensify. Migration speed of these lows is typically 10-12 m/sec off Kodiak Island, but they tend to slow and intensify over the northeast Gulf. Wind speeds during these storms can be high; speeds higher than 48 kt occurred for 1 percent of the samples obtained during November-February over a 15-year period in the coastal region off Yakutat (Brower et al., 1977). Though the statistics have not been rigorously analyzed, time scales for these storms appear to be 4-6 days. During winter the coastal waters are therefore subjected to a series of wind events which, averaged over an entire season, yield a mean southeasterly wind.

During summer the Aleutian Low weakens and is displaced by an atmospheric high pressure system, the North Pacific High. The eastward-migrating low-pressure systems are much weaker than in winter, and the resulting winds are light and variable although there is still a net easterly component in summer. As in winter, the wind field is event-dominated.

The presence of topographically-complex high mountain ranges along the coastline probably has a strong influence on the local near-coastal wind field. While these problems have not been specifically addressed in this study, physical reasoning suggests that winds would be constrained by the coastal

mountains to parallel the coastline within a certain distance offshore. In addition, katabatic or drainage winds commonly blow from valleys breaching the coastal mountains throughout southeast Alaska as relatively dense and cold air from the interior drains through the valleys to sea level. These winds can extend for an indefinite distance seaward and are characterized by high speeds and low air temperatures. Informal sources in southeast Alaska have reported winter wind speeds in excess of 50 m/sec and air temperatures well below freezing.

Finally, mean monthly winter air temperatures in the near-coastal region off Yakutat vary from a minimum of about -10°C to a maximum of about $+8^{\circ}\text{C}$ (Brower et al., 1977).

The above combination of climatological factors leads to an annual freshwater discharge in the coastal band with a maximum approximately in October -- the normal time for onset of the winter storm season prior to the period when most precipitation (due to depressed temperatures) occurs as snow. Freshwater discharge is minimal in February-March, when most near-coastal precipitation occurs as snow. There is a small secondary freshwater discharge maximum in about May, when the onset of above-freezing temperatures leads to melting of the coastal accumulation of snow.* Examination of coastal geography in the northeast Gulf suggests that freshwater discharge will likely come primarily from three sources within the study area: Yakutat Bay, with sources at the glacial streams entering the head of the Bay; Dry Bay, via the Alsek River whose watershed extends through the coastal mountains; and Cross Sound, which has extensive freshwater sources in the southeast Alaska Archipelago to the south.

1.4 Regional Oceanographic Conditions

Circulation in a continental shelf region is expected a priori to be controlled by a number of environmental variables. These variables include

* An up-to-date discussion of coastal freshwater discharge in the northeast Pacific, complete with statistical summaries of discharge data, is presented in Royer (1979).

the current along the shelfbreak seaward of the shelf, which can introduce momentum onto the shelf through lateral transfer either as eddies or mean flow; local winds which drive Ekman current systems; freshwater input as it affects the baroclinic field; and, incident surface waves which generate littoral currents. The resulting circulation is strongly influenced by the local bottom topography. This section first summarizes recent oceanographic exploration and results in the northeast Gulf of Alaska shelf region. Next, the large-scale oceanic circulation which controls flow along the shelfbreak is briefly discussed. Finally, those physical processes expected to be of major importance in the coastal region are summarized.

Research in the northern Gulf of Alaska has been hampered in the past by a lack of field data. The earliest reported study was that of McEwen, Thompson and Van Cleve (1930) who used temperature and salinity data obtained along sections normal to the coastline, including one off Yakutat Bay, to describe and discuss regional hydrographic structure and currents over the shelf and shelfbreak. Little field work was carried out in the northeast Gulf of Alaska between the work of McEwen et al. and the onset of the BLM-sponsored Alaska OCS Program in 1974. This lack of information was pointed out by Favorite, Dodimead and Nasu (1976) who provided a thorough oceanographic summary of the subarctic Pacific covering research through 1972, but found insufficient data to address detailed oceanographic features in the northeast Gulf of Alaska.

A vigorous program of oceanographic data acquisition from the northeast Gulf of Alaska continental shelf region commenced in 1974. This resulted first in a characterization of seasonal variations in the water column in the northern Gulf by Royer (1975). Later, Royer and Muench (1977) discussed some large-scale surface temperature features which were related to the regional circulation and to vertical mixing processes on the shelf. Hayes and Schumacher (1976), Hayes (1978), and Holbrook and Halpern (1977) discussed variations in winds, currents and bottom pressures on the shelf west of Yakutat Bay over February-May 1975. Current observations obtained from the shelf west of Yakutat Bay over 1974 through 1978 were analyzed by Lagerloef, Muench and Schumacher (1981). An assessment of the effect of freshwater input on coastal circulation in the northeast Gulf of Alaska was provided by Schumacher and Reed (1981) and by Royer (1981b). A summary of overall oceanographic conditions in the northeast

Gulf was prepared by Muench and Schumacher (1979). Results of these studies were all consistent with the concept of a general northwesterly mean alongshore flow, with wind-driven events occurring nearer the coastline and current events farther offshore being more closely related to oceanic flow processes at the shelfbreak.

Shelfbreak circulation is controlled by the cyclonic (anticlockwise) mean circulation in the North Pacific subarctic gyre, driven by the large-scale atmospheric flow and leading to northwesterly alongshore flow along the shelfbreak. The subarctic gyre has been indirectly discussed by various researchers (cf. Munk, 1950; Carrier and Robinson, 1962; and numerous others). These largely theoretical studies hypothesized that the gyre was driven by regional wind stress. Only recently, the presence of an actual closed gyral circulation in the Gulf of Alaska was proven using satellite-tracked drogued buoys by Reed (1980). Water for this circulation originates in the North Pacific Drift, which flows eastward from the vicinity of Japan and bifurcates west of Vancouver Island so that the north-flowing branch follows the coastline and eventually becomes the northwest-flowing Alaska Current off Yakutat. The lower-latitude origin of this water gives rise to its characteristic temperature and salinity features, which are then locally modified by severe cooling, wind mixing, and freshwater addition on the northern Gulf of Alaska shelf as discussed by Royer (1975), Royer and Muench (1977), and Royer (1981b and c).

Current speeds and volume transports along the shelfbreak in the northeast Gulf of Alaska remain uncertain, although there is most certainly appreciable seasonal variability in both. Computations of volume transport carried out for the Gulf of Alaska gyre using wind stress curl by Ingraham, Bakun, and Favorite (1976) suggested summer transports of near zero, while winter transports were as great as about $25 \times 10^6 \text{ m}^3/\text{sec}$ (in 1969), and also indicated a large year-to-year variability. Their conclusions were borne out by Reid and Mantyla (1976), who used sealevel data to estimate alongshore flow along the northern Gulf of Alaska coastline. Reed et al. (1980) found, however, that baroclinic transports in the Alaska Current off Kodiak Island show no detectable annual variation. Most recently Royer (1981a) has used all available baroclinic transport data to detect a weak annual signal. These varying results must all be extrapolated to the northeast Gulf shelfbreak with caution, because intensification of the

gyre into a concentrated shelfbreak boundary flow occurs only far to the west off Kodiak Island (Thomson, 1972; Reed et al., 1980).

Shelfbreak flow in the northeast Gulf of Alaska is important to the present study results only inasmuch as energy from this flow is transferred onto the continental shelf. One mechanism for such a transfer is an alongshore sealevel slope, due to the shelfbreak flow, which can in turn drive near-shore currents as has been discussed for the Gulf of Maine by Csanady (1974). Another mechanism is lateral frictional transfer of mean flow energy onto the shelf, e.g., in the form of eddy-like features splitting off from the shelfbreak currents and migrating shoreward as has been observed along the Florida Current (Lee, 1975). This process, discussed in detail by Csanady (1975), can result in transfer of kinetic energy onto the shelf from the shelf edge currents. Such features have been observed on the shelf west of Yakutat Bay by both Hayes (1978) and Royer et al. (1979).

Local winds are of major importance in generating currents on continental shelves. This is expected to be particularly true in the northeast Gulf because of the high intensity of the storm-driven winds during winter. Based upon current data, Hayes (1978) concluded that local winds generated a significant local current response near shore west of Yakutat Bay, but had insignificant effects upon circulation near the shelfbreak. Locally wind-driven circulation on the continental shelves can be classified either as free and forced waves (continental shelf waves) which propagate along the coastline, or as transient responses (storm surges); some knowledge of the behavior of these waves is necessary for understanding and anticipating locally wind-driven shelf circulation features. A vast quantity of research has been carried out on these processes, as reflected in the large amount of pertinent literature; an excellent up-to-date summary has been prepared by Mysak (1980).

In summary, circulation in the northeast Gulf of Alaska region addressed in this study is expected to exhibit a broad spectrum of phenomena which have become commonly accepted as typifying continental shelf behavior. The driving forces for the shelf circulation are a shelfbreak current, an internal baroclinic field due to local coastal freshwater input, and extremely vigorous local winds.

Once established, this integrated circulation is subject to control by a complex bottom topography. Seasonal variations, due to variability both in coastal freshwater input and in intensity of local winds, are also expected to be appreciable. In the remainder of this report, field data obtained in the region in 1980 through 1981 will be analyzed with the intention of clarifying which of these processes are significant in the near-shore area and relating them to the fate of OCS-related contaminants.

2. OBSERVATIONAL PROGRAM

2.1 Program Rationale

Given a relatively simple physical situation, the oceanic velocity field could ideally be recreated from first principles using a computer model. As noted above in Section 1, however, the northeast Gulf of Alaska shelf region poses an extremely complex set of physical problems which combine to make a a priori modeling impractical. The approach which has been used in this study is, rather, application of relatively simple (i.e. when compared to a computer model) analytic theories to carefully chosen observational results in such a way as to extend the results and allow prediction of what might occur under a given set of conditions.

The experimental program discussed below was designed and implemented with the above philosophy in mind. However, the size of the Alaskan continental shelf defies adequate measurement when considered within the context of pollutant transport processes. Therefore, the program was designed to establish statistics of the velocity field at a few selected locations and to supplement these with process-oriented studies addressing both specific dynamical problems and site-specific problems. The dynamical studies relate the observed velocity fields to wind forcing, bathymetry, and freshwater input. The site-specific studies address such problems as flow patterns at the heads of the two major regional cross-shelf troughs and within the surf zone.

The field experiments were planned in such a way as to encompass the extreme seasonal variability due to variations in the forcing parameters such as winds and freshwater input (see Section 1). These experiments were conducted on two separate cruises, each about 12 days in length. The first cruise was in October-November 1980 when maximum annual accumulation of freshwater was assumed to be present in the marine system, prior to the onset of winter storm activity with attendant high local wind speeds. The second cruise took place in March-April 1981 when accumulated freshwater in the system was minimal, following the period of most vigorous winter wind activity. In order to establish a statistical basis for regional wind and current activity, during the October 1980 through April 1981 period, time series of winds were obtained both from Yakutat Airport

and as computed geostrophic winds, and current observations were obtained from a single mid-shelf mooring.

The autumn and spring field experiments were identical to each other in planning, execution, and goals. The intention was to observe the near-shore (inside about 10 km) circulation and to relate these observations to the local winds, coastal freshwater input, circulation farther offshore, and bathymetry. Current observations were made using taut-wire moorings and radar-tracked drogued buoys. Winds were observed using recording instruments deployed on the coastline, from the vessel, and at Yakutat Airport, and were also computed for the entire region as geostrophic winds. Temperature and salinity observations were carried out from shipboard using a CTD and were recorded as time series by the recording current meters on the moorings. Finally, littoral currents were determined using seabed drifters deployed and recovered from a light aircraft. These observational programs are discussed below in detail.

2.2 Current Observation Program

The current observation program in the northeast Gulf of Alaska utilized both current meter moorings and drogued buoys. The moorings provided time-series records at fixed locations and allowed estimation of regional circulation patterns, current variability, and time scales for significant current events. The drogues provided estimates of the trajectories for near-surface water, and thus the pathways likely to be followed by spilled petroleum. The drogue tracks also provided supplementary data on the regional circulation. Finally, seabed drifters were used to estimate littoral currents within a few hundred meters of the beach.

2.2.1 Moored Current Meters

Current meters were deployed on taut-wire moorings in such a manner as to record currents from about 4 km offshore to near the shelfbreak, with emphasis on the region within about 10 km of shore (Figure 2). Six moorings were deployed at the beginning of the autumn 1980 field program. Moorings 1-5 were recovered at the end of the autumn field program, and Mooring 6 was left in throughout the winter and was recovered at the end of the spring 1981 field program. In the

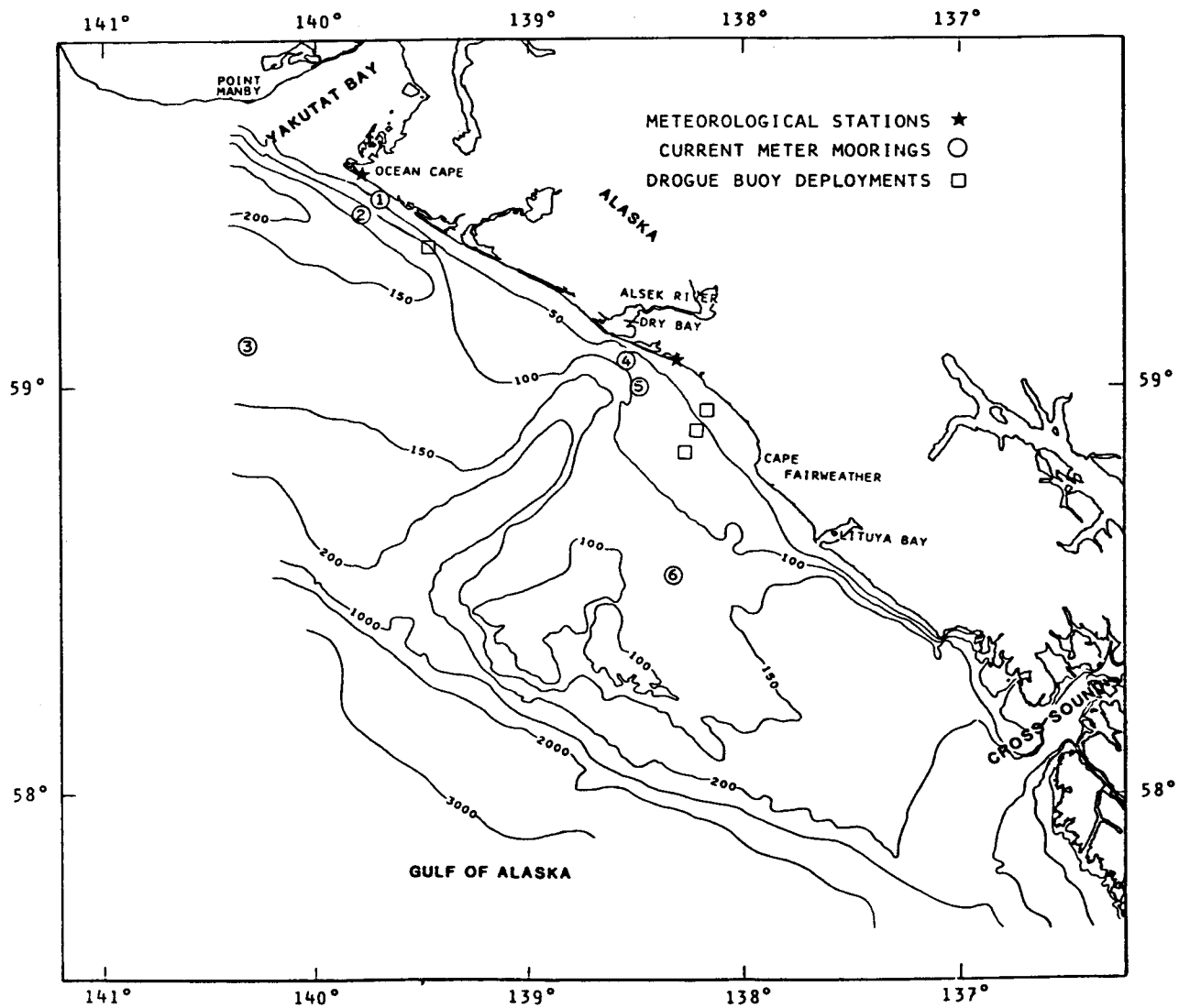


Figure 2. Locations of moored current meter deployments in the northeast Gulf of Alaska. Moorings 1-5 were deployed twice, from October-November 1980 and again from March-April 1981. Mooring 6 was deployed during the entire October 1980-April 1981 period. Drogue deployments are indicated by squares and meteorological stations are indicated by stars.

spring, five moorings were deployed at the same locations as the fall moorings (1-5) and were recovered at the termination of the spring field program along with Mooring 6. Particulars for these moorings are given in Tables 1 and 2.

Mooring configurations were basically similar to those used for previous OCSEAP moorings in the region (documented in Muench and Schumacher, 1979). Each mooring consisted of one or two current meters suspended in a taut-wire configuration using a 41-inch spherical float for primary buoyancy, a 2100-pound anchor constructed from three railroad wheels, and an acoustic release (Figure 3). To aid in mooring recovery in the event of failure of the primary spherical floats, secondary flotation was designed into each mooring in the form of 12-inch vinyl floats. This configuration provided enough tension for the mooring line (about 1000 pound gross positive buoyancy) to minimize chances of mooring noise introducing contamination into the current records.

Two different types of current meters, each having distinctly different modes for recording data, were used. The two near-shore moorings (1 and 4) each utilized a single AMF SeaLink Model 610 vector-averaging current meter to minimize wave contamination of the current records due to interaction of incoming swell with a shoaling bottom. The vector-averaging meters sense speed using a Savonius rotor (east-west and north-south velocity components are sampled eight times per rotor revolution) and sense direction using a vane and compass. For the present study these values were vector-averaged at 7.5-minute intervals and recorded along with temperature; the effect of the averaging is to remove wave- and mooring-induced noise from the recorded data. The remaining moorings each used two Aanderaa Model RCM-4 recording current meters provided by OCSEAP through the Coastal Physics Group, Pacific Marine Environmental Laboratory. These current meters record an average speed, along with an instantaneous direction, at the end of each recording interval. The recording interval for Moorings 2, 3 and 5 was 5 minutes, while the interval at Mooring 6 was 30 minutes to allow acquisition of the considerably longer record from that mooring. The vector-averaging meters had respective minimum threshold speed and accuracy of 3 cm/sec and 2 cm/sec. Corresponding values for the Aanderaa current meters were 1 cm/sec for both parameters.

Table 1

SUMMARY OF INFORMATION CONCERNING DEPLOYMENT OF, AND INFORMATION OBTAINED FROM,
CURRENT METER MOORINGS UTILIZED IN THE AUTUMN 1980
FIELD PROGRAM IN THE NORTHEAST GULF OF ALASKA

MOORING ID	LATITUDE N	LONGITUDE W	DEPLOYMENT DATE/HR	RECORD LENGTH (days)	BOTTOM DEPTH (m)	METER DEPTH (m)
1	59°27.2'	139°44.1'	10-23-80/1909	10	57	26
2	59°24.1'	139°46.4'	10-23-80/2033	10	139	40
2	59°24.1'	139°46.4'	10-23-80/2033	10	139	125
3	59°06.8'	140°20.3'	10-24-80/0030	10	132	37
4	59°04.5'	138°31.1'	10-22-80/1048	11	75	38
5	59°00.0'	138°28.5'	10-22-80/1159	11	65	15
6	58°31.5'	138°19.5'	10-22-80/1500	31	118	29*

* correct speed and direction only for first 31 days

Table 2

SUMMARY OF INFORMATION CONCERNING DEPLOYMENT OF, AND INFORMATION OBTAINED FROM,
CURRENT METER MOORINGS UTILIZED IN THE SPRING 1981
FIELD PROGRAM IN THE NORTHEAST GULF OF ALASKA

MOORING ID	LATITUDE N	LONGITUDE W	DEPLOYMENT DATE/HR	RECORD LENGTH (days)	BOTTOM DEPTH (m)	METER DEPTH (m)
1	59°26.8'	139°43.1'	3-20-81/2355	13	46	17
2	59°24.6'	139°46.2'	3-20-81/2322	2	128 115	27
3	59°06.4'	140°21.2'	3-21-81/0242	13 [†]	132	~ 37 ~120
4	59°04.5'	138°31.8'	3-20-81/1923	13	~ 71	~ 34
5	58°59.9'	138°28.6'	3-20-81/1824	12 [‡]	~ 64	16
6	58°31.5'	138°19.5'	10-22-80/1520	162	118	102

[†] has 6½-day data gap in middle of record

[‡] only temperature, conductivity, and pressure

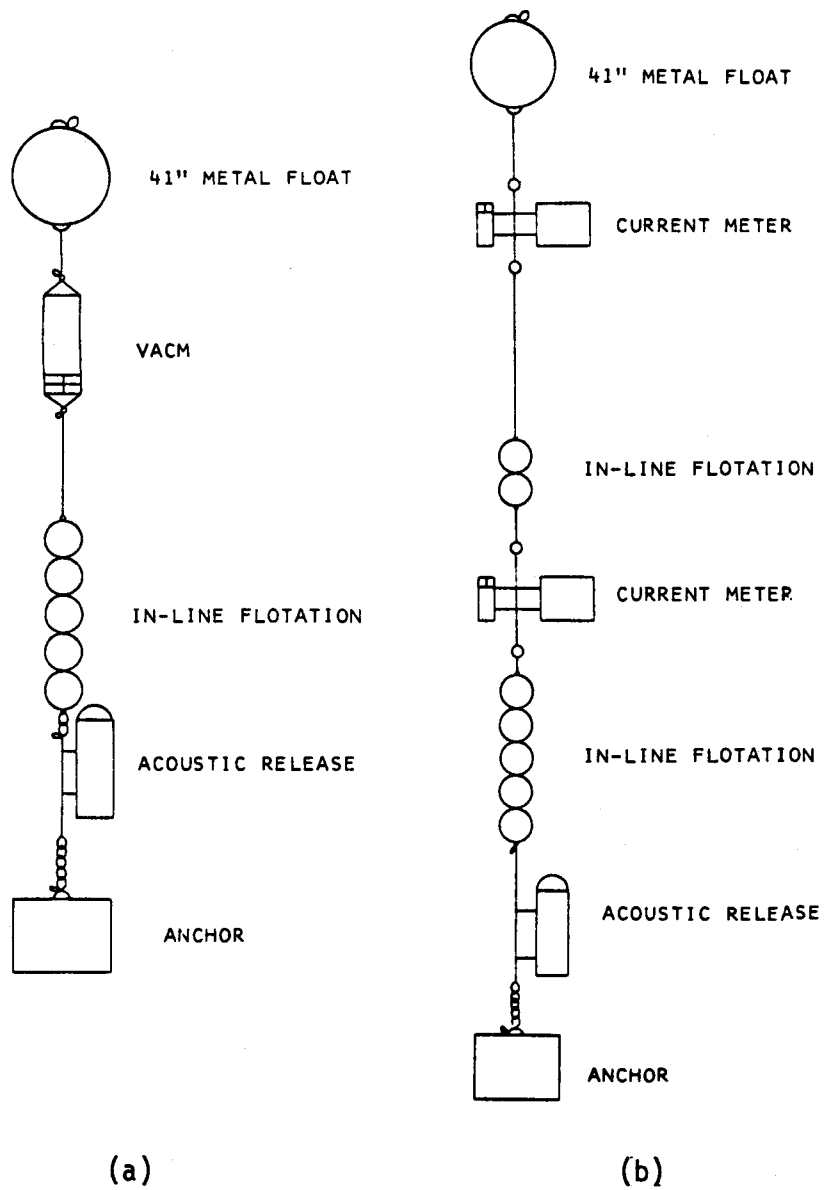


Figure 3. Configurations of current meter moorings using vector-averaging current meters (a) and Aanderaa current meters (b).

Calibration (prior to and following each deployment) and data tape translation were carried out for the vector-averaging current meters by the Technical Services Group at the Graduate School of Oceanography, University of Rhode Island. Data tape translation for the Aanderaa current meters was performed by Marine Data Services of Corvallis, Oregon. After being transcribed onto nine-track tape, all data were processed at SAI/Northwest on a PDP-11/60 computer system.

In evaluating the results of the current meter moorings, the effects upon the resulting records from the two meter types' different recording modes must be kept in mind. As noted above, the vector-averaging meters minimize wave- and mooring-induced noise. On the other hand, the Aanderaa meters are subject to contamination of records by wave and mooring noise. The meters deployed in the northeast Gulf of Alaska were 15 m below the surface or, except for autumn Mooring 5, deeper. Pearson et al. (1981) concluded that, in the case of meters where the surface float was more than 18 m below the water surface, contamination of the records was insignificant insofar as effects upon tidal and lower frequency currents. Based upon this, it is possible that the uppermost meter at autumn Mooring 5 suffered some contamination but that the remaining records are relatively uncontaminated. Detailed intercomparisons between data sets recorded using these different instruments have been reported upon by Halpern and Pillsbury (1976a; 1976b) and Beardsley et al. (1977). Additional commentary on the validity of records from Aanderaa current meters has been provided by Mayer et al. (1979) and Pearson et al. (1981).

2.2.2 Lagrangian Current Observations

Lagrangian current observations were made in the near-shore region of the northeast Gulf of Alaska using window-shade drogues attached to surface buoys. Drogue depths were set so as to follow water motion at about 15 m. The buoys were equipped with radar transponders to allow tracking using the research vessel's radar. Configuration of the drifters is illustrated diagrammatically in Figure 4.

There were two separate and distinct Lagrangian drifter experiments during each of the two field programs. In the first of each pair of experiments, the drogues were deployed about 0.5 km apart and their subsequent separation distances

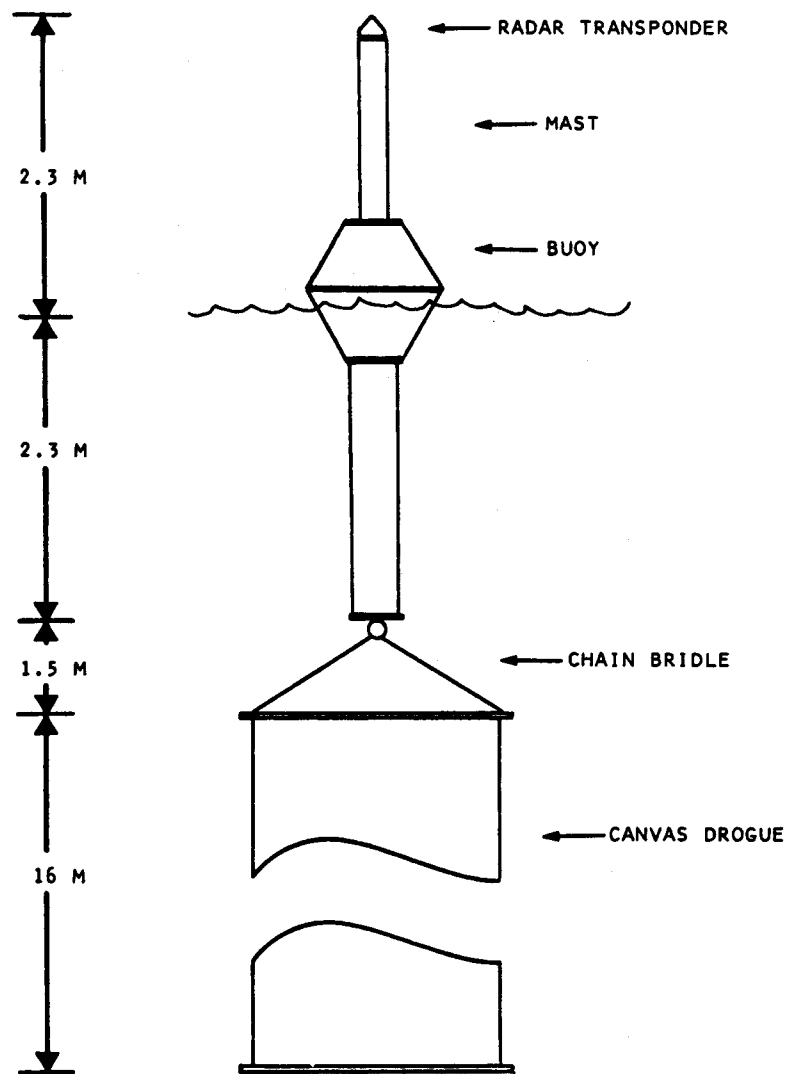


Figure 4. Configuration of radar-tracked drogued drifter used for Lagrangian drift studies.

during the experiment were recorded in an attempt to estimate dispersion. The second experiment of each pair consisted of buoy deployments along a line normal to the longshore current and subsequent tracking to better define the flow field. Deployment locations coincided as closely as possible with current meter mooring sites, to enable later comparison between drifter and current meter results. The approximate areas covered by the autumn and spring drifter experiments are indicated on Figure 2.

Drogued buoy positions were recorded at half-hour intervals during the experiments. Positioning was accomplished by recording the ship's location, determined using Loran C, along with a radar range and bearing to the buoy. In cases where the locations suggested that a drogue was in danger either of running aground or of exceeding the range of the ship's radar, the drogue was recovered and redeployed. The resulting buoy positions were edited for "wild points" which may have been due either to questionable Loran positions or error in recording radar fixes. Such points were generally quite obvious, and were discarded and replaced with interpolated values. The final data set was run through a 5-point 2.5-hour "boxcar" filter to remove high frequencies and facilitate intercomparison with other data.

2.2.3 Littoral Current Observations

Longshore water transports and bottom currents in the region in and just offshore from the surf zone (< 400 m from shore) were addressed using two different methods. First, bottom currents were estimated directly using deployment-recovery results for seabed drifters. Second, longshore wave-induced currents were computed using estimated wave characteristics in conjunction with known empirical formulae.

Seabed drifters were deployed on 18-30 October 1980 and 21-24 March 1981 at the approximate sites shown on Figure 5. These drifters consisted of an 18-cm diameter hemispherical head attached to a weighted tail-like shaft 50 cm long. They were grouped into bundles of 50 each, held together for deployment by a salt block that would dissolve to release them about three hours following deployment. These bundles were launched from a light aircraft just following high tide, in the surf zone along lines normal to the coastline. Three bundles

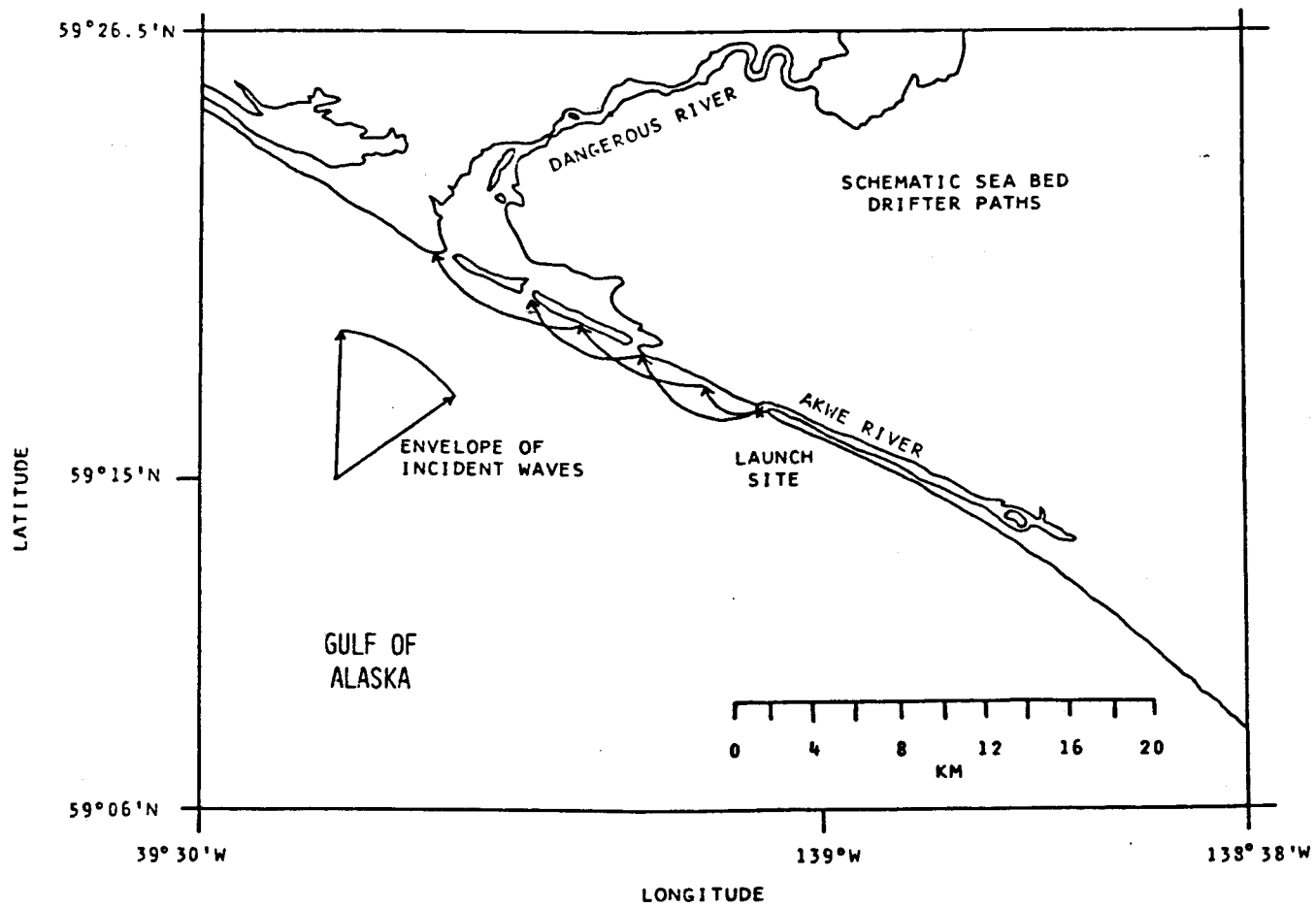


Figure 5. Launch site and schematic sea bed drifter paths from study of littoral currents in October-November 1980 and March-April 1981 (see appropriate sections for actual speeds and directions).

of drifters were released at each deployment. The innermost was deployed shoreward of the breakers, the next group directly in them, and the outermost group about 150 m seaward of the breakers. For three days following each set of launches the beach was searched for drifters during the daylight low tide period using a light aircraft. The relatively uniform and sandy aspect of the beach made spotting of beached drifters easy, suggesting that most of the drifters which actually went ashore were recovered.

Several factors contribute to the uncertainties in longshore speed computed from the drifter recovery and release points. First, time of beaching is not known precisely but is assumed to have been at or near high tide because most of the recovered drifters were found at or near the high tide mark. Because recoveries were limited to the daylight low tide, beaching may have occurred at either of the two high tides between the second- and third-day recoveries. Second, the release time for some drifters is uncertain because, at the time of launching, the airstream generated by the aircraft broke 5-10 drifters loose from the bundle at any given launch. In addition, wave action might have accelerated dissolution of some of the salt blocks more than others. Third, the drifters may somewhat rectify a time-varying current and may therefore show an apparent component due to wave-induced pumping. The magnitude of this effect is uncertain, but it is not felt to be significant here relative to the actual longshore currents. A final consideration stems from the fact that the drifters passed through various regions (depending upon the tidal cycle) en route from their launch site to the beach and that their residence times in each of these regions are unknown. Presumably a pollutant passing through the surf zone would be subject to the same effects, however, so this is not viewed as a critical problem.

In order to provide an independent estimate of longshore currents, in the form of a surface speed rather than the near-bottom velocity resulting from the seabed drifter observations, computations were carried out using empirical equations in conjunction with estimated wave parameters. Estimates of the longshore surface currents produced by breaking waves were calculated using

the equation

$$v = 1.19(gH_b)^{\frac{1}{2}} \sin\alpha \cos\alpha \quad (\text{Komar et al., 1976})$$

where α = angle of breaking wave relative to the coast,

H_b = height of breaking wave, and

g = acceleration of gravity.

The wave height was estimated visually during deployment and recovery of the seabed drifters, and concurrent photographs were taken from a light plane for later determination of the wave angle. Because of the complexity of the surf zone, the wave height and angle measurements were primarily of the dominant wave train. Irregular bottom slope and the contributions from different wave directions make the situation complex, but it is felt that these observations can provide a reasonable order-of-magnitude estimate of longshore currents. Results are presented in Sections 3 and 4.

2.3 Temperature and Salinity Observations

Temperature and salinity observations necessary for determination of water mass interactions such as mixing, for determination of the origins of water types, and to aid in interpretation of current data were obtained from shipboard and as time series from the current moorings. The shipboard sampling pattern encompassed both large-scale shelf-wide spatial scales and small-scale near-shore features through close-spaced sections.

2.3.1 CTD Observations

Temperature and salinity were observed at selected locations as a function of depth using a shipboard conductivity/temperature/depth recording system (CTD). These CTD operations were carried out coincident with the current studies described above. Individual CTD casts were made both on a predetermined grid (Figures 6 and 7) designed to define the regional fields of temperature and salinity, along closely spaced near-coastal sections to define the temperature-salinity structure of the near-coastal currents, and following the radar-tracked drogues described above. Data (such as locations and times) pertinent to these CTD stations are given in Appendix 1.

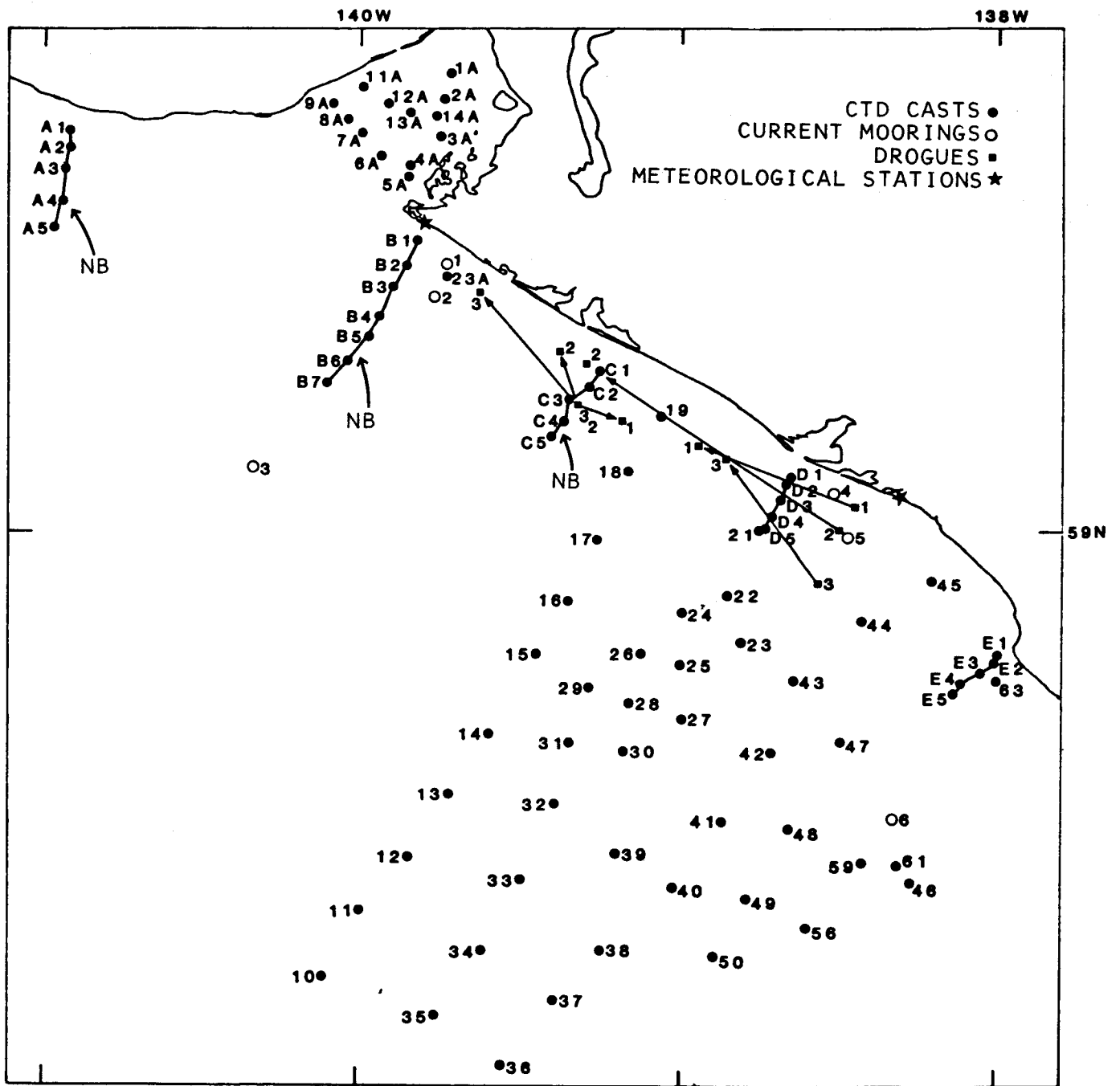


Figure 6. Locations of CTD stations occupied in October-November 1980.

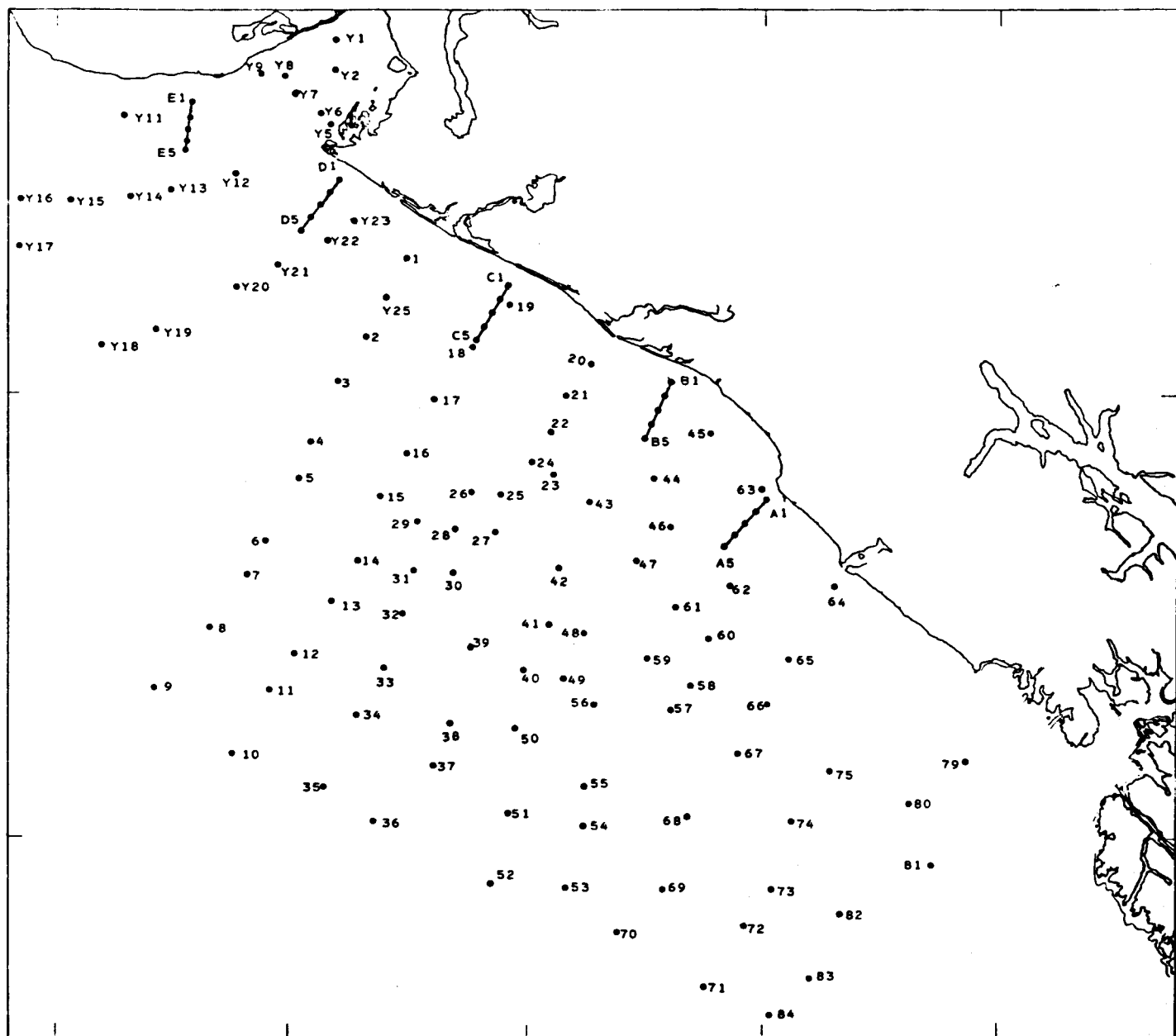


Figure 7. Locations of CTD stations occupied in March-April 1981.

Occupation of the CTD stations followed the general guidelines used in the past for OCSEAP work (cf, for example, Muench and Schumacher, 1979). Data were recorded only on the downcast, and the CTD lowering rate was held to 0.5 m/sec or less to minimize spiking induced by sharp vertical temperature gradients. Sampling was stopped at about 5 m above the bottom in shallow water and at about 10 m in deep water to avoid damage to the sensors. A water sample was obtained for calibration purposes on every third cast. Sample interval during the downcast was 0.1 sec.

Calibrations for the CTD used for both autumn and spring cruises, furnished by the Northwest Regional Calibration Center, provide an estimate of the standard deviation for expected error in the measurements. For the CTD used on the autumn cruise, accuracies for conductivity, temperature and pressure were respectively 0.009 mmho/cm, 0.013 °C and 1 psi. Corresponding values for the CTD used on the spring cruise were 0.011 mmho/cm, 0.009 °C and 1 psi.

Both of the cruises used Plessey Model 9040 CTD systems. For the autumn cruise, data were digitally recorded on a Grundy Model 8400 deck unit and seven-track Kennedy tape recorder. For the spring cruise, data were recorded through a Grundy Model 8700 deck unit and a PDP-11/34 computer onto a DEC Model TS03 nine-track tape recorder. Final processing of the CTD data was carried out on a PDP-11/60 computer located at SAI/Northwest. Processing routines were standard procedures such as utilized for previous OCSEAP work and described in previous documents, and will not be described here.

2.3.2 Temperature and Conductivity Time Series

As described above, each of the Aanderaa recording current meters deployed was equipped with sensors for measuring temperature and conductivity. Throughout the records, these parameters were recorded at the same intervals as the current information, and locations for these time series are the same as for the current records (Figure 2). In contrast, the vector-averaging current meters did not have provision for recording conductivity. They did, however, record temperature throughout the mooring periods.

The accuracy for the temperature and conductivity values recorded on the moorings is approximately 0.1 °C and 0.1 mmho/cm, respectively, which is considerably lower than that obtained from the CTD units. Preliminary comparison between the recorded values and values obtained from adjacent coincident (in time) stations using the CTD suggest that these estimated accuracies are reasonable. Despite the relatively low accuracy, the time series records are capable of detecting variations which can then be compared with coincident events in the current field, making the time series records useful in interpreting the overall data set.

2.4 Wind Observations

During the autumn and spring field experiments, the local wind field was measured through recording of wind speed and direction at two locations along the coastline, at Yakutat Airport and aboard the research vessel, and was computed as geostrophic winds by FNWC in Monterey, California.

Coastal winds were recorded during the field programs at locations along the beach at Dry Bay and Ocean Cape (Figure 2) using Aanderaa automatic recording weather stations. These stations were deployed prior to the beginning of the oceanographic field program for both the autumn and spring cruises and were recovered after the end of the oceanographic program, so that wind data were acquired over the entire period. Station sites were chosen so as to be on flat topography away from significant surface features, hills or forested areas. Locations on the shore just inland from the beach proved particularly satisfactory from this viewpoint because of the flat topography. The weather stations were equipped with 10-meter masts and were set to record at 10-minute intervals. The recording mode was the same as for the Aanderaa current meters, with speed accumulated through the recording interval and wind direction recorded instantaneously once per interval. Minimum threshold wind speed for these instruments is 30-50 cm/sec, with an accuracy of ± 2 percent, with directional accuracy to better than ± 5 degrees.

Data from the Aanderaa weather stations were supplemented with the data recorded by the National Weather Service at Yakutat Airport, which were supplied on a magnetic tape. The airport wind observations were recorded at 3-hour

intervals. Additional supplementary data were available in the form of the computed geostrophic winds, available at six-hour intervals, provided by the Fleet Numerical Weather Central by Mr. A. Bakun and computed according to Bakun (1975). Finally, winds were observed at hourly intervals from the oceanographic vessel during the field programs.

Long-term wind data were obtained in the form of the winds recorded at three-hour intervals at Yakutat Airport, and in the form of six-hourly computed geostrophic winds. These long time-series records coincided with the current record obtained from Mooring 6 during October 1980 to April 1981.

3. THE AUTUMN EXPERIMENT

3.1 Autumn Distributions of Temperature and Salinity

The temperature and salinity distributions for the northeast Gulf of Alaska continental shelf region were determined using a shipborne CTD system and recording current meters equipped with temperature and conductivity sensors (see Section 2). The spatial distributions of temperature and salinity are presented in this section.

The regional temperature and salinity fields are presented here as plan views at depths of 5 m (Figure 8) and 100 m (Figure 9) and as vertical distributions along a transect across the shelf from the coastline to seaward of the shelfbreak (Figure 10). The most prominent feature of the distribution was the narrow (~ 6 km) near-surface coastal band of low temperature (< 8.5 °C) and low salinity (< 31 ‰) water. There was some tendency for the band to widen by about a factor of two into a "bulge" southwest of Dry Bay (Figure 9a) and to be somewhat narrower to the northwest than to the southeast of this widening. On the vertical sections (Figure 10) the band is evidenced as a surface wedge of water which had temperatures below about 8.5 °C and salinities below about 31.0 ‰. The band was not evident at 100 m depth (Figure 9), being constrained generally to depths above ~ 20 m.

Farther offshore, the horizontal distributions of temperature and salinity were irregular (Figure 10). At 5 m the temperature and salinity well offshore south of Dry Bay appeared similar to that in the coastal band but were separated from it by a region of warmer and more saline water. The depressed isohalines at this location were also evident at 100 m depth. Prominent temperature elevations (> 9.5 °C) were evident at 100 m depth overlying Alsek Canyon south of Dry Bay. The general tendency at 5 m was for both temperature and salinity to increase in the offshore direction. At 100 m, salinity increased offshore as temperature decreased.

Because the near-shore band was the dominant feature in the temperature and salinity distributions, it will be investigated in somewhat greater detail. Four close-spaced (~ 5 km between stations) CTD transects occupied in autumn 1980 are

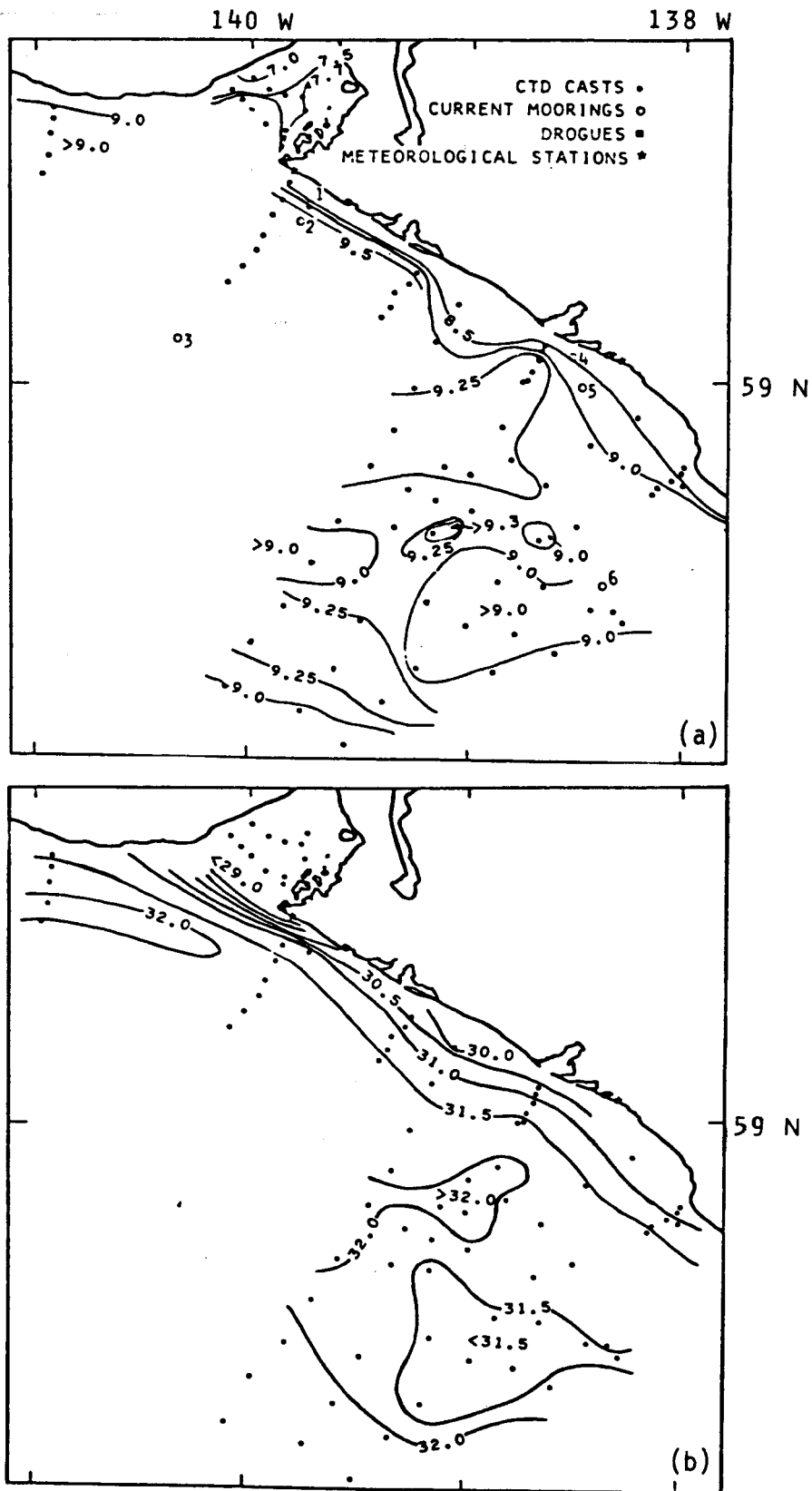


Figure 8. Horizontal distributions of temperature (a) and salinity (b) at 5 m depth for 23 October-4 November 1980. Salinity distribution within Yakutat Bay is not shown, because the contours there are too closely packed for adequate horizontal resolution on this scale.

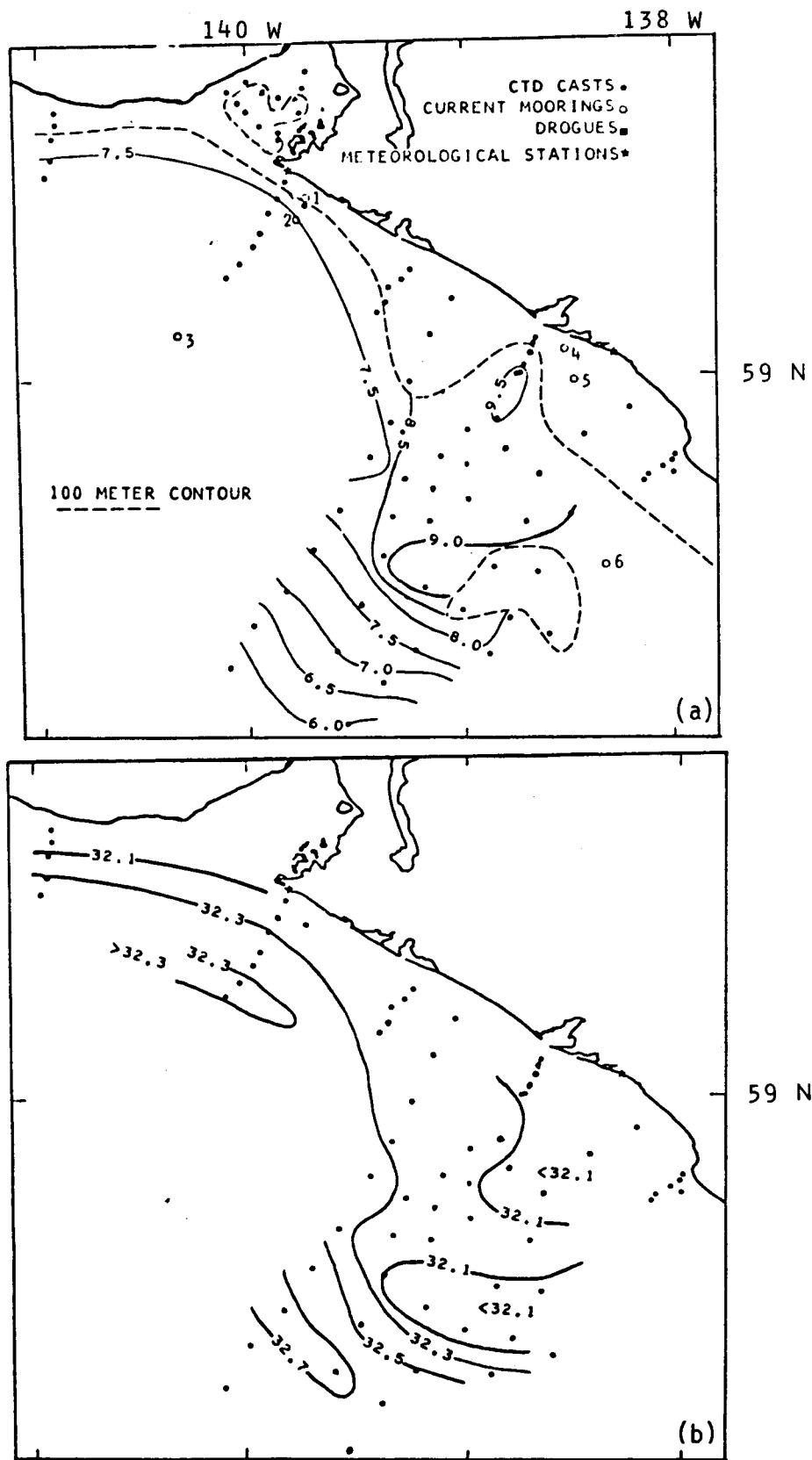


Figure 9. Horizontal distributions of temperature (a) and salinity (b) at 100 m depth for 23 October - 4 November 1980.

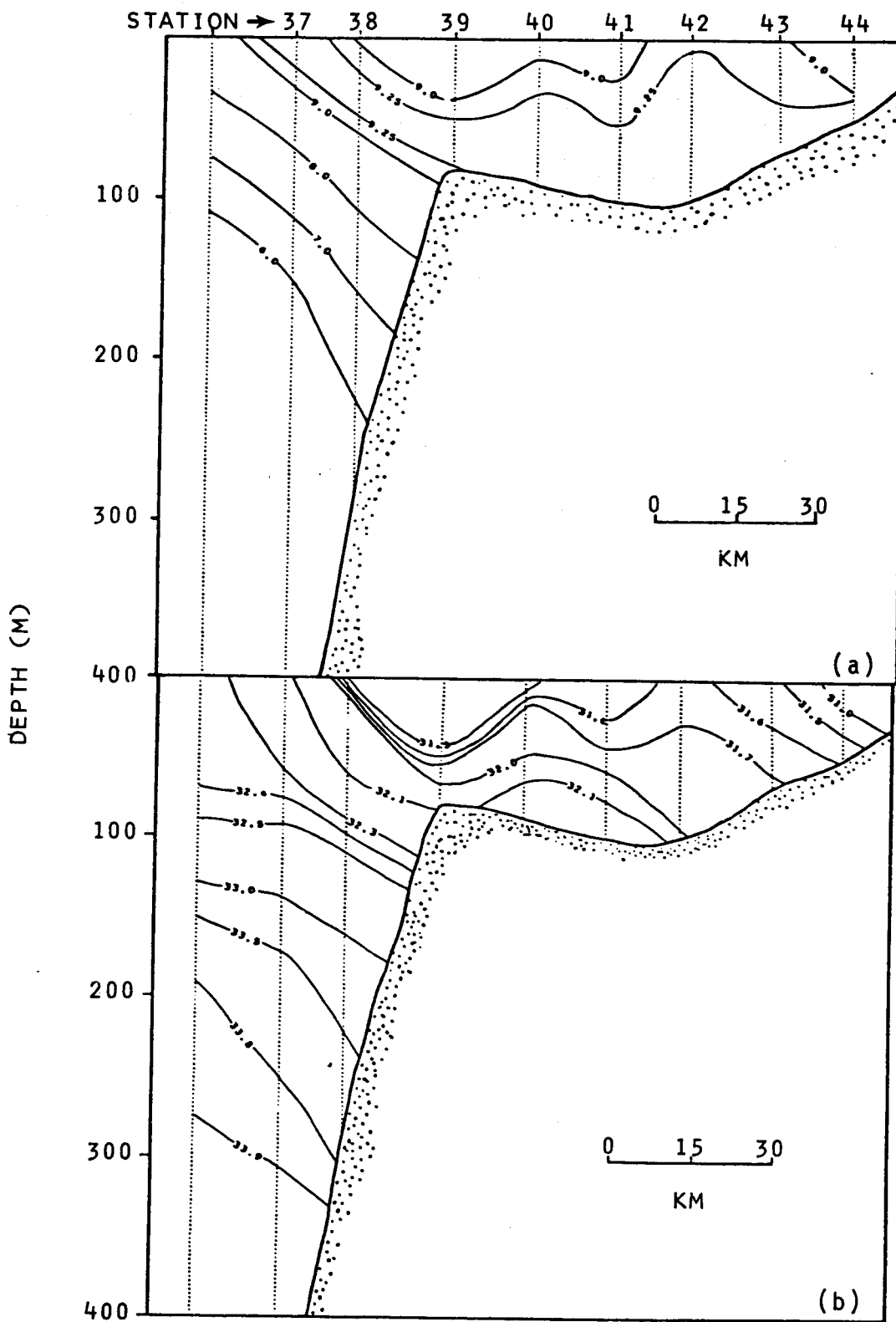


Figure 10. Vertical distributions of temperature (a) and salinity (b) along a transect normal to the coastline on 2 November 1980. See Figure 6 for location of transect.

especially suitable for documenting this feature. The vertical distributions of temperature along these transects are shown on Figure 11. Temperature, rather than salinity, is used as a tracer because it effectively shows the same features and was, in several cases, a better indicator of water mass distribution (cf. for example Figure 10). These CTD transects clearly indicate the relatively constant (5-6 km) offshore extent and spatial continuity of the band in the along-shore direction and its lack of penetration below about 20 m depth. Near-surface temperatures in the band were somewhat lower (typically 8.5 to 9.0 °C) than at depth, although it is probable that observations along Sections C and D (Figures 11b and c) did not extend close enough to the coastline to have detected the lowest temperatures present. Section B (Figure 11a) shows particularly well a thermocline which was present throughout the deeper portions of the study region at about 100 m where the bottom was sufficiently deep.

Features observed in the vertical distributions of temperature, salinity, and density can be better seen in selected vertical profiles (Figures 12-15). The strongest vertical gradients observed occurred in Yakutat Bay, where particularly cold (< 8 °C) and less saline (< 27 ‰) water was underlain by warmer (~ 10 °C) and more saline (> 31 ‰) water (Figure 12). Outside Yakutat Bay in the coastal band just off Ocean Cape, a similar vertical structure was observed with the upper layer having slightly higher salinities than in Yakutat Bay (Figure 13). The deep layer, following the pattern of these two stations, was typified throughout the study region by temperatures of ~ 10 °C and salinities of ~ 31.5 ‰. Farther offshore outside the coastal band, the upper layer of the water column tended toward vertical homogeneity and was underlain by a persistent gradient region at 75 to 125 m depth (Figure 14). Temperature decreased sharply as salinity increased throughout this vertical gradient region. The final profile illustrates the vertical distributions of temperature and salinity near the shelfbreak (Figure 15). At the location of this station, near-surface values were affected by a particularly cold and less saline lens of water which was not present throughout the region as indicated by the patchy upper-level temperature distribution (Figure 8).

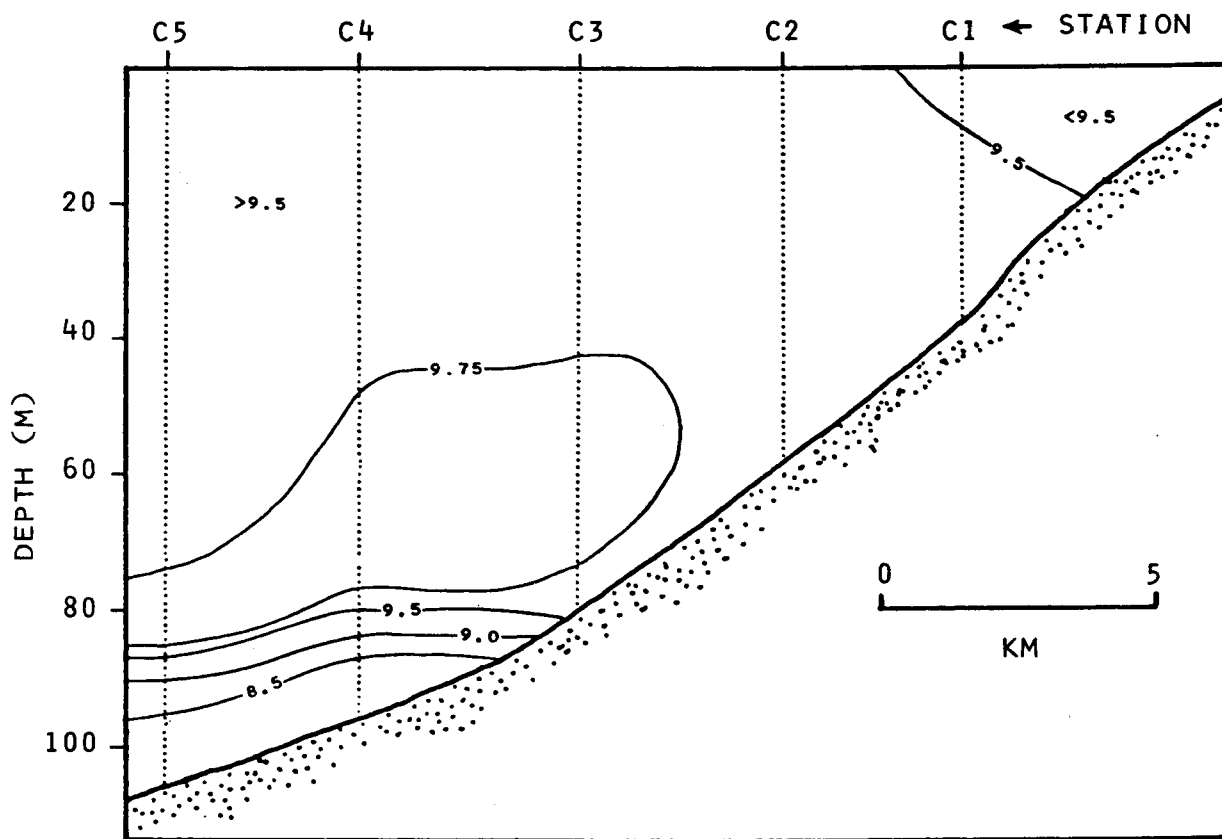
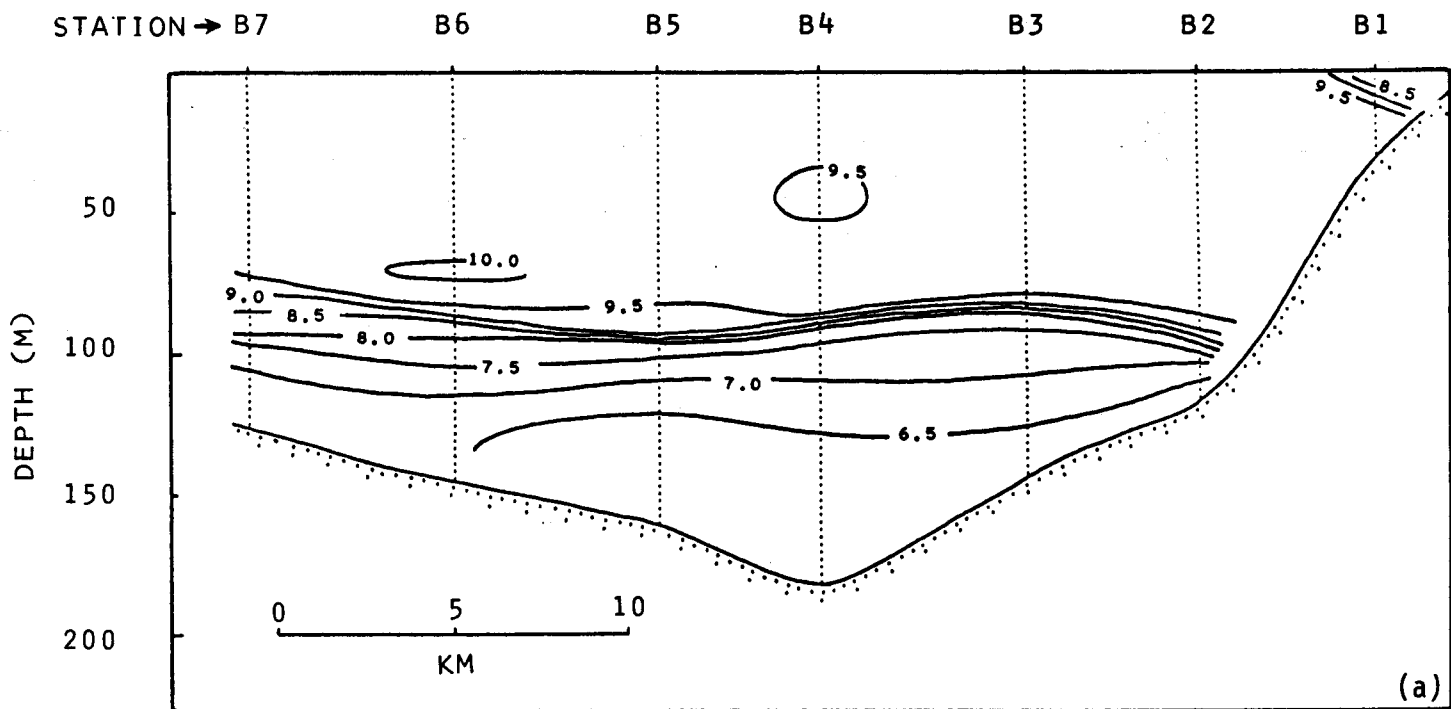


Figure 11. Vertical distributions of temperature along four transects normal to the coast and having closely-spaced stations. See Figure 6 for transect locations.

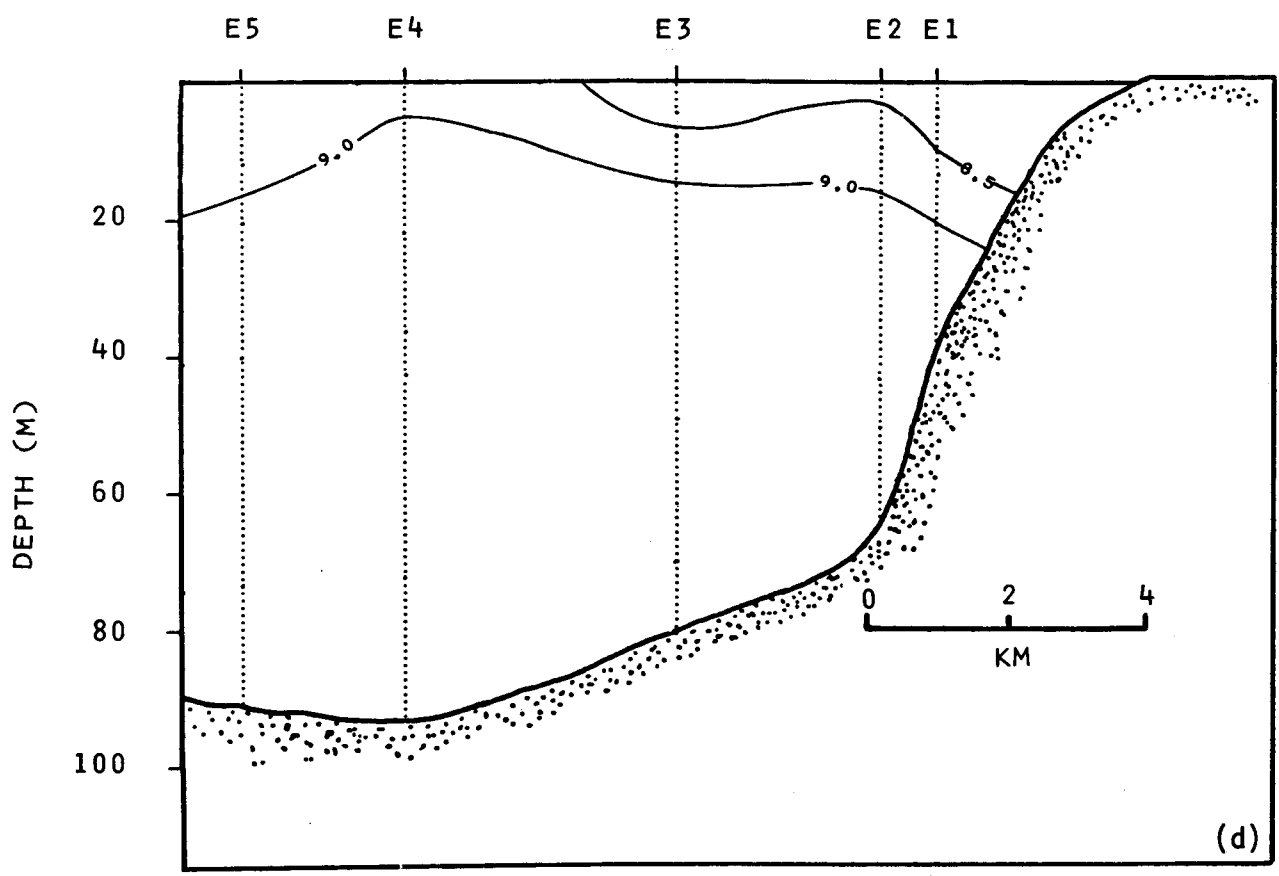
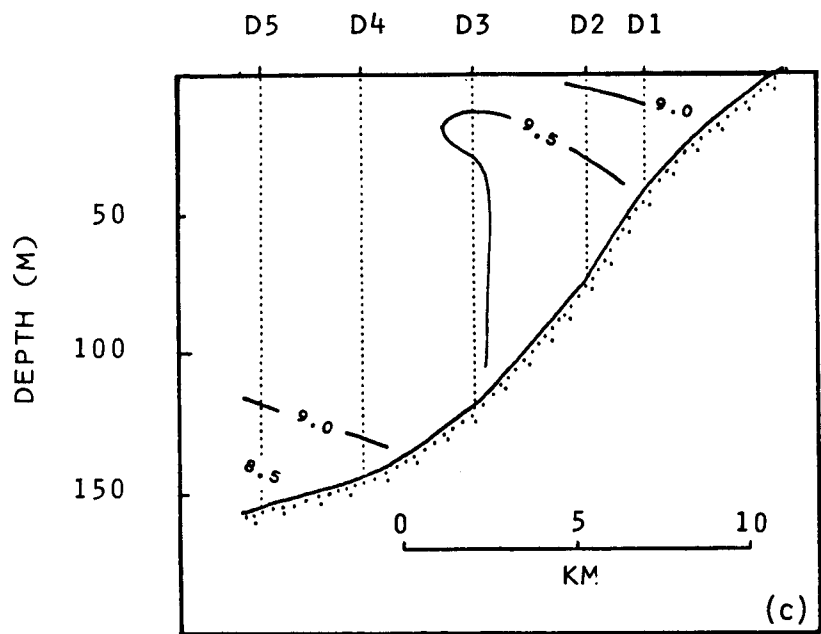


Figure 11 (continued)

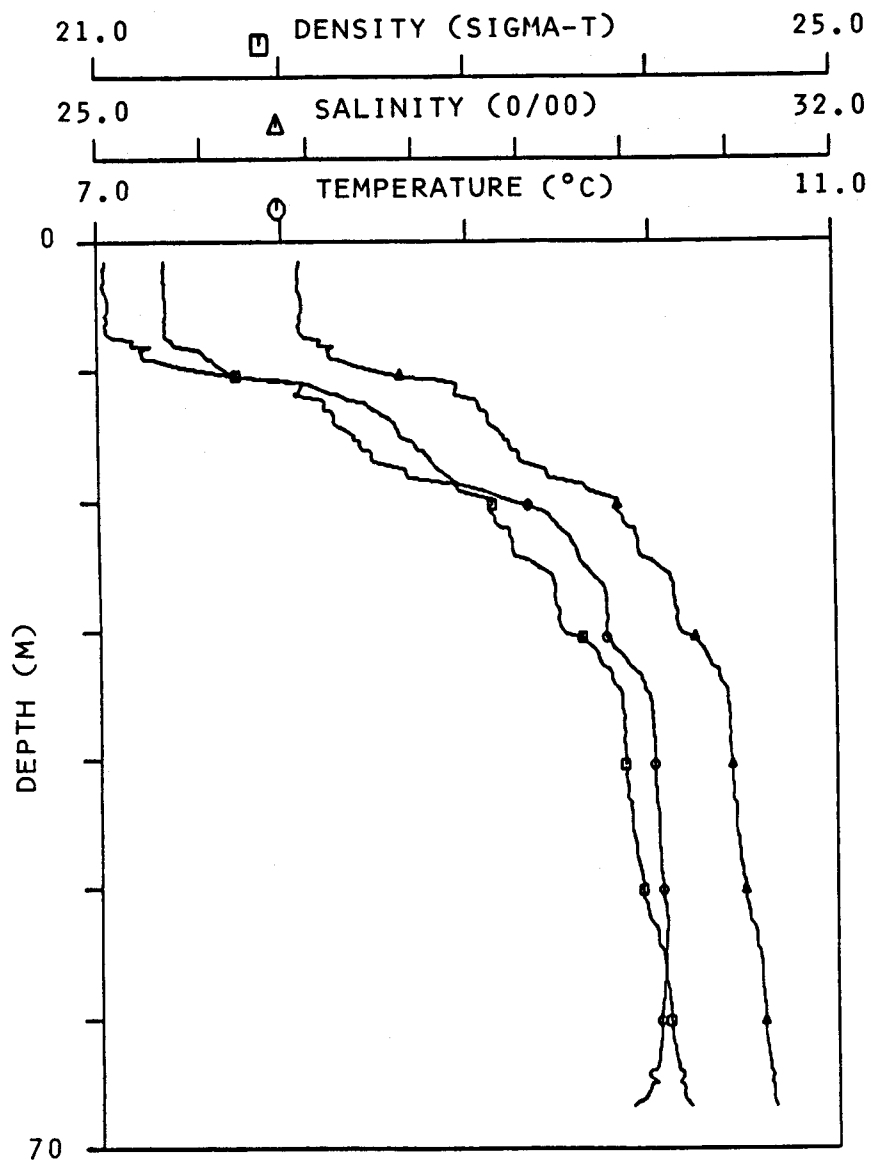


Figure 12. Vertical profiles of temperature, salinity, and density at Station 1a in Yakutat Bay. Station location is shown on Figure 6.

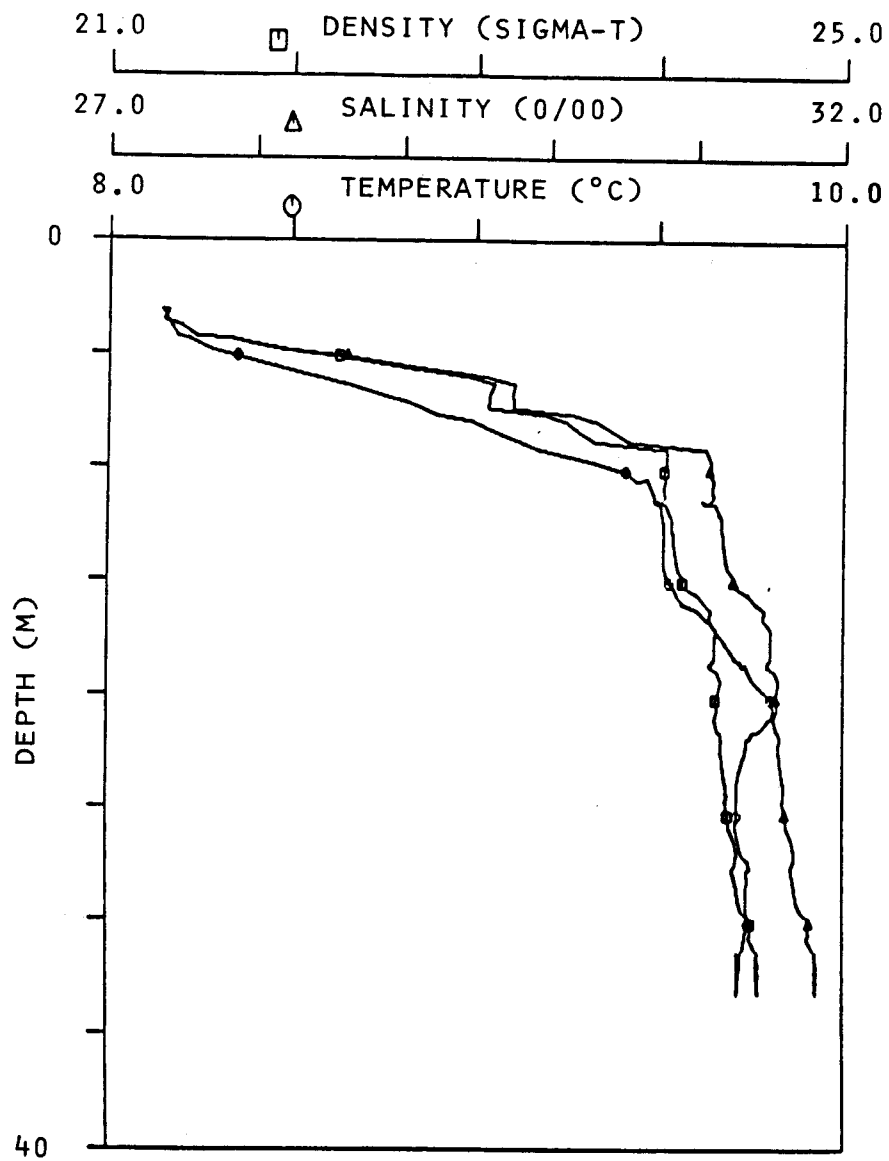


Figure 13. Vertical profiles of temperature, salinity, and density at Station B1 just off Ocean Cape. Station location is shown on Figure 6.

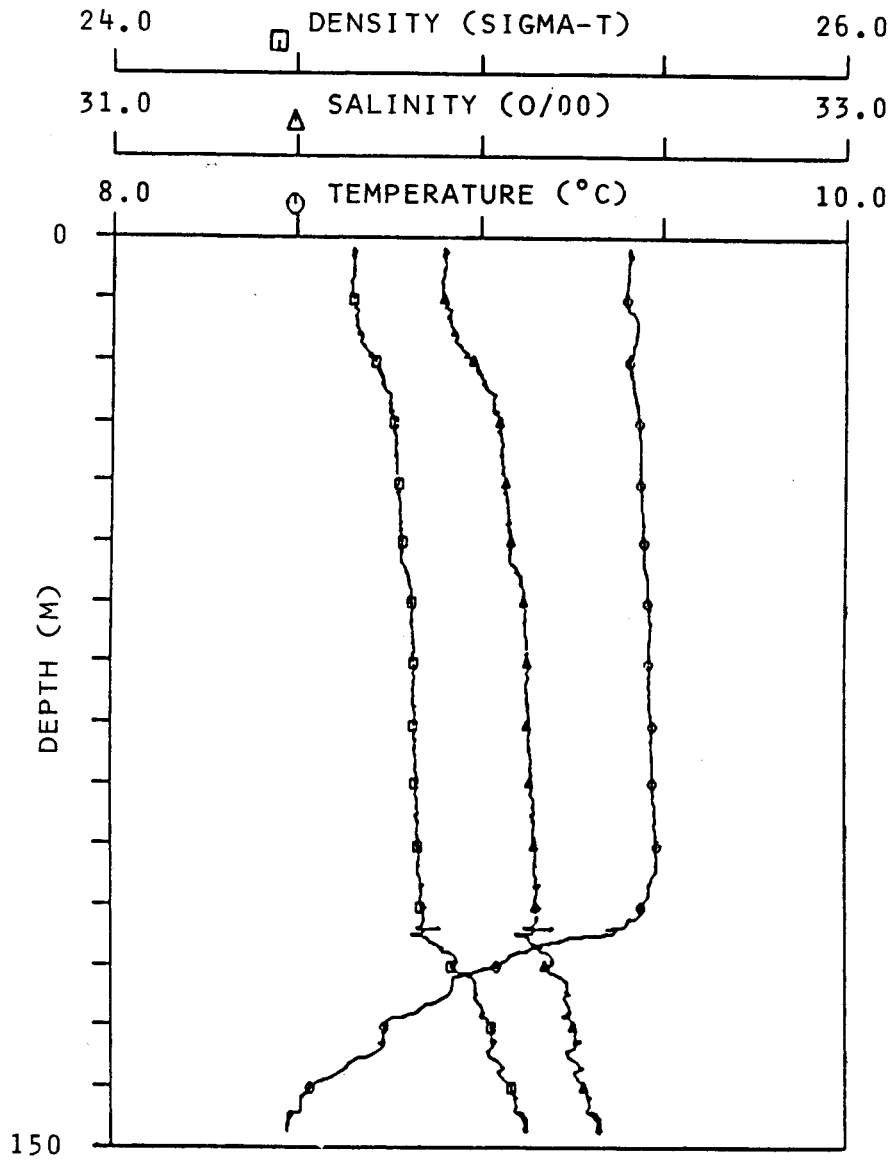


Figure 14. Vertical profiles of temperature, salinity, and density of Station D5 on mid-shelf. Station location is shown on Figure 6.

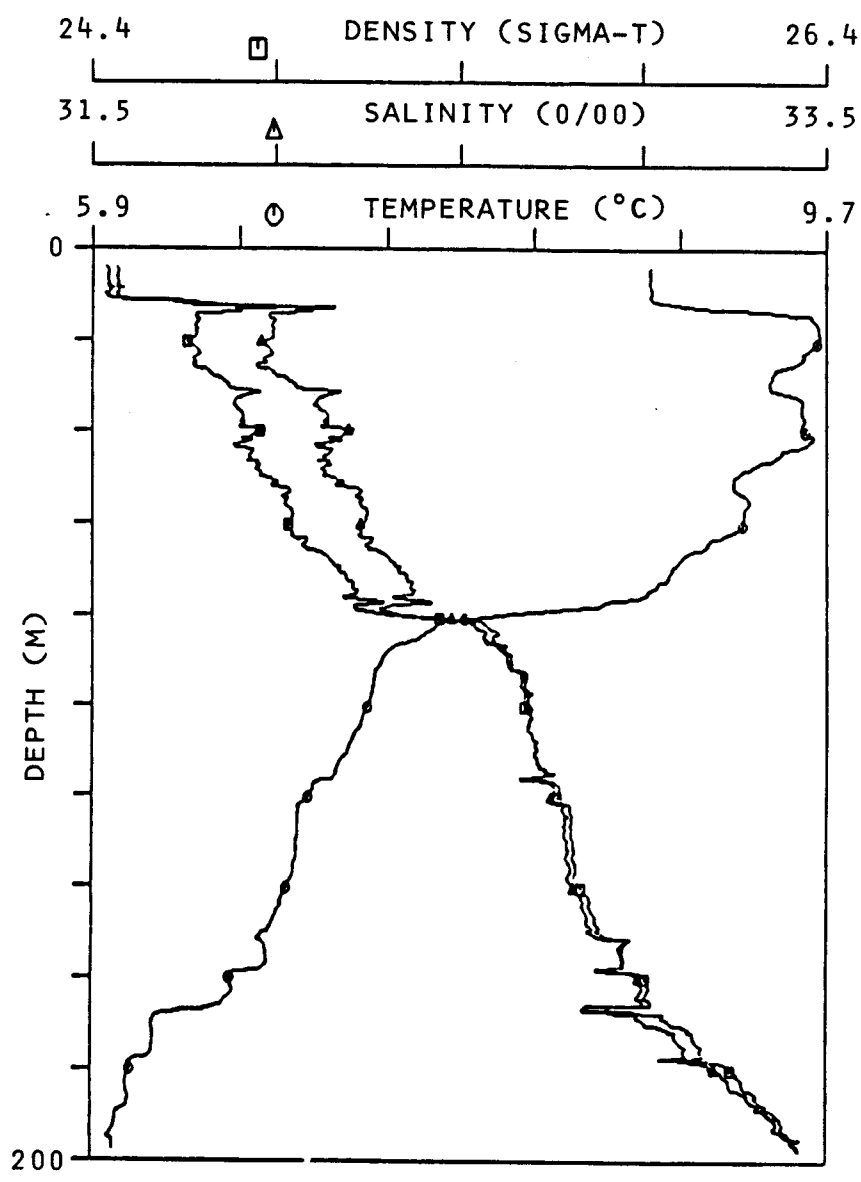


Figure 15. Vertical profiles of temperature, salinity, and density at Station 13 near the shelfbreak. Station location is shown on Figure 6.

To summarize, regional temperature and salinity distributions during October-November 1980 were typified by a two-layered structure seaward from a near-coastal band 10 km from shore. The lower layer was colder and more saline than the upper layer, and the interface between layers occurred at 75-125 m depths. There was a general tendency for salinity to increase, and temperature to decrease, in the offshore direction. Superposed upon this regional distribution was a narrow (< 7 km in most locations), shallow (< 20 m) coastal band of water which was low in salinity and temperature relative to that water immediately beneath and to seaward.

3.2 Observed Autumn Near-Shore Circulation

Water circulation was observed in October-November 1980 using current meters on taut-wire moorings, drogued buoys, and seabed drifters (see Section 2). Results of each of these observation sets will be discussed separately, because each yielded a different type of circulation information.

3.2.1 Autumn Moored Current Observations

There was considerable similarity between the results from near-shore Moorings 1 and 4 (cf. Figure 2), each of which was between 3 and 4 km offshore. Time series from these moorings are presented in Figures 16 and 17. The two records show three prominent flow characteristics. First, cross-shelf current speeds were small relative to longshore current speeds. Second, the along-shore flow was bimodal, with flow to the southeast nearly as frequently as to the northwest (Figure 18). Finally, the currents at each location were dominated by a relatively high speed (about 70 cm/sec at Mooring 4 and slightly less at Mooring 1) along-shore northwest flow event or pulse beginning on 27 October. At both Moorings 1 and 4, flow had been to the southeast prior to this pulse. Another similar event also occurred late on October 31 at Mooring 1, when simultaneous fluctuations in both the along-shore and cross-shelf components indicated a current pulse at the mooring.

Mooring 2, located about 10 km offshore (Figure 2), had current meters at 40 m and 129 m. Data from these meters are presented in similar format (Figures 19 and 20), except that a time series is presented of density instead

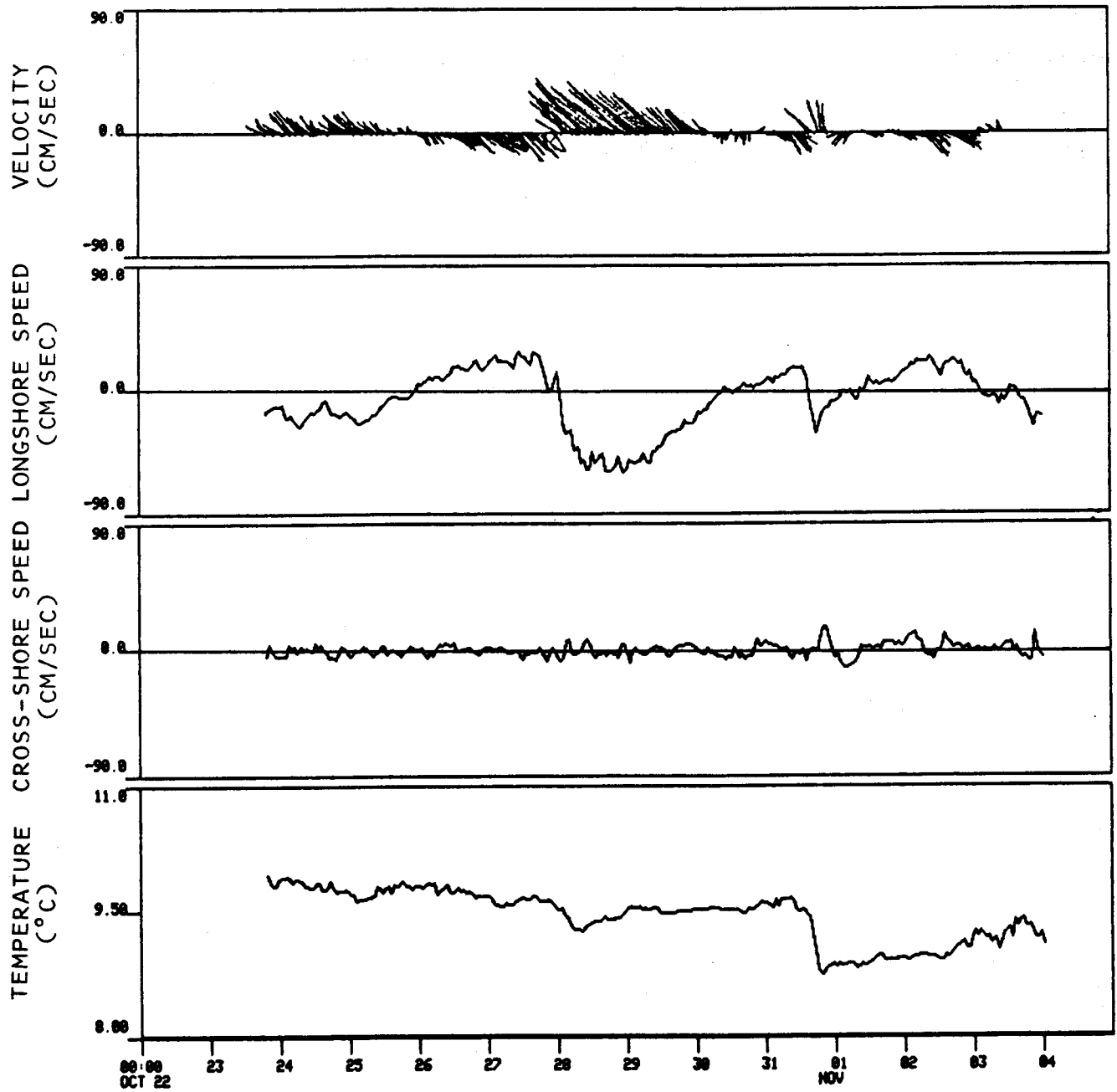


Figure 16. One-hour lowpass-filtered time series of currents (as time-stick vector plot, with vertically upward being north) from autumn Mooring 1. Mooring location is shown on Figure 2.

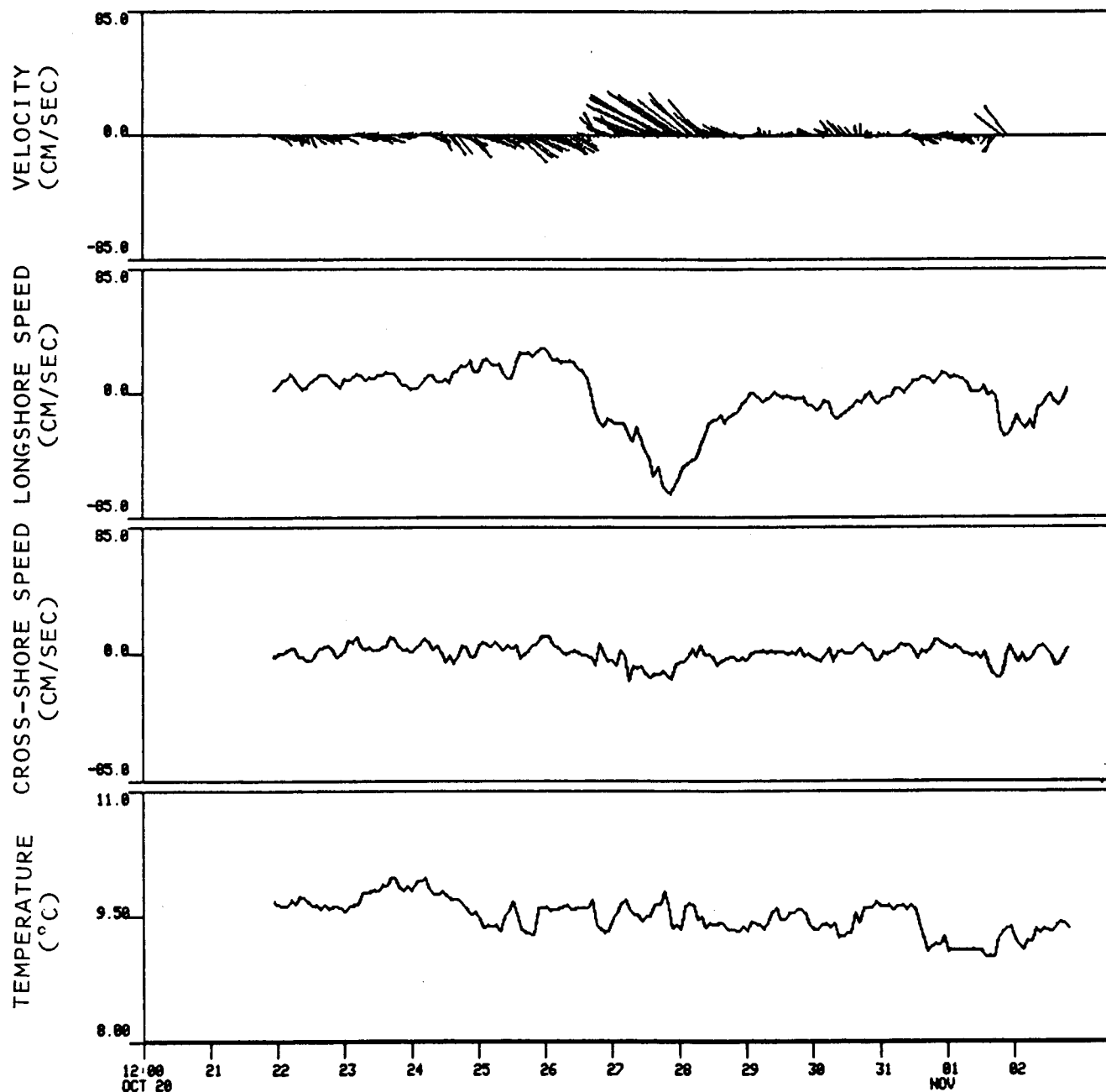


Figure 17. One-hour lowpass-filtered time series of currents (as time-stick vector plot, with vertically upward being north) from autumn Mooring 4. Mooring location is shown on Figure 2.

DIRECTION
MOORING 1 - FALL

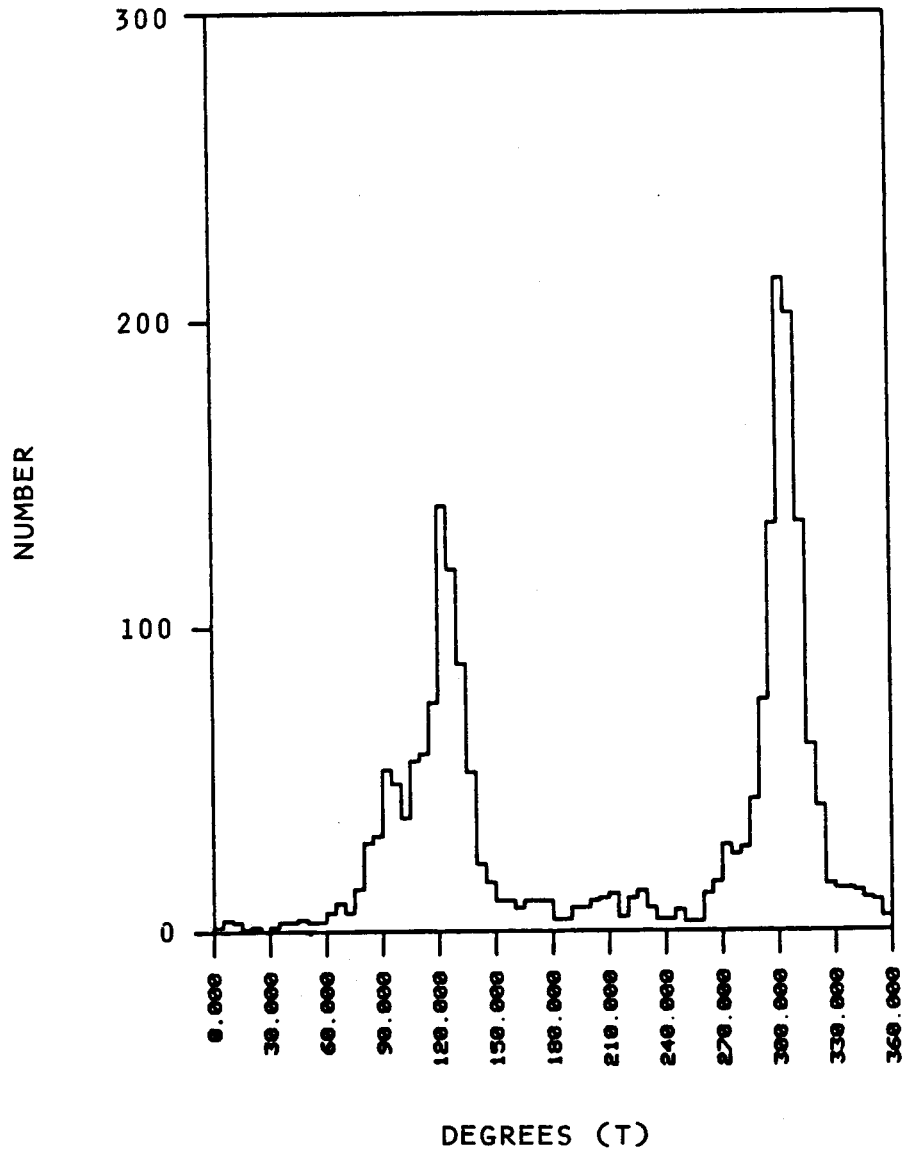


Figure 18. Direction histogram illustrating the bimodal flow direction at autumn Mooring 1. Mooring location is shown on Figure 2.

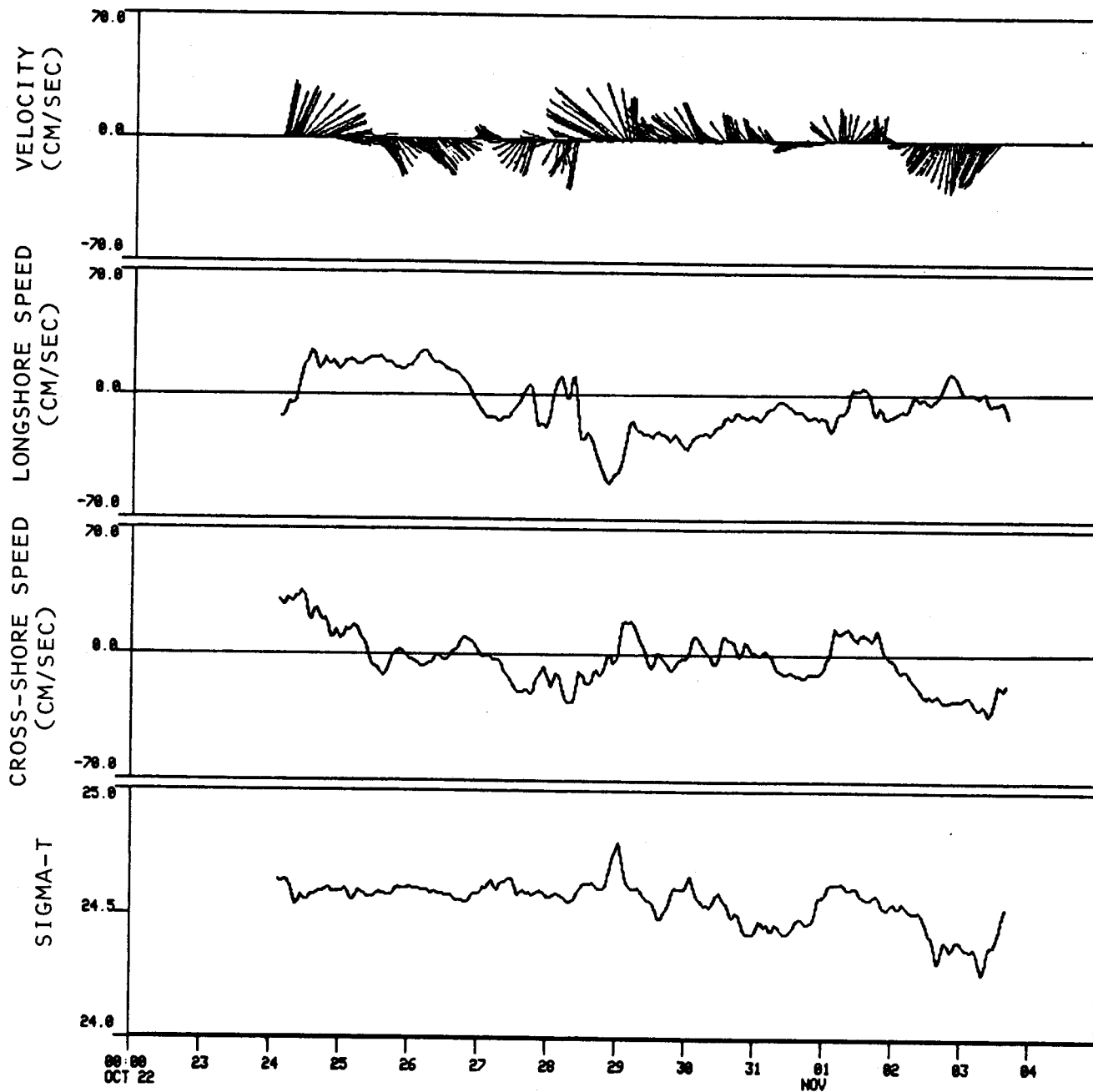


Figure 19. One-hour lowpass-filtered time series of currents as time-stick vector plot, with vertically upward being north, from the 40-m deep meter at autumn Mooring 2. Mooring location is shown on Figure 2.

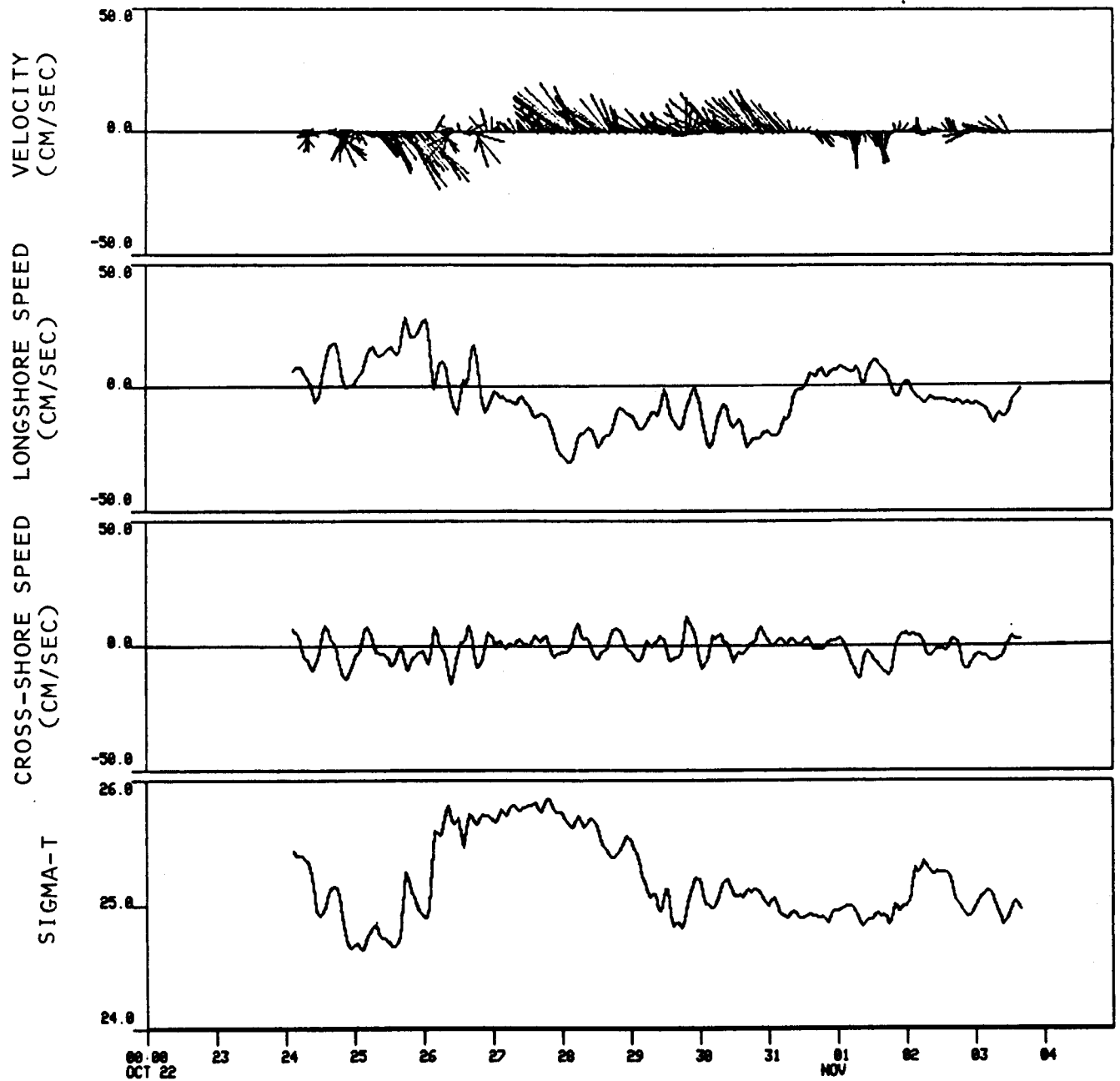


Figure 20. One-hour lowpass-filtered time series of currents as time-stick vector plot, with vertically upward being north, from the 129-m deep meter at autumn Mooring 2.

of temperature as for Moorings 1 and 4. Characteristics of the flow at Mooring 2 were similar to those at Moorings 1 and 4. At the deeper current meter, cross-shelf speeds were very small relative to along-shore speeds, while at the shallower meter this was less evident than at either the deeper meter or at Moorings 1 and 4. The along-shore flow was bimodal at all depths, although the bimodality was far stronger at the upper current meter (Figure 21). Finally, the same current pulse observed at Moorings 1 and 4 on 27 October occurred at the upper meter at Mooring 2 a few hours after it was observed at Mooring 1, reaching peak speeds of about 50 cm/sec. The along-shore pulse was followed by a smaller peak in cross-shelf speed. The current pulse was also observed at the deep current meter at Mooring 2, but was smaller than at the surface and occurred somewhat earlier. The large fluctuations in density which were apparent at the deep meter at Mooring 2 will be discussed in Section 3.3.

Mooring 5 was located about 9.4 km offshore at 65 m depth and had one operational current meter at 17 m; the deeper current meter deployed on this mooring malfunctioned and thus yielded no record. The most apparent difference between the flow at the upper meter at Mooring 5 and those discussed above was the relatively large cross-shelf flow at Mooring 5 (Figure 22). Mooring 5 also detected the northwesterly pulse which was present at the other near-coastal moorings, with a peak speed of about 50 cm/sec. A separate feature, unique to Mooring 5, was a strong (> 50 cm/sec) current to the southeast persisting from October 25 to October 27 prior to the northwesterly pulse.

Mooring 6 was considerably farther offshore -- about 70 km -- than Moorings 1-5. Because it was so much farther offshore than the moorings discussed above, it recorded currents within a basically different mid-shelf current regime than the older moorings discussed above. Results from the Mooring 6 observations are shown on Figures 23 and 24. Both speed and direction at the upper (29 m) meter showed considerable variability; a speed pulse on one occasion (17 November, after the other moorings had been recovered) was greater (nearly 80 cm/sec) than had been recorded elsewhere. Along-shore and cross-shelf speed fluctuations were of the same order, unlike conditions at the moorings nearer the coast where (except for Mooring 5) the flow was predominantly along-shore. Tidal fluctuations are evident on the plots, but these fluctuations were secondary in significance to the longer period (~ 4 days)

DIRECTION
MOORING 2 - FALL

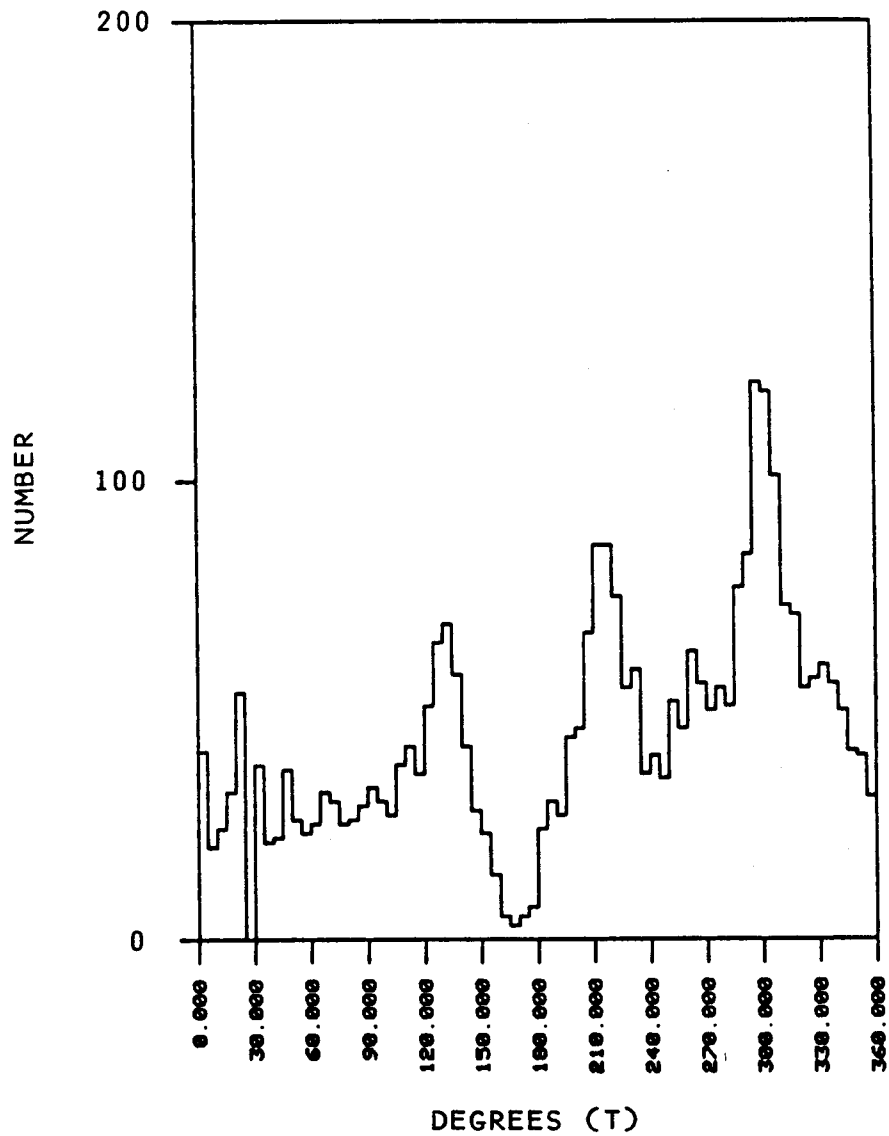


Figure 21. Histogram illustrating the flow direction tendencies at the shallow meter on autumn Mooring 2.

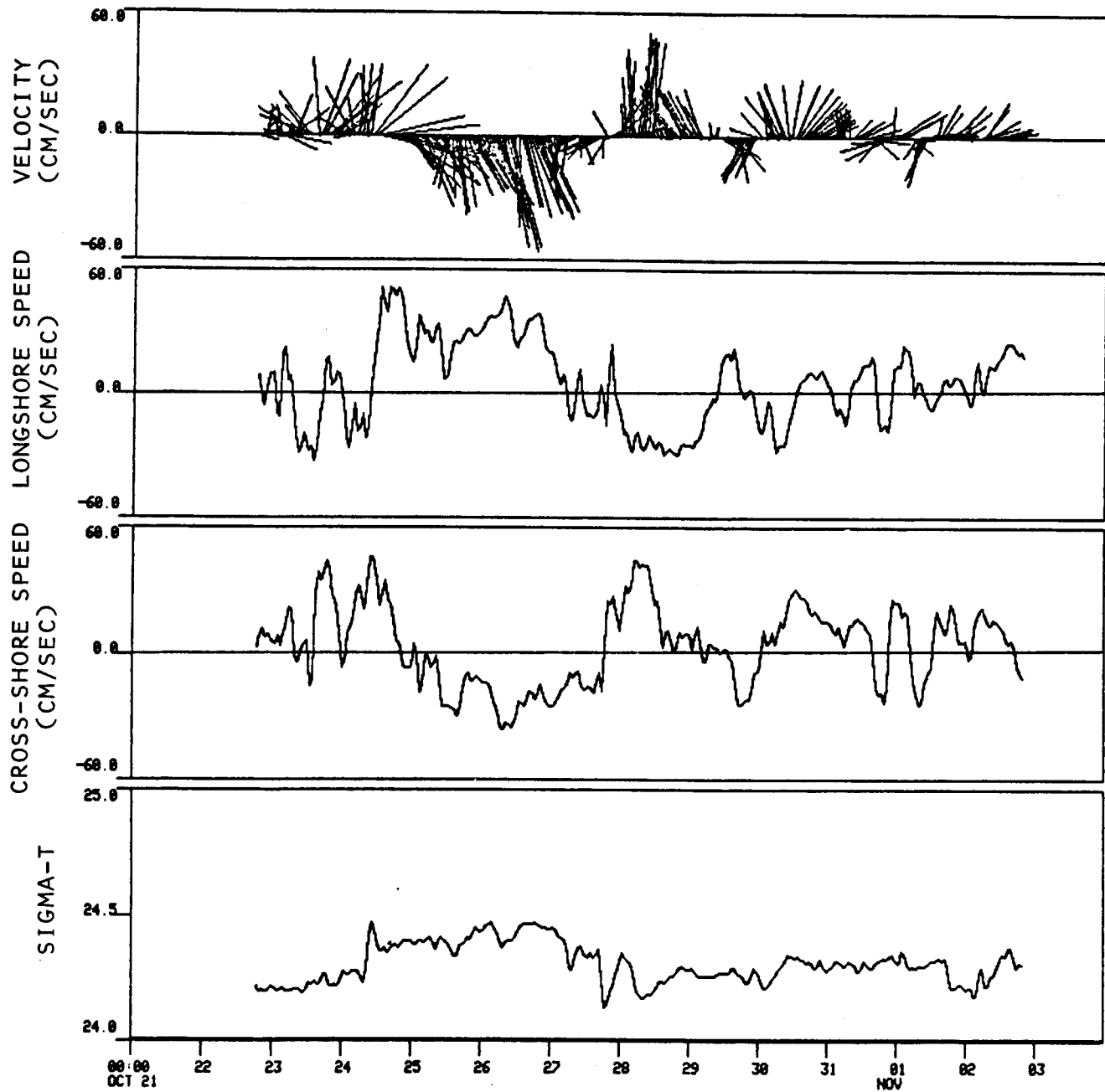


Figure 22. One-hour lowpass-filtered time series of currents as time-stick vector plot, with vertically upward being north, from the 17-m deep meter at autumn Mooring 5. Mooring location is shown on Figure 2.

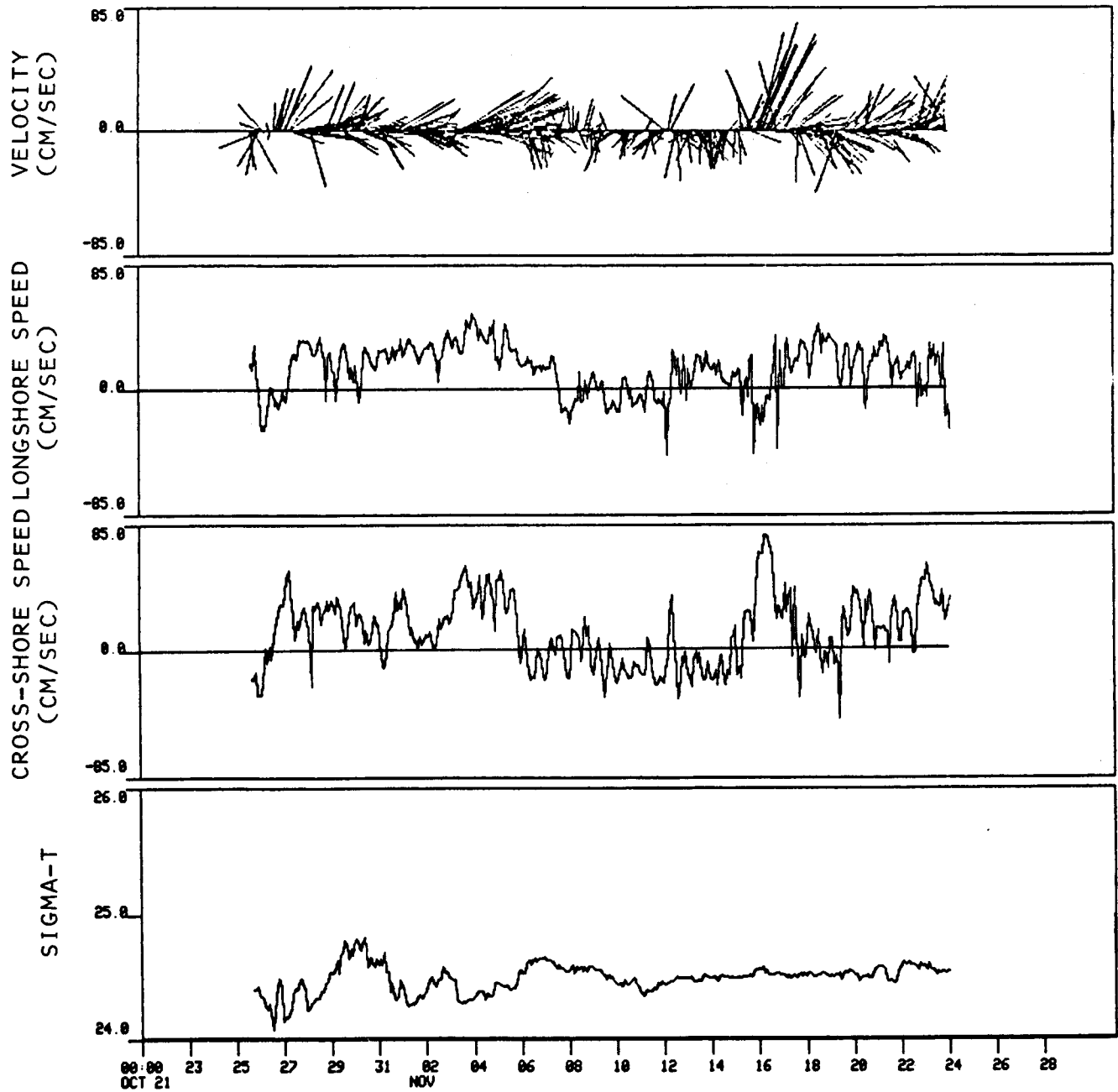


Figure 23. One-hour lowpass-filtered time series of currents as time-stick vector plot, with vertically upward being north, from the 29-m deep meter at autumn Mooring 6. Mooring location is shown on Figure 2.

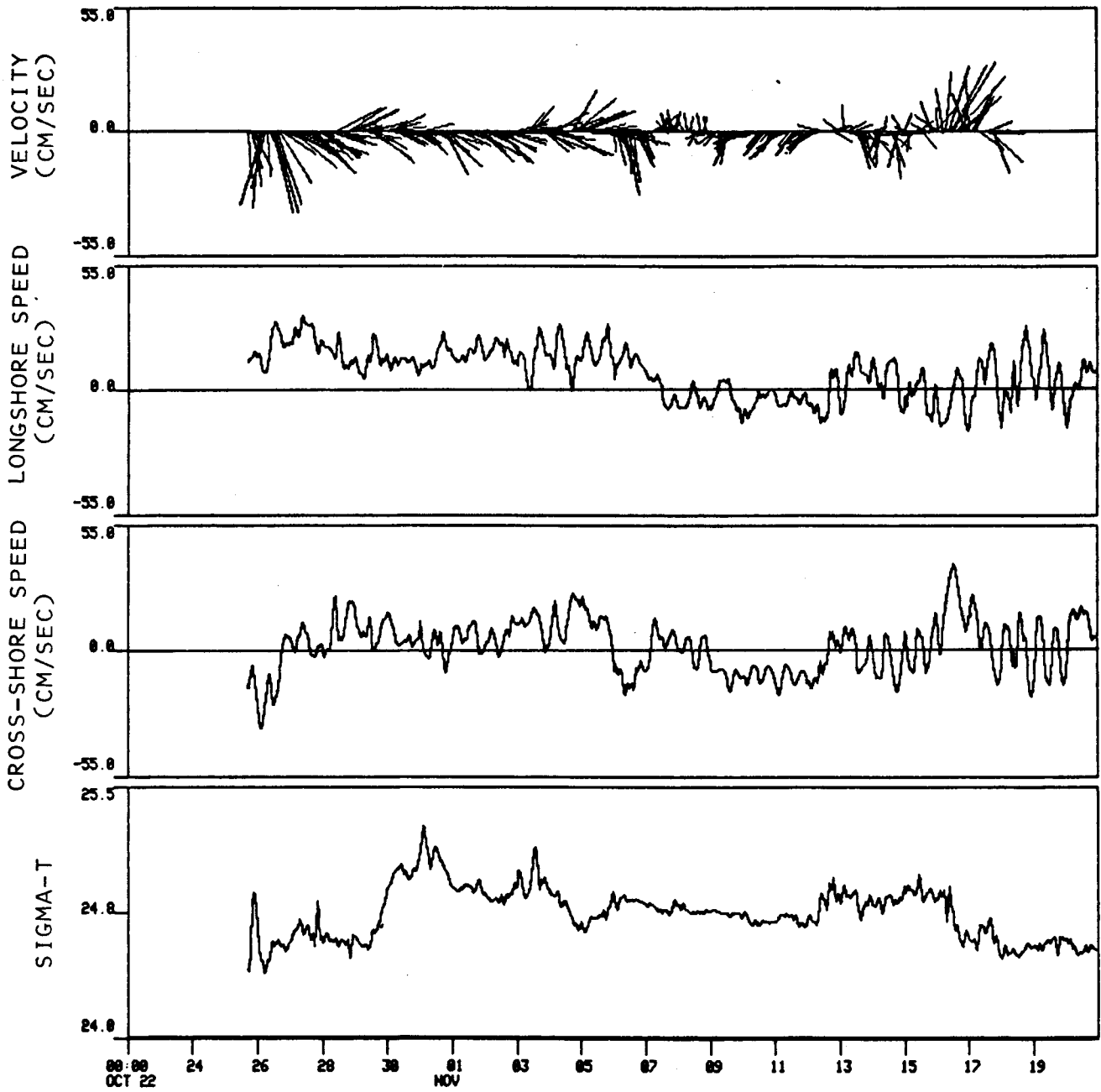


Figure 24. One-hour lowpass-filtered time series of currents as time-stick vector plot, with vertically upward being north, from the 102-m deep meter at autumn Mooring 6. Mooring location is shown on Figure 2.

fluctuations such as that which resulted in the along-shore speed peak on 17 November. The net flow during the period of the autumn experiment was easterly, with a great deal of directional fluctuation. Current speeds at the lower (102 m depth) meter were lower than at the upper meter, and the tidal signal was therefore relatively more significant. Visual inspection of the plots suggests that coherency between the upper and lower records was poor. At Mooring 6 there was no detectable signature of the along-shore current pulse which had been a prominent feature of the nearer-shore records on 27 October.

3.2.2 Autumn Drogued Buoy Observations

The first autumn drogued buoy experiment was conducted 26-28 October 1980. The buoys were deployed within a 0.5-km radius and tracked for approximately one day, after which Buoy 1 was retrieved and the ship broke off operations to drop personnel in Yakutat. Tracking of the remaining two buoys was resumed after a hiatus of approximately 23 hours due to storm conditions. The buoys were subsequently tracked for 15 hours and then retrieved. A composite diagram of all fall buoy tracks is displayed in Figure 25, and more detailed individual buoy tracks are shown in Figures 26 and 27.

During Phase I of the first experiment, the buoys moved briefly in unison due north then reversed direction, turning toward the southeast (Figure 25). Statistically the buoy speeds (Table 3) for Phase I are essentially identical with a mean speed for all three drogues near 13 cm/sec and peak speeds of 20-25 cm/sec. All three buoys initially traveled in the same water parcel for this phase, and the separation distance between the buoys (Figure 28) decreased during the first 12 hours (to ~ 50 m at some times). By 1600 hours on 26 October, 15.5 hours after deployment, the buoys started to disperse more rapidly. The mean separation rates for this last part of Phase I ranged from 1.4 to 5.1 cm/sec.

Buoy 1 was now retrieved and the ship left the area as described above. During its absence current conditions changed considerably. Both remaining buoys (2 and 3) reversed direction and were traveling northwestward with considerably higher speeds (Table 3). In Phase II of the experiment, peak speeds of 47 and 105 cm/sec were reached at approximately 1100 hours on 28 October, thus

Table 3
AUTUMN DROGUED BUOY SPEED STATISTICS

	MIN SPEED (cm/sec)	MAX SPEED (cm/sec)	MEAN SPEED (cm/sec)	SPEED STD DEV (cm/sec)
EXPERIMENT 1				
<u>Phase I: 10/26/80 (0030 hrs) - 10/27/80 (0230 hrs)</u>				
Buoy 1	4.0	24.9	13.3	4.9
Buoy 2	5.0	21.2	13.5	3.9
Buoy 3	4.4	20.2	12.2	3.6
<u>Phase II: 10/28/80 (0200 hrs) - 10/28/80 (1630 hrs)</u>				
Buoy 2	12.5	46.9	29.4	10.6
Buoy 3	24.4	104.7	62.6	28.4

EXPERIMENT 2				
<u>Phase I: 10/29/80 (0230 hrs) - 10/29/80 (1730 hrs)</u>				
Buoy 2	0.6	18.7	8.5	4.4
Buoy 3	4.0	21.7	14.0	5.1
<u>Phase II: 10/29/80 (1800 hrs) - 10/30/80 (1730 hrs)</u>				
Buoy 1	12.3	42.1	28.1	8.3
Buoy 2	13.0	43.7	29.1	8.7
Buoy 3	6.8	49.1	24.1	9.6

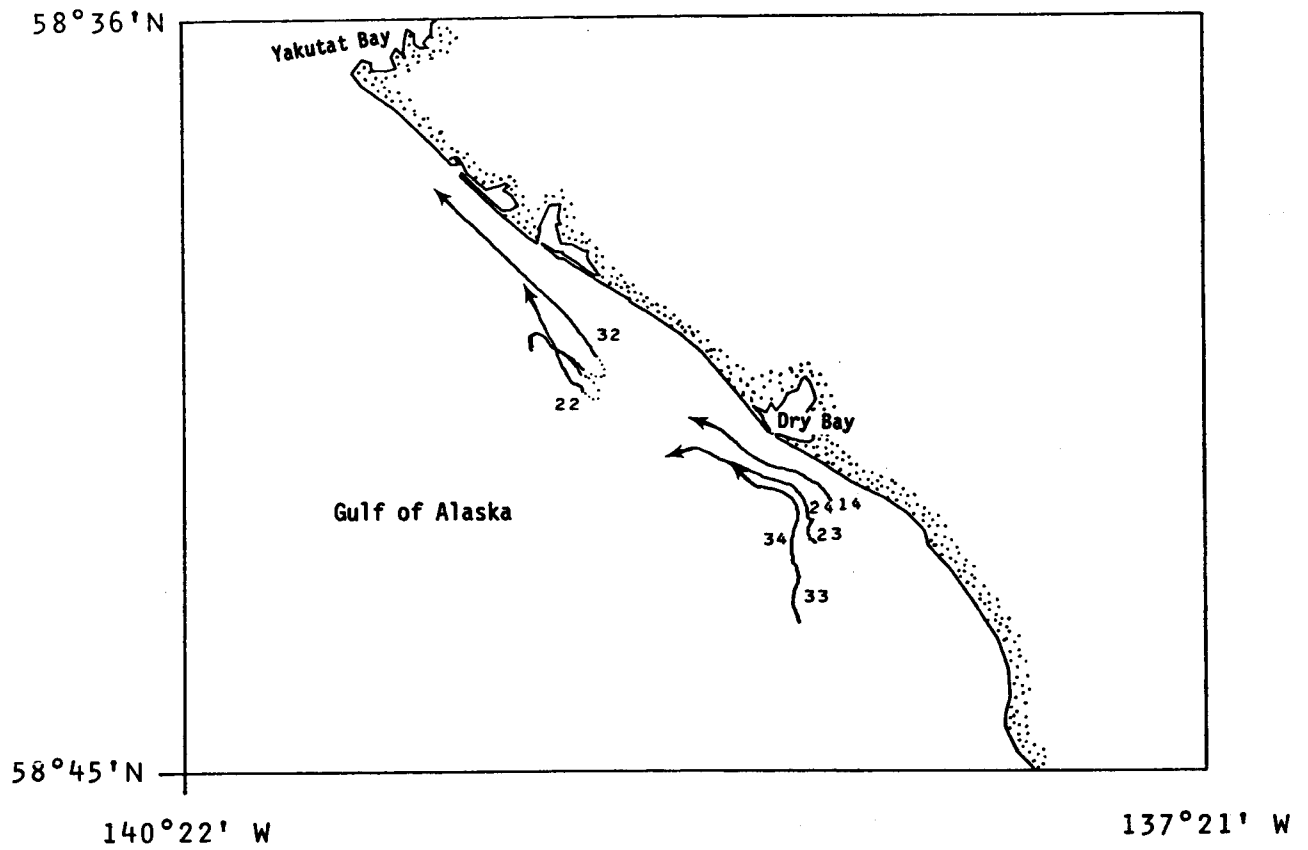


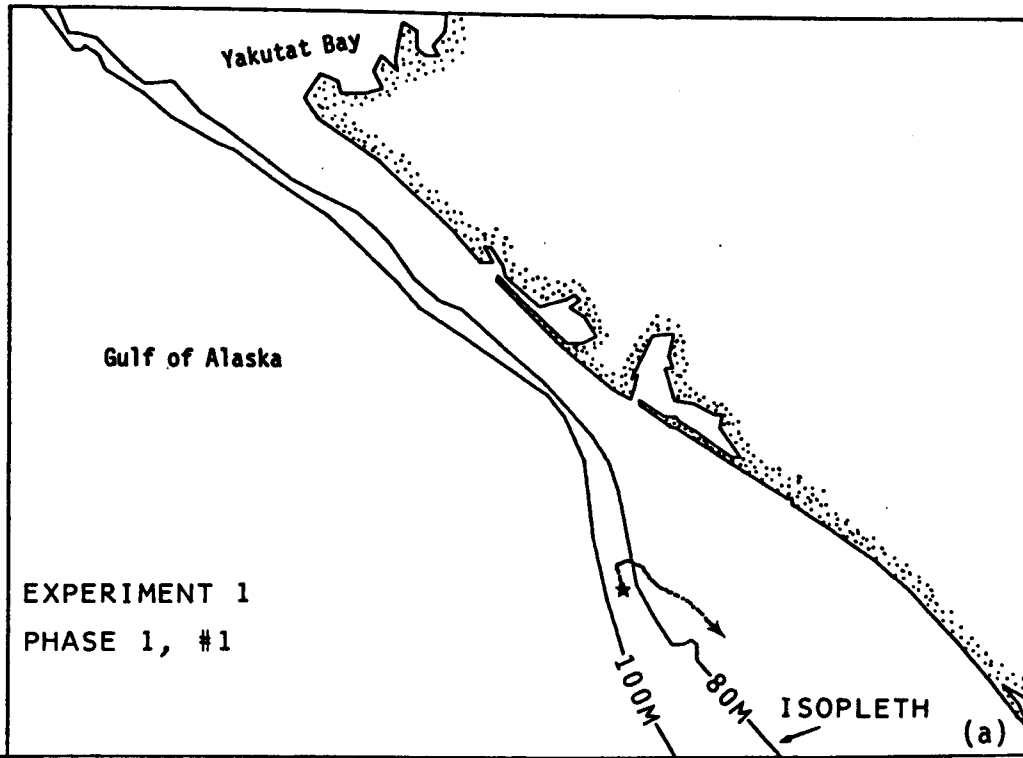
Figure 25. Composite picture showing all drogued drifter tracks observed in autumn 1980.

59°36'N

58°45'N

140°22'W

137°21'W



59°36'N

58°45'N

140°22'W

137°21'W

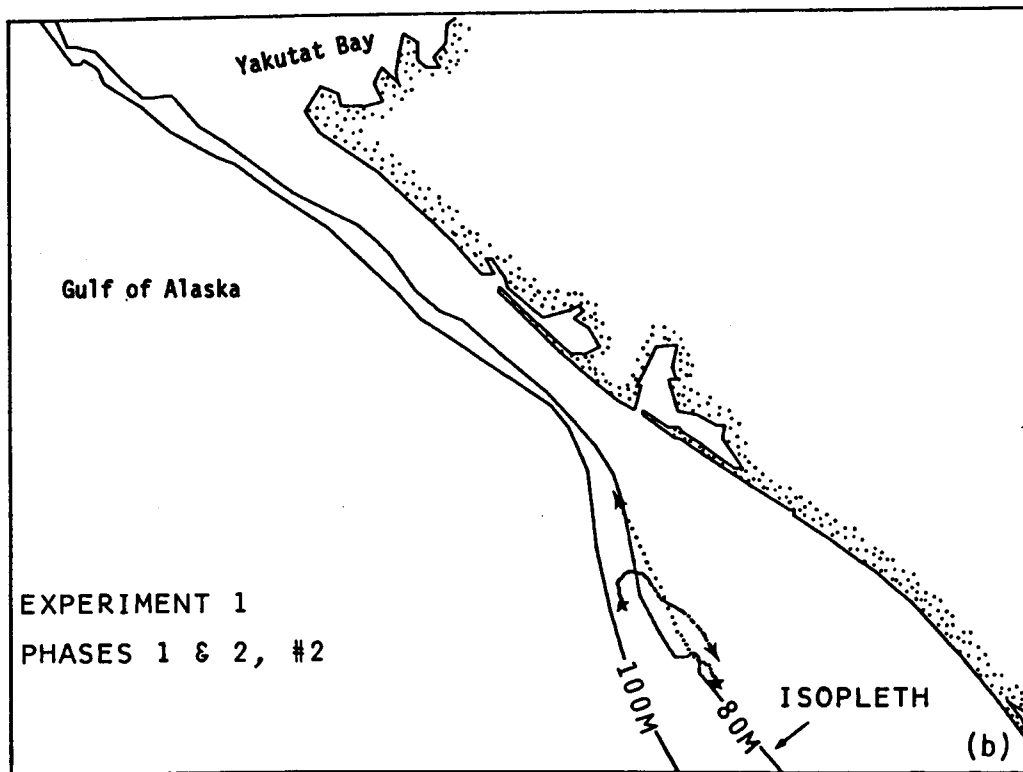


Figure 26. Individual drogue tracks (a), (b), (c) followed by Drifters 1, 2, 3 respectively in the first autumn 1980 drogue experiment. Stars mark start points for each drift track segment.

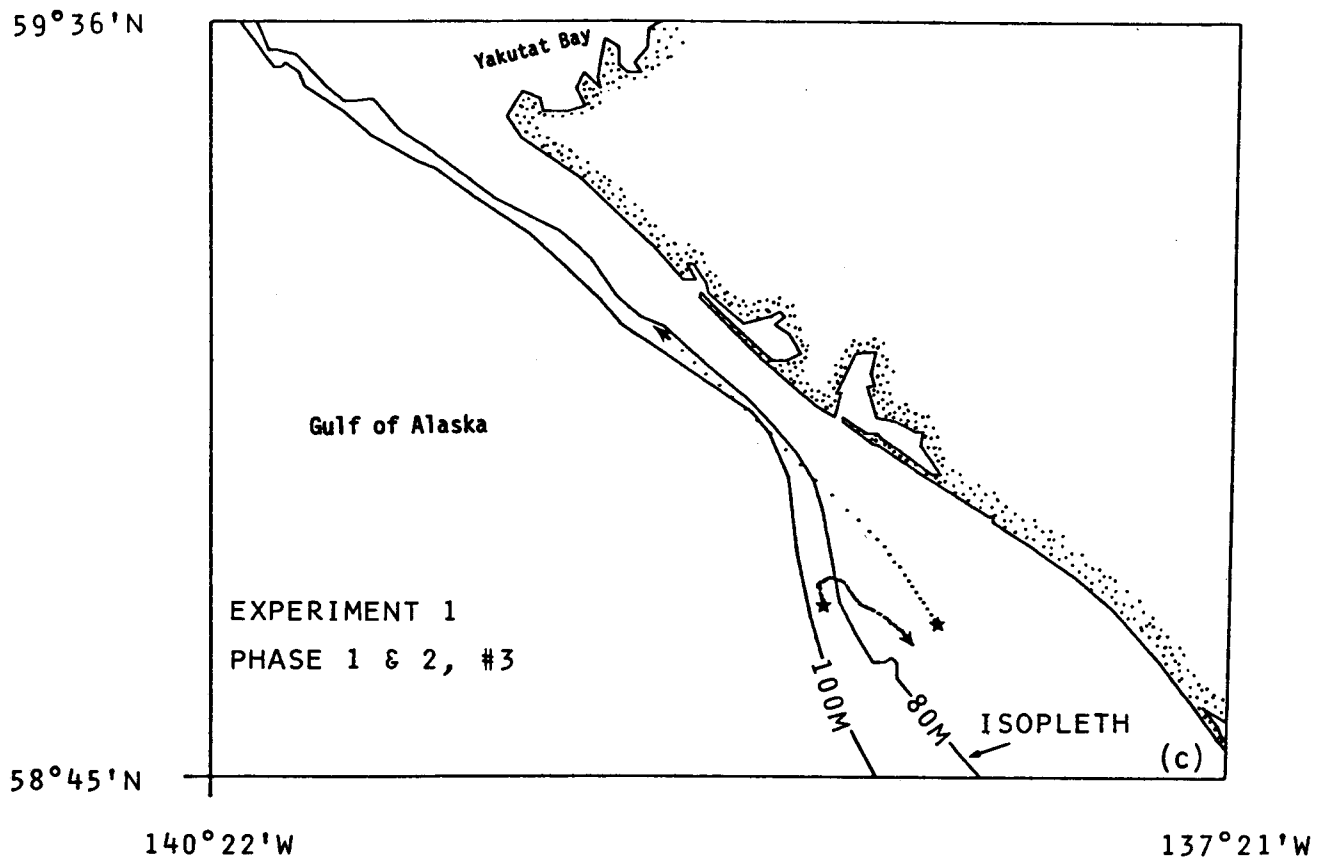
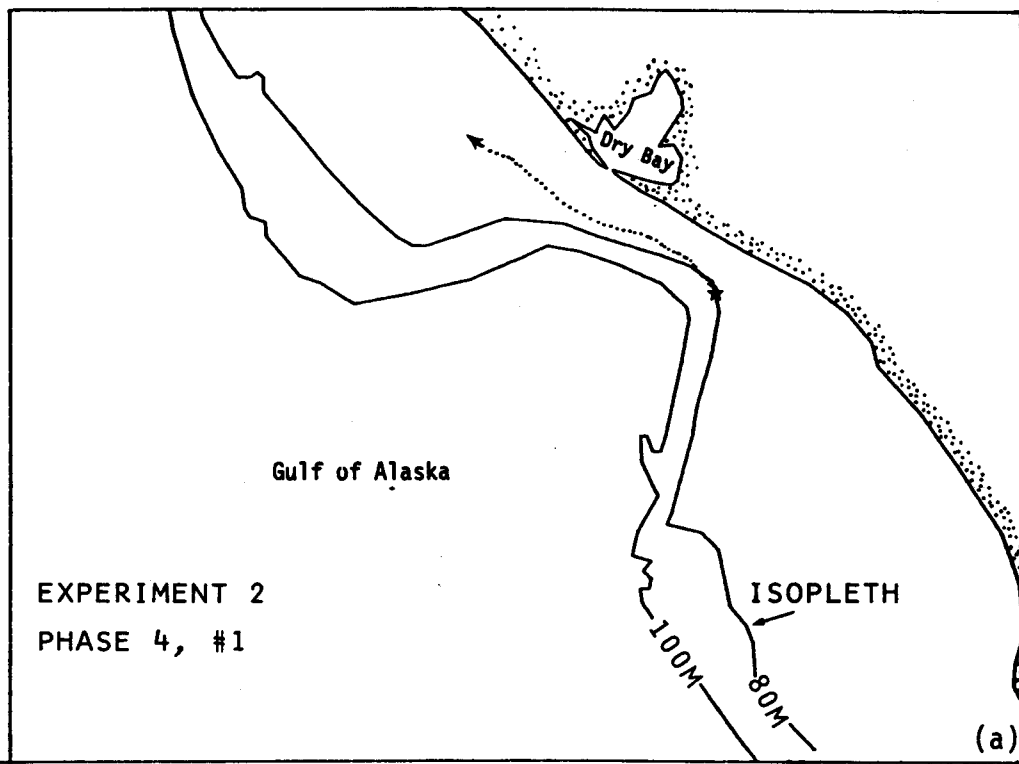


Figure 26 (continued).

59°36'N

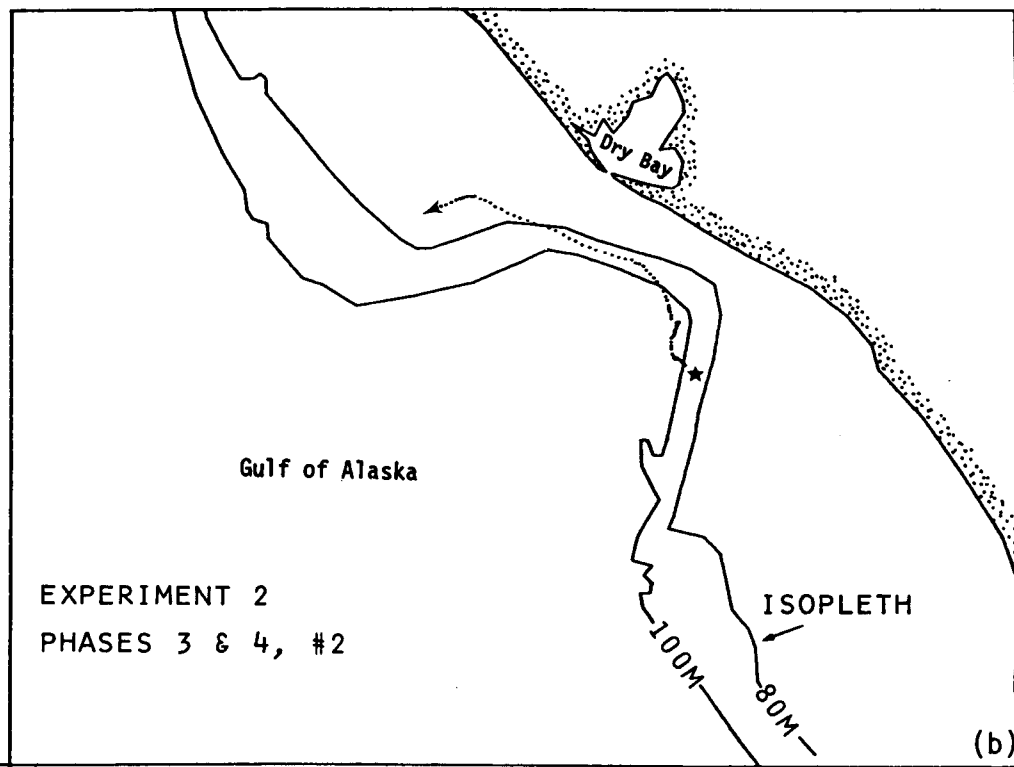


58°45'N

140°22'W

137°21'W

59°36'N



58°45'N

140°22'W

137°21'W

Figure 27. Individual drogue tracks (a), (b), (c) followed by Drifters 1, 2, 3 respectively for the second autumn 1980 drogue experiment. Stars mark start points for each drift track segment.

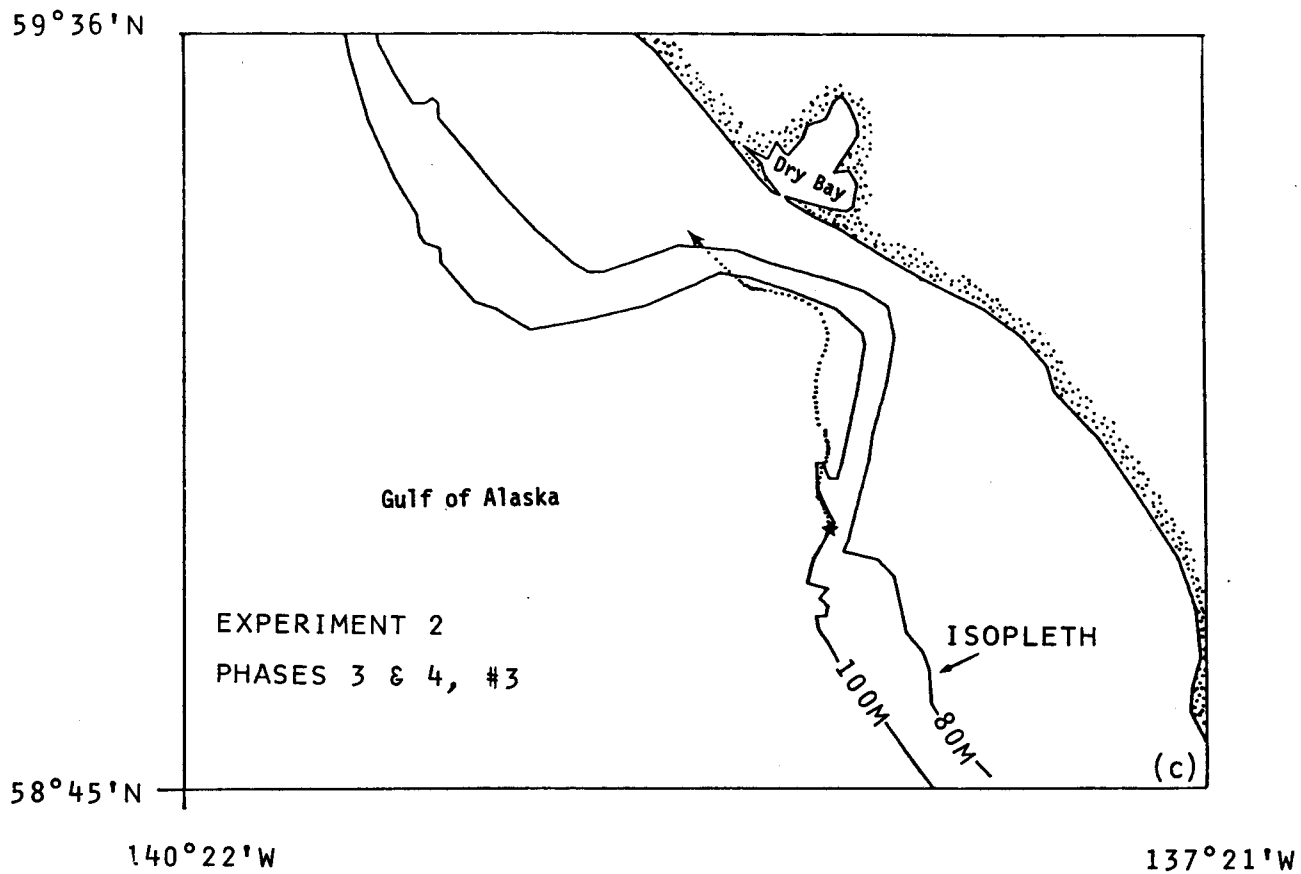


Figure 27 (continued).

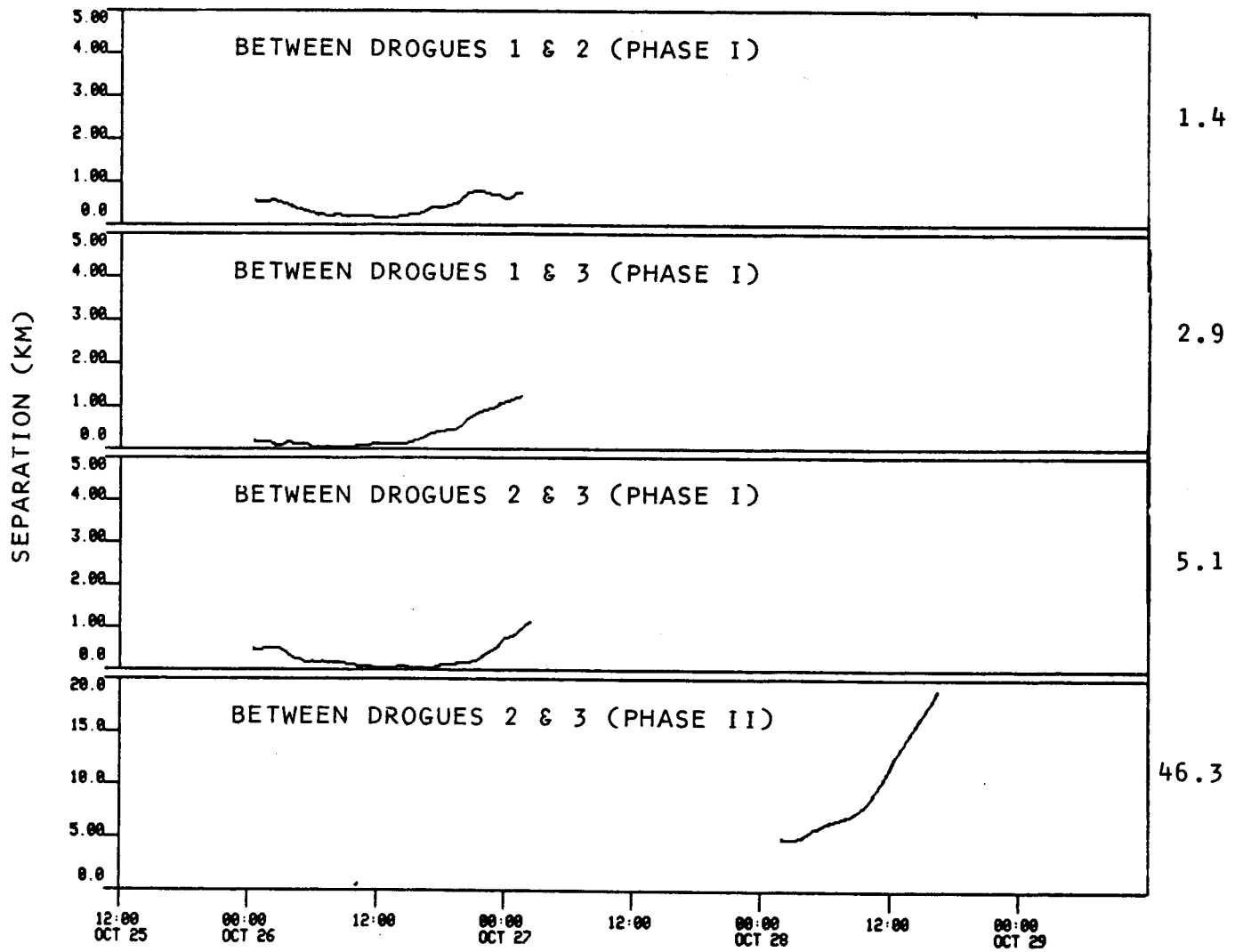


Figure 28. Plot of separation between drogues as a function of time for the autumn 1980 drifter experiment.

lagging the peak winds by 10-12 hours (Figure 29). As Buoy 3 was subjected to higher speeds, the average separation rate between the buoys reached 20 cm/sec (Figure 28). Buoy 2, which was slightly offshore of Buoy 3 at the beginning of Phase II, traveled \sim 50 percent slower and had a stronger northward component than Buoy 3 (Figure 26), suggesting entrainment into a strong near-shore current feature. After 14 hours of tracking, the buoys were retrieved and the ship proceeded southeast for the second experiment.

For the second experiment, the buoys were deployed in a line roughly normal to the coastline (Figure 25). Buoys 2 and 3 were deployed initially (Phase I) with Buoy 1 being deployed approximately 15 hours later (Phase II). The buoy tracks followed the bathymetry closely for both phases of this experiment (see individual buoy tracks in Figure 27). This observed pattern of motion was due to the steering influence of the sharp topography at the head of the Alsek Canyon on the longshore current. Mean speeds (Table 3) were lower for Phase I than for Phase II, as the buoys were turning under the influence of the topographic effect. All three buoys showed increased speeds during Phase II, when mean speeds ranged from 24 to 29 cm/sec and peak speeds reached 40 to 50 cm/sec.

Summarizing the drogued buoy data for the fall survey, considerable variability was found in current speed and direction. A slow (\sim 13 cm/sec) mean drift to the southeast was found to reverse and become quite intense (\sim 63 cm/sec) concurrent with the onset of a storm event. Topography was observed to have considerable influence on current direction at the head of a deep submarine canyon. Buoy drift speeds increased by factors of two to three as buoys appeared to be entrained from offshore into a stronger near-shore along-shore current. Presence of this accelerated flow was probably due in part to shoreward packing of streamlines as the water movement parallels isobaths shoreward along the upstream (southeast) side of Alsek Canyon.

3.2.3 Autumn Littoral Currents

During the period of the littoral zone current study (28-30 October 1980), strong northwestward currents were observed both in surface surf zone (\sim 200 cm/sec) and along the bottom (\sim 30 cm/sec) as estimated using wave measurements and as shown by seabed drifters, respectively. The strong currents were evidently caused

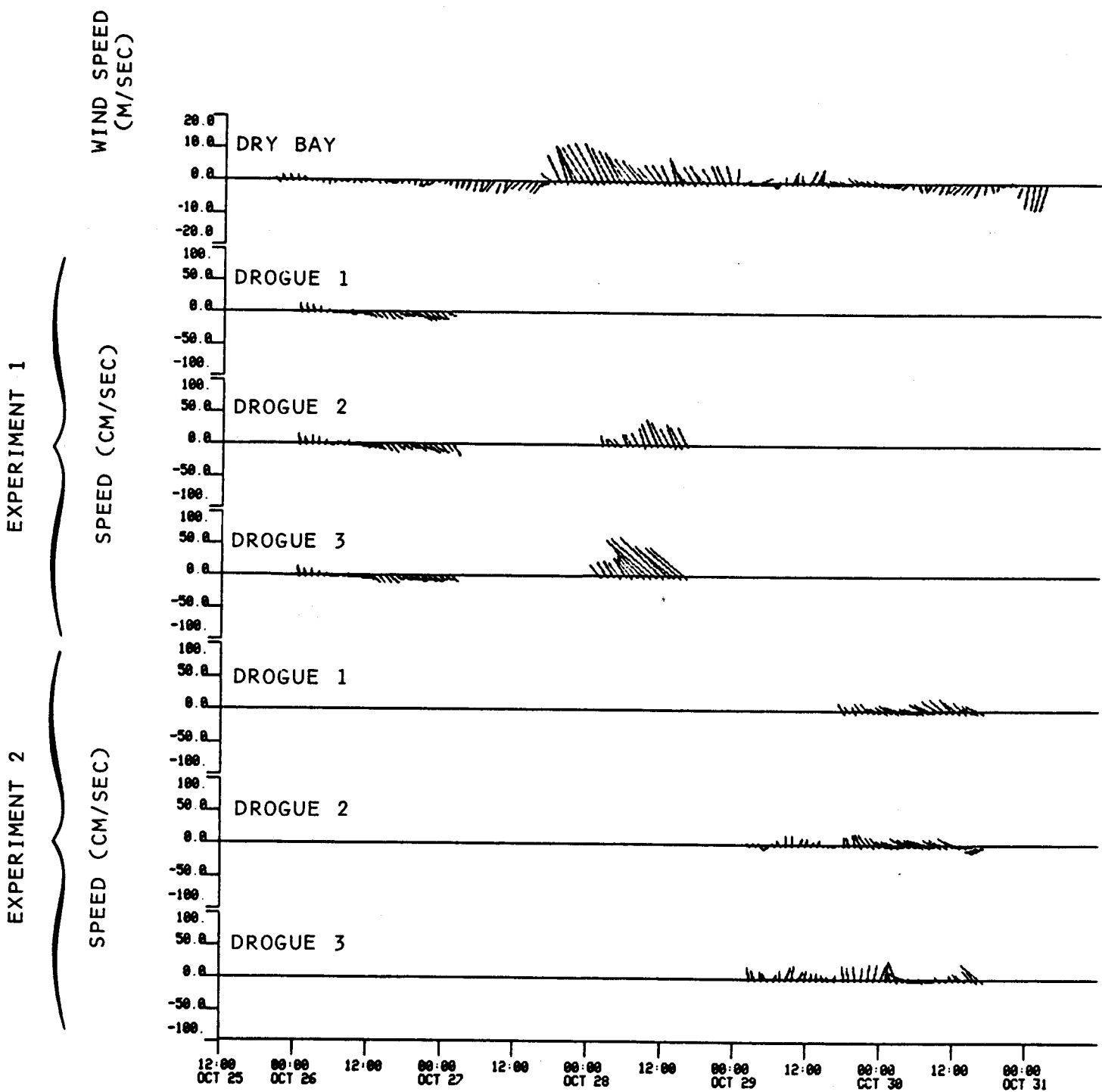


Figure 29. Plot of drogue speeds as a function of time and vector wind observed at Dry Bay.

by storm-induced wave action which was maximum on 28 October, the day the seabed drifters were launched.

The longshore surface currents (Table 4) were computed as described in Section 2. They were highest the day of the launch (~ 196 cm/sec), were lower the next day (~ 93 cm/sec), and eventually reversed direction on the last day (~ -154 cm/sec) (these speed estimates are peak values valid only in the region of breaking waves). Also displayed in Table 4 are vector-averaged along-shore velocity values which should be more easily compared with the bottom velocity values from the seabed drifters. The vector-averaged velocities do show a strong northwestward current pulse on the day of the launch and a subsequent decrease to levels similar to that seen in the seabed drifter velocities discussed below.

Three groups of seabed drifters were also launched on 28 October, and strandings were recorded as described above (Section 2). The three groups of drifters will be discussed progressing from near-shore to offshore. The recoveries from Group 1F occurred generally on the first day close to the launch site, resulting from mean along-shore speeds to the northwest from 0 to 3 cm/sec (Figure 30a); two drifters from this group were recovered on the second day and reflected similar speeds and no seabed drifters from this group were recovered on the third search day.

The recoveries from Group 2F showed a distinct bimodal distribution of mean speeds for the first day (Figure 30b). The lower speed peak ranged from 2 to 30 cm/sec, with a weighted mean value of 15 cm/sec. The higher peak showed speeds ranging from 24 to 34 cm/sec, with a mean value of 29 cm/sec. The second day of recoveries for this group showed two-day mean speeds to be similar to the lower speed peak seen on the first day of recoveries, with speeds to the northwest ranging from 2 to 16 cm/sec with a weighted mean of 12 cm/sec. Again, no drifters were recovered on the third day.

The outermost group, 3F, had a recovery pattern similar to Group 2F (Figure 30c). The first day of recoveries displayed a speed peak at 18 cm/sec with some drifters having speeds up to 35 cm/sec. On the second day, the two-day average speed was 12 cm/sec with values ranging from 8 to 16 cm/sec. No drifters were recovered the third day.

Table 4

AUTUMN SURFACE CURRENT VELOCITY
ESTIMATED FROM WAVE PARAMETERS*

	WAVE ANGLE (°)	WAVE HEIGHT (m)	LONGSHORE SURFACE VELOCITY (cm/sec)	VECTOR- AVERAGED VELOCITY (cm/sec)
Launch	24 (±3)	2.0 (±0.5)	196 (±42)	196
Day 1	15 (±3)	1.0 (±0.5)	93 (±40)	127
Day 2	-28 (±3)	1.0 (±0.5)	-154 (±50)	15

* Error estimates in velocity are those resulting from the uncertainties in angle and height.

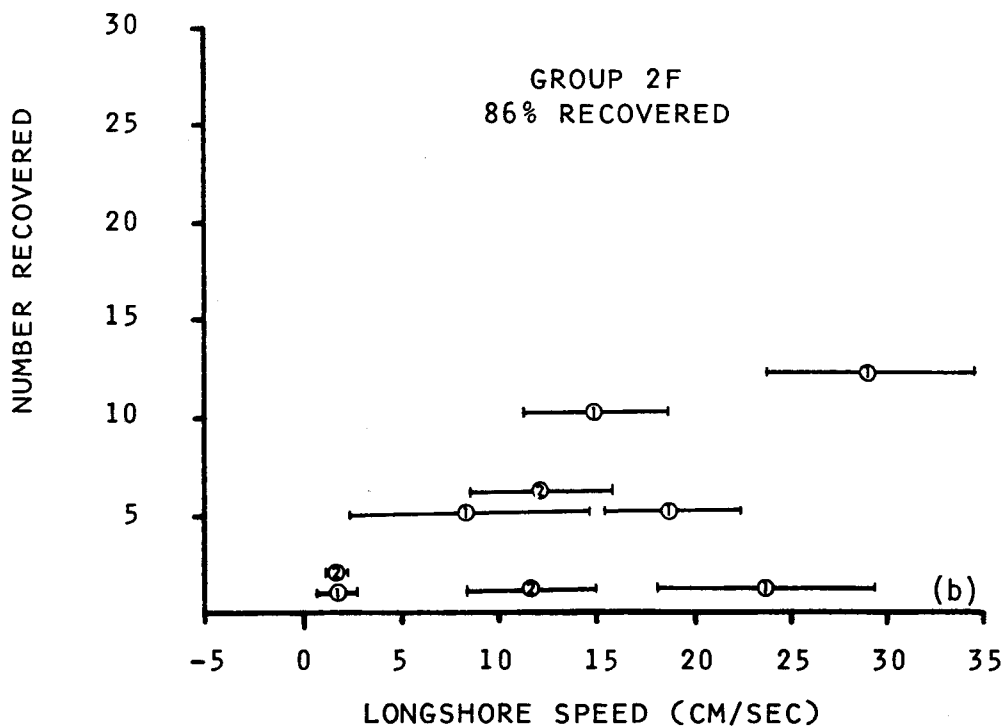
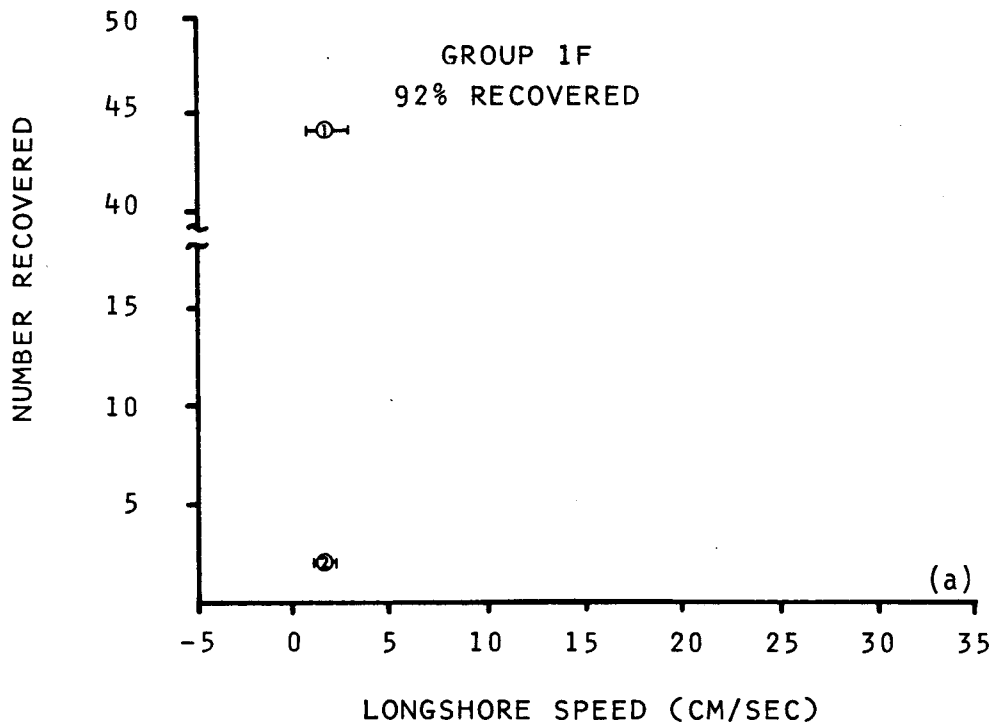


Figure 30. Histograms of longshore speed for Group 1 (a), Group 2 (b) and Group 3 (c) fall 1980 seabed drifter studies. Positive longshore speed is to the northwest. Circles show mean speed for a particular grouping of drifters, and height above horizontal axis reflects number in group. Numbers within circles indicate number of days over which speed was averaged (i.e. day of recovery). Error bars allow for positional uncertainty, release time uncertainty and error in time of stranding (usually the major source of error).

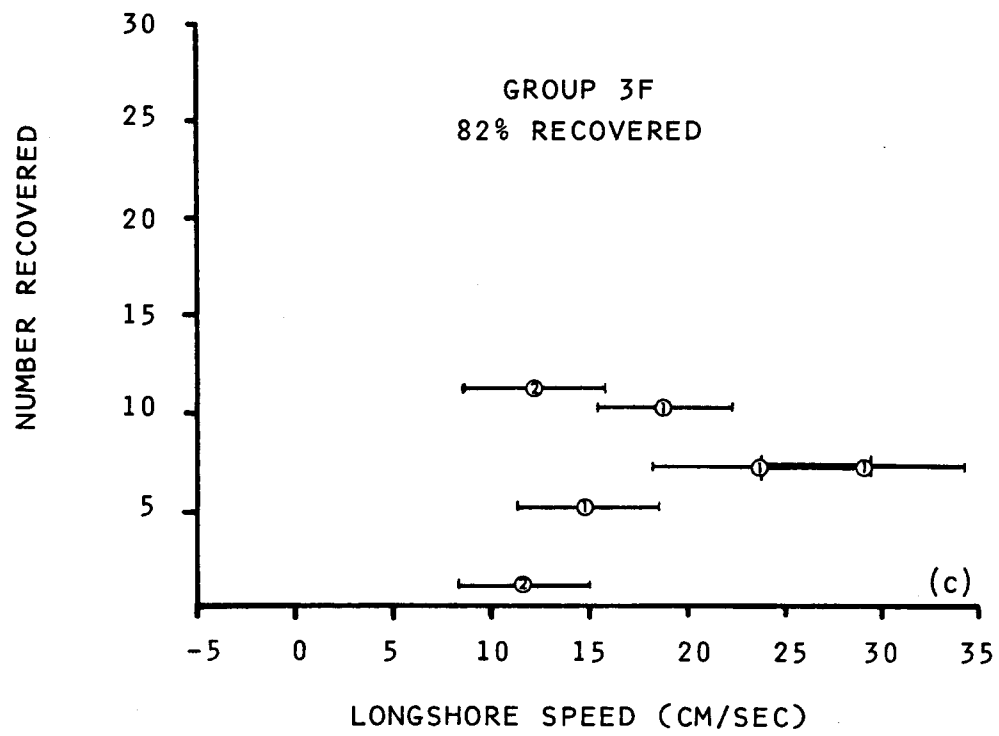


Figure 30 (continued).

The similar recovery patterns for Groups 2F and 3F suggest that some drifters from these groups were subjected to higher current speeds on the first day. The remaining drifters showed similar speeds for the two-day period.

3.2.4 Autumn Wind Observations

The autumn 1980 wind data from the coastal meteorological stations are presented in Figure 31. Coincident winds obtained from Yakutat Airport and as computed geostrophic winds are presented within the context of discussion of the over-winter time series in Section 5. Since these records all show the same features during the autumn field program, it was not felt necessary to include the longer-term time series plots at this point.

The scalar total and cross-shelf speed at Dry Bay (Figure 31a) showed a great deal of fluctuation. In contrast, the along-shore speed showed relatively small values except for three pronounced high-speed (> 20 m/sec) events which occurred on about 17 October, 27-28 October, and 4 November. The wind speed at Ocean Cape had smaller fluctuations than at Dry Bay, both in the along-shore and cross-shelf directions except for the same wind events as observed at Dry Bay -- those on 28 October and 4 November (the Ocean Cape record did not start early enough to have recorded the 17 October pulse which was observed at Dry Bay). As at Dry Bay, the wind pulses were primarily along-shore to the northwest, though there was also a pronounced (7-8 m/sec) on-shore component present during each such event. Since the 4 November wind events occurred after the current moorings (except for Mooring 6, which was relatively far offshore) had been recovered, the 27-28 October wind pulse is of primary concern here. Relations between this pulse and the coincident observed current events are discussed in Section 3.4.

3.3 Discussion of the Autumn Experiment

The foregoing description of the temperature, salinity, and current fields observed in the study region during autumn 1980 reveals a regime which was characterized by strong vertical and horizontal property gradients and by rapid time variability. Prominent features of the temperature and salinity fields included a low-salinity coastal wedge and a persistent deep pycnocline. The

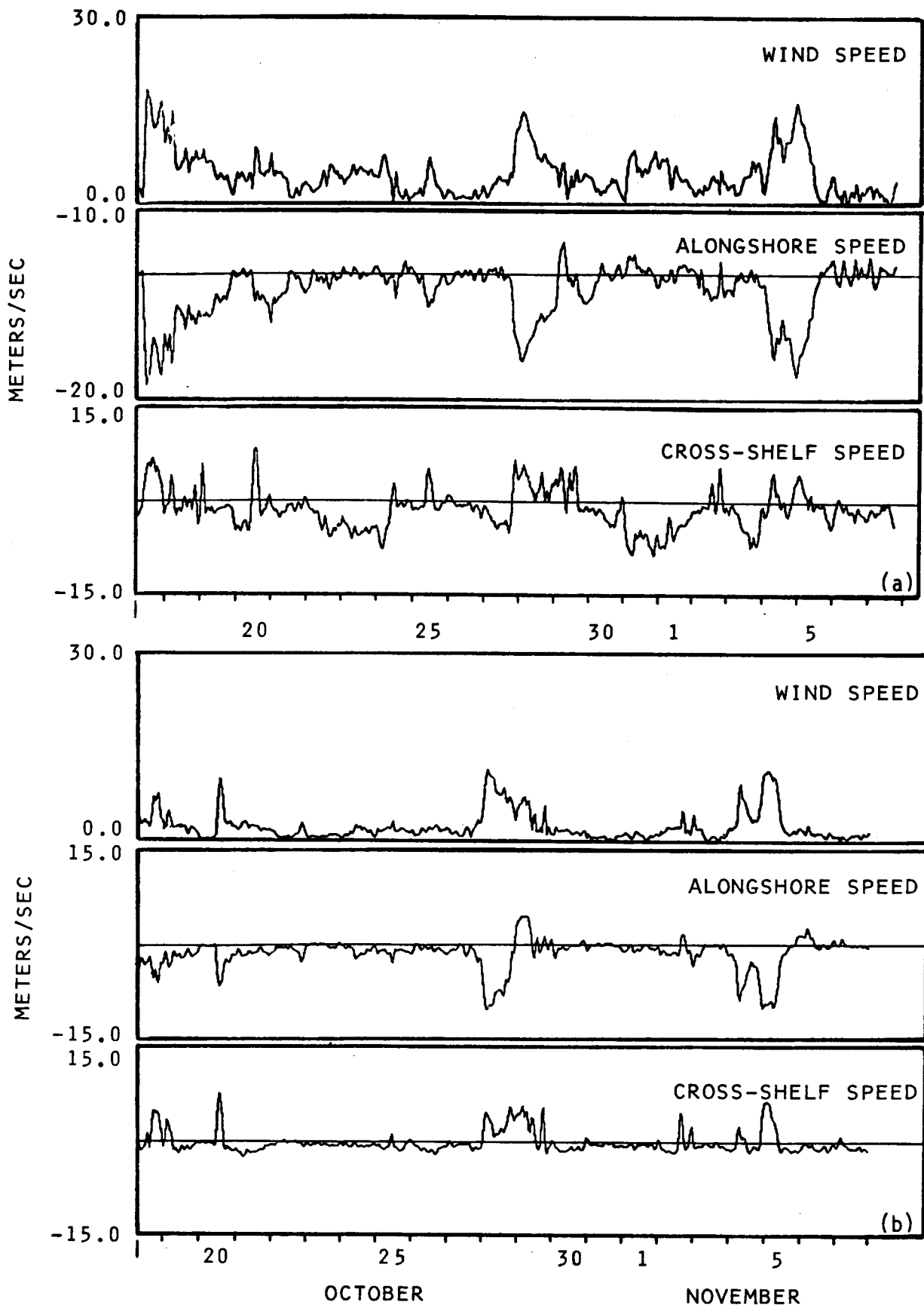


Figure 31. One-hour lowpass-filtered time series plots of wind speed, alongshore and cross-shelf components at the Dry Bay (a) and Ocean Cape (b) meteorological stations during the autumn field program.

variability of the currents, particularly close to the coast, was a prominent feature. These features are discussed below using temperature-salinity and time series analyses.

3.3.1 Temperature-Salinity Analyses

A composite temperature-salinity (T-S) plot has been constructed for the shelf waters off the northeast Gulf of Alaska during autumn 1980 using all stations obtained during the field program (Figure 32). This T-S diagram suggests that the shelf waters may be divided in autumn into three separate masses: (1) coastal water, having salinities of < 28 ‰ and temperatures of 7-8 °C; (2) shelf water, having salinities of 31-32 ‰ and temperatures of 9-10 °C; and, (3) deep ocean water, having salinities of > 32.5 ‰ and temperatures of < 7 °C. The remaining waters in the region can be derived through mixing of these three basic masses.

Coastal water was contained in the low-salinity/low-temperature band which was a permanent feature throughout the study region along the coastline. The temperature-salinity characteristics of this water resulted from admixture of fresh water into the shelf water from the adjacent land. The northeast Gulf of Alaska coastal region is characterized by extremely high rainfall, particularly in autumn just prior to the period when the temperature/salinity data were acquired (cf. Royer, 1979; 1981b; 1981c). Major fresh water sources for this coastal band were Cross Sound (which enters the shelf region to the southeast of the study region and contains freshwater input from southeast Alaska), the Alsek River, the Dangerous River, and the various glacial streams entering Yakutat Bay (cf. Figure 1 for locations). While satellite imagery suggests that freshwater input from these rivers may retain its identity as a plume over a relatively short distance from the source, the horizontal salinity distribution (Figure 8) suggests that bottom topography was as important in controlling the configuration of the coastal band as the locations of major freshwater inputs. For instance, the offshore bulge in the coastal band off the Alsek River was probably due as much to the tendency for the along-shore flow to parallel isobaths around the head of Alsek Canyon, as to the increased local freshwater input from the river. Farther northwest, a steeper bottom topography coincided with a narrower band configuration.

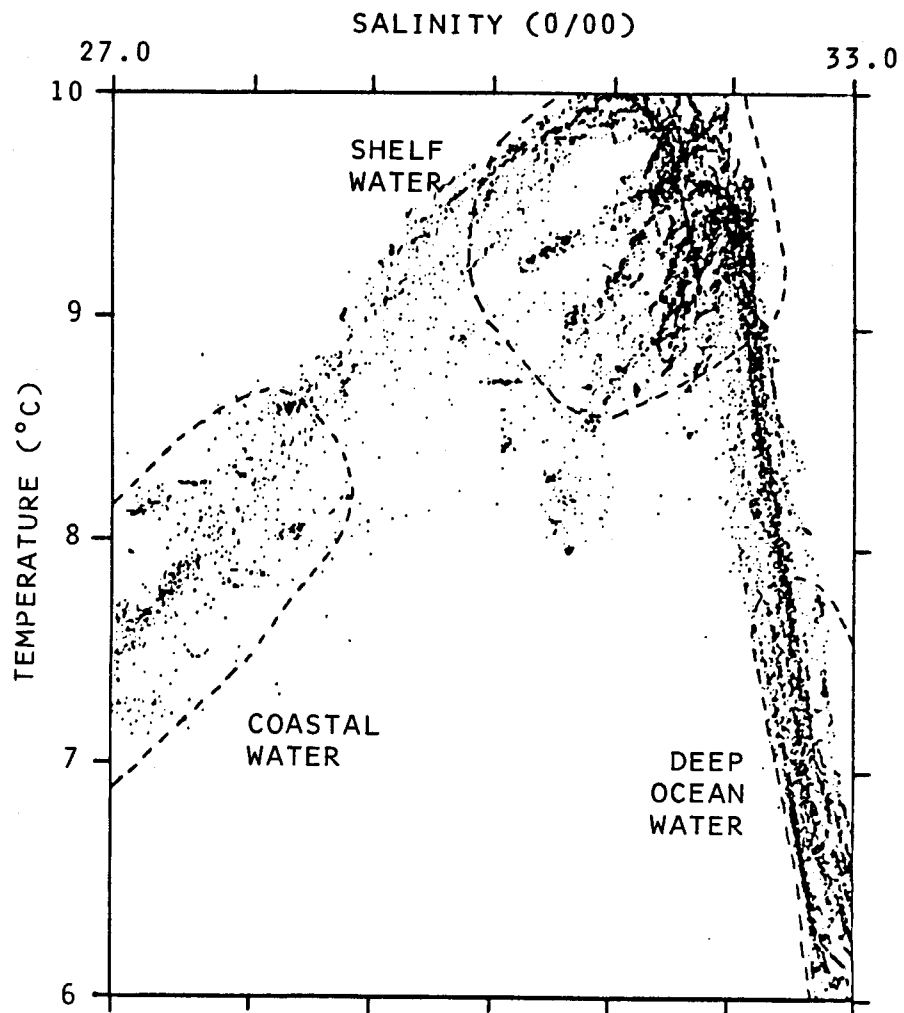


Figure 32. Composite temperature-salinity diagram for autumn 1980, showing the relationships between near-shore, shelf and deep ocean water masses.

These waters defined by their temperature-salinity characteristics as "shelf water" showed considerable variability toward their lower-salinity/lower-temperature ranges, whereas there was a sharply defined cutoff for temperature and salinity values at the high-temperature/high-salinity end (Figure 32). This variability was probably due to the variable nature of the inputs; freshwater, which mixes into the shelf water as low-salinity coastal water, is highly variable in quantity as compared to the relatively constant T-S character of the deep ocean waters. Shelf water occurred throughout the shelf above depths of 75-125 m, where the pycnocline described above in Section 3.1 separated it from deep ocean water. Only in one instance, in the near-surface layers about 50 km south of Dry Bay (Figure 8), was there an indication that coastal water was present at mid-shelf.

Deep ocean water, which was characterized by a relatively narrow range of salinity values, occupied the deeper portions of the shelf and the oceanic regions seaward of the shelfbreak. In particular, it was present in the deeper portions of Yakutat Canyon. Based upon results of other research (Hsueh, 1980; Lavelle et al., 1975; Nelson et al., 1978), a deep up-canyon flow would be expected to occur in response to certain along-shore wind conditions which would advect deep ocean water onto the shelf. The preponderance of along-shore wind events in the study region suggests that such mechanisms were probably responsible in part for shoreward flow of deep ocean water in the cross-shelf valleys. Where shelf bottom depths exceeded about 100 m, a thin layer of deep ocean water was evident in many instances near the bottom (cf. Figure 10). The seaward boundary between deep ocean and shelf waters was marked in some instances by a frontal structure where the shelf water intersected the surface. Such a structure occurred between CTD Stations 37 and 38. Regions of mixing between these water masses were characterized in addition by vertical fine-structure, as illustrated in particular by the zone of interaction between the coastal and shelf waters (Figure 13) and the shelfbreak region where deep ocean and shelf water were interacting (Figure 15). Finestructure is, in a general sense, indicative of dynamic mixing processes associated with sharp property gradients such as occur in this region.

The above depiction of water mass interactions in the study region may be used to speculate qualitatively upon circulation. The general large-scale mass boundaries -- coastal/shelf and shelf/deep ocean -- with local isobaths suggests that the time-mean flow also parallels isobaths except for such instances as on-shelf flow in the deeper portions of the cross-shelf valleys. Such a mean advective regime is necessary for maintenance of these water mass boundaries. This supposition is supported by the current observations except for those at Mooring 6, although except for Mooring 6 these records are too short to rigorously define a "mean" flow. (Lagerloef et al. (1981) have shown that in this region a minimum current record length of 60 days is required to obtain a mean flow value in which we may have confidence at the 95 percent level.) Dynamic considerations also lend credence to our observations; high-latitude conservation of potential vorticity dictates that streamlines of the three basic water mass types parallel isobaths.

Superposed upon the distribution depicted above, there was considerable scatter in the mid-shelf region, as shown particularly clearly on Figures 8 and 9. Of particular interest is the "lens" of coastal type water which occurred 40-50 km south of Dry Bay and was approximately outlined by the 31.5 ‰ isohaline at 5 m (Figure 8b). This lens may have originated from Cross Sound to the southeast and been advected by the mean flow northwest to its observed location. Alternatively, it may have been a remnant of coastal water which was originally present in the coastal band off Dry Bay and was then advected to the observed location by offshore surface flow resulting from relaxation of the shelf waters following a wind-driven downwelling event. (This latter possibility will be more thoroughly discussed below in Section 3.3.2) Because no data were acquired prior to the time when the feature was observed, it is impossible to determine which of these two mechanisms was responsible. Whatever the source, these irregular features are reflected in the composite temperature-salinity plot (Figure 32) as "streamer-like" sets of points extending toward lower temperature/lower salinity values from that portion of the plot defining shelf water. It is possible that the locations of these streamers relative to the portions of the curves connecting shelf water/deep ocean water and shelf water/coastal water reflect the ages of the features. Older features which had been on mid-shelf for a longer period of time, especially those farther seaward, might reflect a greater admixture of shelf-deep ocean water.

3.3.2 Circulation Analyses

This section considers the circulation features observed using the drogues and moorings, and the observed features are correlated with winds and fluctuations in the temperature and salinity fields. Because the moored current records were relatively short compared with the time scale for events -- 12-day records as compared with an event time scale of 5-6 days (cf. Section 5) -- no attempt was made here to compute "mean currents." The main current vectors presented in Section 6, for comparison with a diagnostic model, should be viewed with caution because of the high variability which was observed. To reiterate (see Section 3.3.1 above), Lagerloef et al. (1981) found a minimum recording period of 60 days necessary to obtain meaningful "mean" currents in the northeast Gulf of Alaska shelf region. Therefore, this section will concentrate instead upon the nature of the time variations and will attempt to link these with dynamical processes which may aid in explanation and predictability.

As for computation of "mean" currents, no attempt has been made to construct dynamic topographies. Again, this decision was based on the observed high temporal variability coupled with non-synoptic temperature-salinity sampling. The temperature and density time series observed at the moorings (Figures 16, 17, 19, 20, 22, and 24) reveal that large (as great as 1 °C and 1 sigma-t unit) rapid (time scales of a few hours) fluctuations occurred, particularly at Moorings 2 and 6. Since several days were required to occupy the CTD grid with frequent breaks in the sequence to track drogues, for bad weather and for other operational reasons, significant variations probably occurred in the density field during occupation of the grid. In conjunction with non-synoptic nature of the temperature and salinity data, the noise level introduced by these time variations would be expected to introduce an unacceptable level of uncertainty into an estimate of dynamic topography. These effects would be particularly bad in the near-shore region within about 10 km of the coastline, where the observed fluctuations were greatest and also where experimental results are of most interest to this program.

Near-shore Moorings 1 and 4 exhibited flow which was strongly constrained to flow in the along-shore direction. The flow was thus bimodal, being either to the northwest or to the southeast for about equal portions of the 12-day

record obtained from each mooring. Flow constraint in the along-shore direction was governed by topographic influences both by the sloping bottom and due to the close proximity (< 4 km) to the beach. The small cross-shelf velocity fluctuations appeared upon visual inspection to be due primarily to the tidal currents. Only in one instance (27-28 October at Mooring 4) was there a small (~ 20 cm/sec) offshore current event which coincided with the large (~ 70 cm/sec) north-westward pulse (Figure 17).

Offshore Moorings 2, 5, and 6 showed far less tendency toward solely along-shore flow. Because they were farther from the beach (> 10 km) than Moorings 1 and 4, they were subject to less topographic control. The deeper current record from Mooring 2 is an exception because it was close enough to the bottom that control was imposed by the sloping bottom topography. The near-surface records from Mooring 6 (Figures 23 and 24) showed the greatest cross-shelf fluctuations. In both these cases, the moorings were located in areas where the isobaths were at large angles to the coastline; for Mooring 5, isobaths were nearly normal to the coast as they formed one side of Alsek Canyon. It is likely that a portion of the fluctuations at Moorings 5 and 6 were due to eddying motions resulting from the interaction of a weak mean flow with complex bottom topography.

The reasons for the strong southeasterly flow in the near-shore region (Moorings 1 and 4) are uncertain. The major northwestward current event which was observed at Moorings 1, 2 (upper meter) and 4 on 27-28 October correlated with a storm center which passed over the region and generated strong (~ 15 m/sec) along-shore winds to the northwest (Figure 31). The spatial distribution, magnitude, and along-shore propagation speed of the current event suggested that it behaved as a continental shelf wave generated by the storm (Temple and Muench, 1981). Flow just prior to and (at Mooring 1) just after this northwestward pulse was lower in speed and to the southeast. It is possible that the southeasterly flow may have been due in part to a relaxation of the system following the northwesterly flow, abetted by the curvature of the northeast Gulf of Alaska coastline. This possibility is discussed to greater extent below within the context of the current, temperature, and density time series.

Presence along the coastline of the low-salinity/low-density band of water suggests that a northwesterly along-shore baroclinic flow should have been present rather than the observed bimodal flow with no significant net northwesterly

preference. Because the current meters at Moorings 1 and 4 were, respectively, at 26 and 38 m depths and the density signature of the coastal band did not extend appreciably below about 20 m, it is possible that a northwestward flow associated with the low-density band was present but undetected by our moorings. However, the drogued buoys were set to track water motion at about 15 m depth (cf. Section 2) and so should have detected northwesterly flow of the coastal water. Referral to the drogue velocities (Figure 29) shows that, except for a brief period (< 24 hr) on 26-27 October, the drogues traveled to the northwest with speeds as high as about 70 cm/sec occurring on 28 October. The drogue tracks (Figures 25) indicate the constancy of this northwestward flow except for the single reversal event, and Table 3 indicates mean speeds of order 30 cm/sec. The low mean speeds for Phase I of Experiment 1 reflected incorporation of the reversal into the mean speed computation, whereas the high average speeds for Drogue 3, Phase II were due to incorporation of the northwestward pulse into the means. The consistent 30 cm/sec northwestward drift recorded at 15 m depth by the drogues suggests that the near-surface coastal flow was characterized by speeds of about 30 cm/sec to the northwest.

In conclusion, northwesterly along-shore flow associated with the low density coastal water band (1) had speeds of order 30 cm/sec, (2) was limited primarily to depths above 20 m, and (3) occurred primarily within about 9 km (the approximate offshore distance for Moorings 2 and 5) of the coastline. These observations are consistent with theory, which predicts that this sort of coastal flow will occur primarily within a distance from the coast equal to the computed internal Rossby radius of deformation. In this case, this length scale is about 7 km or approximately the same as the observed width of the low-density band (Figure 11). Based upon observations in previous data bases, Reed and Schumacher (1981) concluded that there was no appreciable coastal flow in the northeast Gulf of Alaska. However, based upon the above analysis, it now appears that such a flow may in fact have been present at the time these data were collected, but was probably contained in too narrow a coastal band to have been detected by their temperature-salinity data, most of which were more than 10 km from the coastline.

3.3.3 Littoral Currents

In Section 3.2.3, results are presented from a field study of littoral currents which was conducted by a seabed drifter experiment and analysis through application of engineering equations to estimated incoming surface wave heights and directions. Both observed longshore seabed drifter speeds to the northwest, and longshore speeds predicted by the analytic equations were greatest when waves approached the beach from the south-southeast, as would be expected. In addition, there was also a southeasterly wind generally present which would have contributed to local wind forcing of a northwest current. At no time was a longshore littoral current observed in the southeasterly direction. This absence was a reflection of the wind stress and the resulting wave field, directed toward the northwest in this region in autumn-winter; in general, a northwesterly littoral current would be expected to exist through most of the winter due to the dominant southeasterly winds. The speeds observed with the seabed drifters -- of order 10-30 cm/sec -- may be considered as a representative estimate of the current speeds. Since these drifters tracked bottom water, this would also represent the longshore speed seen by contaminants which had been introduced into bottom sediments in the surf zone.

3.3.4 Summary

The results of the autumn field experiment can be briefly summarized as follows:

1. The regional temperature-salinity distribution defined coastal, shelf and deep ocean water masses. Coastal water was constrained primarily to a 20-m-deep layer within 10 km of the coast, except for isolated lenses which might be periodically advected well off the coast. Shelf water occupied the bulk of the region from the coast to the shelfbreak. Deep ocean water occurred seaward of the shelfbreak and beneath the shelf water on deeper portions of the shelf. The coastal water had the lowest temperatures and salinities observed; the shelf water had higher temperatures and intermediate salinities, and the deep ocean water had the lowest temperatures and highest salinities.

2. Circulation on the shelf was in general highly variable. Below the 20-m-deep coastal water in the near-coastal region, it was bimodal in the along-shore direction. The wedge of coastal water was characterized by a northwesterly flow of order 30 cm/sec, but was subject to occasional reversals to a southeasterly flow. Strong northwesterly current pulses were driven by southeasterly storm-related winds, with the magnitude of the pulse decreasing in the offshore direction. Currents near Alsek Canyon were particularly variable.
3. Littoral currents were along-shore to the northwest in response to wind waves from the south-southwest and sea surface set-up, and had near-bottom speeds of 10-30 cm/sec.

4. THE SPRING EXPERIMENT

4.1 The Spring Distributions of Temperature and Salinity

The temperature and salinity distributions were determined in the same way for the spring as for the autumn experiment (see Section 2). This section presents the spatial distributions of temperature and salinity observed using the CTD.

The regional temperature and salinity fields are presented as horizontal plan views at depths of 5 m (Figure 33) and 100 m (Figure 34) and as vertical distributions along a transect across the shelf from the coastline to seaward of the shelfbreak (Figure 35). For comparison with the autumn distributions, the transect shown in Figure 35 was chosen to coincide spatially with that shown above in Figure 10 for the autumn distribution.

The 5-m temperatures in spring 1981 were characterized by values which were low relative to those observed in autumn: 6.3 and 7.1 °C compared to 8-9 °C in autumn. Spatial variability in spring was similar to that found in autumn, or about 1 °C, with a tendency for lower temperatures near the coast. The 5-m salinities were about 0.2 ‰ higher off the shelfbreak in spring than in fall but were more than 1 ‰ higher in the coastal band. This was a major difference between the autumn and spring salinity distributions; the low-salinity near-coastal band was highly attenuated in spring.

Shelfbreak temperatures at 100 m in spring were 6-7 °C (Figure 34a), similar to those observed in autumn. Farther onto the shelf, temperatures were 6-7 °C in spring whereas in autumn they had been 8-9 °C. Salinities at 100 m were similar in spring to those observed in autumn; they varied gradually from about 32.0 ‰ near-shore to about 32.8 ‰ near the shelfbreak (Figure 34b).

As in autumn, both the 5-m and the 100-m temperatures and salinities were characterized by horizontal variability on mid-shelf and near the shelfbreak. At 5 m a region of low-temperature (6.5 °C) and low-salinity (31.9 ‰) water lay near the shelfbreak south of Dry Bay. The corresponding feature at 100 m (Figure 34) was characterized by high temperatures (7.3 °C) relative to colder

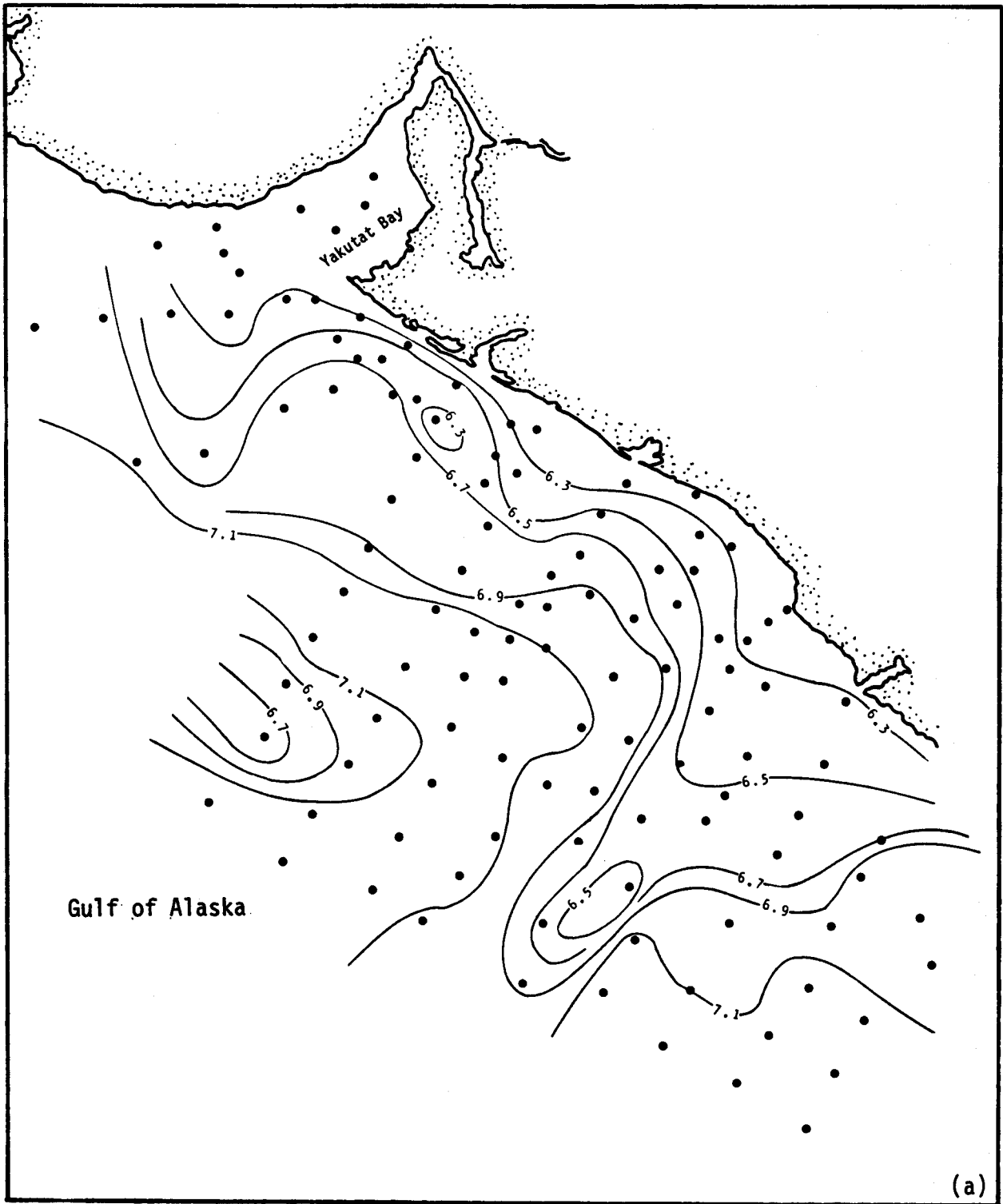


Figure 33a. Horizontal distribution of temperature ($^{\circ}\text{C}$) at 5-m depth, 20 March-3 April 1981.

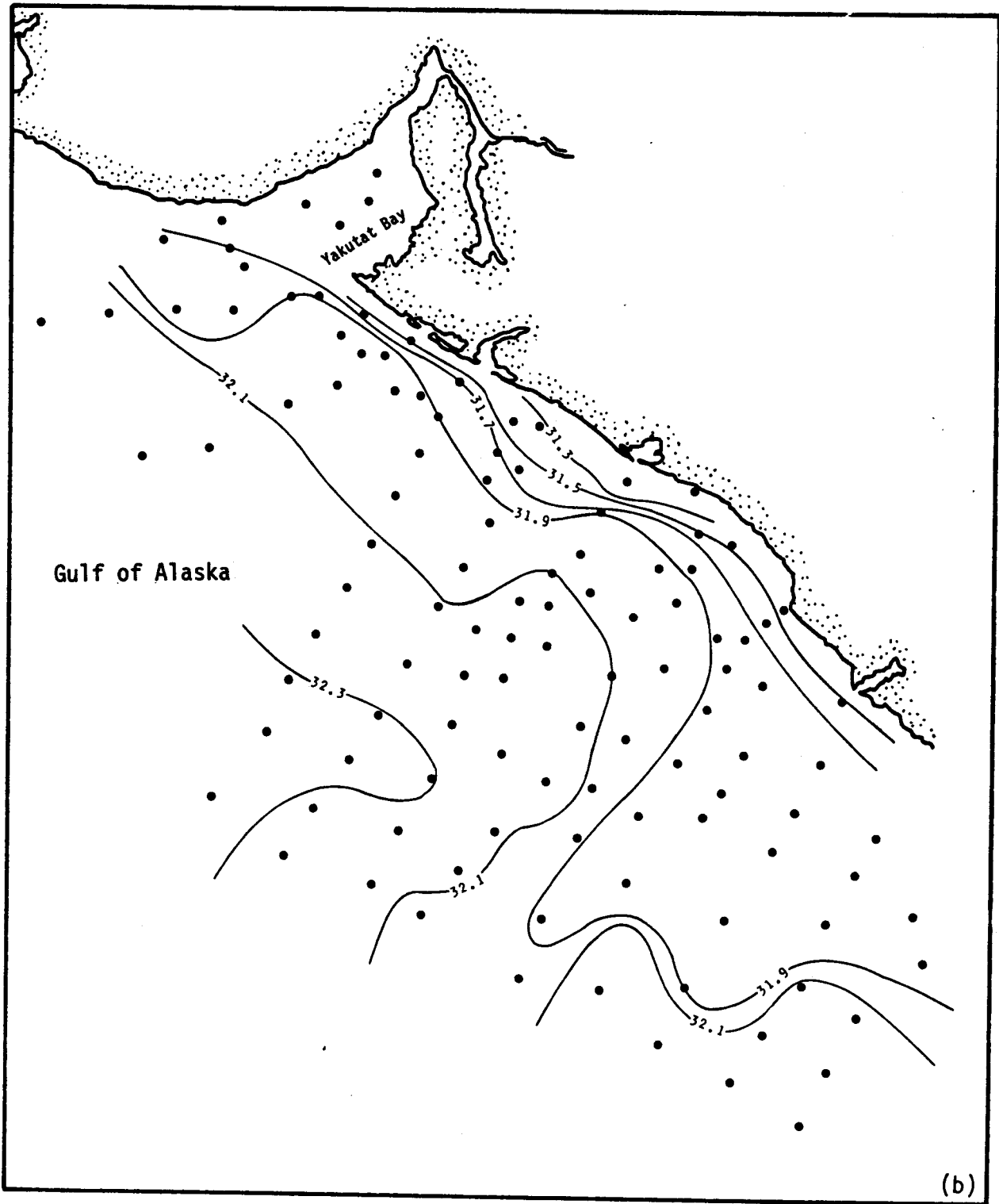


Figure 33b. Horizontal distribution of salinity (‰) at 5-m depth, 20 March-3 April 1981.

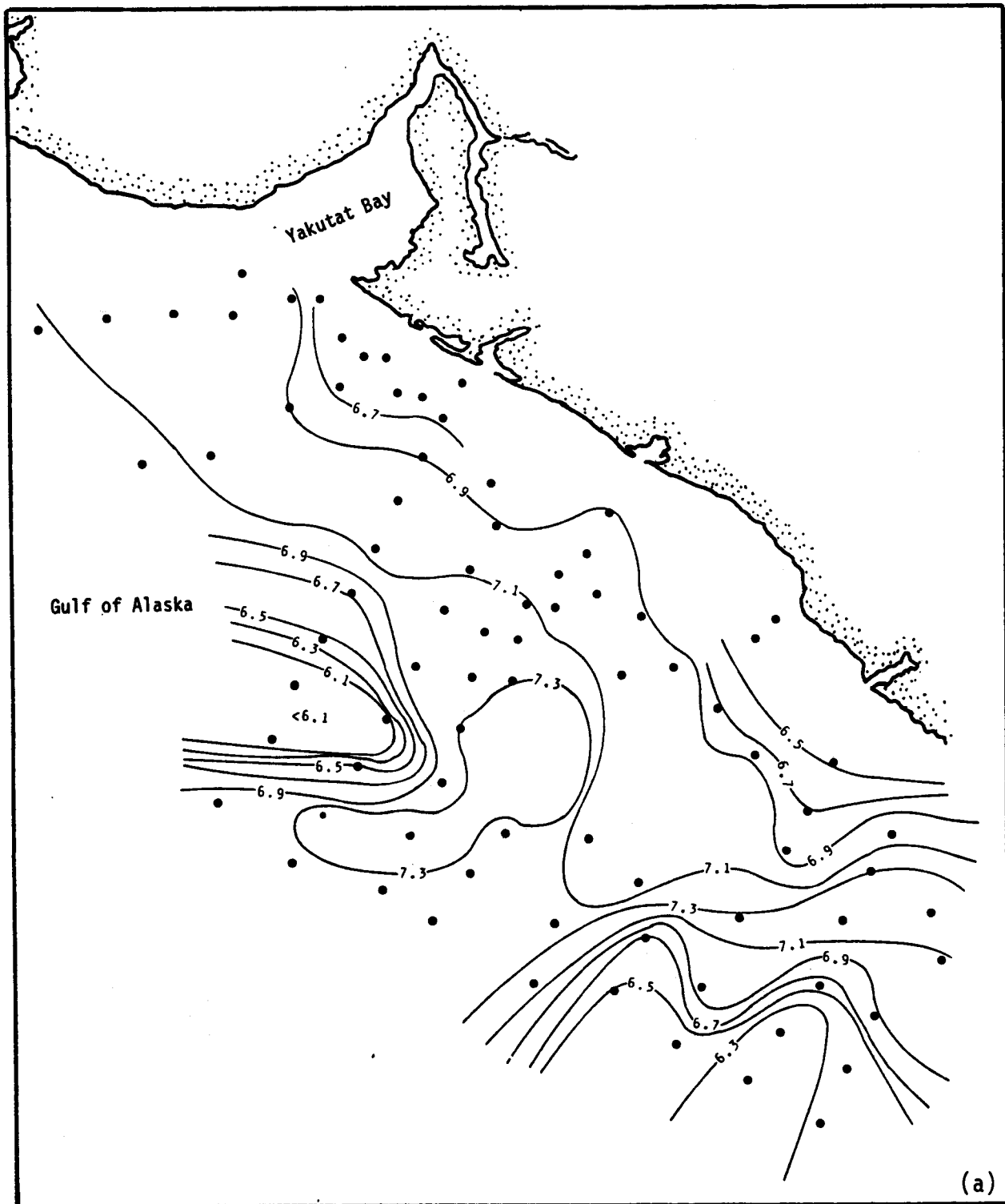


Figure 34a. Horizontal distribution of temperature ($^{\circ}\text{C}$) at 100-m depth, 20 March - 3 April 1981.

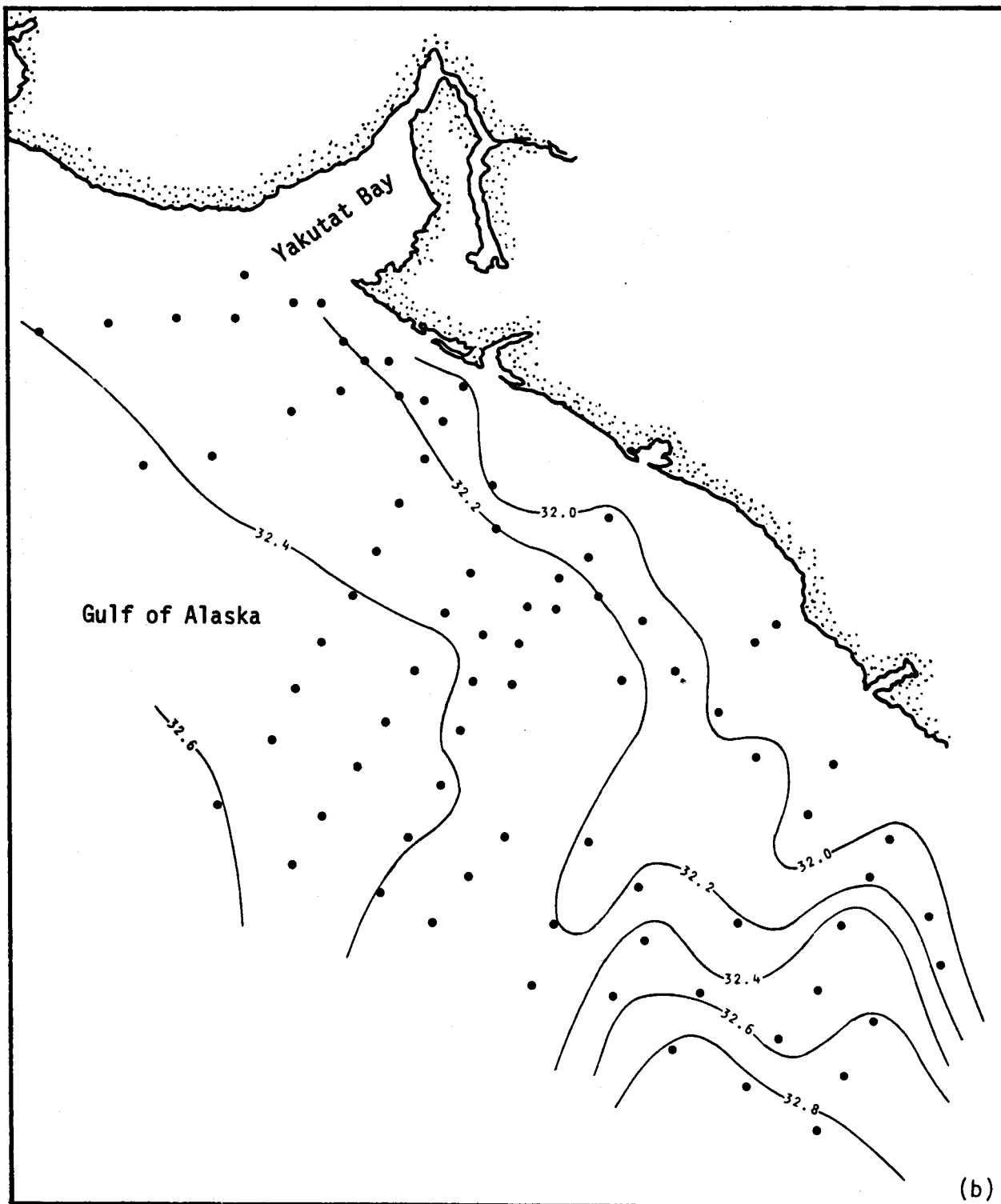


Figure 34b. Horizontal distribution of salinity (‰) at 100-m depth, 20 March - 3 April 1981.

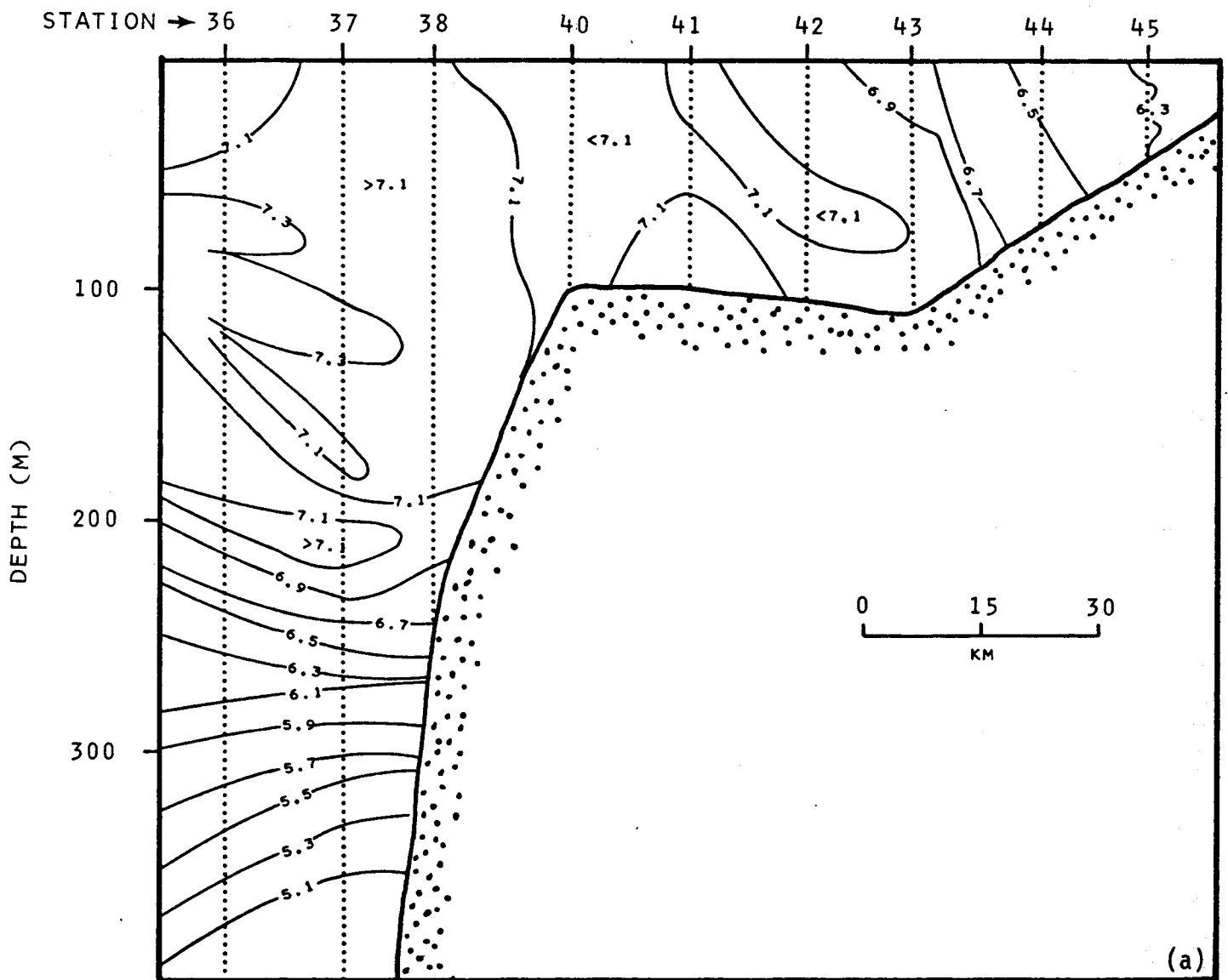


Figure 35a. Vertical distribution of temperature ($^{\circ}\text{C}$) along a cross-shelf transect, 30 March 1981. Location of transect is indicated on Figure 7 by station number.

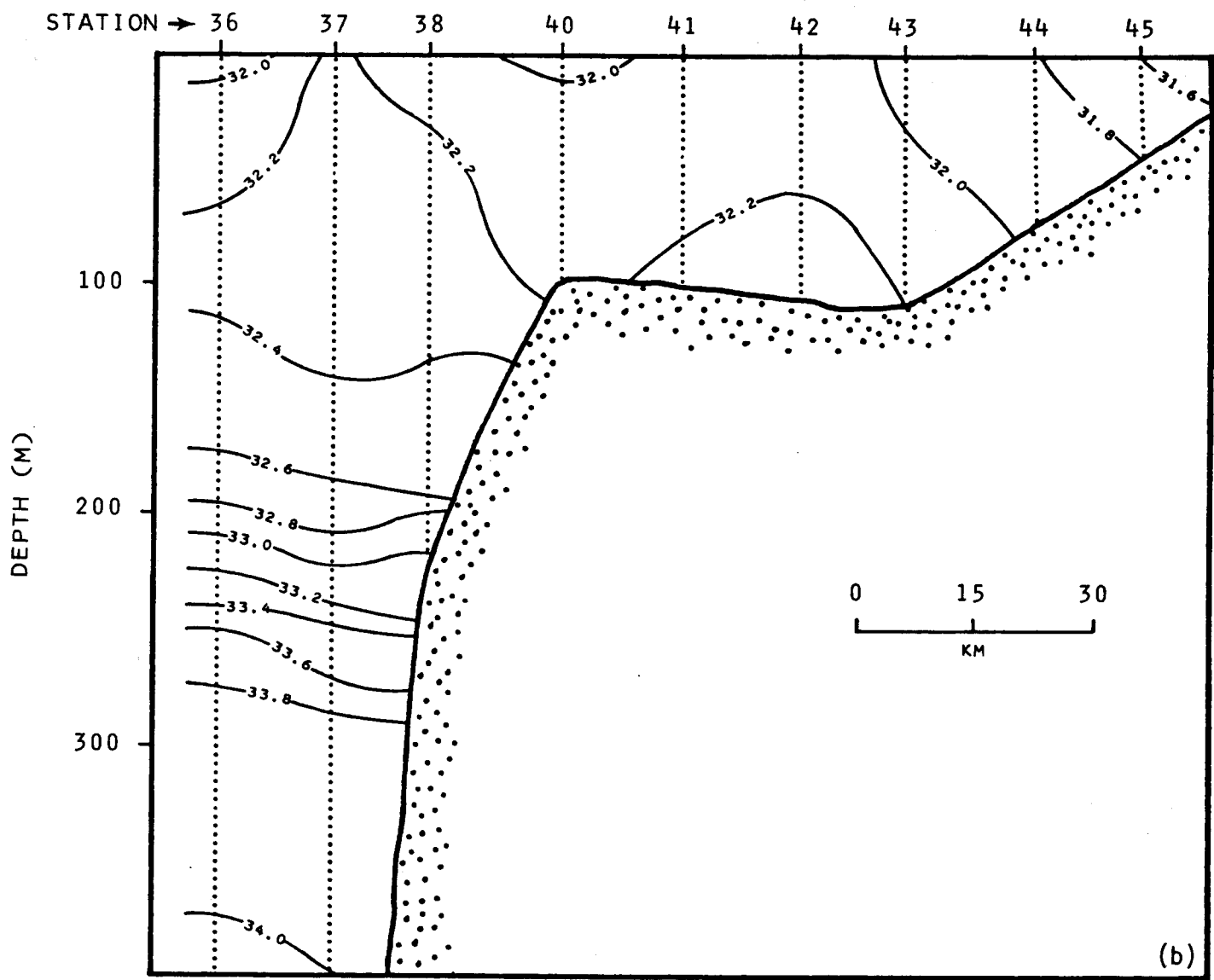


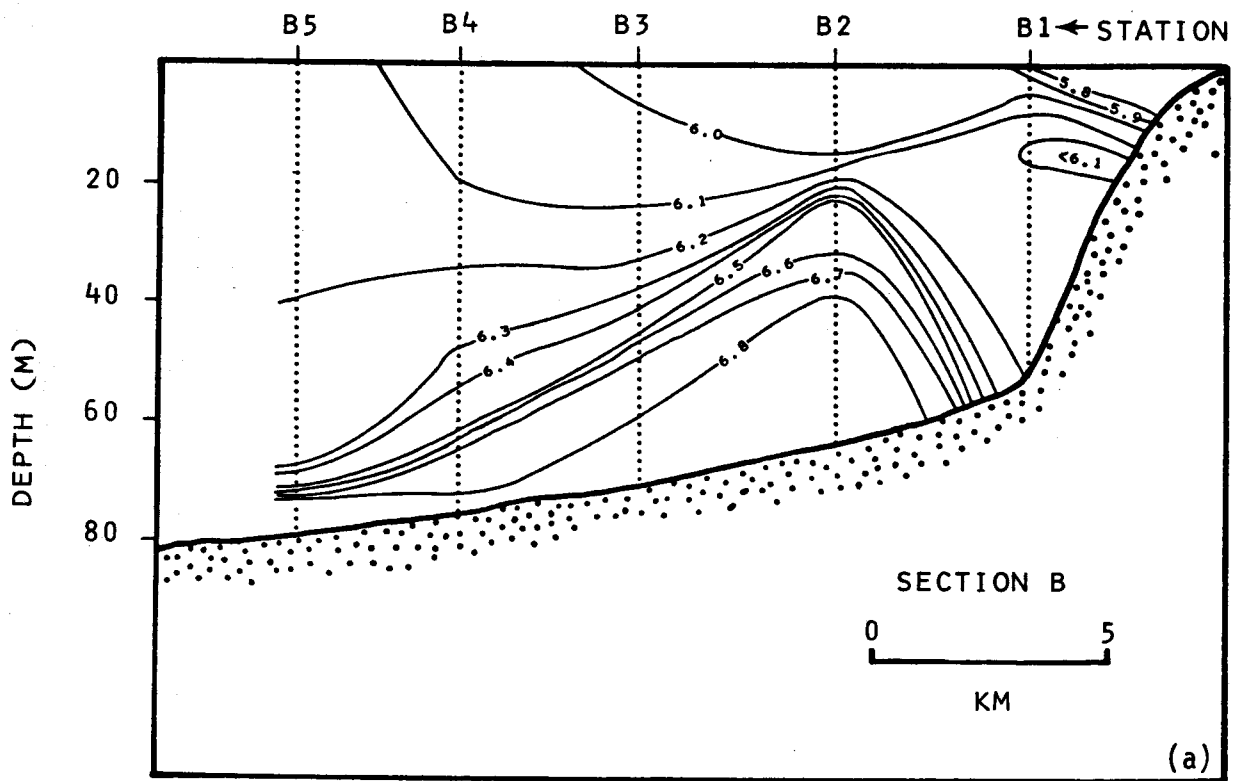
Figure 35b. Vertical distribution of salinity (‰) along a cross-shelf transect, 30 March 1981. Location of transect is indicated on Figure 7 by station number.

water to the northwest and southeast and by lower salinities ($32.2 \text{ }^{\circ}/\text{oo}$). These features coincided approximately with the southeastern side of Alsek Canyon.

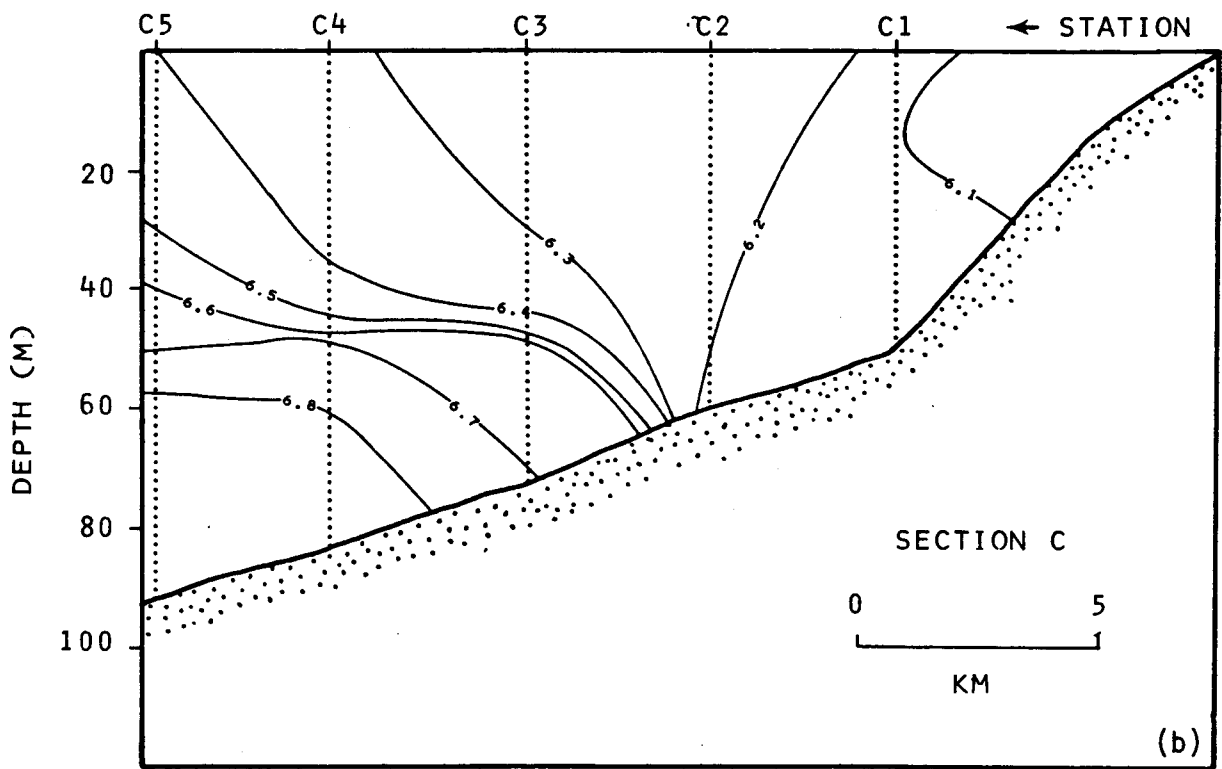
The vertical transects of temperature and salinity (Figure 35) indicate that most of the cross-shelf temperature and salinity gradient occurred within about 30 km of the coast. Temperature increased from 6.3 to $6.9 \text{ }^{\circ}\text{C}$ throughout the water column over this distance, and salinity increased from 31.6 to $32.0 \text{ }^{\circ}/\text{oo}$. Seaward of this zone of horizontal gradient, whose outer bounds were defined approximately by Stations 42-43 (Figure 35), temperature varied by less than $0.1 \text{ }^{\circ}\text{C}$ and salinity by less than $0.2 \text{ }^{\circ}/\text{oo}$ in either the horizontal or vertical. There was no indication in the shelfbreak region of the strong horizontal gradients which were present during autumn (Figure 10) between Stations 37 and 38. In the deeper water ($> 100 \text{ m}$) off the shelfbreak, salinity increased to oceanic values of $33\text{-}34 \text{ }^{\circ}/\text{oo}$, similar to the autumn case. Temperatures below about 350 m were similar to those in autumn, i.e. approximately $5.0\text{-}5.5 \text{ }^{\circ}\text{C}$. Temperatures between about 100 m and 300 m were higher in spring ($5.5\text{-}7.3 \text{ }^{\circ}\text{C}$) than in autumn ($5.2\text{-}5.0 \text{ }^{\circ}\text{C}$), providing the only instance where higher temperatures were present in spring than in autumn.

As in the autumn case (Figure 11), near-shore closely-spaced CTD transects were occupied along the coastline in spring to better define coastal hydrographic features. The temperature distributions along these transects are presented in Figure 36, where B is the easternmost and E is the westernmost transect. Transects B, C, and D (Figures 36a-c) show little or no evidence of the low-temperature coastal wedge which was evident during autumn (Figure 11). Only at Transect E (Figure 36d) was there a region of strong horizontal temperature gradient, found at about $1 \text{ }^{\circ}\text{C}$ over 5 km between Stations E1 and E3. These closely-spaced transects therefore support the observation that the coastal wedge which was a prominent feature in the autumn temperature-salinity field was greatly diminished or absent, depending upon location along the coastline, in the spring.

Details in the vertical distributions of temperature and salinity can be seen, illustrating general features, by referring to selected vertical profiles (Figures 37-40). As in autumn, the maximum stratification was present in Yakutat Bay (Figure 37). The relatively low density of water above $\sim 20 \text{ m}$ was due primarily to its low salinity. Below 20 m the water was relatively uniform



(a)



(b)

Figure 36. Vertical distribution of temperature ($^{\circ}\text{C}$) at four transects normal to the coastline, 20 - 24 March 1981. Locations of transects are indicated on Figure 7.

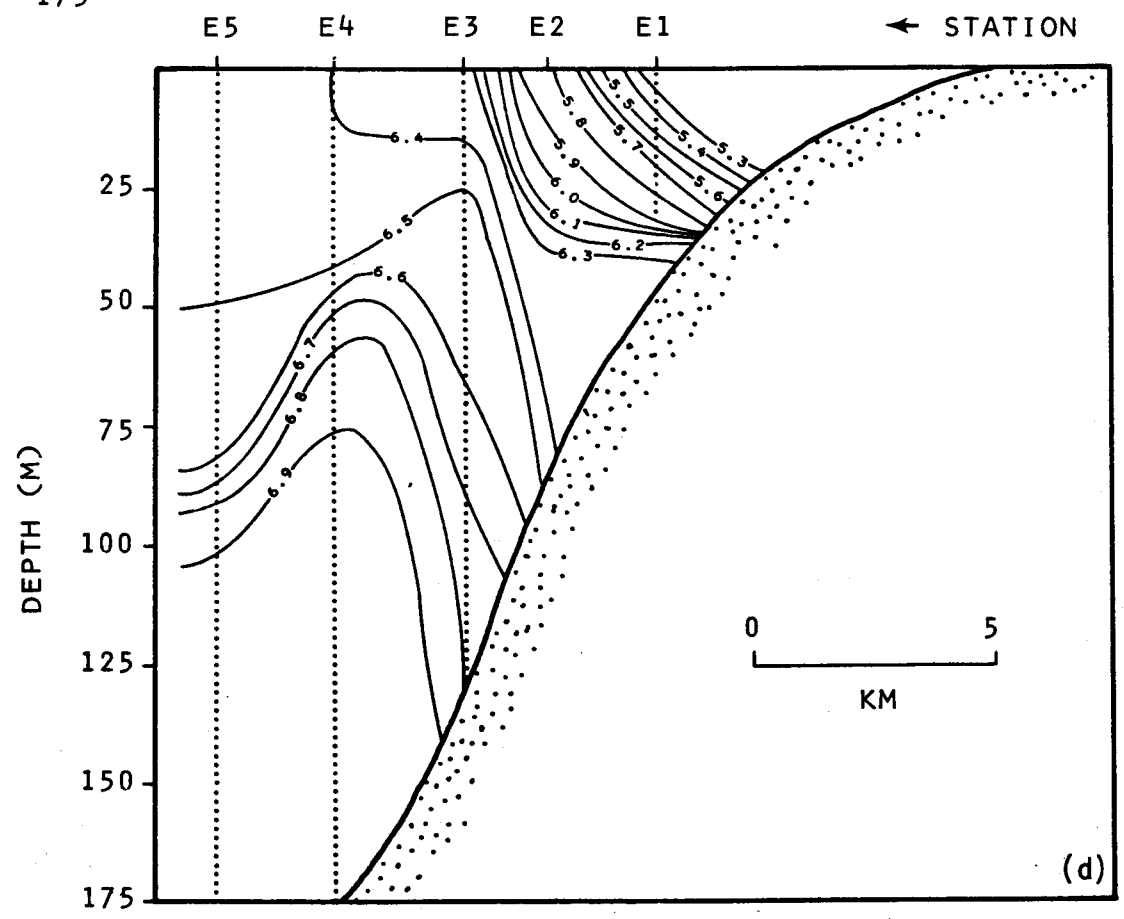
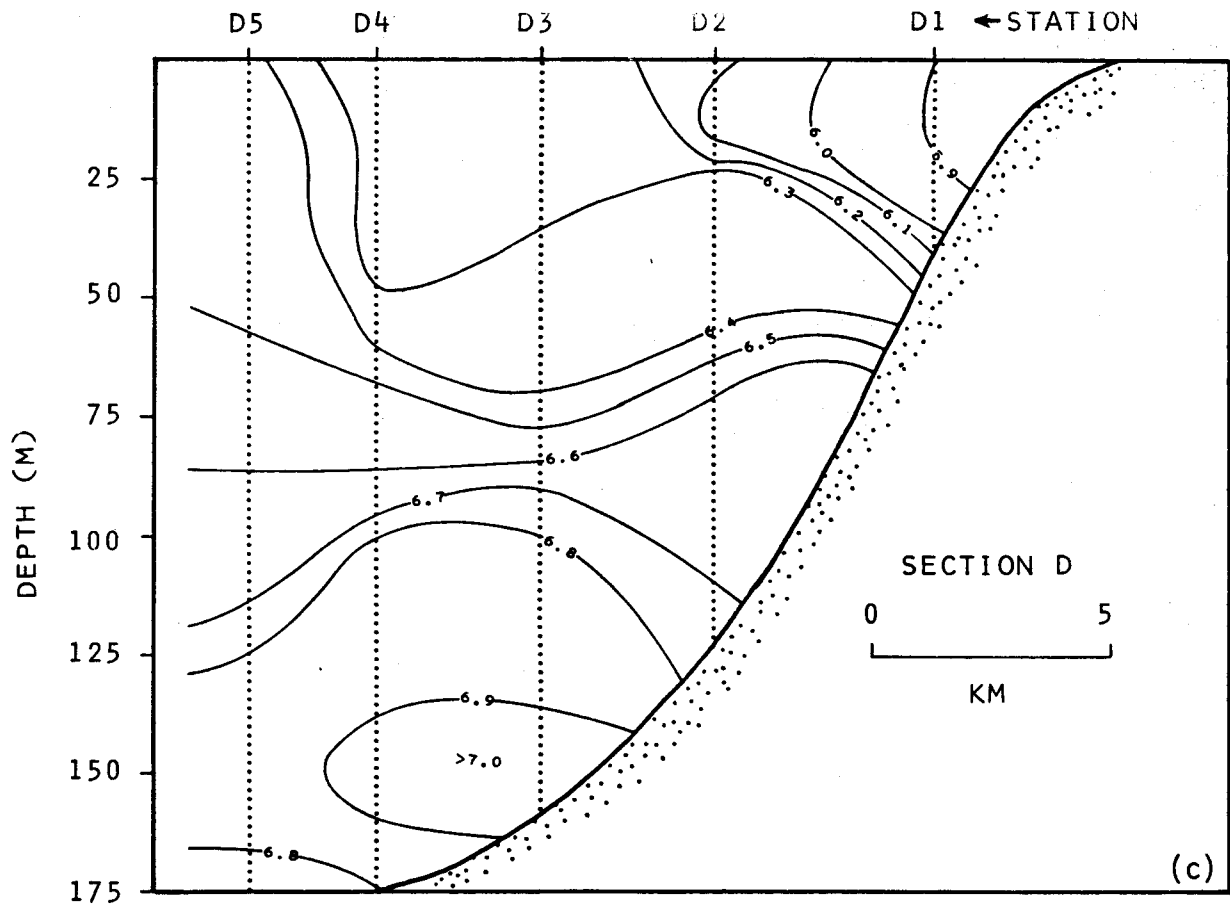


Figure 36 (continued).

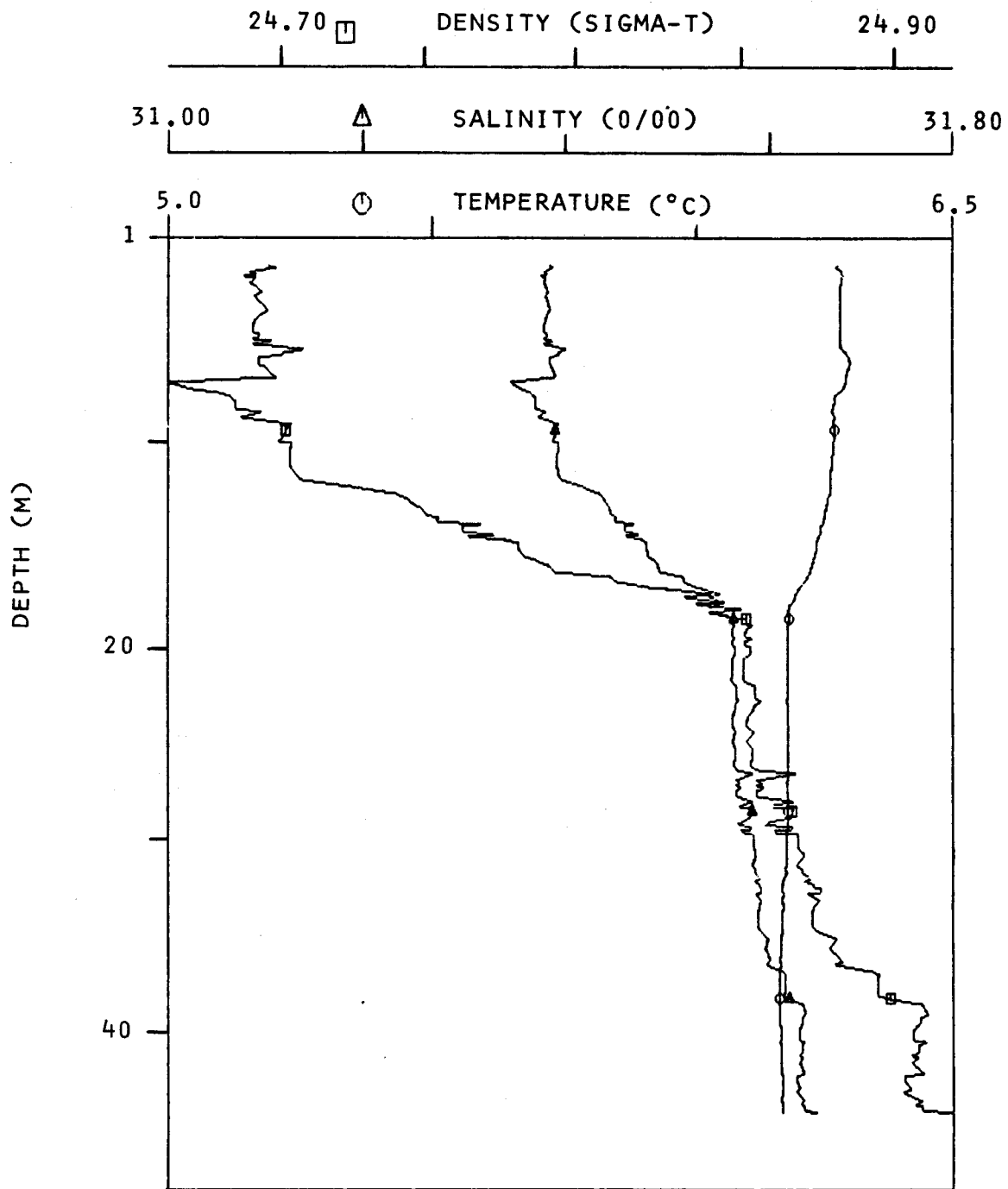


Figure 37. Vertical profiles of temperature, salinity and density at station 18 in Yakutat Bay. Station location is indicated on Figure 7.

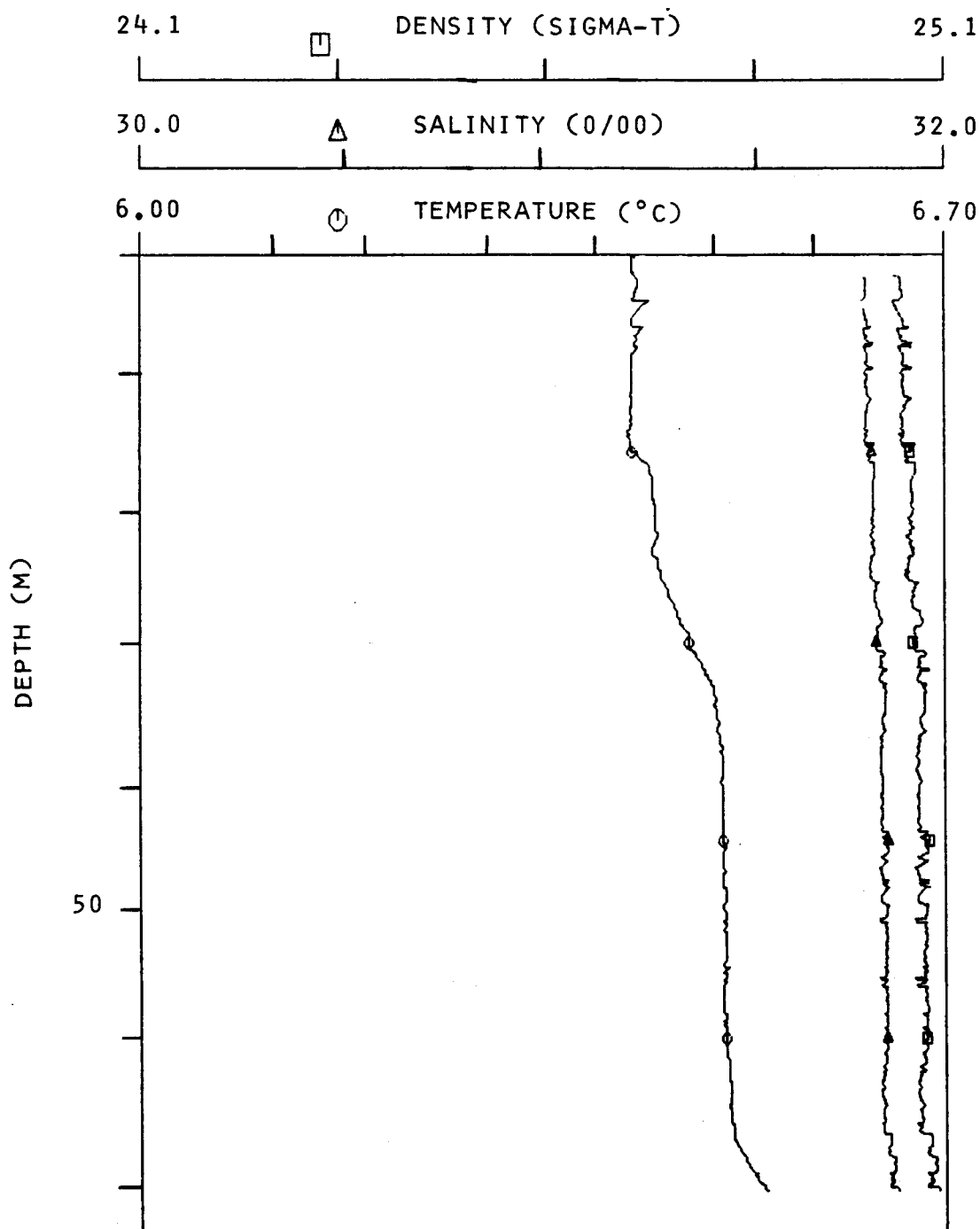


Figure 38. Vertical profiles of temperature, salinity and density at station 43 near the coast. Station location is indicated on Figure 7.

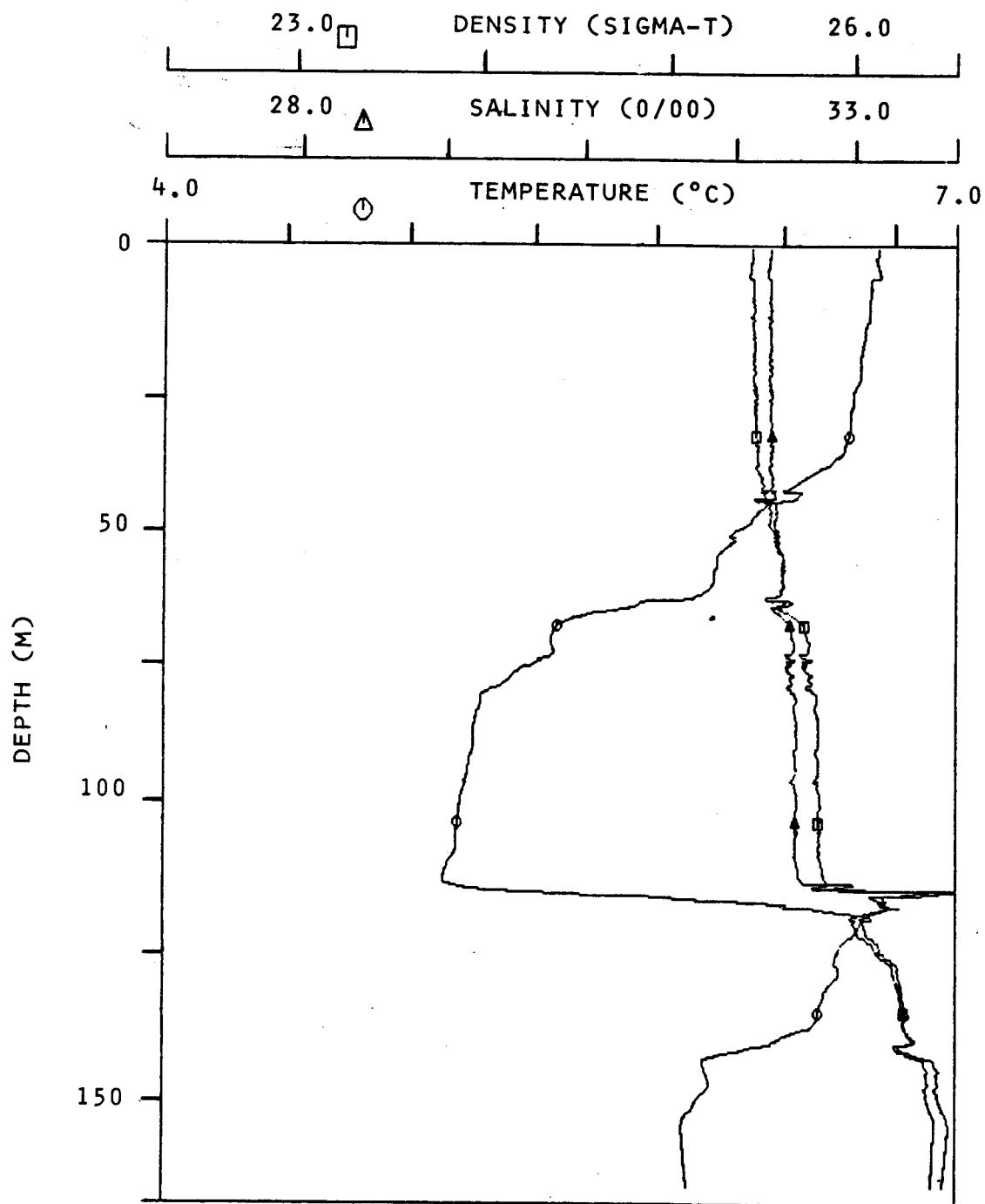


Figure 39. Vertical profiles of temperature, salinity and density at station 6 at mid-shelf. Station location is indicated on Figure 7.

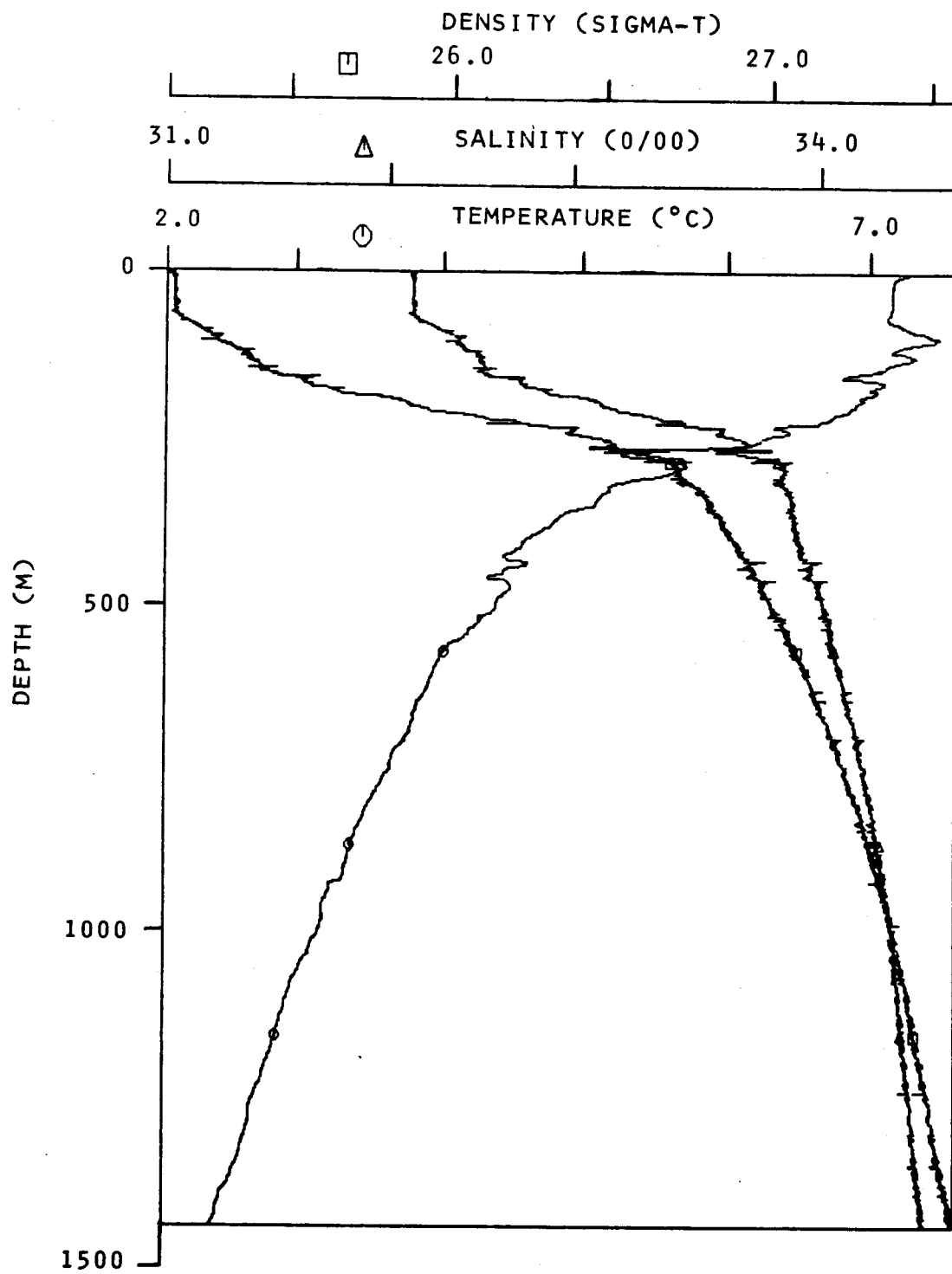


Figure 40. Vertical profiles of temperature, salinity and density at station 40 seaward of the shelfbreak. Station location is indicated on Figure 7.

in the vertical except for a slight near-bottom salinity (and hence density) increase. Station 43 (Figure 38), in the coastal region off Ocean Cape, illustrates the lack of vertical structure in the coastal water. The only significant vertical gradient found was in temperature, which increased by about 0.1 °C from the surface to bottom; farther offshore, mid-shelf Station 6 (Figure 39) reveals that a low-temperature layer was present at about 100 m. Salinity increased by about 1 ‰ from surface to bottom. Finally, Station 33 seaward of the shelfbreak (Figure 40) illustrates the vertical transition to deep ocean water characterized primarily by the gradual temperature decrease with increasing depth and the relatively uniform density below about 200 m. The vertical profiles for spring showed far less finestructure than was observed in autumn.

To summarize, the regional temperature and salinity distributions in March-April 1981 were typified by a far smaller variation in temperature and salinity than was observed the previous autumn, although considerable horizontal variability was still present off the shelfbreak. The autumn coastal band was nearly absent, being evidenced only weakly at Transect B and more strongly at Transect E. Water on the shelf away from the coast was nearly uniform except for perturbations which apparently coincided roughly with the southeastern border of Alsek Canyon. In general, temperature and salinity both decreased with increasing depth and offshore distance.

4.2 Observed Spring Near-shore Circulation

As in the autumn case (Section 3.2), observations obtained using moored current meters, drogued buoys, and seabed drifters will be presented separately here.

4.2.1 Spring Moored Current Observations

The records from Moorings 1 and 4 showed considerable similarity to each other in spring (Figures 41 and 42). Both these moorings were located about 4 km from the coastline. The current meter on Mooring 1 was considerably shallower (17 m) than that on Mooring 4 (34 m), but despite the differences in deployment depth both showed a consistent along-shore flow toward the northwest with only a brief period (1-2 April) of weak reversal to southeasterly

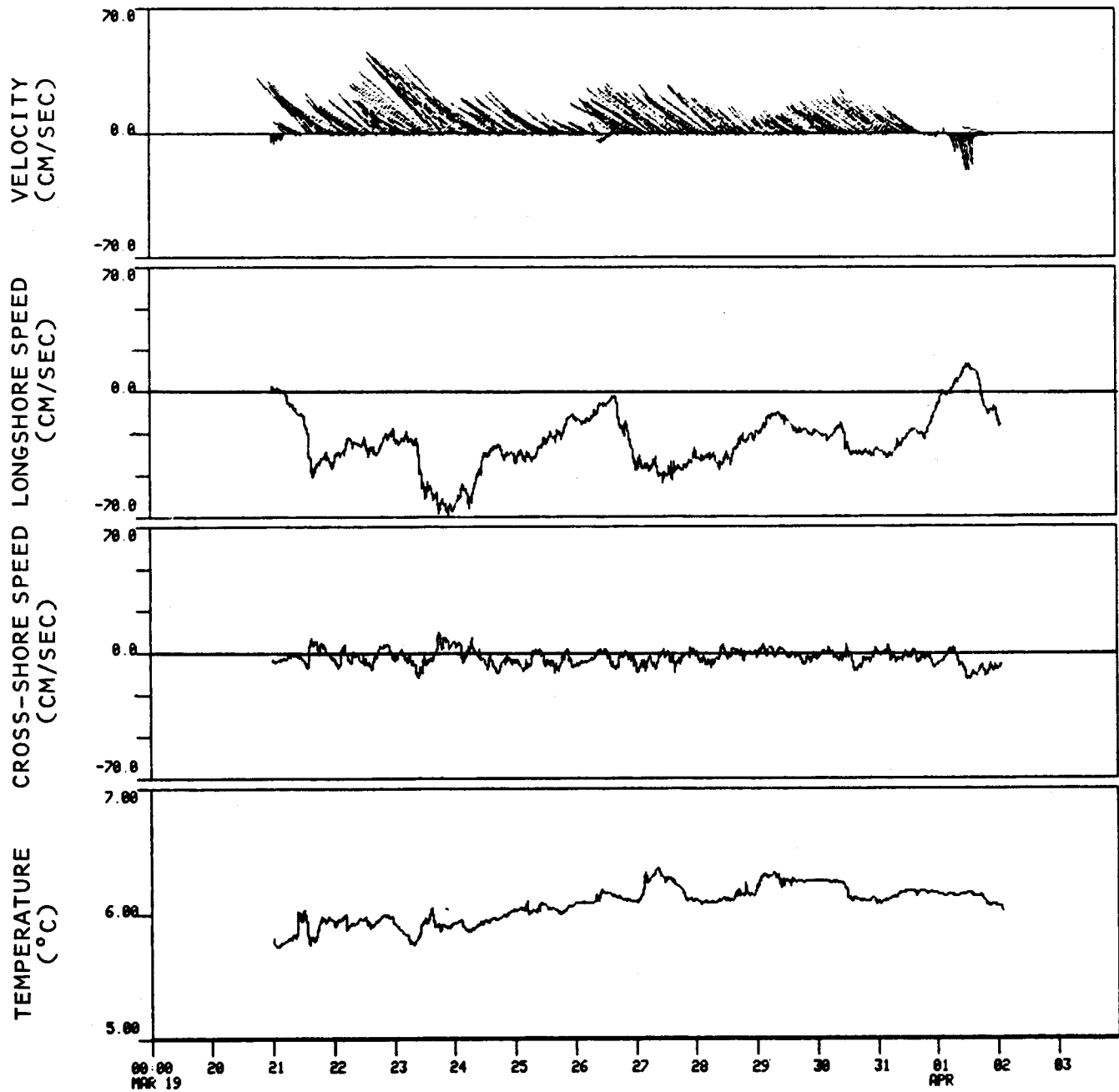


Figure 41. Time-series plots of 1-hour filtered current velocity (north is vertically upward), alongshore and cross-shore speed and temperature at 17 m, mooring 1. Mooring location is indicated on Figure 2.

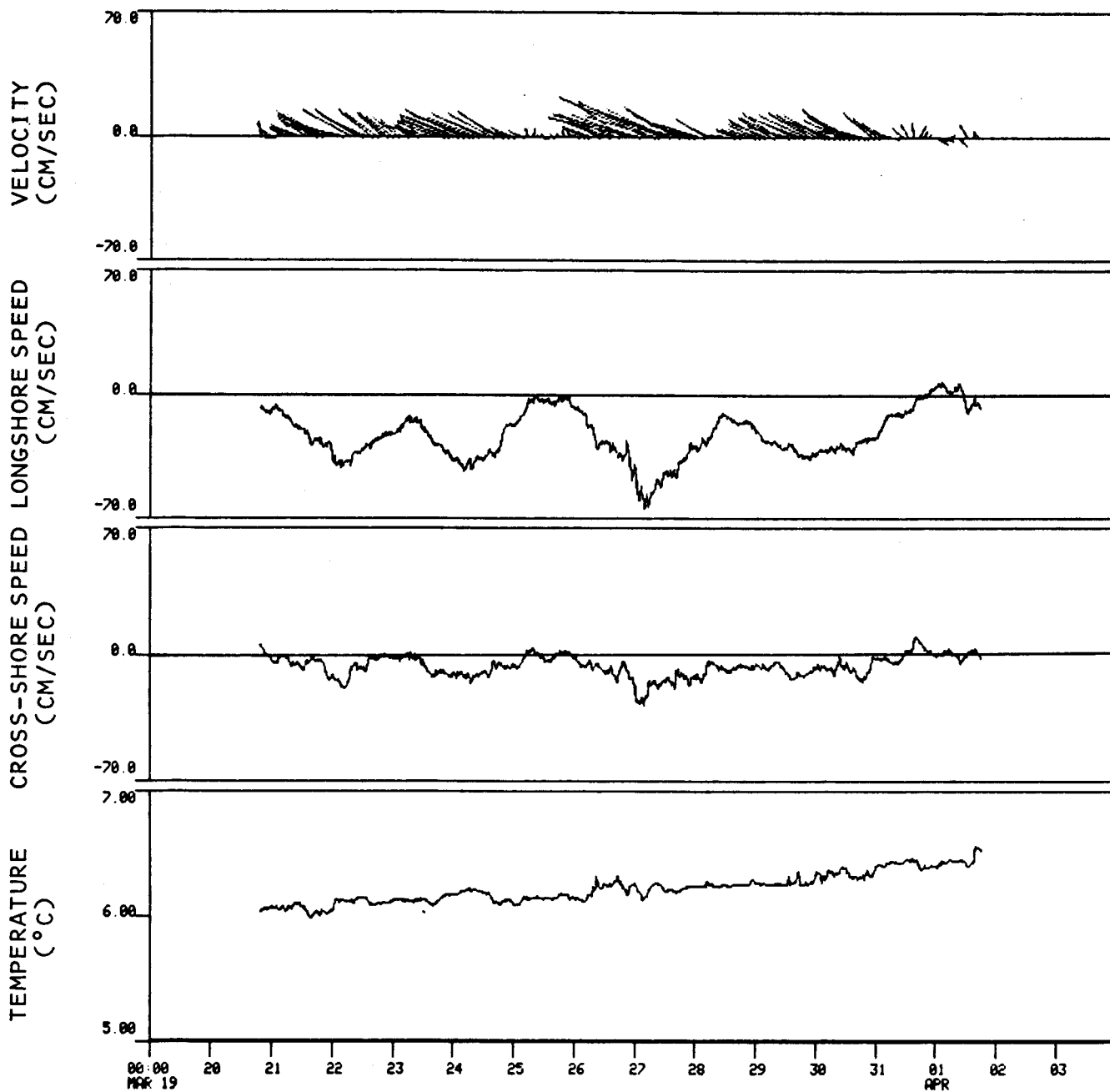


Figure 42. Time-series plots of 1-hour filtered current velocity, alongshore and cross-shore speed and temperature at 34 m, mooring 4. Mooring location is indicated on Figure 2.

flow. This behavior was in sharp contrast to the coastal flow in autumn 1980, when currents were bimodal with flow along-shore in either direction about 50 percent of the time. Flow speeds in spring were highly variable and reached maxima of nearly 70 cm/sec on 23-24 March at Mooring 1 (Figure 41) and on 26-27 March at Mooring 4 (Figure 42). Cross-shelf speeds were usually below about 10 cm/sec, though on 22 and 27 March they exceeded 20 cm/sec at Mooring 4. Visual inspection of the records suggests that a significant portion of the cross-shelf flow at Moorings 1 and 4 was tidal in nature. The records were, however, too short in duration for meaningful computation of energy spectra or tidal constituents. The along-shore flow was correlated at both moorings, with pulses on 22, 24, 27, and 30 March being evident in both records.

Both meters on spring Mooring 2 malfunctioned and yielded no records of significant length, and the upper meter on Mooring 5 also malfunctioned. Therefore, only the deeper (52 m) record from Mooring 5 is available as an indication of flow about 10 km from the coastline (Figure 43). Flow at this location was consistently toward the north, in rough alignment with local isobaths which at that location are strongly influenced by the presence of Alsek Canyon (see Figure 2). While there was some direction fluctuation about the northerly flow, only on 21, 25, and 31 March was there a weak reversal to southerly flow. Maximum flow speeds were about 30 cm/sec, and speeds were in the 15-20 cm/sec range. The maxima in northward flow on 23-24 and 27-28 March coincided with northwesterly flow peaks which were also observed at Moorings 1 and 4 (Figures 41 and 42). Tidal fluctuations appeared to be secondary in magnitude relative to the lower-frequency pulses. As for Moorings 1 and 4, however, the record was too short for quantification of this observation.

Currents recorded on Moorings 3 and 6 provided documentation of mid-shelf currents during the spring field program (Figures 44-46). At Mooring 3 flow was consistently toward the north. Speeds were higher (\sim 25 cm/sec) at the 37-m deep upper current meter (Figure 44) than at the 120-m deep lower meter (Figure 45) where speeds were 10-15 cm/sec. Reversals to southerly flow were infrequent, occurring only on 25 March, 6-7 April, and (at the deep meter only) 21-22 April. Visual inspection of the along-shore and cross-shelf speed plots reveals tidal currents which were appreciable but insufficient to reverse the flow from northerly to southerly.

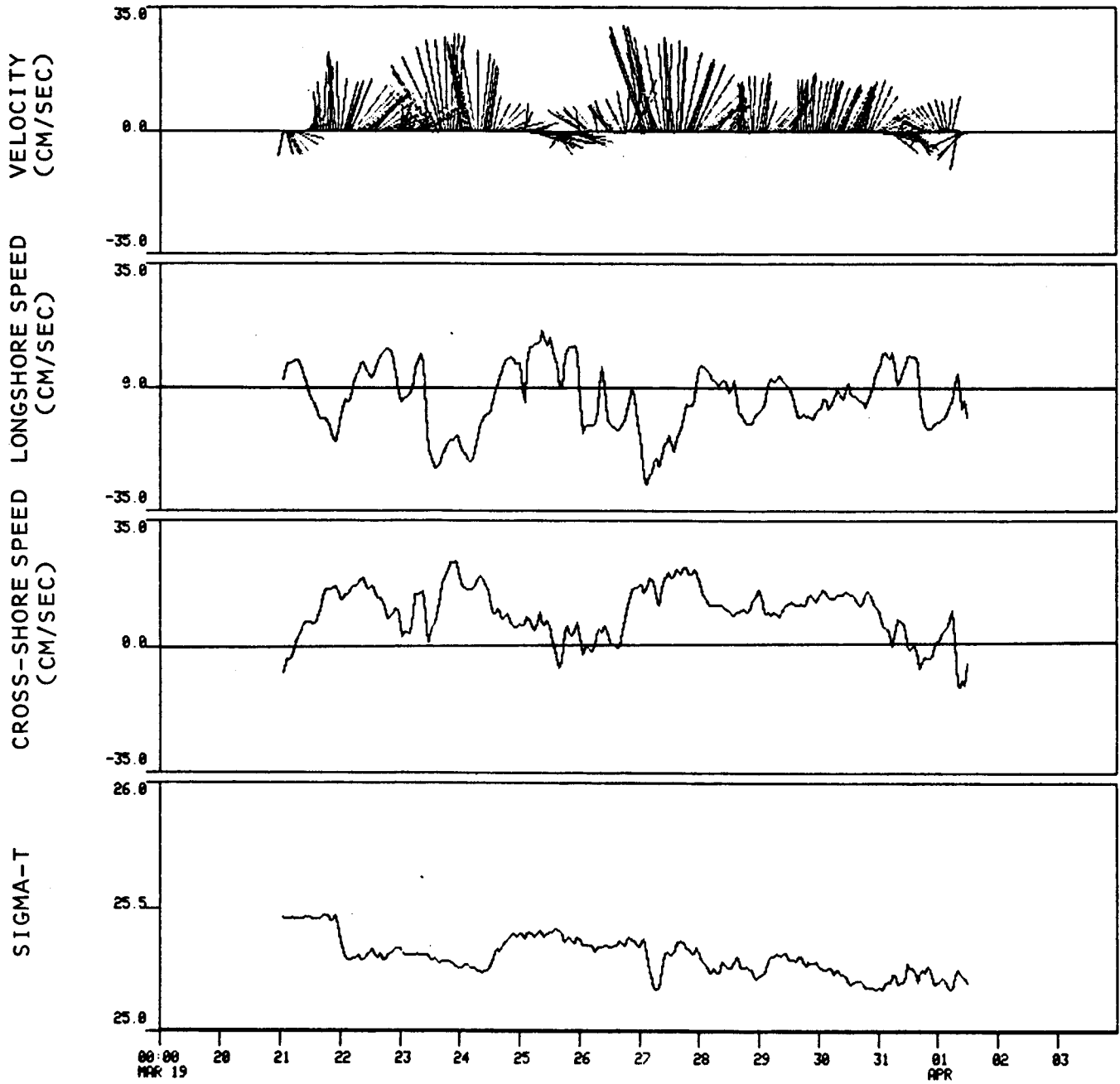


Figure 43. Time-series plots of 1-hour filtered current velocity, alongshore and cross-shore speed, and density (sigma-t) at 52 m, mooring 5. Mooring location is indicated on Figure 2.

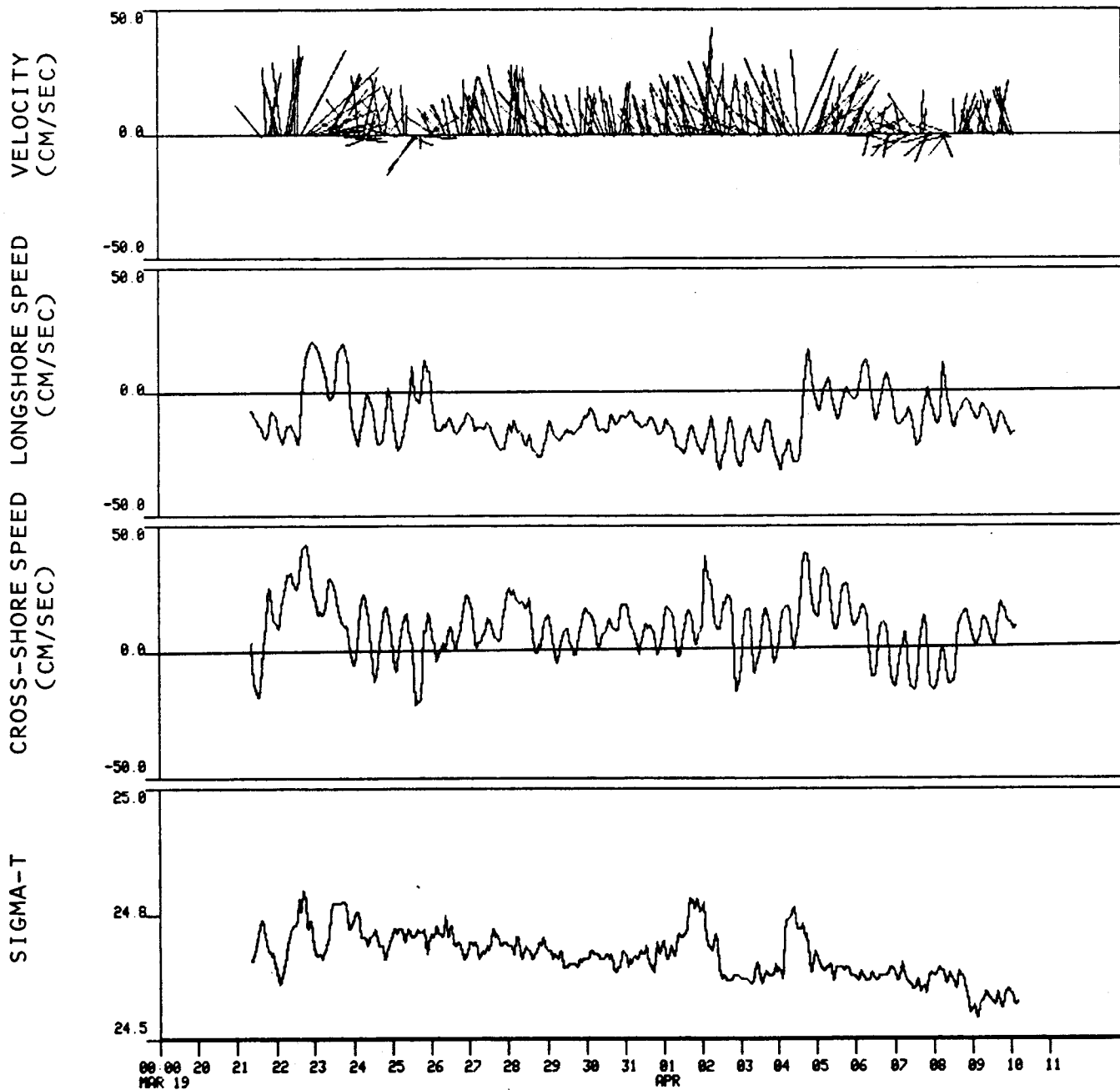


Figure 44. Time-series plots of 1-hour filtered current velocity, alongshore and cross-shore speed, and density (sigma-t) at 37 m, mooring 3. Mooring location is indicated on Figure 2.

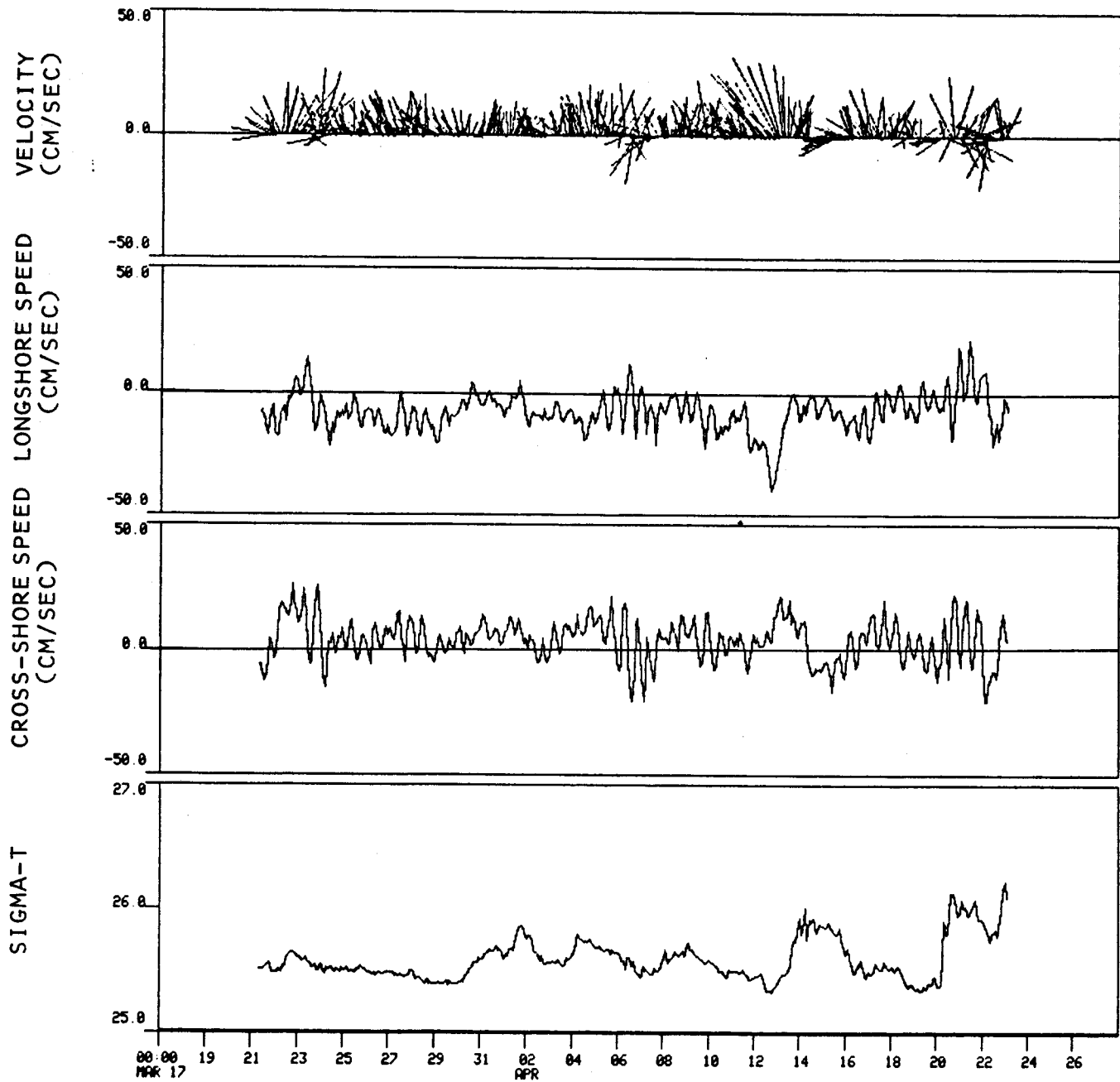


Figure 45. Time-series plots for 1-hour filtered current velocity, alongshore and cross-shore speed, and density (sigma-t) at 120 m, mooring 3. Mooring location is indicated on Figure 2.

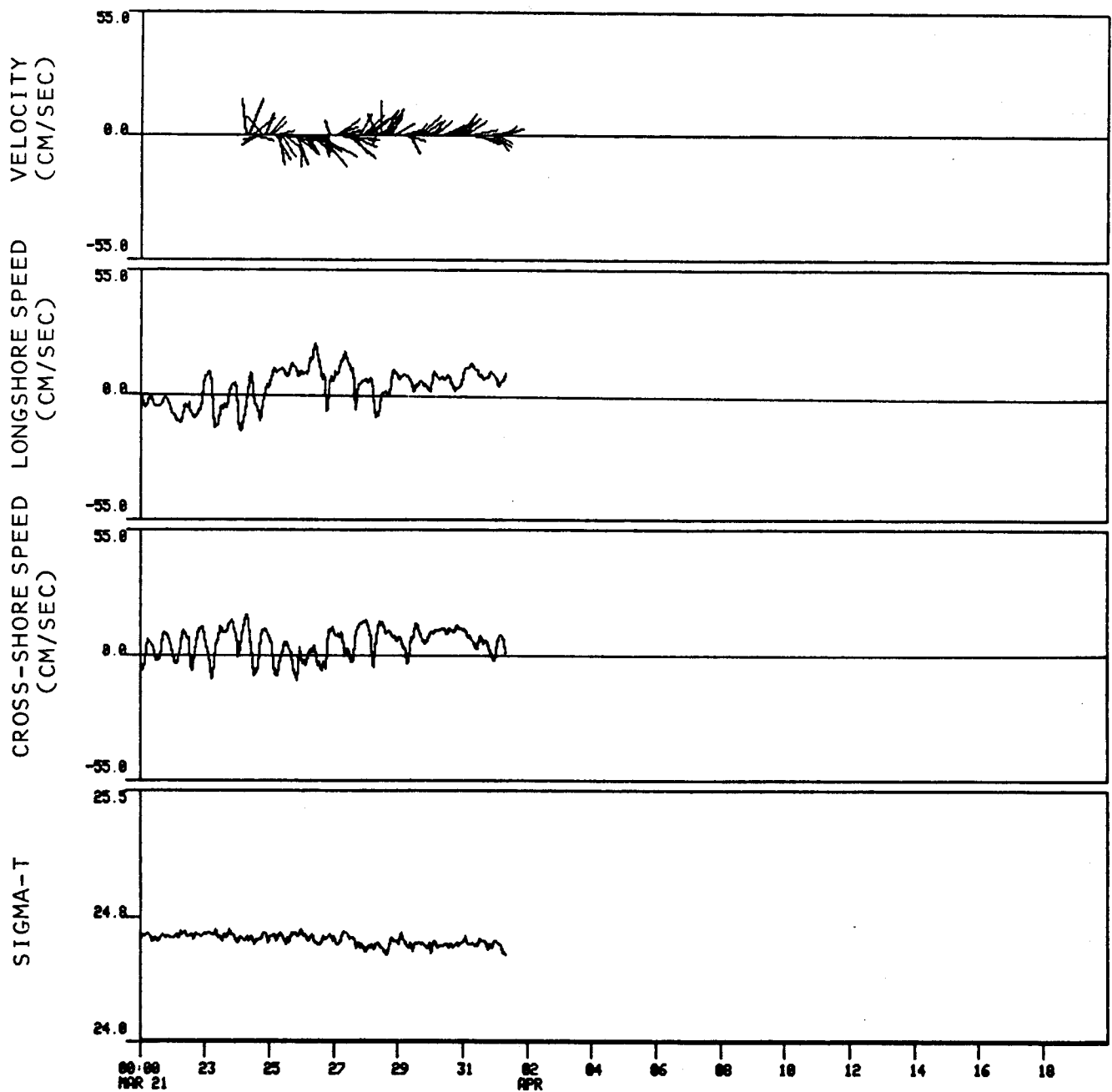


Figure 46. Time-series plots for 1-hour filtered current velocity, alongshore and cross-shore speed, and density (sigma-t) at 102 m, mooring 6. Mooring location indicated on Figure 2.

A current record was available only from the 102-m deep lower current meter on Mooring 6 (Figure 46). This record indicated that flow was fluctuating and generally easterly, varying from northeast to southeast in the same fashion as was observed during the autumn experiment (Figure 24). Speeds were 15-20 cm/sec with an obvious tidal signal as was recorded at Mooring 3. This current record showed by far the greatest directional variability of any of the spring moored current records.

4.2.2 Spring Drogued Buoy Observations

The drogued buoys in the first spring survey were initially separated by 3.5 km (Figure 47), more than the autumn separation distance, to ensure a shorter time period before the buoys started to disperse. After an initial period of moving toward the southwest, both buoys changed to a northwestward direction, Buoy 6 first followed by Buoy 5 (Figure 48). The buoys had similar speed statistics (Table 5), with mean speeds near 20 cm/sec and peak speeds of 40-45 cm/sec. The winds for this period were primarily out of the southeast at 4-5 m/sec. After initially staying within 2-3 km of each other, the two buoys separated at a mean rate of ~ 13 cm/sec; near the end of the experiment this rate returned to zero.

The second spring experiment, conducted from 24-27 March 1981, has been broken up into four phases for statistical purposes. The three buoys were deployed out from the coast in a line approximately 20 km farther southeast than during the autumn survey. Buoy 4, nearest the coast, moved northwestward while Buoys 5 and 6 tracked towards the southwest (Figure 48). The two southwestwardly moving buoys had mean speeds similar to Buoy 4 (10-15 cm/sec), while their peak speeds were higher (34-35 cm/sec as compared to 22 cm/sec; see Table 5) and their directions were more erratic (Figure 50). Because Buoy 4 was moving toward shallow water where recovery would be difficult, it was retrieved and redeployed farther off shore (Figure 49). The frequent gaps in data taken during this experiment were due to equipment problems, position uncertainties, and buoys drifting out of radar range of each other.

Buoys 5 and 6 were redeployed for a short period (Phase II). Although the statistics from this experiment are provided in Table 5, they are probably not particularly meaningful due to the short recording period (three hours).

Table 5
 SPRING SURVEY DROGUED BUOY SPEED STATISTICS

	MIN SPEED (cm/sec)	MAX SPEED (cm/sec)	MEAN SPEED (cm/sec)	SPEED STD DEV (cm/sec)
<u>EXPERIMENT 1</u>				
<u>Phase I: 3/22/81 (0300 hrs) - 3/23/81 (0900 hrs)</u>				
Buoy 5	6.6	45.8	18.1	7.4
Buoy 6	9.9	40.0	22.6	7.0

<u>EXPERIMENT 2</u>				
<u>Phase I: 3/24/81 (2000 hrs) - 3/25/81 (1600 hrs)</u>				
Buoy 4	1.0	22.1	11.0	6.2
Buoy 5	0.3	35.4	10.3	7.3
Buoy 6	2.1	33.8	14.6	7.2
<u>Phase II: 3/25/81 (2000 hrs) - 3/25/81 (2300 hrs)</u>				
Buoy 5	7.1	15.0	10.5	2.8
Buoy 6	2.1	7.9	5.0	1.9
<u>Phase III: 3/26/81 (0130 hrs) - 3/26/81 (1800 hrs)</u>				
Buoy 4	4.7	33.4	15.8	6.2
Buoy 5	2.4	16.9	6.9	3.2
Buoy 6	2.4	17.6	9.1	4.8
<u>Phase IV: 3/27/81 (0630 hrs) - 3/27/81 (2030 hrs)</u>				
Buoy 4	19.2	32.0	26.0	3.5
Buoy 5	4.4	34.8	20.8	9.1

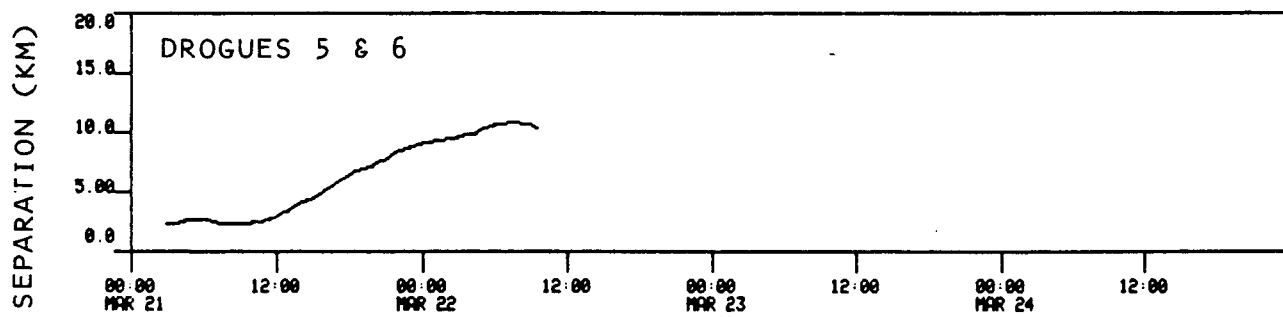


Figure 47. Plot of separation between drogues 5 and 6 as a function of time.

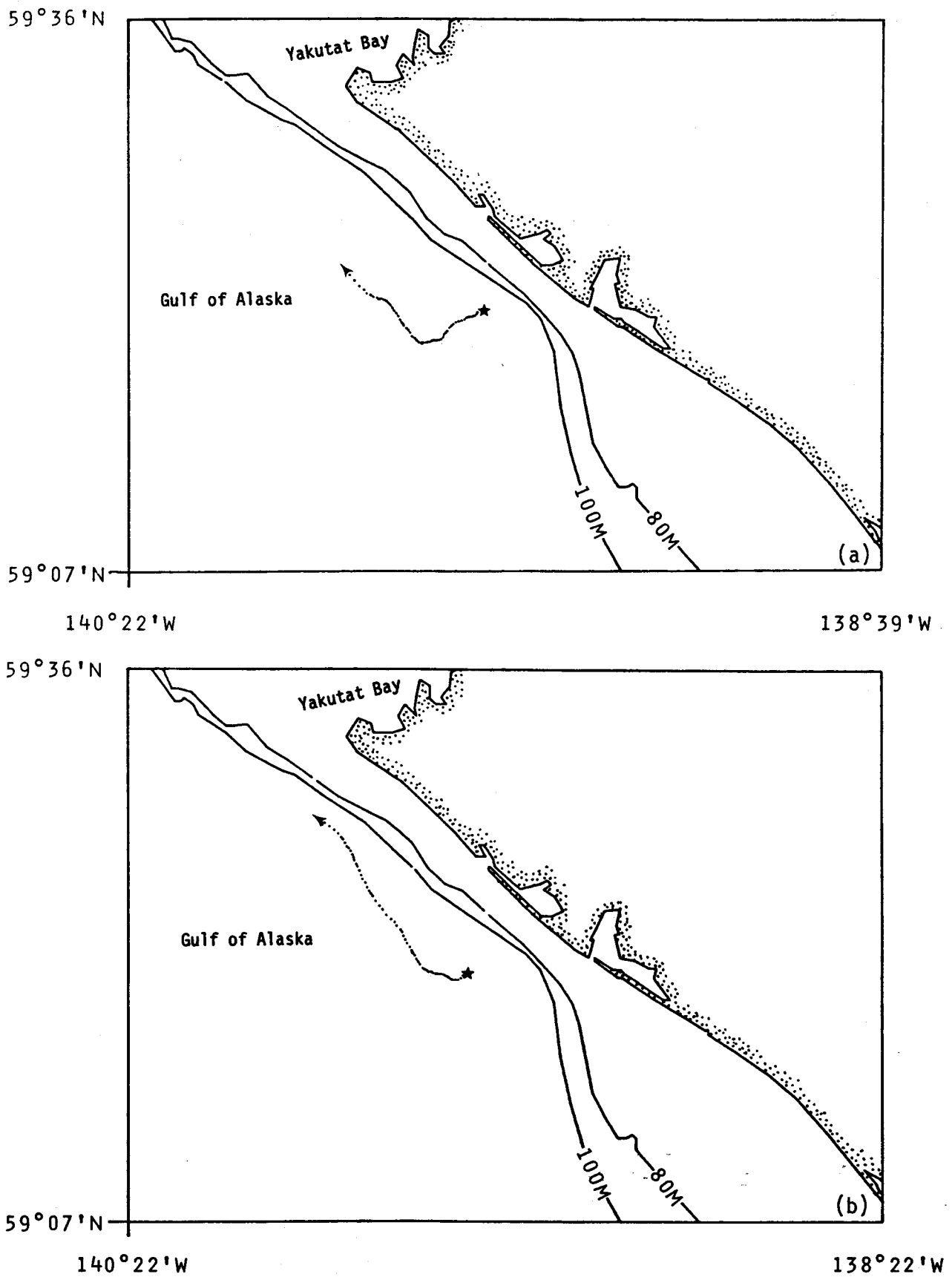
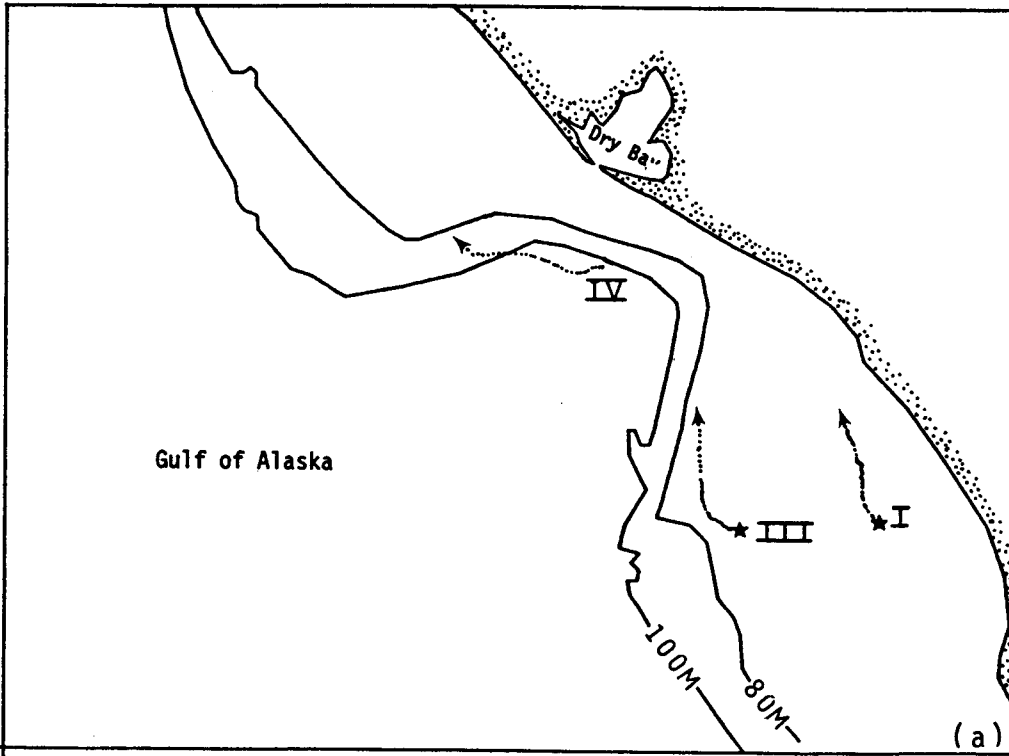


Figure 48. Drift tracks for drogues 5 (a) and 6 (b) during the first spring drogue experiment. Stars indicate deployment locations. See Table 5 for statistics.

59°36'N



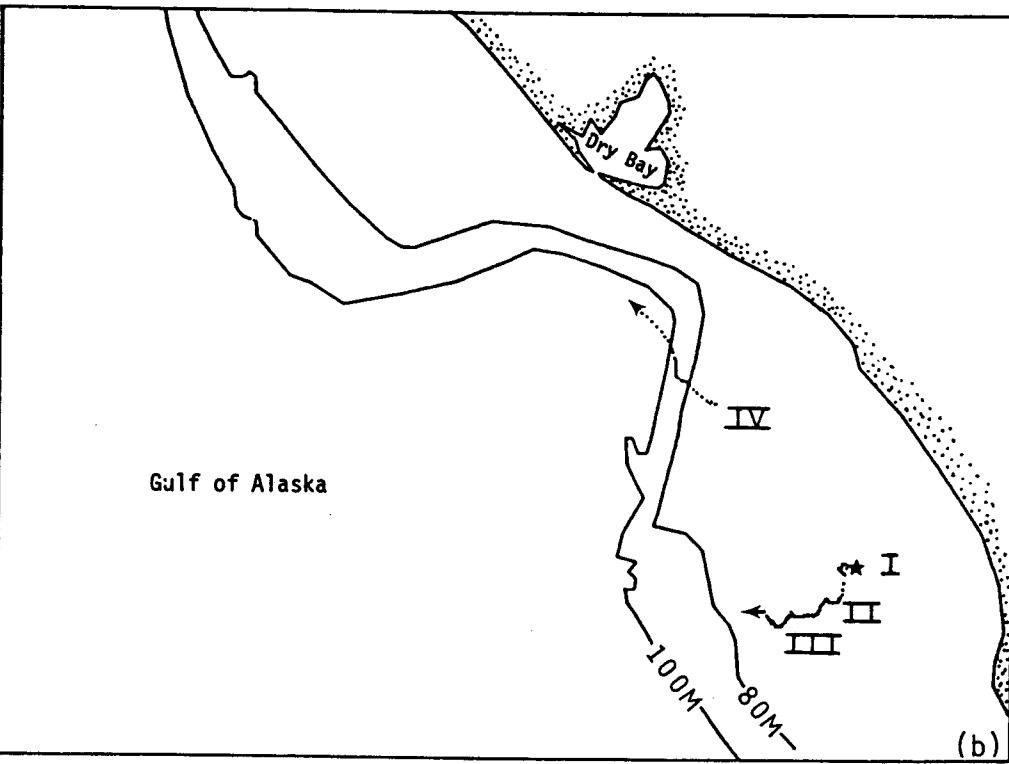
58°45'N

140°22'W

(a)

137°21'W

59°36'N



58°45'N

140°22'W

(b)

137°21'W

Figure 49. Drift tracks for drogues 4 (a), 5 (b) and 6 (c) during the second spring drogoue experiment. Roman numerals (I-IV) refer to different phases of the experiment. Stars indicate deployment locations. See Table 5 for statistics.

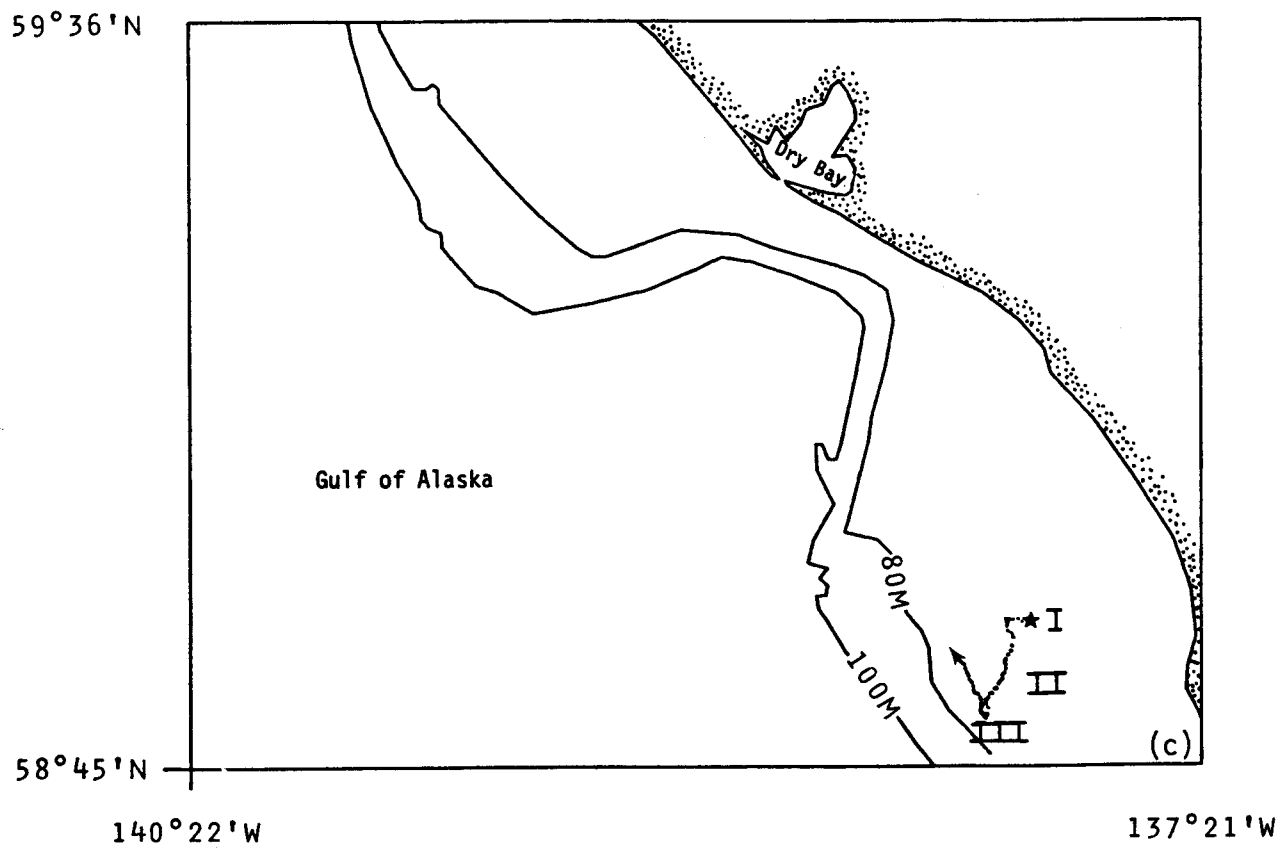


Figure 49 (continued).

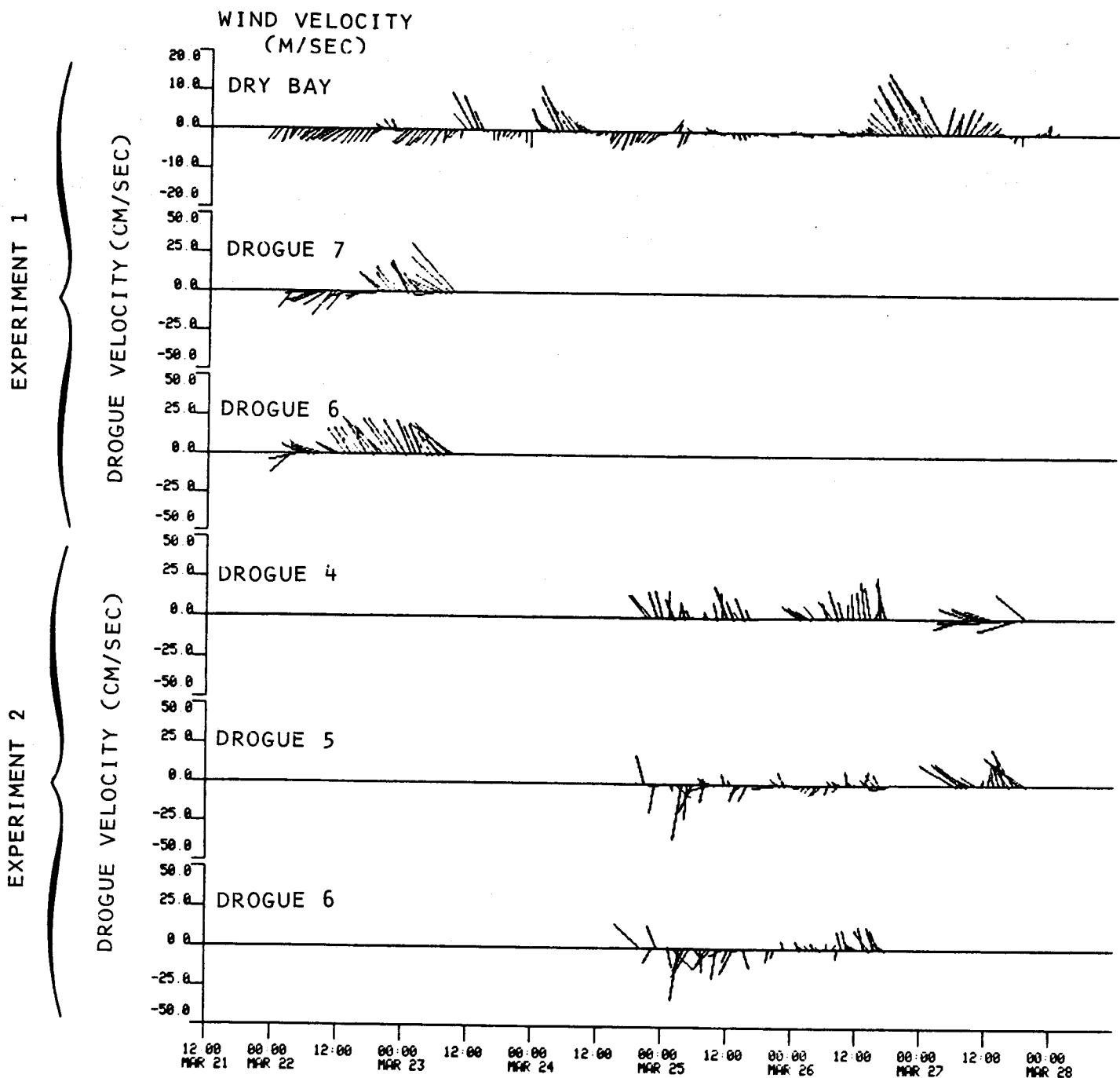


Figure 50. Plots of wind velocity as a function of time (uppermost plot), and drogue velocity derived from trajectories as a function of time. Both wind and drogue velocity vectors are oriented toward direction of movement. North is vertically upwards.

During Phase III all three buoys were redeployed. Buoy 4 was deployed in a region of northwestward flow, as evidenced by its significant mean and peak speeds (16 and 33 cm/sec, respectively). Buoys 5 and 6 changed direction towards the northwest and were entrained into the same strong flow (see Figure 48); this change, which can also be seen in Figure 50 along with the dramatic increase in speed for Buoy 6, happened simultaneously with the onset of a wind event (Figure 50). At this point Buoy 6 was retrieved.

During the final phase (IV) of the experiment, Buoys 4 and 5 moved in the northwesterly current with mean speeds of 20-26 cm/sec and peak speeds of 32-35 cm/sec. These two buoys moved along the coast and displayed the topographic steering effect that was evident during the same experiment of the autumn survey.

In summary, the spring survey showed consistent northwestward flow along the coast for the period of the drogue buoy study, in agreement with the moored current observations. There was some evidence that a storm event influenced the circulation. The topographic steering of the current seen in the autumn was observed at the head of the Alsek Canyon.

4.2.3 Spring Littoral Currents

The longshore surface current speeds and seabed drifter recoveries showed much lower speeds in spring than in the previous autumn's survey, probably as a consequence of the lack of strong storm events during the spring measurement period.

As shown in Table 6, the wave-driven surface current was southeasterly at about 57 cm/sec the day of the launch, reversing to a strong northeasterly flow which subsided the next day and reversed direction again to southeasterly flow on the third day. The vector-averaged velocities (Table 6) show a pattern similar to that seen by the seabed drifters: the first day's average velocity values imply flow to the southeast while all three subsequent days show values which imply flow to the northwest. In a different trend than seen with the seabed drifters, the current speed decreased over those three days, perhaps as a result of uncertainties in estimating the wave parameters.

Table 6

SPRING SURFACE CURRENT VELOCITY
ESTIMATED FROM WAVE PARAMETERS*

	WAVE- ANGLE (°)	WAVE HEIGHT (m)	LONGSHORE SURFACE VELOCITY (cm/sec)	VECTOR- AVERAGED VELOCITY (cm/sec)
Launch	-10 (±3)	0.8 (±0.5)	- 57 (±30)	- 57
Day 1	12 (±3)	1.5 (±0.5)	93 (±37)	62
Day 2	1 (±3)	2.2 (±0.5)	10 (±30)	41
Day 3	-10 (±3)	0.8 (±0.5)	- 57 (±30)	13

* Error estimates in velocity are those resulting from the uncertainties in angle and height of incident waves.

The seabed drifters were launched 21 March 1981, with strandings recovered over the following three-day period. Results from the in-shore group 1S (Figure 51a) show a slight southeast flow for the first-day recoveries, gradually changing to a moderate northwest flow. The drifters showed a range of speeds on the first day from -4 to 2.5 cm/sec, with a weighted mean of -2.5 cm/sec (negative values imply flow to the southeast). By the second day, the flow was to the northwest with a two-day average speed of 1 cm/sec and a range of 0-4 cm/sec. By the third day the northwestward flow was well-established, with one recovery reflecting a speed of 9 cm/sec.

The results from Group 2S (Figure 51b) also reflect this reversal of flow from southeast to the northwest. The first-day recoveries showed southeast flow with a weighted average of -2 cm/sec and a range from -3.5 to 1 cm/sec. On the second day the two-day average speed was 1 cm/sec, with a range from 0-5 cm/sec. The three-day average speeds ranged from 5-11 cm/sec with a mean of 8 cm/sec.

Group 1S and 2S thus showed similar patterns in the reversal from southeast to northwest flow. The third group 3S, which was farthest offshore, did not show this pattern, but its results are consistent with the other groups (Figure 51c). Since there were no recoveries of this group the first day, flow for that period was integrated into the two-day average values which showed a large number of recoveries centered around a mean of 4 cm/sec, slightly higher than the two-day mean values from the other groups. On the third day one drifter was recovered, reflecting a three-day average flow of 8 cm/sec; this is not significantly different from the two-day mean speed, considering the uncertainty in the measurements.

To summarize the spring data, the two in-shore groups of recovered drifters showed a reversal in current direction from southeast to northwest followed by a gradual increase in speed. While the offshore group did not show this reversal, its results are consistent with this pattern.

4.2.4 Spring Wind Observations

Winds recorded at the beach locations near Dry Bay and Ocean Cape during the spring program (Figure 52) showed the same event-dominated wind pattern that had been observed during autumn 1981. Speeds at both locations were generally

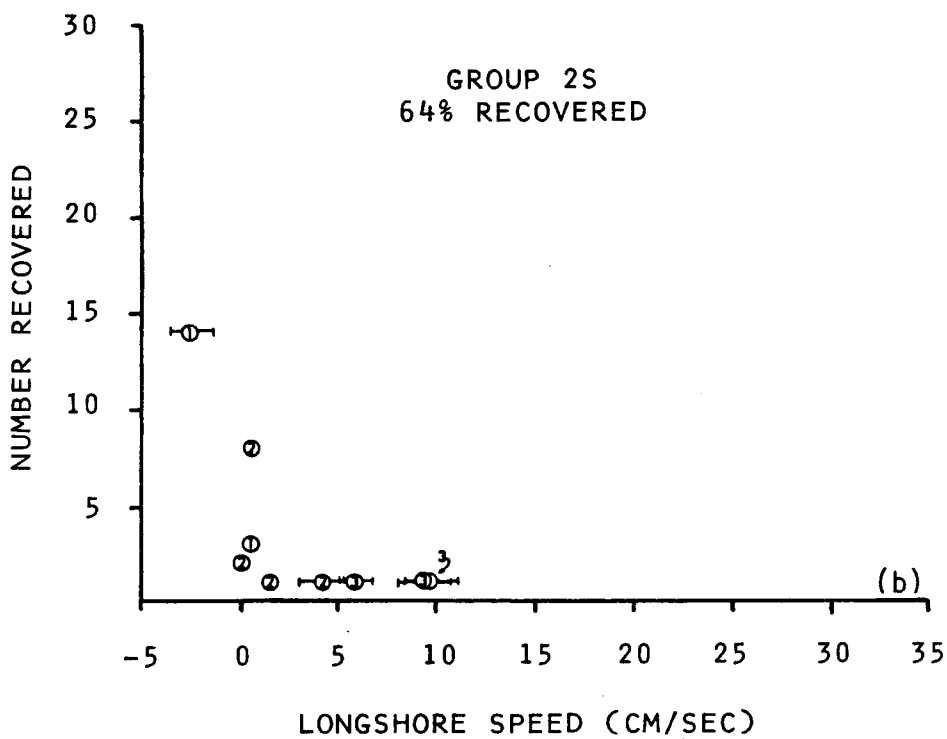
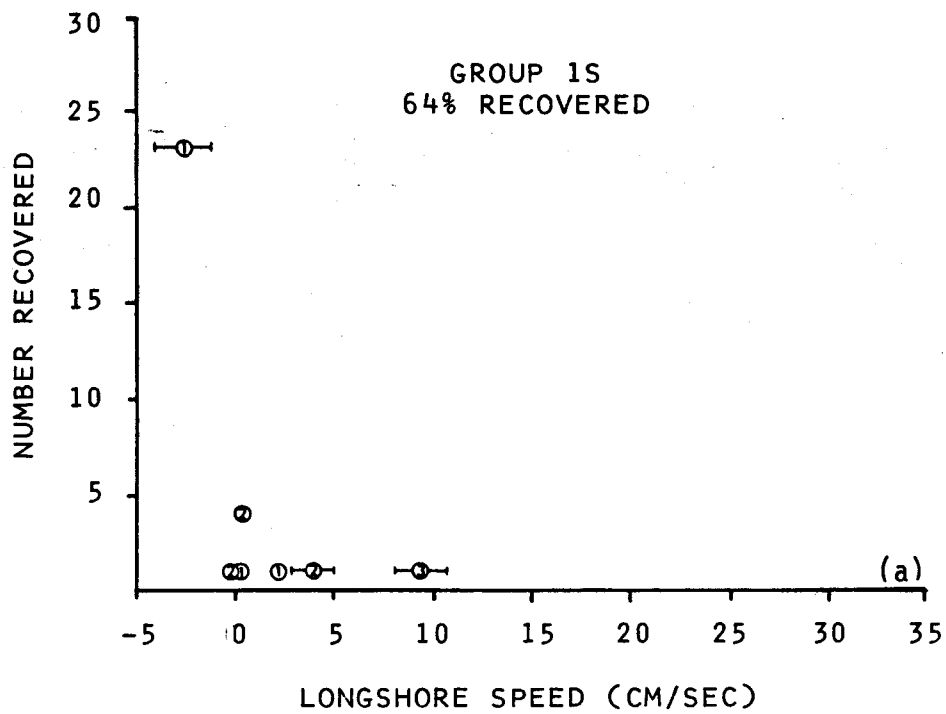


Figure 51. Histogram of alongshore speed for seabed drifters from groups 1 (a), 2 (b) and 3 (c). Positive is northwestward.

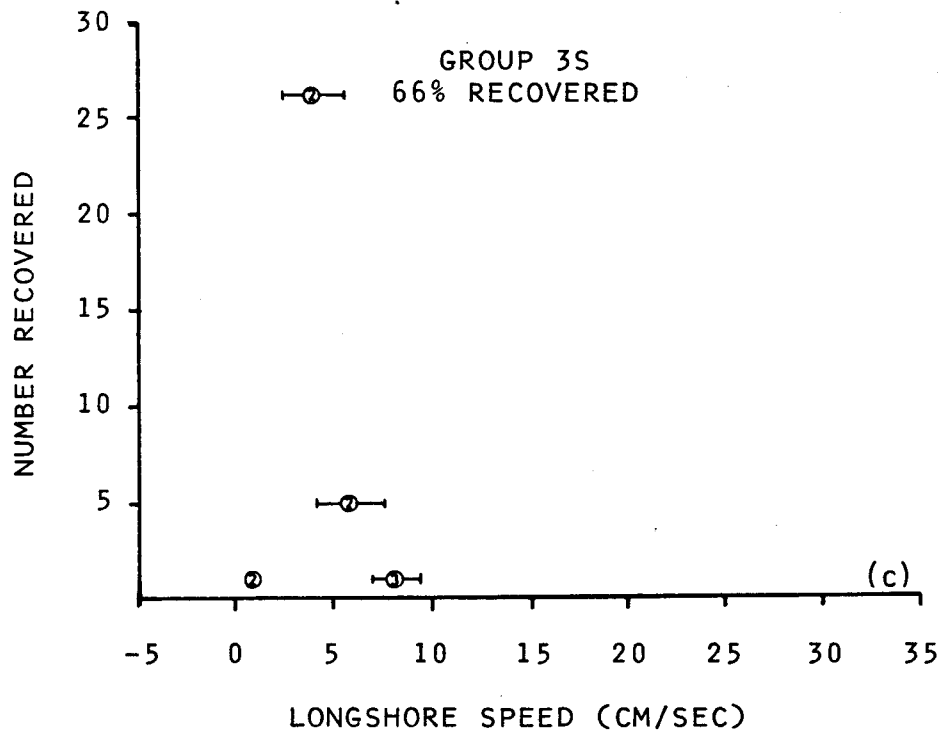


Figure 51 (continued).

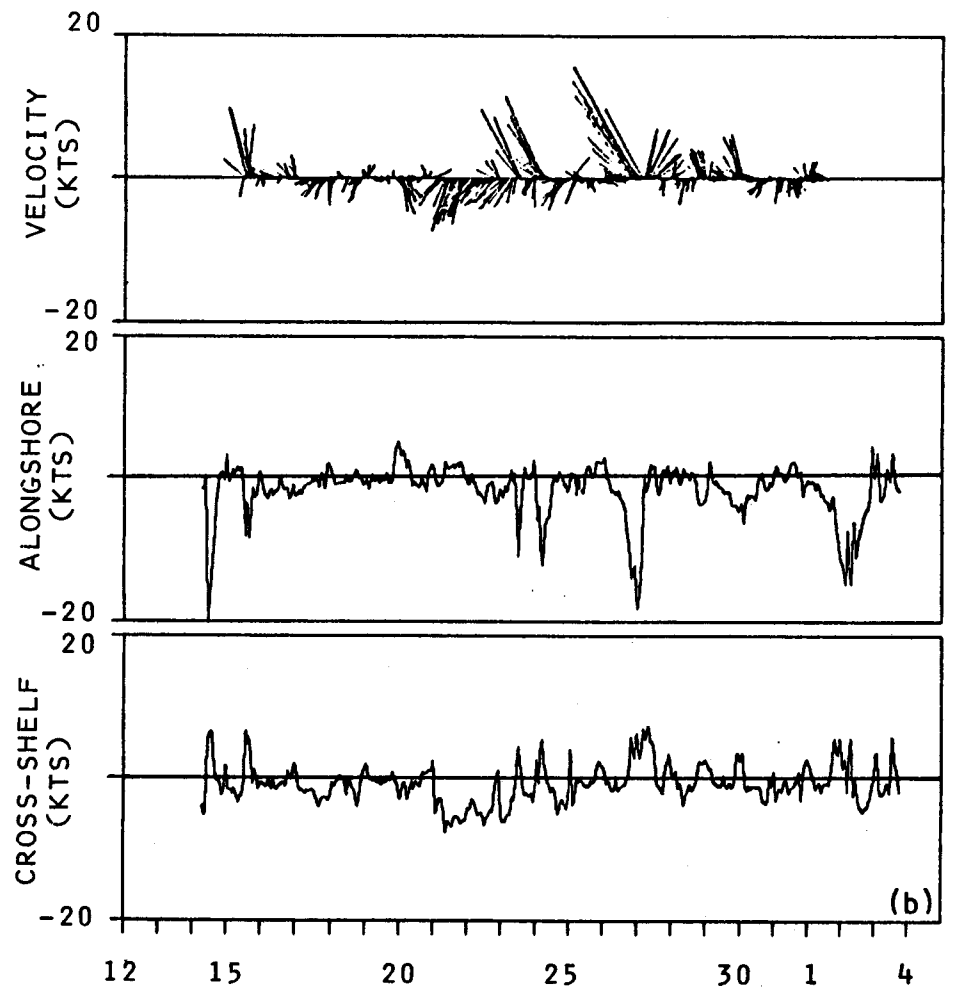
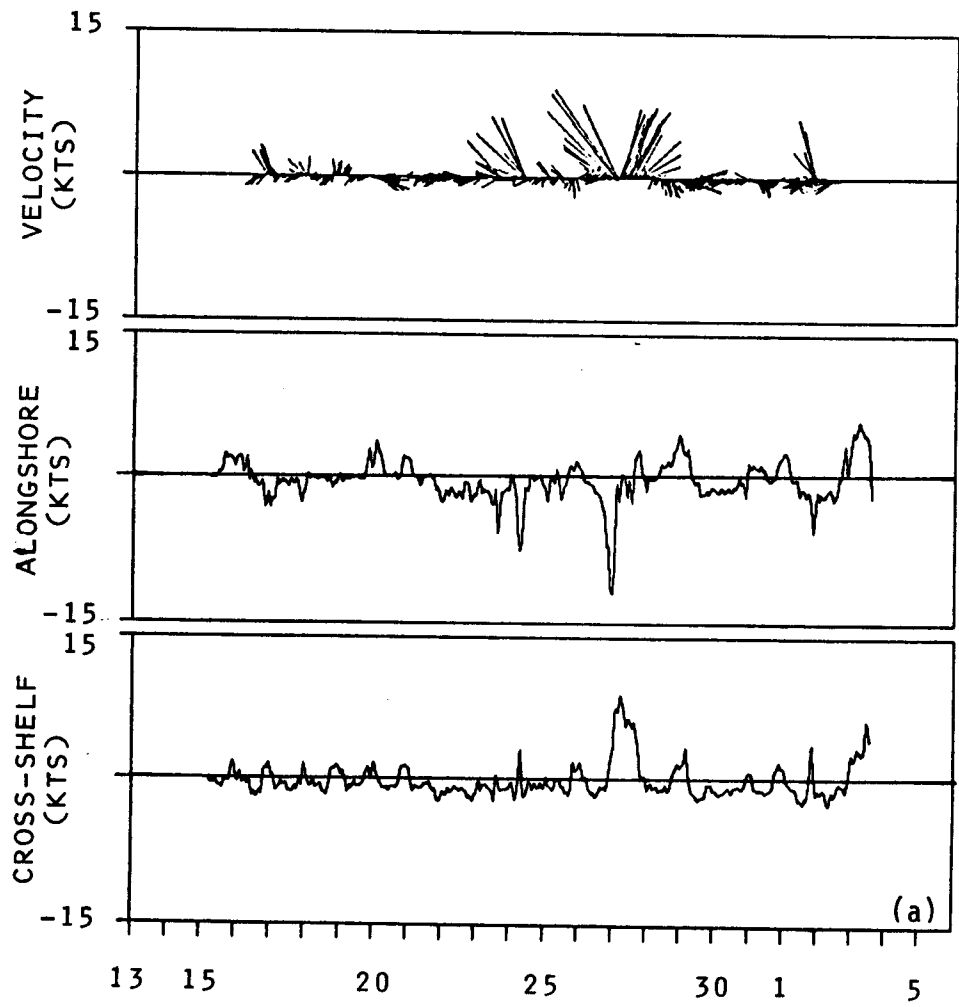


Figure 52. Time-series plots of 1-hour filtered wind velocity (north is vertically upward), alongshore and cross-shelf speed at Ocean Cape (a) and Dry Bay (b). Location of meteorological stations are indicated on Figure 2.

5 m/sec or less except when a storm event passed through the region. During periods of low wind speeds the winds were westerly. Discrete storm events, during which winds became easterly, were observed on 23-24 and 27 March; during these events, wind speeds attained values up to about 15-20 m/sec, with the higher speeds being associated with the later storm event. The storm winds were well correlated between the Ocean Cape and Dry Bay recording stations and were also observed at the vessel which was carrying out the concurrent oceanographic observation program.

4.3 Discussion of the Spring Experiment

The temperature and salinity fields observed in the study region during spring 1981 were characterized by generally lower temperatures, higher salinities, and smaller vertical and horizontal gradients than were observed in autumn 1980 (Section 3). There was, nevertheless, a level of spatial variability similar to that observed in the earlier experiment. Currents in spring exhibited a more consistent flow to the northwest than was present during autumn, although considerable speed variability was still present. The coastal current which had been observed in autumn was greatly diminished during spring. These observations are discussed below using temperature-salinity and time series analyses.

4.3.1 Temperature-Salinity Analyses

A composite temperature-salinity (T-S) plot has been constructed for the shelf waters off the northeast Gulf of Alaska during spring 1981 (Figure 53). For comparison purposes, the water masses which were defined for the autumn 1980 data are indicated on this plot by dashed lines. It is immediately apparent that the only autumn water mass to retain its identity unchanged in spring was the "Deep Ocean" Water having temperatures below about 7.5 °C and salinities greater than 32.0 ‰. The Coastal Water, a major identifiable water mass during autumn, was represented in spring only by the scattered T-S points falling to the left (lower-salinity side) of the Deep Ocean Water. The Shelf Water had salinities between about 31.5 and 32.3 ‰, coincident with the highest salinities observed for this water mass in autumn, and temperatures of 6-7.5 °C.

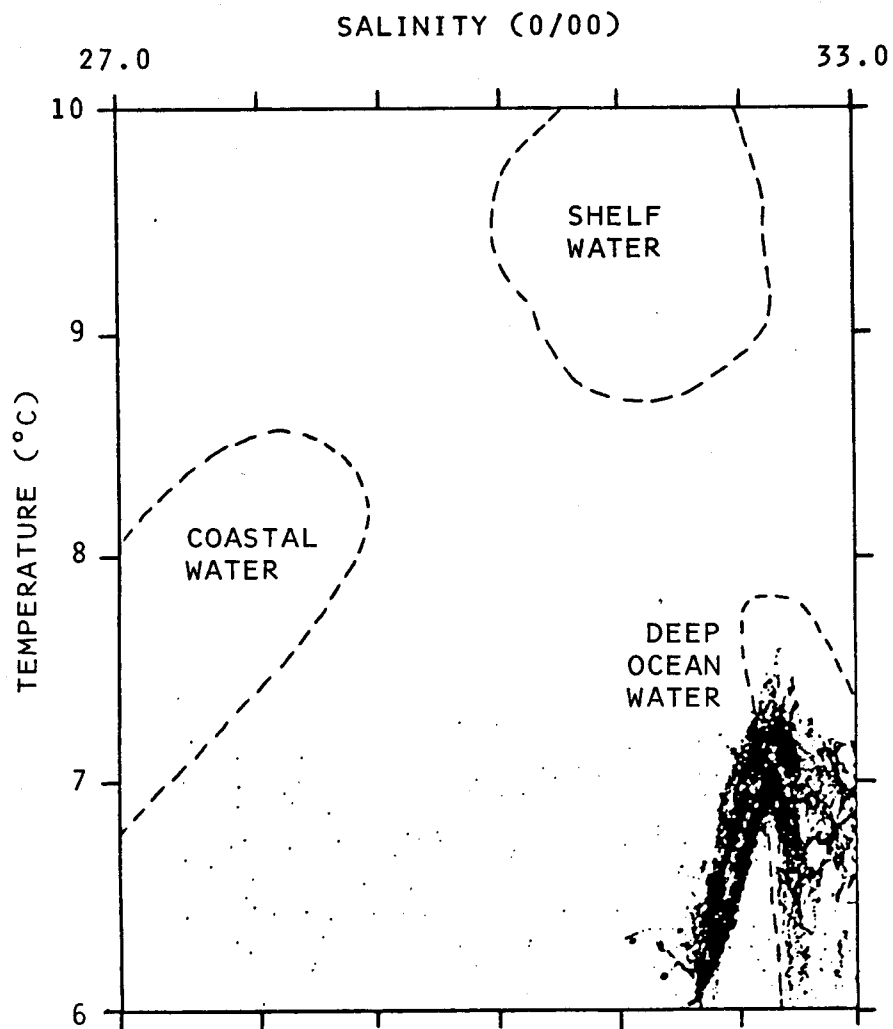


Figure 53. Composite temperature-salinity plot for the northeast Gulf of Alaska in spring 1981. Dashed lines define water masses which were identified during the autumn 1980 field experiment.

The altered (as compared to autumn) temperature-salinity characteristics of the water in spring can be explained qualitatively as due to the combined effects of winter cooling, wind-mixing, and near-cessation of coastal freshwater input to the coastal regions. The nearly complete absence of Coastal Water in spring was due to the lack of coastal freshwater input which was in large part responsible for the presence of this water mass the preceding autumn. The few scattered low-salinity points on Figure 53 were due to samples obtained within the few attenuated coastal river plumes along the coast and off Yakutat Bay. This input was not, however, sufficient to create a well defined low-salinity mass of Coastal Water.

Compression of the Shelf Water into a narrower range of salinities in spring than in autumn was also due in part to lack of freshwater admixture. Lateral mixing with the Coastal Water had been responsible, during autumn, for low-end salinities for the Shelf Water. Absence of the Coastal Water in spring therefore removed the source for low salinities in the Shelf Water, with the result that spring salinities were contained within a relatively narrow range of values.

Winter cooling prior to occupation of the spring CTD stations was responsible for the lower Shelf Water temperatures in spring than in autumn, with the lowest temperatures observed occurring in the near-surface near-coastal waters (see Figures 33-35) and higher temperatures occurring near the bottom at the shelfbreak. The Shelf Water temperature distribution in spring reflected, therefore, the more intense cooling near the coast due to lower air temperatures and shallower depths there, and the admixture of warmer Deep Ocean Water near the shelfbreak. The increase in temperature in the Deep Ocean Water between about 100 and 350 m between autumn and spring (see Section 4.1) was not due to local processes but rather an effect of circulation variations in flow off the shelfbreak. Vertical gradients associated with this feature were at times quite large; an example is shown in Figure 39, which shows a vertical profile from mid-shelf. The strength of the gradients suggests that the feature was being maintained by circulation because, in the absence of strong advection, vertical diffusive processes would have rapidly decreased the gradients.

Unlike the autumn case, spring temperature and salinity distributions were not characterized by well defined horizontal gradients or frontal zones which

separated the water masses (compare, for instance, Figures 10 and 35). This was due to combined cessation of the processes which acted during summer and autumn to maintain the gradients (i.e. warming and freshwater admixing) and an increase in the mixing processes which tend to diminish such gradients. Vertical mixing processes during winter would have been abetted in particular by thermohaline and wind mixing.

The appreciable accumulation of low-salinity near-coastal water at Section E (Figure 36d) suggests that freshwater was still being added to the head of Yakutat Bay through the winter. Since a significant portion of the freshwater addition to this Bay is thought to occur via subglacial streams (Reeburgh et al., 1976), there is no way to verify this contention directly.

Much of the horizontal variability in temperature and salinity at 100 m (Figure 34) can be explained in terms of flow of Deep Ocean water onto the shelf. Such water was evident in Alsek Canyon as 7.3 °C water (Figure 34a) and had probably flowed shoreward along the canyon as was inferred from the autumn 1980 T-S distribution (Section 3). The parcels of relatively cold (6.1-6.7 °C) and saline (32.3-32.6 ‰) water along the shelfbreak south of Yakutat Bay and at the extreme southeastern corner of the study region (Figure 34b) were of the proper characteristics to be Deep Ocean water. The water in Alsek Canyon had originated from slightly greater depths than the water on the shallower portions of the shelf, which explains its higher temperature.

Some of the variability may also have been due to eddy-like structures originating off the shelfbreak. Royer and Muench (1977) have hypothesized the presence of such eddies in the region to the west using satellite data. Hayes (1979) hypothesized, using current data from the Icy Bay region, that current fluctuations near the shelfbreak were due to offshore eddies. Lagerlof et al. (1981) suggest that eddies may explain low frequency current fluctuations observed on the shelf to the west of Dry Bay. Cyclonic "cold-core" eddies might explain presence of the low temperature areas observed off the shelfbreak, and are of the proper horizontal scale (~ 50 km) to be in qualitative agreement with previous work.

As in autumn, there was a general parallelism between the isopleths of temperature and salinity and the isobaths, upon which the above fluctuations were superposed. The parallelism supports the concept of a generally northwesterly flow along the coastline, as for the autumn case, and is in agreement with the dynamic principle that streamlines of flow should be expected to follow isobaths at these latitudes.

4.3.2 Circulation Analyses

In this section, the circulation features observed during the spring deployments of Moorings 1-5 and the final segment of the overwinter deployment of Mooring 6 are considered. The comments provided at the beginning of Section 3.3.2 concerning record length apply also to this section.

In sharp contrast to the autumn records, the spring records from Moorings 1 and 4 nearest the coast indicate that flow was consistently toward the northwest in the along-shore direction (Figures 41 and 42). Large speed variations were present, superposed on this northwest flow. Inspection of the records reveals a good visual correlation between the identifiable current pulses at these moorings. Comparison with the wind records obtained over the same time period indicates that the current pulses on 22, 24, and 27 March were correlated with strong northwesterly wind events (cf. Figure 52), suggesting that these pulses were wind-driven in nature. Coherence between along-shore currents and winds is theoretically to be expected based upon shelf circulation theory (LeBlond and Mysak, 1979). A similar tendency was observed west of Yakutat by Hayes (1979), although his moorings were deployed only beyond about 10 km from the coastline. Hickey (1981) has recently shown a high correlation between coastal current events and local winds off the Pacific Northwest continental shelf.

The small cross-shelf (relative to along-shore) flow reveals a strong bathymetric control over the currents, which paralleled isobaths. While tidal currents were evident in the cross-shelf flow components, they were small (< 10 cm/sec) relative to an along-shore flow which at times approached instantaneous speeds of 70 cm/sec. This small tidal flow near the coast is due to the continuity requirement that currents normal to the coastline go to zero at the coastline. A similar tidal current pattern was observed in the shelf region south of Kodiak Island (Muench and Schumacher, 1980).

Mooring 5 exhibited flow which was northerly except for minor reversals on 21, 25, and 31 March. The northerly orientation paralleled local isobaths which defined the shoreward end of Alsek Canyon (Figure 2). This was particularly pronounced at Mooring 5 because only the deeper of the two records was usable and proximity to the bottom made the tendency to parallel isobaths more pronounced.

Mooring 3, the farthest off the coast, exhibited a strong northward flow at both depths, with instantaneous speeds at 37 m depth of about 40 cm/sec and speeds at 120 m of about 20 cm/sec with one peak (on 12 April) approaching 40 cm/sec. The reason for this strong cross-shelf flow is uncertain, but it is probably related to interaction between the regional northwestward flow and local bathymetry.

The record from Mooring 6 was dominated by the tidal signal, which was considerably stronger than the weak mean flow (cf. Figure 46). This record was in sharp contrast to those from the other spring moorings, all of which had shown relatively consistent flows toward the north-northwest. Conversely, the long-term mean flow at Mooring 6 was easterly (see Section 5.1) and weak relative to the instantaneous current events. As for Mooring 3, the reason for this consistently "reversed" flow is uncertain; it probably is due to topographic effects, in particular the location of the mooring north of Fair-weather Bank.

The overall circulation pattern observed in spring 1981 showed a consistent flow toward the north-northwest, with lower directional variability than in autumn 1980 except for Mooring 6. Results obtained from the moorings were in agreement with those derived from the drogued buoys (Figure 50) and, unlike the autumn case, showed less variation with depth. There was pronounced convergence of streamlines at the heads of the cross-shelf troughs, these being most evident at the head of Alsek Canyon both in currents obtained from the moorings and in the drifter results (Figure 49a). This convergence was responsible for the high currents at Moorings 1 and 4, relative to those observed at other moorings. Reasons for the strong cross-shelf flow component at Mooring 3 and for the small easterly mean flow at Mooring 6 are uncertain.

4.3.3 Littoral Currents

The seabed drifter program and accompanying analytical computations, as described in Section 4.2.3, revealed that the littoral currents were far weaker in spring 1981 than they had been the previous autumn (see Sections 3.2.3 and 3.3.3). This was because most wave activity was directed directly onshore in spring, and there was not therefore an appreciable longshore wave-induced transport. Some reversals to a southeasterly longshore flow in the littoral zone were also observed -- an indication that waves were actually coming from a westerly direction, in sharp contrast to the autumn picture.

Since the littoral currents are a response to waves impinging upon the beach, they reflect both the swell which has propagated for long distances across the North Pacific and the regionally-generated wind waves. Reference to Brower et al. (1977) reveals that in the March-April period the wave field off Yakutat normally is undergoing a transition. Waves tend to come from the east-southeast or the west-southwest, with waves from the south occurring relatively infrequently. This directional bimodality appears to be a consequence of the wind direction field over the same period. By April, however, waves show a marked tendency to be from the west, with about 42 percent from the west-southwest (Brower et al., 1977), and have a height preference from 1 to 3 m. This study's littoral current data, which are a direct reflection of the wave field, show this March-April transition toward eastward wave propagation. The lower littoral current speeds also are in part a reflection of smaller wave heights in March-April than in October-November. Based upon this comparison between the present results and those which would be inferred from the wave fields documented in Brower et al. (1977), the autumn and spring observations made in this study appear to be representative for those times of year.

4.3.4 Summary

The results of the spring field experiment can be briefly summarized as follows:

1. The regional temperature and salinity distribution showed considerably less variability on the continental shelf and near shore in spring than during autumn. Of the three water masses defined on

the basis of their temperature-salinity characteristics in autumn, only the Deep Ocean Water remained relatively unaltered from autumn to spring. The Shelf Water had been cooled and mixed so that it occupied a far smaller temperature-salinity range than in autumn. The Coastal Water was nearly entirely absent, being represented only at a section off Yakutat Bay, and had lower temperatures than in autumn. The area which had been occupied in autumn by Coastal Water revealed presence only of Shelf Water in spring, except for the Yakutat Bay section. Deep Ocean Water occupied the region off the shelfbreak and extended shoreward along the bottom of Alsek Canyon, as it had during autumn. Temperature and salinity irregularities off the shelfbreak suggested the presence there of eddy-like structures associated with the shelfbreak flow.

2. Circulation on the shelf was generally far less variable than during autumn and showed a consistent northwesterly flow upon which were superposed spatial variability due to interactions with the bottom topography and temporal variability due to local wind forcing. In particular, northwesterly flow pulses near shore coincided with strong southeasterly winds. Currents near the heads of Alsek and Yakutat canyons followed the bathymetry and showed accelerated speeds due to convergence of streamlines at the canyon heads. Only at Mooring 6, northeast of Fairweather Bank, was the observed current weak, variable, and tidally dominated, with a weak eastward component throughout the six-month record.
3. Littoral currents were smaller than in autumn and were bimodal in the along-shore direction, in response to the March-April shift in the wave field from southerly-easterly to southeasterly-southwesterly.

5. OVER-WINTER WINDS AND CURRENTS

As described above (Section 2), current mooring 6 was left deployed during the October 1980-April 1981 period in order to detect variations having longer time scales than would have been detectable with the 12-day autumn and spring Moorings 1-5. To supplement the data from Mooring 6, wind data taken at Yakutat Airport and computed geostrophic wind were obtained for the same over-winter period. This section briefly describes and discusses the results of these over-winter observational efforts.

5.1 Over-Winter Currents at Mooring 6

Two current meters were deployed on Mooring 6 (see Figure 2 for location). The shallower of the two malfunctioned early during the mooring period, and the usable portion of its record has been discussed above (Section 3). The current meter at the deeper level (102 m) provided a record nearly 5.5 months long, bracketing the over-winter period October 1980-April 1981; this record is shown in Figure 54. The along-shore and cross-shelf components have been one-hour filtered to remove high-frequency noise. Since, however, the sampling interval of the current meter was 30 minutes, the record is little altered from the raw data. The record is remarkably "clean" and shows no current speeds higher than about 50 cm/sec. Because of the compressed time scale, the tidal components appear as "noise" on the lower frequency fluctuations in Figure 54. The plot of velocity as a function of time (Figure 54, top) was derived from the one-hour filtered values by subsampling every eight hours. Although this probably removed some of the peak current speeds, it has preserved the essentially fluctuating nature of the record.

There were two prominent features of the 102-m deep current record from Mooring 6. The first, seen upon visual inspection of Figure 54, was the tendency for flow events to occur on a time scale of five to six days. These events were of similar magnitude in the along-shore and cross-shelf directions and consisted primarily of fluctuations between northeasterly and southeasterly flow, although reversals to westward flow did occur at infrequent intervals. The second was a net easterly flow which persisted throughout the record. Since the record was longer than 60 days, it satisfied the requirement derived by Lagerloef et al.

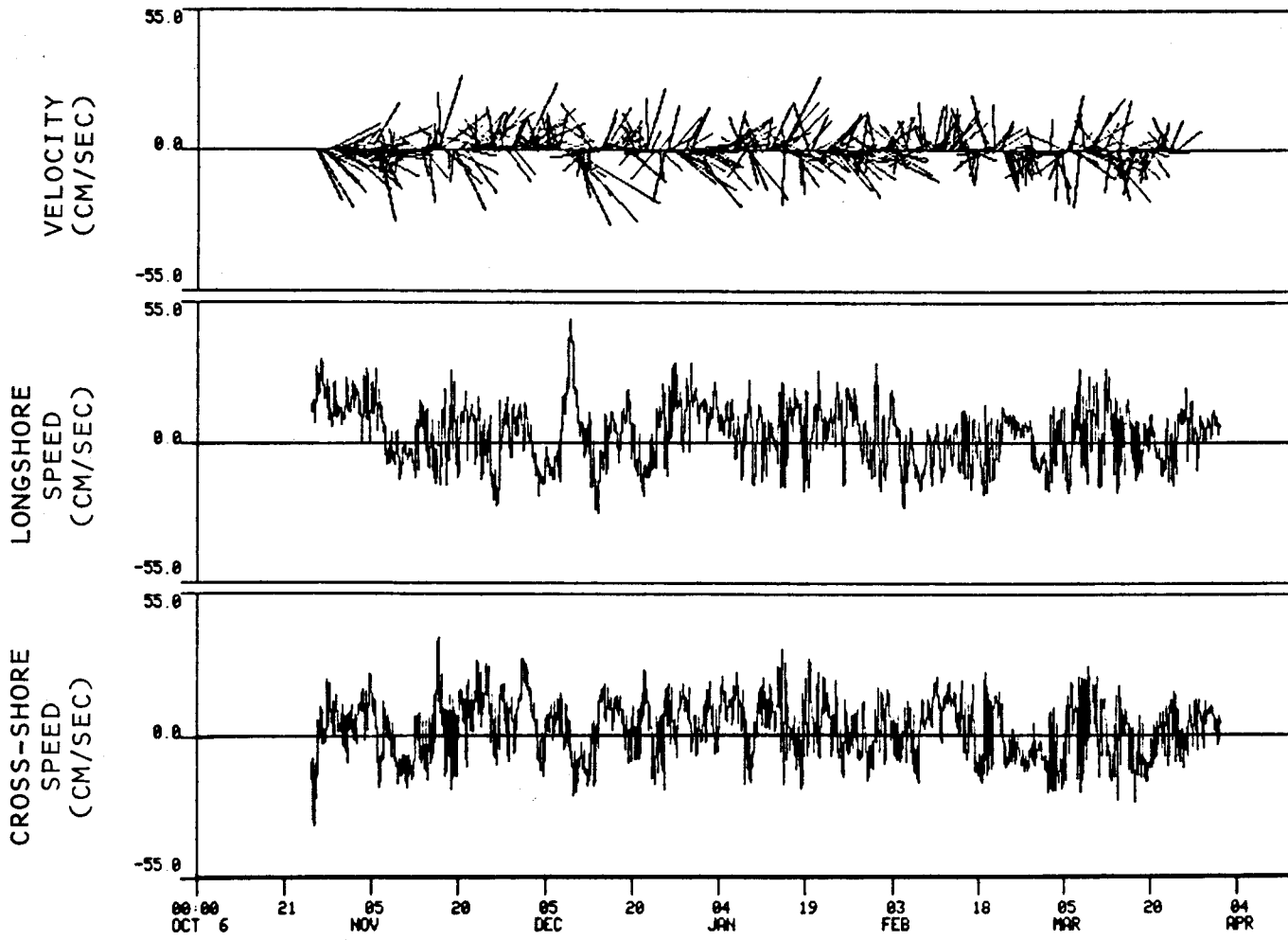


Figure 54. One-hour filtered currents at mooring 6 for the 102-m deep current meter plotted as a function of time.

(1981) for minimum record length needed to yield a mean current velocity valid at the 95 percent confidence level. The vector-averaged over-winter mean velocity at 102 m at Mooring 6 was 6.1 cm/sec at 82 °T.

The 5- to 6-day time scale for flow events was similar to that reported by Hayes (1979) for the continental shelf region off Icy Bay, about 100 km west of Yakutat. Hayes concluded that at the 100 m isobath, a large part of the observed current variability in the 5- to 6-day band was due to local wind forcing. The observations that local winds during the mooring period were characterized by 4- to 6-day time scales (Section 5.2) is also consistent with this contention. However, lack of a long-term cross-shelf array of moorings containing both current meters and pressure gauges precludes a rigorous analysis of local wind/current interaction such as was carried out by Hayes. In addition, Hayes' analysis was carried out on data obtained from a relatively simple (compared to the region of the present field program) shelf area, while the results reported here were subject to probable topographic influences not considered significant in Hayes' analyses.

The reason for the appreciable long-term net eastward flow at Mooring 6 is uncertain. It is probably related to location of the mooring north of Fairweather Bank, a shoal area, and may reflect an anticyclonic circulation around the Bank. A similar weak (5-10 cm/sec) anticyclonic flow over Portlock Bank in the north-west Gulf of Alaska off Kodiak Island was reported by Muench and Schumacher (1980), who speculate that flow over bottom topography in the region was controlled in large part by potential vorticity conservation constraints. A similar mechanism in the present study area would dictate anticyclonic flow about Fairweather Bank and a consequent southeasterly flow north of the Bank as observed at Mooring 6.

5.2 Over-Winter Local Winds

Winds used for the over-winter analysis were obtained from the National Weather Service office at Yakutat Airport in Yakutat (cf. Figure 1) and as computed geostrophic winds from FNWC in Monterey, California. The filtered time series obtained from these two sources are shown in Figures 55-57. The velocity time series (Figure 55) illustrate the overall directional trend of the winds. The easterly and northerly speed components illustrate the agreement

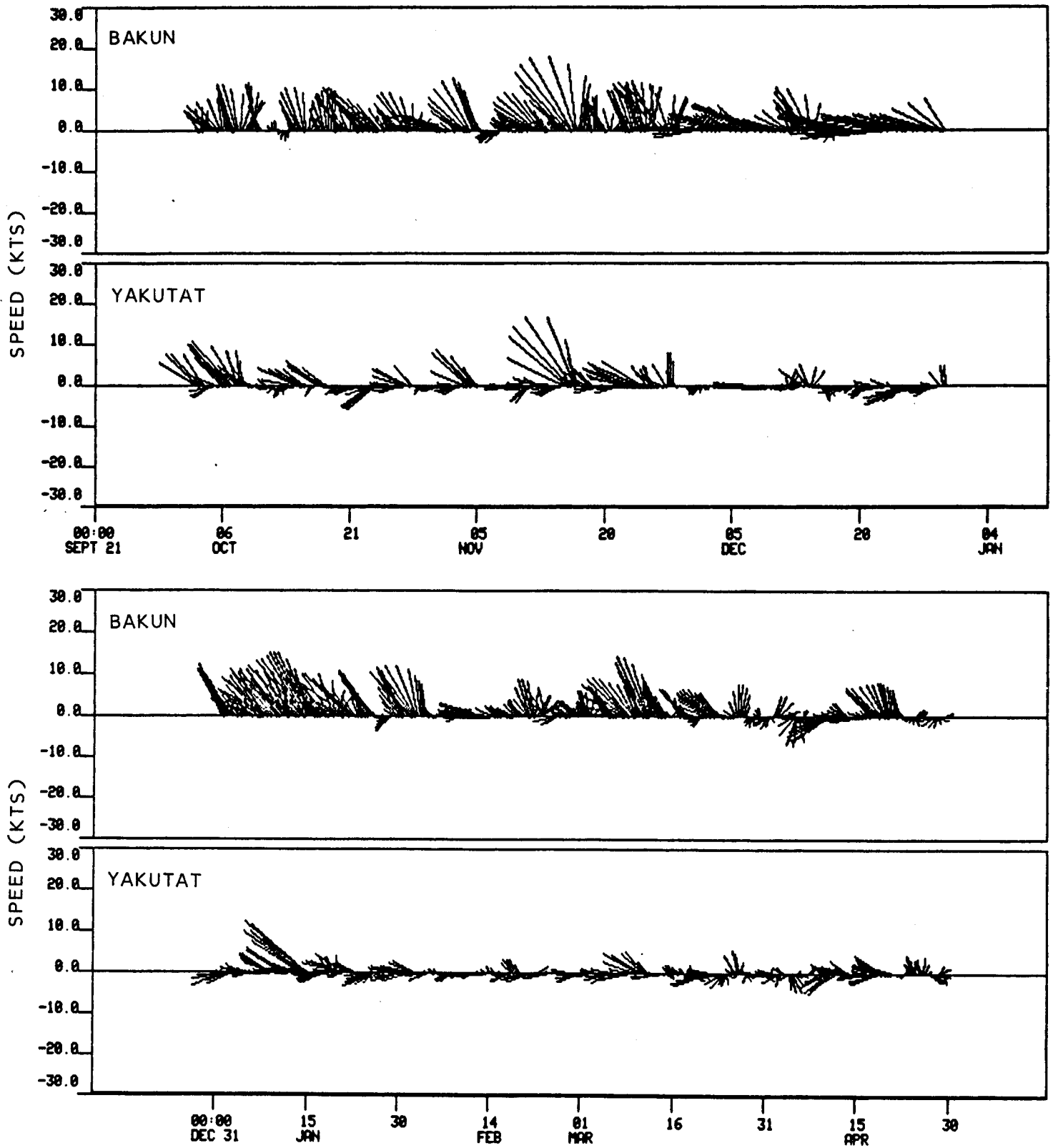


Figure 55. 30-hour filtered winds as observed at Yakutat airport and as computed geostrophic winds plotted as a function of time for September 1980 - April 1981. Wind blowing toward north is up.

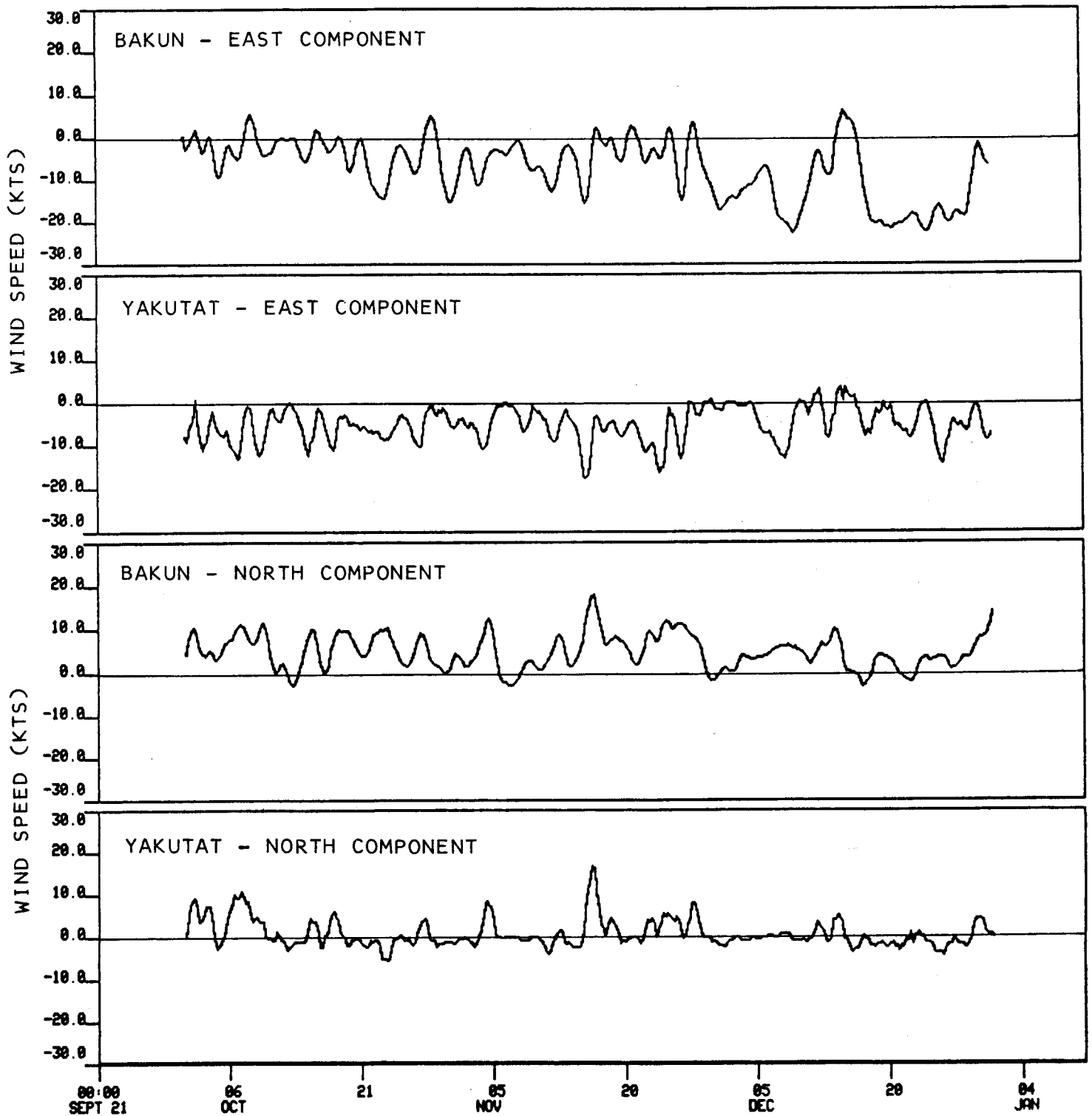


Figure 56. 30-hour filtered east and north wind speed components from Yakutat airport and as computed geostrophic winds plotted as a function of time for September-December 1980. Positive east (north) indicates wind was blowing toward the east (north).

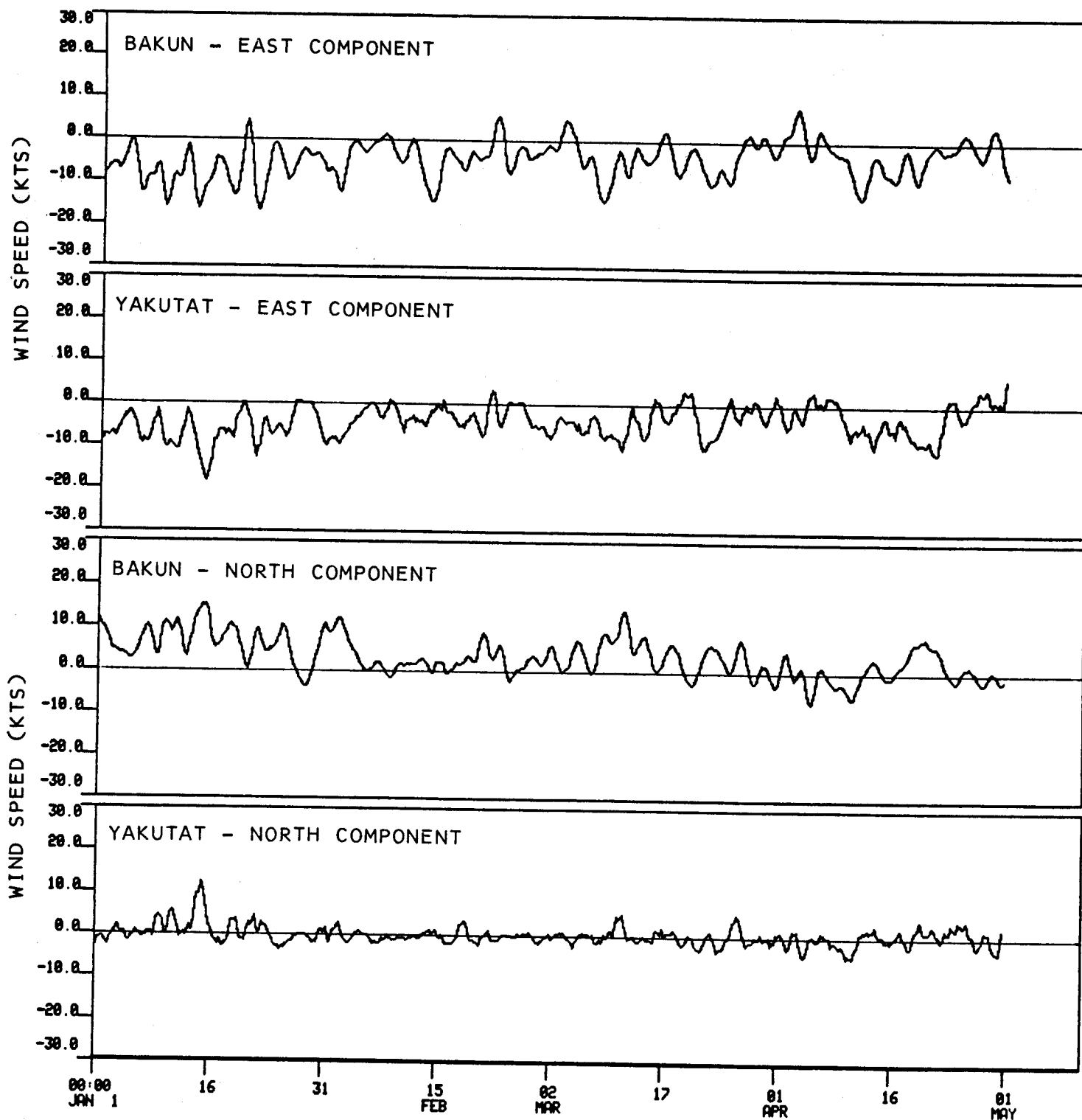


Figure 57. 30-hour filtered east and north wind speed components from Yakutat airport and as computed geostrophic winds plotted as a function of time for January-April 1981. Positive east (north) indicates wind was blowing toward the east (north).

between the Yakutat Airport and computed winds for individual events (Figures 56-57).

Both the wind series show two distinct features. First, the net wind direction through the winter was easterly-southeasterly, with the computed winds having a greater south component than the airport winds. This net direction is because the winds fall along the northeastern portions of cyclones which propagate into the region as part of the Aleutian low-pressure trough. The directional difference between observed and computed winds is due to isobaric blocking by the mountainous coastline which does not affect the computed winds but does, however, cause the observed winds to parallel the coastline. Thus, the computed winds may actually provide the better approximation to the true offshore wind field. Conversely, the observed winds may be more indicative of conditions over the 10-km wide coastal oceanic region focused upon by this program.

The second apparent feature of the winds is the domination by events having time scales of 4-6 days. This observation is in agreement with statistics computed from historical data by Brower et al. (1977). The 4- to 6-day time scale is due to propagation of cyclonic low-pressure systems into the region along the Aleutian Low pressure trough. Visual comparison between the observed and computed winds shows that the majority of wind events were evident on both records. Because the storm systems propagate in a nonstationary fashion, i.e. they occur over time scales varying from about 4 to 6 days, spectral analyses applied to the entire record yield a broad flat energy peak over that range. Application of maximum energy method (MEM) analyses to monthly data sets through the winter yielded, however, more concise information on time scales. The MEM method is capable of resolving time scales (or periods, for periodic functions) given sample intervals which are short -- of order one period or even less. However, this method does not provide reliable estimates of the relative magnitude of energy peaks which are found at different frequencies. An example of a normalized MEM spectrum for the computed geostrophic wind speeds for the month of November 1980 is shown in Figure 58; the spectra for the other months were similar and will not be shown here. The peak at about four days shifted slightly from month to month but was consistent over most of the winter, and represents the most dominant frequency for propagation of high-wind-speed storm events into the area. These spectral estimates therefore are consistent with time scales derived from visual inspection and from the historical data as presented in Brower et al. (1977).

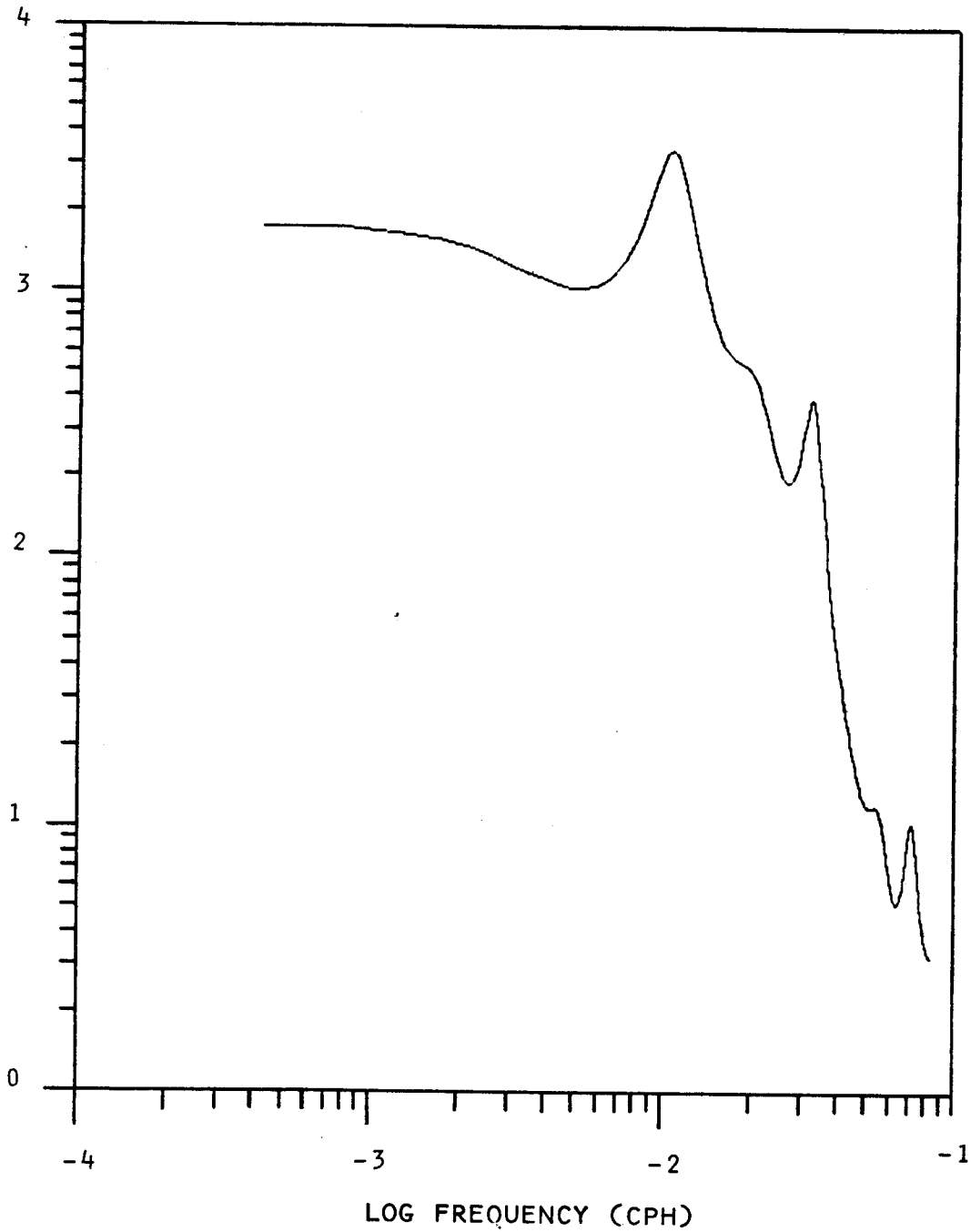


Figure 58. Normalized spectral estimate for computed geostrophic wind speeds during November 1980, computed using a Maximum Entropy Method (MEM) routine.

5.3 Summary

The results from the over-winter current observations from Mooring 6 and the over-winter wind observation program can be summarized as follows:

1. Mean flow at 102 m at Mooring 6 was about 6 cm/sec directed toward 82 °T for the entire October 1980-April 1981 period. Eastward flow at this location was probably due to interaction of a northwesterly regional flow with a rise in the bottom topography.
2. Mean winds for the region were southeasterly (toward the northwest) through the winter. This directional orientation reflects the origin of the winds from eastward-propagating cyclonic low-pressure systems, and is normal for the region.
3. Both currents and winds exhibited events which were large relative to the means and which had dominant time scales of 4-6 days. For the winds, the time scale was that associated with propagation of discrete cyclonic storm systems into the region. Conventional wisdom concerning continental shelf dynamics, coupled with the observed similarity in time scales, suggests that the current variations were a result of wind fluctuations, although complications introduced by a complex bottom topography precluded rigorous analyses of these interactions.

6. SUMMARY AND DISCUSSION

In this section the observational results presented in Sections 3-5 are summarized and discussed briefly within the context of possible effects on the fate of contaminants related to OCS petroleum development activities. Whereas each of the above sections dealt with a specific season, except for the over-winter time series, this section integrates results from the different seasons in order to present as general a depiction of regional transport processes as possible while at the same time retaining information pertinent to major seasonal variability. Finally, autumn and spring mean currents are summarily compared with the results of the Galt and Watabayashi (1980) diagnostic model.

The results of this investigation can be summarized:

1. A coastal band of water relatively low in temperature and low in salinity was present in autumn 1980 but was no longer in evidence in spring 1981. When present, this band was about 7 km wide and 20 m or less thick. Its presence in autumn, but not in spring, was due to admixture into the marine waters of the large autumn coastal freshwater input.
2. Currents within about 5 km from shore were almost entirely along-shore, with small on- and offshore components. In fall these currents were usually to the northwest at about 10 m depth, as shown by drogue studies. At 30 m depth, however, the currents were bimodal and flow was to the southeast and to the northwest for about equal percentages of the time. In spring, flow was consistently toward the northwest at all depths, and current speeds were 10-20 cm/sec.
3. At about 10 km offshore, outside the immediate coastal region, currents were variable with a net flow to the northwest and stronger on- and offshore components than were observed closer to shore. The currents were more consistently northwesterly in spring than during autumn, when reversals to southeasterly flow occurred.
4. The overall large-scale flow over the shelf was to the northwest except at the mooring just north of Fairweather Bank, where a net easterly and highly variable flow regime was observed. The overall northwest flow was due to forcing by northwesterly currents along the shelfbreak and a net northwest-directed winter wind stress. The easterly flow north of Fairweather Bank was due to the influence of the shoal bottom over the banks, with resultant formation of an anticyclonic gyral flow around the Bank.

5. Currents responded to the topographic trough formed by Alsek Canyon by accelerating toward the head of the canyon. Both current meters and drogues revealed a shoreward flow along the southeast side of the canyon which fed an accelerated northwest coastal flow past the canyon head. There was some temperature and salinity evidence of deep shoreward flow in both Alsek and Yakutat canyons.
6. Currents within about 10 km of the coastline were strongly affected by passage of local storms. Strong northwest current pulses coincided with southeast wind events in this zone. Farther offshore, the wind events did not affect the currents as strongly. Long-term over-winter wind and current records revealed a common four- to five-day time scale for both, suggesting wind/current interaction.

The above general results are consistent with existing hypotheses concerning continental shelf circulation for a shelf regime characterized by a large seasonally varying coastal freshwater influx, frequent vigorous along-shore wind events, and a complex bottom topography. For purposes of estimating pollutant transport, the significant aspects are:

- The shelf-wide general net-northwesterly flow except for the location just north of Fairweather Bank where net flow was easterly;
- The large and primarily wind-induced variability superposed upon the net flow;
- Appreciable cross-shelf transport resulting from interaction of the net northwesterly flow with a complex bottom topography.

The first of these points suggests that a pollutant would be transported toward the northwest with the net flow. However, the high wind-induced variability (particularly during autumn) would limit the confidence to be placed in such a prediction for time scales of two to three days. The observed correlation between upper-layer northwesterly flow, at least near the coast, and southeast winds might be used to aid in predicting transports over time scales short relative to net flow. The infrequent occurrence of westerly flow north of Fairweather Bank suggests that pollutants entering the system there might be transported to the southeast. This raises the possibility that they might then circle the Bank in anticyclonic fashion within the suspected flow, increasing the chances of impact upon the Bank itself. The net eastward flow of 6 cm/sec north of the Bank suggests that between one and two weeks might be required for a pollutant to circle completely around the Bank. The probable occurrence of higher-speed flow events during this period could, however, alter this time estimate considerably.

The observed onshore transport along the southeast boundary of Alsek Canyon and at Mooring 3 to the northwest suggests that pollutants released in mid-shelf might find their way into the coastal region. Given the frequent occurrence of 20-30 cm/sec current pulses at virtually all of the moorings, such a cross-shelf transport might occur over a time scale of about two days. The radar-tracked drogues used in the coastal region did not indicate appreciable flow divergence in the along-shore direction. Therefore, it is probable that pollutants in the upper layer near the coast would tend to travel parallel to the coast with the current and would undergo little lateral spreading. Pollutants at the surface would, however, tend to follow the local winds rather than the current. A strong winter regional tendency toward coastal downwelling conditions would drive upper layer pollutants shoreward. As for all wind-driven processes in this region, however, downwelling is event-dominated and so can be predicted only insofar as local winds can be predicted.

Once introduced into the surf zone, it seems likely based upon the results of the seabed drifter studies that pollutants would become mixed into the bottom sediments by wave action and would make their way onto the beach in similar fashion to the drifters. In autumn, a northwesterly motion along the beach would be expected. Movement of pollutants along the beach due to littoral currents could be easily estimated in real time using empirical equations in conjunction with observed wave height and direction.

As elsewhere along the northern Gulf of Alaska coastline, the regime in the northeast Gulf is dominated by variability which has time scales of four to five days. Assuming a current of 30 cm/sec associated with this variability, a net displacement of a pollutant over a single event might be of order 60-70 km or approximately the shelf width. Except for the relatively strong net along-shore flow observed near the coast in spring, this event-driven transport will be greater than that due to the net flow over the same time period. Therefore, prediction of pollutant transport becomes a problem in predicting the local winds inasmuch as we can relate the current events to local wind events. In the absence of appreciable events, most likely to occur during spring, pollutants would tend to move shoreward across the shelf and become entrained in the northwestward along-shore coastal flow.

Results from Galt and Watabayashi's (1980) diagnostic model of the study area compare favorably with our winter 1981 field results. The diagnostic model predicts surface currents using a baroclinic field computed from field observations in conjunction with an imposed, arbitrarily specified surface wind forcing. The model results shown (Figure 59) utilized March 1979 oceanographic data for baroclinic field computation and incorporate a moderate wind stress acting from the southeast. The model yields strong cross-shelf flow associated with Alsek Canyon, a strong northwestward alongshore coastal flow off Yakutat, and large, variable currents near the shelf break.

When comparing modeled and observed currents, it must be borne in mind that the observations were subsurface whereas the model computed surface currents. No attempt will therefore be made here to compare magnitudes. Rather, a qualitative comparison is sought.

Current observations in the northeast Gulf in March-April 1980 showed that, except for mooring 6, subsurface flow was generally along-shore and to the northwest (Figure 60). This northwestward flow was particularly vigorous, with mean speeds approaching 20 cm/sec, nearest shore (moorings 1 and 4). Mooring 5 showed shoreward flow associated with Alsek Canyon, a feature which was also evident in the model output. Mooring 6 observed flow toward the east which was also evident at the same location (north of Fairweather Bank) in the model output. The strong flow at mooring 3 had a shoreward component and was also evident on the model output. Our observations did not extend sufficiently far offshore to allow comparison with the results of the model near the shelf break. Where available for comparison, the agreement between modeled and observed features suggests that the model adequately describes circulation on the inner portion of the shelf during late winter conditions.

The above comparison was between model results computed using late winter (1979) conditions of steady northwesterly wind stress and low runoff, and a set of current observations obtained under similar conditions two years later (1981). As a final comparison, observed currents during a period of high runoff and large, fluctuating northwestward wind stress (October-November 1980) are presented in Figure 61. While the current observations yielded no information seaward of about 10 km from the coastline, they indicate a northwesterly flow

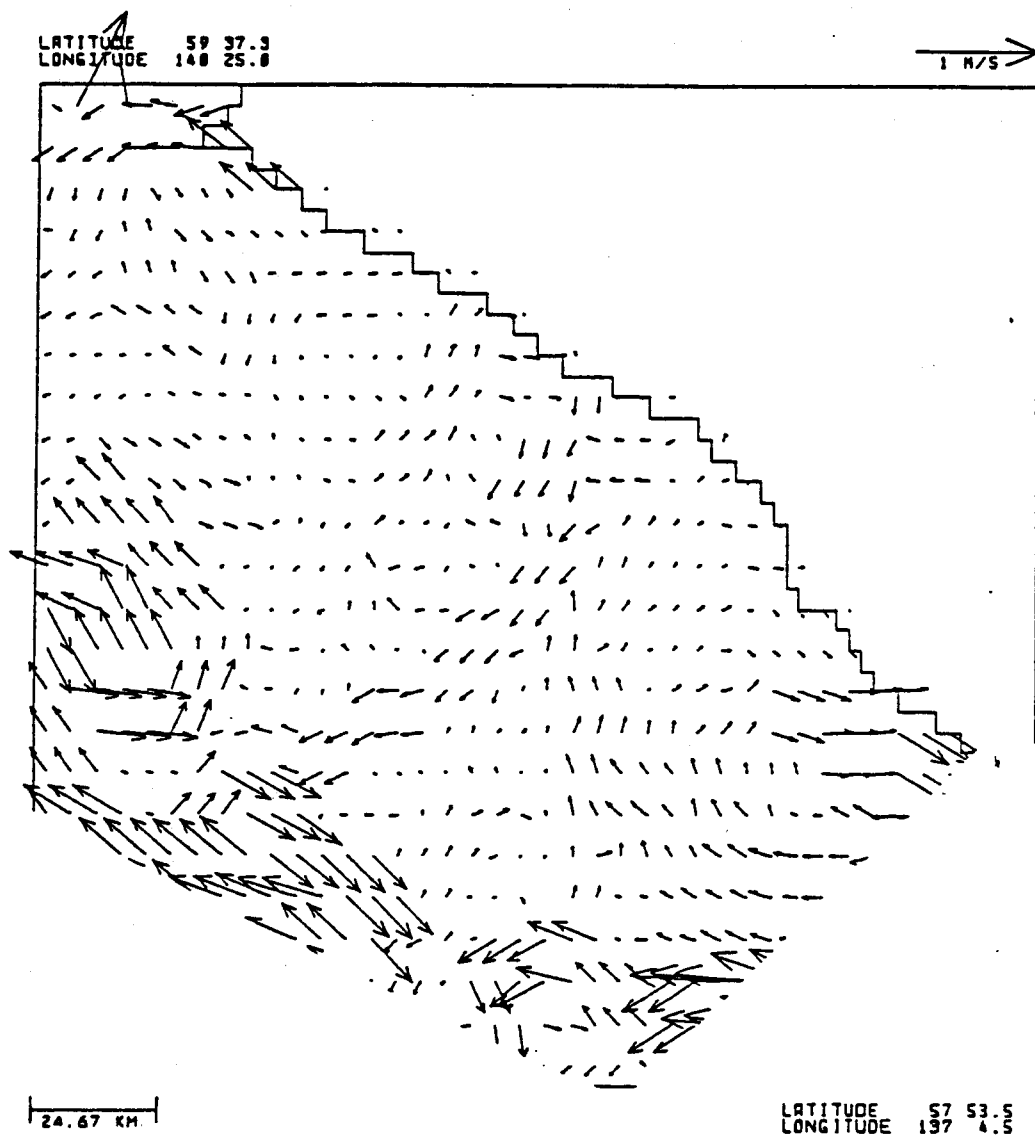


Figure 59. Surface current vectors constructed by application of a diagnostic model to March 1979 density data, assuming presence of a moderate southeasterly (towards the northwest) wind stress (from Galt and Watabayashi, 1980).

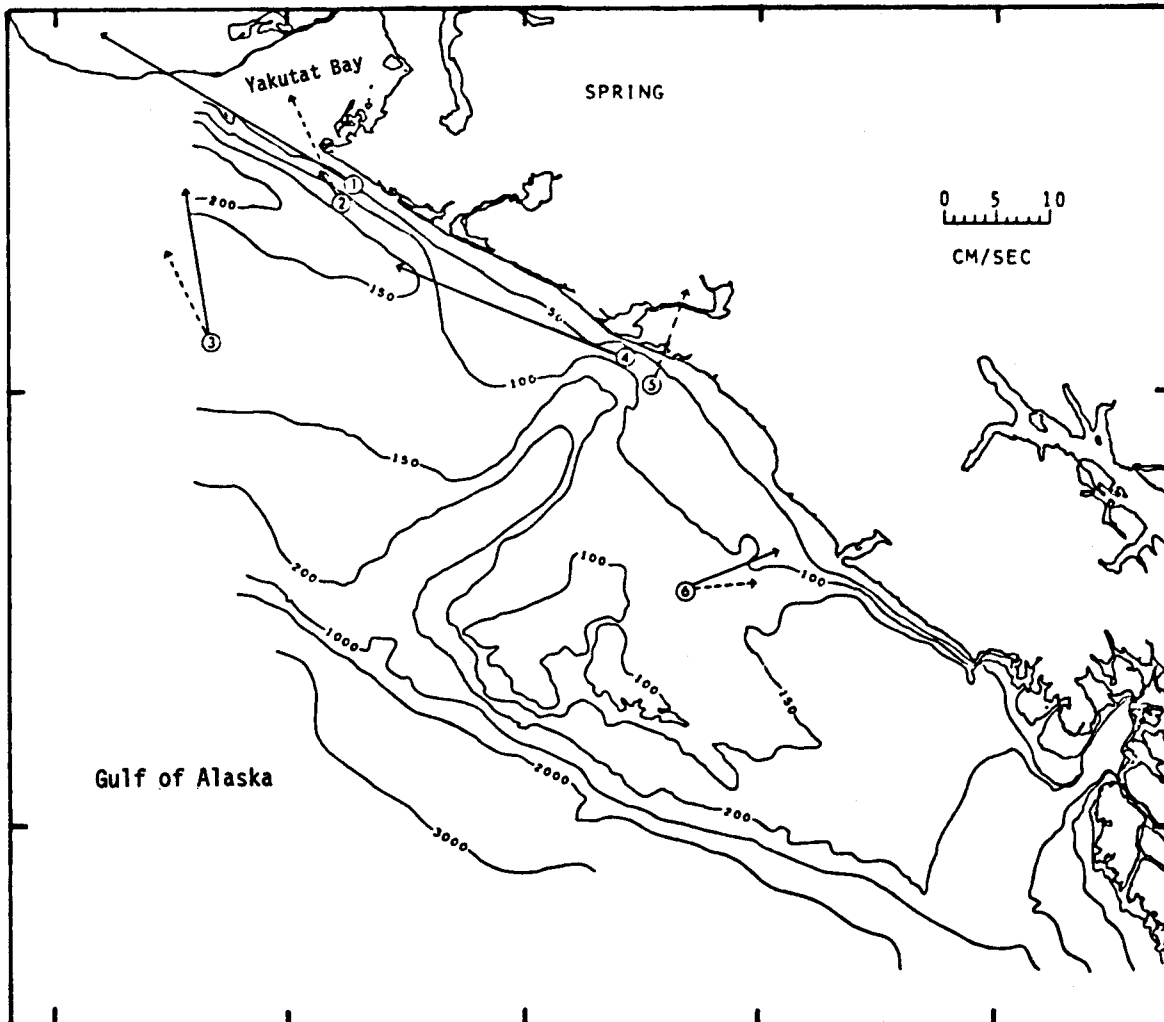


Figure 60. Vector-averaged currents from current meters deployed in March-April 1981 and for the October 1980-April 1981 record obtained at mooring 6. Dashed arrows depict the deeper, where available, of the two observations from a given mooring.

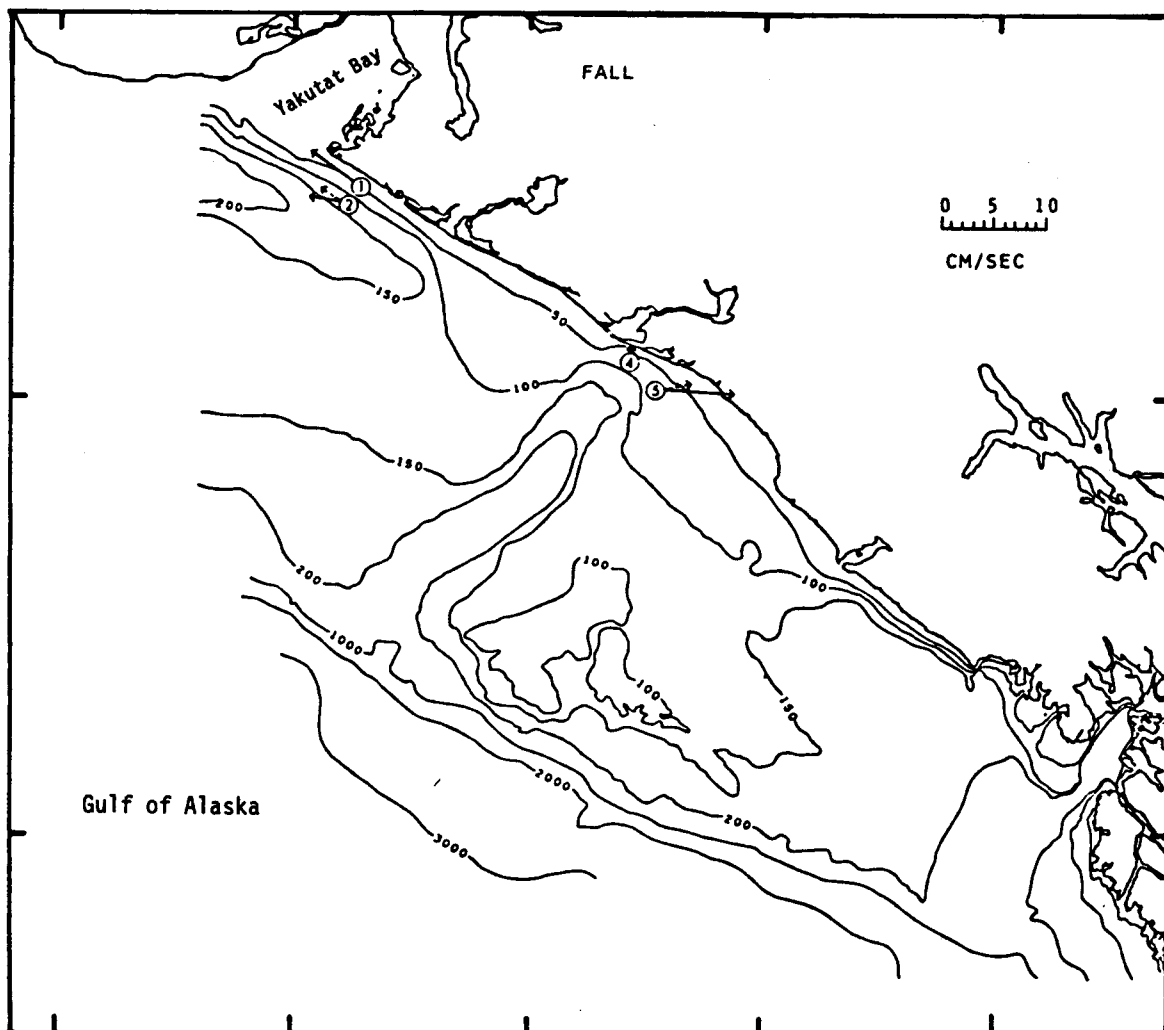


Figure 61. Vector-averaged currents from current meters deployed in October-November 1980. Dashed arrows depict the deeper, where available, of the two observations from a given mooring. These mean currents should be interpreted with caution because of extremely high speed and direction variability during the observation period.

tendency which was similar to that observed in late winter 1981. The "mean" currents in autumn 1981 should, however, be interpreted with considerable caution because the currents were highly variable throughout the observation period. The weak eastward mean flow observed at mooring 5 had superposed upon it a highly variable instantaneous flow. The coastal currents appeared to be dominated during autumn 1980 by wind-driven events as discussed above. Comparison between the observed autumn (Figure 61) and later winter (Figure 60) coastal currents suggests that the circulation became steadier and more consistently towards the northwest during the course of the winter. This seasonal trend may be due to a winter spinup of the entire coastal and offshore circulation by regional wind stress over the northern Gulf of Alaska, which reaches a maximum in mid-winter. The tendency for a mean northwesterly flow remains, however, a consistent regional circulation feature. While our data were inadequate to prove it, the effects of major topographic features such as the Alsek Canyon on the mean shelf circulation would be expected to persist throughout the year.

7. REFERENCES

- Bakun, A., 1975. Wind-driven convergence-divergence of surface waters in the Gulf of Alaska. *EOS*, 56, 1008.
- Beardsley, M.C., W. Boicourt, L.C. Huff and J. Scott, 1977. CMICE 76: A current meter intercomparison experiment conducted off Long Island in February-March 1976. Woods Hole Oceanog. Inst. Tech. Rep. HOI 77-62, 123 pp.
- Brower, W.A., Jr., H.F. Diaz, A.S. Prectel, H.W. Searby and J.L. Wise, 1977. Climatic atlas of the outer continental shelf waters and coastal regions of Alaska; Vol. I - Gulf of Alaska. AEIDC Pub. B-77, Anchorage, Alaska, 439 pp.
- Carrier, G.F. and A.R. Robinson, 1962. On the theory of the wind-driven ocean circulation. *J. Fluid Mech.*, 12, 49-80.
- Csanady, G.T., 1974. Barotropic currents over the continental shelf. *J. Phys. Oceanog.*, 4, 357-371.
- Csanady, G.T., 1975. Lateral momentum flux in boundary currents. *J. Phys. Oceanog.*, 5, 705-717.
- Favorite, F., A.J. Dodimead and K. Nasu, 1976. Oceanography of the subarctic Pacific region, 1960-71. *Internatl. N. Pacific Fish. Comm. Bull.*, 33, 187 pp.
- Galt, J.A. and G. Watabayashi, 1980. Modeling report to OCSEAP from RU 140, January 1980. 57 pp. Unpublished manuscript.
- Halpern, D. and R.D. Pillsbury, 1976a. Influence of surface waves on subsurface current measurements in shallow water. *Limnol. and Oceanog.*, 21, 611-616.
- Halpern D. and R.D. Pillsbury, 1976b.. Near-surface moored current meter measurements. *MTS Journal*, 10, 32-38.
- Hayes, S.P., 1978. Variability of current and bottom pressure across the continental shelf in the northeast Gulf of Alaska. *J. Phys. Oceanog.*, 9, 88-103.
- Hayes, S.P. and J.D. Schumacher, 1976. Description of wind, current and bottom pressure variations on the continental shelf in the northeast Gulf of Alaska from February to May 1975. *J. Geophys. Res.*, 81, 6411-6419.
- Hickey, B.M., 1981. Alongshore coherence on the Pacific Northwest continental shelf (January-April, 1975). *J. Phys. Oceanog.*, 11, 822-835.
- Holbrook, J.R. and D. Halpern, 1977. A compilation of wind, current, bottom-pressure and STD/CTD measurements in the northeast Gulf of Alaska, February-May 1975. NOAA Tech. Memo. ERL/PMEL-10, 11 pp.
- Hsueh, Y., 1980. On the theory of deep flow in the Hudson Shelf Valley. *J. Geophys. Res.*, 85, 4913-4918.
- Ingraham, W.J., Jr., A. Bakun and F. Favorite, 1976. Physical oceanography of the Gulf of Alaska. Northwest Fish. Center Processed Rep., July 1976, 132 pp.
- Komar, P.D., 1976. Beach Processes and Sedimentation. Prentice-Hall, Englewood Cliffs., N.J., 429 pp.

- Lagerloef, G.S., R.D. Muench and J.D. Schumacher, 1981. Low-frequency variations in currents near the shelf break: northeast Gulf of Alaska. *J. Phys. Oceanog.*, 11, 627-638.
- Lavelle, J.W., G.F. Keller and T.L. Clarke, 1975. Possible bottom current response to surface winds in the Hudson shelf channel, *J. Geophys. Res.*, 80, 1953-1956.
- LeBlond, P.H. and L.A. Mysak, 1978. Waves in the Ocean. Elsevier, N.Y., N.Y., 602 pp.
- Lee, T.N., 1975. Florida Current spin-off eddies. *Deep-Sea Res.*, 22, 753-765.
- Mayer, D.C., D.V. Hansen and D.A. Ortman, 1979. Long-term current and temperature observations on the middle Atlantic shelf. *J. Geophys. Res.*, 84, 1776-1792.
- McEwen, G.F., T.G. Thompson and R. Van Cleve, 1930. Hydrographic sections and calculated currents in the Gulf of Alaska, 1927-1928. *Rep. Int. Fish. Comm.*, 4, 36 pp.
- Muench, R.D. and J.D. Schumacher, 1979. Some observations of physical oceanographic conditions on the northeast Gulf of Alaska continental shelf. NOAA Tech. Memo., ERL PMEL-17, 84 pp.
- Muench, R.D. and J.D. Schumacher, 1980. Physical oceanographic and meteorological conditions in the northwest Gulf of Alaska. NOAA Tech. Memo., ERL-PMEL-22, 147 pp.
- Munk, W.H., 1950. On the wind-driven ocean circulation. *J. Met.*, 7, 79-93.
- Mysak, L.A., 1980. Topographically trapped waves. *Ann. Rev. Fluid Mech.*, 12, 45-76.
- Nelsen, T.A., P.E. Gadd and T.L. Clarke, 1978. Wind-induced current flow in the upper Hudson shelf valley. *J. Geophys. Res.*, 83, 6073-6082.
- Pearson, C.A., J.D. Schumacher and R.D. Muench, 1981. Non-effects of wave-induced mooring noise on tidal and low-frequency current observations. *Deep-Sea Res.*, 28, in press.
- Reeburgh, W.S., R.D. Muench and R.T. Cooney, 1976. Oceanographic conditions during 1973 in Russell Fjord, Alaska. *Estuarine and Coastal Mar. Sci.*, 4, 129-145.
- Reed, R.K., 1980. Direct measurement of recirculation in the Alaska Stream. *J. Phys. Oceanog.*, 10, 976-978.
- Reed, R.K., R.D. Muench and J.D. Schumacher, 1980. On baroclinic transport of the Alaskan Stream near Kodiak Island. *Deep-Sea Res.*, 27, 509-523.
- Reed, R.K. and J.D. Schumacher, 1981. Sea level variations in relation to coastal flow around the Gulf of Alaska. *J. Geophys. Res.*, 86, 6543-6546.
- Reid, J.L. and A.W. Mantyla, 1976. The effect of the geostrophic flow upon coastal flow sea elevations in the northern North Pacific Ocean. *J. Geophys. Res.*, 81, 3100-3110.

- Royer, T.C., 1975. Seasonal variation of waters in the northern Gulf of Alaska. *Deep-Sea Res.*, 22, 403-416.
- Royer, T.C., 1979. On the effect of precipitation and runoff on coastal circulation in the Gulf of Alaska. *J. Phys. Oceanog.*, 9, 555-563.
- Royer, T.C., 1981a. Baroclinic transport in the Gulf of Alaska, Part I. Seasonal variations in the Alaska Current. *J. Mar. Res.*, 39, 239-250.
- Royer, T.C., 1981b. Baroclinic transport in the Gulf of Alaska, Part II. A freshwater driven coastal current. *J. Mar. Res.*, 39, 251-266.
- Royer, T.C., 1981c. Coastal freshwater discharge in the northeast Pacific. *J. Phys. Oceanog.*, in press.
- Royer, T.C. and R.D. Muench, 1977. On the ocean temperature distribution in the northern Gulf of Alaska, 1974-1975. *J. Phys. Oceanog.*, 7, 92-99.
- Royer, T.C., D.V. Hansen and D.J. Pashinski, 1979. Coastal flow in the northern Gulf of Alaska as observed by dynamic topography and satellite-tracked drogued drift buoys. *J. Phys. Oceanog.*, 9, 785-801.
- Thomson, R.D., 1972. On the Alaskan Stream. *J. Phys. Oceanog.*, 2, 363-371.